



WORLD
METEOROLOGICAL
ORGANIZATION

WEATHER CLIMATE WATER

Training Materials and Best Practices for Chemical Weather/Air Quality Forecasting

ETR-26

ETR-26

© **World Meteorological Organization, 2020**

The right of publication in print, electronic and any other form and in any language is reserved by WMO. Short extracts from WMO publications may be reproduced without authorization, provided that the complete source is clearly indicated. Editorial correspondence and requests to publish, reproduce or translate this publication in part or in whole should be addressed to:

Chair, Publications Board
World Meteorological Organization (WMO)
7 bis, avenue de la Paix
P.O. Box 2300
CH-1211 Geneva 2, Switzerland

Tel.: +41 (0) 22 730 84 03
Fax: +41 (0) 22 730 80 40
Email: Publications@wmo.int

NOTE

The designations employed in WMO publications and the presentation of material in this publication do not imply the expression of any opinion whatsoever on the part of WMO concerning the legal status of any country, territory, city or area, or of its authorities, or concerning the delimitation of its frontiers or boundaries.

The mention of specific companies or products does not imply that they are endorsed or recommended by WMO in preference to others of a similar nature which are not mentioned or advertised.

The findings, interpretations and conclusions expressed in WMO publications with named authors are those of the authors alone and do not necessarily reflect those of WMO or its Members.

This publication has been issued without formal editing.



WORLD
METEOROLOGICAL
ORGANIZATION

WEATHER CLIMATE WATER

Training Materials and Best Practices for Chemical Weather/Air Quality Forecasting

ETR-26

TABLE OF CONTENTS

Acknowledgements	x
Foreword	xi
Chapter 1. Introduction.....	1
1.1 Purpose, Scope, Focus, and Targeted Audiences	1
1.2 Content and Characteristics	2
1.3 Impacts of Air Pollutants on Health, Ecosystems, and Economy and Importance of CW-AQF in Air Quality Regulation	3
1.4 History and Current Status of CW-AQF	7
1.5 Summary.....	9
Chapter 2. History and Characteristics of CW-AQF	15
2.1 Introduction	15
2.2 Similarities and Differences between Weather Forecasting and CW-AQF.....	15
2.2.1 History of Numerical Weather Prediction	15
2.2.2 History of 3-D CW-AQF.....	17
2.2.3 Similarities and Differences of NWP and AQF	19
2.2.4 Development of an AQF System Based on Existing Practice in NMHSs	20
2.3 Similarities and Differences between CW-AQF and Backcasting Applications	24
2.3.1 History of Chemical Transport Models or Air Quality Models.....	24
2.3.2 Similarities and Differences of Air Quality Backcasting and Forecasting.....	25
2.4 Major Characteristics of CW-AQF	25
2.4.1 Expected Characteristics of CW-AQF.....	25
2.4.2 Coupling of Meteorology and Chemistry.....	28
2.5 Summary.....	29
Chapter 3. Fundamentals of 3-D CW-AQF Models	37
3.1 Introduction.....	37
3.2 Model Types and Existing Models	37
3.2.1 Model Types.....	37
3.2.2 Existing 3-D CW-AQF Models.....	38
3.2.3 Summary.....	50
3.3 Meteorological and NWP Models for Air Quality Forecasting	57
3.3.1 Introduction.....	57
3.3.2 Meteorological Data Requirements for CW-AQF Systems.....	57
3.3.3 Characteristics of Global and Mesoscale Meteorological and NWP models used for AQF.....	59

3.3.4	Different Couplers, Pre/Post-Processing, and Interfaces between NWP and ACT Models.....	59
3.3.5	Methods for The Model Downscaling and Nesting	61
3.3.6	Summary.....	65
3.4	Atmospheric Planetary Boundary Layer and Parameterizations of Boundary-Layer Processes	69
3.4.1	Introduction	69
3.4.2	Representation of Interactions between Atmosphere and Various Earth Surfaces .	70
3.4.3	Turbulence Closures and Boundary-Layer Parameterizations	72
3.4.4	PBL Height and Turbulent Exchanges through the PBL Upper Boundary	73
3.4.5	Parameterizations of Radiation	74
3.4.6	Parameterization of Convection and Clouds	75
3.4.7	Summary.....	76
3.5	Atmospheric Chemistry.....	79
3.5.1	Introduction.....	79
3.5.2	Gas-Phase Chemistry Related to Tropospheric Ozone and Particulate Matter Formation	79
3.5.3	The Relationship Between Gas-Phase Chemistry and Particulate Matter Production.....	83
3.5.4	Gas-Phase Chemistry Mechanisms for Air Quality Modeling	85
3.5.4.1	Carbon Bond Mechanisms	85
3.5.4.2	The Regional Acid Deposition Model and Regional Atmospheric Chemistry Family of Mechanisms.....	90
3.5.4.3	Statewide Air Pollution Research Center (SAPRC) Mechanisms.....	92
3.5.4.4	MOZART	92
3.5.4.5	Emission Inventories and Their Relationship to Chemical Mechanism Schemes	93
3.5.5	Aqueous-Phase Atmospheric Chemistry in Clouds and Aerosols	97
3.5.6	Heterogeneous Atmospheric Chemistry.....	98
3.5.7	Aqueous Phase and Heterogeneous Chemistry Included in CW-AQF Models.....	99
3.5.8	Summary.....	104
3.6	Atmospheric Aerosol	115
3.6.1	Introduction	115
3.6.2	Atmospheric PM Composition, Size Distribution, and Mixing State	115
3.6.3	Modeling of Atmospheric PM Thermodynamics.....	129
3.6.4	Modeling of Atmospheric PM Dynamics	132
3.6.5	Summary.....	135
3.7	Atmospheric Removal.....	145
3.7.1	Introduction.....	145
3.8	Interactions of Aerosol Species with Radiation via the Direct Effect for CW-AQF Models	165
3.8.1	Introduction.....	165
3.8.2	Definitions: the Physics of the Aerosol Direct Effect.....	170
3.8.3	Implementation of Aerosol Optical Properties in CW-AQF Models.....	172
3.8.4	Aerosol Direct Effect Parameterizations Currently Used in CW-AQF Models.....	174
3.8.5	Summary.....	187
3.9	Interactions of Aerosol Chemical Species with Clouds for CW-AQF Models.....	194
3.9.1	Introduction.....	194
3.9.2	Aerosol-Cloud Interaction in CW-AQF Models.....	195
3.9.3	Major Uncertainties on Aerosol-Cloud Interactions	196
3.9.4	Summary.....	201

Chapter 4.	Model Deployment and Application	206
4.1	Introduction	206
4.2	Types and Purposes of CW-AQF Applications	206
4.3	Model Selection	207
4.4	Application Domain	207
4.4.1	Single Domain	208
4.4.2	Nested Domain	208
4.4.3	Defining Domains for Countries	209
4.5	Configurations	209
4.5.1	Coupling Options (1- or 2-way)	209
4.5.2	Time Steps	209
4.5.3	Physical Options	210
4.5.4	Chemical Options	210
4.6	Computing Platforms	211
4.6.1	Multi-Processors	211
4.6.2	Cloud Computing	211
4.7	Downscaling of Global Forecast Products for Regional/Urban Forecasting	211
4.8	Summary	212
Chapter 5.	Special Considerations for Urban Applications	214
5.1	Introduction	214
5.2	Characteristics of Urban Scale Forecast Models	216
5.2.1	Introduction	216
5.2.2	Urban Morphology and Metabolism	216
5.2.3	3-D Urban Structure	217
5.2.4	Initial and Boundary Conditions	219
5.2.5	Resolution Limitations	219
5.2.6	Urban Modeling Science and Supporting Data	220
5.2.7	Interactions with Mesoscale Circulations, and Exacerbations with Respect to Climate Changes	221
5.2.8	Summary	221
5.3	Consideration of Urban Induced Thermal and Air Quality Patterns and Circulations for CW-AQF	223
5.3.1	Introduction	223
5.3.1.1	Scale-dependent photochemistry issues and related urban mixtures	223
5.3.1.2	Characteristics of Urban Morphological Structures	224
5.3.1.3	Treating Intraurban Circulations, UHI, and Climate-Induced Weather Extremes	224
5.3.2	Urban Heat Islands	224
5.3.3	Heat Waves, Air Quality, and Environment Comfort	227
5.3.4	Urban Emissions	229
5.3.6	Summary	233
5.4	Urban Canopy Models	239
5.4.1	Introduction	239
5.4.2	Definition of UCMs	239
5.4.3	Background of UCMs	239
5.4.4	Unique Features	240

5.4.5	Impact of Buildings on AQ and Emissions.....	241
5.4.6	Approaches, Considerations, Advantages and Disadvantages	242
5.4.6.1	Bulk (Flux Profile)	242
5.4.6.2	Urban Canopy	242
5.4.7	Data Requirements and Infrastructure Support.....	243
5.4.8	Modeling System and Applications	244
5.4.9	Summary.....	245
5.5	Coupling with Parameterized or Computational Fluid Dynamics Models	247
5.5.1	Introduction.....	247
5.5.2	Parameterized Microscale Models	248
5.5.3	Full CFD Models.....	248
5.5.3.1	Online Coupling Meteorological/AQ Mesoscale Variables into the CFD Model	249
5.5.3.2	Offline Coupling Meteorological/AQ Mesoscale Variables into the CFD Model	249
5.5.3.3	Coupling Meteorological/AQ Mesoscale Model and Pre-run CFD Simulations.....	250
5.5.4	Summary.....	251
5.6	Urban Data and Tools for CW-AQF Models.....	253
5.6.1	Introduction.....	253
5.6.2	Data Requirements and Tools for Urban Scale Applications	254
5.6.3	Summary.....	259
Chapter 6.	Special Considerations for Extreme Events	262
6.1	Introduction.....	262
6.2	Wildfires and Prescribed Burning.....	262
6.2.1	Predicting the Risk of Vegetation Fires.....	263
6.2.2	Precompiled Global Fire Emission Inventories and Uncertainties.....	263
6.2.3	Satellite Products used for Wildland Fire Monitoring.....	264
6.2.4	Modeling the Fire Impact on Atmospheric Composition and Air Quality	264
6.3	Dust Storms.....	265
6.3.1	Environmental and Health Effects of Dust Storms	265
6.3.2	Global and Regional Trends of Dust Storms.....	266
6.3.3	Overview of Dust Storm Prediction and Forecasting.....	267
6.3.3.1	Dust Prediction Models	267
6.3.3.2	Dust Observations	268
6.3.3.3	WMO Sand and Dust Storm Centers.....	268
6.3.4	Current Challenges	269
6.3.5	Future Research and Recommendations.....	269
6.3.5.1	Dust Mineralogy	269
6.3.5.2	Dust Research for Decision-Making Support	269
6.4	Sudden Release of Air Toxics.....	270
6.4.1	Type of Air Toxics and Those Treated in Current CW-AQF.....	270
6.4.2	Examples of Models Used for Forecasting Air Toxics	270
6.4.2.1	ALOHA Model	270
6.4.2.2	HYSPLIT/ALOHA Model	271
6.5	Volcanic Eruption.....	273
6.5.1	Scope and Mandate for Volcanic Plume Forecasts with CW-AQF	273
6.5.2	Observations of Volcanic Eruptions.....	274
6.5.3	Overview of Modeling Approaches	274
6.5.4	Combining Modeling and Observations for Predicting Volcanic Plumes	275
6.6	Summary.....	276

Chapter 7.	Model Input and Preparation of Simulations	282
7.1	Introduction	282
7.2	Emissions	282
7.2.1	Characteristics of Emission Sources.....	282
7.2.2	Dynamic Emission Models vs. Static Inventories	283
7.2.3	A Few Widely-Used Emission Inventories	284
7.3	Initial and Boundary Conditions	285
7.3.1	Model Initialization.....	285
7.3.2	Boundary Conditions	286
7.3.3	Impact of Chemical Initial and Boundary Conditions	287
7.4	Land Use and Land Cover	289
7.5	Other Model Input Files	290
7.6	Summary.....	290
Chapter 8.	Model Output and Data Management	293
8.1	Introduction	293
8.2	Model Output	293
8.2.1	Horizontal and Vertical Resolution of Model Output	293
8.2.2	Output Frequency and Output Mode.....	293
8.2.3	Chemical Constituents.....	294
8.2.4	Meteorological Variables	294
8.2.5	Process Diagnostics.....	294
8.2.6	Customized Diagnostics.....	294
8.3	Data Management and Access Tools.....	295
8.3.1	Data Format.....	295
8.3.2	Meta data	295
8.3.3	Data Access	296
8.4	Summary.....	297
Chapter 9.	Model Evaluation	299
9.1	Introduction	299
9.2	Observational Dataset	299
9.2.1	Background of CW-AQ Observations.....	299
9.2.2	Summary of Available Observational Data.....	300
9.2.3	Representativeness of CW-AQ Observations	300
9.2.4	Obtaining Observational Data.....	304
9.3	Evaluation Protocols and Criteria for Targeted Performance.....	304
9.3.1	Purposes and Basic Principles of Model Evaluation.....	304
9.3.2	Summary of Techniques	305
9.4	Measures of Forecast Quality.....	306
9.4.1	Description of Discrete and Categorical CW-AQ Forecasting.....	306
9.4.2	Quality Measures Reflecting CW-AQ Regulation.....	306
9.4.3	Summary of Statistical Metrics	306

9.5	Advanced Spatio-Temporal Evaluation.....	310
9.5.1	Background.....	310
9.5.2	Satellite Data	310
9.5.3	Other Remote Sensing Data	311
9.5.4	Ensemble Evaluation Techniques	311
9.6	Model Evaluation Tools and Software.....	312
9.6.1	Availability and Types of Tools and Software	312
9.6.2	Use of Non-Tailored Evaluation Software	312
9.6.3	Use of Tailored Software for Air Quality Evaluation.....	313
9.7	Summary.....	314
Chapter 10. Bias Correction and Forecast Skill Improvement Methods		318
10.1	Introduction	318
10.2	Overview of CW-AQF Model Performance and Biases Reported in the Literature ..	318
10.2.1	CW-AQF Model Performance Skills	318
10.2.2	CW-AQF Model Biases and Likely Causes	326
10.3	Data Fusion.....	327
10.3.1	Fusion with Unbiased Data	327
10.3.2	Data Fusion with Biased Data.....	328
10.3.3	Bias Correction and Weight Modification	329
10.3.4	Examples and Resources	329
10.4	Data Assimilation.....	330
10.4.1	Background.....	330
10.4.2	Summary of Data Assimilation Methods.....	331
10.4.3	Special Considerations Specific to Chemical Data Assimilation	333
10.4.4	Considerations on Observations Assimilated.....	334
10.4.5	Examples and Resources	339
10.5	Inverse Modeling using Data Assimilation	339
10.5.1	Background.....	339
10.5.2	Summary of Inverse Modeling Methods	340
10.5.3	Special Considerations Specific to Inverse Modeling	341
10.5.4	Examples and Resources	342
10.6	Summary.....	343
Chapter 11. Uncertainty Quantification and Probabilistic Forecasting		357
11.1	Introduction	357
11.2	Definitions	357
11.2.1	The Challenge of Uncertainty.....	357
11.2.2	The Power of Probability	357
11.3	Different Forms of Ensembles.....	357
11.3.1	Overview	357
11.3.2	Dynamical Ensembles.....	358
11.3.3	Analog Ensembles.....	359
11.4	Attributes of Probabilistic Prediction	359
11.4.1	Overview	359
11.4.2	Statistical Consistency.....	359

11.4.3	Reliability.....	359
11.4.4	Sharpness.....	362
11.4.5	Resolution and Discrimination	362
11.4.6	Spread-Skill Relationship	362
11.5	Post-Processing and Calibration	363
11.6	Forecast Products from Ensembles.....	365
11.6.1	Deterministic.....	365
11.6.2	Probabilistic	365
Chapter 12.	Demonstration Cases for Real-Time CW-AQF	374
12.1	Introduction	374
12.2	Arctic/Antarctic and High-Latitude Regions.....	374
12.3	Mid-Latitude Regions.....	374
12.4	Tropical Regions of the Hemispheres	375
12.5	Summary of Best Practices	375
12.6	Demonstration Cases	376
12.6.1	Global	417
12.6.2	North America	430
12.6.3	Europe	446
12.6.4	Asia	460
12.6.5	South America.....	486
12.6.6	Oceania.....	493
12.6.7	Africa	500
12.7	Summary.....	520
Appendices	528
List of Tables	538
List of Figures	540
Nomenclature	546

Acknowledgements

This training publication is sponsored by the WMO Education and Training Office and the Global Atmosphere Watch Programme (GAW), with support from the Scientific Advisory Groups on Modeling Applications (GAW SAG APP) and GAW Urban Research Meteorology and Environment (GURME). In particular, we acknowledge the initiative and support from Yinka Rotimi Adebayo, Director of the Education and Training Office throughout the development of this publication. This publication has been developed with support from many researchers in the air quality and meteorology communities worldwide.

We acknowledge the following people for their contributions to this publication:

Scientific editors: Yang Zhang and Alexander Baklanov.

Lead authors (alphabetically): K. Wyatt Appel, Alexander Baklanov, Jason Ching, Edmilson Freitas, Carlos Pérez García-Pando, Daven K. Henze, Oriol Jorba, Christoph A. Keller, Jason C. Knierve, Pius Lee, Paul Makar, Valéry Masson, Luca Delle Monache, Pablo Saide, José Luis Santiago Del Río, Karine Sartelet, Mikhail Sofiev, William Stockwell, Daniel Tong, Shaocai Yu, Yang Zhang, Chunhong Zhou, and Sergej Zilitinkevich.

Co-authors (alphabetically): Dan Aliaga, Maria de Fatima Andrade, Sara Basart, Angela Benedetti, Marc Bocquet, Stefano Calmarini, Gregory Carmichael, Martin Cope, Arlindo da Silva, Hiep Duc, Johannes Flemming, Georg Grell, Antje Inness, Lasse Johansson, Johannes W. Kaiser, Ari Karppinen, Zak Kipling, Alberto Martilli, Gerald Mills, Mariusz Pagowski, Gabi Pfister, Chao Ren, Glenn Rolph, Beatriz Sanchez, Adrian Sandu, and Ranjeet Sokhi.

Case providers (alphabetically): Aboubakr Abdallah, Maria de Fatima Andrade, Charles Chemel, Odón R. Sánchez-Ccoyllo, Martin Cope, Anton Darmenov, Hiep Duc, Aidan R. Farrow, Johannes Flemming, Edmilson Dias de Freitas, Jimmy Chi-Hung Fung, Christopher Gan, Christoph A. Keller, Kenza Khomsi, Youngseob Kim, Pius Lee, Kenneth Leung, Stuart McKeen, Mariusz Pagowski, Matthieu Plu, Chao Ren, Shital Rohekar, Karine Sartelet, Vikas Singh, Mikhail Sofiev, Ranjeet S. Sokhi, Peter Yeung, Melaku Tesfaye Yigiletu, Shaocai Yu, Magdy M. Abdel Wahab, Yang Zhang, and Chunhong Zhou.

Contributors to model descriptions (alphabetically): Maria de Fatima Andrade, Alexander Baklanov, Martin Cope, Hiep Duc, Johannes Flemming, Edmilson Dias de Freitas, Christopher Gan, Christoph A. Keller, Zak Kipling, Rostislav Kouznetsov, Pius Lee, Paul Makar, Karine Sartelet, Mikhail Sofiev, Ashraf Zakey, and Chunhong Zhou.

Reviewers (WMO SAG APP and GURME, alphabetically): Véronique Bouchet, Frank Dentener, Sue Grimmond, Michaela Hegglin, Pablo Saide, Heinke Schluenzen, Ranjeet S. Sokhi, Jianguo Tan, Taichu Tanaka, and Chunhong Zhou.

Reviewers on the outline (alphabetically): Jaakko Kukkonen, Markku Kulmala, Volker Matthias, Steven Pawson, and Ashraf Zakey.

Members of the Secretariat coordinating team Patrick Parrish, Mustafa Adiguzel, Yvette Burnett, and technical editors Catherine Ostinelli-Kelly and Cecilia Cameron.

Foreword

Capacity development of Chemical Weather and Air Quality Forecasting (CW-AQF) attracts considerable attention from research communities and governments worldwide for a number of reasons. Increasing numbers of human mortality rates due to human exposure to ambient and indoor air pollution are reported. Recent scientific advancements in numerical weather prediction (NWP) and CW-AQF have been made using 3-D integrated meteorology-chemistry modeling systems and advanced data assimilation techniques combined with near-real time observations. There is a need for governments to utilize information from CW-AQF to issue health-related alerts, with increasing involvements of National Meteorological and Hydrological Services (NMHSs) and other federal and state-level environmental protection agencies in CW-AQF and Multi-hazard Early Warning Systems (MHEWS). Consequently, a growing number of forecasters use 3-D numerical models worldwide for CW-AQF and MHEWS. On the other hand, those models become progressively complex and would be difficult to adapt for real-time deployment and operation of CW-AQF without adequate training and guiding materials. An important step towards the development of WMO competency for CW-AQF would be to train and guide appropriate experts.

As part of its mandate to contribute to the protection of lives and property, WMO pays attention to the development of the training capacity of experts dealing with atmospheric pollution. Recognizing the urgent need for the successful implementation and application of 3-D numerical models for CW-AQF, WMO, through the Education and Training Office and Global Atmosphere Watch Scientific Advisory Group on Applications (GAW SAG APP), initiated the development of training materials and best practices for CW-AQF. The overarching goals of this initiative are to disseminate some practices from NMHSs and the academic community with the aim of building the scientific capacity of researchers and operational meteorologists in developing countries. Hence this publication aims to help forecasters worldwide, especially those in developing countries, to use 3-D CW-AQF models and NWP for operational forecasting, early warning, policymaking, and action-taking to reduce air pollution and associated human health effects and provide climate co-benefits in the most appropriate and efficient way. It will also provide practical information about the best operational CW-AQF practices and standardized procedures for successful deployment and application. Finally, it will assist in preparing materials that could be adapted for training by NMHSs, WMO training centers, and other users from environmental authorities and academic institutions.

The publication has been developed by some 80 experts on numerical weather prediction, air quality forecasting, anthropogenic and natural emissions (including wildfires, dust storms, air toxics, and volcanic eruptions), data assimilation, as well as ensemble and probabilistic forecasting. It also contains a review of existing worldwide research and development experience and real-time CW-AQF, incorporates existing education materials, recommendations and best practices in recognized meteorological training institutions, and identifies the critical needs for management competence enhancement in CW-AQF. This is the first edition of this publication and efforts will be made to revise it in the future.

We expect that this publication will enhance the capacity of all stakeholders in their efforts to develop and implement chemical weather and air quality forecasting systems by bringing more scientific knowhow into relevant operations on air quality forecasting. In this way, tangible contributions will be made, from the perspective of the science-policy interface, towards the implementation of relevant policy and decision support aimed at improving quality of life and environmental protection.



(Prof. Petteri Taalas)
Secretary-General

Chapter 1. Introduction

1.1 Purpose, Scope, Focus, and Targeted Audiences

Air quality is the state of the atmospheric chemical substances at a given time and place. While weather is the state of the atmosphere with respect to heat or cold, wetness or dryness, calm or storm, and clearness or cloudiness at a given place and time, chemical weather is the ambient air quality conditions at a given place and time. In the forecasting community, the terms of chemical weather and air quality are exchangeable. Chemical weather and air quality forecasting (CW-AQF) has attracted increasing attention from research communities and governmental organizations worldwide, including many National Meteorological and Hydrological Services (NMHSs), for several reasons. This increased attention is driven by several factors including (i) increasing human exposure and associated health impacts and public concerns in many regions where air quality remains poor, particularly in developing countries; (ii) recent scientific advancements in numerical weather prediction (NWP) and CW-AQF using three-dimensional (3-D) integrated meteorology-chemistry modeling systems and advanced data assimilation techniques combined with near-real time observations; (iii) increasing needs for governments to make informed decisions on issuing air quality health alerts for the protection of human health and on taking preventative actions to reduce pollutant emissions; and (iv) increasing involvements of NMHSs and other federal and state-level environmental protection agencies in CW-AQF and Multi-hazard Early Warning Systems (MHEWS) where high pollution episode forecasting (e.g., sand and dust storms) is an important element.

Atmospheric pollution is determined by emissions, chemical transformation, and removal processes, and the latter two are strongly controlled by meteorological processes. Therefore, adequate meteorological forecasting is prerequisite in AQF, and NWP is thus the key and necessary element of any AQF system. For this reason, it is a core task for the World Meteorological Organization (WMO) and NMHSs to engage in CW-AQF related activities, and examples of well-established activities include the volcanic ash advisory and assessment centers (VAACs) and the WMO Emergency Response Activities Programme for nuclear emergencies and extended to other non-nuclear airborne hazardous substances (e.g., dust, smog, volcanic ash, chemicals, bio-aerosols including pollen).

In a number of countries (e.g., Canada, Finland, France, the Russian Federation, Sweden, the United States of America) NMHSs are also responsible for, or collaborating on, air quality monitoring, forecasting, and assessment. In such countries or in countries where an NMHS is closely collaborating with its environmental protection authorities (e.g., Australia) the CW-AQF systems are usually better organized and more efficient and developed. One of the best examples of this is the first operational global atmospheric composition forecasting system (as a service) by the European Copernicus Atmosphere Monitoring Service (CAMS) (<https://atmosphere.copernicus.eu/>) building on the products of the European Center for Medium-range Weather Forecasts (ECMWF). As a result, an increasing number of forecasters are using 3-D numerical models worldwide for CW-AQF and MHEWS. A complicating factor is that these models become increasingly complex and may not be operated easily for real-time deployment and operation of CW-AQF without adequate training and guidance materials.

Recognizing the urgent need for the successful implementation and application of 3-D numerical models for operational CW-AQF, WMO in a collaborative effort of the Education and Training Office and the Global Atmosphere Watch Program, with the Scientific Advisory Groups on Applications (GAW SAG APP) and Urban Research Meteorology and Environment (GURME), initiated the development of guidance materials for training and demonstrating best practices for CW-AQF using 3-D numerical models in late 2017. The overarching goals of this initiative are to provide readers with the best existing experience from NMHSs and the academic community, and to build the scientific capacity of researchers and operational meteorologists in developing countries. This goal will be achieved by bridging research and operations and by making sustained contributions towards the implementation of relevant policy and decision support aimed at improving quality of life through enhancing the science-policy interface. The specific objectives are to (i) help forecasters worldwide, especially those in developing countries, with the use of 3-D CW-AQF models and NWP for operational forecasting, early

warning, policymaking, providing actionable information to reduce air pollution and associated human health effects and climate co-benefits in the most appropriate and efficient way; (ii) provide practical information about the best operational CW-AQF practices and standardized procedures for the successful deployment and application, and (iii) prepare materials that could be adapted for training by NMHSs, WMO training centers, and other users from environmental authorities and academic institutions.

The publication is developed as an effective, long-lasting educational and outreach tool to cover training materials and best practices for 3-D CW-AQF. It includes 12 chapters and 24 demonstration cases. It will target both entry-level and more experienced forecasters, and benefit the meteorological and air quality related communities, such as climate and public health communities. It includes fundamentals of CW-AQF and advanced materials such as applications of computational fluid dynamics (CFDs), chemical data assimilation (CDA), and inverse modeling for 3-D CW-AQF. This is the first version of the publication. It will be updated in the future to reflect the state-of-the-science development and advancement of CW-AQF.

1.2 Content and Characteristics

The publication is developed by experts in numerical weather predictions, air quality forecasting, anthropogenic and natural emissions (including wildfires, dust storms, air pollutants, air toxics (e.g., benzene and 1,3-butadiene), pollen episodes, and volcanic eruptions), observations and data assimilation, as well as ensemble and probabilistic forecasting. The guide will review existing worldwide research, development experience, and real-time 3-D CW-AQF advancements reported in relevant literature and WMO publications. It will also incorporate existing education materials, recommendations and best practice in recognized meteorological training institutions, and identify the most urgent needs for enhancing management competence in CW-AQF related issues. It will (i) describe basic principles, effective methods, and best practices important in the deployment and application of a 3-D model for CW-AQF on different scales: from global to urban; (ii) summarize the current status, the state-of-the-science CW-AQF models and their application and evaluation, special considerations and specific issues for urban applications and extreme pollution events, as well as advanced techniques for improved CW-AQF and uncertainty quantifications; (iii) provide practical recommendations for developing countries and urbanized regions how better build a CW-AQF system on national, regional, or city levels. It will also provide a number of demonstration cases of real-time CW-AQF for WMO regions including Europe, North and South America, Asia, Oceania, and Africa as well as on a global scale.

1.3 Impacts of Air Pollutants on Health, Ecosystems, and Economy and Importance of CW-AQF in Air Quality Regulation

Air quality refers to the chemical state of the atmosphere at a given time and place and how it affects people and ecosystems. Like weather, air quality affects everyone. Air pollutants include gaseous and particulate species that may lead to non-carcinogenic and/or carcinogenic adverse health effects. Numerous studies (e.g., Greenbaum et al., 2001; the World Health Organization (WHO), 2004; Georgopoulos et al., 2009; Phalen and Phalen, 2011; <https://www.apti-learn.net/LMS/EPAHomePage.aspx>) show that acute (short-term) exposure to high levels of these species may pose serious temporary health concerns such as eye irritation, difficulty breathing, pulmonary and cardiovascular health effects and premature death. Chronic (long-term) exposure may lead to health concerns such as cancer, premature death, and damage to the body's immune, neurological, reproductive, and respiratory systems. People with pre-existing heart and lung diseases and diabetics, the elderly, and children (so-called sensitive groups) are at an even greater risk for air pollution-related health effects. In addition, these pollutants and their derivatives can cause many adverse effects on the environment including visibility impairment, acid deposition, global climate change, water quality deterioration, and plant and eco-environmental system damages (e.g., Ecological Society of America (ESA), 2004; Seinfeld and Pandis, 2006; Krupa et al., 2006).

To protect human health and the environment, the WHO has issued guidelines and several countries and states have issued regulations (e.g., WHO, 2010). Most of countries also have enacted national air quality standards, e.g., the U.S. Environmental Protection Agency (EPA) has set the National Ambient Air Quality Standards (NAAQSs) for six air pollutants to protect human health (U.S. EPA, 1996; Seinfeld and Pandis, 2016) and has updated them regularly. These pollutants are sulfur dioxide (SO₂), nitrogen dioxide (NO₂), carbon monoxide (CO), ozone (O₃), lead (Pb), and particulate matter with aerodynamic diameters less than or equal to 2.5 μm (PM_{2.5}) and 10 μm (PM₁₀).

Table 1.1 summarizes air quality standards of major air pollutants implemented by WHO and several countries. In Europe, the European Union (EU) issues directives, which subsequently become air quality standards or goals in 28 member states (EU, 2008) and are still in force. The pollutants regulated by the EU include the six pollutants regulated in the U.S. as well as benzene (C₆H₆), a volatile organic compound (VOC) with known carcinogenic health effects, polycyclic aromatics, and some heavy metals. Despite significant progress in understanding emissions and fates of these pollutants as well as in reducing their ambient levels in urban areas particularly in developed countries in the past half century, air pollution has now become the world's largest single environmental health risk, responsible for human mortality and morbidity. WHO reported that in 2012 ~7 million people deaths (1/8 of total annual global deaths) are linked to exposure to outdoor and indoor air pollution (3.7 and 3.3 million, respectively) (WHO, 2014). In particular, PM pollution has been directly linked to premature deaths in many countries in the world (e.g., Schwartz, 1991; Dockery et al., 1993; Kunzli et al., 2000; Matanoski and Tao, 2002; Millman et al., 2008; Jayachandran, 2009; Zhang et al., 2010). Air pollution has also been responsible for increased hospital admissions and school/work loss days.

To protect citizens from unhealthy air, many countries have real-time air quality forecasting (RT-AQF) programs in place to forecast the concentrations of pollutants of special health concerns such as O₃, NO₂, PM_{2.5}, and PM₁₀ (e.g., Manins, 1999; U.S. EPA, 1999; Pudykiewicz and Koziol, 2001; Baklanov et al., 2007; Kukkonen et al., 2012). Such information has been used to issue early air quality alerts that allow government and people to take precautionary measures such as temporarily banning major emission sources, favoring carpooling or taking public transportation to reduce air pollution and avoid or limit their exposures to unhealthy levels of air pollution (Wayland et al., 2002). It has also been used to issue warnings to avoid outdoor physical exercise and hay fever warnings to avoid exposure to Pollen. Air quality forecasting has been used to schedule and plan numerous field campaigns to effectively track pollutant plume transport and sample pollutant concentrations, which maximizes the usage of expensive instrumented platforms such as airplanes and other limited measurement resources (e.g., Lee et al., 1997; Flatøy et al., 2000). RT-AQF has been deployed during major sport events such as the Olympic Games in Beijing and the 2010 Commonwealth games in Delhi and political summits such as the G-20 in Hangzhou (Wang et al., 2009; Wu et al., 2010; Marrapu et al., 2014; Li et

al., 2017). Accurate RT-AQF can therefore offer tremendous societal and economic benefits by enabling advanced planning for individuals, organizations, and communities in order to avoid exposure, and reduce pollutant emissions and their adverse health impacts. Driven by crucial regulations, societal and economic needs, scientific advancements, and increasing availability of high-performance computing capacity, RT-AQF has evolved from weather forecasting and developed into a new discipline that integrates science and technology from several disciplines including meteorology, atmospheric chemistry/air quality, mathematics, physics, environmental statistics, and computer sciences/engineering.

There are also several specialized applications of CW-AQF system developments for specific atmospheric pollution episodes involving harmful contaminants that affect not only health but many other sectors of economics. In particular, sand and dust storms pose a major challenge to sustainable development in arid and semi-arid regions of the planet. Airborne dust presents serious risks for human health. Sand and dust storms are also detrimental for ecosystems and diverse socio-economic sectors. Surface dust deposits are a source of micro-nutrients for both continental and maritime ecosystems. Although dust can work as fertilizer, it has many negative impacts on agriculture, including reducing crop yields by burying seedlings, causing loss of plant tissue, reducing photosynthetic activity, and increasing soil erosion. Reductions in visibility due to airborne dust also have an impact on air and land transport. Poor visibility conditions are a hazard during aircraft landing and take-off operations – flight landings may be diverted, and departures may be delayed. Dust can also scour aircraft surfaces and damage engines. Reduced radiation at the surface has an impact on the output from solar power plants, especially those that rely on direct solar radiation. Dust deposits on solar panels are a main concern of plants operators. Volcanic eruptions also contribute to natural aerosols directly via emissions of ash and other particulates, or indirectly through the release of sulfur gases that subsequently condense to form sulfate aerosols. Volcanic aerosols are particularly important for aviation safety and climate modeling, as was witness by the eruption of the Icelandic Volcano Eyjafjallajökull, that paralyzed for several days air traffic throughout Europe.

Society is impacted by both long-term and short-term changes to atmospheric composition. Volcanic ash, desert dust, natural and anthropogenic gas emissions are good examples demonstrating both immediate impacts, for example, on aviation and human health – and longer-term, including climate forcing and impacts from the changing atmospheric composition. While both present a range of challenges, the former places considerable additional demands in terms of data timeliness and temporal and spatial resolutions. This near-real-time need for observations is indeed a common requirement across a range of impacts, but one that is not always conducive to the significant processing involved in producing fully assured atmospheric composition data. However, timely data can be produced and has the potential to be of considerable use for a wide range of applications. In recognition of this, the WMO GAW Programme (GAW, 2017) has identified the need for increased support for the development and expanded use of services and research activities concerning the forecasting of atmospheric composition and its induced environmental phenomena.

Such impact-based forecast and assessment systems will help decision-makers to improve air quality and public health, mitigate the occurrence of acute air pollution episodes, particularly in urban areas, and reduce the associated impacts on agriculture, ecosystems, and climate. The suggested approach combines an ensemble of state-of-the-art models, high-resolution emission inventories, space observations and surface measurements of most relevant chemical species to provide hindcasts, analyses, and forecasts of regional air pollution in a specific region (using boundary and initial conditions from global CW-AQF system such as the CAMS) and downscaling for selected countries and urban areas.

Table 1.1 Ambient air quality standards^a of WHO, the European Union (EU), and several countries

Organization or Country	Time Scale	CO	Pb	SO ₂	NO ₂	O ₃	PM _{2.5}	PM ₁₀
WHO ^{1,2}	Short-term	10,000 (8 h) 30,000 (1 h)	-	20 (24 h) 500 (10 min)	200 (1 h)	100 (8 h ^k)	25 (24 h)	50 (24 h)
	Long-term	-	-	-	40 (1 yr)	-	10 (1 yr)	20 (1 yr)
EU ^{3,4}	Short-term	10,000 (8 h ^a)	-	350 (1 h) 125 (24 h)	200 (1 h)	120 (8 h ^a)	-	50 (24 h)
	Long-term	-	0.5 (1 yr)	-	40 (1 yr)	-	25 (1 yr)	40 (1 yr)
U.S.A. ⁵	Short-term	9 ppm (8 h) 35 ppm (1 h)	0.15 (3 mo)	75 ppb (1 h)	100 ppb (1 h)	0.07 ppm (8 h ^a)	35 (24 h)	150 (24 h)
	Long-term	-	-	-	53 ppb (1 yr)	-	12 ^b , 15 ^c (1 yr)	-
China ⁶	Short-term	10,000 (1 h) 4,000 (24 h)	1.5 (3 mo)	150 ^d , 500 ^e (1 h) 50 ^d , 150 ^e (24 h)	200 (1 h) 80 (24 h)	160 ^d , 200 ^e (8 h ^a) 100 ^d , 160 ^e (8 h ^a)	35 ^d , 75 ^e (24 h)	50 ^d , 150 ^e (24 h)
	Long-term		1 (1 yr)	20 ^d , 60 ^e (1 yr)	40 (1 yr)		15 ^d , 35 ^e (1 yr)	40 ^d , 70 ^e (1 yr)
Brazil	Short-term	10,000 (8 h) 40,000 (1 h)	-	365 ^b , 100 ^c (24 h)	320 ^b , 190 ^c (1 h)	160 (1 h)	-	150 (24 h)
	Long-term	-	-	80 ^b , 40 ^c (1 yr)	100 (1 yr)	-	-	50 (1 yr)
Australia ⁷	Short-term	9 ppm (8 h)		0.20 ppm (1 h) 0.08 ppm (24 h)	0.12 ppm (1 h)	0.10 ppm (1 h) ^f 0.08 ppm (4 h) ^f	25 (24 h)	50 (24 h)
	Long-term	-	0.5 (1 yr)	0.02 ppm (1 yr)	0.03 ppm (1 yr)		8 (1 yr)	25 (1 yr)
South Africa ⁸	Short-term	30,000 (1 h) 10,000 (8 h)	-	500 (10 min) 350 (1 h) 125 (24 h)	200 (1 h)	120 (8 h ^a)	-	75 (24 h)
	Long-term	-	0.5 (1 yr)	50 (1 yr)	40 (1 yr)	-	-	40 (1 yr)

The concentration unit is $\mu\text{g m}^{-3}$ unless otherwise noted; all values are primary standards unless otherwise noted.

^amaximum daily 8-h mean;

^bprimary standard (applicable to the health of the population);

^csecondary standard (applicable to the well-being of the population);

^dGrade-I standard (applicable to natural reserves, scenic areas and other specially protected areas in China);

^eGrade-II standard (applicable to residential areas, commercial-traffic-residential areas, cultural areas, industrial areas and rural areas in China);

^fPhotochemical oxidants (as O_3).

¹WHO (2005), Air Quality Guidelines Global Update 2005. Particulate matter, ozone, nitrogen dioxide and sulfur dioxide, WHO/SDE/PHE/OEH/06.02, 2006, ix + 484 pages, ISBN 92 890 2192 6.

²WHO (2000), Air quality guidelines for Europe, 2nd edition, 2000, Second edition, WHO Regional Publications, European Series, No. 91, 2000, x + 273 pages, ISBN 92 890 1358 3.

³<http://ec.europa.eu/environment/air/quality/standards.htm>.

⁴EEA (European Environment Agency) (2017), Air quality standards, available at <https://www.eea.europa.eu/themes/air/air-quality-standards>, European Environment Agency, Kongens Nytorv 6, 1050 Copenhagen K, Denmark.

⁵<https://www.epa.gov/criteria-air-pollutants/naaqs-table>.

⁶Ministry of Environmental Protection (MEP) (2012), Ambient air quality standards. (Document GB 3095-2012) (in Chinese).

⁷<https://soe.environment.gov.au/theme/ambient-air-quality/topic/2016/national-air-quality-standards>.

⁸https://www.environment.gov.za/sites/default/files/legislations/nemaqa_airquality_g32816gon1210_0.pdf.

1.4 History and Current Status of CW-AQF

Many aspects of the history, current status, and major future challenges of CW-AQF have been described in detail in the literature (e.g., Lawrence et al., 2005; Kukkonen et al., 2012; Zhang et al., 2012a, b; Baklanov et al., 2014; Ryan, 2016; Bai et al., 2018). The history of CW-AQF can be traced back to 1960s, when the U.S. Weather Bureau (USWB), i.e., the predecessor of the U.S. National Weather Service (NWS), provided the first forecasts of air stagnation or pollution potential using NWP models to forecast conditions conducive to poor air quality (e.g., Niemeyer, 1960). These forecasts were conducted solely from a meteorological perspective without considering the emissions and chemistry of air pollutants. Two main approaches can be distinguished in CW-AQF: empirical/statistical methods and Chemical Transport Models (CTM). A detailed review of the empirical/statistical approaches can be found in Zhang et al. (2012a) and Bai et al. (2018) and a detailed review of the CTM approaches can be found in Kukkonen et al. (2012), Zhang et al. (2012a), and Ryan (2016).

From the late 1970s to the mid-1990s, real-time CW-AQF has been mainly performed using empirical approaches and statistical models trained with or fitted to historical air quality and meteorological data (e.g., McCollister and Wilson 1975; Wolff and Lioy 1978; Aron, 1980).

The statistical approaches usually require dense and a large quantity of historical measured data under a variety of atmospheric conditions (e.g., 2-3 years observed O₃ or PM_{2.5} concentrations). They are simple to use and generally not computationally expensive. These techniques showed some RT-AQF skill. They, however, have several common drawbacks. For example, they cannot predict concentrations during periods of unusual emissions and/or meteorological conditions that deviate significantly from the historical record (Stockwell et al., 2002). The forecast accuracy typically depends on the skill of commonly used meteorological predictors, which usually neglect or use simplified parameterizations (e.g., turbulence, convection, and precipitation) for some meteorological processes (e.g., morning inversion, regional pollutant transport) that are important to the evolution of air pollutants (Ryan, 1995). These statistical models provide neither the direct linkages between precursor emissions and resultant pollution nor the interrelationships among multiple pollutants (i.e., the interactions among pollutants that may potentially exacerbate one pollution problem while another problem is being alleviated). Explicit treatments for such linkages and interactions in RT-AQF models are essential to the enhancement of understanding of the physical-chemical system, the improvement of short- and long-term RT-AQF skill, and the development of integrated emission control strategies for multi-pollutants.

Since the 1990s, RT-AQF systems based on CTMs have been developed rapidly and are currently in operation in many countries, including Australia, Canada, Japan, the U.S., France, Denmark, Germany, Norway, the U.K., Spain, Belgium, Finland, Turkey, the Netherlands, Brazil, Chile, China, Singapore, Egypt, and South Africa. Progress in CTM development and computing technologies has allowed daily RT-AQFs using simplified (e.g., Vautard et al., 2001) or more comprehensive 3-D CTMs, such as offline-coupled (Tilmes et al., 2002; Honoré et al., 2008; Schaap et al., 2008; Chen et al., 2008; Baldasano et al., 2008; McKeen et al., 2009; Sofiev et al., 2006, 2015; Lawson et al., 2017), and online-coupled meteorology-chemistry models (e.g., Grell et al., 2005; de Freitas et al., 2005; Baklanov et al., 2008; Flemming et al., 2009; Vogel et al., 2009, 2013; Chuang et al., 2011; Zhou et al. 2012; Savage et al., 2013; Li et al., 2017). The use of a coupled meteorology-chemistry model for RT-AQF represents a significant advancement in routine operational RT-AQFs and would greatly enhance understanding of the underlying complex interplay of meteorology, emission, and chemistry. Offline and online coupled models are defined in Chapter 2.3.2. Model evaluation demonstrates that a modeling approach based on CTM has skills consistent with or better than many statistical forecasting tools (McHenry et al., 2004; Manders et al., 2009).

Online-coupled meteorology atmospheric chemistry models have greatly evolved in recent years (Zhang, 2008; Grell and Baklanov, 2011). Although mainly developed by the air quality modeling community, these integrated models are also of interest to numerical weather prediction and climate modeling as they can consider both the effects of meteorology on air quality, and the potentially important effects of atmospheric composition on weather. Migration from offline to online integrated modeling and seamless environmental prediction systems (World Weather Open Science Conference (WWOSC), 2015; Coupled Chemistry-Meteorology/Climate Modeling (CCMM), 2016) is recommended for consistent treatment of processes and allowance of two-way interactions between physical and chemical components, particularly for air quality and NWP communities. Applications that may benefit from CCMM are numerous and include (Baklanov et al., 2017): chemical weather forecasting (CWF), numerical weather prediction for precipitation, visibility, thunderstorms, etc., integrated urban meteorology, environment and climate services, sand and dust storm modeling and warning systems, wildfire atmospheric pollution and effects, volcano ash forecasting, warning and effects, high impact weather and disaster risk, effects of short-lived climate forcers, Earth system modeling and projections, data assimilation for CWF and NWP, and weather modification and geo-engineering. Online integrated models, however, need harmonized formulations of all processes influencing meteorology and chemistry that are not required for offline models.

Multi-model ensemble air quality forecasting has been emerging for CW-AQF on global scale and regional scales (e.g., over Europe and China). For example, the regional air quality production of the CAMS is based on ensemble of seven state-of-the-art numerical air quality models developed in Europe. Under the MarcoPolo – Panda, EU Projects under the Seventh Framework (FP7) Programme (<http://www.marcopolo-panda.eu/>), nine different models are used for multi-model ensemble over China. The most recent the International Cooperative for Aerosol Prediction multi model ensemble (ICAP MME) consists of seven global models (Sessions et al., 2015). Multi-model ensemble results provide a range and an indication of the robustness of the forecasts and help improve the accuracy of CW-AQF. Data assimilation of satellite observations has been implemented in some CW-AQF models such as ECMWF Integrated Forecasting System (IFS)-CTMs developed by ECMWF (Flemming et al., 2009) and the Goddard Earth Observing System Model, Version 5 Earth System Model (GEOS-5 ESM) developed by the National Aeronautics and Space Administration of the U.S. (Nielsen et al., 2017).

There are also already commendable published works that provide a very thorough treatment of meteorological and air pollution modeling (see for example, Jacobson 2005; Seinfeld and Pandis, 2016; Sokhi et al., 2018). The recent publication (Sokhi et al., 2018) combines the fundamental and practical aspects of mesoscale modeling for CW-AQF. It provides an overview of the fundamental concepts of air pollution and meteorological modeling including parameterization of key unresolved processes and then considers equally important aspects such as model integration, performance evaluation, policy relevance, and user training. Therefore, that publication could be used as good complementary material for these training materials, when a reader needs to learn deeper meso-meteorological aspects of CW-AQF. Compared to previous publications, this one covers many aspects of CW-AQF at both introductory and more advanced levels for a variety of users from research and operation communities. It emphasizes the best operational CW-AQF practices and standardized procedures for CW-AQF. Of course, this document does not purport to cover all aspects of CW-AQF modeling but instead its content has been developed around topics that build upon the experience of a large number of meteorological services and air pollution modeling research and user groups from different continents, mainly from Europe, North and South America.

1.5 Summary

- Chemical weather and air quality forecasting has received increased attentions from research communities and governments, including many NMHSs.
- The main goal of this book is to provide training material and best practice on the use of 3-D CW-AQF models and NWP for operational forecasting, early warning, and policymaking for researchers and operational meteorologists, particularly for those in developing countries.
- This book includes fundamentals of CW-AQF and advanced materials such as computational fluid dynamics, chemical data assimilation, and inverse modeling for 3-D CW-AQF.
- This book also provides a number of demonstration cases of real-time CW-AQF for Europe, North and South America, Asia, Oceania, and Africa as well as on a global scale.
- Real-time CW-AQF was based on empirical approaches and statistical models prior to the mid-1990s but since 1990s it has utilized mainly 3-D chemical transport models including online-coupled meteorology atmospheric chemistry models, some with advanced techniques such as multi-model ensemble and chemical data assimilation.

References

- Baklanov, A., O. Hänninen, L. H. Slordal, J. Kukkonen, N. Bjergene, B. Fay, S. Finardi, S. C. Hoe, M. Jantunen, A. Karppinen, A. Rasmussen, A. Skouloudis, R. S. Sokhi, J. H. Sorensen, and V. Ødegaard (2007), Integrated systems for forecasting urban meteorology, air pollution and population exposure, *Atmos. Chem. Phys.*, 7, 855-874 (www.atmos-chem-phys.net/7/855/2007/).
- Baklanov A., U. Korsholm, A. Mahura, C. Petersen, and A. Gross (2008), Enviro-HIRLAM: on-line coupled modelling of urban meteorology and air pollution, *Adv. Sci. Res.*, 2, 41-46, <https://www.adv-sci-res.net/2/41/2008/>
- Baklanov, A., Schlünzen, K., Suppan, P., Baldasano, J., Brunner, D., Aksoyoglu, S., Carmichael, G., Douros, J., Flemming, J., Forkel, R., Galmarini, S., Gauss, M., Grell, G., Hirtl, M., Joffre, S., Jorba, O., Kaas, E., Kaasik, M., Kallos, G., Kong, X., Korsholm, U., Kurganskiy, A., Kushta, J., Lohmann, U., Mahura, A., Manders-Groot, A., Maurizi, A., Moussiopoulos, N., Rao, S. T., Savage, N., Seigneur, C., Sokhi, R. S., Solazzo, E., Solomos, S., Sørensen, B., Tsegas, G., Vignati, E., Vogel, B., and Zhang, Y.: Online coupled regional meteorology chemistry models in Europe: current status and prospects, *Atmos. Chem. Phys.*, 14, 317-398, <https://doi.org/10.5194/acp-14-317-2014>, 2014.
- Baklanov, A., D. Brunner, G. Carmichael, J. Flemming, S. Freitas, M. Gauss, O. Hov, R. Mathur, K. Schlünzen, C. Seigneur, and B. Vogel, 2017: Key issues for seamless integrated chemistry meteorology modelling. *BAMS*, Nov 2017, 2285-2292, [doi: 10.1175/BAMS-D-15-00166.1](https://doi.org/10.1175/BAMS-D-15-00166.1)
- Baldasano, J. M, P. Jiménez-Guerrero, O. Jorba, C. Pérez, E. López, P. Güereca, F. Martin, M. García-Vivanco, I. Palomino, X. Querol, M. Pandolfi, M. J. Sanz, and J. J. Diéguez (2008), CALIOPE: An operational air quality forecasting system for the Iberian Peninsula, Balearic Islands and Canary Islands- First annual evaluation and ongoing developments. *Adv. Sci. Res.*, 2: 89-98, ISSN: 1992-0628, May.
- CCMM, 2016: Coupled Chemistry-Meteorology/Climate Modeling (CCMM): Status and relevance for numerical weather prediction, atmospheric pollution and climate research (Symposium materials). WMO GAW-WWRP-WCRP Report #226, Geneva, https://library.wmo.int/doc_num.php?explnum_id=7938.

- Chen, J., J. Vaughan, J. Avise, S. O'Neill, and B. Lamb (2008), Enhancement and evaluation of the AIRPACT ozone and PM_{2.5} forecast system for the Pacific Northwest, *J. Geophys. Res.*, 113, D14305, doi:10.1029/2007JD009554.
- Chuang, M.-T., Y. Zhang, and D.-W. Kang (2011), Application of WRF/Chem-MADRID for Real-Time Air Quality Forecasting over the South-eastern United States, *Atmos. Environ.*, 45 (34), 6241-6250.
- Cope, M. E., G. D. Hess, S. Lee, K. Tory, M. Azzi, J. Carras, W. Lilley, P. C. Manins, P. Nelson, L. Ng, K. Puri, N. Wong, S. Walsh, and M. Young (2004), The Australian Air Quality Forecasting System. Part I: Project description and early outcomes, *J. of Applied Meteorology*, 43, 649-662.
- de Freitas, E.D., L. D. Martins, P. L. Silva Dias, and M. Fátima Andrade (2005), A simple photochemical module implemented in RAMS for tropospheric ozone concentration forecast in the metropolitan area of São Paulo, Brazil: coupling and validation, *Atmos. Environ.*, 39, 6352–6361.
- Dockery, D., C. Pope, X.P. Xu, J.D. Spengler, J.H. Ware, M.E. Fay, B.G. Ferris, and F. E. Speizer (1993), An Association Between Air-Pollution and Mortality In 6 United-States Cities, *New England Journal of Medicine*, 329 (24): 1753-1759.
- Eder, B., D. Kang, S. T. Rao, R. Mathur, S. Yu, T. Otte, K. Schere, R. Waylard, S. Jackson, P. Davidson, J. McQueen, and G. Bridgers (2010), Using national air quality forecast guidance to develop local air quality index forecasts, *Bull. Amer. Meteor. Soc.*, 91, 313-326.
- Elbern, H., E. Friese, and A. Strunk (2010), EURAD-IM Products, Quality and Background Information, report prepared for MACC, Report D_R-ENS_1.3.2, March.
- Elshout, S. v. d. and K. Léger (2007), Comparing Urban Air Quality Across Borders - A review of existing air quality indices and the proposal of a common alternative, Final Report on the CITEAIR Project of the INTERREG IIIC programme, prepared by DCMR, Environmental Protection Agency Rijnmond, The Netherlands, June.
- Ecological Society of America (ESA), 2004. Impacts of Atmospheric Pollution on Aquatic Ecosystems. In: *Issues in Ecology*, vol. 12. ISSN 1092-8987, The Ecological Society of America, Washington, DC, 20006.
- European Union (EU) (2008), Directive 2008/50/EC of the European Parliament and of the Council of 21 May 2008 on ambient air quality and cleaner air for Europe, *Official Journal of the European Union*, 11.6.2008, L 152, 1-44.
- Flatøy, F., O. Hov, and H. Schlager (2000), Chemical forecasts used for measurement flight planning during POLINAT 2, *Geophys. Res. Lett.*, 27, 951–954.
- Flemming, J., A. Inness, H. Flentje, V. Huijnen, P. Moinat, M. G. Schultz, and O. Stein (2009), Coupling global chemistry transport models to ECMWF's integrated forecast system, *Geosci. Model Dev.*, 2, 253-265.
- GAW, 2017: WMO Global Atmosphere Watch (GAW) Implementation Plan: 2016-2023. WMO GAW Report No. 228, World Meteorological Organization, Geneva, 81 pp.
- Georgopoulos et al. (2009), Air Quality Modelling Needs for Exposure Assessment from the Source-to-Outcome Perspective, *Environmental management*, October Issue, 26-35.
- Greenbaum, D. S., J. D. Bachmann, D. Krewski, J. M. Samet, R. White, and R. E. Wyzga (2001), Particulate Air Pollution Standards and Morbidity and Mortality: Case Study, *American Journal of Epidemiology*, 154 (12), Supplement, S78-S90.
- Grell, G. A., and A. Baklanov, 2011: Integrated modelling for forecasting weather and air quality: A call for fully coupled approaches. *Atmos. Environ.*, 45, 6845–6851, doi:10.1016/j.atmosenv.2011.01.017.
- Grell, G. A., S. E. Peckham, R. Schmitz, and S. A. McKeen, G. Frost, W. C. Skamarock, and B. Eder (2005), Fully coupled "online" chemistry within the WRF model, *Atmos. Environ.*, 39, 6957-6975.
- Honoré, C., L. Rouil, R. Vautard, M. Beekmann, B. Bessagnet, A. Dufour, C. Elichegaray, J.-

M. Flaud, L. Malherbe, F. Meleux, L. Menut, D. Martin, A., Peuch, V.-H. Peuch, and N. Poisson (2008), Predictability of European air quality: Assessment of 3 years of operational forecasts and analysis by the PREV'AIR system, *J. Geophys. Res.*, 113, D04301, doi:10.1029/2007JD008761.

Jacobson, M. Z. (2005) *Fundamentals of Atmospheric Modelling*, Cambridge University Press, Cambridge, UK.

Jayachandran, S. (2009), Air quality and early-life mortality: evidence from Indonesia's wildfires, *The Journal of Human Resources*, 44 (4), 916–954.

Kaminski, J. W., et al. (2008), GEM-AQ, an on-line global multiscale chemical weather modeling system: model description and evaluation of gas phase chemistry processes, *Atmos. Chem. Phys.*, 8, 3255–3281.

Kallos, G., Spyrou, C., Astitha, M., Mitsakou, C., Solomos, S., Kushta, J., Pytharoulis, I.,

Katsafados, P., Mavromatidis, E., Papantoniou, N., 2009. Ten-year operational dust forecasting - Recent model development and future plans. IOP Conf. Ser.: Earth Environ. Sci. 7, 012012. <http://dx.doi.org/10.1088/1755-1307/7/1/012012>.

Krupa, S.V., Grunhage, L., Jager, H.J., Nosal, M., Manning, W.J., Legge, A.H., Hanewald, K., 2006. Ambient ozone (O₃) and adverse crop response: a unified view of cause and effect. *Environ. Pollut.* 87, 119e126.

Kukkonen, J., Olsson, T., Schultz, D. M., Baklanov, A., Klein, T., Miranda, A. I., Monteiro, A., Hirtl, M., Tarvainen, V., Boy, M., Peuch, V.-H., Poupkou, A., Kioutsioukis, I., Finardi, S., Sofiev, M., Sokhi, R., Lehtinen, K. E. J., Karatzas, K., San José, R., Astitha, M., Kallos, G., Schaap, M., Reimer, E., Jakobs, H., and Eben, K.: A review of operational, regional-scale, chemical weather forecasting models in Europe, *Atmos. Chem. Phys.*, 12, 1–87, doi:10.5194/acp-12-1-2012, 2012.

Kunzli, N., R. Kaiser, S. Medina, M. Studnicka, O. Chanel, P. Filliger, M. Herry, F. Horak, V. Puybonnieux-Textier, P. Quenel, J. Schneider, R. Seethaler, J.C. Vergnaud, and H. Sommer (2000), Public-health impact of outdoor and traffic-related air pollution: a European assessment, *LANCET*, 356(9232): 795-801.

Lawrence, M. G., Hov, Ø., Beekmann, M., Brandt, J., Elbern, H., Eskes, H., Feichter, H., and Takigawa, M.: The chemical weather, *Environ. Chem.*, 2, 6–8, doi:10.1071/EN05014, 2005.

Lee, P., D. Kang, J. McQueen, M. Tsisulko, M. Hart, G. DiMego, N. Seaman, and P. Davidson (2008), Impact of domain size on modeled ozone forecast for the Northeastern United States, *Journal of Applied Meteorology and Climatology*, 47, 443-461, doi:10.1175/2007JAMC1408.1.

Li, P.-F., L.-Q. Wang, P. Guo, S.-C. Yu, K. Mehmood, S. Wang, W.-P. Liu, J. H. Seinfeld, Y. Zhang, D. Wong, K. Alapaty, J. Pleim, and R. Mathur, 2017, High reduction of ozone and air particulate matter during the 2016 G-20 summit in Hangzhou by forced emission controls of industry and traffic, *Environmental Chemistry Letters*, doi:10.1007/s10311-017-0642-2.

Lawson, S. J., M. Cope, S. Lee, I. E. Galbally, Z. Ristovski and M. D. Keywood (2017). Biomass burning at Cape Grim: exploring photochemistry using multi-scale modelling. *Atmospheric Chemistry and Physics*, 17(19): 11707-11726.

Manders, A.M.M., M. Schaap, and R. Hoogerbrugge (2009), Testing the capability of the chemistry transport model LOTOS-EUROS to forecast PM₁₀ levels in the Netherlands, *Atmos. Environ.*, 43, 4050-4059, doi:10.1016/j.atmosenv.2009.05.006.

Manins, P. (1999), *Air Quality Forecasting for Australia's Major Cities: 1st Progress Report*; SB/1/407 25; CSIRO Atmospheric Research: Aspendale, Australia, October.

Marrapu, P., Cheng, Y., Beig, G., Srinivas, R., and Carmichael, G. R. (2014) Air quality in Delhi during the Commonwealth Games. *Atmospheric Chemistry and Physics*, 14(19), 10619-10630.

Matanoski, G. M, and X. Tao (2002), Case-cohort study of styrene exposure and ischemic

heart disease, *Research Report/Health Effects Institute*, 108,1-29.

- McHenry, J. N., W. F. Ryan, N. L. Seaman, C. J. Coats Jr., J. Pudykiewics, S. Arunachalam, and J. M. Vukovich (2004), A real-time Eulerian photochemical model forecast system: Overview and initial ozone forecast performance in the Northeast U.S. corridor, *Bull. Amer. Meteor. Soc.*, *85*, 525-548.
- McKeen, S., J. Wilczak, G. Grell, I. Djalova, S. Peckham, E.-Y. Hsie, W. Gong, V. Bouchet, S. Ménard, R. Moffet, J. McHenry, J. McQueen, Y. Tang, G. R. Carmichael, M. Pagowski, A. Chan, t. Dye, G. Frost, P. Lee, and R. Mathur (2005), Assessment of an ensemble of seven real-time ozone forecasts over eastern North America during the summer of 2004, *J. Geophys. Res.*, *110*, D21307, doi:10.1029/2005JD005858.
- McKeen, S., S. H. Chung, J. Wilczak, G. Grell, I. Djalalova, S. Peckham, W. Gong, V. Bouchet, R. Moffet, Y. Tang, G. R. Carmichael, R. Mathur, and S. Yu (2007), Evaluation of several PM_{2.5} forecast models using data collected during the ICARTT/NEAQS 2004 field study, *J. Geophys. Res.*, *112*, D10S20, doi:10.1029/2006JD007608.
- McKeen, S. et al. (2009), An evaluation of real-time air quality forecasts and their urban emissions over eastern Texas during the summer of 2006 Second Texas Air Quality Study field study, *J. Geophys. Res.*, *114*, D00F11, doi:10.1029/2008JD011697.
- Millman, A., D. L. Tang, and F. P. Perera (2008), Air pollution threatens the health of children in China, *Paediatrics*, *122*, 620–628.
- Nielsen, J. E., S. Pawson, A. Molod, B. Auer, A. M. da Silva, A. R. Douglass, B. N. Duncan, Q. Liang, M. E. Manyin, L. D. Oman, W. M. Putman, S. E. Strahan, and K. Wargan, 2017. Chemical Mechanisms and their Applications in the Goddard Earth Observing System (GEOS) Earth System Model. *J. Adv. Model. Earth Sys.* doi:10.1002/2017MS001011.
- Phalen, R.F., and R. N. Phalen (2011), Introduction To Air Pollution Science, ISBN-10: 0763780448, Jones & Bartlett Learning.
- Pudykiewicz, J. A., and A. S. Koziol (2001), The application of Eulerian models for air quality prediction and the evaluation of emission control strategies in Canada, *Int. J. Environ. Pollut.*, *16*, 425– 438.
- Ryan, W.F. (1995), Forecasting ozone episodes in the Baltimore metropolitan area, *Atmos. Environ.*, *29* (17), 2387-2398.
- Ryan, W.F. (2016) The air quality forecast rote: Recent changes and future challenges, *Journal of the Air & Waste Management Association*, *66*:6, 576-596, doi:10.1080/10962247.2016.115146.
- Savage, N. H., Agnew, P., Davis, L. S., Ordóñez, C., Thorpe, R., Johnson, C. E., O'Connor, F. M., and Dalvi, M.: Air quality modelling using the Met Office Unified Model (AQUUM OS24-26): model description and initial evaluation, *Geosci. Model Dev.*, *6*, 353–372, doi:10.5194/gmd-6-353-2013.
- Schaap, M., R.M.A. Timmermans, F. J. Sauter, M. Roemer, G. J. M. Velders, G. A. C. Boersen, J. P. Beck, and P.J.H. Builtjes (2008), The LOTOS-EUROS model: description, validation and latest developments, *International Journal of Environment and Pollution*, *32* (2), 270–289.
- Schwartz J. (1991), Particulate air pollution and daily mortality in Detroit, *Environ. Res.*, *56*, 204-213.
- Seinfeld, J.H. and S.N. Pandis (2006), Atmospheric Chemistry and Physics: from Air Pollution to Climate Change, John Wiley & Sons, Inc., ISBN 978-0-471-72018-8.
- Sessions, W. R., Reid, J. S., Benedetti, A., Colarco, P. R., da Silva, A., Lu, S., Sekiyama, T., Tanaka, T. Y., Baldasano, J. M., Basart, S., Brooks, M. E., Eck, T. F., Iredell, M., Hansen, J. A., Jorba, O. C., Juang, H.-M. H., Lynch, P., Morcrette, J.-J., Moorthi, S., Mulcahy, J., Pradhan, Y., Razinger, M., Sampson, C. B., Wang, J., and Westphal, D. L.: Development towards a global operational aerosol consensus: basic climatological characteristics of the International Cooperative for Aerosol Prediction Multi-Model

- Ensemble (ICAP-MME), *Atmos. Chem. Phys.*, 15, 335-362, <https://doi.org/10.5194/acp-15-335-2015>.
- Sofiev M, Siljamo P, Valkama I, Ilvonen M, Kukkonen J (2006) A dispersion system SILAM and its evaluation against ETEX data. *Atmos. Environ.*, 40, 674-685.
- Sofiev, M., Vira, J., Kouznetsov, R., Prank, M., Soares, J., Genikhovich, E. (2015), Construction of the SILAM Eulerian atmospheric dispersion model based on the advection algorithm of Michael Galperin, *Geosci. Model Dev.*, 8, 3497-3522, <https://doi.org/10.5194/gmd-8-3497-2015>.
- Sokhi et al. (2018), *Air Pollution and Meteorological Modelling for Atmospheric Research and Policy Applications*. Anthem Press.
- Stockwell, W. R. et al. (2002), The scientific basis of NOAA's Air Quality Forecast Program, *Environ. Manage.*, December 20–27.
- Tilmes, S., et al. (2002), Comparison of five Eulerian air pollution forecasting systems for the summer of 1999 using the German ozone monitoring data, *J. Atmos. Chem.*, 42, 91–121.
- U.S. EPA (1999), Guideline for developing an ozone forecasting program. U.S. Environmental Protection Agency Rep. EPA-454/R-99-009, 88 pp. (Available from Office of Air Quality Planning and Standards, EPA, Research Triangle Park, NC 27711.)
- U.S. EPA (2000), *Air Quality Index, A Guide to Air Quality and Your Health*; EPA-454/R-00-005; U.S. Environmental Protection Agency, Office of Air and Radiation: Washington, DC, 2000. <https://www.airnow.gov/all-publications/>.
- U.S. EPA, 2009 U.S. EPA (2009), Technical Assistance Document for Reporting of Daily Air Quality—Air Quality Index (AQI); EPA-454/B-09-001; U.S. Environmental Protection Agency, Office of Air Quality Planning and Standards: Research Triangle Park, NC.
- Vautard, R., M. Beekmann, J. Roux, D. Gombert (2001b), Validation of a deterministic forecasting system for the ozone concentrations over the Paris area, *Atmos. Environ.*, 35, 2449–2461.
- Vogel, B., Vogel, H., Bäumer, D., Bangert, M., Lundgren, K., Rinke, R., Stanelle, T. (2009), The comprehensive model system COSMO-ART - Radiative impact of aerosol on the state of the atmosphere on the regional scale, *Atmos. Chem. Phys.*, 9, 8661-8680.
- Vogel, B., Ferrone, A., Schad, T. (2013): Reducing the Uncertainties of Climate Projections: High-Resolution Climate Modelling of Aerosol and Climate Interactions on the Regional Scale Using COSMO-ART, *High Performance Computing in Science and Engineering '13* 2013, 553-555, [doi:10.1007/978-3-319-02165-2_38](https://doi.org/10.1007/978-3-319-02165-2_38).
- Wang, Z., Wu, Q., Gbaguidi, A., Yan, P., Zhang, W., Wang, W., and Tang, X.: Ensemble air quality multi-model forecast system for Beijing (EMS-Beijing): model description and preliminary application, *J. Nanjing University Inform. Sci. Technol.: Natural Science Edition*, 1, 19–26, 2009 (in Chinese)
- Wayland et al., 2002 Wayland, R. A., J. E. White, P. G. Dickerson, and T. S. Dye (2002), Communicating real-time and forecasted air quality to the public, *Environ. Manage.*, 28–36, December.
- World Health Organization (WHO) (2004), Health Aspects of Air Pollution, Results from the WHO Project "Systematic Review of Health Aspects of Air Pollution in Europe," June, E83080, World Health Organization, Regional Office for Europe Scherfigsvej 8, DK-2100 Copenhagen Ø, Denmark.
- World Health Organization (WHO) (2010), WHO guidelines for indoor air quality: selected pollutants, ISBN: 9789289002134, World Health Organization, Regional Office for Europe Scherfigsvej 8, DK-2100 Copenhagen Ø, Denmark.
- World Health Organization (WHO) (2014), Burden of disease from the joint effects of Household and Ambient Air Pollution for 2012, 25, March 2014; http://www.who.int/phe/health_topics/outdoorair/databases/FINAL_HAP_AAP_BoD_24March2014.pdf?ua=1.

- Wu, Q., Wang, Z., Xu, W., Huang, J., and Gbaguidi, A.: Multi-model simulation of PM₁₀ during the 2008 Beijing Olympic Games: effectiveness of emission restrictions, *Acta Scientiae Circumstantiae*, 30, 1739–1748, 2010 (in Chinese).
- World Weather Open Science Conference (WWOSC), 2015: *Seamless Prediction of the Earth System: From Minutes to Months* – (WMO-No. 1156)
https://library.wmo.int/index.php?lvl=notice_display&id=17276#.XoSX2YgzZPY
- Zhang, K., H. Wan, B. Wang, M. Zhang, J. Feichter and X. Liu: Tropospheric aerosol size distributions simulated by three online global aerosol models using the M7 microphysics module, *Atmos. Chem. Phys.*, 10, 6409–6434 (2010). doi:10.5194/acp-10-6409-2010.
- Zhang, Y., 2008: Online coupled meteorology and chemistry models: history, current status, and outlook, *Atmospheric Chemistry and Physics*, 8, 2895–2932, doi:10.5194/acp-8-2895-2008.
- Zhang, Y., C. Seigneur, M. Bocquet, V. Mallet, and A. Baklanov, 2012a, Real-Time Air Quality Forecasting, Part I: History, Techniques, and Current Status, *Atmospheric Environment*, 60, 632–655, doi:10.1016/j.atmosenv.2012.06.031.
- Zhang, Y., C. Seigneur, M. Bocquet, V. Mallet, and A. Baklanov, 2012b, Real-Time Air Quality Forecasting, Part II: State of the Science, Current Research Needs, and Future Prospects, *Atmospheric Environment*, 60, 656–676, doi:10.1016/j.atmosenv.2012.02.041.
- Zhang, Y., C.-P. Hong, K. Yahya, Q. Li, Q. Zhang, and K.-B. He, 2016, Comprehensive evaluation of multi-year real-time air quality forecasting using an online-coupled meteorology-chemistry model over southeastern United States, *Atmos. Environ.*, 138, 162–182, doi:10.1016/j.atmosenv.2016.05.006.
- Zhou, C.-H., Gong, Sunling., Zhang, Xiao-Ye., Liu, H. L., Xue, M., Cao, G. L., An, X. Q., Che, H. Z., Zhang, Y. M., and Niu, T (2012). Towards the improvements of simulating the chemical and optical properties of Chinese aerosols using an online coupled model CUACE/Aero. *Tellus B* 64: 18965, doi:18910.13402/tellusb.v18964i18960.18965.

Chapter 2. History and Characteristics of CW-AQF

2.1 Introduction

In this chapter, the history and major characteristics of chemical weather-air quality forecasting (CW-AQF) are reviewed. Section 2.2 introduces the history of numerical weather prediction (NWP) and CW-AQF as well as their similarities and differences. It also summarizes the development of an AQF system based on existing practice in National Meteorological and Hydrological Services (NMHSs). Section 2.3 introduces the history of Chemical Transport Models (CTMs) or Air Quality Models (AQMs) as well as similarities and differences of air quality backcasting and forecasting. Section 2.4 describes major characteristics of CW-AQF and defines offline and online coupling of meteorology and chemistry. Finally, Section 2.5 summarizes key points.

2.2 Similarities and Differences between Weather Forecasting and CW-AQF

2.2.1 History of Numerical Weather Prediction

Meteorological conditions control the atmospheric pollution transport, diffusion, and deposition, therefore the prediction of meteorological conditions and fields is a key element for atmospheric pollution forecasting in CW-AQF models. Meteorological processes impacting atmospheric pollution and chemistry are presented in Table 2.1. NWP is the science of forecasting the weather by using the governing physical equations of the atmosphere. The history of NWP has been reviewed and described by several authors including Lynch (2010) and Harper et al. (2007). More fundamental background information about atmospheric processes and NWP methods can be found in most relevant books of Pielke (2002), Jacobson (2005), and the World Weather Open Science Conference (WWOSC) (2015). A brief review of the history of NWP is provided below.

It is interesting to highlight that the first formulation of an NWP model, suggested by L.F. Richardson in 1920s (Richardson, 1922), in addition to the hydrostatic Bjerknes' primitive equations of motion, included also one additional equation for pollutants (dust). However, his attempt to produce by manual calculations a 6-hour forecast for the state of the atmosphere over two points in central Europe took at least six weeks and was not very successful. The first successful NWP was performed using the Electronic Numerical Integrator and Computer (ENIAC) digital computer in 1950 in USA by Charney et al. (1950) and, in 1954, C.-G. Rossby assembled an international group of meteorologists in Stockholm and produced the first operational weather forecast based on the barotropic equation (Harper et al., 2007). Over the following years more powerful computers have been used to increase the size of initial datasets and include more complicated versions of the equations of motion. The development of regional limited area models facilitated advances in forecasting the tracks of [tropical cyclones](#) as well as [air quality](#) in the early 1980s. The first global NWP models, which initialize and forecasts the weather throughout Earth's [troposphere](#), were introduced in 1980 by the U.K. National Meteorological Center's [Global Spectral Model](#) (Kalnay, 2003), and in 1985 by the [European Centre for Medium-Range Weather Forecasts](#) model (ECMWF, 2002). NWP models solve systems of differential equations based on the laws of physics, thermodynamics and fluid motion, and use a coordinate system which divides the planet into a 3-D grid. Winds, heat transfer, radiation, relative humidity, and surface hydrology are calculated within each grid and evaluate interactions with neighboring points. The use of model ensemble forecasts since the 1990s helps to define the forecast uncertainty and extend weather forecasting further into the future than otherwise possible. Nowadays modern NWP systems are being developed in the direction of seamless prediction of the Earth System with coupled models of the atmosphere and ocean covering prediction time scales from minutes (for nowcasting) to seasons (WWOSC, 2015).

Table 2.1 Impacts of meteorology on atmospheric pollution and chemistry (Baklanov et al., 2014).

Variable or process	Impact on air pollution and chemistry
Temperature	<ol style="list-style-type: none"> 1. Modulates chemical reactions and photolytic rates 2. Modulates biogenic emissions (isoprene, terpenes, dimethyl sulfide, etc.) 3. Influences the volatility of chemical species 4. Determines aerosol dynamics (coagulation, condensation, nucleation)
Temperature vertical gradients	Determines vertical diffusion intensity (or turbulent mixing)
Temperature and humidity	Affects aerosol thermodynamics (e.g., gas-particle partitioning, secondary aerosol formation)
Water vapor	Modulates hydroxyl radical (OH) concentrations, size of hydrophilic aerosol
Cloud liquid water	Determines wet scavenging and atmospheric composition
Cloud processes	Affects mixing, transformation and scavenging of chemical compounds
Precipitation	Determines the wet removal of trace gases and aerosol
Land surface parameterization (soil type and vegetation cover, soil moisture, leaf area)	Affects natural emissions (e.g., dust, BVOCs) and dry deposition
Lightning	Determines free troposphere nitrogen oxides (NO _x) emissions
Radiation	Determines photolysis rates and influences many chemical reaction rates; Determines isoprene emissions
Wind speed and direction	Determines horizontal transport and vertical mixing of chemical species; Influences dust and sea-salt emissions
ABL height	Influences mixing in the boundary layer and concentrations

2.2.2 History of 3-D CW-AQF

The history of 3-D CW-AQF has been reviewed in detail in Zhang et al. (2012). Starting in the mid-1990s, building on already existing NWP models, 3-D numerical AQMs have significantly advanced real-time CW-AQF, as those models account for emissions, chemistry, and removal processes that were not included in previous methods. These efforts first began in Germany in 1994 (e.g., Rufeger et al., 1997), Japan in 1996 (e.g., Ohara et al., 1997), Australia in 1997 (e.g., Manins et al., 2002), and Canada in 1998 (e.g., Pudykiewicz and Koziol, 2001) and then expanded into many countries in Europe (e.g., Reimer et al., 2000; Brandt et al., 2001; Jakobs et al., 2002), Asia (Han et al., 2002; Uno et al., 2003; Wang et al., 2009), North America (Pudykiewicz et al., 2003; McHenry et al., 2004; Otte et al., 2005), South America (E.D. Freitas et al., 2005; Andrade et al., 2015; S.R. Freitas et al., 2016), and Africa (see Chapter 9 for several case studies in Africa). In addition to applications for short-term forecasts of air pollution for the public, 3-D AQMs have also been applied to chemical forecasting during field campaigns. Lee et al. (1997) and Flatøy et al. (2000) represent the first CW-AQF to support the planning of field experiments for the troposphere and stratosphere, respectively. Following the two studies, a number of CW-AQFs have been applied before and during field campaigns (e.g., Kang et al., 2005; McKeen et al., 2005, 2007, 2009).

In the mid-to-late 1990s, many countries recognized an increasing need to implement a centralized, national air quality forecasting system. The Minister for the Environment in Australia funded the Air Pollution in Major Cities Program and developed their CW-AQF model in 1998. The Meteorological Service of Canada (MSC) initiated a CW-AQF program for eastern Canada in 1999, which was extended to cover all of subarctic Canada in 2001 (Pudykiewicz et al., 2003). In 1999, the U.S. EPA developed guidelines for O₃ forecasting (U.S. EPA, 1999), which was extended to add PM_{2.5} in 2003 (U.S. EPA, 2003). The U.S. National Oceanic and Atmospheric Administration (NOAA) and EPA collaboratively developed a national CW-AQF model, the National Air Quality Forecast Capability (NAQFC), and provided O₃ forecast guidance to state and local forecasters (Stockwell et al., 2002; Wayland et al., 2002; Dabberdt et al., 2004). They conducted the first pilot studies of predicting O₃ in 2002 and both O₃ and PM_{2.5} in 2004 for the New England region in 2002 using three numerical CW-AQF models (Kang et al., 2005; McKeen et al., 2005, 2007). Region-wide efforts by universities and research organizations are prevalent in the U.S. (e.g., Hogrefe et al., 2007; Chen et al., 2008; Cai et al., 2008; Chuang et al., 2011; Yahya et al., 2014; Zhang et al., 2016), Europe (e.g., San José et al., 2002, 2007; Chenevez et al., 2004; Manders et al., 2009; Rouil et al., 2009; Sofiev et al., 2009), Australia (e.g., Cope et al., 2004; 2005), South America (Freitas et al., 2005; Andrade et al., 2015; S.R. Freitas et al., 2016), and many countries in the world. CW-AQF has also been a focus for several large-scale international projects. For example, the EU-funded Global and regional Earth-system (Atmosphere) Monitoring using Satellite and in-situ data (GEMS) project developed a comprehensive data analysis and modeling system for monitoring the global distribution of atmospheric composition with a focus on Europe (<http://gems.ecmwf.int>). GEMS included 72-h forecasts using 12 state-of-the-art regional chemical weather models on a pre-operational daily basis (<http://gems.ecmwf.int>). These models used the operational meteorological forecasts of the European Centre for Medium-Range Weather Forecasts (ECMWF) and the GEMS global chemical weather data. The European Cooperation in Science and Technology (COST) ES0602 action established the European Chemical Weather Forecasting Portal (<http://www.chemicalweather.eu/>). The portal provided a forum for benchmarking approaches and practices in data exchange and multi-model capabilities for CW-AQF and an access to more than 20 CW-AQF models and their forecasting products over 31 areas in Europe. The action included approximately 30 participants from 20 countries, and its duration is from 2007 to 2011.

Prior to the mid-2000s, CW-AQF has mainly used offline-coupled 3-D air quality models that use pre-calculated meteorological fields. Online-coupled meteorology and chemistry models have been increasingly used for CW-AQF since 2000s (Zhang, 2008; Grell and Baklanov, 2011). Since short-lived pollutants influence climate, weather, and air quality conditions, the AQ community is interested in online-coupled models to understand the feedback mechanisms and to design air quality policies that can maintain future air quality at acceptable levels under changing climate conditions (Alapaty et al., 2012). These online-coupled models can realistically simulate the two-way feedback between meteorology and chemistry in one

atmosphere, representing the-state-of-the-science. More sophisticated techniques such as 4-dimensional variational methods (4D-Var), Kalman-filtering, and ensemble methods have also been used in conjunction with 3-D CW-AQF models to improve CW-AQF results. Elbern and Schmidt (2001) conducted one of the first applications of chemical data assimilation for CW-AQF using 4D-Var to assimilate O₃ and NO₂ observations during August 1997 over central Europe and showed a significant improvement in the associated O₃ forecasts. The first reported ensemble O₃ forecasting was conducted with a three-member CHIMERE ensemble using three global NWP over Europe (Vautard et al., 2001). As one of the early real-time ensemble CW-AQFs, McKeen et al. (2005, 2007) applied several CW-AQF models to forecast O₃ and PM_{2.5}, respectively, during the 2004 NEAQS/ICARTT study and found that multi-model ensemble forecasting outperformed individual forecasting because the average multi-model forecast provides error compensation as well as a greater consistency and reliability than the individual model forecast (Hagedorn et al., 2015). The same set of CW-AQF models was applied to forecast O₃ and PM_{2.5} during the Second Texas Air Quality Study (TexAQS II)/Gulf of Mexico Atmospheric Composition and Climate Study (GoMACCS), with the ensemble forecasting performing better than most individual members (McKeen et al., 2009), which represents the first PM_{2.5} ensemble, bias-corrected, and Kalman filter-corrected forecasting. Doraiswamy et al. (2009) conducted ensemble forecasting of O₃ and PM_{2.5} over the state of New York using the Community Multiscale Air Quality (CMAQ) modeling system with the Weather Research and Forecasting (WRF) and the Mesoscale Model version 5 (MM5) and found that the ensemble forecasts often, but not always, perform better than individual member forecasts and that weighting or bias correction approaches may improve performance. Mallet (2010) coupled an ensemble forecasting of O₃ with chemical data assimilation to overcome the limitations of pure ensemble forecasting and showed a 28% reduction in the root mean square error (RMSE). Hybrid approaches using both statistical and 3-D models have also been applied to improve the accuracy of the CW-AQF (e.g., Eben et al., 2005; Guillas et al., 2008; Kang et al., 2008; Rouil et al., 2009). There are increasing numbers of CW-AQF applications of CTMs coupled with Computational Fluid Dynamical (CFD) models over industrial plants and urban areas at horizontal grid resolutions of 1-10 m (e.g., San José et al., 2006, 2009). These applications predict chemical concentrations in the urban canopy taking into account the complex building structure.

The real-time CW-AQF efforts since the 1990s have focused primarily on O₃ (e.g., Cope et al., 2004; McHenry et al., 2004; McKeen et al., 2005) and have only recently been expanded to include PM_{2.5} and PM₁₀ (e.g., McKeen et al., 2007, 2009; Chuang et al., 2011; Zhang et al., 2016). Some also forecast other pollutants such as SO₂, NO_x, CO, VOCs, air toxics, and dust (e.g., Cope et al., 2004; Baklanov et al., 2007; Kaminski et al., 2008; Kallos et al., 2009; Elbern et al., 2010). For example, in Europe, NO₂ is included in forecasts because of common exceedances of the air quality standard. Because there were no exceedances of the hourly and annual NO₂ standard, NO₂ has typically not been included in the U.S., although the recent promulgation of a 1-h average near-source NO₂ standard may soon generate some interest for NO₂ forecasting in North America. The forecast products are issued in terms of spatial maps or site-specific values of hourly concentrations and time-averaging concentrations (e.g., maximum 8-h average concentrations based on the U.S. National Ambient Air Quality Standard (NAAQS)), as well as the Air Quality Index (AQI) or similar indices.

The U.S. EPA established the Pollutant Standard Index (PSI), also known as the Air Pollution Index (API) in 1978, which was replaced by the Air Quality Index (AQI) to include a simple color scheme in 1997 to link air quality concentrations and associated health effects to a simple color-coded index that can be easily and consistently reported to the public (U.S. EPA, 2000, 2009). Canada established the Air Quality Health Index (AQHI), which uses a 6-hr average of a weighted suite of pollutants (Taylor, 2014). Similar indices exist in more than 37 countries in the world (e.g., Australia, Brazil, Chile, China, Denmark, France, Germany, India, Japan, Mexico, U.K.). Eder et al. (2010) described approaches to use national RT-AQF guidance to develop local AQI forecasts. The AQI used in the U.S. is a dimensionless, six-color-coded index for reporting daily air quality to the public in a manner as easily understood as weather forecasts (U.S. EPA, 2009). It provides a simple, uniform system to relate daily forecasted levels of criteria pollutants (e.g., O₃, PM, NO₂, CO, and SO₂) to health advisories and alerts for sensitive groups and the general public and suggests actions to reduce exposure. The AQI converts a forecasted pollutant concentration to a number on a scale of 0 to 500. A

value of 100 generally corresponds to the NAAQS established for each pollutant under the Clean Air Act. Values below 100 are considered satisfactory. Values above 100 indicate that the air is unhealthy and poses a health concern. For example, the 100-200 level may trigger preventive actions such as limiting certain activities and enforcing potential restrictions on industrial activities by state or local officials. A European AQI, the Common Air Quality Index (CAQI) was developed to compare air quality in different European cities (Elshout and Léger, 2007). An important feature of CAQI is that it accounts for both urban background monitoring conditions at city background sites and traffic (i.e., near-source) pollution at/near traffic monitoring sites. The background index indicates the outdoor air quality in the city experienced by the average citizen. The mandated background index comprises NO₂, PM₁₀, and O₃, with CO and SO₂ as auxiliary components. The traffic index indicates air quality in busy streets, which is generally the poorest air quality in the city. Citizens living in, working in, and visiting these streets as well as those in vehicles are all affected. The mandated traffic index comprises NO₂ and PM₁₀, with CO as an auxiliary component. The two indices provide an improved assessment of current air quality over city averages, because some monitoring networks are designed to monitor areas of poor air quality and others provide an average city picture. CAQI has 5 levels of pollution, using a scale of 0-25 (very low), 25-50 (low), 50-75 (medium), 75-100 (high), and >100 (very high) and the matching colors are green, light green, yellow, red, and dark red, respectively.

Starting in the late 1990s, real-time measurement data became available for validating the CW-AQF model in real-time or near real-time. Real-time data repositories were then developed by environmental agencies to provide an effective platform for communicating RT air quality conditions and forecasts to the public via the Internet and other media. For example, in 1997, the U.S. EPA developed the Aerometric Information Retrieval Now (AIRNow) network (www.airnow.gov) that receives real-time O₃ and PM pollution data from more than 115 U.S. and Canadian agencies as well as CW-AQFs from about 400 U.S. cities and represents a centralized, nationwide, governmental repository for real-time data. Similar programs exist in the EU within the Global Monitoring for Environment and Security (GMES) Programme, the European Commission Seventh Framework Programme, several European COST Actions and EU networks, and various air quality agencies in France, China, and other countries.

2.2.3 *Similarities and Differences of NWP and AQF*

NWP involves the predictions of short-term weather to make more informed daily decisions. Likewise, CW-AQF involves predictions of poor air quality days for public health notification and episodic control programs and for planning specialized air monitoring programs. NWP and AQF are similar in several aspects. For example, they both have certain lead time requirement, typically with 5-10 days in advance for NWP and 1-3 days in advance for CWF. The shorter lead time for CWF is because of a much greater computational demand in terms of CPU time and disk storage required. They both use simplified and optimized parameterizations or mechanisms in numerical models to meet the time requirements, and do not involve any tuning and adjusting of model options. They both use real-time (RT) or near-real time (NRT) datasets for input, which are generated using automatic data downloading and pre-processing. While AQF is built upon NWP and traditional air quality modeling, it differs from them in many aspects including driving force, goals and societal/economic benefits, end users, model inputs and formulation, products and evaluation of products, and special techniques for accuracy and efficiency.

[Table 2.2](#) summarizes these differences.

Weather impacts the lives of many people. NWP information can be used to plan for daily activities such as appropriate dressing, travel, and outdoor activities, for industry and agricultural activities such as power production from wind and solar energy as well as crop planting and harvesting. It minimizes the adverse impact of weather-related hazards and disasters such as lightning, hail, tornadoes, hurricanes, and ice storms. AQF is driven by societal pressures to minimize the human, environmental and economic impacts of air pollution. It provides warnings for sensitive groups and information for actions to reduce exposure and emissions in a timely manner and for planners of large field campaigns to save costs. NWP (0-10 days and beyond) has a much wider user base from many commercial and public service sectors (e.g., industry, transportation, agriculture) and the general public than

AQ forecasts. Compared to end users of the NWP information, AQF includes special end users such as air quality regulators and polluters. NWP forecasts are always needed, for normal conditions as well as for extreme events and hazardous conditions. AQ mainly needs to forecast start, duration and end of extreme pollution events. Correct AQ forecasting of these AQ episodes is mainly controlled by the underlying NWP forecast because the emissions data tends to be mainly climatological, namely, the 'real' emissions tend to be relatively constant over longer timescales (e.g., emissions from power generation). While time-varying emissions are desirable to reflect the variability of real-world emissions, in reality, time-resolved emission information is not always available. Exceptions are wildfire and dust emissions, which can be observed in real time, or modeled dynamically based on the NWP fields.

The model inputs for NWP include the initial and boundary conditions (ICONS and BCONs) for meteorological variables and topographical data. Additional inputs are needed for AQF such as chemical ICONs and BCONs as well as emissions of primary species. NWP simulates all major meteorological processes such as dispersion, transport, turbulence, mixing, radiation, and cloud microphysics, whereas AQF simulates additional physico-chemical processes affecting the fates of air pollutants such as chemistry, aerosol microphysics, and dry and wet deposition. This makes the computational demand for AQ forecasts greater in terms of CPU time and disk storage than NWP at the same resolution. This is particularly true if the CW-AQF is carried out with online-coupled models. AQF is thus more technically and computationally difficult than NWP (Stockwell et al., 2002). The NWP and CW-AQF modeling communities have different targets with respect to temporal and spatial scales, as well as different requirements for the accuracy of the description of the meteorological processes involved in such modeling. For AQ forecasting, the key issue is usually the ground-level concentrations of pollutants, whereas for NWP models, skill is typically based on screen-level temperature, precipitation and wind. Most current NWP models do not incorporate detailed chemical processes, even though aerosols can affect fog formation, visibility and precipitation via radiative and microphysical processes, which in turn can influence forecasting skill.

The products of NWP are weather-related variables including temperature, precipitation, wind speed and direction, fog and visibility, and cloud coverage. Compared to NWP that only forecasts tracer vapor water and its condensates, CW-AQF forecasts much more trace gases and aerosols. The products of CWP include forecasted O₃, NO₂, PM_{2.5}, and PM₁₀ concentrations, additional customized products, and post-calculated AQI and color codes based on forecasted products. NWP products are evaluated using temporal variation and spatial distribution overlaid with observations and discrete statistics. Additional methods such as categorical evaluation have been used to evaluate AQF products. Bias correction, ensemble forecasting, and data assimilation have been used to improve the accuracy and efficiency of NWP. While data assimilation techniques are being extended to AQF (so-called chemical data assimilation), additional techniques such as data fusion using multiple data sources including data from AQF models, surface networks, and satellite retrievals have been used for AQF. In some cases, actual operational NWP forecasting is far more costly than CW-AQF because it is performed at the highest possible resolution and because of the high cost of data assimilation. NWP data assimilation to initialize NWP forecasting with observations is compulsory whereas CW-AQF can also be carried out with initializing the tracer fields with observations. Chemical data assimilation can of course improve AQ forecasts. Because of the need to do NWP data assimilation, networks to exchange weather observations are far more advanced (e.g., synoptic observation, sondes, and satellites) than the AQ observations networks.

2.2.4 *Development of an AQF System Based on Existing Practice in NMHSs*

Operational commitment, ownership of well-tested meteorological model and data assimilation systems and access to powerful high-performance facilities make the National Weather and Hydrological Services (NWHS) well suited to carry out operational CW-AQ forecasting. However, in many countries CW-AQ forecast systems have been developed and run by environmental institutions and not by the NWHS. AQF is often not part of the mandate of the NMWS but falls under the responsibility of national or regional environmental protection agencies (EPAs). A further reason why NWHS sometimes do not engage in CW-AQ forecasting might be the larger uncertainty of the current AQ forecasts compared to NWP forecasts as well

as the lack of operational near real-time access to AQ observations. The mandate of national or regional EPAs is to monitor air quality and to ensure compliance with air quality legislation. This often also motivates the need for AQ forecasts, which can be run in cooperation with other institutions such as NWS. An example of this joint effort is the National Air Quality Forecasting Capability (NAQFC), which runs an AQ forecast system in cooperation between NOAA and the US EPA (Staijner et al., 2012).

Table 2.2 Major differences between weather forecasting and air quality forecasting (Zhang, 2020)

Attribute	Weather forecasting	Air Quality Forecasting
Driving force, goals, and societal/economic benefits	Plan for daily economic and leisure activities such as agriculture, renewable energy, transport, and minimize adverse impact of weather-related disasters	Societal pressures to minimize the human, environmental and economic impacts; Warnings for sensitive groups; actions to reduce exposure and emissions in timely way; cost-saving for large field campaigns for AQ observations
End users	Researchers, forecasters, decision-makers, farmers, the public, the media, many commercial and public service sectors	Researchers, forecasters, air quality regulators, decision-makers, polluters, the public, the media, some commercial sectors
Model inputs	ICONS and BCONs for meteorological variables, topographical data	Additional ICONs and BCONs for chemical species; emissions of primary species
Model formulations	Meteorological processes such as dispersion, transport, turbulence, mixing, radiation, cloud microphysics	Additional physico-chemical processes for chemical species such as chemistry, aerosol microphysics, dry and wet deposition
Products	Temperature, precipitation, wind speed and direction, cloud coverage	Forecasted O ₃ , NO ₂ , PM _{2.5} , and PM ₁₀ concentrations, customized products, and post-calculated AQI and color codes
Evaluation of products	Temporal variation and spatial distribution overlaid with observations; discrete statistical evaluation	Temporal variation and spatial distribution overlaid with observations; discrete statistical evaluation; categorical evaluation
Special techniques for accuracy and efficiency	Bias correction, ensemble forecasting, data assimilation	Bias correction, ensemble forecasting, chemical data assimilation, and post-simulation data fusion

A CW-AQ related area in which NMHSs have been contributing since the 1980s is the modeling of accidental release from nuclear emergencies and the forecast of plume from volcanic eruptions. This activity requires fast response times and high-quality forecasting of the wind fields, which can best be achieved by operational NWHSs. Several NMHSs have included stratospheric O₃ in their global NWP models as a prognostic variable since the mid-1990s (Derber and Wu, 1998) in order to assimilate satellite observations of O₃ within the NWP data assimilation framework. Besides the monitoring of the man-made O₃ depletion, the crucial role of O₃ in the atmospheric radiation budget and its link to wind fields (Allaart et al., 1993) through its tracer characteristics motivated the introduction of O₃ in these NWP models.

Many CW-AQ forecast systems consist of CTMs driven by external meteorological fields, the so-called offline-coupled model system (Kukkonen et al., 2012). In contrast, online-coupled CW-AQ models simulate the tracer transport and the sink and source processes integrated in a meteorological model (Zhang, 2008; Baklanov et al., 2017). This approach has the clear advantage that the meteorological fields are available at much higher temporal resolution, i.e., at every time step, compared to the offline CTMs that use meteorological predictions on an hourly or a longer time scale. A further potential benefit of the online-coupled approach is the possibility to use the chemistry and aerosol fields to simulate the impact of atmospheric composition on the radiative transfer or the cloud micro-physics. For this reason, NMHSs will play a vital role in pursuing CW-AQ activities with online-coupled models. A complication of the online-coupled approach is that NWP models have been optimized to achieve good NWP scores while CW-AQ specific requirements such as mass conservation during the advection, boundary layer diffusion or the interaction with the land surface have often not been given a high priority.

An important but also expensive component of global and regional NWP forecasting systems run by NMHSs is data assimilation. Data assimilation is used to enhance the accuracy of the ICONs, which is vital for the quality of the NWP forecast. Data assimilation of atmospheric composition observations is comparatively less well developed than data assimilation for NWP (Bocquet et al., 2015). On the other hand, reasonable AQ forecasts can be made even without assimilation of composition in-situ and satellite observations to improve CW ICONs or to infer emissions. Still, the expertise in data assimilation methods and the capabilities for observation processing at NMHS centers can be utilized for atmospheric composition assimilation. For example, the Integrated Forecasting System (IFS) of the European Centre for Medium-Range Weather Forecasts has been extended to enable the simulation of atmospheric composition over the last 15 years (Morcrette et al., 2009; Flemming et al., 2015). Hence, the IFS can also be used for the assimilation of atmospheric composition retrievals (Inness et al., 2015). The IFS is the global model of the European Copernicus Atmosphere Monitoring Service, which provides global five-day forecasts of aerosol, reactive and greenhouse gases at a resolution of 40 km as well as reanalysis of atmospheric composition. While the priority of the global CAMS system at ECMWF is the assimilation of satellite retrievals, pioneering developments on the assimilation of in-situ AQ observations to improve AQ forecasting were carried out at Environment Canada, which uses the Global Environmental Multiscale model - Modeling Air quality and CHemistry (GEMS-MACH) model to provide CW-AQ forecasts at different resolutions (Ménard and Robichaud, 2005).

Simulating atmospheric chemistry and aerosol dynamics required by the CW-AQ forecast has a substantial computational cost, which can more than double the run time of the NWP model it is embedded in. This often prohibits online-coupled CW-AQ NWP systems from being run at the same resolution as the operational NWP forecast. To reduce the cost of CW-AQ systems integrated in NWP models, the CW-AQ systems are often run at a lower resolution than the operational NWP forecast. An alternative way to reduce the cost without compromising on the resolution is the application of simplified approaches to simulate atmospheric composition. Using simplified tracers, e.g., wildfire CO or aerosol emissions, is a common approach to make AQ forecasting feasible as an integrated part of the high-resolution NWP model system. An important class of simplified CW-AQ systems is dedicated sand and dust storm forecasting systems, which only include emissions, removal and transport of desert dust without the need for complex chemistry or aerosol physics. Dust is a major natural hazard and its forecasting is of huge societal benefit. That is why WMO has established the Sand and Dust Storm Warning Advisory and Assessment System (SDS-WAS) to improve capabilities for more reliable sand

and dust storm forecasts (<https://public.wmo.int/en/our-mandate/focus-areas/environment/SDS>). Strong dust events are also known to impact the weather, which is further strong motivation to simulate them in coupled CW-AQ-NWP systems.

Table 2.3 provides a few examples of CW-AQ models currently being used by NMHSs. More details of these models such as meteorology and chemistry coupling, grid resolution, physics and chemistry options, and references along with non-NMHS models are provided in Chapter 3.

Table 2.3 Examples of CW-AQ Forecast Models used by NMHSs

NMHS	CW-AQ Forecast Model
DWD, German	EURAD model coupled to EM
UK Met offices, U.K.	UKCA, UKAQ
Met.no, Norway	EMEP
FMI, Finland	SILAM
DMI, Denmark	EnviroHirlam, DERMA
Météo France, France	MOCAGE
SMHI, Sweden	MATCH
KNMI/TNO, Netherlands	LOTOS-EUROS
FMI, SMHI, Météo-France, Met.no, KNMI	CAMS regional AQ ensemble
ECMWF, U.K.	CAMS global model
Many NMHSs	Dust forecast system ¹
Environment Canada, Canada	GEM-MATCH
NOAA/EPA, U.S.A.	NAQFC
CMA, China	GRAPES - CUACE
MSS, Singapore	ASEAN-NAME
SAWS, EMA, Africa	RegCM-CHEM4.5
Maroc Météo, Morocco	ADMS-Urban

¹ <https://public.wmo.int/en/our-mandate/focus-areas/environment/SDS>

2.3 Similarities and Differences between CW-AQF and Backcasting Applications

2.3.1 History of Chemical Transport Models or Air Quality Models

3-D CTMs or AQMs have evolved over five generations since the 1970s, with roughly one generation per decade reflecting the advancements in scientific understanding and numerical and computational technologies. Each generation includes significant upgrades in model formulation and representations of major atmospheric processes. Reviews of some AQMs can be found in the literature (e.g., Seigneur, 1994, 2001; Peters et al., 1995; Russell and Dennis, 2000; Zhang, 2008, 2015; Baklanov et al., 2014).

The first generation AQMs were developed in the early 1970s. Those models treated transport, emissions, and very simple chemistry with a few to ~30 reactions among only a few transported species. The second generation AQMs expanded the chemistry to simulate 50-100 gas-phase reactions and 10-40 aqueous-phase reactions among 30-60 transported species. They treated bulk or internally mixed aerosols, and parameterized dry deposition. Some treated resolved and convective cloud, cloud scavenging, and wet deposition processes. Unlike the 1st and 2nd generation AQMs that focused on a single pollutant/pollution problem, the 3rd generation AQMs were designed to address multi-pollutants and/or pollution problems by including more comprehensive chemistry (typically 100-300 gas-phase reactions and 20-100 aqueous-phase reactions) and aerosol and cloud microphysics. While the 1st generation models used analysed meteorological fields, the 2nd and most of the 3rd generation models used offline calculated meteorological fields that cannot simulate the feedback of chemistry to meteorology. A few 3rd generation models such as GATOR-MMTD (Jacobson et al., 1996; Jacobson, 1997(a), (b) and MCCM (Grell et al., 2000) included coupled meteorology and chemistry. In addition to much more comprehensive chemistry, aerosol, and cloud treatments, the 4th generation AQMs have two distinct features. First, they use online-calculated meteorological fields from an advanced meteorological model (e.g., the WRF model) that allows the simulation of all-important feedback between chemistry and meteorology/climate (Grell et al., 2005; Fast et al., 2006; Zhang et al., 2010, 2012 ; Wong et al., 2012). Secondly, some of them are downscaled by an urban/local scale model such as a human exposure model to simulate the health effect of pollutants (Jacobson, 2007; Baklanov et al., 2007) or an urban traffic model to simulate air pollution on a freeway or neighborhood scale (San José et al., 2009). Examples of the 1st, 2nd, and 3rd generation AQMs include the Sulfur Transport Eulerian Model, version 1 (STEM I) (Carmichael et al., 1986), the Regional Acid Deposition Model (RADM) (Chang et al., 1987; Stockwell et al., 1990), and the CMAQ modeling system (Binkowski and Roselle, 2003; Byun and Schere, 2006), respectively. Examples of 4th generation models include the GATOR-GCMOM (Jacobson, 2001, 2002) and the WRF with Chemistry (WRF/Chem) (Grell et al., 2005).

Since the early 2010s, the 5th generation AQMs have emerged. Their major feature is the use of one model framework across scales with unstructured variable resolution mesh (defined as a network that is formed of cells and points), which allows smoothly-varying mesh transitions and thus overcomes possible abrupt transitions that may be encountered using the traditional one-way and two-way grid nesting techniques. Scale-aware physical parameterizations are being developed to provide seamless simulations from global to local scales. This generation models are designed to simulate the interactions of small-scale phenomena (e.g., clouds, small hydrologic basins, and small estuaries) with large-scale phenomena (e.g., planetary atmospheric waves and Earth-ocean circulations). The Model for Prediction Across Scales for Atmosphere (MPAS-atmosphere) (MPAS-A) released by the U.S. NCAR in 2013 is an example (Duda et al., 2014).

CTMs or AQMs have traditionally been used to retrospectively simulate historical poor air quality scenarios in support of regulation and planning, due primarily to computational constraints and a lack of real-time chemical measurements. Given their relative maturity in sciences and the advancement in computational technology, some of the 2nd, 3rd, and 4th generations AQMs have been deployed for CW-AQF since the mid to late 1990s.

2.3.2 *Similarities and Differences of Air Quality Backcasting and Forecasting*

Compared with traditional air quality modeling for research-grade and regulatory applications aiming at simulations of past high pollution events, AQF has its unique technical challenges and lead time requirements, and involves a number of real-time operational issues that did not exist previously for backcasting. Table 2.4 summarizes major differences between air quality backcasting and forecasting. Different from AQF which is aimed at producing warnings of high pollutant concentrations that will likely pose immediate health threats to the population, air quality backcasting (AQB) is driven by regulatory guidance and compliance aimed at reproducing historic pollution episodes with a high accuracy. The end users for AQF products involve much larger communities than those of AQB. Those differences lead to differences in many aspects of backcasting and AQF. For example, while AQB generally has no specific time window requirements for deliverables, AQF requires a fast-short-term prediction on a day-by-day basis. This delivery-time pressure dictates the implementation of a fully automated system to download and preprocess RT or NRT datasets for AQF model set up and simulations and the use of a fast set of model options or optimized model codes for an efficient deployment of AQF. In contrast, AQB uses the best available historical observational dataset based on pre-processed archived files. AQB often uses the best available model treatments to reproduce the species concentrations observed during a historic pollution episode; AQF typically uses simplified, optimized options for dynamics, chemistry, and physics treatments that are fast enough yet reasonably accurate to meet time requirements for operational forecasting. It involves no mechanisms/options tuning and adjusting. AQF often applies special techniques to achieve accuracy and computational efficiency in a very short turnaround time, which are often not needed for AQB. For product evaluation, while AQF products can be evaluated using evaluation protocols for traditional AQMs, it is more meaningful to use categorical evaluation with threshold statistics (e.g., probability of detection, false alarm ratio) (e.g., McHenry et al., 2004; McKeen et al., 2005, 2007, 2009; Kang et al., 2008), because the primary value of CW-AQFs is their guidance for issuing health advisories and alerts of an air pollution episode and the categorical indices determine the likelihood of such an episode. AQF requires a specific information technology infrastructure that is not always needed for AQB (e.g., web-based interfaces, the construction of application-specific and/or client-oriented datasets, and a timely access to forecast products).

2.4 Major Characteristics of CW-AQF

2.4.1 *Expected Characteristics of CW-AQF*

Figure 2.1 shows a diagram of an RT CW-AQF model system from global to urban scales based on typical configurations available from current CW-AQF models (Zhang et al., 2012a). At each scale, a meteorological model and an air quality model are needed; they may be coupled online or offline. At a global scale, the GCM and the global CTM (GCTM) (e.g., ECHAM5, Roeckner et al., 2006; MOCAGE, Rouil et al., 2009), are initiated with climatological or reanalysis or observational data. The GCM produces the meteorological fields needed by the GCTM. An emission model is required to project real-time emissions based on energy/fuel consumption data, vehicle fleets, and other activities at all scales. An emission processor converts projected emissions into model-ready gridded emission files. Forecasted meteorological information is needed for meteorology-dependent emissions (e.g., biogenic emissions, sea-salt and erodible dust emissions, VOC evaporation).

Table 2.4. Major differences between air quality backcasting and forecasting (Zhang, 2020).

Attribute	Air Quality Backcasting	Air Quality Forecasting
Driving force, Goals and societal/economic benefits	Regulatory guidance and compliance; advancement in sciences, regulatory analyses and policymaking	See Table 2.2
End users	Researchers, regulators, decision-makers,	See Table 2.2
Time requirement for products	No time window requirements	1-3 days in advance Next-day's forecasted products must be available before a specific time (e.g., 2 pm) today
Input datasets and format	Best available historical dataset based on pre-processed archived files	Real-time or near real-time dataset through automatic downloading, quality-assured and quality-controlled, and pre-processing
Model mechanisms and treatments	Best available options	Simplified, optimized options to meet time requirements
Model option tuning and adjusting	Yes, model options or processes are often tuned and improved	No, no tuning and adjusting made to the selected set of model options
Products	Concentrations and deposition fluxes of chemical species	See Table 2.2
Evaluation of products	Temporal variation and spatial distribution overlaid with observations; discrete statistical evaluation	See Table 2.2
Special techniques for accuracy and efficiency	None or rarely use	See Table 2.2
IT infrastructure	No special requirements	Web-based interfaces; interactive, user-friendly virtual environments

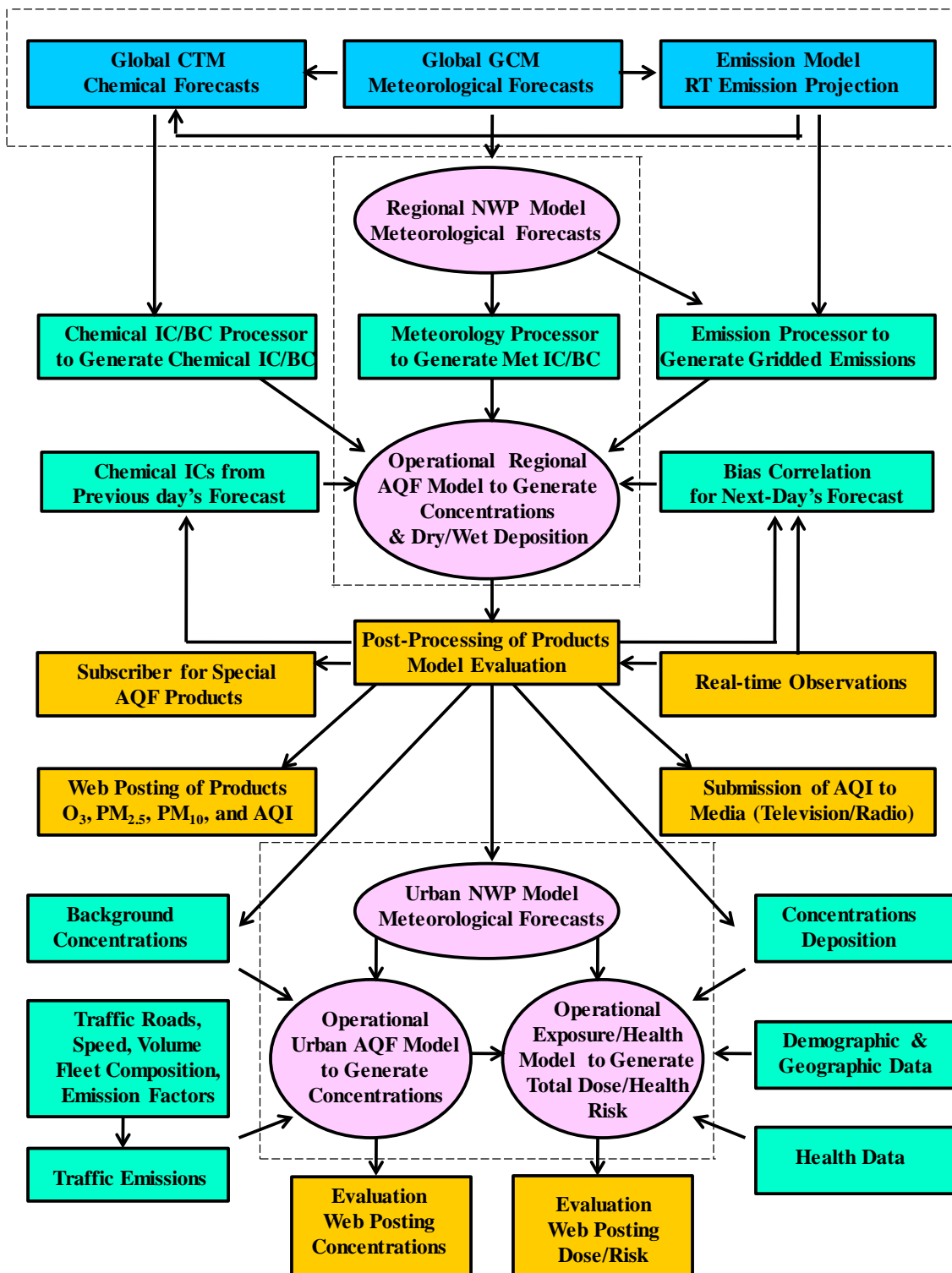


Figure 2.1. An automated RT-AQF system from global to urban scales.

The three model systems at global, regional, and urban scales are shown as offline-coupled meteorology-chemistry models. They can be online-coupled meteorology (climate)_air quality systems (taken from Zhang et al., 2012a).

The regional scale CW-AQF systems (e.g., CHIMERE, Rouil et al., 2009; EURAD, Elbern et al., 2010) use meteorological ICONs and BCONs from a GCM and chemical BCONs from a GCTM. Chemical ICONs from either a GCTM or observations are needed to initiate the first day's forecasting, those for subsequent days will then use previous day's forecast. The forecasting product will be post-processed and evaluated using real-time (or near real-time) observations. Products such as species concentrations and AQIs will be submitted to the media, websites, and subscribers. Some CW-AQF systems employ bias correction techniques to correct large, systematic biases for next day forecasts based on the previous day's forecast and observations (e.g., McKeen et al., 2005, 2007; Kang et al., 2008). The initial CW-AQFs for the current day issued on a previous day may be updated in the morning based on updated meteorological forecasting to improve the accuracy of the forecasting products. Some CW-AQF systems include an extended subsystem for urban scale air quality and/or human exposure and environmental health forecasting (e.g., Tilmes et al., 2002; Baklanov et al., 2007; San José, et al., 2009). The urban CW-AQF requires urban meteorological forecasts, background concentrations forecasted from the regional CW-AQF model, and traffic emissions that are calculated using detailed traffic information. The output includes the spatial and temporal distributions of forecasted concentrations. The neighborhood scale human exposure or environmental health forecasting requires urban meteorological forecasts, forecasted concentrations and deposition from a regional CW-AQF model, demographic and geographic data (e.g., total number of population and age distribution, location and time-activity of people), and health data (e.g., mortality, morbidity, hospital admissions) (Baklanov et al., 2007 and references therein). The output includes the spatial and temporal distributions of the forecasted total dose and relative risks of adverse health outcomes. The entire data retrieval, model simulation, and product processing is automated on a day-to-day basis to ensure completion of forecasts in time.

2.4.2 *Coupling of Meteorology and Chemistry*

Among current AQF models, a meteorological model and an AQM may be coupled online or offline. While an offline meteorological model (e.g., MM5, Grell et al., 1995 or WRF, Michalakes et al., 2001) provides meteorological forecasts separately from a regional AQF model (e.g., CMAQ, Byun and Schere (2006)), an online-coupled meteorology and chemistry model (e.g., WRF/Chem, Grell et al., 2005) generates both meteorological and chemical forecasts within the same time step. The use of offline-coupled meteorology and AQMs does not permit the simulation of meteorology-chemistry feedback such as aerosol feedback to radiation and photolysis, which are important and may affect the next hour's air quality and meteorological predictions (Grell et al., 2004, 2005; Zhang, 2008; Zhang et al., 2010; Baklanov, 2010). Such systems may introduce biases in CW-AQF. For example, Otte et al. (2005) and Eder et al. (2006) reported a poor performance of their offline-coupled Eta/CMAQ modeling system during cloudy periods due to neglecting aerosol feedback to radiation and cloud formation processes. Furthermore, atmospheric information at a time scale smaller than the output time interval of the meteorological model (e.g., 1-h) is lost in the offline-coupled model systems (Grell et al., 2004; Zhang, 2008; Korsholm et al., 2009). Online-coupled models are increasingly used for applications in which the feedback may be important (e.g., locations with high frequencies of clouds and large aerosol loadings), the local scale wind and circulation systems change quickly, and the coupled meteorology-air quality modeling is essential for accurate model simulations (e.g., CW-AQF or simulating the impact of future climate change on air quality). Compared with offline AQMs, online models can provide more realistic treatments of the atmosphere, particularly in regions with a fast local circulation or a high aerosol loading and cloud coverage, where meteorology and radiation may be modified by the presence of chemical species through various feedback mechanisms) (Zhang, 2008; Grell and Baklanov, 2011). Therefore, an AQF system that is based on an online-coupled meteorology-chemistry model can better represent the real atmosphere and thus provide more accurate AQFs.

Two coupling frameworks are conventionally used in all mesoscale and global online-coupled models: online access model (also referred to as separate online model) and online integrated model (also referred to as a unified online model). Online access model couples a meteorology model with an air quality model in which the two systems operate separately but exchange information every time step through an interface (or coupler). Online integrated models integrate an air quality model into a meteorology model as a unified model system in which

meteorology and air quality variables are simulated together in one-time step without an interface between the two models. In models with a unified online coupling, the equations can be solved simultaneously with a nonlinear equation solver or the meteorological and air quality processes can be solved using operator splitting; the latter is more often used at present. The main difference between the two types of coupling is that the transport of meteorological and chemical variables is typically simulated with separate schemes in separate online models but the same scheme in unified online models. In contrast to the online access models, offline CTMs or AQMs do not exchange data between meteorological and chemical calculations, the data flows one way, i.e., meteorology information generated from the meteorological models to the CTM or AQM that uses such information.

2.5 Summary

- Initiated in the 1920s, operational NWP models have evolved from simple formulations to more complicated atmospheric models with ensemble forecasting or coupled atmosphere and ocean models, from regional to global, and from minutes (for nowcasting) to seasons.
- 3-D chemical transport models have been deployed for operational CW-AQF in many countries since the mid-1990s, and online-coupled meteorology and chemistry models as well as advance techniques such as ensemble forecasting and chemical data assimilation have been increasingly used for CW-AQF since the 2000s.
- NWP and CW-AQF are similar in several aspects such as lead time requirement, and the use of simplified and optimized parameterizations or mechanisms. They differ in many aspects including driving force, goals and societal/economic benefits, end users, model inputs and formulation, products and evaluation of products, and special techniques for accuracy and efficiency.
- Since the 1980s, NWHSs have engaged in CW-AQ modeling ranging from the modeling of accidental release to data assimilation as well as sand and dust storm forecasting systems, and they are playing a vital role in pursuing operational CW-AQF with online-coupled models.
- Compared with air quality backcasting for research-grade and regulatory applications, operational CW-AQF has its unique technical challenges, lead time requirements, and evaluation protocols, and it involves a number of real-time operational issues such as the requirement of automatic operations, bias correction, and interactive web-based interfaces;
- An ideal RT-AQF system is an automated model system consisting of a hierarchy of models including both offline- and online-coupled meteorology-chemistry models from global to urban scales. Compared with offline AQMs, an online-coupled meteorology-chemistry model generates both meteorological and chemical forecasts within the same time step and can thus better represent the real atmosphere and thus provide more accurate AQFs.

References

- Alapaty K, R. Mathur, J. Pleim, Ch. Hogrefe, S. T. Rao, V. Ramaswamy, S. Galmarini, M. Schaap, R. Vautard, P. Makar, A. Baklanov, G. Kallos, B. Vogel, R. Sokhi (2012) New Directions: Understanding Interactions of Air Quality and Climate Change at Regional Scales. *Atmospheric Environment*, 49: 419–421.
- Allaart M. A. F., Kelder H., and Heijboer L. C.: On the relation between ozone and potential vorticity, *Geophys. Res. Lett.*, 20, 811–814, 1993.
- Andrade, M. F., Ynoue, R. Y, Freitas, E. D., Todesco, E., Vara Vela, A., Ibarra, S., Martins, L. D., Martins, J. A., Carvalho, V. S. B., 2015. Air quality forecasting system for Southeastern Brazil. *Frontiers in Environmental Science*, 3, 1-14, <http://dx.doi.org/10.3389/fenvs.2015.00009>.
- Aron, R. H. (1980), Forecasting high level oxidant concentrations in the Los Angeles basin. *J. Air Pollut. Control Assoc.*, 20, 1227–1228.
- Baklanov, A. (2010), Chemical weather forecasting: a new concept of integrated modeling, *Adv. Sci. Res.*, 4, 23–27.
- Baklanov et al., (2007) : Urban air flow researches for air pollution, emergency preparedness and urban weather prediction. Chapter 9 in: *Flow and transport processes with complex obstructions*. Editors Ye. A. Gayev and J.C.R. Hunt. NATO Science Series book, Springer, pp. 311-357.
- Baklanov A., Brunner D., Carmichael G., Flemming J., Freitas S., Gauss M., Hov O., Mathur R., Schlünzen K.H., Seigneur C., Vogel B. (2017): Key issues for seamless integrated chemistry-meteorology modeling. *Bull. Amer. Meteor. Soc.*, 2285-2292, [doi: 10.1175/BAMS-D-15-00166...](https://doi.org/10.1175/BAMS-D-15-00166)
- Baklanov, A., K.H. Schlünzen, P. Suppan, J. Baldasano, D. Brunner, S. Aksoyoglu, G. Carmichael, J. Douros, J. Flemming, R. Forkel, S. Galmarini, M. Gauss, G. Grell, M. Hirtl, S. Joffre, O. Jorba, E. Kaas, M. Kaasik, G. Kallos, X. Kong, U. Korsholm, A. Kurganski, J. Kushta, U. Lohmann, A. Mahura, A. Manders-Groot, A. Maurizi, N. Moussiopoulos, S.T. Rao, N. Savage, C. Seigneur, R.S. Sokhi, E. Solazzo, S. Solomos, B. Sørensen, G. Tsegas, E. Vignati, B. Vogel, and Y. Zhang, 2014, Online Coupled Regional Meteorology-Chemistry Models in Europe: Current Status and Prospects, *Atmospheric Chemistry and Physics*, 14, 317-398, [doi:10.5194/acp-14-317-2014](https://doi.org/10.5194/acp-14-317-2014).
- Bocquet, M. H. Elbern, H. Eskes, M. Hirtl, R. Žabkar, G. R. Carmichael, J. Flemming, A. Inness, M. Pagowski, J. L. Pérez Camaño, P. E. Saide, R. San Jose, M. Sofiev, J. Vira, A. Baklanov, C. Carnevale, G. Grell, and C. Seigneur *Atmos. Chem. Phys.*, 15, 5325-5358, <https://doi.org/10.5194/acp-15-5325-2015>.
- Brandt, J., J. H. Christensen, L. M. Frohn, F. Palmgren, R. Berkowicz, and Z. Zlatev (2001), Operational air pollution forecasts from European to local scale, *Atmos. Environ.*, 35, Supplement No. 1, S91-S98.
- Byun, D., and Schere, K.L. (2006), Review of the Governing Equations, Computational Algorithms, and Other Components of the Models-3 Community Multiscale Air Quality (CMAQ) Modeling System, *Appl. Mech. Rev.*, 59, 51– 77.
- Cai, C., C. Hogrefe, P. Katsafados, G. Kallos, M. Beauharnois, J.J. Schwab, X. Ren, W. Brune, X. Zhou, Y. He, and K. Demerjian (2008), Performance evaluation of an air quality forecast modeling system for a summer and winter season – Photochemical oxidants and their precursors, *Atmos. Environ.*, 42, 8585-8599, [doi: 10.1026/j.atmosenv.2008.08.029](https://doi.org/10.1026/j.atmosenv.2008.08.029).
- Charney, J., Fjørtoft, R., von Neumann, J., 1950: Numerical Integration of the Barotropic Vorticity Equation. *Tellus*. 2 (4): 237–254. [doi:10.1111/j.2153-3490.1950.tb00336.x](https://doi.org/10.1111/j.2153-3490.1950.tb00336.x).
- Chen, J., J. Vaughan, J. Avise, S. O'Neill, and B. Lamb (2008), Enhancement and evaluation of the AIRPACT ozone and PM_{2.5} forecast system for the Pacific Northwest, *J. Geophys. Res.*, 113, D14305, [doi:10.1029/2007JD009554](https://doi.org/10.1029/2007JD009554).

- Chenevez, J., Baklanov, A., and Sørensen, J. H.: Pollutant transport schemes integrated in a numerical weather prediction model: model description and verification results, *Meteorol. Appl.*, 11, 265–275, 2004.
- Chuang, M.-T., Y. Zhang, and D.-W. Kang (2011), Application of WRF/Chem-MADRID for Real-Time Air Quality Forecasting over the Southeastern United States, *Atmos. Environ.*, 45 (34), 6241-6250.
- Cope, M. E., Hess, G. D., Lee, S., Tory, K., Azzi, M., Carras, J., Lilley, W., Manins, P. C., Nelson, P., Ng, L., Puri, K., Wong, N., Walsh, S., and Young, M.: The Australian Air Quality Forecasting System. Part I: Project description and early outcomes, *J. Appl. Meteorol.*, 43, 649–662, <https://doi.org/10.1175/2093.1>, 2004.
- Cope, M. E., Hess, G. D., Lee, S., Tory, K. J., Burgers, M., Dewundege, P., and Johnson, M.: The Australian Air Quality Forecasting System: Exploring first steps towards determining the limits of predictability for short-term ozone forecasting, *Bound.-Lay. Meteorol.*, 116, 363–384, <https://doi.org/10.1007/s10546-004-2816-2>
- Dabberdt, W. F., M. A. Carroll, D. Baumgardner, G. Carmichael, R. Cohen, T. Dye, J. Ellis, G. Grell, S. Grimmond, S. Hanna, J. Irwin, B. Lamb, S. Madronich, J. McQueen, J. Meagher, T. Odman, J. Pleim, H. P. Schmid, and D. L. Westphal (2004), Meteorological research needs for improved air quality forecasting: Report of the 11th prospectus development team of the U. S. Weather Research Program, *Bull. Amer. Meteor. Soc.*, 85, 563-586.
- Derber, J. C. and Wu, W.-S.: The Use of TOVS Cloud-Cleared Radiances in the NCEP SSI Analysis System, *Mon. Weather Rev.*, 126, 2287–2299, 1998.
- Dethof, A. and Hólm, E. V.: Ozone assimilation in the ERA-40 reanalysis project, *Q. J. Roy. Meteorol. Soc.*, 130, 2851–2872, 2004.
- Doraiswamy, P., C. Hogrefe, W. Hao, B. Colle, M. Beauharnois, K. Demerjian, J.-Y. Ku, and G. Sistla (2009). Preliminary Experiences with the Multi-Model Air Quality Forecasting System for New York State, paper presented at the 8th Annual Community Modeling and Analysis System (CMAS) Conference, Chapel Hill, NC.
- Eben, K., P. Juruš, J. Resler, M. Belda, E. Pelikán, B. C. Krüger, and J. Keder (2005), An ensemble Kalman filter for short-term forecasting of tropospheric ozone concentrations, *Q. J. R. Meteorol. Soc.*, 131, 3313–3322
- ECMWF, 2002: Brief history of the ECMWF analysis and forecasting system. European Center for Medium Range Forecasts. Reading, UK
- Eder, B. K., D. Kang, R. Mathur, S. Yu, and K. Schere (2006), An operational evaluation of the Eta-CMAQ air quality forecast model, *Atmos. Environ.*, 40, 4894–4905.
- Eder, B., D. Kang, S. T. Rao, R. Mathur, S. Yu, T. Otte, K. Schere, R. Waylard, S. Jackson, P. Davidson, J. McQueen, and G. Bridgers (2010), Using national air quality forecast guidance to develop local air quality index forecasts, *Bull. Amer. Meteor. Soc.*, 91, 313-326.
- Elbern, H., and H. Schmidt (2001), Ozone episode analysis by four-dimensional variational chemistry data assimilation, *J. Geophys. Res.*, 106, 3569– 3590.
- Flatøy, F., O. Hov, and H. Schlager (2000), Chemical forecasts used for measurement flight planning during POLINAT 2, *Geophys. Res. Lett.*, 27, 951–954.
- Flemming, J., Huijnen, V., Arteta, J., Bechtold, P., Beljaars, A., Blechschmidt, A.-M., Diamantakis, M., Engelen, R. J., Gaudel, A., Inness, A., Jones, L., Josse, B., Katragkou, E., Marecal, V., Peuch, V.-H., Richter, A., Schultz, M. G., Stein, O., and Tsikerdekis, A.: Tropospheric chemistry in the Integrated Forecasting System of ECMWF, *Geosci. Model Dev.*, 8, 975–1003, [doi:10.5194/gmd-8-975-2015](https://doi.org/10.5194/gmd-8-975-2015), 2015.
- Freitas, E. D., Martins, L. D., Silva Dias, P. L., and Andrade, M. F. (2005). A simple photochemical module implemented in RAMS for tropospheric ozone concentration forecast in the metropolitan area of Sao Paulo, Brazil: coupling and validation. *Atmos. Environ.* 39, 6352–6361. [doi: 10.1016/j.atmosenv.2005.07.017](https://doi.org/10.1016/j.atmosenv.2005.07.017)

- Freitas, S. R., Panetta, J., Longo, K. M., Rodrigues, L. F., Moreira, D. S., Rosário, N. E., Silva Dias, P. L., Silva Dias, M. A. F., Souza, E. P., Freitas, E. D., Longo, M., Frassoni, A., Fazenda, A. L., Santos e Silva, C. M., Pavani, C. A. B., Eiras, D., França, D. A., Massaru, D., Silva, F. B., Cavalcante, F., Pereira, G., Camponogara, G., Ferrada, G. A., Campos Velho, H. F., Menezes, I., Freire, J. L., Alonso, M. F., Gácita, M. S., Zarzur, M., Fonseca, R. M., Lima, R. S., Siqueira, R. A., Braz, R., Tomita, S., Oliveira, V., Martins, L. D., 2016. The Brazilian developments on the Regional Atmospheric Modeling System (BRAMS 5.2): an integrated environmental model tuned for tropical areas, *Geoscientific Model Development Discussion*, 1-55, doi: [10.5194/gmd-2016-130](https://doi.org/10.5194/gmd-2016-130).
- Grell, G. and A. Baklanov, 2011: Integrated Modeling for Forecasting Weather and Air Quality: A Call for Fully Coupled Approaches. *Atmospheric Environment*, doi: [10.1016/j.atmosenv.2011.01.017](https://doi.org/10.1016/j.atmosenv.2011.01.017)
- Grell, G., J. Dudhia, and D. Stauffer (1995), A Description of the Fifth-Generation Penn State/NCAR Mesoscale Model (MM5), NCAR Technical Note, NCAR/TN-398+STR.
- Grell, G.A., R. Knoche, S.E. Peckham, and S.A. McKeen (2004), Online versus offline air quality modeling on cloud-resolving scales, *Geophys. Res. Lett.*, 31, L16117, doi: [10.1029/2004GL020175](https://doi.org/10.1029/2004GL020175).
- Grell, G. A., S. E. Peckham, R. Schmitz, and S. A. McKeen, G. Frost, W. C. Skamarock, and B. Eder (2005), Fully coupled “online” chemistry within the WRF model, *Atmos. Environ.*, 39, 6957-6975.
- Guillas, S., J. Bao, Y. Choi, and Y. Wang (2008), Statistical correction and downscaling of chemical transport model ozone forecasts over Atlanta, *Atmos. Environ.*, 42, 1338-1348, doi: [10.1016/j.atmosenv.2007.10.027](https://doi.org/10.1016/j.atmosenv.2007.10.027).
- Hagedorn, R., F. J. Doblas-Reyes, and T.N. Palmer (2015), The rationale behind the success of multi-model ensembles in seasonal forecasting — I. Basic concept, *Tellus A: Dynamic Meteorology and Oceanography*, 57:3, 219-233, DOI: [10.3402/tellusa.v57i3.14657](https://doi.org/10.3402/tellusa.v57i3.14657)
- Han, Z.-W., S.-Y., Du, X.-E., Lei, L.-X., Ju, and Q.-G. Wang (2002), Numerical model system of urban air pollution prediction and its application, *China Environmental Science* (in Chinese), 22(3), 202-206.
- Han, Z.-W., S.-Y., Du, X.-E., Lei, L.-X., Ju, and Q.-G. Wang (2002), Numerical model system of urban air pollution prediction and its application, *China Environmental Science* (in Chinese), 22(3), 202-206.
- Harper, K., Uccellini, L.W., Kalnay, E., Carey, K., Morone, L., 2007: 50th Anniversary of Operational Numerical Weather Prediction. *Bulletin of the American Meteorological Society*. 88 (5): 639–650. doi: [10.1175/BAMS-88-5-639](https://doi.org/10.1175/BAMS-88-5-639).
- Inness, A., Blechschmidt, A.-M., Bouarar, I., Chabrillat, S., Crepulja, M., Engelen, R. J., Eskes, H., Flemming, J., Gaudel, A, Hendrick, F., Huijnen, V., Jones, L., Kapsomenakis, J., Katragkou, E., Keppens, A., Langerock, B., de Mazière, M., Melas, D., Parrington, M., Peuch, V. H., Razinger, M., Richter, A., Schultz, M. G., Suttie, M., Thouret, V., Vrekoussis, M., Wagner, A., and Zerefos, C.: Data assimilation of satellite retrieved ozone, carbon monoxide and nitrogen dioxide with ECMWF's Composition-IFS, *Atmos. Chem. Phys.*, 15, 5275–5303, doi: [10.5194/acp-15-5275-2015](https://doi.org/10.5194/acp-15-5275-2015), 2015.
- Jakobs, H. J., S. Tilmes, A. Heidegger, K. Nester, and G. Smiatek (2002), Short-term ozone forecasting with a network model system during summer 1999, *J. Atmos. Chem.*, 42, 23–40.
- Jacobson, M. Z., 2005: *Fundamentals of Atmospheric Modeling*, 2nd edn., Camb. Univ. Press, New York, 813 pp.
- Kalnay, E. (2003). *Atmospheric modeling, data assimilation and predictability*. Cambridge University Press. ISBN 0-521-79179-0.

- Kang, D., B. K. Eder, A. F. Stein, G. A. Grell, S. E. Peckham, and J. McHenry (2005), The New England Air Quality Forecasting Pilot Program: Development of an evaluation protocol and performance benchmark, *J. Air & Waste Manage. Assoc.*, *55*, 1782-1796.
- Kang, D., R. Mathur, S. T. Rao, and S. Yu (2008), Bias adjustment techniques for improving ozone air quality forecasts, *J. Geophys. Res.*, *113*, D23308, doi: 10.1029/2008JD010151.
- Korsholm U.S., A. Baklanov, A. Gross and J.H. Sørensen (2009), On the importance of the meteorological coupling interval in dispersion modeling during ETEX-1, *Atmospheric Environment*, doi: 10.1016/j.atmosenv.2008.11.0117., *43*(31), 4805–4810
- Kukkonen, J., Olsson, T., Schultz, D. M., Baklanov, A., Klein, T., Miranda, A. I., Monteiro, A., Hirtl, M., Tarvainen, V., Boy, M., Peuch, V.-H., Poupkou, A., Kioutsioukis, I., Finardi, S., Sofiev, M., Sokhi, R., Lehtinen, K. E. J., Karatzas, K., San José, R., Astitha, M., Kallos, G., Schaap, M., Reimer, E., Jakobs, H., and Eben, K.: A review of operational, regional-scale, chemical weather forecasting models in Europe, *Atmos. Chem. Phys.*, *12*, 1-87, <https://doi.org/10.5194/acp-12-1-2012>, 2012.
- Lawrence, M. G., Hov, Ø., Beekmann, M., Brandt, J., Elbern, H., Eskes, H., Feichter, H., and Takigawa, M.: The chemical weather, *Environ. Chem.*, *2*, 6–8, doi: 10.1071/EN05014, 2005.
- Lee, A. M., G. D. Carver, M. P. Chipperfield, J. A. Pyle (1997), Three-dimensional chemical forecasting: A methodology, *J. Geophys. Res.*, *102*, 3905-3919.
- Mallet, V. (2010), Ensemble forecast of analyses: Coupling data assimilation and sequential aggregation, *J. Geophys. Res.*, *115*, D24303, doi: 10.1029/2010JD014259.
- Manders, A. M. M., Schaap, M., and Hoogerbrugge, R.: Testing the capability of the chemistry transport model LOTOS-EUROS to forecast PM10 levels in The Netherlands, *Atmos. Environ.*, *43*, 4050–4059, doi: 10.1016/j.atmosenv.2009.05.006, 2009.
- Manins, P. C., M. E. Cope, G. D. Hess, P. F. Nelson, K. Puri, N. Wong, and M. Young (2002), The Australian Air Quality Forecasting System: prognostic air quality forecasting in Australia, *Clean Air and Environmental Quality*, *36* (2): 43-48.
- McCollister, G., and K. Wilson (1975), Linear stochastic models for forecasting daily maxima and hourly concentrations of air pollutants, *Atmos. Environ.*, *9*, 417–423.
- McHenry, J. N., W. F. Ryan, N. L. Seaman, C. J. Coats Jr., J. Pudykiewics, S. Arunachalam, and J. M. Vukovich (2004), A real-time Eulerian photochemical model forecast system: Overview and initial ozone forecast performance in the Northeast U.S. corridor, *Bull. Amer. Meteor. Soc.*, *85*, 525-548.
- McKeen, S., J. Wilczak, G. Grell, I. Djalova, S. Peckham, E.-Y. Hsie, W. Gong, V. Bouchet, S. Ménard, R. Moffet, J. McHenry, J. McQueen, Y. Tang, G. R. Carmichael, M. Pagowski, A. Chan, t. Dye, G. Frost, P. Lee, and R. Mathur (2005), Assessment of an ensemble of seven real-time ozone forecasts over eastern North America during the summer of 2004, *J. Geophys. Res.*, *110*, D21307, doi: 10.1029/2005JD005858.
- McKeen, S., S. H. Chung, J. Wilczak, G. Grell, I. Djalalova, S. Peckham, W. Gong, V. Bouchet, R. Moffet, Y. Tang, G. R. Carmichael, R. Mathur, and S. Yu (2007), Evaluation of several PM_{2.5} forecast models using data collected during the ICARTT/NEAQS 2004 field study, *J. Geophys. Res.*, *112*, D10S20, doi: 10.1029/2006JD007608.
- McKeen, S. et al. (2009), An evaluation of real-time air quality forecasts and their urban emissions over eastern Texas during the summer of 2006 Second Texas Air Quality Study field study, *J. Geophys. Res.*, *114*, D00F11, doi: 10.1029/2008JD011697.
- Ménard R, Robichaud A 2005. The chemistry-forecast system at the Meteorological Service of Canada. In: ECMWF Seminar proceedings on Global Earth-System Monitoring, Reading, UK, pp 297–308.

- Michalakes, J., Chen, S., Dudhia, J., Hart, L., Klemp, J., Middlecoff, J., Skamarock, W. (2001), Development of a next-generation regional weather forecast model, *Devel.. In Teracomputing: Proceedings of the Ninth ECMWF Workshop on the Use of High-Performance Computing in Meteorology*, Eds. Walter Zwiefelhofer and Norbert Kreitz, World Scientific, Singapore, pp. 269-276.
- Morcrette, J.-J., Boucher, O., Jones, L., Salmond, D., Bechtold, P., Beljaars, A., Benedetti, A., Bonet, A., Kaiser, J. W., Razinger, M., Schulz, M., Serrar, S., Simmons, A. J., Sofiev, M., Suttie, M., Tompkins, A. M., and Untch, A.: Aerosol analysis and forecast in the ECMWF Integrated Forecast System, Part I: Forward modeling, *J. Geophys. Res.*, 114, D06206, doi:10.1029/2008JD011235, 2009.
- Niemeyer, L. E. (1960), Forecasting Air Pollution Potential, *Mon. Wee. Rev.*, 88(3), 88-96.
- Ohara T., A. Fujita, T. Kizu and S. Okamoto (1997), Advanced air quality forecasting system for Chiba Prefecture, *Proceedings of the 22nd NATO/CCMS International Technical Meeting on Air Pollution Modeling and its Application*, Clermont- Ferrand, France, 2-6 June.
- Otte, T. L., G. Pouliot, J. E. Pleim, J. O. Young, K. L. Schere, D. C. Wong, P. C. S. Lee, M. Tsidulko, J. T. McQueen, P. Davidson, R. Mathur, H.-Y. Chuang, G. DiMego, and N. L. Seaman (2005), NCEP Notes: Linking the Eta model with the Community Multiscale Air Quality (CMAQ) Modeling System to build a national air quality forecasting system, *Weather and Forecasting*, 20, 367-384.
- Pielke, R.A. (2002). *Mesoscale Meteorological Modeling*. Academic Press. ISBN 0-12-554766-8.
- Pudykiewicz, J. A., and A. S. Koziol (2001), The application of Eulerian models for air quality prediction and the evaluation of emission control strategies in Canada, *Int. J. Environ. Pollut.*, 16, 425– 438.
- Pudykiewicz, J. A., et al. (2003), Operational air quality forecasting in Canada: Numerical model guidance for ground-level ozone and particulate matter, Preprints, *Fifth Conf. on Atmospheric Chemistry: Gases, Aerosols, and Clouds*, Long Beach, CA, Amer. Meteor. Soc., the 83rd Annual Meeting CD-ROM, 3.2.
- Reimer, E., Wiegand, G., Flemming, J., Dlabka, M., Enke, W., Berendorf, K., Weiß, W., and Stern, R.: Development of an Ozone Short Range Forecast for the Smog Warning system, Final Report, UBA F&E project 29543817, Berlin, Germany, 2000 (in German).
- Richardson, L. F. (1922). *Weather Prediction by Numerical Process*. Cambridge University Press. 2nd Edn. (2007).
- Rouil, L., C. Honoré, R. Vautard, M. Beekmann, B. Bssagnet, L. Malherbe, F. Meleux, A. Dufour, C. Elichegaray, J.-M. Flaud, L. Menut, D. Martin, A. Peuch, V.-H. Peuch, and N. Poisson (2009), Prev'air: An operational forecasting and mapping system for air quality in Europe, *Bull. Amer. Meteor. Soc.*, 90, 73-83, doi:10.1175/2008BAMS2390.1.
- Rufeger, W., P. Mieth, and T. Lux (1997), Applying the DYMOSS system in conurbations, *Proc. Modsim 97*, 4, Hobart, TAS, Australia, International Congress on Modeling and Simulation, 1797–1801.
- Ryan, W.F. (2016) The air quality forecast rote: Recent changes and future challenges, *Journal of the Air & Waste Management Association*, 66:6, 576-596, DOI:10.1080/10962247.2016.1151469
- San José, R., Salas, I., Martín, A., Pérez, J. L., Carpintero, A. B., Ramos, M. C., Peña, J. I., and González, R. M.: Development of a global-through-urban scale nested air quality forecast model (RSM-ANA): Application over the Madrid domain, *SAMS*, 42, 1551–1560, 2002.

- San José, R., J. L. Pérez, and R.M. González (2006), CFD and mesoscale air quality application in urban environment: MADRID case study, Proceedings of the 4th WSEAS International Conference on Environment, Ecosystems, and Development (EED '06), Venice, Italy, November 20-22, 2006.
- San José, R., Pérez, J. L., and González, R. M.: An operational real time air quality modeling system for industrial plants, *Environ. Model. Softw.*, 22, 297–307, 2007.
- San José, R. & J. L. Pérez, J. L. Morant, and R. M. González Barras (2009), The Use of Modern Third-Generation Air Quality Models (MM5-EMIMO-CMAQ) for Real-Time Operational Air Quality Impact Assessment of Industrial Plants, *Water, Air, & Soil Pollution: Focus*, 9 (1-2), 27-37, DOI: [10.1007/s11267-008-9196-4](https://doi.org/10.1007/s11267-008-9196-4)
- Sofiev, M., Vankevich, R., Lotjonen, M., Prank, M., Petukhov, V., Ermakova, T., Koskinen, J., and Kukkonen, J.: An operational system for the assimilation of the satellite information on wildland fires for the needs of air quality modeling and forecasting, *Atmos. Chem. Phys.*, 9, 6833–6847, doi:[10.5194/acp-9-6833-2009](https://doi.org/10.5194/acp-9-6833-2009), 2009.
- Stajner I., P. Davidson, D. Byun, J. McQueen, R. Draxler, P. Dickerson, and J. Meagher (2012), US National Air Quality Forecast Capability: Expanding Coverage to Include Particulate Matter, NATO/ITM Air Pollution Modeling and Its Application XXI, Douw G. Steyn & Silvia Trini Castelli (ed.), Springer, Netherlands, pp 379-384, DOI: [10.1007/978-94-007-1359-8_64](https://doi.org/10.1007/978-94-007-1359-8_64).
- Stockwell, W. R. et al. (2002), The scientific basis of NOAA's Air Quality Forecast Program, *Environ. Manage.*, December 20–27.
- Taylor, E. 2014. The Canadian Air Quality Health Index. In *Air Quality Management*, ed. E. Taylor and A. McMillan, 351–363. Dordrecht, The Netherlands: Springer.
- Tilmes, S., Brandt, J., Flatøy, F., Bergström, R., Flemming, J., Langner, J., Christensen, J. H., Frohn, L. M., Hov, O., Jacobson, I., Reimer, E., Stern, R., and Zimmermann, J.: Comparison of five Eulerian air pollution forecasting systems for the Summer of 1999 using the German Ozone monitoring data, *J. Atmos. Chem.*, 42, 91–121, 2002.
- Uno, I., et al. (2003), Regional chemical weather forecasting system CFORS: Model descriptions and analysis of surface observations at Japanese island stations during the ACE-Asia experiment. *J. Geophys. Res.*, 108, 8668, doi:[10.1029/2002JD002845](https://doi.org/10.1029/2002JD002845).
- U.S. EPA (1999), Guideline for developing an ozone forecasting program. U.S. Environmental Protection Agency Rep. EPA-454/R-99-009, 88 pp. (Available from Office of Air Quality Planning and Standards, EPA, Research Triangle Park, NC 27711.)
- U.S. EPA (2000), *Air Quality Index, A Guide to Air Quality and Your Health*; EPA-454/R-00-005; U.S. Environmental Protection Agency, Office of Air and Radiation: Washington, DC, 2000. <https://www.airnow.gov/all-publications/>.
- U.S. EPA (2003), Guideline for developing an air quality (ozone and PM_{2.5}) forecasting program. U.S. Environmental Protection Agency Rep. EPA-456/R-03-002, 126 pp. (Available from Office of Air Quality Planning and Standards, EPA, Research Triangle Park, NC 27711; also available online at <https://www.airnow.gov/all-publications/>)
- U.S. EPA (2009), Technical Assistance Document for Reporting of Daily Air Quality—Air Quality Index (AQI); EPA-454/B-09-001; U.S. Environmental Protection Agency, Office of Air Quality Planning and Standards: Research Triangle Park, NC.
- Vautard, R., N. Blond, H. Schmidt, C. Derognat, and M. Beekmann (2001), Multi-model ensemble ozone forecasts over Europe: Analysis of uncertainty. In *Mesoscale Transport of Air Pollution*. OA15, ed. J. Brandt. EGS XXXVI General Assembly. Nice, France: European Geophysical Society, Katlenburg-Lindau, Germany, 26 March.

- Wang, Z.-F., Q.-Z. Wu, A. Gbaguidi, P.-Z. Yan, W. Zhang, W. Wang, and X. Tang (2009), Ensemble air quality multi-model forecast system for Beijing (EMS-Beijing): Model description and preliminary application, *Journal of Nanjing University of Information Science and Technology: Natural Science Edition* (in Chinese), 1(1), 19-26.
- Wayland, R. A., J. E. White, P. G. Dickerson, and T. S. Dye (2002), Communicating real-time and forecasted air quality to the public, *Environ. Manage.*, 28–36, December.
- Wolff, G. T., and P. J. Liroy (1978), An empirical model for forecasting maximum daily ozone levels in the north-eastern United States, *J. Air Pollut. Control Assoc.*, 28, 1034–1038.
- World Weather Open Science Conference (WWOSC), 2015: Seamless Prediction of the Earth System: From Minutes to Months. WMO-No. 1156. 471 pp.
https://library.wmo.int/index.php?lvl=notice_display&id=17276#.XoWu3lgzZPY
- Yahya, K., Y. Zhang, and J. M. Vukovich, 2014, Real-Time Air Quality Forecasting over the Southeastern United States using WRF/Chem-MADRID: Multiple-Year Assessment and Sensitivity Studies, *Atmospheric Environment*, 92, 318-338,
[doi: 10.1016/j.atmosenv.2014.04.024](https://doi.org/10.1016/j.atmosenv.2014.04.024).
- Zhang, Y., 2008, Online Coupled Meteorology and Chemistry models: History, Current Status, and Outlook, *Atmospheric Chemistry and Physics*, 8, 2895-2932,
[doi: 10.5194/acp-8-2895-2008](https://doi.org/10.5194/acp-8-2895-2008).
- Zhang, Y., 2021, Air Quality in a Changing Climate: Science and Modeling, Cambridge University Press, in preparation.
- Zhang, Y., P. Liu, X.-H. Liu, B. Pun, C. Seigneur, M.Z. Jacobson, and W.-X. Wang (2010b), Fine Scale Modeling of Wintertime Aerosol Mass, Number, and Size Distributions in Central California, *J. Geophys. Res.*, 115, D15207, [doi: 10.1029/2009JD012950](https://doi.org/10.1029/2009JD012950).
- Zhang, Y., C. Seigneur, M. Bocquet, V. Mallet, and A. Baklanov, 2012, Real-Time Air Quality Forecasting, Part I: History, Techniques, and Current Status, *Atmospheric Environment*, 60, 632-655, [doi: 10.1016/j.atmosenv.2012.06.031](https://doi.org/10.1016/j.atmosenv.2012.06.031).
- Zhang, Y., C.-P. Hong, K. Yahya, Q. Li, Q. Zhang, and K.-B. He, 2016, Comprehensive evaluation of multi-year real-time air quality forecasting using an online-coupled meteorology-chemistry model over southeastern United States, *Atmos. Environ.*, 138, 162-182, [doi: 10.1016/j.atmosenv.2016.05.006](https://doi.org/10.1016/j.atmosenv.2016.05.006).

Chapter 3. Fundamentals of 3-D CW-AQF Models

3.1 Introduction

Deterministic, 3-D chemical weather and air quality forecasting (CW-AQF) models explicitly solve the mathematical equations that describe physical and/or chemical relations among the chemical species concentrations and the governing atmospheric processes, based on the mass conservation principle. Along with information about the meteorological state, which may be specified or computed, CW-AQF systems require initial and boundary conditions (ICONS and BCONs, respectively) for atmospheric constituents. In this chapter, fundamentals of CW-AQF models are described. Section 3.2 introduces the major types of CW-AQF models. Current 3-D CW-AQF models on global, regional, and urban/local scales are reviewed in terms of component models, spatial scale, and coupling between meteorology and chemistry. Section 3.3 introduces major meteorological and NWP models. These models were developed for their applications on various spatial and temporal scales. Major characteristics of representative models are reviewed. Section 3.4 describes atmospheric planetary boundary layer and parameterizations of key boundary-layer processes. Section 3.5 describes atmospheric gas-phase, aqueous-phase, and heterogeneous reactions, as well as major chemical mechanisms that are most commonly used in CW-AQF models. Section 3.6 describes chemical composition, size distribution, mixing state, and major thermodynamic and dynamic processes of atmospheric aerosol as well as common modeling approaches for aerosol properties and processes used in CW-AQF models. Section 3.7 describes atmospheric removal processes of gases and aerosols including dry deposition, wet deposition, and gravitational settling and major formulations used in CW-AQF models. Sections 3.8 and 3.9 describe the interactions of chemical species with radiation through direct effects and with cloud through indirect effects, respectively. The representations of aerosol direct and indirect effects as well as feedback in representative CW-AQF models are reviewed.

3.2 Model Types and Existing Models

3.2.1 Model Types

CW-AQF models can be grouped, in several different ways, into different categories (Zhang, 2020).

- Based on the underlying model framework, CW-AQF models can be grouped into three categories: Eulerian, Lagrangian, and hybrid models. Eulerian models use fixed grids (both vertically and horizontally) and solve the appropriate mathematical equations simultaneously in all grid cells. While most CW-AQF models are Eulerian, some are Lagrangian (e.g., NAME, DERMA) and a few have a hybrid structure (e.g., SILAM). Lagrangian models use moving grids and follow individual air parcels over time using the meteorological field to advect and disperse the pollutants. Lagrangian models are typically computationally more efficient than Eulerian models, but less suitable for data assimilation. Because of limitations in their formulations, they struggle to properly characterize the interaction of a large number of individual sources when nonlinear chemistry is involved.
- Based on spatial scale, CW-AQF models can be grouped into four types in terms of horizontal grid resolution: local (< 1 km), urban (1 km – 12 km), mesoscale (12 -1 000 km), and global (1 000-20 000 km). A CW-AQF model can be coupled with a street-network model to forecast air pollutant concentrations at street level. An example is the Street-in-Grid (SinG) model that is composed of the CTM Polair3D of the Polyphemus air quality modeling platform (Mallet et al., 2007) and of the street-network model, MUNICH (Model of Urban Network of Intersecting Canyons and Highways) (Kim et al., 2018). Some (Eulerian) models adopt a hybrid approach to scale, using nested or adaptive grids. In the nested grid models, a fine-resolution grid is nested over a region of interest (e.g., an urban center) inside a mode using a coarse grid over a larger domain. In the adaptive grid models, the grids are periodically refined or coarsened, with a finer mesh retained in regions with sharp concentration gradients. This method effectively reduces the number of grid points without losing overall accuracy.

- Based on temporal scale, CW-AQF models can be grouped into two types: episodic (or short-term) and long-term models. They are designed for simulations of hours to days, or weeks to months, respectively. Most CW-AQF models are episodic models, aimed at forecasting atmospheric composition or extreme air-quality events up to a few days or one week ahead of time. Longer-term models can be used for forecasting air quality in the context of weeks or seasons, or can be used for retrospective studies (reanalyses) of air quality. Here we are not considering AQ assessment models based on diagnostic equations or semi-empirical methods.
- Based on the chemistry coupling with the meteorology, there are two main types: online-coupled models and offline models. The main characteristics of these models are described in detail in Kukkonen et al, (2012) and Baklanov et al. (2014). In online-coupled models, the meteorological fields are generated internally in the CW-AQF model itself (also called online integrated models, e.g., WRF/Chem) or externally by a coupled meteorological model (also called online-access models, e.g., two-way coupled WRF/CMAQ), or offline-coupled models in which meteorological fields are generated externally by a meteorological model that is not coupled with AQM (e.g., SILAM or CAMx coupled offline with NWP models). As defined in Chapter 2, online-coupled models can be grouped into online-access and online-integrated models. WRF/Chem, Meso-NH-C, COSMO-Art, Enviro-HIRLAM, and GEM-MACH15 are examples of online-integrated models. The two-way coupled WRF-CMAQ, COSMO-MUSCAT, and RAMS/ICLAMS are examples of online-access models.
- Based on community involvement, CW-AQF models may be a community-based model or a non-community based model. They differ in their development, support, and availability to the users. A community-based model is a model that is first developed by one or more institutions to address the community's needs and then released to the research community free of charge. Researchers in the community may further develop or improve modules in the released model, which may be included in the next version of the model for public release. Examples of community models include CMAQ, WRF/Chem, and Polyphemus. This type of model is also referred to as an open-source model. A non-community based model is developed and used by one or more institutions only. An agreement or a contract is usually required to use a non-community model. Payment is often required. It may be provided to a small number of collaborators free of charge but it is not intended for public release. In some cases, those models are closed sources or proprietary. Examples of non-community models include GRAPES-CUACE.

3.2.2 Existing 3-D CW-AQF Models

A number of 3-D global and regional models have been deployed for RT CW-AQF. Tables 3.1 and 3.2 summarize 17 global and 56 regional/urban RT CW-AQF models that are currently used in Australia, North America, South America, Europe, Asia, and Africa in terms of component models (i.e., meteorological models, air quality models, microscale models), spatial scale, and coupling between meteorology and chemistry. Case studies using some of these CW-AQFs along with detailed model descriptions over all six continents are given in Chapter 9. The full names of models and associated organizations are provided in a [list of acronyms](#) and symbols in an appendix in the supplementary material. Among these models, nine global models and twenty-three regional models are multiscale models. Eleven global models (i.e., GEM-AQ, GEM-MACH, GRAPES-CUACE, LMDzt-INCA, ECHAM5, MASINGAR, NMMB/BSC-CTM, ECMWF/CAMs, MetUM, NCEP-NGAC, and GEOS-5 ESM) and twenty-one regional models (e.g., WRF/Chem, WRF/Chem-MADRID, GEM-MACH15, COSMO-Art, Enviro-HIRLAM, and CFORS) are online-coupled models. Most online coupled models are online-integrated models, which represent the direction of current CW-AQF model development. Three global models (LMDzt – INCA, NMMB/BSC-CTM, ECMWF/CAMS) and eight regional models (i.e., two-way coupled WRF-CMAQ, DACFOS, COSMO-MUSCAT, MEMO/MARS, BOLCHEM, ADMS URBAN, LOTOS-EUROS, and RAMS/ICLAMS) are online-access models.

For global models, meteorological fields are produced by reanalysis data such as National Centers for Environmental Prediction (NCEP) or general circulation models such as GEM, ECMWF/IFS, LMDzt, ECHAM5, and GEOS-5. In online-integrated models such as GEM-AQ, ECHAM5, and GEOS-5 ESM, a chemistry module is incorporated into a GCM. In offline or online-access models, an AQM is driven by data from meteorological reanalysis (e.g., BSC-CTM) or used in conjunction with a GCM (e.g., MOCAGE, MOZART-3, TM5), respectively.

Table 3.1 Component Models, Spatial Scale, and Coupling of Meteorology and Chemistry in Global CW-AQF Model Systems (modified from Zhang et al., 2012).

Country/ Organization	Model System	Meteorological Model (MetM)	Air Quality Model (AQM)	Microscale Models	Scale	MetM -AQM coupling	References
Canada/Environ Canada	GEM-MACH	GEM	GEM-MACH15	None	Global/ Regional	Online- Integrated	Talbot et al., 2008; Moran et al., 2010; Anselmo et al., 2010
Canada/ York Univ.	GEM-AQ	GEM	AQ	None	Global/ Regional	Online- Integrated	Neary et al., 2007; Kaminski et al., 2008; http://ecoforecast.eu/index.php?id=2
China/CMA and CAMS	GRAPES- CUACE	GRAPES	CUACE	None	Global/ Regional	Online- Integrated	Wang et al., 2010, 2018 https://www.sciencedirect.com/science/article/pii/S1352231017308026 ; Zhou et al., 2016, 2018
Finland/FMI	SILAM	ECMWF/IFS; WRF; HIRLAM; AROME; COSMO HARMONIE	SILAM	None	Global/ Regional	Offline	Sofiev et al., 2006, 2015; Sofiev and Vira, 2010; Kukkonen et al., 2011; Kuznetsov and Sofiev (2012); Marecal et al., 2015; http://silam.fmi.fi/
France/LMD	LMDzt -INCA	ECMWF/IFS; LMDzt v4.0 with nudged with NCEP	INCA v3	None	Global	Online-Access	Hauglustaine et al., 2004; Folberth et al., 2006;
France/Météo- France-CNRM	MOCAGE	ARPEGE (global) ALADIN (regional) ECMWF	MOCAGE	None	Global/ Regional	Offline	Dufour et al., 2004; Rouil et al., 2009; http://www2.prevaire.org/
Germany/MPIM	ECHAM5	ECHAM5	ECHAM5	None	Global	Online- Integrated	Roeckner et al., 2006; K. Zhang et al., 2010; http://www.mpimet.mpg.de/en/science/models/echam.html
Norway NIAR/ FLEXPART	FLEXPART	ECMWF NCEP	FLEXPART	None	Global	Offline	Forster et al., 2004; Stohl et al., 2005; https://www.nilu.no/flexpart
Japan-FRCGC	GR-RT CW- AQF	CCSR/NIES/FRCG C atmospheric GCM (global) WRF (regional)	CHASER (global) WRF/Chem (regional)	None	Global/ Regional	Offline for global/regional Online- Integrated for regional	Takigawa et al., 2007

Country/ Organization	Model System	Meteorological Model (MetM)	Air Quality Model (AQM)	Microscale Models	Scale	MetM -AQM coupling	References
Japan/JMA	MASINGAR	AGCM	MASINGAR	None	Global	Online	Tanaka et al., 2003; http://www.jma.go.jp/en/kosa/
Spain, BSC-CNS	NMMB/BSC- CTM	NMMB	BSC-CTM (dust module)	None	Global/ regional	Online-Access	Pérez et al. (2011); Jorba et al., 2012; Spada et al., 2013; Badia and Jorba (2014); Spada (2015); https://dust.aemet.es/ mineral-dust-forecast-system
UK/ECMWF, MACC	ECMWF-IFS CTMs; ECMWF/CAMS	IFS	MOZART-3, TM5, or MOCAGE; C-IFS	None	Global/ Regional	Online-Access	Flemming et al., 2009; Mangold et al., 2011; https://atmosphere.copernicus.eu/
UK/Met Office	MetUM	MetUM	Dust module	None	Global/ Regional	Online- Integrated	Johnson et al. (2011); https://www.metoffice.gov.uk/resear ch/
US/FNMOC/NRL	NAAPS	NOGAPS	NAAPS	None	Global	Offline	http://www.nrlmry.navy.mil/aerosol/ ; http://www.usno.navy.mil/FNMOC/
US/NASA	GEOS-ESM	GEOS	GEOS-Chem GOCART	None	Global	Online- Integrated	Chin et al., 2002; Rienecker et al. 2008; Colarco et al., 2010; Long et al., 2015; Nielsen et al., 2017; https://gmao.gsfc.nasa.gov/
US/NCAR, Germany/MPIC	MATCH-NCAR	NCEP/NCAR	MATCH-NCAR	None	Global	Offline	Rasch et al.,1997; Lawrence et al., 2003;
US/NOAA-NCEP	NEMS GFS- NGAC	NEMS GFS	NGAC (dust only)	None	Global	Online- Integrated	Lu et al., 2010, 2013, 2016

Table 3.2 Component Models, Spatial Scale, and Coupling of Meteorology and Chemistry in Regional/Urban CW-AQF Model Systems (modified from Zhang et al., 2012 and Kukkonen et al., 2012).

Country/ Organization	Model System	Meteorological Model (MetM)	Air Quality Model (AQM)	Microscale Models	Scale	MetM - AQM coupling	References
Australia/CSIRO	AAQFS Or AQFx	LAPS, UM, CCAM; ACCESS	CSIRO's CTM C-CTM	None	Regional	Offline	Manins, 2002; Cope et al., 2004; Lawson et al. 2017, https://www.epa.vic.gov.au/for-community/airwatch/air-notice
Austria/ZAMG	ALADIN- CAMx	ALADIN- Austria	CAMx	None	Regional	Offline	http://www.umr-cnrm.fr/aladin/ http://www.camx.com
Brazil/CPTEC	CCATT-BRAMS	BRAMS	CCATT	None	Regional	Online- Integrated	Freitas et al., 2009, 2011,2017; Longo et al., 2013 http://meioambiente.cptec.inpe.br/index.php?lang=en
Canada/Environment Canada	GEM-AURAMS	regional GEM	AURAMS	None	Regional	Offline	McKeen et al., 2005, 2007, 2009;
Canada/Environment Canada	GEM-CHRONOS	regional GEM	CHRONOS	None	Regional	Offline	Pudykiewicz and Koziol, 2001; McKeen et al., 2005, 2007, 2009;
Canada/Environment Canada	GEM-MACH15	GEM	chemistry from AURAMS	None	Regional	Online- Integrated	Talbot, 2007
China/IAP-CAS	EMS-Beijing	MM5	NAQPMS, CMAQ, CAMx	None	Regional	Offline	Wang et al., 2009
China/ Zhejiang Univ.	Two-way coupled WRF- CMAQ	WRF (ARW)	CMAQ	None	Regional	Online- Access	Li et al., 2017
Denmark/ DMU-ATMI	THOR	The US NCEP, Eta	DEOM DEHM (UPM, OSPM)	BUM OSPM DREAM	Regional	Offline	Brandt et al. (2001); Tilmes et al., 2002; https://envs.au.dk/en/
Denmark/DMI	Enviro-HIRLAM	HIRLAM	DERMA, CAMx, Enviro- HIRLAM	M2UE	Continental/ Regional/ urban	Online- Integrated/ Access	Chenevez and Jensen, 2001; Sørensen et al., 2007, Baklanov et al., 2011; 2017 and references therein; http://hirlam.org/index.php/documentation/chemistry-branch

Country/ Organization	Model System	Meteorological Model (MetM)	Air Quality Model (AQM)	Microscale Models	Scale	MetM - AQM coupling	References
Denmark, Finland, Norway, Spain, Italy/ FUMAPEX UAQIFS ³	1. UAQIFS- Norway 2. UAQIFS- Finland 3. UAQIFS- Spain 4. UAQIFS- Italy1 5. UAQIFS- Italy2 6. UAQIFS- Denmark	1. HIRLAM 2. HIRLAM 3. RAMS 4. RAMS 5. LAMI 6. HIRLAM	1. AirQUIS (dispersion) 2. CAR-FMI (dispersion) 3. CAMx (O ₃ only) 4. FARM 5. NINFA- OPPIO/ADAM 6. DERMA- ARGOS	Some include population exposure models, some include urban dispersion/ statistical models	Regional/ local	Offline	Baklanov, 2006; Baklanov et al., 2006
Egypt/EMA; South Africa/ SAWS	RegCM-CHEM	RegCM4.6	RegCM- CHEM4.6	None	Regional	Online- Integrated	Zakey et al, 2006, 2008, Shalaby et al., 2012, and Salah et al., 2018
France/AIRPA RIF ²	ESMERALDA	MM5	CHIMERE	None	Regional	Offline	Vautard et al., 2001a, b; http://www.esmeralda-web.fr
France/INERIS	Prev'air	MM5, WRF, ECMWF/IFS	CHIMERE, MOCAGE, Polair3D	None	Regional	Offline	Vautard et al., 2001a; Rouil et al., 2009; http://www2.prevoir.org/
France/CEREA	POLYPHEMUS	ECMWF, MM5, WRF	Polair3D	MUNICH	Regional/ urban	Offline	Mallet and Sportisse, 2006; Mallet et al., 2007; Debry et al, 2007; Sartelet et al. 2007, 2012; Zhu et al. (2016); Chrit et al. (2017), http://cerea.enpc.fr/polyphemus/
France/CNRS, Météo-France	Meso-NH-C	Meso-NH-C	Meso-NH-C	None	Continental/ regional/ urban/local	Online- Integrated	http://mesonh.aero.obs- mip.fr/mesonh; http://www.cnrm.meteo.fr /surfex/; Tulet et al., 2003
Germany/FRIU UK,RIU, Cologne	EURAD-RIU	MM5	EURAD-IM	None	Regional	Offline	Elbern et al., 2010; www.eurad.uni-koeln.de
Germany/FU- Berlin,	RCG	GME	REM- CALGRID	None	Regional	Offline	http://www.trumf.de; Stern (2003)

Country/ Organization	Model System	Meteorological Model (MetM)	Air Quality Model (AQM)	Microscale Models	Scale	MetM - AQM coupling	References
Institute for Meteorology							
Germany/KIT	COSMO- ART	COSMO	ART	None	Continental/ regional	Online- Integrated	Vogel et al., 2009, 2013;
Germany/LIT R	COSMO- MUSCAT	COSMO	MUSCAT	None	Continental/ regional	Online- Access	Wolke et al., 2004; 2012; http://projects.tropos.de/cosmo_muscat/
Germany/ Uni. of Hamburg	M-SYS	METRAS	MECTM	MITRAS- MICTM	Regional/ urban/local	Online- Integrated	Trukenmuller et al., 2004; Schatzmann et al., 2006; https://www.mi.uni-hamburg.de/en/arbeitsgruppen/me mi/modelle.html
Germany/IMK- IFU	MCCM (MM5-Chem)	MM5	Chem	None	Continental/ regional/ urban	Online- Integrated	Grell et al. (2000)
Greece/Aristot le University	MEMO/MARS	MEMO	MARS-aero	None	Regional/ urban	Online- Access	Moussiopoulos et al., 2012
Greece/NKUA	CAMx-AMWFG	SKIRON/Dust	CAMx	None	Regional	Offline	http://www.mg.uoa.gr/ICLAMS/index.php ; http://www.camx.com
Greece/NKUA , AUT	MM5-CAMx	MM5	CAMx	None	Regional	Offline	http://lap.phys.auth.gr/gems.asp
Greece/Univer sity of Athens	SKIRON/TAPM	SKIRON/dust; Eta	CAMx v4.31	None	Regional	Offline	Kallos et al., 2007, 2009; Mitsakou et al., 2008; Spyrou et al., 2010; https://forecast.uoa.gr/en/
Italy/CETEMPS	ForeChem	MM5	CHIMERE	None	Regional	Offline	Curci et al., 2010; pumpkin.aquila.infn.it/forechem/
Italy/ARIANE T s.r.l.	FARM	RAMS	FARM	None	Regional	Offline	http://www.aria-net.it/
Italy/CNR- ISAC	BOLCHEM	BOLAM	CHEMistry modules	None	Continental/ regional	Online- Access	http://bolchem.isac.cnr.it
Italy/ITCP	RegCM-Chem	RegCM4	RegCM- Chem4	None	Continental/ regional	Online- Integrated	http://gforge.ictp.it/gf/project/regcm

Country/ Organization	Model System	Meteorological Model (MetM)	Air Quality Model (AQM)	Microscale Models	Scale	MetM - AQM coupling	References
Japan/Kyushu University	CFORS	RAMS	Parameterize d chemical tracers in RAMS	None	Regional	Online- Integrated	Uno et al., 2003; Carmichael et al., 2003; Hadley et al., 2007
Morocco/Maroc Météo	ADMS URBAN 3.1	ALADIN	GRS Chemical Model	Urban canopy	Regional/loca l	Offline	Carruthers et al., 1997; McHugh et al., 1997
Netherlands/ KNMI, TNO, RIVM, PBL/KN	LOTOS-EUROS	Archived analyses, ECMWF, RACMO2	LOTOS- EUROS	None	Regional	Online- Integrated/ Access	Schaap et al., 2008; Manders et al., 2009; http://www.lotos- euros.nl/
Norway/MET- NO	EMEP-Unified	ECMWF/IFS	Unified EMEP-CWF	None	Regional	Offline	Valdebenito and Benedictow, 2010; www.emep.int
Singapore/MS S	ATLAS-NAME	UM	NAME	None	Regional	Offline	Jones et al., 2007; Redington et al., 2009
Spain/BSC- CNS	CALIOPE	WRF, MM5	CMAQ, DREAM, CHIMERE,	None	Regional	Offline	Baldasano et al., 2008; www.bsc.es/caliope
Spain/TUM, LHTEE, AUT, NCAR/Pen	OPANA v4.0	MM5 MEMO	CMAQ	MICROSYS	Regional/ local	Offline	San José, et al., 2006, 2009; artico.lma.fi.upm.es
Sweden/SMHI	MATCH	ECMWF/IFS HIRLAM	MATCH	None	Regional	Offline	Robertson et al. (1999), Langner et al. (2005), Robertson, 2010; www.smhi.se/en/Research/Researc h-departments/Air-quality/ ; www.smhi.se/sgn0106/if/meteorolo gi/match.htm ;
UK/Uni. Of Hertfordshire	WRF-CMAQ	WRF(ARW)	CMAQ v5.02	None	Regional/ national	Offline	Chemel et al., 2010
UK/AEA	WRF/CMAQ	WRF	CMAQ	None	Regional	Offline	Allen and Fraser, 2009; Fraser et al., 2010 https://uk-air.defra.gov.uk/

Country/ Organization	Model System	Meteorological Model (MetM)	Air Quality Model (AQM)	Microscale Models	Scale	MetM - AQM coupling	References
UK Met Office	AQUM	MetUM	UKCA	None	Sub-regional/ national	Online- Integrated	Savage et al., 2013
UK/Met Office	NAME-III	ECMWF, Met Office Unified Model	NAME-III	None	Regional/ local	Offline	Jones et al., 2004; http://www.metoffice.gov.uk/research/
US/BAMS	MAQSIP-RT CMAQ	BAMS-MM5, WRF	MAQSIP CMAQ	None	Regional	Offline	McHenry et al., 2004; McKeen et al., 2009,
US/WSU	AIRPACT3	MM5	CALGRID, CMAQ	None	Regional	Offline	Vaughan et al., 2004; Chen et al., 2008;
US/SUNY- Albany	AQFMS	SKIRON/Eta; WRF (NMM and ARW)	CAMx, CMAQ	None	Regional	Offline	Hogrefe et al., 2007, Cai et al., 2008; Doraiswamy et al https://www.albany.edu/asrc/
US/University of Iowa	STEM-2K3	MM5, WRF	STEM	None	Regional	Offline	Carmichael et al., 2003; nas.cgrer.uiowa.edu/
US/NOAA, ARL	NAQFC (NAM- CMAQ)	Eta, WRF (NMM), NAM	CMAQ	None	Regional/ national	Offline	Otte et al., 2005; Ryan et al., 2005; Yu et al., 2007, 2008; Lee et al., 2008; Eder et al., 2010; www.weather.gov/aq/ ; airnow.gov/
US/NCAR, Greece	MM5-CHIMERE	MM5	CHIMERE	None	Regional	Offline	https://www.mmm.ucar.edu/
US, Greece	RAMS/ICLAMS	RAMS	ICLAMS	None	Continental/ urban	Online- Access	http://www.mg.uoa.gr/ICLAMS/index.php
US/NOAA, EMSL	WRF/Chem	WRF (ARW)	WRF/Chem	None	Regional/ urban	Online- Integrated	McKeen et al., 2005, 2007; 2009 https://rapidrefresh.noaa.gov/RAPchem/Welcome.cgi
US/NEU	WRF/Chem- MADRID	WRF (ARW)	WRF/Chem	None	Regional/ urban	Online- Integrated	Zhang et al., 2010a; Chuang et al., 2011, Yahya et al., 2014; Zhang et al., 2016, https://coe.northeastern.edu/Research/CASCADE/Real_Time.html

Nine out of 17 global models are multiscale models and have been applied to regional domains for RT CW-AQF. They use two methods for downscaling. While some models (e.g., GEM-AQ, GEM-MATH, MOCAGE, NMMB/BSC-CTM, and SILAM) were directly downscaled to a regional domain at a finer horizontal grid resolution (Neary et al., 2007; Rouil et al., 2009), the global-regional RT CW-AQF model system (GR-RT CW-AQF) was used to provide ICONs and BCONs to drive a regional online-integrated model, WRF/Chem (Takigawa et al., 2007). Among the 17 global RT CW-AQF models, two of them offer an integrated flexible, advanced global forecasting modeling tool with data assimilation of satellite observations: ECMWF/IFS-CTMs developed by ECMWF and GEOS-5 ESM developed by U.S. NASA. In ECMWF/IFS-CTMs, the IFS is coupled via a coupler software to one of the global CTMs: MOCAGE, MOZART-3, and TM5 for global forecasting and assimilation of reactive chemical species. The selection of multiple CTMs and their ensemble results provides a range and an indication of the robustness of the forecasts. In the latest version of IFS developed by ECMWF, C-IFS supersedes MOZART-3, and the system is named as ECMWF/CAMS. The coupled system can directly utilize the IFS 4D-Var algorithm to assimilate atmospheric observations (Flemming et al., 2009). In GEOS-5 ESM, a variety of aerosol and chemistry components are available (Nielsen et al., 2017). For example, two chemical model configurations have been implemented: the chemistry-climate model (CCM) that simulates the feedback between circulation and chemical composition and the chemistry-transport model (CTM) that simulates air quality without considering such feedback. GEOS-5 generates near real-time analysed data products, reanalyses, and short-term and seasonal forecasts. Global forecasts of aerosol concentrations that incorporate satellite observations are available in near real-time (<https://fluid.nccs.nasa.gov/weather/>). The most recent ICAP multi-model ensemble (ICAP MME) consists of seven global models including four comprehensive global aerosol models (NASA GEOS-5, FNMOC/NRL NAAPS, ECMWF MACC, JMA MASINGAR), and three dust-only global models (NOAA NGAC, BSC NMMB/BSC-CTM, UKMO Unified Model) (Sessions et al., 2015). The ICAP-MME is run daily at 0Z for 6 hourly forecasts at one degree resolution out to 120 hours.

For regional models, many of them use the most popular meteorological models such as MM5, WRF, and ECMWF/IFS. Other NWP models include Eta, SKIRON, UM, RAMS, GEM, GME, ALADIN, RegCM, HIRLAM, HARMONIE, COSMO, and BRAMS. The major NWP models used for AQF have been reviewed in Kukkonen et al. (2012). Many AQMs (e.g., CHIMERE and Polyphemus/Polair3D) can be driven by several meteorological models. The most commonly-used regional AQMs include CMAQ, CAMx, WRF/Chem, and CHIMERE. Other AQMs include C-CTM, STEM, AURAMS, CHRONOS, Polair3D, DEOM, MATCH, LOTOS-EUROS, DREAM, NAQPMS, and NAME. Many AQMs have been reviewed in Kukkonen et al. (2012), Zhang et al. (2012a), and Baklanov et al. (2014). All regional CW-AQF models that use CMAQ, CAMx, and CHIMERE as the CTM are offline-coupled models with one exception, i.e., the two-way coupled WRF-CMAQ, originally developed by the U.S. NOAA/EPA, which has been applied for RT CW-AQF over eastern China by Zhejiang University, China (Li et al., 2017). CMAQ has been used in CW-AQF models in China, Spain, the U.K. and the U.S. CAMx has been used in CW-AQF models in Austria, China, Greece, Spain and the U.S. CHIMERE has been used in CW-AQF models in France, Greece, Italy, Spain, and the U.S. Among offline CW-AQF models, AAQFS is one of the earliest offline CW-AQF models developed by the Bureau of Meteorology, CSIRO, and the Australian EPA in the late 1990s to provide hourly air quality forecasting in Melbourne, Sydney and Adelaide, Australia (Manins, 2002; Cope et al., 2004). AQFx is a three-tiered numerical smoke forecasting system recently developed by CSIRO, Australia (Lawson et al. 2017). The first tier is an ensemble forecast of fire weather and fire danger indices extending over a 5–10 day outlook. The second tier is a traditional AQF system for a multi-species air quality forecast for the Australian region for a 24–72 hour outlook, and the third tier provides a tagged tracer forecast for any likely hazard reduction burning within 24 hour outlook. The National Air Quality Forecasting Capability (NAQFC) developed by U.S. NOAA and EPA is one of the first offline CW-AQF models implemented in the U.S. and has evolved numerous updates in its meteorological and air quality models. It uses the meteorological fields from Eta and WRF (NMM) in the earlier versions and from the North American Mesoscale Forecasting System (NAM) in the latest version. Its air quality model is based on CMAQ which has been updated in many aspects of chemical and physical process representations of the atmosphere. Similar to the global ECMWF-IFS-CTMs, the French national air quality forecasting and monitoring system, Prev'air, consists of three CTM models: CHIMERE, MOCAGE, and polyphemus/Polair3D

(<http://www2.prevoir.org/> ; Rouil et al., 2009), which allows ensemble RT CW-AQFs. Since spring 2003, Prev'air has been in operational forecasting. Several RT CW-AQF systems are being used by regional air quality agencies (e.g., the Associations agréées de surveillance de la qualité de l'air, AASQAs) in France (e.g., AIRPARIF for the Paris region); those regional RT CW-AQF systems typically use CHIMERE.

Among the online-coupled regional CW-AQF models, WRF/Chem (Grell et al., 2005) and WRF/Chem-MADRID (Zhang et al., 2010a) include the most coupled meteorological, microphysical, chemical, and radiative processes and allow the simulation of aerosol direct, semi-direct, and indirect effects, thus representing the state-of-the-science online-coupled regional CW-AQF models. Since its first release in 2002, WRF/Chem has been further developed and improved by many researchers in the community (e.g., Fast et al., 2006; Zhang et al., 2010a; Shrivastava et al., 2010) and increasingly applied to many regions of the world (e.g., Tie et al., 2009; Fast et al., 2009; Misenis and Zhang, 2010; Zhang et al., 2010a, b, 2011b; Li et al., 2011). Compared to WRF/Chem, WRF/Chem-MADRID includes two additional gas-phase mechanisms (i.e., the 2005 version of carbon bond gas-phase mechanism (CB05) and the 1999 Statewide Air Pollution Research Center gas-phase mechanism (SAPRC-99)), one aerosol module (i.e., the model of aerosol dynamics, reaction, ionization, and dissolution (MADRID)), one aerosol activation scheme (i.e., Fountoukis and Nenes, 2005), and several nucleation algorithms (e.g., Sihto et al., 2006; Merikanto et al., 2007; Yu, 2010). CB05 and SAPRC-99 are coupled with MADRID and two existing aerosol modules (i.e., the Modal Aerosol Dynamics Model for Europe/the Secondary Organic Aerosol Model (MADE/SORGAM) and Model for Simulating Aerosol Interactions and Chemistry (MOSAIC)) as well as the CMU aqueous-phase chemistry in WRF/Chem-MADRID (Zhang et al., 2010a, c, 2012). WRF/Chem-MADRID has been applied retrospectively over the continental U.S. and its sub-regions (e.g., Zhang et al., 2010a, 2012, 2016), and Europe (Zhang et al., 2011a) and also for RT CW-AQF at a horizontal resolution of 12 km over the southeastern U.S. since summer 2009 (Chuang et al., 2011). WRF/Chem and its variants have been used for CW-AQF in many regions of the world including North America (McKeen et al., 2005, 2007, 2009; Chuang et al., 2011; Yahya et al., 2014; Zhang et al., 2016) and South America (Saide et al., 2011; Vara-Vela et al., 2016). CCATT-BRAMS is a new online model developed by the Brazilian Center for Weather Forecasts and Climate Studies (CPTEC) from the National Institute of Spatial Research (INPE) for RT CW-AQF in South America (Freitas et al., 2009, 2011, 2017; Longo et al., 2013). The meteorological model is the Brazilian developments on the Regional Modeling System (BRAMS), which treats sub-grid vertical transport associated with wet, deep and shallow convection, by applying a 1-D cloud resolving model in each column. CCATT-BRAMS contains an emission module that takes into account anthropogenic and natural emissions due to human activities and biomass burning, including gases and particles. Special attention is given to carbon monoxide (CO) and fine particulate matters (PM_{2.5}), over tropical forests, grassland and "cerrado" (a kind of Brazilian savanna). Emission sources are distributed over the interest domain along the time according to information retrieved from a set of satellites (GOES, EOS-TERRA, EOS-AQUA), which identify biomass burning locations. Anthropogenic sources of CO are based on EDGAR/RETRO/CETESB databases. The online regional integrated coupled RegCM-CHEM is being used for CW-AQF in Italy, Egypt, and South Africa (Zakey et al., 2006, 2008, Shalaby et al., 2012, and Salah et al., 2018). Its climate model, the RegCM4.5, developed at the Abdus Salam International Center for Theoretical Physics (ICTP) (Giorgi et al., 2012) includes both Mesoscale Model (MM5) hydrostatic and non-hydrostatic dynamical cores, with a sigma vertical coordinate system. By solving the tracer mass continuity equation within the RegCM dynamical core, RegCM-CHEM can simulate emissions, transport, chemical transformation, and removals of gaseous and aerosol species (Solmon et al., 2006; Zakey et al., 2006, 2008; Shalaby et al., 2012).

There have been two major regional ensemble air quality forecasts ongoing in Europe and China. The regional air quality production of the Copernicus Atmosphere Monitoring Service (CAMS) is based on ensemble of seven state-of-the-art numerical air quality models developed in Europe: CHIMERE from INERIS (France), EMEP from MET Norway (Norway), EURAD-IM from University of Cologne (Germany), LOTOS-EUROS from KNMI and TNO (Netherlands), MATCH from SMHI (Sweden), MOCAGE from METEO-FRANCE (France) and SILAM from FMI (Finland). While MOCAGE and SILAM are global models downscaled for regional CW-AQF, the rest are

regional models. All models are offline models. They use the same meteorological data from the ECMWF global weather operating system, the same chemical boundary conditions from the CAMS IFS-MOZART global production), and the same emissions from CAMS emission. These regional air quality models provide 4-day, daily forecasts of the concentrations of main atmospheric pollutants at surface at a horizontal grid space of 10 to 20 km over Europe. The forecasted species include nitrogen dioxide (NO₂), sulfur dioxide (SO₂), ozone (O₃), CO, and particulate matter (PM₁₀ and PM_{2.5}). Under the MarcoPolo – Panda, EU FP7 Programme (<http://www.marcopolo-panda.eu/>), RT CW-AQF is being performed by nine different models and an ensemble. These models include CHIMERE by CNRS, France, C-IFS by ECMWF, UK, WRF-Chem and WARMS-CMAQ by SMS, China, WRF-Chem by MPI, Germany, SILAM by FMI, Finland, EMEP by met.no, Norway, LOTOS-EUROS by TNO, The Netherlands, and WRF-CMAQ by Nanjing University, China.

Among 56 regional models, eight are suitable for urban/local scale applications at a spatial resolution of 1 km or less. These models include THOR, DACFOS, M-SYS, ADMS URBAN 3.1, the operational version of the Atmospheric Numerical pollution model for urban and regional Areas (OPANA), and four Urban Air Quality Information and Forecasting Systems (UAQIFS) models (i.e., UAQIFS – Norway, UAQIFS-Finland, UAQIFS-Italy2, and UAQIFS-Denmark), and the Polyphemus air quality modeling platform. THOR includes the background urban model (BUM), the Operational Street Pollution Model (OSPM), and the Danish Rimpuff and Eulerian Accidental release Model (DREAM). Enviro-HIRLAM is a fully online integrated meteorology-chemistry model for CW and pollen forecasting on regional and urban scales. It includes several urban sublayer parameterization modules (Baklanov et al., 2008; Mahura et al., 2008) to simulate urbanization effects and a possibility to downscale with the Microscale Model for Urban Environment (M2UE) to consider street scale effects (Baklanov and Nuterman, 2009; Nuterman et al., 2011). M-SYS includes MITRAS- MICTM to simulate flow and transport regimes as well as chemistry within the urban boundary layer. ADMS URBAN 3.1 includes an urban canopy model. OPANA includes the microscale air quality modeling system (MICROSYS) to forecast air concentrations for urban areas with street level details at a 5–10 m spatial resolution and up to 200–300 m in height over the maximum building heights in one 1-km grid cell that is nested in a regional simulation domain (San José et al., 2006, 2009). The UAQIFS models were developed as part of the Integrated Systems for Forecasting Urban Meteorology, Air Pollution, and Population Exposure - UAQIFS (FUMAPEX-UAQIFS) project sponsored by the EU (Baklanov, 2006). They include six separate UAQIFS that are further developed and applied in six cities in Europe (Baklanov et al., 2006). While these UAQIFS use advanced meteorological models such as HIRLAM and RAMS, the level of sophistication in AQMs varies from the simplest dispersion model with no or very simple chemistry, to the most complex 3-D AQMs such as FARM and CAMx. Their common feature lies in that they integrate the latest developments in urban meteorology, air quality, and population exposure modeling via an offline coupling approach to enhance the model's forecasting capability in urban areas. The enhanced modeling capabilities include one or more areas in urban RT CW-AQF, urban management and planning, public health assessment and exposure prediction, and urban emergency preparedness. The Polyphemus has recently been extended to include a street network model, the Model of Urban Network of Intersecting Canyons and Highways (MUNICH), which is online-coupled with a 3-D Eulerian chemical-transport model (Polair3D) within Polyphemus. The resulting model system is referred to as a Street-in-Grid (SinG) model (Kim et al., 2018). MUNICH is based conceptually on the SIRANE general formulation (Soulhac et al., 2011). MUNICH consists of two main components: the street-canyon component, which represents the atmospheric processes in the volume of the urban canopy, and the street-intersection component, which represents the processes in the volume of the intersection. These components are connected to the Polair3D model at roof level and are also interconnected. The combined model system, SinG, aims at improving urban street-level pollutant concentrations by modeling both background and street-level concentrations at the same time. One example of an application of SinG is given in [Chapter 9](#).

3.2.3 Summary

- CW-AQF models can be grouped into three types (Eulerian, Lagrangian, and hybrid models) based on model framework, four types (local, urban, mesoscale, and global) based on horizontal grid resolution, two types (short- and long-term) based on temporal scale, two types (online- and offline-coupled) based on the chemistry coupling with the meteorology, and two types (community- and non-community) based on community involvement.
- Current CW-AQF models differ in many aspects including their component models (i.e., meteorological models, air quality models, microscale models), spatial scale, and coupling between meteorology and chemistry.
- Among 17 global and 56 regional/urban real-time CW-AQF models reviewed in this section, 9 global models and 23 regional models are suitable for multiscale applications and 8 regional models can be applied on urban/local scale at a spatial resolution of 1 km or less. 11 global models and 21 regional models are online-coupled models.
- Regional ensemble air quality forecasting has been increasingly applied. Examples include the Copernicus Atmosphere Monitoring Service (CAMS) for Europe and the MarcoPolo – Panda, EU FP7 Programme for China.

References

- Andrade, M. F., R. Y. Ynoue, E. D. Freitas, E. Todesco, A. Vara Vela, S. Ibarra, L. D. Martins, J. A. Martins, and V. S. B. Carvalho (2015), Air quality forecasting system for southeastern Brazil, *Frontiers in Environmental Science*, 3, 14, [doi: 10.3389/fenvs.2015.00009](https://doi.org/10.3389/fenvs.2015.00009)
- Baklanov, A.: 2006: Overview of the European project FUMAPEX. *Atmos. Chem. Phys.*, 6, 2005-2015.
- Baklanov, A. and R. Nuterman, 2009: Multi-scale atmospheric environment modeling for urban areas. *Advances in Science and Research*, 3, 53-57.
- Baklanov A., O. Hänninen, L. H. Størdal, J. Kukkonen, J. H. Sørensen, N. Bjergene, B. Fay, S. Finardi, S. C. Hoe, M. Jantunen, A. Karppinen, A. Rasmussen, A. Skouloudis, R. S. Sokhi, V. Ødegaard, 2006: Integrated systems for forecasting urban meteorology, air pollution and population exposure, *Atmos. Chem. Phys.*, 7, 855–874.
- Baklanov A., P. Mestayer, A. Clappier, S. Zilitinkevich, S. Joffre, A. Mahura, N.W. Nielsen, 2008: Towards improving the simulation of meteorological fields in urban areas through updated/advanced surface fluxes description. *Atmospheric Chemistry and Physics*, 8, 523-543.
- Baklanov, A., Schlünzen, K., Suppan, P., Baldasano, J., Brunner, D., Aksoyoglu, S., Carmichael, G., Douros, J., Flemming, J., Forkel, R., Galmarini, S., Gauss, M., Grell, G., Hirtl, M., Joffre, S., Jorba, O., Kaas, E., Kaasik, M., Kallos, G., Kong, X., Korsholm, U., Kurganskiy, A., Kushta, J., Lohmann, U., Mahura, A., Manders-Groot, A., Maurizi, A., Moussiopoulos, N., Rao, S. T., Savage, N., Seigneur, C., Sokhi, R. S., Solazzo, E., Solomos, S., Sørensen, B., Tsegas, G., Vignati, E., Vogel, B., and Zhang, Y.: Online coupled regional meteorology chemistry models in Europe: current status and prospects, *Atmos. Chem. Phys.*, 14, 317-398, <https://doi.org/10.5194/acp-14-317-2014>, 2014.
- Baklanov, A., Korsholm, U. S., Nuterman, R., Mahura, A., Nielsen, K. P., Sass, B. H., Rasmussen, A., Zakey, A., Kaas, E., Kurganskiy, A., Sørensen, B., and González-Aparicio, I.: The Enviro-HIRLAM online integrated meteorology–chemistry modeling system: strategy, methodology, developments, and applications (v. 7.2), *Geosci. Model Dev.*, 10, 2971-2999, <https://doi.org/10.5194/gmd-10-2971-2017>, 2017.

- Chemel, C., Sokhi, R.S., Yu, Y., Hayman, G.D., Vincent, K.J., Dore, A.J., Tang, Y. S., Prain, H.D., and Fisher, B. E. A., 2010, Evaluation of a CMAQ simulation at high resolution over the UK for the calendar year 2003, *Atmos. Environ.*, 44, 2927-2939, doi: [10.1016/j.atmosenv.2010.03.029](https://doi.org/10.1016/j.atmosenv.2010.03.029).
- Chin, M., Ginoux, P., Kinne, S., Torres, O., Holben, B., Duncan, B.N., Martin, R.V., Logan, J., Higurashi, A., Nakajima, T., 2002. Tropospheric aerosol optical thickness from the GOCART model and comparisons with satellite and sun photometer measurements. *J. Atmos. Sci.* 59, 461–483
- Colarco, P. R., da Silva, A., Chin, M., & Diehl, T. (2010). Online simulations of global aerosol distributions in the NASA GEOS-4 model and comparisons to satellite and ground-based aerosol optical depth. *Journal of Geophysical Research*, 115, D14207.
- Chuang, M.-T., Y. Zhang, and D.-W. Kang, 2011, Application of WRF/Chem-MADRID for Real-Time Air Quality Forecasting over the Southeastern United States, *Atmospheric Environment*, 45 (34), 6241-6250, doi: [10.1016/j.atmosenv.2011.06.071](https://doi.org/10.1016/j.atmosenv.2011.06.071). Cotton, W. R., et al. (2003), RAMS 2001: Current status and future directions, *Meteorology and Atmospheric Physics*, 82(1-4), 5-29, doi: [10.1007/s00703-001-0584-9](https://doi.org/10.1007/s00703-001-0584-9).
- Grell, G. S. Emeis, W.R. Stockwell, T. Schoenemeyer, R. Forkel, J. Michalakes, R. Knoche, W. Seidl (2000) Application of a Multiscale, Coupled MM5/Chemistry Model to the Complex Terrain of the VOTALP Valley Campaign. *Atmospheric Environment*, 34, 1435-1453
- Grell, G. A., and D. Devenyi (2002), A generalized approach to parameterizing convection combining ensemble and data assimilation techniques, *Geophysical Research Letters*, 29(14), 38-31–38-34, doi: [10.1029/2002GL015311](https://doi.org/10.1029/2002GL015311).
- Grell, G. and A. Baklanov, 2011: Integrated Modeling for Forecasting Weather and Air Quality: A Call for Fully Coupled Approaches. *Atmospheric Environment*, doi: [10.1016/j.atmosenv.2011.01.017](https://doi.org/10.1016/j.atmosenv.2011.01.017).
- Fast, J. D., W. I. Gustafson Jr., R. C. Easter, R. A. Zaveri, J. C. Barnard, E. G. Chapman, G. A. Grell, and S. E. Peckham (2006), Evolution of ozone, particulates, and aerosol direct radiative forcing in the vicinity of Houston using a fully coupled meteorology-chemistry-aerosol model, *J. Geophys. Res.*, 111, D21305, doi: [10.1029/2005JD006721](https://doi.org/10.1029/2005JD006721).
- Fast, J., et al. (2009), Evaluating simulated primary anthropogenic and biomass burning organic aerosols during MILAGRO: implications for assessing treatments of secondary organic aerosols, *Atmos. Chem. Phys.*, 9, 6191–6215, doi: [10.5194/acp-9-6191-2009](https://doi.org/10.5194/acp-9-6191-2009), 2009.
- Freitas, S. R., Longo, K. M., Silva Dias, M. A. F., Chatfield, R., Silva Dias, P., Artaxo, P., Andreae, M. O., Grell, G., Rodrigues, L. F., Fazenda, A., and Panetta, J.: The Coupled Aerosol and Tracer Transport model to the Brazilian developments on the Regional Atmospheric Modeling System (CATT-BRAMS) – Part 1: Model description and evaluation, *Atmos. Chem. Phys.*, 9, 2843-2861, doi: [10.5194/acp-9-6191-2009](https://doi.org/10.5194/acp-9-6191-2009), 2009.
- Freitas, S. R., et al. (2017), The Brazilian developments on the Regional Atmospheric Modeling System (BRAMS 5.2): an integrated environmental model tuned for tropical areas, *Geosci. Model Dev.*, 10(1), 189-222, doi: [10.5194/gmd-10-189-2017](https://doi.org/10.5194/gmd-10-189-2017).
- Johnson, B. T., Brooks, M. E., Walters, D., Christopher, S., and Schepanski, K.: Assessment of the Met Office dust forecast model using observations from the GERBILS campaign, *Q. J. Roy. Meteor. Soc.*, 137, 1131–1148, doi: [10.1002/qj.736](https://doi.org/10.1002/qj.736), 2011.
- Jorba, O., D. Dabdub, D., Blaszcak-Boxe, C., Pérez, C., Janjic, Z., Baldasano, J. M., Spada, M., Badia, A., and Gonçalves M.: Potential Significance of Photoexcited NO₂ on Global Air Quality with the NMMB/BSC Chemical Transport Model, *J. Geophys. Res.*, 117, D13301, doi: [10.1029/2012JD017730](https://doi.org/10.1029/2012JD017730), 2012.

- Kim, Y., Wu, Y., Seigneur, C., and Roustan, Y.: Multi-scale modeling of urban air pollution: development and application of a Street-in-Grid model (v1.0) by coupling MUNICH (v1.0) and Polair3D (v1.8.1), *Geosci. Model Dev.*, 11, 611-629, <https://doi.org/10.5194/gmd-11-611-2018>, 2018.
- Kukkonen, J., Olsson, T., Schultz, D. M., Baklanov, A., Klein, T., Miranda, A. I., Monteiro, A., Hirtl, M., Tarvainen, V., Boy, M., Peuch, V.-H., Poupkou, A., Kioutsioukis, I., Finardi, S., Sofiev, M., Sokhi, R., Lehtinen, K. E. J., Karatzas, K., San José, R., Astitha, M., Kallos, G., Schaap, M., Reimer, E., Jakobs, H., and Eben, K.: A review of operational, regional-scale, chemical weather forecasting models in Europe, *Atmos. Chem. Phys.*, 12, 1–87, [doi: 10.5194/acp-12-1-2012](https://doi.org/10.5194/acp-12-1-2012), 2012.
- Kuo, H. L. (1974), Further Studies of the Parameterization of the Influence of Cumulus Convection on Large-Scale Flow, *Journal of the Atmospheric Sciences*, 31(5), 1232-1240, [doi: 10.1175/1520-0469\(1974\)031<1232:FSOTPO>2.0.CO;2](https://doi.org/10.1175/1520-0469(1974)031<1232:FSOTPO>2.0.CO;2).
- Li, P.-F., L.-Q. Wang, P. Guo, S.-C. Yu, K. Mehmood, S. Wang, W.-P. Liu, J. H. Seinfeld, Y. Zhang, D. Wong, K. Alapaty, J. Pleim, and R. Mathur, 2017, High reduction of ozone and air particulate matter during the 2016 G-20 summit in Hangzhou by forced emission controls of industry and traffic, *Environmental Chemistry Letters*, [doi: 10.1007/s10311-017-0642-2](https://doi.org/10.1007/s10311-017-0642-2).
- Long, M. S., Yantosca, R., Nielsen, J. E., Keller, C. A., da Silva, A., Sulprizio, M. P., Pawson, S., and Jacob, D. J.: Development of a grid-independent GEOS-Chem chemical transport model (v9-02) as an atmospheric chemistry module for Earth system models, *Geosci. Model Dev.*, 8, 595-602, <https://doi.org/10.5194/gmd-8-595-2015>, 2015.
- Lu, S., Huang, H.-C., Hou, Y.-T., Tang, Y., McQueen, J., da Silva, A., Chin, M., Joseph, E., and Stockwell, W.: Development of NCEP Global Aerosol Forecasting System: an Overview and its Application for Improving Weather and Air Quality Forecasts, *NATO Science for Peace and Security Series: Air Pollution Modeling and Its Application XX*, [doi: 10.1007/978-90-481-3812-8](https://doi.org/10.1007/978-90-481-3812-8), 2010.
- Lu, S., da Silva, A., Chin, M., Wang, J., Moorthi, S., Juang, H., Chuang, H.-Y., Tang, Y., Jones, L., Iredell, M., and McQueen, J.: The NEMS GFS Aerosol Component: NCEP's global aerosol forecast system, NCEP Office Note 472, Washington DC, 2013.
- Mahura, A., Petersen, C., Baklanov, A., Amstrup, B., Korsholm, U. S., and Sattler, K., 2008: Verification of long-term DMI-HIRLAM NWP model runs using urbanization and building effect parameterization modules, *HIRLAM Newsl.*, 53, 50–60.
- Mallet, V., D. Quélo, B. Sportisse, M. Ahmed de Biasi, É. Debry, I. Korsakissok, L. Wu, Y. Roustan, K. Sartelet, M. Tombette and H. Foudhil: Technical Note: The air quality modeling system Polyphemus, *Atmos. Chem. Phys.*, 7 (20), 2007.
- Marécal, V., Peuch, V.-H., Andersson, C., Andersson, S., Arteta, J., Beekmann, M., Benedictow, A., Bergström, R., Bessagnet, B., Cansado, A., Chéroux, F., Colette, A., Coman, A., Curier, R.L., Denier van der Gon, H. A. G., Drouin, A., Elbern, H., Emili, E., Engelen, R. J., Eskes, H. J., Foret, G., Friese, E., Gauss, M., Giannaros, C., Joly, M., Jaumouillé, E., Josse, B., Kadygrov, N., Kaiser, J.W., Krajsek, K., Kuenen, J., Kumar, U., Liora, N., López, E., Malherbe, L., Martinez, I., Melas, D., Meleux, F., Menut, L., Moinat, P., Morales, T., Parmentier, J., Piacentini, A., Plu, M., Poupkou, A., Queguiner, S., Robertson, L., Rouil, L., Schaap, M., Segers, A., Sofiev, M., Thomas, M., Timmermans, R., Valdebenito, A., van Velthoven, P., van Versendaal, R., Vira, J., Ung, A. (2015) A regional air quality forecasting system over Europe: the MACC-II daily ensemble production. *Geosci. Model Dev.*, 8, 2777-2813, 2015 www.geosci-model-dev.net/8/2777/2015/ [doi: 10.5194/gmd-8-2777-2015](https://doi.org/10.5194/gmd-8-2777-2015).
- McKeen, S., J. Wilczak, G. Grell, I. Djalova, S. Peckham, E.-Y. Hsie, W. Gong, V. Bouchet, S. Ménard, R. Moffet, J. McHenry, J. McQueen, Y. Tang, G. R. Carmichael, M. Pagowski, A. Chan, t. Dye, G. Frost, P. Lee, and R. Mathur (2005), Assessment of an ensemble of seven real-time ozone forecasts over eastern North America during the summer of 2004, *J. Geophys. Res.*, 110, D21307, [doi: 10.1029/2005JD005858](https://doi.org/10.1029/2005JD005858).

- McKeen, S., S. H. Chung, J. Wilczak, G. Grell, I. Djalalova, S. Peckham, W. Gong, V. Bouchet, R. Moffet, Y. Tang, G. R. Carmichael, R. Mathur, and S. Yu (2007), Evaluation of several PM_{2.5} forecast models using data collected during the ICARTT/NEAQS 2004 field study, *J. Geophys. Res.*, *112*, D10S20, doi: [10.1029/2006JD007608](https://doi.org/10.1029/2006JD007608).
- McKeen, S. et al. (2009), An evaluation of real-time air quality forecasts and their urban emissions over eastern Texas during the summer of 2006 Second Texas Air Quality Study field study, *J. Geophys. Res.*, *114*, D00F11, doi: [10.1029/2008JD011697](https://doi.org/10.1029/2008JD011697).
- Mellor, G.L. and Yamada, T., (1974), A hierarchy of turbulence closure models for planetary boundary layers. *J. Atmos. Sci.*, *31*, 1791-1806.
- Meyers, M. P., R. L. Walko, J. Y. Harrington, and W. R. Cotton (1997), New RAMS cloud microphysics parameterization. Part II: The two-moment scheme, *Atmospheric Research*, *45*(1), 3-39, doi: [http://dx.doi.org/10.1016/S0169-8095\(97\)00018-5](http://dx.doi.org/10.1016/S0169-8095(97)00018-5).
- Moussiopoulos, N., I. Douros, G. Tsegas, S. Kleanthous, and E. Chourdakis, 2012, An Air Quality Management System for Policy Support in Cyprus, *Advances in Meteorology*, Volume 2012, Article ID 959280, 8 pages, <http://dx.doi.org/10.1155/2012/959280>.
- Neariy, L., J. W. Kaminski, A. Lupu, and J. C. McConnell (2007), Developments and Results from a Global Multiscale Air Quality Model (GEM-AQ), *Air Pollution Modeling and Its Application XVII*, *5*, 403-410, doi: [10.1007/978-0-387-68854-1_44](https://doi.org/10.1007/978-0-387-68854-1_44).
- Nielsen, J. E., S. Pawson, A. Molod, B. Auer, A. M. da Silva, A. R. Douglass, B. N. Duncan, Q. Liang, M. E. Manyin, L. D. Oman, W. M. Putman, S. E. Strahan, and K. Wargan, 2017. Chemical Mechanisms and their Applications in the Goddard Earth Observing System (GEOS) Earth System Model. *J. Adv. Model. Earth Sys.*, . doi: [10.1002/2017MS001011](https://doi.org/10.1002/2017MS001011).
- Nuterman R., A. Starchenko, A. Baklanov, 2011. Numerical Model of Urban Aerodynamics and Pollution Dispersion. *International Journal of Environment and Pollution*, 2011, *44* (1-4): 385 – 393.
- Pérez, C., Haustein, K., Janjic, Z., Jorba, O., Huneus, N., Baldasano, J. M., Black, T., Basart, S., Nickovic, S., Miller, R. L., Perlwitz, J. P., Schulz, M., and Thomson, M.: Atmospheric dust modeling from meso to global scales with the online NMMB/BSC-Dust model – Part 1: Model description, annual simulations and evaluation, *Atmos. Chem. Phys.*, *11*, 13001–13027, doi: [10.5194/acp-11-13001-2011](https://doi.org/10.5194/acp-11-13001-2011), 2011.
- Pielke, R. A., et al. (1992), A Comprehensive Meteorological Modeling System - RAMS, *Meteorology and Atmospheric Physics*, *49*(1-4), 69-91, doi: [10.1007/BF01025401](https://doi.org/10.1007/BF01025401).
- M.M. Rienecker, M.J. Suarez, R. Todling, J. Bacmeister, L. Takacs, H.-C. Liu, W. Gu, M. Sienkiewicz, R.D. Koster, R. Gelaro, I. Stajner, and J.E. Nielsen (2008), The GEOS-5 Data Assimilation System— Documentation of Versions 5.0.1, 5.1.0, and 5.2.0, Technical Report Series on Global Modeling and Data Assimilation, Volume 27 (edited by Max J. Suarez), NASA/TM–2008–104606.
- Rienecker, M. M., M. J. Suarez, and co-authors, 2011: MERRA: NASA's Modern-Era Retrospective Analysis for Research and Applications. *J. Clim.*, *24*, 3624–3648, doi: [10.1175/JCLI-D-11-00015.1](https://doi.org/10.1175/JCLI-D-11-00015.1)
- Rouil, L., C. Honoré, R. Vautard, M. Beekmann, B. Bssagnet, L. Malherbe, F. Meleux, A. Dufour, C. Elichegaray, J.-M. Flaud, L. Menut, D. Martin, A. Peuch, V.-H. Peuch, and N. Poisson (2009), Prev'air: An operational forecasting and mapping system for air quality in Europe, *Bull. Amer. Meteor. Soc.*, *90*, 73-83, doi: [10.1175/2008BAMS2390.1](https://doi.org/10.1175/2008BAMS2390.1).
- Saide, P.E., Gregory R. Carmichael, Scott N. Spak, Laura Gallardo, Axel E. Osses, Marcelo A. Mena-Carrasco, Mariusz Pagowski (2011), Forecasting urban PM10 and PM2.5 pollution episodes in very stable nocturnal conditions and complex terrain using WRF-Chem CO tracer model. *Atmospheric Environment* *45*, 2769-e2780
- Salah, Z., Ahmed Shalaby, Allison L. Steiner, Ashraf S. Zakey, Ritesh Gautam, and M. M.

- Abdel Wahab (2018), Study of Aerosol Direct and Indirect Effects and Auto-conversion Processes over the West African Monsoon Region Using a Regional Climate Model, *Advances in Atmospheric Sciences*, 35:182-194, doi:10.1007/s00376-017-7077-3.
- Savage, N. H., Agnew, P., Davis, L. S., Ordóñez, C., Thorpe, R., Johnson, C. E., O'Connor, F. M., and Dalvi, M.: Air quality modeling using the Met Office Unified Model (AQUM OS24-26): model description and initial evaluation, *Geosci. Model Dev.*, 6, 353–372, doi:10.5194/gmd-6-353-2013, 2013.
- Schatzmann, M., W. Bächlin, S. Emeis, J. Kühlwein, B. Leitl, W. J. Müller, K. Schäfer, and H. Schlünzen, 2006, Development and validation of tools for the implementation of European air quality policy in Germany (Project VALIUM), *Atmos. Chem. Phys.*, 6, 3077–3083, <https://doi.org/10.5194/acp-6-3077-2006>.
- Sessions, W. R., Reid, J. S., Benedetti, A., Colarco, P. R., da Silva, A., Lu, S., Sekiyama, T., Tanaka, T. Y., Baldasano, J. M., Basart, S., Brooks, M. E., Eck, T. F., Iredell, M., Hansen, J. A., Jorba, O. C., Juang, H.-M. H., Lynch, P., Morcrette, J.-J., Moorthi, S., Mulcahy, J., Pradhan, Y., Razinger, M., Sampson, C. B., Wang, J., and Westphal, D. L.: Corrigendum to "Development towards a global operational aerosol consensus: basic climatological characteristics of the International Cooperative for Aerosol Prediction Multi-Model Ensemble (ICAP-MME)" published in *Atmos. Chem. Phys.*, 15, 335–362, 2015, *Atmos. Chem. Phys.*, 15, 2533-2534, <https://doi.org/10.5194/acp-15-2533-2015>, 2015.
- Sessions, W. R., Reid, J. S., Benedetti, A., Colarco, P. R., da Silva, A., Lu, S., Sekiyama, T., Tanaka, T. Y., Baldasano, J. M., Basart, S., Brooks, M. E., Eck, T. F., Iredell, M., Hansen, J. A., Jorba, O. C., Juang, H.-M. H., Lynch, P., Morcrette, J.-J., Moorthi, S., Mulcahy, J., Pradhan, Y., Razinger, M., Sampson, C. B., Wang, J., and Westphal, D. L.: Corrigendum to "Development towards a global operational aerosol consensus: basic climatological characteristics of the International Cooperative for Aerosol Prediction Multi-Model Ensemble (ICAP-MME)" published in *Atmos. Chem. Phys.*, 15, 335–362, 2015, *Atmos. Chem. Phys.*, 15, 2533-2534, <https://doi.org/10.5194/acp-15-2533-2015>, 2015.
- Shalaby A., A.S. Zakey, A.B. Tawfik, F. Solmon, F. Giorgi, F. Stordal, S. Sillman, R. Zaveri, and A.L. Steiner (2012) "Implementation and evaluation of online gas phase chemistry within a regional climate model (RegCMChem4)." *Geoscientific Model Development*, doi:10.5194/gmdd51492012.
- Smagorinsky, J. (1963), General circulation experiments with the primitive equations: 1. The basic experiment, *Monthly Weather Review*, 91, 99-164.
- Sofiev M, Siljamo P, Valkama I, Ilvonen M, Kukkonen J (2006) A dispersion system SILAM and its evaluation against ETEX data. *Atmos. Environ.*, 40, 674-685.
- Sofiev M., Galperin M., Genikhovich E. (2008) A Construction and Evaluation of Eulerian Dynamic Core for the Air Quality and Emergency Modeling System SILAM. In: Borrego C., Miranda A.I. (eds) *Air Pollution Modeling and Its Application XIX*. NATO Science for Peace and Security Series C: Environmental Security. Springer, Dordrecht.
- Solmon, F., F. Giorgi, and C. Liousse, 2006: Aerosol modeling for regional climate studies: Application to anthropogenic particles and evaluation over a European/African domain. *Tellus*, 58B, 51–72, <https://doi.org/10.1111/j.1600-0889.2005.00155.x>
- Spada, M., Jorba, O., Pérez García-Pando, C., Janjic, Z., and Baldasano, J. M.: Modeling and evaluation of the global sea-salt aerosol distribution: sensitivity to size-resolved and sea-surface temperature dependent emission schemes, *Atmos. Chem. Phys.*, 13, 11735–11755, doi:10.5194/acp-13-11735-2013, 2013.
- Sørensen, J. H., A. Baklanov and S. Hoe. 2007: The Danish Emergency Response Model of the Atmosphere. *J. Envir. Radioactivity*, 96: 122-129.
- Tanaka, T. Y., Orito, K., Sekiyama, T. T., Shibata, K., Chiba, M., and Tanaka, H.: MASINGAR, a global tropospheric aerosol chemical transport model coupled with MRI/JMA98 GCM:

Model description, *Pap. Meteorol. Geophys.*, 53, 119–138, 2003.

- Tripoli, G.J., and W.R. Cotton, 1982: The Colorado State University three-dimensional cloud/mesoscale model -- 1982. Part I: General theoretical framework and sensitivity experiments. *J. de Rech. Atmos.*, 16, 185-220.
- Trukenmuller, A., Grawe, D., and Schlünzen, K. H.: A model system for the assessment of ambient air quality conforming to EC directives, *Meteorol. Z.*, 13, 387–394, 2004.
- Tulet, P, V. Crassier, F. Solmon, D. Guedalia, R. Rosset, 2003: Description of the Mesoscale Nonhydrostatic Chemistry model and application to a transboundary pollution episode between northern France and southern England, *J. Geophys. Res.*, 108(D1), 4021, doi: [10.1029/2000JD000301](https://doi.org/10.1029/2000JD000301);
- Vogel, B., Vogel, H., Bäumer, D., Bangert, M., Lundgren, K., Rinke, R., Stanelle, T. (2009), The comprehensive model system COSMO-ART - Radiative impact of aerosol on the state of the atmosphere on the regional scale, *Atmos. Chem. Phys.*, 9, 8661-8680.
- Vogel, B., Ferrone, A., Schad, T. (2013): Reducing the Uncertainties of Climate Projections: High-Resolution Climate Modeling of Aerosol and Climate Interactions on the Regional Scale Using COSMO-ART, *High Performance Computing in Science and Engineering '13* 2013, 553-555, doi: [10.1007/978-3-319-02165-2_38](https://doi.org/10.1007/978-3-319-02165-2_38).
- Wolke, R., O. Knoth, O. Hellmuth, W. Schröder and E. Renner, 2004, The parallel model system LM-MUSCAT for chemistry-transport simulations: Coupling scheme, parallelization and application, in: G.R. Joubert, W.E. Nagel, F.J. Peters, and W.V. Walter, Eds., *Parallel Computing: Software Technology, Algorithms, Architectures, and Applications*, Elsevier, Amsterdam, The Netherlands, 363-370.
- Wolke, R., W. Schroeder, R. Schroedner, E. Renner, 2012, Influence of grid resolution and meteorological forcing on simulated European air quality: A sensitivity study with the modeling system COSMO-MUSCAT. *Atmos. Env.*, 53, 110-130.
- Walko, R. L., et al. (2000), Coupled atmosphere-biophysics-hydrology models for environmental modeling, *Journal of Applied Meteorology*, 39(6), 931-944, doi: [10.1175/1520-0450\(2000\)039<0931:CABHMF>2.0.CO;2](https://doi.org/10.1175/1520-0450(2000)039<0931:CABHMF>2.0.CO;2).
- Walko, R. L., W. R. Cotton, M. P. Meyers, and J. Y. Harrington (1995), New RAMS cloud microphysics parameterization Part I: the single-moment scheme, *Atmospheric Research*, 38(1), 29-62, doi: [10.1016/0169-8095\(94\)00087-T](https://doi.org/10.1016/0169-8095(94)00087-T).
- WMO CCMM, 2016: Coupled Chemistry-Meteorology/Climate Modeling (CCMM): Status and relevance for numerical weather prediction, atmospheric pollution and climate research (Symposium materials). WMO GAW Report, Geneva, Switzerland. [Available online at https://library.wmo.int/doc_num.php?explnum_id=7938]
- WWRP, 2015: Seamless Prediction of the Earth System: From Minutes to Months. WMO-No. 1156. 471 pp. [Available online at http://library.wmo.int/pmb_ged/wmo_1156_en.pdf.]
- VARA-VELA, A; ANDRADE, M. F.; KUMAR, P.; YNOUE, R. Y.; MUÑOZ, A. G. Impact of vehicular emissions on the formation of fine particles in the Sao Paulo Metropolitan Area: a numerical study with the WRF-Chem model. *Atmospheric Chemistry and Physics (Online)*, v. 16, p. 777-797, 2016
- Yahya, K., Y. Zhang, and J. M. Vukovich, 2014, Real-Time Air Quality Forecasting over the Southeastern United States using WRF/Chem-MADRID: Multiple-Year Assessment and Sensitivity Studies, *Atmospheric Environment*, 92, 318-338, doi: [10.1016/j.atmosenv.2014.04.024](https://doi.org/10.1016/j.atmosenv.2014.04.024).
- Zakey, A.S., Solmon, F. and F. Giorgi, 2006 "Implementation and testing of a desert dust module in a regional climate model", *Atmos. Chem. Phys.*, 6, 4687-4704.
- Zakey, A. S, Giorgi, F, and Bi, X., 2008 "Modeling of sea salt in a regional climate model: Fluxes and radiative forcing", *Journal of Geophysical Research*, Vol. 113, D14221, [http://doi: 10.1029/2007JD009209](http://doi.org/10.1029/2007JD009209)

- Zeinab SALAH, Ahmed SHALABY, Allison L. STEINER, Ashraf S. ZAKY, Ritesh GAUTAM, and Mohamed M. ABDEL WAHAB (2018), Study of Aerosol Direct and Indirect Effects and Auto-conversion Processes over the West African Monsoon Region Using a Regional Climate Model, *ADVANCES IN ATMOSPHERIC SCIENCES*, VOL. 35, FEBRUARY 2018, 1–13
- Zhang, Y., C.-P. Hong, K. Yahya, Q. Li, Q. Zhang, and K.-B. He, 2016, Comprehensive evaluation of multi-year real-time air quality forecasting using an online-coupled meteorology-chemistry model over southeastern United States, *Atmos. Environ.*, 138, 162-182, doi: [10.1016/j.atmosenv.2016.05.006](https://doi.org/10.1016/j.atmosenv.2016.05.006).
- Zhang, Y., C. Seigneur, M. Bocquet, V. Mallet, and A. Baklanov, 2012, Real-Time Air Quality Forecasting, Part I: History, Techniques, and Current Status, *Atmospheric Environment*, 60, 632-655, doi: [10.1016/j.atmosenv.2012.06.031](https://doi.org/10.1016/j.atmosenv.2012.06.031).
- Zhang, Y., 2021, *Air Quality in a Changing Climate: Science and Modeling*, Cambridge University Press, in preparation.

3.3 Meteorological and NWP Models for Air Quality Forecasting

3.3.1 Introduction

Meteorology or numerical weather prediction (NWP) is one of the key components of 3-D CW-AQF models (e.g., integrated in online coupled systems or providing the necessary input data for offline atmospheric chemical transport (ACT) models). Historically, AQF and NWP systems were developed separately, and the corresponding communities had limited contact and cooperation. Although this situation could be tolerated in previous decades when NWP data was rarely available operationally for AQF models, and the resolution of NWP models was too coarse for mesoscale air-pollution forecasting, this has changed during this century as modern NWP models include mesoscale and city-scale resolution. This progress has been made possible due to advances in computing power, high-speed computing networks, and the availability of land-use databases and remote-sensing data on a finer resolution (Sokhi et al., 2018). As a result, the conventional concepts of CW-AQF is revised, as greater integration and interfacing between NWP models and ACT models is needed. Several NMHSs have suggested extending meteorological weather forecasting to environment forecasting that includes both NWP and CW-AQF.

In this sub-section, we address important characteristics of numerical models used for weather and air quality forecast models. Besides the complexity of physical and chemical processes that are present in any numerical model, other features are of crucial importance in order to produce valuable forecasts on weather or air quality in different time and space scales. Therefore, features related to initial and boundary conditions, different scale processes transfer, among others, are an important step required for the correct use of numerical models. The sub-section discusses some meteorological data requirements for CW-AQF models; characteristics of global and mesoscale models; couplers, pre-processing and post-processing systems; interfaces between NWP and ACT models; and methods for model downscaling and nesting.

3.3.2 Meteorological Data Requirements for CW-AQF Systems

Weather forecasting, as an initial value problem, requires the definition of initial values for some of the atmospheric variables (e.g., wind components, temperature, humidity, pressure, precipitation) in every grid point (horizontal and vertical) of the interest domain. These initial conditions for NWP systems are obtained from data assimilation procedures based on the observational network globally available. Examples of data sources are surface stations, instrumented balloons, atmospheric soundings, airplanes, ships, retrievals from satellites, among others.

Table 3.3 summarizes major meteorological observational networks. The measured variables include sky conditions, such as cloud cover, cloud height, and visibility, air temperature, dew point temperature, precipitation, humidity, solar radiation, soil temperature and moisture, atmospheric pressure, wind speed and direction, among others. The traditional observational network was mainly concerned with "atmospheric variables", without considering the necessity of providing information about more complex atmospheric chemical constituents, such as primary and secondary pollutants (e.g., carbon oxides (CO_x), Sulphur oxides (SO_x), volatile organic compounds (VOCs), ozone (O₃), and particulate matter (PM)). Nowadays, with the advent of air quality forecast, the traditional observational network needed to be improved. Over urban areas it is very common to find air quality measurement networks, mainly dedicated to emission control or the establishment of new policies with the goal of air quality improvement. Such data are now part of the data assimilation systems in some locations, but they are still very sparse and, therefore, not sufficient for the complex task of numerical air quality forecasting. Also, although these measurements made inside some cities can provide us with some ideas of the atmospheric constitution in a specific period of time, in most cases, there is very limited information available in rural areas and no data over large water bodies, as over oceans, for example. For the improvement of global and regional models dedicated to air quality forecasting, an increase in the number of observations available must be a main concern. Chapter 9 summarizes some commonly used regional and global observational networks for chemical constituents.

Table 3.3 Some meteorological observational networks used for CW-AQF models

Network	Full Name	Spatial Coverage	Species Measured	Temporal Frequency	Website
ASOS	Automated Surface Observing Systems	Entire U.S.	Cloud height and amount (clear, scattered, broken, overcast) up to 12 000 feet, visibility, basic present weather information: type and intensity for rain, snow, and freezing rain, fog, haze, sea-level pressure, ambient temperature, dew point temperature, wind speed and direction, speed (gusts, squalls), accumulated precipitation.	Every minute	https://www.weather.gov/asos
INMET	Brazilian National Institute of Meteorology	Entire Brazil	Wind, precipitation, temperature, dew point, humidity, solar radiation, pressure	Hourly	http://www.inmet.gov.br/portal/index.php?r=estacoes/estacoesAutomaticas
JMA	Japan Meteorological Agency	Entire Japan	Wind, precipitation, type and base height of cloud, visibility, temperature, humidity and atmospheric pressure.	Every ten minutes	https://www.jma.go.jp/jma/en/Activities/observations.html
KMA	Korean Meteorological Administration	Entire Korea	Pressure, temperature, humidity, precipitation, cloud coverage, wind, solar radiation, among others	Every 3 hours	https://web.kma.go.kr/eng/biz/observation_01.jsp
Metoffice	UK Met Office	Entire UK	Air temperature at 1.25 m above the ground, over a grass surface or its artificial equivalent, and over a concrete surface; Soil temperature at 0.1 m, 0.3 m and 1.0 m below the ground level, Relative humidity at 1.25 m above the ground, rainfall, depth of snow, mean wind speed, direction and maximum gust at 10m above the ground, pressure, visibility, amount of cloud.	Hourly	https://www.metoffice.gov.uk/weather/guides/observations-guide/uk-observations-network
MSS	Singapore's Meteorological Observing Network	Entire Singapore	Rainfall, temperature, humidity, surface wind and air pressure	Hourly	http://www.weather.gov.sg/learn_observations/

These meteorological and chemical observations are necessary to prepare initial and boundary conditions for weather and air quality models. In addition, they are required to evaluate models' ability to reproduce atmospheric observations and improve models' forecasting skills.

3.3.3 *Characteristics of Global and Mesoscale Meteorological and NWP models used for AQF*

Meteorology is one of the main drivers for atmospheric pollution processes and many atmospheric variables and processes impact on trace gases and aerosols. A meteorological or NWP model calculates three-dimensional fields of wind, temperature, relative humidity, pressure, and, in some cases, turbulent diffusivity, clouds, and precipitation, which are used for ACT modeling. The main meteorology and chemistry/aerosol interacting processes and effects, which could be considered in CW-AQF models, are summarized in Tables 3.4 and 3.5. The order, relevance, and importance of specific meteorological variables and processes in Table 3.4 for CW-AQF depend on the model applications.

There are a large number of global and mesoscale models around the world dedicated to weather and air quality forecasting as well as climate studies. Although many of those models have a large similarity among them, oftentimes specific characteristics of some locations requires the development of different physical parameterizations, which results in a variety of models available. Table 3.6 presents some of the models available in all continents with their most important characteristics, such as convective processes, boundary layer treatments, and types of vertical coordinate and pressure components. The application of each of these models will depend mainly on local features and on the purpose of model use. More specific characteristics of these NWP models, that affect the ability of the CW-AQF models to produce accurate forecasts of air quality, can be found in several review papers (e.g., Zhang, 2008; Zhang et al., 2012; Kukkonen et al., 2012; and Sokhi et al., 2018).

3.3.4 *Different Couplers, Pre/Post-Processing, and Interfaces between NWP and ACT Models*

For CW-AQF systems interfacing, integration or coupling of NWP and ACP models can be achieved in different ways using the online and offline modeling approaches, as briefly described in Chapter 2. There are a number of factors that have to be considered, including (Sokhi et al., 2018):

- input data (measurements or prognostic model data including input data formats and coupling time step);
- downscaling/nesting with high-resolution requirements for special topographies and circulation conditions, achieved through (self-) nesting of NWP and/or ACT models, including two-way interactive nesting for NWP models;
- modularity (requirements for high modularity and high compatibility);
- flexible input-output (IO) strategies;
- interfaces (described in the following).

Table 3.4 The impact of atmospheric variables and processes on atmospheric composition (after Baklanov et al., 2014).

Variable	Impact
Temperature	Modulates chemical reaction and photolytic rates
	Modulates biogenic emissions (isoprene, terpenes, dimethyl sulfide, etc.)
	Influences biogenic and anthropogenic emissions (isoprene, monoterpenes, VOCs from solvents and fuel)
	Influences the volatility of chemical species
	Determines aerosol dynamics (coagulation, condensation, nucleation) Determines atmospheric stability, turbulence and mixing potential
Temperature and humidity	Affect aerosol thermodynamics (e.g., gas-particle partitioning, secondary aerosol formation) Influence pollen emissions
Water vapor	Modulates OH radicals, size of hydrophilic aerosol
Liquid water	Determines wet scavenging and aqueous phase chemistry
Wind vector	Determines horizontal and vertical transport of trace gases and aerosols
	Influences dust-, sea-salt-, and pollen emissions
Atmospheric turbulence	Determines turbulent diffusion of trace gases and aerosols
ABL height	Influences concentrations
Radiation	Determines photolysis rates
	Determines biogenic VOC emissions
Cloud processes	Affect in-cloud scavenging of aerosols and trace gases
Precipitation	Determines the wet removal of trace gases and aerosol
Surface-vegetation-atmosphere exchange processes (depending on soil type, vegetation cover, soil moisture, and leaf area)	Affect natural emissions (e.g. dust, sea salt, pollen, nitrogen compounds, biogenic VOCs, CO ₂ , water vapor) and dry deposition
Lightning	Contributes to natural NO _x emissions

Table 3.5 Impacts of atmospheric pollutants on atmospheric variables and processes (after Baklanov et al., 2014).

Pollutant	Impact
Aerosols	Modify radiation transfer (SW scattering/absorption, LW absorption, LW scattering by large particles like dust)
	Affect ABL meteorology (temperature, humidity, wind speed and direction, stability)
	Affect haze formation and atmospheric humidity
	Modify physical properties of clouds (size distribution, extinction coefficient, phase function and single scattering albedo)
	Influence cloud droplet and ice crystal number concentrations
	Influence precipitation (initiation, intensity)
Soot	Influences surface albedo (e.g., ice surfaces)
Trace gases	Modify radiation transfer

The communication between offline-coupled meteorological and ACT models is a problem of often underestimated importance. The multitude of modeling systems previously introduced gives rise to different approaches and methods implemented within interface modules. Tasks covered by interfaces are minimized in coupled systems relying on surface fluxes, turbulence, and dispersion parameters (i.e., eddy viscosity) provided by the meteorological driver already on the grid used in the ACT model. Other systems use interface modules implementing surface and boundary-layer parameterizations to estimate dispersion and other required parameters. Sometimes these last choices are due to the need to rely on 'standard' meteorological products and to guarantee air quality modeling robustness for practical applications. In other cases, interfaces are used to enhance local physiographic data resolution and possibly introduce advanced parameterizations (e.g., urbanization). Atmospheric physics parameterizations, and even default or limit values assumed for some key parameters, can have relevant effects on pollutant concentration fields in critical conditions (e.g., low wind and stable stratification conditions). Moreover, interface modules may involve the evaluation of emissions of some relevant species that can be strongly influenced by meteorology, like biogenic VOCs, wind-blown dust, and sea salt spray.

3.3.5 *Methods for The Model Downscaling and Nesting*

As for roving numerical results, computational resources can be a limitation factor, requiring for most of the world the use of regional or limited area models in higher resolution grids. As in global models, higher resolution limited area models (LAM) also need data for their initial conditions and, as they have limited boundaries, the continuous supply of boundary conditions as well. For that task the usual procedure is to use global model results as a base for initial and boundary conditions for LAM. However, we need to note the existence of a large resolution difference between the two type of models. Therefore, it is necessary to apply some procedures of extrapolation or interpolation of global model data into the high-resolution grid of the LAM in use. This procedure is known as "downscaling". In a few words, we can define downscaling as the mathematical procedure of taking the information from large scale or global models to make predictions at local scales, usually with limited area models (meso or microscale).

Downscaling can be divided into two main types: dynamical and statistical. Statistical downscaling is made in two steps. First, it is necessary to develop statistical relationships between local variables (e.g., air temperature) and large-scale predictors (e.g., wind and pressure fields). Second, it is necessary to apply these relationships to the output of global models to simulate local characteristics in the future. As mentioned by Hoar and Nychka (2008), additional information on downscaling procedures is available in Haylock et al (2006),

Fowler et al (2007), and other articles published in the 2007 special issue of International Journal of Climatology (Volume 27, Issue 12, Downscaling and hydrology: progress in assessing impacts and adaptation to climate change, Pages: 1543-1705, October 2007).

Besides downscaling, there is another procedure used in models in order to represent different spatial scales. The procedure known by "nesting" consists of simulating different grid meshes almost simultaneously, using the same time step or fractions of it. Each higher resolution grid inside a coarser grid, called "parent grid", is provided with information from the lower resolution grid at predefined intervals of time. In such cases, initial and boundary conditions are provided by the coarser grid to the inner grids, successively, during the whole integration time. Figure 3.1 shows an example of the nesting procedure in models. Examples of models that apply nesting procedures are the Nested Grid Model (NGM) from the formerly National Climatic Data Center (NCDC), actual NOAA (Hoke et al., 1989), the fifth generation Penn State/NCAR Mesoscale Model (MM5, Grell et al., 1994), the Regional Atmospheric Modeling System (RAMS, Cotton et al., 2003; Pielke et al., 1992), the Weather Research and Forecasting (WRF) Model (Skamarock et al., 2008), and its chemical version (WRF/Chem, Grell et al., 2005), among others.

Table 3.6 Selected main characteristics of the numerical weather prediction models used for CTMs (mostly in Europe based on Kukkonen et al., 2012).

Model name	Hydrostatic/nonhydrostatic	Vertical coordinate	Reference	Cloud microphysics	Convective parameterization scheme	PBL scheme	Global or Limited-area model
ALADIN	Hydrostatic	Pressure or Sigma-pressure hybrid	http://www.umr-cnrm.fr/aladin/	Kessler (1969)	Bougeault (1985)	First order turbulence closure (Louis, 1979; Louis et al., 1982)	Limited-area
ECMWF IFS	Nonhydrostatic	Hybrid	https://www.ecmwf.int/en/research	Tiedtke (1993)	Modified Tiedtke (1989) scheme (Nordeng, 1994)	Modified Louis et al. (1982) <i>K</i> -theory scheme (Beljaars and Viterbo 1999)	Global
Eta	Nonhydrostatic	Eta	Mesinger et al. (1988), Janjic' (1990, 1994), Majewski et al. (2002)	Ferrier et al. (2002)	Betts-Miller-Janjic' and Kain-Fritsch Tiedke (1989)	Mellor-Yamada 2.5-order	Limited-area
GME	Hydrostatic	Sigma-pressure hybrid		Kessler-type scheme (Doms and Schättler, 1997)		2nd order, Mellor and Yamada (1974)	Global
HIRLAM	Hydrostatic/nonhydrostatic	Sigma-pressure hybrid	http://hirlam.org	STRACO (Soft Transition Condensation)	STRACO (modified Kuo scheme), Rasch and Kristjánsson (1998), Kain-Fritsch	Cuxart Bougeault Lacarrere, order 1.5 TKE scheme	Limited-area
MEMO	Nonhydrostatic	Sigma	Kunz and Moussiopoulos (1995), Moussiopoulos et al. (1997)	No moist processes	No moist processes	<i>K</i> -theory	Limited-area
MM5	Nonhydrostatic	Sigma	Dudhia (1993), Grell et al. (1995)	Various possible schemes	Various possible schemes	Various possible schemes	Limited-area

Model name	Hydrostatic/nonhydrostatic	Vertical coordinate	Reference	Cloud microphysics	Convective parameterization scheme	PBL scheme	Global or Limited-area model
Unified Model	Nonhydrostatic	Height	Cullen et al. (1997), Davies et al. (2005)	Wilson and Ballard extended by Forbes	Gregory and Rowntree (1990)	Lock et al. (2000)	Limited-area or global
WRF	Nonhydrostatic	Sigma or sigma-pressure hybrid	Janjic et al. (2001), Janjic (2003), Skamarock et al. (2005)	Various possible schemes	Various possible schemes	Level 2.5 Mellor and Yamada Janjic, or non-local YSU scheme	Limited-area
RAMS	Nonhydrostatic	Height, sigma or eta	Pielke et al. (1992), Cotton et al. (2003)	Various possible schemes	Various possible schemes	Various possible schemes	Limited-area

The nesting procedure can be used in two different ways. In the simple one, only the inner grid receives information from the coarser grid. This method is called one-way interaction. In this type of method large scale features can be transferred to the small scales, but higher resolution phenomena will not be sensed by the large scale. The second way of nesting grids involves the feedback between different grids (or processes) and it is called two-way interaction. In this method both large and mesoscale phenomena provide feedback to each other, being a more consistent and appropriate procedure to represent different scales in a model. However, it is important to remember that two-way nesting is more expensive computationally.

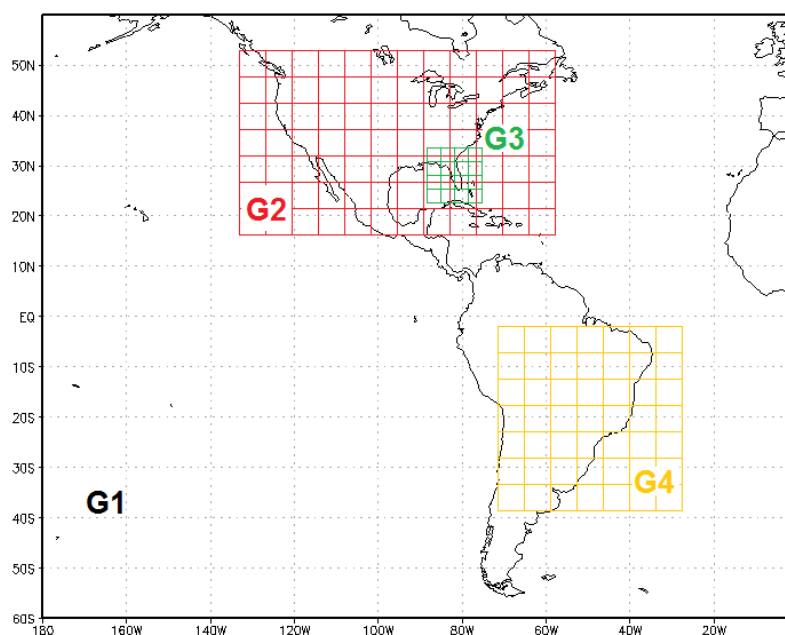


Figure 3.1. Illustration of the nesting grid procedure in numerical models.

G1 indicates the “parent” grid, which will provide initial and boundary conditions for the inner grids, G2 (covering the United States) and G4 (covering part of South America). Initial and boundary conditions to grid G3 (covering the Florida peninsula, U.S.) will be provided by grid G2, which will be considered as its parent grid during the integration.

3.3.6 Summary

- CW-AQF systems require detailed data, based on observational networks globally available, for its initial and boundary conditions. The necessary information includes meteorological variables and atmospheric chemical constituents.
- Although global and mesoscale models differ in many features, due to the different spatial and timescales these models can represent, both types of models provide the meteorological bases for atmospheric pollution processes, through a variety of physical parameterizations that allow us to analyse atmospheric interacting processes and their effects. A list of models used worldwide was presented.
- Integration or coupling of NWP and ACP models can be achieved in different ways using the online and offline modeling approaches. The communication of different models is of great importance and constitutes a great problem for the scientific community.

- Despite the great development of computational resources, allowing the use of models in higher resolution, it is still necessary to improve and develop new methods for downscaling of global models to mesoscale or higher resolution models. This process of downscaling provides the necessary information on the different scales of the phenomena of interest. Also, nesting of computational grids, allowing the passage of information between different scales is an important process to be improved and applied in activities related to weather and air quality forecasting and diagnosis.

References

- Baklanov, A., Schlünzen, K., Suppan, P., Baldasano, J., Brunner, D., Aksoyoglu, S., Carmichael, G., Douros, J., Flemming, J., Forkel, R., Galmarini, S., Gauss, M., Grell, G., Hirtl, M., Joffre, S., Jorba, O., Kaas, E., Kaasik, M., Kallos, G., Kong, X., Korsholm, U., Kurganskiy, A., Kushta, J., Lohmann, U., Mahura, A., Manders-Groot, A., Maurizi, A., Moussiopoulos, N., Rao, S. T., Savage, N., Seigneur, C., Sokhi, R. S., Solazzo, E., Solomos, S., Sørensen, B., Tsegas, G., Vignati, E., Vogel, B., and Zhang, Y.: Online coupled regional meteorology chemistry models in Europe: current status and prospects, *Atmos. Chem. Phys.*, 14, 317-398, doi: [10.5194/acp-14-317-2014](https://doi.org/10.5194/acp-14-317-2014), 2014.
- Beljaars, A. C. M., P. Viterbo (1999). Soil moisture-precipitation interaction: Experience with two land surface schemes in the ECMWF model. *Global energy and water cycles*.
- Bougeault, P., 1985: A Simple Parameterization of the Large-Scale Effects of Cumulus Convection. *Mon. Wea. Rev.*, 113, 2108–211, [https://doi.org/10.1175/1520-0493\(1985\)113<2108:ASPOTL>2.0.CO;2](https://doi.org/10.1175/1520-0493(1985)113<2108:ASPOTL>2.0.CO;2)
- Cotton, W. R., et al. (2003), RAMS 2001: Current status and future directions, *Meteorology and Atmospheric Physics*, 82(1-4), 5-29, doi: [10.1007/s00703-001-0584-9](https://doi.org/10.1007/s00703-001-0584-9).
- Cullen, M. J. P., T. Davies, M. H. Mawson, J. A. James, and S. Coulter, 1997: An overview of numerical methods for the next generation UK NWP and climate model. *Atmos.–Ocean Special*, 35,425–444.
- Davies, T., M. J. P. Cullen, A. J. Malcolm, M. H. Mawson, A. Staniforth, A. A. White, and N. Wood (2005), A new dynamical core for the Met Office's global and regional modeling of the atmosphere. *Quart. J. Roy. Meteor. Soc.*, 131, 1759–1782.
- Doms, G., and U. Schättler (1997), The nonhydrostatic limited-area model LM (Lokal-Model) of DWD. Part I: Scientific documentation. *Deutscher Wetterdienst Rep. LM F90 1.35*, 172 pp. [Available from Deutscher Wetterdienst, P.O. Box 100465, 63004 Offenbach, Germany.]
- Dudhia, J., 1993: A Nonhydrostatic Version of the Penn State–NCAR Mesoscale Model: Validation Tests and Simulation of an Atlantic Cyclone and Cold Front. *Mon. Wea. Rev.*, 21, 1493–1513,
- Ferrier, B. S., Y. Jin, T. Black, E. Rogers, and G. DiMego, 2002: Implementation of a new grid-scale cloud and precipitation scheme in NCEP Eta model. *Preprints, 15th Conf. on Numerical Weather Prediction, San Antonio, TX, Amer. Meteor. Soc.*, 280–283.
- Fowler, H. J., Blenkinsop, S. and Tebaldi, C. (2007), Linking climate change modeling to impacts studies: recent advances in downscaling techniques for hydrological modeling. *Int. J. Climatol.*, 27: 1547-1578. doi: [10.1002/joc.1556](https://doi.org/10.1002/joc.1556).
- Grell, G. A., Dudhia, J., Stauffer, D. R. (1994) A description of the fifth generation Penn State/NCAR Mesoscale Model (MM5). NCAR Technical note. NCAR/TN-398+STR, December 1994.
- Grell G, Dudhia J, Stauffer D (1995) A description of the fifth-generation Penn State/NCAR mesoscale model (MM5). TN-398+STR, NCAR, Boulder, CO.
- Grell, G. A., S. E. Peckham, R. Schmitz, S. A. McKeen, G. Frost, W. C. Skamarock, and B. Eder (2005), Fully coupled “online” chemistry within the WRF model, *Atmospheric Environment*, 39(37), 6957-6975,

- Gregory, D. and P.R. Rowntree, 1990: A Mass Flux Convection Scheme with Representation of Cloud Ensemble Characteristics and Stability-Dependent Closure. *Mon. Wea. Rev.*, 118, 1483–1506,
- Haylock, M. R., Cawley, G. C., Harpham, C., Wilby, R. L. and Goodess, C. M. (2006), Downscaling heavy precipitation over the United Kingdom: a comparison of dynamical and statistical methods and their future scenarios. *Int. J. Climatol.*, 26: 1397-1415. doi: [10.1002/joc.1318](https://doi.org/10.1002/joc.1318).
- Hoar, T., and Nychka, D. (2008) Statistical downscaling of the Community Climate System Model (CCSM) monthly temperature and precipitation projections. White Paper – NCAR, April 2008. Available at <https://gisclimatechange.ucar.edu/sites/default/files/users/Downscaling.pdf>. Last access on 5 April 2018.
- Hoke, J.E., N. A. Phillips, G.J. DiMego, J.J. Tuccillo, and J.G. Sela, 1989: The Regional Analysis and Forecast System of the National Meteorological Center. *Weather and Forecasting*, 4 (323-334).
- Janjic, Z. I., 1990: The step-mountain coordinate: physical package, *Mon. Wea. Rev.*, 118, 1429–1443.
- Janjic, Z. I., 1994: The step-mountain eta coordinate model: further developments of the convection, viscous sublayer and turbulence closure schemes, *Mon. Wea. Rev.*, 122, 927–945.
- Janjic, Z. I., J. P. Gerrity, Jr. and S. Nickovic, 2001: An alternative approach to nonhydrostatic modeling. *Mon. Wea. Rev.*, 129, 1164-1178.
- Janjic, Z. I., 2003: A nonhydrostatic model based on a new approach. *Meteorol. Atmos. Phys.*, 82, 271-285.
- Kessler E. (1969) On the Distribution and Continuity of Water Substance in Atmospheric Circulations. In: *On the Distribution and Continuity of Water Substance in Atmospheric Circulations*. Meteorological Monographs, vol 10. American Meteorological Society, Boston, MA. https://doi.org/10.1007/978-1-935704-36-2_1.
- Kukkonen, J., et al. (2012), A review of operational, regional-scale, chemical weather forecasting models in Europe, *Atmos. Chem. Phys.*, 12(1), 1-87, doi: [10.5194/acp-12-1-2012](https://doi.org/10.5194/acp-12-1-2012).
- Kunz, R., and N. Moussiopoulos (1995), Simulation of the wind field in Athens using refined boundary conditions, *Atmospheric Environment*, 29(24), 3575-3591, [https://doi.org/10.1016/1352-2310\(94\)00361-N](https://doi.org/10.1016/1352-2310(94)00361-N).
- Lock, A. P., Brown, A. R., Bush, M. R., Martin, G. M., and Smith, R. N. B.: A new boundary layer mixing scheme, Part I: Scheme description and single-column model tests, *Mon. Weather Rev.*, 128, 3187–3199, 2000.
- Louis, J. F. (1979), Parametric model of vertical eddy fluxes in the atmosphere, *Boundary-Layer Meteorology*, 17(2), 187-202, doi: [10.1007/BF00117978](https://doi.org/10.1007/BF00117978)
- Louis J, Tiedtke M, Geleyn J. 1982. A short history of the operational PBL-parameterization at ECMWF. In: Proc. Workshop on planetary boundary-layer parameterization. ECMWF: Reading, UK. 59–79.
- Majewski, D., D. Liermann, P. Prohl, B. Ritter, M. Buchhold, T. Hanisch, G. Paul, W. Wergen, and J. Baumgardner, 2002: The Operational Global Icosahedral–Hexagonal Gridpoint Model GME: Description and High-Resolution Tests. *Mon. Wea. Rev.*, 130, 319–338, [https://doi.org/10.1175/1520-0493\(2002\)130<0319:TOGIHG>2.0.CO;2](https://doi.org/10.1175/1520-0493(2002)130<0319:TOGIHG>2.0.CO;2)
- Mellor, G.L. and T. Yamada, 1974: A Hierarchy of Turbulence Closure Models for Planetary Boundary Layers. *J. Atmos. Sci.*, 31, 1791– 806, [https://doi.org/10.1175/1520-0469\(1974\)031<1791:AHOTCM>2.0.CO;2](https://doi.org/10.1175/1520-0469(1974)031<1791:AHOTCM>2.0.CO;2)

- Mesinger, F., Z. I. Janjic, S. Nickovic, D. Gavrilov, and D. G. Deaven, 1988: The step mountain coordinate: Model description and performance for cases of Alpine cyclogenesis and for a case of an Appalachian redevelopment. *Mon. Wea. Rev.*, 116, 1493–1518.
- Moussiopoulos, N., Sahm, P., Karatzas, K., Papalexidou, S., Karagiannidis, A., 1997. Assessing the impact of the new Athens airport to urban air quality with contemporary air pollution models. *Atmospheric Environment* 31, 1497–1511.
- Nordeng, T. E.: Extended versions of the convective parametrization scheme at ECMWF and their impact on the mean and transient activity of the model in the tropics, Tech. Rep. 206, ECMWF, 1994
- Pielke, R. A., et al. (1992), A Comprehensive Meteorological Modeling System - RAMS, *Meteorology and Atmospheric Physics*, 49(1-4), 69-91, doi:10.1007/BF01025401
- Rasch, P.J. and J.E. Kristjánsson, 1998: A Comparison of the CCM3 Model Climate Using Diagnosed and Predicted Condensate Parameterizations. *J. Climate*, 11, 1587–1614, [https://doi.org/10.1175/1520-0442\(1998\)011<1587:ACOTCM>2.0.CO;2](https://doi.org/10.1175/1520-0442(1998)011<1587:ACOTCM>2.0.CO;2)
- Skamarock, W. C., J. B. Klemp, J. Dudhia, D. O. Gill, D. M. Barker, W. Wang, and J. G. Powers, 2005: A Description of the Advanced Research WRF Version 2. NCAR Technical Note NCAR/TN-468+STR, doi:10.5065/D6DZ069T.
- Skamarock, W. C., J. B. Klemp, J. Dudhia, D. O. Gill, D. M. Barker, M. G. Duda, X. Huang, W. Wang, and J. G. Powers (2008), A description of the Advanced Research WRF Version 3Rep.
- Sokhi, R.S. et al., 2018: *Mesoscale Modeling for Meteorological and Air Pollution Applications*. Anthem Press.
- Tiedtke, M., 1989: A Comprehensive Mass Flux Scheme for Cumulus Parameterization in Large-Scale Models. *Mon. Wea. Rev.*, 117, 1779–1800,
- Tiedtke, M., 1993: Representation of Clouds in Large-Scale Models. *Mon. Wea. Rev.*, 121, 3040–3061,
- Zhang, Y., C. Seigneur, M. Bocquet, V. Mallet, and A. Baklanov, 2012, Real-Time Air Quality Forecasting, Part I: History, Techniques, and Current Status, *Atmospheric Environment*, 60, 632-655, doi:10.1016/j.atmosenv.2012.06.031.
- Zhang, Y.: Online-coupled meteorology and chemistry models: history, current status, and outlook, *Atmos. Chem. Phys.*, 8, 2895– 2932, doi:10.5194/acp-8-2895-2008, 2008.

3.4 Atmospheric Planetary Boundary Layer and Parameterizations of Boundary-Layer Processes

3.4.1 Introduction

The Planetary boundary layer (PBL) is the lower, essentially turbulent atmospheric layer that responds to special or temporal changes in properties of or impacts from Earth's surface (see Figure 3.2). PBL creates an interface between the surface and free troposphere extended up to the tropopause. The PBL upper boundary is defined as the height at which wind velocity approaches 95% of its value in the free-flow. It is strongly variable in space and time, ranging from hundreds of meters to a few kilometers.

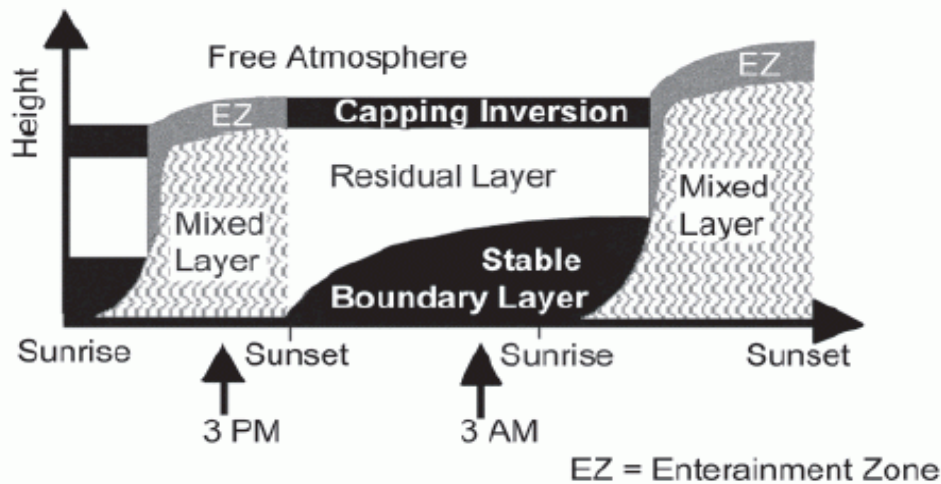


Figure 3.2. Diurnal evolution of PBL (after Stull, 2000).

Adequate representation of PBL processes is crucial for numerical modeling of weather, climate, air pollution, and atmospheric dispersion. Thanks to persistently increasing computer power, the model-grid resolution is continually enhancing. This allows for better representation of PBL processes and calls for better knowledge of physical, chemical, and biological mechanisms controlling these processes. Thus, development of and requirements to advanced PBL parameterizations in NWP and CW-AQF models are closely connected with advances in computing capability, so should be fit for purpose and for computer possibilities. A short summary of PBL parameterizations or schemes is given in the following sections. Wider treatments of these issues can be found in Stull (1988), Garratt (1994), COST-710 (1998), Baklanov and Grisogono (2007), Baklanov et al. (2011), Holton (2012), Salby (2012), Zilitinkevich (2013), Pielke (2013), and Sokhi et al. (2018). In spite of increasing resolution in mesoscale models, it remains insufficient to resolve crucially-important processes controlling the heat and mass transfer. Some examples where the resolution of models can be a particularly limiting factor include deep canopies, complex terrain or stormy seas, PBLs in very stable stratification typical of winter time at high latitudes, and long-lived PBLs typical of polar night (stable stratification) or polar day (unstable stratification), not to mention the incapability of contemporary models to resolve the PBL upper boundary and to quantify vertical exchanges between the PBL and free troposphere.

In numerical models, PBL can be considered as single layer (usually in global or simplified models (see Deardorff, 1972; Mahrt, 1974; Smith and Mahrt, 1981)). In most regional models, the PBL is resolved into several sub-layers to more realistically reproduce specific features over complex terrain or across land-water borders characterized by large horizontal gradients of meteorological variables (see overview in Sokhi et al., 2018). Traditionally, PBL consists of three essentially different parts: roughness layer, surface layer, and PBL core:

- Roughness layer, immediately adjacent to Earth's surface, is defined for shallow canopies as $0 < z < z_0$ where z_0 is roughness length for momentum (usually an order of magnitude larger than typical height of roughness elements, h_0). Deep canopy causes a kind of stagnation zone quantified by so-called displacement height, D (essentially shallower than the canopy depth, h_0), so that the roughness layer is defined as $0 < z < (D + z_0)$ (e.g., Pielke, 2013).
- Surface layer is defined as the layer where vertical turbulent fluxes are practically independent of height. It is described by the Monin-Obukhov (1954) similarity theory (MOST). It is conventionally defined as the lower 10% of PBL.
- PBL core is defined as the upper 90% of PBL up to the PBL upper boundary.

Notably, the free troposphere above PBL is characterized by typically weak velocity shears and very stable stratification, which strongly reduces the intensity of turbulence. This in turn strongly reduces vertical exchange processes at the PBL upper boundary, so that any impacts from Earth's surface, such as warming or cooling, stronger or weaker surface drag, emissions of pollutants, almost immediately affect the entire PBL, but penetrate into the free troposphere with essential time lag and considerably weakened. Especially dramatic is the difference in nature between the free troposphere and unstably stratified and, hence, strongly mixed PBL. In this case, the PBL height is clearly seen in vertical profiles of mean potential temperature and concentration of pollutants emitted at Earth's surface (which almost completely remain within PBL).

3.4.2 Representation of Interactions between Atmosphere and Various Earth Surfaces

Correct parameterizations of surface fluxes of heat, moisture, and momentum play a vital role in modeling of practically all meteorological processes via the control of the mass energy, and momentum exchanges between the atmosphere and Earth's surface. Turbulent fluxes and turbulent energies close to the surface and in the interior of the PBL, to a large extent, control meteorological fields, namely, the mean flow and turbulent mixing. Hence in practice this includes the transport and dispersion of pollutants, thermal and moisture regimes, and practically the most important near-surface phenomena, such as fogs, frosts, storms and gustiness essential for aviation, energy sector, transport and agriculture. Surface fluxes are the key factors of initiation and development of hurricanes. Below, we briefly describe the parameterization of turbulent fluxes over various surfaces of Earth for CW-AQF models. Additional information can be found, e.g., in Chapter 3 of Sokhi et al. (2018).

In a broad framework, vertical turbulent fluxes of momentum (τ_0), heat (H_0), and moisture (E_0)-at Earth's surface are calculated through the mean flow characteristics using the drag and heat- or moisture-transfer coefficients derived from different (usually first-order) turbulence closure models. Presently, only vertical turbulent fluxes are parameterized for the grids of mesoscale models, whereas very little is known about horizontal fluxes. As emphasized by Pielke (2013), subgrid-scale fluctuations of modeled variables can be of the same order or even larger than resolvable variations. As an example, the resolved wind speed and fluctuations of wind-speed could both be of the order of 5 m s^{-1} . Similarly, in a grid volume with the averaged vertical wind speed close to zero, vertical turbulent heat flux can be significant due to pronounced vertical-velocity and potential-temperature fluctuations (especially in convective PBLs).

For homogeneous terrains the widely-used instrument for calculating surface fluxes is MOST treated as a kind of first-order closure model and, thus, expressing turbulent fluxes via the calculated vertical profiles of mean-flow parameters. Examples of the surface flux schemes commonly used in mesoscale meteorological models, e.g., in the Weather Research and Forecast (WRF) model, are discussed in Jimenez et al. (2012) and ARW-WRF (2015). Most parameterizations, e.g., Blackadar (1962), MRF and Eta schemes, employ MOST. Instead, Burk and Thompson (1989) PBL scheme, e.g., used in HIRLAM model, employs Mellor–Yamada (1982) closure level-2.5 including the prognostic equation for turbulent kinetic energy (TKE). Quante et al. (2009) and Gryning et al. (2011) have shown large spread in the ability of models to calculate the surface fluxes of sensible heat and momentum. It is not surprising that

modern NWP and CW-AQF models, e.g., WRF-Chem, are equipped with many different options for the surface-layer scheme to be chosen by the user.

The following paragraphs briefly explore how different surfaces are treated in air quality forecasting models.

Urban air pollution and atmospheric chemical transport models have different primary requirements when including urbanization effects. These depend on the scale of the models and functional requirements such as if they are to be used for forecasting or assessment, for environmental and air quality applications or emergency preparedness. In the case of incorporating urban effects into urban- and regional-scale atmospheric pollution models, a key primary requirement is to improve the urban meteorological fields. Urban cases are essential for air pollution forecasting applications, especially if the information is targeted at the public, and considered separately in Section 3.3.

As forests are taller than other vegetation surface types, air flow is also subject to larger aerodynamic roughness and displacement heights (Finnigan 2000; Dupont and Patton 2012). Both height and density of the forest are important for the flow (Gayev and Hunt, 2007). Forest canopy reduces shortwave radiation received on the ground but emits and absorbs longwave radiation as a function of forest type, which is characterized by the leaf area index (LAI). The aerodynamic and thermal parameters change during the year; for example, snow cover strongly affects the surface albedo. Recent advances in micrometeorological studies which have resulted in improved parameterizations (e.g., Ershadi et al., 2014) include: (i) exchange of heat and moisture between trees and air, (ii) local momentum flux over the forest, including stability effects on it, and (iii) transfer of solar radiation within the forest.

It seems that while there are improvements in horizontal resolution of models, less attention has been paid to the treatment of surface heterogeneity within a grid square. Heterogeneity is often present in a range of environments such as forest, field, swamp, and lakes with scales smaller than a few kilometers. In particular for forests and cities many models do not take into account certain important effects, such as displacement height; roughness sublayer, which presents a major challenge for the parameterization of turbulent surface fluxes, especially in conditions of stable stratification, when the constant-flux layer may be very thin or entirely missing. Other effects that need further attention include:

- effects of forest on the transfer of longwave and shortwave radiation;
- simulation of vertical profiles within the forest (instead, the forest effects are treated as a part of the exchange between the surface and the lowest model level, even if the forest in reality reaches altitudes higher than the lowest model level);
- application of the tile/mosaic method in its simplest form, without paying attention to the subgrid-scale variability at the lowest atmospheric model level.

Turbulent flux parametrizations over the inhomogeneous surface are realized in different models through different surface layer formulations and canopy models (see overview in Zhang, 2008; Kukkonen et al., 2012; Baklanov et al., 2014). Surface fluxes depend considerably on the land cover. Some models only consider one land cover type per grid cell, but others parameterize the effects of subgrid scale land use on turbulent fluxes (e.g., Schlünzen and Katzfey, 2003). Above the sea surface, drag is often parameterized using the Charnock (1955) formula, due to missing wave data. It works reasonably well for flat coastal regions, while for deeper water recent studies suggest a different approach (Foreman and Emeis, 2010).

3.4.3 Turbulence Closures and Boundary-Layer Parameterizations

The key aspect of PBL is its turbulent nature. Turbulence is several orders of magnitude more effective at transporting quantities than is molecular diffusivity. It is turbulence that allows the PBL to respond to changing surface forcing (as frictional drag, evaporation and transpiration, heat transfer, pollutant emission, and terrain induced modification). As a result, about fifty percent of the atmosphere's kinetic energy is dissipated in the PBL. Understanding the PBL is fundamental for the numerical modeling of meteorological and transport processes, from micro to global scales.

The levels of turbulence in an atmospheric boundary layer with zero heat flux at the surface in uniform, homogeneous, steady conditions are determined by the following fundamental parameters (COST-710, 1998):

- wind velocity at the upper boundary of the layer (often identified with geostrophic wind speed G);
- Coriolis parameter f quantifying the influence of Earth's rotation;
- roughness lengths for momentum and scalars characterizing the surface drag and heat/mass transfer and dependent on the height and geometry of roughness elements from very small (sand particles in a desert) to very large (buildings);
- the background thermal stratification of the atmosphere characterized by the Brunt-Väisälä frequency in the atmosphere above PBL layer.

When the surface heating is non-zero, the surface heat flux H is the other driving force setting up the structure of the boundary layer. During the day, when the flux of heat carried from the surface into the atmosphere by convection is usually positive, the heat flux acts as an extra source of turbulence over and above that caused by the wind. At night the heat flux is usually negative, and this tends to drain energy down from the wind-induced turbulence, leading to much reduced turbulence levels for a given wind speed. Since the interests of boundary layer meteorology and dispersion modeling are in the main velocity and length scales, it is usual to introduce a new length scale L_* into the equations describing wind, temperature, and turbulence profiles. L_* is the Monin-Obukhov length, equal to u_*^3/H apart from some constant of proportionality. In convective boundary layers it is usual to introduce the convective velocity scale w_* , which is proportional to $(hH)^{1/3}$.

Most of the operationally-used closures employ the concept of down-gradient turbulent transport, implying that turbulent fluxes are proportional to and oriented along mean gradients of the transporting properties. The proportionality coefficients in such relations, called eddy viscosity K_M , eddy conductivity K_H and eddy diffusivity K_D , are considered as the major (or only) unknowns to be determined from turbulence closure theory. The modern content of this theory is based on the paradigm originated from Kolmogorov (1941, 1942). His turbulence closure theory was based on (i) budget equation for the TKE, E_K , (ii) definition of turbulent velocity scale, u_T , as the square root of TKE: $u_T = E_K^{1/2}$ Prandtl's vision of turbulent exchange coefficients, $K_M \sim K_H \sim K_D$, as proportional to product $u_T l_T$, where l_T is turbulent length scale identified in neutrally stratified boundary-layer flow with the height over the surface, z . This revolutionary idea has resolved the problem of dissipation rate of TKE: $\epsilon_K \sim E_K^{3/2} / l_T$ and yielded constructive turbulence-closure theory for neutrally stratified sheared flows.

In due time, this vision of turbulence has revolutionized the understanding and modeling of turbulence in neutrally stratified flows. Later on, followers of Kolmogorov have extended it without proof to stably and unstably stratified flows. This extended version gave rise to the streamline in turbulence closure theory, in particular, to the models in operational use. In moderately stable or unstable stratifications this approach shows quite good results. However, it fails in strongly stable stratification. In particular, the conventional approach erroneously prescribes degeneration of turbulence in supercritical stratification typical of free troposphere and ocean thermocline (yet corrected only approximately and without physical explanation). Moreover, conventional theory and closure models become fully erroneous as applied to horizontal diffusion in unstable stratification. The problem of stratified turbulence typical of the

atmosphere problem is now being resolved – for stable stratification via the Energy- and Flux-Budget turbulence closure theory (Zilitinkevich et al., 2007, 2009, 2013), and for unstable stratification via the concept of self-organization of convective turbulence (Zilitinkevich, 2013).

Parameterization of processes in stable PBL constitutes a considerable source of uncertainty in modeling air pollution. Despite their sophistication, schemes used in NWP models have limitations, that are critical in CW-AQF applications. For example, CW-AQF models need greater vertical resolution within PBLs and improved surface-layer parameterizations, especially in urban-scale air-pollution modeling where low-level emissions (e.g., from traffic) within the surface layer are typical.

3.4.4 PBL Height and Turbulent Exchanges through the PBL Upper Boundary

The PBL upper boundary acts as a barrier preventing (or strongly reducing) vertical dispersion in most of air quality and dispersion models and essentially controlling extreme weather events and microclimates in NWP and climate models. Methods of calculation of PBL height, h_{PBL} , have been the subject of numerous theoretical and experimental studies since Ekman (1905), who identified PBL as the steady-state boundary layer in rotating fluid and derived the relation: $h_{PBL} \sim \sqrt{K_M / f}$, where K_M is a reference value of eddy viscosity and f is Coriolis parameter quantifying the effect of Earth's rotation; and Rossby and Montgomery (1935) whose formulation; $h_{PBL} \sim u_* / f$, where u_* is friction velocity, is still used in meteorological practice as a rough approximation. In reality, the PBL height (as well as other features of PBL) strongly depends on static stability. Its effect is traditionally characterized by just one parameter: vertical turbulent flux of buoyancy at Earth's surface, $F_B = (g/T)F_\theta + 0.61gF_q$, where $g = 9.81 \text{ ms}^{-2}$ is the acceleration due to gravity, T is absolute temperature, F_θ is vertical turbulent flux of potential temperature, F_q is vertical turbulent flux of specific humidity.

Accordingly, the three basic types of PBL are distinguished, namely, stable: $F_B < 0$ reducing turbulence, neutral: $F_B = 0$, and unstable (or convective): $F_B > 0$ enhancing turbulence.

For convective PBL (CPBL), Zubov (1945) has derived prognostic equation for the CPBL height, h_{CPBL} , implying its growth until F_B remains positive: $dh_{CPBL}^2/dt = 2F_B/N^2 = 0$, where N is Brunt-Vaisala frequency in the free flow beyond the ever developing CPBL. More general formulation of the CPBL height equation accounting for turbulent entrainment and the CPBL upper boundary can be found in Zilitinkevich (1991, 2012).

For the stable PBL (SPBL) that forms in the atmosphere over land after sunset due to the change from $F_B > 0$ to $F_B < 0$, Zilitinkevich (1972) has derived diagnostic formulation:

$$h_{SPBL} = C_{SPBL} u_*^2 (F_B f)^{-1/2}, \text{ where } C_{SPBL} = 0.5 \text{ is dimensionless empirical constant.}$$

In later publications, it has been revealed that major properties of PBLs, in particular their heights, are essentially different for the two principally different PBL types (Zilitinkevich and Esau, 2002; Zilitinkevich et al., 2007): (i) Short-lived mid- and low-latitude continental PBLs subjected to pronounced diurnal variations and, therefore, almost fully controlled by the surface buoyancy flux, F_B , and (ii) Long-lived high-latitude PBLs and PBLs over open ocean keeping their type of stratification (stable or unstable) over long periods from several days or weeks (over ocean) to more than a month (over both ocean and land during polar night or polar day). We recall that long-lived PBLs are essentially controlled by persistent stable stratification inherent to the free troposphere and characterized the Brunt-Vaisala frequency, N , (typically of order 10^{-2} s^{-1}) which makes them very shallow and, hence, very sensitive to any external impacts.

In practical CW-AQF applications the height of PBL can be derived from meteorological measurements as well as model data. Several methods have also been suggested based on analysis of turbulence processes, e.g., see overview in: COST-710, 1998; Zilitinkevich and Baklanov, 2002:

- Bulk Richardson number method;
- Gradient Richardson number method;
- Profiles of TKE, momentum and heat fluxes;
- Theoretical approaches.

For example, Gryning and Batchvarova (1990) have suggested an often used in models analytical formulation for the CPBL height, z_i , accounting for mechanical and convective turbulence mixing and including a diagnostic parameterization for $\Delta\theta_i$ in the jump model:

$$\frac{dz_i}{dt} = \frac{(1+2A)Q_0}{\gamma h} + \frac{2B}{\gamma\beta} \frac{u_*^3}{z_i^2} \quad (1)$$

where A and B are model constants, β is the buoyancy parameter and γ is the potential temperature gradient. Batchvarova and Gryning (1994) also introduced an additional parameterization of Δz_i , the depth of the entrainment zone.

In CW-AQF models the turbulent mixing takes place within the PBL and therefore the PBL height is estimated at each time step in order to define up to which model level turbulence mixing exists. When first order closure is used, the height of the PBL is an essential parameter (implicit or explicit) in the description of mixing of meteorological properties (see overview in Seibert et al., 2000).

3.4.5 Parameterizations of Radiation

The presence of longwave and shortwave radiation in the atmosphere profoundly influences weather conditions and correspondingly atmospheric pollution processes in all spatial and temporal scales. Differential heating of Earth's surface by the sun creates horizontal temperature gradient, and thus pressure differences driving the circulation of the atmosphere.

Numerical weather prediction (NWP) models usually utilize two separate radiation schemes: for the shortwave (SW) and for the longwave (LW) radiation. Shortwave and longwave radiation schemes must both simulate the absorption of radiation by water vapor, ozone, carbon dioxide (and other greenhouse gases), clouds, and Earth's surface. In addition, models must demonstrate other phenomena such as reflection of radiation by clouds and Earth's surface, scattering by clouds and aerosols, and re-emission of longwave radiation by greenhouse gases (see also Section 3.8). Radiation schemes, although different in various models (see overview and Tables for different AQF models in Kukkonen et al., 2012; Baklanov et al., 2014), perform similar functions. Dealing appropriately with the energy input and the energy budget of the atmosphere is essential for the accuracy of model results. Most radiation schemes currently used are column (one-dimensional) schemes, so each column is treated independently, and the fluxes correspond to those in infinite horizontally uniform planes, which is a good approximation if the vertical thickness of the model layers is much less than the horizontal grid length. This assumption would become less accurate at high horizontal resolution.

In the case of meteorological models used as the drivers (i.e., for offline models) or as host models (i.e., for online models) for CW-AQF, the formulation of the radiation parameterization is of lesser importance in terms of atmospheric dispersion, although the methodology of coupling constant value (J) calculation in chemical solver might have significant impacts on modeled chemical processes. The concentrations and the distribution of the trace species that affect the radiative transfer in the atmosphere is derived from the climatological datasets.

As the understanding of the radiative properties of chemical compounds (especially aerosols) increases as well as the continuous increase in available computation resources, further additions and improvements can be introduced to radiation schemes. The ongoing development of the fully-coupled online atmospheric modeling systems focuses mainly on feedback, namely, the effects of the scattering on aerosols as well as absorption of atmospheric gases are treated interactively. Studies with the advanced coupled CW-AQF models show the mechanism and the magnitude of meteorological and chemical responses to aerosol radiative forcings. During short-term air quality episodes, the interactive treatment of the direct aerosol effect leads to a decrease in the solar radiation flux, a decrease in the daytime diurnal temperature amplitude, an increase in night-time temperature, and a decrease in the PBL height (see Section 3.8).

3.4.6 *Parameterization of Convection and Clouds*

A correct representation of convection in NWP, air quality, and climate models has long been recognized as one of the most important challenges in meteorological research. Cloud processes are extremely important for air quality as well as for weather prediction. Clouds couple dynamical and hydrological processes in the atmosphere and on the ground through the heat of condensation and evaporation, through redistributions of sensible and latent heat and momentum, and through precipitation. Clouds also may be the most important link between weather/air quality and climate by coupling radiative, microphysical, and aerosol processes in the atmosphere through the reflection, absorption, and emission of radiation as well as the interaction of cloud condensation nuclei (CCN) with the microphysical properties. Additionally, photolysis rates directly influence chemical transformations, and wet deposition by rainout removes pollutants. Even though most of these processes are highly coupled, most modeling systems artificially separate them, or leave some of them out completely.

Clouds span many different scales of motion, starting from shallow convection, deep convection, and larger-scale stable stratiform clouds. Almost all types of clouds require some type of parameterizations, even in the most high-resolution NWP models. The increase in resolution of the models, however, has introduced additional problems for cloud parameterizations. As the grid resolution increases, more and more of the convective clouds can be resolved by the model. The resulting heating and moistening profiles from the microphysics in a cloud resolving model are very different than the tendencies from a convective parameterization. A large part of the parameterized heating and drying tendencies are caused by compensating subsidence. In cloud resolving models the subsidence is caused by explicit vertical motion away from the heat and moisture source from the microphysical parameterization. This scale separation problem is one of the biggest challenges with current NWP and online integrated CW-AQF models. Previously, clouds were commonly classified as (a) large scale stable precipitating clouds, (b) deep convective clouds, and (c) shallow non-precipitating convection. With the increase in resolution (b) are now partially resolved in NWP models. A better classification - which is used in models (Sokhi et al., 2018) - would therefore be:

- (1) Unresolved precipitating convective clouds;
- (2) Resolved precipitating and non-precipitating clouds (microphysical parameterizations);
- (3) Non-precipitating shallow convection.

Classes (1) and (3) require convective parameterizations, (2) and possibly (1) require microphysical parameterizations. The most difficult challenge is usually the parameterization of precipitating convective clouds (1). Additional attention will be given to parameterization of cloud cover, which is a very important parameter for air quality and climate applications, since it links the clouds with the radiation schemes (both atmospheric radiation and photolysis schemes). In Sokhi et al. (2018), different approaches for (1) through (3) are described. While a number of studies focusing on specific aspects of convection are cited in the following sections, the reader is directed to works that provide an overview of convection parameterization for online CW-AQF, meteorological and climate models (e.g., Plant and Yano, 2015; Yano et al., 2015 and references therein).

Mechanisms of interaction of clouds with aerosols and gases are also one of the key components of modern CW-AQF and NWP models. These issues are considered in Section 3.9.

3.4.7 Summary

- Adequate representation of atmospheric PBL processes is crucial for numerical modeling of weather, climate, air pollution, and atmospheric dispersion.
- Development of and requirements to advanced PBL parameterizations in NWP and CW-AQF models are closely connected with advances in computing capability, so should be fit for purpose and for computer possibilities.
- The section considers key PBL processes described or parameterized in meteorological and atmospheric pollution models for CW-AQF.
- Representation of interactions between atmosphere and various Earth surfaces in CW-AQF models requires different schemes of turbulence closure and parameterizations of surface and boundary-layers.
- PBL upper boundary acts as a barrier preventing (or strongly reducing) vertical dispersion in most air quality and dispersion models, so the PBL height is extremely important for CW-AQF modeling.
- Parameterizations of radiation processes, convection and cloud microphysics are also important for CW-AQF.

References

- ARW-WRF (2015): ARW-WRF Weather Forecasting and Research Modeling System Version 3 User's Guide. 2015.
- Baklanov, A., and B. Grisogono, eds. 2007. Atmospheric Boundary Layers: Nature, Theory and Applications to Environmental Modeling and Security. *Boundary- Layer Meteorology* 125: 157– 397.
- Baklanov, A., A. Mahura and R. Sokhi, eds. 2011. Integrated Systems of Meso-Meteorological and Chemical Transport Models. Springer. doi:10.1007/978-3-642-13980-2.
- Baklanov A., K. Schlünzen, P. Suppan, J. Baldasano, D. Brunner, S. Aksoyoglu, G. Carmichael, J. Douros, J. Flemming, R. Forkel, S. Galmarini, M. Gauss, G. Grell, M. Hirtl, S. Joffre, O. Jorba, E. Kaas, M. Kaasik, G. Kallos, X. Kong, U. Korsholm, A. Kurganskiy, T. Rao, N. Savage, C. Seigneur, R. S. Sokhi, E. Solazzo, S. Solomos, B. Sørensen, G. Tsegas, E. Vignati, B. Vogel and Y. Zhang. 2014. 'Online Coupled Regional Meteorology Chemistry Models in Europe: Current Status and Prospects'. *Atmospheric Chemistry and Physics* 14: 317– 98.
- Batchvarova, E., and S. E. Gryning (1994) 'An Applied Model for the Height of the Daytime Mixed Layer and the Entrainment Zone'. *Boundary- Layer Meteorology* 71: 311– 23.
- Blackadar AK (1962) The vertical distribution of wind and turbulent exchange in a neutral atmosphere. *J Geophys Res.* 67: 3095–3102
- Burk, S. D., and W. T. Thompson, 1989. 'A Vertically Nested Regional Numerical Prediction Model with Second- Order Closure Physics'. *Monthly Weather Review* 117: 2305– 24.
- Charnock, H. (1955) 'Wind Stress on a Water Surface'. *Q.J.R. Meteorol. Soc.* 81: 639–640.
- COST-710, 1998: Harmonisation of the pre-processing of meteorological data for atmospheric dispersion models. Final report of COST Action 710. Directorate-General for Research and Innovation, European Commission, ISBN: 92-828-3302-X, 456 p.
- Deardorff, J. W., 1972. Parameterization of the Planetary Boundary Layer for Use in General Circulation Models. *Monthly Weather Review*, 100: 93–106.
- Dupont S., and E. G. Patton. 2012. 'Influence of Stability and Seasonal Canopy Changes on Micrometeorology within and above an Orchard Canopy: The CHATS Experiment'.

Agricultural and Forest Meteorology 157: 11– 29.

- Ekman V.W., 1905-1906: On the influence of the Earth's rotation on ocean currents, *Arkiv Mat. Astron. Fys.*, Uppsala – Stockholm, 2, No.11, 1-52
- Ershadi, A., M. F. McCabe, J. P. Evans, N. W. Chaney and E. F. Wood. 2014. 'Multi- Site Evaluation of Terrestrial Evaporation Models Using FLUXNET Data'. *Agricultural and Forest Meteorology* 187: 46– 61.
- Finnigan, J. 2000. 'Turbulence in Plant Canopies'. *Annu. Rev. Fluid Mech.* 32: 519– 71.
- Foreman, Richard J., and Stefan Emeis. 2010. 'Revisiting the Definition of the Drag Coefficient in the Marine Atmospheric Boundary Layer'. *Journal of Physical Oceanography* 40, no. 10: 2325– 32.
- Garratt, J. R. 1994. *The Atmospheric Boundary Layer*. Cambridge: Cambridge University Press.
- Gayev, Ye.A. and J.C.R. Hunt, 2007: *Flow and transport processes with complex obstructions*. NATO Science Series book, Springer, 414 p.
- Gryning, S.- E., and E. Batchvarova (1990) 'Analytical Model for Growth of the Coastal Internal Boundary Layer during Onshore Flow'. *Quart J Roy Meteorol Soc* 116: 187– 203.
- Gryning, S.- E., E. Batchvarova, M. Quante and V. Matthias 2011. 'Evaluation of Vertical Profiles in Mesoscale Meteorological Models Based on Observations for the COST728 Study of Winter 2003 PM Episodes in Europe'. In *Air Pollution Modeling and Its Application XXI*, edited by D. G. Steyn and S. Trini- Castelli, 499– 503. Dordrecht: Springer.
- Holton, J. R. 2012. *Introduction to Dynamic Meteorology*. 5th ed. Amsterdam, Boston, Heidelberg, London, New York, Oxford, Paris, San Diego, San Francisco, Singapore, Sydney, Tokyo: Elsevier.
- Jimenez, P. A., J. Dudhia, J. F. González-Rouco, J. Navarro, J. P. Montavez and E. Garcia– Bustamante, 2012. 'A Revised Scheme for the WRF Surface Layer Formulation'. *Monthly Weather Review* 140: 898– 918.
- Kolmogorov, A.N., 1941: The local structure of turbulence in incompressible viscous fluid for very large Reynolds numbers. *C. R. Acad. Sci. URSS*, 30:301, 1941.
- Kolmogorov A.N., 1942: Equations of turbulent motion in an incompressible fluid. *Izv. AN SSSR, Ser. Fiz.* 6, No. 1-2, 56-58.
- Kukkonen, J., T. Balk, A. D. M. Schultz, A. Baklanov, T. Klein, A. I. Miranda, A. Monteiro, M. Hirtl, V. Tarvainen. M. Boy, R. Sokhi, K. Lehtinen K. Karatzas R. San José, M. Astitha, G. Kallos, M. Schaap, E. Reimer, H. Jakobs and K. Eben. 2012. 'A Review of Operational, Regional- Scale, Chemical Weather Forecasting Models in Europe'. *Atmospheric Chemistry and Physics*. 01/ 2012; 12, no. (12): 1– 87. <https://doi.org/10.5194/acp-12-1-2012>.
- Mahrt, L. J. 1974. 'Time-Dependent Integrated Planetary Boundary Layer Flow'. *Journal of the Atmospheric Sciences* 31: 457–64.
- Mellor GL, Yamada T (1982) Development of a turbulence closure model for geophysical fluid problems. *Rev Geophys* 20(4):851–875.
- Monin, A. S., and Obukhov, A. M., 1954: Main characteristics of the turbulent mixing in the atmospheric surface layer, *Trudy Geophys. Inst. AN. SSSR*, 24(151), 153-187.
- Pielke, R. A. 2013. *Mesoscale Meteorological Modeling*. 2nd ed. San Diego: Academic Press.
- Plant, R. S., and J.-I. Yano, eds. 2015. *Parameterization of Atmospheric Convection*. Volume 1: Theoretical Background and Formulation. World Scientific, Imperial College Press.
- Quante, M., V. Matthias, S.E. Gryning, E. Batchvarova, A. Aulinger, C. Chemel, G. Geertsema, B. Geyer, H. Jakobs, A. Kerschbaumer, M. Frank, R. San José, H. Schlünzen, J. Struzewska, B. Szintai and R. Wolke . 2009. 'Using Wind profiler Data in Time and Frequency Domain for the Evaluation of Meteorological Drivers Employed in Chemistry Transport Modeling'. *Proceedings: 8th International Symposium on Tropospheric Profiling*. Delft (NL), 18– 23 October 2009 – Delft: RIVM.

- Rossby, C. G. and Montgomery, R. B., 1935: The Layer of Frictional Influence in Wind and Ocean Currents, *Pap. Phys. Oceanogr. Meteorol.* 3(3), 1–101.
- Salby, M. L. 2012. *Physics of the Atmosphere and Climate*. Cambridge: Cambridge University Press.
- Schlünzen, K. H., and J. J. Katzfey, 2003. 'Relevance of Sub- Grid- Scale Land- Use Effects for Mesoscale Models'. *Tellus* 55A: 232– 46. [doi:10.1034/j.1600-0870.2003.00017.x](https://doi.org/10.1034/j.1600-0870.2003.00017.x).
- Seibert, P., Beyrich, F., Gryning, S.-E., Joffre, S., Rasmussen, A., and Tercier, Ph.: 2000, 'Review and Intercomparison of Operational Methods for the Determination of the Mixing Height', *Atmos. Environ.* 34, 1001–1027.
- Smith, B., and L. Mahrt. 1981. 'A Study of Boundary-Layer Pressure Adjustments'. *Journal of the Atmospheric Sciences* 38: 334–46.
- Sokhi, R., Baklanov, A., Schlunzen, H. (Eds), 2018: *Mesoscale Modeling for Meteorological and Air Pollution Applications*. Anthem Press, 376 pp. ISBN-10: 1-78308-826-5.
- Stull, R. B. 1988. *An Introduction to Boundary Layer Meteorology*. Dordrecht: Kluwer Academic Publishers.
- Yano, J.-I., J. F. Geleyn, M. Köller, D. Mironov, J. Quaas, P. M. M. Soares, V. T. J. Phillips et al. 2015. 'Basic Concepts for Convection Parameterization in Weather Forecast and Climate Models: COST Action ES0905 Final Report'. *Atmosphere* 6: 88–147. [doi: 10.3390/atmos6010088](https://doi.org/10.3390/atmos6010088)
- Zhang, Y. 2008. 'Online- Coupled Meteorology and Chemistry Models: History, Current Status, and Outlook'. *Atmospheric Chemistry and Physics* 8: 2895– 2932.
- Zilitinkevich, S.S., 1972: On the determination of the height of the Ekman boundary layer. *Boundary-Layer Meteorol.*, **3**, 141-145.
- Zilitinkevich, S. (2013) *Atmospheric turbulence and planetary Boundary Layers*. Moscow: FIZMATLIT, 252 p., ISBN 978-5-9221-1519-3.
- Zilitinkevich, S.S., 1991: *Turbulent Penetrative Convection*, Avebury Technical, Aldershot, 180 pp.;
- Zilitinkevich S.S., 2012: The Height of the Atmospheric Planetary Boundary layer: State of the Art and New Development – Chapter 13 in "National Security and Human Health Implications of Climate Change", edited by H.J.S. Fernando, Z. Klaić, J.L. McKulley, NATO Science for Peace and Security Series – C: Environmental Security (ISBN 978-94-007-2429-7), Springer, 147-161.
- Zilitinkevich, S. and A. Baklanov, 2002: Calculation of the height of stable boundary layers in practical applications. *Boundary-Layer Meteorology*, 105(3), pp. 389-409.
- Zilitinkevich S.S., and Esau, I.N., 2002: On integral measures of the neutral, barotropic planetary boundary layers. *Boundary-Layer Meteorol.* 104, 371-379.
- Zilitinkevich, S., Esau, I. and Baklanov, A., 2007: Further comments on the equilibrium height of neutral and stable planetary boundary layers. *Quart. J. Roy. Met. Soc.* 133, 265-271.
- Zilitinkevich, S.S., Elperin, T., Kleeorin, N., and Rogachevskii, I., 2007: Energy- and flux-budget (EFB) turbulence closure model for the stably stratified flows. Part I: Steady-state, homogeneous regimes. *Boundary-Layer Meteorol.* **125**, 167-192.
- Zilitinkevich, S.S., Elperin, T., Kleeorin, N., L'vov, V., and Rogachevskii, I., 2009: Energy- and flux-budget (EFB) turbulence closure model for stably stratified flows. Part II: The role of internal gravity waves. *Boundary-Layer Meteorol.* 133, 139-164.
- Zilitinkevich, S.S., Elperin, T., Kleeorin, N. et al. (2013) A hierarchy of energy- and flux-budget (EFB) turbulence closure models for stably stratified geophysical flows. *Boundary-Layer Meteorol.* 146: 341. <https://doi.org/10.1007/s10546-012-9768-8>.
- Zubov N.N., 1945: "Arctic ice", Glavsevmorput, Moscow, 360 pp.

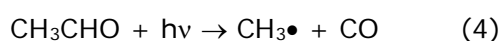
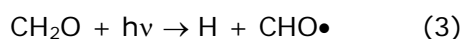
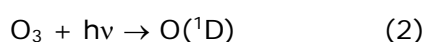
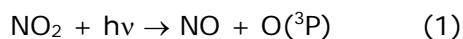
3.5 Atmospheric Chemistry

3.5.1 Introduction

Atmospheric chemistry is important because it affects the production, loss and concentrations of ozone (O₃), particulate matter (PM), atmospheric acids and other air pollutants. Important chemistry occurs in the gas-phase, aqueous-phase and heterogeneously (multiple phases are involved). Much of the gas-phase chemistry involves the oxidation of nitrogen oxides (NO_x = NO + NO₂) and volatile organic compounds (VOCs). Gas-phase chemistry plays a key role in determining the lifetime and distribution of O₃, hydrogen peroxide (H₂O₂) and other oxidants. Other gas-phase oxidants include the hydroxyl radical (HO) and the hydroperoxyl radical (HO₂); intermediates that are collectively known as odd hydrogen (HO_x). The gas-phase reactions that produce O₃, H₂O₂ and inorganic aerosols are linked to the chemistry that occurs in the aqueous and heterogeneous phases. HO reacts with NO₂ and SO₂ to produce nitric acid and sulfuric acid which both react with ammonia (NH₃) to produce ammonium nitrate, ammonium bisulfate and ammonium sulfate. Sulfuric acid, ammonium nitrate, ammonium bisulfate and ammonium sulfate are constituents of secondary inorganic aerosols. The gas-phase reactions of HO_x with VOCs may lead to the formation of secondary organic aerosol (SOA). Different gas-phase chemical mechanisms may lead to different predictions of gases, aerosols, and the resulting aerosol direct and indirect effects that will in turn affect the radiation, cloud and precipitation formation, as well as climate. Aqueous-phase chemistry can occur in various hydrometeors such as cloud, rain, and fog droplets following the dissolution of gas-phase species. Heterogeneous reactions involving two or more phases such as gas and aqueous-phase or solid phase may also occur at the surface of fog or cloud droplets and aerosol particles. Similar to gas-phase reactions, aqueous-phase and heterogeneous reactions can produce or consume the mass of a chemical species, therefore affecting their atmospheric concentrations and lifetimes. Many of these reactions also produce acids that result in acidic precipitation and acid deposition (Calvert et al., 2015; Seinfeld and Pandis, 2016). The aqueous-phase production of acids on cloud water droplets and aerosol particles adds mass to particles but it does not create new particles (Calvert et al., 2015). In this Section, the fundamentals of atmospheric gas-phase, aqueous-phase, and heterogeneous chemical reactions are introduced. Major gas-phase, aqueous-phase, and heterogeneous chemical mechanisms that are most commonly used in CW-AQF models are described.

3.5.2 Gas-Phase Chemistry Related to Tropospheric Ozone and Particulate Matter Formation

The photolysis of nitrogen dioxide, ozone, formaldehyde and other aldehydes are major causes of photochemical air pollution in urban regions (Gao et al., 1995; Calvert et al., 2015). Four of the most important reactions are given below:



In these reactions the symbol $h\nu$ indicates that the reaction is photochemical; NO₂ is nitrogen dioxide; NO is nitric oxide; O(³P) is a ground state oxygen atom, O₃ is ozone, O(¹D) is an energetically excited oxygen atom; CH₂O (or HCHO) is formaldehyde; H is a hydrogen atom; CHO• is a formyl radical; CH₃CHO is acetaldehyde; CH₃• is a methyl radical and CO is carbon monoxide. The formyl radical and the methyl radical are examples of free radicals and these react rapidly with atmospheric molecular oxygen (O₂) as discussed below (Calvert et al., 2015) to produce CH₂O and CH₃O₂. Also, the H atom combines quickly with O₂ to form the HO₂ radical.

One of the most important factors in determining the importance of an atmospheric reaction is its rate. The calculation of reaction rates is very necessary in air quality models to forecast air quality. The rate of a photolysis reaction, $\frac{d[X]}{dt}$, is given by the concentration of the photolyzing compound, $[X]$ and the reaction's photolysis frequency, J , as shown below (Kim et al., 2007),

$$\frac{d[X]}{dt} = J[X] \quad (5)$$

The unit of J is reciprocal time such as s^{-1} , and therefore, $\frac{d[X]}{dt}$, is in units of concentration per unit of time, such as molecules s^{-1} .

Radiation transfer models are used to estimate photolysis frequencies for air quality modeling (Madronich, 1987). A photolysis frequency at any point in the atmosphere is determined by the flux of photons entering an infinitesimal sphere surrounding the point and by two sets of molecular properties: absorption cross-sections and quantum yields. Briefly, photons must be available, they must be absorbed, and they react following the probability of the process.

The photon flux, absorption cross-sections and quantum yields are all wavelength-dependent. The equation given below is used to calculate photolysis frequencies and it is integrated between the wavelength limits of the available photon flux, λ_1 to λ_2 ,

$$J = \int_{\lambda_1}^{\lambda_2} I(\lambda) \times \sigma(\lambda, T, P) \times \phi(\lambda, T) d\lambda \quad (6)$$

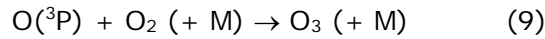
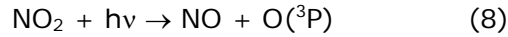
This photon flux is commonly known as spectrally resolved solar actinic flux or more simply, actinic flux and it is defined by the following equation (Madronich, 1987; Kim et al., 2007),

$$I(\lambda) = \int_{\omega} L(\lambda, \theta, \varphi) d\omega \quad (7)$$

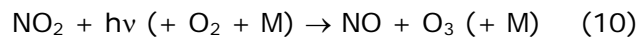
where $L(\lambda, \theta, \varphi)$ is the solar radiance at wavelength λ , θ is the angle between the incident solar beam and a line normal to the surface and φ is the azimuth angle. The integral of the solar radiance is integrated over a spherical solid angle, $\omega = 4\pi$. Photolysis frequencies depend only on the absorption of photons by a molecule and not on their specific path. The solar radiation entering Earth's atmosphere is known as the extraterrestrial flux. Absorption and scattering by atmospheric gases, clouds, and other PM impact the downward and upward welling components of the solar radiance. For example, the absorption of radiation by ozone prevents highly energetic radiation from reaching Earth's surface. At Earth's surface there is very little radiation below 300 nm (Calvert et al., 2015). Another important component of upward welling components is the reflection of solar radiation from Earth's surface and this is strongly affected by the surface albedo. The surface albedo varies greatly depending on location. For example, it is very high (i.e., close to 1) for snow covered surfaces and very low (close to 0) for dark sooty surfaces (Madronich, 1987). A typical unit of actinic flux is photons cm^{-2} , s^{-1} , nm^{-1} where nm^{-1} is the spectral resolution of the flux.

Absorption cross-sections and quantum yields are obtained from laboratory measurements. The absorption cross-section is the absorption spectrum of a gas (with absorption defined in terms of natural logarithms) given in units of area such as cm^2 . Absorption cross-sections are wavelength-dependent and, for some gases, absorption cross-sections are pressure- and temperature-dependent, $\sigma(\lambda, T, P)$. The quantum yield is the probability that a gas will react through a specified process following the absorption of a photon, $\phi(\lambda, T)$, it is wavelength-dependent and it is dimensionless. Quantum yields may be temperature-dependent. The relative importance of a photolysis pathway depends on the wavelength of the absorbed radiation. For example, formaldehyde has two different photolysis reactions; one that produces radicals and another that produces the molecular products CO and molecular hydrogen (H_2). At some wavelengths the radical producing path is the dominant reaction pathway while at others the molecular product producing pathway is dominant.

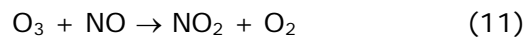
Prognostic air quality models must utilize chemical mechanisms for ozone and PM. Photolysis of NO_2 by ultraviolet radiation from the sun is the major source of ozone in the lower troposphere (Stockwell et al., 2012; Calvert et al., 2015). The photolysis of NO_2 produces NO and $\text{O}(^3\text{P})$ that reacts with O_2 to yield O_3 . The overall process is pressure dependent because a third molecule (M) such as N_2 or O_2 is required to stabilize the formation of O_3 by carrying away excess energy from the collision that produces O_3 . These processes are represented by reactions 8 and 9,



Reaction 9 is very fast due to the high oxygen concentration in the troposphere, therefore, reactions 8 and 9 may be combined to give reaction 10 as the overall reaction,



These reactions alone are insufficient to produce much O_3 in the troposphere because NO reacts with O_3 to reproduce NO_2 and O_2 . Additional chemistry that leads to the conversion of NO to NO_2 is required to produce high O_3 concentrations,



Because of the relationship between NO and NO_2 the total sum of their concentrations is referred to as NO_x and it will be seen that NO_x can be considered as a catalyst for tropospheric ozone production.

Suppose the rate of O_3 formation by reaction 10 is equal to its destruction rate by reaction 11. The following equation may be written,

$$J_{\text{NO}_2}[\text{NO}_2] = k[\text{O}_3][\text{NO}] \quad (12)$$

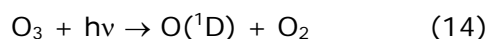
where J_{NO_2} is the photolysis frequency of NO_2 , $[\text{NO}_2]$ is the concentration of NO_2 , k is the rate coefficient of reaction 11, $[\text{O}_3]$ is the concentration of O_3 and $[\text{NO}]$ is the concentration of NO. Rearranging reaction 5 yields the ozone photo-stationary state equation (e.g., Stockwell et al., 2012),

$$[\text{O}_3] = \frac{J_{\text{NO}_2} [\text{NO}_2]}{k [\text{NO}]} \quad (13)$$

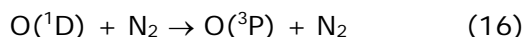
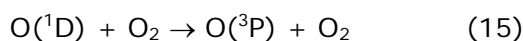
Equation 13 is an approximation, but it provides important insights into tropospheric ozone production. The O_3 concentration is directly related to J_{NO_2} . J_{NO_2} is related to solar radiation. Higher O_3 concentrations are related to higher rates of NO_2 photolysis and this increases with higher levels of solar radiation flux. The O_3 concentration is also related to the concentration ratio of NO_2 to NO. Chemical processes that convert NO to NO_2 produce greater O_3 concentrations. This occurs because greater NO_2 concentrations increase the rate of production by reaction 10 and lower NO concentrations decrease its destruction rate by reaction 11. This chemistry involves NO_x , HO, VOCs, and peroxy radicals (Stockwell et al., 2012; Calvert et al., 2015).

The hydroxyl radical is produced during the daytime by the photolysis of ozone, CH_2O and subsequent reactions of their reaction products (Stockwell et al., 2012; Calvert et al., 2015). Additionally, some HO is produced through the photolysis of nitrous acid (HONO) during the early morning hours. Some HO is produced during the day and night-time by reactions of ozone with alkenes.

One of the photolysis reactions of O_3 produces an excited oxygen atom, $\text{O}(^1\text{D})$,



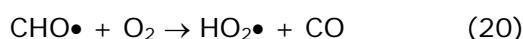
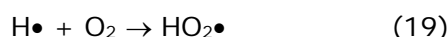
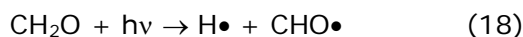
Most of the excited oxygen atoms collide with O₂, N₂ and other air molecules to lose energy to become ground state oxygen atoms that react to reproduce O₃ by reactions 15 and 16,



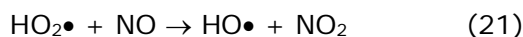
A few of the excited oxygen atoms react with water vapor to produce HO,



Photolysis of CH₂O also leads to the production of HO. There are two photolysis reactions of CH₂O; one of these reactions produces atomic hydrogen and a CHO radical. Both react with O₂ to produce the hydroperoxy radical (HO₂) (Calvert et al., 2015),

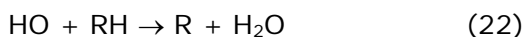


The hydroperoxy radical reacts with NO to convert it to NO₂ and to produce HO (Calvert et al., 2015),

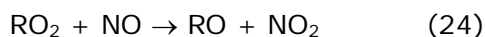


Reaction 21 is very important because it converts large amounts of NO to NO₂ that produces O₃ while also producing HO.

Hydroxyl radicals react with VOCs (also referred to as reactive hydrocarbons (RH)) to produce organic peroxy radicals (RO₂), reactions 22 and 23. For hydrocarbons R represents an alkyl radical that reacts to produce an organic peroxy radical.



Organic peroxy radicals react with NO to convert it to NO₂ and in the case of hydrocarbons an alkoxy radical (RO) is produced,

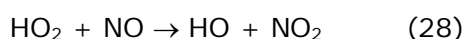
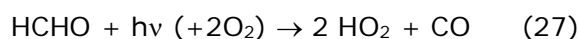
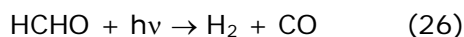


These reactions increase NO₂ concentrations and increase the rate of O₃ production through photolysis. Lower NO concentrations result in lower rates of O₃ loss through reaction 11. The resulting increase in the rate of O₃ production and the reduced rate of O₃ loss results in increases in O₃ concentrations. Therefore, O₃ concentrations depend very strongly on both NO_x and VOCs (Stockwell et al., 2012).

The RO may react with O₂ to produce carbonyl-containing compounds such as aldehydes (compounds with an HCO group) or ketones (compounds with a CO group). In reaction 25 these compounds are represented by CARBONYL,



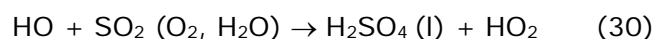
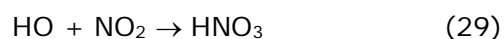
Aldehyde and ketones react further with HO or photolyse to produce additional peroxy radicals that lead to the production of O₃. For example, one of the photolysis reactions of formaldehyde produces hydroperoxy radicals that convert NO to NO₂,



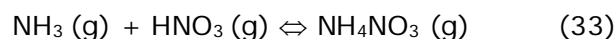
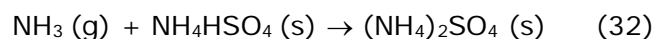
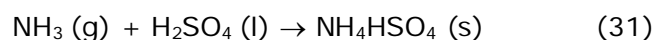
Higher molecular VOC may have much more complicated reaction mechanisms that include rearrangements, fragmentation and the formation of organic nitrates that occur in the oxidation reactions of high molecular weight organic compounds (Calvert et al., 2015). The overall tropospheric production of O₃ is a chain mechanism where HO radicals are produced and react with VOCs to produce organic peroxy radicals and the hydroperoxy radical. The peroxy radicals convert NO to NO₂ and reproduce HO radicals. The produced NO₂ photolyses to produce more ozone. Different organic compounds have different degradation mechanisms where each VOC produces different numbers of NO to NO₂ conversions and so each organic compound produces different amounts of ozone. Table 3.7 shows some of the most important gas-phase reactions that affect ozone concentrations.

3.5.3 *The Relationship Between Gas-Phase Chemistry and Particulate Matter Production*

Chemical reactions involving NO_x and VOCs produce low vapor products that condense to form secondary PM_{2.5} (Saunders, 2017; Stewart, 2017). Reactions of NO_x and VOCs lead to the production of O₃ and HO radicals. The HO radicals initiate reactions with NO₂, SO₂, and VOCs to produce PM_{2.5}. HO reacts with NO₂ and SO₂ to produce nitric acid (HNO₃) and sulfuric acid (H₂SO₄) that react with atmospheric ammonia (NH₃) to produce chemical components contributing to PM_{2.5},



Note that the H₂SO₄ produced by reaction 30 immediately condenses into a liquid aerosol. Ammonium bisulfate (NH₄HSO₄), ammonium sulfate ((NH₄)₂SO₄) and ammonium nitrate (NH₄NO₃) aerosol particles are formed when ammonia reacts with HNO₃ and H₂SO₄ through reactions 31 – 34,



where reactions (31) - (33) are heterogeneous reactions involving two different phases and ⇌ indicates a chemical equilibrium. The extent of the reactions that produce aerosol particles consisting of NH₄HSO₄, (NH₄)₂SO₄, and NH₄NO₃ depends on the relative concentrations of HNO₃, H₂SO₄ and NH₃, relative humidity, and temperature (Kim et al., 1993a, b; Kim and Seinfeld, 1995; Kuhns et al., 2003). No NH₄NO₃ is formed until almost all of the available sulfate (SO₄) reacts (Seinfeld and Pandis, 2016). When NH₄NO₃ is formed its partitioning between the gas and solid aerosol phases is a function of temperature and relative humidity. Cooler temperatures and higher humidity favor the partitioning of NH₄NO₃ to the solid aerosol-phase (Kim et al., 1993a, b; Kim and Seinfeld, 1995). Therefore, the season for high aerosol concentrations occurs during late fall and early for urban regions, such as Los Angeles.

Table 3.7 A summary of highly significant reactions that affect ozone concentrations over a range of polluted conditions

Full results are presented in Gao et al. (1995) and Calvert et al. (2015). The order represents the relative importance of the reaction or process.

Relative Importance	Reaction
1.	Xylene + HO → RO ₂ + products
2.	HO + NO ₂ (+ O ₂) → HNO ₃
3.	NO ₂ + hv → O ₃ + NO
4.	O ₃ + NO → NO ₂ + O ₂
5.	CH ₂ O + hv (+ 2 O ₂) → 2 HO ₂ + CO
6.	RO ₂ (from primary alkenes) + NO → NO ₂ + products
7.	RO ₂ (from xylene) + NO → NO ₂ + products
8.	CH ₃ CO ₃ + NO → NO ₂ + CH ₃ O ₂ + CO ₂
9.	CH ₃ CO ₃ + NO ₂ → PAN
10.	RO ₂ (from ethene) + NO → NO ₂ + products
11.	DCB (dicarbonyl compounds from aromatic oxidation) + hv → RO ₂
12.	PAN → CH ₃ CO ₃ + NO ₂
13.	HO + CO (+ O ₂) → HO ₂ + CO ₂
14.	HO ₂ + NO → HO + NO ₂
15.	O ₃ + hv → O(¹ D) + O ₂
16.	O(¹ D) + H ₂ O → 2 HO
17.	RO ₂ (from alkanes) + NO → NO ₂ + products

The reactions of HO with higher molecular VOCs lead to the production of highly oxygenated organic compounds with low vapor pressure that condense to produce SOA (Donahue et al., 2006; Zhang et al., 2007; de Gouw et al., 2008; Lee-Taylor et al., 2011). These VOCs are oxidized through reactions that are the same or similar to those that produce O₃ by converting NO to NO₂, reactions 22 – 25 (Lee-Taylor et al., 2011). Additional oxidation of alkenes may occur through ozonolysis or additional reactions with nitrate radical (NO₃) to the alkene's double bonds. High molecular weight VOCs may undergo multiple oxidation cycles that produce oxygenated compounds with high molecular weights and low vapor pressures (Fuentes et al., 2000).

SOA consists of many organic compounds (Ketseridis et al., 1976; Middlebrook et al., 1998; Hamilton et al., 2004; Lee-Taylor et al., 2011) and measurements show that a large fraction of SOA are composed of organic compounds with more than six carbon atoms (Volkamer et al., 2006; Hallquist et al., 2009; Hodzic et al., 2010a, b; Virtanen et al., 2010; Lee-Taylor et al., 2011; Zhang et al., 2013). Higher molecular weight VOCs with greater numbers of carbon atoms (C₁₁ to C₂₅) are important precursors for the formation of SOA. These VOCs are emitted by anthropogenic and biogenic sources (Heisler and Friedlander, 1977; Pandis et al., 1991, 1992; Turpin et al., 1991; Griffin et al., 1999; Aumont et al., 2000; Claeys et al., 2004; Goldstein and Galbally, 2007; de Gouw and Jimenez, 2009; Lee-Taylor et al., 2011). Many of the compounds emitted from biogenic sources are alkenes (Fuentes et al., 2000). There remains much to be learned about this organic chemistry and more detailed treatment of the chemistry and vapor pressure of products improves model performance for SOA (Lee-Taylor et al., 2011).

Meteorology is another very important factor that affects the concentrations of O₃ and PM (Calvert et al., 2015). Summer days that are warm, clear and with calm winds are associated with stagnant high-pressure conditions and absence of cloudiness. On these days NO_x and VOC concentrations rise in a polluted urban atmosphere and the resulting photochemistry increases O₃ concentrations. On the other hand, cool fall days are associated with low mixing heights and cooler temperatures promote the condensation of ammonium nitrate particles from gas-phase ammonia and nitric acid (Kim et al., 1993a, b; Kim and Seinfeld, 1995; Kuhns et al., 2003) and these conditions can cause dangerously high concentrations of PM. High O₃ and PM days are associated with health effects that are observed particularly in sensitive populations. Therefore, air quality modeling systems that combine meteorology, emission source modeling, and atmospheric chemistry are used to predict the concentrations of air pollutants that include ozone, and particulate matter (Stockwell et al., 2012).

3.5.4 Gas-Phase Chemistry Mechanisms for Air Quality Modeling

The treatment of organic compounds is the major difference between the gas-phase chemical mechanisms used for air quality forecasting. Millions of reactions and chemical species would be required to completely describe the gas-phase organic chemistry of the atmosphere. Therefore, aggregated mechanisms are used where groups of similar chemical compounds are aggregated into the model species. Table 3.8 lists some of the available gas-phase mechanisms for air quality forecasting. Using a box model, Knote et al. (2014) intercompared seven gas-phase mechanisms that are commonly used in 3-D CW-AQF models including CB05Cix, CB05-TUL, CBM-Z, RADM2, RADMK, RACM-ESRL, and MOZART-4.

They reported differences in predicted O₃, HO₂, HO, NO_x, PAN, and CH₂O are 4 ppbv (by 5%), 20%, 40%, 25%, 50%, and 20%, respectively, among all selected mechanisms. Largest differences (by 100%) are found for major species involved in the night-time chemistry such as NO₃ and N₂O₅ and BVOCs such as isoprene. These results indicate that the choice of gas-phase mechanism introduces non-negligible uncertainty in not only the gas-phase concentrations of gaseous and radical species, but also the concentrations of secondary aerosol species.

Several most commonly-used gas-phase mechanisms are described below.

3.5.4.1 Carbon Bond Mechanisms

The Carbon Bond series of mechanisms was based on a very innovative approach to the treatment of atmospheric chemistry of the polluted urban atmosphere (Whitten et al., 1980; Whitten et al., 1999). The Carbon Bond Mechanism series began with an aggregated-structure approach where model species represent concentrations of constituent molecular groups regardless of the molecule to which they are attached.

For example, the hundreds of organic compounds consisting of only hydrogen and carbon atoms, linked together by single bonds (alkanes), might be grouped into the model species PAR. Among the species included in the Carbon Bond Mechanism are PAR (alkane carbon atoms), OLE (double bonded carbon atoms), ARO (aromatic rings) and CAR (carbonyl group). As a further example, imagine that there is a mixture that consists of 1.0 ppmV of butane (CH₃CH₂CH₂CH₃) and 1.0 ppmV of propene (CH₃HC=CH₂). The butane is represented by 4.0 ppmC PAR and the propene is represented by 1.0 ppmC PAR and 1.0 ppmC OLE so the mixture is represented as a total of 5.0 ppmC PAR and 1.0 ppmC of OLE. The original Carbon Bond approach had several advantages that include its relative ease in grouping emissions into model species, the conservation of carbon atoms and the relatively low number of chemical species required to represent atmospheric organic chemistry.

Although the Carbon Bond results in forecasts that are less accurate than other mechanisms (Sarwar et al., 2013), the Carbon Bond is popular among air pollution meteorologists because of its relative ease of use and its lower demands on computational resources due to its relatively small size, resulting in comparatively faster model execution times.

Table 3.8 Gas-phase chemical mechanisms used in 3-D air quality models (modified from Baklanov et al., 2014)

The symbol + indicates that the information was not apparent from the mechanism description.

No.	Mechanism	Number of Chemical Species	Number of Chemical Reactions	Number of Photochemical Reactions	Number of Heterogeneous Reactions	Aqueous Chemistry	Model(s)	Reference
1	ADOM-IIb	50	100	+	NA	NA	GEM	Venkatram et al. (1988)
2	CACM	189	349	+	NA	NA	Meso-NH, CMAQ-MADRID	Griffin et al. (2002)
3	CBM-IV/CB4	33	70	11	NA	NA	NMMB/BSC-CTM, BOLCHEM, RACMO2/LOTOS-EUROS, WRF-Chem	Gery et al. (1989)
4	CBM-05/CB05	52	133	23	NA	NA	NMMB/BSC-CTM, WRF-CMAQ, C-IFS, CAMx	Sarwar et al. (2008)
5	CBM-Z	55-56	156	+	NA	NA	RegCM-Chem, WRF-Chem	Zaveri and Peters (1999)
6	CB06	77	190	28	NA	NA	CAMx	Yarwood et al. (2010)
7	GACM	107	352	41	NA	NA	WRF-Chem	Saunders (2017)
8	GEOS-CHEM	80	>300	+	N ₂ O ₅ & NO ₃ → HNO ₃ in sulfate	NA	RegCM-Chem	Bey et al. (2001)
9	CRIMech	240	652	+	NA	NA	WRF-Chem	Watson et al. (2008)
10	EMEP-EmChem09	69	137	26	NA	NA	EMEP MSC-W	Simpson et al. (2012)
11	MECCA1	116	295	+	NA	NA	MESSy(ECHAM5)	Sander et al. (2005)
12	MELCHIOR1	87	>300	+	HONO formation from deposition of NO ₂ on wet surfaces	NA	MELCHIOR	Lattuati (1997)

No.	Mechanism	Number of Chemical Species	Number of Chemical Reactions	Number of Photochemical Reactions	Number of Heterogeneous Reactions	Aqueous Chemistry	Model(s)	Reference
13	MELCHIOR2	<87	~120	+	HONO formation from deposition of NO ₂ on wet surfaces	NA	MELCHIOR	Derognat et al. (2003)
14	MOZART2	63	132	32	N ₂ O ₅ & NO ₃ on sulfate	NA	ECHAM5/6-HAMMOZ	Horowitz et al. (2003)
15	MOZART3	108	218	18	71	NA	IFS-MOZART	Kinnison et al. (2007)
16	MOZART4	85	157	39	4	NA	ECHAM5/6-HAMMOZ, WRF-Chem	Emmons et al (2010)
17	NWP-Chem	17-28	27-32	4	NA	17	Enviro-HIRLAM v1	Korsholm et al. (2008)
18	RADMK	86	171	22	1	NA	COSMO-ART	Vogel et al. (2008, 2009)
19	RADM2	63	136	21	NA	NA	MCCM, M-SYS, REMO, WRF-Chem, M-SYS	Stockwell et al. (1990)
20	RACM	77	214	23	NA	NA	COSMO-LM-MUSCAT, MCCM, Meso- NH, RegCM-Chem, MEMO/MARS, WRF- Chem	Stockwell et al. (1997)
21	RACM2	119	321	42	NA	NA	CMAQ, WRF-Chem, Polair3D	Goliff et al. (2013)
22	RACM-MIM	84	221	23	NA	NA	MCCM, WRF-Chem	Geiger et al. (2003)
23	RAQ (plus CLASSIC)	61	115	23	NA	SO ₂ Oxidation by H ₂ O ₂ & O ₃	MetUM	Collins et al. (1997; 1999)
24	ReLACS	37	128	+	NA	NA	Meso-NH	Crassier et al. (2000)
25	ReLACS2	82	343	+	NA	NA	Meso-NH	Tulet et al. (2006)

No.	Mechanism	Number of Chemical Species	Number of Chemical Reactions	Number of Photochemical Reactions	Number of Heterogeneous Reactions	Aqueous Chemistry	Model(s)	Reference
26	ReLACS-AQ	41	128	+	NA	Detailed Aq. phase chemistry	Meso-NH	Crassier et al. (2000), Leriche et al. (2013)
27	SAPRC90 SOA	43	131	16	NA	NA	BOLCHEM	Carter (1990)
28	SAPRC99	72	182	35	NA	NA	RAMS/ICLAMS, CMAQ, CAMx, WRF-Chem	Carter (2000)
29	SAPRC07	44-207	126-640	+	NA	NA	CMAQ, CHIMERE	Carter (2010)
30	StdTrop (plus CLASSIC)	42	96	25	NA	SO ₂ Oxidation by H ₂ O ₂ & O ₃	MetUM	Law et al. (1998)

More recent versions of the Carbon Bond Mechanism rely less on the original Carbon Bond approach and more on an aggregated-structure approach because constituent groups on the same molecule and the total molecular weight strongly affect atmospheric chemistry (Gery et al., 1989; Yarwood et al., 2005a, b). In the Aggregated Molecule Approach similar chemical compounds are aggregated into grouped model species. Although the Carbon Bond Mechanisms work reasonably well for ozone, a mechanism with a pure aggregated-structure approach cannot model the formation of secondary aerosol well because of the importance of the molecular weight of an organic compound in determining its vapor pressure. However, minor modifications to recent versions of the Carbon Bond Mechanism allow them to estimate secondary organic aerosol concentrations very similar to those of more complex mechanisms (Kim et al., 2011).

Three specific carbon bond mechanisms are discussed in modeling scenarios below. These include the Carbon Bond Mechanism (CBM-Z), the Carbon Bond Mechanism, Version 5 (CB05) and the Carbon Bond Mechanism, Version 6 (CB06).

- CBM-Z with the Computationally Rapid Radical Balance Method (RBM)

CBM-Z was developed by Zaveri and Peters (1999) and it is based on the Carbon Bond Mechanism version 4 (CB04; Gery et al., 1989). CB04 was originally designed for the modeling of highly polluted urban regions. CBM-Z was designed to be computationally faster than other mechanisms while applying to larger spatial regions and longer timescales that are necessary if it is to be used to model regional domains. Regional domains include areas with lower levels of emissions and lower concentrations of nitrogen oxides. Therefore CBM-Z has more detailed chemistry than CB04 that includes revised inorganic chemistry and explicit treatment of less reactive organic compounds, such as methane and ethane. Compared to CB04, CBM-Z includes improved parameterizations of alkenes, aromatics, isoprene (a biogenically emitted compound). CBM-Z includes a more detailed treatment of the interactions of organic chemistry with nitrogen compounds such as nitrate radical and it includes the formation of organic nitrates.

CBM-Z simulations were compared with simulations made with CB04 and another regional scale mechanism, the Regional Acid Deposition Mechanism, version 2 (RADM2; Stockwell et al., 1990). The simulations were made for a period of thirty simulated days for a number of hypothetical urban and rural scenarios. CBM-Z and RADM2 mechanisms produced results that were within 20% of each other while there were significant differences between CBM-Z and CB04. The simulations made with CBM-Z required somewhat less computational time than those made with RADM2. The computationally rapid Radical Balance Method (RBM; Sillman, 1991) has been used in air quality models with the CBM-Z mechanism to reduce the computational time required for air quality model simulations (i.e., Shalaby et al., 2012).

- CB05 and CB06

CB05 (Yarwood, et al., 2005a) was developed from the earlier CB04 (Gery et al., 1989) as corrected by Milford et al. (1995) and its more recent updates (Yarwood, et al., 2005b). CB05 included updated rate coefficients. More significantly, although CB04 was focused on urban regions, CB05 was designed to apply to conditions ranging from urban to remote. This means that CB05 may be used in models to simulate air quality over the regional scale. This required several important additions to CB04 to develop CB05. The standard CB05 mechanism is composed of 51 model species and 156 reactions. The mechanism was evaluated by comparing its simulation with environmental chamber data obtained from the University of North Carolina and the University of California at Riverside.

In order to extend the Carbon Bond Mechanism to a wider range of atmospheric conditions a number of inorganic reactions were added (Yarwood et al., 2005a). Similar to CBM-Z, explicit methane and ethane organic chemistry is included in CB05. Explicit treatment of the methylperoxy radical was included to allow CB05 to better characterize lower nitrogen oxide concentration conditions. Treatment of more reactive organic compounds was improved also in CB05. A more detailed treatment of alkenes with an internal double bond (of the form: R-HC=CH-R) was added along with an aggregated species for terpene and similar biogenically

emitted compounds. CB05 includes reactions that produce oxygenated products such as aggregated higher organic peroxides, formic acid, and organic acids that may enter the aqueous-phase and react there.

CB05 includes more explicit treatments of acetaldehyde and an aggregated species for aldehydes with higher molecular weights than acetaldehyde (Yarwood et al., 2005a). CB05 includes peroxyacetyl nitrate (PAN) and a higher molecular weight analog (PANX). PAN and PANX are formed from acetaldehyde and higher molecular weight aldehydes, respectively, and nitrogen oxides. Additional reactions were added to account for the recycling of nitrogen oxides. PAN, PANX, and the nitrogen oxides recycling reactions are critical for simulating polluted air masses over long-distances (Real et al., 2010).

There are two extensions available for CB05 (Yarwood, et al., 2005a). One extension is a set of reactions that allows the simulation of the effects of reactive chlorine chemistry on air quality. Chlorine chemistry affects ozone formation and the decomposition of organic compounds. It is expected that chlorine chemistry will be most important around oceanic coasts. The other is a set of more explicit reactions that allows CB05 to simulate air-toxics and precursors to SOA.

CB06 is an update and further extension of CB05. CB06 includes explicit chemistry for propane, benzene, acetone and other ketones to better simulate ozone over the regional spatial scale. Explicit chemistry for acetylene, benzene glyoxal, glycolaldehyde and methylglyoxal were added to allow the mechanism to better represent precursors for SOA formation. The carbon bond series of mechanisms are well suited for the modeling of O₃. However, if the forecaster's goal is to model SOA, the use of chemical mechanisms that have a more explicit treatment of VOC should be carefully considered.

3.5.4.2 *The Regional Acid Deposition Model and Regional Atmospheric Chemistry Family of Mechanisms*

The family of gas-phase mechanisms includes the Regional Acid Deposition Model mechanism, version 2 (RADM2; Stockwell et al., 1990; Middleton et al., 1990), the Regional Atmospheric Chemical Mechanism, version 1 (RACM1; Stockwell et al., 1997), the Regional Atmospheric Chemical Mechanism, version 2 (RACM2; Goliff et al., 2013), and the Global Atmospheric Chemistry Mechanism (GACM; Saunders, 2017). These mechanisms use the aggregated molecule approach to aggregate chemical species into model species. In the aggregated molecule approach similar chemical compounds are aggregated into a grouped model species. For example, the model species "ALD" could represent all aldehydes while "PRO" might represent propane and all less reactive alkanes. Weighting factors to account for differences in chemical reactivity or carbon mass have been applied within molecular aggregation schemes (e.g., (Stockwell et al., 1990). The RADM/RACM family of mechanisms was designed from the beginning to model both regional and urban regions while GACM is an extension of RACM2 for the modeling of global atmospheric chemistry (RACM2; Goliff et al., 2013; Saunders, 2017). These mechanisms were designed to model a wider range of pollutant concentrations than the original Carbon Bond and SAPRC mechanisms. Another overall guiding design goal of the RADM/RACM family of mechanisms is to supply a mechanism that is a little more detailed than SAPRC and the Carbon Bond mechanism families that may be used efficiently in 3-D chemical transport models.

Regional domains include locations where NO_x concentrations are lower and where more slowly reacting organic compounds have greater effects than in urban areas. When the concentrations of NO become lower over suburban and rural areas and aloft the reactions of peroxy radicals with each other become more important. The reactions of RO₂ with HO₂, the reactions of RO₂ with the methylperoxy radical (CH₃O₂), and the reactions of RO₂ with acyl peroxy radicals (RCO₃) become increasingly important as NO concentrations and these peroxy-radical with peroxy-radical reactions produce organic peroxides. It was important to include these reactions in the mechanism for an acid deposition model because hydrogen peroxide and organic peroxides react in the aqueous phase to oxidize sulfur dioxide to sulfate. The peroxy-radical with peroxy-radical reactions have some influence on ozone concentrations so they need to be included in a regional model. It is noted that the treatment of regional conditions was added to more recent versions of the SAPRC and Carbon Bond mechanisms.

Two specific RADM mechanisms and three specific RACM mechanisms are discussed below. These include RADM1 and RADM2, RACM1 and RACM2, and GACM.

- RADM1 and RADM2

The RADM mechanisms were designed to represent the chemistry required to model the gas-phase formation of acids and to provide oxidants of sulfur dioxide, such as hydrogen peroxide, to the aqueous-phase modules (Stockwell, 1986; Stockwell et al., 1990). Their application to the regional scale required that the RADM mechanisms simulate everything from highly polluted conditions through much cleaner, remote conditions. At the time the first RADM mechanism was developed the carbon bond and SAPRC were designed to simulate surface-level, urban conditions such as those that occur over Los Angeles and similar cities. They were not designed to simulate cleaner atmospheric conditions. For example, in SAPRC all organic peroxy radicals decomposed to give the same products as their reactions with nitric oxide and there was little treatment of other organic peroxy radicals' reactions. At that time, during the 1980s, these mechanisms included only very superficial operator approaches to treat the reactions of organic peroxy radicals. The RACM mechanisms have always included an explicit but reduced set of reactions to treat the reactions of organic peroxy radicals.

The number of primary emitted compounds that were explicitly included in the available emissions inventory was limited (Middleton et al., 1990). For this reason, the organic chemistry in RADM1 was limited to the organic compound emissions in the inventory. This limited organic chemistry RADM1 made it desirable to develop a mechanism with a more comprehensive treatment of the organic chemistry and the new mechanism was RADM2 (Stockwell et al., 1990). RADM2 supersedes RADM1 and now RADM2 is much more widely used.

- RACM1, RACM2, and GACM

RACM1 (Stockwell et al., 1997) is an update of RADM2 and RACM2 (Goliff et al., 2013) is an updated version of RACM1. These mechanisms were designed to be valid for chemical conditions that range from the clean air found in remote locations to highly urban air and for air at Earth's surface through the upper troposphere.

RACM1 reaction rate coefficients and reaction products were updated from RADM2 and it included new data from laboratory measurements. Significant revisions were made to the chemistry of alkanes, alkenes and aromatic compounds. The representation of night-time chemistry was improved by increasing the production of hydroxyl radical from the ozonolysis of alkenes and revisions were made to the reactions of nitrate radical with alkenes and its reactions with organic peroxy radicals. RACM1 includes more complete treatment of the chemistry of biogenically emitted compounds with reaction schemes for three classes of biogenic compounds that are represented as isoprene, α -pinene, and d-limonene. The RACM was tested against an environmental chamber.

RACM2 is the most recent regional mechanism in this family and it includes updated reaction schemes, rate constants, and product yields (Goliff et al., 2013). Its reaction schemes for aromatic compounds, isoprene and alcohols were very heavily revised and expanded based on recent data. Acetaldehyde and acetone were added as explicit species to improve the simulation of the decomposition of organic compounds and including acetone improves RACM2's simulations of the upper troposphere. Revisions to alcohol chemistry include explicit treatment of methanol, ethanol, and a higher molecular weight alcohol species in RACM2 and allows RACM2 to better simulate rural regions. The new species for acetaldehyde, acetone and others required that RACM2's set of inorganic and organic photolysis reactions be expanded and updated.

The RACM2 mechanism was tested against environmental chamber experiments and compared with RACM1 simulations. RACM2 simulated the environmental chamber experiments better than RACM1 (Goliff et al., 2013). RACM2 forecasts lower ozone concentrations for ambient conditions than RACM1 but RACM2's forecasts appear to be more realistic. RACM2 was implemented in the Community Multiscale Air Quality Model (CMAQ) and it was more accurate

in its forecasts than the SAPRC and Carbon Bond Mechanisms (Sarwar et al., 2013). RACM2 is more complex than RACM1 but its computational requirements are well within the acceptable range for use within a comprehensive Eulerian air quality model.

The GACM mechanism is the most recent member of this family of mechanisms (Saunders, 2017). GACM was developed from RACM2. GACM was developed to be used in global atmospheric chemistry models to supply lateral chemical boundary conditions to regional air quality models using RACM2. If global and regional air quality models use a highly compatible set of chemical mechanisms some uncertainty in the representation of the chemical boundary conditions for the regional model is reduced.

Chemistry for simulating air over oceans was added to RACM2 while its detailed organic chemistry for simulating highly polluted urban regions was condensed (Saunders, 2017). The new chemistry included chlorine and reduced sulfur compounds. This process helped insure that GACM and RACM2 are highly compatible while keeping GACM simple enough for global modeling. Test simulations for the California Coast have been made with GACM implemented in the Weather Research and Forecasting model coupled with Chemistry (WRF-Chem).

3.5.4.3 *Statewide Air Pollution Research Center (SAPRC) Mechanisms*

The SAPRC series of mechanisms was named after that Statewide Air Pollution Research Center located at the University of California, Riverside. This series of mechanisms follows the aggregated molecule approach. The SAPRC series includes SAPRC-90, SAPRC-99, SAPRC-07, and SAPRC-11 (Carter, 1990, 2000, 2010 and Carter and Heo, 2013). The SAPRC chemical mechanism has its roots in the modeling of highly polluted urban atmospheres and, like Carbon Bond, SAPRC had been highly updated to be able to simulate regional atmospheric chemistry.

SAPRC07 included revisions to the rate coefficients for reactions involving NO₂, HO, HO₂, HNO₃, CH₂O, and PAN and more explicit representation of peroxy-peroxy reactions and hydroperoxide formation (Cai et al., 2011). The revisions of the peroxy-peroxy reactions and hydroperoxide formation allow the mechanism to more accurately simulate the effects of changes in NO_x concentrations on the formation of organic products. Atmospheric aromatic chemistry is very complicated, and research continues to require updates to this chemistry. The mechanisms for aromatic chemistry were revised in SAPRC07 and further revised in SAPRC-11. Some research versions of SAPRC have an adjustable number of species to allow very explicit representations of organic reactions. The most explicit version of SAPRC can represent about 400 categories of VOCs. This version is used to estimate the ozone forming reactivity of individual VOC compounds. The versions of SAPRC used in 3-D air quality models are much more condensed.

The SAPRC series of mechanisms have been tested against environmental chamber data (e.g., Carter and Lurmann, 1991; Carter, 1995). Simulations using CMAQ with SAPRC have been compared with field data (Cai et al., 2011; Sarwar et al., 2013).

3.5.4.4 *MOZART*

The Model for Ozone and Related chemical Tracers (MOZART) mechanism (Emmons et al., 2010) includes a very comprehensive set of chemical reactions for troposphere and stratosphere. The standard chemical mechanism includes 85 gas-phase species, 39 photolytic reactions, and 157 gas-phase reactions. It treats explicitly many VOCs such as ethane, propane, formaldehyde, acetaldehyde, acetone, methanol, isoprene), and includes three lumped species for higher hydrocarbons, namely, BIGALK and BIGENE that represent alkanes and alkenes with four or more carbon atoms and other higher-carbon VOCs with similar reactivity, TOLUENE that represents lumped aromatic species (including toluene, benzene and xylenes). The MOZART mechanisms have been used in the offline MOZART global chemical transport model, which has been used to supply lateral chemical boundary conditions to regional air quality models such as WRF-Chem.

3.5.4.5 Emission Inventories and Their Relationship to Chemical Mechanism Schemes

The development of detailed emissions inventories is beyond the scope of this chapter. More information on the management of emissions inventory databases is available (e.g., U.S. EPA, 2018). This section discusses the translation between an emission inventory and a particular chemical mechanism using Middleton et al. (1990) as a template example. Note that each mechanism and its implementation in a model may have its own rules for this translation. The documentation for the chosen model and mechanism should be checked carefully. There are software systems that support the development and management of emissions inventories such as the Sparse Matrix Operator Kerner Emissions (SMOKE) modeling system (CMAS, 2018). SMOKE may be used to format emissions inventories into formats that are directly readable by air quality models. Readers should consult the CMAS website for detailed documentation.

Usually emissions inventories are constructed in units of mass per time while a gas-phase chemistry module usually calculates in terms of concentration units (molecules volume⁻¹). This conversion must be made either in the inventory or in the air quality model (depending on the modeling system being used). Translation between the emissions of inorganic compounds such as NO, NO₂, SO₂ and NH₃ and their representation by a chemical mechanism's model species is usually direct and one for one because most schemes have explicit treatments of inorganic compounds. For NO_x there is one important note of caution because NO_x emissions are often reported as total NO_x with mass emission rate given as NO₂. A splitting factor giving the fraction of NO_x emitted as NO is required and typically over 90% of NO_x is emitted as NO. Therefore, the fraction of NO_x emitted as NO must be weighted by the mass ratio 1.53 (the molecular weight of NO₂, 46 g mole⁻¹ divided by the molecular weight of NO, 30 g mole⁻¹).

The greater difficulty is to translate between a VOC emissions inventory and the chemical mechanism's model species. This process would be easy for chemical mechanisms that treat the chemistry of individual VOC compounds as explicitly (e.g., Master Chemical Mechanism (MCM), 2018) but explicit mechanisms place demands on computational resources that are much too high for routine air quality forecasting applications. Condensed chemical mechanisms simplify atmospheric chemistry by aggregating individual compounds into grouped model species that represent the chemistry of classes and subcategories of similar compounds. The representation of the chemistry similar compounds by a grouped model species drastically reduces the number of chemical species and reactions required to represent atmospheric chemistry. In fact, the main differences between the available chemical mechanisms used in air quality modeling are due to the developers' approach to condensing VOC chemistry.

The application of condensed chemical mechanisms for air quality forecasting requires that the compounds in a VOC emission inventory be aggregated together into the model species of the condensed chemical mechanism. Middleton et al. (1990) provide a detailed procedure for aggregating compounds in a VOC emission inventory for the RADM2 chemical mechanism. Here we present this scheme as a general template for translating emission inventories into model species in a condensed chemical mechanism. A VOC-emissions inventory typically will be grouped into broad classes with subcategories within the classes. Broad classes include alkanes, alkenes, aromatics, aldehydes and ketones, mixtures and other classes as shown in Table 3.9. For example, alkanes are saturated hydrocarbons; compounds consisting of hydrogen and carbon atoms that are bonded together by single bonds only. Subcategories are defined based on the alkanes' rate coefficient for their reactions with the HO radical as shown in Table 3.9. The HO rate coefficient is used for aggregation because reaction of HO is the major oxidation reaction for alkanes in the lower troposphere. The definition of subcategories may depend on high atmospheric concentrations and on the details of the chemical mechanism. For example, methane is usually assigned to its own subcategory due to its high concentration, low HO-rate coefficient and the fact that its chemistry is treated explicitly in most chemical mechanisms. Ethane and propane are often assigned to their own subcategories for the same reasons. Table 3.9 shows four categories where the remainder of the alkanes are grouped together by ranges of their rate coefficients for their reactions with the HO-radical. When the emission rates of compounds are aggregated together into subcategory totals, the emission rates should be converted from mass emission rates to molar emission rates; this is accomplished by dividing the organic compound emission rates in grams per unit time by the

molecular weight of the compound. In the case of mixtures, an average molecular weight for the organic compounds in the subcategory must be estimated.

Table 3.9 An example of typical assignments of VOCs in an emissions inventory to classes and subcategories.

Numbers in parenthesis are the range in rate constants ($\text{cm}^3 \text{ molecules s}^{-1}$) for the reactions of HO with the compounds in the subcategory.

Chemical Class / Chemical Subcategory	Chemical Class / Chemical Subcategory
<p>Alkanes (Saturated Hydrocarbons)</p> <p>Methane</p> <p>Ethane</p> <p>Propane</p> <p>Alkanes ($1.7 \times 10^{-12} - 3.4 \times 10^{-12}$)</p> <p>Alkanes ($3.4 \times 10^{-12} - 6.8 \times 10^{-12}$)</p> <p>Alkanes ($6.8 \times 10^{-12} - 1.4 \times 10^{-11}$)</p> <p>Alkanes ($>1.4 \times 10^{-11}$)</p>	<p>Aldehydes, Ketones and Organic Acids (Compounds with a -CO Group)</p> <p>Formaldehyde</p> <p>Higher Aldehydes</p> <p>Acetone</p> <p>Higher Ketones</p> <p>Organic Acids</p>
<p>Alkenes (Unsaturated Hydrocarbons)</p> <p>Ethene</p> <p>Propene</p> <p>Primary Alkenes</p> <p>Internal Alkenes</p>	<p>Mixtures and Others</p> <p>Alkane/Aromatic Mixtures</p> <p>Alkenes (Primary/Internal Mixtures)</p> <p>Acetylene</p> <p>Haloalkanes</p> <p>Others ($<0.17 \times 10^{-12}$)</p> <p>Others ($1.7 \times 10^{-12} - 3.4 \times 10^{-12}$)</p> <p>Others ($3.4 \times 10^{-12} - 6.8 \times 10^{-12}$)</p> <p>Others ($>6.8 \times 10^{-12}$)</p>
<p>Aromatics</p> <p>Benzene</p> <p>Aromatics ($<1.4 \times 10^{-11}$)</p> <p>Aromatics ($>1.4 \times 10^{-11}$)</p> <p>Phenols and Cresols</p> <p>Styrenes</p> <p>Halobenzenes</p>	<p>Non-Assignable</p> <p>Unidentified</p> <p>Unassignable</p>

Alkenes are unsaturated hydrocarbons; compounds consisting of hydrogen and carbon atoms that are bonded together by at least one double carbon-carbon bond. Ethene and propene are grouped within their own subcategories. However, in this example higher molecular weight alkenes are grouped into their subcategories by structure. The subcategory "primary alkenes" includes all alkenes where the double bond is at the end of a molecule. The subcategory "internal alkenes" includes all alkenes where the double bond is contained within the molecule. In general, primary and internal alkenes have different mechanisms for their reactions with HO and O_3 .

The assignment of VOCs to subcategories in the classes, "Aromatics" and "Aldehydes, Ketones and Organic Acids", is analogous to the procedures described for alkanes and alkenes. Common aromatic compounds contain at least one six-carbon aromatic ring. Aldehydes, ketones and organic acids all contain at least one carbonyl group ($\text{C}=\text{O}$). Some compounds in an emissions inventory may be reported as mixtures that will require further treatment when

these are assigned to model chemical species. For mixtures, a mixing factor must be estimated for the split between two VOC classes - Table 3.10. Some compounds in an emissions inventory may be difficult or impossible to assign, these may be designated as "Unidentified" or "Unassignable".

The assignment of VOCs into classes and subcategories helps make the assignment of these compounds into model species more systematic. The next step is to align emission subcategories with model species as shown in Table 3.10. In this case, the RADM chemical species are used as an example. These species are: methane (CH₄), ethane (ETHA), low reactive alkane based on HO-rate coefficients (HC3), middle reactive alkane (HC5), high reactive alkane (HC8), ethene (ETH), primary alkenes (OLT), internal (OLI), lower reactive aromatic compounds (TOL), high reactive aromatic compounds (XYL), cresols and phenols (CSL), formaldehyde (HCHO), higher aldehydes (ALD), higher ketones (KET) and organic acids (ORA).

The details of aggregating the emissions subcategories into model species are mechanism dependent. Reactivity weighting is a common approach although, for the earlier versions of the carbon bond mechanism, assignments of emissions into model species is done by chemical moiety. When aggregation is performed by chemical moiety, the model species represent the chemical functional groups regardless of the molecules they are attached to. Therefore, VOC emissions are assigned to model species by breaking the VOCs down by their functional groups.

One advantage is that the carbon bond mechanism conserves carbon better than mechanisms that use reactivity weighting.

Reactivity weighting helps represent the effect of a VOC on atmospheric chemistry at the expense of carbon mass balance and it is used for the SAPRC and the RADM/RACM series of mechanisms. The rate constant for the reaction of a VOC with HO is typically used at the standard for reactivity weighting. One way to define an aggregation factor, F , based on reactivity weighting is given by the following equation.

$$F = \frac{1 - e^{-k_{HO(emit)} \times INT(HO)}}{1 - e^{-k_{HO(model)} \times INT(HO)}}$$

where $k_{HO(emit)}$ is the HO rate coefficient of the emitted VOC, $k_{HO(model)}$ is the HO rate coefficient for the model species in the mechanism, $INT(HO) = \int_{t_i}^{t_f} [HO]_t dt$ is the domain average integrated HO concentration for the simulation period, $[HO]_t$ is the time dependent HO concentration, t_i is the initial simulation time and t_f is the final simulation time. The numerator represents the fraction of the emitted VOC that reacts during the simulation and the denominator represents the fraction of the model VOC that reacts during the simulation. The domain average integrated HO concentration is difficult to estimate, but 6×10^{26} molecules cm⁻³ s has been used for episodic regional simulations (Middleton et al., 1990). The aggregation factor will be 1 for VOC and model species that react rapidly. If both react slowly, F is proportional to the ratio of the rate constants and independent of the estimated INTOH parameter. Sources of HO rate constants include: Burkholder et al. (2015), Calvert et al. (2015) and the Master Chemical Mechanism (2018). The final VOC emissions inventory is a field of emissions for each model VOC species that is determined by the sum of the product of the molar emission rate (E_{VOC}) for each VOC aggregated into the model species, its mixing factor (M_x) and the aggregation factor based on reactivity weighting.

$$E_{Model_Species} = \sum M_x F E_{VOC}$$

Table 3.10 The assignment of chemical subcategories into model species using the RADM chemistry mechanism as an example.

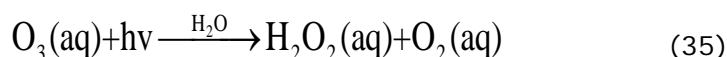
RADM Model Species	Chemical Subcategory	Mixing Factor	Aggregation Factor
CH ₄	Methane	1.00	1.000
ETHA	Ethane	1.00	1.000
HC3	Propane	1.00	0.519
(Low Reactive Alkane)	Alkanes ($1.7 \times 10^{-12} - 3.4 \times 10^{-12}$)	1.00	0.964
	Acetylene	1.00	0.343
	Haloalkanes	1.00	0.078
	Others ($<0.17 \times 10^{-12}$)	1.00	0.404
(Middle Reactive Alkane)	Others ($1.7 \times 10^{-12} - 3.4 \times 10^{-12}$)		1.215
	Alkanes ($3.4 \times 10^{-12} - 6.8 \times 10^{-12}$)	1.00	0.956
(High Reactive Alkane)	Others ($3.4 \times 10^{-12} - 6.8 \times 10^{-12}$)	1.00	1.075
	Alkanes ($6.8 \times 10^{-12} - 1.4 \times 10^{-11}$)	1.00	0.945
ETH	Alkanes ($>1.4 \times 10^{-11}$)	1.00	1.141
	Alkane/Aromatic Mixtures	0.91	1.002
	Others ($>6.8 \times 10^{-12}$)	1.00	1.011
OLT	Ethene	1.00	1.000
	Propene	1.00	1.000
OLI	Primary Alkenes	1.00	1.000
	Alkenes (Primary/Internal Mixtures)	0.50	0.500
	Styrenes	1.00	1.000
	Internal Alkenes	1.00	1.000
TOL	Alkenes (Primary/Internal Mixtures)	0.50	0.500
	Benzene	1.00	0.293
	Halobenzenes	1.00	0.293
	Aromatics ($<1.4 \times 10^{-11}$)	1.00	1.000
XYL	Styrenes	1.00	1.000
	Aromatics ($>1.4 \times 10^{-11}$)	1.00	1.000
CSL	Alkane/Aromatic Mixtures	0.09	0.090
	Phenols and Cresols	1.00	1.000
HCHO	Formaldehyde	1.00	1.000
ALD	Higher Aldehydes	1.00	1.000
KET	Acetone	1.00	0.253
	Higher Ketones	1.00	1.000

RADM Model Species	Chemical Subcategory	Mixing Factor	Aggregation Factor
ORA	Organic Acids	1.00	1.000

3.5.5 Aqueous-Phase Atmospheric Chemistry in Clouds and Aerosols

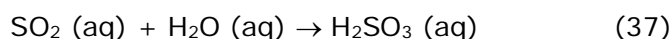
Compared to gas-phase chemistry, aqueous-phase chemistry is much more complex. It includes aqueous-phase dissolution and dissociation equilibria, photolytic reactions, catalytic reactions, radical chemistry, and organic chemistry. Aqueous-phase dissolution and dissociation equilibria processes occur when a gas dissolves in a liquid droplet to form a solution that consists of a solute (e.g., the dissolving gas) and a solvent (e.g., water). Dissolved chemical species may partially or completely dissociate into ions in the solution. The aqueous-phase concentration of dissolved species, A , can be determined based on the so-called Henry's law, which states that the amount of dissolved gas is proportional to its partial pressure in the gas phase with a proportionality factor of the Henry's law constant, H_A . Species with $H_A < 1,000 \text{ M atm}^{-1}$, are relatively insoluble or slightly soluble and they are present mainly in the gas phase. Examples for slightly soluble species include NO_2 , O_3 , CO_2 , SO_2 , NH_3 , HO , and many organic species. Species with $1,000 \text{ M atm}^{-1} < H_A < 10,000 \text{ M atm}^{-1}$ are moderately soluble with significant fractions in both phases. HO_2 , HCHO , HCOOH , and CH_3COOH are examples in this category. Species with $H_A \geq 10,000 \text{ M atm}^{-1}$ are highly soluble and they are mainly present in the liquid phase. HNO_4 , hydrogen peroxide (H_2O_2), HNO_3 , and H_2SO_4 are highly soluble species.

Many dissolved species can undergo various aqueous-phase reactions including photolytic reactions and kinetic reactions. For example, dissolved O_3 and H_2O_2 can photolyse as follows,

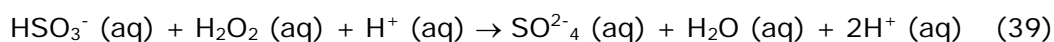


These reactions provide important sources for H_2O_2 and HO in the aqueous-phase. Aqueous kinetic reactions involving oxygen-hydrogen chemistry, and chemistry of sulfur, nitrogen, chlorine, mercury, and organic compounds. While the aqueous-phase oxidation of dissolved sulfur compounds (S(IV) and NO_x) is relatively well understood, considerable uncertainty exists for aqueous-phase catalytic reactions, radical chemistry, and organic chemistry. For those reasons, most air quality models include simplified aqueous-phase chemistry that mainly focuses on sulfur chemistry. Some models include nitrogen and chlorine chemistry. Very few models include aqueous-phase mercury and organic chemistry. The most important aqueous-phase sulfur and nitrogen chemistry is described below.

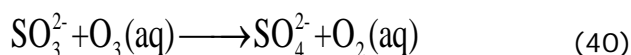
Sulfur dioxide may be oxidized in cloud water droplets or aerosol particles by many dissolved oxidants such as H_2O_2 , O_3 , and O_2 catalysed by metals (e.g., Fe^{3+} and Mn^{2+}) (Jacobson, 2005; Seinfeld and Pandis, 2016). The bisulfate anion, HSO_3^- is produced when sulfur dioxide dissolves in liquid water reactions 37 and 38,



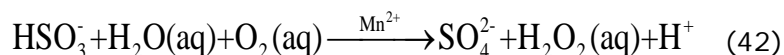
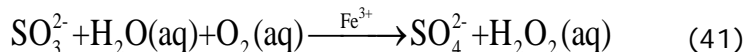
The overall reaction of H_2O_2 with bisulfate to sulfate is given by reaction 39 (Jacobson, 2005; Seinfeld and Pandis, 2016),



The reaction of H_2O_2 with bisulfate is much more important in the atmosphere because reaction 39 is acid-catalysed allowing it to be important at low pH values (< 6) that shut down the reaction of bisulfate with O_3 . At $\text{pH} > 6$, is the prevalent species for dissolved sulfur, the dominant reaction to convert to is,

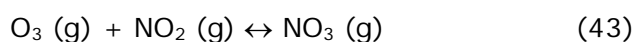


The reaction (40) is extremely fast in solution, with a faster rate at higher pH. Because of its fast reaction rate and the omnipresence of O_3 in the atmosphere, it has been identified as one of the main pathways to deplete O_3 in cloud droplets. At $\text{pH} < 12$, can also be oxidized by O_2 catalysed by metal species such as iron (Fe^{3+}) and manganese (Mn^{2+}),

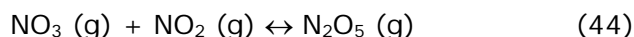


Reaction (41) occurs much faster than (42). The reactions (39)-(42) are the dominant aqueous oxidation reactions of dissolved SO_2 that have been included in nearly all aqueous-phase chemical mechanisms used in the atmospheric models. Dissolved SO_2 can also be oxidized to form sulfate by additional aqueous species such as HO , NO_2 , NO_3 , HNO_4 , Cl_2^- , Br_2^- , and several organic compounds.

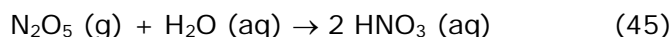
The atmospheric production of nitric acid by aqueous-phase reactions is less important than in the gas-phase (Calvert et al., 2015). Much of the aqueous-phase production of nitric acid occurs due to night-time gas-phase chemistry. During the night gas-phase O_3 reacts with NO_2 to produce the nitrate radical (NO_3),



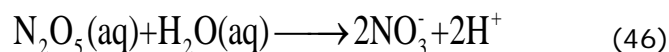
During the day NO_3 photolyses rapidly but during the night it reacts with nitrogen dioxide to produce dinitrogen pentoxide, N_2O_5 ,



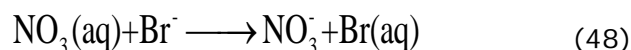
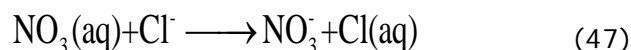
Dinitrogen pentoxide (N_2O_5) is not stable. It is in equilibrium with nitrate radical and nitrogen dioxide. N_2O_5 reacts with liquid water to produce nitric acid,



Dissolved N_2O_5 can react rapidly in the aqueous phase to produce,



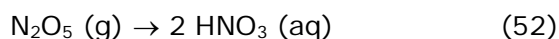
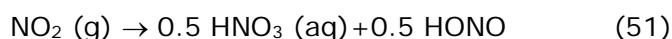
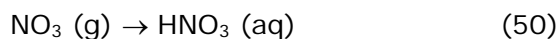
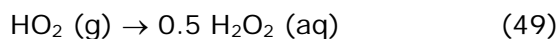
A similar reaction occurs between N_2O_5 and H_2O in the gas-phase, but its rate is much slower than the reactions (45) and (46). The NO_3 radical in the aqueous phase can be removed through their reactions with the halogenide anions Cl^- and Br^- in a halogen-rich environment, which account for more than 90% of the total loss flux:



Both reactions produce active halogen species, Cl and Br , under night-time conditions. They may be important in coastal areas.

3.5.6 Heterogeneous Atmospheric Chemistry

Heterogeneous chemical reactions involving gas species uptaken onto the surfaces of aerosol particles and cloud droplets may significantly contribute to atmospheric chemistry. In addition to several heterogeneous reactions mentioned above such as reactions 31, 32, 34, and 45, a minimal set of reactions is recommended by Jacob (2000) for O_3 modeling:



Uptake coefficient is an important parameter used to calculate the above heterogeneous reaction rates, which is defined as the fraction of collisions with a particle that leads to irreversible loss of species on the surface of a droplet or an aerosol particle. The suggested uptake coefficients for reactions (49-52) are 0.2, 10⁻³, 10⁻⁴, and 0.1, respectively. These reactions are included in some CW-AQF models.

3.5.7 Aqueous Phase and Heterogeneous Chemistry Included in CW-AQF Models

Several aqueous-phase chemical mechanisms have been developed since the early 1980s. These include the mechanisms of Chameides and Davis (1982), Chameides (1984) (C84), Graedel and Goldberg (1983), Walcek and Taylor (1986) (WT86), Jacob (1986) (J86), Pandis and Seinfeld (1989) (PS89), Strader et al. (1998) (S98), Zaveri (1997)/Zhang et al. (1998)/Zhang et al. (2005) (Z97/Z98/Z05), Ervens et al. (2003) (E03), Herrmann et al. (2005) (H05), and Deguillaume et al. (2009) (D09). These mechanisms have different numbers of aqueous species and reactions.

Table 3.11 compares several aqueous-phase chemical mechanisms in terms of species and equilibrium and kinetic reactions treated.

A majority of CW-AQF only simulate inorganic sulfate production by aqueous chemistry through several oxidation pathways. Only a few models include aqueous-phase SOA formation pathways. Table 3.12 summarizes the aqueous-phase chemical mechanisms used in some regional CW-AQF models. These mechanisms vary in their levels of detail in terms of aqueous-phase species, the number of equilibria and kinetic reactions included, and the size resolution used in solving aqueous-phase chemistry, ranging from highly-simplified to condensed or more detailed full chemical mechanisms. Among them, COSMO-MUSCAT and LOTUS-EUROS use highly parameterized oxidation of S(IV) to S(VI), and AQFx, NAQFC (NAM-CMAQ), CHIMERE, GEM-MACH, and GRAPES-CUACE use condensed mechanisms with a focus on aqueous-phase sulfur chemistry that is based on WT86, or a simpler version of SP89. For comparison, CCATT-BRAMS, Polyphemus, STEM-2K3, and WRF-Chem include more complete aqueous-phase chemical mechanisms that consider radical chemistry and the formation of sulfate and nitrate based on C84, SP89, S98, although these models except for CCATT-BRAMS and STEM-2K3 also offer options to use simpler or condensed aqueous-phase chemistry. Among these models, aqueous-phase SOA formation pathways were only included in NAQFC and Polyphemus. Although VRSM has been implemented in Polyphemus and WRF-Chem, only the bulk version of VRSM has been applied.

STEM-2K3 includes most detailed heterogeneous chemistry SO₂, O₃, HO, HO₂, H₂O₂, N₂O₅, NO₃, and HNO₃ at the surface of aerosols and cloud droplets following Zhang and Carmichael (1999). CHIMERE, Polyphemus, and WRF-Chem included the heterogeneous reactions for HO₂, NO₂, N₂O₅ and NO₃ at the surface of aerosols and cloud droplets following Jacob (2000). NAQFC, GEM-MACH15, and LOTOS-EUROS include only the N₂O₅ hydrolysis on aerosol and cloud droplets. AQFx, CCATT-BRAMS, and GRAPES-CUACE do not include any heterogeneous reactions.

Table 3.11 Comparison of several aqueous-phase chemical (Zhang, 2020)

Mechanism	Aqueous-phase species	Gas/liquid equilibria	Dissociation equilibria	Aqueous photolysis	Kinetic aqueous reactions	Total number of reactions
C84	27	13	10	0	31	54
WT86: RADM	27	10	9	0	5	24
J86	40	19	12	7	90	127
PS89: CMU (full/cond)	49/49	21/21	16/16	7/2	106/58	147/97
S98: CMU	27	17	17	7	99	134
Z97/Z98/Z05 (full/cond_p/cond_c)	58/58/58	29/29/29	18/18/18	7/2/1	113/64/47	167/113/95
FP01: VRSM	50	21	17	7	102	147
H99: CAPRAMv2.3	88	34	31	6	197	268
E03: CAPRAMv2.4 (full/reduced)	153/118	34/33	57/39	11/4	313/108	415/184
H05/D09: CAPRAMv3.0 (full/reduced)	380/130	51/42	89/55	12/5	676/138	828/240

WT86- Walcek and Taylor (1986); J96-Jacob (1986); PS89-Pandis and Seinfeld (1989); S98-Strader et al. (1998); Z97/Z98/Z05- Zaveri (1997)/Zhang et al. (1998)/Zhang et al. (2005); FP01: Fahey and Pandis (2001); H99- Herrmann et al. (1999); E03-Ervens et al. (2003); H05-Herrmann et al. (2005); D09- Deguillaume et al. (2009). RADM - regional acid deposition model; CMU-Carnegie Mellon University; VRSM- variable size-resolution model; CAPRAM - Chemical Aqueous Phase Radical Mechanism; Full - full mechanism, cond-condensed mechanism; cond_p and cond_c-condensed mechanisms under polluted and clean conditions, respectively; reduced - reduced mechanism.

Table 3.12 Aqueous-phase and heterogeneous chemical mechanisms used in CW-AQF models (Zhang, 2020)

Model	Aqueous-Phase Chemistry	Heterogeneous Chemistry	Reference
AQFx	Highly simplified bulk sulfur chemistry with S(IV) oxidation by O ₃ (aq) and H ₂ O ₂ (aq) based on Seinfeld and Pandis (2016)	None	Lawson et al., 2017
ATLAS-NAME	Simplified chemistry involving H ₂ O, HNO ₃ , SO ₂ , HSO ₃ ⁻ , NH ₃ , CO ₂ , OH, NO ₃ ⁻ , SO ₃ ²⁻ , NH ₄ ⁺ , HCO ₃ ⁻ . It contains 6 dissolution equilibria, 3 kinetic oxidation reactions for sulfate formation, and one reaction to form (NH ₄) ₂ SO ₄ , based on STOCHEM (Collins et al., 1997) and (Redington and Derwent, 2002)	Heterogeneous reactions for N ₂ O ₅ and HNO ₃ at a fixed rate	Jones et al., 2007, Redington and Derwent, 2002, 2013; Redington et al., 2009
CCATT-BRAMS	Aqueous-phase chemistry with 28 aqueous phase species based on the Strader et al. (1999)	None	Longo et al., 2013
CHIMERE	Highly simplified bulk sulfur chemistry with S(IV) oxidation by H ₂ O ₂ , O ₃ , NO ₂ , O ₂ (catalysed by Fe ³⁺ and Mn ²⁺); 7 aqueous-phase species and 7 kinetic reactions	Heterogeneous reactions for HO ₂ , NO ₂ , N ₂ O ₅ and NO ₃ at the surface of aerosols and fog droplets following Jacob (2000)	Bessagnet et al. 2004, http://www.lmd.polytechnique.fr/chimere/
COSMO-MUSCAT	Bulk, parameterized aqueous-phase production of SO ₄ ²⁻ based on the approach in LOTOS-EUROS	None	http://projects.tropos.de/cosmo_muscat/ Wolke et al., 2012
ENVIRO-HIRLAM	NWPChem-Liquid aqueous-phase chemistry mechanism involving up to 17 aqueous species, simplified thermodynamic equilibrium model, (Korsholm et al., 2008).	13 reactions (Korsholm et al., 2008)	Korsholm et al., 2008
GEM-MACH15	25 aqueous-phase reactions among 13 species including oxidation of S(IV) to S(VI) by dissolved O ₃ , H ₂ O ₂ , ROOH, and O ₂ (catalysed by Fe ³⁺ and Mn ²⁺), based on ADOM-II aqueous phase mechanism (Venkatram et al., 1988; Fung et al., 1991)	Parameterized N ₂ O ₅ hydrolysis as part of gas-phase mechanism	Gong et al., 2015
G5CHEM	It includes simplified chemistry of HNO ₃ , NO ₃ , NH ₃ , NH ₄ ⁺ , and SO ₄ ²⁻ . The original sulfate-nitrate-ammonium aerosol simulation coupled to gas-phase chemistry was developed by Park et al. [2004]. Cloudwater pH for in-cloud sulfate formation is as given by Alexander et al. (2012).	Heterogeneous reactions for HO ₂ , NO ₂ , N ₂ O ₅ , and NO ₃ at the surface of aerosols and fog droplets following Jacob (2000)	Hu et al. (2018)

Model	Aqueous-Phase Chemistry	Heterogeneous Chemistry	Reference
GRAPES- CUACE	AQCHEM in CMAQ with SO ₂ , CO ₂ , NH ₃ , H ₂ O ₂ , O ₃ , HNO ₃ , MHP, PAA, FO equilibrium reactions and kinetic reactions with 22 aqueous-phase aerosol species and intermediates	None	Wang et al. 2010; Zhou et al., 2016, Zhou, et al., 2018
IFS (ECMWF/CAMS)	It includes simplified chemistry of HNO ₃ , NO ₃ , NH ₃ , NH ₄ ⁺ , and SO ₄ ²⁻ based on EQSAM (Metzger et al., 2002) but not linked to aerosol scheme.	Heterogeneous reactions of N ₂ O ₅ (Evans and Jacob, 2005) and H ₂ O ₂ (Huijnen et al., 2014) on aerosol surfaces	Flemming et al. (2015), Morcrette et al. (2009)
LOTOS-EUROS	Parameterized by a single pseudo first order reaction for aqueous-phase SO ₂ oxidation to SO ₄ , with a reaction rate as a function of cloud cover and relative humidity; 2 aqueous-phase species	Heterogeneous N ₂ O ₅ chemistry with an uptake coefficient of 0.05	Schapp et al., 2004; Barbu et al., 2009
NAQFC (NAM-CMAQ)	the bulk RADM chemistry based on Walcek and Taylor (1986) and two SOA-forming reactions from glyoxal and methylglyoxal based on Carlton et al. (2008); 12 aqueous-phase species	N ₂ O ₅ hydrolysis on aerosol and cloud droplets	Byun and Schere, 2006; Fahey et al. (2017)
NMMB-MONARCHv1.0	Formation of sulfate from SO ₂ and DMS, and oxidation of S(IV) to S(VI) by dissolved O ₃ and H ₂ O ₂	Heterogeneous hydrolysis of N ₂ O ₅	Pérez et al. (2011); Badia and Jorba (2015); Spada (2015)
Polyphemus	1. A bulk, simple mechanism with S(IV) oxidation by S(VI) (Roustan et al., 2010) 2. The bulk VRSM of Fahey and Pandis (2001), aqueous-phase chemistry of SOA formation based on Couvidat et al. (2013)	Heterogeneous reactions for HO ₂ , NO ₂ , N ₂ O ₅ and NO ₃ at the surface of aerosols and cloud droplets following Jacob (2000)	Sartelet et al. (2007), Debry et al. (2007), Couvidat et al. (2013)
SILAM v.5.5	Highly simplified aqueous-phase chemistry accounting for sulfate formation from SO ₂	None	Sofiev (2000); Kouznetsov and Sofiev (2012)
STEM-2K3	Bulk chemistry of sulfate and nitrate formation based on Chameides and Davis (1982) and Chameides (1984), with rate constants updated based on Jacob (1986)	Heterogeneous reactions for SO ₂ , O ₃ , HO, HO ₂ , H ₂ O ₂ , N ₂ O ₅ , NO ₃ , and HNO ₃ at the surface of aerosols and cloud droplets following Zhang and Carmichael (1999)	Carmichael et al., 1991; Zhang and Carmichael, 1999; Tang et al., 2003

Model	Aqueous-Phase Chemistry	Heterogeneous Chemistry	Reference
WRF-Chem	1. Bulk RADM mechanism based on AQCHEM in CMAQ 2. Bulk VSRM (Fahey and Pandis, 2001) 3. MOZART AQ 4. CAM MAM7 AQ 27 aqueous-phase species, 5-99 kinetic reactions, depending on the mechanism selected	Heterogeneous reactions for HO ₂ , NO ₂ , N ₂ O ₅ and NO ₃ at the surface of aerosols and cloud droplets following Jacob (2000)	WRF-Chem (2018) Chapman et al., 2009; Tie et al., 2001; Liu et al., 2012

3.5.8 Summary

- O₃, PM, acid deposition, and other air pollutants are produced through gas-phase, aqueous-phase, and heterogeneous chemical reactions.
- Meteorology is a very important factor that affects O₃ and PM concentrations. O₃ concentrations are the greatest usually on warm, clear summer days with calm winds; these are associated with stagnant high-pressure conditions. PM concentrations are the greatest usually on cool fall days with low mixing heights and cooler temperatures.
- The photochemical production of air pollutants is driven by solar radiation. Photolysis frequencies (J-values) are used to calculate the rates of photochemical reactions.
- J-values are calculated through the use of radiation transport models. These models calculate J-values from spherically integrated flux of photons and two sets of molecular properties: absorption cross-sections and quantum yields.
- Key atmospheric reactive intermediates are HO and HO₂, collectively known as HO_x that oxidize NO_x and VOCs. Emissions of nitrogen oxides and VOCs are the key gas-phase chemical reactants that lead to the production of O₃ and PM.
- O₃ concentrations depend upon solar actinic flux and the ratio of the concentration of NO₂ to the concentration of NO. Realistically accurate emissions inventories of NO_x and VOCs are critical for air quality forecasting with prognostic air quality models.
- Ammonia emissions from animal and human waste react with the atmospheric acids, nitric acid and sulfuric acid, to produce inorganic aerosols. If inorganic PM are to be forecasted, the emissions inventory must include NH₃ and SO₂. The oxidation products of VOCs can form secondary organic aerosol.
- There are several available gas-phase, aqueous-phase, and heterogeneous chemical mechanisms employed by air quality models. These range from highly detailed to very condensed. Condensed mechanisms describe the chemistry of groups of similar chemical compounds aggregated into a very limited number of model species. The aggregation scheme for VOCs and the level of detail are the major differences between the gas-phase chemical mechanisms.
- In general, O₃ may be forecasted well with very condensed mechanisms (fewer than a couple hundred reactions) while the accurate forecasting of PM requires more chemical detail, especially if SOA is to be forecasted.
- Aqueous-phase and heterogeneous chemical mechanisms are necessary for the forecasting of acid deposition.
- An air quality forecast may be affected by the scheme used to translate between an emission inventory and a particular chemical mechanism. Each chemical mechanism will have its own rules for this translation. There are emissions inventory management software systems that may be used to develop emissions inventories, translate between the inventory and the particular chemical mechanism used, and format the inventory to be read by the air quality model.

References

- Alexander, B., D.J. Allman, H.M. Amos, T.D. Fairlie, J. Dachs, D.A. Hegg and R.S. Sletten, Isotopic constraints on sulfate aerosol formation pathways in the marine boundary layer of the subtropical northeast Atlantic Ocean, *J. Geophys. Res.*, 117, D06304, doi:10.1029/2011JD016773 (2012)
- Aumont B, Madronich S, Bey I, Tyndall GS. Contribution of secondary VOC to the composition of aqueous atmospheric particles: A modeling approach. *J. Atmos. Chem.*; 2000:35,59-75.
- Badia, A. and O. Jorba, 2015, Gas-phase evaluation of the online NMMB/BSC-CTM model over Europe for 2010 in the framework of the AQMEII-Phase2 project, *Atmos. Environ.*, 115, 657-669.
- Baklanov, A, K. Schlünzen, P. Suppan, J. Baldasano, D. Brunner, S. Aksoyoglu, G. Carmichael, J. Douros, J. Flemming, R. Forkel, S. Galmarini, M. Gauss, G. Grell, M. Hirtl, S. Joffre, O. Jorba, E. Kaas, M. Kaasik, G. Kallos, X. Kong, U. Korsholm1, A. Kurganskiy, J. Kushta, U. Lohmann, A. Mahura, A. Manders-Groot, A. Maurizi, N. Moussiopoulos, S. T. Rao, N. Savage, C. Seigneur, R. S. Sokhi, E. Solazzo, S. Solomos, B. Sørensen, G. Tsegas, E. Vignati, B. Vogel, and Y. Zhang, Online Coupled Regional Meteorology Chemistry Models in Europe: Current Status and Prospects, *Atmos. Chem. Phys.*, 14, 317–398 (2014). www.atmos-chem-phys.net/14/317/2014/ doi:10.5194/acp-14-317-2014
- Barbu, A.L.; Segers, A.J.; Schaap, M.; Heemink, A.W.; Builtjes, P.J.H. A multi-component data assimilation experiment directed to sulphur dioxide and sulfate over Europe. *Atmos. Environ.* 2009, 43, 1622–1631.
- Bessagnet, B., A. Hodzic, R. Vautard, M. Beekmann, S. Cheinet, C. Honoré, C. Liousse, L. Rouil, Aerosol modeling with CHIMERE—preliminary evaluation at the continental scale, *Atmospheric Environment*, Volume 38, Issue 18, June 2004, Pages 2803-2817, ISSN 1352-2310, 10.1016/j.atmosenv.2004.02.034, 2004.
- Bey, I., Jacob, D. J., Yantosca, R. M., Logan, J. A., Field, B., Fiore, A. M., Li, Q., Liu, H., Mickley, L. J., and Schultz, M.: Global modeling of tropospheric chemistry with assimilated meteorology: model description and evaluation, *J. Geophys. Res.*, 106, 23073–23096, 2001.
- Burkholder, J. B., S. P. Sander, J. Abbatt, J. R. Barker, R. E. Huie, C. E. Kolb, M. J. Kurylo, V. L. Orkin, D. M. Wilmouth, and P. H. Wine "Chemical Kinetics and Photochemical Data for Use in Atmospheric Studies, Evaluation No. 18," JPL Publication 15-10, Jet Propulsion Laboratory, Pasadena, 2015 <http://jpldataeval.jpl.nasa.gov>. Last accessed November 10, 2018.
- Byun, D. and K.L. Schere. Review of the governing equations, computational algorithms, and other components of the Models-3 Community Multiscale Air Quality (CMAQ) Modeling System, *Appl. Mech. Rev.*, 59, 51-77, 2006. doi:10.1115/1.2128636.
- Cai, C., J.T. Kelly, J.C. Avise, A.P. Kaduwela and W.R. Stockwell, Photochemical Modeling in California with the SAPRC07C and SAPRC99 Chemical Mechanisms: Model Intercomparison and Response to Emission Reductions, *J. Air and Waste Management Association*, 61, 559 –572, 2011.
- Calvert, J.G., J.J. Orlando, W.R. Stockwell and T.J. Wallington, *The Mechanisms of Reactions Influencing Atmospheric Ozone*, Oxford University Press, Oxford, May 2015.
- Carlton, A. G., Turpin, B. J., Altieri, K. E., Seitzinger, S. P., Mathur, R., Roselle, S. J., and Weber, R. J.: CMAQ model performance enhanced when in-cloud secondary organic aerosol is included: comparisons of organic carbon predictions with measurements, *Environ. Sci. Technol.* 42, 8798–8802, doi:10.1021/es801192n, 2008.

- Carmichael, G.R.; Peters, L.K.; Saylor, R.D. The STEM-II regional scale acid deposition and photochemical oxidant model: I. An overview of model development and applications. *Atmos. Environ.* 1991, 25A, 2077–2090.
- Carter, W.P.L. A detailed mechanism for the gas-phase atmospheric reactions of organic compounds. *Atmos. Environ.* 1990, 24A, 481-518, doi:10.1016/0960-1686(90)90005-8.
- Carter, W.P.L., 1995, Computer modeling of environmental chamber measurements of maximum incremental reactivities of volatile organic compounds, *Atmos. Environ.*, 29, 2513–2527.
- Carter, W.P.L. Documentation of the SAPRC-99 Chemical Mechanism for VOC Reactivity Assessment. Final Report to California Air Resources Board Contract No. 92-329, and 95-308: California Air Resources Board, Sacramento, California, United States, 2000.
- Carter, W.P.L. Development of the SAPRC-07 chemical mechanism. *Atmos. Environ.* 2010, 44, 5324-5335.
- Carter, W.P.L. and G. Heo, Development of revised SAPRC aromatics mechanisms. *Atmos. Environ.* 2013, 77, 404-414.
- Carter, W.P.L., and F.W. Lurmann, 1991, Evaluation of a detailed gas phase atmospheric reaction mechanism using environmental chamber data, *Atmos. Environ.*, 25, 2771–2806.
- Chapman, E. G., W. I. Gustafson Jr, R. C. Easter, J. C. Barnard, S. J. Ghan, M. S. Pekour, and J.D. Fast (2009), Coupling aerosol-cloud-radiative processes in the WRF-Chem model: Investigating the radiative impact of elevated point sources, *Atmos. Chem. Phys.*, 9, 945-964.
- Chameides, W.L., 1984, The Photochemistry of a Remote Marine Stratiform Cloud, *J. of Geophys. Res.*, 89, D3, 4739-4755, June 20.
- Chameides, W.L., Davis, D.D., 1982. The free radical chemistry of cloud droplets and its impact upon the composition of rain. *Journal of Geophysical Research* 87, 4863-4877.
- Claeys, M, Graham B, Vas G, Wang W, Vermeylen R, Pashynska V, Cafmeyer J, Guyon P, Andreae MO, Artaxo P, Maenhut W. Formation of secondary organic aerosols through photooxidation of isoprene. *Science*, 2004:303,1173-1176.
- CMAS (2018) Community Modeling and Analysis System, SMOKE (Sparse Matrix Operator Kerner Emissions) Modeling System, <https://www.cmascenter.org/smoke/>. Last accessed November 10, 2018.
- Collins, W. J., Stevenson, D. S., Johnson, C. E., and Derwent, R. G.: Role of convection in determining the budget of odd hydrogen in the upper troposphere, *J. Geophys. Res.*, 104, 26927–26941, 1999.
- Collins, W. J., Stevenson, D. S., Johnson, C. E., and Derwent, R. G., 1997: Tropospheric ozone in a global-scale three-dimensional Lagrangian model and its response to NOx emission controls, *J. Atmos. Chem.*, 26, 223-274.
- Couvidat, F., K. Sartelet, and C. Seigneur, 2013, Investigating the Impact of Aqueous-Phase Chemistry and Wet Deposition on Organic Aerosol Formation Using a Molecular Surrogate Modeling Approach, *Environ. Sci. Technol.*, 47, 914–922, dx.doi.org/10.1021/es3034318.
- Crassier, V., Suhre, K., Tulet, P., and Rosset, R.: Development of a reduced chemical scheme for use in mesoscale meteorological models, *Atmos. Environ.*, 34, 2633–2644, 2000.
- Debry E., Fahey K., Sartelet K., Sportisse B. and Tombette M. (2007), Technical Note: a new Size REsolved Aerosol Model: SIREAM. *Atmos. Chem. Phys.*, 7, 1537-1547.

- de Gouw, JA, Brock CA, Atlas EL, Bates TS, Fehsenfeld FC, Goldan PD, Holloway JS, Kuster WC, Lerner BM, Matthew BM, Middlebrook AM, Onasch TB, Peltier RE, Quinn PK, Senff CJ, Stohl A, Sullivan AP, Trainer M, Warneke C, Weber RJ, Williams EJ. Sources of particulate matter in the north-eastern United States in summer: 1. Direct emissions and secondary formation of organic matter in urban plumes. *J. Geophys. Res.-Atmos.*; 2008;13,D08301.
- de Gouw J, Jimenez JL. Organic aerosols in the Earth's atmosphere. *Environ. Sci. Technol.*, 2009;43, 7614-7618.
- Deguillaume, L., A. Tilgner, R. Schrödner, R. Wolke, N. Chaumerliac, H. Herrmann, 2009, Towards an operational aqueous phase chemistry mechanism for regional chemistry-transport models: CAPRAM-RED and its application to the COSMO-MUSCAT model, *J Atmos Chem* (2009) 64:1–35, doi:10.1007/s10874-010-9168-8.
- Derognat, C., Beekmann, M., Baeumle, M., Martin, D., and Schmidt, H. Effect of biogenic volatile organic compound emissions on tropospheric chemistry during the atmospheric pollution over the Paris area (esquif) campaign in the Ile-de-France region. *J. Geophys. Res.-Atmospheres*, 108(D17), 2003.
- Donahue NM, Robinson AL, Stanier CO, Pandis SN. Coupled partitioning, dilution, and chemical ageing of semi-volatile organics. *Environ. Sci. Technol.*; 2006;40,2635-2643.
- Emmons, L. K.; S. Walters, P. G. Hess., J.-F. Lamarque, G. G. Pfister, D. Fillmore, C. Granier, A. Guenther, D. Kinnison, T. Laepple, J. Orlando, X. Tie, G. Tyndall, C Wiedinmyer, S. Baughcum and S. Kloster, 2009: Description and evaluation of the Model for Ozone and Related chemical Tracers, version 4 (MOZART-4), *Geoscientific Model Development*, **3**, 43-67, 2010, doi:10.5194/gmd-3-43-2010.
- Ervens, B.; George, C.; Willams, J. E.; Buxton, G. V.; Salmon, G .A.; Bydder, M.; Wilkinson, F.; Dentener, F.; Mirabel, P. and Herrmann, H.; CAPRAM 2.4 (MODAC mechanism): An extended and condensed tropospheric aqueous phase mechanism and its application, *J. Geophys. Res.* 108 (D14), 4426. (2003).
- Evans, M. J., and D. J. Jacob (2005), Impact of new laboratory studies of N₂O₅ hydrolysis on global model budgets of tropospheric nitrogen oxides, ozone, and OH, *Geophys. Res. Lett.*, 32, L09813, doi:10.1029/2005GL022469.
- Fahey, K. M., and S. N. Pandis, Optimizing model performance: Variable size resolution in cloud chemistry modeling, *Atmos. Environ.*, 35, 4471–4478, 2001.
- Fahey, K.M., A. G. Carlton, H. O. T. Pye, J. Baeka, W. T. Hutzell, C. O. Stanier, K. R. Baker, K. W. Appel, M. Jaoui, and J. H. Offenberg, 2017, A framework for expanding aqueous chemistry in the Community Multiscale Air Quality (CMAQ) model version 5.1, *Geosci. Model Dev.*, 10, 1587–1605, 2017, doi:10.5194/gmd-10-1587-2017.
- Flemming, J., Huijnen, V., Arteta, J., Bechtold, P., Beljaars, A., Blechschmidt, A.-M., Diamantakis, M., Engelen, R. J., Gaudel, A., Inness, A., Jones, L., Josse, B., Katragkou, E., Marecal, V., Peuch, V.-H., Richter, A., Schultz, M. G., Stein, O., and Tsikerdekis, A.: Tropospheric chemistry in the Integrated Forecasting System of ECMWF, *Geosci. Model Dev.*, 8, 975-1003, <https://doi.org/10.5194/gmd-8-975-2015>, 2015.
- Fuentes, JD, Lerdau M, Atkinson R, Baldocchi D, Botteneheim JW, Ciccioli P, Lamb B, Geron C, Gu L, Guenther A, Sharkey TD, Stockwell WR. Biogenic hydrocarbons in the atmospheric boundary layer: a review. *Bull. Amer. Meteor. Soc.*; 2000;81,1537-1575.
- Fung, C.S.; Misra, P.K.; Bloxam, R.; Wong, S. A numerical experiment on the relative importance of H₂O₂ and O₃ in aqueous conversion of SO₂ to SO₄²⁻. *Atmos. Environ.* **1991**, 25, 411–423.
- Gao, D., W.R. Stockwell and J. B. Milford, First Order Sensitivity and Uncertainty Analysis for a Regional Scale Gas-Phase Chemical Mechanism, *J. Geophys. Res.*, 100, 23153-23166, 1995.

- Geiger, H., Barnes, I., Bejan, I., Benter, T., and Spittler, M.: The tropospheric degradation of isoprene: an updated module for the regional atmospheric chemistry mechanism, *Atmos. Environ.*, 37, 1503–1519, doi:10.1016/S1352-2310(02)01047-6, 2003.
- Gery, M. W., Whitten, G. Z., Killus, J. P., and Dodge, M. C.: A photochemical kinetics mechanism for urban and regional scale computer modeling, *J. Geophys. Res.*, 94, 12925–12956, 1989.
- Goldstein AH, Galbally IE. Known and unexplored organic constituents in the Earth's atmosphere. *Environ. Sci. Technol.*; 2007;41,1514-1521.
- Goliff, W.S., W.R. Stockwell and C.V. Lawson, The Regional Atmospheric Chemistry Mechanism, Version 2, *Atmos. Environ.*, 68, 174-185, 2013.
- Gong, W., Makar, P.A., Zhang, J., Milbrandt, J., Gravel, S., Hayden, K.L., MacDonald, A.M., and Leaitch, W.R., Modeling aerosol-cloud-meteorology interaction: A case study with a fully coupled air quality model (GEM-MACH), *Atm. Env.*, 115, 695-715, 2015.
- Graedel, T. E., and K. I. Goldberg, Kinetic studies of raindrop chemistry, I, Inorganic and organic processes, *J. Geophys. Res.*, 88, 10,865-10,882, 1983.
- Griffin, RJ, Cocker DR, Flagan RC, Seinfeld JH (1999), Organic aerosol formation from the oxidation of biogenic hydrocarbons. *J. Geophys. Res.-Atmos.*; 1999:104,3555-3567.
- Griffin, R. J., Dabdub, D., and Seinfeld, J. H.: Secondary organic aerosol 1. Atmospheric chemical mechanism for production of molecular constituents, *J. Geophys. Res.*, 107, 4342, doi:10.1029/2001JD000541, 2002.
- Hallquist M, Wenger JC, Baltensperger U, Rudich Y, Simpson D, Claeys M, Dommen J, Donahue NM, George C, Goldstein AH, Hamilton JF, Herrmann H, Hoffmann T, Iinuma Y, Jang M, Jenkin ME, Jimenez JL, Kiendler-Scharr A, Maenhaut W, McFiggans G, Mentel ThF, Monod A, Prévôt ASH, Seinfeld JH, Surratt JD, Szmigielski R, Wildt J. The formation, properties and impact of secondary organic aerosol: current and emerging issues. *Atmos. Chem. Phys.*; 2009;9,5155–5236.
- Hamilton JF, Webb PJ, Lewis AC, Hopkins JR, Smith S, Davy P. Partially oxidized organic components in urban aerosol using GCXGC-TOF/MS. *Atmos. Chem. Phys.*; 2004;4,1279-1290.
- Heisler SL, Friedlander SK. Gas-to-particle conversion in photochemical smog: aerosol growth laws and mechanisms for organics. *Atmos. Environ.*; 1977;11, 157-168.
- Herrmann, H.; Ervens, B., et al., A chemical aqueous phase radical mechanism for tropospheric chemistry, *Chemosphere* 38, 1223-1232. (1999)
- Herrmann, H.; Tilgner, A.; Barzagli, P.; Majdik, Z.; Gligorovski, S.; Poulain, L. and Monod, A.; Towards a more detailed description of tropospheric aqueous phase organic chemistry: CAPRAM 3.0. *Atmos. Environ.*, 39 (23-24), 4351-4363. (2005)
http://projects.tropos.de/capram/capram_30.html
- Hodzic A, Jimenez JL, Prévôt ASH, Szidat S, Fast JD, Madronich S., Can 3-D models explain the observed fractions of fossil and non-fossil carbon in and near Mexico City? *Atmos. Chem. Phys.*; 2010a:10,10997-11016.
- Hodzic A, Jimenez JL, Madronich S, Canagaratna MR, DeCarlo PF, Kleinman L, Fast J. Modeling organic aerosols in a megacity: potential contribution of semi-volatile and intermediate volatility primary organic compounds to secondary organic aerosol formation. *Atmos. Chem. Phys.*; 2010b:10,5491-5514.
- Horowitz, L. W.: A global simulation of tropospheric ozone and related tracers: description and evaluation of MOZART, version 2, *J. Geophys. Res.*, 108, 4784, doi:10.1029/2002JD002853, 2003.

- Hu, L., C.A. Keller, M.S. Long, T. Sherwen, B. Auer, A. Da Silva, J.E. Nielsen, S. Pawson, M.A. Thompson, A.L. Trayanov, K.R. Travis, S.K. Grange, M.J. Evans, and D.J. Jacob (2018), Global simulation of tropospheric chemistry at 12.5 km resolution: performance and evaluation of the GEOS-Chem chemical module within the NASA GEOS Earth System Model, *Geosci. Model Dev.*, 11, 4603-4620, <https://doi.org/10.5194/gmd-11-4603-2018>.
- Huijnen, V., Williams, J. E., and Flemming, J.: Modeling global impacts of heterogeneous loss of HO₂ on cloud droplets, ice particles and aerosols, *Atmos. Chem. Phys. Discuss.*, 14, 8575-8632, <https://doi.org/10.5194/acpd-14-8575-2014>, 2014.
- IUPAC (2018) International Union of Pure and Applied Chemistry, Task Group on Atmospheric Chemical Kinetic Data Evaluation, URL: <http://iupac.pole-ether.fr>. Last accessed November 10, 2018.
- Jacob, D.J., 1986. The chemistry of OH in remote clouds and its role in the production of formic acid and peroxymonosulfate, *Journal of Geophysical Research* 91, 9807-9826.
- Jacob, D.J., 2000, Heterogeneous chemistry and tropospheric ozone, *Atmospheric Environment* 34, 2131-2159.
- Jacobson, 2005, *Fundamentals of Atmospheric Modeling*, Cambridge University Press, New York, 2005, 813 pp., ISBN 9780521548656.
- Jones, A., D. Thomson, M. Hort, and B. Devenish, 2007: The U.K. Met Office's next-generation atmospheric dispersion model, NAME III, in *Air Pollution Modeling and Its Application XVII*, edited by C. Borrego and A.-L. Norman, 580–589, Springer, New York.
- Ketseridis G, Hahn J, Jaenicke R, Junge C. The organic constituents of atmospheric particulate matter. *Atmos. Environ.*; 1976:10, 603-610.
- Kim, Y.; Sartelet, K.; Seigneur, C. Formation of secondary aerosols over Europe: comparison of two gas-phase chemical mechanisms. *Atmos. Chem. Phys.* 2011, 11, 583–598.
- Kim YP and Seinfeld JH. Atmospheric gas–aerosol equilibrium III. Thermodynamics of crustal elements Ca²⁺ ; K⁺ ; and Mg²⁺. *Aerosol Science and Technology*; 1995: 22, 93-110.
- Kim YP, Seinfeld JH, Saxena P. Atmospheric gas-aerosol equilibrium I. Thermodynamic model. *Aerosol Science and Technology*; 1993a:19,157-181.
- Kim YP, Seinfeld JH, Saxena P. Atmospheric gas-aerosol equilibrium II. Analysis of common approximations and activity coefficient calculation methods. *Aerosol Science and Technology*; 1993b: 19,182-198.
- Kim, D., C. Loughner, M.A. Wetzell, W.S. Goliff and W.R. Stockwell, A Comparison of Photolysis Rate Parameters Estimated from Measured and Simulated Actinic Flux for Wintertime Conditions at Storm Peak Laboratory, Colorado, *J. Atmos. Chem.*, 57, 59-71, 2007. doi:10.1007/s10874-007-9061-2.
- Kinnison, D. E., Brasseur, G. P., Walters, S., Garcia, R. R., Marsh, D. R, Sassi, F., Harvey, V. L., Randall, C. E., Emmons, L., Lamar- que, J. F., Hess, P., Orlando, J. J., Tie, X. X., Randel, W., Pan, L. L., Gettelman, A., Granier, C., Diehl, T., Niemeier, U., and Simmons, A. J.: Sensitivity of chemical tracers to meteorological parameters in the MOZART-3 chemical transport model, *J. Geophys. Res.*, 112, D03303, doi:10.1029/2008JD010739, 2007.
- Knote, C., P. Tuccella, G. Curci, L. Emmons, J. J. Orlando, S. Madronich, R. Baro, P. Jiménez-Guerrero, D. Luecken, C. Hogrefe, R. Forkel, M. Hirtl, R. San José, L. Giordano, D. Brunner, K. Yahya, and Y. Zhang, 2014, Influence of the choice of gas-phase mechanism on predictions of key pollutants during the AQMEII phase-2 intercomparison, *Atmospheric Environment*, doi:10.1016/j.atmosenv.2014.11.066.
- Korsholm, U. S., Baklanov, A., Gross, A., Mahura, A., Hansen Sass, B., and Kaas, E.: Online coupled chemical weather forecasting based on HIRLAM – overview and prospective of Enviro- HIRLAM, *HIRLAM Newsletter*, 54, 151–168, 2008.

- Kouznetsov, R., Sofiev, M. (2012) A methodology for evaluation of vertical dispersion and dry deposition of atmospheric aerosols. *JGR*, 117. doi: [10.1029/2011JD016366](https://doi.org/10.1029/2011JD016366).
- Kuhns H, Bohdan V, Chow J, Etyemezian V, Green M, Herlocker D, Kohl S, McGown M, Ramsdell J, Stockwell WR, Toole M, Watson J. The treasure valley secondary aerosol study I: measurements and equilibrium modeling of inorganic secondary aerosols and precursors for southwestern Idaho. *Atmos. Environ.*; 2003;37,511-524.
- Lattuati, M. (1997). Contribution à l'étude du bilan de l'ozone troposphérique à l'interface de l'Europe et de l'Atlantique Nord : modélisation lagrangienne et mesures en altitude. PhD thesis, Université P.M.Curie, Paris, France.
- Law, K. S., Plantévin, P.-H., Shallcross, D. E., Rogers, H. L., Pyle, J. A., Grouhel, C., Thouret, V., and Marenco, A.: Evaluation of modeled O₃ using Measurement of Ozone by Airbus In-Service Aircraft (MOZAIC) data, *J. Geophys. Res.*, 103, 25721–25737, 1998.
- Lawson, S. J., M. Cope, S. Lee, I. E. Galbally, Z. Ristovski and M. D. Keywood (2017). "Biomass burning at Cape Grim: exploring photochemistry using multi-scale modeling." *Atmospheric Chemistry and Physics* 17(19): 11707-11726.
- Lee-Taylor J, Madronich S, Aumont B, Baker A, Camredon M, Hodzic A, Tyndall GS, Apel E, Zaveri RA. Explicit modeling of organic chemistry and secondary organic aerosol partitioning for Mexico City and its outflow plume. *Atmos. Chem. Phys.*; 2011;11,13219-13241.
- Leriche, M., Pinty, J.-P., Mari, C., and Gazen, D.: A cloud chemistry module for the 3-D cloud-resolving mesoscale model Meso-NH with application to idealized cases, *Geosci. Model Dev.*, 6, 1275–1298, doi:[10.5194/gmd-6-1275-2013](https://doi.org/10.5194/gmd-6-1275-2013), 2013.
- Liu, X., R. C. Easter, S. J. Ghan, R. Zaveri, P. Rasch, X. Shi, J.-F. Lamarque, A. Gettelman, H. Morrison, F. Vitt, A. Conley, S. Park, R. Neale, C. Hannay, A. M. L. Ekman, P. Hess, N. Mahowald, W. Collins, M. J. Iacono, C. S. Bretherton, M. G. Flanner, and D. Mitchell (2012), Toward a minimal representation of aerosols in climate models: description and evaluation in the Community Atmosphere Model CAM5, *Geosci. Model Dev.*, 5, 709-739, doi: [10.5194/Gmd-5-709-2012](https://doi.org/10.5194/Gmd-5-709-2012).
- Longo, K. M.; Freitas, S. R.; Pirre, M.; Marécal, V.; Rodrigues, L. F.; Panetta, J.; Alonso, M. F.; Rosário, N. E.; Moreira, D. S.; Gácita, M. S.; Arteta, J.; Fonseca, R.; Stockler, R.; Katsurayama, D. M.; Fazenda, A.; Bela, M., The Chemistry CATT-BRAMS model (CCATT-BRAMS 4.5): a regional atmospheric model system for integrated air quality and weather forecasting and research. *Geoscientific Model Development*, 6, p. 1389-1405, 2013.
- Madronich, S., Photodissociation in the atmosphere; 1. Actinic flux and the effects on ground reflections and clouds. *J. Geophys. Res.* 92, 9740–9752, 1987.
- Master Chemical Mechanism (2018). URL <http://mcm.leeds.ac.uk/MCMv3.3.1/home.htm>. Last accessed November 10, 2018.
- Metzger, S., Dentener, F., Pandis, S., and Lelieveld, J.: Gas/aerosol partitioning, 1, A computationally efficient model, *J. Geophys. Res.*, 107, 16, doi: [10.1029/2001JD001102](https://doi.org/10.1029/2001JD001102), 2002.
- Middlebrook AM, Murphy DM, Thomson DS. Observations of organic material in individual marine particles at Cape Grim during the First Aerosol Characterization Experiment (ACE 1). *J. Geophys. Res.-Atmos.*; 1998;103,16475-16483.
- Middleton, P.; Stockwell, W.R.; Carter, W.P.L. Aggregation and analysis of volatile organic compound emissions for regional modeling. *Atmos. Environ.* 1990, 24A, 1107-1133.
- Milford, J.B., D. Gao, A.G. Russell, and G.J. McRae, Use of sensitivity analysis to compare chemical mechanisms for air-quality modeling, *Environ. Sci. Technol.*, 26, 1179–1189, 1992.

- Morcrette, J.-J., et al. (2009), Aerosol analysis and forecast in the European Centre for Medium-Range Weather Forecasts Integrated Forecast System: Forward modeling, *J. Geophys. Res.*, 114, D06206, doi:10.1029/2008JD011235.
- Pandis, S.N. and J.H. Seinfeld, 1989, Sensitivity analysis of a chemical mechanism for aqueous-phase atmospheric chemistry, *J. Geophys. Res.*, 94, 1105-1126.
- Pandis SN, Harley RA, Cass GR, Seinfeld JH. Secondary organic aerosol formation and transport, *Atmos. Environ.*; 1992:26A, 2269-2282.
- Pandis SN, Paulson SE, Seinfeld JH, Flagan RC. Aerosol formation in the photooxidation of isoprene and beta-pinene. *Atmos. Environ.*; 1991:25A,997-1008.
- Pérez, C., Hausteijn, K., Janjic, Z., Jorba, O., Huneus, N., Baldasano, J. M., Black, T., Basart, S., Nickovic, S., Miller, R. L., Perlwitz, J. P., Schulz, M., and Thomson, M.: Atmospheric dust modeling from meso to global scales with the online NMMB/BSC-Dust model – Part 1: Model description, annual simulations and evaluation, *Atmos. Chem. Phys.*, 11, 13001-13027, <https://doi.org/10.5194/acp-11-13001-2011>, 2011.
- Real, E, E. Orlandi, K.S. Law, F. Fierli, D. Josset, F. Cairo, H. Schlager, S. Borrmann, D. Kunkel, C.M. Volk, J.B. McQuaid, D.J. Stewart, J. Lee, A.C. Lewis, J.R. Hopkins, F. Ravegnani, A. Ulanovski and C. Liousse, Cross-hemispheric transport of central African biomass burning pollutants: implications for downwind ozone production, *Atmos. Chem. Phys.*, 10, 3027-3046, 2010.
- Redington, A. L., and R. G. Derwent, 2002: Calculation of sulfate and nitrate aerosol concentrations over Europe using a Lagrangian dispersion model, *Atmos. Environ.*, 36, 4425-4439.
- Redington, A.L., Derwent, R.G., Witham, C.S., Manning, A.J., 2009: Sensitivity of modeled sulfate and nitrate aerosol to cloud, pH and ammonia emissions, *Atmos. Environ.*, 43, 3227-3234.
- Redington, A. L., and R. G. Derwent, 2013: Modeling secondary organic aerosol in the United Kingdom, *Atmos. Environ.*, 63, 349-357.
- Roustan Y., Sartelet K.N., Tombette M., Debry É. and Sportisse B. (2010), Simulation of aerosols and gas-phase species over Europe with the POLYPHEMUS system. Part II: Model sensitivity analysis for 2001. *Atmospheric Environment*, 44 (34), p4219-4229, doi:10.1016/j.atmosenv.2010.07.005.
- Sander, R., Kerkweg, A., Jöckel, P., and Lelieveld, J.: Technical note: The new comprehensive atmospheric chemistry module MECCA, *Atmos. Chem. Phys.*, 5, 445–450, doi:10.5194/acp-5-445-2005, 2005.
- Sartelet K., Debry E., Fahey K., Roustan Y., Tombette M., Sportisse B. (2007), Simulation of aerosols and gas-phase species over Europe with the Polyphemus system. Part I: model-to-data comparison for 2001. *Atmospheric Environment*, 41 (29), p6116-6131, doi:10.1016/j.atmosenv.2007.04.024.
- Sarwar, G., Luecken, D., Yarwood, G., Whitten, G. Z., and Carter, W. P. L.: Impact of an updated carbon bond mechanism on predictions from the CMAQ modeling system: preliminary assessment, *J. Appl. Meteorol. Clim.*, 47, 3–14, 2008.
- Sarwar, G., J. Godowitch, B. Henderson, K. Fahey, G. Pouliot, W. Hutzell, R. Mathur, D. Kang, W.S. Goliff and W.R. Stockwell. A Comparison of Atmospheric Composition using the Carbon Bond and Regional Atmospheric Chemistry Mechanisms, *Atmos. Chem. Phys.*, 13, 1–18, 2013. doi:10.5194/acp-13-1-2013.
- Saunders E. Modeling Regional & Global Atmospheric Chemistry Mechanisms: Observing Adverse Respiratory Health Effects due to Tropospheric Ozone Air Pollution from Modeling Output. Ph.D. Dissertation. Washington, DC: Howard University; May 2017.
- Schaap, M.; van Loon, M.; ten Brink, H.M.; Dentener, F.J.; Builtjes, P.J.H. Secondary inorganic aerosol simulations for Europe with special attention to nitrate. *Atmos. Chem. Phys.* 2004, 4, 857–874.

- Seinfeld, J.H. and S.N. Pandis (2016), *Atmospheric Chemistry and Physics: from Air Pollution to Climate Change*, John Wiley & Sons, Inc., ISBN: 978-1-118-94740-1, 2016 (the 3rd edition).
- Shalaby, A.K., A.S. Zakey, A.B. Tawfik, F. Solmon, F. Giorgi, F. Stordal, S. Sillman, R.A. Zaveri and A.L. Steiner, Implementation and evaluation of online gas-phase chemistry within a regional climate model (RegCM-CHEM4), *Geosci. Model Dev. Discuss.*, 5, 149–188, 2012.
- Sillman, S., A Numerical Solution for Equations of Tropospheric Chemistry Based on an Analysis of Sources and Sinks of Odd Hydrogen, *J. Geophys. Res.*, 96, 20735–20744, 1991.
- Simpson, D., Benedictow, A., Berge, H., Bergström, R., Emberson, L. D., Fagerli, H., Flechard, C. R., Hayman, G. D., Gauss, M., Jonson, J. E., Jenkin, M. E., Nyíri, A., Richter, C., Semeena, V. S., Tsyro, S., Tuovinen, J.-P., Valdebenito, Á., and Wind, P.: The EMEP MSC-W chemical transport model – technical description, *Atmos. Chem. Phys.*, 12, 7825–7865, <https://doi.org/10.5194/acp-12-7825-2012>, 2012
- Sofiev, M. (2000) A model for the evaluation of long-term airborne pollution transport at regional and continental scales. *Atmospheric Environment*. 34, No.15, pp. 2481-2493.
- Spada, M., 2015. Development and evaluation of an atmospheric aerosol module implemented within the NMMB/BSC-CTM. PhD Thesis, BarcelonaTech, Spain.
- Stewart, D.R., E. Saunders, R.A. Perea, R. Fitzgerald, D.E. Campbell and W.R. Stockwell, Linking Air Quality and Human Health Effects Models: An Application to the Los Angeles Air Basin, *Environmental Health Insights*, 11, 1-13, 2017.
[doi:10.1177/1178630217737551](https://doi.org/10.1177/1178630217737551)
- Stockwell, W.R., A Homogeneous Gas Phase Mechanism for use in a Regional Acid Deposition Model, *Atmos. Environ.*, 20, 1615-1632, 1986.
- Stockwell, W.R., F. Kirchner, M. Kuhn, and S. Seefeld, A New Mechanism for Regional Atmospheric Chemistry Modeling, *J. Geophys. Res.*, 102, 25847-25879, 1997.
- Stockwell WR, Lawson CV, Saunders E, Goliff WS. A Review of Tropospheric Atmospheric Chemistry and Gas-Phase Chemical Mechanisms for Air Quality Modeling. *Atmosphere*; 2012: 3,1-32.
- Stockwell, W.R.; Middleton, P.; J.S. Chang; Tang, X. The second generation regional acid deposition model chemical mechanism for regional air quality modeling. *J. Geophys. Res.* 1990, 95, 16343-16367.
- Strader, R., C. Gurciullo, S. Pandis, N. Kumar and F.W. Lurmann, 1998. Development of gas-phase chemistry, secondary organic aerosol, and aqueous-phase chemistry modules for PM modeling, Technical Report, STI, Contract A-21-2, Coordinating Research Council, Atlanta, GA.
- Strader, R., Lurmann, F., and Pandis, S. N., 1999, Evaluation of secondary organic aerosol formation in winter, *Atmos. Environ.*, 39, 4849–4864.
- Tang, Y., et al. (2003), Impacts of aerosols and clouds on photolysis frequencies and photochemistry during TRACE-P: 2. Three-dimensional study using a regional chemical transport model, *J. Geophys. Res.*, 108(D21), 8822,
[doi:10.1029/2002JD003100](https://doi.org/10.1029/2002JD003100).
- Tie, X., G. Brasseur, L. Emmons, L. Horowitz, and D. Kinnison, Effects of aerosols on tropospheric oxidants: A global model study, *J. Geophys. Res.*, 106, 22,931–22,964, 2001.
- Tulet, P., Grini, A., Griffin, R., and Petitcol, S.: ORILAM-SOA: a computationally efficient model for predicting secondary organic aerosols in 3-D atmospheric models, *J. Geophys. Res.*, 111, D23208, [doi:10.1029/2006JD007152](https://doi.org/10.1029/2006JD007152), 2006.
- Turpin BJ, Huntzicker JJ, Larson SM, Cass GR. Los-Angeles summer midday particulate carbon – primary and secondary aerosol. *Environ. Sci. Technol.*, 1991:25,1788-1793.

- U.S. EPA (2018), United States Environmental Protection Agency, Managing Air Quality - Emissions Inventories, <https://www.epa.gov/air-quality-management-process/managing-air-quality-emissions-inventories#dev>
- Venkatram, A., Karamchandani, P. K., and Misra, P. K.: Testing a comprehensive acid deposition model, *Atmos. Environ.*, **22**, 737–747, 1988.
- Virtanen A, Joutsensaari J, Koop T, Kannosto J, Yli-Pirila P, Leskinen J, Makela JM, Holopainen JK, Pöschl U, Kulmala M, Worsnop DR, Laaksonen A. An amorphous solid state of biogenic secondary organic aerosol particles. *Nature*, 2010: 467, 824-827//.
- Vogel, B., Vogel, H., Bäumer, D., Bangert, M., Lundgren, K., Rinke, R., and Stanelle, T.: The comprehensive model system COSMO- ART – Radiative impact of aerosol on the state of the atmosphere on the regional scale, *Atmos. Chem. Phys.*, **9**, 8661–8680, doi: 10.5194/acp-9-8661-2009, 2009.
- Vogel, H., Pauling, A., and Vogel, B.: Numerical simulation of birch pollen dispersion with an operational weather forecast system, *Int. J. Biometeorol.*, **52**, 805–814, doi: 10.1007/s00484-008-0174-3, 2008.
- Volkamer R, Jimenez JL, Martini FS, Dzepina K, Zhang Q, Salcedo D, Molina LT, Worsnop DR, Molina MJ. Secondary organic aerosol formation from anthropogenic air pollution: Rapid and higher than expected. *Geophys. Res. Lett.*, 2006: 33, L17811, doi: 10.1029/2006GL026899.
- Walcek, C.J. and G.R. Taylor, 1986. A theoretical method for computing vertical distributions of acidity and sulfate production within cumulus clouds, *J. Atmos. Sci.*, **43**, 339-355.
- Wang, H., X. Y. Zhang, S. L. Gong, et al., 2010: Radiative feedback of dust aerosols on the East Asian dust storms. *J. Geophys. Res.*, **115**, D23214, doi: 10.1029/2009JD013430.
- Watson, L. A., Shallcross, D. E., Utembe, S. R., and Jenkin, M. E.: A Common Representative Intermediates (CRI) mechanism for VOC degradation – Part 2: Gas phase mechanism reduction, *Atmos. Environ.*, **42**, 7196–7204, doi: 10.1016/j.atmosenv.2008.07.034, 2008.
- Whitten, G.Z.; Hogo, H. Mathematical Modeling of Simulated Photochemical Smog, EPA Report Number EPA-600/3-77-011, Washington DC, United States, 1999.
- Whitten, G.Z.; Hogo, H.; Killus, J.P. The carbon-bond mechanism: a condensed kinetic mechanism for photochemical smog, *Environ. Sci. Technol.* 1980, **14**, 690 – 700.
- Wolke, R., W. Schroeder, R. Schroedner, E. Renner, 2012, Influence of grid resolution and meteorological forcing on simulated European air quality: A sensitivity study with the modeling system COSMO-MUSCAT. *Atmos. Env.*, **53**, 110-130.
- WRF-Chem (2018), WRF-Chem Version 3.9.1.1 users' Guide, https://ruc.noaa.gov/wrf/wrf-chem/Users_guide.pdf
- Yarwood, G., J. Jung, G. Z. Whitten, G. Heo, J. Mellberg, and E. Estes, 2010. Updates to the Carbon Bond Mechanism for Version 6 (CB6), Presented at the 9th Annual CMAS Conference, Chapel Hill, October 2010. Available: http://www.cmascenter.org/conference/2010/abstracts/emery_updates_carbon_2010.pdf
- Yarwood, G.; Rao, S.; Yocke, M.; Whitten, G.: Updates to the carbon bond chemical mechanism: CB05. Final report to the US EPA, EPA Report Number: RT-0400675, ENVIRON International Corporation, Novato, California, available at: www.camx.com, December 8, 2005a
- Yarwood, G., G.Z. Whitten and S. Rao, Updates to the Carbon Bond 4 Photochemical Mechanism, ENVIRON International Corporation, Novato, California, March 2005b.
- Zaveri, R., 1997. Development of a comprehensive tropospheric chemistry model for regional and global applications, Ph.D. thesis, Virginia Polytechnic Institute and State University, Blacksburg, VA.

- Zaveri, R.A. and L.K. Peters, A New Lumped Structure Photochemical Mechanism for Large-Scale Applications, *J. Geophys. Res., Atmospheres*, *104*, 30387-30415, 1999.
- Zhang, Y. and G.R. Carmichael, 1999, The Role of Mineral Aerosol in Tropospheric Chemistry in East Asia - a Model Study, *Journal of Applied Meteorology*, *38* (3), 353-366, doi: [10.1175/1520-0450\(1999\)038<0353:TROMAI>2.0.CO;2](https://doi.org/10.1175/1520-0450(1999)038<0353:TROMAI>2.0.CO;2).
- Zhang, Y., C.H. Bischof, R.C. Easter, and P.-T. Wu, 2005, Sensitivity analysis of photochemical indicators for O₃ chemistry using automatic differentiation, *Journal of Atmospheric Chemistry*, *51*, 1-41, doi: [10.1007/s10874-005-5440-8](https://doi.org/10.1007/s10874-005-5440-8).
- Zhang Q, Jimenez JL, Canagaratna MR, Allan JD, Coe H, Ulbrich I, Alfarra MR, Takami A, Middlebrook AM, Sun YL, Dzepina K, Dunlea E, Docherty K, DeCarlo PF, Salcedo D, Onasch T, Jayne JT, Miyoshi T, Shimojo A, Hatakeyama S, Takegawa N, Kondo Y, Schneider J, Drewnick F, Borrmann S, Weimer S, Demerjian K, Williams P, Bower K, Bahreini R, Cottrell, L, Griffin R.J., Rautiainen, J., Sun J.Y., Zhang Y.M. Worsnop D.R., Ubiquity and dominance of oxygenated species in organic aerosols in anthropogenically-influenced Northern Hemisphere midlatitudes, *34*, L13801, doi: [10.1029/2007GL029979](https://doi.org/10.1029/2007GL029979), 2007.
- Zhang, Y., C.H. Bischof, R.C. Easter and P.T. Wu, 1998. Sensitivity analysis of a mixed-phase chemical mechanism using automatic differentiation, *J. Geophys. Res.*, **103**, 18953-18979.
- Zhang Q.J., Beekmann M, Drewnick F, Freutel F, Schneider J, Crippa M, Prévôt ASH, Baltensperger U, Poulain L, Wiedensohler A, Sciare J, Gros V, Borbon A, Colomb A, Michoud V, Doussin J-F, Denier-van der Gon HAC, Haeffelin M, Dupont J-C, Siour G, Petetin H, Bessagnet B, Pandis SN, Hodzic A, Sanchez O, Honoré C, Perrussel O. Formation of organic aerosol in the Paris region during the MEGAPOLI summer campaign: evaluation of the volatility-basis-set approach within the CHIMERE model. *Atmos. Chem. Phys.*; 2013;13, 5767-5790.
- Zhang, Y., 2021, Air Quality in a Changing Climate: Science and Modeling, Cambridge University Press, in preparation.
- Zhou C., X. Zhang, S. Gong, Y. Wang, and M. Xue, Improving aerosol interaction with clouds and precipitation in a regional chemical weather modeling system, *Atmos. Chem. Phys.* *16*, 145-160, 2016, doi: [10.5194/acp-16-145-2016](https://doi.org/10.5194/acp-16-145-2016)
- Zhou, C. H., X. J. Shen, Z. R. Liu., et al., 2018: Simulating aerosol size distribution and mass concentration with simultaneous nucleation, condensation/coagulation, and deposition with the GRAPES-CUACE. *J. Meteor. Res.*, *32*(2), 1-14, doi: [10.1007/s13351-018-7116-8](https://doi.org/10.1007/s13351-018-7116-8).

3.6 Atmospheric Aerosol

3.6.1 Introduction

Atmospheric aerosols play an important role in air quality, climate, and public health. For example, they are a major component of smog and haze, adversely impacting air quality and visibility. They can enter nose/mouth and penetrate human lungs, causing nose and throat irritation, lung damage, respiratory diseases such as bronchitis, and premature death. They can also influence climate directly through absorbing or scattering atmospheric radiation and indirectly through affecting cloud formation by acting as cloud condensation nuclei. Forecasting atmospheric aerosols is technically very challenging because of their broad size spectrum from a few nanometers to tens of micrometers, multiple chemical components, and complex physical and chemical formation mechanisms and processes. A series of modules has been developed and implemented in CW-AQF models to represent the PM size distribution, chemical composition, and the physical and chemical processes that determine the spatial and temporal distributions of aerosol concentrations. Due to limitations in our understanding and computational resources, many processes are necessarily simplified or parameterized based on detailed formulations. The mass of particles is regulated for particulate matter of aerodynamic diameter lower than and equal to 2.5 μm and 10 μm (PM_{2.5} and PM₁₀, respectively). Atmospheric PM is made of a variety of components. PM diameters vary over a wide size range of a few nanometers to several tens of micrometers. Ultrafine particles (of diameter lower than 0.1 μm) have very low mass concentrations, but their number concentrations may be very high. Although these particles may penetrate deep in the respiratory tract, they are not regulated as they do not contribute much to mass concentration but mostly to number concentration.

Because of the chemical transformations, aerosol processes are strongly linked to the gas-phase processes through various gas-to-particle conversion processes such as heterogeneous reactions (see Section 3.5), nucleation, condensation/evaporation (see Section 3.6.4). Gaseous precursors, for example, can condense onto particles, which requires the modeling of the interactions between different phases at the particle surface. The modeling of the dynamic evolution of the PM size distribution of particles affects the concentrations of particles through different processes such as deposition, which removes pollutants from the atmosphere and transfers them to other media (see Section 3.7). Fundamentals of PM composition, size distribution, thermodynamics, and dynamics are introduced below. Common modeling approaches for representing aerosol properties and processes in current CW-AQF models are discussed. Tables 3.13 and 3.14 summarize the main characteristics of aerosol modules used in CW-AQF models. These aerosol modules will also be reviewed.

3.6.2 Atmospheric PM Composition, Size Distribution, and Mixing State

Particle Composition

Particulate matter (PM) includes primary and secondary components. Primary PM is emitted directly from various sources (e.g., anthropogenic sources such as industry, combustion, vehicles, and household, and natural sources such as biomass burning, sea salt (SS), and dust). Secondary PM is formed in the atmosphere through chemical transformations of organic or inorganic precursor gases. Atmospheric PM is a complex mixture of chemical species including inorganic (e.g., sodium, sulfate, ammonium, nitrate, chloride, water, trace metals), mineral dust, elemental carbon (EC) (also referred to as black carbon (BC) or light-absorbing carbon when it is estimated using optical measurements), and organic aerosol (OA). OA can be further classified as primary organic aerosol (POA) and secondary organic aerosol (SOA). Most CW-AQF models treat all major PM species other than trace metals. The GLOMAP aerosol model used in Australian CW-AQF model, AQFx, also treats trace metals speciated from sea salt and dust. Some only consider a subset of these species. For example, the global CW-AQF model developed by ECMWF, IFS, does not treat nitrate.

Representation of PM Size Distribution

The PM size distribution may be modeled by different approaches, among which the most commonly used approaches in CW-AQF are the sectional and the modal size distributions. In the sectional approach, the size distribution is discretized into sections or “bins”, e.g., in the aerosol model MADRID (Zhang et al., 2004) used in WRF/Chem-MADRID and SIREAM (Debry et al., 2007) or SCRAM (Zhu et al., 2015) used in Polyphemus. The sectional representation of the particle size distribution used in most CW-AQMs is based on the mass distribution of particles. In the modal approach, the size distribution is represented by several log-normally distributed modes, e.g., in the modal model MAM (Sartelet et al., 2006). The modal approach typically uses three modes including Aitken nuclei mode, accumulation mode, and coarse mode. The log-normal approximation allows one to simulate the evolution of both the number and volume (or mass). Each size representation method has its own merits. While the modal approach is computationally more efficient than the sectional approach that consists of more than two sections, it is usually less accurate than the sectional approach. The accuracy of the sectional representation strongly depends on the size resolution. CW-AQMs typically use 6-16 size sections (Zhang et al., 1999). CW-AQF models based on the sectional size representation include IFS, AQFx, CHIMERE, Polyphemus, and NAQFC. Some models such as WRF/Chem and RegCM-CHEM offer options to use either the sectional or the modal size representations. A few models simulate the bulk aerosol mass without distinguishing the size range or a mix of bulk and sectional approach. For example, LOTOS-EUROS offers options to use bulk representation or sectional representation with two sections (fine and coarse). CCATT-BRAMS uses sectional representation for dust and sea salt and the bulk treatment for other aerosols. GRAPES-CUACE uses 12 bins from 10 nm to 40 μm in diameter for all aerosol components except for ammonium which is in bulk representation.

Table 3.13 Representation of aerosol processes in global CW-AQF models

Attribute/Model	G5CHEM (GEOS-5 with GEOS-Chem)	IFS (ECMWF/CAMS) (ECMWF)	SILAM v.5.5
Aerosol model name	The original carbonaceous aerosol simulation was developed by Park et al. (2003). Wang et al. (2014) gives an overview of the current BC simulation in GEOS-Chem. SOA formation follows the simplified Volatility Basis Set (VBS) scheme of Pye et al. (2010). The dust simulation in GEOS-Chem is described by Fairlie et al. (2007). The sea salt aerosol simulation in GEOS-Chem is described by Jaegle et al. (2011).	LOA/LMDz (Reddy et al., 2005; Morcrette et al., 2009)	Four models: (i) DMAT bulk inorganic aerosol formation, equilibrium-based, (ii) VBS for secondary organics, (iii) stratospheric PSC, (iv) SALSA-type dynamic scheme, research-only
Aerosol species	Dust, sea salt, black and organic carbon (BC and OC), sulfate, nitrate, ammonium	Desert dust, sea salt, organic matter (OM), BC SO_4^{2-}	Reactive: SO_4^{2-} , NH_4NO_3 , NH_4HSO_4 (NH_4) $_2\text{SO}_4$, coarse NO_3^- on sea salt. Non-reactive: Sea salt, Fire PM, desert dust, OC, EC, mineral anthropogenic
Size representation	Bin/bulk scheme (4 bins for dust, 2 bins for sea salt, bulk hydrophilic/hydrophobic for BC and OC)	Bin/bulk scheme (3 size bins for DD and SS; bulk hydrophilic/hydrophobic for OM and BC; bulk for SO_4^{2-})	Sectional. User-defined bins (typically 2-15 bins over 0.01-30 μm)
Aerosol mixing state	Internally mixed	Externally mixed	External mixture
Aerosol mass/number	Diagnosed	Predicted/diagnosed	Mass only
Aerosol hygroscopicity	Prescribed	Prescribed radius and mass growth factors for each species	Species-dependent
Aerosol radiative properties	Aerosol optical depth is calculated using RH-dependent aerosol optical properties from Martin et al. (2003). Dust optics are from Ridley et al. (2012).	Lookup tables based on offline Mie scattering calculations using prescribed refractive indices for each species/bin at a range of wavelengths and relative humidities, as described in Bozzo et al. (2017)	Mie scheme for sections
Inorganic aerosol thermodynamic module	ISORROPIA-II (Fountoukis and Nenes, 2007), as implemented by Pye et al. (2009).	EQSAM for the nitrate partitioning	Gas-particle equilibrium, Sofiev (2000)

Attribute/Model	G5CHEM (GEOS-5 with GEOS-Chem)	IFS (ECMWF/CAMS) (ECMWF)	SILAM v.5.5
Organic precursors	Biogenic SOA is produced with a yield of 3% from isoprene and 5% from monoterpenes. Anthropogenic VOCs are emitted in proportion to CO.	None	Biogenic: isoprene, monoterpene. Anthropogenic: toluene, xylene, and 7 volatility bins of unspciated VOCs.
SOA module	Described in Marais et al. (2016). SOA formation follows the simplified Volatility Basis Set (VBS) scheme of Pye et al. (2010).	Prescribed biogenic SOA sources, Anthropogenic SOA sources based on CO emissions as proxy	1D VBS with 7 volatility bins, for anthropogenic and 5 for biogenic (Shrivastava et al., 2011)
Interactions organic/inorganic compounds	Via competition for OH in the gas phase. Via nucleation/condensation competition in the aerosol phase.	Ageing of hydrophobic OM (and BC) to hydrophilic with fixed timescale	None
Aerosol water content	ZSR correlation	Prescribed fixed radius and mass growth factors for each species at different relative humidities	Hygroscopic growth (Lewis and Schwartz, 2006)
Online photolysis calculation accounting for aerosol feedbacks	Yes, computed based on Mie theory as described in Wild et al. (2000).	Yes, CBO5 calculations updated to use prognostic fields from the aerosol scheme rather than climatologies and its own sulfate tracer.	None
Nucleation	Homogeneous nucleation of H ₂ SO ₄	None	None
Condensation/Evaporation	Dynamic condensation of SO ₂ following Chameides and Stelson (1992).	Temperature and latitude-dependent irreversible conversion of SO ₂ to form SO ₄ ²⁻	None
Redistribution or mode merging schemes	N/A	N/A	None
Coagulation	N/A	N/A	None
Gas-to-particle mass transfer	Thermodynamic equilibrium for HNO ₃ and NH ₃ . Dynamic equilibrium for SO ₂ (Chameides and Stelson, 1992). Organics equilibrium based on VBS approach (Pye et al., 2010).	None	equilibria, Sofiev (2000)
Reference	Hu et al. (2018)	Flemming et al. (2015); Morcrette et al. (2009)	Sofiev (2000); Kouznetsov and Sofiev (2012)

Table 3.14 Representation of aerosol processes in 11 regional/urban CW-AQF models.

Attribute/Model	AQFx	NAQFC (WRF-CMAQ)	WRF/Chem
Aerosol model name	Option of GLOMAP or a simple fixed 2-bin scheme. The description below primarily refers to GLOMAP	Aero6	MADE, MOSAIC, GOCART, MADRID, MAM3 or MAM7
Aerosol species	Sulfate, nitrate, ammonium, OC, sea salt, dust, water. Trace metals speciated from sea salt and dust.	Sulfate, nitrate, ammonium, BC, OC, sea salt, dust, water	Sulfate, nitrate, ammonium, BC, OC, sea salt, dust, water
Size Representation	Modal (4 soluble modes, 3 insoluble modes). nucleation 0.001-0.1 μm ; Aitken 0.01-0.10 μm ; accumulation 0.10-1.0 μm ; coarse 1.0-10 μm . Log-normal distributions; dynamical geometric mean diameters, fixed geometric standard deviations (Mann et al., 2010).	Modal (3 log-normal distributions over 0-10 μm)	Modal (3 modes in MADE and 3 or 7 modes in MAM) Sectional (4-8 sections for MOSAIC and 8 sections for MADRID over 0-10 μm) Bulk (GOCART)
Aerosol mixing state	Internal mixture	Internal mixture	Internal mixture
Aerosol mass/number	Predicted/Predicted	Predicted/Predicted	Predicted/Predicted
Aerosol hygroscopicity	Water uptake is based on the soluble inorganic components and an equivalent hygroscopicity for the soluble organic components.	Water uptake based on inorganic components (Binkowski and Roselle, 2003)	Simulated (volume averaged) with prescribed hygroscopicities for OC and dust
Aerosol radiative properties	These are used only for the calculation of aerosol optical depth and attenuated backscatter.	Mass Reconstruction and Mie Schemes (Binkowski and Roselle, 2003)	Parameterized Refractive Index (RI) and optical properties based on wet radius and RI of each mode
Inorganic aerosol thermodynamic module	ISORROPIA-II (Fountoukis and Nenes, 2007)	ISORROPIA	MARS-A (MADE) MESA-MTEM (MOSAIC) ISORROPIA (MADRID) a highly simplified inorganic aerosol thermodynamics treatment that only simulates particulate-phase sulfate and ammonium (MAM7) No thermodynamic module (MAM3 and GOCART)
Organic precursors	Anthropogenic and ambient smoke SVOCs are tracked using (for CB05) five VOC species. Biogenic SVOCs are tracked using two VOC species.	8 classes of condensable SVOCs resulting from five classes of parent VOCs 6 classes of the condensable	SORGAM: (8 classes VOCs) MADRID1: 2 anthropogenic VOC precursors, 4 surrogate anthropogenic

Attribute/Model	AQFx	NAQFC (WRF-CMAQ)	WRF/Chem
		SVOCs arise from anthropogenic precursor VOCs (from 3 classes of aromatics including xylene, toluene, and cresol, and 1 class of higher alkanes) and two classes from biogenic monoterpenes.	species representing their condensable products, 12 biogenic VOC (BVO) precursors and 34 surrogate biogenic species representing their condensable products; MADRID 2 includes 10 surrogate for 42 explicit compounds, grouped according to their affinity. for water; VBS (9 bins) includes 36 POA gases, 32 SI-SOA gases, and 8 V-SOA gases, VBS (2 bins) includes 8 POA gases, 4 SI-SOA gases, and 2 V-SOA gases.
SOA module	Volatility Basis Set (Tsimpidi et al., 2014).	1. Reversible Absorption based on SORGAM 2. VBS (Robinson et al., 2007)	SORGAM: reversible absorption based on smog-chamber data () VBS (9 bins) includes 144 POA aerosols, 128 SI-SOA aerosols resulted from semi- and intermediate VOCs, and 32 V-SOA aerosols resulted from VOCs, VBS (2 bins) includes 32 POA aerosols, 16 SI-SOA aerosols, and 8 V-SOA aerosols MADRID1: absorption MADRID2: combined absorption and dissolution. MOSAIC: no SOA treatment with CBM-Z, VBS with SAPRC99
Interactions organic/inorganic	Via competition for OH in the gas phase. Via perturbation to aerosol water; nucleation/condensation competition in the aerosol phase.	None	Only available in MADRID2
Aerosol water content	The ZSR method	Water uptake based on inorganic components (Binkowski and Roselle 2003)	The ZSR method
Online photolysis calculation accounting for aerosol feedbacks	None	Binkowski et al. (2007)	Grell et al. (2005)
Nucleation	Binary homogeneous nucleation- with options for 4 different mechanisms based on H ₂ SO ₄ and (for 2 mechanisms) H ₂ SO ₄ and organic vapor (Reddington et al., 2011).	Binary homogeneous nucleation of H ₂ SO ₄ and H ₂ O of Kulmala et al. (1998)	Binary homogeneous nucleation of H ₂ SO ₄ and H ₂ O of Kulmala et al. (1998 b) (SORGAM) and of McMurry and Friedlander (1979) (MADRID); T- and RH-dependent; sectional; different equations in different aero modules

Attribute/Model	AQFx	NAQFC (WRF-CMAQ)	WRF/Chem
Condensation / Evaporation	Dynamic condensation of H ₂ SO ₄ (Mann et al., 2010). Condensation/evaporation for other semi-volatile organic and inorganic species follows (Capaldo et al., 2000).	Dynamic condensation of H ₂ SO ₄ and VOCs using the modal approach of Binkowski and Shankar (1995) (SORGAM)	Dynamic condensation of H ₂ SO ₄ and VOCs using the modal approach of Binkowski and Shankar (1995) (SORGAM), of H ₂ SO ₄ , MSA, and NH ₃ using the ASTEEM method (MOSAIC), and of volatile inorganic species using the APC with moving center scheme (MADRID)
Redistribution or mode merging schemes	GLOMAP- mode merging occurs after the coagulation-nucleation step if the geometric mean diameter of a mode falls above of a prescribed range. In this case, a fraction of the particle number and mass is moved to the next largest mode (Mann et al., 2010).	The condensed mass is redistributed using the mode merging following Binkowski and Roselle (2003)	The condensed mass is redistributed using the mode merging following Binkowski and Roselle (2003) in MADE, and the moving-center scheme of Jacobson (1997) in MADRID
Coagulation	Intra-modal and inter-modal coagulation is treated (Mann et al., 2010)	Modal approach	Modal/Sectional (MADE/SORGAM, MOSAIC, MADRID), single size distribution, fine modes only
Gas-to-particle mass transfer	Inorganics- equilibrium for HNO ₃ , NH ₃ , and HCl for fine modes; dynamic mass transfer for coarse modes (Pilinis et al., 2000; Capaldo et al., 2000; Kelly et al., 2010). Organics- equilibrium using the VBS approach (Tsimpidi et al., 2014).	Full equilibrium for HNO ₃ and NH ₃	1. Full equilibrium for HNO ₃ and NH ₃ in MADE/SORGAM and all species in MADRID 2. Dynamic for H ₂ SO ₄ in MADE/SORGAM; Dynamic for all species in MOSAIC and MADRID 3. Hybrid in MADRID
References	Mann et al. (2010)	Lee et al. (2017)	Grell et al. (2005); Fast et al. (2006); Zhang et al. (2010)

Attribute	GEM-MACH15	NMMB/BSC-CTM	DERMA & ENVIRO- HIRLAM
Aerosol model name	Canadian Aerosol Module (CAM)	in-house (Spada, 2015)	2 aerosol dynamics modules: Old modal CAC (Baklanov, 2003; Gross and Baklanov, 2004) and new version is based on M7 (Vignati et al., 2004) with aerosol removal processes (Stier et al., 2005).
Aerosol species	Sulfate, nitrate, ammonium, primary OC, SOA, BC, sea salt, crustal material, water	Dust, sea salt, BC, OM, sulfate, nitrate and ammonium	4 predominant aerosol types are included: BC and primary OC, sulfate, mineral dust and sea salt in the key version, pollen aerosols in the version for pollen forecast.

Attribute	GEM-MACH15	NMMB/BSC-CTM	DERMA & ENVIRO- HIRLAM
Size representation	Sectional (2 or 12-bin distributions)	8 sectional bins for dust and 8 for sea salt, and bulk for the rest.	Insoluble and mixed (water-soluble) particles. 7 classes by particle size and solubility. 4 classes to represent mixed particles, i.e. nucleation, Aitken, accumulation and coarse modes, and another 3 classes are for the insoluble (Aitken, accumulation and coarse modes).
Aerosol mixing state	Internal mixture	Externally mixed	External mixture of insoluble and internally mixed populations
Aerosol mass/number	Predicted/prognosed	Only mass is predicted	Predicted/prognosed
Aerosol hygroscopicity	Two approaches: (a) based on inorganic heterogeneous chemistry (HETV, Makar et al., 2003); (b) Hanel (1976) empirical functions plus Kohler equation (Gong et al., 2003).	Hygroscopic factors following Chin et al. (2002)	Species-dependent
Aerosol radiative properties	Mie scattering assuming a homogeneous mixture, water and typical anthropogenic aerosol refractive indices (Makar et al., 2015a; Bohren and Huffman, 1983)	OPAC (Hess et al., 1998) or in-house (Obiso, 2017)	Nielsen et al. (2014); Rontu et al. (2017)
Inorganic aerosol thermodynamic module	HETV (Makar et al., 2003)	Equilibrium Simplified Aerosol Model (EQSAM) (Metzger et al., 2002, 2006)	Thermodynamic equilibrium NWP-Chem-Liquid, described in Korsholm et al. (2008).
Organic precursors	Isoprene, lumped species: mono-substituted alkyl aromatics, di,tri-substituted alkyl aromatics, higher carbon number alkanes, higher carbon number alkenes; subversions with monoterpenes as separate species.	Isoprene and α -pinene	HCHO and a lumped HC representing all remaining organics
SOA module	(1) Operational code: 2 product fit to chamber data (Pankow, 1994; Griffin et al., 1999); initial products assumed to be converted rapidly to non-volatile organic particulate mass. (2) Volatility basis set (experimental code), Robinson et al. (2007)	Two-product scheme (Tsigaridis and Kanakidu, 2003)	simplified parametrization

Attribute	GEM-MACH15	NMMB/BSC-CTM	DERMA & ENVIRO- HIRLAM
Interactions organic/inorganic	None	None	Under development
Aerosol water content	Two approaches: (a) based on inorganic heterogeneous chemistry (HETV, Makar et al., 2003); (b) Hanel (1976) empirical functions plus Kohler equation (Gong et al., 2003).	Not treated	Simplified liquid-phase equilibrium mechanism included in NWP-Chem-Liquid.
Online photolysis calculation accounting for aerosol feedbacks	Yes, based on the approach of Makar et al. (2015a, b)	No	Yes
Nucleation	Kumala et al. (1998) ($H_2SO_4 + H_2O$); Gong et al. (2003)	None	Yes, with 2 aerosol dynamics models: CAC and M7
Condensation/Evaporation	Modified Fuchs-Sutugin (1971) equation for H_2SO_4 , organic gases assumed to partition similar to H_2SO_4 (Gong et al., 2003)	None	Yes, with 2 aerosol dynamics models: CAC and M7
Redistribution or mode merging schemes	Sectional approach	None	Yes, as in M7
Coagulation	Semi-implicit numerical solution following Jacobson et al. (1994); Gong et al. (2003)	None	Yes, with 2 aerosol dynamics models: CAC and M7
Gas-to-particle mass transfer	Bulk equilibrium followed by rebinning for inorganics; Sulfate explicit redistribution according to condensation equation, condensable organics assumed to partition similar to organics.	Equilibrium	equilibria
References	Makar et al. (2015a, b)	Pérez et al. (2011); Badia and Jorba (2014); Spada (2015)	Baklanov and Sørensen (2001); Sørensen et al. (2007); Korsholm et al. (2008); Baklanov et al. (2017)

Attribute	CHIMERE	Polyphemus	LOTOS-EUROS
Aerosol model name	A sectional aerosol module	Two aerosol models: the Size Resolved Aerosol Model (SIREAM) (Debry et al., 2007) or the size and composition resolved aerosol model (SCRAM) (Zhu et al., 2015)	Simplified aerosol model assuming equilibrium
Aerosol species	primary particulate matter, sulfate, nitrate, ammonium, biogenic and anthropogenic SOA, and water. Sea salt is an optional species	Sulfate, ammonium, nitrate, chloride., sodium, BC, OC, dust, water	sulfate, nitrate, ammonium), SOA, primary PM _{2.5} and PM _{2.5-10} , BC, sea salt
Size Representation	Sectional, 6-10 bins (0.01–40 μm)	Sectional for both SIREAM and SCRAM with size sections between 1 nm and 10 μm and composition fraction section between 0 and 1.	Bulk (or 2 sections/modes): fine (primary and all secondary components) and coarse (primary)
Aerosol mixing state	Internal mixture	Internal mixture or mixture explicitly resolved	Internal mixture
Aerosol mass/number	Predicted/diagnostic	Predicted/Predicted	Predicted/diagnostic
Aerosol hygroscopicity	Simulates the diameter and the density of aerosols change with humidity due to the amount of water absorbed into the particles.	Explicitly calculated for inorganics and organics (possibility to use the Gerber et al. (1985) approximation)	None
Aerosol radiative properties	Simulates aerosol effects through absorption and Mie diffusion; calculates aerosol optical depth, LIDAR backscatter	Computed in the post-processing of the simulation	Aerosol direct effect on radiation based on Savenije et al. (2012) and on CCN based on Van Meijgaard et al. (2012)
Inorganic aerosol thermodynamic module	online ISORROPIA	ISORROPIA (equilibrium or dynamic approach)	ISORROPIA or EQSAM options
Organic precursors	3 anthropogenic: TOL, TMB, NC4H10), 5 biogenic surrogate: isoprene, APINEN, BPINEN, LIMONE, OCI	Anthropogenic: I/S-VOCs (3 precursor surrogates), aromatics (2 precursor surrogates). Biogenic: isoprene, monoterpenes and sesquiterpenes (5 surrogates). These precursors are oxidized to form compounds that can partition to the particle or aqueous phases.	5 anthropogenic: xylene, toluene, alkanes, alkenes, primary OM, 2 biogenic species: isoprene, terpene

Attribute	CHIMERE	Polyphemus	LOTOS-EUROS
SOA module	Pun scheme of Pun et al. (2006): a single-step oxidation of the relevant precursors and gas-particle partitioning of the condensable oxidation products based on absorption approach	Gas/particle phase partitioning with Secondary Organic Aerosol Processor (SOAP) (Couvidat and Sartelet, 2015).	VBS with 9 bins
Interactions organic/inorganic	None	AIOMFAC (Zuend et al., 2008, 2011), formation of organic nitrate (Chrit et al., 2017)	None
Aerosol water content	The amount of water in each bins is computed with the "reverse mode" of ISORROPIA by using the composition of particles	The ZSR method for inorganics and SOAP for organics.	Calculated based on aerosol thermodynamic equilibrium
Online photolysis calculation accounting for aerosol feedbacks	Online FastJX	FAST-JX, as described in Real and Sartelet (2011)	None
Nucleation	Binary nucleation parameterization of (Kulmala et al., 1998)	for inorganics (binary or ternary)	None
Condensation/Evaporation	No condensation treatment; simulations the evaporation of secondary inorganic aerosols	Thermodynamic equilibrium or scheme for inorganics (ISOROPPIA, Nenes et al. 1998) and organics (SOAP, Couvidat and Sartelet, 2015). For organics, hydrophilicity and activity coefficients are taken into account.	None
Redistribution or mode merging schemes	None	Moving-center approach (Jacobson, 1997), or Euler-coupled or HEMEN (Devilliers et al. 2013)	None
Coagulation	Section approach (Gelbard and Seinfeld, 1980)	Sectional approach (Dergaoui et al., 2013)	None
Gas-to-particle mass transfer	Simulates through absorption, nucleation, gas/particle partitioning	SAME as treatments in condensation/evaporation	None
References	Vivanco et al. (2009), CHEMERE (2017)	Chrit et al. (2017); Zhu et al. (2016); Sartelet et al. (2007, 2012); Debry et al. (2007)	Schaap et al. (2008); LOTOS-EUROS (2016)

Attribute	CATT-BRAMS	GRAPES-CUACE	ASEAN Tropical Lagrangian Atmospheric System (ATLAS)
Aerosol model name	Simple aerosol model (Longo et al., 2013) or MATRIX aerosol model (Bauer et al., 2008)	CUACE aerosol model is called CAM, (Gong et al., 2003).	None
Aerosol species	Sulfate, nitrate, ammonium, OC, BC, dust, and sea salt	BC, OC, dust, sulfate, sea salt, ammonium and nitrate	Sulfate, nitrate, ammonium, sea salt, dust, anthropogenic and biogenic SOA, primary PM
Size representation	Sections for dust and sea salt otherwise bulk mass 16 mixed modes in MATRIX	12 bins from 10 nm to 40 μ m in diameter for all aerosol components except for ammonium which is in bulk mass concentration	User-defined with arbitrary number of non-interacting size range bins
Aerosol mixing state	Internal and external mixtures	Internal mixture	External mixture
Aerosol mass/number	Two-moment (2M) microphysical parameterization (Freitas et al., 2017)	Mass predicted, number diagnosed	Only aerosol mass predicted
Aerosol hygroscopicity	(Petters and Kreidenweis, 2007; Gácita et al., 2017)	Hygroscopicity for sulfate, nitrate, ammonium, sea salt and OC	Not included
Aerosol radiative properties	The BRAMS radiation module includes two additional schemes to treat atmospheric radiative transfer consistently for both longwave and shortwave spectra. The first scheme is a modified version of the Community Aerosol and Radiation Model for Atmospheres (CARMA) (Toon et al., 1989), and the second one is the Rapid Radiation Transfer Model (RRTM) version for GCMs (RRTMG, Mlawer et al., 1997; Iacono et al., 2008). Optical properties especially for the South American continent derives from the use of climatological size distribution and the complex refractive index from several measurement sites of the Aerosol RObotic NETwork (AERONET, Holben et al., 1998) in the southern area of the Amazon Basin.	Parameterized Refractive Index (RI) and optical properties based on wet radius and RI of each bin	Not included

Attribute	CATT-BRAMS	GRAPES-CUACE	ASEAN Tropical Lagrangian Atmospheric System (ATLAS)
Inorganic aerosol thermodynamic module	<ol style="list-style-type: none"> 1. IMAGES model (Müller and Brasseur, 1995) 2. EQSAM and ISORROPIA in MATRIX 	ISORROPIA-II	Malcolm et al. (2000); Redington and Derwent (2002); nitrate-sulfate-Ammonia equilibrium based on Ackermann et al. (1995)
Organic precursors	Under development	<p>19 VOCs which have been sorted into four surrogate anthropogenic, natural species representing their condensable products.</p> <p>RADMII: five anthropogenic VOC precursors, five surrogate anthropogenic species representing their condensable products (from three classes of aromatics including xylene, toluene, and cresol, one class of higher alkanes, and one class of higher alkenes), one biogenic VOC (BVOC) precursors and one surrogate biogenic species representing their condensable products (from one class of monoterpenes)</p>	Parameterizations to represent the formation of both anthropogenic and biogenic SOA (Redington and Derwent, 2013)
SOA module	None	The production rate of SOA for 19 VOCs species (also with a simplified natural VOCs production scheme based on LAI) from RADMII has been put into the aerosol model and condensed onto different bins.	Secondary biogenic organic aerosol precursor is formed from α -pinene ($C_{10}H_{16}$), followed by a simple rate coefficient to model the subsequent gas to particle conversion of the precursor to biogenic SOA. Loss of the precursor also occurs via oxidation by OH. Toluene is used (scaled to represent the total of VOCs that form anthropogenic SOA) in a simple scheme for production of anthropogenic SOA (Redington and Derwent, 2013).
Interactions organic/inorganic	None	None	Not included
Aerosol water content	aerosol equilibrium partitioning among inorganic species (including water)	ZSR	Not included

Attribute	CATT-BRAMS	GRAPES-CUACE	ASEAN Tropical Lagrangian Atmospheric System (ATLAS)
Online photolysis calculation accounting for aerosol feedbacks	None	None	None
Nucleation	Five nucleation parameterizations can be defined, two for binary homogeneous nucleation of sulfuric acid and water, one for sulfuric acid, water and ammonia, one for ion-ion recombination, and one for particles 3 nm diameter (MATRIX scheme, Bauer et al., 2008)	Sulfate-H ₂ O nucleation parameterization for sulfate based on the work of Kulmala et al (1998)	Not included
Condensation/Evaporation	The total production rate of species in population due to condensation of non-volatile species and subsequent gas-particle mass transfer due to equilibration (Bauer et al., 2008) Scheme that predicts condensation as to formation of CCN and IN explicitly (Thompson and Eidhammer, 2014)	Condensation parameterization for second organic aerosol based on the work of Fuchs and Sutugin, 1971	Not included
Redistribution or mode merging schemes	Use of quadrature methods of moments to simulation of aerosols. (Bauer et al., 2008; (Thompson and Eidhammer, 2014)	The moving scheme of Jacobson (1997) is used to calculate the mass transfer between bins	None
Coagulation	Particles from two populations coagulate such that the resulting particle is placed into the mixed population (MATRIX scheme). (Bauer et al., 2008)	Binary coagulation between 12 bins on the based of Fuchs and Davies, 1964	None
Gas-to-particle mass transfer	All populations undergo condensational growth and self-coagulation, and all but the mixed population undergo loss due to hetero-coagulation with other populations (Bauer et al., 2008)	Gas to particle mass transfer for SOA on base of Schell et al. (2001)	Ammonium nitrate and ASOA assumes equilibrium, ammonium sulfate, coarse mode nitrate and BSOA are assumed irreversible
References	Freitas et al. (2009, 2011, 2017); Longo et al. (2013)	Wang et al. (2010); Zhou et al. (2016, 2018)	Jones et al., 2007; Redington and Derwent, 2002, 2013; Redington et al., 2009

Representation of PM Mixing State

Atmospheric PM may exist in different mixing states, including external mixing, internal mixing, and core-shell structure. External mixing refers to the state in which aerosol components are not mixed. Example species existing in an external state include freshly-emitted primary OC, EC, dust, and fly ash. Internal mixing refers to the state in which the aerosol components are well mixed with the same composition. Example species existing in an internal state include sulfate, nitrate, and ammonium. Aerosols are external mixtures at or near the sources, and become internal mixtures through various processes such as coagulation, condensation, and cloud processing as they are transported downwind. In the core-shell structure, the core may be composed of insoluble particles such as dust and black carbon, the shell may contain H₂O and other soluble salts such as sulfate and ammonium. While the core-shell structure may be the most realistic under typical ambient conditions, internal mixing is often assumed in aerosol models for simplicity. The internal mixture is the mixing state most commonly used in CW-AQF models. SILAM is one of the models that treats aerosol species as external mixtures. In the M7 aerosol module (Vignati et al., 2004), which is used in Enviro-HIRLAM and several other models, the aerosol population is divided into two externally mixed populations: an internally mixed water-soluble particle population and a population of insoluble particles. Polyphemus is the only model that can simulate the evolution of the aerosol mixing state from external mixture to internal mixture. This is achieved using the aerosol model SCRAM (Zhu et al. 2015): based on a comprehensive combination of all chemical species and their mass-fraction sections, both the composition and the size distribution of particles are discretized.

3.6.3 Modeling of Atmospheric PM Thermodynamics

Inorganic Compounds: Thermodynamic Equilibrium or Dynamic Evolution

Among inorganic compounds, some compounds such as sodium or sulfate have a low saturation vapor pressure and exist mostly in the particulate phase. They may be neutralized by compounds such as chloride, ammonium, and nitrate, with partition between the gas and particle phases. As particles may be solid or in an aqueous solution, departure from thermodynamic equilibrium drives the mass transfer of species between gas and particulate phases. Thermodynamic models are used to compute the concentrations of gas and particles at equilibrium. A number of inorganic aerosol thermodynamic models have been reviewed in several papers (e.g., Ansari and Pandis, 1999; Zhang et al., 2000), which described the strengths and limitations of several thermodynamic models along with recommendations of their applications. MARS-A is the simplest thermodynamic module that was used in an earlier version of CMAQ and is still used in conjunction with SORGAM in the current version of WRF/Chem. It is computationally very efficient however it does not treat sodium chloride, excluding its application over coastal areas where sea salt is significant. Some models, such as AIM2 (Wexler and Clegg, 2002), use a Gibbs free energy minimization method to determine the thermodynamic equilibrium state. As this method is computationally expensive, other models (e.g., EQUISOLVII Jacobson (1999), ISORROPIA Nenes et al. (1999)) instead solve a reduced set of equilibrium reactions. As the particulate phase may be highly acidic or alkaline, it is a non-ideal solution (intermolecular interactions between chemical compounds are strong) and the equilibrium constants of reactions depend on activity coefficients, leading the set of equilibrium equations to be highly nonlinear. To reduce the computational time, these coefficients may be tabulated depending on the composition (e.g., as in the case of ISORROPIA), and/or only equations involving components which are in non-negligible quantities are considered (e.g., ISORROPIA, SCAPE2 of Meng et al. (1995)). Most thermodynamic models compute the equilibrium between gas and the bulk particulate phases, i.e., from the total concentration of a component (e.g., ammonium in the particulate phase and ammonia in the gas phase), it will determine the concentrations of the gas (ammonia) and the particulate ion (ammonium). Others, such as ISORROPIA, may also solve the reverse problem and provide the surface concentrations of gases at equilibrium from the particulate concentrations, allowing to compute dynamically the exchange between the gas and the particulate phases. The modeling of the mass transfer of condensable species (inorganic and organic) from the gas phase to the particulate phase is important, because it determines the

fraction of the condensable species in the particulate phase, and therefore the overall particle concentration.

ISORROPIA is used in many CW-AQF models such as AQF_x, NAOFC, Polyphemus and GRAPES-CUACE. WRF/Chem offers three thermodynamic modules, depending on the aerosol module selected. It uses MARS-A in SORGAM, MESA-MTEM in MOSAIC, and ISORROPIA in MADRID. LOTOS-EUROS offers three thermodynamic modules including ISORROPIA, MARS-A, or EQSAM. RegCM-CHEM also offers three thermodynamic modules including MARS-A, SEQUILIB, and ISORROPIA. CCATT-BRAMS offers three modules to simulate inorganic aerosol thermodynamic partitioning including the IMAGES model of Müller and Brasseur (1995), EQSAM, and ISORROPIA. SILAM uses the DMAT module of Sofiev (2000), which simulates the thermodynamics of all major secondary inorganic aerosol species including SO_4^{2-} , NH_4NO_3 , NH_4HSO_4 , $(\text{NH}_4)_2\text{SO}_4$, and sea salt. Enviro-HIRLAM uses the NWP-Chem-Liquid module with a simplified liquid-phase thermodynamic equilibrium mechanism, described in Korsholm et al. (2008).

Organic Compounds

Simulating organic aerosols is technically more challenging than inorganic aerosols due to complex formation mechanisms that involve many organic precursors and large uncertainties in chemical kinetics (Hallquist et al., 2009). The oxidation of volatile organic compounds (VOCs) leads to semi-volatile and low-volatile organic compounds (SVOCs and LVOCs, respectively) that have increasingly complicated chemical functions, high polarizations, and lower saturation vapor pressure, and that may condense onto particles to form secondary organic aerosol (SOA). Precursors of SOA in the models typically include anthropogenic compounds (e.g., aromatics and long-chain alkanes and alkenes) and biogenic compounds (e.g., isoprene, monoterpenes, and sesquiterpenes).

SOA modules in CW-AQF models have a varying degree of complexity. The simplest module is to prescribe biogenic SOA sources via climatology (e.g., Dentener et al., 2006 based on terpene emissions as used in AeroCom Phase I, or an offline vegetation model such as MEGAN), and use the CO emissions as proxy for anthropogenic SOA sources (as in Spracklen et al., 2011), which is used in the global model, IFS. Several CW-AQF models use the SOA modules with intermediate complexity that are based on an absorptive method for several classes of SVOCs which resulted from the gas-phase oxidation of several classes of anthropogenic and biogenic precursor VOCs.

SOA models can be grouped into three major categories: (1) models based on the absorption partitioning theory with an empirical two-product representation of SOA formation, (2) models based on the volatility basis set approach (VBS), and (3) models based on a mechanistic representation of SOA formation. The first type of model is based on the aerosol yield and partitioning coefficients obtained from the smog chamber experiments of Odum et al. (1996) and has been widely used in many global and regional models because of its simplicity and computational efficiency (e.g., Schell et al., 2001; Zhang et al., 2004, 2007; Binkowski and Roselle, 2003). It, however, significantly underpredicts observed OA or SOA (e.g., Binkowski and Roselle, 2003; Zhang et al., 2004, 2007; Henze et al., 2006; Carlton et al., 2010) due to missing SOA precursors and formation processes.

The VBS model simulates gas-aerosol partitioning and chemical ageing of a set of semi-volatile OA species with volatility equally-spaced in a logarithmic scale (the basis set) and (Donahue et al., 2006). In the one-dimensional (1-D) VBS approach, organic compounds are divided into logarithmically-spaced bins of similar saturation concentration (i.e., volatility). Oxidation moves organic compounds from one bin to the other. In the 2-D VBS approach, organic compounds are described not only by their saturation concentration but also by their oxygen content O:C, i.e., their oxidative state (Jiménez et al., 2009; Donahue et al., 2011, 2012a). The 1-D VBS approach has been increasingly implemented in many regional models such as PMCAMx (Lane et al., 2008; Shrivastava et al., 2008; Murphy and Pandis, 2009; Tsimpidi et al., 2010; Fountoukis et al., 2011), CHIMERE (Hodzic et al., 2010; Zhang et al., 2013), WRF-Chem (Shrivastava et al., 2011; Ahmadov et al., 2012), EMEP (Bergström et al., 2012), COSMO-ART (Athanasopoulou et al., 2013) and global models such as GISS GCM II (Farina et

al., 2010; Jathar et al., 2011), GEOS-CHEM (Jo et al., 2013), and CESM (Shrivastava et al., 2015). The 2-D VBS approach has been used to simulate SOA from chamber experiments (Jimenez et al., 2009; Donahue et al., 2012b; Chacon-Madrid et al., 2012; Chen et al., 2013) and implemented in a Lagrangian trajectory model (Murphy et al., 2011, 2012). It has, however, not been implemented in a 3-D air quality model because of its high computational cost. A hybrid approach, referred to as the 1.5-D VBS, has been developed for 3-D applications, which is based on the 1-D VBS framework but accounts for changes in the oxidation state of OA in addition to its volatility using multiple reaction trajectories defined in the 2-D VBS space. This 1.5-D VBS approach combines the simplicity of the 1-D VBS with the ability of the 2-D VBS in a computational efficient framework and has been implemented in CAMx and CMAQ (Koo et al., 2014). A variant 1.5-D VBS approach is to add a dimension of oxidation generation to the gas-phase SVOCs but keep only 1-D in the particulate phase (e.g., volatility) as implemented in a global model, CESM (Glotfelty et al., 2017) and a regional model, WRF/Chem (Yahya et al., 2017). Compared to the traditional two-product approach, the 1-D or 1.5-D VBS approach has significantly improved the current model's capability in simulating SOA (Lane et al., 2008; Murphy and Pandis, 2009; Shrivastava et al., 2011; Tsimpidi et al., 2010; Jathar et al., 2011; Wang et al., 2015; Yahya et al., 2017; Glotfelty et al., 2017). The 1-D or 1.5-D VBS SOA module is coupled with the gas-phase chemical mechanisms of CB05 or SPARC99 in WRF/Chem. The 1-D VBS SOA module is also used in SILAM.

Models of the third category use experimental data of smoke chamber experiments (or theoretical mechanism data), and differentiate high NO_x from low NO_x environments for the oxidation of SOA precursors. These models also use molecular composition data of SOA and represent the formation of SOA using surrogate molecules with representative physico-chemical properties (Pun et al., 2006, Chrit et al., 2017). The gas/particle partitioning can include both absorption into hydrophobic organic particles and dissolution into aqueous particles. Absorption of SOA into organic particles follows Raoult's law, while absorption into aqueous particles follows Henry's law. Absorption depends on the average molecular weight of the organic particulate mixture, the saturation vapor pressure of the condensing SOA surrogate and its activity coefficient in the particle. Activity coefficients are often computed by the universal functional activity coefficient (UNIFAC) method (Fredenslund et al., 1975) or AIOMFAC (Zuend et al. 2008), which deduces the intermolecular interactions from the molecules' groups contribution. Examples of SOA models for this category include MADRID 2 (Pun et al., 2003), AEC (Pun et al., 2006), and the SOAP model (Couvidat and Sartelet, 2015). This surrogate approach was implemented in several CW-AQF models such as CMAQ, Polyphemus (SOAP), MADRID 2 (WRF/Chem), and compares well to measurements of SOA concentrations and properties, particularly for biogenic SOA (Sartelet et al. 2012, Chrit et al. 2017).

Interactions between Organic and Inorganic Compounds

Inorganic aerosols influence the SOA formation in several ways. They constitute an absorbing mass onto which hydrophilic organic aerosols can condense, but they also interact with organic species. These interactions are taken into account in the MADRID 2, AEC, and SOAP models, which compute the partitioning between organic gas and particles using a surrogate approach. In the aqueous phase, for hydrophilic organic species, due to the presence of ions, such as inorganic ions, medium and long-range activity coefficients (resulting from electrostatic interactions) may also influence the partitioning between gas and particles. These medium and long-range activity coefficients may be described by the Aerosol Inorganic–Organic Mixtures Functional groups Activity Coefficient AIOMFAC model (Zuend et al., 2008). Among all CW-AQF models, CMAQ, WRF/Chem (with MADRID 2) and Polyphemus are the only models that include the interactions between organic and inorganic compounds.

Modeling Aerosol Water Content

The aerosol water content from inorganic aerosols is often approximated by the Zdanovskii-Stokes-Robinson (ZSR) relation, which states that the total aerosol water content at a particular relative humidity is the sum of the water content of each chemical component of the particle. This is the case in the thermodynamic model ISORROPIA. Absorption of water by the organic phase may also be computed in the SOA models based on the mechanistic approach such as the SOAP model (Couvidat and Sartelet, 2015) or MADRID 2. Almost all CW-AQF models use the ZSR to calculate aerosol water content. The only two models that account for additional water absorbed by organic SOA are WRF/Chem (with MADRID 2) and Polyphemus.

Other Interactions between the Gas and Particulate Phases

Interactions between the gas and particle phases may occur through other processes such as heterogeneous reactions and impact of particles on photolysis rates. The heterogeneous reactions at the surface of condensed matter (particles and cloud or fog droplets) may significantly impact gas-phase photochemistry and particles (see Section 3.5). Heterogeneous reactions for HO₂, NO₂, N₂O₅ and NO₃ at the surface of aerosols and cloud droplets are often modeled following Jacob (2000). Those reactions have been included in some CW-AQF models such as WRF/Chem-MADRID and Polyphemus.

Photolysis reactions play a major role in the atmospheric composition. In the troposphere, they drive both O₃ production through NO₂ photolysis, and O₃ destruction through its own photolysis. The photolysis of O₃ is also the main source of OH radicals, which are involved in the formation of secondary aerosols as the main oxidant of their gas precursors. In an aerosol layer, light beams can be scattered and/or absorbed depending on aerosol optical characteristics, i.e., their optical properties at the beam wavelengths, and their optical depths which, given their OP, depend on the aerosol loading. Photolysis rates can be modified by aerosols and clouds inside the layer but also below and above it. In clouds, actinic fluxes may be enhanced by not only the reflection within droplets but also the scattering between cloud droplets. This can enhance photolysis rates strongly in upper parts for clouds. In most offline air quality forecasting (AQF) models, the impact of aerosols on photolysis rates is not taken into account, while the impact of clouds on photolysis rates is calculated through an attenuation coefficient applied to clear-sky photolysis rate coefficients (Roselle et al., 1999). Photolysis rates may, however, be computed online (e.g., Binkowski et al., 2007; Real and Sartelet, 2011)) using for example the photolysis scheme FAST-J (Wild et al., 2000). The photolysis rate is calculated online in all online-coupled CW-AQF models and several offline CW-AQF models such as NAQFC and Polyphemus. In Polyphemus, the photolysis can be calculated using offline or online options. The online option calculates photolysis rates by solving the radiative transfer equation for the needed actinic fluxes.

3.6.4 Modeling of Atmospheric PM Dynamics

Major aerosol dynamical processes include nucleation, condensation, coagulation, and gas-particle mass transfer. These processes affect the mass concentrations and size distribution of aerosols. Accurate predictions of the evolution of the aerosol require accurate representations of these processes in the CW-AQF models. Numerical methods for simulating each of the dynamic processes were reviewed in Zhang et al. (1999). The fundamentals of these processes along with common approaches used in simulating those processes in the CW-AQF models are reviewed below. The PM dynamics is governed by gas/particle mass transfer, which is a process that transfers the mass of condensable species from bulk gas phase to the particle surface or the reversed process. It generates mass fluxes of chemical species for heterogeneous nucleation, condensation/evaporation, heterogeneous chemistry on the surface of particles, aqueous-phase chemistry within droplets, and particle formation. It is a combination of multiple processes. Examples of processes include gas-phase diffusion, interfacial mass transfer, collision and subsequent accommodation, chemical thermodynamics converting a species from the gaseous phase to the particulate phase, heterogeneous nucleation, condensation, adsorption, and absorption.

Nucleation

Nucleation is a process by which gas molecules aggregate to form clusters. If the radius of the cluster reaches a critical size, the cluster becomes stable and can grow further. Nucleation increases the number and volume concentrations of particles in the atmosphere. Depending on the availability of the pre-existing particles, nucleation can be classified into two categories: homogeneous nucleation that occurs in a supersaturated vapor phase when gases nucleate without the aid of an existing surface, and heterogeneous nucleation that occurs when gases nucleate on a pre-existing surface. The former provides a source of new particle, whereas the latter does not result in new particles. Depending on the number of species involved, homogeneous or heterogeneous nucleation can be further grouped into three categories: homomolecular nucleation that involves only one gas species, binary nucleation that involves molecules of two gases (e.g., H_2SO_4 and H_2O), and ternary nucleation that involves molecules of three gases (e.g., H_2SO_4 , H_2O , NH_3). Aerosol mass increases through gas-to-particle conversion during all types of nucleation processes, aerosol number increases through the formation of new particles in the homogeneous nucleation. Nucleation may not always form new particles because some nucleated particles are lost by coagulation with pre-existing particles before they grow to a size that can be detected. While nucleation could occur on a daily basis, new particle formation occurs only when ambient conditions favor the growth to the minimum detectable size before loss of nucleated particles. New particles formed have a size at the lower end of the particle size distribution. Nucleation is negligible when existing aerosol concentration is high (i.e., when condensation prevails). The formation mechanisms and growth properties of new particles have been reviewed in several papers (Kulmala et al., 2004a; Zhang et al., 2010a).

Several nucleation mechanisms have been reported, for example, binary, ternary, and ion-mediated nucleation. While binary nucleation theory tends to underpredict observed nucleation rates, ternary nucleation enhances nucleation rates. It is impractical to represent the detailed nucleation mechanisms in the 3-D models because this requires detailed knowledge of the system and kinetic data such as the collision kernels for each cluster and the sticking coefficient of a molecule on clusters. The classical theory of nucleation is simple but may lead to high uncertainty and inaccuracy because it lacks a sound microscopic foundation and often fails to produce correct atmospheric nucleation rates. Computationally-efficient parameterizations have therefore been developed for their implementation in 3-D models. Zhang et al. (2010a) evaluated seven binary, three ternary, two power law nucleation parameterizations, and one ion-mediated nucleation parameterization under a variety of hypothetical and observed atmospheric/laboratory conditions.

Binary homogeneous nucleation is the most common mechanism implemented in CW-AQFs. For example, AQFx includes four different binary homogeneous nucleation mechanisms based on H_2SO_4 and two additional mechanisms based on H_2SO_4 and organic vapor (Reddington et al. 2011). NAQFC, WRF/Chem (SORGAM), and GRAPES-CUACE include the binary homogeneous nucleation of H_2SO_4 and H_2O of Kulmala et al. (1998). WRF/Chem also includes the binary homogeneous nucleation of H_2SO_4 and H_2O of McMurry and Friedlander, (1979) in MADRID. Polyphemus includes the binary homogeneous nucleation of Kuang et al. (2008), Vehkamäki et al. (2002), the ternary nucleation of Napari et al. (2002). IFS does not explicitly simulate nucleation, but it has a combined semi-empirical parameterization of total SO_2 -to-sulfate conversion. SILAM does not simulate nucleation.

Coagulation

Coagulation occurs when two particles collide and stick (coalesce) together. It reduces the aerosol number concentration but conserves the aerosol volume concentration. Particle size distribution shifts toward larger sizes as a result of coagulation. There are five types of coagulation. Brownian motion is the random movement of particles suspended in a fluid. It dominates all five coagulation processes when at least one of the two colliding particles is small. Convective Brownian diffusion enhancement refers to the enhanced diffusion due to eddies created in their wake when particles fall through the air. Gravitational collection is a process during which larger particles catch up and collide with smaller ones during gravitational settling. It is an important mechanism for producing raindrops. It dominates

when both particles are large (but not exactly the same size). Turbulent inertial motion is a process in which turbulence enhances the rate by which particles of different size falling through the air coagulate. Turbulent shear is the wind shear that allows particles at different heights to move at different velocities, causing faster particles to catch up and coagulate with slower particles. Most CW-AQM models only simulate coagulation due to Brownian motion. The particle mass change due to coagulation is obtained by solving coagulation equation using either the sectional approach or the modal approach. In the sectional approach, the sectional coagulation coefficients are integrated only once and the coagulation equation is then reduced from an integro-differential equation to a set of ordinary differential equations (ODEs). In the modal approach, the coagulation equations consist of a set of 6 ODEs for the total number and volume concentrations of each mode, as described in Binkowski and Shankars (1995).

Coagulation is simulated using the modal approach of Mann et al. (2010) in AQFx and Binkowski and Shankar (1995) in NAQFC, and the sectional approach of Debry et al. (2007) or Zhu et al. (2015) in Polyphemus and that of Fuchs and Davies (1964) in GRAPES-CUACE. WRF/Chem offers both the modal and sectional approaches in solving the coagulation equation, depending on the aerosol modules selected. Coagulation is not treated in IFS and SILAM.

Condensation/Evaporation

Condensation is a process in which gas molecules continuously condense (change state from gas to liquid) onto existing particle surfaces. The reverse process is evaporation during which liquid molecules continuously evaporate (change state from liquid to gas) from existing particle surfaces. Condensation or evaporation causes particles to grow or shrink, respectively. During the condensation process, aerosol mass increases, aerosol number remains unchanged, and particle size distribution shifts toward larger sizes. Gaseous species may condense or evaporate depending on their saturation vapor pressure. The mass transfer depends on the gradient between the gaseous concentrations and the concentrations at the particle surface.

Solving the equation for gas/particle mass transfer is numerically challenging. Several approaches have been developed to simulate gas/particle mass transfer through condensation/evaporation (Sartelet et al., 2006). The first approach is the equilibrium approach that assumes an instantaneous chemical equilibrium between the bulk gas phase and the particulate phase. It can be divided into two subgroups. Bulk equilibrium assumes that an equilibrium occurs between a gas species and bulk particulate phase. Non-bulk equilibrium assumes that an equilibrium occurs between a gas species and a single particle or particles in a specific size range. The second approach is the dynamic (also referred to as kinetic) approach that explicitly simulates gas/particle mass transfer for each size section by solving the equation for mass fluxes between the bulk gas-phase and individual particles or particles in a given size range. The third approach is the hybrid approach that combines both dynamic and equilibrium approaches. Among the three approaches, the equilibrium approach is the most computationally efficient approach but it introduces errors. It is the most commonly used in 3-D models. The dynamic approach is the most accurate approach but it is the most computationally expensive. The hybrid approach provides a compromise between the equilibrium approach and the dynamic approach.

The IFS aerosol scheme includes only the conversion of SO₂ to sulfate aerosol, although the gas-phase chemistry scheme also uses EQSAM to determine the phase partitioning of nitrates. AQFx assumes inorganics equilibrium for HNO₃, NH₃, and HCl for fine modes and treats dynamic mass transfer for coarse modes following the approach of Pilinis et al. (2000), Capaldo et al. (2000), and Kelly et al. (2010). NAQFC assumes full equilibrium for HNO₃ and NH₃. WRF/Chem offers three approaches, (1) full equilibrium for HNO₃ and NH₃ in MADE/SORGAM and all species in MADRID, (2) a dynamic approach for H₂SO₄ in MADE/SORGAM, and for all species in MOSAIC and MADRID, and (3) a hybrid approach in MADRID. Polyphemus simulates condensation/evaporation using the sectional approach (models SIREAM and SCRAM described in Debry et al. (2007) and Zhu et al. (2015)). Different assumptions can be made depending on the users' choice and the CPU time required: thermodynamic equilibrium between gas and particle phases (bulk approach), fully dynamic approach or hybrid resolution (thermodynamic equilibrium for particles of low diameter and

dynamic approach for particles of high diameter). The thermodynamic model used in Polyphemus is ISORROPIA for inorganics (forward mode of ISORROPIA for equilibrium and reverse mode of ISORROPIA for dynamic) and SOAP for organics. GRAPES-CUACE uses the gas-to-particle mass transfer for SOA based on Schell et al. (2001). SILAM assumes the full equilibrium approach and does not explicitly simulate gas/particle mass transfer.

AQF_x simulates the dynamic condensation of H₂SO₄ using the modal approach of Mann et al. (2010) and condensation/evaporation for other semi-volatile organic and inorganic species follows the method of Capaldo et al. (2000). NAQFC simulates the dynamic condensation of H₂SO₄ and SVOCs using the modal approach of Binkowski and Shankar (1995). WRF/Chem simulates the dynamic condensation of H₂SO₄ and VOCs using the modal approach of Binkowski and Shankar (1995) in MADE/SORGAM, the dynamic condensation of H₂SO₄, MSA, and NH₃ using the Adaptive Step Time-split Explicit Euler Method (ASTEEM) method in MOSAIC, and dynamic condensation of volatile inorganic species using the APC with moving center scheme in MADRID. GRAPES-CUACE uses a condensation parameterization for second organic aerosol based on the work of Fuchs and Sutugin (1971). Condensation is not explicitly simulated in IFS, although the IFS has a combined semi-empirical parameterization of total SO₂-to-sulfate conversion. Condensation is not simulated in SILAM.

Redistribution or Mode-Merging Schemes

The PM size sections or modes may be of distinct size ranges throughout the simulations in 3-D applications of a CW-AQF model. As particles grow via condensation or shrink via evaporation, the bounds of the sections or modes evolve, introducing numerical errors. It is thus necessary to redistribute the number and mass or moments to minimize such numerical errors. In the sectional approach, the section bounds are usually fixed. The number and mass concentrations as well as the diameter of each section are linked. Redistribution occurs when the diameter of a section increases or decreases beyond the section boundaries. The key point in redistributing sections after condensation/evaporation is to choose which of the two variables amongst mass, number, and diameter to conserve and which to diagnose. Different approaches exist depending on whether the mean diameter of the section is allowed to vary or not (Devilliers et al. (2013)). In the section approach, the moving diameter approach (Jacobson, 1997) is an example to redistribute PM number and mass. In the modal approach, different mode merging schemes have been used, often based on that of Binkowski and Roselle (2003), where a threshold diameter between the two modes to be merged is chosen as the diameter where the number distributions of the two modes overlap. Mode merging may also be applied for each mode when the diameter of the distribution exceeds a fixed diameter (Sartelet et al., 2007).

The condensed mass is redistributed over modes using the mode merging schemes of Mann et al. (2010) in AQF_x and the mode merging scheme of Binkowski and Roselle (2003) in NAQFC. WRF/Chem uses the same scheme as that of NAQFC in MADE/SORGAM and the moving diameter approach of Jacobson (1997) in MOSAIC and MADRID. Polyphemus also uses the moving diameter approach of Jacobson et al. (1997), or the Euler-coupled scheme or the HEMEN scheme of Devilliers et al. (2013). GRAPES-CUACE uses the moving diameter approach of Jacobson et al. (1997). IFS represents sulfate as bulk aerosol in a single bin, so has no redistribution. Since SILAM does not simulate condensation, no scheme is used to redistribute condensed mass over the particle size sections.

3.6.5 Summary

- Atmospheric aerosols are made of multiple inorganic and organic chemical compounds, some of them being directly emitted, while others are formed in the atmosphere. Their size ranges from a few nanometers to tens of micrometers. Small particles tend to have higher particle number than large particles and large particles tend to have higher particle mass. Particles may exist in different mixing states, including external mixing, internal mixing, and core-shell structure. The core-shell structure may be the most realistic state, the internal mixture is, however, the mixing state most commonly used in CW-AQF models.

- The most commonly used aerosol size distribution representations in CW-AQF are the sectional and the modal size distributions. The former discretizes the size distribution into sections, the latter represents the size distribution using several log-normally distributed modes, e.g., three modes (Aitken nuclei, accumulation, and coarse). The modal approach is computationally more efficient than the sectional approach but usually less accurate. The sectional size representation that can simulate both particle mass and number accurately is recommended. Modeling of particle number is important for climate effect and understanding of ultrafine particles. The size distribution at emission is an important parameter to model particle number concentration, but it is not well characterized.
- Aerosol processes include thermodynamic equilibrium and dynamic processes such as nucleation, condensation/evaporation, coagulation, and gas-particle mass transfer. A number of aerosol modules with varying degrees of complexity have been implemented in CW-AQF models to represent these processes, explaining the large differences in simulated aerosol mass concentrations. To represent accurately the formation of secondary compounds, the exchange between the gas and the particle phases (condensation/evaporation and heterogeneous reactions) and thermodynamics need to be modeled.
- Thermodynamics describes the partitioning of a volatile species in the gas- and particulate-phase at equilibrium. A number of thermodynamic models have been developed to compute the concentrations of gas and inorganic aerosol at equilibrium. The departure from thermodynamic equilibrium (i.e., non-equilibrium) may occur, which will require the simulation of explicit mass transfer of a chemical species between gas and particulate phases.
- The completeness of aerosol precursors and formation mechanisms in CW-AQF models determines the ability of the model to represent a wide range of situations, such as urban, rural, summer, winter, etc. There are still large uncertainties on the emissions of precursors of organic aerosols from various sources such as combustion processes and vegetation, which need to be better characterized. These precursors are oxidized in the atmosphere, generating low vapor pressure organic compounds that may undergo particle-phase transformations to form secondary organic aerosol. The properties of the aged precursors, such as their affinity to water, is important to determine the phase changes and aerosol optical properties. Complex models are required to simulate the formation of secondary organic aerosol because of many organic precursors and formation mechanisms, as well as large uncertainties in chemical kinetics.
- Major aerosol dynamical processes are governed by gas/particle mass transfer, which generates mass fluxes of chemical species for heterogeneous nucleation, condensation/evaporation, heterogeneous chemistry on the surface of particles, aqueous-phase chemistry within droplets, and particle formation. Binary homogeneous nucleation is the most common mechanism implemented in CW-AQFs. The smaller the spatial scale, the more refined the algorithm modeling condensation/evaporation needs to be. At small scales, close to sources, a dynamic approach is required to represent condensation/evaporation, and the mixing state of particles impacts aerosol composition and radiative properties.

References

- Abdul-Razzak, H. and Ghan, S. J.: A parameterization of aerosol activation: 2. Multiple aerosol types, *J. Geophys. Res.-Atmos.*, 105, 6837–6844, <https://doi.org/10.1029/1999JD901161>, 2000.
- Ahmadv, R., McKeen, S.A., Robinson, A.L., Bahreini, R., Middlebrook, A.M., de Gouw, J.A., Meagher, J., Hsie, E.-Y., Edgerton, E., Shaw, S., Trainer, M., 2012. A volatility basis set model for summertime secondary organic aerosols over the eastern United States in 2006. *J. Geophys. Res.* 117, D06301.
- Ansari, A.S., Pandis, S.N., 1999, An analysis of four models predicting the partitioning of semi-volatile inorganic aerosol components, *Aerosol Science and Technology* 31 (2-3), 129-153.
- Athanasopoulou, E., Vogel, H., Vogel, B., Tsimpidi, A.P., Pandis, S.N., Knote, C., Fountoukis, C., 2013. Modeling the meteorological and chemical effects of secondary organic aerosols during an EUCAARI campaign. *Atmos. Chem. Phys.* 13, 625-645.
- Baklanov, A.: Modeling of formation and dynamics of radioactive aerosols in the atmosphere, in: *Research on a Theory of Elementary Particles and Solid State*, 4, 135–148, 2003.
- Baklanov, A. and Sørensen, J.: Parameterization of radionuclide deposition in atmospheric long-range transport modeling, *Phys. Chem. the Earth Pt. B*, 26, 787–799, [https://doi.org/10.1016/S1464-1909\(01\)00087-9](https://doi.org/10.1016/S1464-1909(01)00087-9), 2001.
- Bergström, R., Denier van der Gon, H.A.C., Prévôt, A.S.H., Yttri, K.E., Simpson, D., 2012. Modeling of organic aerosols over Europe (2002-2007) using a volatility basis set (VBS) framework: application of different assumptions regarding the formation of secondary organic aerosol. *Atmos. Chem. Phys.* 12, 8499-8527.
- Binkowski, F.S., Shankar, U., 1995. The Regional Particulate Matter Model .1. Model description and preliminary results. *J Geophys Res-Atmos* 100, 26191-26209.
- Binkowski, F.S., and S.J. Roselle: Models-3 Community multiscale air quality (CMAQ) model aerosol component, 1. Model description, *J. Geophys. Res.*, 108(D6), 4183, doi: 10.1029/2001JD001409, 2003.
- Binkowski, F.S., S. Arunachalam, Z. Adelman, and J. P. Pinto, 2007, Examining Photolysis Rates with a Prototype Online Photolysis Module in CMAQ, *Journal of Applied Meteorology and Climatology*, 46 (8, August 2007), 1252-1256.
- Bohren, C.F., Huffman, D.R., 1983. *Absorption and Scattering of Light by Small Particles*. Wiley and Sons, New York, p. 530.
- Bozzo, A, Remy, S, Benedetti, A, Flemming, J, Bechtold, P, Rodwell, MJ, Morcrette, J.-J. (2017), Implementation of a CAMS-based aerosol climatology in the IFS, ECMWF Technical Memorandum 801, <https://www.ecmwf.int/en/elibrary/17219-implementation-cams-based-aerosol-climatology-ifs>
- Capaldo, K.P., Pilinis, C., Pandis, S.N., 2000. A computationally efficient hybrid approach for dynamic gas/aerosol transfer in air quality models. *Atmospheric Environment* 34, 3617-3627.
- Carlton, A. G., Bhave, P. V., Napelenok, S. L., Edney, E. D., Sarwar, G., Pinder, R. W., Pouliot, G. A., and Houyoux, M.: Model Representation of Secondary Organic Aerosol in CMAQv4.7, *Environ. Sci. Technol.*, 44, 8553–8560, <https://doi.org/10.1021/es100636q>, 2010. Chacon-Madrid, H.J., Murphy, B.N., Pandis, S.N., Donahue, N.M., 2012. Simulations of smog-chamber experiments using the two-dimensional volatility basis set: linear oxygenated precursors. *Environ. Sci. Technol.* 46, 11179-11186.
- Chen, S., Brune, W.H., Lambe, A.T., Davidovits, P., Onasch, T.B., 2013. Modeling organic aerosol from the oxidation of α -pinene in a Potential Aerosol Mass (PAM) chamber. *Atmos. Chem. Phys.* 13, 5017-5031.
- Chen, Y., Y. Zhang, J.-W. Fan, L.R. Leung, Q. Zhang, and K.-B. He, 2015, Application of an Online-Coupled Regional Climate Model, WRF-CAM5, over East Asia for Examination of Ice Nucleation Schemes: Part I. *Comprehensive Model Evaluation and Trend Analysis*

for 2006 and 2011, *Climate*, 3(3), 627-667; doi:10.3390/cli3030627.

- Couvidat F. and Sartelet K. (2015), The Secondary Organic Aerosol Processor (SOAP) model: a unified model with different ranges of complexity based on the molecular surrogate approach. *Geosci. Model Dev.*, 8, 1111-1138.
- Debry E., Fahey K., Sartelet K., Sportisse B. and Tombette M. (2007), Technical Note: a new Size REsolved Aerosol Model: SIREAM. *Atmos. Chem. Phys.*, 7, 1537-1547.
- DeMott, P.J.; Prenni, A.J.; McMeeking, G.R.; Sullivan, R.C.; Petters, M.D.; Tobo, Y.; Niemand, M.; Möhler, O.; Snider, J.R.; Sever, G.; Kreidenweis, S.M. Integrating laboratory and field data to quantify the immersion freezing ice nucleation activity of mineral dust particles, *Atmos. Chem. Phys.* 2015, 15, 393-409, doi:10.5194/acp-15-393-2015.
- Dergaoui H., Sartelet K.N., Debry E. and Seigneur C. (2013), Modeling coagulation of externally mixed particles: sectional approach for both size and chemical composition. *Journal of Aerosol Science*, 58, 17-32.
- Devilliers M., Debry E., Sartelet K. and Seigneur, C. (2013), A New Algorithm to Solve Condensation/Evaporation for Ultra Fine, Fine, and Coarse Particles. *Journal of Aerosol Science*, 55, 116-136.
- Donahue, N.M., Robinson, A.L., Stanier, C.O., Pandis, S.N., 2006. Coupled partitioning, dilution, and chemical ageing of semi-volatile organics. *Environ. Sci. Technol.* 40, 2635-2643.
- Donahue, N.M., Epstein, S.A., Pandis, S.N., Robinson, A.L., 2011. A two-dimensional volatility basis set: 1. organic-aerosol mixing thermodynamics. *Atmos. Chem. Phys.* 11, 3303-3318.
- Donahue, N.M., Kroll, J.H., Pandis, S.N., Robinson, A.L., 2012a. A two-dimensional volatility basis set e part 2: diagnostics of organic-aerosol evolution. *Atmos. Chem. Phys.* 12, 615-634.
- Donahue, N.M., Henry, K.M., Mentel, T.F., Kiendler-Scharr, A., Spindler, C., Bohn, B., Brauers, T., Dorn, H.P., Fuchs, H., Tillmann, R., Wahner, A., Saathoff, H., Naumann, K.-H., Möhler, O., Leisner, T., Müller, L., Reinnig, M.-C., Hoffmann, T., Salo, K., Hallquist, M., Frosch, M., Bilde, M., Tritscher, T., Barmet, P., Praplan, A.P., DeCarlo, P.F., Dommen, J., Prevôt, A.S.H., Baltensperger, U., 2012b. Ageing of biogenic secondary organic aerosol via gas-phase OH radical reactions. *Proc. Natl. Acad. Sci. U. S. A.* 109, 13503-13508.
- Donahue, N.M., Chuang, W., Epstein, S.A., Kroll, J.H., Worsnop, D.R., Robinson, A.L., Adams, P.J., Pandis, S.N., 2013. Why do organic aerosols exist? Understanding aerosol lifetimes using the two-dimensional volatility basis set. *Environ. Chem.* 10, 151-157.
- Erisman, J.W., van Pul, A., Wyers, P., 1994. Parameterization of surface resistance for the quantification of atmospheric deposition of acidifying pollutants and ozone. *Atmospheric Environment* 28, 2595-2607.
- Farina, S.C., Adams, P.J., Pandis, S.N., 2010. Modeling global secondary organic aerosol formation and processing with the volatility basis set: Implications for anthropogenic secondary organic aerosol. *J. Geophys. Res.* 115, D09202.
- Flemming, J., Huijnen, V., Arteta, J., Bechtold, P., Beljaars, A., Blechschmidt, A.-M., Diamantakis, M., Engelen, R. J., Gaudel, A., Inness, A., Jones, L., Josse, B., Katragkou, E., Marecal, V., Peuch, V.-H., Richter, A., Schultz, M. G., Stein, O., and Tsikerdekis, A.: Tropospheric chemistry in the Integrated Forecasting System of ECMWF, *Geosci. Model Dev.*, 8, 975-1003, <https://doi.org/10.5194/gmd-8-975-2015>, 2015.
- Fountoukis, C., Nenes, A., 2007. ISORROPIA II: a computationally efficient thermodynamic equilibrium model for K^+ - Ca^{2+} - Mg^{2+} - NH_4^+ - Na^+ - SO_4^{2-} - NO_3^- - Cl^- - H_2O aerosols. *Atmos Chem Phys* 7, 4639-4659.
- Fountoukis, C., Racherla, P.N., Denier van der Gon, H.A.C., Polymeneas, P., Charalampidis, P.E., Pilinis, C., Wiedensohler, A., Dall'Osto, M., O'Dowd, C., Pandis, S.N., 2011. Evaluation of a three-dimensional chemical transport model (PMCAMx) in the European domain during the EUCAARI May 2008 campaign. *Atmos. Chem. Phys.* 11,

10331-10347.

- Freitas, S. R., K. Longo, M. Dias, R. Chatfield, P. Dias, P. Artaxo, M. Andreae, G. Grell, L. Rodrigues, A. Fazenda and J. Panetta. (2009), The Coupled Aerosol and Tracer Transport model to the Brazilian developments on the Regional Atmospheric Modeling System (CATT-BRAMS). Part 1: Model description and evaluation. *Atmos. Chem. Phys.*, 9., 2843-2861.
- Fuchs, N. A., and C. N. Davies, 1964: Aerosol mechanics. (Book Reviews: The Mechanics of Aerosols). *Science*, 146, 1033–1034, doi: 10.1126/science.146.3647.1033.
- Fuchs, N. A., and A. G. Sutugin, Highly dispersed aerosols, in *Topics in Current Aerosol Research*, edited by G. M. Hidy and J. R. Brock, pp. 1 –60, Pergamon, New York, 1971.
- Glotfelty, T., J. He, and Y. Zhang, 2017, Improving Organic Aerosol Treatments in CESM/CAM5: Development, Application, and Evaluation, *Journal of Advances in Modeling Earth Systems*, 9(2), 1506–1539, DOI: 10.1002/2016MS000874.
- Gong, S. L., L. A. Barrie, and J.-P. Blanchet, 1997: Modeling sea salt aerosols in the atmosphere: 1. Model development. *J. Geophys. Res.*, 102, 3805–3818, doi: [10.1029/96JD02953](https://doi.org/10.1029/96JD02953).
- Gong, S.L., Barrie, L.A., Blanchet, J.-P., von Salzen, K., Lohmann, U., Lesins, G., Spacek, L., Zhang, L.M., Girard, E., Lin, H., Leaitch, R., Leighton, H., Chylek, P., Huang, P. (2003), Canadian Aerosol Module: a size-segregated simulation of atmospheric aerosol processes for climate and air quality models. 1. Module development. *J. Geophys. Res.* 108, 4007. <http://dx.doi.org/10.1029/2001JD002002>.
- Gong, W.; Dastoor, A.P.; Bouchet, V.S.; Gong, S.; Makar, P.A.; Moran, M.D.; Pabla, B.; Ménard, S.; Crevier, L.-P.; Cousineau, S.; et al. Cloud processing of gases and aerosols in a regional air quality model (AURAMS). *Atmos. Res.* 2006, 82, 248–275.
- Grell, G. A., S. E. Peckham, R. Schmitz, S. A. McKeen, G. Frost, W. C. Skamarock, and B. Eder (2005), Fully coupled “online” chemistry within the WRF model, *Atmos. Environ.*, 39(37), 6957–6975, doi: [10.1016/j.atmosenv.2005.04.027](https://doi.org/10.1016/j.atmosenv.2005.04.027).
- Griffin, R.J., Cocker III, D.R., Flagan, R.C., Seinfeld, J.H., Organic aerosol formation from the oxidation of biogenic hydrocarbons, (1999) *Journal of Geophysical Research Atmospheres*, 104 (D3), art. no. 1998JD100049, pp. 3555-3567.
- Gross, A. and Baklanov, A.: Modeling the influence of dimethyl sulfide on aerosol production in the marine boundary layer, *Int. J. Environ. Pollut.*, 22, 51–71, <https://doi.org/10.1504/IJEP.2004.005492>, 2004.
- Hallquist, M., Wenger, J.C., Baltensperger, U., Rudich, Y., Simpson, D., Claeys, M., Dommen, J., Donahue, N.M., George, C., Goldstein, A.H., Hamilton, J.F., Herrmann, H., Hoffmann, T., Iinuma, Y., Jang, M., Jenkin, M.E., Jimenez, J.L., Kiendler-Scharr, A., Maenhaut, W., McFiggans, G., Mentel, Th.F., Monod, A., Prévôt, A.S.H., Seinfeld, J.H., Surratt, J.D., Szmigielski, R., Wildt, J., 2009. The formation, properties and impact of secondary organic aerosol: current and emerging issues. *Atmos. Chem. Phys.* 9, 5155-5236.
- Hanel, G., The properties of atmospheric aerosol particles as functions of the relative humidity at thermodynamic equilibrium with the surrounding moist air, *Adv. Geophys.*, 19, 73– 188, 1976.
- Henze, D.K. and J.H. Seinfeld (2006), Global secondary organic aerosol formation from isoprene oxidation, *Geophys. Res. Lett.*, 33, L09812, doi: [1029/2006GL025976](https://doi.org/10.1029/2006GL025976).
- Hodzic, A., Jimenez, J.L., Madronich, S., Canagaratna, M.R., DeCarlo, P.F., Kleinman, L., Fast, J., 2010. Modeling organic aerosols in a megacity: potential contribution of semi-volatile and intermediate volatility primary organic compounds to secondary organic aerosol formation. *Atmos. Chem. Phys.* 10, 5491-5514.
- Hu, X.-M., Y. Zhang, M.Z. Jacobson, and C.K. Chan, 2008, Coupling and evaluating gas/particle mass transfer treatments for aerosol simulation and forecast, *Journal of Geophysical Research*, 113, D11208, doi: [10.1029/2007JD009588](https://doi.org/10.1029/2007JD009588).
- Jacobson, M. Z. (1997), Development and application of a new air pollution modeling

- system-II. Aerosol module structure and design, *Atmos. Environ.*, 31, 131– 144.
- Jacobson, M. Z., R. P. Turco, E. J. Jensen, and O. B. Toon, Modeling coagulation among particles of different composition and size, *Atmos. Environ.*, 28(7), 1327– 1338, 1994.
- Jathar, S.H., Farina, S.C., Robinson, A.L., Adams, P.J., 2011. The influence of semi-volatile and reactive primary emissions on the abundance and properties of global organic aerosol. *Atmos. Chem. Phys.* 11, 7727-7746.
- Jiménez, J.L., Canagaratna, M.R., Donahue, N.M., Prévôt, A.S.H., Zhang, Q., Kroll, J.H., DeCarlo, P.F., Allan, J.D., Coe, H., Ng, N.L., Aiken, A.C., Docherty, K.S., Ulbrich, I.M., Grieshop, A.P., Robinson, A.L., Duplissy, J., Smith, J.D., Wilson, K.R., Lanz, V.A., Hueglin, C., Sun, Y.L., Tian, J., Laaksonen, A., Raatikainen, T., Rautiainen, J., Vaattovaara, P., Ehn, M., Kulmala, M., Tomlinson, J.M., Collins, D.R., Cubison, M.J., Dunlea, E.J., Huffman, J.A., Onasch, T.B., Alfarra, M.R., Williams, P.I., Bower, K., Kondo, Y., Schneider, J., Drewnick, F., Borrmann, S., Weimer, S., Demerjian, K., Salcedo, D., Cottrell, L., Griffin, R., Takami, A., Miyoshi, T., Hatakeyama, S., Shimojo, A., Sun, J.Y., Zhang, Y.M., Dzepina, K., Kimmel, J.R., Sueper, D., Jayne, J.T., Herndon, S.C., Trimborn, A.M., Williams, L.R., Wood, E.C., Middlebrook, A.M., Kolb, C.E., Baltensperger, U., Worsnop, D.R., 2009. Evolution of organic aerosols in the atmosphere. *Science* 326, 1525-1529.
- Jo, D.S., Park, R.J., Kim, M.J., Spracklen, D.V., 2013. Effects of chemical ageing on global secondary organic aerosol using the volatility basis set approach. *Atmos. Environ.* 81, 230-244.
- Kelly, J.T., Bhave, P.V., Nolte, C.G., Shankar, U., Foley, K.M., 2010. Simulating emission and chemical evolution of coarse sea-salt particles in the Community Multiscale Air Quality (CMAQ) model. *Geosci Model Dev* 3, 257-273.
- Koo, B., E. Knipping, and G. Yarwood, 2014, 1.5-Dimensional volatility basis set approach for modeling organic aerosol in CAMx and CMAQ, *Atmospheric Environment*, 95, 158-164, DOI: 10.1016/j.atmosenv.2014.06.031
- Kim Y., Couvidat F., Sartelet K. and Seigneur C. (2011), Comparison of different gas-phase mechanisms and aerosol modules for simulating particulate matter formation. *J. Air Waste Manage. Assoc.*, 61, 1218-1226, doi:10.1080/10473289.2011.603999.
- Korsholm, U. S., Baklanov, A., Gross, A., Mahura, A., Sass, B. H., and Kaas, E.: Online-coupled chemical weather forecasting based on HIRLAM – overview and prospective of Enviro-HIRLAM, *HIRLAM Newsletter*, 54, 151–168, 2008.
- Kouznetsov, R., Sofiev, M. (2012) A methodology for evaluation of vertical dispersion and dry deposition of atmospheric aerosols. *JGR*, 117. doi: 10.1029/2011JD016366.
- Kuang, C., McMurry, P. H., McCormick, A. V., Eisele, F. L., 2008. Dependence of nucleation rates on sulfuric acid vapor concentration in diverse atmospheric locations. *J. Geophys. Res.* 113 (D10209).
- Kulmala, M., A. Laaksonen, L. Pirjola, 1998: Parameterizations for sulfuric acid/water nucleation rates. *J. Geophys. Res.*, 103, 8301–8307, doi: 10.1029/97JD03718.
- Lane, T.E., Donahue, N.M., Pandis, S.N., 2008. Simulating secondary organic aerosol formation using the volatility basis-set approach in a chemical transport model. *Atmos. Environ.* 42, 7439-7451.
- Lewis, E. R. & Schwartz, S. E. Comment on “Size distribution of sea-salt emissions as a function of relative humidity” *Atmospheric Environment*, 2006, 40, 588 – 590.
- Lim, K.-S. J.-W. Fan, L. R. Leung, P.-L. Ma, B. Singh, C. Zhao, Y. Zhang, G. Zhang, and X.-L. Song, 2014, Investigation of Aerosol Indirect Effects Using A Cumulus Microphysics Parameterization in A Regional Climate Model, *Journal of Geophysical Research*, 116, D02204, DOI: 10.1002/2013JD020958.
- Makar, P.A., Bouchet, V.S., and Nenes, A. (2003), Inorganic Chemistry Calculations using HETV – A Vectorized Solver for the SO₄²⁻-NO₃⁻-NH₄⁺ system based on the ISORROPIA Algorithms, *Atmos. Environ.* (37): 2279-2294.

- Makar, P.A., Gong, W., Milbrandt, J., Hogrefe, C., Zhang, Y., Curci, G., Zabkar, R., Im, U., Balzarini, A., Baro, R., Bianconi, R., Cheung, P., Forkel, R., Gravel, S., Hirtl, H., Honzak, L., Hou, A., Jimenez-Guerrero, P., Langer, M., Moran, M.D., Pabla, B., Perez, J.L., Pirovano, G., San Jose, R., Tuccella, P., Werhahn, J., Zhang, J., Galmarini, S. Feedbacks between air pollution and weather, part 1: Effects on weather. *Atmospheric Environment*, 115, 442-469, 2015a.
- Makar, P.A., Gong, W., Hogrefe, C., Zhang, Y., Curci, G., Zabkar, R., Milbrandt, J., Im, U., Balzarini, A., Baro, R., Bianconi, R., Cheung, P., Forkel, R., Gravel, S., Hirtl, H., Honzak, L., Hou, A., Jimenez-Guerrero, P., Langer, M., Moran, M.D., Pabla, B., Perez, J.L., Pirovano, G., San Jose, R., Tuccella, P., Werhahn, J., Zhang, J., Galmarini, S. Feedbacks between air pollution and weather, part 2: Effects on chemistry. *Atmospheric Environment*, 115, 499-526, 2015b.
- Mann, G.W., Carslaw, K.S., Spracklen, D.V., Ridley, D.A., Manktelow, P.T., Chipperfield, M.P., Pickering, S.J., Johnson, C.E., 2010. Description and evaluation of GLOMAP-mode: a modal global aerosol microphysics model for the UKCA composition-climate model. *Geosci Model Dev* 3, 519-551.
- Meyers, M.P.; DeMott, P.J.; Cotton, W.R. New primary ice-nucleation parameterizations in an explicit cloud model. *J. Appl. Meteorol.* 1992, 31, 708–721, doi:10.1175/1520-0450(1992)031<0708:NPINPI>2.0.CO;2.
- Morcrette, J.-J., et al. (2009), Aerosol analysis and forecast in the European Centre for Medium-Range Weather Forecasts Integrated Forecast System: Forward modelling, *J. Geophys. Res.*, 114, D06206, doi:10.1029/2008JD011235.
- Murphy, B.N., Pandis, S.N., 2009. Simulating the formation of semivolatile primary and secondary organic aerosol in a regional chemical transport model. *Environ. Sci. Technol.* 43, 4722e4728.
- Murphy, B.N., Donahue, N.M., Fountoukis, C., Pandis, S.N., 2011. Simulating the oxygen content of ambient organic aerosol with the 2D volatility basis set. *Atmos. Chem. Phys.* 11, 7859-7873.
- Murphy, B.N., Donahue, N.M., Fountoukis, C., Dall'Osto, M., O'Dowd, C., Kiendler-Scharr, A., Pandis, S.N., 2012. Functionalization and fragmentation during ambient organic aerosol aging: application of the 2-D volatility basis set to field studies. *Atmos. Chem. Phys.* 12, 10797-10816.
- Napari, I., Noppel, M., Vehkamäki, H., Kulmala, M., 2002. An improvement model for ternary nucleation of sulfuric acid-ammonia-water. *J. Comp. Phys.* 116 (10), 4221–4227.
- Nielsen, K. P., Gleeson, E., and Rontu, L.: Radiation sensitivity tests of the HARMONIE 37h1 NWP model, *Geosci. Model Dev.*, 7, 1433–1449, <https://doi.org/10.5194/gmd-7-1433-2014>, 2014.
- Oshima, N., M. Koike, Y. Zhang, Y. Kondo, N. Moteki, N. Takegawa, and Y. Miyazaki, 2009, Aging of Black Carbon In Outflow From Anthropogenic Sources Using A Mixing State Resolved Model: 2. Aerosol optical properties and cloud condensation nuclei activities, *Journal of Geophysical Research*, 114, D18202, doi:10.1029/2008JD011681.
- Oshima, N., M. Koike, Y. Zhang, Y. Kondo, N. Moteki, N. Takegawa, and Y. Miyazaki, 2009, Aging of Black Carbon In Outflow From Anthropogenic Sources Using A Mixing State Resolved Model: Model Development and Evaluation, *Journal of Geophysical Research*, 114, D06210, doi:10.1029/2008JD010680.
- Pankow, J.F., An absorption model of the gas/aerosol partitioning involved in the formation of secondary organic aerosol, (1994) *Atmospheric Environment*, 28 (2), pp. 189-193.
- Phillips, V.T.J.; Demott, P.J.; Andronache, C.; Pratt, K.A.; Prather, K.A.; Subramanian, R.; Twohy, C. Improvements to an empirical parameterization of heterogeneous ice nucleation and its comparison with observations. *J. Atmos. Sci.* 2013, 70, 378–409.
- Pilinis, C., Capaldo, K.P., Nenes, A., Pandis, S.N., 2000. MADM - A new multicomponent aerosol dynamics model. *Aerosol Sci Tech* 32, 482-502.
- Pleim, J. E., Clarke, J. F., Finkelstein, P. L., Cooter, E. J., Ellestad, T. G., Xiu, A., and Angevine, W. M., 1996, "Comparison of Measured and Modeled Surface Fluxes of

Heat, Moisture and Chemical Dry Deposition," Air Pollution Modelling and its Applications XI, S. Gryning and F. Schiermeier, eds., Plenum Press, New York.

- Redington, A. L., and R. G. Derwent, 2002: Calculation of sulphate and nitrate aerosol concentrations over Europe using a Lagrangian dispersion model, *Atmos. Environ.*, 36, 4425-4439.
- Redington, A.L., Derwent, R.G., Witham, C.S., Manning, A.J., 2009: Sensitivity of modelled sulphate and nitrate aerosol to cloud, pH and ammonia emissions, *Atmos. Environ.*, 43, 3227-3234.
- Redington, A. L., and R. G. Derwent, 2013: Modelling secondary organic aerosol in the United Kingdom, *Atmos. Environ.*, 63, 349-357.
- Reddington, C.L., Carslaw, K.S., Spracklen, D.V., Frontoso, M.G., Collins, L., Merikanto, J., Minikin, A., Hamburger, T., Coe, H., Kulmala, M., Aalto, P., Flentje, H., Plass-Duelmer, C., Birmili, W., Wiedensohler, A., Wehner, B., Tuch, T., Sonntag, A., O'Dowd, C.D., Jennings, S.G., Dupuy, R., Baltensperger, U., Weingartner, E., Hansson, H.C., Tunved, P., Laj, P., Sellegri, K., Boulon, J., Putaud, J.P., Gruening, C., Swietlicki, E., Roldin, P., Henzing, J.S., Moerman, M., Mihalopoulos, N., Kouvarakis, G., Zdimal, V., Zikova, N., Marinoni, A., Bonasoni, P., Duchi, R., 2011. Primary versus secondary contributions to particle number concentrations in the European boundary layer. *Atmos Chem Phys* 11, 12007-12036.
- Reddy, M. S., O. Boucher, N. Bellouin, M. Schulz, Y. Balkanski, J.-L. Dufresne, and M. Pham (2005), Estimates of global multicomponent aerosol optical depth and direct radiative perturbation in the Laboratoire de Météorologie Dynamique general circulation model, *J. Geophys. Res.*, 110, D10S16, doi:10.1029/2004JD004757.
- Rontu, L., Gleeson, E., Räisänen, P., Pagh Nielsen, K., Savijärvi, H., and Hansen Sass, B.: The HIRLAM fast radiation scheme for mesoscale numerical weather prediction models, *Adv. Sci. Res.*, 14, 195-215, <https://doi.org/10.5194/asr-14-195-2017>, 2017.
- Sartelet K., Hayami H., Albriet B., and Sportisse B. (2006), Development and preliminary validation of a modal aerosol model for tropospheric chemistry: MAM. *Aerosol Science and Technology*, 40 (2), p188-127. doi:10.1080/02786820500485948.
- Schell B, Ackermann I J, Hass H, et al. Modelling the formation of secondary organic aerosol within a comprehensive air quality model system. *Journal of Geophysical Research Atmospheres*, 2001, 106(D22):28275-28293.
- Shrivastava, M.K., Lane, T.E., Donahue, N.M., Pandis, S.N., Robinson, A.L., 2008. Effects of gas-particle partitioning and aging of primary emissions on urban and regional organic aerosol concentrations. *J. Geophys. Res.* 113, D18301.
- Shrivastava, M., Fast, J., Easter, R., Gustafson Jr., W.I., Zaveri, R.A., Jimenez, J.L., Saide, P., Hodzic, A., 2011. Modelling organic aerosols in a megacity: comparison of simple and complex representations of the volatility basis set approach. *Atmos. Chem. Phys.* 11, 6639-6662.
- Shrivastava, M., et al. (2015), Global transformation and fate of SOA: Implications of low-volatility SOA and gas-phase fragmentation reactions, *J. Geophys. Res. Atmos.*, 120, 4169–4195, doi:10.1002/2014JD022563.
- Slinn, W. G. N., 1982: Predictions for particle deposition to vegetative canopies. *Atmos. Environ.*, 16, 1785–1794, doi: 10.1016/0004-6981(82)90271-2.
- Slinn, W. G. N. (1977). Some approximations for the wet and dry removal of particles and gases from the atmosphere.
- Sofiev, M. (2000) A model for the evaluation of long-term airborne pollution transport at regional and continental scales. *Atmospheric Environment*. 34, No.15, pp. 2481-2493.
- Spracklen, D.V., Pringle, K.J., Carslaw, K.S., Chipperfield, M.P., Mann, G.W., 2005. A global off-line model of size-resolved aerosol microphysics: II. Identification of key uncertainties. *Atmos Chem Phys* 5, 3233-3250.
- Stier, P., Feichter, J., Kinne, S., Kloster, S., Vignati, E., Wilson, J., Ganzeveld, L., Tegen, I.,

- Werner, M., Balkanski, Y., Schulz, M., Boucher, O., Minikin, A., and Petzold, A.: The aerosol-climate model ECHAM5-HAM, *Atmos. Chem. Phys.*, 5, 1125–1156, <https://doi.org/10.5194/acp-5-1125-2005>, 2005.
- Tiedtke, M., 1989. A Comprehensive Mass Flux Scheme for Cumulus Parameterization in Large-Scale Models. *Mon Weather Rev* 117, 1779-1800.
- Tompkins, A. M. (2005), A revised cloud scheme to reduce the sensitivity to vertical resolution, Tech. Memo. 0599, 25 pp., Res. Dep., Eur. Cent. for Medium-Range Weather Forecasts, Reading, U. K.
- Tsimpidi, A.P., Karydis, V.A., Zavala, M., Lei, W., Molina, L., Ulbrich, I.M., Jimenez, J.L., Pandis, S.N., 2010. Evaluation of the volatility basis-set approach for the simulation of organic aerosol formation in the Mexico City metropolitan area. *Atmos. Chem. Phys.* 10, 525-546.
- Tsimpidi, A.P., Karydis, V.A., Pozzer, A., Pandis, S.N., Lelieveld, J., 2014. ORACLE (v1.0): module to simulate the organic aerosol composition and evolution in the atmosphere. *Geosci Model Dev* 7, 3153-3172.
- Vehkamäki, H., Kulmala, M., Napari, I., Lehtinen, K., Timmreck, C., 2002. An improved parameterization for sulfuric acid-water nucleation rates for tropospheric and stratospheric conditions. *J. Geophys. Res.* 107 (D22), 4622
- Vignati, E., J. Wilson, and P. Stier (2004), M7: An efficient size-resolved aerosol microphysics module for large-scale aerosol transport models, *J. Geophys. Res.*, 109, D22202, [doi: 10.1029/2003JD004485](https://doi.org/10.1029/2003JD004485).
- Wang, H., X. Y. Zhang, S. L. Gong, et al., 2010: Radiative feedback of dust aerosols on the East Asian dust storms. *J. Geophys. Res.*, 115, D23214, [doi: 10.1029/2009JD013430](https://doi.org/10.1029/2009JD013430)
- Wang, K., Y. Zhang, K. Yahya, S.-Y. Wu, and G. Grell, 2015, Implementation and Initial Application of New Chemistry-Aerosol Options in WRF/Chem for Simulating Secondary Organic Aerosols and Aerosol Indirect Effects for regional air quality, *Atmospheric Environment*, 115, 716-732, [doi: 10.1016/j.atmosenv.2014.12.007](https://doi.org/10.1016/j.atmosenv.2014.12.007).
- Wild, O., Zhu, X., and Prather, M. J., 2000: Fast-J: Accurate simulation of in- and below-cloud photolysis in tropospheric chemical models, *J. Atmos. Chem.* 37, 245–282.
- Yahya, K., T. Glotfelty, K. Wang, Y. Zhang, and A. Nenes, 2017, Modelling Regional Air Quality and Climate: Improving Organic Aerosol and Aerosol Activation Processes in WRF/Chem version 3.7.1, *Geoscientific Model Development*, 10, 2333-2363, [doi: 10.5194/gmd-10-2333-2017](https://doi.org/10.5194/gmd-10-2333-2017).
- Yu, Shaocai, R. Mathur, J. Pleim, D. Wong, R. Gilliam, K. Alapaty, C. Zhao, and X. Liu, 2014. Aerosol indirect effect on the grid-scale clouds in the two-way coupled WRF-CMAQ: model description, development, evaluation and regional analysis. *Atmos. Chem. Phys.* 14, 11247–11285, [doi:10.5194/acp-14-1-2014](https://doi.org/10.5194/acp-14-1-2014).
- Zhang, L. M., S. L. Gong, J. Padro, et al., 2001: A size-segregated particle dry deposition scheme for an atmospheric aerosol module. *Atmos. Environ.*, 35, 549–560, [doi: 10.1016/S1352-2310\(00\)00326-5](https://doi.org/10.1016/S1352-2310(00)00326-5).
- Zhang, Q.J., Beekmann, M., Drewnick, F., Freutel, F., Schneider, J., Crippa, M., Prévôt, A.S.H., Baltensperger, U., Poulain, L., Wiedensohler, A., Sciare, J., Gros, V., Borbon, A., Colomb, A., Michoud, V., Doussin, J.-F., Denier van der Gon, H.A.C., Haeffelin, M., Dupont, J.-C., Siour, G., Petetin, H., Bessagnet, B., Pandis, S.N., Hodzic, A., Sanchez, O., Honoré, C., Perrussel, O., 2013. Formation of organic aerosol in the Paris region during the MEGAPOLI summer campaign: evaluation of the volatility-basis-set approach within the CHIMERE model. *Atmos. Chem. Phys.* 13, 5767-5790.
- Zhang, Y., C. Seigneur, J.H. Seinfeld, M. Jacobson, and F.S. Binkowski, 1999, Simulation of Aerosol Dynamics: A Comparative Review of Algorithms used in Air Quality Models, *Aerosol Science and Technology*, 31 (6), 487-514, [doi: 10.1080/027868299304039](https://doi.org/10.1080/027868299304039).
- Zhang, Y., C. Seigneur, J.H. Seinfeld, M. Jacobson, S.L. Clegg, and F.S. Binkowski, 2000, A Comparative Review of Inorganic Aerosol Thermodynamic Equilibrium Modules: Similarities, Differences, and Their Likely Causes, *Atmospheric Environment*, 34, 117-137, [doi: 10.1016/S1352-2310\(99\)00236-8](https://doi.org/10.1016/S1352-2310(99)00236-8).

- Zhang, Y., B. Pun, K. Vijayaraghavan, S.-Y. Wu, C. Seigneur, S. Pandis, M. Jacobson, A. Nenes and J.H. Seinfeld, 2004, Development and Application of the Model of Aerosol Dynamics, Reaction, Ionization and Dissolution (MADRID), *Journal of Geophysical Research*, 109, D01202, doi: [10.1029/2003JD003501](https://doi.org/10.1029/2003JD003501).
- Zhang, Y., P. McMurry, F. Yu, and M.Z. Jacobson, 2010, A Comparative Study of Nucleation Parameterizations: 1. Examination and Evaluation of the Formulations, *Journal of Geophysical Research*, 115, D20212, doi: [10.1029/2010JD014150](https://doi.org/10.1029/2010JD014150).
- Zhang, Y., P. Liu, X.-H. Liu, M.Z. Jacobson, P. McMurry, F. Yu, S.-C. Yu, and K. Schere, 2010, A Comparative Study of Nucleation Parameterizations: 2. Three-Dimensional Model Application and Evaluation, *Journal of Geophysical Research*, 115, D20213, doi: [10.1029/2010JD014151](https://doi.org/10.1029/2010JD014151).
- Zhang, Y., J.-P. Huang, D. K. Henze, and J. H. Seinfeld, 2007, Role of Isoprene in Secondary Organic Aerosol Formation on a Regional Scale, *Journal of Geophysical Research*, 112, D20207, doi: [10.1029/2007JD008675](https://doi.org/10.1029/2007JD008675).
- Zhang, Y., X. Zhang, K. Wang, J. He, L. R. Leung, J.-W. Fan, and A. Nenes, 2015a, Incorporating An Advanced Aerosol Activation Parameterization into WRF-CAM5: Model Evaluation and Parameterization Intercomparison, *Journal of Geophysical Research*, 120 (14), 6952–6979, DOI: [10.1002/2014JD023051](https://doi.org/10.1002/2014JD023051).
- Zhang, Y., Y. Chen, J.-W. Fan, and L.R. Leung, 2015b, Application of an Online-Coupled Regional Climate Model, WRF-CAM5, over East Asia for Examination of Ice Nucleation Schemes: Part II. Sensitivity to Ice Nucleation Parameterizations and Dust Emissions, *Climate*, 2015, 3(3), 753-774; doi: [10.3390/cli3030753](https://doi.org/10.3390/cli3030753).
- Zhou, C. H., X. J. Shen, Z. R. Liu., et al., 2018: Simulating aerosol size distribution and mass concentration with simultaneous nucleation, condensation/coagulation, and deposition with the GRAPES–CUACE. *J. Meteor. Res.*, 32(2), 1–14, doi: [10.1007/s13351-018-7116-8](https://doi.org/10.1007/s13351-018-7116-8).
- Zhu, S., Sartelet K., Seigneur C. (2015), A size-composition resolved aerosol model for simulating the dynamics of externally mixed particles: SCRAM (v 1.0) *Geosci. Model Dev.*, 8, 1595-1612.

3.7 Atmospheric Removal

3.7.1 Introduction

Atmospheric gases and particles can be removed through dry and wet deposition processes. Dry deposition is the transport of gaseous and particulate species from the atmosphere onto surfaces in the absence of precipitation. Wet deposition is the natural processes by which material is scavenged by atmospheric hydrometeors (e.g., cloud and fog drops, rain, snow) and is consequently delivered to Earth's surface. Tables 3.15 and 3.16 summarize model treatments of dry and wet deposition in CW-AQF models. The fundamentals of dry and wet deposition processes along with their model treatments in CW-AQF models are reviewed below.

Dry Deposition and Sedimentation

Turbulent motion in the lowest part of the planetary boundary layer may result in particles coming into contact with the surface and being deposited there. Dry deposition involves gas-phase diffusion for gases or Brownian motion for particles, turbulent diffusion, gravitational sedimentation, interception, and impaction. Dry deposition is affected by several factors. First, the level of turbulence can govern the rate at which species are delivered down to the surface. Second, the chemical and physical properties of the depositing species can affect the uptake at the surface including solubility and chemical reactivity for gases and size, density, and shape for particles. Third, the properties of the surface such as land cover and moisture can affect the capture of a species through absorption or adsorption or desorption. For example, a natural surface with a variety of vegetation generally promotes dry deposition, whereas a smooth surface may lead to particle bounce-off.

The dry deposition process is usually modeled by a serial resistance approach analogous to electrical resistance. The resistances include an aerodynamic resistance based on the turbulent diffusion within the boundary layer, a quasi-laminar resistance due to the thin non-turbulent layer adjacent to the surface, and a canopy resistance due to the surface type and roughness. The inverse of the sum of the three resistances gives a dry deposition velocity at which particles are transferred to the surface. The resistances may be prescribed or computed dynamically based on the boundary layer and surface schemes within a model; while simplified or offline schemes may use fixed climatology for the deposition velocity. A number of dry deposition parameterizations or models have been developed to estimate the dry deposition fluxes of gases and aerosols. Some of them have been intercompared in the literature (e.g., Petroff et al., 2008; Hicks et al., 2016; Khan and Perlinger, 2017). Table 3.15 summarizes the model treatments of dry deposition for gases and particles that are currently used in 3-D CW-AQF models. Commonly-used schemes include Slinn (1982), Wesely (1989), and Zhang et al. (2001), and their updated formulations. Separate implementations are often used within a model for gases and aerosols.

Additionally, sedimentation (gravitational settling) can be important for coarse particles with aerodynamic diameters larger than 10 μm (e.g., for sand and dust storm forecasting systems), and is typically implemented as a downward flux according to the Stokes velocity for particles of a given size and density. Stokes law is suitable for particle diameters less than approximately 3.5 μm (Hinds, 1999). However, for larger particles, Stokes law is not valid, and in the turbulent regime. Baklanov and Sørensen (2001) suggested to use for the DERMA model an iterative procedure to solve the equation for the terminal settling velocity according to Nöslund & Thaning (1991). For particles smaller than 1 μm the Cunningham correction factor for the Stokes velocity is suggested (Zanetti, 1990). For fine-mode particles, this velocity is typically small and models may neglect the process entirely.

Table 3.15 Representation of atmospheric removal processes in global CW-AQF models

Attribute	G5CHEM (GEOS-5 with GEOS-Chem)	IFS (ECMWF/CAMS) (ECMWF)	SILAM v.5.5
Dry deposition/ sedimentation	Dry deposition is based on the resistance-in-series scheme of Wesely (1989) as implemented by Wang et al. (1998a). Aerosol deposition is from Zhang et al. (2001). Aerosol deposition to snow/ice is described by Fisher et al. (2011). Gravitational settling is from Fairlie et al. (2007) for dust and Alexander et al. (2005) for coarse sea salt.	Deposition velocity calculated interactively following Zhang et al. (2001), applied at surface boundary of diffusion scheme. Sedimentation using implicit scheme based on IFS ice sedimentation (Tompkins, 2005).	Gaseous: Wesely (1989) adapted for SILAM surface treatment, aerosols: (Kouznetsov and Sofiev, 2012); Settling with Stokes-Cunningham approximation.
In-cloud impaction scavenging	The wet deposition scheme is described by Liu et al. (2001) for water-soluble aerosols and by Amos et al. (2012) for gases. Scavenging of aerosol by snow and cold/mixed precipitation is described by Wang et al. (2011, 2014)	No explicit treatment, using prescribed scavenged fractions covering all types of in-cloud scavenging.	Particles assumed to be inside cloud droplets/ice crystals, so rainout coefficients (cloud water/ice content over rain increment through a layer) apply. Gas-water equilibrium for cloud droplets. pH-sensitive solubility for SO ₂ , absorption for falling droplets same as below-cloud
In-cloud nucleation scavenging	See above	Prescribed fraction of each species/size bin removed in proportion to removal of cloud water as precipitation.	All particles are inside droplets/ice crystals
Ice nucleation scavenging	See above	Prescribed fraction of each species/size bin removed in proportion to removal of cloud ice as precipitation.	Same as above, the model does not distinguish between droplet and crystal. If hydrometeors present, particles are considered within them.
Below-cloud impaction scavenging	See above	Proportional to precipitation rate, with prescribed collection efficiencies for each species/bin for rain and snow.	3-D scavenging based on rain intensity profile, distinguishes between rain and snow, in- and sub-cloud. Gases: solubility-based, pH-sensitive, dynamically computed absorption to droplets; particles: impaction
References	Hu et al. (2018)	Flemming et al. (2015); Morcrette et al. (2009)	Sofiev (2000); Kouznetsov and Sofiev (2012)

Table 3.16 Representation of atmospheric removal processes in regional/urban CW-AQF models

Attribute	AQFx	NAQFC (WRF-CMAQ)	WRF/Chem
Dry deposition/ sedimentation	Wesely (1989) for gases. For aerosols, GLOMAP uses Slinn (1982) for the dry deposition velocity and Binkowski and Shankar (1995) for the removal of mode number density and mass.	Wesely (1989) for gases and the RPM approach (Binkowski and Shankar, 1995) for particles	Wesely (1989) for all species except for sulfate; sulfate dry deposition based on Erisman et al. (1994); aerosol settling velocity and deposition based on Slinn and Slinn (1980) and Pleim et al. (1984)
In-cloud impaction scavenging	Henry's law approach for gases, Spracklen et al. (2005) for large-scale rain removal and Tiedtke et al. (1989) for convective-scale rain	For reactive species, the amount of scavenging depends on Henry's law constants, dissociation constants, and cloud water pH. For species that do not react in aqueous-phase, the model uses the effective Henry's law equilibrium equation to calculate ending concentrations and deposition amounts. For aerosol, accumulation and coarse mode aerosols completely absorbed by cloud and rainwater, Aitken mode aerosols slowly absorbed into cloud and rainwater. The wet deposition algorithm is described in Chang et al. (1987) and Roselle and Binkowski, 1999)	Autoconversion and collection for bulk cloud droplets, precipitation rate independent of aerosols; in-cloud wet removal of aerosol particles involves removal of the cloud-borne aerosol particles collected by rain, graupel, and snow, using the same first-order rate that cloud water is converted to precipitation. For trace gases, the same removal rate is applied to the fraction of each gas that is dissolved in cloud water.
In-cloud nucleation scavenging	Calculated for large-scale and convective-scale rainfall as described in Spracklen et al. (2005)	Accretion with empirical uptake coefficient	Activation (nucleation) scavenging and Brownian diffusion (for activated particles) are included. Activation parameterizations are based AR&G00 and AR&G02 (Abdul-Razzak and Ghan, 2000, 2002) or the FN series (Fountoukis and Nenes, 2005)
Ice nucleation scavenging	None	Accretion with empirical uptake coefficient	Two heterogeneous ice nucleation parameterizations for mixed-phase clouds: Meyers et al. (1992) in WRF/Chem and Niemand et al. (2012) in WRF/Chem-CAM5

Attribute	AQFx	NAQFC (WRF-CMAQ)	WRF/Chem
Below-cloud impaction wet scavenging	Mann et al. (2010) for particle number and mass.	The accumulation mode and coarse mode aerosols are assumed to be completely absorbed; the Aitken mode aerosols are treated as interstitial aerosol and are slowly absorbed into the cloud/rainwater	Below-cloud wet removal of aerosol particles by impaction scavenging via convective Brownian diffusion and gravitational or inertial capture. Calculated scavenging coefficient using a parameterization of the collection efficiency of aerosol particles by raindrops, with size dependence. Irreversible uptake of H ₂ SO ₄ , HNO ₃ , HCl, NH ₃ , and simultaneous reactive uptake of SO ₂ , H ₂ O ₂ (Easter, 2004)
References	Mann et al. (2010)	Lee et al. (2017)	Grell et al. (2005); Fast et al. (2006); Zhang et al. (2010); Yahya et al. (2017)

Attribute	GEM-MACH15	MOCAGE	NMMB/BSC-CTM	DERMA & Enviro-HIRLAM
Dry deposition/ sedimentation	Based on Wesely (1989) for gases, Zhang et al. (2001) for particles, detailed description in Makar et al. (2018)	Resistance approach: for gases, it is based upon (Wesely, 1989) with refinements for stomatal resistance (Michou et al., 2004); Aerosol settling velocity and deposition is described in (Nho-Kim et al., 2004);	Wesely (1989) for all species except for sulfate; sulfate dry deposition based on Erisman et al. (1994); Zhang (2001) for aerosol dry deposition. Settling velocity following the Stokes-Cunningham approximation.	Separate resistance models for gases and aerosols. Three regimes gravitational settling parameterizations for different size aerosols follow N�aslund and Thaning (1991)
In-cloud impaction wet scavenging	Impaction of size-distributed aerosol particles by precipitation; scavenging rate parameterized by precipitation rate and a mean collision frequency (Gong et al., 2006; Gong et al., 2003; Slinn, 1984)	For scavenging by large-scale precipitation and below convective cloud, the parameterization is based upon (Giorgi and Chameides, 1986), with a special treatment for snowflakes. For scavenging within convective clouds, it is done within the convective parameterization as described in (Mari et al., 2000); convective (Mari et al., 2000) and stratiform precipitation (Giorgi and Chameides, 1986)	For reactive species, the amount of scavenging depends on Henry's law constants, dissociation constants, and cloud water pH. For species that do not react in aqueous-phase, the model uses the effective Henry's law equilibrium equation to calculate ending concentrations and deposition amounts. Wet deposition algorithms taken from RADM (Chang et	Scavenging coefficients for gases following Seinfeld and Pandis (1998); in-cloud scavenging of aerosols dependent on the aerosol radius and rain rate (Baklanov and S�orensen, 2001). Separate 3-D scavenging models for gases and aerosols, and for rainout and washout with particle size-dependent parameterizations (Baklanov and S�orensen, 2001).

Attribute	GEM-MACH15	MOCAGE	NMMB/BSC-CTM	DERMA & Enviro-HIRLAM
			al., 1987); wet deposition of chemical species depending on precipitation rate and cloud water concentration (Roselle and Binkowski, 1999)	
In-cloud nucleation scavenging	Default (operational forecast) mode makes use of Jones et al. (1994) parameterization where aerosols with a radius larger than a critical value are assumed to be activated in the chemistry to create an assumed droplet number, while droplet nucleation in the microphysics is treated using the Cohard et al (1998) scheme with a time and spatially invariant CCN concentration. Indirect effect feedback mode: CCN activation based on Abdul-Razzak and Ghan, 2002) using the Hoose et al. (2010) updraft velocity linked to cloud liquid water content.	All particles are inside droplets	Parameterized for aerosols using a solubility parameter, the conversion rate of cloud water to rain. For subgrid-scale clouds following same adjustment scheme BMJ (Pérez et al., 2011).	Activation (nucleation) scavenging and Brownian diffusion (for activated particles) are included. Activation parameterizations are based AR&G00 (Abdul-Razzak and Ghan, 2000)
Ice nucleation scavenging	Currently under development; no "aerosol-aware" ice nucleation in GEM-MACH operational.	All particles are inside ice crystals	Parameterized for aerosols using a solubility parameter, the conversion rate of cloud ice to precipitation through melting. For subgrid-scale clouds following same adjustment scheme BMJ (Pérez et al., 2011).	Empirical uptake coefficient
Below-cloud impaction wet scavenging	Scavenging of soluble gases by precipitation (both irreversible and reversible processes included; former through a Sherwood number parameterization, latter through aqueous phase equilibrium. Soluble gas scavenging for snow and ice for HNO ₃ and NH ₃) based on the H ₂ SO ₄ scavenging rate. Scavenging of	Giorgi and Chameides (1986)	Parameterized for aerosols following Slinn (1984).	Scavenging coefficients for gases following Seinfeld and Pandis (1998); below-cloud scavenging of aerosols dependent on the aerosol radius and rain rate (Baklanov and Sørensen, 2001). In the latest version of Enviro-HIRLAM, fixed size- and composition-dependent

Attribute	GEM-MACH15	MOCAGE	NMMB/BSC-CTM	DERMA & Enviro-HIRLAM
	aerosol particles by snow and ice is included. Cloud and raindrop scavenging parameterized by precipitation rate and mean collision frequency. Overview of precipitation scavenging used in GEM-MACH appears in Gong et al (2006).			scavenging parameters for wet deposition and for stratiform and convective clouds (Stier et al., 2005).
References	Makar et al. (2015a, b)	Mari et al. (2000); Nho-Kim et al. (2004)	Pérez et al. (2011); Badia and Jorba (2015); Spada (2015)	Baklanov and Sørensen (2001); Sørensen et al. (2007); Korsholm et al. (2008); Baklanov et al. (2017)

Attribute	CHIMERE	Polyphemus	MATCH	LOTOS-EUROS
Dry deposition/ sedimentation	Considered for model gas species and is parameterized as a downward flux out of the lowest model layer. The deposition velocity is described through a resistance analogy (Wesely 1989). Aerosol settling velocity and deposition follow Seinfeld and Pandis (1998); Zhang et al. (2001); Giorgi (1986); Peters and Eiden (1992)	Following Zhang et al. (2001) for particles and Zhang et al. (2003) for gases. As in Simpson et al. (2003), the surface resistance is modeled following Wesely (1989) for sub-zero temperatures, and the surface resistance of HNO ₃ is assumed to be zero for positive temperatures. Following Cherin et al. (2015) in urban areas.	Modeled using a resistance approach; deposition schemes with different degrees of sophistication are available. Aerosol settling velocity and deposition follow Seinfeld and Pandis (1998)	Resistance approach DEPAC 3.11 (Zanten et al., 2010) for gases, Aerosol settling velocity and deposition follow Zhang et al. (2001)
In-cloud impaction wet scavenging	Dissolution of gases in cloud droplets (Seinfeld and Pandis, 1998); aerosol nucleation (Tsyro, 2002; Guelle et al., 1998). The scheme is based on Loosmore and Cederwall (2004)	Loosmore and Cederwall (2004)	O ₃ , H ₂ O ₂ and SO ₂ in-cloud scavenging is calculated by assuming Henry's law equilibrium in the clouds; for sulfate particles, in-cloud scavenging is assumed to be 100% effective. Assumed to be proportional to the precipitation intensity using species-specific scavenging coefficients. For particles, several different schemes are available	The approach of Banzhaf et al. (2012)

Attribute	CHIMERE	Polyphemus	MATCH	LOTOS-EUROS
In-cloud nucleation scavenging	None	Following Strader et al. (1997)	None	None
Ice nucleation scavenging	None	None	None	None
Below-cloud impaction wet scavenging	Dissolution of gases in precipitating drops (Mircea and Stefan, 1998); scavenging by raining drops (Loosmore and Cederwall, 2004)	Following Sportisse and Dubois (2002). Ion dissociation during dissolution in water is taken into account for soluble gaseous species via their Henry coefficients	For sulfate particles, Berge (1993); neglected for O ₃ , H ₂ O ₂ and SO ₂ ; for other species proportional to the precipitation intensity and a species-specific scavenging coefficient	Gases: scavenging rates depending on Henry's law constant and precipitation intensity (Simpson et al., 2003); aerosols following Scott (1978)
References	Vivanco et al. (2009); CHEMERE (2017)	Chrit et al. (2017); Zhu et al. (2016); Sartelet et al. (2007, 2012); Debry et al. (2007)	Robertson et al. (1999); Langner et al. (2005)	Schaap et al. (2008); LOTOS-EUROS (2016)

Attribute	CCATT-BRAMS	GRAPES-CUACE	ASEAN Tropical Lagrangian Atmospheric System (ATLAS)
Dry deposition/ sedimentation	Aerodynamic, quasi-laminar layer and canopy resistances (Wesely, 1989; Seinfeld and Pandis, 1998) with updates from Wesely and Hicks (2000) and Zhang et al. (2003).	This scheme combines the effects of gravitational settling, aerodynamic resistance, and the collection efficiency of the surface and mass transfer between layers (Slinn 1982; Gong and Barrie, 1997; Zhang et al., 2001)	Option between simple deposition velocity scheme and scheme based on a resistance analogy parameterization to calculate a species-dependent deposition velocity applied to all air parcels within the boundary layer (Webster and Thomson, 2011)
In-cloud impaction wet scavenging	Wet deposition accounts for the scavenging of aerosols in convective updrafts and rainout/washout in large-scale precipitation (Giorgi and Chameides, 1986; Balkanski et al., 1993)	Sectional activation and precipitation rate independent of aerosols (Gong et al., 2003)	Bulk parameterizations for aerosols representing the mean wet scavenging rate for the whole aerosol size range (Webster and Thomson, 2014); option for aerosol size-dependent scheme (Webster and Thomson, 2017)
In-cloud nucleation scavenging	two-moment (2M) microphysical parameterization (Freitas et al., 2017)	AR&G00 and AR&G02 (Abdul-Razzak&Ghan, 2000, 2002)	Webster and Thomson, 2014; option for aerosol size-dependent scheme (Webster and Thomson, 2017)

Attribute	CCATT-BRAMS	GRAPES-CUACE	ASEAN Tropical Lagrangian Atmospheric System (ATLAS)
Ice nucleation scavenging	two-moment (2M) microphysical parameterization (Freitas et al., 2017)	None	Webster and Thomson, 2014, option for aerosol size-dependent scheme (Webster and Thomson, 2017)
Below-cloud impaction wet scavenging	Wet deposition accounts for the scavenging of aerosols in convective updrafts and rainout/washout in large-scale precipitation (Giorgi and Chameides, 1986; Balkanski et al., 1993)	Calculated sectional scavenging coeff. using a parameterization of the collection efficiency of aerosol particles by rain, snow or graupel (Slinn, 1977)	Webster and Thomson, 2014, option for aerosol size-dependent scheme, (Webster and Thomson, 2017)
References	Freitas et al. (2009); Freitas et al. (2011); Longo et al. (2013)	Wang et al. (2010); Zhou et al. (2016, 2018)	Jones et al. (2007); Redington and Derwent (2002); Redington et al. (2009, 2013)

Many CW-AQF models used the formulation of Wesely (1989) for dry deposition of gases, including G5CHEM, GEM-MACH15, MOCAGE, AQFx, NAQFC, NMMB/BSC-CTM, CHIMERE, CCATT-BRAMS, and SILAM. Many models use the formulation of Zhang et al. (2001) for dry deposition of particles including G5CHEM, GEM-MACH15, NMMB/BSC-CTM, Polyphemus, IFS, and LOTOS-EUROS. Other formulations have also been used for gas and particle dry deposition and settling. For example, for gas deposition, Polyphemus uses the formulation of Zhang et al. (2003), MATCH uses the formulation of Seinfeld and Pandis (1998), and LOTOS-EUROS uses the formulation of Zanten et al. (2010). For particle settling velocity and deposition, AQFx uses Slinn (1982) for the dry deposition velocity and Binkowski and Shankar (1995) for the removal of mode number density and mass of aerosols, NAQFC uses the RPM approach of Binkowski and Shankar (1995), DERMA uses the formulation of Baklanov and Sørensen (2001), MOCAGE uses the formulation of Nho-Kim et al. (2004), and LOTOS-EUROS uses the formulation of Erisman and Draaijers (1995). AQFx uses the formulation of Slinn (1982) for particle dry deposition velocity and Binkowski and Shankar (1995) for the removal of mode number density and mass. WRF/Chem uses the formulation of Wesely (1989) for both gases and particles except for sulfate. It also offers the formulations of Slinn and Slinn (1980) and Pleim et al. (1984) for particles. GRAPES-CUACE uses those of Slinn (1982), Gong and Barrie (1997), and Zhang et al. (2001) for both gases and particles. IFS simulates sedimentation using implicit scheme based on IFS ice sedimentation (Tompkins, 2005).

Large uncertainties exist in the formulation of the dry deposition calculation due to limited understanding of the complex processes involved in dry deposition, technical difficulties in measuring dry deposition velocities and fluxes, and a lack of extensive measurements for model validation (Sportisse, 2007; Seinfeld and Pandis, 2016). The largest uncertainty in many dry deposition parameterizations has been reported for particles with diameters in the range of 0.1– 1.0 μm , due to the different representations of major processes such as Brownian diffusion (Petroff and Zhang, 2010; Zhang et al., 2014). Hicks et al. (2016) evaluated five deposition models using observations over forest canopies and reported a large discrepancy between measurements and model calculation of dry deposition velocities for particle sizes of 0.3-5.0 μm , particularly in the accumulation size range. Textor et al. (2007) compared the fractions of sulfate and sea salt removed through dry deposition simulated by 24 global atmospheric models and found a large difference in those removed fractions across these models, ranging from 4-29% for sulfate and 45-95%, respectively.

Wet Deposition/Scavenging by Cloud and Precipitation

All gaseous and aerosol species may be collected via collision by or dissolution in hydrometeors including cloud droplets, raindrops, ice and snow crystals (referred to as in-cloud impaction scavenging, or rainout) or falling precipitation (referred to as below-cloud impaction scavenging, or washout). Hygroscopic aerosols can also be incorporated into cloud droplets when liquid cloud forms (referred to as in-cloud nucleation scavenging or aerosol activation). Aerosol particles can act as cloud condensation nuclei (CCN) or ice nuclei (IN) to provide the initial sites for condensation of water vapor into cloud droplets or cloud ice particles at a given supersaturation (often $< 2\%$). Following cloud scavenging, the soluble gaseous and aerosol species may undergo aqueous-phase dissociation and chemical reactions. The relevant aqueous-phase chemical mechanisms used in CW-AQF models are reviewed in Section 3.5. The chemical species incorporated into cloud droplets through in-cloud scavenging may be transferred from cloud droplets to raindrops through autoconversion that produces precipitation. The gaseous and aerosol species captured in raindrops are removed from the atmosphere once the raindrops reach the ground. However, a substantial part or all of the precipitation may evaporate before reaching the ground, releasing the chemical species back to the atmosphere from the evaporating hydrometeors. For many gaseous and aerosol species, especially those that are soluble or hygroscopic, the dominant removal process is via precipitation scavenging and subsequent wet deposition. Many factors can affect wet deposition including precipitation intensity and frequency, the properties of hydrometeors such as size, velocity, and temperature, as well as the chemical properties of depositing species such as gas-phase diffusivity, solubility and chemical reactivity for gases and shape, size, and density for particles.

The in-cloud impaction scavenging rate of gases is estimated by using the product of their concentrations and scavenging coefficients. The scavenging coefficient is an effective first-order removal rate constant through the cloud scavenging process. It is a function of mass transfer coefficient, cloud droplet size distribution, and droplet diameter. For less soluble gases, the Henry's law aqueous-phase equilibrium, aqueous-phase chemical reactions, and their dependence on the pH of the droplet need to be accounted for in calculating their surface uptake. The in-cloud impaction scavenging of gases is treated in all CW-AQF models, but with different degrees of complexity. For example, AQFx uses the Henry's law approach for gases, with the formulation of Spracklen et al. (2005) for large scale rain removal and that of Tiedtke et al. (1989) for convective-scale rain. In WRF/Chem, for trace gases, the same removal rate is applied to the fraction of each gas that is dissolved in cloud water. In NAQFC, for reactive gaseous species, the amount of scavenging depends on Henry's law constants, dissociation constants, and cloud water pH. For species that do not react in the aqueous-phase, the model uses the effective Henry's law equilibrium equation to calculate aqueous-phase concentrations and deposition amounts through dissolution and dissociation. In SILAM, in-cloud scavenging of gas is estimated by accounting for gas-water equilibrium in cloud, rainout coefficient, and pH-dependent solubility of SO₂.

Atmospheric aerosols can be removed through both nucleation scavenging and impaction scavenging in cloud. Nucleation scavenging can remove all large and mid-size particles (Zhang et al., 2002; Jacobson, 2005). The remaining particles are referred to interstitial particles, primarily small particles. Compared to nucleation scavenging, impaction scavenging of interstitial particles is a slow process, removing certain aerosol number but negligible aerosol mass (Seinfeld and Pandis, 2016). The representations of in-cloud scavenging of particles in CW-AQF models vary from simple to detailed parameterizations. In the simple parameterization, in-cloud scavenging of aerosol is usually parameterized by assuming that a prescribed fraction of a given aerosol type/bin/mode becomes dissolved or embedded within cloud droplets or ice particles, and this fraction is removed at the same rate as the cloud water/ice. This simple parameterization is used in some models such as ECMWF's IFS. An intermediate approach applies a fixed lower size cut-off for in-cloud nucleation, as in the sectional size discretization of Polyphemus (approach detailed in Strader et al., 1997). In Polyphemus, in-cloud wet scavenging is modeled following Loosmore and Cederwall (2004). A similar parameterization is used in NAQFC with the modal size discretization, in which accumulation and coarse mode aerosols are completely absorbed by cloud and rainwater, Aitken mode aerosols are slowly absorbed into cloud and rainwater. In more complex parameterizations, an empirical or explicit parameterization of the activation of aerosol particles as CCN (e.g., Abdul-Razzak & Ghan, 2000, 2002 (AR&G00 and AR&G02); Nenes & Seinfeld, 2003; Fountoukis and Nenes, 2005 (FN05)) is used together with detailed representations of both the aerosol and cloud-droplet size distributions. The parameterizations of AR&G00 and AR&G02 have been implemented in several CW-AQF models such as WRF/Chem (Grell et al., 2005), two-way coupled WRF-CMAQ (Yu et al., 2014), GEM-MACH15, DERMA, Enviro-HIRLAM, and GRAPES-CUACE. The FN05 and its updated version that accounts for insoluble particles as CCN, the effect of giant CCN, and cloud entrainment have been implemented in WRF-CAM5 (Zhang et al., 2015a) and WRF/Chem (Yahya et al., 2017). WRF/Chem and its variants such as WRF/Chem-MADRID, offline and online-coupled WRF-CMAQ, and WRF-CAM5 have been deployed for RT CW-AQF in the U.S. (Kang et al., 2005; McKeen et al., 2005, 2007, 2009; Chuang et al., 2011; Zhang et al., 2016; Li et al., 2017), and southeast Atlantic (Shinozuka et al., 2020). Therefore, the in-cloud scavenging in both WRF/Chem and WRF-CAM5 represents the most detailed description in CW-AQF models. In both models, in-cloud impaction scavenging of aerosol particles involves removal of the cloud-borne aerosol particles collected by rain, graupel, and snow, using the same first-order rate that cloud water is converted to precipitation. They offer two options for in-cloud nucleation scavenging: one based on AR&G00 and AR&G02 and one based on the FN05 and its updated version. While WRF-CAM5 includes explicit nucleation scavenging of aerosol by both warm clouds and cumulus clouds (Lim et al., 2014), most other models include explicit nucleation scavenging of aerosol by warm clouds but use simple nucleation scavenging parameterizations based on an assumed scavenging fraction of each aerosol type. For sub-grid-scale convective cloud, there is an important distinction between wet removal coupled with convective mass transport, and wet removal at the grid-scale.

Aerosol particles can be scavenged through heterogeneous nucleation to act as ice nuclei (IN), affecting the microphysical properties of mixed-phase clouds. Compared to aerosol nucleation scavenging by liquid clouds to form CCN used in CW-AQF models, the parameterizations of ice nucleation remain largely empirical in nature (e.g., DeMott et al., 2010), and large uncertainties exist in the ice nucleation parameterizations (INPs) used in current climate models. WRF/Chem and WRF-CAM5 simulates ice nucleation through homogeneous and heterogeneous freezing for cirrus clouds based on Liu et al. (2007). WRF/Chem simulates heterogeneous INPs based on Meyers et al. (1992). WRF-CAM5 offers two heterogeneous INPs for mixed-phase cloud regimes including the default INP based on Meyers et al. (1992) and a new INP based on Niemand et al. (2012). An evaluation of the INPs of Meyers et al. (1992) and Niemand et al. (2012) can be found in Chen et al. (2015) and Zhang et al. (2015b). Most CW-AQF models do not treat ice nucleation. IFS uses a prescribed fraction of each species/bin removed in proportion to removal of cloud ice as precipitation. SILAM and NMMB/BSC-CTM use a parameterization for aerosols using a solubility parameter. The representations of in-cloud and ice nucleation scavenging of aerosol particles will be reviewed in more detail in Section 3.9.

For below-cloud scavenging of gases and particles, the rate of transfer into rain droplets can also be estimated using the product of their concentrations and scavenging coefficients. The scavenging coefficient is a function of precipitation, mass transfer coefficient, terminal velocity of a falling raindrop, and droplet diameter. Scavenging coefficient and mass transfer coefficient are larger for smaller droplets, whereas the terminal velocity is larger for larger droplets. Below-cloud scavenging of gases can be estimated by a mass balance between the rate of mass increase of a species in the droplet and the rate of transport of the species to the droplet. Henry's law equilibrium is assumed. The treatment of below-cloud scavenging of particles by rain is usually based on the aerodynamic collision probabilities between particles and droplets at different sizes, depending on their terminal velocities. Raindrop size distribution is typically assumed to be Marshall-Palmer or similar, unless explicitly available from a very detailed cloud scheme. More empirical power-law parameterizations are often used for scavenging by snow and other forms of ice, where terminal velocity is very dependent on the type of ice. The representations of below-cloud scavenging in CW-AQF models vary from simple to detailed parameterizations. For example, the scavenging rate in IFS is proportional to precipitation rate, with prescribed collection efficiencies for each species/bin for rain and snow, which is the simplest below-cloud scavenging parameterization. AQF_x uses Mann et al. (2010) for below-cloud scavenging of both particle number and mass. Polyphemus simulates below-cloud scavenging following Sportisse and Dubois (2002), and dissociation during dissolution in water is taken into account for soluble gaseous species via their Henry coefficients. NAQFC uses the RADM wet deposition algorithms (Chang et al., 1987), in which the wet deposition of chemical species is calculated as a function of precipitation rate and cloud water concentration (Roselle and Binkowski, 1999). WRF/Chem assumes an irreversible uptake of H₂SO₄, HNO₃, HCl, NH₃ and simultaneous reactive uptake of SO₂, H₂O₂ (Easter et al., 2004). It includes below-cloud wet removal of aerosol particles by impaction scavenging via convective Brownian diffusion and gravitational or inertial capture. In DERMA and ENVIRO-HIRLAM, the below-cloud scavenging of aerosols depend on the aerosol radius and rain/snow rates following the parameterization of Baklanov and Sørensen (2001). In SILAM, 3-D scavenging based on the rain intensity profile, distinguishes between rain and snow, in- and sub-cloud. Below-cloud scavenging is calculated through solubility-based, pH-sensitive, dynamically computed absorption to droplets for gases and impaction for particles. Most models also account for the fact that some or all of the precipitation may evaporate below the cloud, resulting in downward transport rather than removal of scavenged aerosol.

Similar to dry deposition, large uncertainties are associated with the formulation of the wet deposition calculation, due mainly to a limited understanding of the complex processes involving surface uptake, dissolution, cloud formation, and aqueous-phase chemistry and parameters such as properties of dissolving chemical species, cloud cover and liquid water content, and scavenging coefficients, as well as technical difficulties in representing those processes (e.g., impaction and nucleation scavenging, subgrid-scale cloud formation, aqueous-phase chemistry) (Seinfeld and Pandis, 2016). In addition, there is a lack of field studies in and below clouds for evaluation of simulated wet deposition. Textor et al. (2007) compared the fractions of sulfate and sea salt removed through wet deposition simulated by

24 global atmospheric models and found a large difference in those removed fractions across these models, ranging from 4-54%. Wang et al. (2008) intercompared nine different regional chemical transport models applied over East Asia and evaluated simulated wet deposition amounts of sulfate, nitrate, and ammonium against the observations from the Acid Deposition Monitoring Network in East Asia. They found large discrepancies between observed and simulated amounts of wet deposition of these species and among all models included (may be up to one to two orders of magnitude for the monthly values).

Summary

- Dry and wet deposition are important removal processes for atmospheric gases and particles. Sedimentation (gravitational settling) can be important for coarse particles.
- Dry deposition is affected by several factors such as the level of turbulence, the chemical and physical properties of the depositing species, and the properties of the surface. The dry deposition process is usually modeled by the resistance approach analogous to electrical resistance, considering an aerodynamic resistance, a quasi-laminar resistance, and a canopy resistance. Large uncertainties exist in the formulation of the dry deposition calculation.
- Wet deposition is affected by many factors such as precipitation intensity and frequency, the properties of hydrometeors, and the chemical properties of depositing species. Modeling of wet deposition requires representations of complex processes including in-cloud impaction scavenging (rainout), below-cloud impaction scavenging (or washout), and in-cloud nucleation scavenging (aerosol activation).
- All CW-AQF models treat the in-cloud and below-cloud scavenging of gases and particles, but with different degrees of complexity and large uncertainties in several parameters. Among them, scavenging coefficient is a key parameter in simulating the in-cloud and below-cloud scavenging for both gases and particles.

References

- Abdul-Razzak, H., and S. J. Ghan: A parameterization of aerosol activation. 2. Multiple aerosol types, *J. Geophys. Res.*, 105, 6837-6844, 2000.
- Abdul-Razzak, H., Ghan, S.J., 2002. A parameterization of aerosol activation 3. Sectional representation. *J. Geophys. Res. Atmos.* 107 (D3) <http://dx.doi.org/10.1029/2001JD000483>. AAC 1-1 to AAC 1-6.
- Alexander, B., R.J. Park, D.J. Jacob, Q.B. Li, R.M. Yantosca, J. Savarino, C.C.W. Lee, and M.H. Thiemens, Sulfate formation in sea-salt aerosols: Constraints from oxygen isotopes, *J. Geophys. Res.*, 110, D10307, 2005.
- Amos, H. M., D. J. Jacob, C. D. Holmes, J. A. Fisher, Q. Wang, R. M. Yantosca, E. S. Corbitt, E. Galarneau, A. P. Rutter, M. S. Gustin, A. Steffen, J. J. Schauer, J. A. Graydon, V. L. St. Louis, R. W. Talbot, E. S. Edgerton, Y. Zhang, and E. M. Sunderland, Gas-Particle Partitioning of Atmospheric Hg(II) and Its Effect on Global Mercury Deposition, *Atmos. Chem. Phys.*, 12, 591-603, 2012.
- Badia, A. and O. Jorba (2015), Gas-phase evaluation of the online NMMB/BSC-CTM model over Europe for 2010 in the framework of the AQMEII-Phase2 project, *Atmos. Environ.*, 115, 657-669.
- Balkanski, Y.J.; Jacob, D. J.; Gardner, G.M.; Graustein, W.C.; Turekian, K. K. (1993). Transport and residence times of tropospheric aerosols inferred from a global three-dimensional simulation of 210Pb. *Journal of Geophysical Research, Atmosphere*, 98, 20573-20586, <https://doi.org/10.1029/93JD02456>.

- Baklanov, A., and J. H. Sørensen. 2001. 'Parameterization of Radionuclide Deposition in Atmospheric Long-Range Transport Modeling'. *Physics and Chemistry of the Earth: (B)* 26, no. 10: 787–99.
- Baklanov, A., Korsholm, U. S., Nuterman, R., Mahura, A., Nielsen, K. P., Sass, B. H., Rasmussen, A., Zakey, A., Kaas, E., Kurganskiy, A., Sørensen, B., and González-Aparicio, I.: The Enviro-HIRLAM online integrated meteorology–chemistry modeling system: strategy, methodology, developments, and applications (v. 7.2), *Geosci. Model Dev.*, 10, 2971–2999, <https://doi.org/10.5194/gmd-10-2971-2017>, 2017.
- Banzhaf, S., M. Schaap, A. Kerschbaumer, E. Reimer, R. Stern, E. van der Swaluw, and P. Builtjes, 2012, Implementation and evaluation of pH-dependent cloud chemistry and wet deposition in the chemical transport model REM-Calgrid, *Atmos. Environ*, 49, 378–390, <https://doi.org/10.1016/j.atmosenv.2011.10.069>
- Berge, E.: Coupling of wet scavenging of sulphur to clouds in a numerical weather prediction model, *Tellus*, 45B, 1–22, 1993.
- Binkowski, F.S., Shankar, U., 1995. The Regional Particulate Matter Model .1. Model description and preliminary results. *J Geophys Res-Atmos* 100, 26191–26209.
- Binkowski, F.S., and S.J. Roselle: Models-3 Community multiscale air quality (CMAQ) model aerosol component, 1. Model description, *J. Geophys. Res.*, 108(D6), 4183, [doi: 10.1029/2001JD001409](https://doi.org/10.1029/2001JD001409), 2003.
- Chang, J. S., Brost, R. A., Isaksen, I. S. A., Madronich, S., Middleton, P., Stockwell, W. R., and Walcek, C. J.: A three-dimensional Eulerian acid deposition model: physical concepts and formulation, *J. Geophys. Res.*, 92, 14681–14700, 1987.
- Chen, Y., Y. Zhang, J.-W. Fan, L.R. Leung, Q. Zhang, and K.-B. He, 2015, Application of an Online-Coupled Regional Climate Model, WRF-CAM5, over East Asia for Examination of Ice Nucleation Schemes: Part I. Comprehensive Model Evaluation and Trend Analysis for 2006 and 2011, *Climate*, 3(3), 627–667; [doi: 10.3390/cli3030627](https://doi.org/10.3390/cli3030627).
- CHEMERE (2017), Documentation of the chemistry-transport model, CHIMERE, <http://www.lmd.polytechnique.fr/chimere/>
- Cherin, N., Y. Roustan, L. Musson-Genon, C. Seigneur. Modeling atmospheric dry deposition in urban areas using an urban canopy approach *Geosci. Model Dev.* 8, 893–910 (2015), [doi: 10.5194/gmd-8-893-2015](https://doi.org/10.5194/gmd-8-893-2015).
- Chrit, M. and Sartelet, K. and Sciare, J. and Pey, J. and Marchand, N. and Couvidat, F. and Sellegri, K. and Beekmann, M. (2017), Modeling organic aerosol concentrations and properties during ChArMEx summer campaigns of 2012 and 2013 in the western Mediterranean region *Atmos. Chem. Phys.*, 17, 12509–12531, [doi: 10.5194/acp-2017-312](https://doi.org/10.5194/acp-2017-312).
- Chuang, M.-T., Y. Zhang, and D.-W. Kang, 2011, Application of WRF/Chem-MADRID for Real-Time Air Quality Forecasting over the Southeastern United States, *Atmospheric Environment*, 45 (34), 6241–6250, [doi: 10.1016/j.atmosenv.2011.06.071](https://doi.org/10.1016/j.atmosenv.2011.06.071).
- Cohard, J.-M., Pinty, J.-P., Bedos, C., 1998. Extending Twomey's analytical estimate of nucleated cloud droplet concentrations from CCN spectra. *J. Atmos. Sci.* 55, 3348–3357.
- Debry E., Fahey K., Sartelet K., Sportisse B. and Tombette M. (2007), Technical Note: a new Size REsolved Aerosol Model: SIREAM. *Atmos. Chem. Phys.*, 7, 1537–1547.
- DeMott, P. J., A. J. Prenni, X. Liu, S. M. Kreidenweis, M.D. Petters, C. H. Twohy, M. S. Richardson, T. Eidhammer, and D. C. Rogers (2010), Predicting global atmospheric ice nuclei distributions and their impacts on climate. *Proc. Natl. Acad. Sci. (USA)*, 107, 11217–11222, [doi: 10.1073/pnas.0910818107](https://doi.org/10.1073/pnas.0910818107).
- Easter, R. C., S. J. Ghan, Y. Zhang, R. D. Saylor, E. G. Chapman, N. S. Laulainen, H. Abdul-Razzak, L. R. Leung, X. Bian, and R. A. Zaveri: MIRAGE: Model description and evaluation of aerosols and trace gases, *J. Geophys. Res.*, 109(D2), 0210, [doi: 10.1029/2004JD004571](https://doi.org/10.1029/2004JD004571), 2004.

- Erisman, J.W., van Pul, A., Wyers, P., 1994. Parameterization of surface resistance for the quantification of atmospheric deposition of acidifying pollutants and ozone. *Atmospheric Environment* 28, 2595–2607.
- Erisman, J. W. and Draaijers, G. P. J.: Atmospheric deposition in relation to acidification and eutrophication, in: *Studies in Environmental Science 63*, edited by: Erisman, J. W. and Draaijers, G. P. J., Elsevier, Amsterdam, The Netherlands, 91 pp., 1995.
- Fairlie, T.D., D.J. Jacob, and R.J. Park, The impact of transpacific transport of mineral dust in the United States, *Atmos. Environ.*, 1251-1266, 2007.
- Fast, J.D., W.I. Gustafson Jr., R.C. Easter, R.A. Zaveri, J.C. Barnard, E.G. Chapman, and G.A. Grell: Evolution of ozone, particulates, and aerosol direct forcing in an urban area using a new fully-coupled meteorology, chemistry, and aerosol model, *J. Geophys. Res.*, 111, D21305, doi:10.1029/2005JD006721, 2006.
- Fisher, J.A., D.J. Jacob, Q. Wang, R. Bahreini, C.C. Carouge, M.J. Cubison, J.E. Dibb, T. Diehl, J.L. Jimenez, E.M. Leibensperger, M.B.J. Meinders, H.O.T. Pye, P.K. Quinn, S. Sharma, A. van Donkelaar, and R.M. Yantosca, Sources, distribution, and acidity of sulfate-ammonium aerosol in the Arctic in winter-spring, *Atmos. Environ.*, 45, 7301-7318, 2011.
- Flemming, J., Huijnen, V., Arteta, J., Bechtold, P., Beljaars, A., Blechschmidt, A.-M., Diamantakis, M., Engelen, R. J., Gaudel, A., Inness, A., Jones, L., Josse, B., Katragkou, E., Marecal, V., Peuch, V.-H., Richter, A., Schultz, M. G., Stein, O., and Tsikerdekis, A. (2015), Tropospheric chemistry in the Integrated Forecasting System of ECMWF, *Geosci. Model Dev.*, 8, 975-1003, <https://doi.org/10.5194/gmd-8-975-2015>.
- Freitas, S. R., Longo, K. M., Silva Dias, M. A. F., Chatfield, R., Silva Dias, P., Artaxo, P., Andreae, M. O., Grell, G., Rodrigues, L. F., Fazenda, A., and Panetta, J.: The Coupled Aerosol and Tracer Transport model to the Brazilian developments on the Regional Atmospheric Modeling System (CATT-BRAMS) – Part 1: Model description and evaluation, *Atmos. Chem. Phys.*, 9, 2843–2861, doi:10.5194/acp-9-2843-2009, 2009.
- Freitas, S. R. ; FREITAS, S. R. ; ALONSO, M. F. ; Longo, K. M. ; Pirre, M. ; Marecal, V. ; Grell, G. ; STOCKLER, R. ; Mello, R. F. ; Sánchez Gácita, M. . PREP-CHEM-SRC 1.0: a pre-processor of trace gas and aerosol emission fields for regional and global atmospheric chemistry models, *Geosci. Model Dev.*, 4, 419-433, 2011.
- Freitas, S.R., J. Panetta, K. M. Longo, L. F. Rodrigues, D. S. Moreira, N. E. Rosário, P. L. Silva Dias, M. A. F. Silva Dias, E. P. Souza, E. D. Freitas, M. Longo, A. Frassoni, A. L. Fazenda, C. M. S. e Silva, C. A. B. Pavani, D. Eiras, D. A. França, D. Massaru, F. B. Silva, F. C. Santos, G. Pereira, G. Camponogara, G. A. Ferrada, H. F. C. Velho, I. Menezes, J. L. Freire, M. F. Alonso, M. S. Gácita, M. Zarzur, R. M. Fonseca, R. S. Lima, R. A. Siqueira, R. Braz, S. Tomita, V. Oliveira, and L. D. Martins (2017), The Brazilian developments on the Regional Atmospheric Modeling System (BRAMS 5.2): an integrated environmental model tuned for tropical areas, *Geosci. Model Dev.*, 10, 189-222, <https://doi.org/10.5194/gmd-10-189-2017>.
- Fountoukis, C. and Nenes, A.: Continued development of a cloud droplet formation parameterization for global climate models, *J. Geophys. Res.*, 110, D11212, doi:10.1029/2004JD005591, 2005.
- Giorgi, F.: A particle dry deposition parameterization scheme for use in tracer transport models, *J. Geophys. Res.*, 91, 9794–9806, 1986.
- Giorgi, F. and Chameides, W. L.: Rainout lifetimes of highly soluble aerosols and gases as inferred from simulations with a general circulation model, *J. Geophys. Res.*, 91, 14367–14376, 1986.
- Gong, S. L., Barrie, L. A., and Blanchet, J.-P.: Modeling sea salt aerosols in the atmosphere: 1. Model development, *J. Geophys. Res.*, 102, 3805–3818, 1997.
- Gong, S.L., Barrie, L.A., Blanchet, J.-P., von Salzen, K., Lohmann, U., Lesins, G., Spacek, L., Zhang, L.M., Girard, E., Lin, H., Leaitch, R., Leighton, H., Chylek, P., Huang, P.

- (2003b), Canadian Aerosol Module: a size-segregated simulation of atmospheric aerosol processes for climate and air quality models. 1. Module development, *J. Geophys. Res.*, 108, 4007. <http://dx.doi.org/10.1029/2001JD002002>.
- Gong, W.; Dastoor, A.P.; Bouchet, V.S.; Gong, S.; Makar, P.A.; Moran, M.D.; Pabla, B.; Ménard, S.; Crevier, L.-P.; Cousineau, S.; et al. Cloud processing of gases and aerosols in a regional air quality model (AURAMS). *Atmos. Res.* 2006, 82, 248–275.
- Grell, G. A., S. E. Peckham, R. Schmitz, S. A. McKeen, G. Frost, W. C. Skamarock, and B. Eder (2005), Fully coupled “online” chemistry within the WRF model, *Atmos. Environ.*, 39(37), 6957–6975, [doi:10.1016/j.atmosenv.2005.04.027](https://doi.org/10.1016/j.atmosenv.2005.04.027).
- Guelle, W., Balkanski, Y. J., Dibb, J. E., Schulz, M., and Dulac, F.: Wet deposition in a global size-dependent aerosol transport model, 2. Influence of the scavenging scheme on Pb vertical profiles, and deposition, *J. Geophys. Res.*, 103, 28875–28891, 1998.
- Hicks, B. B., Saylor, R. D., and Baker, B. D.: Dry deposition of particles to canopies – A look back and the road forward, *J. Geophys. Res.-Atmos.*, 121, 14691–14707, <https://doi.org/10.1002/2015JD024742>, 2016.
- Hinds, W. C. 1999. *Aerosol Technology*. New York: Wiley.
- Hoose, C., Kristjansson, J.E., Arabas, S., Boers, R., Pawlowska, H., Puygrenier, V., Siebert, H., Thouron, O., 2010. Parameterization of in-cloud vertical velocities for cloud droplet activation in coarse-grid models: analysis of observations and cloud resolving model results. In: *Proceedings of the 13th AMS Conference on Atmospheric Radiation*, Portland, OR, USA, 28 June–2 July 2010. Paper # 6.4.
- Hu, L., C.A. Keller, M.S. Long, T. Sherwen, B. Auer, A. Da Silva, J.E. Nielsen, S. Pawson, M.A. Thompson, A.L. Trayanov, K.R. Travis, S.K. Grange, M.J. Evans, and D.J. Jacob (2018), Global simulation of tropospheric chemistry at 12.5 km resolution: performance and evaluation of the GEOS-Chem chemical module within the NASA GEOS Earth System Model, submitted to *Geosci. Model Dev.*
- Jacobson, M. Z.: *Fundamentals of Atmospheric Modeling*, Second Edn., Cambridge University Press, New York, 813 pp., 2005.
- Jones, A.; Roberts, D.L.; Slingo, J. A climate model study of indirect radiative forcing by anthropogenic sulfate aerosols. *Nature* 1994, 370, 450–453.
- Jones, A., D. Thomson, M. Hort, and B. Devenish, 2007: The U.K. Met Office’s next-generation atmospheric dispersion model, NAME III, in *Air Pollution Modeling and Its Application XVII*, edited by C. Borrego and A.-L. Norman, 580–589, Springer, New York.
- Khan, T.R. and J. A. Perlinger (2017), Evaluation of five dry particle deposition parameterizations for incorporation into atmospheric transport models, *Geosci. Model Dev.*, 10, 3861–3888, <https://doi.org/10.5194/gmd-10-3861-2017>.
- Kang, D., B. K. Eder, A. F. Stein, G. A. Grell, S. E. Peckham, and J. McHenry (2005), The New England Air Quality Forecasting Pilot Program: Development of an evaluation protocol and performance benchmark, *J. Air & Waste Manage. Assoc.*, 55, 1782–1796.
- Korsholm, U. S., Baklanov, A., Gross, A., Mahura, A., Sass, B. H., and Kaas, E.: Online coupled chemical weather forecasting based on HIRLAM – overview and prospective of Enviro-HIRLAM, *HIRLAM Newsletter*, 54, 151–168, 2008.
- Kouznetsov, R., Sofiev, M. (2012) A methodology for evaluation of vertical dispersion and dry deposition of atmospheric aerosols. *JGR*, 117. [doi: 10.1029/2011JD016366](https://doi.org/10.1029/2011JD016366).
- Langner, J., Bergström, R., and Foltescu, V. L.: Impact of climate change on surface ozone and deposition of sulphur and nitrogen in Europe, *Atmos. Environ.*, 39, 1129–1141, 2005.
- Li, P.-F., L.-Q. Wang, P. Guo, S.-C. Yu, K. Mehmood, S. Wang, W.-P. Liu, J. H. Seinfeld, Y. Zhang, D. Wong, K. Alapaty, J. Pleim, and R. Mathur, 2017, High reduction of ozone and air particulate matter during the 2016 G-20 summit in Hangzhou by forced emission controls of industry and traffic, *Environmental Chemistry Letters*, DOI

[10.1007/s10311-017-0642-2](https://doi.org/10.1007/s10311-017-0642-2).

- Liu, H., Jacob, D.J., Bey, I., Yantosca, R.M., 2001. Constraints from ^{210}Pb and ^7Be on wet deposition and transport in a global three-dimensional chemical tracer model driven by assimilated meteorological fields. *Journal of Geophysical Research* 106, 12109–12128.
- Liu, X.H.; Penner, J.E.; Das, B.; Bergmann, D.; Rodriguez, J.M.; Strahan, S.; Wang, M.; Feng, Y. Uncertainties in global aerosol simulations: Assessment using three meteorological datasets. *J. Geophys. Res.* 2007, 112, D11212.
- Longo, K. M., Freitas, S. R., Pirre, M., Marécal, V., Rodrigues, L. F., Panetta, J., Alonso, M. F., Rosário, N. E., Moreira, D. S., Gácita, M. S., Arteta, J., Fonseca, R., Stockler, R., Katsurayama, D. M., Fazenda, A., and Bela, M.: The Chemistry CATT-BRAMS model (CCATT-BRAMS 4.5): a regional atmospheric model system for integrated air quality and weather forecasting and research, *Geosci. Model Dev.*, 6, 1389-1405, <https://doi.org/10.5194/gmd-6-1389-2013>, 2013.
- Loosmore, G., Cederwall, R., 2004. Precipitation scavenging of atmospheric aerosols for emergency response applications: testing an updated model with new real-time data. *Atmospheric Environment* 38, 993–1003.
- LOTOS-EUROS (2016), LOTOS-EUROS v2.0 Reference Guide, TNO Report, TNO 2016 R10898, pp. 77.
- Makar, P.A., Gong, W., Milbrandt, J., Hogrefe, C., Zhang, Y., Curci, G., Zabkar, R., Im, U., Balzarini, A., Baro, R., Bianconi, R., Cheung, P., Forkel, R., Gravel, S., Hirtl, H., Honzak, L., Hou, A., Jimenez-Guerrero, P., Langer, M., Moran, M.D., Pabla, B., Perez, J.L., Pirovano, G., San Jose, R., Tuccella, P., Werhahn, J., Zhang, J., Galmarini, S. Feedbacks between air pollution and weather, part 1: Effects on weather. *Atmospheric Environment*, 115, 442-469, 2015a.
- Makar, P.A., Gong, W., Hogrefe, C., Zhang, Y., Curci, G., Zabkar, R., Milbrandt, J., Im, U., Balzarini, A., Baro, R., Bianconi, R., Cheung, P., Forkel, R., Gravel, S., Hirtl, H., Honzak, L., Hou, A., Jimenez-Guerrero, P., Langer, M., Moran, M.D., Pabla, B., Perez, J.L., Pirovano, G., San Jose, R., Tuccella, P., Werhahn, J., Zhang, J., Galmarini, S. Feedbacks between air pollution and weather, part 2: Effects on chemistry. *Atmospheric Environment*, 115, 499-526, 2015b.
- Makar, P. A., Akingunola, A., Aherne, J., Cole, A. S., Aklilu, Y.-A., Zhang, J., Wong, I., Hayden, K., Li, S.-M., Kirk, J., Scott, K., Moran, M. D., Robichaud, A., Cathcart, H., Baratzedah, P., Pabla, B., Cheung, P., Zheng, Q., and Jeffries, D. S.: Estimates of Exceedances of Critical Loads for Acidifying Deposition in Alberta and Saskatchewan, *Atmos. Chem. Phys.* 18, 9897-9927, 2018, <https://doi.org/10.5194/acp-18-9897-2018>.
- Mann, G.W., Carslaw, K.S., Spracklen, D.V., Ridley, D.A., Manktelow, P.T., Chipperfield, M.P., Pickering, S.J., Johnson, C.E., 2010. Description and evaluation of GLOMAP-mode: a modal global aerosol microphysics model for the UKCA composition-climate model. *Geosci. Model Dev.* 3, 519-551.
- Mari, C., Jacob, D. J., and Bechtold, P.: Transport and scavenging of soluble gases in a deep convective cloud, *J. Geophys. Res.*, 105, 22255–22267, 2000.
- McKeen, S., J. Wilczak, G. Grell, I. Djalova, S. Peckham, E.-Y. Hsie, W. Gong, V. Bouchet, S. Ménard, R. Moffet, J. McHenry, J. McQueen, Y. Tang, G. R. Carmichael, M. Pagowski, A. Chan, t. Dye, G. Frost, P. Lee, and R. Mathur (2005), Assessment of an ensemble of seven real-time ozone forecasts over eastern North America during the summer of 2004, *J. Geophys. Res.*, 110, D21307, doi: [10.1029/2005JD005858](https://doi.org/10.1029/2005JD005858).
- McKeen, S., S. H. Chung, J. Wilczak, G. Grell, I. Djalalova, S. Peckham, W. Gong, V. Bouchet, R. Moffet, Y. Tang, G. R. Carmichael, R. Mathur, and S. Yu (2007), Evaluation of several PM_{2.5} forecast models using data collected during the ICARTT/NEAQS 2004 field study, *J. Geophys. Res.*, 112, D10S20, doi: [10.1029/2006JD007608](https://doi.org/10.1029/2006JD007608).

- McKeen, S. et al. (2009), An evaluation of real-time air quality forecasts and their urban emissions over eastern Texas during the summer of 2006 Second Texas Air Quality Study field study, *J. Geophys. Res.*, 114, D00F11, doi:10.1029/2008JD011697.
- Meyers, M.P.; DeMott, P.J.; Cotton, W.R. New primary ice-nucleation parameterizations in an explicit cloud model. *J. Appl. Meteorol.* 1992, 31, 708–721, doi:10.1175/1520-0450(1992)031<0708:NPINPI>2.0.CO;2.
- Michou, M., Laville, P., Serça, D., Fotiadi, A., Bouchou, P., and Peuch, V.-H.: Measured and modeled dry deposition velocities over the ESCOMPTE area, *Atmos. Res.*, 74, 89–116, 2004.
- Mircea, M. and Stefan, S.: A theoretical study of the microphysical parameterization of the scavenging coefficient as a function of precipitation type and rate, *Atmos. Environ.*, 32, 2931–2938, 1998.
- Morcrette, J.-J., et al. (2009), Aerosol analysis and forecast in the European Centre for Medium-Range Weather Forecasts Integrated Forecast System: Forward modeling, *J. Geophys. Res.*, 114, D06206, doi:10.1029/2008JD011235.
- Näslund E. and L. Thaning (1991), On the settling velocity in a nonstationary atmosphere, *Aerosol Sci. Tech.*, 14, 247–256, 1991.
- Nenes, A. and Seinfeld, J. H.: Parameterization of cloud droplet formation in global climate models, *J. Geophys. Res.*, 108, 4415, doi:10.1029/2002JD002911, 2003.
- Nho-Kim, E.-Y., Michou, M., and Peuch, V.-H.: Parameterization of size dependent particle dry deposition velocities for global modeling, *Atmos. Environ.*, 38, 1933–1942, 2004.
- Niemand, M.; Mohler, O.; Vogel, B.; Vogel, H.; Hoose, C.; Connolly, P.; Klein, H.; Bingemer, H.; DeMott, P.; Skrotzki, J.; Leisner, T. A particle-surface-area-based parameterization of immersion freezing on desert dust particles. *J. Atmos. Sci.* 2012, 69, 3077–3092.
- Peters, K. and Eiden, R.: Modeling the dry deposition velocity of aerosol particles to a spruce forest, *Atmos. Environ.*, 26A, 2555–2564, 1992.
- Pleim, J. E., Venkatram, A., and Yamartino, R.: ADOM/TADAP Model Development Program, The Dry Deposition Module, Vol. 4, Ontario Ministry of the Environment, Rexdale, Canada, 1984.
- Pérez, C., K. Haustein, Z. Janjic, O. Jorba, N. Huneus, J. M. Baldasano, T. Black, S. Basart, S. Nickovic, R. L. Miller, J. P. Perlwitz, M. Schulz, and M. Thomson (2011), Atmospheric dust modeling from meso to global scales with the online NMMB/BSC-Dust model – Part 1: Model description, annual simulations and evaluation, *Atmos. Chem. Phys.*, 11, 13001-13027, <https://doi.org/10.5194/acp-11-13001-2011>.
- Petroff, A., and L. Zhang (2010), Development and validation of a size-resolved particle dry deposition scheme for application in aerosol transport models, *Geosci. Model Dev.*, 3, 753–769.
- Redington, A. L., and R. G. Derwent, 2002: Calculation of sulfate and nitrate aerosol concentrations over Europe using a Lagrangian dispersion model, *Atmos. Environ.*, 36, 4425-4439.
- Redington, A.L., Derwent, R.G., Witham, C.S., Manning, A.J., 2009: Sensitivity of modeled sulfate and nitrate aerosol to cloud, pH and ammonia emissions, *Atmos. Environ.*, 43, 3227-3234.
- Redington, A. L., and R. G. Derwent, 2013: Modeling secondary organic aerosol in the United Kingdom, *Atmos. Environ.*, 63, 349-357.
- Robertson, L., Langner, J., and Engardt, M.: An Eulerian limited area atmospheric transport model, *J. Appl. Meteorol.*, 38, 190–210, 1999.
- Roselle, S. J. and Binkowski, F. S.: Chapt. 11: Cloud dynamics and chemistry, in: Science Algorithms of the EPA Models-3, Technical Report 600/R-99/030, EPA, Research Triangle Park, NC, 1999.

- Sartelet K., Debry E., Fahey K., Roustan Y., Tombette M., Sportisse B. (2007), Simulation of aerosols and gas-phase species over Europe with the Polyphemus system. Part I: model-to-data comparison for 2001. *Atmospheric Environment*, 41 (29), p6116-6131, doi: [10.1016/j.atmosenv.2007.04.024](https://doi.org/10.1016/j.atmosenv.2007.04.024).
- Sartelet K.N., Couvidat F., Seigneur, C. and Roustan Y. (2012), Impact of biogenic emissions on air quality over Europe and North America. *Atmospheric Environment*, 53, 131-141, doi: [10.1016/j.atmosenv.2011.10.046](https://doi.org/10.1016/j.atmosenv.2011.10.046).
- Schaap, M., Timmermans, R. M. A., Roemer, M., Boersen, G. A. C., Builtjes, P. J. H., Sauter, F. J., Velders, G. J. M., and Beck, J. P.: The LOTOS-EUROS model: description, validation and latest developments, *Int. J. Environ. Pollut.*, 32, 270–290, 2008.
- Seinfeld, J. and Pandis, S.: *Atmospheric Chemistry and Physics*, John Wiley & Sons Inc., New York, 1998.
- Seinfeld, J.H. and S.N. Pandis (2016), *Atmospheric Chemistry and Physics: from Air Pollution to Climate Change*, John Wiley & Sons, Inc., ISBN: 978-1-118-94740-1, 2016 (the 3rd edition).
- Shinozuka, Y., P. E. Saide, G. A. Ferrada, S. P. Burton, R. Ferrare, S. J. Doherty, H. Gordon, K. Longo, M. Mallet, Y. Feng, Q.-Q. Wang, Y.-F. Cheng, A. Dobracki, S. Freitag, S. G. Howell, S. LeBlanc, C. Flynn, M. Segal-Rosenhaimer, K. Pistone, J. R. Podolske, E. J. Stith, J. Ryan Bennett, G. R. Carmichael, A. da Silva, R. Govindaraju, R. Leung, Y. Zhang, L. Pfister, J.-M. Ryoo, J. Redemann, R. Wood, and P. Zuidema, 2020, Modeling the smoky troposphere of the southeast Atlantic: a comparison to ORACLES airborne observations from September of 2016, *Atmo. Chem. Phys.*, 20, 11491–11526, <https://doi.org/10.5194/acp-20-11491-2020>.
- Simpson, D., Fagerli, H., Jonson, J.E., Tsyro, S., Wind, P., Tuovinen, J.-P., 2003. Transboundary acidification, eutrophication and ground level ozone in Europe. Part I: unified EMEP model description. Technical Report, EMEP.
- Slinn, W. G. N. (1977). Some approximations for the wet and dry removal of particles and gases from the atmosphere.
- Slinn, W. G. N., 1982: Predictions for particle deposition to vegetative canopies. *Atmos. Environ.*, 16, 1785–1794, doi: [10.1016/0004-6981\(82\)90271-2](https://doi.org/10.1016/0004-6981(82)90271-2).
- Slinn, S. A. and Slinn, W. G. N.: Predictions for particle deposition on natural waters, *Atmos. Environ.*, 14, 1013–1026, 1980.
- Sofiev, M. (2000) A model for the evaluation of long-term airborne pollution transport at regional and continental scales. *Atmospheric Environment*. 34, No.15, pp. 2481-2493.
- Sørensen, J. H., Baklanov, A., and Hoe, S.: The Danish emergency response model of the atmosphere, *J. Environ. Radioactiv.*, 96, 122–129, 2007.
- Spada, M., 2015. Development and evaluation of an atmospheric aerosol module implemented within the NMMB/BSC-CTM. PhD Thesis, BarcelonaTech, Spain.
- Sportisse, B. (2007), A review of parameterizations for modeling dry deposition and scavenging of radionuclides, *Atmos. Environ.*, 41, 2683–2698.
- Sportisse, B., Dubois, L., 2002. Numerical and theoretical investigation of a simplified model for the parameterization of below-cloud scavenging by falling raindrops. *Atmospheric Environment* 36, 5719–5727.
- Spracklen, D.V., Pringle, K.J., Carslaw, K.S., Chipperfield, M.P., Mann, G.W., 2005. A global offline model of size-resolved aerosol microphysics: II. Identification of key uncertainties. *Atmos Chem Phys* 5, 3233-3250.
- Stier, P., Feichter, J., Kinne, S., Kloster, S., Vignati, E., Wilson, J., Ganzeveld, L., Tegen, I., Werner, M., Balkanski, Y., Schulz, M., Boucher, O., Minikin, A., and Petzold, A.: The aerosol-climate model ECHAM5-HAM, *Atmos. Chem. Phys.*, 5, 1125–1156, <https://doi.org/10.5194/acp-5-1125-2005>, 2005. Strader et al. (1997)
- Strader, R., Gurciullo, C., Pandis, S., Kumar, N., and Lurmann, F.: Development of gas-phase chemistry, secondary organic aerosol and aqueous-phase chemistry modules

for PM modeling, Tech. rep., STI, 1998. Savijärvi, H.: Shortwave optical properties of rain, *Tellus*, 49a, 177–181, 1997.

- Textor, C., M. Schulz, S. Guibert, S. Kinne, Y. Balkanski, S. Bauer, T. Berntsen, T. Berglen, O. Boucher, M. Chin, F. Dentener, T. Diehl, J. Feichter, D. Fillmore, P. Ginoux, S. Gong, A. Grini, J. Hendricks, L. Horowitz, P. Huang, I. S. A. Isaksen, T. Iversen, S. Kloster, D. Koch, A. Kirkevåg, J. E. Kristjansson, M. Krol, A. Lauer, J. F. Lamarque, X. Liu, V. Montanaro, G. Myhre, J. E. Penner, G. Pitari, M. S. Reddy, Ø. Seland, P. Stier, T. Takemura, and X. Tie (2007), The effect of harmonized emissions on aerosol properties in global models – an AeroCom experiment, *Atmos. Chem. Phys.*, 7, 4489–4501.
- Tiedtke, M., 1989. A Comprehensive Mass Flux Scheme for Cumulus Parameterization in Large-Scale Models. *Mon Weather Rev* 117, 1779-1800.
- Tompkins, A. M. (2005), A revised cloud scheme to reduce the sensitivity to vertical resolution, Tech. Memo. 0599, 25 pp., Res. Dep., Eur. Cent. for Medium-Range Weather Forecasts, Reading, U. K.
- Tsyro, S.: First Estimates of the Effect of Aerosol Dynamics in the Calculation of PM10 and PM2.5, EMEP/MSC-W Note 4/2002, Norwegian Meteorological Institute, Oslo, Norway, Research Note no. 76.
- Vivanco, Marta G. and Palomino, Immaculada and Vautard, Robert and Bessagnet, Bertrand and Martin, Fernando and Menut, Laurent and Jimenez, Santiago, Multi-year assessment of photochemical air quality simulation over Spain, *Environmental Modeling and Software*, 24, 1, 63-73, 2009.
- Wang, Y., D.J. Jacob, and J.A. Logan, Global simulation of tropospheric O₃-NO_x-hydrocarbon chemistry, 1. Model formulation, *J. Geophys. Res.*, 103/D9, 10,713-10,726, 1998a.
- Wang, H., X. Y. Zhang, S. L. Gong, et al., 2010: Radiative feedback of dust aerosols on the East Asian dust storms. *J. Geophys. Res.*, 115, D23214, doi: 10.1029/2009JD013430.
- Wang, Q., D.J. Jacob, J.A. Fisher, J. Mao, E.M. Leibensperger, C.C. Carouge, P. Le Sager, Y. Kondo, J.L. Jimenez, M.J. Cubison, and S.J. Doherty, Sources of carbonaceous aerosols and deposited black carbon in the Arctic in winter-spring: implications for radiative forcing, *Atmos. Chem. Phys.*, 11, 12,453-12,473, 2011.
- Wang, Q., D.J. Jacob, J.R Spackman, A.E. Perring, J.P. Schwarz, N. Moteki, E.A. Marais, C. Ge, J. Wang, and S.R.H. Barrett, Global budget and radiative forcing of black carbon aerosol: constraints from pole-to-pole (HIPPO) observations across the Pacific, *J. Geophys. Res.*, 119, 195-206, 2014
- Wang, Z., Xie, F., Sakurai, T., Ueda, H., Han, Z., Carmichael, G. R., Streets, D., Engardt, M., Holloway, T., Hayami, H., Kajino, M., Thongboonchoo, N., Bennet, C., Park, S. U., Fung, C., Chang, A., Sartelet, K., Amann, M.: MICS-Asia II: Model intercomparison and evaluation of acid deposition, *Atmos. Environ.*, 42, 3528–3542, 2008.
- Webster, H.N. and Thomson, D.J., 2011: Dry deposition modeling in a Lagrangian dispersion model, *Int. J. Environ. Pollut.*, 47(1-4), 1-9.
- Webster, H.N. and Thomson, D.J., 2014: The NAME wet deposition scheme, Forecasting Research Technical Report 584, Met Office.
- Webster, H.N. and Thomson, D.J., 2017: A particle size dependent wet deposition scheme for NAME, Forecasting Research Technical Report 624, Met Office.
- Wesely, M. L., 1989, Parametrization of Surface Resistances to Gaseous Dry Deposition in Regional-Scale Numerical Models, *Atmos. Environ.*, 23, pp. 1293–1304.
- Wesely, M. L. and Hicks, B. B. A.: A review of the current status of knowledge on dry deposition, *Atmos. Environ.*, 34, 2261–2282, 2000.
- Yahya, K., T. Glotfelty, K. Wang, Y. Zhang, and A. Nenes, 2017, Modeling Regional Air Quality and Climate: Improving Organic Aerosol and Aerosol Activation Processes in WRF/Chem version 3.7.1, *Geoscientific Model Development*, 10, 2333-2363, doi:10.5194/gmd-10-2333-2017.

- Yu, Shaocai, R. Mathur, J. Pleim, D. Wong, R. Gilliam, K. Alapaty, C. Zhao, and X. Liu, 2014. Aerosol indirect effect on the grid-scale clouds in the two-way coupled WRF-CMAQ: model description, development, evaluation and regional analysis. *Atmos. Chem. Phys.* 14, 11247–11285, doi:10.5194/acp-14-1-2014.
- Zannetti, P., ed. 1990. *Air Pollution Modeling: Theories, Computational Methods and Available Software*. Springer.
- Zanten, M.C. van, F.J. Sauter R.J. Wichink Kruit J.A. van Jaarsveld, PBL W.A.J. van Pul (2010), Description of the DEPAC module, Dry deposition modeling with DEPAC_GCN2010, RIVM Report 680180001/2010, RIVM, P.O. Box 1, 3720 BA Bilthoven, the Netherlands.
- Zhang, J., Y. Shao, and N. Huang (2014), Measurements of dust deposition velocity in a wind-tunnel experiment, *Atmos. Chem. Phys.*, 14, 8869–8882.
- Zhang, L. M., S. L. Gong, J. Padro, et al., 2001: A size-segregated particle dry deposition scheme for an atmospheric aerosol module. *Atmos. Environ.*, 35, 549–560, doi: 10.1016/S1352-2310(00)00326-5.
- Zhang, L., Brook, J., Vet, R., 2003. A revised parameterization for gaseous dry deposition in air-quality models. *Atmos. Chem. Phys.*, 3, 2067-2082, <https://doi.org/10.5194/acp-3-2067-2003>
- Zhang, Y., R.C. Easter, S.J. Ghan, and H. Abdul-Razzak, 2002, Impact of Aerosol Size Representation on Modeling Aerosol-Cloud Interactions, *Journal of Geophysical Research*, 107, 4558, doi:1029/2001JD001549.
- Zhang, Y., Y. Pan., K. Wang, J. D., Fast, and G. A. Grell, 2010, WRF/Chem-MADRID: Incorporation of an Aerosol Module into WRF/Chem and Its Initial Application to the TexAQS2000 Episode, *Journal of Geophysical Research*, 115, D18202, doi: 10.1029/2009JD013443.
- Zhang, Y., X. Zhang, K. Wang, J. He, L. R. Leung, J.-W. Fan, and A. Nenes, 2015a, Incorporating An Advanced Aerosol Activation Parameterization into WRF-CAM5: Model Evaluation and Parameterization Intercomparison, *Journal of Geophysical Research*, 120 (14), 6952–6979, DOI: 10.1002/2014JD023051.
- Zhang, Y., Y. Chen, J.-W. Fan, and L.R. Leung, 2015b, Application of an Online-Coupled Regional Climate Model, WRF-CAM5, over East Asia for Examination of Ice Nucleation Schemes: Part II. Sensitivity to Ice Nucleation Parameterizations and Dust Emissions, *Climate*, 2015, 3(3), 753-774; doi:10.3390/cli3030753.
- Zhang, Y., C.-P. Hong, K. Yahya, Q. Li, Q. Zhang, and K.-B. He, 2016, Comprehensive evaluation of multi-year real-time air quality forecasting using an online-coupled meteorology-chemistry model over southeastern United States, *Atmos. Environ.*, 138, 162-182, doi:10.1016/j.atmosenv.2016.05.006.
- Zhou C., X. Zhang, S. Gong, Y. Wang, and M. Xue, Improving aerosol interaction with clouds and precipitation in a regional chemical weather modeling system, *Atmos. Chem. Phys.* 16, 145-160, 2016, doi:10.5194/acp-16-145-2016
- Zhou, C. H., X. J. Shen, Z. R. Liu., et al., 2018: Simulating aerosol size distribution and mass concentration with simultaneous nucleation, condensation/coagulation, and deposition with the GRAPES–CUACE. *J. Meteor. Res.*, 32(2), 1–14, doi: 10.1007/s13351-018-7116-8.
- Zhu S., Sartelet K., Seigneur C. (2015), A size-composition resolved aerosol model for simulating the dynamics of externally mixed particles: SCRAM (v 1.0) *Geosci. Model Dev.*, 8, 1595-1612.

3.8 Interactions of Aerosol Species with Radiation via the Direct Effect for CW-AQF Models

3.8.1 Introduction

The “radiative direct effect” describes the impact of airborne atmospheric particles (aerosols) on the radiative balance of the atmosphere.

Particles may *scatter* light: the direction of motion of incoming photons incident to a particle may change due to the particle’s presence. Some of the incident energy may continue in the forward direction (*forward scattering*); some component of the energy still continues in the original direction of the incoming light, while some component of the energy may return in the direction of the incoming light (*backscattering*).

Particles may also *absorb* incoming light; some fraction of the total incoming energy may remain with the particle as opposed to travelling onward or backwards after the particle is encountered.

These optical properties of particles allow them to have a key role in the atmosphere’s response to incoming and outgoing solar and infrared radiation. The optical properties of particles are highly dependent on the wavelength of light, as well as the particles’ size, chemical composition, and morphology (the latter describes how the different chemical species are physically arranged within the particle). These variations may result in significant differences in how the particles affect the atmosphere’s radiative balance. For example, particles located in the stratosphere that happen to backscatter a large amount of the incoming ultraviolet light from the sun reduce the amount of this radiation reaching the surface of Earth, and hence may cool the atmosphere below the particle layer. This effect is sometimes seen with major volcanic eruptions. Particles which contain a significant fraction of black carbon may absorb a relatively large amount of the incoming ultraviolet and visible radiation. This may in turn heat the atmospheric layers containing the black carbon particles, while preventing solar radiation from reaching the surface, resulting in surface cooling. Black carbon is known as a short-lived climate pollutant, due to its ability to influence global warming, and due to its relatively short residence time in the atmosphere compared to carbon dioxide. In a recent review of the impacts of black carbon aerosols on climate, Bond *et al.* (2013) estimated the black carbon direct effect radiative forcing¹ at $+0.71 \text{ W m}^{-2}$, with an additional $+0.23 \text{ W m}^{-2}$ and $+0.13 \text{ W m}^{-2}$ associated with cloud interactions with black carbon, and snow plus sea-ice black carbon effects, respectively. Myhre *et al.* (2013) summarized the direct effect impacts of different aerosols by composition, as global 2013 radiative forcing values (Table 3.17).

Table 3.17 shows that, globally, different chemicals found in atmospheric particles can have very different effects on the atmosphere’s radiative balance, with black carbon particles contributing the most to warming of the atmosphere, and sulfate particles contributing most to atmospheric cooling. The table also shows that the range of estimates for the radiative forcing associated with each component is high, with the total aerosol impact ranging from -0.81 W m^{-2} (cooling) to $+0.19 \text{ W m}^{-2}$ (warming). This may be compared to the current estimate of the radiative forcing associated with carbon dioxide of $+1.8 \text{ W m}^{-2}$. Reductions of emissions of black carbon particles have been put forward as one means of combating global warming, due to their positive radiative forcing. The range of estimated impacts of the different chemical components found in atmospheric particles may in part be due to the range of methods used to simulate particle direct effects in atmospheric models – these methods are discussed in detail later in this section.

¹ *Radiative forcing* is the difference between the incoming solar radiation absorbed by Earth and the energy radiated back into space, with positive values indicating a net warming effect, negative values indicating a net cooling effect.

Table 3.17 Radiative forcing impact of different aerosol components by composition (after Figure 8.8 of Myhre et al. (2013)).

Chemical component of global aerosol	Radiative Forcing (Range) (W m^{-2})
Black Carbon	+0.40 (0.05 to 0.80)
Secondary Organic Aerosol	-0.03 (-0.27 to +0.20)
Primary Organic Carbon	-0.09 (-0.03 to -0.15)
Nitrate	-0.11 (-0.03 to -0.30)
Sulfate	-0.40 (-0.60 to -0.20)
Total Aerosols	-0.31 (-0.81 to +0.19)

Different classes of atmospheric models simulate aerosol direct effects to different degrees of complexity. At the time of writing, most regional and global *weather forecast* models make use of *specified optical properties* – that is, rather than simulating the particles and the details of their chemistry, tabulated “typical values” or climatologies of their optical properties are used in the weather forecast model’s radiative transfer code. General Circulation Models have a greater level of detail for chemical speciation of particles, with a main focus of these models in recent years being the accurate simulation of the optical properties of black carbon (c.f. Bond *et al.*, 2013). However, General Circulation Models usually do not describe the complexities of secondary particle formation due to the high level of computational resources required for these detailed chemical simulations. Chemical Weather – Air-Quality Forecast (CW-AQF) models provide the most detailed description of particle emissions, chemistry and speciation as a function of time – however, the level of complexity of the assumptions and algorithms used in these models to describe the aerosol direct effect varies widely, as will be discussed later in this section.

Recent studies utilizing CW-AQF models illustrate the potentially large impact of the direct effect on weather forecast accuracy (Figure 3.3). Prediction accuracy of the average vertical temperature profile over the continental USA was significantly improved utilizing a configuration of the Weather Research Forecast model with Chemistry (WRF-Chem) which incorporated the direct effect for forest fire smoke using a single transported species to represent the smoke (Figure 3.3 (a, b); Ahmadov *et al.*, 2018). In this application, the optical properties of the transported variable were chosen to follow the observed properties of forest fire smoke. These were added to the standard climatological aerosol optical properties used in the WRF weather forecast model, and no impacts of the smoke on cloud formation were assumed (i.e. the improvement to the forecast bias was due solely to the incorporation of the direct effect of forest fire smoke within WRF). The effect of forest fire smoke on weather forecasts was also the focus of a study using the Global Environmental Multiscale – Modeling Air-quality and CHemistry (GEM-MACH) model (Figure 3.3 (c), (d); Makar *et al.*, 2018), which incorporated both emitted and chemically-formed particulate matter as well as both the direct and indirect effects with a speciated aerosol size distribution (albeit with a generic set of complex refractive index values to describe locally calculated aerosol optical properties). These GEM-MACH simulations significantly improved the forecast surface temperature and pressure bias, the temperature and wind speed mean average error, the surface temperature, pressure and wind speed root mean square error, and the wind speed standard deviation over the western USA. Conditions were simulated for a period and location where low cloud conditions prevailed, during a month in which forest fire emissions of particulate matter were high. These examples illustrate the potential for CW-AQF models to improve weather forecasts through simulating the direct effect under conditions when the atmospheric loading of particles is high, such as during large forest fire events.

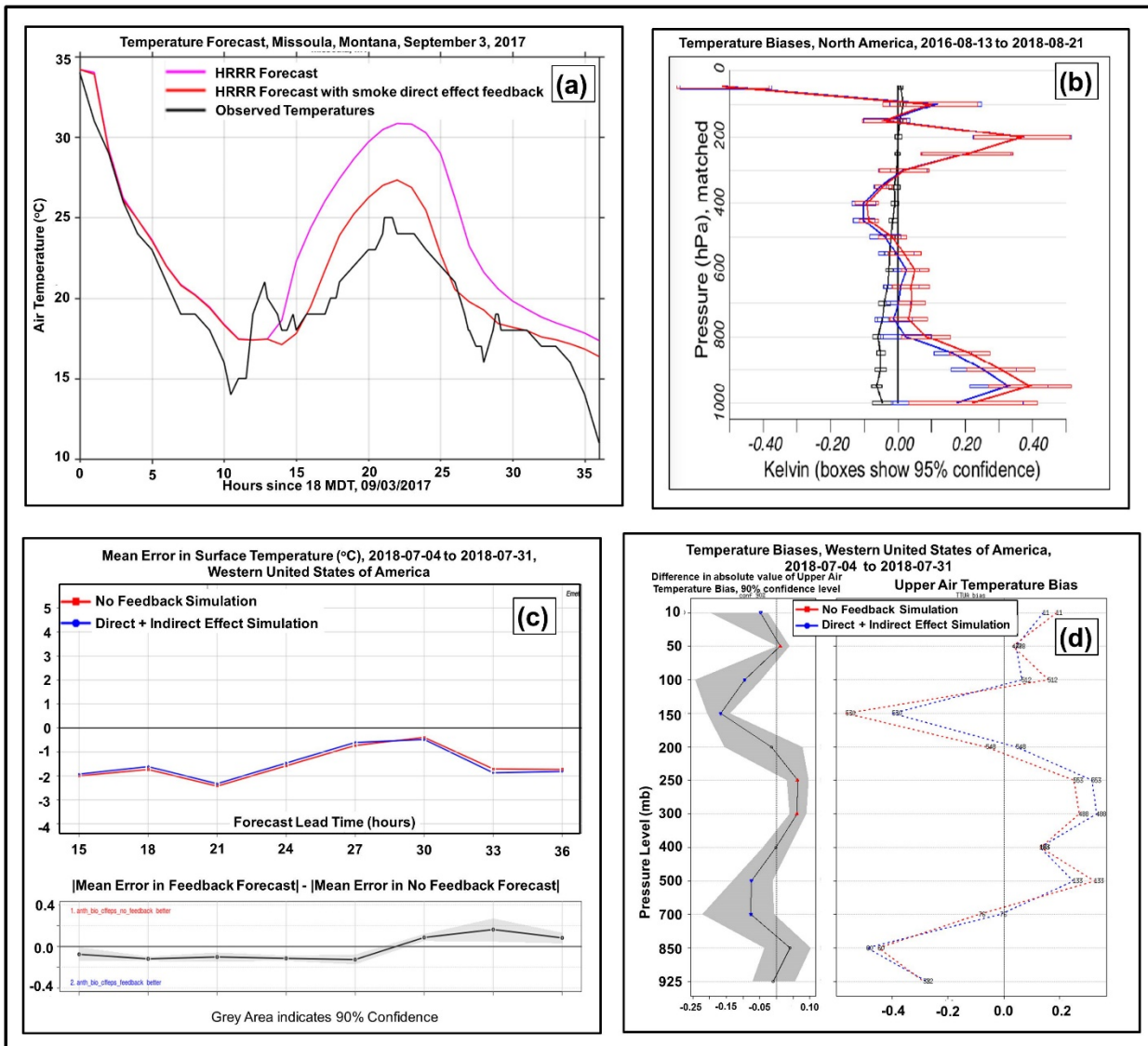


Figure 3.3. Recent Evaluations of Aerosol Feedback CW-AQF models for Forest Fire Smoke.

- (a) WRF-Chem time series for Missoula, Montana;
- (b) WRF-Chem Continental United States Temperature Biases;
- (c) GEM-MACH surface temperature biases, western U.S.A.;
- (d) GEM-MACH temperature profile biases, western USA.

After Ramanadov *et al.* (2018) and Makar *et al.* (2018).

However, it must also be acknowledged that the aerosol *indirect* effect (the cloud formation properties of particles, discussed elsewhere in this report), when incorporated into CW-AQF models, may act in opposition to and have stronger effects on weather forecasts than the direct effect. Another forest fire example using two versions of WRF-Chem (Figure 3.4, Makar *et al.*, 2015(a)) shows the downward ultraviolet radiation and resulting surface temperature response over Europe for a case study simulating the impacts of large forest fires in Russia in the summer of 2010 using the WRF-Chem model. The simulation using the direct effect only (Figure 3.4 (a), (c)) shows a significant surface cooling associated with the forest fire smoke, while the simulation incorporating both the direct and indirect effects (Figure 3.4 (b)) has a more muted response to the fires. The indirect effect reduced the impact of the direct effect on the forest fire forecast, in this example. Further work simulating the direct effect impact of the Russian fires of 2010 showed that the absence of direct effect parameterizations would result in errors in global shortwave irradiance of +15 W m⁻² or +10 W m⁻² with the use of standard climatological aerosols (Gleeson *et al.*, 2016).

Nevertheless, the direct effect has been shown to have a significant impact on chemical weather and air-quality forecasts. Sea salt aerosols have been found to have a negative radiative forcing on the order of -2 to -3 Wm^{-2} over the southern ocean, and -0.65 W m^{-2} globally (Ayash *et al.*, (2008). Xing *et al.* (2015) carried out a 21-year simulation subsequent to incorporating the direct effect into the CMAQ model, and found that the direct effect could account for increases in the concentrations of SO_2 , NO_2 , O_3 , SO_4^{2-} , NO_3^- and $\text{PM}_{2.5}$ of up to 10.6, 6.7, 3.0, 18.6 and 10.1%, respectively, on polluted days. This study also noted that the direct effect resulted in reduced boundary layer height, and that reductions in emissions increased boundary layer heights, further reducing pollutant concentrations beyond what would be expected in the absence of direct effect feedbacks. Wang *et al.* (2016) used the WRF-Chem model to show that the direct effect decreased incoming surface shortwave radiation by 20 Wm^{-2} over an East Asian domain, consistent with observations, and that this meteorological impact resulted in subregion surface $\text{PM}_{2.5}$ concentration increases of 2.3 to 10%. Reducing SO_2 emissions decreased both surface $\text{PM}_{2.5}$ and ozone, though reducing black carbon emissions specifically resulted in some increases in ozone. The relative balance between ozone formation and destruction as a result of the direct effect was examined further by Xing *et al.* (2017) , who found that direct effect-induced changes in atmospheric dynamics and photolysis reduced the 1 hour daily maximum O_3 in January in China by $39 \mu\text{gm}^{-3}$, while enhancing July O_3 by $4 \mu\text{gm}^{-3}$. The direct effect of biomass burning has been shown to reduce the amount of solar energy reaching the surface, cooling the surface and increasing the relative fraction of diffuse radiation over the Amazon rainforest, in turn resulting in Amazonia becoming a net carbon sink (Moreira *et al.*, 2017). CW-AQF simulations of dust storms show that these sources of atmospheric particles also reduce incoming solar radiation, resulting in more stable thermal stratification of the atmosphere, weaker wind speeds, and hence constraining dust emissions (Remy *et al.*, 2015). However, night-time long-wave fluxes were enhanced by the presence of particles, leading to less stable stratification at night due to higher minimum surface temperatures, resulting in stronger surface winds. All of these studies show the importance of the aerosol direct effect in forecasts of both weather and air-quality.

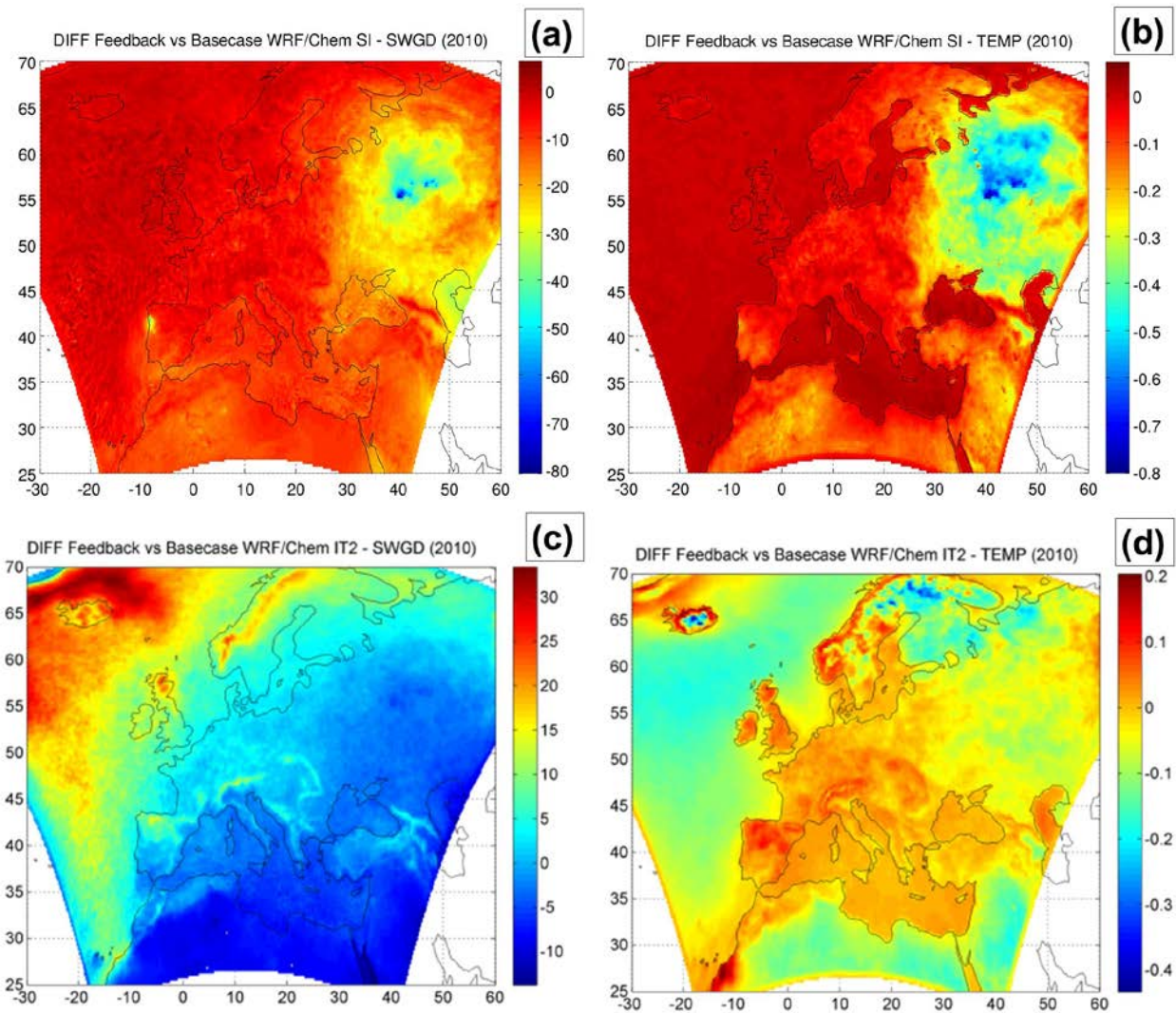


Figure 3.4. WRF-Chem simulations comparing (a, b) direct effect only simulations with (c, d) direct + indirect effect simulations, during the Russian forest fires of 2010.

(a, c): Change in short wave radiation reaching the ground compared to a no-aerosol simulation. (b, d): Change in surface temperature differences reaching the ground compared to a no-aerosol simulation. After Makar et al. (2015 a).

While the direct effect has been shown to have a high level of importance for Chemical Weather – Air Quality Forecasting, the manner in which this effect has been parameterized in current CW-AQF models varies greatly, and may have a significant impact on simulation results.

The following sections summarize the theoretical basis for the aerosol direct effect, and some of the main considerations in building parameterizations for these processes in atmospheric models. The discussion begins with a summary of the underlying theory of radiative transfer, is followed by considerations for implementation of the direct effect in models, and ends with a description and Table of the main methodologies used to simulate the aerosol direct effect in current CW-AQF models.

3.8.2 Definitions: the Physics of the Aerosol Direct Effect

The background theory summary provided here is largely based on the textbooks of Jacobson (2005), and Bohren and Huffman (1983) and Curci *et al.* (2015)'s investigation of the impact of assumptions for aerosol mixing state and composition on the resulting aerosol optical properties; the reader is directed to these sources for more in-depth information. This section also summarizes the direct effect parameterizations in some of the main online air-quality models in the current literature.

The aerosol direct effect is the process by which particles suspended in the atmosphere (aerosol) forward- or backscatter and/or absorb light. This process is dependent on the wavelength of the incident light, and the size, composition and internal structure of the particles. For all wavelengths, particles will scatter light. Absorption of light is more strongly dependent on wavelength, with light absorption being the strongest for wavelengths greater than 760 nm, the dividing line between the shorter wavelength ultra-violet and visible parts of the solar spectrum and the longer wavelength near-infrared to infrared. As noted by Jacobson (2005), if the scattering properties of light are ignored, then to a reasonable approximation, the transmission of light through a single particle may be given by:

$$\frac{I}{I_0} = e^{-4\pi d m_i(\lambda)/\lambda} \quad (1)$$

Where I_0 is the incident radiant energy, I is the radiant energy exiting the particle, d is the particle's diameter, $m_i(\lambda)$ is the imaginary component of the complex index of refraction of the particle (itself a function of the particle composition and internal structure, or "morphology"), and λ is the wavelength of light. The refraction of light through a particle is a function of the real component of the complex refractive index of the particle, where the net complex refractive index is given by (where subscripts "r" and "i" designate the real and imaginary components of the complex refractive index):

$$m(\lambda) = m_r(\lambda) \pm i m_i(\lambda) \quad (2)$$

Most atmospheric models will tend to ignore the wavelength dependence of equation (2). However, some observation-based studies have suggested that the imaginary component, $m_i(\lambda)$, which dominates absorption, significantly increases in magnitude with increasing wavelength (e.g., Ghan *et al.*, 2001). Jacobson (2005) provides a table of complex refractive indexes at wavelengths of 0.51 and 10.0 μm to illustrate this point; in [Figure 3.5](#) these values and equation (1) have been used to show the key features of absorption as a function of wavelength, particle size, and particle composition.

It should also be noted that the sign of the imaginary component varies depending on the reference consulted, as a result of two different conventions being used in the disciplines of electrical engineering and physics (Bradley, 2007). The underlying issue is that the plane wave amplitude equation can be defined using either sign, and the two possibilities may also be combined as a single equation,

$$\begin{aligned} E_y &= \frac{E_0}{2} \exp[i(\omega t - \beta z)] \exp[-i(\omega t - \beta z)] \exp(-\alpha z); \text{ ie.} \\ E_y &= \frac{E_0}{2} \exp[i(\omega t - (\beta - i\alpha)z)] \exp[-i(\omega t - (\beta + i\alpha)z)] \end{aligned} \quad (3)$$

That is, if $+i$ has been used in the initial definition of the plane wave, the complex refractive index may be defined as:

$$m = \frac{c}{\omega}(\beta - i\alpha) = m_{r,\lambda} - i m_{i,\lambda} \quad (4)$$

Similarly, if $-i$ has been used in the initial definition of the plane wave, the complex refractive index may be defined as:

$$m = \frac{c}{\omega}(\beta + i\alpha) = m_{r,\lambda} + i m_{i,\lambda} \quad (5)$$

Definition (4) is usually used in electrical engineering, while (5) is used in physics. Either definition results in the $m_{i,\lambda}$ term describing an exponential decay of the energy with increasing positive distance z into the refracting medium. We mention both formats here since different chemical weather/air-quality codes and the references for complex refractive index values they cite make use of *either* of these definitions, sometimes tabulating the $m_{i,\lambda}$ term as having a positive sign, sometimes as a negative sign. Mie scattering codes such as that of Bohren and Huffman (1983) take the *magnitude* of the imaginary term $m_{i,\lambda}$ as input and provide a consistent definition within the subsequent calculations. The issue has been identified here as a caution to the reader that a common sign convention should be employed when comparing or combining different sources of complex refractive index values.

Several important features of light absorption and transmission by atmospheric particles may be seen in Figure 3.5:

- The large imaginary component of the complex refractive of soot (one form of black carbon) results in this particle component having the lowest light transmission (highest light absorbance), and this increase in absorption becomes more pronounced, and occurs at smaller particle sizes, as the wavelength is decreased. Figure 3.5(a) shows 510 nm transmission, in the visible part of the spectrum, while Figure 3.5(b) shows 10 μm transmission, in the infrared; note that the soot transmission line drops to zero at smaller particle sizes at the visible light wavelength of Figure 3.5(a) than at the infrared light wavelength of Figure 3.5(b).
- While the transmission through soot at a given particle size increases with increasing wavelength, the transmission through all other particle components decreases with increasing wavelength.
- Transmission decreases (absorption increases) as particle size increases, at a given wavelength

Soot particles are thus strongly absorptive at visible light wavelengths and particle sizes for particles with diameters between 0.1 to 2.0 μm . These optical properties of soot, along with the result from particle microphysics that accumulation mode particles have the longest residence time in the atmosphere, results in soot contributing strongly to global warming, and the identification of soot as a "short-lived climate pollutant" (SLCP), in that the visible light energy intercepted by accumulation mode soot particles may be released as infrared. Reductions in the emissions of soot have thus been identified as a possible means of ameliorating the effects of global warming, in the short-term (decades) time frame.

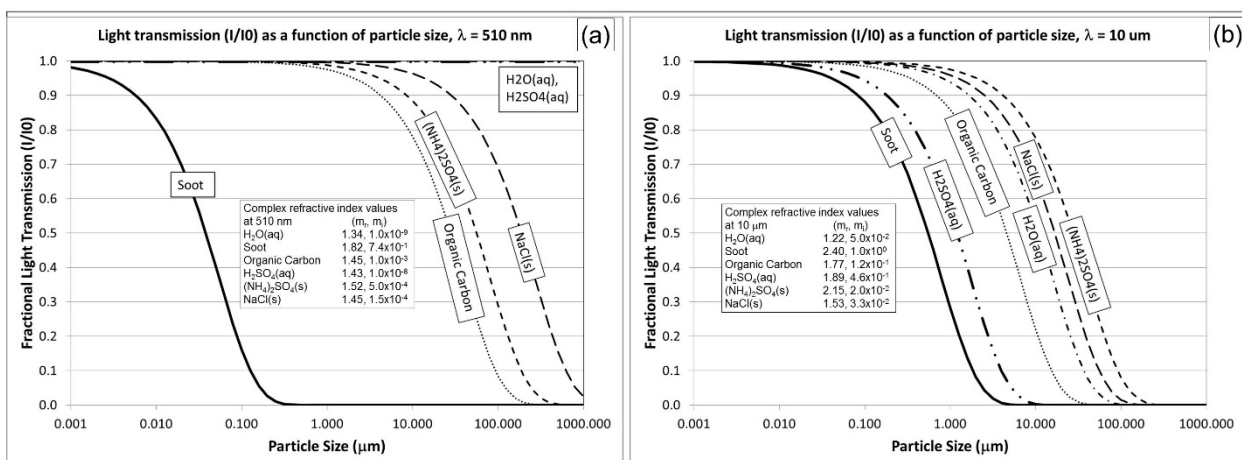


Figure 3.5. Approximate fractional light transmission from equation (1) using the data of Hale and Query (1973) and Krekov (1993) presented in Jacobson (1999).

3.8.3 Implementation of Aerosol Optical Properties in CW-AQF Models

Absorption, extinction, and scattering of light are included in atmospheric models. Usually, the particles are assumed to be spherical in shape – this assumption has been observed to be more correct as particles age. Freshly emitted primary particles may have a high fractal dimension (particularly for soot), as condensable gases coat these particles (condensation) and/or other particles impact against them (coagulation): the initial fractal structure becomes more compressed, and the accuracy of the spherical assumption improves with increasing particle age. The absorption, extinction, and scattering efficiencies are described using extinction coefficients in turn dependent on effective absorption, extinction, and scattering cross-sections:

$$\sigma_a(\lambda) = \sum_{i=1}^{N_b} \pi r_i^2 n_i Q_{a,i}(\lambda) ; \sigma_e(\lambda) = \sum_{i=1}^{N_b} \pi r_i^2 n_i Q_{e,i}(\lambda) ; \sigma_s(\lambda) = \sum_{i=1}^{N_b} \pi r_i^2 n_i Q_{s,i}(\lambda) \quad (6)$$

where $\sigma_a(\lambda)$ is the aerosol absorption coefficient, $\sigma_e(\lambda)$ is the aerosol extinction coefficient, $\sigma_s(\lambda)$ is the aerosol scattering coefficient, N_b is the number of particle bins, n_i is the number of particles in the i -bin, $Q_{a,i}(\lambda)$ is the dimensionless single particle absorption efficiency and $Q_{s,i}(\lambda)$ is the dimensionless single particle scattering efficiency. Equations (6) may also be expressed as integral over the particle radius size range at a given height (z) in the atmosphere (Curci *et al.*, 2015; Lesins *et al.*, 2002):

$$\sigma_{a,z}(\lambda) = \int_{r_{min}}^{r_{max}} \pi r^2 n(r) Q_a(r, \lambda) dr \quad (7)$$

With similar equations for $\sigma_{e,z}(\lambda)$ and $\sigma_{s,z}(\lambda)$. If the particle size distribution at height z corresponds to a (model) layer of thickness Δz , then the value of the *aerosol optical depth* (AOD) at the given wavelength may be given by:

$$AOD_z(\lambda) = \sigma_{e,z}(\lambda) \Delta z \quad (8)$$

Two other parameters in addition to the extinction define the aerosol properties required for radiative transfer calculations. The first of these is the single scattering albedo (SSA), defined as the ratio of scattering to extinction cross-sections:

$$SSA_z(\lambda) = \frac{\sigma_{s,z}}{\sigma_{s,z} + \sigma_{a,z}} = \frac{\sigma_{s,z}}{\sigma_{e,z}} \quad (9)$$

The third parameter is the average of the cosine of the scattering angle θ (the angle between the vector of the light incident to the particle and the vector of the scattered light leaving the particle):

$$g_z(\lambda) = \frac{1}{4\pi} \int_{4\pi} P\left(\theta, \frac{2\pi r}{\lambda}, m\right) d\Omega \quad (10)$$

where P is the phase function of the particle, which varies with the scattering angle, the radius of the particle (r), the wavelength of light and the complex refractive index of the particle (m), and the integration is over the solid angle Ω . Equations (7 and/or 8), (9) and (10) are the usual aerosol optical properties used in model radiative transfer codes to estimate the impact of scattering, extinction and absorption of light on the atmosphere's radiative balance.

The single particle absorption, extinction and scattering efficiencies Q are size and wavelength dependent. For very small particles ($2\pi r/\lambda < 0.1$), and as the imaginary component of the complex refractive index approaches zero (conditions usually met for atmospheric gas molecules), the particle is said to be in the Rayleigh size regime, and the values of $Q_{a,i}(\lambda)$ and $Q_{s,i}(\lambda)$ are known as the Tyndall absorbing and scattering efficiencies. These are given by (Jacobson, 1999):

$$Q_{a,i}(\lambda) = \frac{2\pi r_i}{\lambda} \left[\frac{24m_r(\lambda)m_i(\lambda)}{((m_r(\lambda))^2 + 2)^2} \right], Q_{s,i}(\lambda) = \frac{8}{3} \left(\frac{2\pi r_i}{\lambda} \right)^4 \left| \frac{(m_r(\lambda))^2 - 1}{(m_r(\lambda))^2 + 2} \right|^2 \quad (11)$$

Equations (11) imply that at sufficiently small particle sizes relative to the wavelength, the absorption efficiency will be much greater than the scattering efficiency. When the particle to wavelength ratio is such that $(0.1 \leq \frac{2\pi r_i}{\lambda} \leq 100)$, the particle is in the “Mie regime”, and the scattering and extinction efficiencies are defined via a series solution to Maxwell’s equations with complex coefficients a_k and b_k :

$$Q_{s,i}(\lambda) = \frac{\lambda}{\pi r_i} \sum_{k=1}^{\infty} (2m_i(\lambda) + 1) (|a_k|^2 + |b_k|^2); \quad Q_{e,i}(\lambda) = \frac{\lambda}{\pi r_i} \sum_{k=1}^{\infty} (2m_i(\lambda) + 1) \text{Re}(a_k + b_k) \quad (12)$$

Note that $Q_{a,i}(\lambda) = Q_{e,i}(\lambda) - Q_{s,i}(\lambda)$. The solution methods for determining the coefficients a_k and b_k in equation (12) can be computationally expensive, due to the rapid variation in the coefficients as a function of wavelength, particle size, and composition. An example is given in Figure 3.6, comparing a dry aerosol with a typical industrial atmosphere complex refractive index and the same aerosol with significant water uptake. Both axes on Figure 3.6 are logarithmic, showing relatively small changes in r_i and λ may lead to large changes in the extinction coefficient. One approach frequently used in atmospheric models is to calculate coefficients for a large number of possible values of $(\frac{2\pi r_i}{\lambda})$ and/or complex refractive index values *a priori*, placing these in a “lookup table” for subsequent use by the chemical transport model.

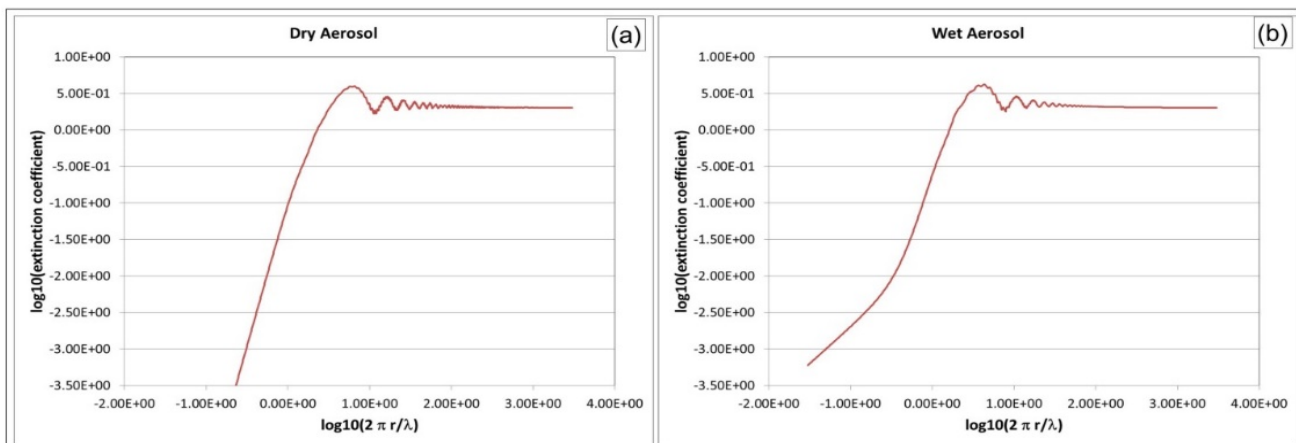


Figure 3.6. Comparison of extinction coefficient values for a dry (a) and wet (b) aerosol, as a function of $(\frac{2\pi r_i}{\lambda})$. Note that both scales are logarithmic.

As noted above with reference to Table 3.17 and Figure 3.5, the optical properties of the particles are dependent on the particle composition. A mixture of particles occupying the same volume of air with each particle being composed of a single substance, though the substance may vary between individual particles, is referred to as a heterogeneous or external mixture. Multiple chemical species contained within the same particle are said to be internally mixed, with two variations. Homogeneous internal mixtures describe the state of particles for which all of the components are well mixed throughout the particle. Core-shell internal mixtures refer to multi-component particles for which the different components form spherical shells about a core.

External mixtures are usually found for cases of relatively fresh emissions of primary particulate matter, examples being emissions of fresh soot and sea salt aerosols, and the formation of sulfuric acid particles through nucleation. With increasing time, the processes of condensation (in which condensable gases such as sulfuric acid and condensable organic gases coat pre-existing aerosols) and coagulation (in which particles collide and stick to each other, forming larger particles) ensure that the residence time of external mixtures in the atmosphere is relatively low. The mixing state of the particles may have an impact on their resulting radiative properties. For example, Lesins et al (2002) and Jacobson (2001) showed that the

absorption efficiency of soot increases as it becomes coated with a spherical shell of other material through condensation, due to refraction of light onto the inner carbon core.

The process by which a complex refractive index is assigned to a homogeneous mixture may vary between models. A common assumption in models is to use two volume-weighted summations, of the real and imaginary components of the contributing chemical species in the mixture (volume refractive index mixing), though other methods include volume weighting of the complex dielectric constants (which are then used to create a net complex refractive index), and the Maxwell Garnett and Bruggeman mixing rules (which provide refractive index values for particles containing absorbing inclusions imbedded in a homogeneous mixture of the other components, using different assumptions).

These assumptions regarding particle mixing state and refractive index behavior can influence the resulting predicted values of the aerosol optical properties in Chemical Weather Air-Quality Forecast models. Curci *et al.* (2015) examined the influence of several common mixing state assumptions using PM_{2.5} particle composition data from a suite of online feedback air-quality models. These mass composition amounts were used in sensitivity tests of mixing state, density, refractive index and hygroscopicity (water uptake). The radiative transfer parameters were found to be the most sensitive to the assumed mixing state. SSA variations of up to 30-35% were found going from homogeneous internal mixtures to core-shell mixtures, though 15% if all insoluble species are assumed to form a homogeneous core, and 10% if all species other than black carbon form the shell coating). The other factors such as the use of different sources of data for the complex refractive indexes of the components, different assumptions on particle density, and different hygroscopic growth factors for water uptake, resulted in variations of AOD, SSA and g of less than 10%.

The changes in optical properties associated with mixing state assumptions studied in Curci *et al.* (2015) resulted largely from a comparison between an external mixture and internal mixtures. External mixtures for the shorter visible wavelengths for example had a 37% higher AOD than a homogeneous internal mixture, and a 32% higher AOD than a (mixed) core-shell internal mixture. The use of a core-shell assumption with a black carbon core also reduced SSA by about 30% relative to an external mixture.

While these differences in particle optical properties associated with mixing state assumptions are significant, it should be noted that the optical properties will also depend on the composition of the particles, since the latter determines the complex refractive index or indexes used in calculating scattering and absorption. The current state of accuracy of predictions of the composition of aerosols thus has an influence on the accuracy of direct effect predictions by CW-AQF models. These errors in composition may be of a similar or greater magnitude to the differences resulting from the choice of an assumed aerosol mixing state. For example, in a multi-model comparison of feedback models for annual simulations in North America and Europe (Makar *et al.*, 2015a,b), the range in normalized mean bias relative to observations for the predicted European PM_{2.5}, and the PM_{2.5} components sulfate, ammonium, and nitrate was -45 to 9%, -58 to 1.7%, -61 to 37%, and -79 to 14%, respectively. For North American PM_{2.5}, and components sulfate, ammonium, nitrate, and total organic carbon, the normalized mean bias ranges were -15 to 37%, -6.9 to 134%, -50 to 29%, -78 to 56%, and -39 to 53%, respectively. Thus, for some models and some species, the range of errors in prediction of particle speciation and mass are often larger than the errors associated with different assumptions on mixing state towards the resulting optical properties. The two optical model parameterization choices having a similar impact on results were: (1) the use of an internal versus external mixing state with regards to AOD, and (2) the use of a black carbon core for SSA.

3.8.4 Aerosol Direct Effect Parameterizations Currently Used in CW-AQF Models

Although most online coupled meteorology-chemistry models consider the aerosol direct effect, the level of details for considering this effect differs largely between models. There are also major differences between the models with respect to the inclusion of the radiative effect of trace gases, aerosol particles and cloud droplets. An overview of some of the different models and approaches may be found in Zhang (2008) and Baklanov *et al.*, (2014). Tables 3.18 and

3.19 provide a detailed summary of the main features of direct effect parameterizations appearing in a number of global and regional/urban chemical weather/air-quality models. Complex refractive index values have been stated as provided in the original references (and hence may be using either the "electrical engineering" or "physics" definitions; a negative or positive sign for the complex refractive index $m_{i,\lambda}$, respectively). There are a large number of different approaches currently used in different models. All models at some level have made use of Mie scattering algorithms to define aerosol optical properties, but usually this is done via offline or *a priori* calculations, due to the computation expense associated with explicitly solving the Mie solutions to Maxwell's equations.

Table 3.18 Methodologies used in simulating aerosol direct and indirect effects and feedbacks in global CW-AQF models

Model and References for Direct Effect Approach Taken	Direct Effect Methodology	Aerosol Size Representation and Processes	Aerosol Speciation	Aerosol Mixing Representation in Radiative Transfer	Treatment of Complex Refractive Indexes, and Model Details	Radiative Transfer Scheme	Complex Refractive Index Values Used
ECHAM5-HAM (Stier et al., 2005)	Mie Scattering	Modal	Sulfate, black carbon, primary organic carbon, sea salt, dust, water		Aerosol optical properties are pre-computed in 24 bands, 3-dimensional lookup tables are constructed a priori as a function of $(\frac{2\pi r}{\lambda}, m_r, m_i)$, where r is the number median radius of the log-normal mode. A volume-weighted average of the component refractive indices is used to provide the m_r, m_i values used to access the lookup table.	Rapid Radiative Transfer Model (RRTM, Wild and Roeckner, 2005; Mlawer et al. (1997))	Sulfate: $1.43 + 1 \times 10^{-8} i$ BC: $1.75 + 0.44 i$ POM: $1.53 + 5.5 \times 10^{-3} i$ Sea salt: $1.49 + 1.0 \times 10^{-6} i$ Dust: $1.52 + 1.1 \times 10^{-3} i$ Water: $1.33 + 2.0 \times 10^{-7} i$
GEOS-CHEM (Ma et al., 2012; Yu et al., 2012)	Mie scattering (Ackermann and Toon, 1981)	Modal	Sulfate, nitrate, ammonium, water, secondary organic aerosol, primary organic carbon, black carbon, sea salt, dust	Core-shell approach	Lookup tables based on a priori Mie calculations (Yu et al, 2012), with the axes of the 3 optical parameter lookup tables being λ , core diameter, shell diameter, m_r and m_i . Different axes have different numbers of intervals, ranging from 1 to 91. Bilinear multivariant interpolation is used to determine the final values of the properties. Core is assumed to be black carbon; shell m_r and m_i are volume weighted averages of the shell components.	Li and Barker (2005)	550nm values: Sulfate: $1.52 - 5.0 \times 10^{-4} i$ Nitrate: $1.53 - 5.0 \times 10^{-3} i$ Ammonia: $1.52 - 5.0 \times 10^{-4} i$ Water: $1.33 - 1.8 \times 10^{-8} i$ SOA: $1.45 - 0.001 i$ POC: $1.45 - 0.001 i$ BC: $1.85 - 0.71 i$ Sea salt: $1.45 - 1.5 \times 10^{-4} i$ Dust: $1.519 - 1.6 \times 10^{-3} i$

Model and References for Direct Effect Approach Taken	Direct Effect Methodology	Aerosol Size Representation and Processes	Aerosol Speciation	Aerosol Mixing Representation in Radiative Transfer	Treatment of Complex Refractive Indexes, and Model Details	Radiative Transfer Scheme	Complex Refractive Index Values Used
CCATT-BRAMS (Longo et al., 2013)	Mie scattering (Rosario et al., 2013; Toon et al., 1989)	Not described. Apparently passive tracer advection of emitted biomass aerosols with an assumed size distribution; no description of the means of resolving aerosol size mentioned in the literature consulted.	Biomass burning emitted aerosols only	Mie scattering mentioned, but details missing; likely homogeneous mixture	Prescribed aerosol optical properties based on AERONET observations for specific field study purposes. From the information in Longo et al (2013), it is unclear whether CCATT-BRAMS includes an option for online aerosol calculations.	CARMA (Toon et al., 1988, 1989)	Not provided in literature
GEM-MACH v2 (Moran et al., 2010; Makar et al., 2015a,b)	Mie scattering; Bohren and Huffman (1983)	Sectional, 2 and 12 bins; Gong et al. (2003a,b); feedback mode uses the 12 bin configuration.	Sulfate, nitrate, ammonium, primary organic carbon, secondary organic carbon, elemental carbon, sea salt, crustal material, water	Homogeneous internal mixture	A lookup table is generated using the BHMIE program of Bohren and Huffman (1983). The range of possible values of $\log_{10}\left(\frac{2\pi r}{\lambda}\right)$ is divided into 1001 intervals, from -1.5228 to 3.4772, while the range of $\log_{10}(w_f)$ is divided into 100 intervals from -5 to 0. The resulting lookup tables of Q_{ext} , SSA and g thus have axes of $\log_{10}\left(\frac{2\pi r}{\lambda}\right)$ and $\log_{10}(w_f)$, the dry aerosol ($w_f = 1 \times 10^{-5}$) has a complex refractive index of $1.49 + 0.01 i$, and water has a complex refractive index of $1.33 + 0 i$.	Li and Barker (2005)	The complex refractive index values are taken from a bilinear interpolation between water and a standard dry aerosol refractive index: $m_r = 1.5 - 0.17 w_f$ and $m_i = 0.01 (1.0 - w_f)$ where w_f is the water mass fraction of the aerosol.

Table 3.19 Methodologies used in simulating aerosol direct and indirect effects and feedbacks in regional/urban CW-AQF models

Model and References for Direct Effect Approach Taken	Direct Effect Methodology	Aerosol Size Repres. and Processes	Aerosol Speciation	Aerosol Mixing Repres. in Radiative Transfer	Treatment of Complex Refractive Indexes, and Model Details	Radiative Transfer Scheme	Complex Refractive Index Values Used
WRF-Chem 3.4.1 (Grell et al., 2005; Skamarock et al., 2008)	Fast-Chapman: Fast et al. (2006), Chapman et al. (2009)	<p>Multiple options:</p> <p>Modal (3 modes) (1) MADE3 (Ackerman et al., 1998; Grell et al., 2005) (2) MADE-SORGAM (Ackermann et al., 1998; Schell et al., 2001) (3) MADE-VBS aerosol scheme (Ahmadov et al., 2012)</p> <p>Sectional: MOSAIC (Fast et al., 2006)</p>	<p>Depends on the option chosen: MADE originally included sulfate, nitrate, ammonium and water. MADE-SORGAM added secondary organic aerosol and primary organic aerosol. MADE-VBS includes a more detailed secondary organic aerosol formation module. MOSAIC includes sulfate, nitrate, ammonium, chloride, sodium, "other inorganics", organic carbon, elemental carbon, and includes options for the inclusion of calcium, carbonate, and methyl sulfonic acid.</p>	Different options possible; homogeneous internal mixture, core-shell or Maxwell-Garnet (inclusions)	<p>Mie calculations and/or the Ghan et al (2001)¹ parameterization are available options. e.g., WRF-CHEM-MOSAIC/Ghan et al. (2001): volume weighted averaging of complex refractive indexes of the components is carried out to determine the net refractive index. Mie theory is used to determine the values of Q_e, Q_s and g: The approach of Ghan et al. (2001) is used: Mie calculations as a function of $\frac{2\pi r}{\lambda}$ and m are carried out <i>a priori</i> for a range of complex refractive index values; these are used to determine lookup table coefficients for Chebyshev polynomials describing the three optical parameters. Bilinear interpolation between the seven sets of stored coefficients is used to determine the values of the polynomial coefficients to be used for the optical properties at individual model grid points. The details of the matching between the Ghan et al. (2001) aerosol composition and the (differing) composition used in the driving air-quality model is not described.</p>	RRTMG: Clough et al. (2005). Some versions also reference Iacono et al. (2008)	<p>Ghan et al. (2001) refractive indices for 7 species, Solar Radiation:</p> <p>Water 1.33+0.0 i</p> <p>Ammonium Sulfate 1.53+0.0 i</p> <p>Methyl sulfonic acid 1.53+0.0 i</p> <p>Sea Salt 1.50+0.0 i</p> <p>Soil Dust 1.50+0.002 i</p> <p>Organic Carbon 1.55+0.0 i</p> <p>Black Carbon 1.90 + 0.60 i</p> <p>Ghan et al. (2001) refractive indices for 7 species, Infrared Radiation:</p> <p>Water 1.18+0.68 i</p> <p>Ammonium Sulfate 1.98+0.06 i</p> <p>Methyl sulfonic acid 1.98+0.06 i</p> <p>Sea Salt 1.50+0.01 i</p> <p>Soil Dust 1.62+0.12 i</p> <p>Organic Carbon 1.70+0.07 i</p> <p>Black Carbon 2.22 + 0.73 i</p>

Model and References for Direct Effect Approach Taken	Direct Effect Methodology	Aerosol Size Repres. and Processes	Aerosol Speciation	Aerosol Mixing Repres. in Radiative Transfer	Treatment of Complex Refractive Indexes, and Model Details	Radiative Transfer Scheme	Complex Refractive Index Values Used
Enviro-HIRLAM (Baklanov et al., 2017)	Mie Scattering	Two options: Modal CAC (Baklanov, 2003; Gross and Baklanov, 2004) and Pseudo-modal M7 (Vignati et al., 2004)	BC (soot), minerals (nucleus, accumulation, coarse and transported modes), sulfuric acid, sea salt (accumulation and coarse modes), "water soluble" and "water insoluble" aerosols.	Homogeneous internal mixture or external mixture	Direct and semi-direct effects are simulated using a modification of the Savijärvi radiation scheme (Savijärvi, 1990; Wyser et al., 1999) with implementation of new fast analytical SW and LW aerosol transmittances, reflectances and absorbances (Nielsen et al., 2014; Rontu et al., 2017). The two-stream approximation equations for anisotropic non-conservative scattering described by Thomas and Stamnes (2002) are used.	Nielsen et al. (2014); Rontu et al. (2017)	The Global Aerosol Data Set/Optical Properties of Aerosols and Clouds (GADS/OPAC) aerosols of Köpke et al. (1997) are used as input to the routine.
<p>¹ In Ghan et al (2001), seven complex refractive index values (for water, ammonium sulfate, methyl sulfonic acid, sea salt, soil dust, organic carbon, and black carbon) are used to describe the <i>range</i> of possible values of the m_r and m_i. A log-normal size distribution is assumed from 0.01 to 10 μm (the number of intervals was not stated) and full Mie calculations are for the range of particle sizes and complex refractive index values. The resulting values of extinction coefficient, single scattering albedo and the asymmetry factor are then fit using Chebyshev polynomials for the size distribution as a function of complex refractive index. For subsequent calculations at model grid points, the water content of the components is calculated, the volume weighted values of the complex refractive indexes of these (wet) aerosol components are calculated, and bilinear interpolation is used to determine the appropriate values of the Chebyshev polynomial coefficients based on the tabulated values, which are functions of the real and imaginary components of the complex refractive index values in creating the table. Solar radiation values are taken from the range of complex refractive index values for the 7 components at 550nm (m_r from 1.33 to 1.90, m_i from 0 to 0.62) and infrared values from the range at 10 μm wave length (m_r 1.18 to 2.22, m_i from 0.01 to 0.73). Note that in Ghan et al (2001), all imaginary components are assumed to have a positive sign; $m = m_r + i m_i$. It is unclear in subsequent applications of Ghan et al (2001) whether the air-quality model aerosol composition, which differs from the 7 components used in Ghan et al (2001) provides complex refractive index values which are then used with the Ghan et al (2001) coefficients, or the air-quality model must <i>a priori</i> assign mass to each of the 7 components assumed by Ghan et al (2001) in their original application of this approach.</p>							
WRF-CMAQ 5.0.1 (Byun and Schere, 2006; Foley et al., 2010; Wong et al., 2012; Appel et al., 2013)	CMAQ Feedback: Bohren and Huffman (1998); Wong et al. (2012)	AERO6 3-modal (Appel et al., 2013)	Speciation is dependent on the particle mode: Coarse mode: sulfate, nitrate, soil dust, chloride	Homogeneous internal mixture or external mixtures possible for water-soluble,	Extinction optical depth, single scattering albedo, asymmetry parameter and forward scattering fraction are calculated for 19 bands if the Community Atmosphere Model is in use, 14 bands for the Rapid Radiative Transfer Model for GCMs	RRTMG: Clough et al. (2005)	Based on Hess et al. (1998); refractive indices from three sources (d'Almeida et al., 1991; Shettle and Fenn, 1979; Koepke et al., 1997).

Model and References for Direct Effect Approach Taken	Direct Effect Methodology	Aerosol Size Repres. and Processes	Aerosol Speciation	Aerosol Mixing Repres. in Radiative Transfer	Treatment of Complex Refractive Indexes, and Model Details	Radiative Transfer Scheme	Complex Refractive Index Values Used
			Accumulation mode : sulfate, nitrate, chloride, ammonium, sodium, calcium, potassium, primary organic carbon, secondary organic carbon, iron, aluminum, silicon, titanium, manganese, magnesium, other Aitken mode: sulfate, nitrate, ammonium, primary organic carbon, non-carbon organic matter	insoluble, components	(RRTMG). CMAQ's chemical species are combined into 5 groups: water-soluble, insoluble, sea salt, black carbon, and water. The OPAC model of Hess et al (1998) is used to estimate the aerosol optical properties; pre-calculated values of the optical properties for the 5 aerosol types (along with assumptions regarding the size distribution for the modes for those components) are provided as a lookup table for each of the 5 groups, normalized to 1 particle cm ⁻³ ; multiplication by the number density of each group is used to derive net aerosol optical properties. The matching and assignment from the original CMAQ speciation to the OPAC species is not described in the reference material cited here.		
GRAPES-CUACE (Wang et al., 2004, 2006, 2015)	Mie Scattering	Sectional, 12 bins (Gong et al., 2003a, b).	Sulfate, nitrate, ammonium, organic carbon, elemental carbon, sea salt, crustal material, water.	The model assumes a homogeneous internal mixture, but aerosol optical properties are calculated as an external mixture.	An external mixture is first assumed for each of the particle bins within a given aerosol species, and Mie theory is used to calculate the optical properties for each bin of the given species, with 10 relative humidity levels being used along with the Kohler equation to estimate water uptake for the hygroscopic components. Aerosol optical properties are thus calculated <i>a priori</i> as functions of relative humidity	Goddard model (Chou et al., 1998, 2001)	Each chemical constituent of an aerosol is associated with a set of complex refractive index (CRI) data as a function of wavelength. The CRI data of 6 aerosol species are mainly derived from the Hitran2008 database (Rothman et al., 2009) and the optical properties of aerosols and clouds database (OPAC) (Hess et al., 1998). Dust CRI data

Model and References for Direct Effect Approach Taken	Direct Effect Methodology	Aerosol Size Repres. and Processes	Aerosol Speciation	Aerosol Mixing Repres. in Radiative Transfer	Treatment of Complex Refractive Indexes, and Model Details	Radiative Transfer Scheme	Complex Refractive Index Values Used
					and wavelength for each median particle size and species for each bin. Net optical properties may thus be generated as summations of externally mixed totals. A radiation model has been implemented in GRAPES-CUACE to work on the aerosol and radiation interactions (Wang et al. 2004, 2006, 2015).		is used for representing dust aerosol from Chinese deserts in an international research project ADEC (Wang et al., 2004; 2006). Based on the CRI dataset of 7 aerosols species of 12 size bins, Mie theory is used to calculate the key optical parameters of extinction coefficient, SSA and ASY depending on different relative humidity (only for Hygroscopic aerosol). The composite aerosol AOD, SSA and ASY are calculated based on an external mixture of 7 aerosol species and 12 size bins in each model grid.
COSMO-Art (Vogel et al., 2009)	Mie scattering (Bohren and Huffman, 1983)	Modal, 5 modes	Speciation is dependent on mode: Mode Species <i>if</i> sulfate, nitrate, ammonium, water, secondary organic aerosol <i>ic</i> sulfate, nitrate, ammonium, water, secondary organic aerosol, soot	Homogeneous internal mixture for 4 modes, plus two independent modes for fresh soot and primary PM ₁₀ emissions, respectively.	Bohren and Huffman (1983) Mie code was used to calculate optical properties from a dataset built from offline (no feedback) simulations using the COSMO-ART model. Within a given mode, and at each of 8 wavelengths, the relationship between the total aerosol mass of the mode and the three aerosol optical properties was assumed to be linear; the summation of these linear functions across all five modes for a given set of wet mode	General Radiative Algorithm Adapted to Linear-type Solutions (GRAALS) (Ritter and Geleyn, 1992)	Complex refractive index values assigned to the modes for the initial Mie calculation were not described in Vogel et al. (2009).

Model and References for Direct Effect Approach Taken	Direct Effect Methodology	Aerosol Size Repres. and Processes	Aerosol Speciation	Aerosol Mixing Repres. in Radiative Transfer	Treatment of Complex Refractive Indexes, and Model Details	Radiative Transfer Scheme	Complex Refractive Index Values Used
			<i>jf</i> sulfate, nitrate, ammonium, water, secondary organic aerosol <i>jc</i> sulfate, nitrate, ammonium, water, secondary organic aerosol, soot <i>s</i> soot <i>c</i> Primary PM10		masses was thus used in subsequent estimations of the aerosol optical properties in subsequent model simulations.		
CSU-RAMS (Saleeby and Heever, 2013)	Mie scattering (Bohren and Huffman, 1983)	Main model assumes a modal approach. Optical properties calculated using 17 sections to represent the modes.	Ammonium sulfate, sea salt, mineral dust	Modes are externally mixed; 3 modes for sulfate, two for mineral dust, 3 for sea salt, 2 for "regenerated aerosols" (the latter represent aerosols regenerated as a result of evaporation of hydrometeors)	Four-dimensional lookup tables were generated offline, with the axes of aerosol type (ammonium sulfate, sea salt, and mineral dust), radiation band (three solar, five infrared), aerosol radius (17 bin diameters used to span the modes), and relative humidity (1% increments from 80 to 100%; deliquescence is assumed to occur at 80% RH, and particles are dry below this value). Model estimates of the number of particles within each radius are then used to generate net optical parameters within each aerosol type. Optical depth is the sum over all species, while the single scattering albedo values are weighted by the component optical depths, and the asymmetry factors are weighted by the product of the	Stokowski (2005)	Not stated

Model and References for Direct Effect Approach Taken	Direct Effect Methodology	Aerosol Size Repres. and Processes	Aerosol Speciation	Aerosol Mixing Repres. in Radiative Transfer	Treatment of Complex Refractive Indexes, and Model Details	Radiative Transfer Scheme	Complex Refractive Index Values Used
					individual species optical depth and asymmetry factors (Liou et al, 1978; Slingo and Schrecker, 1982)		
RegCM (Tsikerdekis et al., 2013)	Mie scattering or prescribed optical properties	Sectional, 4 and 12 bins	Dust emissions only in the reference consulted. Other information (http://indico.ictp.it/event/a09151/session/46/contribution/33/material/0/0.pdf) implies that black carbon, total carbon and a total PM _{2.5} are included as passive tracers.	Single component (dust)	Pre-calculated or prescribed optical properties for each bin and spectral band of whichever of the two radiative transfer options (CCM3 or RRTM) is being used.	CCM3 (Kiehl et al., 1996) or RRTM (Wild and Roeckner, 2005)	Not provided in literature; net extinction, single scattering albedo, and asymmetry factors are prescribed as a function of particle size, based on either observations or Mie calculations. The complex refractive index values used for the latter option are not stated.

Model and References for Direct Effect Approach Taken	Direct Effect Methodology	Aerosol Size Repres. and Processes	Aerosol Speciation	Aerosol Mixing Repres. in Radiative Transfer	Treatment of Complex Refractive Indexes, and Model Details	Radiative Transfer Scheme	Complex Refractive Index Values Used
Meso-NH (Aouizerats et al., 2010)	Mie scattering (Mie, 1908 ; unclear whether a specific existing implementation was used for their tests or a new implementation of Mie's 1908 work was used)	Modal – the methodology assumes a standard deviation of particle size specified by a median radius.	Primary organic carbon, black carbon, dust, nitrate, sulfate, ammonium, water, secondary organic aerosol.	Core-shell; core is composed of primary organic carbon, black carbon and dust.	Maxwell-Garnett mixing rule used to build net refractive index. Lookup tables created using Mie calculations within input values of complex refractive index and geometric standard deviation. Mie calculations were fit in two sections of the size range using 5 th degree polynomials in particle radius for a given complex refractive index. The two sections were defined for either side of the median radius for the maximum value of the given optical parameter (effectively splitting the optical parameter function of radius into upper and lower halves, each with their own 5 th order polynomial. Eight real refractive index values, 6 imaginary refractive index values, eight standard deviations of aerosol size distribution, and 6 wavelengths were used; each combination resulted in a different set of coefficients for the two 5 th order polynomials used to describe the 3 aerosol optical properties. Bilinear interpolation between these 4 axes were then used to construct the final values of the coefficients of the two fifth order polynomials used in the subsequent tests.	Not stated in the given reference (which focuses on the aerosol optical property creation and comparison of the resulting aerosol optical properties with observations).	Values at 5 wavelengths (217.5, 345, 550, 925, 2285, 3190 nm) specified from Krekov (1993) and Tulet et al (2008) were tabulated for black carbon, organic carbon, dust, water, nitrate, ammonium, sulfate and secondary organic aerosol. The values of m_r , m_i and σ_r used in the lookup table construction were $m_r = \{1.45, 1.50, 1.55, 1.60, 1.65, 1.70, 1.75, 1.80\}$, $m_i = \{-0.001, -0.006, -0.008, -0.02, -0.1, -0.4\}$, and $\sigma_r = \{1.05, 1.25, 1.45, 1.64, 1.85, 2.05, 2.25, 2.45\}$

Model and References for Direct Effect Approach Taken	Direct Effect Methodology	Aerosol Size Repres. and Processes	Aerosol Speciation	Aerosol Mixing Repres. in Radiative Transfer	Treatment of Complex Refractive Indexes, and Model Details	Radiative Transfer Scheme	Complex Refractive Index Values Used
UKCA (Bellouin, 2010)	Depends on aerosol scheme chosen: "Classic" option: Mie parameters computed offline UKCA-MODE	Modal; mass is distributed into one or two optically active modes, dependent on species	Dependent on mode: Nucleation soluble: sulfate Aitken soluble: sulfate, black carbon, organic carbon Aitken insoluble: black carbon, organic carbon Accumulation soluble: sulfate, black carbon, organic carbon, sea salt, dust. Accumulation insoluble: dust Coarse soluble: sulfate, black carbon, organic carbon, sea salt, dust. Coarse insoluble: dust.	Internal mixtures assumed within each mode.	Pre-computed lookup tables of monochromatic optical properties, as a function of modal radii and refractive index values. Fifty-one values each of m_r , m_i , and $\log_{10}\left(\frac{2\pi r}{\lambda}\right)$ were found sufficient to represent the variable space; the ranges of $\log_{10}\left(\frac{2\pi r}{\lambda}\right)$, m_r and m_i varied for shortwave and long-wave calculations, and between the accumulation and coarse modes. (presumably Aitken modes were assumed to be Rayleigh scatterers; this was not discussed).	Not described in the reference.	The complex refractive index values used for the components within the modes, and the manner in which they were combined to create a net refractive index prior to the use of the lookup tables, were not presented in the reference.

The aerosol optical properties generated may have a large degree of variation, in part dependent on the level of information available in the models. In order to speed up costly calculations of radiative feedbacks, some radiation modules use externally stored data in the form of a pre-computed parameter cache (e.g. tabulated results of a priori Mie calculations or from the Optical Properties of Aerosols and Clouds (OPAC) software library module (d'Almeida et al., 1991)). OPAC defines a dataset of typical cloud components as well as aerosol components and component mixtures, in order to calculate the optical properties from the concentration fields of simulated PM compositions. Other options include calling a Mie code a limited number of times to generate an online lookup table of aerosol optical properties as a function of composition and particle size (this approach is used in the GEM-MACH and WRF-CMAQ models).

Modal approach models tend to make use of complex refractive index values which apply for typical modes in the atmosphere; and sectional models tend to make use of species-specific complex refractive index values, but there are variations within those options. The aerosol morphology assumptions employed vary from external mixtures to homogeneous internal mixtures (the most common assumption) through to core-shell internal mixtures. For the core-shell approaches, which are generally recognized as being the most rigorous, the assumptions regarding which species form the core vary; usually black carbon is treated as the core, though sometimes other species are included.

At this point in time there does not appear to be a universally applied approach to simulating the aerosol direct effect in CW-AQF models, particularly with regards to mixing state. However, model intercomparisons such as Makar et al. (2015a,b) suggest that, despite the variety of different approaches, the incorporation of the direct effect results in a similar direction of impact on CW-AQF model predictions (Makar et al. (2015a,b)), and the differences in the assumptions made for aerosol morphology result in at most a 30% difference in the resulting radiative transfer properties (Curci et al., 2015). From arguments presented in Jacobson (2005), some form of the core-shell approach, with the black carbon forming all or part of the core, is probably the most realistic relative to conditions in the actual atmosphere, and is recommended for future implementations of the direct effect.

An overview of CW-AQF models employed in Europe (Baklanov et al., 2014) provides the following analysis of a large variability among models and the complexity of the treatment of the effect of simulated aerosol concentrations on shortwave and longwave radiation fluxes. For example, MCCM (Grell et al., 2000; Forkel & Knoche, 2006) makes use of only the simulated total mass of dry aerosol in each layer along with a "typical" mass extinction coefficient, and the water attached to the aerosol in order to calculate the extinction of shortwave radiation. Different chemical species, which include BC, organic matter (OM), water and various ionic species, such as sulfate and nitrate, can be included in direct effect calculations in WRF-Chem, Enviro-HIRLAM and COSMO-Art. Within WRF-Chem an aerosol optical property module (Barnard et al., 2010) treats bulk, modal, and sectional aerosol size distributions using a similar methodology for refractive indices and multiple mixing rules, to prepare 3-D distributions of aerosol optical thickness, single scattering albedo and asymmetry parameters. These aerosol optical variables are then passed into some of the SW and LW radiation schemes available in WRF. WRF-Chem has different options for the aerosol direct effect, including runtime Mie calculations for the optical parameters (using bulk, modal, or sectional aerosol modules) as well as BOLCHEM (Russo et al., 2010) and COSMO-MUSCAT (Heinold et al., 2008) for dust aerosols. The Enviro-HIRLAM radiation module can account for the effects of dissolved sulfate, speciated PM, as well as trace gases within cloud droplets. In COSMO-ART, aerosol optical parameters are calculated based on tabulated values derived from aerosol distributions of a previous COSMO-ART simulation, and the current simulated aerosol masses of each mode (Vogel et al., 2009). A slightly different approach is employed in MEMO/MARS-aero, where radiative effects of aerosol particles are introduced using the OPAC software library.

Few consistent assumptions about the mixing state of pollutants exist among different models and radiation modules, most of which tend to employ widely differing approaches. For example, soot is considered as externally and internally mixed and its ageing process is explicitly simulated in the model COSMO-Art. In WRF/Chem all soot compounds are simulated as being internally mixed. The OPAC speciation, on the other hand, defines a set of internally

mixed aerosol components, which are subsequently externally mixed in order to represent PM concentration fields of a given composition. The WMO CCMM symposium (CCMM, 2016) summarized a few key application areas and associated challenges of aerosol-radiation interaction in coupled meteorology-composition models, including the following.

Online coupling imposes additional requirements on the set-up and implementation of radiation parameterizations. Most of these requirements reflect the need to maintain physical and numerical consistencies between the various modules and computational schemes of the model, against the increased frequency of interactions and the multitude of simulated effects. The complexity of the treatment of the effect of simulated aerosol concentrations on shortwave and longwave radiation fluxes differs strongly among the models. SW radiation in existing modern CW-AQFs is perhaps the best represented radiative feedback process, while LW radiation is less well represented. Cloud-aerosol interactions (indirect effects) are described elsewhere in this report, but have also been shown to have a large degree of variability in response across different models. The direct and indirect effects sometimes act in opposite direction in terms of their impact on both weather and air-quality predictions.

3.8.5 Summary

- The aerosol direct effect can have a significant impact on the outcome of weather forecast and chemical weather forecast model simulations. Accurate estimation of aerosol optical properties is largely controlled by aerosol composition, size distribution, mixing state and the knowledge of the refractive index of the individual species.
- The incorporation of the aerosol direct effect has been shown to:
 - Improve weather forecasts resulting from large biomass burning events;
 - Result in negative climate forcings of -3 W m^{-2} over oceans;
 - Change the predicted concentrations of a host of pollutants between 3 and 19%;
 - Reduce shortwave radiation reaching the surface of East Asia by 20 W m^{-2} ;
 - Reduce wintertime and increase summertime O_3 in China;
 - Cool the surface of Amazonia during biomass burning events, resulting in a net carbon sink for this region due to biological feedbacks with plant growth;
 - Reduce the intensity of daytime desert dust storms, and increase the intensity of night-time desert dust emissions.
- Model assumptions on particle morphology seem to account for a 30% variation in the resulting optical properties. This is smaller than the typical range of error associated with predictions of individual particle components from different models, at the current time. However, models incorporating the direct effect nevertheless show a similar direction of meteorological response, suggesting that the morphology and composition differences in direct effect approaches are sufficiently small that the results of the models have some confidence.
- Pollution events with high particle number densities have the largest direct effect impacts; (such as urban areas with high pollution, sand and dust storms, forest fires and other large plume emissions events).

References

- Ackerman, T. P. and Toon O. B., Absorption of visible radiation in atmosphere containing mixtures of absorbing and non-absorbing particles, *Appl. Opt.*, 20, 3661–3668, 1981.
- Ackerman, I. J., H. Hass, M. Memmesheimer, A. Ebel, F. S. Binkowski, U. Shankar, Modal aerosol dynamics model for Europe: development and first applications, *Atmospheric Environment*, 32, 17, 2981 – 2999, 1998.
- Ahmadov, R., McKeen, S.A., Robinson, A., Bahreini, R., Middlebrook, A., de Gouw, J., Meagher, J., Hsie, E., Edgerton, E., Shaw, S., Trainer, M., A volatility basis set model for summertime secondary organic aerosols over the eastern United States in 2006, *J. Geophys. Res.*, 117, D06301, doi:10.1029/2011JD016831, 2012.
- Ahmadov, R., James, E., Grell, G., Alexander, C., Albers, S., Csiszar, I., Tsidulko, M., Graw, R., McKeen, S., Kondragunta, S., Pereira, G., Pierce, B., Freitas, S., Forecasting smoke transport and its impact on weather in high-resolution (3km) HRRR-Smoke model over the US. 10th International Aerosol Conference (IAC), St. Louis, Missouri, <http://aaarabstracts.com/2018IAC/AbstractBook.pdf> (last accessed November 5, 2018).
- Appel, K. W., Pouliot, G. A., Simon, H., Sarwar, G., Pye, H. O. T., Napelenok, S. L., Akhtar, F., and Roselle, S. J., Evaluation of dust and trace metal estimates from the Community Multiscale Air Quality (CMAQ) model version 5.0, *Geosci. Model Dev.*, 6, 883-899, doi:10.5194/gmd-6-883-2013, 2013.
- Aouizerats, B., Thouron, O., Tulet, P., Mallet, M., Gomes, L., and Henzing, J.S., Development of an online radiative module for the computation of aerosol optical properties in 3-D atmospheric models: validation during the EUCAARI campaign, *Geosci. Model Dev.*, 3, 553-564, 2010.
- Ayash, T., Gong, S., Jia, C.Q., Direct and indirect shortwave radiative effects of sea salt aerosols, *J. of Climate*, 21, 3207-3220, 2008.
- Baklanov, A.: Modeling of formation and dynamics of radioactive aerosols in the atmosphere, in: *Research on a Theory of Elementary Particles and Solid State*, 4, 135–148, 2003.
- Baklanov, A., Schlünzen, K., Suppan, P., Baldasano, J., Brunner, D., Aksoyoglu, S., Carmichael, G., Douros, J., Flemming, J., Forkel, R., Galmarini, S., Gauss, M., Grell, G., Hirtl, M., Joffre, S., Jorba, O., Kaas, E., Kaasik, M., Kallos, G., Kong, X., Korsholm, U., Kurganskiy, A., Kushta, J., Lohmann, U., Mahura, A., Manders-Groot, A., Maurizi, A., Moussiopoulos, N., Rao, S.T., Savage, N., Seigneur, C., Sokhi, R.S., Solazzo, E., Solomos, S., Sørensen, B., Tsegas, G., Vignati, E., Vogel, B., Zhang, Y., Online coupled regional meteorological chemistry models in Europe: current status and prospects, *Atmos. Chem., Phys.*, 14, 317-398, 2014.
- Baklanov, A., Korsholm, U. S., Nuterman, R., Mahura, A., Nielsen, K. P., Sass, B. H., Rasmussen, A., Zakey, A., Kaas, E., Kurganskiy, A., Sørensen, B., and González-Aparicio, I.: The Enviro-HIRLAM online integrated meteorology–chemistry modeling system: strategy, methodology, developments, and applications (v. 7.2), *Geosci. Model Dev.*, 10, 2971-2999, <https://doi.org/10.5194/gmd-10-2971-2017>, 2017.
- Barnard, J. C., Fast, J. D., Paredes-Miranda, G., Arnott, W. P., and Laskin, A.: Technical Note: Evaluation of the WRF-Chem “Aerosol Chemical to Aerosol Optical Properties” Module using data from the MILAGRO campaign, *Atmos. Chem. Phys.*, 10, 7325–7340, doi:10.5194/acp-10-7325-2010, 2010.
- Bellouin, N., Interaction of UKCA aerosols with radiation: UKCA_RADAER, internal report, Met. Office Hadley Center, 13 pp, 2010 (http://www.ukca.ac.uk/images/d/dc/UKCA_RADAER.pdf, last accessed June 27, 2018).

- Bohren, C.F., and Huffman, D.R., *Absorption and scattering of light by small particles*, Wiley and Sons, New York, 530 pp., 1983
- Bohren, Craig F. and Donald R. Huffman, *Absorption and scattering of light by small particles*, 2nd Edition, New York: Wiley, 530 p., 1998.
- Bond, T.C., Doherty, S.J., Fahey, D.W., Forster, P.M., Bernsten, T., DeAngelo, B.J., Flanner, M.G., Ghan, S., Karcher, B., Koch, D., Kinne, S., Kondo, Y., Quinn, P.K., Sarofim, M.C., Schultz, M.G., Schulz, M., Venkataraman, C., Zhang, H., Bounding the role of black carbon in the climate system: A scientific assessment. *J. Geophys. Res., Atm.*, 118, 5380-5552, 2013.
- Bradley, S., Sign Conventions in Electromagnetic Waves, https://ocw.mit.edu/courses/electrical-engineering-and-computer-science/6-007-electromagnetic-energy-from-motors-to-lasers-spring-2011/readings/MIT6_007S11_sign.pdf, 5pp. last accessed July 2nd, 2018.
- Byun, D. W. and Schere, K. L., Review of the governing equations, computational algorithms, and other components of the Models- 3 Community Multiscale Air Quality (CMAQ) Modeling System, *Appl. Mech. Rev.*, 59, 51–77, 2006.
- CCMM, 2016: Coupled Chemistry-Meteorology/Climate Modeling (CCMM): status and relevance for numerical weather prediction, atmospheric pollution and climate research (Symposium materials). WMO GAW Report #226, WMO, Geneva, Switzerland, https://library.wmo.int/doc_num.php?explnum_id=7938
- Chapman E.G., Gustafson Jr, W.I., Barnard, J.C., Ghan, S.J., Pekour, M.S., and Fast, J.D., Coupling aerosol-cloud-radiative processes in the WRF-Chem model: Investigating the radiative impact of large point sources. *Atmos. Chem. Phys.*, 9:945-964, 2009.
- Chou, M. D., Suarez, M. J., Ho, C. H., Yan, M. M. H., and Lee, K. T., Parameterizations for Cloud Overlapping and Shortwave Single-Scattering Properties for Use in General Circulation and Cloud Ensemble Models, *J. Clim.*, 11, 202–214, 1998.
- Chou, M. D., Suarez, M. J., Liang, X. Z., and Michael M.-H. Y., A Thermal Infrared Radiation Parameterization for Atmospheric Studies, Technical Report Series on Global Modeling and Data Assimilation, NASA/TM-2001-104606, 19, America, Goddard Space Flight Center, Greenbelt, Maryland, 55, 2001.
- Clough, S. A., Shephard, M. W., Mlawer, E. J., Delamere, J. S., Iacono, M. J., Cady-Pereira, K., Boukabara, S., Brown, P. D., Atmospheric radiative transfer modeling: a summary of the AER codes. *J. Quant. Spectrosc. Radiat. Transfer* 91 (2): 233 244, [doi:10.1016/j.jqsrt.2004.05.058](https://doi.org/10.1016/j.jqsrt.2004.05.058), 2005.
- Curci, G., Ferrero, L., Tuccella, P., Barnaba, F., Angelini, F., Bolzacchini, E., Carbone, C., Denier van der Gon, H. A. C., Facchini, M. C., Gobbi, G. P., Kuenen, J. P. P., Landi, T. C., Perrino, C., Perrone, M. G., Sangiorgi, G., and Stocchi, P.: How much is particulate matter near the ground influenced by upper-level processes within and above the PBL? A summertime case study in Milan (Italy) evidences the distinctive role of nitrate, *Atmos. Chem. Phys.*, 15, 2629-2649, <https://doi.org/10.5194/acp-15-2629-2015>.
- D’Almeida, G. A., Koepke, P., and Shettle E. P.: *Atmospheric aerosols: global climatology and radiative characteristics*, A. Deepak Publishing, 561 pp., 1991.
- Fast, J. D., Gustafson, Jr., W. I., Easter, R. C., Zaveri, R. A., Barnard, J. C., Chapman, E. G., Grell, G. A., and Peckham, S. E., Evolution of Ozone, Particulates and Aerosol Direct Radiative Forcing in the Vicinity of Houston Using a Fully Coupled Meteorology-Chemistry-Aerosol Model, *J. Geophys. Res.*, 111, D21305, [doi:10.1029/2005JD006721](https://doi.org/10.1029/2005JD006721), 2006.

- Foley, K. M., Roselle, S. J., Appel, K. W., Bhave, P. V., Pleim, J. E., Otte, T. L., Mathur, R., Sarwar, G., Young, J. O., Gilliam, R. C., Nolte, C. G., Kelly, J. T., Gilliland, A. B., and Bash, J. O., Incremental testing of the Community Multiscale Air Quality (CMAQ) modeling system version 4.7, *Geosci. Model Dev.*, 3, 205–226, doi:10.5194/gmd-3-205-2010, 2010.
- Forkel, R. and Knoche, R.: Regional climate change and its impact on photooxidant concentrations in southern Germany: simulations with a coupled regional climate–chemistry model, *J. Geophys. Res.*, 111, D12302, doi:10.1029/2005JD006748, 2006.
- Ghan, S., Laulainen, N., Easter, R., Wagener, R., Nemesure, S., Chapman, E., Zhang, Y., Leung, R., Evaluation of aerosol direct radiative forcing in MIRAGE, *J. Geophys. Res.*, 106, 5295-5316, 2001.
- Gleeson, E., Toll, V., Nielsen, K.P., Rontu, L., and Masek, J., Effects of aerosols on clear-sky solar radiation in the ALADIN-HIRLAM NWP system, *Atmos. Chem. Phys.*, 16, 5933-5948, 2016.
- Grell, G. A., Emeis, S., Stockwell, W. R., Schoenemeyer, T., Forkel, R., Michalakes, J., Knoche, R., and Seidl, W.: Application of a multiscale, coupled MM5/chemistry model to the complex terrain of the VOTALP valley campaign, *Atmos. Environ.*, 34, 1435–1453, 2000.
- Grell, G.A., Peckham, S.E., Schmitz, R., McKeen, S.A., Frost, G., Skamarock, W.C., Eder, B., Fully coupled online chemistry within the WRF model. *Atmos. Environ.* 39, 6957-6975, 2005.
- Gross, A. and Baklanov, A.: Modeling the influence of dimethyl sulfide on aerosol production in the marine boundary layer, *Int. J. Environ. Pollut.*, 22, 51–71, <https://doi.org/10.1504/IJEP.2004.005492>, 2004.
- Heinold, B., Tegen, I., Schepanski, K., and Hellmuth, O.: Dust radiative feedback on Saharan boundary layer dynamics and dust mobilization, *Geophys. Res. Lett.*, 35, L20817, doi:10.1029/2008GL035319, 2008.
- Hess, M., Koepke, P., and Schult, I., Optical Properties of Aerosols and clouds: The software package OPAC, *Bull. Am. Met. Soc.*, 79, 831–844, 1998.
- Iacono, M. J., Delamere, J. S., Mlawer, E. J., Shephard, M. W., Clough, S. A., and Collins, W. D.: Radiative forcing by long-lived greenhouse gases: Calculations with the AER radiative transfer models, *J. Geophys. Res.-Atmos.*, 113, D13103, <https://doi.org/10.1029/2008JD009944>, 2008.
- Jacobson, M.Z. Fundamentals of atmospheric modeling, 2nd Edition, Cambridge University Press, 813pp., 2005. Schell, B., Ackermann, I.J., Hass, H., Binkowski, F.S., Ebel, A., Modeling the formation of secondary organic aerosol within a comprehensive air quality model system. *Journal of Geophysical Research* 106, 28275–28293, 2001, Skamarock, W. C., Klemp, J. B., Dudhia, J., Gill, D. O., Barker, D. M., Duda, M. G., Huang, X.-Y., Wang, W., and Powers, J. G., A description of the Advanced Research WRF version 3, National Center for Atmospheric Research Tech. Note, NCAR/TN-475+STR, 113 pp., 2008.
- Kiehl, J. T., Hack, J. J., Bonan, G. B., Boville, B. A., Briegleb, B. P., Williamson, D. L., and Rasch, P. J.: Description of the NCAR Community Climate Model (CCM3), National Center for Atmospheric Research, Boulder, Colorado, 1996.
- Köpke, P., Hess, M., Schult, I., and Shettle, E.P., Global Aerosol Data Set (GADS), Tech. Rep. 243, Max-Planck-Institut für Meteorologie, Hamburg, Germany, 1997.
- Krekov, M., Aerosols Effects on Climate, University of Arizona Press, USA, 9-72, 1993.
- Liou, K. N., K. P. Freeman, and T. Sasamori, Cloud and aerosol effects on the solar heating rate of the atmosphere. *Tellus*, 30, 62–70, 1978.
- Longo, K.M., Freitas, S.R., Pirre, M., Marecal, V., Rodrigues, L.F., Panetta, J., Alonso, M.F., Rosario, N.E., Moreira, D.S., Gacita, M.S., Areteta, J., Fonseca, R., Stockler, R., Katsurayama, D.M., Fazenda, A., and Bela, M., The Chemistry CATT-BRAMS model (CCATT-BRAMS 4.5): a regional atmospheric model system for integrated air quality

and weather forecasting and research, *Geosci. Model Dev.*, 6, 1389-1405, 2013.

- Ma, X., Yu, F., and Luo, G., Aerosol direct radiative forcing based on GEOS-Chem-APM and uncertainties, *Atmos. Chem. Phys.*, 12, 5563-5581, 2012.
- Makar, P.A., Gong, W., Milbrandt, J., Hogrefe, C., Zhang, Y., Curci, G., Zabkar, R., Im, U., Balzarini, A., Baro, R., Bianconi, R., Cheung, P., Forkel, R., Gravel, S., Hirtl, H., Honzak, L., Hou, A., Jimenez-Guerrero, P., Langer, M., Moran, M.D., Pabla, B., Perez, J.L., Pirovano, G., San Jose, R., Tuccella, P., Werhahn, J., Zhang, J., Galmarini, S. Feedbacks between air pollution and weather, part 1: Effects on weather. *Atmospheric Environment*, 115, 442-469, 2015a.
- Makar, P.A., Gong, W., Hogrefe, C., Zhang, Y., Curci, G., Zabkar, R., Milbrandt, J., Im, U., Balzarini, A., Baro, R., Bianconi, R., Cheung, P., Forkel, R., Gravel, S., Hirtl, H., Honzak, L., Hou, A., Jimenez-Guerrero, P., Langer, M., Moran, M.D., Pabla, B., Perez, J.L., Pirovano, G., San Jose, R., Tuccella, P., Werhahn, J., Zhang, J., Galmarini, S. Feedbacks between air pollution and weather, part 2: Effects on chemistry. *Atmospheric Environment*, 115, 499-526, 2015b.
- Makar, P.A., Gong, W., Stroud, C.A., Akingunola, A., Pabla, B., Chen, J., Pavlovic, R., Moran, M.D., McLinden, C., Zhang, J., Milbrandt, J., Sills, D., Hayden, K., Li, S.-M., Cheung, P. and Zheng, Q., Modeling the effects of natural and anthropogenic sources of aerosols on weather, 10th International Aerosol Conference (IAC), St. Louis, Missouri, <http://aaarabstracts.com/2018IAC/AbstractBook.pdf> (last accessed November 5, 2018), 2018.
- Myhre, G., Shindell, D., Bréon, F.-M., Collins, W., Fuglestedt, J., Huang, J., Koch, D., Lamargue, J.-F., Lee, D., Mendoza, B., Nakajima, T., Robock, A., Stephens, G., Takemura, T., and Zhang, H., 2013: Anthropogenic and Natural Radiative Forcing. In: *Climate Change 2013: The Physical Science Basis. Contribution of Working Group I to the Fifth Assessment Report of the Intergovernmental Panel on Climate Change* [Stocker, T.F., Qin, D., Plattner, G.-K., Tignor, M., Allen, S.K., Borschung, J., Nauels, A., Xia, Y., Bex, V., and Midgley, P.M. (eds.)]. Cambridge University Press, Cambridge, United Kingdom and New York, NY, USA.
- Mlawer, E. J., S. J. Taubman, P. D. Brown, M. J. Iacono, and S. A. Clough, Radiative transfer for inhomogeneous atmospheres: RRTM, validated correlated-k model for the longwave. *J. Geophys. Res.*, **102**, 16 663–16 682, 1997.
- Moran M.D., S. Ménard, D. Talbot, P. Huang, P.A. Makar, W. Gong, H. Landry, S. Gravel, S. Gong, L-P. Crevier, A. Kallaur, M. Sassi, Particulate-matter forecasting with GEM-MACH15, a new Canadian air-quality forecast model. In: Steyn DG, Rao ST (eds) *Air Pollution Modeling and Its Application XX*, Springer, Dordrecht, pp. 289-292, 2010.
- Moreira, D.S., Longo, K.M., Freitas, S.R., Yamasoe, M.A., Mercado, L.M., Rosario, N.E., Gloor, E., Viana, R.S.M., Miller, J.B., Gatti, L.V., Wiedemann, K.T., Domingues, L.K.G, and Correia, C.C.S., Modeling the radiative effects of biomass burning aerosols on carbon fluxes in the Amazon region, *Atmos. Chem. Phys.*, 17, 14,785-14,810, 2017.
- Nielsen, K. P., Gleeson, E., and Rontu, L.: Radiation sensitivity tests of the HARMONIE 37h1 NWP model, *Geosci. Model Dev.*, 7, 1433–1449, <https://doi.org/10.5194/gmd-7-1433-2014>, 2014.
- Remy, S., Benedetti, A., Bozzo, A., Haiden, T., Jones, L., Razinger, M., Flemming, J., Engelsen, R.J., Peuch, V.H., and Thepaut, J.N., Feedbacks of dust and boundary layer meteorology during a dust storm in the eastern Mediterranean, *Atmos. Chem., Phys.*, 15, 12,909-12,933, 2015.
- Ritter, B. and Geleyn, J.-F., A comprehensive scheme for numerical weather prediction models with potential applications in climate simulations, *Mon. Weather Rev.*, 120, 303–325, 1992.
- Rontu, L., Gleeson, E., Räisänen, P., Pagh Nielsen, K., Savijärvi, H., and Hansen Sass, B.: The HIRLAM fast radiation scheme for mesoscale numerical weather prediction models, *Adv. Sci. Res.*, 14, 195-215, <https://doi.org/10.5194/asr-14-195-2017>, 2017.

- Rosario, N. E., Longo, K. M., Freitas, S. R., Yamasoe, M. A., and Fonseca, R. M., Modeling the South American regional smoke plume: aerosol optical depth variability and surface shortwave flux perturbation, *Atmos. Chem. Phys.*, 13, 2923–2938, 2013.
- Rothman L.S., I.E. Gordon, A. Barbe, D. Chris Benner, P.F. Bernath, M. Birk, V. Boudon, L.R. Brown, A. Campargue, J.-P. Champion, K. Chance, L.H. Coudert, V. Dana, V.M. Devi, S. Fally, J.-M. Flaud, R.R. Gamache, A. Goldman, D. Jacquemart, I. Kleiner, N. Lacome, W.J. Lafferty, J.-Y. Mandin, S.T. Massie, S.N. Mikhailenko, C.E. Miller, N. Moazzen-Ahmadi, O.V. Naumenko, A.V. Nikitin, J. Orphal, V.I. Perevalov, A. Perrin, A. Predoi-Cross, C.P. Rinsland, M. Rotger, M. Šimečková, M.A.H. Smith, K. Sung, S.A. Tashkun, J. Tennyson, R.A. Toth, A.C. Vandaele, J. Vander Auwera, 2009, The HITRAN 2008 molecular spectroscopic database, *Journal of Quantitative Spectroscopy & Radiative Transfer*, 110, 533–572.
- Russo, F., Maurizi, A., D'Isidoro, M., and Tampieri, F.: Introduction of the aerosol feedback process in the model BOLCHEM, in: EGU General Assembly 2010, Vienna, Austria, 2–7 May 2010, EGU2010-8561, 2010.
- Saleeby, S.M. and van den Heever, S.C., Developments in the CSU-RAMS aerosol model: emissions, nucleation, regeneration, deposition and radiation, *J. Appl. Met. Clim.*, 52, 2601-2622, 2013.
- Savijärvi, H., Fast radiation parameterization schemes for mesoscale and short-range forecast models, *J. Appl., Meteorol.*, 20, 437-447, 1990.
- Schell B., I.J. Ackermann, H. Hass, F.S. Binkowski, and A. Ebel, Modeling the formation of secondary organic aerosol within a comprehensive air quality model system, *Journal of Geophysical research*, 106, 28275-28293, 2001.
- Slingo, A., and H. M. Schrecker, On the shortwave radiative properties of stratiform water clouds. *Quart. J. Roy. Meteor. Soc.*, 108, 407–426, 1982.
- Stier, P., Feichter, J., Kinne, S., Kloster, S., Vignati, E., Wilson, J., Ganzeveld, L., Tegen, I., Werner, M., Balkanski, Y., Schultz, M., Boucher, O., Minikin, A., Petzold, A., The aerosol-climate model ECHAM5-HAM, *Atmos. Chem. Phys.*, 5, 1125-1156, 2005.
- Stokowski, D., The addition of the direct radiative effect of atmospheric aerosols into the Regional Atmospheric Modeling System (RAMS). M.S. thesis, Dept. of Atmospheric Science, Colorado State University, Atmospheric Science Paper 637, 89 pp., 2005
- Toon, O. B., Turco, R. P., Westphal, D., Malone, R., and Liu, M., A Multidimensional Model for Aerosols: Description of Computational Analogs, *J. Atmos. Sci.*, 45, 2123–2144, 1988.
- Toon, O. B., McKay, C. P., Ackerman, T. P., and Santhanam, K.: Rapid Calculation of Radiative Heating Rates and Photodissociation Rates in Inhomogeneous Multiple Scattering Atmospheres, *J. Geophys. Res.*, 94, 16287–16301, doi:10.1029/JD094iD13p16287, 1989.
- Tsikerdekis, A., Zanis, P., Steiner, A.L., Solmon, F., Amirdis, V., Marinou, E., Katragkou, E., Karacostas, T., and Foret, G., Impact of dust size parameterizations on aerosol burden and radiative forcing in RegCM4, *Atmos. Chem. Phys.*, 17, 769-791, 2017.
- Tulet, P., Mallet, M., Pont, V., Pelon, J., and Boone, A.: The 7– 13 March 2006 dust storm over West Africa: generation, transport, and vertical stratification, *J. Geophys. Res.*, 113, D00C08, doi:10.1029/2008JD009871, 2008.
- Vignati, E., J. Wilson, and P. Stier (2004), M7: An efficient size-resolved aerosol microphysics module for large-scale aerosol transport models, *J. Geophys. Res.*, 109, D22202, doi:10.1029/2003JD004485.
- Vogel, B., Vogel, H., Bäumer, D., Bangert, M., Lundgren, K., Rinke, R., and Stanelle, T., The comprehensive model system COSMO-ART – radiative impact of aerosol on the state of the atmosphere on the regional scale, *Atmos. Chem. Phys.*, 9, 8861-8680, 2009.
- Wang, H., G.-Y. Shi, A. Teruo, B. Wang, T.-L. Zhao, 2004, Radiative forcing due to dust aerosol over east Asia-north Pacific region during spring, 2001, *Chinese Science Bulletin*, 49 (20) 2212-2219.

- Wang, H., G.-Y. Shi, S.-Y. Li, W. Li, B. Wang, Y.-B. Huang, 2006, The Impacts of Optical Properties on Radiative Forcing Due to Dust Aerosol, *Advances in Atmospheric Sciences*, 23 (3), 431-441.
- Wang, H., Xue, M., Zhang, X.Y., Liu, H.L., Zhou, C.H., Tan, S.C., Che, H.Z., Chen, B., and Li, T., Mesoscale modeling study of the interactions between aerosols and PBL meteorology during a haze episode in Jing–Jin–Ji (China) and its nearby surrounding region – Part 1: Aerosol distributions and meteorological features, *Atm. Chem., Phys.*, 15, 3257-3275, 2015.
- Wang, J., Allen, D.J., Pickering, K.E., Li, Z., He, H., Impact of aerosol direct effect on East Asian air quality during the EAST-AIRE campaign, *J. Geophys. Res. Atmos.*, 121, 6634-6554, doi: [10.1002/2016JD025108](https://doi.org/10.1002/2016JD025108), 2016.
- Wild, M., and Roeckner, E., Radiative fluxes in the ECHAM5 general circulation model, *J. Climate*, 19, 3792-3809, 2006.
- Wong, D. C., Pleim, J., Mathur, R., Binkowski, F., Otte, T., Gilliam, R., Pouliot, G., Xiu, A., Young, J. O., and Kang, D., WRF-CMAQ two-way coupled system with aerosol feedback: software development and preliminary results, *Geosci. Model Dev.*, 5, 299-312, doi: [10.5194/gmd-5-299-2012](https://doi.org/10.5194/gmd-5-299-2012), 2012.
- Wyser, K., Ronto, L., and Savijärvi, H., Introducing the effective radius into a fast radiation scheme of a mesoscale model, *Atmos. Chem. Phys.*, 6, 4687-4704, 2006.
- Xing, J., Mathur, R., Pleim, J., Hogrefe, C., Gan, C.-M., Wong, D.C., Wei, C., and Wang, J., Air pollution and climate response to aerosol direct radiative effects: a modeling study of decadal trends across the northern hemisphere, *J. Geophys. Res. Atmos.*, 120, 12,221-12,236, doi: [10.1002/2015JD023933](https://doi.org/10.1002/2015JD023933), 2015.
- Xing, J., Wang, J., Mathur, R., Wang, S., Sarwar, G., Pleim, J., Hogrefe, C., Zhang, Y., Jiang, J., Wong, D.C., and Hao, J., Impacts of aerosol direct effects on tropospheric ozone through changes in atmospheric dynamics and photolysis rates, *Atmos. Chem. Phys.*, 17, 9869-9883, 2017.
- Yu, F., Luo, G., and Ma, X., Regional and global modeling of aerosol optical properties with a size, composition and mixing state resolved particle microphysics model, *Atmos. Chem. Phys.*, 12, 5719-5736, 2012.
- Zhang, Y., 2008: Online-coupled meteorology and chemistry models: history, current status, and outlook, *Atmos. Chem. Phys.*, 8, 2895–2932, doi: [10.5194/acp-8-2895-2008](https://doi.org/10.5194/acp-8-2895-2008).

3.9. Interactions of Aerosol Chemical Species with Clouds for CW-AQF Models

3.9.1 Introduction

Aerosols can serve as cloud condensation nuclei (CCN) and ice nuclei (IN) upon which cloud droplets and ice crystals form. The microphysical and radiative properties, amount, and lifetime of clouds are modified thus by aerosols. The parameters that determine cloud properties include updraft speeds of air that form the clouds, chemical and physical properties of aerosol particles on which cloud particles nucleate, and cloud microphysical processes. The largest uncertainties in current estimates of climate forcing are associated with the poor knowledge on the aerosol-cloud interactions (ACI), traditionally referred to as aerosol indirect effects (IPCC, 2013). The 'first indirect effect' is the microphysically induced effect on the cloud droplet number concentration and hence the cloud droplet size, with the liquid water content held fixed. This effect is also known as the 'cloud albedo effect' or the 'Twomey effect'. The 'second indirect effect' is the microphysically induced effect on the liquid water content, cloud height, and lifetime of clouds. This second effect is also known as the 'cloud lifetime effect' or the 'Albrecht effect'. The semi-direct effect is the mechanism by which absorption of shortwave radiation by tropospheric aerosols leads to heating of the troposphere that in turn changes the relative humidity and the stability of the troposphere and thereby influences cloud formation and lifetime. Figure 3.7 schematizes the different effects considered as most relevant in IPCC (2007).

The ACI effect on cloud properties and precipitation strongly varies among cloud types (Fan et al., 2016). The effects on warm clouds comprise the first and second indirect effects. Many different aerosol indirect effects have been suggested since 'Twomey effect' (Twomey, 1974), such as increased cloud lifetime and cloudiness (Albrecht, 1989) and suppressed rain (Rosenfeld, 1999) that are both controlled by reduced droplet size and narrower droplet spectrum. A recent review on ACI presented in Fan et al. (2016) indicates that current research on warm clouds mainly focuses on how aerosols change microphysics and dynamic feedbacks in maritime stratocumulus clouds and affect cloud macrophysics such as the transitions between open and closed cells and from shallow to deep clouds.

For deep convective clouds, aerosol impacts are extremely complex and not as well understood as those for shallow clouds (Fan et al., 2016). It is still not clear if the effect of suppressing warm rain by aerosols invigorates the convection in deep clouds. This has been suggested by Rosenfeld et al. (2008) with the idea that reduction of warm precipitation allows more cloud water being lifted higher in the atmosphere, where freezing of the larger amount of cloud water releases more latent heat and invigorates convection. However, many modeling studies suggested that this thermodynamic invigoration is insignificant or even suppression of convection is seen, especially for clouds with cold cloud base, or strong wind shear, or dry conditions (e.g., Fan et al., 2013). On the other hand, observational studies showed the increased cloud-top height and cloud cover with an increase of aerosol loading (e.g., Niu and Li, 2012).

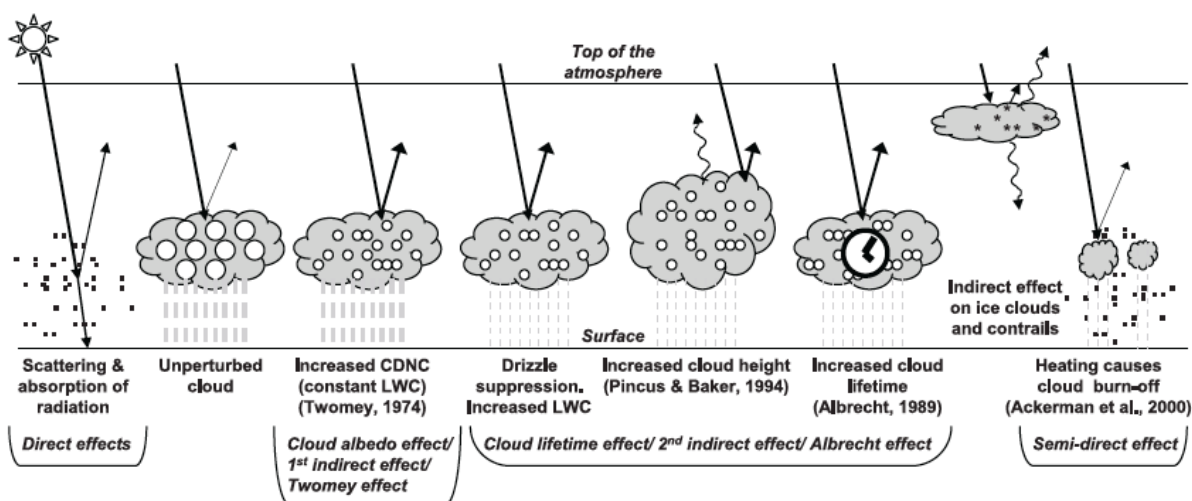


Figure 3.7. Radiative mechanisms associated with cloud effects identified as significant in relation to aerosols (IPCC, 2007)

Many recent studies also investigated aerosol impacts on clouds by acting as IN. IN directly change ice nucleation processes that determines the initial number concentration and size distribution of ice crystals. Various insoluble or partially insoluble aerosol particles can act as IN, such as mineral dust, carbonaceous aerosol, biological particles, and volcanic ash. Apart from mineral dust, the relevance of the other species acting as IN is still under discussion. Ice nucleation processes connected to IN are the homogeneous freezing of hazy aerosols, the heterogeneous ice nucleation through deposition, immersion or condensation, or direct contact (Fan et al., 2016).

The ACI mechanisms are nowadays been implemented in CW-AQF as a potential source of performance improvements. In this section, we will discuss the different approaches followed in CW-AQF when aerosols affect cloud processes.

3.9.2 Aerosol-Cloud Interaction in CW-AQF Models

The treatment of ACI in CW-AQF models depends on the degree of coupling between the meteorology and the chemistry. Aerosols are a necessary condition for cloud formation and influence cloud microphysical and physical properties as well as precipitation release. Thus, two approximations are found in models: (1) no coupling between prognostic aerosols and clouds, and (2) interactive coupling of prognostic aerosols with the cloud scheme. The first group has cloud schemes that implicitly represent the effect of aerosols on clouds through diagnostic calculation of CCN number concentration or even simpler approaches assuming a constant droplet number to close the cloud droplet radiation interaction equations. Such cloud schemes are known as one-moment schemes and only solve the mixing ratio of water species within and below the cloud. The second group of models use more physically-based schemes that explicitly resolve the activation of CCN into cloud droplets (e.g. Abdul-Razzak and Ghan, 2002) and describe both number and mass of water species. Such cloud schemes are the two-moment schemes (e.g., Morrison et al., 2009). The coupling of two-moment cloud schemes with prognostic aerosols allows a more physically-based description of the aerosol activation for both number and mass depending on aerosol size and composition (Abdul-Razzak and Ghan, 2002).

Cloud droplet number concentration may be calculated based on a prognostic representation of aerosol size and chemical composition within the framework of an ascending adiabatic cloud parcel (Nenes and Seinfeld, 2003). This scheme can be extended to include: (a) adsorption activation from insoluble CCN (Kumar et al., 2009), (b) giant CCN equilibrium-timescales on aerosol activation (Barahona et al., 2010), or (c) the effect of entrainment on activation (Barahona and Nenes, 2007). The supersaturation needed for activating condensation nuclei is determined by the modified Köhler theory that takes the effects of surfactants and slightly

soluble species into account. Most models assume specific size distributions for cloud droplets and raindrops (Seifert and Beheng, 2001).

Tables 3.20 and 3.21 summarize the treatment of cloud properties in global and regional/urban CW-AQF models that have an interactive coupling of prognostic aerosols with the cloud formation. Most models use a bulk two-moment microphysics scheme to treat the ACI (e.g., Morrison et al., 2009; Seifert and Beheng, 2001). For subgrid-scale clouds, there is still no common approach to parameterize the aerosol effects and all the models exclude this process. Thus, the effect of aerosols on convective clouds are studied only with model resolution that explicitly develops convection with the microphysics schemes used.

In most models, the activation of CCN is based on a parameterized scheme that solves the Köhler theory, where the important parameters for activation are calculated following Abdul-Razzak and Ghan (2000). Only the MetUM model uses an empirical expression for cloud droplet number based on Jones et al. (2001), while RAMS/ICLAMS implements the explicit cloud droplet nucleation parameterization scheme of Nenes and Seinfeld (2003), and Fountoukis and Nenes (2005).

A common gamma distribution is assumed for the size distribution of the cloud droplets. Most models consider all aerosol species as CCN, and only WRF-CMAQ deals with IN species (sulfate, black carbon, dust and organic aerosols). There is still a lack of aerosol-ice interaction treatment in most models, and current developments have been focused on warm cloud ACI processes.

Aerosols that have been activated as CCN to form cloud droplets are removed from the atmosphere through wet deposition following in- and below-cloud scavenging. After activation, cloud droplets are removed via autoconversion (i.e., the collision/coalescence of cloud drops to become raindrops and get into precipitation) and via collection/accretion by (existing) precipitation (i.e., rain, snow, graupel). Complexity of such processes significantly varies among models as shown in Tables 3.20 and 3.21. Some models implement detailed schemes for in-cloud scavenging considering activation (nucleation) scavenging, Brownian diffusion (for activated particles), autoconversion, and collection (i.e., WRF/Chem). On the other side, simplified approaches are chosen using prescribed fractions for collection efficiencies (i.e., C-IFS).

3.9.3 *Major Uncertainties on Aerosol-Cloud Interactions*

A major shortcoming when coupling prognostic aerosols with a cloud scheme in an operational model is that aerosol mass and number are difficult to predict accurately due to uncertainties in emissions and deposition. Hence, although this coupling is more physically correct, in practice it may be difficult to achieve better verification scores than without prognostic aerosols (Baklanov et al., 2014).

Fan et al. (2016) identified the most important uncertainties associated with aerosol-cloud interactions. There are still large variability in simulated convective and cloud properties among cloud schemes, even with cloud resolved model scales. Under the same conditions, cloud microphysical parameterizations produce large differences in simulated convection and clouds. Current CW-AQF models are based on bulk cloud schemes, due to the reduced computational cost compared with more precise bin cloud schemes. Bulk schemes have been shown that are not well configured for studying ACI (Khain et al., 2015).

Table 3.20 Treatments of Cloud Properties in Global CW-AQF Models

Model System	Hydrometeor Types in Clouds	Cloud Droplet Size Distribution	Cloud Droplet Number	CCN/IDN Composition	CCN/IDN Spectrum	Cloud Radiative Properties
G5CHEM (GEOS-5 with GEOS-Chem) (Hu et al., 2018) (Global)	Water vapor, cloud liquid water, cloud ice, rain, snow	Prescribed	Prescribed	N/A	N/A	Prognostic
GEM-MACH (Moran et al., 2010; Makar et al., 2015a, b) (Global/Regional)	Depends on the resolution employed for the model; 2.5 km resolution uses explicit 2-moment microphysics scheme of Milbrandt and Yau (2005a,b), with 6 hydrometeor categories (cloud droplets, rain, pristine ice, snow, graupel and hail 10km and lower resolution uses Sundqvist and Kain-Fritsch parameterizations for grid-scale condensation and sub-grid-scale convection, respectively.	Feedback mode: bulk cloud water is distributed evenly to all activated aerosol particles, determining the droplet sizes for cloud processing. (Gong et al., 2015)	One-way coupling (no feedbacks): empirical activation scheme is used to determine cloud droplet number (Jones et al, 1994), microphysics uses Cohard et al (1998) hyperbolic function with fixed CCN numbers. Two-way coupling (feedbacks): sectional representation aerosol activation scheme of Abdul-Razzak and Ghan (2002) used to determine cloud droplet number from number of activated aerosols	Feedback mode using Abdul-Razzak and Ghan (2002) scheme uses $(\text{NH}_4)_2\text{SO}_4$, NH_4HSO_4 , H_2SO_4 , NH_4NO_3 , HNO_3 , NaCl , secondary organic aerosol treated as adipic acid, primary organic aerosol, elemental carbon, and crustal material all treated as insoluble.	Feedback mode: CCN spectrum from Abdul-Razzak and Ghan (2002) activation of particles. Ice Nucleation currently under development.	Cloud droplets, solar spectrum: 4-band model of Dobbie et al (1999), based on the work of Slingo (1989). Cloud droplets, infrared: based on Lindner and Li (1999): fitting to Mie theory, accurate to 5% of exact calculations. Cirrus/ice clouds, solar spectrum: aircraft-observation based parameterization of ice water content and effective ice crystal size (Fu, 1996). Cirrus/ice clouds, infrared: functions of the cloud ice water content and generalized effective crystal size (Fu et al., 1998).
IFS-MOZART; C-IFS (Flemming et al., 2015) (Global)	Water vapor, cloud liquid water, cloud ice, rain, snow	Prescribed exponential distribution	Prescribed	N/A	N/A	Calculated online from prognostic hydrometeors and cloud cover as described in Hogan and Bozzo (2016).

Model System	Hydrometeor Types in Clouds	Cloud Droplet Size Distribution	Cloud Droplet Number	CCN/IDN Composition	CCN/IDN Spectrum	Cloud Radiative Properties
MetUM (Mulcahy et al. 2014) (Global/Mesoscale)			Prognostic based on aerosol mass and prescribed size distribution CCN and following Jones et al. (2001) expression for CDN	All except BC and dust; CCN only	large-scale precipitation scheme uses the CDNC to calculate the autoconversion rate of cloud water to rainwater based on the Tripoli and Cotton (1980) autoconversion scheme.	radiation scheme uses the CDNC to obtain the cloud effective radius and cloud albedo

Table 3.21 Treatments of Cloud Properties in Regional/Urban CW-AQF Models

Model System	Hydrometeor Types in Clouds	Cloud Droplet Size Distribution	Cloud Droplet Number	CCN/IDN Composition	CCN/IDN Spectrum	Cloud Radiative Properties
WRF-Chem (Mesoscale) (Grell et al., 2005; Fast et al., 2006)	bulk water vapor, rain, snow, cloud ice, cloud water, and graupel or a subset of them, depending on microphysics schemes used in both stratiform and subgrid convective clouds	Prognostic, modal, single size distribution (MOSAIC)	Prognostic, aerosol size- and composition dependent, parameterized	All treated species; CCN only	Function of aerosol size and hygroscopicity based on Köhler theory; CCN only	Prognostic, parameterized in terms of cloud water, ice mass, and number
NAQFC (NAM-CMAQ) (Lee et al., 2017)	Cloud ice, graupel and cloud droplets	CMAQ in NAQFC re-diagnose cloud layers with a single size distribution	Re-diagnosed from specific humidity profile with an assumed single size	Water uptake and activation in aero6	Water uptake and activation in aero6	Cloud attenuation diagnosed from ratio between short wave under clear sky conditions and cloudy conditions

Model System	Hydrometeor Types in Clouds	Cloud Droplet Size Distribution	Cloud Droplet Number	CCN/IDN Composition	CCN/IDN Spectrum	Cloud Radiative Properties
Two-way coupled WRF-CMAQ (Mesoscale)	bulk two-moment water vapor, rain, snow, cloud ice, cloud water, and graupel	Gamma size distribution	Diagnosed from the activation of the aerosol particles based on Abdul-Razzak and Ghan (2000, 2002)	All types of aerosols treated for both CCN/IDN	Function of aerosol size and hygroscopicity based on Köhler theory;	Prognostic, parameterized in terms of cloud water, ice mass, and number
GCCATT-BRAMS (Mesoscale) (Freitas et al., 2009, 2011, 2017)	Two-moment (2M) microphysical parameterization used in RAMSv6 and Thompson microphysics parameterization	Gamma size distribution	Prognostic based on aerosol solubility; activation based on Abdul-Razzak and Ghan (2000)	Aerosol species lumped into "water friendly" and "ice friendly" contribute to CCN/IDN	Function of aerosol size and hygroscopicity based on Köhler theory	Cloud physical and optical properties in the CARMA radiative scheme have been parameterized according to Sun and Shine (1994), Savijärvi (1997), and Savijärvi et al. (1997, 1998) using liquid and ice water content. For the RRTMG, the optical properties of liquid and ice water are from Hu and Stamnes (1993) and Ebert and Curry (1992)
COSMO-ART (Bangert et al., 2011) (Mesoscale)	Bulk water, rain, ice and snow for grid-scale clouds. Two-moment parameterization of Seifert and Beheng (2001). No microphysics for subgrid scale clouds (Tiedke et al, 1989)	Gamma distribution function	Prognostic equation; activation of the aerosol particles based on Abdul-Razzak and Ghan (2000)	All treated species; CCN only	Function of aerosol size and hygroscopicity based on Köhler theory; CCN only	Mie theory with different liquid and ice cloud properties

Model System	Hydrometeor Types in Clouds	Cloud Droplet Size Distribution	Cloud Droplet Number	CCN/IDN Composition	CCN/IDN Spectrum	Cloud Radiative Properties
Enviro-HIRLAM (Baklanov et al., 2017) (Mesoscale)	Bulk liquid, ice, rain, snow; simplified microphysics; subgrid-scale clouds and mixing	Gamma distribution with Geoffroy et al. (2010) shape parameter.	Prognostic based on aerosol size, number and solubility; activation based on Abdul-Razzak and Ghan (2000)	All treated species; CCN only	N/A	Modification of the Savijärvi radiation scheme (Savijärvi, 1990) with implementation of new fast analytical shortwave (SW) and longwave (LW) aerosol transmittances, reflectances and absorptances (Nielsen et al., 2014; Rontu et al., 2017).
GRAPES-CUACE (Mesoscale) (Wang et al., 2010; Zhou et al., 2016; Zhou et al., 2018)	Two-moment or bulk mass and number concentration for water vapor, cloud water, rain, snow, cloud ice, cloud water, and graupel or snow a subset of them, depending on microphysics schemes	Gamma distribution in WDM6	Predicted	Sectional activation of all aerosols by AR&G00 and AR&G02 (Abdul-Razzak&Ghan, 2000, 2002) or bulk parameterization by Twomey scheme	Bulk number	Prognostic, parameterized in terms of cloud water, ice mass, and number
RAMS/ICLAMS (Solomos et al., 2011) (Mesoscale)	Bulk liquid, pristine ice, snow, aggregates, graupel and hail; Two-moment bulk scheme	None, bulk approach	lookup table derived from bin-parcel model to compute CCN or explicit cloud droplet nucleation parameterization scheme (Nenes and Seinfeld, 2003; Fountoukis and Nenes, 2005)	Soil dust, sea salt spray and secondary pollutants contribute to the CCN population; insoluble	CCN concentrations are expressed as a function of supersaturation using Köhler theory (Köhler, 1936; Nenes and Seinfeld, 2003)	The optical properties of liquid and ice water in RRTMG are from Hu and Stamnes (1993) and Ebert and Curry (1992)

Main limitations of bulk schemes are that they generally 1) do not include a CCN budget, which can cause unrealistic results for aerosol impact; 2) do not explicitly calculate diffusional growth based on supersaturation and droplet sizes, but they employ the saturation adjustment approach, which eliminates supersaturation and decreases the sensitivity of bulk schemes to aerosols; 3) employ autoconversion parameterizations that were generally developed under a narrow range of conditions and do not take into account the time evolution of autoconversion to convert cloud water to rainwater; 4) use average fall velocities for collision processes of hydrometeors, which is a big problem for self-collections and for collisions between different hydrometeor types with the similar average fall velocities; 5) use average fall velocities over the particle size distribution for sedimentation, which does not account for smaller particles that fall slower and larger particles that fall faster; and 6) use two sets of averaged fall velocities, mass-mean and number-mean fall velocities, in two-moment schemes that would result in cloud area with significant mass but negligible number or with significant number but negligible mass as shown in Fan et al. (2015).

Another major issue in current CW-AQF and climate models is how to accurately parameterize the effect of aerosols in subgrid clouds. None of the CW-AQF models revised considers the interaction of aerosols in such clouds. However, positive impacts have been shown in studies that consider some types of aerosol impacts on subgrid parameterizations (e.g., Song and Zhang, 2011; Berg et al., 2015). Future developments in CW-AQF models should focus on this direction and have a complete implementation of ACI in both grid- and subgrid-scale clouds.

3.9.4 Summary

- Cloud formation is tightly related with aerosol presence in the atmosphere;
- Aerosols can act as cloud condensation nuclei (CCN) and ice nuclei (IN) representing a key element in the development of clouds;
- A summary of the main processes related with the interaction of clouds and aerosols, with a main emphasis on the formation process is presented;
- A review of the different methodologies implemented in state-of-the-art CW-AQF models are presented and the main uncertainties highlighted.

References

- Abdul-Razzak, H. and Ghan, S. J.: A parameterization of aerosol activation: 2. Multiple aerosol types, *J. Geophys. Res.-Atmos.*, 105, 6837–6844, 2000.
- Abdul-Razzak, H. and Ghan, S. J.: Parameterization of aerosol activation. 3. Sectional representation, *J. Geophys. Res.*, 107, 4026, 2002.
- Albrecht, B. A., 1989: Aerosols, cloud microphysics, and fractional cloudiness. *Science*, 245, 1227–1230, [doi:10.1126/science.245.4923.1227](https://doi.org/10.1126/science.245.4923.1227).
- Baklanov, A., Schlünzen, K., Suppan, P., Baldasano, J., Brunner, D., Aksoyoglu, S., Carmichael, G., Douros, J., Flemming, J., Forkel, R., Galmarini, S., Gauss, M., Grell, G., Hirtl, M., Joffre, S., Jorba, O., Kaas, E., Kaasik, M., Kallos, G., Kong, X., Korsholm, U., Kurganskiy, A., Kushta, J., Lohmann, U., Mahura, A., Manders-Groot, A., Maurizi, A., Moussiopoulos, N., Rao, S. T., Savage, N., Seigneur, C., Sokhi, R. S., Solazzo, E., Solomos, S., Sørensen, B., Tsegas, G., Vignati, E., Vogel, B., and Zhang, Y.: Online coupled regional meteorology chemistry models in Europe: current status and prospects, *Atmos. Chem. Phys.*, 14, 317–398, <https://doi.org/10.5194/acp-14-317-2014>, 2014.

- Baklanov, A., Smith Korsholm, U., Nuterman, R., Mahura, A., Nielsen, K. P., Sass, B. H., Rasmussen, A., Zakey, A., Kaas, E., Kurganskiy, A., Sørensen, B., and González-Aparicio, I.: Enviro-HIRLAM online integrated meteorology–chemistry modeling system: strategy, methodology, developments and applications (v7.2), *Geosci. Model Dev.*, 10, 2971–2999, <https://doi.org/10.5194/gmd-10-2971-2017>, 2017.
- Bangert, M., Kottmeier, C., Vogel, B., and Vogel, H.: Regional scale effects of the aerosol cloud interaction simulated with an online coupled comprehensive chemistry model, *Atmos. Chem. Phys.*, 11, 4411–4423, <https://doi.org/10.5194/acp-11-4411-2011>, 2011.
- Barahona, D., West, R. E. L., Stier, P., Romakkaniemi, S., Kokkola, H., and Nenes, A.: Comprehensively accounting for the effect of giant CCN in cloud activation parameterizations, *Atmos. Chem. Phys.*, 10, 2467–2473, [doi: 10.5194/acp-10-2467-2010](https://doi.org/10.5194/acp-10-2467-2010), 2010.
- Barahona, D. and Nenes, A.: Parameterization of cloud droplet formation in large scale models: including effects of entrainment, *J. Geophys. Res.*, 112, D16026, [doi: 10.1029/16207JD008473](https://doi.org/10.1029/16207JD008473), 2007.
- Berg, L.K., M. Shrivastava, R. C. Easter, J.D. Fast, E.G. Chapman, Y. Liu, and R. A. Ferrare, 2015: A new WRF-Chem treatment for studying regional-scale impacts of cloud processes on aerosol and trace gases in parameterized cumuli. *Geosci. Model Dev.*, 8, 409–429, [doi: 10.5194/gmd-8-409-2015](https://doi.org/10.5194/gmd-8-409-2015).
- Dobbie, J.S., Li, J., and Chylek, P., Two- and four-stream optical properties for water clouds and solar wavelengths, *J. Geophys. Res.*, 104, 2067–2079, 1999.
- Ebert, E. E. and Curry, J. A.: A parameterization of ice cloud optical properties for climate models, *J. Geophys. Res.*, 97, 3831–3836, 1992.
- Fan, J., L. R. Leung, D. Rosenfeld, Q. Chen, Z. Li, J. Zhang, and H. Yan, 2013: Microphysical effects determine macrophysical response for aerosol impacts on deep convective clouds. *Proc. Natl. Acad. Sci. USA*, 110, E4581–E4590, [doi: 10.1073/pnas.1316830110](https://doi.org/10.1073/pnas.1316830110).
- Fan, J., D. Rosenfeld, Y. Yang, C. Zhao, L. R. Leung, and Z. Li, 2015: Substantial contribution of anthropogenic air pollution to catastrophic floods in Southwest China. *Geophys. Res. Lett.*, 42, 6066–6075, [doi: 10.1002/2015GL064479](https://doi.org/10.1002/2015GL064479).
- Fan J., Wang Y., Rosenfeld D., Liu X., 2016: Review of aerosol–cloud interactions: mechanisms, significance, and challenges. *J Atmos Sci* 73:4221–4252
- Fast, J. D., W. I. Gustafson Jr., R. C. Easter, R. A. Zaveri, J. C. Barnard, E. G. Chapman, G. A. Grell, and S. E. Peckham (2006), Evolution of ozone, particulates, and aerosol direct radiative forcing in the vicinity of Houston using a fully coupled meteorology-chemistry-aerosol model, *J. Geophys. Res.*, 111, D21305, [doi: 10.1029/2005JD006721](https://doi.org/10.1029/2005JD006721).
- Flemming, J., Huijnen, V., Arteta, J., Bechtold, P., Beljaars, A., Blechschmidt, A.-M., Diamantakis, M., Engelen, R. J., Gaudel, A., Inness, A., Jones, L., Josse, B., Katragkou, E., Marecal, V., Peuch, V.-H., Richter, A., Schultz, M. G., Stein, O., and Tsikerdekis, A.: Tropospheric chemistry in the Integrated Forecasting System of ECMWF, *Geosci. Model Dev.*, 8, 975–1003, <https://doi.org/10.5194/gmd-8-975-2015>, 2015.
- Fountoukis, C. and Nenes, A.: Continued development of a cloud droplet formation parameterization for global climate models, *J. Geophys. Res.*, 110, D11212, [doi: 10.1029/2004JD005591](https://doi.org/10.1029/2004JD005591), 2005.

- Freitas, S. R., Longo, K. M., Silva Dias, M. A. F., Chatfield, R., Silva Dias, P., Artaxo, P., Andreae, M. O., Grell, G., Rodrigues, L. F., Fazenda, A., and Panetta, J.: The Coupled Aerosol and Tracer Transport model to the Brazilian developments on the Regional Atmospheric Modeling System (CATT-BRAMS) – Part 1: Model description and evaluation, *Atmos. Chem. Phys.*, 9, 2843–2861, doi:10.5194/acp-9-2843-2009, 2009.
- Freitas, S. R., Panetta, J., Longo, K. M., Rodrigues, L. F., Moreira, D. S., Rosário, N. E., Silva Dias, P. L., Silva Dias, M. A. F., Souza, E. P., Freitas, E. D., Longo, M., Frassoni, A., Fazenda, A. L., Santos e Silva, C. M., Pavani, C. A. B., Eiras, D., França, D. A., Massaru, D., Silva, F. B., Santos, F. C., Pereira, G., Camponogara, G., Ferrada, G. A., Campos Velho, H. F., Menezes, I., Freire, J. L., Alonso, M. F., Gácita, M. S., Zarzur, M., Fonseca, R. M., Lima, R. S., Siqueira, R. A., Braz, R., Tomita, S., Oliveira, V., and Martins, L. D.: The Brazilian developments on the Regional Atmospheric Modeling System (BRAMS 5.2): an integrated environmental model tuned for tropical areas, *Geosci. Model Dev.*, 10, 189–222, <https://doi.org/10.5194/gmd-10-189-2017>, 2017.
- Fu, Q., An accurate parameterization of the solar radiative properties of cirrus clouds for climate models, *J. Climate*, 9, 2058–2082, 1996.
- Fu, Q., Yang, P., and Sun, W.B., An accurate parameterization of the infrared radiative properties of cirrus clouds for climate models, *J. Climate*, 11, 2223–2236, 1998.
- Grell, G. A., S. E. Peckham, R. Schmitz, and S. A. McKeen, G. Frost, W. C. Skamarock, and B. Eder (2005), Fully coupled “online” chemistry within the WRF model, *Atmos. Environ.*, 39, 6957–6975.
- Gong, W., Makar, P.A., Zhang, J., Milbrandt, J., Gravel, S., Hayden, K.L., MacDonald, A.M., and Leaitch, W.R., Modeling aerosol-cloud-meteorology interaction: A case study with a fully coupled air quality model (GEM-MACH), *Atm. Env.*, 115, 695–715, 2015.
- Hu, L., Keller, C. A., Long, M. S., Sherwen, T., Auer, B., Da Silva, A., Nielsen, J. E., Pawson, S., Thompson, M. A., Trayanov, A. L., Travis, K. R., Grange, S. K., Evans, M. J., and Jacob, D. J.: Global simulation of tropospheric chemistry at 12.5 km resolution: performance and evaluation of the GEOS-Chem chemical module (v10-1) within the NASA GEOS Earth system model (GEOS-5 ESM), *Geosci. Model Dev.*, 11, 4603–4620, <https://doi.org/10.5194/gmd-11-4603-2018>, 2018.
- Hu, Y. X. and Stamnes, K.: An accurate parameterization of the radiative properties of water clouds suitable for use in climate models, *J. Climate*, 6, 728–742, 1993.
- IPCC, 2007: *Climate Change 2007: The Physical Science Basis*. Cambridge University Press, 996 pp.
- IPCC, 2013: *Climate Change 2013: The Physical Science Basis*. Cambridge University Press, 1535 pp., doi:10.1017/CBO9781107415324.
- Lee, P., McQueen, J., Stajner, I., Huang, J., Pan, L., Tong, D., Kim, H., Tang, Y., Shafran, P., Huang, H.-C., Gorline, J., Upadhyay, S., and Artz, R., 2017: NAQFC developmental forecast guidance for fine particulate matter (PM_{2.5}), *Weather and Forecasting*, 32(1): 343–360.
- Jones, A., Roberts, D. L., Woodage, M. L., and Johnson, C. E.: Indirect sulfate forcing in a climate model with an interactive sulphur cycle, *J. Geophys. Res.*, 106, 20293–20310, 2001.
- Khain A. P., and Co-authors, 2015: Representation of microphysical processes in cloud-resolving models: Spectral (bin) microphysics versus bulk parameterization. *Rev. Geophys.*, 53, 247–322, doi:10.1002/2014RG000468.
- Kumar, P., Sokolik, I. N., and Nenes, A.: Parameterization of cloud droplet formation for global and regional models: including adsorption activation from insoluble CCN, *Atmos. Chem. Phys.*, 9, 2517–2532, doi:10.5194/acp-9-2517-2009, 2009.

- Lindner, T.H., and Li, J., Parameterization of the optical properties for water clouds in the infrared, *J. Climate*, 13, 1797-1805, 2000.
- Makar, P.A., Gong, W., Milbrandt, J., Hogrefe, C., Zhang, Y., Curci, G., Zabkar, R., Im, U., Balzarini, A., Baro, R., Bianconi, R., Cheung, P., Forkel, R., Gravel, S., Hirtl, H., Honzak, L., Hou, A., Jimenez-Guerrero, P., Langer, M., Moran, M.D., Pabla, B., Perez, J.L., Pirovano, G., San Jose, R., Tuccella, P., Werhahn, J., Zhang, J., Galmarini, S. Feedbacks between air pollution and weather, part 1: Effects on weather. *Atmospheric Environment*, 115, 442-469, 2015a
- Makar, P.A., Gong, W., Hogrefe, C., Zhang, Y., Curci, G., Zabkar, R., Milbrandt, J., Im, U., Balzarini, A., Baro, R., Bianconi, R., Cheung, P., Forkel, R., Gravel, S., Hirtl, H., Honzak, L., Hou, A., Jimenez-Guerrero, P., Langer, M., Moran, M.D., Pabla, B., Perez, J.L., Pirovano, G., San Jose, R., Tuccella, P., Werhahn, J., Zhang, J., Galmarini, S. Feedbacks between air pollution and weather, part 2: Effects on chemistry. *Atmospheric Environment*, 115, 499-526, 2015b
- Milbrandt, J.A., Yau, M.K., 2005a. A multimoment bulk microphysics parameterization. Part I: analysis of the role of the spectral shape parameter. *J. Atmos. Sci.* 62, 3051-3064.
- Milbrandt, J.A., Yau, M.K., 2005b. A multimoment bulk microphysics parameterization. Part II: a proposed three-moment closure and scheme description. *J. Atmos. Sci.* 62 (9), 3065-3081.
- Moran, M. D., Ménard, S., Talbot, D., Huang, P., Makar, P. A., Gong, W., Landry, H., Gravel, S., Gong, S., Crevier, L.-P., Kallaur, A., and Sassi, M.: Particulate-matter forecasting with GEM-MACH15, a new Canadian air-quality forecast model, in: *Air pollution modeling and its application XX*, edited by: Steyn, D. G. and Rao, S. T., Springer, Dordrecht, 289–292, 2010.
- Mulcahy, J. P., Walters, D. N., Bellouin, N., and Milton, S. F.: Impacts of increasing the aerosol complexity in the Met Office global numerical weather prediction model, *Atmos. Chem. Phys.*, 14, 4749-4778, <https://doi.org/10.5194/acp-14-4749-2014>, 2014.
- Morrison, H., Thompson, G., and Tatarskii, V.: Impact of Cloud Microphysics on the Development of Trailing Stratiform Precipitation in a Simulated Squall Line: Comparison of One- and Two-Moment Schemes, *Mon. Weather Rev.*, 137, 991–1007, 2009.
- Nenes, A. and Seinfeld, J. H.: Parameterization of cloud droplet formation in global climate models, *J. Geophys. Res.*, 108, 4415, [doi:10.1029/2002JD002911](https://doi.org/10.1029/2002JD002911), 2003.
- Niu, F., and Z. Li, 2012: Systematic variations of cloud top temperature and precipitation rate with aerosols over the global tropics. *Atmos. Chem. Phys.*, 12, 8491–8498, [doi:10.5194/acp-12-8491-2012](https://doi.org/10.5194/acp-12-8491-2012).
- Rosenfeld, D., 1999: TRMM observed first direct evidence of smoke from forest fires inhibiting rainfall. *Geophys. Res. Lett.*, 26, 3105–3108, [doi:10.1029/1999GL006066](https://doi.org/10.1029/1999GL006066).
- Rosenfeld, D., U. Lohmann, G. B. Raga, C. D. O'Dowd, M. Kulmala, S. Fuzzi, A. Reissell, and M. O. Andreae, 2008: Flood or drought: How do aerosols affect precipitation? *Science*, 321, 1309–1313, [doi:10.1126/science.1160606](https://doi.org/10.1126/science.1160606).
- Savijärvi, H.: Shortwave optical properties of rain, *Tellus*, 49a, 177– 181, 1997.
- Savijärvi, H. and Raisanen, P.: Long-wave optical properties of water clouds and rain, *Tellus*, 50A, 1–11, 1998.
- Savijärvi, H., Arola, A., and Räisänen, P.: Short-wave optical properties of precipitating water clouds, *Q. J. Roy. Meteor. Soc.*, 123, 883–899, [doi:10.1002/qj.49712354005](https://doi.org/10.1002/qj.49712354005), 1997.
- Seifert, A. and Beheng, K. D.: A double-moment parameterization for simulating autoconversion, accretion and self-collection, *Atmos. Res.*, 59, 265–281, 2001.

- Solomos, S., Kallos, G., Kushta, J., Astitha, M., Tremback, C., Nenes, A., and Levin, Z.: An integrated modeling study on the effects of mineral dust and sea salt particles on clouds and precipitation, *Atmos. Chem. Phys.*, 11, 873-892, <https://doi.org/10.5194/acp-11-873-2011>, 2011.
- Song, X., and G. J. Zhang, 2011: Microphysics parameterization for convective clouds in a global climate model: Description and single-column model tests. *J. Geophys. Res.*, 116, D02201, [doi:10.1029/2010JD014833](https://doi.org/10.1029/2010JD014833).
- Sun, Z. and Shine, K. P.: Studies of the radiative properties of ice and mixed-phase clouds, *Q. J. Roy. Meteor. Soc.*, 120, 111–137, [doi:10.1002/qj.49712051508](https://doi.org/10.1002/qj.49712051508), 1994.
- Twomey, S., 1974: Pollution and the planetary albedo. *Atmos. Environ.*, Vol. 8, 12, 1251-1256.
- Wang, H., X. Y. Zhang, S. L. Gong, Y. Chen, G. Shi, and W. Li, 2010: Radiative feedback of dust aerosols on the East Asian dust storms. *J. Geophys. Res.*, 115, D23214, [doi:10.1029/2009JD013430](https://doi.org/10.1029/2009JD013430).
- Zhou, C. H., X. J. Shen, Z. R. Liu., et al., 2018: Simulating aerosol size distribution and mass concentration with simultaneous nucleation, condensation/coagulation, and deposition with the GRAPES–CUACE. *J. Meteor. Res.*, 32(2), 1–14, [doi: 10.1007/s13351-018-7116-8](https://doi.org/10.1007/s13351-018-7116-8).
- Zhou C., X. Zhang, S. Gong, Y. Wang, and M. Xue, Improving aerosol interaction with clouds and precipitation in a regional chemical weather modeling system, *Atmos. Chem. Phys.* 16, 145-160, 2016, [doi:10.5194/acp-16-145-2016](https://doi.org/10.5194/acp-16-145-2016)

Chapter 4. Model Deployment and Application

4.1 Introduction

In this section, major types of CW-AQF applications along with differences in purposes for research and operational forecasting are introduced. Important aspects of CW-AQF model deployment and application along with factors to be considered are described. These include types and purposes of CW-AQF applications (Section 4.2), model selection (Section 4.3), model domain (Section 4.4), configurations in terms of coupling options, time steps, physical and chemical options (Section 4.5), computing platforms (Section 4.6), and downscaling from global to regional/urban scale (Section 4.7). Finally, Section 4.8 summarizes key points.

4.2 Types and Purposes of CW-AQF Applications

There are many possible applications of CW-AQF systems, e.g.:

- Air quality forecasting, assessments, and management
- Chemical composition analysis on global, regional, and local levels
- Haze/smog and chemical weather forecasting
- Numerical weather prediction for precipitation, visibility, thunderstorms, etc.
- Urban air quality and integrated urban meteorology, environment, and climate services
- Sand and dust storm modeling and warning systems
- Wildfire atmospheric pollution and effects
- Volcano ash forecasting, warning, and effects
- Multi-hazard early warning systems and disaster risk reduction
- Nuclear (and other chemical, biological) emergency preparedness
- Assessments and prediction of effects of short-lived climate forcings
- Earth system modeling and projections
- Data assimilation for CWF and NWP
- Weather modification and geo-engineering

The purpose of each of the above applications is different, which determines the model type and configuration used. This section will demonstrate the strategies and approaches on how to deploy and apply a global or a regional/urban CW-AQF model. The first step is to define the goal of a study.

For research purposes, the scientific representation is of great importance for a CW-AQF modeling system. The modeling system should have an ability to represent the microphysics of chemical and physical processes and large-scale transport of air pollutants. It should also have the ability to launch applications with a specific scientific focus such as the microphysics of aerosol nucleation, heterogeneous reactions, direct or indirect feedbacks from air quality to weather/climate, etc. A CW-AQF model with a detailed representation of aerosol microphysics and comprehensive gas chemistry would be more feasible for applications and the air pollutants impacting on air quality and climate. The online-coupled model framework would facilitate accurately forecasting the air pollutants in connecting the meteorology and air quality and has been used in the applications focusing on meteorology-air quality feedbacks.

For operational forecast purposes, the forecasting accuracy and stability, as well as the computational efficiency, should be more important for a CW-AQF modeling system. The model cannot be too complex and every component should be consistent with each other to promise a smooth run and ensure a stable and relatively high accuracy output routinely. This does not mean that it is easy to establish an operational CW-AQF modeling system. Before operational applications of the CW-AQF model, sufficient sensitive simulations and evaluation of prediction results should be performed for the modeling system to meet expected forecasting accuracy and time requirements. Even in operational simulations, it still needs a persistent improvement to ensure better accuracy and smooth running in the long term.

Many institutes can establish their own CW-AQF models. For those who do not have this kind of capability, the next step is to select the model and its physics and chemistry options, as well as running configurations once the purpose is determined.

4.3 Model Selection

The models can be categorized in different ways such as temporal and spatial scales and application purposes. In this part, we mainly focus on the temporal and spatial scales, which are a concept from meteorology. The spatial scale of a model means how much area the model domain can cover. Since the time scale has relations with the spatial scale, it would match with the spatial scale automatically. There are three types of CW-AQF modeling systems according to the spatial scale: global, regional, and urban. The global CW-AQF model covers the whole Earth, from -90°N to 90°S , from -180°W to 180°E . It can make simulations for at least 7 days, which is compatible with the lifetime of Rossby waves. The regional model can cover areas up to continental scales and usually extends to 3-day simulations, which are consistent with meso-scale weather systems. As for the urban scale, the covered area is relatively small, however, with a very high resolution to resolve the targeted urban area with enough detail to make the forecast information as useful as possible. It can simulate pollutants in small scale circulation systems and phenomena in the urban area such as the heat island, the urban canopy, or more detailed street canyon streams. This type of model is more important for air quality and health impact warnings.

We can either choose one model for one scale or for different scales. There is not much to say about a model for fixed one scale and we would stress a little more for a model for different scales. A model useable at different scales is called a multi-scale CW-AQF model, and has been developed on the basis of comprehensive multi-scale weather models. It can be applied from global to urban scale, and all scales in between (e.g., global to regional or regional to urban). As it is tailored to simulate both weather systems and air quality at different scales in one model, self-adaptation of downscaling can be realized in one such model from a larger scale to a smaller one or vice versa.

4.4 Application Domain

A model domain is a more or less rectangular area, for which the weather is calculated in three dimensions. The model domain of CW-AQF is the same as that of a weather model for which chemical weather is calculated. It should be set at the very beginning of the model application. The horizontal size of a domain is determined according to the spatial scale of the application with the targeting area in the heart of the domain. The domain is divided into grid cells shaped as triangles, rectangles, pentagons or hexagons and the length of the cell line is called model resolution. The smaller the length of the grid line, the higher the model domain resolution. For one fixed model domain, the higher the resolution, the more precise the results are in general but more computationally expensive. Therefore, a balance exists between the two. The vertical length of a domain should be tailored for the size of the horizontal size to cover most vertical motion of the air and the physical and chemical processes the model represents. It is usually unequally divided into different layers, denser near the surface layers. Chemical transformation, physics changes, and transport of tracers and atmospheric fields are calculated on the grid for each layer of the model.

Global models do not have lateral boundaries but regional and urban scale models do. For these models, the horizontal domain size should be as large as it could be to reduce the truncation error from the boundaries and to include the impacts of transport from upstream areas to the targeting area.

One also needs to determine if a single domain or nested domains should be used.

4.4.1 *Single Domain*

A model runs at least in one single domain. In the regional model, there is only one set of boundary conditions for four bilateral boundaries, the top, and the surface. The single domain can be uniformly gridded or graded gridded. For uniform domains, the only way to improve the precision from the point of numerical calculation is to increase the model resolution to meet the model application precision. The resolutions cannot be set as high as we expect because of the computing limitations. While for a graded resolution model, it can increase the resolution of the targeting center area and keep coarse resolution for the outline areas to keep the balance between the accuracy and the computing requirements. Examples of a single uniform and graded domain are shown in Figures 4.1 and 4.2.

4.4.2 *Nested Domain*

Some models run in nested domains. The nested domains are like Matryoshka dolls, the larger one contains the inner one. The inner one should be at a higher resolution than the larger one. We can set the domain in several nested domains to get as high resolution as computationally possible to meet the model application precision. It is another way to save computing but still to get precise results. It is important to handle the boundaries of these neighboring Matryoshka dolls to reduce truncation errors. The grid length can be three times between the neighboring nested domains which can promise a geometric series integration time steps and more adaptive boundaries between the mother domain and the nested domain. An example of a nested domain is shown in Figure 4.1.

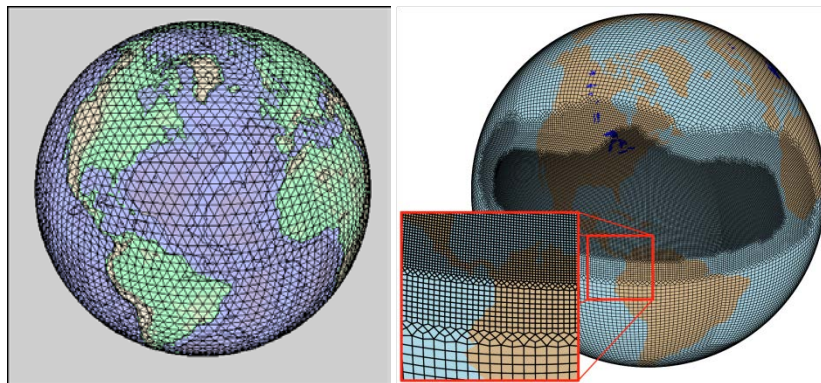


Figure 4.1 A uniform domain (left) and graded domain or adaptive mesh refinement (right) (Zarzycki and Jablonowski, 2014, 2015).

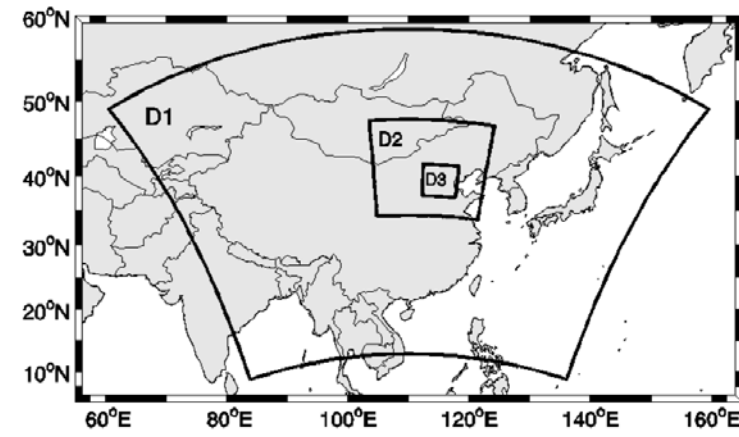


Figure 4.2 A nested domain covering most of China and parts of East Asia (An et al., 2011).

4.4.3 Defining Domains for Countries

The size of a model domain is usually in quadrilateral and cannot be exactly tailored to the boundaries of one country, hence the targeting domain for a country may be the center part of a single domain or the innermost domain of the nested domains. In terms of application, outputs for the targeting domain can be interpolated exactly to the size of one country just as most national weather forecast bureaus do.

4.5 Configurations

CW-AQF models are comprehensive modeling systems that usually contain numerical ways to solve atmospheric and chemistry processes. There is always a parameter table in which we can set the configurations, one of which represents one process or one numerical scheme or the model domain settings. Here we would go a little further to try to understand how to choose some of the configurations.

4.5.1 Coupling Options (1- or 2-way)

The 1-way coupling for CW-AQF is mostly used in offline and some online-coupled modeling systems. The driving weather model supplies atmospheric boundary conditions and initial conditions for the coupled chemical models and the chemical model would not feedback the chemical fields to the mother weather model.

The 2-way coupling for CW-AQF modeling is mostly used in air quality and weather and climate interactions. In 2-way coupling, the chemical fields can be exchanged through the interface between the weather model and air quality modules. It is more feasible for chemical weather modeling since the atmospheric compositions can change the atmospheric state by interacting with radiation, cloud, and precipitation processes in the meteorological models.

It is very important to choose the right interpolation schemes to get more correct meteorology and more adaptive conditions for the air quality fields just as described in previous chapters.

4.5.2 Time Steps

Time step is the time difference to integrate the discrete differential equations of the air quality fields. It is another decisive element for resulting model precision and computing time. Larger time step means shorter computing wall time to run the model but coarse precision, and vice versa. There is also a balance between the shorter time step, stability, and precision. The time step must first satisfy the stability conditions in case the model overflows and breaks into chaos. The time step should meet the Courant-Friedrichs-Lewy (CFL) stability condition which

is in proportion to the model grid length and is inversely proportional to the characteristic wind speed. The higher model resolution means smaller time steps and a longer computing time. The time step is also adjusted to the integration schemes of a model. In an implicit scheme, it can be much longer than the basic time step decided by the CFL conditions.

For CW-AQF modeling systems, basically the time step is the same as that in the weather model. But for some microphysics like aerosol coagulations, the time steps can be set to be half an hour or longer, much longer than the time step in general used by weather models. For some fast chemical reactions, the time step must be much shorter than the time step in the weather model.

4.5.3 *Physical Options*

The principle to select the schemes for PBL, radiation, cloud physics, and sub-grid parameterizations for a weather model depends on the ability of the weather model itself. In a comprehensive weather model, there should be several choices for each of these physics schemes. Sensitive simulations are necessary to get the "best" meteorology. The offline and 1-way coupling CW-AQF modeling system can share the "best" meteorology. For online modeling system, there is a different meaning for the "best" meteorology. Because weather models pay more attention to basic fields of wind, temperature, humidity, wind and pressure, the best meteorology means these variables can favor the simulations of extreme weather events such as heavy rainstorms or gales, etc. While in the CW-AQF modeling system, the extreme weather is the static condition which favors pollutant formation and accumulation, in this case the weather is peaceful without any rains or gales. Furthermore, there are many uncertainties for the static weather simulation especially for the diffusion in the PBL. The basis to determine the physics schemes for the best meteorology for a CW-AQF modeling system is different from that for the pure weather model.

As the aerosol interactions with the cloud and radiation are more important currently and in the near future, the ability to include the feedback of air quality in the schemes of the PBL, radiation, cloud physics, and sub-grid parameterizations would be more demanding in CW-AQF model applications.

4.5.4 *Chemical Options*

Almost every CW-AQF modeling system provides chemical options of gas, aqueous and aerosol schemes. Most detailed options include the ability to simulate the heterogeneous chemistry and thermodynamics to get better simulations. Some models may have the ability to simulate the aerosol feedback on weather through radiation and interactions with clouds and precipitation. The complexity of the chemical options depends on the number of gaseous species and the resolution of the size distribution of aerosols. The types of gases such as VOCs and non-VOCs have not been clearly identified by scientists. For aerosols, there are three ways to depict the size distribution: continuous, sectional (or bin), or modal among which the continuous way is the most complex and the modal is the least complex while the sectional approach lies in between. The complexity of the chemical choices also depends on the complexity of the radiation schemes and the cloud physics since cloud physics can also be described in bulk, moments, or bin approaches. The interactions between aerosol and ice nucleus remain poorly understood. Table 4.1 shows the chemical options selected for GRAPES-CUACE applications.

Table 4.1 Chemical Options selected for GRAPES-CUACE.

Chemical options	
Gas Chemistry	RADM2
Aqueous-Phase Chemistry	RADM
Aerosol Module	CAM
Inorganic Aerosol Thermodynamics	ISORROPIA
Secondary Organic Model	AERO6
Aerosol Direct Effect	Yes
Aerosol Indirect Effect	Yes

4.6 Computing Platforms

Many comprehensive CW-AQF modeling systems can be run in a parallel way which means that they can run with multiple processors on a single computer or on supercomputers with many nodes and many processors at one node. It also comes from the way the weather model runs. If the weather model can run in parallel mode, the air pollutants and the feedbacks can run in the same way. In a way, the chemical or aerosol module seems like one physical scheme in a weather model. All the computing for this special physics module can be performed on one grid. As the weather model compiles and runs in a parallel way, the chemical modules can also run in parallel automatically.

4.6.1 Multi-Processors

In parallel way, the model domain is divided into several sections like many rooms in one building. Each 'room' contains some model grids and run in it. When some numerical calculations need the data from the neighboring room, they would be transferred by the computers automatically with no need for artificial interference. It is an art to select how many processors should run the model since although more processors mean fast computing, the time to transfer the data between the boundaries of the processors would grow. There is an optimal option to select how many processors by considering the model domain grids and computing speed of one processor and the data transfer speed between processors. Sensitive tests should be performed to achieve an optimal choice of computing node and efficient computing time before a routine operation.

4.6.2 Cloud Computing

Cloud computing is to do computation on more than just one supercomputer. It can select the computer sources from everywhere it can. Nowadays it is not so widely used in weather and climate computing, more precisely, it is more like an expanded idea from traditional one supercomputer computing.

4.7 Downscaling of Global Forecast Products for Regional/Urban Forecasting

In this section, downscaling means the application of the numerical model results to even smaller spatial and temporal scales. As described above, the outputs can be downscaled to the targeting domain directly by increasing the resolution of the whole uniformed grids and the center part of graded grids in one single domain. The downscaling can also be done in the innermost domain for the nested domains.

The outputs of larger spatial scale models can also be interpolated to the targeting smaller areas or shorter time periods. It can be used more widely through statistical methods to obtain high resolution and high precision results. It can also be further improved to higher precision by considering the synoptic pattern by the forecaster.

4.8 Summary

- The strategies and approaches on how to deploy and apply a global or a regional/urban CW-AQF model are demonstrated;
- For research purposes, the scientific representation is of great importance for a CW-AQF modeling system;
- For operational forecast purposes, the forecasting accuracy and stability, as well as the computational efficiency, should be more important for a CW-AQF modeling system;
- The steps for the model selection, model domain, model configurations are described;
- The information about computing platforms and downscaling of global forecast products to the applications of regional/urban forecasting is presented.

References

- Drake, J B , and I. T. Foster . Introduction to the Special Issue on Parallel Computing in Climate and Weather Modeling. Elsevier Science Publishers B. V. 1995.
- Gong, S. L., L. A. Barrie, J.-P. Blanchet, et al., 2003: Canadian aerosol module: A size-segregated simulation of atmospheric aerosol processes for climate and air quality models 1. Module development. *J. Geophys. Res.*, 108, 4007, doi: 10.1029/2001JD002002
- Li, P.F., Wang, L.Q., Guo, P., Yu, S.C., Mehmood, K., Wang, S., Liu, W.P., Seinfeld, J.H., Zhang, Y., Wong, D.C., Alapaty, K., Pleim, J., Mathur, R.(2017) High reduction of ozone and particulate matter during the2016 G-20 summit in Hangzhou by forced emission controls of industry and traffic. *Environ Chem Lett* 15: 709–715.
- Li, Y. , An, J. , Min, M. , Zhang, W. , Wang, F. , & Xie, P. . (2011). Impacts of HONO sources on the air quality in Beijing, Tianjin and Hebei province of China. *Atmospheric Environment*, 45(27), 4735-4744. doi: 10.1016/j.atmosenv.2011.04.086
- Niu, T., S. L. Gong, et al. (2008). Data assimilation of dust aerosol observations for the CUACE/dust forecasting system. *Atmos. Chem. Phys.* 8: 3437-3482.
- Ridwan, R. , Imam, A. , Kistijantoro, Kudsy, M. , & Gunawan, D. (2015). Performance Evaluation of Hybrid Parallel Computing for WRF Model with CUDA and OpenMP. *International Conference on Information & Communication Technology*. IEEE.
- Wong, D. C., Pleim, J., Mathur, R., Binkowski, F., Otte, T., & Gilliam, R., et al. (2012). WRF-CMAQ two-way coupled system with aerosol feedback: software development and preliminary results. *Geoscientific Model Development Discussions*, 5(2), 299-312. Wang, H., X. Y. Zhang, S. L. Gong, et al., 2010: Radiative feedback of dust aerosols on the East Asian dust storms. *J. Geophys. Res.*, **115**, D23214, doi: 10.1029/2009JD013430.
- Yu, S., Mathur, R., Pleim, J., Wong, D., Gilliam, R., and Alapaty, K., et al. (2014). Aerosol indirect effect on the grid-scale clouds in the two-way coupled WRF-CMAQ: model description, development, evaluation and regional analysis. *Atmospheric Chemistry & Physics*, 13(10), 25649-25739.
- Zarzycki, Colin M. , and C. Jablonowski . A multidecadal simulation of Atlantic tropical cyclones

using a variable-resolution global atmospheric general circulation model. *Journal of Advances in Modeling Earth Systems* 6.3(2014):805-828.

- Zarzycki, C.M., C. Jablonowski, D. R. Thatcher, and M. A. Taylor (2015), Effects of localized grid refinement on the general circulation and climatology in the Community Atmosphere Model. *J. Clim.*, 28(7), 2777-2803. doi:10.1175/JCLI-D-14-00599.1.
- Zarzycki, Colin M. , and C. Jablonowski . Experimental Tropical Cyclone Forecasts Using a Variable-Resolution Global Model. *Monthly Weather Review* 143.10(2015): 4012-4037.
- Zhou, C., X. Zhang, et al. (2016). Improving aerosol interaction with clouds and precipitation in a regional chemical weather modeling system. *Atmospheric Chemistry and Physics*, 16(1): 145-160.
- Zhou, C.-H., Gong, S., Zhang, X.-Y., Liu, H. L., Xue, M., Cao, G. L., An, X. Q., Che, H. Z., Zhang, Y. M., and Niu, T.: Towards the improvements of simulating the chemical and optical properties of Chinese aerosols using an online coupled model CUACE/Aero, *Tellus B*, 64, 18965, <http://dx.doi.org/10.3402/tellusb.v64i0.18965>, 2012.
- Zhou, C. H., Gong, S. L., Zhang, X. Y., Wang, Y. Q., Niu, T., Liu, H. L., Zhao, T. L., Yang, Y. Q., and Hou, Q.: Development and Evaluation of an Operational SDS Forecasting System for East Asia: CUACE/Dust Atmos. Chem. Phys, 8, 1-12, 2008.

Chapter 5. Special Considerations for Urban Applications

5.1 Introduction

In this chapter, we recognize the need for myriad “Fit-for-Purpose” urban model applications with applicability on a worldwide basis to address climate change, population growth, urban planning needs and a host of other issues. Optimally, for each and every model application, the fitness for purpose context must necessarily be scale (spatial) and seasonally appropriate, applicable to specific geographic and climatic conditions. Model results are resolved according to their grid sizes, i.e., the subgrid resolution is unresolved; typically, model nesting is based on fixed rectangular grid structure or adaptive-type gridding thus providing the means to improve the resolution of such variations. Even so, it is important that all inputs including initial and boundary conditions, model physics and land use descriptions are appropriate to the scale being used. This is especially important for the unique challenges posed in urban contexts due to the inherent complexities of the built form and materials of the multiple and heterogeneous urban morphological structures distributed throughout the urban surface, and their wide variety of use and functional activities. Recent insights and developments have introduced grid-based urban canopy parameterization (UCP) schemes thus providing explicit treatment of flow and thermodynamic effects of complex building morphology distributions in modeling urban boundary layers (described in Chen et al. 2010 and Ching (2013). This framework ameliorates the limitation of roughness and stability-based Reynolds-Average Navier Stokes (RANS) model-based physics that typically ignore these grid-by-grid morphological variations. Figure 5.1 lists and depicts schematically a variety of important urban effects including radiative trapping, turbulent transport and drag effects, and the anthropogenic energy production attributable to the presence of the morphological structure of buildings (and in the presence of vegetation) in the urban canopy. The degree of variation in the form and function of these features will control these effects and their role throughout the canopy layer; the resulting impact of spatially varying morphological characteristics (introduced as UCPs) on the urban boundary layer is a function of the speed and direction of the flow modulated by the presence of clouds and is moreover, scale and height dependent. Likewise, the input data must be commensurate in scale, geography, and climate appropriate. Given the infra-spatial complexity of urban areas for each grid resolution in models, there can be a significant degree of subgrid variations. By scale-dependent resolution, we mean that various models have incorporated the atmospheric processes appropriate to the grid resolution for the predicted variables, e.g., meteorological fields, chemical species, pollutant deposition, etc. By subgrid, we mean to indicate significant variations to such fields present at finer grid sizes, but clearly not made explicit at the parent grid. Likewise, different model treatments may be required for local to regional differences in terrain and climate.

In Section 5.2 we present some characteristics of urban scale forecasting primarily advanced in current operational schemes. Section 5.2 introduces the provisions for incorporating the canopy framework including information on urban morphology and metabolism, three-dimensional urban structure, some insights on initial and boundary condition issues, resolution limitations, supporting data, interactions with mesoscale circulations and possible relations to climate change. Section 5.3 shows some features related to urban meteorology such as urban heat islands, including air quality, urban parameterizations and environmental comfort issues, the very complex problem of urban emissions (heat and pollution), the consequences of urban growth, especially on atmospheric patterns. Section 5.4 introduces urban canopy models (UCM) and focuses on the reasons behind the meteorological impacts of cities and urban settlements on the local and mesoscale flows. UCM is presented, stressing approaches, considerations, advantages and disadvantages on its use, some data requirements and infrastructure support, and applicability of the local climate zones (LCZ) approach. Also, this section presents modeling systems and some applications. In Section 5.5, we discuss the interaction between atmosphere and urban surfaces’ induced complex flow patterns in the urban canopy layer. This fact, linked to the irregular distribution of emissions, mainly from traffic, throughout a city produces strong spatial heterogeneities (on the order of meters) in pollutant concentrations at pedestrian level. To capture these heterogeneities and quantify population exposure to air pollution, the coupling between a mesoscale and a microscale model, whose spatial resolution is of the order of 1 m, is necessary. Section 5.6 addresses

model input data requirements on urban canopy features including the building’s morphological form, material composition and activity. In particular, they are demonstrated with an example of a major international community-based project, the World Urban Database and Access Port Tool (WUDAPT). WUDAPT is, by conceptual design and scope, to provide the means, framework and infrastructure capable of supporting a wide range of “fit for purpose, and scale dependent ” grid-based environmental modeling applications (such as air quality forecasts) customized for use anywhere in the world. The suggested implementation strategy is based upon a hierarchical structure to provide increasing information and precision, yet responsive towards addressing climate change and urbanization issues in a reasonable time frame.

References

Ching, J., D. Aliaga, G. Mills, V. Masson, L. See, M. Neophytou, A. Middel, C. Ren, E. Ng, Y. Huang, I. Stewart, J. Fung, M. Wong, X. Zhang, A. Shehata, A. Martilli, S. Miao, X. Wang, D. Duarte, L. Schwandner, W. Wang, Y. Li, B. Bechtel, and 24 others, 2019, Pathway using WUDAPT’s Digital Synthetic City tool towards generating urban canopy parameters for multi-scale urban atmospheric modeling. In press: WUDAPT Special Issue of Urban Climate.

Oke, T.R. 1997, Urban Climates and Global Environmental Change. In: Thompson, R.D. and A. Perry (eds.) Applied Climatology: Principles & Practices. New York, NY: Routledge. pp. 273-287.

Oke, T., G. Mills, A. Christen, and J.A. Voogt, 2017, Urban Climates, Cambridge University Press, DOI: 9780521849500.

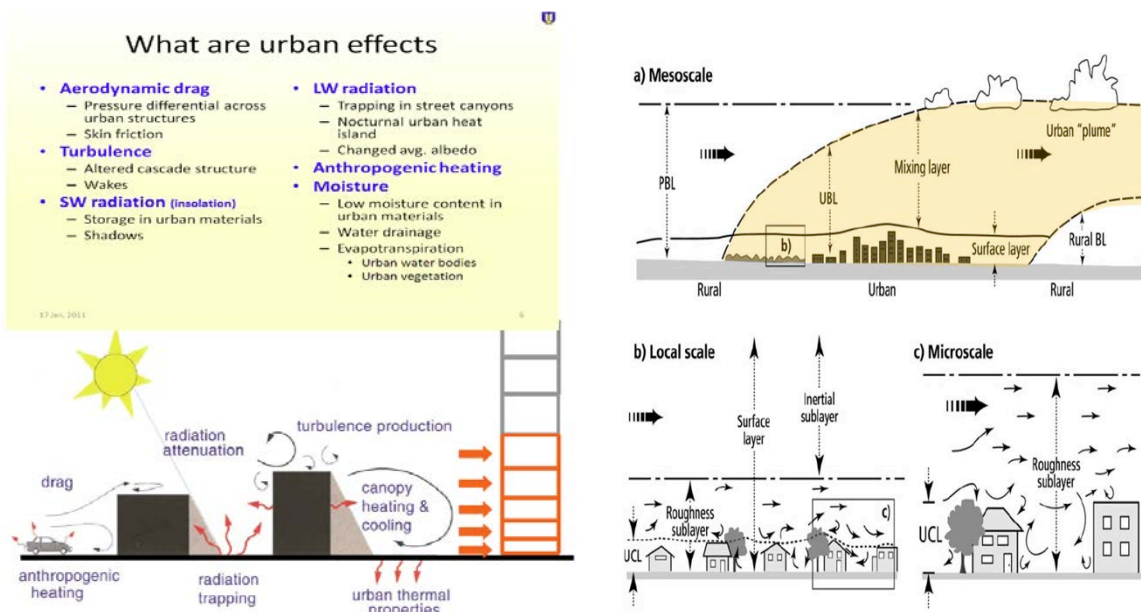


Figure 5.1. Urban effects and idealized urban canopy structure and scales incorporated as science codes into urbanized mesoscale forecasting modeling systems (Source: Ching et al., 2019; Oke, 1997; and Oke et al., 2017).

5.2 Characteristics of Urban Scale Forecast Models

5.2.1 Introduction

Urban models provide an important means to assess the nexus of (a) population growth and (b) climate change, two of the major issues confronting today's society. Urbanization and climate change on regional and global scales are linked. Urban areas are major contributors to the atmospheric greenhouse burden, including carbon, non-methane hydrocarbon (NMHC) and photochemical species (e.g., ozone). In turn, it is believed that climate change will be manifested in cities and elsewhere in a variety of direct and subtle ways, e.g., by more extreme and adverse weather events, such as heat waves, droughts, and increases in the degree of thunderstorm severity. It is also highly probable that the intensity of heat islands coupled with the degree of imperviousness and building heights and density will further modulate convective activity, the initiation and/or severity of thunderstorm activity and thus, its hydrology. Computer models provide the tools for predicting climate and air quality.

Air quality is one of the most pressing urban issues, which has long been studied and modeled for planning purposes. Air pollution is a mixture of different chemicals both locally emitted and from transported regional sources. The concentrations of air pollution from local sources as well as the mixing of pollution from regional sources are controlled by the transport and dispersion capability of the flow field in the urban canopy layers and in turn by the vertical structure of the urban mixed layer.

Weather and air quality forecasts are known to be a great challenge not only for scientists but also for policy makers, rulers, and other people that depend on such forecasts for managing their activities. Much of the difficulties found in making a forecast are related to the grid scale of the forecast, the physical representation of urban features, such as its three-dimensional structures, type of construction materials, artificial sources of heat, among others. In this section, some characteristics of urban areas and the supporting state of science options for forecast models will be addressed. While this section focuses on describing the considerations and specific processes necessary to address weather and air quality forecasts, much of the same applies in developing a model to predict climate and air quality.

In this sub-section, we address important features regarding urban scale forecast models. The main goal is to focus on describing considerations and specific processes important to weather and air quality forecasting, although much of the information can be applied as well to climate studies. Main topics of the sub-section include: details on urban morphology and metabolism; 3-D structure; initial and boundary conditions; resolution limitations; urban modeling science and supporting data; and interactions with mesoscale circulations, and exacerbations with respect to climate change.

5.2.2 Urban Morphology and Metabolism

Urban areas interact at many scales with the atmosphere through their morphological form and metabolisms from human activities and functions. Urban morphology is the physical form of the city including the dimensions and fabric of roads, buildings, parks, etc. and their geographical distribution. Urban metabolism refers to the human activities and transits requiring and releasing energy and pollutant wastes into the overlying atmosphere. The extent and the morphological structure of cities create a unique spatial and temporal influence on the vertical thermal and turbulence layers, which induces complex intra urban flows (ventilation). These changes regulate the transport and dispersion of pollution from local and upwind regional sources, which affects human comfort and health.

5.2.3 3-D Urban Structure

In any type of urban area, small or a megacity, its three-dimensional structure and complexity of the underlying surface constitutes a huge scientific and computational challenge in numerical models used for forecasts. Part of this challenge is linked to the scale of urban structure and those allowed in the models in order to provide the interested meteorological (temperature, moisture, wind, etc.) and chemical (ozone, particles, and others) fields of interest in time. Since model resolution improvement implies smaller time steps, there is a practical limit for the inclusion of many urban features. Usually, horizontal grid spacing from the order of a few kilometers is used in the forecast centers around the world. At such horizontal scale, some urban features cannot be explicitly represented; that is the case for features such as walls, roofs, street width and orientation (Figure 5.2), and the differences among a large number of buildings or any kind of construction, cannot be explicitly considered.

A way of representing urban structure in the models is to consider a model grid with mean characteristics found in an idealized urban canyon approach (e.g., Masson, 2000). In this approach urban features are predetermined for a specific urban type, identified in the model through its land use file, a database that “tells” the model what the surface is composed of. Each predefined urban type has a specification of construction material properties, such as thermal conductivity, heat capacity, albedo, emissivity, and depth of walls, roofs and roads, among others. Table 5.1 shows some characteristics of materials used in urban areas.

Besides building materials, three-dimensional urban structure is also a very important feature in urban areas when one needs to consider the complex interaction with solar and terrestrial radiation, as shown in Figure 5.3. Basically, two processes must be taken into account to consider this interaction: 1) multiple or simple reflections of solar radiation by walls, roads, and roofs; 2) absorption of solar radiation (short wave) by the same surfaces and re-emission of the absorbed energy in the form of terrestrial radiation (long wave). The energy stored in an urban canyon is increased by some anthropogenic sources. Examples of these sources are air conditioning systems, coal or wood burning for industrial, commercial or domestic use, vehicle engines, and animal metabolism, among others. Finally, another important feature that must be considered in urban areas, especially because of its interaction with short and long wave radiation, is the emission of air pollutants, mainly by vehicles and industries. Some gases like carbon monoxide, sulfur oxides, nitrogen oxides, volatile organic compounds, and particulate matter of different sizes ($PM_{2.5}$ and PM_{10}), participate in the tropospheric energy budget by absorbing solar and terrestrial radiation and modifying the vertical thermal structure of the urban boundary layer.



Figure 5.2. View of the city of São Paulo, Brazil, illustrating the very complex 3-D structure of an urban area.

Table 5.1 Properties of Building Materials

Material	Density (g cm ⁻³) ¹	Porosity (%) ¹	Thermal Conductivity (W m ⁻¹ K ⁻¹) ²
Steel	7.85	--	16-43
Granite	2.5~2.7	0~0.3	1.7-4.0
Limestone	2.6~2.8	0.5~3.0	1.26-1.33
Gravels	2.6~2.9	--	0.7
Ordinary Sand	2.6~2.8	--	0.15-4
Sintered Clay Brick	2.5~2.7	20~40	0.15-1.31
Ordinary Concrete	2.1~2.6	5~20	0.1-1.8
Asphalt Concrete	2.3~2.4	2~4	0,75
Wood	1.55	55~75	0.055-0.17

1. adapted from Zhang (2011)
2. adapted from www.engineeringtoolbox.com

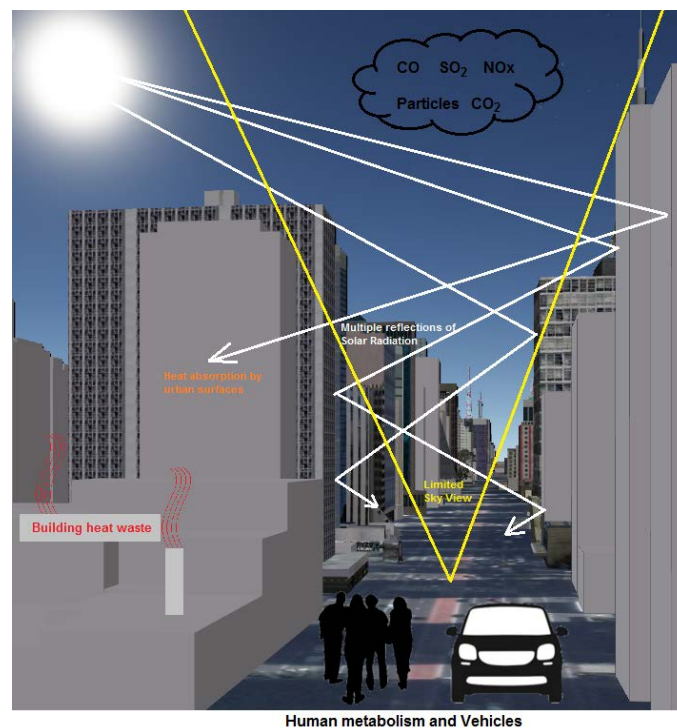


Figure 5.3. Three-dimensional urban structure and the main components of energy budget.

5.2.4 Initial and Boundary Conditions

As an initial value problem, weather and air quality forecasts are very dependent on the observational network available. Although it is impossible to have a real observed value of temperature, wind, pressure and any atmospheric compound in every horizontal or vertical grid point, data assimilation systems must be developed in order to provide the appropriate initial conditions for the models. In the case of regional or limited area models (also known as mesoscale models), where a small part of the global domain is considered for the forecast in a higher horizontal resolution (in the order of a few kilometers), it is also necessary to provide boundary conditions, not only during the initial time but also along the whole period of integration. In this case, the use of atmospheric fields provided by global models is the normal procedure during weather and air quality forecasting. Examples of global models are the Global Forecast System (GFS, <https://www.ncdc.noaa.gov/data-access/model-data/model-datasets/global-forecast-system-gfs>), from the National Centers for Environmental Prediction (NCEP), and the Integrated Forecast System (IFS) from the European Centre for Medium-Range Weather Forecasts (ECMWF, <https://www.ecmwf.int/>) and others.

5.2.5 Resolution Limitations

Most of the urban features are at the scale of a few meters. For example, mean values for constructions in suburban areas are on the order of 5 or 10 meters. High-rise buildings have a height of 50 to 100 meters. Of course, these values are very dependent on several factors, like economy, topography, climate, and social development. However, independent of these factors, one key feature is a common limitation to weather and air quality forecast: it is not possible to integrate the models operationally in such high resolution. The limitation is mostly due to the technology and computational resources available and, in some degree, to the lack of knowledge on urban scale processes, such as turbulence and nonlinear interactions among surface fluxes. In that sense, mean grid spacing applied in weather and air quality forecasts are around 5 to 10 kilometers. In some cases, urban canopy models are now available based on horizontal grid spaces as low as 1 km or less (Chen et al., 2010). Considering the current situation, with models using grid spacing of this order, how well can urban features be represented by the models?

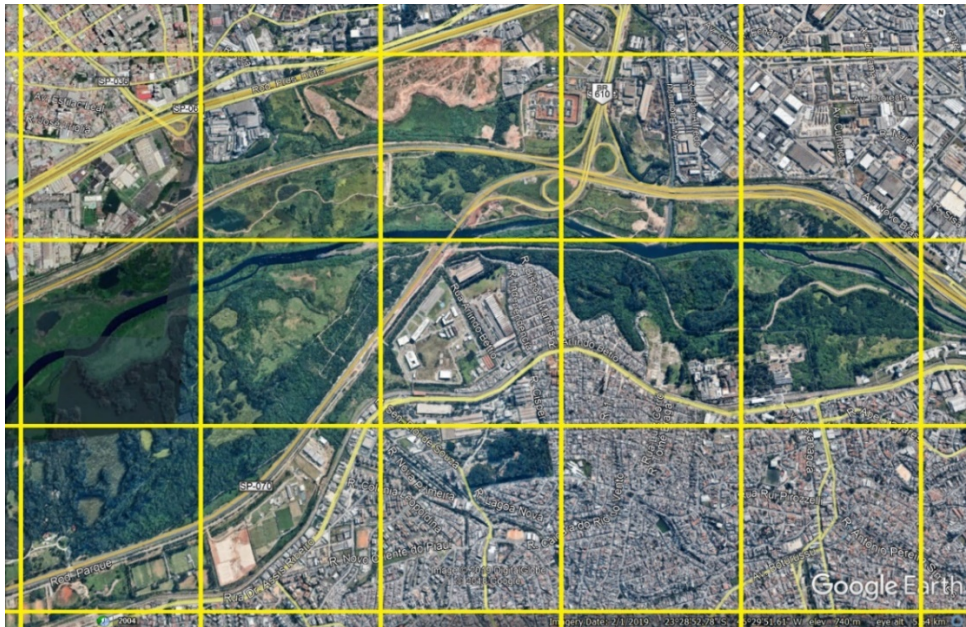


Figure 5.4. Satellite picture in a very heterogeneous urban region. Yellow line grid was constructed using 1 km spacing.

Source: Adapted from Google Earth Pro V 7.3.2.5776. (March 5, 2019). São Paulo, Brazil. 23° 28' 52.78" S, 46° 29' 51.61"W, Eye alt 5.54 km. Digital Globe 2019, Google 2018. <https://www.google.com/earth/> (Jan 2, 2019).

In Figure 5.4 we can see a very heterogeneous urban region in South America, from which it is possible to identify green areas, very dense residential areas, commercial and industrial regions, roads, streets, water bodies and many other features. For a numerical model this high number of different aspects cannot be explicitly treated; a current approach is to establish mean characteristics for each grid horizontal volume. A common procedure for determining these mean features is made through the use of land use/land class files. Figure 5.5 shows an example of a land use/land class file constructed based on the urban area presented in Figure 5.4. Instead of representing each urban feature, each grid volume is defined by its mean or predominant characteristics, including vegetation and water fraction, building height, roughness, albedo, emissivity, and other characteristics, based on observations. These characteristics are then listed in a lookup table available in the models' code. In that sense, a green box in Figure 5.5, for example, would be representative of a green area, such as a park, while a red grid box would be representative of a residential area, and so on.

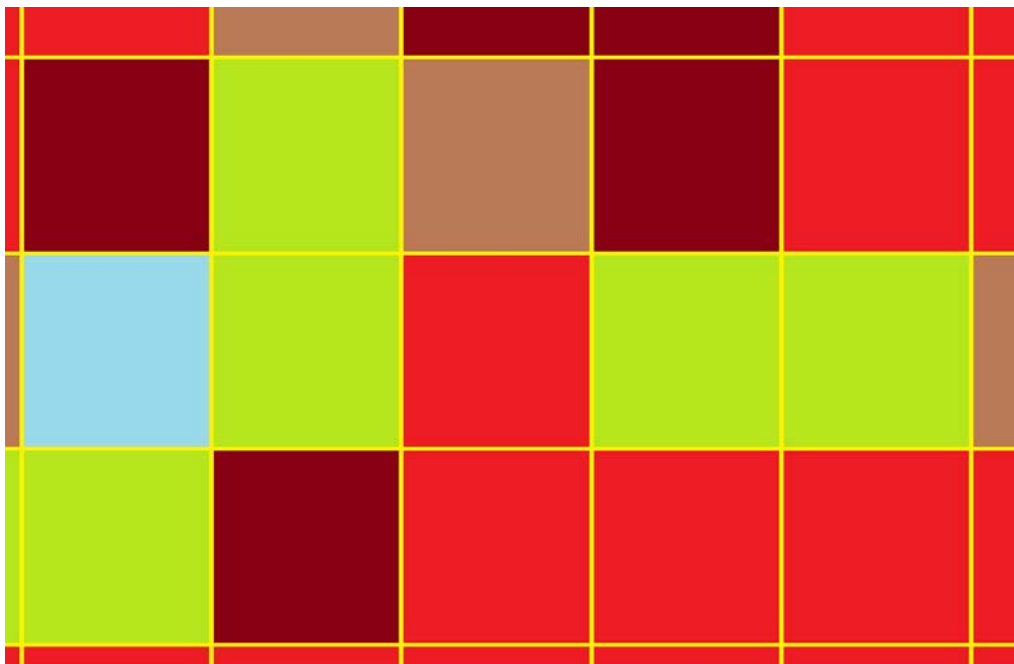


Figure 5.5. Example of a land use/land class file used in numerical models to identify surface characteristics, including urban features. As in Figure 5.4, grid was constructed using 1 km spacing.

5.2.6 *Urban Modeling Science and Supporting Data*

The development of models dedicated to address urban issues requires a good set of data regarding urban structure and many other characteristics. There are important initiatives in that direction providing a more detailed atmospheric dataset, e.g., temperature, wind, pressure, and moisture from different sources, like surface observations or satellite retrieved values, and also providing important parameters that describe urban features in an aggregate manner that can be introduced into urban scale models with corresponding physical options in single and multi-layer urban canopy models (Ching et al., 2018). Data is currently being generated to support such modeling (<http://www.wudapt.org/>) on a worldwide basis. Further details can be found in Section 5.6.

5.2.7 *Interactions with Mesoscale Circulations, and Exacerbations with Respect to Climate Changes*

Many studies have addressed the interactions between urban-caused circulations, the so-called urban heat island circulation, and other mesoscale circulations like land and sea breezes and mountain-valley ones. These interactions sometimes can be the cause of thunderstorm development (Freitas et al., 2009; Vemado and Pereira Filho, 2016) or of very critical air pollution episodes (Yoshikado and Tsuchida, 1996). Yoshikado (1994), in a study for the urban region near Tokyo Bay, identified that the urban heat island may persist and interact with the sea breeze, causing convergent outflow patterns, appearing more clearly in coastal cities. Inland penetration of sea breeze can be accelerated by several hours due to the urban thermal effect, which produces a similar flow to the sea breeze, as identified in some studies (e.g., Khan and Simpson, 2001; Freitas et al., 2007). It can also be decelerated, depending on the location of the sea breeze front in relation to the urban heat island (UHI) (Freitas et al., 2007). Interactions with the region's topography can also modify the sea-breeze-front propagation by its association with mountain-valley circulations (Freitas, 2003). Effects of the interactions between UHI and other mesoscale circulations can be critically increased if we consider that most cities are growing. Intensification of urban effects would contribute to regional and global climate change, including the intensification of floods, heat waves, air quality issues, and other extreme weather events. Therefore, the development of better modeling tools for air quality and weather forecasts represents a great demand for scientists and governmental policies.

5.2.8 *Summary*

- Urban areas interact at many scales with the atmosphere through their physical form, geographical distribution and metabolisms from human activities and functions.
- Three-dimensional structure is an important feature to define temperature, humidity, wind flow and pollutant concentrations inside urban areas. In most cases, this feature cannot be explicitly considered, being necessary some approaches, such as the canyon one, to deal with it.
- Weather and air quality forecasts are very dependent on initial and boundary conditions. Data assimilation systems must be developed in order to provide the ideal information for the models.
- Although computational resources have greatly improved, time and spatial resolution is still imposing some limitations on the correct representation of urban features.
- Urban areas are responsible for mesoscale circulations, the urban heat island circulation, which interacts with other mesoscale circulations, such as the sea-breeze and mountain-valley circulations. Since cities are still growing, intensification of urban effects are expected to increase, contributing to regional or global climate change, including intensification of floods, heat waves, air quality issues, and other extreme weather events.

References

- Chen, F., Kusaka, H., Bornstein, R., Ching, J., Grimmond, C.S.B., Grossman-Clarke, S., Loridan, T., Manning, K.W., Martilli, A., Miao, S., Sailor, D., Salamanca, F.P., Taha, H., Tewari, M., Wang, X., Wyszogrodzki, A.A., Zhang, C., 2010. The integrated WRF urban modeling system: development, evaluation, and applications to urban environmental problems. *Int. J. Climatol.* 31, 273–288.
- Ching, J., G. Mills, B. Bechtel, L. See, J. Feddema, X. Wang, C. Ren, O. Brousse, A. Martilli, M. Neophytou, P. Mouzourides, I. Stewart, A. Hanna, E. Ng, M. Foley, P. Alexander, D. Aliaga, D. Niyogi, A. Shreevastava, P. Bhalachandran, V. Masson, J. Hidalgo, J. Fung, M. Andrade, A. Baklanov, W. Dai, G. Milcinski, M. Demuzere, N. Brunzell, M. Pesaresi, S. Miao, Q. Mu, F. Chen, and N. Theeuwes (2018): World Urban Database and Access Portal Tools (WUDAPT), an urban weather, climate and environmental modeling infrastructure for the Anthropocene. *Bull. Amer. Meteor. Soc.*, <https://doi.org/10.1175/BAMS-D-16-0236.1>.
- Ching, J. K. S. (2013): A perspective on urban canopy layer modeling for weather, climate, and air quality applications, *Urban Climate* (3), 13-39.
- Freitas, E. D. (2003), *Circulações locais em São Paulo e sua influência sobre a dispersão de poluentes*, 157 pp, PhD Thesis. University of São Paulo, Institute of Astronomy, Geophysics and Atmospheric Sciences.
- Freitas, E. D., C. M. Rozoff, W. R. Cotton, and P. L. S. Dias (2007), Interactions of an urban heat island and sea-breeze circulations during winter over the metropolitan area of Sao Paulo, Brazil, *Boundary-Layer Meteorology*, 122(1), 43-65, [doi: 10.1007/s10546-006-9091-3](https://doi.org/10.1007/s10546-006-9091-3).
- Freitas, E. D., P. L. Silva Dias, V. S. B. Carvalho, C. R. Mazzoli, L. D. Martins, J. A. Martins, and M. F. Andrade (2009), Factors involved in the formation and development of severe weather conditions over the Megacity of São Paulo, in *89th American Meteorological Society Meeting*, edited, AMS, Phoenix, AZ.
- Khan, S., and R. Simpson (2001), Effect of a heat island on the meteorology of a complex urban airshed, *Boundary-Layer Meteorology*, 100(3), 487-506, [doi: 10.1023/A:1019284332306](https://doi.org/10.1023/A:1019284332306)
- Masson, V. (2000), A physically-based scheme for the urban energy budget in atmospheric models, *Boundary-Layer Meteorology*, 94(3), 357-397, [doi: 10.1023/A:1002463829265](https://doi.org/10.1023/A:1002463829265).
- Vemado, F., and A. J. Pereira Filho (2016), Severe Weather Caused by Heat Island and Sea Breeze Effects in the Metropolitan Area of São Paulo, Brazil, *Advances in Meteorology*, 2016, 13, [doi: 10.1155/2016/8364134](https://doi.org/10.1155/2016/8364134).
- Yoshikado, H. (1994), Interaction of the Sea-Breeze with Urban Heat Islands of Different Sizes and Locations, *Journal of the Meteorological Society of Japan*, 72(1), 139-143.
- Yoshikado, H., and M. Tsuchida (1996), High levels of winter air pollution under the influence of the urban heat island along the shore of Tokyo Bay, *Journal of Applied Meteorology*, 35(10), 1804-1813, [doi: 10.1175/1520-0450\(1996\)035<1804:HLOWAP>2.0.CO;2](https://doi.org/10.1175/1520-0450(1996)035<1804:HLOWAP>2.0.CO;2)
- Zhang, H. (2011), 2 - The Basic Properties of Building Materials A2 - Zhang, Haimei, in *Building Materials in Civil Engineering*, edited, pp. 7 -423, Woodhead Publishing, [doi: https://doi.org/10.1533/9781845699567.7](https://doi.org/10.1533/9781845699567.7)

5.3 Consideration of Urban Induced Thermal and Air Quality Patterns and Circulations for CW-AQF

5.3.1 Introduction

Air quality in urban areas is a dynamic mixture of regional, advected distributions of pollutants, newly emitted and different primary types of VOCs and NO_x as well as other emissions and formed secondary pollutants, all undergoing complex atmospheric processes for which the urban morphology is relevant. The goals, capabilities, and capacities for CW-AQFs require attention to dealing with exacerbation of air quality issues to large and mesoscale circulations induced by various phenomena on sub-grid and small scales. These phenomena are attributable to urbanization and varieties of morphological features. Here we identify and examine a few important aspects that require special modeling treatments and attention, including:

- (1) methods for handling scale-dependent photochemistry issues;
- (2) atmospheric processes of morphological-related dispersion, turbulent mixing, pollutant deposition, particle re-suspension;
- (3) in light of recent and new insights about local climate zones (LCZ)² classification schemes on urban heat island (UHI), and
- (4) spatial aspects of climate induced heat wave enhancements and other related issues.

In Section 5.4 these challenges are reflected by recommendations for improved urban canopy modules.

In this sub-section, we consider some urban features related to the influence of thermal gradients on atmospheric patterns, showing how they can generate important circulations that must be considered when studying chemical weather and air quality forecast models. The sub-section addresses features relating different scales that determine photochemical processes and influences of urban morphological structures on air mixture in the boundary layer, including atmospheric circulations, urban heat islands and climate-induced weather extremes. Important topics include: urban heat islands; heat waves, air quality and environment comfort; urban emissions, and urban growth and changes in the atmospheric patterns.

5.3.1.1 Scale-dependent photochemistry issues and related urban mixtures

Urban residents are exposed to diverse air quality and mixtures of different airborne pollutant compounds in urban areas; the urban mixed layer contains constantly evolving mixtures of both aged pollutants and new primary (time of day, seasonal, week end and weekday dependent) emissions from traffic, industrial waste, biogenic and of indoor origin, some are photochemically produced secondary products including ozone and organic particulates resulted from semi-volatile VOCs (SVOC). Photochemical oxidants are an important class of pollution and their modeling is very complex. For example, traffic NO_x emissions will titrate ambient ozone along streets and highways, modulated by the presence of street canyons. Away from traffic sources, traffic emitted NO_x and VOCs will produce ozone and nitrogen oxide products. Thus, the type of compounds and spatial patterns affecting exposure to traffic emissions will strongly depend on proximity to distance from traffic sources. For example, spatial patterns for ozone and NO_x will be correlated to the road network and traffic loads, and modeling such patterns (Figure 5.11) and will be at best, coarsely resolved even with fine grid mesh models. Exceptions would be very high-resolution microscale meteorology models (Schlunzen et al., 2011) and CFD models (Section 5.5).

² the local climate zones (LCZ) classification scheme was suggested for urban climate studies (see, e.g., Stewart and Oke, 2012). Important to stress that it is representing a morphological structure, not the climate. So, to avoid a misunderstanding by readers, it is better to use terms of urban morphology classification, instead of LCZ.

Regarding SVOC exposures, a wide variety of health impacting SVOCs, each originated from a variety of different indoor and outdoor sources, e.g., polycyclic aromatic hydrocarbons (PAHs), endocrine disrupting chemicals, etc. Some are gaseous, some become attached to airborne particles, the latter can be resuspended after deposition and their composition span a range of acidity and thus require the introduction of ammonia emissions as inputs. This set of pollutants are emitted and transported as gas and particles in multi-size modes, and involve heterogeneous and aqueous chemistry treatments. Model treatments may require hybrid grid and local scale modeling, e.g., street in grid (Kim et al., 2018; Shi et al., 2018; and C-Tools: <https://www.cmascenter.org>).

5.3.1.2 *Characteristics of Urban Morphological Structures*

Current multiscale emission-based chemistry and transport modeling systems such as CMAQ (<https://www.cmascenter.org>) provide a comprehensive science-based system that treats scale-dependent atmospheric processes for policy-relevant regional to mesoscale air quality modeling. However, in the urban context, a modified and innovative treatment of subgrid-scale atmospheric processes is needed, which considers the complex urban morphological structures and canopy structures. Within urban areas, atmospheric processes of dispersion, turbulent mixing, pollutant deposition and particle re-suspension are strongly influenced by building compactness, mean and variations in building height and degree of perviousness and vegetation coverage. This depends on the underlying morphological structure as likely found in the different neighborhoods across cities. For example, this heterogeneity in LCZs across the city will modulate the turbulence intensities, drag properties and 3-D dispersion of pollutant emissions unlikely to be captured by roughness and displacement height scaling parameterizations but more aptly by urban canopy schemes (Masson, 2000; Kusaka et al., 2001; Masson et al., 2002; Martilli et al., 2002; Baklanov et al., 2008; and Salamanca et al., 2010). Incoming and outgoing radiation-controlling surface and canopy energy budgets, and pollution photochemistry will be modulated by multiple wall and street level reflections. The fluxes of the surface energy budget will be influenced by canopy structures and perviousness of surfaces as well as additional anthropogenic heat contributions. The deposition of gases and particles, as well as particle re-suspension, will be influenced by the nature of the building walls, the extent of impervious cover by roads and other paved surfaces. Further details on urban canopy modules are given in Section 5.4.

5.3.1.3 *Treating Intraurban Circulations, UHI, and Climate-Induced Weather Extremes*

Given recent developments in urban-scale high-resolution atmospheric systems (see Section 5.4 on models and Section 5.6 on descriptions of the urban structure), there is now an improved means and framework for CW-AQF modeling to reflect intracity circulations and spatial variability enhancements to the phenomena of UHI and heat waves based on land surface and building morphological features on top of the synoptic-mesoscale expectations, which is described below.

5.3.2 *Urban Heat Islands*

Land use changes are known to be responsible for significant changes in Earth's Energy Budget near the surface and are associated with possible climate change (IPCC, 2013). Deforestation, substitution of forests by crops, and the increase of urban areas are some of the examples of changes in the landscape resulting in local urban climate change. Due to the extreme modification of surface characteristics, urbanization (or urban growing) is one of the most extreme among them, causing the so-called UHI, which is the focus of this section.

The average annual temperature in an urban center is typically higher than the surrounding areas (Oke, 1997). This anomalous heating occurs on the surface and in the atmosphere. During the summer, in some extreme situations, solar radiation can heat up exposed urban surfaces, such as roofs and pavements, to temperatures 27–50°C higher than the air (Berdahl and Bretz, 1997), while shaded or moist surfaces remain close to air temperatures. In the atmosphere, during appropriate conditions, thermal contrast can be as high as 12°C (Oke,

1988). Recent studies illustrate that an accurate temperature range is between 5 and 15°C (Santamouris, 2013). The temperature contrast, and correspondingly the UHI, forms a convective circulation that usually, especially in calm conditions, increases mixing within PBL and reduces air pollution concentrations. But in specific cases the effect can be the opposite and it contributes to harmful conditions for the population, such as the increase of pollutant concentrations at night-time (Zhang and Rao, 1999), or due to the recirculation of pollutants through the UHI circulation cell (Freitas 2003; Freitas and Silva Dias 2005; Yoshikado and Tsuchida, 1996) or the intensification of convective systems (Freitas et al., 2007; Silva Dias et al., 2013; Vemado and Pereira Filho 2016). Several factors contribute to the development of a UHI. One is the relatively high concentration of anthropogenic heat sources in the cities. The thermal properties of urban building materials also facilitate heat conduction faster than soil and vegetation in rural areas, contributing to an increase in the temperature contrast between these regions. Heat loss at night, through infrared radiation into the atmosphere and into space, is partially offset in cities by the release of heat from anthropogenic sources such as light and heavy-duty vehicles, industries and commercial activities, residences, people, air conditioning systems, among others. For example, Ichinose et al. (1999) showed that the contribution of anthropogenic sources can exceed 50% of the total heat flux during the day in the winter period in the city of Tokyo. In addition, tall buildings between relatively narrow streets, the “urban canyons”, reduce the natural ventilation of streets and trap solar energy through multiple reflections of the solar rays, acting as an energy storage element. Figure 5.6 shows a view of the Metropolitan Area of São Paulo, Brazil, where some of these features can be seen. In the cities, the typically lower evapotranspiration rate further accentuates the temperature contrast with its surroundings. The drainage system quickly removes most of the rainwater, so that only a small fraction of the absorbed radiation is used for evaporation (latent heat) and most of that radiation is used to heat up the surface and the urban fabric, and by this the air (sensible heat). On the other hand, the moist surfaces of rural areas (lakes, streams, soil and vegetation) increase the fraction of absorbed radiation that is used for evaporation. Bowen's ratio (the ratio of the sensible heat flux to the latent heat flux) is therefore higher in the city than in the rural adjacent areas.

A UHI develops most often when winds of synoptic scale are weak (strong winds would mix the air of the city and rural areas and decrease the temperature contrast). Under these conditions, in some large metropolitan areas the relative heating of the city compared to its surroundings can promote convective air circulation: relatively warm air rises above the center of the city and is replaced by colder and denser air from the rural areas, forming UHI circulation cells. Figure 5.7 shows two examples of UHI. The first one (Left panel) shows the horizontal thermal gradient over the Metropolitan Area of São Paulo, where differences up to 4 °C are usually observed, when comparing the central urban temperature with the temperature of the surrounding areas. This thermal gradient favors convective cells formation, like the ones shown in the right panel of Figure 5.7. In this panel we see the circulation cells (between 113.6° E and 114° E), provided by model simulations, caused by the convergence zone due to the urban area of Hong Kong, reaching as high as 1200 m at 1400 Local Time.

The urban elements that form large urban conglomerates of many megacities around the world are very heterogeneous, having areas of high-rise buildings with very sparse vegetation in the vicinity of commercial or residential areas where constructions are more spaced and the vegetation is in a larger portion. Figure 5.8 shows an example of such heterogeneous land use inside the city of São Paulo, Brazil.



Figure 5.6. View of the city center of the Metropolitan Area of São Paulo, Brazil.

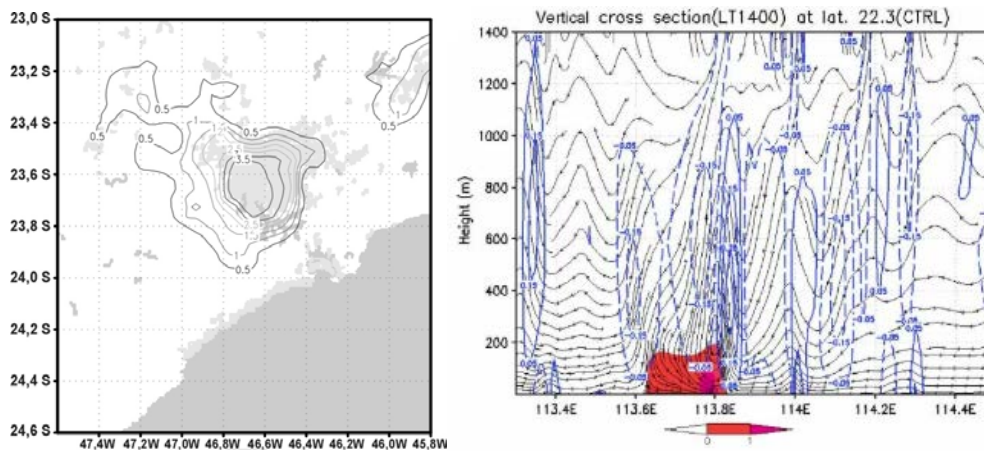


Figure 5.7. Left panel - Urban Heat Island Intensity over the Metropolitan Area of São Paulo, Brazil.

(Source: Freitas and Silva Dias, 2005). Right panel – Vertical cross section at latitude 22.3°N over the Pearl River Delta, China, showing the u - w streamlines, vertical velocities (m s^{-1} , contours) and magnitudes of westerly winds (m s^{-1} , shadings) at LT 1400. (Source: adapted from Lu et al., 2010).

UHI-generated circulations can interact with other microscale, mesoscale, and synoptic scale systems, such as gravity waves, sea-breezes, topography-induced circulations, and cold fronts. Nair et al. (2004) studied an occurrence of such interactions in a case where boundary layer processes were modified by the interaction among a low-level jet, gravity waves and a cold front. As they mentioned, these interactions are of great importance in the pollution dispersion process. Freitas et al. (2007) made numerical simulations and showed that the effects of UHI circulations can be intensified by sea breezes and interact with them, intensifying the vertical movement associated with the sea-breeze front. Khan and Simpson (2001) also identified influences of the UHI on sea-breeze propagation, with propagations being accelerated in several hours due to the urban thermal effect. The more pronounced the interactions, the more intense the anthropogenic heat contribution of the urban area is (Freitas, 2003) and are also dependent on the city size and location, as mentioned by Yoshikado (1994). Deceleration of sea-breeze propagation is also possible, as reported in some studies over coastal megacities (Ohashi and Kida, 2002; von Glasow et al., 2013) or over inland megacities where both effects can be observed (Freitas et al., 2007). As the tendency of urbanization is to increase the area occupied by artificial materials, we can expect hazardous urban effects to increase in the next decades over such areas, making the situation in terms of urban dispersion or severe weather more complex.



Figure 5.8. View of heterogeneity observed in the city of São Paulo, Brazil, showing a region of a large number of high-rise buildings in the vicinity of low-rise constructions in a greener area.

5.3.3 Heat Waves, Air Quality, and Environment Comfort

Heat stress, occurring especially in warm climate cities, should be considered together with air pollution and other environmental hazards within the concepts of multi-hazards early warning systems (MHEWS, see: WMO-MHEWS, 2018) and Urban Integrated Hydro-meteorological, Climate and Environmental Services (WMO, 2018).

A 'heatwave' often refers to a prolonged period of several days under excessively hot or unusually hot weather (WMO-WHO, 2015). The development of heatwaves not only depends on a location, but also on its large scale, stagnant, high-pressure systems influencing the weather on a regional scale and on its local meteorological conditions. Although there is no universally acceptable definition of heatwaves (WMO-WHO, 2015), there are three heat event metrics widely adopted in heatwave studies such as magnitude, duration, and frequency especially for developing heat-health weather warning systems (Horton et al., 2016; Lam et al., 2013; WMO-WHO, 2015). Heatwaves are known as a natural climate hazard since they can have a notable impact on the natural physical environment, human systems, and ecosystems (IPCC et al., 2012a). A large number of worldwide research studies focuses on examining heatwaves' potential and consequential impacts on cooling energy requirements and heat risks on well-being, such as heat-related mortality and morbidity (Endlicher et al., 2008; Harlan and Ruddell, 2011; Heaviside et al. 2016; Heaviside et al. 2017; Johnson et al. 2012; Kovats 2013). Correspondingly spatial and temporal patterns of heat events is another research interest recently since mapping and exploring the heat-related risk might meet the needs of stakeholders and decision-makers (ARUP 2014; Aubrecht and Özceylan 2013; Macintyre et al., 2018). The effects of heatwaves may be exacerbated in urban areas due to the UHI effect (Heaviside et al., 2017; IPCC 2012b). Li and Bou-Zeid (2013) even found that not only do heatwaves increase the ambient temperature, but they also intensify the UHI intensity. Ward et al. (2016) examined the causes for the emergence of surface UHIs and their change during heatwaves in 70 European cities and found out that the northern European cities with cooler climates are more affected by additional heat during heatwaves than southern European cities with hot climates (Ward et al., 2016).

The IPCC report on 'Future Climate Extremes and Their Effects' stated that as a result of anthropogenic warming a rise of extreme daily minimum and maximum temperatures is expected on a global scale, and the length, frequency and/or intensity of heatwaves would likely increase over most land areas in the 21st century under climate change (IPCC, 2012a, 2012b). At the regional level, using Europe as an example, based on the projections, it

concludes that ‘*Likely* more frequent, longer and/or intense heat waves or warm spells in Europe; *Very likely* increase in warm days and nights’ (IPCC 2012b). Liu et al.’s work (2017) echoed the same results, and they adopted bias-corrected and downscaled projections of Coupled Model Intercomparison Project Phase 5 (CMIP5) to characterize future climate change of 2071-2100 and to capture spatial distribution patterns of heatwaves at both the global and regional scale under RCP8.5-SSP3 (Figure 5.9). From their study results, at the regional level, it is expected in certain low latitude areas that annual Heat Wave Days (HWDs) will increase dramatically by over 150 days during 2071-2100, while HWDs will increase by 80–120 days in the mid-latitudes and 40–80 days in the sub-polar regions (Liu et al., 2017).

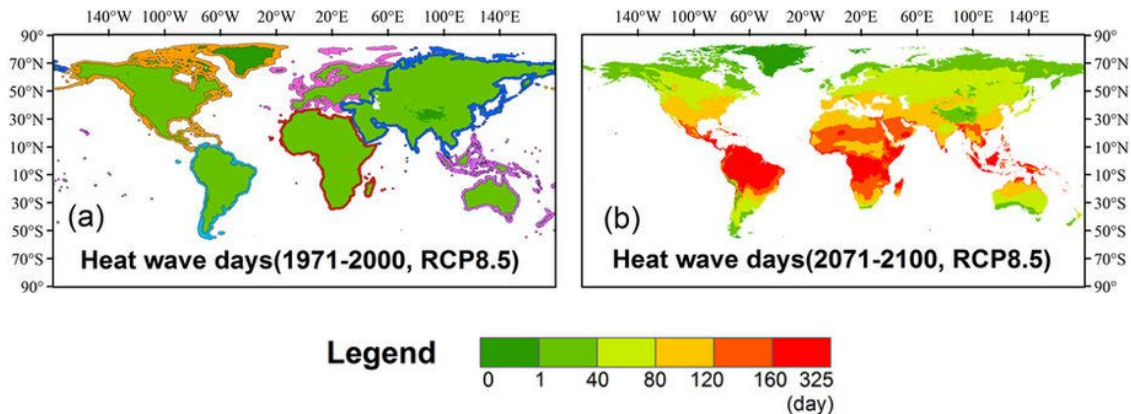


Figure 5.9. Multi-model average of heat wave days (averaged for the period 1971–2000 (left: a) and the 2071–2100 period (right: b) under scenario RCP8.5-SSP3

Source: Liu et al. (2017).

Because of a combination of weather factors, such as high temperatures and radiation, stagnation of air masses, intensive photochemistry mechanisms and weak dry deposition, extremely hot weather events and heatwaves may occur together with high air pollution episodes, especially with intensified ‘ground-level ozone (or smog)’ (Guerova and Jones, 2007; Harlan and Ruddell, 2011; Tressol et al., 2008). There are many such combined heatwaves and air pollution episodes with observed health effects, e.g.,

- Heatwaves and peak tropospheric ozone episodes (due to the favoring of photochemical reactions) in Central Europe during the summer of 2003 (Solberg et al., 2008)
- Heatwaves and mortality rates in France during August 2003 (Douset et al., 2011; Fouillet et al., 2006)
- Heatwaves and peat wildfires due to long-term dry and hot weather in the Moscow region, during the summer of 2010 (Konovalov et al., 2011).

So, combined integrated systems for high impact weather, air quality and combined health impacts are needed, like the FUMAPEX integrated system for forecasting urban meteorology, air pollution and population exposure (UAQIFS) realized for several European cities (Baklanov et al., 2006; 2012) or the SAFAR System for Indian cities (Beig et al., 2015).

Furthermore, given the recent LCZ framework of Stewart and Oke (2012) which has been shown to be able to capture and explain intracity spatial variation in morphology, given WUDAPT protocols (see Section 5.6), there is now an improved means and framework for CW-AQF modeling to reflect intracity circulations’ spatial variability enhancements to the phenomena of UHI and heat waves based on land surface and building morphological features on top of the synoptic-mesoscale expectations.

There is a large number of models dedicated to representing surface energy balance over

urban areas. The main goal of these models is to represent accurately the surface fluxes of heat, moisture and momentum at the local scale. Other features such as pollution emissions, net heat storage, inside canyon temperature, moisture, and wind are also desirable. Figure 5.10 shows some characteristics of different urban canopy models (UCM). For surface fluxes, some models consider all fluxes, some consider all fluxes but QE and QF, while others consider only QE or QF. For more details on this figure and for a comprehensive comparison among 33 UCM we strongly invite the reader to access the work by Grimmond et al. (2010).

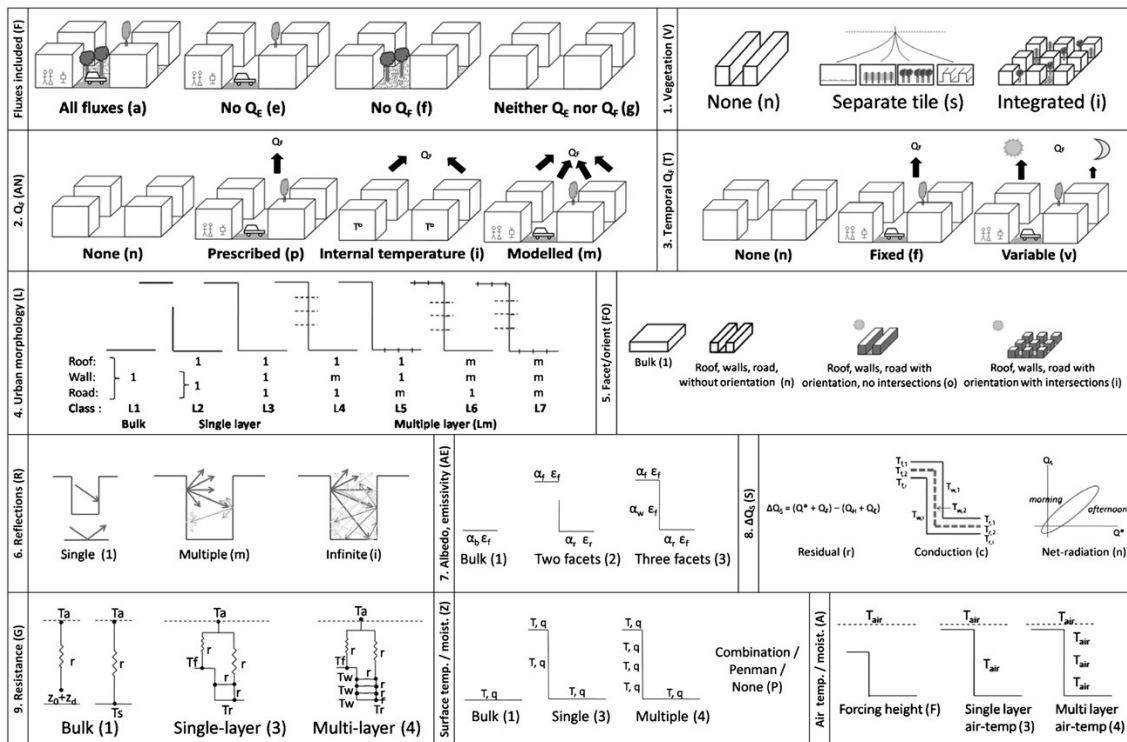


Figure 5.10. Characteristics used to classify models. QF is the anthropogenic heat flux, QH is the sensible heat flux, QE is the latent heat flux, Q* is the net all-wave radiation, and ΔQS is the net heat storage.

Source: Grimmond et al. (2010).

5.3.4 Urban Emissions

One of the key features on representing urban-related processes is to consider artificial contributions for heat anomalies inside cities. As already mentioned, the large number of vehicles can contribute to increased UHI intensity, being an important heat source (engine temperatures range from 363 to 378 K). Also, these vehicles are responsible for the emission of many air pollutants, such as carbon oxides (CO), sulfur oxides (SO_x), volatile organic compounds (VOCs), nitrogen oxides (NO_x), and particulate matter (PM). In most cities we also have to take into account emissions due to industrial activities, such as paper mills, refineries, steelworks, among others. For such features we use emission inventories globally and locally built, originated from all types of sources in a certain location during a specific time period, ranging from hours to a specific year. Examples of emission inventories are the National Emissions Inventory (NEI) published every three years by the United States Environmental Protection Agency (U.S. EPA) (<https://www.epa.gov/air-emissions-inventories/national-emissions-inventory-nei>), the European Union emission inventory provided by the European Environmental Agency (EEA) (<https://www.eea.europa.eu/data-and-maps/dashboards/air-pollutant-emissions-data-viewer>), and Global emission fields of air pollutants and Green House Gases, developed with the Greenhouse Gas and Air Pollution Interactions and Synergies (GAINS) model, provided by the International Institute for Applied Systems Analysis (IIASA) (http://www.iiasa.ac.at/web/home/research/researchPrograms/air/Global_emissions.html).

In general, UCMs are introduced in the models as part of its Soil-Vegetation-Atmosphere-Transfer schemes, being all related variables evaluated when an urban grid point is identified. In such cases, UCMs provide surface fluxes over urban areas as a bottom boundary condition to the atmospheric component of the model, getting feedback from pertinent processes from it. Those fluxes are simultaneously calculated with many other processes in the whole model system. Emissions of pollutants can also be made by using land use files, considering emissions over urban areas and roads and highways. However, they are mostly provided to the models in different data sets containing the emission sources based on their location or, in the case of vehicular emissions, based on statistical procedures applied to streets, roads, highways, etc., considering the number and types of vehicles.

Higher resolution models dedicated to local scale applications usually consider a bottom-up emissions approach as a base for their emission inventory. Bottom-up emission inventories must consider all near surface sources of pollutant emissions. For the case of vehicular emissions, these sources are due to the gases and particles that come from vehicle exhausts, including the first few minutes of engine functioning (cold-start exhaust, CE) and emissions after the engine reaches a certain temperature limit (hot exhaust, HE), fuel evaporation in the vehicle system, comprising the tank, pipes and engine (evaporative, EV). These emissions will also depend on deterioration factors and other specific features of each vehicle (Ibarra-Espinosa et al., 2018). Also, besides vehicle characteristics, it is necessary to identify in the domain of interest how vehicular traffic behaves, which will depend on the number of streets, avenues, roads, and other links that a vehicle can be in at a given time, as well as some of their characteristics, such as length, width, type of pavement, etc. In other words, it is necessary to complement vehicle emission information with traffic flow. Traffic flow simulations will provide spatial and time distributions of vehicles over the interest domain, making the task of creating a vehicular emission inventory possible. Although many details can be provided to the AQM, some unknowns will always remain. For example, although one may know the number of vehicles by age, in a spatial domain we will not know in advance where a certain type of vehicle will be at a given time. Those uncertainties can be reduced by means of statistical methods, but they will always exist. For lower resolution models, the top-down approach is usually the best way of representing emissions. An example of vehicular emission information is shown in Figure 5.11.

Great efforts have been made to improve the emissions in different time and space scales. One of the examples of such efforts is the MEGAPOLI project (<http://megapoli.dmi.dk/index.html>), developed by European research groups. Objectives were assessing the impacts of megacities and large air-pollution hot spots on air quality in different spatial scales (local, regional and global), quantifying feedbacks among megacities' air quality and climate from local up to global scales and, to develop integrated tools for air pollution prediction in megacities. The main results of this project include multi-scale gridded emission and heat flux inventories, as well as European and Megacity baseline scenarios for 2020, 2030 and 2050. A hierarchy of nesting anthropogenic emission databases for Global, Pan-European and urban scales were developed. These datasets, built by TNO, include high-resolution (1 km) emission inventories for four European megacities/urban agglomerations (London, Paris, Rhine-Ruhr, and Po Valley) nested into the Pan European MEGAPOLI emission dataset (6x7 km² resolution), represented by local bottom-up emission inventories. On the global scale, 36 megacities around the world were identified and used to provide a global emission inventory. The inventory was based on population data and used the global gridded dataset by Lamarque et al. (2010), used in the IPCC Fifth Assessment Report (AR5). The Representative Concentration Pathways 8.5 (RCP 8.5) developed by Riahi et al. (2007) was selected as the scenario to derive a global emission inventory for the base year of 2005, in a grid of 0.5 degree × 0.5 degree (Butler et al., 2011).

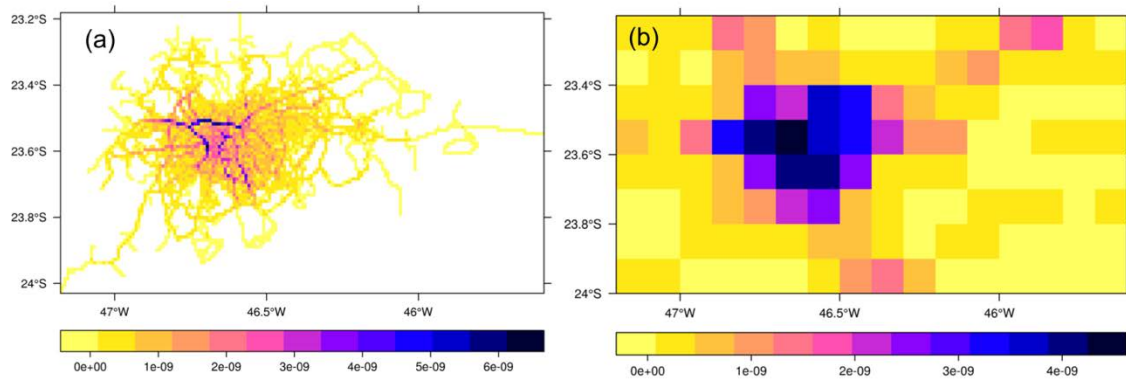


Figure 5.11. Vehicular CO emissions ($\text{kg}\cdot\text{m}^{-2}\cdot\text{s}^{-1}$) in the Metropolitan Area of Sao Paulo for (a) Monday at 00:00:00 LT, estimated with the VEIN model (Ibarra-Espinosa et al., 2018), and (b) the emissions of road transport for the same area from the Emission Database for Global Atmospheric Research (EDGAR).

Source: Ibarra-Espinosa et al. (2018).

Emission sources in the MEGAPOLI inventory include contributions from energy production and distribution, industrial processes and combustion, land transport, residential and commercial, solvent production and use, agriculture, agricultural waste burning, waste treatment and disposal, biomass burning in forest and grassland, navigation, aviation, biogenic, volcanic, and oceanic sources, and dust (Butler et al., 2011). Pollutants in the global inventory include all those necessary for the simulation of tropospheric ozone and aerosols, including CH_4 , CO, NO_x , total and speciated non-methane volatile organic compounds (NMVOCs), NH_3 , SO_2 , organic carbon (OC) and black carbon (BC) (Butler et al., 2011).

Anthropogenic heat sources are a fundamental part of UCM, since it will provide surface heat fluxes from artificial materials in an urban area. The main heat sources include the vehicles' engines (combustion), industrial processes, the conduction of heat through building walls, air conditioning systems, and the metabolic heat produced by humans (Sugawara and Narita, 2009). MEGAPOLI was also dedicated to that matter (Allen et al., 2010).

In order to define anthropogenic contributions to heat fluxes, the **Large scale Urban Consumption of energy** model (LUCY), was used in the MEGAPOLI project. LUCY simulates all components of anthropogenic heat flux (Q_f) from the global to individual city scale at 0.25×0.25 arc-minute resolution (Allen et al., 2010). The model considers different working patterns, public holidays, energy consumption, and vehicle use for each country considered. Detailed information on specific diurnal and seasonal vehicle and energy consumption patterns, local holidays and flows of people within a city can be provided to the model to improve the surface fluxes definition (Allen et al., 2010).

Fuel combustion by motor vehicles is one of the main sources of heat in urban areas. The contribution will depend on the use of the vehicle, traffic flow, type of fuel, among other factors. For example, Smith et al. (2009) found that the amounts of energy released from fuel combustion in the UK are 45.85 kJ g^{-1} for petrol and 46 kJ g^{-1} for diesel, respectively. Lower values were found by Pigeon et al. (2007) for France, being the energy released 43.8 kJ g^{-1} for petrol and 42.5 kJ g^{-1} for diesel. In some cases, an average of 45 kJ g^{-1} over an entire fleet has also been used (Sailor and Lu, 2004; Sailor et al., 2007).

The heat released from buildings is identified to be the largest contributor (89 to 96%) to heat emissions globally (Allen et al., 2010). Estimations of this contribution use both top-down and bottom-up approaches. For top-down estimates, energy consumption is frequently used, and it allows the construction of an annual distribution behavior. For bottom-up estimates it is

necessary to have more detailed information, considering energy consumption in individual buildings. The contribution can be divided into different classes or sectors of activity (e.g., industries, residencies, commerce) (Pigeon et al., 2007; Hamilton et al., 2009), as well as fuel type (electric or combustion of oil or gas). Heiple and Sailor (2008) estimated that the largest part of energy consumption in buildings in the USA (60 to 70%) is used for heating, air-conditioning and water heating. Considering that many factors can contribute to differences in energy consumption in a city, in the MEGAPOLI project, the application of LUCY allowed estimations for several megacities around the world. The highest individual grid cell values for heat fluxes in urban areas were located in New York (577 W m^{-2}), Paris (261.5 W m^{-2}), Tokyo (178 W m^{-2}), San Francisco (173.6 W m^{-2}), Vancouver (119 W m^{-2}) and London (106.7 W m^{-2}) (Allen et al., 2010).

As mentioned in Allen et al. (2010) metabolic heat emissions can be determined using population data with an assumption of average human metabolic rate. Some models consider a constant rate of 100 W per person (Makar et al., 2006), while other models use different contributions during the day or night. For example, Sailor and Lu (2004) considered different metabolic rates for night periods (between 2300 and 0500), as 75 W per person, and in the daytime (between 0700 and 2100), as 175 W per person, with transitional values for the hours in between.

5.3.5 Urban Growth and Changes in the Atmospheric Patterns

As mentioned before, city size is determinant for the UHI intensity. As population is growing in most cities around the globe, it is expected that urban areas will increase proportionally. Therefore, the intensification of the harmful effects of UHI is of great concern. Levermore et al. (2017) analysed modifications in the UHI intensity in the city of Manchester, U.K. Cloud cover and wind speed were found to have a trend of decreasing as consequence of urbanization. They also estimated an increase of 2.4 K to the average annual urban temperature by the end of the 21st century, which will increase UHI intensity. As mentioned by Watkins et al. (2007), in a temperate climate, this increase in temperature can have beneficial effects during the winter, but can increase heat stress and energy consumption for cooling during summer. Also, as pointed out by the U.S. Environmental Protection Agency (U.S. EPA, 2018), electricity demand, which generally occurs on hot summer weekday afternoons, can be significantly affected by UHI. With the increase of UHI intensity, this effect can be even worse. They also call attention to the fact that in many countries, companies responsible for electricity supply use fossil fuels in their power plants, which in turn would lead to an increase in air pollutant and greenhouse gas emissions. Considering that there is a projection that heat waves will become more frequent (Li and Bou-Zeid, 2013), together with urban growing, one might expect serious heat-related health risks for urban dwellers in the near future. Another consequence of increasing UHI intensity is the effects that temperature has on thunderstorm formation. UHI was associated with the severity of thunderstorms (Silva Dias et al., 2013) where more extreme precipitation occurrence has been observed, including high lightning activity (e.g., Bourscheidt et al., 2016; Westcott, 1995). Zhang et al. (2011) identified UHI effects on downstream urban areas, with more unstable conditions, and pointed out that judicious land use and urban planning, especially in rapidly developing countries, could help to alleviate UHI consequences, including heat stress and smog, and also improve weather forecasts over urban areas. Stone et al. (2010) found that the rate of increase in the annual number of extreme heat events (EHEs) between 1956 and 2005 in the most sprawling metropolitan regions was more than double the rate of increase observed in the most compact metropolitan regions, associating urban size to the intensity of UHI. One of the main features related to climate change is also temperature increase. In this way, urban areas have even more intense consequences. McCarthy et al. (2010) argued that climate change has the capacity to modify the climatic potential for UHI. In some places they estimate a 30% increase, although they found a 6% global average reduction in the potential for UHI. They also mentioned that warming and extreme heat events due to urbanization and consequent increased energy consumption were simulated to be as large as the impact of doubled CO_2 in some regions, and climate change increases the disparity in extreme hot nights between rural and urban areas.

5.3.6 Summary

- Air quality in urban areas is a dynamic mixture of regional, advected distributions of pollutants, newly emitted from different sources, and it is subject to complex atmospheric processes for which urban morphology is important.
- Extreme land use changes are known to be responsible for significant changes in Earth's Energy Budget near the surface and are associated with possible climate changes.
- Urbanization is one of the most prominent examples of changes in the landscape resulting in local climate change and responsible for the UHI effect. UHI are associated with many atmospheric modifications and can influence pollutant concentrations, thunderstorm formation and other harmful conditions over cities and surrounding areas.
- Heat waves are prolonged periods of several days under excessive heat or unusually hot weather. This type of extreme weather condition constitutes a natural climate hazard and can be exacerbated in urban areas due to the UHI effect and can intensify air pollution episodes, especially those of ground-level ozone (or smog), and impact environmental human comfort.
- Urban emissions are responsible for a large amount of pollutants in the atmosphere, the main sources being associated with vehicles and industries. They represent a key feature on urban-related features. Air quality models depend on the creation and maintenance of emission inventories worldwide.

References

- Allen L., S Beevers, F Lindberg, Mario Iamarino, N Kitiwiroon, CSB Grimmond (2010): Global to City Scale Urban Anthropogenic Heat Flux: Model and Variability. Deliverable 1.4, MEGAPOLI Scientific Report 10-01, MEGAPOLI-04-REP-2010-03, 87p, ISBN: 978-87-992924-4-8; http://megapoli.dmi.dk/publ/MEGAPOLI_sr09-03.pdf
- ARUP, 2014: Reducing Urban Heat Risk: A study on urban heat risk mapping and visualization.
- Aubrecht, C., and D. Özceylan, 2013: Identification of heat risk patterns in the U.S. National Capital Region by integrating heat stress and related vulnerability. *Environment International*, 56, 65-77.
- Baklanov A, Hänninen O, Slørdal LH, Kukkonen J, Sørensen JH, Bjergene N, Fay B, Finardi S, Hoe SC, Jantunen M, Karppinen A, Rasmussen A, Skouloudis A, Sokhi RS, Ødegaard V, 2006: Integrated systems for forecasting urban meteorology, air pollution and population exposure. *Atmos Chem Phys* 7: 855–874.
- Baklanov A., P. Mestayer, A. Clappier, S. Zilitinkevich, S. Joffre, A. Mahura, N.W. Nielsen, 2008: Towards improving the simulation of meteorological fields in urban areas through updated/advanced surface fluxes description. *Atmospheric Chemistry and Physics*, 8, 523-543.

- Baklanov, A., 2012. Megacities: Urban Environment, Air Pollution, Climate Change and Human Health Interactions. Chapter 10 in: National Security and Human Health Implications of Climate Change. In: NATO Science for Peace and Security Series C: Environmental Security, pp. 103e114. http://dx.doi.org/10.1007/978-94-007-2430-3_10.
- Beig, G. et al., 2015. System of Air Quality Forecasting and Research (SAFAR-India). WMO GAW Report No. 217. https://library.wmo.int/doc_num.php?explnum_id=7182
- Berdahl P. and S. Bretz. 1997. Preliminary survey of the solar reflectance of cool roofing materials. *Energy and Buildings* 25: 149-158.
- Bourscheidt, V., O. Pinto, and P. Naccarato Kleber, 2016: The effects of Sao Paulo urban heat island on lightning activity: Decadal analysis (1999–2009). *Journal of Geophysical Research: Atmospheres*, 121, 4429-4442.
- Butler T., H.A.C. Denier van der Gon, J. Kuenen (2011): The Base Year (2005) Global Gridded Emission Inventory used in the EU FP7 Project MEGAPOLI (Final Version). MEGAPOLI Scientific Report 11-02, MEGAPOLI-28-REP-2011-01, 27p.
- Dousset, B., and Co-authors, 2011: Satellite monitoring of summer heat waves in the Paris metropolitan area. *International Journal of Climatology*, 31, 313-323.
- Endlicher, W., G. Jendritzky, J. Fischer, and J.-P. Redlich, 2008: Section III-Heat waves, urban climate and human health. *Urban Ecology*, Springer Link, 269-278.
- Fouillet, A., and Co-authors, 2006: Excess mortality related to the August 2003 heat wave in France. *International Archives of Occupational and Environmental Health*, 80, 16-24.
- Freitas, E. D., 2003: Circulações locais em São Paulo e sua influência sobre a dispersão de poluentes, Department of Atmospheric Sciences, University of São Paulo, 157 pp.
- Freitas, E. D., and P. L. Silva Dias, 2005: Alguns efeitos de áreas urbanas na geração de uma ilha de calor. *Revista Brasileira de Meteorologia*, 20, 355-366.
- Freitas, E. D., C. M. Rozoff, W. R. Cotton, and P. L. S. Dias, 2007: Interactions of an urban heat island and sea-breeze circulations during winter over the metropolitan area of Sao Paulo, Brazil. *Boundary-Layer Meteorology*, 122, 43-65.
- Grimmond, C. S. B., and Co-authors, 2010: The International Urban Energy Balance Models Comparison Project: First Results from Phase 1. *Journal of Applied Meteorology and Climatology*, 49, 1268-1292.
- Guerova, G., and N. Jones, 2007: A global model study of ozone enhancement during the August 2003 heat wave in Europe. *Environmental Chemistry*, 4, 285-292.
- Hamilton IG, Davies M, Steadman P, Stone A, Ridley I, Evans S. 2009. The significance of the anthropogenic heat emissions of London's buildings: A comparison against captured shortwave solar radiation. *Building and Environment*. 44: 807-817.
- Harlan, S. L., and D. M. Ruddell, 2011: Climate change and health in cities: impacts of heat and air pollution and potential co-benefits from mitigation and adaptation. *Current Opinion in Environmental Sustainability*, 3, 126-134.
- Heaviside, C., S. Vardoulakis, and X.-M. Cai, 2016: Attribution of mortality to the urban heat island during heatwaves in the West Midlands, UK. *Environmental Health*, 15, 50-59.
- Heaviside, C., H. L. Macintyre, and S. Vardoulakis, 2017: The Urban Heat Island: Implications for Health in a Changing Environment. *Current Environ Health Rep*.
- Heiple S, Sailor DJ. 2008. Using building energy simulation and geospatial modeling techniques to determine high resolution building sector energy consumption profiles. *Energy and Buildings*. 40: 1426-1436.
- Horton, R. M., J. S. Mankin, C. Lesk, E. Coffel, and C. Raymond, 2016: A Review of Recent Advances in Research on Extreme Heat Events. *Current Climate Change Reports*, 1-18.

- Ibarra-Espinosa, S., R. Ynoue, S. O'Sullivan, E. Pebesma, M. D. F. Andrade, and M. Osses, 2018: VEIN v0.2.2: an R package for bottom-up vehicular emissions inventories. *Geosci. Model Dev.*, 11, 2209-2229.
- Ichinose, T., K. Shimodozono, and K. Hanaki, 1999: Impact of anthropogenic heat on urban climate in Tokyo. *Atmospheric Environment*, 33, 3897-3909.
- IPCC, 2012a: The IPCC on Future Climate Extremes and Their Effects. *Population and Development Review*, 38, 383-386.
- IPCC, 2012b: Managing the Risks of Extreme Events and Disasters to Advance Climate Change Adaptation: Special Report of the Intergovernmental Panel on Climate Change. Cambridge University Press, .
- IPCC, 2013: Climate Change 2013: The Physical Science Basis. Contribution of Working Group I to the Fifth Assessment Report of the Intergovernmental Panel on Climate Change [Stocker, T.F., D. Qin, G.-K. Plattner, M. Tignor, S.K. Allen, J. Boschung, A. Nauels, Y. Xia, V. Bex and P.M. Midgley (eds.)]. Cambridge University Press, Cambridge, United Kingdom and New York, NY, USA, 1535 pp.
- IPCC, WMO, and UNEP, 2012a: Managing the risks of extreme events and disasters to advance climate change adaptation, Special Report of the Intergovernmental Panel on Climate Change, 20 pp.
- , 2012b: Managing the risks of extreme events and disasters to advance climate change adaptation - summery for policymakers, Special Report of the Intergovernmental Panel on Climate Change, 20 pp.
- Johnson, D. P., A. Stanforth, V. Lulla, and G. Luber, 2012: Developing an applied extreme heat vulnerability index utilizing socio-economic and environmental data. *Applied Geography*, 35, 23-31.
- Khan, S. M. and Simpson, R. W., 2001. Effect of a heat island on the meteorology of complex urban airshed. *Bound-Layer Meteorol.*, 100, 487-506.
- Kim, Y., Y. Wu., C. Seigneur, Y. Roustan 2018: SING Multi-scale modeling of urban air pollution: development and application of a Street-in-Grid model (v1.0) by coupling MUNICH (v1.0) and Polair3D (v1.8.1) *Geosci. Model Dev.*, 11, 611–629, 2018 <https://doi.org/10.5194/gmd-11-611-2018>
- Konovalov, I. B., M. Beekmann, I. N. Kuznetsova, A. Yurova, and A. M. Zvyagintsev, 2011: Atmospheric impacts of the 2010 Russian wildfires: integrating modeling and measurements of an extreme air pollution episode in the Moscow region. *Atmos. Chem. Phys.*, 11, 10031-10056.
- Kovats, S., 2013: 1.08 - Heat-Related Mortality A2 - Pielke, Roger A. *Climate Vulnerability*, Academic Press, 95-103.
- Kusaka, H. Kondo, Y. Kikegawa, and F. Kimura, 2001: A simple single-layer urban canopy model for atmospheric models: Comparison with multi-layer and slab models. *Bound. Layer Meteorol.*, 101, 329–358, doi:10.1023/A:1019207923078.
- Lam, C. K. C., M. E. Loughnan, and N. J. Tapper, 2013: An exploration of temperature metrics for further developing the heat-health weather warning system in Hong Kong. *ISRN Atmospheric Sciences*, 1-9.
- Lamarque, J.-F., Bond, T. C., Eyring, V., Granier, C., Heil, A., Klimont, Z., Lee, D., Liousse, C., Mieville, A., Owen, B., Schultz, M. G., Shindell, D., Smith, S. J., Stehfest, E., Van Aardenne, J., Cooper, O. R., Kainuma, M., Mahowald, N., McConnell, J. R., Naik, V., Riahi, K., and van Vuuren, D. P. (2010), Historical (1850–2000) gridded anthropogenic and biomass burning emissions of reactive gases and aerosols: methodology and application, *Atmos. Chem. Phys. Discuss.*, 10, 4963-5019, doi:10.5194/acpd-10-4963-2010.

- Levermore, G., J. Parkinson, K. Lee, P. Laycock, and S. Lindley, 2017: The increasing trend of the urban heat island intensity. *Urban Climate*.
- Li, D., and E. Bou-Zeid, 2013: Synergistic Interactions between Urban Heat Islands and Heat Waves: The Impact in Cities Is Larger than the Sum of Its Parts. *Journal of Applied Meteorology and Climatology*, 52, 2051-2064.
- Liu, Z., B. Anderson, K. Yan, W. Dong, H. Liao, and P. Shi, 2017: Global and regional changes in exposure to extreme heat and the relative contributions of climate and population change. *Scientific Reports*, 7, 43909.
- Lu, X., K. Chow, T. Yao, A. K. H. Lau, and J. C. H. Fung, 2010: Effects of urbanization on the land sea breeze circulation over the Pearl River Delta region in winter. *International Journal of Climatology*, 30, 1089-1104.
- Macintyre, H. L., C. Heaviside, J. Taylor, R. Picetti, P. Symonds, X. M. Cai, and S. Vardoulakis, 2018: Assessing urban population vulnerability and environmental risks across an urban area during heatwaves – Implications for health protection. *Science of The Total Environment*, 610, 678-690.
- Makar P A, Gravel S, Chirkov V, Strawbridge KB, Froude F, Arnold J, Brook J. 2006. Heat flux, urban properties, and regional weather. *Atmospheric Environment*. 40: 2750-2766.
- Martilli, A, A. Clappier, M. Rotach, 2002: An Urban Surface Exchange Parameterization for Mesoscale Models. *Boundary Layer Meteor.* 104, 261-304.
- Masson, Valery, 2000: A Physically Based Scheme for the Urban Energy Budget in Atmospheric Models, *Bound Layer Meteorology* 94: 357–397, 2000.
- Masson, V., C. S. B. Grimmond, and T. R. Oke, 2002: Evaluation of the Town Energy Balance (TEB) Scheme with Direct Measurements from Dry Districts in Two Cities. *Journal of Applied Meteorology*, 41, 1011-1026.
- McCarthy, M. P., M. J. Best, and R. A. Betts, 2010: Climate change in cities due to global warming and urban effects. *Geophysical Research Letters*, 37.
- Nair, K. N., E. D. Freitas, O. R. Sánchez-Ccoyllo, M. Dias, P. L. S. Dias, M. F. Andrade, and O. Massambani, 2004: Dynamics of urban boundary layer over Sao Paulo associated with mesoscale processes. *Meteorology and Atmospheric Physics*, 86, 87-98.
- Ohashi, Y., and H. Kida, 2002: Local circulations developed in the vicinity of both coastal and inland urban areas: A numerical study with a mesoscale atmospheric model. *Journal of Applied Meteorology*, 41, 30-45.
- Oke, T. R. *Boundary Layer Climates*. Second Edition. Routledge Kegan & Paul. 1988. 435 pp.
- Oke, T.R. 1997. *Urban Climates and Global Environmental Change*. In: Thompson, R.D. and A. Perry (eds.) *Applied Climatology: Principles & Practices*. New York, NY: Routledge. pp. 273-287.
- Pigeon G, Legain D, Durand P, Masson V. 2007. Anthropogenic heat release in an old European agglomeration (Toulouse, France). *International Journal of Climatology*. 27: 1969-1981.
- Riahi, K., A. Gruebler, and N. Nakicenovic (2007), Scenarios of long-term socio-economic and environmental development under climate stabilization. *Greenhouse Gases – Integrated Assessment. Special Issue of Technological Forecasting and Social Change*, 74(7), 887–935, doi:10.1016/j.techfore.2006.05.026.
- Sailor DJ, Lu L. 2004. A top-down methodology for developing diurnal and seasonal anthropogenic heating profiles for urban areas. *Atmospheric Environment*. 38: 2737-2748.

- Sailor DJ, Brooks A, Hart M, Heiple S. 2007. A bottom-up approach for estimating latent and sensible heat emissions from anthropogenic sources. In: Seventh Symposium on the Urban Environment, San Diego 10-13 September 2007. [Online]. Available from: http://ams.confex.com/ams/7Coastal7Urban/techprogram/paper_127290.htm [Accessed 02 September 2018].
- Salamanca, F., Krpo, A., Martilli, A., Clappier, A., 2010: A new building energy model coupled with an urban canopy parameterization for urban climate simulation-Part 1. formulation verification, and sensitivity analysis of the model. *Theor. Appl. Climatol.* 99: 331-344.
- Santamouris, M. 2013. *Energy and Climate in the Urban Built Environment*, Routledge, Abingdon-on-Thames, UK (2013).
- Schlünzen, K.H., D. Grawe, S.I. Bohnenstengel, I. Schlüter, R. Koppmann 2011: Joint modeling of obstacle induced and mesoscale changes – current limits and challenges. *J Wind Eng. Ind. Aerodynamics*, 99, 217–225, doi:10.1016/j.jweia.2011.01.009.
- Shi Y., X.L. Xie, J.C.H. Fung and E. Ng (2018) Identifying critical building morphological design factors of street-level air pollution dispersion in high-density built environment using mobile monitoring. *Building and Environment* 128, 248-259.
- Silva Dias, M. A. F., J. Dias, L. M. V. Carvalho, E. D. Freitas, and P. L. S. Dias, 2013: Changes in extreme daily rainfall for So Paulo, Brazil. *Climatic Change*, 116, 705-722.
- Smith C, Lindley S, Levermore G. 2009. Estimating spatial and temporal patterns of urban anthropo- genic heat fluxes for UK cities: the case of Manchester. *Theoretical Applied Climatology*. 98: 19- 35.
- Solberg, S., and Co-authors, 2008: European surface ozone in the extreme summer 2003. *Journal of Geophysical Research: Atmospheres*, 113.
- Stone, B., J. J. Hess, and H. Frumkin, 2010: Urban Form and Extreme Heat Events: Are Sprawling Cities More Vulnerable to Climate Change Than Compact Cities? *Environmental Health Perspectives*, 118, 1425-1428.
- Stewart, I. D., & Oke, T. R. (2012). Local climate zones for urban temperature studies. *Bulletin of the American Meteorological Society*, 93(12), 1879-1900.
- Sugawara H, Narita K. 2009. Roughness length for heat over an urban canopy. *Theoretical and Applied Climatology*. 95: 291-299.
- Tressol, M., and Co-authors, 2008: Air pollution during the 2003 European heat waves as seen by MOZAIC airliners. *Atmos. Chem. Phys.*, 8, 2133-2150.
- USEPA, 2018. Heat Islands Impacts. Available from: <https://www.epa.gov/heat-islands/heat-island-impacts>. Last access on 28 March, 2019.
- Vemado, F., and A. J. Pereira Filho, 2016: Severe Weather Caused by Heat Island and Sea Breeze Effects in the Metropolitan Area of São Paulo, Brazil. *Advances in Meteorology*, 2016, 13.
- von Glasow, R., T.D. Jickells, A. Baklanov, G.R. Carmichael, T.M. Church, L. Gallardo, C. Hughes, M. Kanakidou, P.S. Liss, L. Mee, R. Raine, P. Ramachandran, R. Ramesh, K. Sundseth, U. Tsunogai, M. Uematsu, T. Zhu (2013) Megacities and Large Urban Agglomerations in the Coastal Zone: Interactions Between Atmosphere, Land, and Marine Ecosystems. *AMBIO, A Journal of the Human Environment*, 42 (1), 13-28.
- Ward, K., S. Lauf, B. Kleinschmit, and W. Endlicher, 2016: Heat waves and urban heat islands in Europe: A review of relevant drivers. *Science of The Total Environment*, 569, 527-539.
- Watkins, R., J. Palmer, and M. Kolokotroni, 2007: Increased Temperature and Intensification of the Urban Heat Island: Implications for Human Comfort and Urban Design. *Built Environment (1978-)*, 33, 85-96.
- Westcott, N. E., 1995: Summertime Cloud-to-Ground Lightning Activity around Major Midwestern Urban Areas. *Journal of Applied Meteorology*, 34, 1633-1642.

- WMO-WHO, 2015: Heatwaves and Health: Guidance on Warning System Development, [WMO-No. 1142](#).
- WMO, 2018: WMO, 2018: Guidance on Integrated Urban Hydrometeorological, Climate and Environmental Services - Volume I: Concept and Methodology. World Meteorological Organization, WMO- No. 1234. web-link: https://library.wmo.int/doc_num.php?explnum_id=9903
- WMO-MHEWS, 2018: Multi-hazard Early Warning Systems: A Checklist: Outcome of the first Multi-hazard Early Warning Conference. WMO, https://library.wmo.int/doc_num.php?explnum_id=4463
- Yoshikado, H., 1994. Interaction of the sea breeze with urban heat islands of different sizes and locations, *J. Meteor. Soc. of Japan*, 72, 139-143.
- Yoshikado, H. and Tsuchida, M., 1996. High levels of winter air pollution under the influence of the urban heat island along the shore of Tokyo Bay. *J. Appl. Meteor.*, 35, 18.04-1813.
- Zhang, D.-L., Y.-X. Shou, R. R. Dickerson, and F. Chen, 2011: Impact of Upstream Urbanization on the Urban Heat Island Effects along the Washington–Baltimore Corridor. *Journal of Applied Meteorology and Climatology*, 50, 2012-2029.
- Zhang J., Rao, S. T. 1999: The role of vertical mixing in the temporal evolution of the ground-level ozone concentrations. *Journal of Applied Meteorology*, 38:1674–1691.

5.4 Urban Canopy Models

5.4.1 Introduction

Section 5.3 has presented the impacts of cities and urban settlements on the local and mesoscale flows. This section focuses on the reasons behind these meteorological impacts: they are induced by the modification of the surface dynamical and energetic processes compared to rural areas. This section also describes the way to represent these specific urban surface processes using Urban Canopy Models (UCM).

5.4.2 Definition of UCMs

Urban canopy models, UCMs (such as Masson, 2000; Kusaka et al., 2001; Masson et al., 2002; Martilli et al., 2002; Baklanov et al., 2008; and Salamanca et al., 2010), are surface schemes that first aim to represent the energy, water, momentum exchanges between the urban surface and the atmosphere. As explained in the previous section and hereafter, urban features strongly modify the boundary layer structure, and hence, the behavior of chemical components and potentially the AQ.

In the frame of AQ modeling, some advanced features, such as building energy modules or urban vegetation, are also able to evaluate some emissions linked to a specific sector, the buildings, biogenic urban emissions, or chemical pollutants' lifetime in street canyons. However, such features are not often activated in 3-D modeling yet, and are currently mostly a way of researching and doing test studies.

5.4.3 Background of UCMs

3-D AQ modeling in cities presents some major differences with the traditional way of chemistry-inclusive mesoscale models (either in offline CTM mode, or in coupled online mode). While urban chemical emissions are of course taken into account in such modeling, other aspects also need to be modeled.

As described in the previous section, the urban climate is very specific, especially during night-time, when the UHI strengthens. Contrary to what people unfamiliar with urban climate may think, it is not the change in air temperature in itself that may change the chemistry significantly (by changing photosynthesis rates, for example). The heat fluxes from the surface are in fact drastically changing the stability within the boundary layer at night over cities. A classical nocturnal stable boundary layer is most of the time encountered over the countryside, which strongly inhibits the vertical turbulent exchanges of chemistry components. However, over cities at night, heat fluxes are often positive, realizing heat towards the atmosphere, and creating a mixed layer of typically 100 to 200 m of height. While such a mixed boundary layer height is much smaller than during daytime by up to one order of magnitude, it is enough to increase vertical mixing.

Therefore, if no specific urban modeling is performed over cities in the 3-D AQ modeling system, then all emitted chemical components, even if emissions are generally reduced compared to daytime, will accumulate unrealistically near the ground. This may, for example, destroy all ozone produced during the day by NO_x , while some ozone concentration is still observed. UCMs are mandatory to reproduce such a mixed unstable boundary layer over cities at night.

Another urban effect on the boundary layer is more straightforward. The complex 3-D shape of urban tissue, composed of many infrastructures (some of them above ground) as well as the buildings, directly modify the air flow. While for most parts of the cities, a roughness approach is reasonable to represent the friction effect on the flow in 3-D AQ mesoscale models, high-rise buildings may present a challenge for some cities, such buildings interacting with the flow even high in the boundary layer. Sometimes, it can even interact directly above the thermal inversion layer at boundary layer top, for example, at night or for coastal cities with flow coming from the sea). In such conditions, drag approaches may be necessary to improve the accuracy of the exchanges of chemistry components within the urban boundary layer. However, there is still no extensive evidence of the impact on AQ of the representation of these turbulent processes in 3-D AQ mesoscale modeling systems, especially no comparison in relation to the uncertainties on emissions. Recently developments are underway that introduce and treat dispersal and chemical reactions of emissions introduced in urban street canyons (Kim et al., 2018; Shi et al., 2018). This approach explicitly recognizes and introduces street canyons providing flow constraints and thus a framework for street level AQ exposure assessments. The feasibility and potential links to the generation of street canyon morphology data in WUDAPT levels 1 and 2 are an avenue of investigation underway as part of the WUDAPT Testbed (c.f. Section 5.6). Inherent is the need for multiscale urban morphology and real-time traffic emissions data to realize the potential of this methodology.

5.4.4 *Unique Features*

UCMs have to represent unique processes, which are not present in classical Soil-Vegetation-Atmosphere-Transfer schemes (that are dedicated to vegetation). As will be presented in subsection 3.3.3.3, there are many ways to represent them and the simpler models will not represent them all.

Here are some unique processes to take into account in UCM:

- 3-D shape of the city

Of course, the first particularity of cities that comes to mind when thinking about the impact on the flow is the 3-D shape of the city, that will produce a strong friction. Typical roughness lengths and displacement heights in cities are of the order of 1 m or more. As explained above, the presence of high-rise buildings is to be taken into account, if necessary. The 3-D shape of the urban fabric, often modeled as 'urban canyons' in UCM, may also influence the way emitted pollutants at road levels are transferred to the upper boundary layer at roof level.

- Strong heat storage

The night-time urban heat island (UHI) is mainly caused by the heat released by the urban material in evening and night. This heat reduces the cooling of the air, and modifies the structure of the boundary layer. This heat comes from a strong heat storage flux during daytime, especially in clear-sky conditions. This day-night interaction is the most important process that all UCMs tend to simulate. The storage heat flux in the soil and urban material is, in many city centers, the most important component of the energy balance, larger than sensible and latent heat fluxes combined. The 3-D shape of the city favors this storage flux, because of the larger amount of the surfaces in contact with the air, and by the type of mineral materials – bricks, concrete, stone, asphalt, tiles, etc., that have a much greater heat storage capacity than vegetation or soil.

- Radiative trapping

The 3-D shape of the buildings also induces shadows and a reduction of the amount of sky seen by each surface (the 'sky view factor'), which limits the energy loss by infra-red radiation. This tends to limit the cooling of urban surfaces during night-time, contributing to maintaining the UHI.

- Imperviousness

Cities are mostly composed of impervious surfaces, such as roads, pavements, and buildings. This has a strong impact on the energy balance, favoring sensible heat flux over evaporation. In addition to the impact on energy fluxes, the percentage imperviousness will have an impact on the re-suspension of particles to the atmosphere.

- Anthropogenic heat

Human activities also release heat directly towards the atmosphere, by traffic, industries, domestic heating or air-conditioning. Such heat translates directly into sensible heat flux (or latent heat flux). Such heat contributes to the daytime heat island (which is generally much less than daytime, but also has an impact on the population). Still, this amount of heat is typically much less than that released by the storage flux at night. Anthropogenic heat fluxes can either be prescribed to UCM (for all or part of the sector, e.g., traffic), or simulated (for buildings when a Building Energy Module (BEM) is used).

- Anthropogenic modification of the water cycle

Many activities, such as road washing (or watering for coolness), vegetation irrigation, snow removal, also modify the energy balance and the subsequent contrast between urban and rural boundary layers.

- Architecture and building materials

The way buildings are built (typologies), the alignment of streets and street canyons, and the materials used also have an impact on many flow, dispersive and radiative processes.

- Citizens

A very specific process is the one linked to human activities and building uses, that may interact subtly with the urban physics. People's behavior, e.g., by domestic heating or air-conditioning settings, modulate anthropogenic heat fluxes and related emissions. The variety of uses inside buildings, especially in densely populated areas, is necessary to be able to simulate correct energy consumption and the potential subsequent emissions.

- Urban vegetation in interaction with the urban fabric

Urban vegetation has several effects. It impacts the overall energy balance, by increasing latent heat fluxes hence reducing, at least locally, the UHI. It can reduce energy consumption by shading buildings in summer. It can also, from an AQ point of view, modify the vertical transport of pollutants, potentially keeping them near the ground longer. Biogenic emissions and their photochemical oxidation and carbon uptake by urban vegetation are also to be accounted for. While the first UCM did not simulate the interactions between urban vegetation and buildings (either by neglecting the vegetation or by treating it separately in the model grid mesh), the necessity to better represent the vegetation impacts in cities (including potentially on AQ), recent developments in UCM included the vegetation (green roofs, gardens, street trees, city parks and water bodies), within the 3-D shape of the UCM, interacting with the buildings and impervious surfaces.

5.4.5 *Impact of Buildings on AQ and Emissions*

Aerosols may also modify the urban meteorology, either influencing the amount of solar and infra-red radiation reaching the ground or by modifying the microphysics, and hence the behavior of clouds and fog over the city. UCM models do not have at present any specific processes linked to aerosols. The 3-D shape of buildings may impact the deposition of gases or aerosols, but a simple deposition velocity approach is still used in the UCM. Another aspect that some state-of-the-art UCM may contribute to is on the meteorologically-dependent emissions for some sectors (e.g., buildings, urban vegetation). Energy consumption by

domestic heating is simulated by BEM, that are present is some UCM of a medium or high degree of complexity. Energy demand could then be linked to emissions, but this is not implemented in any 3-D AQ model yet.

5.4.6 *Approaches, Considerations, Advantages and Disadvantages*

UCMs have been developed since the year 2000. They contain different levels of details in the processes as well as in the morphological representation of the city. The latter follows mainly three approaches: bulk (as in the simplest vegetation model, there is one slab layer representing the whole surface), and two approaches using a simplified urban geometry, interacting with either one atmospheric layer above the urban canopy, or with many atmospheric layers intersecting the canopy.

5.4.6.1 *Bulk (Flux Profile)*

Bulk UCMs have the sole objective to simulate the energy and momentum fluxes from the city towards the atmosphere. The number of processes is reduced, limiting their applicability, especially regarding the possibility of evaluating impacts in the urban canopy on citizens, but it is also simpler to initialize with fewer parameters. They are efficient in terms of computer time.

One example of such a model is the Surface Urban Energy and Water balance Schemes (SUEWS). It computes the energy and water fluxes towards the atmosphere, using several empirical statistical approaches (for the different fluxes) calibrated on a large number of experimental sites. The heat storage is computed using a time-hysteresis relation with net radiation.

5.4.6.2 *Urban Canopy*

Each building cannot be represented in the UCM. This is actually not necessary as they are applied to represent grid meshes in mesoscale atmospheric models, at horizontal resolution of a few hundreds of meters at best. Therefore, the urban structure is simplified in such models. There are two ways to do this simplification: to use an 'urban canyon' (a long road, bordered by walls of 2 buildings), which is the most popular, or an 'urban block', where identical blocks of one building are repeated.

These models have three main advantages:

- They are based on physical equations. In that sense, they follow the same approach as atmospheric and chemical models, they can be applied anywhere (provided that urban data are available), and can be coupled to various atmospheric models.
- The fact of representing the 3-D shape of the city (even if in a simplified way), makes it possible to take into account many processes that can be physical (e.g., radiation trapping, shadows, conduction, convection, water reservoirs, urban snow), biochemical (for urban vegetation), or sociological (e.g., buildings use, human behavior).
- Because of the large number of processes and the relatively realistic geometry, it is possible to evaluate impacts, such as microclimate and human comfort within the canyon, inside temperature and energy consumption by buildings, water consumption, etc.

- Single layer

Single layer models interact with the atmosphere at only one layer, located several meters above roof level. In such models, the urban canyon climate is in general deduced by analytical laws (such as logarithmic-exponential laws), that is in equilibrium with the fluxes coming from the various surfaces (e.g. walls and road) and the atmospheric conditions above. These models generally do not describe the buildings vertically.

One can further consider these models in two categories. There are those that treat the canyon as a whole (SM2U, TERRA-URB), where there is no distinction between walls and roads, but they are limited in processes, especially they must treat urban vegetation relatively simply and cannot include a building energy module.

Most of the single layer models treat the different surfaces separately (walls that can be distinct depending on orientation, roofs, road). This allows a very large number of processes to be considered. The single-layer version of the Town Energy Balance (TEB, Masson 2000) model for example, in addition to the simulation of energy fluxes, treats urban snow on roofs and roads, green roofs, street trees (with their shadowing effects), low vegetation in the canyon, has a BEM that includes several buildings' use within the same grid mesh and simulates inhabitants' energetic behavior.

A main interest of single layer models is that they are efficient in terms of CPU time. When they are coupled within a mesoscale atmospheric model, the extra cost is generally of the order of 1%. This explains why many Numerical Weather Prediction (NWP) models at kilometric resolution use this type of UCM (e.g., WRF, GEM in Canada, Enviro-HIRLAM in Denmark, COSMO consortium, ALADIN-HIRLAM consortia models have one).

- Multi-layer

A multi-layer model interacts with the atmosphere on several layers. An example of such model is the Building Environment Parameterization (BEP) (Martilli et al., 2001), which has been designed for such applications from the start. BEP also describes the vertical variability of the height of the buildings within the grid mesh, and simulates several buildings floors, corresponding to the atmospheric model's layers. BEP also has a BEM. TEB now also has a multi-layer version (but without discretizing the walls themselves on the vertical, Hamdi and Masson, 2008). The need for input urban data is similar as for single-layer models.

The main advantage of multi-layer models is that the influence of the urban canopy on the boundary layer follows a more realistic approach than single layer models, by use of a drag approach instead of the classical roughness length. This allows for example to simulate the direct impact of high-rise buildings.

However, multi-layer UCMs have drawbacks: they are more complicated so it is more difficult to add new processes, and they are computationally expensive, mainly because of the refined vertical grid mesh (typically 5m near the ground) within the atmosphere.

5.4.7 *Data Requirements and Infrastructure Support*

There is often a lack of data to physically represent the city in the model (it is represented chemically by emissions). This indeed is a crucial problem, especially in developing countries where urban data may not exist, or exist but not be useable or reachable. Global databases from satellites often lack a description of urban classes (until recently, only one or at most three urban classes were present).

UCMs need many specific parameters that in general are not available in databases for atmospheric models, because of the specificity of the processes treated. The UCM parameters encompass land use and land cover information (e.g., the fraction of buildings), morphological parameters (e.g., mean height of buildings), architectural parameters (e.g., albedo of surfaces for example), socio-economical parameters (e.g., building use), and information on urban vegetation, when the latter is represented in the UCM.

Several methods exist to define these parameters. When building and/or road databases are available, these can be used to derive a very fine description of the city and countryside at a scale suitable for the UCM. However, for most locations, and even for most parameters, such a database does not exist. For example, extensive databases on construction materials is something very rare, even on the scale of a city.

An approach based on the 'Local Climate Zone' (LCZ) classification is defined by the urban climate scientist's community. The LCZ classifies the urbanized covers in 10 classes (dense and open high-rise, medium-rise and low-rise buildings, informal settlements, sparsely built, open low-rise and large industries) and also describes the countryside. It is possible to classify these LCZs using satellite data, and then to assign UCM parameters to each urban LCZ. This is the methodology of the WUDAPT (Section 3.3.5) initiative, in which a common methodology is used by many institutions to map cities in the world. For some parameters that are not accessible (such as construction materials, colors of wall, etc.), a value is given for each LCZ, by an expert methodology involving architects or by crowdsourcing.

5.4.8 *Modeling System and Applications*

Any modeling system should contain, and apply, both UCM and AQ chemistry to be used for 3-D AQ mesoscale modeling within cities. This is especially true when the city is large enough compared to the resolution of the model to occupy several grid meshes of the model. Indeed, in such modeling conditions, this will allow the simulation of the meteorological specificities of the urban climate (UHI, mixed layer at night, high roughness), and the subsequent impacts on the AQ within the city itself. Note that these considerations hold for modeling systems with grid meshes as fine as a few hundred meters. At finer scales, models should represent the buildings individually, and UCMs are no more adapted at those scales.

When urban AQ at city or neighborhood scales is to be evaluated, UCMs should be used, whatever the mesoscale modeling approach used:

- Mesoscale atmospheric model with an offline CTM model
- A coupled inline atmospheric-chemistry model

Indeed, the urban dynamical impact on the AQ is mostly due to strong alterations of the boundary layer. Therefore, it is necessary to activate the UCM within the atmospheric part of the system: either the coupling atmospheric model for the CTM, or the atmospheric-chemistry model itself for the inline approach.

Indeed, even if UCMs often now exist within the atmospheric model, this is often not activated, and this for various reasons:

- The resolution of the AQ forecast system is coarse (of the order of 10 km). At such a scale, UCMs could be turned off, but this strongly limits the interpretation of the model result for AQ in large cities.
- As stated above, there is a lack of data to physically represent the city in the model.
- There is a lack of expertise, and the need to activate the UCM is not obvious. This section of the guide aims to improve this aspect.

There are many possible applications on cities with atmospheric mesoscale models using an UCM. For example, one can cite: UHI studies, meteorological and air quality forecasting, energy balance modeling, risk assessment, climate change assessment, urban planning and design. Air quality aspects could be incorporated in all of these. How does the UHI modify the AQ? How will AQ specifically evolve in the future climate, in link with urban climate, urban design and chemistry emission scenarios?

There are many systems with both a specific representation of urban processes using a UCM, as well as an atmospheric chemistry module. The main message here is that whatever your system (offline or online), if you want to address AQ questions within cities, an UCM module should be activated in the atmospheric model that you use.

5.4.9 Summary

- Urban Canopy Models simulate unique radiative, energetic, anthropogenic, hydrologic processes linked to city-atmosphere interactions.
- The structure of the urban boundary layer is fundamentally different to the rural one, especially at night (when it is neutral or even convective), leading to a strongly modified mixing of pollutants.
- Mesoscale models now often include one state-of-the-art UCM, but description of urban data is still an issue. The description of the urban structure with the Local Climate Zones approach helps to have access to a better urban representation in atmospheric models.
- Whatever the chemistry approach (offline or online), to address AQ questions within cities, an UCM should be activated in the atmospheric model used.

References

- Baklanov A., P. Mestayer, A. Clappier, S. Zilitinkevich, S. Joffre, A. Mahura, N.W. Nielsen, 2008: Towards improving the simulation of meteorological fields in urban areas through updated/advanced surface fluxes description. *Atmospheric Chemistry and Physics*, 8, 523-543.
- Brown, M.J., 2000. Urban parameterizations for mesoscale meteorological models. *Mesoscale atmospheric dispersion*, pp.193-255.
- Dupont, S., Otte, T.L. and Ching, J.K., 2004. Simulation of meteorological fields within and above urban and rural canopies with a mesoscale model. *Boundary-Layer Meteorology*, 113(1), pp.111-158.
- Dupont, S. and Mestayer, P.G., 2006. Parameterization of the urban energy budget with the submesoscale soil model. *Journal of Applied Meteorology and Climatology*, 45(12), pp.1744-1765.
- Freitas, E. D.; Rozoff, C; Cotton, W. R.; Silva Dias, P. L., Interactions of urban heat island and sea breeze circulations during winter over the Metropolitan Area of São Paulo – Brazil. *Boundary-Layer Meteorology*, v. 122, n. 1, p. 43-65, 2007.
- Freitas, S. R., et al. (2017), The Brazilian developments on the Regional Atmospheric Modeling System (BRAMS 5.2): an integrated environmental model tuned for tropical areas, *Geosci. Model Dev.*, 10(1), 189-222, doi: 10.5194/gmd-10-189-2017
- Grimmond, C.S.B. and T. Oke, 1991: An evaporation-interception model for urban areas, *Water resources Res.*, 27, 1739-1755.
- Hamdi, R. and V. Masson, 2008 : Inclusion of a drag approach in the town energy balance (TEB) scheme : offline 1-d validation in a street canyon. *Journal of Applied Meteorology and Climatology*, 47, 2627-2644.
- Kim, Y., Y. Wu., C. Seigneur, Y. Roustan 2018: SING Multi-scale modeling of urban air pollution: development and application of a Street-in-Grid model (v1.0) by coupling MUNICH (v1.0) and Polair3D (v1.8.1) *Geosci. Model Dev.*, 11, 611–629, 2018 <https://doi.org/10.5194/gmd-11-611-2018>
- Kondo, H., Genchi, Y., Kikegawa, Y., Ohashi, Y., Yoshikado, H. and Komiyama, H., 2005. Development of a multi-layer urban canopy model for the analysis of energy

consumption in a big city: Structure of the urban canopy model and its basic performance., *Boundary-Layer Meteorology*, 116(3), pp.395-421.

- Kusaka, H., Kimura, F., 2004, "Coupling a Single-Layer Urban Canopy Model with a Simple Atmospheric Model: Impact on Urban Heat Island Simulation for an Idealized Case.", *Journal of the Meteorological Society of Japan*, Vol. 82, No. 1, pp. 67-80., doi: 10.2151/jmsj.82.67.
- Kusaka, H., Kondo, H., Kikegawa, Y. and Kimura, F., 2001. A simple single-layer urban canopy model for atmospheric models: comparison with multi-layer and slab models. *Boundary-Layer Meteorology*, 101(3), pp.329-358.
- Lemonsu, A.; Grimmond, C. S. B.; Masson, V., Modeling the Surface Energy Balance of the Core of an Old Mediterranean City: Marseille, *Journal of Applied Meteorology*, 2004, vol. 43, p. 312-327.
- Lemonsu, A.; Masson, V.; Shashua-Bar, L.; Erell, E.; Pearlmutter, D., Inclusion of Vegetation in the Town Energy Balance model for modeling urban green areas, *Geoscientific Model Development*, 2012, vol. 5, p. 1377-1393.
- Martilli, A.; Clappier, A.; Rotach, M. W., An urban surface Exchange parameterization for mesoscale models. *Boundary-Layer Meteorology*, 2002, vol. 104, p. 261-304.
- Martilli, A., A two-dimensional numerical study of the impact of a city on atmospheric circulation and pollutant dispersion in a coastal environment, *Boundary-Layer Meteorology*, 2003, v. 41, p. 1247-1266.
- Martilli, A., Current Research and future challenges in urban mesoscale modeling, *International Journal of Climatology*, 2007, vol. 27, n. 14, p. 1909-1918.
- Masson, V., A physically-based scheme for the urban energy budget in atmospheric models. *Boundary-Layer Meteorology*, 2000, vol. 94, p. 357-397.
- Otte, T.L., Lacser, A., Dupont, S. and Ching, J.K., 2004. Implementation of an urban canopy parameterization in a mesoscale meteorological
- Salamanca, F., Krpo, A., Martilli, A. and Clappier, A., 2010. A new building energy model coupled with an urban canopy parameterization for urban climate simulations—Part I. formulation, verification, and sensitivity analysis of the model. *Theoretical and Applied Climatology*, 99 (3-4), p.331.
- Salamanca, F. and Martilli, A., 2010. A new Building Energy Model coupled with an Urban Canopy Parameterization for urban climate simulations—Part II. Validation with one dimension online simulations. *Theoretical and Applied Climatology*, 99(3-4), p.345.
- Salamanca, F., Martilli, A., Tewari, M. and Chen, F., 2011. A study of the urban boundary layer using different urban parameterizations and high-resolution urban canopy parameters with WRF. *Journal of Applied Meteorology and Climatology*, 50(5), pp.1107-Sarrat, C., A. Lemonsu, V. Masson, and G. Guédalia, 2006: Impact of urban heat island on regional atmospheric pollution. *Atmos. Environ.*, 40, 1743-1758.
- Schoetter R., V. Masson, A. Bourgeois, M. Pellegrino, and J.-P. Lévy (2017): Parametrization of the variety of human behaviour related to building energy consumption in TEB (SURFEX v. 8.2), *Geoscientific Model Development*, 10, 2801–2831, doi: 10.5194/gmd-10-2801-2017
- Shi Y., X.L. Xie, J.C.H. Fung and E. Ng (2018) Identifying critical building morphological design factors of street-level air pollution dispersion in high-density built environment using mobile monitoring. *Building and Environment* 128, 248-259.
<https://doi.org/10.1016/j.buildenv.2017.11.043>.
- Ward H.C., Y. Tan, A. M. Gabey, S. Kotthaus, W.T.J. Morrison, C.S.B. Grimmond, 2017: Impact of temporal resolution of precipitation forcing data on modeled urban-atmosphere exchanges and surface conditions, *Int. J. Climatol* 10.1002/joc.5200.

5.5 Coupling with Parameterized or Computational Fluid Dynamics Models

5.5.1 Introduction

In urban environments, interaction between the atmosphere and urban obstacles (e.g., buildings, trees, vehicles) induces complex flows within streets and squares. This fact, linked to the irregular emission sources in the city, mainly traffic, produces strong gradients of pollutant concentration within the streets. For example, in a recent study in an urban zone of Madrid (Spain), Borge et al. (2016) recorded differences up to a factor four in 3-week average NO_2 concentrations at distances of less than 300m ($200 \mu\text{g m}^{-3}$ vs. $50 \mu\text{g m}^{-3}$). Therefore, a detailed air quality assessment or forecasting in urban areas would need microscale models to capture this type of pollutant distribution. It is important to quantify population exposure to air pollution that has an impact on health. This will provide useful information for public, e.g., which route to take when walking or riding a bicycle.

The scales of atmospheric processes involved inside the urban canopy layer (UCL) range from street scale to a scale greater than the city, including processes at neighborhood scale (Britter and Hanna, 2003; Schlünzen et al., 2011). Horizontal spatial resolution of mesoscale models is not usually higher than 1 km to a few hundred meters. In urban environments, these models use urban canopy modules (UCM) (see Section 5.4) to represent the dynamical effects and heat exchanges between urban surfaces and atmosphere. However, urban obstacles cannot be resolved explicitly and UCM provides variable representatives of the spatial average over mesoscale grid cells. Therefore, the coupling with a microscale model, whose spatial resolution can be of the order of 1 m is needed to model processes at lower spatial scale and provide more accurate concentration at street levels. As an example, Figure 5.12 illustrates the concentration distribution provided by a microscale model in a $1 \text{ km} \times 1 \text{ km}$ domain corresponding to an urban area of Madrid (Spain).

Microscale models are classified in two types:

- Parameterized models. These models are based on parametric relations between simplified descriptions of urban geometry and the dispersion of pollutants.
- Full computational fluid dynamics (CFD) models. These models consider explicitly the urban obstacles, solving the momentum, turbulence and energy equation at high spatial resolution (order of meters).

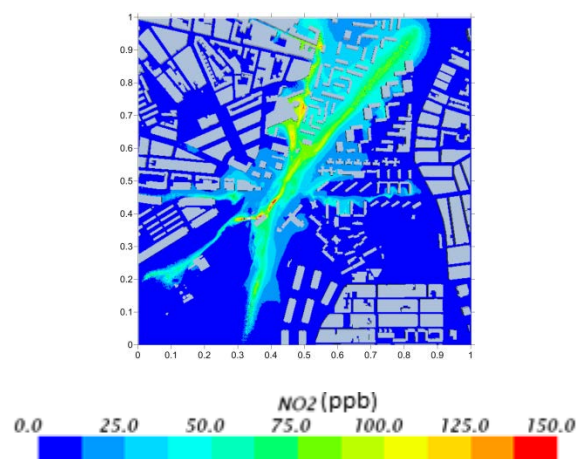


Figure 5.12. Spatial distribution of pollutant concentrations in $1 \text{ km} \times 1 \text{ km}$ with a full CFD model. This domain is the equivalent to a grid cell of a mesoscale model.

5.5.2 *Parameterized Microscale Models*

Parameterized microscale models are semi-empirical models based on assumptions about the characteristics of the flow and dispersion of pollutants within and above the urban canopy layer as a function of the urban geometry of the study area. The input data of these models are urban morphology, forcing meteorological parameters, background concentration of pollutants and the emissions in each street within the domain. Some examples of parameterized models are OSPM, SIRANE, QUIC or MUNICH. The Danish Operational Street Pollution Model (OSPM) provides the pollutant concentrations by means of the combination of a plume model and a box model taking into account the direct contribution from vehicle exhausts and the recirculation in the streets (Berkowicz, 2000). The SIRANE model is an urban dispersion model that computes the flow and dispersion in two regions: the overlying atmospheric boundary layer and the urban canopy, represented by a simplified network of connected streets modeled as boxes (Souhac, 2011). Conceptually based on the general formulation of SIRANE is the Model of Urban Network of Intersecting Canyons and Highways (MUNICH) (Kim et al., 2018). This street-network model consists of two main components: a street-canyon component and a street-intersection component. Finally, the QUIC model (Quick Urban and Industrial Complex model) computes three-dimensional wind, concentration, and deposition fields around buildings in a short time. The wind solver is an empirical diagnostic model and the dispersion model is a Lagrangian random-walk code that computes the 3-D trajectories of a great number of markers that represent gases and aerosol dispersion in the air (Brown et al., 2015).

Multiscale systems of models have been developed using these parameterized models to simulate the concentration at street level. For example, the MUNICH model is coupled to the Polair3D Chemical Transport Model of Polyphemus air quality modeling platform to constitute a Street-in-Grid model (Kim et al., 2018). Another instance is the THOR system, an Integrated Air Pollution Forecasting and Scenario Management System which uses the OSPM model to provide air pollution concentration (NO, NO₂, NO_x, O₃, CO and benzene) at both sides of the streets.

These parameterized models do not resolve explicitly the wind flow and dispersion around the buildings, however the main advantage is the low computational cost required. Therefore, the use of these models is suitable for AQ forecasting, despite the loss in accuracy in comparison with CFD models, in particular in complex urban configurations.

5.5.3 *Full CFD Models*

CFD models solve the momentum, turbulence, energy and pollutant transport equations within the urban canopy and above. The turbulent flow around the urban obstacles (e.g., buildings, trees, etc.) is explicitly resolved by means of numerical methods over a computational mesh of the order of a few meters in horizontal and vertical directions. Then, the main processes involved within the urban canopy are solved with an appropriate spatial resolution to capture the pollutant distribution in a city. For a study zone of 1 km², the grid would be of several millions of cells, and thereby requires large computational resources. This fact makes it difficult to directly use these models for forecasting.

Two approaches are mainly used: Reynolds-Averaged Navier-Stokes (RANS) where the whole turbulence spectrum is parameterized and Large-Eddy Simulations (LES) that resolves explicitly the unsteady dynamics of large-scale turbulent motions while modeling the effects of subgrid motions by means of a spatial filtered operator applied to the Navier-Stokes equations. LES are considered more accurate but the CPU time required is much higher than RANS (about two orders of magnitudes).

To simulate an urban zone using a CFD model, details of the building geometry of the area are required. Additionally, at the inlet of the domain, vertical profiles of all variables are needed. For example, a RANS model with k - ϵ turbulence closure needs inlet vertical profiles of wind speed and direction, turbulent kinetic energy (TKE), turbulence dissipation rate (ϵ), temperature and pollutant concentration. The mesoscale model can provide the time evolution

of these profiles for each variable. However, several difficulties arise like in the interpolation of mesoscale outputs for CFD model inlet conditions due to differences in the spatial resolution between models or the fact that CFD needs variables like the turbulence dissipation rate that are not always computed by the mesoscale model. In this section, different types of coupling between mesoscale (e.g., Enviro-HIRLAM, WRF) and CFD models, that could be applied now or in the future, are described.

5.5.3.1 *Online Coupling Meteorological/AQ Mesoscale Variables into the CFD Model*

The multiscale modeling system from mesoscale to urban scale comprising the building effects is a big challenge for the assessment and forecasting of the air quality in cities. The downscaling considering nested domains from different types of models requires high computational resources and accuracy in the representation of the scale interaction. An example of nested models is the Environment-High Resolution Limited Area Model (Enviro-HIRLAM) at city-scale and the Microscale Model for Urban Environment (M2UE) (Baklanov et al., 2009). In urban environments, the mesoscale model parameterizes the building effects using BEP (Martilli et al., 2002), whereas the M2UE solves the flow and dispersion among urban obstacles based on the RANS equations with a k- ε turbulence closure (Nuterma et al., 2010). In this way, the coupled system of the Enviro-HIRLAM and the M2UE allows the up- and down- scaling transfer (two-way nesting) between both models (Baklanov et al., 2009). Test realization of such a coupled system in a simplified (one-way nesting) configuration was performed for street-scale AQ forecasting in Copenhagen within the European MACC project (Nuterma et al., 2011). Preliminary outcomes of this test showed a notable improvement of AQ forecasts at urban and street scales.

An integrated multiscale system has also been developed through the Weather Research and Forecasting (WRF) model and microscale urban models for the transport and dispersion of pollutants, e.g., CFD-Urban and EULAG. CFD-Urban is a model based on the RANS equations with the standard k- ε turbulence closure. It simulates the fields of wind, turbulence, and dispersion in urban areas taking into account the building structures (Coirier et al., 2006). The buildings that are not explicitly resolved are simulated by means of the drag terms in the equations of momentum, and turbulent kinetic energy and its dissipation. The WRF data (wind components, temperature, TKE and the momentum diffusion coefficient, μ_t) are used to provide the initial and boundary conditions to the CFD-Urban model, unlike the dissipation rate that is computed from μ_t relation ($\varepsilon = \rho C_\mu \frac{tke^2}{\mu_t}$). Hence, the one-way nesting is carried out in real time (Tewari et al., 2010). Similar to the CFD-Urban model, EULAG is an EULERian/semi-LAGRangian model based on LES, which has also been coupled with the WRF model. The downscaling modeling from WRF to the EULAG is performed and validated for pollutant dispersion at urban scale (Wyszogrodzki et al., 2012). A good accuracy of microscale simulation is usually found, even if, obviously, the microscale model performance depends on the quality of the mesoscale weather forecast.

A key aspect of the online coupling is the scale ratio between the grid resolutions where the main limitation is also the choice of the interpolation for the meteorological variables from coarse to fine mesh because it can modify the results in the streets. In addition, this aggregated system may allow transferring the features of the microscale flow to the mesoscale model. However, the upscaling modeling requires large computational resources (Baklanov et al., 2009).

5.5.3.2 *Offline Coupling Meteorological/AQ Mesoscale Variables into the CFD Model*

The offline coupling consists of the use of outputs derived from a mesoscale model as boundary conditions of the CFD models without running both models at the same time. To that end, the inlet conditions are obtained from the mesoscale grid point corresponding to the microscale computational domain. In that regard, the meteorological mesoscale and air quality models provide the time-dependent conditions for the CFD simulation.

The vertical profiles of the meteorological variables, e.g., horizontal wind components, air

temperature and turbulent kinetic energy can be imposed as inlet of the CFD simulation. Nevertheless, depending on the turbulence closure used in the CFD model, the additional variables have to be computed keeping the relation to the turbulent kinetic energy. In the case of the k - ϵ turbulent closure, the turbulent dissipation rate (ϵ) is calculated as follows, $\epsilon_{in} = C_{\mu}^{3/4} k_{in}^{3/2} / (\kappa z)$ or by means of the expression of turbulent viscosity ($\mu_t = \rho C_{\mu} k^2 / \epsilon$), C_{μ} is a model constant, κ is the von Karman's constant (0.4) and z is the height above ground. The difference in the turbulence closure between the mesoscale and microscale models is one of the limitations of this kind of coupling. However, an alternative solution is to simulate the mesoscale processes well upwind of the buildings area in the CFD domain and thus to hold the inlet vertical profiles until the research area. Finally, the finest resolution and accuracy of solving the turbulent processes in the CFD model improve the outcomes at local scale.

Additionally, the background pollutant concentrations are derived from air quality models. Hence, the concentration profiles are directly imposed at the inlet of the CFD domain and are properly transported and mixed with the local sources with a higher spatial resolution of the CFD models. An example of this type of coupling could be found in Borge et al. (2018) where WRF/CMAQ mesoscale models were coupled with a CFD model to simulate one hour of a high pollution episode in Madrid (Spain).

5.5.3.3 Coupling Meteorological/AQ Mesoscale Model and Pre-run CFD Simulations

In order to avoid the computational cost problem of running a CFD model for air quality forecasting but keeping the advantages of CFD simulations (e.g., spatial resolution, atmospheric processes resolved, etc.), pre-run CFD simulations could be used for the downscaling of mesoscale results. The methodology is based on creating a database of CFD simulations with wind flow and dispersion over the studied zone for different conditions. Mesoscale simulations provide hourly meteorological and air quality predictions at a spatial resolution from 1 km to a few hundred meters. These predictions are used to select the appropriate pre-run CFD simulation from the database and to modify it depending on the mesoscale conditions. Figure 5.13 illustrates the description of this type of downscaling.

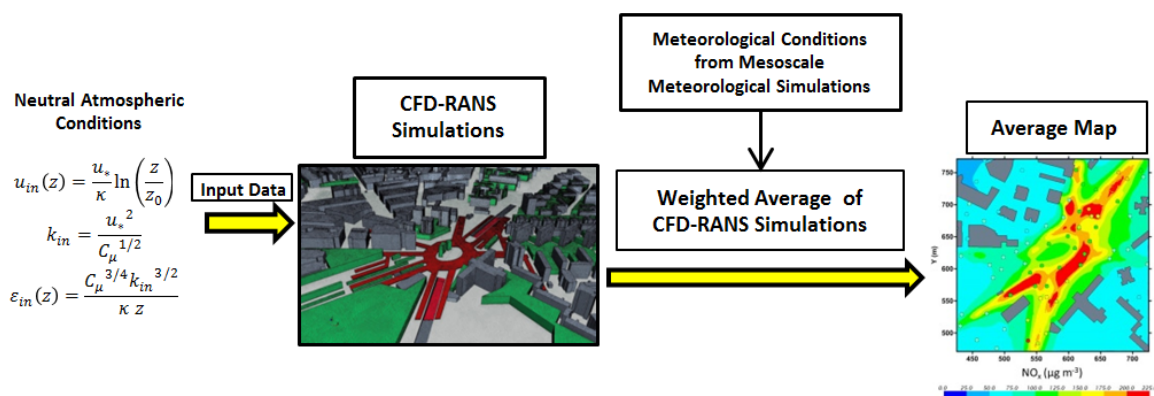


Figure 5.13. Simplified scheme of the numerical approach of the multiscale system.

This methodology has been already evaluated for air quality assessment (Santiago et al., 2013; Vranckx et al., 2015; Santiago et al., 2017; Sanchez et al., 2017). In these studies, 16 CFD-RANS simulations were performed for different wind directions (N, NNE, NW and so on). Logarithm vertical profiles of velocity (neutral conditions) considering a reference wind speed were used. In addition, for each wind direction, several emission scenarios are simulated representing hourly traffic emissions for each day. Firstly, mesoscale wind direction is used to select from the database the CFD simulation closest to this direction. In addition, the wind flow is modified by the ratio between the mesoscale reference wind velocity (u_{meso}) and the inlet wind speed used in the selected CFD simulation ($u_{refmicro}$). Concerning pollutant concentrations, two contributions should be considered:

- (1) Background concentration (C_{backg}). Concentration transported from other areas not

simulated by CFD model.

- (2) Local concentration (C_{local}). Concentration due to local emissions considered in CFD simulations.

The $C_{local}(u_{refmicro})$ map obtained by the selected CFD simulation for $u_{refmicro}$ is transformed by the ratio $u_{refmicro}/u_{meso}$, taking into account that this concentration is inversely proportional to wind speed for non-reactive pollutants. Concerning the background concentration, previous works obtained this value from recorded concentrations at urban background stations close to the studied zone. However, for air quality forecasts, C_{backg} should be taken from a mesoscale model at a certain height that represents the urban background. Therefore, the hourly concentration at each cell of the microscale domain is computed as,

$$C = (C_{local}(u_{refmicro}) * u_{refmicro}/u_{meso}) + C_{backg}$$

Regarding the reference wind speed, Santiago et al. (2013) and Santiago et al. (2017) used the wind speed at a reference height (usually employed 10 m, the height where wind speed and direction were recorded by the urban meteorological stations), however, Sanchez et al. (2017) observed a better agreement with experimental data when friction velocity from mesoscale simulation is used as reference wind speed. In this way, the same vertical flux at the top of the canopy is imposed by means of the ratio of friction velocities. This coupling has several limitations. Firstly, it can only be applied for non-reactive pollutants as particulate matter or NO_x . However, NO_2 could also be computed in winter conditions where highest levels are recorded (Sanchez et al., 2016; Santiago et al., 2017; Rivas et al., 2019). Usually, chemistry is neglected in CFD simulations because of the increase in computational time. This issue is a limitation for NO_2 forecasts, especially important in urban environments in summer conditions. However, the continuous increase of computational resources has made it possible that CFD studies including chemical reactions of nitrogen oxides and ozone are becoming more frequent (e.g., Kwak et al., 2015; Sanchez et al., 2016). Finally, CFD simulations are run for neutral conditions. These issues can be addressed increasing the number of simulations considering different inlet conditions and reactive pollutants for the database of simulated scenarios by CFD model.

5.5.4 Summary

- High spatial resolution is needed to capture pollutant concentration spatial variability at pedestrian level in an urban environment.
- Microscale models are useful for this purpose.
- CFD models coupled with mesoscale models resolve the turbulent flow and pollutant dispersion around urban obstacles but require high computational resources.
- A database created with CFD simulations of several scenarios can be an alternative way to do the downscaling of mesoscale variables.
- Parameterized microscale models do not explicitly resolve flow and dispersion within the urban canopy but can provide a simplified representation in reasonable CPU time.
- In the near future, CFD can become an appropriate tool for forecasting purposes due to the continuous increase of computational resources.

References

Baklanov, A.A., Nuterman R.B., 2009. Multi-scale atmospheric environment modeling for urban areas. *Advance in Science Research*, 3, 53-57.

- Berkowicz, 2000. OSPM - A Parameterized Street Pollution Model. *Environmental Monitoring and Assessment*, 65, 323-331.
- Britter RE, Hanna SR (2003) Flow and dispersion in urban areas. *Annu Rev Fluid Mech* 35:469–496.
- Borge, R., Narros, A., Artiñano, B., Yagüe, C., Gomez-Moreno, F.J., de la Paz, D., Román-Cascon, C., Díaz, E., Maqueda, G., Sastre, M., Quaassdorff, C., Dimitroulopoulou, C., Vardoulakis, S., 2016. Assessment of micro- scale spatio-temporal variation of air pollution at an urban hot spot in Madrid (Spain) through an extensive field campaign. *Atmospheric Environment* 140, 432-445.
- Borge, R., Santiago, J.L., de la Paz, D., Martín, F., Domingo, J., Valdés, C., Sanchez, B., Rivas, E., Rozas, M.T., Lázaro, S., Pérez, J., Fernández, A., 2018. Application of a short term air quality action plan in Madrid (Spain) under a high-pollution episode- Part II: Assessment form multi-scale modeling. *Science of the Total Environment*, 635, 1574-1584.
- Brown, M.J., Williams, M.D., Nelson, M.A., Werley, K.A., 2015. QUIC Transport and Dispersion Modeling of Vehicle Emissions in Cities for Better Public Health Assessments. *Environmental Health Insights* 9, 55-65.
- Coirier W, Kim S., 2006. CFD Modeling for Urban Area Contaminant Transport and Dispersion: Model Description and Data Requirements. *American Meteorological Society's 6th Symposium on the Urban Environment, Atlanta, GA, Amer. Meteor. Soc.*, 11.
- Kim, Y., Wu, Y., Seigneur, C., Roustan, Y., 2018. Multi-scale modeling of urban air pollution: development and application of a Street-in-Grid model (v1.0) by coupling MUNICH (v1.0) and Polair3D (v1.8.1). *Geoscientific Model Development* 11, 611-629.
- Kwak, K.H., Baik, J.-J., Ryu, Y.-H., Lee, S.-H., 2015. Urban air quality simulation in a high-rise building area using a CFD model coupled with mesoscale meteorological and chemistry-transport models. *Atmospheric Environment*, 100, 167-177.
- Martilli, A., Clappier, A., Rotach, M., 2002. An urban surface exchange parameterization for mesoscale models. *Boundary-Layer Meteorology*, 104 (261–304).
- Nuterman R.B., Starchenko A., Baklanov A.A., 2010. Prediction of air flow and pollution dispersion above urban obstacles on the basis of microscale model resolved arrays of vegetation and buildings. *CLIMAQS Workshop Local Air Quality and its Interactions with Vegetation, January 21-22, 2010, Antwerp, Belgium*.
- Nuterman, R., B. Amstrup, A. Mahura, A. Baklanov, A. Zakey, D. Banciu, O. Diaconu, S. Tascu, M. Pietrisi, R. Dumitrache, 2011: Core-downstream processing chain test cases. Running the full downscaling model systems based on the MACC forecasts. Report D_OINT_2.7.1-2, October 2011, 27pp.
- Rivas, E., Santiago, J.L., Lechón, Y., Martín, F., Ariño, A., Pons, J.J., Santamaría, J.M., 2019. CFD modeling of air quality in Pamplona City (Spain): Assessment, stations, spatial representativeness and health impacts valuation. *Science of the Total Environment*, 649, 1362-1380.
- Sanchez, B., Santiago, J.L., Martilli, A., Martín, F., Borge, R., Quaassdorff, C., de la Paz, D., 2017. Modeling NO_x Concentrations through CFD-RANS in an Urban Hot Spot Using High Resolution Traffic Emissions and Meteorology from a Mesoscale Model. *Atmospheric Environment*, 163, 155-165.
- Sanchez, B., Santiago, J.-L., Martilli, A., Palacios, M., Kirchner, F., 2016. CFD modeling of reactive pollutant dispersion in simplified urban configurations with different chemical mechanisms. *Atmospheric Chemistry and Physics*, 16 (18), 12143-12157
- Santiago, J.L., Borge, R., Martín, F., de la Paz, D., Martilli, A., Lumbreras, J., Sanchez, B. (2017). Evaluation of a CFD-based approach to estimate pollutant distribution within a real urban canopy by means of passive samplers. *Science of the Total Environment*, 576, 46-58.

- Santiago, J.L., Martin, F., Martilli, A., 2013. A computational fluid dynamic modeling approach to assess the representativeness of urban monitoring stations. *Science of The Total Environment*, 454-455, 61-72.
- Schlünzen, K. H., D. Grawe, S. I. Bohnenstengel, I. Schlüter and R. Koppmann. 2011. 'Joint Modeling Of Obstacle Induced And Mesoscale Changes – Current Limits and Challenges'. *Journal of Wind Engineering and Industrial Aerodynamics*. *Wind Eng. Ind. Aerodyn.* 99: 217–25. doi: 10.1016/j.jweia.2011.01.009.
- Soulhac, L., Salizzoni, P., Cierco, F.-X., and Perkins, R., 2011. The model SIRANE for atmospheric urban pollutant dispersion; Part I, presentation of the model, *Atmos. Environ.*, 45, 7379 – 7395.
- Tewari M, Kusaka H, Chen F, Coirier W., Kim S., Wyszogrodzki A., Warner T., 2010. Impact of coupling a microscale computational fluid dynamics model with a mesoscale model on urban scale contaminant transport and dispersion. *Atmospheric Research*, 96 (656-664).
- Vranckx, S., Vos, P., Mahieu, B., Janssen, S., 2015. Impact of trees on pollutant dispersion in street canyons: A numerical study of the annual average effects in Antwerp, Belgium. *Science of The Total Environment* 532, 474-483.
- Wyszogrodzki, A., Miao, S., Chen, F., 2012. Evaluation of the coupling between mesoscale-WRF and LES-EULAG models for simulating fine-scale urban dispersion. *Atmospheric Research* 118 (324–345).

5.6 Urban Data and Tools for CW-AQF Models

5.6.1 Introduction

A wide variety of input data is required to support air quality modeling systems performing myriad of applications, and purposes, and contexts. Such data need to be appropriate to the spatial and temporal resolutions and land use complexities of the application problem. This section focuses on data inputs and tools to support AQ modeling systems applications in urban areas and urban modules as in Section 5.4. The modeling of the transport, chemical transformation, composition (speciation) and concentration, and surface exchange processes are scale dependent. The model inputs, meteorological, emission and characterization of land surfaces are also scale and time dependent. Underlying surface roughness and vegetative coverage serve as sources or sinks for chemical species via deposition and re-suspension processes. Modeling frameworks are basically either fixed or on moving coordinates; the increased scale resolution requires careful attention, albeit commonly based on nesting techniques. Given the inherent nonlinearities that can occur between transport and chemistry and also on all scales, model results will depend on the degree to which these feedbacks are allowed. AQF modeling systems will be particularly challenged when handling scale- dependent issues due to the complex nature of the surfaces. In urban modeling applications, issues of complexities and heterogeneities of the myriad of morphological features, emission sources, and scale-dependent nonlinearities between transport and chemistry are considerably enhanced.

5.6.2 *Data Requirements and Tools for Urban Scale Applications*

The purpose of this section is on the data requirements and tools to support the needs of models in urban context. We provide a framework capable of supporting modern model treatments of urban air quality models given the context of wide range, diversity and complexity of the underlying city surfaces. It is important to also appreciate that these complexities will impact to varying extents the flow and thermal characteristics of cities, e.g., urban heat and cool islands, which will influence the chemistry and depositional aspects in models. Further classes of applications such as street level pollutant exposure is morphology dependent in cities where the channelling effect of street canyons prevail and even dominate. The characteristics and diversity of morphological features that distinguish urban from their rural counterparts are exemplified in Figure 5.14.

While a scaling roughness length for models is suitably appropriate for homogeneous surfaces, it can be inadequate for situations characterized by high degrees of heterogeneity in areas such as in cities. For urban modeling, an alternative to the roughness scaling approach more appropriate to handling the highly heterogeneous urban surfaces is proposed and details can be found in Section 5.4. Cities are characterized with complex land cover consisting of morphological elements to create impervious surfaces containing 2-D-3-D buildings of varying typological characteristics of building density, size, composition and heights, road and sidewalk systems, and pervious surfaces including trees, lawns, parks, and water bodies. Buildings in urban models can be parameterized by various combinations of morphological parameters shown in Figure 5.14(b). Canopy modeling will be based on some combinations of parameters including:

- Average building height, standard deviation/maximum height
- Aspect ratios and standard deviation (distribution)
- Fraction of buildings, green, paved, water (e.g., river, lake, ocean, ...), open soil
- Type and size of green (leaf area index and phenology)
- Building materials: radiative (e.g., albedo, emissivity) and thermal (e.g., heat capacity, diffusivity)
- Speciated vegetative cover that influences gaseous and particulate matter uptakes (deposition) and biogenic emissions of oxidizing VOCs such as isoprene and terpenes that contribute to gas and particulate phase pollution.

Urban areas are characterized by the presence of varying amounts of non-natural morphological elements and their material composition. In turn, variations in their parameter values will influence the overlying wind, temperature, and moisture fields. Recently, a classification system called Local Climate Zones (or LCZ) (Figure 5.15) devised by Stewart and Oke (2010) has been developed having potential applicability to climate, weather, and air quality models. Bechtel et al. (2012, 2015, 2017 a, b), has devised a method that generates LCZ maps for any city in the world. Not surprisingly, LCZ maps for cities within and between regions and throughout the world are each unique in their spatial distinctions. By invoking a lookup table of urban canopy parameters (UCPs) as ranges of values for each LCZ class (see below), it follows that each and every city throughout the world will have their own distinct and unique spatial distributions of UCPs that will induce its very own distinctive intraurban meteorological field. Examples of LCZ maps are shown in Figure 5.16. It follows that the resulting emission-based air quality fields will be similarly influenced. Given this, modeling schemes using LCZ-based air quality emissions-based modeling systems with linked or coupled sub-models for chemistry and meteorology should provide an improved basis to roughness length approaches.

Thus, given the science basis and data requirements of urban climate and forecasting, models vary according to scale. Regional-mesoscale modeling performed at grid sizes of the order of

5 to 20 km or so limit the intracity spatial resolution and only require coarse scale representation of the urban areas as land use parameterizations. Finer grid sizes of the order of 100 m to 2 km provide greater spatial resolution forecasts, but model structures are more complex with various urban canopy parameterization treatments (e.g., Kusaka et al., 2001; Martilli et al., 2002; Salamanca et al., 2010; Masson, 2000) and commensurate UCP information requirements as well as computer resources. Unfortunately, available UCP data have typically been expensive to obtain; and currently been generated for a limited number of cities for specialized projects.

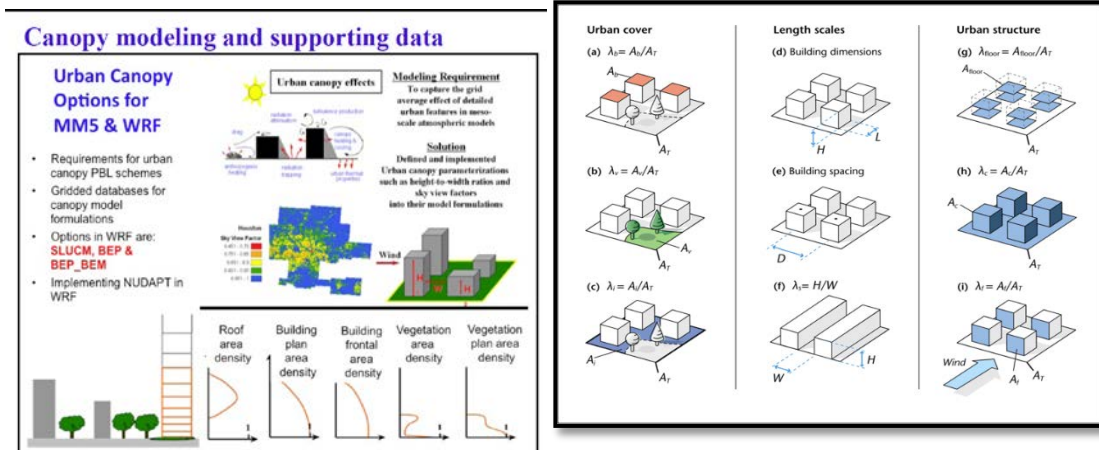


Figure 5.14 (a) Schematic depicting the role of UCPs to represent urban effects incorporated into science options in contemporary urban canopy models. (b) Form based building UCPs (from Oke et al., 2017).




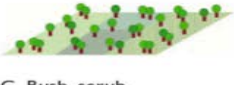












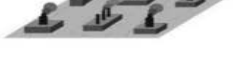
Built types	Definition	Land cover types	Definition
1. Compact high-rise 	Dense mix of tall buildings to tens of stories. Few or no trees. Land cover mostly paved. Concrete, steel, stone, and glass construction materials.	A. Dense trees 	Heavily wooded landscape of deciduous and/or evergreen trees. Land cover mostly pervious (low plants). Zone function is natural forest, tree cultivation, or urban park.
2. Compact midrise 	Dense mix of midrise buildings (3–9 stories). Few or no trees. Land cover mostly paved. Stone, brick, tile, and concrete construction materials.	B. Scattered trees 	Lightly wooded landscape of deciduous and/or evergreen trees. Land cover mostly pervious (low plants). Zone function is natural forest, tree cultivation, or urban park.
3. Compact low-rise 	Dense mix of low-rise buildings (1–3 stories). Few or no trees. Land cover mostly paved. Stone, brick, tile, and concrete construction materials.	C. Bush, scrub 	Open arrangement of bushes, shrubs, and short, woody trees. Land cover mostly pervious (bare soil or sand). Zone function is natural scrubland or agriculture.
4. Open high-rise 	Open arrangement of tall buildings to tens of stories. Abundance of pervious land cover (low plants, scattered trees). Concrete, steel, stone, and glass construction materials.	D. Low plants 	Featureless landscape of grass or herbaceous plants/crops. Few or no trees. Zone function is natural grassland, agriculture, or urban park.
5. Open midrise 	Open arrangement of midrise buildings (3–9 stories). Abundance of pervious land cover (low plants, scattered trees). Concrete, steel, stone, and glass construction materials.	E. Bare rock or paved 	Featureless landscape of rock or paved cover. Few or no trees or plants. Zone function is natural desert (rock) or urban transportation.
6. Open low-rise 	Open arrangement of low-rise buildings (1–3 stories). Abundance of pervious land cover (low plants, scattered trees). Wood, brick, stone, tile, and concrete construction materials.	F. Bare soil or sand 	Featureless landscape of soil or sand cover. Few or no trees or plants. Zone function is natural desert or agriculture.
7. Lightweight low-rise 	Dense mix of single-story buildings. Few or no trees. Land cover mostly hard-packed. Lightweight construction materials (e.g., wood, thatch, corrugated metal).	G. Water 	Large, open water bodies such as seas and lakes, or small bodies such as rivers, reservoirs, and lagoons.
8. Large low-rise 	Open arrangement of large low-rise buildings (1–3 stories). Few or no trees. Land cover mostly paved. Steel, concrete, metal, and stone construction materials.	VARIABLE LAND COVER PROPERTIES	
9. Sparsely built 	Sparse arrangement of small or medium-sized buildings in a natural setting. Abundance of pervious land cover (low plants, scattered trees).	<i>b. bare trees</i>	Leafless deciduous trees (e.g., winter). Increased sky view factor. Reduced albedo.
10. Heavy industry 	Low-rise and midrise industrial structures (towers, tanks, stacks). Few or no trees. Land cover mostly paved or hard-packed. Metal, steel, and concrete construction materials.	<i>s. snow cover</i>	Snow cover > 10 cm in depth. Low admittance. High albedo.
		<i>d. dry ground</i>	Parched soil. Low admittance. Large Bowen ratio. Increased albedo.
		<i>w. wet ground</i>	Waterlogged soil. High admittance. Small Bowen ratio. Reduced albedo.

Figure 5.15. Local Climate Zones

Given the need to provide specialized data to support state-of-science regional, mesoscale climate and AQ models for urban applications, the urban climate community has recently been engaged in the World Urban Database and Access Portal Tools or WUDAPT Project (www.wudapt.org). As indicated, every urban area is unique due to its geographical, terrain and climatic location, size, emissions, and morphological content. WUDAPT's LCZ-based method can provide morphology information for the world's urban settlements that has formerly impeded the application of these models. WUDAPT's database and portal infrastructure system are specifically designed to support intra-urban climate assessments, surface energy budget, and mesoscale to urban weather, CW and AQ forecasting applications. For modeling purposes, it focuses on generating urban canopy data suitable for running "fit-for-purpose" urban scale science-based meso to urban scale meteorological forecast, climate, and AQ models. Applications range from chemical weather, AQ forecasting, weather forecasting, urban climate analyses, UHI studies, urban planning response to climate change, etc. and is capable of being generated for any city in the world according to a common standard protocol. It is anticipated to provide an infrastructure for WMO mandated Urban Integrated Hydro-Meteorological, Climate and Environmental Services (WMO, 2018). The WUDAPT approach is to create levels of information on a hierarchical framework with increasing degrees of precision and information content described next.

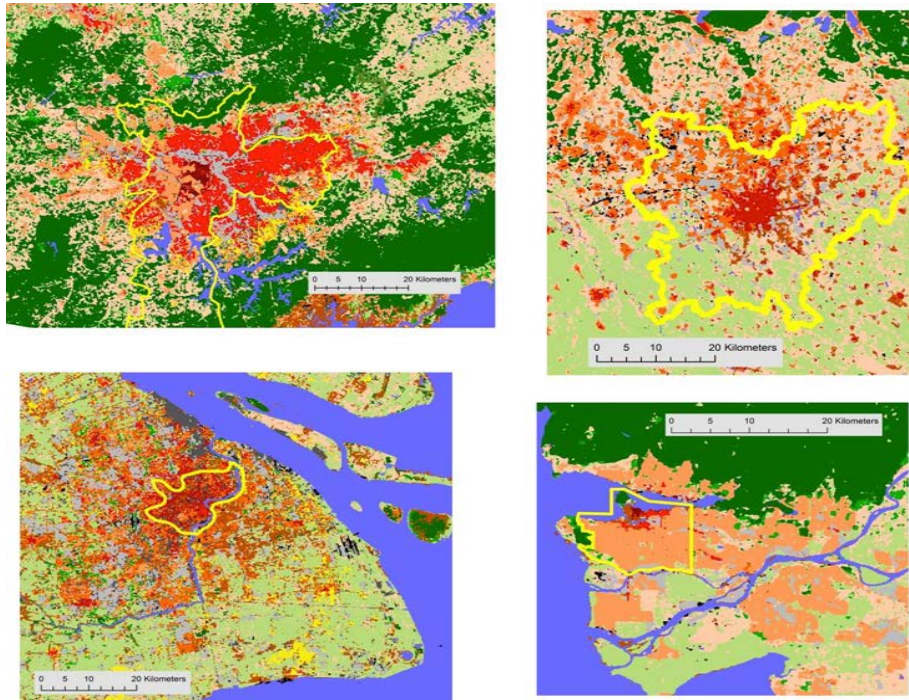


Figure 5.16. Examples of classifying LCZs: (a) Sao Paulo, (b) Madrid, (c) Shanghai, (d) Mumbai.

WUDAPT Level 0, is based on the Local Climate Zone paradigm devised by Stewart and Oke (2012) (Figure 5.15). The methodology for generating LCZ maps has been developed and tested by Bechtel (2012, 2015, 2017a, b) and a summary of the approach has been described in Mills et al. (2015) and Ching et al. (2018). Modeling at level 0 utilizes lookup tables with a range of values for each LCZ and UCP shown in Table 5.2 from Stewart and Oke (2012) (W2W, www.wudapt.org) and Brousse et al. (2016) have been created, residing and accessible in the WUDAPT Portal for running the single layer and canopy layer urban option in the WRF (Weather Research and Forecasting model) as discussed in Chen et al. (2010) and Ching et al. (2018).

The objective of WUDAPT Level 1 and 2 is to generate georeferenced and rasterized (gridded) UCP values instead of depending on some procedures required using the Lookup table and procedures from Level 0 approach (Ching et al., 2018, 2019). For this, we will be employing a customized Digital Synthetic City (DSC) tool with the capability to digitize high resolution imagery (such as Google Earth), with block level accuracy being customized based on Crowdsourced APPs (CSAPPs) (See et al., 2015) to reflect regional and cultural architectural differences worldwide. As these form features of the imagery are digitized, all morphological form-based UCPs can be computer generated and to any grid size (Figure 5.17). The figure also shows examples of products generated by the generic DSC tool. Application of the DSC provides a "top down" approach to making feasible computing the form-based urban canopy parameters. The testing and methods protocols will synthesize the efforts and recommendations arising from a number of urban testbeds located around the world each led by urban experts. These testbeds will incorporate baseline data from actual building data as well as other independently generated UCPs such as Sky View Factors (Middel et al., 2017, 2018) serving to calibrate the outcomes.

Table 5.2 Urban canopy parameter (UCP) values associated with Local Climate Zone (LCZ) types from Stewart and Oke (2012)

Columns represent the percentage of impervious (λ_i), built (λ_b) and vegetated (λ_v) land-cover and mean height of building elements (z), sky view factor (λ_s), albedo (α) and anthropogenic heat flux (Q_F in $W m^{-2}$).

LCZ	λ_i	λ_b	λ_v	z (m)	λ_s	α	Q_F
1. Compact high-rise	40–60	40–60	<10	>25	0.2–0.4	0.10–0.20	50–300
2. Compact mid-rise	40–70	30–50	<20	10–25	0.3–0.6	0.10–0.20	<75
3. Compact low-rise	40–70	20–50	<30	3–10	0.2–0.6	0.10–0.20	<75
4. Open high-rise	20–40	30–40	30–40	>25	0.5–0.7	0.12–0.25	<50
5. Open mid-rise	20–40	30–50	20–40	10–25	0.5–0.8	0.12–0.25	<25
6. Open low-rise	20–40	20–50	30–60	3–10	0.6–0.9	0.12–0.25	<25
7. Lightweight low-rise	60–90	<20	<30	2–4	0.2–0.5	0.15–0.35	<35
8. Large low-rise	30–50	40–50	<20	3–10	>0.7	0.15–0.25	<50
9. Sparsely built	10–20	<20	60–80	3–10	>0.8	0.12–0.25	<10
10. Heavy industry	20–30	20–40	40–50	5–15	0.6–0.9	0.12–0.20	>300
101. Dense trees	<10	<10	>90	3–30	<0.4	0.10–0.20	0
102. Scattered trees	<10	<10	>90	3–15	0.5–0.8	0.15–0.25	0
103. Bush, scrub	<10	<10	>90	<2	0.7–0.9	0.15–0.30	0
104. Low plants	<10	<10	>90	<1	0.2–0.4	0.15–0.25	0
105. Bare rock or paved	<10	>90	<10	<0.25	>0.9	0.15–0.30	0
106. Bare soil or sand	<10	<10	>90	<0.25	>0.9	0.20–0.35	0
107. Water	<10	<10	>90	–	>0.9	0.02–0.10	0

The WUDAPT approach to generating information on building materials and energy use will adopt a complementary “bottoms-up” approach; incorporating deep learning techniques applied to crowdsourced pictorial building data sampled to sets of architectural/building typology classes with further links to data pictorial building dictionaries such as in TABULA-Episcopal. Each testbed will also be employed to test, evaluate and apply various models based upon results of these top-down and bottoms-up approaches. The shared experiences with other testbeds will provide the base for the community-based protocol for the methodology. As this is a portal-based approach, the results will become part of WUDAPT’s global urban database and contribute to the dissemination of urban climate knowledge. Results from the testing phase will provide proof-of-concept impetus and guidance for a variety of fit-for-purpose model applications. They may include mesoscale to urban models, e.g., WRF modeling (3 urban physics options) for UHI studies, air quality urban to block scale modeling and links or extensions to local and street-in-grid (SinG) exposure modeling, risk assessments, climate

change assessments, input to UMEP, Surface Energy Budget modeling such as SUEWS, urban planning, design and climate analyses mapping links to ENVI-Met.

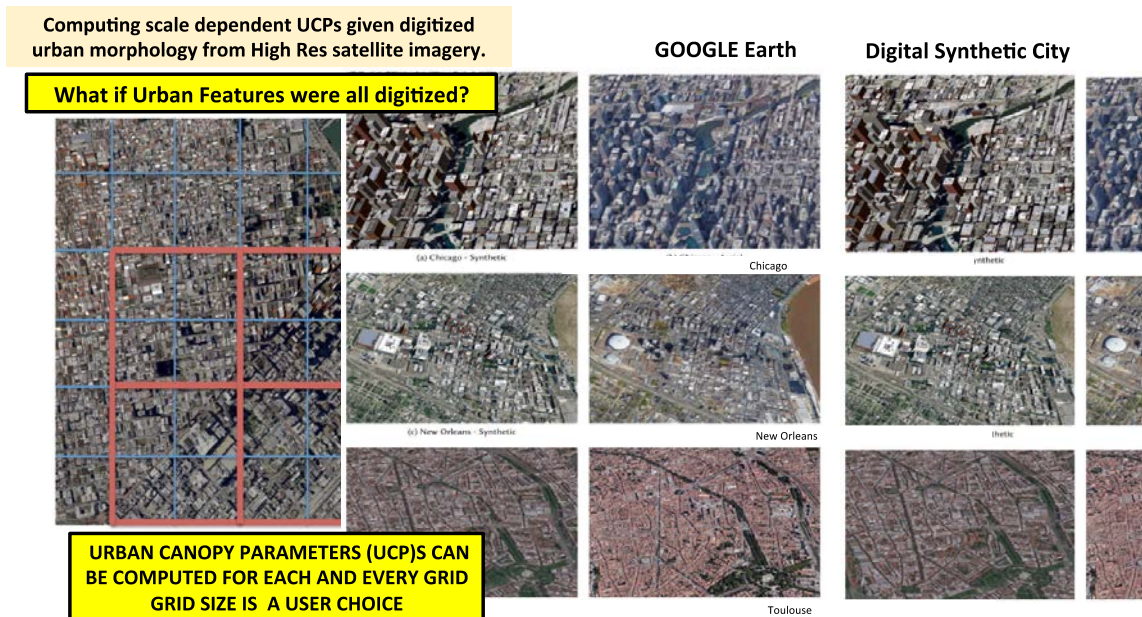


Figure 5.17. Computing scale dependent UCPs based on outputs of DSC

5.6.3 Summary

- A framework based on incorporating urban canopy parameters to weather and AQ modeling at the km to block scale is becoming attractive and viable for handling complexities and heterogeneities in building morphology in cities.
- The World Urban Database and Access Port Tool (WUDAPT) is a major and unique international community-based project initiated by and for the worldwide urban community to provide the means, framework, and infrastructure capable of supporting a wide range of “fit-for-purpose, and scale dependent ” grid-based environmental modeling applications (such as air quality forecasts) customized for use anywhere in the world.
- WUDAPT methodology can generate modeling data hierarchically at Levels 0, 1, and 2. It can be achieved based on readily accessible and available data inputs everywhere, its outcomes are unrestricted and the quality levels are known. This implementation strategy is based upon a hierarchical structure, which allows data to be generated with increasing precision on information so as to be responsive to addressing climate change and urbanization issues in a reasonable time frame. The time frame from concept to prototype to implementation of Level 0 was about 3 or so years; a similar time frame is anticipated for advancing Levels 1 and 2 staged to generate form-based UCPs based on implementing the DSC followed by information on building material and energy usage. Success at each level has required creative methodological innovations and international collaborations among and by urban experts.
- Level 0 is based on characterizing urban areas into Local Climate Zones and associated lookup tables provide a range of values of UCPs; a tool, W2W is designed to enable mesoscale modeling. Levels 1 and 2 are designed to directly generate a gridded set of UCP, material and functional information at succeeding greater levels of precision and coverage, based on the implementation of its Digital Synthetic Tool. Testbeds are being established throughout the world to establish the best practice methodology for customization, testing and model demonstration

of the Levels 1 and 2 outputs. The quality of the initial results is encouraging (Ching et al., 2019).

- A portal provides both a means to facilitate the generation of Levels 0, 1, and 2 data, and tools for interfacing to various types of modeling needs.

References

- Aliaga D., C. Vanegas, M. Lei, D. Niyogi. Visualization-based Decision Tool for Urban Meteorological Modeling, *Environment and Planning B: Planning and Design (EPB)*, 40(2), 271-288, 2013.
- Bechtel, B., Alexander, P., Böhner, J., Ching, J., Conrad, O., Feddema, J., Mills, G., See, L. and Stewart, I. 2015: Mapping local climate zones for a worldwide database of form and function of cities. *Int'l J. of Geographic Information*, 4(1), 199-219. doi:10.3390/ijgi4010199.
- Bechtel B, C. Daneke, 2012: Classification of local Climate Zones based on multiple Earth Observation Data. *IEEE Journal of Selected Topics in Applied Earth Observations and Remote Sensing*, 5(4): 1191-1202 [doi:10.1109/JSTARS.2012.2189873]
- Bechtel, B., Demuzere, M., Xu, Y., Verdonck, M., Lopes, P., See, L., Ren, C., Van Coillie, F., Tuia, D., Fonte, C., Cassone, A., Kaloustian, N., Conrad, O., Tamminga, M & Mills, G. 2017: Beyond the Urban Mask: Local Climate Zones as a Generic Descriptor of Urban Areas – Potential and Recent Developments. Joint Urban Remote Sensing Event (JURSE). Dubai, 5-7 March 2017a.
- Bechtel B., Matthias Demuzere, Panagiotis Sismanidis, Daniel Fenner, Oscar Brousse, Christoph Beck, Frieke Van Coillie, Olaf Conrad, Iphigenia Keramitsoglou, Ariane Middel, Gerald Mills, Dev Niyogi, Marco Otto, Linda See, and Marie-Leen Verdonck. (2017) Quality of Crowdsourced Data on Urban Morphology—The Human Influence Experiment (HUMINEX). *Urban Science* 1:2, 15. Online publication date: 9-May-2017b.
- Brousse O, Martilli A, Foley M, Mills G, Bechtel B, 2016: WUDAPT, an efficient land use producing data tool for mesoscale models: Integration of urban LCZ in WRF over Madrid. *Urban Climate*, 17, 116-134.
- Chen, F., H. Kusaka, R. Bornstein, J. Ching, C.S.B. Grimmond, S. Grossman-Clarke, T. Loridan, K.W. Manning, A. Martilli, S. Miao, D. Sailor, F.P. Salamanca, H. Taha, M. Tewari, X. Wang, A.A. Wyszogrodzki, C. Zhang, 2010: The integrated WRF urban modeling system: development, evaluation, and applications to urban environmental problems. *Int. J. Climatol.*, 31, 273–288.
- Ching, J. G. Mills, B. Bechtel, L See, J. Feddema, X. Wang, C. Ren, O. Brousse, A. Martilli9, M. Neophytou, P. Mouzourides, I. Stewart, A. Hanna, E. Ng, M. Foley, P. Alexander, D. Aliaga, D. Niyogi, A. Shreevastava, P. Bhalachandran, V. Masson, J. Hidalgo, J. Fung, M. Andrade, A. Baklanov, W. Dai, G. Milcinski, M. Demuzere, N. Brunsell, M. Pesaresi, S. Miao, Q. Mu, F. Chen, N. Theeuwes, 2018: World Urban Database and Access Portal Tools (WUDAPT), an urban weather, climate and environmental modeling infrastructure for the Anthropocene. Online, *Bulletin of American Meteorological Society*.
- Ching, J., D. Aliaga, G. Mills, V. Masson, L. See, M. Neophytou, A. Middel, C. Ren, E. Ng, Y. Huang, I. Stewart, J. Fung, M. Wong, X. Zhang, A. Shehata, A. Martilli, S. Miao, X. Wang, D. Duarte, L. Schwandner, W. Wang, Y. Li, B. Bechtel, and 24 others, Pathway using WUDAPT's Digital Synthetic City tool towards generating urban canopy parameters for multi-scale urban atmospheric modeling. In press: WUDAPT Special Issue of *Urban Climate* (2019).
- Kusaka, H. Kondo, Y. Kikegawa, and F. Kimura, 2001: A simple single-layer urban canopy model for atmospheric models: Comparison with multi-layer and slab models. *Bound.*

Layer Meteor., 101, 329–358, doi:10.1023/A:1019207923078.

- Martilli, A., A. Clappier, M. Rotach, 2002: An Urban Surface Exchange Parameterization for Mesoscale Models. *Boundary Layer Meteor.* 104, 261-304.
- Masson, Valery, 2000: A Physically Based Scheme for the Urban Energy Budget in Atmospheric Models, *Bound Layer Meteorology* 94: 357–397, 2000.
- Middel, A., Lukasczyk, J., Maciejewski, R., 2017, Sky View Factors from Synthetic Fisheye Photos for Thermal Comfort Routing—A Case Study in Phoenix, Arizona, *Urban Planning* 2(1): 19-30.
- Middel, A., J. Lukasczyk, R. Maciejewski, M. Demuzere and M. Roth, 2018: Sky View Factor footprints for urban climate modeling, *Urban Climate*, WUDAPT special Issue, (25) 120-134.
- Mills, G., Ching, J., See, L., Bechtel, B., Feddema, J., Masson, V., Stewart, I., Neophytou, M., O'Connor, M., Chen, F., Martilli, A., Grimmond, S., Alexander, P., Foley, M., Gal, T., Wang, X., Mitra, C., Pereira, N., Steeneveld, G.-J., 2015: Introduction to the WUDAPT Project. *Proceedings, 9th International Conference on Urban Climate (jointly with 12th Symposium on the Urban Environment)*, Toulouse, France, July 2015.
- Oke, T., G. Mills, A. Christen, and J.A. Voogt, 2017: *Urban Climates*, Cambridge University Press, DOI: 9780521849500.
- Salamanca, F., Krpo, A., Martilli, A., Clappier, A., 2010: A new building energy model coupled with an urban canopy parameterization for urban climate simulation-Part 1. formulation verification, and sensitivity analysis of the model. *Theor. Appl. Climatol.* 99: 331-344.
- See, L., Ching, J., Masson, V., Feddema, J., Mills, G., Neophytou, M., Foley, M., O'Connor, M., Perger, C., Duerauer, M., Fritz, S., Bechtel, B. 2015: Generating WUDAPT's Specific Scale-dependent Urban Modeling and Activity Parameters: Collection of Level 1 and Level 2 Data. *Proceedings, 9th International Conference on Urban Climate (jointly with 12th Symposium on the Urban Environment)*, Toulouse, France, July 2015.
- Stewart, I, T. Oke, 2012: Local Climate Zones for Urban Temperature Studies, *Bull. Amer. Meteor. Soc.* doi: <http://dx.doi.org/10.1175/BAMS-D-11-00019>.
- Tornay N., R. Schoetter, M. Bonhomme, S. Faraut, A. Lemonsu and V. Masson (2017) : GENIUS : A methodology to define a detailed description of buildings for urban climate and building energy consumption simulations, *Urban Climate*, 10, 75-93, doi:10.1016/j.uclim.2017.03.002
- WMO, 2018: *Guidance on Integrated Urban Hydrometeorological, Climate and Environmental Services - Volume I: Concept and Methodology*. World Meteorological Organization, WMO- No. 1234. web-link: https://library.wmo.int/doc_num.php?explnum_id=9903

Chapter 6. Special Considerations for Extreme Events

6.1 Introduction

Extreme events, such as wildfires, dust storms and volcanoes, can wield drastic effects on air quality and human health. In contrast to recurring sources, these events emit air pollutants with distinct patterns, often abruptly and in large quantities. Air quality models utilize various techniques to predict the emissions, transformation, transport and removal of pollutants or other hazardous substances from these extreme events. Such forecasting information is vital in order to issue predictions, early warnings and multi-hazard early warning systems to impacted populations, and to design responses to mitigate environmental and health effects of harmful exposure to primary (directly emitted) and secondary (formed in the air) pollutants. WMO strategies and requirements for such early warning and forecasting systems are realized within the concepts of the Global Data-Processing and Forecasting System (GDPFS) (WMO GDPFS, 2017) and the multi-hazard early warning systems (MHEWSs) (WMO MHEWS, 2018).

In this chapter, extreme events such as wildfires, dust storms and volcanoes along with special considerations for emissions and modeling of these events are introduced. The status and challenges in air quality forecasts during extreme events, including wildfires, dust storms, volcanic eruptions, and sudden release of air toxics are summarized. The topics include wildfires and prescribed burning and their modeling, as well as global fire emission inventories (Section 6.2), dust storms, their impacts, trends, and modeling (Section 6.3), sudden release of air toxics and modeling (Section 6.4), and volcanic eruption and modeling (Section 6.5). Finally, Section 6.6 summarizes the key points.

6.2 Wildfires and Prescribed Burning

Vegetation fires are widely present on all continents except Antarctica. Their smoke contains large quantities of fine mode particulate matter (PM) and reactive gases, which has the potential to impact human health. The PM consists of organic matter (OM), black carbon (soot) (BC) and brown carbon (BrC). It contributes significantly to the global premature mortality due to outdoor air pollution (Lelieveld et al., 2015). The atmospheric pollution typically occurs in fire episodes during dry periods. During strong fire events, atmospheric concentrations of PM are often many times larger than the WHO interim targets (WHO, 2006); the 2015 peat fires in Indonesia were an extreme example with widespread PM concentrations of 1000-2000 $\mu\text{g m}^{-3}$ for several weeks. On a global average, fires contribute ~66% of the OM and > 40% of the carbon monoxide to the atmosphere.

Vegetation fires are an essential part of many natural ecosystems with fire repeat periods between 1 year, e.g., in the African savanna, and several hundred years, e.g., in boreal forests. They are ignited naturally by lightning and volcanic eruptions. Today, most fires are ignited on purpose or accidentally by humans. Agricultural burning is a widespread practice that helps to remove remaining plant material from fields after harvesting in preparation for the sowing of new crops. Fire is also used during deforestation or when old trees are replaced in various plantations. Accidental and uncontrollable vegetation fires are called *wildfires*. On the other hand, humans can also suppress fires. Excessive fire suppression, and also abandonment of agricultural land, leads to fuel build-up and subsequently more intense and destructive fires. Therefore, *prescribed burning* in safe conditions is increasingly used to manage the available fuel load or as a tool to prevent forestation of open landscapes. During the planning of prescribed burns, air quality forecasting systems are being used to predict the impact on air quality for the population downwind of the planned fire and ensure that the burning only takes place when the air quality threshold will not be exceeded. A number of regional, national and international agencies (e.g., the Commonwealth Scientific and Industrial Research Organization (CSIRO) in Australia, the National Oceanic and Atmospheric Administration (NOAA) in the U.S.) are operating the air quality forecasting systems for this purpose.

Arising from the keen interest of WMO members in several impacted regions, the WMO Global Atmosphere Watch (GAW) Programme together with the Interdisciplinary Biomass Burning Initiative (IBBI) provided guidance for addressing the issues of vegetation fire and smoke pollution. They highlighted some of the challenging aspects related to the estimation of emissions from biomass burning and prediction of fire danger conditions. It also proposed the establishment of a Vegetation Fire and Smoke Pollution Warning and Advisory System (VFSP-WAS) and to support the potential foundation of regional centers on the topic (WMO VFSP-WAS, 2018, <https://community.wmo.int/activity-areas/gaw/science/modelling-applications/vfsp-was>). The overall structure of a potential Vegetation Fire and Smoke Pollution Warning and Advisory System is presented in Figure 6.1.

6.2.1 Predicting the Risk of Vegetation Fires

The risk of vegetation fires can be estimated several days ahead from regular weather forecasts. In some regions, with skillful seasonal weather forecasting, even seasonal predictions are feasible. Mostly, the Canadian Fire Weather Index (FWI) is used for the calculation. However, it needs to be calibrated for the local vegetation types in different regions before being interpreted. Fire danger ratings are available from national and regional institutions as well as globally, e.g., at

- <http://data.giss.nasa.gov/impacts/gfwed>
- <http://apps.ecmwf.int/datasets/data/geff-reanalysis/>
- http://gwis.jrc.ec.europa.eu/static/gwis_current_situation/public/index.html

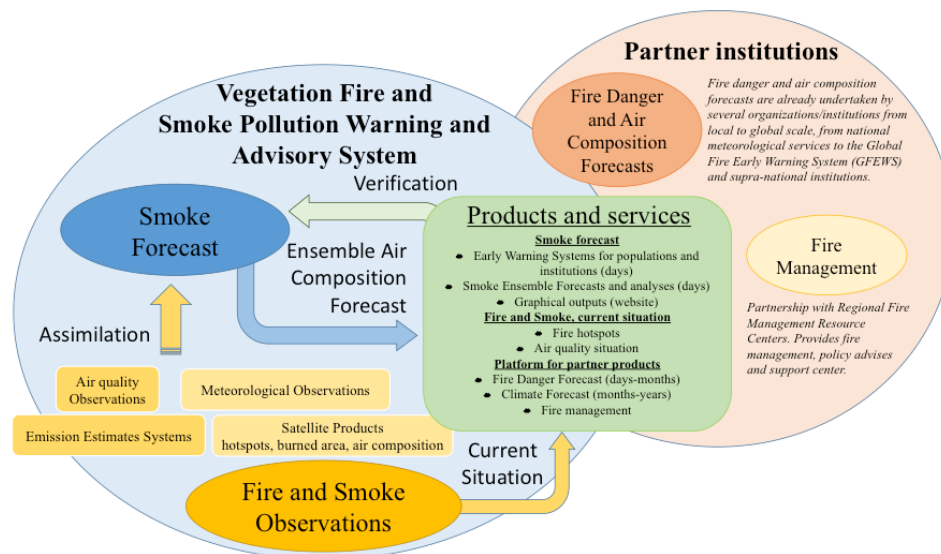


Figure 6.1. Overview of a potential Vegetation Fire and Smoke Pollution Warning and Advisory System (WMO VFSP-WAS, 2018).

6.2.2 Precompiled Global Fire Emission Inventories and Uncertainties

The most widely-used fire emission inventory for scientific applications is the Global Fire Emission Database. Its latest version (GFED4s, van der Werf et al., 2017) is based on MODIS burnt area estimates with a correction for small fires that is based on MODIS hot spots. The data are freely available at <http://www.globalfiredata.org>.

The most widely-used fire emission inventory for operation real-time applications is the Global Fire Assimilations System (GFAS, Kaiser et al., 2012). It is based on fire radiative power (FRP) observations of MODIS. Starting in late 2018, FRP observations from the SEVIRI and VIIRS instruments will also be included and the temporal resolution will be improved to 1 hour. It is freely available at <https://atmosphere.copernicus.eu/catalogue>. Similar FRP-based

inventories are the Integrated Monitoring and Modeling System for wildland fires (IS4FIRES) (Sofiev et al., 2009) and the Quick Fire Emissions Dataset (QFED) (Darmenov et al., 2013). Another real-time inventory is based on scaling hot spot observations to a burnt area: Fire INventory from NCAR (FINN) (Wiedinmyer et al., 2011).

Being based on a burnt area and FRP observations, all inventories are highly uncertain for peat fires because the burn depth cannot be inferred from the observations. Also, fire on the ground below tree coverage is poorly observed from satellites and the detection thresholds of satellites lead to a systematic underestimation of small fires.

6.2.3 *Satellite Products used for Wildland Fire Monitoring*

Vegetation fires are observed with satellites by detecting the burnt area or the thermal radiation. The *burnt area* can be detected as a change in reflectance immediately after the fire: the albedo and directional effects are reduced. The reduction generally lasts for several weeks, so that most observation gaps, e.g., due to cloud cover, can be bridged. The most widely-used global burnt area products are derived from observations by NASA's MODIS instrument and date back to the year 2000: MCD64 (Giglio et al., 2013) and MCD45 (Roy et al., 2008). An alternative product for 2005-2011 has been produced by the Fire_cci project based on ESA's MERIS instrument (Alonso-Canas and Chuvieco, 2015). For longer time periods, the AVHRR instruments might be used to derive burnt areas with less than global monthly coverage but dating back to 1982.

Active fire products are detections of the thermal radiation released by fires, which is typically observed in the middle infrared (MIR) near 4 mm wavelength. The signal is so strong in this spectral range that fire in even a few percent of the satellite pixel can saturate the MIR channel in many satellite instruments. Thus, binary *hot spot* products are available since the mid-1990s, from the ATSR-2 and VIRS instruments. The polar orbiting MODIS, VIIRS and SLSTR instruments have fire-dedicated MIR channels with a large saturation level. These allow the quantitative characterization of biomass burning with FRP products (Giglio et al., 2016; Wooster et al., 2012). Compared to burnt area products, advantages of the active fire products are availability in near-real time and a lower detection threshold, e.g. for detecting agricultural burning. A disadvantage is that fires can only be detected while still burning. The products are thus affected by the observation gaps due to cloud cover and observation periods. The above-mentioned satellite instruments are in polar orbits. Fire radiative power is also observed by geostationary meteorological satellites, namely the Meteosat Second Generation and GOES satellites, as well as Himawari-8. These satellites provide a high observation frequency of up to six observations per hour, but some suffer from a higher detection threshold than MODIS, for example.

6.2.4 *Modeling the Fire Impact on Atmospheric Composition and Air Quality*

The precompiled fire emission inventories can be readily used to drive Chemical Transport Models (CTMs) and global circulation models (GCMs). However, recalculation with higher-resolution land cover maps helps to improve regional accuracy. Also, smoke aerosol undergoes rapid evolution during the first few hours in the high concentration smoke plumes; it has been observed that different atmospheric models require a calibration with observations of the target aerosol quantity (AOD or PM) to derive individual aerosol enhancement factors.

Due to the high variability of fires, a resolution of at least one day is recommended. Peat fires burn throughout day and night. All other fires have a very pronounced variability at sub-daily scales and most display a strong maximum in the early afternoon local time at the regional scale. Typical diurnal cycles for tropical fires are displayed in Giglio (2007). Such diurnal cycles may be superimposed on daily emission estimates.

Due to the heat release of the fire, emissions are generally injected well above the ground level. The bulk of the emissions stays in the boundary layer (Veira et al., 2015). However, occasional fire emissions can reach up to the lower stratosphere, when wet pyro-convection is

induced. The injection height can be estimated with a simple parameterization based on the atmospheric stability (Sofiev et al., 2012) or with a 1-D plume rise model (Freitas et al., 2007; Paugam et al., 2015). The former is less dynamic and thus more accurate than the latter, but the latter is more likely to estimate extreme cases realistically. Daily injection height estimates from both methods are produced operationally and freely available (Remy et al., 2017).

6.3 Dust Storms

6.3.1 *Environmental and Health Effects of Dust Storms*

Dust storms impose myriad effects on the environment and society, including air quality, atmospheric chemistry, climate, human health, agriculture, transportation, and solar energy productivity. As one of the major components of atmospheric aerosols, dust contributes approximately 37% of the global aerosol loading (IPCC, 2001). Globally, emissions of mineral dust have been estimated to range between 1 000 to 5 000 Mt/yr with large spatial and temporal variability from year to year (Tegen and Miller, 1998; Zender et al., 2003; Shao, 2008). By providing surfaces for heterogeneous reactions, atmospheric mineral dust can alter the concentrations of ozone and other photochemical oxidants in the atmosphere (Dentener et al., 1996; Usher et al., 2003). Suspended dust particles affect regional and global climate directly through scattering and the absorption of solar radiation (Tegen and Lacis, 1996; Sokolik and Toon, 1996; Chin et al., 2002; Pérez et al., 2006), and indirectly through acting as cloud condensation nuclei (CCN), and through supplying bio-available iron that increases primary productivity and hence sink carbon dioxide (CO₂) (Zhuang et al., 1992; Duce, 1995; Buesseler et al., 2004). Mineral dust is also reported to suppress precipitation (Rosenfeld et al., 2000), although more recent studies have shown that dust can increase precipitation locally over desert regions (Miller et al., 2004) and the net impact varies from day to night during the Western African Monsoon season (Zhao et al., 2011; Yu et al., 2015; Nivkovic et al., 2016).

Dust storms pose imminent threats to aviation and highway transportation (Pauley et al., 1996; Goudie, 2009; Baddock et al., 2013; Lader et al., 2016; Middleton, 2017; Li et al., 2017). Desert dust can cause significant problems in aviation such as rerouting due to poor visibility, disturbances in airport operations, massive canceling of scheduled flights and mechanical problems such as erosion or corrosion (Lekas et al., 2011). A major incident occurred in 1991 in the San Joaquin Valley of California, where blowing dust caused a 164 car pile-up, killing or injuring 168 people on the U.S. Interstate Highway 5 (Pauley et al., 1996). Goudie (2014) reported that dust-related fatal highway accidents happened in six states in the U.S. during 2012-2013. Lader et al. (2016) reported that dust storms are the third largest cause of weather fatalities and dust-related incidents have killed 157 and injured 1 324 people over the last 50 years in the state of Arizona alone, making dust storms the third deadliest weather hazard in the southwestern U.S. Dust storms also pose adverse effects on human health (Crooks et al., 2016; Zhang et al., 2016; Tong et al., 2017). Reported health effects of desert dust include injuries and death from non-accidental death, respiratory diseases (e.g., rhinitis, asthma, tracheitis, pneumonia, coccidiomycosis), cardiovascular diseases (e.g., stroke, arrhythmia, ischemic heart disease, cerebrovascular disease), cardiopulmonary diseases (e.g., chronic obstructive pulmonary disease, COPD), and, more rarely, conjunctivitis, meningococcal meningitis, dermatological disorders, skin allergies, and an exacerbated cough (Zhang et al., 2016). A global assessment in 2014 estimated that exposure to dust particles caused about 400 thousand premature deaths by cardiopulmonary disease in the population of individuals over 30 years old (Giannadaki et al., 2014). For instance, Crooks et al. (2016) found that dust storms are associated with increases in non-accidental and cardiovascular mortalities in the Southwestern states such as California and Arizona where dust storms are frequently observed. Dust, along with wind, is shown to be indicative of the seasonal occurrence of meningitis, an infection of the thin lining that surrounds the brain and spinal cord, in the sub-Saharan Africa region (Perez García-Pando et al., 2014).

Dust storms accelerate soil erosion in agricultural zones. Dust can act at times as a powerful vehicle to cascade the impacts of global climate variations onto the environment and society on a local scale. In the 1930s, an extended drought in the U.S., coupled with high winds,

economic depression, and poor land management, led to numerous large dust storms – collectively producing an environmental catastrophe known as the “Dust Bowl” (Lee and Gill, 2015). These storms have devastated thousands of farms and forced millions of farmers to migrate (Worster, 1979). An episodic version of a Dust Bowl lasted for 50 years (1895–1945) in southeastern Australia where marginal lands were actively cropped and grazed by domestic and wild animals (rabbits) (Cattle, 2016). Similar widespread soil deflation occurred in the Argentine Pampas during the 1930s and 1940s, and after the 1950s Virgin Lands Scheme in the former Union of Soviet Socialist Republics due to an analogous expansion of cultivation into native grasslands (Middleton, 2016 and references therein). Climate model projections suggest a consistent trend towards an increasingly arid climate in the subtropics, including the southwestern United States (Schubert et al., 2004; Seager et al., 2007; Cook et al., 2015). The predicted drying trend over arid and semi-arid regions aids speculation of more frequent dust storms and even another “Dust Bowl” in the coming decades. For instance, Romm (2011) has argued that the combination of precipitation shift from subtropics, greater evaporation, less snow/ice, and an earlier onset of spring can amplify the effects of natural climatic variations (e.g., the El Niño-La Niña cycle). The amplified climatic effects may in turn intensify droughts and lead to “dust-bowlification” rather than desertification in the Americas.

As renewable energy becomes increasingly important, dust storms can cause serious repercussions for electricity generation and distribution (Middleton, 2016). Deserts offer large unused land and strong solar radiation conditions. Dust deposition, however, adversely affects two of the main technologies used in solar energy generation: photovoltaic (PV) and concentrating solar-thermal power (CSP) systems (Kosmopoulos et al., 2017). Dust decreases the efficiency of both PV modules and the highly reflective mirrors in CSP systems to generate electricity by 15% to 100% (Middleton, 2016). Dust can also affect the reliability of power distribution grids in deserts or adjacent regions by interfering with porcelain insulators on high-voltage transmission lines (Maliszewski et al., 2012).

6.3.2 *Global and Regional Trends of Dust Storms*

The dust frequency trend is a simple but powerful indicator to describe how the dryland ecosystem responds to changes in weather and climate conditions. Assessment of global and regional dust trends reveals large spatial and temporal variations, which have broad implications on the environmental and health effects discussed earlier. Although there are inconsistent reports over different timescales (e.g., Mahowald et al., 2007; Ginoux et al., 2012; Shao et al., 2013), a decreasing dust trend has been reported during the past decades in major dust regions of the world. For instance, a decreasing dust trend has been observed by satellite and ground monitoring in the Saharan region (Evan et al., 2006), where a negative correlation between dust and tropical cyclone activity is linked to the trend of North Atlantic sea surface temperatures (SST) (Foltz et al., 2008). Long-term observations of dust frequency show a remarkable declining trend in northern China (Zhu et al., 2008; Guan et al., 2015). Using observations with visibility less than 5 km (known as VIS5), Shao et al. (2013) showed that mean dust concentration has decreased by 1.2% per year between 1974 and 2012, due largely to reduced dust activities in Africa, north-eastern Asia, and South America that outweigh increases in other source regions. A strong anti-correlation is found between Atlantic Multidecadal Oscillation (AMO) and Saharan dust, the dominant source of global dust loading, suggesting that the present global dust trend is largely determined by the climate systems governing the Atlantic and North African regimes (Shao et al., 2013).

Regardless of the downward global trend, upward trends are found in several regions, including North America and the Middle East. In North America, multiple lines of evidence suggested that the western U.S. has become dustier in recent decades. A significant increase in rainwater calcium (Ca^{2+}) was detected by the National Atmospheric Deposition Network from 1994 to 2010 in the western U.S. (Brahney et al., 2013). Using snowpack Ca^{2+} as a surrogate, Clow et al. (2016) showed that aeolian dust deposition to snow has increased 80% in the southern Rockies during 1993-2014. The most direct evidence came from the NASA Dust Climate Indicator project which found that the frequency of locally originated wind-blown dust storms has increased 240% in 1990-2011 in the Southwest U.S. (Figure 6.2) (Tong et al.,

2017). Compared to the global trend, U.S. dust storms have increased tenfold faster in the opposite direction (Shao et al., 2013; Tong et al., 2017).

6.3.3 Overview of Dust Storm Prediction and Forecasting

6.3.3.1 Dust Prediction Models

In recent years, a number of dust forecasts have become available from numerical weather prediction (NWP) and research centers around the world. An overview of current dust prediction models and related analysis systems can be found in Benedetti et al. (2014). Many of these forecasts are now delivered through the regional nodes of the WMO Sand and Dust Storms Warning Advisory and Assessment System (SDS-WAS) programme (WMO SDS-WAS, 2015). Other forecasts are delivered through dedicated web interfaces to serve the purposes of the individual operational centers. Global models have a typical spatial resolution around 1° , but can also be found with spacing grids finer than 50 km (i.e., CAMS, NASA-GEOS5, and MASINGAR). These models are capable of reproducing the seasonal cycles and large-scale transport patterns of dust into the atmosphere, which are synoptic scale phenomena. On the contrary, regional models offer important advantages in comparison with global models due to their higher spatio-temporal resolution and even multiple physical parameterizations (i.e., NMMB-MONARCH, CHIMERE, and WRF-Chem).

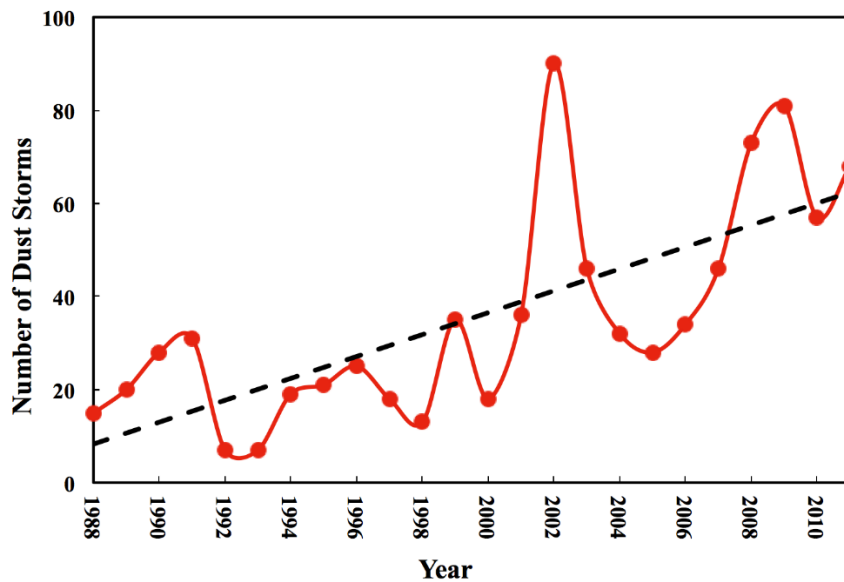


Figure 6.2 Interannual variability and trend of dust storms from the NASA NCA Dust Indicator observations (Tong et al., 2017).

The Multi-model ensemble (i.e., ensemble prediction) aims to better describe the future state of the atmosphere from a probabilistic point of view. Multiple simulations are run to account for the uncertainty of the initial state and/or for the inaccuracy of the model and the mathematical methods used to solve its equations. The use of ensemble forecasting is especially encouraged in situations associated with unstable weather patterns or in extreme conditions. Two examples of multi-model ensembles for dust prediction are the WMO SDS-WAS multi-model ensemble which considers global and regional models; as well as the International Cooperative for Aerosol Prediction (ICAP) multi-model ensemble (Sessions et al., 2015) which only considers operational global models.

6.3.3.2 Dust Observations

In recent years, a growing number of centers have been producing aerosol analysis for model initialization. Different assimilation techniques are employed, ranging from 3-D and 4-D variational approaches to Ensemble Kalman Filter with different flavors. Assimilation has been shown to be a powerful tool to improve model skills in predicting dust events by providing observational constraints for the model simulation. However, assimilation of dust observations presents specific challenges. On the one hand, there is the paucity of suitable in-situ observations: the location of the main dust sources in unpopulated areas complicates the establishment of observing networks. On the other hand, extracting specific dust signals from satellite radiances, which are affected by all aerosol species and other atmospheric quantities, is a complex issue (Benedetti et al., 2014). Similar problems arise when addressing the forecast evaluation. Ideally, for dust model evaluation, it would be necessary to have accurate observations of dust only.

6.3.3.3 WMO Sand and Dust Storm Centers

- (i) Research: WMO Sand and Dust Storm Warning Advisory and Assessment system (SDS-WAS): Objectives and Regional Centers (NA-ME-E, Asian, and Pan-American) (WMO SDS-WAS, 2015);

Over the last decade, there has been a growing recognition of the crucial role of sand and dust storms (SDS) on weather, climate, and ecosystems, along with their substantial adverse impacts on life, health, property, economy and other strategic sectors.

Reacting to the concerns about SDS by its most affected member states, in 2007, the World Meteorological Organization (WMO) endorsed the launch of the Sand and Dust Storm Warning Advisory and Assessment System (SDS-WAS; <https://public.wmo.int/en/our-mandate/focus-areas/environment/SDS>). The SDS-WAS mission is to enhance the delivery of timely and quality SDS forecasts, observations, information and knowledge to users through an international partnership of research and operational communities. The SDS-WAS is established as a federation of partners organized around regional nodes. The SDS-WAS Regional Centers support a node, which consists of a network of research and operational partners implementing the SDS-WAS objectives in a region. At present, three nodes are established: the Northern Africa-Middle East-Europe (NA-ME-E) node (hosted by Spain, <https://sds-was.aemet.es/>), the East Asia node (hosted by China, <http://www.asdf-bj.net/>) and the recent Pan-American node (hosted by Barbados, <http://sds-was.cimh.edu.bb/>).

- (ii) Operations: WMO Regional Specialized Meteorological Centers with activity specialization on Atmospheric Sand and Dust Forecast (RSMC-ASDF): Barcelona Dust Forecast Center and Beijing Dust Forecast Center.

In view of the demand of many national meteorological services and the achievements of the SDS-WAS Regional Centers, the 65th session of the WMO executive council designated Spain to create in Barcelona the first regional specialized meteorological center with activity on atmospheric SDS forecasts for the NA-ME-E region, known as the Barcelona Dust Forecast Center (BDFC, <https://dust.aemet.es/>). The Center was created in February 2014 and its mandate is to generate and distribute operational dust forecasts. Recently, a second specialized center in Beijing (China) has been approved.

6.3.4 Current Challenges

A critical issue in dust models is the simulation of dust fluxes. Dust emission depends not only on surface properties but also on surface meteorology. On the soil side, we often lack sufficient information on soil characteristics such as size distribution and binding energies between particles in sufficiently high resolution. Otherwise, in general, some subscale processes important for dust generation are not explicitly resolved by the (global or regional) models. These processes include evaporation-driven, cold, near-surface outflows from organized moist convection and turbulent circulation in dry convective boundary layers. One of the most challenging aspects are convective dust storms called haboobs (from the Arab word for wind). They are particularly frequent over the Sahel and southern Sahara in summer but have been observed in many other desert regions, too. Cold pool outflows are downdrafts caused by the evaporation and cooling of rain from thunderstorms which, near the surface, cause gravity currents where strong winds can uplift dust. It has been shown that haboobs are largely missed by models using parameterized convection, as this does not allow a realistic representation of the organization from individual convective cells to larger squall lines with more intense cold pools that can reach a several hundred kilometer extension. Models using explicit convection can better represent cold-pool dust emission, but even those show discrepancies to observations due to the stochastic nature of the initial convective development. A second critical phenomenon is the formation of nocturnal low-level jets related to the reduced surface friction during stable nighttime conditions that allows the air in several hundred meters above ground to accelerate (and turn if an inertial oscillation takes place).

Once lifted into the air, the dust particles are subject to vertical and horizontal transport or mixing as well as deposition. Deposition, which can be dry (sedimentation, turbulence) or wet (in- or below-cloud scavenging) is another critical process in the dust cycle. There are relatively few observations of deposition and the underlying theory has not evolved much in recent years. Wet deposition is closely related to the representation of precipitation in models, which tends to be too light and too frequent due to simplifications such as convective parameterizations. This can potentially remove too much dust from the atmosphere, as suggested by a general tendency of too much dust lost during long-range transport. This is particularly critical in the Saharan trans-Atlantic transport.

6.3.5 Future Research and Recommendations

6.3.5.1 Dust Mineralogy

The mineral composition of dust affects various processes, such as processes in atmospheric, ocean and terrestrial environments, and it also affects human health (Tong et al., 2017). Including mineral dust transport interacting with the atmosphere in numerical models can improve the accuracy of weather forecasts and climate simulations and contribute to a better understanding of the environmental processes caused by mineral dust. Motivated by the interest of the modeling community to study impacts of dust mineralogy, several studies have been recently performed focused on dust mineralogy.

6.3.5.2 Dust Research for Decision-Making Support

Dust storms impose a myriad of detrimental effects on human societies. Efforts have been made to utilize air quality forecasting systems to support decision-making activities to mitigate these effects. For instance, several dust control and health surveillance programs have been set up to address health effects of dust storms at local, state, national and international levels, such as the public health tracking systems by Centers for Disease Control and Prevention (CDC). Certain populations are more vulnerable to the health impacts associated with exposure to *Coccidioides* and the vulnerability changes based on the demographics of the county. Air quality forecasting systems have been used to provide early warning for elevated PM_{2.5} concentrations for sensitive groups. In addition, dust storms are one of the deadliest weather hazards in many arid and semi-arid regions, with a death toll exceeded only by extreme heat and flooding (e.g., Ladder et al., 2016). Transportation agencies in the United States have established active Highway Dust Mitigation programs. The public is alerted to blowing dust

hazards by Dust Storm Warnings and Blowing Dust Advisories via cell phones, a “zone based” technology. Other decision-making entities address these issues, such as the wind erosion and soil conservation programs by the U.S. Department of Agriculture (USDA), and the Sand and Dust Storm Advisories coordinated by the World Meteorological Organization (WMO).

6.4 Sudden Release of Air Toxics

6.4.1 *Type of Air Toxics and Those Treated in Current CW-AQF*

Air toxics are chemical species that are suspected of causing or known to cause cancer or other serious health effects. In the U.S., the Clean Air Act requires the U.S. Environmental Protection Agency to regulate air toxics and works with state, local, and tribal leaders to reduce their emissions. Some examples of toxic air pollutants include benzene, dioxin, toluene, mercury, and lead compounds (<https://www.epa.gov/haps/health-effects-notebook-hazardous-air-pollutants>). Regional air quality models such as the Community Multiscale Air Quality Modeling System (CMAQ, Byun and Schere, 2006), and local scale models such as ALOHA (Areal Locations of Hazardous Atmospheres; Jones et al., 2013), can be used to predict the concentrations and depositions of harmful materials released into the atmosphere.

6.4.2 *Examples of Models Used for Forecasting Air Toxics*

In this section two atmospheric dispersion models will be presented in more detail to provide examples of the types of inputs and outputs that can be expected by air toxic models. Further information on air toxic models can be found in several recent publications (Bauer, 2011; Brzozowska, 2016, 2013; Dev et al., 2017; Gunatilaka et al., 2014; Kukkonen et al., 2017; Tauseef et al., 2017; Truong et al., 2016).

6.4.2.1 *ALOHA Model*

The ALOHA (Areal Locations of Hazardous Atmospheres; Jones et al., 2013) model is designed to provide emergency response personnel with a quick estimate of the spatial extent of harmful pollutants associated with a short-term, short-range accidental release of volatile and flammable chemicals to the atmosphere. ALOHA, the atmospheric modeling portion of the CAMEO® software suite, has been developed over the last 30 years by the U.S. National Oceanic and Atmospheric Administration's (NOAA) Office of Response and Restoration (OR&R) in collaboration with the Office of Emergency Management of the U.S. Environmental Protection Agency (EPA) and is currently available for both Windows and Mac computers (<https://www.epa.gov/cameo/aloha-software>).

To be useful to an emergency responder during a real event, the model was designed to require a minimum amount of information from the user that would be readily available in an emergency, such as the local weather and information on the chemical and its storage state at the time of its release. Defaults are provided if some of these parameters are not known so that a conservative result will be projected by the model. In addition, the model is designed to run quickly and provide the results in a form that is understandable and familiar to decision makers.

To estimate the amount of pollutant released, either from a physical container, or from a spill, ALOHA has multiple time-dependent chemical source models. These include a tank, puddle, gas pipeline, and a direct release to the atmosphere. Based on the weather conditions at the time of the release, the physical dimensions of the container, the storage state of the chemical, and the dimensions of the release point or spill area, ALOHA calculates the time-varying emission rate of the chemical vapor to the atmosphere. For example, ALOHA will calculate the evaporation rate of a chemical spill and how it varies as the spill area decreases. ALOHA contains its own chemical library of approximately 1 000 common hazardous chemicals that includes the physical properties needed to calculate the chemical release rate.

ALOHA contains both a Gaussian and a Heavy Gas dispersion algorithm, either of which can be selected by the user or the model can decide based on the chemical and its storage state at the time of release. Once the release rate has been calculated, ALOHA uses the appropriate atmospheric dispersion model to calculate the toxic Level of Concern (LOC), or threshold concentration values, from exposure to a chemical that is harmful to people if breathed in for a defined length of time. ALOHA provides the user with several LOC values that are commonly used in the emergency response community or the user can specify their own.

ALOHA also contains five types of fire and explosion scenarios (i.e., jet fires, pool fires, BLEVEs, flammable areas, and vapor cloud explosions) most frequently associated with chemical releases and can help the user to choose the appropriate type based on the chemical being modeled. ALOHA can create LOC plots of flammability, thermal radiation, or overpressure for these non-dispersion scenarios.

Model results can be presented as a plot of toxic threat zones in the downwind direction of the plume which indicate areas that exceed the LOC values defined by the user. The toxic threat zone plot also contains wind direction confidence lines surrounding the threat zone that encloses the region within which the chemical cloud is expected to remain 95% of the time, providing a measure of certainty. The user can also create a time series of the pollutant concentration at a point for the first hour of the calculation, which can be helpful to know the expected peak concentration at a point of interest such as a school or hospital. In addition, maps of contoured LOCs with detailed map backgrounds can be produced by exporting the ALOHA results to another program in the CAMEO Suite called MARPLOT.

Limitations of ALOHA include conditions of very light wind speeds or very stable atmospheric conditions and in areas of wind shifts or terrain-induced flows where the Gaussian plume model does not apply. The model also does not account for the byproducts from fires, explosions, or chemical reactions, chemical mixtures, particulates (deposition), hazardous fragments from explosions, or terrain (pooling of chemicals).

Since ALOHA is designed primarily for the emergency responder or planner, many training materials have been created and made available on the OR&R website at:

<https://response.restoration.noaa.gov/aloha>

Technical resources can be found at:

<https://response.restoration.noaa.gov/oil-and-chemical-spills/chemical-spills/resources/aloha-technical-resources.html>

6.4.2.2 *HYSPLIT/ALOHA Model*

NOAA National Weather Service (NWS) forecasters have an operational need to provide local and state emergency responders with plume forecasts tailored to their specific needs, such as a wildfire event or a chemical or radiological release. In 2013, a web-based modeling system was developed to provide NWS forecasters with the ability to first simulate a release of a hazardous chemical to the atmosphere, using the extensive scenario-based source term configuration of the ALOHA model developed by OR&R and the U.S. EPA, and then simulate the resulting plume, using the HYSPLIT atmospheric transport and dispersion model (Stein, 2015) developed by the NOAA Air Resources Laboratory. Based on user input, ALOHA creates a time-varying release rate that is used by HYSPLIT for transport and dispersion calculations. The HYSPLIT system also has menu-driven capabilities to simulate the release of other hazardous pollutants to the atmosphere, such as smoke and radiological contaminants.

The HYSPLIT model is a complete system for computing simple air parcel trajectories, as well as complex transport, dispersion, chemical transformation, and deposition simulations. The model calculation method is a hybrid between the Lagrangian approach, using a moving frame of reference for the advection and diffusion calculations as the trajectories or air parcels move from their initial location, and the Eulerian methodology, which uses a fixed three-dimensional grid as a frame of reference to compute pollutant air concentrations. HYSPLIT has evolved over

more than 30 years, from estimating simplified single trajectories based on radiosonde observations to a system accounting for multiple interacting pollutants transported, dispersed, and deposited over local to global scales.

The dispersion of a pollutant is calculated by assuming either puff or particle dispersion. In the puff model, puffs expand until they exceed the size of the meteorological grid cell (either horizontally or vertically) and then split into several new puffs, each with its share of the pollutant mass. In the particle model, a fixed number of particles are advected about the model domain by the mean wind field and spread by a turbulent component. The model is available for the Windows, Mac, and LINUX platforms from the READY (Rolph, 2017) website (<https://www.ready.noaa.gov/HYSPLIT.php>).

ARL and OR&R collaborated to combine the strengths of each of their models to produce a new system that provides NWS forecasters with a better forecast of the location of hazardous areas from the release of chemicals to the atmosphere. The source strength models of ALOHA (tank, puddle, gas pipeline, and direct release to the atmosphere) were extracted from ALOHA, converted to the LINUX platform, and used to produce a time-varying chemical emission rate for HYSPLIT. The system uses the meteorological model's weather parameters as input to the ALOHA source term model instead of manual entry by the user. HYSPLIT is then used to transport and disperse the chemical using its three-dimensional particle dispersion algorithms to provide a more realistic concentration estimate, especially at farther distances than is recommended by ALOHA alone. In addition, HYSPLIT has the advantage of being able to use archived and forecast three-dimensional gridded meteorological data in its calculations thereby allowing for wind shear and vertical mixing that ALOHA's Gaussian model does not allow.

The HYSPLIT/ALOHA modeling system is currently only available to NOAA personnel, however, the NWS forecasters have an option to create a web link to provide to outside clients that will enable them to see the products on a web page similar to the one provided to the forecasters. This enables the forecasters to be able to brief the local emergency manager on the products in the same formats (web interface) as is available to him or her. Forecasters enter information on the meteorological data to use, the details on the chemical and its storage conditions, the time of release, and the number of hours to run HYSPLIT. Similar to ALOHA, the HYSPLIT/ALOHA system provides the user with the same toxic LOC options and produces similar maps of contoured concentrations at each of the LOC values selected by the forecaster on a detailed GIS-based map background. Additional options allow the results to be output as PDF, GIF, Shapefiles, and KMZ files.

The HYSPLIT/ALOHA system has the same chemical limitations as ALOHA (no chemical reactions, byproducts from fires, explosions or chemical reactions), and at this time does not incorporate the effects of dense gases, non-neutrally buoyant materials, particulate deposition (unless particle parameters are specified at run time), or complex terrain other than what is resolved through the meteorological model's terrain.

A training course designed for NWS forecasters on the combined HYSPLIT/ALOHA system titled "HYSPLIT Applications for Emergency Decision Support, 2nd Edition" is available on the COMET MetEd website at: <https://www.meted.ucar.edu>. COMET is part of the University Corporation for Atmospheric Research's (UCAR's) Community Programs and is sponsored by the NWS. Additional training resources for HYSPLIT are available on the ARL HYSPLIT website at: <https://www.ready.noaa.gov/HYSPLIT.php> or the HYSPLIT Forum at: <https://hysplitbbs.arl.noaa.gov/>.

6.5 Volcanic Eruption

After the comparatively moderate eruption of Eyjafjallajökull volcano in Iceland in 2010, volcanoes attract primary attention as the sources of potentially major and widespread disruptions of air traffic, worldwide. They also have a potentially strong impact on climate, and devastating effects on the environment in their proximity (sometimes, spanning over hundreds of kilometers from the crater).

The amount of material and energy released makes volcanoes practically unrivaled in the list of natural disasters. To date, there is absolutely no way to influence the eruptions and very limited and uncertain means to predict their occurrence, strength, and type. Information on the volcanic unrest, i.e. the changes in seismicity, ground deformation, release of gases, etc., which can be used as indicators of approaching eruption can be found in:

<http://www.wovodat.org>.

From the atmospheric standpoint, the most important characteristics of eruptions are:

- (i) amount of sulphur dioxide SO₂ released during the eruption – important for climate change,
- (ii) amount of fine (smaller than 10 mm in diameter) volcanic ash particles – important for aviation, and
- (iii) height to which volcanic ash is brought by the explosions – important for aviation.

It should be pointed out that the term “volcanic ash” is often misunderstood and somehow related to ash from biomass burning. In reality, these two have nothing in common: volcanic ash consists of melted and/or crushed pieces of rocks (e.g., basalt) and minerals, less than 2 mm in diameter. They often have an irregular shape with sharp edges. Not all eruptions release large amounts of ash – usually these are explosive eruptions, contrary to effusive ones, which are characterized by a comparatively calm outflow of lava with few or no explosions.

The eruption’s strength is quantified via the Volcanic Explosivity Index (VEI), which, similar to the scale measuring earthquakes, has a range from 0 to 8. The scale is logarithmic with a base of 10, i.e. each next gradation is 10 times stronger than the previous one. The VEI 1 eruption produces less than 0.0001 km³ of ejecta (ash, tephra, etc.), a VEI 2 eruption produces from 0.001 km³ up to 0.01 km³ ejecta, etc., up to VEI 8, which releases a stunning 1 000 km³ of ejecta. On this scale, the Eyjafjallajökull eruption has VEI 4, i.e., it released about 1 km³ of ejecta.

It is generally considered that eruptions of VEI 5 or higher can have significant effects on climate. It was also shown that for many eruptions, VEI is related to a characteristic height reached by the initial explosive and thermal uplift of the released material. The most cited work relating to the amount of released material and the typical height of release is the work of Mastin et al. (2009). Being indeed a very useful source for a quick assessment, this relation has strong limitations: Mastin et al. themselves stressed that the envelope enclosing half of the considered eruptions reaches a factor of four in either direction from the best fit. Thus, for Eyjafjallajökull, this formula provides quite reasonable estimates but fails for the Grimsvotn eruption in Iceland a few years later.

6.5.1 Scope and Mandate for Volcanic Plume Forecasts with CW-AQF

The high impact of volcanoes on aviation called for the establishment of a network of Volcanic Ash Advisory Centers (VAAC), which was set up by the International Civil Aviation Organization ICAO (<http://www.icao.int>). The nine VAACs together cover the whole globe (except for Antarctica) and are responsible for issuing warnings if an eruption occurs in their area of responsibility. VAACs also perform basic services on forecasting the plumes from the ongoing eruptions for a period of up to a couple of days and issue the corresponding information bulletins for the aviation authorities, airlines, military services, etc. VAACs also serve as

centers collecting and distributing information on the ongoing eruptions, their characteristics, available observations, etc.

Apart from the VAAC information and its important role in decision-making, a large variability and poor predictability of volcanic plumes leaves a wide area for improvement and services with more complete and comprehensive information. Therefore, information of operational CW-AQF systems can comprise a significant contribution. Apart from evaluation and model intercomparison purposes, availability of several independent model predictions opens the possibility for ensemble approaches, which were shown to outperform all individual models comprising the ensemble.

6.5.2 *Observations of Volcanic Eruptions*

Eruptions are spectacular events, which makes them highly visible and easily observable at least in the area of the volcano. However, the spontaneous nature of eruption variations and wide danger zones around the crater make direct observations impossible. Secondly, the ash and SO₂ clouds released in the air can remain dangerous far beyond the local area. As a result, two types of observations presently dominate: local and space-born remote sensing instruments.

On a local scale, radars, cameras, lidars, etc., are the most useful tools providing the initial height of the plume and, in some cases, giving some hints on the composition of the released clouds. Some of these instruments also serve as early-warning systems because they can be set up around the volcano in advance, e.g., when the seismic activity shows the possibility of eruption. Some of them can be used as permanent posts monitoring the activity of the volcano.

Satellite information has already become a vital part of volcano-related decision support systems. Both SO₂ and ash clouds are well observed by modern instruments and, in combination with ground-based monitoring, can provide previously unprecedented levels of detail. The limitations of space-born monitors include cloud obscuration, which can hide the plumes of even a relatively powerful eruption or make them hard to distinguish from the clouds themselves.

Geostationary satellites (e.g., SEVIRI, GOES, and HIMAWARI) provide excellent temporal resolution (10-15 minutes) and consequently have little problem with clouds – even losing 80% of images, the instrument still can provide a lot of information on the plumes. However, the location above the Equator makes their viewing area limited with a radius of about 60°-65° (ca. 7 000 km) from the nadir point. As a consequence, Icelandic or Alaskan volcanoes are barely visible by such instruments. Low-orbit satellites can provide global coverage every day but they have just a few overpasses over each specific place. Cloud obscuration then becomes arguably the most serious problem.

6.5.3 *Overview of Modeling Approaches*

Modeling the volcanic plumes poses strict requirements to the models: they should have sufficient horizontal and vertical resolution to reproduce narrow plumes, low-diffusive transport schemes enabling the simulation of compact clouds with sharp boundaries, and be capable of quickly handling varying strengths and a vertical injection of the source.

Initially, the main instrument for predicting the volcanic plumes were Lagrangian models, i.e. the numerical systems representing the plumes and clouds as a collection of independent Lagrangian particles, each representing a certain limited volume of the air, transported with the mean wind and randomly relocated in both horizontal and vertical directions due to turbulence. Being a convenient and quite natural instrument for representing the volcanic plumes, these models have difficulties at very large scales of dispersion when the required number of Lagrangian particles becomes too large even for modern supercomputers. Secondly, these models by their construction cannot handle non-linear chemical and physical

transformations, which can be a significant weakness for climate-related studies or when there are strong gaseous emissions from the crater.

Eulerian chemical transport models, unlike Lagrangian ones, have no problem with the comprehensive physics and chemistry but have substantial difficulties with the spatial resolution, which is often not sufficient near the volcano and requires nested simulations. The second problem is that many Eulerian models have diffusive transport routines, which further exacerbate the resolution limitation. In modern schemes, the diffusivity problem is practically resolved but such solutions can be quite expensive computation-wise and require a good understanding from the model developers and operators.

Here we provide as an example the application of a full-chemistry Eulerian model - Community Multiscale Air Quality (CMAQ) - to predict the volcanic plume during the recent eruption of the Kilauea volcano in Hawaii. The Kilauea volcano has been degassing with a relatively constant emission rate for the past three decades until May 2018. A large eruption occurred first on 6 May, followed by several episodes of varying magnitude. Elevated levels of toxic gases and particles were detected at several monitoring stations, suggesting that the volcanic plumes can potentially impose severe health stress on the people living in the impacted areas and further downwind. Advanced air quality forecasting systems, such as CMAQ, can be equipped with near-real time emission estimates to provide critical air quality data to assess population exposure to volcanic smog (vog) and to assist in developing effective evacuation plans, if necessary. The CMAQ prediction (Figure 6.3) shows that the health-based air quality standard for sulfur dioxide (SO_2) was frequently exceeded in the areas downwind to the Kilauea volcano on 19 May 2018. This highlights the need to provide predictive air quality data for emergency response activities.

6.5.4 *Combining Modeling and Observations for Predicting Volcanic Plumes*

High levels of uncertainty of both monitoring and model-based predictions of volcanic plumes call for the blending of the strong features of both approaches. A series of research and application projects resulted in the development of advanced technologies in this area. The primary questions to be answered when one tries to predict the volcano plume dispersion are: (i) how much was emitted? (ii) what is the vertical injection profile? Answers have to be provided with sufficient temporal resolution in order to capture variations in the eruption strength.

One of the possible approaches characterizes the volcanic source term explicitly: it searches for the emission rate as a function of vertical height and time, for each released species. The collection of the corresponding mathematical methods is commonly described as "source inversion technologies". They can be made via the direct inversion of transport matrices (developed mainly for Lagrangian models) or via data assimilation extended to include emission strength as a control variable. Under this paradigm, observations are used only to reconstruct the characteristics of the eruption whereas prediction of the plume dispersion is left completely to models.

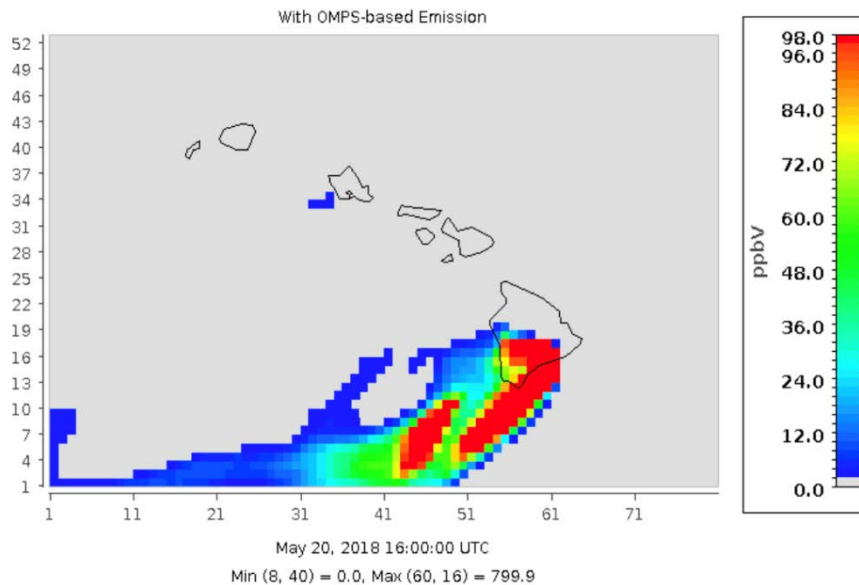


Figure 6.3. Surface SO_2 concentration predicted on 19 May 2018 over Hawaii, United States.

The alternative approach almost ignores the features of the source term and concentrates exclusively on transport of the once-observed plumes. These methods follow the classical data assimilation paradigm and use observations to initialize the models with the observed clouds, which are then transported by the model.

Both “pure” methods above have their strong and weak points originating from incompleteness of information coming from the observations and limited predictability of the single-cloud dispersion process. Therefore, their combined application is probably the most promising approach. Indeed, having a reasonably accurate characterization of the eruption behavior, one can apply the transport model, which is then additionally adjusted towards the newly available observations, which correct the model predictions further away from volcano.

Observations are also indispensable for evaluation of the model predictions. One only has to keep in mind that the assimilated set of observations must be independent from the one used for evaluation, preferably coming from a different instrument.

6.6 Summary

- In contrast to recurring sources, these events emit air pollutants with distinct patterns, often abruptly and in large quantities. These intermittent sources can impose drastic effects on air quality, human health and transportation safety.
- Contemporary predicting and warning systems employ a variety of techniques to predict the emissions, transformation, transport and removal of pollutants or other hazardous substances from these extreme events. Forecasts of these extreme events provide vital information to many decision-making activities.
- The WMO Global Atmosphere Watch (GAW) Programme together with the Interdisciplinary Biomass Burning Initiative (IBBI) provided guidance for addressing the issues of vegetation fire and smoke pollution. They also proposed the establishment of a Vegetation Fire and Smoke Pollution Warning and Advisory System (VFSP-WAS) to support the potential foundation of regional centers.
- Several dust control and health surveillance programs have been set up to address the health effects of dust storms at local, state, national and international levels, such as the public health tracking systems by CDC.

- Transportation agencies have established active Highway Dust Mitigation programs. The public is alerted to blowing dust hazards by Dust Storm Warning and Blowing Dust Advisories via cell phones, a “zone based” technology.
- Other decision-making entities address these issues, such as the Sand and Dust Storm Advisories coordinated by WMO. The high impact of volcanoes on aviation called for the establishment of a network of VAAC, which was set up by the International Civil Aviation Organization ICAO (<http://www.icao.int>). The nine VAACs together cover the whole globe (except for Antarctica) and are responsible for issuing warnings when an eruption occurs in their area of responsibility.

References

- Alonso-Canas, I. and Chuvieco, E. (2015). Global burned area mapping from envisat-meris and modis active fire data. *Remote Sensing of Environment*, 163: 140–152.
- Bauer, T. J. (2011). Software User’s Manual for the RAILCAR4 Toxic Industrial Chemical Source Characterization Program, NSWCDD/TR-12/68, Naval Surface Warfare Center, Dahlgren Division, Dahlgren, VA.
- Benedetti, A., Baldasano, J. M., Basart, S., Benincasa, F., Boucher, O., Brooks, M. E., ... & Jones, L. (2014). Operational dust prediction. In *Mineral Dust* (pp. 223-265). Springer, Dordrecht.
- Brahney, J., A. P. Ballantyne, S. Sievers, and J. C. Neff (2013), Increasing Ca²⁺ deposition in the western US: The role of mineral aerosols, *Aeolian Res.*, 10, 77–87.
- Brzozowska, L. (2016). Computer simulation of impacts of a chlorine tanker truck accident, *Transportation Research Part D: Transport and Environment*. 43, 107-122. <https://doi.org/10.1016/j.trd.2015.12.001>
- Brzozowska, L. (2013). Modeling the propagation of smoke from a tanker fire in a built-up area, *Sci. Total Environ.*, 472, 901-911. <https://doi.org/10.1016/j.scitotenv.2013.11.130>
- Byun, D., and K.L. Schere (2006). Review of the governing equations, computational algorithms, and other components of the models-3 Community Multiscale Air Quality (CMAQ) modeling system. *Appl. Mech. Rev.* 59 (1–6), 51–77. <http://dx.doi.org/10.1115/1.2128636>.
- Chin, M., P. Ginoux, S. Kinne, B. N. Holben, B. N. Duncan, R. V. Martin, J. A. Logan, A. Higurashi, and T. Nakajima, Tropospheric aerosol optical thickness from the GOCART model and comparisons with satellite and sun photometer measurements, *J. Atmos. Sci.* 59, 461-483, 2002.
- Clow, David W., Mark W. Williams, and Paul F. Schuster. "Increasing aeolian dust deposition to snowpacks in the Rocky Mountains inferred from snowpack, wet deposition, and aerosol chemistry." *Atmospheric Environment* 146 (2016): 183-194.
- Cook, B.I., Ault, T.R., & Smerdon, J.E. Unprecedented 21st century drought risk in the American Southwest and Central Plains. *Science Advances* 1(1): e1400082 (2015).
- Crooks JL, Cascio WE, Percy MS, Reyes J, Neas LM, Hilborn ED. 2016. The association between dust storms and daily non-accidental mortality in the United States, 1993–2005. *Environ Health Perspect.* 124:1735–1743; <http://dx.doi.org/10.1289/EHP216>.
- Darmenov, A. and da Silva, A. (2013). The quick-fire emissions dataset (QFED) - documentation of versions 2.1, 2.2 and 2.4. NASA Technical Report Series on Global Modeling and Data Assimilations 32, NASA.
- Dentener, F.J., G.R. Carmichael, Y. Zhang, J. Lelieveld and P. J. Crutzen, Role of mineral aerosol as a reactive surface in the global troposphere, *J. Geophys. Res.*, 101, 22,860-22,889, 1996.
- Dev D.J., M. Wilson, J.K. Wickliffe, J. Shaffer, T. Middleton, R. Rando, E.R. Svendsen (2017)

Assessment of an irritant gas plume model for epidemiologic study. *International Journal of Environmental Health Research*, 27:4, 276-292.
<https://doi.org/10.1080/09603123.2015.1020414>.

- Duce, R. A. (1995), Sources, distributions, and fluxes of mineral aerosols and their relationship to climate, in *Aerosol Forcing of Climate*, edited by R. J. Charlson and J. Heintzenberg, pp. 43– 72, John Wiley, New York.
- Evan, A.T., Dunion, J., Foley, J.A., Heidinger, A.K., & Velden, C.S. New evidence for a relationship between Atlantic tropical cyclone activity and African dust outbreaks. *Geophysical Research Letters* 33(19) (2006).
- Foltz, G.R., & McPhaden, M.J. Trends in Saharan dust and tropical Atlantic climate during 1980–2006. *Geophysical Research Letters* 35: L20706, doi:10.1029/2008GL035042 (2008).
- Freitas, S., Longo, K., Chatfield, R., Latham, D., Silva Dias, M., Andreae, M., Prins, E., Santos, J., Gielow, R., and Carvalho Jr., J. (2007). Including the sub-grid scale plume rise of vegetation fires in low resolution atmospheric transport models. *Atmos. Chem. Phys.*, 7: 3385–3398.
- Ginoux, P., Prospero, J.M., Gill, T.E., Hsu, N.C., & Zhao, M. Global-scale attribution of anthropogenic and natural dust sources and their emission rates based on MODIS Deep Blue aerosol products. *Reviews of Geophysics* 50: RG3005, doi:10.1029/2012RG000388 (2012).
- Giglio, L. (2007). Characterization of the tropical diurnal fire cycle using VIRS and MODIS observations. *RSE*, 108(4):407–421.
- Giglio, L., Randerson, J. T., and van der Werf, G. R. (2013). Analysis of daily, monthly, and annual burned area using the fourth-generation global fire emissions database (GFED4). *Journal of Geophysical Research: Biogeosciences*, 118(1):317–328.
- Giglio, L., Schroeder, W., and Justice, C. O. (2016). The collection 6 MODIS active fire detection algorithm and fire products. *Remote Sensing of Environment*, 178:31–41.
- Guan, Q., Yang, J., Zhao, S., Pan, B., Liu, C., Zhang, D., & Wu, T. (2015). Climatological analysis of dust storms in the area surrounding the Tengger Desert during 1960–2007. *Climate Dynamics*, 45(3-4), 903-913.
- Goudie, A. S. (2014). Desert dust and human health disorders. *Environment international*, 63, 101-113.
- Gunatilaka A., A. Skvortsov, and R. Gailis (2014). A review of toxicity models for realistic atmospheric applications, *Atmospheric Environment*, 84, 230-243.
<https://doi.org/10.1016/j.atmosenv.2013.11.051>
- Intergovernmental Panel on Climate Change (IPCC), *Climate Change 2001*, edited by J. T. Houghton et al., Cambridge Univ. Press, New York, 2001.
- Jones, R., W. Lehr, D. Simecek-Beatty, R. Michael Reynolds (2013). ALOHA® (Areal Locations of Hazardous Atmospheres) 5.4.4: Technical Documentation. U. S. Dept. of Commerce, NOAA Technical Memorandum NOS OR&R 43. Seattle, WA: Emergency Response Division, NOAA. 96 pp.
- Kaskaoutis, D. G., E. E. Houssos, A. Rashki, P. Francois, M. Legrand, D. Goto, A. Bartzokas, H. D. Kambezidis, and T. Takemura (2016), The Caspian Sea–Hindu Kush Index (CasHKI): A regulatory factor for dust activity over southwest Asia, *Global and Planetary Change*, 137(C), 10–23, doi:10.1016/j.gloplacha.2015.12.011.
- Kaiser, J. W., Heil, A., Andreae, M. O., Benedetti, A., Chubarova, N., Jones, L., Morcrette, J.-J., Razinger, M., Schultz, M. G., Suttie, M., and van der Werf, G. R. (2012). Biomass burning emissions estimated with a global fire assimilation system based on observed fire radiative power. *Biogeosciences*, 9:527–554.
- Kukkonen, J., J. Nikmo, K. Riikonen (2017). An improved version of the consequence analysis model for chemical emergencies, *ESCAPE*, *Atmospheric Environment*, 150,

198-209. <https://doi.org/10.1016/j.atmosenv.2016.11.050>

- Lader, Glenn, Aishwarya Raman, Jeffrey T. Davis, Ken Waters, 2016. Blowing Dust and Dust Storms: One of Arizona's Most Underrated Weather Hazards. NOAA Technical Memorandum NWS-WR 290. Published in July 2016.
- Lee, J.A., & Gill, T.E. Multiple causes of wind erosion in the Dust Bowl. *Aeolian Research* 19: 15–36 (2015).
- Lelieveld, J., Evans, J. S., Fnais, M., Giannadaki, D., and Pozzer, A. (2015). The contribution of outdoor air pollution sources to premature mortality on a global scale. *Nature*, 525(7569):367– 371.
- Mahowald, N. M., Ballantine, J. A., Feddema, J., and Ramankutty, N.: Global trends in visibility: implications for dust sources, *Atmos. Chem. Phys.*, 7, 3309-3339, [doi: 10.5194/acp-7-3309-2007](https://doi.org/10.5194/acp-7-3309-2007), 2007.
- Mastin, L.G. et al., 2009. A multidisciplinary effort to assign realistic source parameters to models of volcanic ash-cloud transport and dispersion during eruptions. *Journal of Volcanology and Geothermal Research*, 186(1–2), pp.10–21.
- Nickovic, S., Cvetkovic, B., Madonna, F., Rosoldi, M., Pejanovic, G., Petkovic, S., & Nikolic, J. (2016). Cloud ice caused by atmospheric mineral dust—Part 1: Parameterization of ice nuclei concentration in the NMME-DREAM model. *Atmospheric Chemistry and Physics*, 16(17), 11367-11378.
- Paugam, R., Wooster, M., Atherton, J., Freitas, S. R., Schultz, M. G., and Kaiser, J. W. (2015). Development and optimization of a wildfire plume rise model based on remote sensing data inputs - part 2. *Atmospheric Chemistry and Physics Discussions*, 15(6):9815–9895.
- Perez, Laura, Aurelio Tobias, Xavier Querol, Nino Künzli, Jorge Pey, Andrés Alastuey, Mar Viana, Natalia Valero, Manuel González-Cabré, and Jordi Sunyer. "Coarse particles from Saharan dust and daily mortality." *Epidemiology* 19, no. 6 (2008): 800-807.
- Remy, S., Veira, A., Paugam, R., Kaiser, J., Marenco, F., Burton, S., Benedetti, A., Engelen, R., Ferrare, R., and Hair, J. (2017). Two global climatologies of daily fire emission injection heights since 2003. *Atmos. Chem. Phys.*, 17(4):2921–2942.
- Rolph, G., A. Stein, and B. Stunder (2017). Real-time Environmental Applications and Display sYstem: READY, *Environ. Model. Softw.*, 95, 210-228. [doi: 10.1016/j.envsoft.2017.06.025](https://doi.org/10.1016/j.envsoft.2017.06.025).
- Rosenfeld, D. (2000). Suppression of Rain and Snow by Urban and Industrial Air Pollution. *Science*, 287(5459): 1793-1796.
- Roy, D. P., Boschetti, L., Justice, C. O., and Ju, J. (2008). The collection 5 MODIS burned area product: Global evaluation by comparison with the MODIS active fire product. *Journal of Geophysical Research*, 112(9):3690– 3707.
- Sessions, W. R., Reid, J. S., Benedetti, A., Colarco, P. R., da Silva, A., Lu, S., ... & Brooks, M. E. (2015). Development towards a global operational aerosol consensus: basic climatological characteristics of the International Cooperative for Aerosol Prediction Multi-Model Ensemble (ICAP-MME). *Atmos. Chem. Phys.*, 15, 335-362.
- Schubert, S.D., Suarez, M.J., Pegion, P.J., Koster, R.D., & Backmeister, J.T. On the cause of the 1930s Dust Bowl. *Science* 303: 1855–1859 (2004).
- Seager, R., Ting, M., Held, I., Kushnir, Y., Lu, J., Vecchi, G., et al. Model projections of an imminent transition to a more arid climate in southwestern North America. *Science* 316(5828): 1181–1184 (2007).
- Shao, Y., Klose, M., & Wyrwoll, K.H. (2013). Recent global dust trend and connections to climate forcing. *Journal of Geophysical Research: Atmospheres* 118(19), 11107-11118 (2013).
- Shao, Y. (2008), *Physics and modeling of wind erosion*. Springer, ISBN 978-1-4020-8894-0, 452pp.

- Sofiev, M., Vankevich, R., Lotjonen, M., Prank, M., Petukhov, V., Ermakova, T., Koskinen, J., and Kukkonen, J. (2009). An operational system for the assimilation of the satellite information on wildland fires for the needs of air quality modeling and forecasting. *Atmospheric Chemistry and Physics*, 9(18):6833–6847.
- Sofiev, M., Ermakova, T., and Vankevich, R. (2012). Evaluation of the smoke injection height from wildland fires using remote sensing data. *ACP*, 12:1995–2012.
- Sokolik, I.N. and O.B. Toon (1996), Direct radiative forcing by anthropogenic airborne mineral aerosols, *Nature*, 381, 681-683.
- Son C.H. Truong, M. Lee, G. Kim, D. Kim, J. Park, S. Choi, G. Cho (2016). Accidental benzene release risk assessment in an urban area using an atmospheric dispersion model, *Atmospheric Environment*, 144, 146-159.
<https://doi.org/10.1016/j.atmosenv.2016.08.075>
- Stein, A.F., R.R. Draxler, G.D. Rolph, B.J.B. Stunder, M.D. Cohen, and F. Ngan (2015). NOAA's HYSPLIT atmospheric transport and dispersion modeling system, *B. Am. Meteorol. Soc.*, 96, 2059–2077, [doi:10.1175/BAMS-D-14-00110.1](https://doi.org/10.1175/BAMS-D-14-00110.1)
- Tauseef, S. M., Tasneem Abbasi, R. Suganya and S.A. Abbasi (2017). A critical assessment of available software for forecasting the impact of accidents in chemical process industry, *International Journal of Engineering, Science and Mathematics*, 6, Issue 7, 269-289.
- Tegen, I., and A. Lacis, 1996: Modeling of particle size distribution and its influence on the radiative properties of mineral dust aerosol. *J. Geophys. Res.*, 101, 19 237–19 244.
- Tong, D. Q., Dan, M., Wang, T., and Lee, P., 2012. Long-term dust climatology in the western United States reconstructed from routine aerosol ground monitoring, *Atmos. Chem. Phys.*, 12, 5189-5205.
- Tong, D. Q., et al. (2017). Intensified dust storm activity and Valley fever infection in the southwestern United States. *Geophysical Research Letters*, 44(9), 4304-4312.
- Usher C.R., A.E. Michel, V.H. Grassian, 2003. Reactions on Mineral Dust. *Chem. Rev.*, 103: 4883-4939.
- Van Der Werf, G. R., Randerson, J. T., Giglio, L., Van Leeuwen, T. T., Chen, Y., Rogers, B. M., Mu, M., Van Marle, M. J., Morton, D. C., Collatz, G. J., et al. (2017). Global fire emissions estimates during 1997-2016.
- Veira, A., Kloster, S., Schutgens, N. A. J., and Kaiser, J. W. (2015). Fire emission heights in the climate system - part 2: Impact on transport, black carbon concentrations and radiation. *Atmospheric Chemistry and Physics*, 15(13):7173–7193.
- Wiedinmyer, C., Akagi, S. K., Yokelson, R. J., Emmons, L. K., Al-Saadi, J. A., Orlando, J. J., and Soja, A. J. (2011). The fire inventory from ncar (finn); a high-resolution global model to estimate the emissions from open burning. *Geosci. Model Dev.*, 4:625–641.
- Wooster, M. J., Xu, W., and Nightingale, T. (2012). Sentinel-3 SLSTR active fire detection and FRP product: Pre-launch algorithm development and performance evaluation using MODIS and ASTER datasets. *RSE*, 120:236–254.
- Worster, D. Dust Bowl. The Southern Great Plains in the 1930s. Oxford University Press, New York (1979).
- World Health Organization (WHO) (2006). Air Quality Guideline Global Update 2005. WHO Regional Office for Europe, Copenhagen, Denmark. ISBN 92-890-2192-6.
- WMO SDS-WAS, 2015: Sand and Dust Storm Warning Advisory and Assessment System (SDS–WAS): Science and Implementation Plan 2015-2020, (S. Nickovic, E. Cuevas, J. Baldasano, E. Terradellas, T. Nakazawa and A. Baklanov), WWRP Report 2015-5, World Meteorological Organization, Geneva, 37 pp. Available at:
https://library.wmo.int/doc_num.php?explnum_id=3383

- WMO GDPFS, 2017: Revised Manual on the Global Data-Processing and Forecasting System, WMO No. 485, https://library.wmo.int/doc_num.php?explnum_id=10164
- WMO MHEWS, 2018: Multi-hazard Early Warning Systems: A Checklist: Outcome of the first Multi-hazard Early Warning Conference. WMO, https://library.wmo.int/doc_num.php?explnum_id=4463
- WMO VFSP-WAS, 2018: Vegetation Fire and Smoke Pollution Warning and Advisory System (VFSP-WAS): Concept Note and Expert Recommendations, WMO GAW Report 235, 45 pp., https://library.wmo.int/opac/index.php?lvl=notice_display&id=20244.
- Yu, H., Chin, M., Yuan, T., Bian, H., Remer, L. A., Prospero, J. M., Zhang, Z. (2015). The fertilizing role of African dust in the Amazon rainforest: A first multiyear assessment based on data from Cloud-Aerosol Lidar and Infrared Pathfinder Satellite Observations. *Geophysical Research Letters*, 42(6), 1984-1991.
- Zender, C.S., H. Bian, and D. Newman (2003), Mineral Dust Entrainment and Deposition (DEAD) model: Description and 1990s dust climatology, *J. Geophys. Res.*, 108(D14), 4416, [doi:10.1029/2002JD002775](https://doi.org/10.1029/2002JD002775).
- Zhu, C., Wang, B., & Qian, W. (2008). Why do dust storms decrease in northern China concurrently with the recent global warming? *Geophysical Research Letters*, 35(18).
- Zhuang, G.S., Z. Yi, R.A. Duce, and P. R Brown, (1992). Link between iron and sulfur suggested by the detection of Fe(II) in remote marine aerosols, *Nature*, 355, 537-539.

Chapter 7. Model Input and Preparation of Simulations

7.1 Introduction

Atmospheric composition and air quality modeling problems are largely driven by the external forcing: (i) emission of trace constituents, (ii) for offline chemistry transport models, meteorological input, and (iii) for limited-area applications, boundary conditions. These three inputs vary with time and their dynamics decide the evolution of the simulations. Other input data, such as land-use characteristics, local time zone, population maps, etc., are predominantly static. Finally, initial conditions prescribing the model state at the beginning of the simulations are the instant fields. Meteorological input was considered in the previous chapters (see Sections 3.3 and 3.4), therefore in this chapter we will concentrate on emissions and initial and boundary conditions, briefly outlining auxiliary information that might be of use for some applications.

In this chapter, important aspects of model inputs such as emissions and initial and boundary conditions as well as simulation preparation are described. These include anthropogenic and natural emissions (Section 7.2), initial and boundary conditions (Section 7.3), land use and land cover (Section 7.4), and other model input files (Section 7.5). Finally, Section 7.6 summarizes key points.

7.2 Emissions

The importance of knowing about the emission of atmospheric compounds is recognized since the very beginning of studies related to atmospheric composition. It started with the application for local air quality problems helping to implement programs for local- or city-level emission control. With the growing understanding of the variety of spatial scales of air pollution problems, local emission estimates turned into regional and global inventories covering tens of pollutants and providing a detailed distribution of the emission fluxes in both space and time.

7.2.1 Characteristics of Emission Sources

The emission input for an atmospheric composition model is the 4-D flux of species: the data needed to resolve all three spatial dimensions and reflect the temporal variability of the fluxes. The vertical profiles of emissions and the temporal variations, often neglected in the past, are now considered to be as important as the mapping of the source locations. The variety of species released into the atmosphere is very large. In practical applications, models are provided with a subset of pollutants, which selection depends on the problem at hand.

One can roughly identify the following groups:

- acidifying (SO_x and NO_x , also forming secondary aerosols),
- eutrophication-responsible NH_3 ,
- ozone-producing volatile organic compounds and NO_x ,
- toxic species, such as heavy metals and some organic species,
- primary aerosols,
- semi-volatile organic species largely responsible for the formation of secondary organic aerosols and affecting ozone formation,
- long-living halogenated compounds that are active in the stratosphere,
- long-living climate forcers, such as CO_2 , which practically do not participate in tropospheric chemistry but readily interact with vegetation and are important for the radiative budget.

Many species belong to several groups, so that the selection of the consistent subset of the species can be quite tedious work but in many cases the models have such sets predefined.

Apart from the chemical speciation, emission inventories are structured along the type of the sources, anthropogenic activity sectors, and the governing natural processes. For each sector, one can develop temporal profiles of emissions and estimate the vertical injection. Among the most important anthropogenic sectors, large combustion sources – power plants and industry – are characterized by comparatively stable release rates, high stacks, and extensive emission reduction technologies. Closer to the surface, especially in the cities, traffic pollution is the most important – and is characterized by a strong diurnal cycle with peaks of concentrations during rush hour. With emission reduction technologies also improving the situation with traffic exhausts, the residential combustion gradually emerges as a strong distributed source of pollution with limited control measures. Finally, a specific source of pollution is agriculture. It releases the bulk of ammonia, substantial amounts of dust and also combustion exhausts.

The most important sources governed by natural processes are wind-blown dust, sea salt, biogenic gases and aerosols, pollen particles, smoke from vegetation fires, and plume from volcanic eruptions. The latter, however, in many cases can be considered as anthropogenic: about 90% of fires worldwide are human-induced. They are set as part of agricultural processes, forest management or accidentally. The only significant natural source of fires is lightning, which is responsible for about 10% of the total number of fires.

7.2.2 *Dynamic Emission Models vs. Static Inventories*

Historically, the standard way to obtain emission data is to make a bottom-up inventory of the anthropogenic activities and natural processes, then estimate the emission factors for each activity sector, finally ending up with the set of annual emission estimates gridded in accordance with the locations of the sources. The bulk of anthropogenic emissions is computed via this approach. For this, emission factors from different processes were cataloged by leading international and national authorities, such as IPCC, EMEP, EPA, EEA, Copernicus, etc.

Apart from the static bottom-up inventories, physical models were developed for several strongly varying sources of pollution: wind-blown dust, biogenic volatile organic compounds, sea salt, vegetation fires, etc. The primary factors driving these models are meteorological parameters: wind, temperature, humidity, precipitation. The complexity of these models varies but it has been shown repeatedly that even approximate representation of the emission variability leads to a strong improvement of the computation results. The new direction today is to develop dynamic models to describe the impact of weather conditions on anthropogenic emissions. Promising results were obtained, for instance, for residential combustion influenced by ambient temperature. Another example is the adjustment of vertical profiles of emissions in relation to boundary layer thickness and intensity of mixing. Various injection-height models were developed to reproduce the impact of buoyancy effects on the plume rise from the strong thermal sources (e.g., power plants, factories, vegetation fires) starting from the classical works of Briggs suggesting empirical plume-rise formulas for industrial stacks (Briggs, 1969, 1984, 1975). The approach was further developed producing more formulas but also suggesting some semi-empirical and dynamic models, e.g., Brown et al. (1997); Berlyand (1991); Hanna and Chang (1991); Nikmo et al. (1999); Freitas et al. (2007); Sofiev et al. (2012, 2013); and Kukkonen et al. (2014)

An emerging approach of top-down emission estimation involves chemistry transport models – a so-called inverse dispersion modeling. In essence, it looks for the changes in emissions that would result in a better agreement of the model results with the observations. Under the assumption that the model is sufficiently accurate and the observational data are sufficiently extensive and accurate, the outcome can indeed see improved emission estimates. Arguably, the most important role in the inverse modeling rise was played by the satellite information that became comparatively abundant and accurate during the last decades. In many regions of the globe, satellites are the only available source of information regarding the atmospheric state and composition. However, data provided by satellites are indirect and usually require substantial processing before submitting them to the models. The challenges gave rise to

whole new fields of mathematical modeling, including highly sophisticated data assimilation algorithms, observational operators, source inversions, etc.

For the AQ forecasting, emissions also need to be forecasted. For the static inventories, the solution is straightforward, albeit not accurate, while dynamic meteorology-driven models provide ready solutions online with the chemistry transport simulations. However, for highly dynamic sources affected by both anthropogenic activity and meteorological factors, the problem is much more complicated. For instance, to date, there is no adequate methodology for predicting the regional-scale evolution of vegetation fires. These strong nearby-point sources can have a short lifetime (a few hours) while the place of the next ignition is hard to predict. Efforts are being undertaken to improve the situation but an acceptable solution has yet to be found.

7.2.3 *A Few Widely-Used Emission Inventories*

There are many initiatives to compile and improve emission inventories, some covering the globe, some concentrating on high-resolution detailed descriptions of regional and local emissions. Arguably, the largest collection of emission data is available from the ECCAD portal (Emissions of atmospheric Compounds and Compilation of Ancillary Data, <http://eccad.aeris-data.fr/>). It provides access to a large number of datasets on a global and regional scale also allowing the download of the emission time series.

For Europe, a compilation of national emission inventories provided by the authorities is maintained by the Cooperative Programme for monitoring and assessment of the long-range transboundary air pollution in Europe (EMEP, <http://www.emep.int>). For the U.S., the National Emissions Inventory (NEI) is provided by the Environment Protection Agency (EPA, <http://www.epa.gov>). The responsible authorities also provide guidance suggesting the best practices for the emission calculation. Thus, the European Environment Agency EEA (2016) gives guidelines at continental and national scales for reporting the emissions data under the UNECE Convention on Long-range Transboundary Air Pollution.

Several large-scale multi-pollutant assessment efforts have been undertaken to homogenize, evaluate and intercompare the existing inventories. Thus, the simulations for the IPCC AR5 considered the Emissions for Atmospheric Chemistry and Climate Model (ACCMIP) Intercomparison Project historical emissions (Lamarque et al., 2010). Granier et al. (2011) analysed the evolution of the emissions of air pollutants at global and regional scales for 1980-2010. They compared ACCMIP with MACCity, RCPs, EDGAR, HYDE, RETRO and GAINS for global emissions and some regional inventories: EMEP (Europe), TNO (Europe), INERIS (Europe), EPA (USA), REAS (Asia), ACCESS (Asia) and Garg (India). The report highlighted the similarities and inconsistencies of the inventories, also showing the lowest and the highest emissions for each species.

Some regions have very scarce data concerning emissions, for instance Africa and South America, where top-down approaches can be particularly useful for evaluating and improving the existing data. Corresponding methodology and multi-annual top-down emission datasets were developed by the GlobEmission project of the European Space Agency ESA (<http://www.globemission.eu>).

The project ECLIPSE (Evaluating the Climate and Air Quality Impacts of Short-Lived Pollutants) developed in Europe (Stohl et al., 2015) studied the effects of mitigation for short-lived climate pollutants and the quantification of the climate and air quality impacts. Several scenarios were built for Earth System Models (ESM) and Chemistry Transport Models (CTM). Global and European inventories are compiled within the scope of Copernicus Atmospheric Monitoring Service CAMS – and presented in the ECCAD database. Several research initiatives also significantly contribute to the development and harmonization of the area (e.g., Kuenen et al., 2014).

The European project MEGAPOLI (Megacities: Emissions, urban, regional and Global Atmospheric POLLution and climate effects, and Integrated tools for assessment and mitigation) (<http://megapoli.dmi.dk/>, MEGAPOLI, 2010, 2011) developed a hierarchy of nesting anthropogenic emission databases for Global, Pan-European and urban scales. These datasets, built by TNO, include high-resolution (1 km) emission inventories for four European megacities/urban agglomerations (London, Paris, Rhine-Ruhr, and the Po Valley) nested into the Pan European MEGAPOLI emissions dataset (6x7 km resolution), represented by local bottom-up emission inventories. Significant differences were found when comparing the local bottom-up inventories of the megacities with the European downscaled estimates for the same domain. Part of this is caused by different estimation methodologies, but the choices made to spatially distribute emissions were another important explaining variable. Often the local emissions for the megacity were considerably lower than the emissions allocated to their domain in the European downscaled inventory. This suggested that the share of national emissions allocated to the cities is overestimated in the spatial distribution procedure used to downscale the European inventory. In the final inventory the country, total emissions are kept in line with the official reported emissions by each country to EMEP. This was done by adding or removing emissions, at the source sector level, from that part of the country which is not in the megacity. The result is that the emission inventory is consistent with local megacity level inventories as well as the national inventories.

7.3 Initial and Boundary Conditions

Initial and (for limited-area applications) boundary conditions are two important drivers of the atmospheric composition simulations, on a par with the above-mentioned emissions and (for offline models) meteorological input. The roles of these drivers vary during the progress of the model run. At the beginning, the model state is completely decided by the initial conditions. With time, the other three drivers gradually take over, so that after some spin-up intervals, the influence of the initial conditions becomes negligible and simulations started from different points converge. This period is much shorter than in the meteorological simulations, where, especially on global scales, the influence of initial conditions can in principle last indefinitely: two runs with different initial states may never converge (only their statistical properties will be similar but phase trajectories never come together). For air quality problems, a long-lasting impact of initial conditions can only be seen in the stratosphere.

7.3.1 Model Initialization

There are several ways of initializing the simulations. The selection of the specific method depends on computer resources, model capabilities, and observational data availability.

The simplest initialization is the cold-start: the model is initialized with zeroes. It allows the starting of simulations with no readily available initialization dataset. Evidently, the spin-up period (preferably, a period several times longer than that) has to be computed before the simulation results become useful.

A more consistent way is pre-emption or warm-start: the next run starts from the fields of the previous one. Such chain of runs is convenient for operational forecasts or similar tasks with a series of sequential identical simulations with overlapping periods. Today, this is the most commonly used approach in AQ forecasting.

An extension of the pre-emption method is a warm-start from the fields of another model. This is a less convenient approach because different models usually have different species, grids, verticals, etc., so that massive interpolation and chemical cross-mapping have to be performed prior to starting the run. For such runs, it is highly advisable to use a time period comparable with the spin-up time in order to let the model shake off the initial inconsistencies and reach its own forecast trajectory.

An evident disadvantage of the pre-emption method is that the chain of runs can drift far from reality, depending on emission input and boundary conditions. If the simulation period is comparable with the model spin-up time or shorter, it may be useful to involve the assimilation

of the model's initial state using one of the data assimilation methods: point-wise nudging towards the observations, Optimal Interpolation of the observed concentrations, 3-D and 4-D Var, or EnKF (see Section 7.4 for explanations of the data assimilation procedures). All initialization options will interfere with the feedback between meteorology and chemistry in online AQ models, which needs to be considered when the objective of a study is such a feedback. A longer spin-up period is probably necessary in this case.

7.3.2 *Boundary Conditions*

Limited-area AQ applications require a definition of the exchange of the considered domain with the outer regions. The most common boundary conditions for CTMs are of Dirichlet type: the outer-area concentration at the border of the domain is prescribed to a fixed or space-time-varying value. Then, if the wind direction at the domain edge is directed inwards, the inflow mass is the product of the normal wind component and the outer-area concentration. If the normal wind vector component is directed outwards, the boundary is transparent.

In comparison with Dirichlet-type boundary conditions, a less common type is Neumann, which prescribes an in/out flux at the boundary rather than the concentrations. Periodic boundary conditions require that concentrations at the left and right borders are always equal to each other. This is practically never used in limited-area chemistry transport simulations but standard for global runs and also widely used for large eddy and direct numerical simulations.

Obtaining the boundary condition fields can be a challenge for limited-area applications if the outer-domain simulations are too bulky to make. One can consider a fixed value obtained from observations but spatial representativeness of such a solution is low. Climatological boundary conditions from some large-scale model runs are somewhat better but can still be far from reality because long-range transport exhibits large spatio-temporal variability. A solution can be to use one of the available datasets offered by organizations performing regular global atmospheric composition hind- and forecasts. For instance:

- Copernicus Atmospheric Monitoring Service (CAMS) (<http://atmosphere.copernicus.eu>) distributes global forecasting, hindcasting, and reanalysis products of the Integrated Forecasting System IFS. The reanalysis time series covers the period starting from 2003 and forecasts for reactive species and aerosols for up to 120 hours.
- CAMS also provides European forecasts for up to 96 hours, analysis and interim (two weeks delay) reanalysis with high spatial resolution (0.1°). The forecasts originate from the CAMS multi-model ensemble, which currently includes 7 European models.
- MOZART-4 global fields starting from 2007 are available from the National Center for Atmospheric Research (NCAR) Atmospheric Chemistry Observations and Modeling Laboratory (ACOM, <https://www2.acom.ucar.edu/acresp/forecasts>)
- NCAR-ACOM also provides forecasts since February 2018 with the whole-atmosphere WACCM model: <https://www2.acom.ucar.edu/gcm/waccm> and the "mozbc" tool to use these forecasts in WRF-Chem: <https://www2.acom.ucar.edu/wrf-chem>
- From the same website, users can also download a tool and data to set climatological upper boundary conditions, i.e., a method to constrain stratospheric concentration fields in a regional model.
- Global tropospheric and stratospheric forecasts up to 120 hours are available from the Finnish Meteorological Institute (FMI) model SILAM (<http://silam.fmi.fi/>). The same site also provides European forecasts for up to 96 hours covering the troposphere with 0.1° resolution.
- Global SILAM and European hindcasts starting from 1980 are available from FMI on a request basis.

- ICAP ensemble of global atmospheric aerosol forecasting models (<http://icap.atmos.und.edu/>).

When the boundary conditions are taken from a different model, care must be taken to map the chemical species of the foreign model to the ones used in the simulations. Only longer-lived species and aerosols need to be taken into account while the constraint of short-lived species (e.g. OH or HO₂ radicals) will not provide any benefit.

The specific way the inflow mass is introduced into the computation domain is almost completely determined by the model construction. One of the commonly-used procedures involves gradual relaxation of the outer-area values towards the inner-model fields (Davie's relaxation). More accurate approaches, however, are available for many CTMs, which can, for instance, treat the boundary inflows as a special type of emission source.

7.3.3 *Impact of Chemical Initial and Boundary Conditions*

The first CTMs used for air quality studies and forecasts used fixed concentration profiles for the whole period of study as chemical initial or boundary conditions (ICONS and BCONs). In some cases, such profiles were constructed based on mean values of observed concentration time series or chosen based on clean atmospheric conditions. Although observations would be the most appropriate information for chemical ICONs and BCONs, they are rarely available in an adequate spatial and temporal resolution, which leads to interpolation errors and low representability of timescales and, consequently, impact simulation results (Pfister et al., 2011). For chemical ICONs this impact can be reduced considering a spin-up time large enough for the simulation period, depending on each pollutant of interest. Some pollutants have "short memory" and a few hours will be enough for spin-up time while others have "longer memory" and will require more time to reduce the impact of chemical ICONs. For chemical BCONs three ways of minimizing the impact are usually applied (Seinfeld and Pandis, 1998). The first one is to use grid domains that are large enough to consider all emission sources of importance. The great limitation of this procedure is the high computational resources required and, therefore, it is rarely used. The second method applies time-independent (static) boundary conditions (e.g., mean pollutant profiles). The third method referred to as the nesting procedure, is the most used one and is based on outputs of lower resolution models, whose coarse-grid concentrations are reprojected to the higher resolution grids at the border of the domain of interest.

The nesting procedure requires information from some larger scale models, such as a global model. Examples of chemical global models that can be used for this task are RAQMS (Pierce et al., 2003), GEOS-CHEM (Shim et al., 2009), MOZART (Lin et al., 2010) and SILAM (Sofiev et al., 2015). Data from these models are downscaled into mesoscale air quality models to provide both initial and boundary conditions that represent the chemical state of the atmosphere outside the model domain (Curci, 2012). In this way, the intrusion of stratospheric air masses, intercontinental air advection and the influence of remote pollution sources, such as biomass burning, can be introduced in the regional model domain and interact with other atmospheric constituents (Tang et al., 2009). Independently of what kind of method is applied, there is no perfect procedure to provide chemical initial and boundary conditions, which makes it necessary to evaluate the impacts of such procedures.

One of the first studies to address this matter was made by Liu et al. (2001). They found that chemical ICONs influences decay exponentially with time, disappearing after the spin-up period. They also found that local emissions and chemical BCONs' influence increases with time and dominates the evolution of the concentrations after the spin-up time. The authors analysed 3-D ozone concentrations over California, U.S., using different idealized conditions and concluded that the chemical BCONs' influence is inversely proportional to the domain border distance and that the chemical BCONs can contribute from 30 to 40% of ozone formation in a polluted boundary layer. Samaali et al. (2009) studied the impact of the type of chemical BCONs in the spin-up period on an annual simulation of ozone and PM_{2.5} for a domain that covers the entire U.S. territory using the AURAMS offline model (Gong et al., 2006). The authors performed the simulation in three periods with two overlapping segments. The spin-up

period would be given by the convergence of the simulations in these overlapping periods. They found that the choice of chemical BCONs has a strong influence on the spin-up period mainly for ozone. When using chemical BCONs that do not consider the entry of concentrations from outside the simulation domain, i.e., a closed boundary, the daily averages of ozone concentration within the domain do not converge in the overlapping periods. The opposite behavior is observed by using an open boundary using static chemical BCONs, when the values of ozone are best represented and converge within the first three days of simulation. Their results also suggest the use of a spin-up period of longer than one week for a large (continental) domain and long-term simulation of $PM_{2.5}$ and O_3 rather than the 2–4 days commonly used.

Another important body of work was done by Tang et al. (2007), which used the STEAM -2K3 model to evaluate the effects of the chemical BCONs generated by three global models: MOZART/NCAR, MOZART/GFDL and RAQMS in the CO and O_3 simulations over the United States. They found that chemical BCONs improved model predictions, since they incorporate time-varying external values within the regional simulation domain, for example: biomass burning, stratospheric intrusion, and air masses from Asia. They also showed that the vertical distribution of ozone in the initial 3 km is not very sensitive to chemical BCONs, but the values in the middle and upper troposphere are dominated by them. These results show that ozone formation processes in the lower troposphere are dominated by local processes, such as emission sources and chemical production/deposition. But for long-lived species like CO , there is an impact throughout the troposphere.

Tang et al. (2009) compared six chemical BCONs in the United States National Air Quality Forecasting System (NOAA-EPA National air quality forecast guidance): the standard profile, three dynamic BCONs constructed with information from three different models (i.e., MOZART-4, RAQMS and GFS-O3), and two BCONs with information from ozone soundings conducted in the summer of 2006. The results showed that the choice of chemical BCONs affects the simulation throughout the whole domain especially at higher levels. They also showed that the use of dynamic BCON improves the correlation coefficients, however, it can increase mean bias and errors. For the surface O_3 simulations, the use of the MOZART-4 outputs generated the best simulations and the BCONs made with the soundings information improved the ozone representation at higher levels.

Using the CMAQ model, Borge et al. (2010) tested three types of chemical BCONs in high-resolution simulations (3 km): the standard profile, BCONs generated by a CMAQ coarser domain (parent grid) and the BCONs from GEOS-Chem, and found that the type of chemical BCON does not significantly influence the representation of nitrogen oxides, and sulfur, with their influence being more restricted to the vicinity of the boundaries of the model, but affecting the representation of ozone and particulate matter. They also mentioned that GEOS-Chem dynamic BCON improved the O_3 and PM_{10} representation, while the CMAQ BCON slightly improved the simulations of NO_2 and PM_{10} .

Over Europe, Ritter et al. (2013) evaluated the influence of boundary conditions, both chemical and meteorological, on the representation of O_3 and PM_{10} for a domain with a 50 km grid spacing. They compared simulations made using the standard BCONs with the BCONs generated using monthly averages of the simulations of the LMDZ-INCA global model (1997–2001). The results showed an improvement in the O_3 simulations using the new chemical BCONs, when higher values of the Pearson correlation coefficient and smaller mean deviations and errors were obtained. In addition, Žabkar et al. (2013) in the development of sensitivity tests for WRF-Chem in the simulation of a high O_3 concentration in Slovenia and the northern part of the Adriatic Sea, found that using BCONs generated by MOZART-4 produced an improvement in the representation of surface O_3 concentrations.

Pendlebury et al. (2018), using the GEM-MACH model with four different chemical BCONs, examined the conditions under which a limited-area air quality model could accurately forecast near-surface ozone concentrations during stratospheric intrusions over North America. They showed that the mean bias and correlation in surface ozone over the course of a season can be improved by using time-varying chemical BCONs, particularly through the correct assignment

of stratospheric vs. tropospheric ozone along the western lateral boundary. They attribute part of the improvement in surface ozone forecast results to a better characterization of near-surface ozone along the lateral boundaries that then directly impact surface locations near the boundaries.

7.4 Land Use and Land Cover

The surface is the lower boundary of the computational domain. The two key processes there are dry deposition and surface-specific emissions (e.g., wind-blown dust or sea salt). Depending on the model at hand, a description of these processes can require input varying from a simple land-sea mask up to a comprehensive set of land-cover characteristics, type and state of vegetation, water temperature and salinity, etc. In most cases, the corresponding maps are included in the model package but if the application is specific, such maps may need to be specific too. Then, one of the important issues is the compatibility of the external land-cover classification and the model internal surface typology. It is therefore recommended to use global datasets, which provide homogeneous classification across the continents and time periods.

Sources of the land-cover information may vary but it is important to keep in mind that utilization of very specific local datasets can make the computations non-reproducible and prevent the expansion of the work to other areas. Currently available global datasets practically do not compromise between the coverage and resolution: Landsat products have ~30m resolution (<https://www.usgs.gov/>). The project spans from the 1970s to the present day, albeit with different sets of products available for different times. A more detailed land-use dataset with 100 land-use categories is available from the Global Land Cover Characteristics (<https://lta.cr.usgs.gov/>). The dataset has 1 km spatial resolution and refers to 1992-1993.

Specific and much more detailed (depending on the model resolution) information about land cover, land use and urban morphology is needed for urban weather and air pollution modeling. See more about this in Section 5.6.

A specific class of the land-cover information refers to urban areas, which are particularly important for urban climate and air quality applications. An Initiative of the International Association for Urban Climate (IAUC), the World Urban Database (WUDAPT), is an international community-based borderless system generated by and for the urban community (www.wudapt.org). A detailed description of WUDAPT is provided in Section 5.6, here a brief outline is provided.

The WUDAPT database and portal are designed to support intraurban climate assessments, surface energy budget, and meso- to urban weather, chemical weather and AQ forecasting applications. Its scope encompasses urban areas around the world. For modeling purposes, it focuses on generating urban canopy data suitable for running “fit-for-purpose” urban scale science-based meso to urban scale meteorological forecast, climate, and AQ models. The data available in WUDAPT start from level 0 built on the Local Climate Zone (LCZ) concept (Stewart and Oke, 2012). Higher levels of integration (levels 1 and 2) aim at the generation of specific values of urban canopy parameterization (UCP) for each LCZ. At Level 2, generalized georeferenced rasterized UCPs are generated.

7.5 Other Model Input Files

Apart from the above-mentioned major input datasets, CTMs also require auxiliary data, which are usually problem-specific. Some examples are shown below.

The diurnal variation of anthropogenic emission rates raises the question of an adequate determination of the anthropogenic activity and its timing. Models always run using some universal standard time definition: Coordinated Universal Time UTC, Greenwich Mean Time GMT, Pacific Standard Time PST, etc. However, at regional and, especially, global scales, this has to be accompanied with the astronomical local time (needed for solar radiation calculations) and the “conventional” local time, i.e. the one that is introduced by the local authorities. The latter time is characterized as a time zone and usually just states the difference in hours from one of the universal times. This very time defines the anthropogenic activities and, consequently, controls the anthropogenic emission rates.

There exists a global list of all time zones used worldwide – and also the exhaustive list of all differences ever applied in these time zones (<http://www.timeanddate.com>). For long simulations, changes in daylight saving time have to be accounted for, as well as the changes in the time zone features, their appearance and disappearance depending on the decisions of the time-setting authorities. Corresponding functionality is available from operational systems.

Many AQ problems include tasks of evaluation of the population exposure to air pollutants, which requires availability of population density maps valid during the computed period. Global country-level maps can be obtained from, for instance, the World Bank (<http://databank.worldbank.org>). Population maps with high spatial resolution covering the period 1975-c.m. are available from <http://ghsl.jrc.ec.europa.eu> and other sources.

7.6 Summary

- Atmospheric composition and air quality forecasting based on chemistry transport models involve several types of input data, and their quality and completeness largely decides the success of the exercise.
- The most important datasets are:
 - Emission inventories and emission models describing the release of pollutants into the atmosphere from anthropogenic and natural sources
 - For offline models, meteorological information from numerical weather prediction models
 - Initial conditions for the model to start from
 - For regional applications, boundary conditions to accurately describe the inflow of pollutants into the computation domain
 - A variety of auxiliary input datasets: land use, vegetation type and state, urbanized areas' characteristics, population density, etc.

References

- Borge, R., J. López, J. Lumbreras, A. Narros, and E. Rodríguez, 2010: Influence of boundary conditions on CMAQ simulations over the Iberian Peninsula. *Atmospheric Environment*, 44, 2681-2695.
- Curci, G., 2012. On the Impact of Time-Resolved Boundary Conditions on the Simulation of Surface Ozone and PM10 In: Khare, M. (Ed.), *Air Pollution: Monitoring, Modeling and Health IntechOpen*, Rijeka. DOI:10.5772/33703
- EMEP EEA Air Pollutant Emission Inventory Guidebook. (2016). <http://www.eea.europa.eu/publications/emep-eea-emission-inventory-guidebook-2009>
- Gong, W. et al., 2006. Cloud processing of gases and aerosols in a regional air quality model (AURAMS). *Atmospheric Research*, 82(1): 248-275. DOI: <https://doi.org/10.1016/j.atmosres.2005.10.012>
- Granier C. et al., 2011. Evolution of anthropogenic and biomass burning emissions of air pollutants at global and regional scales during the 1980–2010 period. *Climatic Change*, 109:163–190 DOI 10.1007/s10584-011-0154-1.
- Kuenen et al., *Atmos. Chem. Phys.*, 14, 10963–10976, 2014, doi:10.5194/acp-14-10963-2014
- Lin, M., Holloway, T., Carmichael, G.R., Fiore, A.M., 2010. Quantifying pollution inflow and outflow over East Asia in spring with regional and global models. *Atmos. Chem. Phys.*, 10(9): 4221-4239. DOI:10.5194/acp-10-4221-2010.
- Liu, T.-H., Jeng, F.-T., Huang, H.-C., Berge, E., Chang, J.S., 2001. Influences of initial conditions and boundary conditions on regional and urban scale Eulerian air quality transport model simulations. *Chemosphere - Global Change Science*, 3(2): 175-183. DOI: [https://doi.org/10.1016/S1465-9972\(00\)00048-9](https://doi.org/10.1016/S1465-9972(00)00048-9)
- MEGAPOLI, 2011: Megacities: Emissions, urban, regional and Global Atmospheric POLLution and climate effects, and Integrated tools for assessment and mitigation. Final project report. Coordinator A. Baklanov, Danish Meteorological Institute. Deliverable 9.6, MEGAPOLI Final Report Part 1, 43p., http://megapoli.dmi.dk/publ/MEGAPOLI_FinalReport_Part1.pdf
- MEGAPOLI, 2010: A Base Year (2005) MEGAPOLI European Gridded Emission Inventory (Final Version). Kuenen J., H. Denier van der Gon, A. Visschedijk, H. van der Brugh, S. Finardi, P. Radice, A. d'Allura, S. Beevers, J. Theloke, M. Uzbisich, C. Honoré, O. Perrussel. Deliverable D1.6, MEGAPOLI Scientific Report 10-17, MEGAPOLI-20-REP-2010-10, 39p., http://megapoli.dmi.dk/publ/MEGAPOLI_sr10-17.pdf
- Pendlebury, D., Gravel, S., Moran, M.D., Lupu, A., 2018. Impact of chemical lateral boundary conditions in a regional air quality forecast model on surface ozone predictions during stratospheric intrusions. *Atmospheric Environment*, 174: 148-170. DOI: <https://doi.org/10.1016/j.atmosenv.2017.10.052>
- Pfister, G.G. et al., 2011. Characterizing summertime chemical boundary conditions for airmasses entering the US West Coast. *Atmos. Chem. Phys.*, 11(4): 1769-1790. DOI:10.5194/acp-11-1769-2011
- Pierce, R.B. et al., 2003. Regional Air Quality Modeling System (RAQMS) predictions of the tropospheric ozone budget over east Asia. *Journal of Geophysical Research: Atmospheres*, 108(D21). DOI:10.1029/2002JD003176
- Ritter, M., Müller, M.D., Jorba, O., Parlow, E., Liu, L.J.S., 2013. Impact of chemical and meteorological boundary and initial conditions on air quality modeling: WRF-Chem sensitivity evaluation for a European domain. *Meteorology and Atmospheric Physics*, 119(1): 59-70. DOI:10.1007/s00703-012-0222-8

- Samaali, M. et al., 2009. On the influence of chemical initial and boundary conditions on annual regional air quality model simulations for North America. *Atmospheric Environment*, 43(32): 4873-4885. DOI: <https://doi.org/10.1016/j.atmosenv.2009.07.019>
- Seinfeld, J.H., Pandis, S.N., 1998. *Atmospheric chemistry and physics: from air pollution to climate change*. John Wiley & Sons, 1326 pp.
- Shim, C. et al., 2009. Satellite observations of Mexico City pollution outflow from the Tropospheric Emissions Spectrometer (TES). *Atmospheric Environment*, 43(8): 1540-1547. DOI: <https://doi.org/10.1016/j.atmosenv.2008.11.026>
- Sofiev, M., Vira, J., Kouznetsov, R., Prank, M., Soares, J., Genikhovich, E. (2015) Construction of the SILAM Eulerian atmospheric dispersion model based on the advection algorithm of Michael Galperin, *Geosci. Model Developm.* 8, 3497-3522, doi: [10.5194/gmd-8-3497-2015](https://doi.org/10.5194/gmd-8-3497-2015)
- Stewart, I, T. Oke, 2012: Local Climate Zones for Urban Temperature Studies, *Bull. Amer. Meteor. Soc.* doi: <http://dx.doi.org/10.1175/BAMS-D-11-00019>.
- Stohl, A., Aamaas, B., Amann, M., Baker, L. H., Bellouin, N., Bernsten, T. K., Boucher, O., Cherian, R., Collins, W., Daskalakis, N., Dusinska, M., Eckhardt, S., Fuglestvedt, J. S., Harju, M., Heyes, C., Hodnebrog, Ø., Hao, J., Im, U., Kanakidou, M., Klimont, Z., Kupiainen, K., Law, K. S., Lund, M. T., Maas, R., MacIntosh, C. R., Myhre, G., Myriokefalitakis, S., Olivie, D., Quaas, J., Quennehen, B., Raut, J.-C., Rumbold, S. T., Samset, B. H., Schulz, M., Seland, Ø., Shine, K. P., Skeie, R. B., Wang, S., Yttri, K. E., and Zhu, T.: Evaluating the climate and air quality impacts of short-lived pollutants, *Atmos. Chem. Phys.*, 15, 10529-10566, <https://doi.org/10.5194/acp-15-10529-2015>, 2015.
- Tang, Y. et al., 2007. Influence of lateral and top boundary conditions on regional air quality prediction: A multiscale study coupling regional and global chemical transport models. *Journal of Geophysical Research: Atmospheres*, 112(D10). DOI: [10.1029/2006JD007515](https://doi.org/10.1029/2006JD007515)
- Tang, Y. et al., 2009. The impact of chemical lateral boundary conditions on CMAQ predictions of tropospheric ozone over the continental United States. *Environmental Fluid Mechanics*, 9(1): 43-58. DOI: [10.1007/s10652-008-9092-5](https://doi.org/10.1007/s10652-008-9092-5)
- Travis, K. R., Jacob, D. J., Fisher, J. A., Kim, P. S., Marais, E. A., Zhu, L., Yu, K., Miller, C. C., Yantosca, R. M., Sulprizio, M. P., Thompson, A. M., Wennberg, P. O., Crouse, J. D., St. Clair, J. M., Cohen, R. C., Laughner, J. L., Dibb, J. E., Hall, S. R., Ullmann, K., Wolfe, G. M., Pollack, I. B., Peischl, J., Neuman, J. A., and Zhou, X.: Why do models overestimate surface ozone in the Southeast United States?, *Atmos. Chem. Phys.*, 16, 13561-13577, <https://doi.org/10.5194/acp-16-13561-2016>, 2016.
- Žabkar, R., Koračin, D., Rakovec, J., 2013. A WRF/Chem sensitivity study using ensemble modeling for a high ozone episode in Slovenia and the Northern Adriatic area. *Atmospheric Environment*, 77: 990-1004. doi: <https://doi.org/10.1016/j.atmosenv.2013.05.065>

Chapter 8. Model Output and Data Management

8.1 Introduction

Model output and data management are an integral part of a chemical weather-air quality forecasting (CW-AQF) model system. Ideally, all relevant model fields such as constituent concentrations and meteorological conditions are archived at native model resolution and at the highest available time interval. These fields may then be further aggregated in space and/or time to fulfil end user needs. For example, important metrics in the context of air quality are daily maximum 8-hour average ozone (MDA8, Rieder et al., 2013), aerosol optical depth (AOD), or visibility, and it is advisable for an air quality forecasting system to provide these metrics directly instead of requiring end users to compute them individually.

In practice, the amount of model output that can be archived is dictated by soft- and hardware limitations, most importantly the amount of available disk space. The challenge for every air quality model archiving strategy is thus to find the right balance between completeness and practicality. The overarching goal should always be to provide as much information as possible to guide interpretation of the observed model features. For example, model output showing a high pollution event is much more valuable if it comes with information on what causes it, e.g., emission fields, boundary layer heights, etc.

In this chapter, important topics on the model outputs and the needs and purposes for data management are described. These include a model output along with its main characteristics such as major types, horizontal and vertical resolution, frequency, mode, and variables (Section 8.2) and data management including data format and access tools (Section 8.3). Finally, Section 8.4 summarizes key points.

8.2 Model Output

Output provided by a CW-AQF model can be broadly grouped into four categories: constituent concentrations, meteorological conditions, process diagnostics, and customized products. Individual features of these categories are discussed below. For any output diagnostics, a data archiving strategy must take into consideration a number of factors, such as horizontal and vertical resolution of the output fields, output frequency, and output mode.

8.2.1 *Horizontal and Vertical Resolution of Model Output*

The resolution of the model output is dictated by the resolution of the model. It is good practice to provide output on a rectilinear (lat-lon) grid at a resolution as close as possible to the native model grid. Model output should only be remapped onto a (much) coarser grid if it can be demonstrated that there is no significant loss of information. Using the highest possible horizontal resolution is particularly important for air pollutants with strong spatial gradients, such as NO₂.

Similar considerations apply to the vertical resolution. For air quality applications, it can be sufficient to output only the lowest model level. However, if possible it is recommended to archive the entire 3-dimensional field - or at least to capture the vertical structure up to the tropopause. This enables an analysis of physical processes that impact atmospheric chemistry, such as boundary layer dynamics and long-range transport of smoke plumes (e.g., Liang et al., 2007; Weiss-Panzias et al., 2004).

8.2.2 *Output Frequency and Output Mode*

Model fields should be archived at a frequency that is sufficient to capture the variability of the variables of interest. For example, surface concentrations of air pollutants can exhibit very strong diurnal cycles (e.g., Nieuwenhuijsen et al., 2015; Schneider et al., 2017) and it is thus critical to provide these quantities at an hourly temporal resolution. This is further critical for air quality applications that focus on afternoon concentrations (e.g., Fiore et al., 2003). For

chemically less reactive species and/or at higher altitudes, longer time-averages up to 24 hours are sufficient.

The output mode is tightly linked to the output frequency. For most applications, archiving the time-averaged quantity is the most sensible solution. Time-averaged values should always be used for diagnostics that are typically compared against annual totals, e.g., emission fluxes. For diagnostics that are archived at time intervals of one hour or less, outputting the instantaneous fields (model snapshot) can offer an additional level of detail. This is particularly the case for variables with large temporal variability that use air quality metrics based on minimum/maximum concentrations, such as NO_x. Directly outputting the minimum or maximum value is only recommended for specialty diagnostics.

8.2.3 *Chemical Constituents*

It goes without saying that for CW-AQFs, the most important model outputs are the concentration fields of the chemical constituents. Given the large number of chemical species typically present in an atmospheric chemistry model (often more than 200 species), it is unfeasible to output all model species and priority should thus be given to regulatory species (e.g., PM_{2.5}, O₃, NO₂, CO, SO₂). An effective tool to combine multiple species into a single model output is lumped species diagnostics, e.g., NO_y and total organic carbon. Especially for hydrocarbons, providing total carbon instead of individual species concentrations facilitates model inter-comparisons as it offers a diagnostic that is independent of the species classification scheme (e.g., Emmons et al., 2015).

Chemical constituents are typically output in units of volume mixing ratio (mol/mol) or mass mixing ratio (kg/kg). It is good practice to use dry air mixing ratios. For PM_{2.5}, it is also common to provide concentrations in units of kg/m³. In any case, the meteorological variables required to perform unit conversions should be provided alongside the chemical species.

8.2.4 *Meteorological Variables*

Information about the meteorological state of the atmosphere is critical to put the chemical concentrations into context, for local source apportionment analysis, and to convert output units. At a minimum, the model temperature, (relative and/or specific) humidity, pressure, and wind speed (u and v direction) should be provided. Other meteorological variables relevant for atmospheric chemistry and air quality include precipitation, cloud cover, radiation, thermal stability (e.g., buoyancy), and boundary layer height. For coupled chemistry-meteorology models, many more variables (all of them can be available on each time step) can be considered as output for the chemistry part of the modeling system.

8.2.5 *Process Diagnostics*

The most common process diagnostics are flux diagnostics such as emission, dry and wet deposition fluxes. Other process diagnostics include fields related to chemical processes, such as reaction and photolysis rates or chemical production and loss rates. These diagnostics can greatly facilitate the interpretation of species concentrations, and often help explain the differences among models and/or compared to observations (e.g., Zhang et al., 2012). Unfortunately, they are less commonly provided and their definitions tend to vary substantially from one model to another.

8.2.6 *Customized Diagnostics*

Customized diagnostics encompass model outputs specifically tailored towards air quality applications. These include exposure metrics, source-receptor relationships, and information on particle speciation.

Some of the most commonly used air quality metrics such as MDA8, sum of means over 35 ppbv (SOMO35), accumulated ozone exposure over 40 ppbv (AOT40), or sum of all hourly

average concentrations at or above 60 ppbv (SUM60) require long integration windows or rolling averages (Avnery et al., 2011; Rieder et al., 2013; Shen et al., 2016; Carter et al., 2017), and are more easily computed at a post-processing stage. A frequently-used metric for human health applications is the Air Quality Health Index (AQHI). The AQHI pays particular attention to people who are sensitive to air pollution, providing a number from 1 to 10+ to indicate the level of health risk associated with local air quality. Numerous definitions of the AQHI (e.g., Eder et al., 2010) exist, which makes it particularly important for AQHI outputs to come with proper documentation.

Providing detailed information on the composition of particulate matter and/or the origin of air pollutants through tagged species (e.g., black carbon from forest fires, NO_x from traffic sources) can offer some of the most useful information for scientists and policymakers (e.g., Pfister, 2004; Duncan 2007). However, such information can be difficult to derive from the model without adding significant complexity and computational cost (especially for tagged species diagnostics).

8.3 Data Management and Access Tools

The means by which end users can access model output greatly determines the usefulness of an air quality forecast. The easiest solution is to show selected model output online in the form of visualizations, most importantly surface concentration maps of air pollutants such as ozone and PM_{2.5}. Such visualizations are already openly available, e.g., from the Copernicus Atmosphere Monitoring Service (CAMS) or the NASA Global Modeling and Assimilation Office (GMAO) (Figure 8.1).

While useful for a large group of users, concentration maps do not provide enough information for sophisticated applications, i.e., to study the link between air quality and human health or for a detailed analysis of air quality at a target location. It is thus good practice to also make available the actual model output. This can be done by providing download tools for the full (3-dimensional) output files or through an Application Programming Interface (API) that allows the user to pre-select values of interest. One of the key challenges for every data access platform is to be powerful enough to give quick access to large amounts of data while also being simple enough to be suitable for end users with limited technical resources.

8.3.1 Data Format

Given the high density of air quality model outputs, data needs to be saved in file formats that are able to handle geospatial information very efficiently. The most commonly used data formats are the Network Common Data Form (netCDF), Hierarchical Data Format 5 (HDF5), and GRIBbed Binary or General Regularly-distributed Information in Binary form (GRIB, GRIB2). These formats are well established in the scientific community and supported by standard data analysis software languages, such as IDL, MATLAB, Python, or R. However, netCDF is not commonly used outside of the atmospheric community. To broaden the reach of air quality model outputs, it is thus advisable to also provide selected model outputs in more commonly used data formats such as comma separated values (csv) or text format (txt). Since these formats are much less efficient in dealing with large data volumes, they should only be used to provide the most relevant information, e.g., surface concentrations of selected species.

8.3.2 Meta data

A detailed description of the model output should be included in every data file (meta data). At the very least this should include information on location (lon/lat/altitude), time (in Coordinated Universal Time (UTC)), and units corresponding to the values stored on file.

8.3.3 Data Access

Ideally, the web interface that offers users access to air quality model output is designed such that it supports both high-performance users as well as end users with limited technical resources. The requirements for these two user groups are very different: high-end users are interested in using scripting protocols to access large swaths of model output, while others wish to work with just small batches of model information.

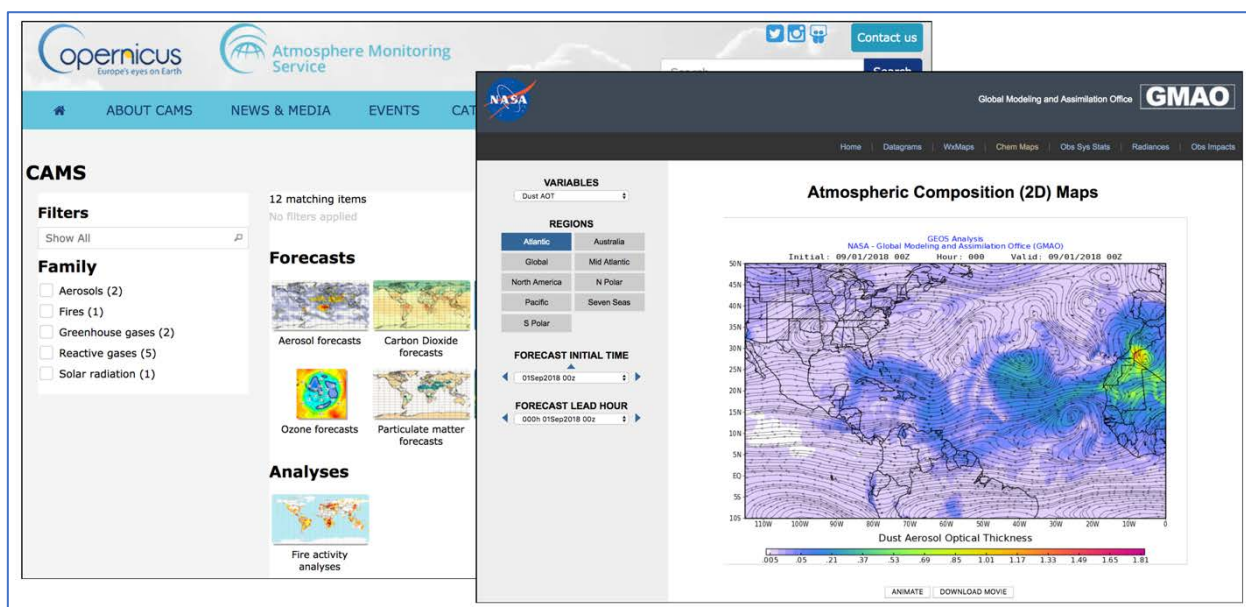


Figure 8.1. Global air quality model forecasts are available online from a variety of sources, such as the Copernicus Atmosphere Monitoring Service (CAMS, <https://atmosphere.copernicus.eu/charts/cams/>) or the NASA Global Modeling and Assimilation Office (GMAO, <https://fluid.nccs.nasa.gov/wxmaps/chem2d/>).

The easiest solution is to provide access to the native model output files (i.e., in netCDF format) via standard transfer protocols such as File Transfer Protocol (FTP) or Hypertext Transfer Protocol (HTTPs), and to expect the users to store the files locally and perform analysis on those files with their software of choice. This is often the preferred method for sophisticated end users that are interested in a comprehensive analysis of the entire model output. However, this approach requires a high level of programming knowledge and is not suitable for the common user. It is also very inefficient if users are interested in only small subsamples of the model output (i.e., concentrations at just one particular location) or output averaged over long time periods, which requires downloading an excessive amount of data only to extract comparatively little information from it. Especially as file sizes grow due to improved model resolution, downloading the full files can become a significant restriction. In recent years, there has thus been a trend towards data access strategies that offer the ability to perform data selection and/or analysis remotely (i.e., without having to download the complete files onto a local computer) and to then retrieve these pre-processed data values for further analysis. This trend is exacerbated by an increased switch to cloud-based storage solutions, which often offer embedded data analytics options.

For users that are interested in quick visualizations of model output and/or need to access just small amounts of information (e.g., forecast at a given location), Application Programming Interfaces (API) offer an interesting alternative that are now increasingly provided along with the raw model output. API's are easy-to-use web interfaces designed to facilitate the selection of user-specified model output that can either be visualized online or saved in ubiquitously used data formats such as text file (txt), comma separated values (csv), or Microsoft Excel

(xls). While API's are not yet very common, they have the potential to make air quality model outputs available to a much broader user community.

8.4 Summary

- Model output can be broadly categorized into four categories: constituent concentrations, meteorological conditions, process diagnostics, customized end-user products.
- Concentrations of regulatory air pollutants are the most important model outputs. They should be made available at the highest possible temporal and spatial resolution.
- Detailed information on modeled meteorological conditions and chemical processes are less commonly provided, but are critical for an in-depth analysis of air quality.
- Most models make their results accessible via online visualizations and netCDF data files. More efficient ways to access selected data need to be explored in order to broaden the use of air quality forecasts.

References

- Avnery, S., Denise L. Mauzerall, D. L., Liu, J., Horowitz, L.W. (2011), Global crop yield reductions due to surface ozone exposure: 2. Year 2030 potential crop production losses and economic damage under two scenarios of O₃ pollution, *Atmospheric Environment*, Volume 45, Issue 13, 2011, Pages 2297-2309, <https://doi.org/10.1016/j.atmosenv.2011.01.002>.
- Carter, C. A., Cui, X., Ding, A., Ghanem, D., Jiang, F., Yi, F., Zhong, F. (2017), Stage-specific, Nonlinear Surface Ozone Damage to Rice Production in China. *Sci. Rep.* 7, 44224; doi: 10.1038/srep44224.
- Duncan, B. N., Logan, J. A., Bey, I., Megretskaia, I. A., Yantosca, R. M., Novelli, P. C., Jones, N. B., and Rinsland, C. P. (2007), Global budget of CO, 1988–1997: Source estimates and validation with a global model, *J. Geophys. Res.*, 112, D22301, doi: 10.1029/2007JD008459.
- Eder, B., D. Kang, S.T. Rao, R. Mathur, S. Yu, T. Otte, K. Schere, R. Wayland, S. Jackson, P. Davidson, J. McQueen, and G. Bridgers (2010), Using national air quality forecast guidance to develop local air quality index forecasts. *Bull. Am. Meteorol. Soc.* 91:313–26. doi:10.1175/2009BA MS2734.1.
- Emmons, L. K., Arnold, S. R., Monks, S. A., Huijnen, V., Tilmes, S., Law, K. S., Thomas, J. L., Raut, J.-C., Bouarar, I., Turquety, S., Long, Y., Duncan, B., Steenrod, S., Strode, S., Flemming, J., Mao, J., Langner, J., Thompson, A. M., Tarasick, D., Apel, E. C., Blake, D. R., Cohen, R. C., Dibb, J., Diskin, G. S., Fried, A., Hall, S. R., Huey, L. G., Weinheimer, A. J., Wisthaler, A., Mikoviny, T., Nowak, J., Peischl, J., Roberts, J. M., Ryerson, T., Warneke, C., and Helmig, D. (2015), The POLARCAT Model Intercomparison Project (POLMIP): overview and evaluation with observations, *Atmos. Chem. Phys.*, 15, 6721-6744, <https://doi.org/10.5194/acp-15-6721-2015>.
- Fiore, A., D. J. Jacob, H. Liu, R. M. Yantosca, T. D. Fairlie, and Q. Li (2003), Variability in surface ozone background over the United States: Implications for air quality policy, *J. Geophys. Res.*, 108, 4787, doi:10.1029/2003JD003855, D24.
- Liang, Q., L. Jaeglé, et al. (2007), Summertime influence of Asian pollution in the free troposphere over North America, *J. Geophys. Res.*, doi:10.1029/2006JD007919, 112, D12S11, doi:10.1029/2006JD007919.
- Nieuwenhuijsen, M.J., Donaire-González, D., Rivas, I., de Castro, M., Cirach, M., Hoek, G., Seto, E., Jerrett, M., Sunyer, J.J., 2015. Variability in and agreement between modeled and personal continuously measured black carbon levels using novel smartphone and sensor technologies. *Environ. Sci. Technol.* 49, 2977–2982.

<http://dx.doi.org/10.1021/es505362x>.

- Rieder, H.E., A M Fiore, L M Polvani, J-F Lamarque, and Y Fang (2013), Changes in the frequency and return level of high ozone pollution events over the eastern United States following emission controls. *Environmental Research Letters*, Vol 8, Number 1.
- Pfister, G., G. Pétron, L. K. Emmons, J. C. Gille, D. P. Edwards, J.-F. Lamarque, J.-L. Attie, C. Granier, and P. C. Novelli (2004), Evaluation of CO simulations and the analysis of the CO budget for Europe, *J. Geophys. Res.*, 109, D19304, doi: [10.1029/2004JD004691](https://doi.org/10.1029/2004JD004691).
- Shen, L., L. J. Mickley, and E. Gilleland (2016), Impact of increasing heat waves on U.S. ozone episodes in the 2050s: Results from a multimodel analysis using extreme value theory, *Geophys. Res. Lett.*, 43, 4017–4025, doi: [10.1002/2016GL068432](https://doi.org/10.1002/2016GL068432).
- Schneider, P., Castell, N., Vogt, M., Dauge, F. R., Lahoz, W.A., Bartonova, A. (2017), Mapping urban air quality in near real-time using observations from low-cost sensors and model information, *Environmental International*, 106, 234-247.
- Weiss-Penzias, P., D. Jaffe, A. McClintick, L. Jaeglé, and Q. Liang (2004), The influence of long-range transported pollution on the annual and diurnal cycles of carbon monoxide and ozone at Cheeka Peak Observatory, *J. Geophys. Res.*, 109(D23), D23S14, doi: [10.1029/2004JD004505](https://doi.org/10.1029/2004JD004505).
- Zhang, L., D.J. Jacob, E.M. Knipping, N. Kumar, J.W. Munger, C.C. Carouge, A. van Donkelaar, Y. Wang, and D. Chen (2012), Nitrogen deposition to the United States: distribution, sources, and processes, *Atmos. Chem. Phys.*, 12, 4,539-4,4554.

Chapter 9. Model Evaluation

9.1 Introduction

The evaluation of chemical weather air quality (CW-AQ) numerical models is in some ways as much an art as it is a science. This is because many methods/protocols are available for evaluating CW-AQ models, and the interpretation of the results of these methods is dependent on many factors, including but not limited to the nature of the model application (e.g., forecasting, model development, rule-making), the CW-AQ network being used and so on. As such, few absolute targets exist for CW-AQ numerical model performance, and what targets do exist are frequently associated with CW-AQ model performance as it applies to AQ regulation development and/or demonstration of the attainment of AQ regulations. Understanding of the availability of observational data is the first step of the model evaluation. Such data come from routine surface networks, special field campaigns, satellites, and aircraft. The second step is to understand the model output variables and establish the evaluation protocols and criteria for targeted variables. The third step is to select methods of model evaluation, which include conventional methods such as the discrete and categorical evaluation of the CW-AQ forecast products and more advanced spatio-temporal evaluation. Whenever possible, using existing model evaluation tools and software can greatly facilitate the evaluation.

In this chapter, all important aspects of model evaluation and the observational data used in model evaluation are described in detail. Topics include available observational datasets (Section 9.2), evaluation protocols and criteria for targeted performance (Section 9.3), measures of forecast quality (Section 9.4), advanced spatio-temporal evaluation (Section 9.5), and model evaluation tools and software (Section 9.6). Finally, Section 9.7 summarizes the key points.

9.2 Observational Dataset

9.2.1 Background of CW-AQ Observations

CW-AQ observational data consist of a wide range of observations, including surface-based observations, vertical profiles (e.g., sondes), surface-based vertical measurements (e.g., LIDAR), aircraft-based measurements and satellite observations. The temporal availability of these measurements varies considerably, with some measurements being made at hourly or sub-hourly intervals, while other measurements are made at weekly or even longer intervals. Likewise, the spatial density of measurements also varies widely, ranging from some surface-based networks consisting of over 1 000 sites across a country (e.g., United States AQS network) to some networks with only a handful of sites across the globe. Furthermore, the representativeness of the observations also varies depending on the source of the data, with some observations representative of many 10s or 100s of square kilometers (e.g., some satellite measurements), while other measurements are representative of only a small area (typical of urban-based measurements). In contrast to meteorological observations designed to capture large, representative areas, air quality observations are often designed to capture times and areas of increased pollutant concentrations, although some air quality measurements are specifically cited to capture background pollutant concentrations.

The Global Atmosphere Watch (GAW) Programme of WMO focuses on building a single coordinated global understanding of atmospheric composition and its change. It coordinates high-quality atmospheric composition observations across global to local scales to drive high-quality and impact science while co-producing a new generation of research enabled products and services. About 100 countries are participating in the GAW Programme. Currently GAW coordinates observation activities and data from 31 Global stations, more than 400 Regional stations, and around 100 Contributing stations operated by Contributing networks (see: https://library.wmo.int/doc_num.php?explnum_id=7938 and GAW SIS: <https://gawsis.meteoswiss.ch/GAW SIS/#/>).

In addition to variations in the temporal and spatial coverage of CW-AQ observational data, the types of measurements made across the various networks also differ, with some networks focused primarily on measuring the concentration of atmospheric gases, while others focus on measuring particles, and still others focus on measurement deposition. Examples of routine gas measurements include O_3 , NO , NO_2 , CO and SO_2 . Particle measurements include particulate SO_4^{2-} , NO_3^- and NH_4^+ , EC , OC , total fine particulate matter ($PM_{2.5}$) and total particulate matter (PM_{10}). Examples of deposition species include the wet and dry deposition of SO_4^{2-} , NO_3^- and NH_4^+ , Cl^- , Na^+ , and O_3 . Measurements of gases are typically made by mass or volume and are reported in units of parts per million/billion or micrograms per cubic meter, although the exact units reported can vary depending on species. Particle measurements are often reported in either unit of per volume or by mass, depending on the observational network. Likewise, the units of deposition measurements also vary by network, with the most typical units being concentration per volume or mass per area. A variety of other CW-AQ measurements are available (e.g., deposition flux), however, they tend to be much less common than those described above.

Most, if not all, of these species are standard outputs from numerical air quality models and therefore represent critical elements in the evaluation of these models. The availability of CW-AQ observations varies based on network and species measured, with gas species generally being the most readily available measurement, with some networks providing these measurements in near-real time (e.g., AirNow; <https://airnow.gov/>). Some measurements of total particulate mass are also available in near-real time, however the majority of total particulate mass measurements and nearly all speciated mass measurements are filter-based and therefore must undergo significant processing before measurement data are available. While this inhibits the near-real time evaluation of numerical models for speciated PM components, these measurements are nonetheless vital for a retrospective evaluation of these models.

9.2.2 Summary of Available Observational Data

Table 9.1 summarizes available observational data from routine surface-level network primarily in North America and Europe.

9.2.3 Representativeness of CW-AQ Observations

Because of their different character air quality observations are often classified according to air quality regimes such as rural, urban, traffic, or mountain. The classification shall help to give information about the strength of and distance to emissions that influence the site. The AQ regime classification is often provided by the network operator and is based on expert judgement. Alternatively, different automated methods have been suggested to classify the AQ sites. The methods are mainly based on the specifics of the observations such as the mean value or the strength of the diurnal cycle (Flemming et al., 2005). More complex automated methods consider the land use or even use backward-trajectory calculation (Henne et al., 2010).

One very important consideration when using in-situ observations to evaluate numerical models is the representativeness of the observations compared to that of the model. It is therefore commonly assumed that stations of the rural or sub-urban type have a larger spatial representativeness than stations of the traffic regime. Numerical model values are representative of the entire grid cell, which can vary in size from relatively fine-scale (e.g., 1 km × 1 km) to very coarse hemispheric/global scales up to 100 or more kilometers. For the more common regional-scale CW-AQ applications, horizontal grid sizes typically range from roughly 10-40 square kilometers. Just as the representativeness of the model, values can differ depending on the application, so to do the CW-AQ observations, with very urban-based observations representative of only a very small area (often less than square kilometer) to very rural/remote observations which can be representative of larger background values. In addition to the spatial variability of the observations, the temporal variable is also an important consideration when comparing model values. Typically, observations with high temporal

frequency (one hour or smaller) will not compare as well to the model values as longer-duration observations (e.g., daily or weekly). This is due in part to the inherent nature of numerical models being representative of the average conditions, and they will typically struggle to capture the potentially extreme fluctuations that can occur from hour to hour.

Table 9.1 Example routine surface-level observation data available

Network	Full Name	Spatial Coverage	Species Measured	Temporal Frequency	Data Availability	Website
GAW	Global Atmosphere Watch	Global	Gas, Aerosol, Met	Hourly	1989-present	https://public.wmo.int/en/programmes/global-atmosphere-watch-programme https://community.wmo.int/activity-areas/gaw
AQS	Air Quality System	Entire U.S. (primarily urban)	Gas, Aerosol, Met	Hourly, Daily	Pre-1980 to present	https://aq5.epa.gov/aqsweb/airdata/download_files.html
AirNow	AirNow	Entire U.S.	Gas, Aerosol	Hourly, Daily	N/A	https://www.airnow.gov/
CSN	Chemical Speciation Network	Entire U.S.	Aerosol	Daily (1,3,6 days)	1990-present	https://www3.epa.gov/ttnamti1/speciepg.html
IMPROVE	Interagency Monitoring of Protected Environments	Entire U.S. (primarily rural)	Aerosol, Extinction	Daily (1,3,6 days)	1985-present	http://vista.cira.colostate.edu/Improve/
CASTNET	Clean Air Status and Trends Network	Entire U.S. (Eastern U.S. centric)	Gas, Aerosol, Dry Deposition	Hourly, Weekly	1987-present	https://www.epa.gov/castnet
NTN	National Trends Network	Entire U.S.	Wet Deposition, Met	Weekly	1978-present	http://nadp.slh.wisc.edu/ntn/
AMON	Ammonia Monitoring Network	Contiguous U.S.	Ammonia Wet Deposition	Weekly	2010-present	http://nadp.slh.wisc.edu/AMoN/
AERONET	Aerosol Network	Global	Aerosol Optical Depth	Hourly	1994-present	https://aeronet.gsfc.nasa.gov/
FLUXNET	FLUXNET	Global	Various Fluxes	Hourly		https://daac.ornl.gov/cgi-bin/dataset_lister.pl?p=9
SEARCH	Southeastern Aerosol Research and Characterization	Southeastern U.S.	Gas, Aerosol, Met	Hourly (some 5-minute), Daily	1992-2016	https://my.usgs.gov/gcmp/program/show/943855

Network	Full Name	Spatial Coverage	Species Measured	Temporal Frequency	Data Availability	Website
NAPS	National Air Pollution Surveillance	Entire Canada	Gas, Aerosol	Hourly, Daily	1974-present	https://open.canada.ca/data/en/dataset/1b36a356-defd-4813-acea-47bc3abd859b
EMEP	European Monitoring and Evaluation Programme	Across Europe	Gas, Aerosol	Hourly, Daily	Pre-1990 to present	http://www.emep.int/
AirBase		Across Europe	Gas, Aerosol, Met	Hourly, Daily		https://www.eea.europa.eu/data-and-maps/data/aqereporting-2

Similar to the issues of representativeness of in-situ observations compared to numerical model output, remote observations (e.g., satellite data) also have inherent representativeness that must be considered when comparing them to numerical model values. Satellite observations can be representative of a wide range of spatial and temporal conditions, typically ranging from 10-100 kilometers in spatial resolution. Current satellite instruments for composition monitoring are carried by polar-orbiting satellites, which allow observations only at a specific time of the day, which may not coincide with the daily pollution maximum. It is also important to consider the nature of the satellite observation when comparing to CW-AQ model values, as satellite observations have a very limited vertical resolution, and often employ their own retrieval algorithms to obtain final data values from the satellite measurements, and therefore the satellite data themselves represent modeled values as well. It is important to weigh these factors when evaluating CW-AQ models against satellite measurements.

9.2.4 *Obtaining Observational Data*

Obtaining historical and/or near-real time CW-AQ observational data can be accomplished in several ways. Table 9.1 includes a link to the observational network website (where available), which typically explains how to obtain archived data from the network. Some networks provide directly downloadable zip archives containing historic data, while other networks provide an interactive query system for obtaining data. In most instances these data are provided as delimited (typically comma delimited) ASCII files.

In addition to obtaining the network observational data directly from each network website, some sources provide access to data from multiple networks. One example of this type of site is the Federal Land Manager Environmental Database (<http://views.cira.colostate.edu/fed/DataWizard/>), which provides a JAVA-based web interface for accessing data from multiple CW-AQ networks. Observational data from many different U.S.-based AQ networks can be obtained using that website. The AQS maintained by the EPA is another example of a data source where data from multiple networks can be obtained in a single location. The EPA's AQS contains historical data from EPA's very large national AQ network for observing ozone and particulate matter, but also contains historical data from the CSN and IMPROVE networks (see Table 9.1).

Observational data are available from other sources as well. The Atmospheric Model Evaluation Tool (AMET, see Section 9.6) provides a set of comma-separated CW-AQ observational data files for North America. These data files are designed to be directly compatible with the AMET software, but they are simply comma-separated ASCII files that can be used with any software or self-written tool. These AMET data are the same data available directly from the network websites (e.g. AQS, IMPROVE, NAPS, etc.) but have been processed into a common data format to be compatible with the AMET software. These data files are available directly from the CMAS Center website (<https://www.cmascenter.org/amet/>).

9.3 *Evaluation Protocols and Criteria for Targeted Performance*

9.3.1 *Purposes and Basic Principles of Model Evaluation*

For the purposes of CW-AQ forecasting, model performance must be sufficient to adequately inform/protect the public. Model performance is often assessed in terms of bias/error (the deviation of the forecast value from the observed value) and correlation (assessment of the linear relationship between observed and forecast values). Large values of bias/error metrics typically indicate a large deviation between the observed and forecast values, either positive (overestimation of observed value) or negative (underestimation of observed value) when considering bias, and absolute when considering error. Correlation values typically range from -1 to 1, with larger positive numbers indicating a good linear relationship between the observed and forecast values, while smaller and negative values indicate a poor linear relationship between observed and forecast values. While it may be tempting to consider a numerical model with large bias/error and poor correlation valueless, these models can still provide useful information in the CW-AQ forecast process.

As stated previously, numerical CW-AQ models can simulate a large range of atmospheric species. The evaluation protocols and performance targets for these large range of species can vary, and therefore must be appropriate for the species being considered. The concentration of atmospheric CW-AQ species can vary widely across space, time and species. As such, the evaluation protocol and performance criteria targets used must not only be appropriate for the species being considered but must also be appropriate for the application spatial scale and time period. For example, tropospheric O₃ concentrations are typically highest in summer and lowest in winter, and therefore absolute and percentage bias/error values can be considerably different between the two seasons. So, a 10% bias in O₃ in summer often represents a much different absolute value than a 10% bias in winter. A similar situation can exist for the same species for different regions (e.g., urban vs. rural environments) and for different species (e.g., particulate matter).

Finally, the relatively recent implementation of coupled (or “two-way”) meteorology-chemistry models (e.g., WRF-Chem and WRF-CMAQ) has added additional factors to consider when evaluating CW-AQ models (e.g., Baklanov et al., 2014). Traditionally, CW-AQ models are driven by “offline” meteorological inputs. These offline meteorological inputs, created entirely separately from the CW-AQ model, are used by CW-AQ models in a completely static form. With coupled meteorology-chemistry models, the meteorology and chemistry models are run simultaneously (referred to as “online”), allowing for feedback between the meteorology and chemistry. This is an important advancement in CW-AQ modeling, as it allows for better representation of the total atmospheric environment from both a meteorological and air quality standpoint.

While the techniques described throughout this chapter are applicable to these coupled models, additional care should be used when evaluating these models due to the potential for significant feedback between the meteorology and chemistry, which can potentially complicate the evaluation of CW-AQ models. Particularly, the interaction of atmospheric aerosols from the CW-AQ model on solar radiation and cloud formation in the meteorology model can have significant impact on the performance of both modeling systems (e.g., Palacios-Peña et al., 2018). While the use of these coupled models is relatively new, several studies have begun examining these models in depth. Such efforts include the second phase of the Air Quality Model Evaluation International Initiative (AQMEII; <https://doi.org/10.1016/j.atmosenv.2015.06.009>), which focused specifically on the evaluation of coupled models (e.g., Im et al., 2014a, b), and EuMetChem (<http://eumetchem.info/>), a group focused on creating a framework for online integrated air quality and meteorological modeling in Europe.

9.3.2 *Summary of Techniques*

One important difference between the evaluation of numerical weather prediction (NWP) models and CW-AQ models is the spatial and temporal distribution of available observations. There is typically a great deal more NWP relevant observations available spatially (and temporally) than CW-AQ observations. In addition, NWP vertical observations (e.g., vertical soundings) are routinely available, while these types of observations are relatively rare for CW-AQ applications. Satellite data are also widely available (both spatially and temporally) to evaluate NWP models, but are again relatively scarce for CW-AQ model evaluation, although such products are becoming more routinely available. As such, while similar protocols can be applied to both NWP and CW-AQ evaluation efforts, it is important to consider the differences in available observations when formulating a CW-AQ evaluation protocol.

The skill scores calculated through the evaluation protocols can be used to determine the forecasting skill of a particular CW-AQ model as compared to a baseline forecast, which includes persistence and statistical equation-based forecasts (without the use of numerical models or human determination). A numerical model can be considered useful if the skill scores calculated using the forecasts from the model are an improvement over those calculated from the baseline forecast (e.g. persistence forecast). It is likely that under some conditions the numerical model will outscore the baseline forecast, while under other conditions the baseline forecast will outscore the model.

9.4 Measures of Forecast Quality

9.4.1 *Description of Discrete and Categorical CW-AQ Forecasting*

Various metrics exist to measure the quality of a CW-AQ forecast. The particular metric applied depends on the application, however, many metrics can be applied to many different applications. This section and the following sections aim to briefly describe several broad categories of evaluation metrics that can be applied, as well as several different types of applications they can be applied to. This is by no means a comprehensive list of the many different metrics used to evaluate forecast quality, nor do the applications presented represent all the various applications that exist.

As touched upon in the previous section on evaluation protocols, a variety of metrics with which to assess forecast quality/skill exist. Here, two primary classifications of metrics are used, specifically discrete metrics and categorical metrics. Discrete metrics represent the more widely applied metrics to model evaluation, consisting of commonly known values such as bias, error, and correlation, and are routinely found in analyses of both meteorology and CW-AQ models. Categorical metrics are less commonly known and are generally applied when evaluating a model in a forecast capacity, although nothing prevents categorical metrics from being applied to retrospective simulations.

9.4.2 *Quality Measures Reflecting CW-AQ Regulation*

For AQ regulatory applications, forecast (often retrospective simulations) quality is most typically assessed using discrete metrics such as bias, error, and correlation, and not categorical metrics. This is due to the particular nature of these CW-AQ model applications for the purposes of applying future regulatory scenarios, which are almost always in the form of changes in emissions (either increasing or decreasing). As such, discrete metrics help determine the overall quality of the model simulation for the regulatory application, which can have forecast (regulatory) value despite the presence of any large biases/errors, since these model simulations are applied to assess the relative, and not absolute, change in pollutant concentrations. Therefore, if a CW-AQ model can accurately simulate the relative change in pollutant concentrations given a known change in model inputs (e.g., emissions), even a simulation with a large bias can be applied to a regulatory scenario. Categorical metrics are not routinely applied to regulatory applications, since the CW-AQ model is not being assessed against another type of forecast (e.g., persistence) and the model's performance against a "bright-line" value is not particularly valuable.

9.4.3 *Summary of Statistical Metrics*

Tables 9.2-9.4 summarize examples of absolute and relative bias/error metrics, as well as categorical forecast metrics. A list of verification metrics for forecasting products along with their definitions can be found at http://www.nws.noaa.gov/oh/rfcdev/docs/Glossary_Verification_Metrics.pdf.

Table 9.2 Example absolute bias/error metrics

Metric	Definition	Unit	Range
Mean Bias (MB)	$\frac{1}{N} \sum_{i=1}^N (C_m - C_o)$	Absolute	$\pm\infty$
Mean Error (ME)	$\frac{1}{N} \sum_{i=1}^N C_m - C_o $	Absolute	$+\infty$
Root Mean Square Error (RMSE)	$\sqrt{\frac{\sum_{i=1}^N (C_m - C_o)^2}{N}}$	Absolute	$+\infty$

Table 9.3 Example relative bias/error metrics

Metric	Definition	Unit	Range
Normalized Mean Bias (NMB)	$\frac{1}{N} \sum_{i=1}^N \frac{(C_m - C_o)}{\sum_{i=1}^N C_o}$	%	-100% to $+\infty$
Normalized Mean Error (NME)	$\frac{1}{N} \sum_{i=1}^N \frac{ C_m - C_o }{\sum_{i=1}^N C_o}$	%	0% to $+\infty$
Mean Normalized Bias (MNB)	$\frac{1}{N} \sum_{i=1}^N \left(\frac{C_m - C_o}{C_o} \right)$	%	-100% to $+\infty$
Mean Normalized Error (MNE)	$\frac{1}{N} \sum_{i=1}^N \left \frac{C_m - C_o}{C_o} \right $	%	0% to $+\infty$
Mean Fractional Bias (MFB)	$\frac{1}{N} \sum_{i=1}^N \frac{(C_m - C_o)}{\left(\frac{C_o + C_m}{2} \right)}$	%	-200% to +200%
Mean Fractional Error (MFE)	$\frac{1}{N} \sum_{i=1}^N \frac{ C_m - C_o }{\left(\frac{C_o + C_m}{2} \right)}$	%	0% to +200%
Correlation (r)	$\frac{n(\sum C_m C_o) - (\sum C_m)(\sum C_o)}{\sqrt{[n \sum C_m^2 - (\sum C_m)^2][n \sum C_o^2 - (\sum C_o)^2]}}$	None	-1 to 1

Table 9.4 Example categorical forecast metrics

Metric	Definition	Unit	Range
Hit Rate (HR)	(True Positives + True Negatives) / All Values	%	0% to 100%
False Alarm Rate (FAR)	False Positives/(False Positives + True Positives)	%	0% to 100%
Probability of Detection (POD)	True Positives/(True Positives + False Positives)	%	0% to 100%
Critical Success Index (CSI) (Threat Score)	True Positives/(True Positives + False Positives + False Negatives)	None	0 to 1
Brier Score (BS)	The mean square error of probabilistic two-category forecasts where the observations are either 0 (no occurrence) or 1 (occurrence) and forecast probability may be arbitrarily distributed between occurrence and non-occurrence	None	BS=0 for perfect (deterministic) forecasts. BS=1 for forecasts that are always incorrect.
Skill Score	A measure of the relative improvement of the forecast over some (usually 'low-skilled') benchmark forecast. Commonly used reference forecasts include climatology, persistence, or output from an earlier version of the forecast	%	Typically, skill scores are the percentage difference between verification scores for two sets of forecasts (e.g., operational forecasts versus climatology). Perfect score: 1
Uncertainty	The degree of variability in the observations. Most simply measured by the variance of the observations (e.g.): $\frac{\sum(C - \bar{C})^2}{N - 1}$	Absolute	0 to $+\infty$

It is apparent from the metrics example presented in Tables 9.2-9.4 that many statistical metrics exist for evaluating CW-AQ numerical model performance. While the use of any particular metric depends on many factors, the application will generally dictate which metrics are the most useful. Absolute and relative metrics are commonly used when evaluating model performance for development and/or regulatory model applications, while the categorical skill metrics are more commonly used in forecasting applications.

Absolute metrics are valuable, but it can be difficult to assess model bias/error when species concentrations vary considerably across time and space. For example, a large seasonal variation in species concentration can make a relatively moderate bias/error in one season seem like a relatively large bias/error in another season. Relative evaluation metrics are particularly useful for assessing model performance under conditions of changing species concentration as they attempt to account for fluctuations in concentration. However, relative metrics alone may not be sufficient to inform model performance, as large bias/error can occur when concentrations are very low, potentially indicating relatively poor model performance, but the bias/error may in fact be very small in an absolute sense and not necessarily indicate an overall poor performing model. As such, it is recommended that absolute and relative evaluation metrics be used together to provide a more comprehensive evaluation of model performance.

Examples of CW-AQ model evaluations can be found in the literature (e.g., Zhang et al., 2006a, b, 2009; Foley et al., 2010; Appel et al., 2007, 2008, 2011a, 2012, 2013, 2017; Solazzo et al., 2012a; Yahya et al., 2014, 2015a,b, 2016, 2017; Chen et al., 2015; He et al., 2017; Campbell et al., 2017, 2018).

9.5 Advanced Spatio-Temporal Evaluation

9.5.1 Background

Advanced spatio-temporal evaluation of CW-AQ models incorporates non in-situ measurements (e.g., remote sensing) and more advanced statistical analysis techniques (e.g., ensemble models) into the model evaluation process. While these advanced techniques have existed for quite some time, their application to the evaluation of CW-AQ models is relatively new. This is due to the recent advances in remote sensing as it relates to species relevant to CW-AQ numerical modeling and advances in computing power which have made possible the creation of ensemble CW-AQ models, which tend to be much more computationally intensive than numerical meteorology models for example. Applying these advanced techniques to the evaluation of CW-AQ models can be extremely valuable, as remote sensing can provide measurements when and where no measurements would otherwise exist, while the application of advanced ensemble evaluation techniques can provide, among other things, a range of uncertainty for a particular model application.

9.5.2 Satellite Data

Satellite-based measurements have several advantages and disadvantages with respect to their use in the evaluation of CW-AQ models. The primary advantages of satellite measurements tend to be their spatial, and for some satellite products temporal, coverage. They can also provide unique routine measurements that are otherwise not routinely available from in-situ measurements, as well as potentially providing information throughout the entire troposphere. The same reasons that provide advantages for the use of satellite measurements can also be disadvantages. Some satellite products only provide measurements across narrow swaths, and/or require several days to produce a full-coverage product from multiple swaths. In addition, many satellite products are hindered by the presence of dense cloud cover and data will often be flagged as unreliable or missing entirely when clouds are present.

From the AQ perspective the biggest limitation of satellite retrievals is the lack of sensitivity to the surface level where AQ regulation is applied. A further limitation is the lack of temporal resolution, i.e., the observations can only be made at the overpass time. Geostationary

satellites such as TEMPO and Sentinel 4 will provide satellite observations at high temporal resolution in the future. It is important to keep in mind that many satellite products also employ their own regression algorithms and/or numerical models to produce their user end-product measurements. As such, most satellite measurements should be treated in their own way as models, with the potential for significant bias/error to exist, and therefore should not necessarily be considered “ground-truth” when comparing to CW-AQ numerical model forecasts. However, these satellite products are nonetheless still vital tools in evaluating CW-AQ models, particularly since satellite measurements are often available in real time or near-real time and therefore can be used to evaluate true CW-AQ forecasts (as opposed to retrospective model simulations).

A number of different satellite products exist that are applicable to CW-AQ model evaluation, and new CW-AQ relevant satellite products are continuing to be developed and deployed. Here we provide several examples of current satellite products that may be useful for the evaluation of CW-AQ models. Current satellite products include measurements of tropospheric column and surface NO and NO₂, O₃, Aerosol Optical Depth (AOD), as well as fire/smoke-related products. The AOD products are valuable for assessing the ability of the CW-AQ model to reproduce the aerosol loading throughout the troposphere and can be used indirectly to estimate surface level aerosol concentrations. Likewise, the fire/smoke satellite products are extremely valuable for assessing fire-related aerosol, and can be used to identify large sources of particulate matter, which would not be captured in CW-AQ forecasts, unless the models were actively assimilating real-time fire/smoke information (a rare but evolving feature in CW-AQ model forecasts).

Examples of CW-AQ model evaluations using satellite products can be found in Zhang et al. (2009), Liu and Zhang (2011), and Wang et al. (2015).

9.5.3 *Other Remote Sensing Data*

In addition to satellite data, other remote sensing data exist that are useful for CW-AQ model evaluation efforts. Examples include LIDAR measurements, which are often made using equipment that is either fixed at the surface or mounted on an aircraft, and can provide estimates of particle concentrations. More recently, NASA has implemented Pandora spectrophotometers to measure trace gases, including NO, NO₂ and O₃. Commercial aircraft are also equipped to measure atmospheric conditions such as temperature, pressure and humidity using the aircraft communications addressing and reporting system (ACARS). Some aircraft have also been specially equipped with instrumentation that measures trace gases relevant to CW-AQ models, although these types of data are generally rare.

9.5.4 *Ensemble Evaluation Techniques*

Ensemble models (and correspondingly the evaluation of those ensembles) is yet another technique that can be used to assess the quality of a CW-AQ numerical model forecast. Ensemble evaluation entails creating multiple simulations for a single time period and location, while varying certain other aspects of the model simulation. These variations can include meteorology (e.g., different meteorology models, different meteorology configuration options, etc.), different emission inputs, different boundary conditions, or different CW-AQ model configuration options. These simulations together form a range of model solutions to a single event, from which one can ascertain a range of uncertainty in the model estimates, with a small range suggestive of good confidence in the model forecast, while a large range would be suggestive of low confidence in the model forecast.

Several different techniques exist for creating ensemble models. Probably the most common method of producing a model ensemble is “brute force”, where the model is simply run many times, each time varying some aspects of the model simulation (e.g., Gilliam et al., 2015; Solazzo et al., 2012b). The brute force method has several advantages, namely it is conceptually simple (i.e., change something in the model and run it again) and is free from assumptions. The primary disadvantage of brute-force ensembles is that they are

computationally expensive, as the model must be run many times in order to create a robust ensemble.

Other ensemble techniques employ various numerical methods to produce ensemble results without having to run the model in a brute-force configuration. One such technique, the so called decoupled direct method (DDM; Napelenok et al., 2006), is a “sensitivity analysis technique for computing sensitivity coefficients simultaneously while air pollutant concentrations are being computed”. Put simply, DDM allows for the computation of the impact (sensitivity) of the model to an input perturbation (typically emission perturbations) using a single model simulation. The DDM method is much more computationally efficient than running the equivalent brute-force simulations that would be needed. However, since DDM is a numerical technique, the results can differ from brute-force, although this difference is often small enough to justify the use of the technique over brute-force. Other statistical techniques (e.g., Monte Carlo simulation) can be used to create an ensemble without the use of brute-force simulations.

Pinder et al. (2009) describes the types of uncertainty that can be addressed using model ensembles, namely structure and parametric uncertainties. Structure uncertainty refers to the lack of knowledge regarding the fundamental mechanisms underlying an environmental process, which can be addressed by ensembles that vary a single process. Parametric uncertainty refers to uncertainty in the inputs and parameter values employed, which can similarly be addressed using ensembles by varying an input or parameter used.

Pinder et al. employed several metrics to evaluate the model estimated probability, reliability, resolution, and sharpness. Reliability refers to the skill of the ensemble’s estimated probability, calculated by aggregating together all the times and locations with a similar estimated probability of exceeding a threshold and comparing the result with the observed frequency. Resolution is a measure of differentiation, i.e., how well does the ensemble categorize observed events into groups that are different from each other. Sharpness is an inherent feature that is not dependent on observed data, and can be evaluated using the absolute mean difference between the ensemble estimated probability of exceeding a threshold value and some reference value (e.g., climatological average).

9.6 Model Evaluation Tools and Software

9.6.1 Availability and Types of Tools and Software

A number of different tools and software exist for aiding in the evaluation of CW-AQ models, with seemingly no preferred software or tool. These tools/software range from widely available, non-tailored software for reading, manipulating and processing ASCII files (e.g., Microsoft Excel) to tools developed specifically for evaluating CW-AQ models (e.g., AMET). Other software that is frequently utilized for CW-AQ numerical model evaluation includes statistical programs such as SAS and R. In order for non-tailored tools such as Excel, SAS, and R to be useful for the model being used, they must either be capable of reading the numerical model output in its native format (e.g., NetCDF) or the model output must first be converted to a format that software can read (e.g., delimited ASCII). Conversely, tailored tools are often designed to work directly with the output from one or more numerical models and therefore are often preferred if available for the model being used.

9.6.2 Use of Non-Tailored Evaluation Software

Non-tailored software for CW-AQ model evaluation, which includes Excel, Python, SAS and R, can be useful evaluation tools once the observational and model data are imported into the software. This often first requires converting the model data from the native output format into a format that is readable by the software. Often this requires separate software designed specifically to convert the model data into a more common, easily readable format. However, in some cases non-tailored software is able to read the model data directly (e.g., IOAPI/ NetCDF library for R). When attempting to use non-tailored software for CW-AQ model

evaluation it is advised that one first determines if (a) the software has the ability to read the model data output directly or (b) other software exists to convert the model data into a format readable by the non-tailored software. Non-tailored software can also be used in conjunction with tailored software to broaden the suite of evaluation products available.

9.6.3 Use of Tailored Software for Air Quality Evaluation

Here, tailored software refers to those tools/software that are designed specifically to work with CW-AQ numerical model outputs for the purposes of evaluating the model using observational data. While only a few of these tailored software tools exist, when available they typically have the advantage of streamlining the evaluation process, speeding up the time required to evaluate the model. Some tools contain the built-in ability to read and process the native model data, while other tools require the user to preprocess the model data before utilizing the tool. These tailored tools provide built-in analysis products (e.g., statistics, plots) with which to evaluate the model output against observational data. Examples of existing tailored tools (and the models they are designed to work with) are provided in Table 9.5. More details can be found in Foley et al. (2010), Appel et al. (2011, 2012, 2013, 2017), and Solazzo et al. (2012a).

Table 9.5 Examples of existing air quality modeling specific evaluation tools/software

Software Name	Developer	Application	Supported Models	Availability	Website	Reference
AMET	EPA	Meteorology, Air Quality	CMAQ directly, other models indirectly	Open Source	https://www.cmascenter.org/amet/	Appel et al., 2010
MET	NCAR	Meteorology, Air Quality	WRF, MPAS	Open Source	https://dtcenter.org/met/users/index.php	
ENSEMBLE	JRC	Meteorology, Air Quality	Multiple models indirectly	Online	https://ec.europa.eu/jrc/en/scientific-tool/model-evaluation-platform-ensemble	Galmarni et al., 2012
OPENAIR	NERC	Air Quality	Model independent	Open Source (R package)	http://davidcarslaw.github.io/openair/	Carslaw and Ropkins, 2011
MONET	NOAA	Air Quality	CMAQ directly	Open Source	https://github.com/noaa-oar-arl/MONET	Baker and Pan, 2017

9.7 Summary

- Model evaluation is a critical and necessary step in the effective use of numerical CW-AQ models.
- Criteria for a model simulation to meet at least the minimum thresholds for acceptable performance should be well established before the model data are used, although certain model applications may allow for more leeway in what constitutes acceptable model performance.
- For CW-AQ forecasting applications, the models should meet the minimum performance thresholds to provide forecasters with reassurance that the model can be a useful tool in their forecasting process. While thoroughly evaluating a model's performance can in some cases be a time-consuming endeavor, it is nonetheless a critical component of applying models.
- Numerous resources exist to aid in model evaluation, with new and existing tools being continually developed and greater access to new and existing observation data sources being made.

References

- Appel, K.W., Gilliland, A.B., Sarwar, G., Gilliam, R.C., 2007. Evaluation of the Community Multiscale Air Quality (CMAQ) model version 4.5: Sensitivities impacting model performance; Part I – ozone, *Atmospheric Environment*, doi:10.1016/j.atmosenv.2007.08.044.
- Appel, K.W., Bhawe, P.V., Gilliland, A.B., Sarwar, G., Roselle, S.J., 2008. Evaluation of the Community Multiscale Air Quality (CMAQ) model version 4.5: Sensitivities impacting model performance; Part II - particulate matter, *Atmospheric Environment* (2008), doi:10.1016/j.atmosenv.2008.03.036.
- Appel, K.W., Foley, K.M., Bash, J.O., Pinder, R.W., Dennis, R.L., Allen, D.J., and Pickering, K.: A multi-resolution assessment of the Community Multiscale Air Quality (CMAQ) model v4.7 wet deposition estimates for 2002–2006, *Geosci. Model Dev.*, 4, 357-371, doi:10.5194/gmd-4-357-2011, 2011a.
- Appel, K.W., Gilliam, R.C., Davis, N., Zubrow, A., and Howard, S.C.: Overview of the Atmospheric Model Evaluation Tool (AMET) v1.1 for evaluating meteorological and air quality models, *Environ. Model. Softw.*, 26, 4, 434-443, doi:10.1016/j.envsoft.2010.09.007, 2011b.
- Appel, K.W., Chemel, C., Roselle, S.J., Francis, X.V., Sokhi, R.S., Rao, S.T., and Galmarini, S.: Examination of the Community Multiscale Air Quality (CMAQ) model performance over the North American and European Domains, *Atmos. Environ.*, doi:10.1016/j.atmosenv.2011.11.016, 2012.
- Appel, K. W., Pouliot, G. A., Simon, H., Sarwar, G., Pye, H. O. T., Napelenok, S. L., Akhtar, F., and Roselle, S. J.: Evaluation of dust and trace metal estimates from the Community Multiscale Air Quality (CMAQ) model version 5.0, *Geosci. Model Dev.*, 6, 883-899, doi:10.5194/gmd-6-883-2013, 2013.
- Appel, K. W., Napelenok, S. L., Foley, K. M., Pye, H. O. T., Hogrefe, C., Luecken, D. J., Bash, J. O., Roselle, S. J., Pleim, J. E., Foroutan, H., Hutzell, W. T., Pouliot, G. A., Sarwar, G., Fahey, K. M., Gantt, B., Gilliam, R. C., Kang, D., Mathur, R., Schwede, D. B., Spero, T. L., Wong, D. C., and Young, J. O.: Description and evaluation of the Community Multiscale Air Quality (CMAQ) model version 5.1, *Geosci. Model Dev.*, 10, 1703-1732, doi:10.5194/gmd-1703-2017, 2017.
- Baker, B.; Pan, L. Overview of the Model and Observation Evaluation Toolkit (MONET) Version 1.0 for Evaluating Atmospheric Transport Models. *Atmosphere* 2017, 8, 210.
- Baklanov, A., Schlünzen, K., Suppan, P., Baldasano, J., Brunner, D., Aksoyoglu, S.,

- Carmichael, G., Douros, J., Flemming, J., Forkel, R., Galmarini, S., Gauss, M., Grell, G., Hirtl, M., Joffre, S., Jorba, O., Kaas, E., Kaasik, M., Kallos, G., Kong, X., Korsholm, U., Kurganskiy, A., Kushta, J., Lohmann, U., Mahura, A., Manders-Groot, A., Maurizi, A., Moussiopoulos, N., Rao, S. T., Savage, N., Seigneur, C., Sokhi, R. S., Solazzo, E., Solomos, S., Sørensen, B., Tsegas, G., Vignati, E., Vogel, B., and Zhang, Y.: Online coupled regional meteorology chemistry models in Europe: current status and prospects, *Atmos. Chem. Phys.*, 14, 317-398, <https://doi.org/10.5194/acp-14-317-2014>, 2014.
- Campbell, P., Y. Zhang, K. Wang, R. Leung, J.-W. Fan, B. Zheng, Q. Zhang, and K.-B. He, 2017, Evaluation of a Multi-scale WRF-CAM5 Simulation during the 2010 East Asian Summer Monsoon, *Atmospheric Environment*, 169, 204-217, doi.org/10.1016/j.atmosenv.2017.09.008.
- Campbell, P., F. Yan, Z.-F. Lu, Y. Zhang, and D. Streets, 2018, Impacts of Transportation Sector Emissions on Future U.S. Air Quality in a Changing Climate. Part I: Projected Emissions, Simulation Design, and Model Evaluation, *Environmental Pollution*, 238:903-917. doi: 10.1016/j.envpol.2018.04.020.
- Chen, Y., Y. Zhang, J.-W. Fan, L.R. Leung, Q. Zhang, and K.-B. He, 2015, Application of an Online-Coupled Regional Climate Model, WRF-CAM5, over East Asia for Examination of Ice Nucleation Schemes: Part I. Comprehensive Model Evaluation and Trend Analysis for 2006 and 2011, *Climate*, 3(3), 627-667; doi:10.3390/cli3030627.
- Flemming J, Stern R, and Yamartino R, A new air quality regime classification scheme for O₃, NO₂, SO₂ and PM₁₀ observations sites. *Atmos. Environ.*, 39, 6121–6129, 2005.
- Foley, K.M., Roselle, S.J., Appel, K.W., Bhave, P.V., Pleim, J.E., Otte, T.L., Mathur, R., Sarwar, G., Young, J.O., Gilliam, R.C., Nolte, C.G., Kelly, J.T., Gilliland, A.B., and Bash, J.O.: Incremental testing of the Community Multiscale Air Quality (CMAQ) modeling system version 4.7, *Geosci. Model Dev.*, 3, 205-226, [10.5194/gmd-3-205-2010](https://doi.org/10.5194/gmd-3-205-2010), 2010.
- Galmarini, S., Bianconi, R., Appel, K.W., Solazzo, E., Mosca, S., Grossi, P., Moran, M., Schere, K., and Rao, S.T., ENSEMBLE and AMET: two systems and approaches to a harmonized, simplified and efficient assistance to air quality models development and evaluation, *Atmos. Environ.*, 53, 51-59, [10.1016/j.atmosenv.2011.08.076](https://doi.org/10.1016/j.atmosenv.2011.08.076), 2012.
- Gilliam, R.C., Hogrefe, C., Godowitch, J.M., Napelenok, S., Mathur, R., Rao, S.T.: Impact of inherent meteorology uncertainty on air quality model predictions, *J. Geophys. Res.*, 120 (23), 12259-12280, <https://doi.org/10.1002/2015JD023674>, 2015.
- He, J., Y. Zhang, K. Wang, Y. Chen, L. R. Leung, J.-W. Fan, M. Li, Bo Zheng, Q. Zhang, F.-K. Duan, and K.-B. He, 2017, Multi-Year Application of WRF-CAM5 over East Asia-Part I: Comprehensive Evaluation and Formation Regimes of O₃ and PM_{2.5}, *Atmospheric Environment*, 165, 122–142 [10.1016/j.atmosenv.2017.06.015](https://doi.org/10.1016/j.atmosenv.2017.06.015).
- Henne, S., Brunner, D., Folini, D., Solberg, S., Klausen, J., and Buchmann, B.: Assessment of parameters describing representativeness of air quality in-situ measurement sites, *Atmos. Chem. Phys.*, 10, 3561-3581, <https://doi.org/10.5194/acp-10-3561-2010>, 2010.
- Im, U., R. Bianconi, E. Solazzo, I. Kioutsioukis, A. Badia, A. Balzarini, R. Baró, R. Bellasio, D. Brunner, C. Chemel, G. Curci, J. Flemming, R. Forkel, L. Giordano, P. Jiménez-Guerrero, M. Hirtl, A. Hodzic, L. Honzak, O. Jorba, C. Knote, J. J.P. Kuenen, P. A. Makar, A. Manders-Groot, L. Neal, J. L. Pérez, G. Pirovano, G. Pouliot, R. San Jose, N. Savage, W. Schroder, R. S. Sokhi, D. Syrakov, A. Torian, P. Tuccella, J. Werhahn, R. Wolke, K. Yahya, R. Zabkar, Y. Zhang, J.-H. Zhang, C. Hogrefe, S. Galmarini, 2014a, Evaluation of operational online-coupled regional air quality models over Europe and North America in the context of AQMEII phase 2. Part I: Ozone, 115, 404-420, *Atmospheric Environment*, doi: 10.1016/j.atmosenv.2014.09.042.
- Im, U., R. Bianconi, E. Solazzo, I. Kioutsioukis, A. Badia, A. Balzarini, R. Baró, R. Bellasio, D. Brunner, C. Chemel, G. Curci, H. D. van der Gon, J. Flemming, R. Forkel, L. Giordano,

- P. Jiménez-Guerrero, M. Hirtl, A. Hodzic, L. Honzak, O. Jorba, C. Knote, P. Makar, A. Manders-Groot, L. Neal, J. L. Pérez, G. Pirovano, G. Pouliot, R. San Jose, N. Savage, W. Schroder, R. S. Sokhi, D. Syrakov, A. Torian, P. Tuccella, K. Wang, J. Werhahn, R. Wolke, R. Zabkar, Y. Zhang, J.-H. Zhang, C. Hogrefe, and S. Galmarini, 2014b, Evaluation of operational online-coupled regional air quality models over Europe and North America in the context of AQMEII phase 2. Part II: Particulate Matter, *Atmospheric Environment*, 115, 421-441, doi: 10.1016/j.atmosenv.2014.08.072.
- Liu, P. and Y. Zhang, 2011, Use of a Process Analysis Tool for Diagnostic Study on Fine Particulate Matter Predictions in the U.S. Part I: Model Evaluation Using Surface, Aircraft, and Satellite Data, *Atmospheric Pollution Research*, 2 (1), 49-60, doi: 10.5094/APR.2011.007.
- Napelenok, S., Cohan, D.S., Yongtao, H., Armistead, R.G.: Decoupled direct 3-D sensitivity analysis for particulate matter (DDM-3D/PM), *Atmos. Environ.*, 40 (32), 6112-6121, <https://doi.org/10.1016/j.atmosenv.2006.05.039>, 2006.
- Palacios-Peña, L., Baró, R., Baklanov, A., Balzarini, A., Brunner, D., Forkel, R., Hirtl, M., Honzak, L., López-Romero, J. M., Montávez, J. P., Pérez, J. L., Pirovano, G., San José, R., Schröder, W., Werhahn, J., Wolke, R., Žabkar, R., and Jiménez-Guerrero, P.: An assessment of aerosol optical properties from remote-sensing observations and regional chemistry-climate coupled models over Europe, *Atmos. Chem. Phys.*, 18, 5021-5043, <https://doi.org/10.5194/acp-18-5021-2018>, 2018.
- Pinder, R.W., R.C. Gilliam, K.W. Appel, S.L. Napelenok, A.B. Gilliland. Efficient probabilistic estimates of surface ozone concentration using an ensemble of model configurations and direct sensitivity calculations, *Environ. Sci. Technol.*, 2009, 43 (7), pp 2388-2393, DOI: 10.1021/es8025402.
- Solazzo, E., Bianconi, R., Pirovano, G., Matthias, V., Vautard, R., Appel, K.W., Bessagnet, B., Brandt, J., Christensen, J.H., Chemel, C., Coll, Ferreira, J., Forkel, R., Francis, X.V., Grell, G., Grossi, P., Hansen, Miranda, A.I., Moran, M.D., Nopmongcol, U., Parnk, M., Sartelet, K.N., Schapp, M., Silver, J.D., Sokhi, R.S., Vira, J., Werhahn, J., Wolke, R., Yarwood, G., Zhang, J., Rao, S.T., Galmarini, S.: Operational model evaluation for particulate matter in Europe and North America in the context of the AQMEII project, *Atmos. Environ.*, 53, 75-92, 2012a.
- Solazzo, E., Bianconi, R., Vautard, R., Appel, K.W., Bessagnet, B., Brandt, J., Christensen, J.H., Chemel, C., Coll, I., Denier van der Gon, H., Ferreira, J., Forkel, R., Francis, X.V., Grell, G., Grossi, P., Hansen, A., Jericevic, A., Kraljevic, L., Miranda, A.I., Moran, M.D., Nopmongcol, U., Pirovano, G., Parnk, M., Riccio, A., Sartelet, K.N., Schapp, M., Silver, J.D., Sokhi, R.S., Vira, J., Werhahn, J., Wolke, R., Yarwood, G., Zhang, J., Rao, S.T., Galmarini, S.: Model evaluation and ensemble modeling for surface-level ozone in Europe and North America, *Atmos. Environ.*, 53, 60-74, 2012b.
- Wang, K., K. Yahya, Y. Zhang, C. Hogrefe, G. Pouliot, C. Knote, A. Hodzic, R. San Jose and J. L. Perez, P. J. Guerrero, R. Baro, and P. Makar, 2015, A Multi-Model Assessment for the 2006 and 2010 Simulations under the Air Quality Model Evaluation International Initiative (AQMEII) Phase 2 over North America, Part 2. Evaluation of Column Variable Predictions Using Satellite Data, *Atmospheric Environment*, 115, 587-603, doi: 10.1016/j.atmosenv.2014.07.044.
- Yahya, K., K. Wang, M. Gudoshava, T. Glotfelty, and Y. Zhang, 2014, Application of WRF/Chem over North America under the AQMEII Phase 2. Part I. Comprehensive Evaluation of 2006 Simulation, *Atmospheric Environment*, 115, 773-755, doi: 10.1016/j.atmosenv.2014.08.063.
- Yahya, K., J. He, and Y. Zhang, 2015a, Multiyear Applications of WRF/Chem over Continental U.S.: Model Evaluation, Variation Trend, and Impacts of Boundary Conditions, *Journal of Geophysical Research*, 120, 12748-12777, doi: 10.1002/2015JD023819.
- Yahya, K., K. Wang, Y. Zhang, and T. E. Kleindienst, 2015b, Application of WRF/Chem over North America under the AQMEII Phase 2-Part 2: Evaluation of 2010 Simulation and Responses of Air Quality and Meteorology-Chemistry Interactions to Changes in

Emissions and Meteorology from 2006 to 2010, *Geoscientific Model Development*, 8, 2095-2117, doi:10.5194/gmd-8-2095-2015.

- Yahya, K., K. Wang, P. Campbell, T. Glotfelty, J. He, and Y. Zhang, 2016, Decadal Evaluation of Regional Climate, Air Quality, and Their Interactions using WRF/Chem version 3.6.1, *Geoscientific Model Development*, 9, 671-695, doi:10.5194/gmd-9-671-2016.
- Yahya, K., K. Wang, P. Campbell, Y. Chen, T. Glotfelty, J. He, M. Pirhalla, and Y. Zhang, 2017, Decadal Application of WRF/Chem for Regional Air Quality and Climate Modeling over the U.S. under the Representative Concentration Pathways Scenarios. Part 1: Model Evaluation and Impact of Downscaling, *Atmospheric Environment*, 152: 562–583, doi: 10.1016/j.atmosenv.2016.12.029.
- Zhang, Y., P. Liu, B. Pun, and C. Seigneur, 2006a, A Comprehensive Performance Evaluation of MM5-CMAQ for the Summer 1999 Southern Oxidants Study Episode, Part-I. Evaluation Protocols, Databases and Meteorological Predictions, *Atmospheric Environment*, 40, 4825-4838, doi: 10.1016/j.atmosenv.2005.12.043.
- Zhang, Y., P. Liu, A. Queen, C. Misenis, B. Pun, C. Seigneur, and S.-Y. Wu, 2006b, A Comprehensive Performance Evaluation of MM5-CMAQ for the Summer 1999 Southern Oxidants Study Episode, Part-II. Gas and Aerosol Predictions, *Atmospheric Environment*, 40, 4839-4855, doi:10.1016/j.atmosenv.2005.12.048.
- Zhang, Y., K. Vijayaraghavan, X.-Y. Wen, H. E. Snell, and M.Z. Jacobson, 2009, Probing Into Regional Ozone and Particulate Matter Pollution in the United States: 1. A 1-year CMAQ Simulation and Evaluation Using Surface and Satellite Data, *Journal of Geophysical Research*, 114, D22304, doi:10.1029/2009JD011898.

Chapter 10. Bias Correction and Forecast Skill Improvement Methods

10.1 Introduction

The forecasting skills of CW-AQF models depend on their representations of major atmospheric processes and the simulation configurations such as horizontal and vertical grid resolutions and nesting methods used in their applications. In this chapter, the performance of CW-AQF models, model biases and associated likely causes are first reviewed. Several methods that will improve their forecasting skills will then be introduced, including data fusion, data assimilation, and inverse modeling.

In this chapter, bias correction and forecast skill improvement methods are described in detail. Topics include common model biases reported in the literature (Section 10.2), data fusion to correct model biases (Section 10.3), chemical data assimilation (Section 10.4), and inverse modeling using data assimilation (Section 10.5). Finally, Section 10.6 summarizes key points.

10.2 Overview of CW-AQF Model Performance and Biases Reported in the Literature

10.2.1 CW-AQF Model Performance Skills

Most evaluations of forecasted O₃ and its precursors focus on summer, and very few include winter (e.g., Manins et al., 2002; Cai et al., 2008; Findari et al., 2008; Doraiswamy et al., 2009; Yahya et al., 2014; Zhang et al., 2016). Forecasting particulate matter (PM) is more difficult than forecasting O₃ because PM consists of multiple chemical components over a broad size spectrum and also because surface O₃ generally shows a distinct diurnal cycle driven by photochemistry that models can properly capture. PM modeling is starting to reach sufficient maturity for transition from research to operational use. Several PM models have been transferred into operational models to forecast PM since 2003 (Carmichael et al., 2003; McHenry et al., 2004; McKeen et al., 2005, 2007; Yu et al., 2008; Chuang et al., 2011), but very few studies provide detailed evaluations of forecasted PM and its composition and precursors (e.g., McKeen et al., 2007, 2009; Yu et al., 2008; Chen et al., 2008; Manders et al., 2009; Yahya et al., 2014; Zhang et al., 2016). Similar to O₃ forecasts, most evaluations are conducted for summer episodes, and very few for winter episodes (e.g., Mathur et al., 2008; Findari et al., 2008; Konovalov et al., 2009; Yahya et al., 2014; Zhang et al., 2016) or a full year (e.g., Manders et al., 2009). Limited evaluation was performed for coarse particles such as mineral dust (e.g., Jiménez-Guerrero et al., 2008; Niu et al., 2008; Menut et al., 2009) that may be of major concerns for PM₁₀ attainment in some regions such as Asia, southern Europe, and the western U.S. Jiménez-Guerrero et al. (2008) showed that the inclusion of a dust emission module substantially increases the accuracy of both discrete and categorical statistics in the Iberian Peninsula in Europe where the influence of Saharan dust cannot be neglected.

Tables 10.1 and 10.2 summarize the evaluation of a number of RT-AQF systems in terms of domain and period and discrete and categorical performance statistics. While maximum 1-h O₃ average statistics are generally satisfactory, those for maximum 8-h average and hourly O₃ sometime exceed normalized mean bias (NMB) of 15% and normalized mean error (NME) of 30% for some models (e.g., Eta/CMAQ, WRF-NMM/CMAQ) over the eastern or north-eastern U.S. in the O₃ season during 2004-2006, indicating a relatively poor performance. The overpredictions in the low O₃ range (< 50 ppb) were reported in several studies (e.g., Yu et al., 2007; Chen et al., 2008). Several factors may contribute to such overpredictions. These include a poor representation of the nocturnal PBL mixing height (Gilliam et al., 2006; Zhang et al., 2006b; Eder et al., 2006); an excessive downward transport of high level O₃ aloft and too much photolysis under high cloud conditions (Eder et al., 2006); a high O₃ production rate with the SAPRC-99 chemical mechanism (Arnold and Dennis, 2006); the model limitation in resolving titration of O₃ by NO in urban plumes (Yu et al., 2007); and the chemical boundary conditions from global models (Chen et al., 2008). Chuang et al. (2011) applied WRF/Chem-MADRID for RT-AQF and found that O₃ overprediction in most regions in the southeastern U.S. is likely caused by inaccurate emissions of precursors such as biogenic volatile organic compounds (VOCs), positive biases in 2-m temperature and negative biases in wind speed at 10-m. O₃ underpredictions in some regions could be due in part to the uncertainties in lateral boundary conditions.

For categorical evaluation, different threshold values were used for the same variables. For example, the threshold values used for maximum 1-h average O_3 , maximum 8-h average O_3 , and hourly O_3 are 60-125 ppb, 65-85 ppb, and 80 ppb, respectively. Some of these values are lower than the former U.S. NAAQS of 120 ppb for maximum 1-h average O_3 and the current U.S. NAAQS of 70 ppb for maximum 8-h O_3 , respectively, for the reasons stated previously (e.g., Hogrefe et al., 2007; Yu et al., 2007; Chuang et al., 2011), although higher thresholds were used in some earlier applications (e.g., Kang et al., 2005). For maximum 1-h average O_3 , accuracy (A), critical success index (CSI), probability of detection (POD), bias (B), and false alarm ratio (FAR) range from 15-99.8%, 5.2-21.6%, 6.9-89%, 0.1-5.3 ppb, and 0.3-94.1%, respectively. Prev'air gives the lowest A of 15-41%, because it underestimates O_3 daily maxima at high O_3 concentrations (Honoré et al., 2008). All RT-AQFs give low values of CSI and POD but higher values of FAR because they fail to forecast exceedance (i.e., a low value of b) but overpredict low O_3 (i.e., a high value of a). A, CSI, POD, B, and FAR for maximum 8-h average O_3 range from 76.2-99.8%, 0-53.2%, 0-84.8%, 0.3-17.0 ppb, and 13-99.1%, respectively. Compared with maximum 1-h O_3 , the values of CSI and POD are higher and those of FAR are lower for corresponding maximum 8-h O_3 . The categorical evaluation for hourly O_3 was conducted by only one model (i.e., WRF/Chem-MADRID), with A, CSI, POD, B, and FAR of 99.2%, 2.5%, 18.8%, 6.8 ppb, and 97.2%, respectively. Very few evaluations were conducted for precursors of O_3 and other gaseous species (e.g., Cai et al., 2008) and vertical profiles of forecasted concentrations (e.g., Yu et al., 2007). Yu et al. (2007) reported that Eta/CMAQ reproduced O_3 vertical distributions on most of the days at low altitudes, but overpredictions occurred at altitudes > 6 km because of a combination of effects related to the specifications of meteorological lateral boundary conditions as well as the model's coarse vertical resolution in the upper free troposphere.

Surface PM forecasts are evaluated in terms of 24-h average $PM_{2.5}$, hourly $PM_{2.5}$, and 24-h average PM_{10} . These evaluations, however, have been very limited to date and a consistent evaluation protocol has not yet been well established (Seigneur, 2001; Zhang et al., 2006a). The forecasting skill for $PM_{2.5}$ is overall poorer than that for O_3 . For 24-h average $PM_{2.5}$, mean biases (MBs), root mean square errors (RMSEs), NMBs, and NMEs range from -3.2 to 6.2 $kg\ m^{-3}$, 1.7-15.9 $kg\ m^{-3}$, -21 to 32%, and 37-81%, respectively. The NMB of -21% using Eta/CMAQ over the eastern U.S. during 14 July-18 August 2004 was reported by Yu et al. (2008), who attributed underpredictions to underestimated total carbonaceous PM at both urban and rural sites and a significant underestimation of unspecified anthropogenic PM mass (mainly consisting of primary emitted trace elements) at rural sites. On the other hand, Hogrefe et al. (2007) showed that Eta/CMAQ overpredicted $PM_{2.5}$ in New York City due to overpredictions in organic aerosols and crustal material. Factors contributing to such overpredictions include underpredictions of nocturnal vertical mixing, inaccurate temporal allocation of primary OM emissions, and underestimates of deposition processes. Chen et al. (2008) reported the NMB of 17-32% over the Pacific Northwest during August–November 2004. The overpredictions in $PM_{2.5}$ were attributed to uncertainties in wildfire emission estimates and the modeling error in fire plume transport due to errors in MM5-predicted wind direction and wind speed. McKeen et al. (2007) evaluated RT-AQF of 6 models including WRF/Chem at two grid resolutions (12- and 36-km), CHRONOS, AURAMS, STEM-2K3, and Eta/CMAQ. They found that most models did not reproduce the observed diurnal variation at urban and suburban sites, particularly during the nighttime to early morning period and the ensemble mean based on 6 models with equal weighting gave the best possible forecast in terms of statistics. Chuang et al. (2011) showed slight underpredictions of $PM_{2.5}$ in the O_3 season over the southeastern U.S. by WRF/Chem-MADRID, which were attributed to uncertainties in emissions such as those of biogenic VOCs and NH_3 , overpredictions of precipitation, and uncertainties in the boundary conditions. Only two studies evaluated hourly $PM_{2.5}$, giving MBs, RMSEs, NMBs, and NMEs of -3.3 to -0.6 $kg\ m^{-3}$, 8.3-11.3 $kg\ m^{-3}$, -21.1 to -5.2%, and 49.8-51.4%, respectively. For 24-h average PM_{10} , MBs and RMSEs range from -29 to 13.8 $kg\ m^{-3}$ and 8.3-47.2 $kg\ m^{-3}$, respectively. Berge et al. (2002) reported forecasted PM_{10} performance over Oslo with an MB of -20.9 $kg\ m^{-3}$ and an NMB of -36.5% at Kirkeveien due to inaccurate emissions of PM_{10} from the surface (i.e., the re-suspension of dust deposited at the roadside) on dry days and an MB of 13.8 $kg\ m^{-3}$ and an NMB of 24% at Furuset due to errors in simulated grid-averaged wind fields.

Table 10.1. Discrete and categorical evaluation of RT-AQF results for O₃ predictions (modified from Zhang et al., 2012)

Pollutants	Area	Period	MB	RMSE	NMB (%)	NME (%)	Threshold	A (%)	CSI (%)	POD (%)	B	FAR (%)	Model	Reference
maximum 1-h average O ₃	W EU Melbourne/ Sydney, Australia	5/1- 9/30,1998 March 7-9, 2001 1/1-5/31, 2001 Summer, 2001-2003	1.5 -6 to -1	11.0	— -12 to -14	— 17-24	— 60 60 80	—	—	— 30-70 33-89 37-53	—	— 14-63	ECMWF/CHIMERE AAQFS AAQFS AAQFS AAQFS	SC01 MA01b CO04 CH05 ^a CH05 ^a
	NE US	8/5- 29,2002	1.4	14.6	2.2	18.0	125	99.2	9.7	14.0	0.6	76	MAQSIP-RT	KA05
	NE US	8/5- 29,2002	9.5	21.3	15.0	25.8	125	97.0	9.8	29.8	2.3	87.2	MM5/Chem	KA05
	NIP	8/13- 16,2000	—	—	—	—	60	89.7- 92.2	6.7- 15.0	6.9- 22.1	0.1- 0.7	33.3- 69.6	MM5/CMAQ	J106
	E US.	7/1- 8/15,2004	8.5	16.9	16.4	25.3	—	—	—	—	—	—	Eta/CMAQ ^a	YU07
	EU	Spring/ summer, 2004-2006	0-5.6 kg m ⁻³	0.83- 20.1 kg m ⁻³			180 kg m ⁻³	15-41				0.3- 0.9	PREV'AIR	HO08
	EU S US	7/1- 8/31,2005 5/1- 9/30,2009 5/1- 9/30,2009- 2011	-0.7 4.5 -3.0 – 7.3 -1.5 – 8.0	— 16.8 11.6- 17.0 12.1- 15.9	— 9.5 -5.5 – 15.5 -3.0 – 17.0	— 26.7 17.6- 27.4 19.0- 27.0	— 80 60 80 80	— 94.0 75.3 94.6- 96 94.2- 97.7	— 5.2 21.7 5.2- 13.8 3.6- 15.5	— 31.3 46.1 17- 31.3 18.8- 30.5	— 5.3 1.6 0.6- 5.3 0.9- 7.9	— 94.1 71.1 67- 94.1 71.5- 96.1	CHIMERE WRF/Chem- MADRID WRF/Chem- MADRID WRF/Chem- MADRID	SZ09 CH11 YA14 ZH16

Pollutants	Area	Period	MB	RMSE	NMB (%)	NME (%)	Threshold	A (%)	CSI (%)	POD (%)	B	FAR (%)	Model	Reference
		5/1-9/30,2012-2014												
maximum 8-h	NE US	8/1-10,2001					85	80.0	34.0	49.0	1.1	13.0	MM5/MAQSIP-RT	MC04
average O₃	NE US.	8/5-29,2002	8.3	18.2	15.1	25.4	85	85.8	18.1	26.7	0.7	64.0	MAQSIP-RT	KA05
	NE US	8/5-29,2002	2.8	13.0	5.0	18.6	85	76.2	17.6	36.4	1.4	74.6	MM5/Chem	KA05
	NE US	6/1-9/30,2004	10.2	15.7	22.8	28.1	85	98.9	14.2	41.0	2.3	82.1	Eta/CMAQ	ED06
	E US	7/1-8/15,2004	10.4	16.6	22.6	28.8	—	—	—	—	—	—	Eta/CMAQ	YU07
	NY	7/1-9/30,2004	6.5	12.8	—	—	—	—	—	—	—	—	Eta/CMAQ	HO07
	NY	7/1-9/30,2004	—	—	—	—	65	84.0-95.2	31.4-53.2	46.5-84.8	—	32.9-55.2	Eta/CMAQ	HO07
	NE US	7/14-8/17,2004	10.0	14.0	—	—	—	—	—	—	—	—	7-model ensemble ^b	MK05
	PN	8/1-9/30,2004	2.7	—	6	17	—	—	—	—	—	—	MM5/CMAQ	CH08
	E US	8/12,2005	—	—	—	—	85	90.4	24.3	37.5	0.9	59.1	Eta/CMAQ	LE08
	CONUS	8/12,2005	—	—	—	—	85	87.4	26.0	54.2	1.6	66.7	Eta/CMAQ	LE08
	E US	6/1-9/30,2005	7.9-10.9	14.5-16.3	16.5-22.4	24.1-27.1	—	—	—	—	—	—	WRF-NMM/CMAQ	ED09
		2006, 2007												
	CONUS	6/1-8/31,2007	4.3	13.0	8.7	20.4	75	92.4	23.2	42.5	1.2	66.3	WRF-NMM/CMAQ	ED09
	CONUS		—	—	—	—	85	96.9	15.4	32.2	1.4	77.3	WRF-NMM/CMAQ	ED09
	E. Texas		6.0	13.1	—	—	75	—	18.0	32.0	—	59.0	—	DJ10

Pollutants	Area	Period	MB	RMSE	NMB (%)	NME (%)	Threshold	A (%)	CSI (%)	POD (%)	B	FAR (%)	Model	Reference
	S US	6/1-8/31,2007	3.5	13.6	8.3	25.0	85	91.5	6.0	10.0		70.0	7-model ensemble ^c	CH11
		8/31-10/12,2006					65	97.2	9.2	28.4	2.4	88.0		
							75	99.0	0.9	15.6	5.8	95.6	WRF/Chem-MADRID	YA14
			-2.2 – 6.1	10.5– 13.9	-4.5 – 14.6	17.8– 26.1	85	81.4– 85.7	14– 24.9	29.1– 33.3	0.6– 1.7	48.6– 80.6		ZH16
		5/1-9/30, 2009	-0.8 – 8.8	10.3– 15.1	-2.0 – 22.0	21.0– 29.0	60	98.7– 100	9.9– 25.3	26.6– 46.7	0.8– 4.2	54.9– 88.9	WRF/Chem-MADRID	
													WRF/Chem-MADRID	
		5/1-9/30,2009-2011												
		5/1-9/30,2012-2014												

1. MB: Mean Bias; RMSE: Root Mean Square Error; NMB: Normalized Mean Bias; NME: Normalized Mean Error; A: Accuracy; CSI: Critical Success index; POD: Probability Of Detection; B: Bias; FAR: False Alarm Ratio.
2. The unit for MB, RSME, and threshold are ppb for O₃ (except those indicated).
3. Superscripts a: all data pairs are included without cut-off threshold value; b: the seven models include: WRF/chem (27 km), BAMS (15-km), BAMS (45-km), CHRONOS (21 km), AURAMS (42 km), STEM-2K3 (12 km), and CMAQ/Eta(12-km); c: the seven models include: WRF/chem-2 (27-km), WRF/chem-2 (12-km), CHRONOS, AURAMS, STEM-2K3, BAMS (15-km), and NMM/CMAQ.
4. S US: Southeastern U.S.; E US: Eastern U.S., NE US: North-eastern U.S.; PN: Pacific Northwest; NY: New York State; EU: Europe; W EU: Western Europe; SE CA: southeastern Canada; LP-S: La Plana, Spain; SP-B: São Paulo, Brazil; NIP: North-eastern Iberian Peninsula; IP: Iberian Peninsula; NA: North America; ME: Melbourne, Australia; OS: Oslo, Norway; NE: the Netherlands.
5. See a list of acronyms in the [appendix](#) for all model names
6. CH11: Chuang et al. (2011); MA01a: Manins (2001a); MA01b: Manins (2001b); SC01: Schmidt et al. (2001); CO04: Cope et al. (2004); MC04: McHenry et al. (2004); CH05: Cope and Hess (2005); KA05: Kang et al. (2005); ED06: Eder et al. (2006); HO07: Hogrefe et al. (2007); JI06: Jiménez et al. (2006); MK05: McKeen et al. (2005); YU07: Yu et al. (2007); CH08: Chen et al. (2008); ED09: Eder et al. (2009); LE08: Lee et al. (2008); HO08: Honoré et al., 2008; SZ09: Szopa et al. (2009); DJ10: Djalalova et al. (2010), YA14: Yahya et al. (2014), ZH16: Zhang et al. (2016).

**Table 10.2. Discrete and categorical evaluation of RT-AQF results for PM_{2.5} predictions
(modified from Zhang et al., 2012)**

Pollutants	Area	Period	MB	RMSE	NMB (%)	NME (%)	Threshold	A (%)	CSI (%)	POD (%)	B	FAR (%)	Model	Reference
24-h	NY	7/1-9/30,2004	5.4	13.2	—	—	—	—	—	—	—	—	Eta/CMAQ	HO07
average PM _{2.5}	NY	1/1-3/31,2005	6.2	14.5	—	—	—	—	—	—	—	—	Eta/CMAQ	HO07
	NY	6/1-7/31,2005	4.4	13.6	—	—	—	—	—	—	—	—	Eta/CMAQ	HO07
	NY	7/1-9/30,2004		—	—	—	15.5	60.8 - 89.7	22.5- 53.7	24.3- 90.9	—	25.0- 55.0	Eta/CMAQ	HO07
	EUS	1/1-3/31, 6/1-7/31,2005 7/14-8/17, 2004		— 1.69	—	—	45.5	91.4 - 99.7	0-3.6	0- 44.7	—	N/A ^a , 96.2- 100	Eta/CMAQ 6-model ensemble ^a	HO07 MK07
	PN	8/1-11/30,2004	2.1-2.2	—	17-32	70-81	—	—	—	—	—	—	MM5/CMAQ	CH08
	E US eastern Texas NA NA NA NA NA NA S US	7/14-8/18,2004 8/31-10/12,2006 Summer 2008 Winter 2008 Summer 2009 Summer 2008 Winter 2008 Summer 2009 5/1-9/30,2009	-3.2 -1.3 -2.08 0.86 -0.70 0.69 -0.18 2.08 -0.6	8.8 5.5 12.8 14.1 12.9 13.5 15.9 13.6 5.9	-21.0 -5.6	41.2 37.0	— 31.5 16.5 15.5 45.5 15.0 15.0 15.0 15.0	— 78.0 99.5 70.7 - 76.2 77.5 - 83.2 82.2	— 20.6 0.0 8.0 20.6 0.0 22.3- 27.9 10.3- 21.3 14.8- 22.2	— 29.1 0.0 14 29.1 0.0 31.5- 36 15.3- 40.1 27.7- 38.3	— 0.7 1.9 0.6- 0.7 0.6- 1.3 0.7- 1.2	— 58.8 100.0 44.6- 56.7 68.3- 75.9 61.3- 76.6	Eta/CMAQ 7-model ensemble ^b GEM-CHRONOS GEM-CHRONOS GEM-CHRONOS GEM-MACH15 GEM-MACH15 GEM-MACH15 WRF/Chem- MADRID WRF/Chem- MADRID WRF/Chem- MADRID WRF/Chem-	YU08 DJ10 MA09 MA09 MA09 MA09 MA09 MA09 CH11 YA14 ZH16 YA14 ZH16

Pollutants	Area	Period	MB	RMSE	NMB (%)	NME (%)	Threshold	A (%)	CSI (%)	POD (%)	B	FAR (%)	Model	Reference
		5/1-9/30, 2009-2011 5/1-9/30, 2012-2014 winter, 2009-2012 winter, 2012-2015	0.1 – 5.2	4.9– 10.5	4.9 – 68.4	37.3 – 89.0		- 85.9 83.5 - 85.3	14.7- 17.1	25.5- 31.8	1.0- 1.2	72.1- 74.1	MADRID WRF/Chem- MADRID	
Hourly PM_{2.5}	E US	7/14- 8/18, 2004	-3.3	11.3	-21.1	51.4	—	—	—	—	—	—	Eta/CMAQ	YU08
	S US	5/1- 9/30, 2009	-0.6	8.3	-5.2	49.8	15.0	72.1	20.5	29.2	0.7	59.1	WRF/Chem- MADRID	CH11/12
24-h average PM₁₀	ME OS EU	March, June, July, 2001 11/01, 1999 – 04/30, 2000 Summer, 2004-2006 Winter, 2004-2006	-20.9 to 13.8 ^c -3.5 to -1.3 -5.7 to -1.5	37.9- 47.2 8.3-8.9 12.5- 14.3	-36.5 to 24 ^c					31-65		78-98	AAQFS MM5- AirQUIS PREV'AIR	MA01b BE02 HO08
	IP NE NE NE	6/19-7/12, 2006 2005 2004-2006 2004-2006	-29 -7 -13.2 -0.03 to -1.3	15.4 16.3 9.1-9.6			30.0 50.0 30.0 50.0	29.2 - 54.2 16.7 - 79.2 95.8 -100 70.8 - 95.8	15.0- 54.2 9.1- 16.7 - 95.2- 100 68.2- 83.3 8.3 44.5- 49.2	15.0- 54.2 9.1- 16.7 100.0 68.2- 83.3	0.5- 0.9 0.8- 0.9 0.9 0.9	0 0 0-4.8 0	MM5/CMAQ MM5/CMAQ/ DREAM LOTOS-EUROS LOTOS-EUROS With bias correction	JI08 MAN09

1. MB: Mean Bias; RMSE: Root Mean Square Error; NMB: Normalized Mean Bias; NME: Normalized Mean Error; A: Accuracy; CSI: Critical Success index; POD: Probability Of Detection; B: Bias; FAR: False Alarm Ratio.

2. The unit for MB, RSME, and threshold are kg m⁻³ for PM_{2.5}.

3. Superscripts **a**: the six models include: WRF/chem (36-km), WRF/chem. (12-km), CHRONOS, AURAMS, STEM-2K3, and Eta/CMAQ; **b**: the seven models include: WRF/chem-2 (27-km), WRF/chem-2 (12-km), CHRONOS, AURAMS, STEM-2K3, BAMS (15-km), and NMM/CMAQ; **c**: calculated based on data reported in this paper.
4. S US: Southeastern U.S.; E US: Eastern U.S., NE US: North-eastern U.S.; PN: Pacific Northwest; NY: New York State; EU: Europe; W EU: Western Europe; SE CA: Southeastern Canada; LP-S: La Plana, Spain; SP-B: São Paulo, Brazil; NIP: North-eastern Iberian Peninsula; IP: Iberian Peninsula; NA: North America; ME: Melbourne, Australia; OS: Oslo, Norway; NE: the Netherlands.
5. See a list of acronyms in the [appendix](#) for all model names
6. CH11: Chuang et al. (2011); MA01b: Manins (2001b); HO07: Hogrefe et al. (2007); MK07; McKeen et al. (2007); CH08: Chen et al. (2008); MA09: Makar et al. (2009); YU08: Yu et al. (2008); HO08: Honoré et al. (2008); BE02: Berge et al. (2002); JI08: Jiménez et al. (2008); MAN09: Manders et al. (2009); DJ10: Djalalova et al. (2010), YA14: Yahya et al. (2014), ZH16: Zhang et al. (2016).

Very few evaluations were conducted for PM components. McKeen et al. (2007) found that all six of the RT-AQF models significantly underpredicted OM at the surface and overestimated SO_4^{2-} above 2 km. The overpredictions in SO_4^{2-} were attributed to overestimates of SO_2 by WRF/Chem and CHRONOS and the inclusion of aqueous-phase oxidation of SO_2 by AURAMS, CMAQ/ETA, and STEM-2K3. Yu et al. (2007) reported that Eta/CMAQ overpredicted SO_4^{2-} due to too much in-cloud SO_2 oxidation as a result of overestimated H_2O_2 concentrations in the model, underpredicted NH_4^+ at the rural sites and aloft due to the exclusion of some sources of NH_3 in the real-time emission inventory, underpredicted NO_3^- due to overpredictions of SO_4^{2-} , and underpredicted OC due to missing sources of primary OC in the emissions inventory and missing secondary organic aerosol (SOA) formation from the gas-phase oxidation of isoprene and sesquiterpenes and aqueous-phase oxidation of glyoxal and methylglyoxal. Chen et al. (2008) reported that AIRPACT-3 reproduced OC well but significantly overpredicted EC and significantly underpredicted SO_4^{2-} , NO_3^- , and NH_4^+ , due to underestimations of emissions of primary PM species (e.g., sulfate) and precursors of secondary PM (e.g., SO_2 , NH_3 , and NO_x), insufficient spatial resolution, and the model's inability to capture the hourly PM variations. Zhang et al. (2014) showed an overall good performance of WRF/Chem-MADRID during 2012-2014 for $\text{PM}_{2.5}$ composition except for relatively larger biases for NH_4^+ against Speciation Trend Network (STN), EC against SEARCH, and OC against IMPROVE. They attributed these biases to the inaccurate primary PM emissions and the emissions of $\text{PM}_{2.5}$ precursors, as well as uncertainties in the spatial allocations of those emissions used in the simulations. For categorical evaluation of PM, some studies used threshold values of 15-31.5 $\mu\text{g m}^{-3}$ for 24-h average $\text{PM}_{2.5}$ and 30-50 $\mu\text{g m}^{-3}$ for 24-h average PM_{10} that are lower than the NAAQSs of 24-h average $\text{PM}_{2.5}$ of 35 $\mu\text{g m}^{-3}$ and 24-h average PM_{10} of 150 $\mu\text{g m}^{-3}$ for the same reason as mentioned previously. For 24-h average $\text{PM}_{2.5}$, A, CSI, POD, B, and FAR range from 60.8-99.7%, 0-53.7%, 0-90.9%, 0.7-1.9 $\mu\text{g m}^{-3}$, and 25-100%, respectively. Those for 24-h average PM_{10} range from 16.7-100%, 9.1-100%, 15.0-100%, 0.5-0.9 $\mu\text{g m}^{-3}$, and 0-4.8%, respectively. A categorical evaluation of hourly $\text{PM}_{2.5}$, was conducted only with WRF/Chem-MADRID, with A, CSI, POD, B, and FAR of 72.1%, 20.5%, 29.2%, 0.7 $\mu\text{g m}^{-3}$, and 59.1%, respectively.

10.2.2 CW-AQF Model Biases and Likely Causes

Several inaccuracies in RT-AQF and their possible causes have been reported in the literature. Factors related to meteorology include an inaccurate characterization of the transport (e.g., Eder et al., 2006; Yu et al., 2007, 2008) and planetary boundary layer (PBL) meteorological processes such as turbulent mechanisms and vertical convection, cloud attenuation of photolysis (e.g., Eder et al., 2006), local drainage and sea-breeze circulations (e.g., Hess et al., 2004; Honoré et al., 2008) and variables such as temperature, water vapor, inversion, and PBL heights (e.g., Berge et al., 2002; Hess et al., 2004; McKeen et al., 2007; Hogrefe et al., 2007). Factors related to boundary conditions include inadequate representations of boundary conditions of O_3 , $\text{PM}_{2.5}$, and PM_{10} (e.g., McKeen et al., 2005; Yu et al., 2007; Chen et al., 2008; Chuang et al., 2011). Factors related to emissions include uncertainties in anthropogenic emissions of SO_2 (e.g., McKeen et al., 2007), NO_x (e.g., McKeen et al., 2005, 2009), and VOCs (e.g., Shrivastava et al., 2010), NH_3 (e.g., McKeen et al., 2007; Yu et al., 2008; Chuang et al., 2011), biogenic VOC emissions (e.g., McKeen et al., 2005, 2007; Yu et al., 2008; Hu et al., 2008; Chuang et al., 2011; Yahya et al., 2014), wildfire emissions (e.g., Snow et al., 2003; McKeen et al., 2007; Chen et al., 2008; Yahya et al., 2014), primary PM (e.g., Berge et al., 2002; Manins et al., 2002; McKeen et al., 2007; Hogrefe et al., 2007; Manders et al., 2009; Shrivastava et al., 2010; Chuang et al., 2011; Zhang et al., 2016), dust (e.g., Jiménez-Guerrero et al., 2008), and pollen emissions (e.g., Sofiev et al., 2006). Factors related to model process treatments include inaccurate model treatments such as urban processes (Baklanov et al., 2002), gas-phase chemistry (e.g., Chen et al., 2008; Cai et al., 2008), in-cloud oxidation of SO_2 (Yu et al., 2008; Cai et al., 2008), SOA formation (McKeen et al., 2009; Shrivastava et al., 2010; Chuang et al., 2011), dry and wet deposition (McKeen et al., 2007; Hogrefe et al., 2007). A factor related to model configuration is the use of a coarse grid resolution (e.g., Cope et al., 2004).

These studies indicate a need for improvement regarding several aspects of RT-AQF. A number of methods and techniques have been developed to improve RT-AQF performance skills. Several methods that are commonly used to improve the forecasting skills of CW-AQF models including data fusion, data assimilation, and inverse modeling are introduced below.

10.3 Data Fusion

For air-quality (AQ) modeling there are nowadays a large number of relevant environmental datasets available. Most large urban areas have multiple air-quality measurement sites with real-time data accessibility. Simultaneously, there are several global-regional chemical-transport models that provide open-access data. After the introduction of affordable complementary air-quality sensors, the coverage of monitoring networks in urban areas can be increased substantially. For comprehensive predictions, however, fusion of information must be used to capture the highly variable nature of urban air quality in dispersion modeling and air-quality forecasting.

Air quality, especially in an urban landscape, has a strong temporal and spatial variability, which can make the interpretation and utilization of heterogeneous data difficult. Fortunately, the use of data-fusion algorithms makes it possible to assimilate data from multiple sensors and measurement stations with variable quality standards. Additionally, variable measurement heights can be taken into account, the spatial distribution of the available data in the area can be considered and the maturity of data points (older data) will have an effect on its assigned weighting. The methodology can also be used for modeled data as well; however, for modeled data points there are additional factors that must be taken into account.

10.3.1 Fusion with Unbiased Data

Practically all measured and modeled data used in AQ modeling, including meteorological data, are imprecise and the given values deviate around the actual value they are meant to describe. As an example, when two different measurement devices are installed to measure at the same location, the data from these measurements are not in total agreement; commonly the observed correlation of the two signals is affected by the price/quality difference of the equipment, and modeled data can have a very low correlation with respect to high quality measurement data. However, from a data-fusion point-of-view, high deviation and low correlation of data is not a major concern. In fact, data fusion with unbiased yet imprecise data with any number of data points is straightforward once the deviation of error for data points has been quantified.

One basis for a data-fusion algorithm is presented in Potempski and Galmarini (2009). The data fusion is done in a way that theoretically minimizes the expected mean squared error for fused information. For instance, the prediction of a model ensemble, which can be considered a special case of data fusion, will in most cases be of a better quality than the prediction of individual models, if specific assumptions about the statistical distribution of error and variance in the source data hold true.

Assuming all data sources to be independent and the estimators to be unbiased, an optimal fused value θ_F can be calculated according to Potempski and Galmarini (2009) as follows:

$$\theta_F = \sum_{i=1}^n w_i \theta_i, \quad (1)$$

here θ_i is the most recent datapoint from a data source i (e.g., a measurement station or a model) and w_i is the assigned weight for the data point. It is important to note that the data-fusion algorithm is always *with respect to a selected point of interest* (POI) in time and space and the selection of the POI affects not only the weight w_i but also which data points are selected for the fusion from data sources. As an example, since there is a requirement for independence for the data points, only one data point -- the temporally nearest one -- is taken from each source. For modeled data, which is commonly provided in gridded form, we simply use the temporally nearest layer of the grid and take the closest point from it with respect to

the POI. In this context we call θ_i an *estimator* for the fused value at the POI. Weights w_i in Eq. 1 are given by,

$$w_i = \frac{VAR[\varepsilon_i]^{-1}}{\sum_{i=1}^n VAR[\varepsilon_i]^{-1}} \quad (2)$$

where $VAR[\varepsilon_i]$ is the expected variance for data point θ_i error, taking into account the temporal and spatial distances to the POI as well as the data source's inherent quality. The assessment of $VAR[\varepsilon_i]$ can be done, for instance, by using empiric variograms as presented in Johansson et al. (2015).

10.3.2 Data Fusion with Biased Data

A general approach for data fusion allows very different types of data (e.g., model results, measurements, emission data, land use data). Although this in general is a strength in comparison to ordinary data-assimilation methods, this has also a price. Sources providing the data points in the data fusion can exhibit substantial bias terms, and the nature of the bias is always strongly related to the data source. The existence of bias in data fusion can be problematic and it is important to understand and classify possible sources of bias in the data. Here we classify a couple of different sources for bias and then proceed to solutions on how to deal with them in the data fusion. However, it is important to note that most of the bias classes discussed below are not 'bias' in its classical meaning, but biased with respect to a selected POI.

(1) Technological bias

It is not uncommon for a measurement device's capability to measure to be affected by underlying meteorological conditions, e.g., temperature or humidity. Alternatively, the measurement device could fail to capture local emission sources due to long averaging periods, or the device could simply be malfunctioning and require recalibration or maintenance. A similar kind of technological bias can be associated with AQ models that commonly have incomplete and coarse emission inventories and meteorological data at their disposal, and are forced to simplify complex physical and chemical processes due to computational limitations. This kind of bias, that is independent of the selection of POI, is what traditionally is meant by 'bias'.

(2) Resolution bias

Most air-quality models have native resolution of the order from several tens of meters to tens of kilometers and can thus completely fail to capture local phenomena in contrast to measured data. Therefore, the data points from such models can be biased with respect to a selected POI by their coarse resolution. Naturally this source of bias does not exist for measurement data.

(3) Environment bias

For pollutant concentrations, another important source of bias for any θ_i acting as an estimator for concentration in POI is the local environment. Quite simply, a pollutant concentration in one specific environment can be a poor estimate for concentration in another location due to local known emission sources, geography and buildings. Furthermore, differences in measurement (or modeling) height can cause bias in a similar manner. As an example, measurement devices can be installed on rooftops, and if the POI is set to ground level the bias due to this difference in measurement height must be dealt with.

(4) Local short-term/temporary bias

In some cases, there can be strong, local, and temporary phenomena that can affect measurements unexpectedly. As an example, there can be construction sites near the measurement location, street kitchens or small-scale private combustion activities nearby. In a data-fusion approach such as the one presented here, such phenomena are desired to be kept very local so that the bias of this kind does not propagate far from the measurement point's location.

10.3.3 Bias Correction and Weight Modification

In the case of data fusion with biased data, one can attempt to modify θ_i into an *unbiased estimator* for POI before computing Eqs. 1 and 2. In Johansson et al. (2015) this process has been described. Briefly, there is a master air-quality model (the authors use the FMI-ENFUSER) that classifies the data sources and the local environment in a way that the resolution bias and the environment bias can be identified and quantified. The master model provides the expected values in all estimator locations as well as the POI and based on the differences of expectancies and estimator values, all estimators are converted into non-biased ones. This approach has been observed to work well when the measured data originates from a heterogeneous set of environments (strong differences in local emission sources and measurement heights). For model data with resolution bias, the corrections can be performed in a similar manner once the expected values given by the master model have been adjusted to fit the model data's resolution and capabilities to capture local phenomena.

The data-fusion algorithm can further be refined with a modification that we call here the *penalty on disagreement* –modification, which targets specifically the technological bias and the local contemporary bias. In essence, the θ_F is computed for each θ_i while leaving θ_i out from the pool of used data. Then the sum of squared error ($\theta_{Fi} - \theta_i$)² (SSE) is computed by iterating over the data points. Finally, we assign penalties to each weight w_i in an iteration that seeks to minimize the SSE. Broadly speaking, this iteration assigns penalties to data point weights in such cases that a data point deviates from the “big picture” indicated by the rest of the data points; in cases where the deviation is strong (e.g., the data source is not working properly) its contribution to the fused product is effectively filtered out. Technically, for the iteration there are several possibilities: for example, a simple brute-force search can be used since the computation is relatively lightweight. Alternatively, a more sophisticated gradient descent approach (e.g., Nesteroy, 2004) could be used, in which incremental changes to the weights are made towards the direction that reduces the SSE the most until no more improvements can be made to the weights.

10.3.4 Examples and Resources

FMI_EnFuser provides an example of a model extending the traditional data fusion methods to cover a large set of available data relevant to air quality concentrations:

- local sensor network results
- local air quality model(s)
- regional air quality model(s)
- meteorological data
 - meteorological measurements, in addition to basic parameters, also e.g., mixing height estimates from ceilometers
 - data from meteorological (NWP) models
- satellite data (including SENTINEL-data)
- various GIS-datasets:
 - OSM-information

- o land-use/road network
- o terrain maps
- o population information
- o traffic volumes
- o emission information also directly/not only through model calculations

A key strength of the EnFuser system is the ability to fuse many complex types of information to generate high resolution air quality concentration fields. The concept has already been demonstrated in the Helsinki metropolitan area (starting in 2018 EnFuser produces the official air quality information - including forecast - for the Helsinki Metropolitan Area), and the next, much more challenging proof-of-concept target is Nanjing, China.

Similar developments with operative/official data-fusion modeling have been performed in Belgium, with the RIO modeling system (<http://www.irceline.be/en/documentation/models>). The spatial resolution of the RIO interpolation technique is $4 \times 4 \text{ km}^2$. RIO calculates the air quality every hour in all the $4 \times 4 \text{ km}^2$ grid cells in Belgium. The RIO method is used on the IRCEL website to show real-time air quality data. RIO is an intelligent interpolation technique in which the local influence per measuring site is removed first, in order to obtain a spatially homogenous dataset of air quality measurements.

The values received as such can then be interpolated via ordinary Kriging. The local character of a measuring site is determined by a statistical analysis of a long time series of concentrations at the measuring sites and the land use in the vicinity of the stations.

From this analysis it becomes clear that a robust correlation exists between land use and concentration levels. This correlation between the concentrations and the land use is summarized in trend functions. Because land use is known for all of Belgium, the local character of every place where an interpolation occurs can be taken into account. For the interpolation of $\text{PM}_{2.5}$ aerosol optical depth (AOD) was used in addition to land use for the determination of the local character.

The spatial resolution of the RIO interpolation technique is $4 \times 4 \text{ km}^2$. Using RIO, it is possible to calculate the air quality at every hour in all the $4 \times 4 \text{ km}^2$ grid cells in Belgium. The RIO method is used on the IRCEL website to show the real-time air quality data.

Most of the other existing methods dealing with model results and measurements fall (by our own definition) within the category of data assimilation (see next section). Additional examples of data fusion methods and systems for total atmospheric deposition can be found in the GAW Report No. 234 (WMO, 2017).

10.4 Data Assimilation

10.4.1 Background

Chemical Transport Models (CTMs) are used to predict the chemical composition of the atmosphere at urban, regional and global scales. These predictions are used for a variety of important applications including air quality management, estimating health and ecosystem impacts, and the management of solar energy production. Forecasts of air quality are being used more and more for public health applications and transportation management during severe pollution episodes, and to help improve weather forecasts. While our ability to predict air quality continues to improve, there are still significant uncertainties associated with: incomplete and/or inaccurate emissions information; lack of key measurements to impose initial and boundary conditions; missing science elements; and poorly parameterized processes.

Improvements in air quality predictions require better constraints using observational data. The close integration of observational data is essential in weather/climate analysis, and it is

accomplished by a mature experience/infrastructure in data assimilation – the process by which models use measurements to produce an optimal representation of the state of the atmosphere. (e.g. Marchuk, 1995; Kalnay, 2003; Navon, 2009; Lahoz et al., 2010). Borrowing on the experiences gained in data assimilation applications in numerical weather prediction, there are growing numbers of applications of atmospheric composition assimilation in air quality predictions (Bocquet et al., 2015).

Data assimilation combines information from three different sources: the physical and chemical governing equations (encapsulated in the model), the reality (as captured by the observations), and the current best estimate of the distribution of pollutants in the atmosphere (all with associated errors). As more chemical observations in the troposphere are becoming available, chemical data assimilation is expected to play an essential role in air quality forecasting, similar to the role it has in numerical weather prediction. For atmospheric applications, the objective of data assimilation is to obtain a better representation of the atmosphere in terms of meteorological and atmospheric composition variables. The goals of data assimilation in numerical weather prediction are to find the optimal initial conditions that produce the best forecast. In air quality applications, the impacts of the initial conditions on the prediction skill are often short-lived (typically less than 24 hours (Carmichael et al., 2008)). Emissions have a significant impact on the prediction skills. Therefore, atmospheric composition data assimilation applications have also included inverse modeling to improve emission rates (e.g., Elbern et al., 2007; Vira and Sofiev, 2012; Yumimoto et al., 2012). Chemical data assimilation is expected to play an essential role in air quality forecasting, similar to the role it has in numerical weather prediction. In addition to helping to improve forecasts of atmospheric composition, it has important uses in producing reanalyses of atmospheric composition (Borrego et al., 2015; OJEU, 2008).

Three-dimensional fields constrained by observations are needed to reduce uncertainties in estimates of impacts of air pollutants on human and ecosystem health (Gao et al., 2017) and to detect trends in atmospheric composition in response to conventions and policies aimed at reducing emissions. Furthermore, as air quality predictions rely heavily on meteorological predictions and the important impact that atmospheric composition (e.g., aerosols) can have on weather prediction (e.g., Saide et al., 2016), there is a growing interest in coupled chemistry meteorology models (CCMM), which simulate meteorology and atmospheric chemistry jointly (Zhang, 2008; Baklanov et al., 2014). Data assimilation in CCMMs is thus an active area of research. In spite of the availability of previous experience in data assimilation for meteorological modeling on the one hand and chemical transport modeling on the other hand, conducting data assimilation in CCMM can be challenging because of interactions among meteorological and chemical variables (Bocquet, et al., 2015; Baklanov et al., 2017; Hov, 2017).

10.4.2 *Summary of Data Assimilation Methods*

Data assimilation fuses information from priors (encapsulating our current knowledge of quantities of interest such as the atmospheric composition and its sources and sinks, chemical reaction rates, and other model parameters), computational models (encapsulating our knowledge about the physical laws that govern the evolution of the atmospheric composition), and measurements (sparse, noisy snapshots of tracer distribution), all with their associated uncertainties. Based on this information data assimilation computes a best estimate (in a statistically rigorous sense) of the quantities of interest.

The data assimilation problem is formulated in a Bayesian framework (Sandu et al., 2011). The analysis probability density is the probability density of the quantities of interest conditioned by all the available observations. Two approaches to solving data assimilation have gained wide popularity: variational methods (Penenko and Obraztsov (1976), rooted in control theory), and ensemble-based methods (rooted in statistical estimation theory). Under certain commonly posited assumptions, these solutions are mathematically equivalent. Practical data assimilation approaches can be classified as filters (where the analysis is conditioned by all prior observations) and smoothers (where the solution is conditioned by all past and future observations in a certain time window). In earlier applications, optimal interpolation, a filtering

method that seeks to determine “optimal” weights for priors and observations, was often employed. Direct bias correction methods, as described in Section 10.3, are also frequently applied.

In a variational approach the “best estimate” of the quantity of interest is considered to be a maximum likelihood solution of the posterior probability density. It is computed by minimizing a cost function that represents the negative logarithm of the posterior pdf. In operational practices the errors are assumed to be Gaussian, and consequently the cost function minimization leads to a least squares problem. To impose bounds on a solution (e.g., to assure non-negative tracer concentration or geostrophic balance) penalty terms can be included in the cost function. Also, model error can be accounted for (weak constraint).

In the variational filtering approach, named 3D-Var, the cost function does not allow time variation of model errors and observations are clustered in the middle of the assimilation window. First guess at appropriate time extends this approach to calculate innovations from priors and observations that are matched in time. Model error covariances are static, usually represented in terms of zonally-dependent standard deviation and spatial scales and are determined heuristically and tuned seasonally in operational implementations. The minimization methods often rely on the Gauss-Newton algorithm and incremental approach for linear inner and non-linear outer loops (Courtier et al., 1994).

The variational smoothing approach, named 4D-Var, minimizes the cost function over both space and time. Because of the time dimension, the procedure to obtain the analysis traditionally requires the use of tangent-linear and adjoint models so that the minimization spans the model trajectory within the assimilation window. The construction and upkeep of these models is highly labor-intensive, and specialized tools to assist in their development are available (Sandu et al., 2010). Another level of complexity is brought by the different mathematical properties of different types of adjoint models (Gou et al., 2011), and by different approximations that can be employed in practice (Singh et al., 2012). Only at the beginning of the iteration process are model error covariances prescribed, but they depend on the model state afterwards. Elbern and collaborators (Elbern and Schmidt 1999, 2001; Elbern et al., 2007) and Carmichael and collaborators (Chai et al., 2006; Chai et al., 2007; Carmichael et al., 2008) describe applications of variational methods in chemical data assimilation. 4D-Var data assimilation can also be achieved without an adjoint model by restricting the analysis to consider only a small number of parameters (usually emissions scaling factors across large spatial domains, e.g., Park et al., 2013) or using other approaches such as tagging to track emissions' influences (Saide et al., 2015).

Because of the high dimensionality of the data assimilation problem for the atmosphere, ensemble-based methods employ a Monte Carlo approach to advancing the error covariance during a forecast. Evensen (1994) introduced the ensemble Kalman filter (EnKF), and since then, multiple variants have been proposed (Houtekamer and Mitchell 2001; Whitaker and Hamill 2002; Anderson 2003; Zupanski 2005). Ensemble members may use different initial and boundary conditions and account in varying ways for deficiencies of model components (e.g., a numerical scheme or physical parameterizations). For each member, increments to the prior are obtained by matrix algebra (scaled innovations multiplied by Kalman gain) rather than in an iterative process. Consensus analysis is usually obtained as an average of the member analyses. Availability of multiple analyses provides a characterization of posterior uncertainty. The quality of the analysis is quantified by the spread of the ensemble, which relates to the actual error of a model. Inherent deficiency of ensemble Kalman filtering derives from the limited number of realizations and, consequently, large sampling errors. This can lead to a diminished impact of observations and divergence of the analysis from reality. To prevent filter divergence, constraints on covariances can be imposed (localization) and/or covariances can be inflated (additive or multiplicative). Constraints on the solutions are more difficult to impose compared to variational methods. Examples of applications of ensemble methods for chemical data assimilation include Constantinescu et al. (2007 a, b, and c, 2011).

Hybrid methods (Lorenc, 2003) combine static and ensemble covariances and re-center ensemble mean on the control analysis that is obtained by variational methods (e.g., Schwartz

et al., 2014). Buenher (2010 a and b) documented that model error covariances derived from an ensemble can be used within a minimization procedure similar to 4D-Var and provide skill comparable to the assimilation that requires tangent-linear and adjoint models. Error subspace approaches seek to combine 4D-Var and EnKF at a fundamental level; these include the construction of 4D-Var analysis error covariances (Cheng et al., 2010) and the use of 4D-Var as a look-ahead mechanism for EnKF (Sandu et al., 2015).

10.4.3 *Special Considerations Specific to Chemical Data Assimilation*

There are several aspects that need to be taken into consideration when building and employing a chemical data assimilation system. Some of them are described below.

Dynamics. The properties of the dynamics of the forecast model have an impact on the efficiency of data assimilation methods. Whereas meteorological models are chaotic, and as such characterized by critical unstable directions, the transport and chemistry of atmospheric constituents are mostly stable. Yet, chemical models can exhibit significant nonlinearities. Moreover, compared to meteorological models, the constituents' dynamics, physics, and chemistry as well as the many input parameters are much more uncertain, yielding significant model errors. As a consequence, the performance of classical data assimilation schemes (EnKF, 3D-Var, and 4D-Var) in atmospheric chemistry is not driven by the same mechanisms as in meteorological data assimilation. The strong stability of chemical kinetics causes ensemble filtering methods to be prone to divergence, unless special precautions are taken (Constantinescu et al., 2007). For instance, smoothing (e.g., 4D-Var) is primarily of interest in atmospheric chemistry for a consistent parameter estimation within a time frame, whereas it is mainly of interest in meteorological data assimilation for estimating the initial condition on the unstable manifold (Haussaire and Bocquet, 2016).

Background error covariances. Their estimation typically depends on the type of data assimilation used. While they are estimated from the ensemble perturbations in ensemble-based methods (e.g., Miyazaki et al., 2012), they are generally static in variational methods and implemented by assuming horizontal and vertical correlation lengths. These lengths can be computed with methods such as comparing the differences between 24-h and 48-h forecasts valid at the same time (e.g., Liu et al., 2011; Inness et al., 2013). Techniques proposed to construct error covariances in air quality assimilation include autoregressive models (Constantinescu et al., 2007d), tensor products (Singh et al., 2011), and subspace approaches (Cheng et al., 2010). Tools such as GEN_BE (Descombes et al., 2015) are available to the community to perform these computations.

(1) Multiple species and size

The data assimilated usually observes a few key gas and aerosol species, while multiple species remain unobserved. However, due the chemical interactions and co-emission between these multiple species, chemical data assimilation systems can assume co-variations between species in order to expand the constraints. Multiple methods have been used to determine the cross-correlation between species including expert knowledge or ad-hoc procedures (Elbern and Schmidt, 1999) and the use of ensembles (Arellano et al., 2010; Miyazaki et al., 2012). Another strategy is not to assume cross-variation (Inness et al., 2013). An added difficulty is that the spatial correlation lengths depend on the chemical lifetimes, and are therefore different for different species (Constantinescu et al., 2007c). For data assimilation of aerosols, depending on the aerosol model used there could be multiple aerosol size bins resolved by the model, in which case cross-correlation between aerosol sizes can also be prescribed (Saide et al., 2013). These difficulties explain how delicate it is to specify background covariances for multi species models (see previous point).

(2) Verification

Chemical data assimilation systems can be verified in multiple ways. One way used in the development stage is to perform an Observing System Simulation Experiment (OSSE), consisting of the generation of synthetic observations based on model simulations and then try to recover the reference fields using data assimilation (e.g., Barré et al., 2016; Messina et al., 2011). The observing system simulation experiments (OSSEs) can also be useful in the planning stage of new observing systems to show their value when added to the already existent observations (e.g., Zoogman et al., 2014; Bousserez et al., 2016). Another strategy consists of evaluating the reanalysis and/or forecast to observations not assimilated and compare that to the evaluation of a control run. Some options for the control run include a simulation without data assimilation (e.g., Miyazaki et al., 2012), and a simulation including data assimilation of a reduced set of observations (e.g., Saide et al., 2014) or using a different data assimilation method (Schwartz et al., 2014). For reanalyses, observations used for evaluation can include data that are not collected regularly such as that from field campaigns and data that their impact in assimilation is not expected to be large, such as infrequent soundings and satellite retrievals with coarser resolution, larger uncertainties, and/or reduced spatial coverage (Arellano et al., 2010; Miyazaki et al., 2012; Randles et al., 2017). For forecasts, observations used for evaluation can also include those not yet assimilated (Saide et al., 2013). Refer to Chapter 9 of this guide for a description of evaluation metrics that can be used.

(3) Constraining concentrations and emissions simultaneously

Air quality predictions are highly influenced by the emission forcing, which explains why improvements due to data assimilation can rapidly diminish within 1-2 days of forecasts (e.g., Schwartz et al., 2012; Carmichael et al., 2008). Applications have been developed to simultaneously constrain the concentrations and emissions, which are generally only possible with advanced data assimilation methods such as 4D-VAR (Elbern et al., 2007; Vira and Sofiev, 2012) or ensemble methods (Miyazaki et al., 2016). Refer to Section 10.5 for additional information on the inverse modeling of emissions. The joint data assimilation of atmospheric dynamics, tracer concentrations, and sources and sinks, remains an important research goal, likely to be facilitated by the high density of chemical constituent measurements afforded by upcoming geostationary remote sensing instruments (Liu et al., 2017).

10.4.4 Considerations on Observations Assimilated

Although chemical data assimilation is a relatively recent branch of assimilation, the rapid development of models to predict air quality and pollution at regional and global scales in the last 15 years has prompted the development of related analysis systems which are sustained by a wealth of observations from current space-borne instruments and ground-based networks. Observations currently assimilated in aerosol forecast models include AOD at 550 nm from satellite images (e.g., Zhang et al., 2008; Benedetti et al., 2009; Rubin et al., 2016; Di Tomaso, 2017) and ground-based sun photometers (Rubin et al., 2017), aerosol reflectance (Randles et al., 2017), backscatter from space-borne lidars (Sekiyama et al., 2010) and PM from air quality networks in regional models (i.e., Tombette et al., 2009). A detailed list of remote sensing observations is reported in Table 10.3. Observations of chemical compounds include total column, partial column and profile retrievals for the major gases such as ozone, NO₂, CO, SO₂, formaldehyde as well as column averaged concentrations of the greenhouse gases CO₂ and CH₄ retrieved from various sensors (see Table 10.4 for a full overview). Many of these observations are available in near-real time (NRT), i.e., within 3 hours of the measurements. For reanalyses, reprocessed data sets are used to ensure consistency of the data over longer time periods.

Observation operators vary from simple interpolation for data related to surface concentrations or PM to more complex neural network systems to derive AOD from aerosol reflectances. The operator for AOD often makes use of pre-computed lookup tables of aerosol optical properties to calculate extinction at the given wavelength and from its integral over the vertical column, the AOD. Visible reflectances can be assimilated directly via the use of a radiative transfer

model coupled with a surface reflectance model (Weaver et al., 2007) or can be treated to derive for example AOD. The lidar backscatter operator, similarly to AOD, can be based on a lookup table approach in which the backscatter coefficient for the various aerosol species is tabulated and used during the model run. The aerosol optical properties are usually computed using the Mie approach for spherical particles, but more sophisticated operators also account for non-sphericity of certain species, such as dust (Colarco et al., 2014).

For chemical compounds, the simplest operator is an integration over the total or partial columns or direct insertion of concentration profiles. To exploit the data to their full potential the averaging kernels of the retrievals should be used in the observation operators (e.g., Miyazaki et al., 2012).

Given the complexity of current aerosol/chemical models with several tracers, chemical data assimilation often suffers from under-determination. For example, AOD only provides information on the 2-D distribution of the total aerosols and does not contain information on the vertical distribution of the aerosol concentrations for each species modeled. Any redistribution of the information coming from AOD into the individual aerosol species is hence largely determined by the model. For reactive gases, it is also complicated because observations often do not have large sensitivity to the lower troposphere where the bulk of the pollutants reside and there is not enough vertically resolved information in the data that are often total or partial columns. Therefore, the vertical distribution of analysis increments depends strongly on the model's background error standard deviation profiles. A further complication for reactive gases is that, depending on the lifetime of the gas, the assimilation will have little impact if only the initial conditions are corrected and that more benefit could be derived from adding emissions to the control vector and correcting those. Furthermore, many retrievals that are currently used come from LEO satellites and are based on UV/VIS sensors. They do not give information during the night, including the polar night and also do not capture the daily cycle. Exceptions here are MOPITT, IASI, MLS and MIPAS. Fields of pollutants can vary over several orders of magnitude (e.g. volcanic plumes, dust storms) and data are needed to resolve such features adequately. The recently-launched S5P satellite which has a horizontal resolution of 7 km × 3.5 km will help to better resolve such features and after the launch of the constellation of geostationary satellites covering Europe (S4), North America (TEMPO) and East Asia (GEMS) planned for 2019-2022 there will also be hourly temporal coverage providing information about atmospheric composition.

Finally, not all observations are equally valuable for constraining the models. Techniques for determining information content and data impact in the context of chemical data assimilation have been proposed (Cioaca et al., 2013; Sandu et al., 2013).

Table 10.3 Aerosol remote-sensing observations

Type of observation	Platform	Sensor	Name of product	Provider	Reference
Aerosol Optical Depth at 550nm	Terra/Aqua	MODIS	Dark Target/Deep Blue	NASA/LANCE (https://earthdata.nasa.gov/earth-observation-data/near-real-time)	Levy, R. C., et al., 2018: The Collection 6 MODIS aerosol products over land and ocean. Atmospheric Measurement Techniques, vol. 6, no. 11, 2013, p. 2989
Aerosol Optical Depth at 550nm	Metop-A/Metop-B	GOME-2/AVHRR/IASI	Polar Multi-sensor Aerosol properties product (PMAp)	EUMETSAT	Polar Multi-Sensor Aerosol Product: User Guide, available at https://www.eumetsat.int/website/home/Data/TechnicalDocuments/index.html
Aerosol Reflectance	Terra/Aqua	MODIS		NASA	See Levy et al, 2018
Aerosol index	Aura	OMI		NASA	OMI Data User's Guide, available at https://disc.gsfc.nasa.gov/datasets/OMTO3d_V003/summary
Lidar backscatter	CALIPSO	CALIOP		NASA	CALIPSO Data User Guide, available at: https://www-calipso.larc.nasa.gov/resources/calipso_users_guide/
Aerosol Optical Depth at 550nm	Envisat	AATSR		ESA, CCI (Swansea)	Popp, T et al, 2016: Development, Production and Evaluation of Aerosol Climate Data Records from European Satellite Observations (Aerosol_cci). Remote Sens. 2016, 8, 421.
Aerosol Optical Depth at 550nm	COMS, H8	GOCI, AHI		Yonsei University, JMA	Choi et al, 2018: GOCI Yonsei aerosol retrieval version 2 products: An improved algorithm and error analysis with uncertainty estimation from 5-year validation over East Asia. Atmospheric Measurement Techniques. 11. 385-408. 10.5194/amt-11-385-2018. http://www.eorc.jaxa.jp/tree/userguide.html
Aerosol Optical Depth at 550nm	S-NPP, GOES-R	VIIRS, ABI		NOAA	Jackson et al, 2013: Suomi-NPP VIIRS aerosol algorithms and data products. Journal of Geophysical Research: Atmospheres. 118. 10.1002/2013JD020449. https://www.goes-r.gov/products/RIMPs/RIMP_ABI-L2_AOD_v1.0.pdf

Table 10.4 Reactive and GHG remote sensing retrievals. TC: Total column, TRC: Tropospheric column, PROF: profiles, PC: Partial columns, ColAv: Column average mixing ratio

Type of observation	Platform	Sensor	Product type	Data provider	Reference
O ₃	Envisat	SCIAMACHY	TC	ESA, CCI (BIRA)	http://www.esa-ozone-cci.org/
O ₃	Envisat	MIPAS	PROF	ESA, CCI (KIT)	von Clarmann et al. (2003, 2009)
O ₃	Aura	MLS	PROF	NASA	Froidevaux et al. (2008)
O ₃	Aura	OMI	TC	KNMI/NASA	Liu et al. (2010)
O ₃	Metop-A	GOME-2	TC	ESA, CCI (BIRA) AC SAF	http://www.esa-ozone-cci.org/ ; Hassinen et al. (2016)
O ₃	Metop-B	GOME-2	TC	ESA, CCI (BIRA) AC SAF	http://www.esa-ozone-cci.org/ ; Hassinen et al. (2016)
O ₃	NOAA-14	SBUV/2	PC	NASA	Bhartia et al. (1996)
O ₃	NOAA-16	SBUV/2	PC	NASA	Bhartia et al. (1996)
O ₃	NOAA-17	SBUV/2	PC	NASA	Bhartia et al. (1996)
O ₃	NOAA-18	SBUV/2	PC	NASA	Bhartia et al. (1996)
O ₃	NOAA-19	SBUV/2	PC	NASA	Bhartia et al. (1996)
O ₃	SNPP	OMPS	PC	NOAA/Eumetsat	https://ozoneaq.gsfc.nasa.gov/omps/
O ₃	S5P	TROPOMI	TC	DLR	http://www.tropomi.eu/data-products
CO	Terra	MOPITT	TC (TIR)	NCAR	https://www2.acom.ucar.edu/mopitt Deeter et al. (2017)
CO	Metop-A and Metop-B	IASI	TC	LATMOS/ULB	George et al. (2009); Clerbaux et al. (2009)
CO	S5P	TROPOMI	TC	SRON	Borsdorff et al. (2018) http://www.tropomi.eu/data-products
NO ₂	Envisat	SCIAMACHY	TRC	KNMI	Boersma et al. (2004)
NO ₂	Aura	OMI	TRC	KNMI	Vlemmix et al. (2010)

Type of observation	Platform	Sensor	Product type	Data provider	Reference
NO ₂	Metop-A and Metop-B	GOME-2	TRC	AC SAF, GDP4.8 NRT	https://acsaf.org/index.html Hassinen et al. (2016)
NO ₂	S5P	TROPOMI	TRC	KNMI	http://www.tropomi.eu/data-products
SO ₂	Envisat	SCIAMACHY	TC	KNMI	Lee et al. (2008)
SO ₂	Aura	OMI	TC	NASA	Yang et al. (2007)
SO ₂	Metop-A and Metop-B	GOME-2	TC	AC-SAF (DLR)	https://acsaf.org/index.html Hassinen et al. (2016)
CO ₂	Envisat	SCIAMACHY	CoIAv	ESA CCI (Bremen)	http://www.esa-ghg-cci.org/sites/default/files/documents/public/documents/GHG-CCI_DATA.html
CO ₂	Metop-A and Metop-B	IASI	CoIAv	LMD v8.0	Crevoisier et al. (2009a)
CO ₂	GOSAT	Tanso	CoIAv	ESA CCI (SRON)	http://www.esa-ghg-cci.org/sites/default/files/documents/public/documents/GHG-CCI_DATA.html
CH ₄	Envisat	SCIAMACHY	CoIAv	ESA CCI (SRON)	http://www.esa-ghg-cci.org/sites/default/files/documents/public/documents/GHG-CCI_DATA.html
CH ₄	Metop-A and Metop-B	IASI	CoIAv	LMD	Crevoisier et al. (2009b)
CH ₄	GOSAT	Tanso	CoIAv	ESA CCI (SRON)	Butz et al. (2010)
CH ₄	S5P	TROPOMI	CoIAv	SRON	http://www.tropomi.eu/data-products

10.4.5 Examples and Resources

Multiple institutions provide reanalysis and forecasting products that have been initialized using data assimilation. Some examples include some of the models described in Tables 3.1 and 3.2, including the Copernicus Atmosphere Monitoring System (CAMS, <https://atmosphere.copernicus.eu/>), GEOS-5 forecasts and MERRA reanalysis from NASA GMAO (<https://gmao.gsfc.nasa.gov/>), NAAPS forecasts provided by NRL (<https://www.nrlmry.navy.mil/aerosol/>) and RAQMS forecasts provided by NOAA/NESDIS/STAR (<http://raqms-ops.ssec.wisc.edu/>).

There are several tools publicly available to the community to perform data assimilation. Some of them include the Gridpoint Statistical Interpolation (GSI) system (<https://dtcenter.org/com-GSI/users/index.php>) that is a variational data assimilation tool originally developed for meteorological applications but that has been extended to air quality (Pagowski et al., 2014), the Data Assimilation Research Testbed (DART, <https://www.image.ucar.edu/DAReS/DART/>) that is a community facility for ensemble data assimilation supporting many models, and the Polyphemus air quality modeling system (<http://cerea.enpc.fr/polyphemus/>) which implements multiple variational and ensemble methods for performing data assimilation.

10.5 Inverse Modeling using Data Assimilation

10.5.1 Background

Inverse modeling is a name used by the atmospheric chemistry community for the process of estimating key parameters of an atmospheric chemistry transport model or its input, such as pollutant emissions. In particular, the goal is not to forecast atmospheric species concentrations, but rather to estimate model parameters or input data for their own sake or with the goal to improve the model. Joint parameter and state variable estimation is nonetheless possible. This is especially important in atmospheric data assimilation since the models depend on many key physical and statistical parameters, much more than dynamical models of the atmosphere or the ocean. Typical parameters are kinetic constants, deposition parameters, etc. Estimation of the emission fluxes, or boundary conditions for regional models, also fall within the scope of inverse modeling.

Most of the techniques used for inverse modeling in atmospheric chemistry are borrowed from data assimilation, even though the focus is different. They also borrow from the pioneering solid Earth community (e.g., Tarantola, 2005) where state variables coincide with non-observable parameters, from techniques developed in the mathematics of inverse problems (Groetsch, 1993), and from the remote sensing community, where retrieval of information from radiances is considered an inverse problem (e.g., Rodgers, 2000)

A key difference between inversion problems and forecasting problems is the source of prior information on parameters. Forecasting data assimilation routines always rely on a previous forecast, whereas most inverse modeling constraints on parameters must rely on some external expertise (e.g., uncertainty of the emission inventories). Hence, regularization techniques of the inverse problems, which correct and balance prior information in the analysis, are key to the quality of the inversions. They have been one of the weakest point of most inverse modeling studies, questioning their reliability for many years, although continued research on the use and understanding of regularization techniques (e.g., Bocquet, 2014; Bousserrez and Henze, 2018) may improve their utility.

The estimation of greenhouse gas emissions and sinks using inverse modeling techniques, at global, mesoscale, and down to urban scales, has become a huge subject with a large community, where emissions themselves are the primary object of the studies. For point sources such as in accidental atmospheric releases, the problem is often called a source term estimation. These techniques have now been applied to many other species such as dust, aerosols and aerosol precursors, ozone precursors, carbon monoxide, radionuclides, volatile organic compounds, wildfire emission, volcanic emissions, etc.

10.5.2 Summary of Inverse Modeling Methods

There are many approaches to solving inverse problems in the field of air quality (Bocquet, 2014; Brasseur and Jacob, 2017). Many have been adapted specifically for constraining emissions and fluxes of atmospheric constituents, which is the most common objective of inverse modeling in this field. Such emission estimates are often referred to as “top-down” (in contrast to “bottom-up” emission inventories derived from detailed accounting of emissions’ processes and activities). Inverse methods range in complexity from simple statistical relationships to application of air quality models and sophisticated optimization and estimation algorithms. The choice of method is often heavily influenced by the available computational resources and type of data, from sparse in situ monitoring or data-rich yet spatially localized field campaigns, to spatially more comprehensive yet indirect measurements of concentrations from satellite-based remote sensing instrument.

One of the simplest inverse modeling methods is the mass-balance approach. When used with data from a field campaign (primarily with aircraft measurements), observations upwind are used to determine background concentrations and extensive measurements are made downwind of sources under meteorologically steady conditions. Changes in concentrations detected above background levels are then translated directly into emission estimates using mass closure, without the use of statistical relationships or atmospheric models (e.g., Peischl et al., 2015). When the mass-balance method is applied to satellite data, a model is used to simulate the column concentrations derived from the satellite measurements; the ratio of the simulated to observed column is used to estimate adjustments to the model’s bottom-up emissions. This approach requires model grid cells that are larger than the smearing length (distance over which a species is transported, accounting for wind speed and atmospheric residence time) of the species being inverted (Palmer et al., 2003; Martin et al., 2003; Turner et al., 2015), yet it is computationally expedient and can be applied incrementally and iteratively to reduce errors associated with smearing (Cooper et al., 2017).

Atmospheric chemistry models may also be used to more directly relate emissions (or other parameters) to estimated observations. This relationship, often referred to as the Jacobian, is utilized in several inverse modeling methods. These methods may be distinguished based on how this Jacobian is calculated. For a small number of variable parameters, these relationships are often evaluated through several simulations wherein each parameter is perturbed individually; these methods are thus often used when working with sparse networks of in situ observations that only contain enough information to adjust a small (<100) number of parameters (e.g., Park et al., 2003; Fu et al., 2012). A tangent linear model can be used for increased computational efficiency (e.g., Mendoza-Dominguez and Russell, 2000). For a small number of observations but a large number of parameters, Lagrangian back-trajectory models can be used to quantify the “emissions footprint” of each measurement; this method is thus often applied to aircraft or timeseries measurements for species that can be treated as chemically conservative over the time period being simulated (Brioude et al., 2012; de Foy et al., 2014). For models that can very quickly be run several thousand times, approaches such as Markov Chain Monte Carlo methods for calculating solutions as probability distributions become computationally tractable (e.g., DelleMonache et al., 2008).

For inverse problems that involve both a large number of measurements and variable parameters, the challenges and methods become very similar or even identical to the DA methods described in Section 10.4.2. The difference between their use for inverse modeling compared to data assimilation is primarily in terms of the result of interest – for inverse modeling, the objective is to obtain improved estimates of the variable parameters, rather than making an improved simulation or forecast with these parameters. Often, as discussed in the previous section, the parameters of interest from the perspective of inverse modeling are separate from those of data assimilation (i.e., an emphasis on emissions, rather than initial conditions). While DA methods such as ensemble and variational techniques may again be applied directly to estimating sources, methodological differences arise in terms of assimilation windows and error propagation. For example, Wells et al. (2018) used 4D-Var to estimate N₂O emissions with a year-long assimilation window; in contrast, DA methods for air quality forecasting typically use assimilation windows of 24h or less (Vira and Sofiev, 2012, 2015).

Longer assimilation windows allow for the maximization of the influence of the source terms on the state estimates. The goals of inverse modeling and state estimation can be combined through augmented state vectors, wherein the typical goals of data assimilation (improved concentration) and inverse modeling (improved emissions) are achieved simultaneously (e.g., Penenko et al., 2012; Vira and Sofiev, 2012; Liu et al., 2017; Miyazaki et al., 2017).

Another difference when using DA methods for emission estimates is that variable parameters are not propagated forwards in time by the prediction model itself; prior information about these parameters is thus drawn from outside sources of information, other models, or adjusted using statistical regularization techniques. Geostatistical inverse modeling avoids the use of prior emission estimates through application of proxy data to evaluate spatial and temporal correlations (Michalak et al., 2004). Hierarchical Bayesian inversions have been developed to include estimation of error characteristics as part of the inversion itself (e.g., Ganesan et al., 2014).

10.5.3 *Special Considerations Specific to Inverse Modeling*

The following specific aspects need to be considered when developing and using inverse modeling systems:

(1) Evaluation of emissions

The vast majority of inverse problems are ill-posed. One of the consequences is that comparatively small uncertainties in the model or observational data can be amplified by the inversion and lead to a degradation of the constrained emissions compared to the initial ones. It is therefore imperative to evaluate the inversion results. In a similar way as described in Section 10.3.3, OSSES could be used to test the system in the development stage by comparing the constrained emissions with the ones used to drive the model from where the synthetic observations are sampled (e.g., Meirink et al., 2006). Also, some part of observations can be withheld from the inversion computations and used to compare the skill of a simulation driven by the updated emissions versus that of the simulation driven by the a-priori emissions (e.g., Kopacz et al., 2010). As emissions should be model-independent, a more rigorous approach consists of switching the model when performing the test just described (e.g., Chen et al., 2018). Other tests consist of comparing the optimized emissions to emission estimates other than the a-priori one (e.g., Zhang et al., 2018; Davoine and Bocquet, 2007).

(2) Non-Gaussianity

This refers to changing the cost function from the typical normal distribution assumption to a different one. In inverse modeling of atmospheric composition this is typically performed when the distribution of the prior is non-Gaussian, for instance, when emissions are positive or when the emissions values can differ by several orders of magnitude. The most frequent approach used consists of using log-normal statistics (e.g., Fletcher and Zupanski, 2006; Henze et al., 2009; Saide et al., 2015), which can be interpreted as optimizing for scaling factors applied over the prior emissions. Other approaches consist of using other distributions such as uniform, Poisson or Bernoulli (Bocquet, 2005). An in-depth analysis on the subject is provided by Bocquet et al. (2010). Non-Gaussianity can also be considered for the observational error term (Fletcher and Zupanski, 2006)

(3) Emission error covariance matrix

Many studies estimate emissions errors based on expert judgement, which is usually applied as a percentage of the emission quantity. On top of these estimates, there are usually regularization parameters in the variational methods (e.g., Henze et al., 2009; Saide et al., 2015) or inflation factors in ensemble method (Miyazaki et al., 2012a) that are applied to balance the emission and observation terms of the cost function. These factors can be selected by expert knowledge or trial and error, or through the use of more objective criteria for selection (Wu et al., 2013), such as L-curve, chi-square, maximum likelihood estimation, expectation-maximization (Michalak et al., 2005; Davoine and Bocquet, 2007; Liu et al., 2017) or minimizing the total error (Henze et al., 2009).

(4) Dimension reduction and information content of inversions

Emissions typically have spatial and temporal distributions that are too fine to recover via an inversion methodology due to the sparsity of the observation system. In such cases, the spatial and/or temporal resolution needs to be coarsened (i.e., its dimensions need to be reduced) when performing the inversion, which in turn can lead to aggregation errors (Kaminski et al., 2001; Bocquet et al., 2011; Wu et al., 2011; Turner and Jacob, 2015). Other reasons for coarsening the emissions being constrained include being able to treat the emissions error covariance matrix explicitly (Bousserez and Henze, 2018), being able to derive an analytical solution to the inverse problem (Turner and Jacob, 2015), and to overcome computational limitations for inversion methodologies based on computing brute-force sensitivities (Saide et al., 2015). Multiple methods exist for reducing the dimensionality going from expert knowledge, ad-hoc criteria or trial and error, to more sophisticated methods such as clustering using principal component analysis, using a Gaussian mixture model (Turner and Jacob, 2015), applying an optimality criteria on the grid (Bocquet and Wu, 2011), or maximizing the information content of the inversion (Bocquet et al., 2011; Bousserez and Henze, 2018).

(5) Constraining emissions and concentrations simultaneously

While errors in the emissions can be used to explain part of the misfits between model and observations, other issues could exist including misrepresentation of atmospheric transport, removal processes, or chemical transformation. A way to account for such errors is to include constraints on the three-dimensional concentrations in the inversion methodology (Miyazaki et al., 2012b), which has been shown to improve results compared to only constraining emissions (Elbern et al., 2007). Another approach is to explicitly treat model error in the inversion (the so-called weak-constraint formulation). Refer to Section 10.4 for additional information on chemical data assimilation.

10.5.4 Examples and Resources

Multiple systems provide greenhouse gas surface flux inversions allowing the monitoring of the evolution in time of these fluxes. Some examples include the Copernicus Atmosphere Monitoring Service (<http://atmosphere.copernicus.eu>) and the CarbonTracker systems (<https://www.esrl.noaa.gov/gmd/ccgg/carbontracker/>, <http://www.carbontracker.eu/>).

A dedicated effort towards estimating poorly known emissions over the globe and, in particular, in Africa and Asia, were undertaken within the GlobEmission project of the European Space Agency (<http://www.globemission.eu/>). Building on GlobEmission technology, MarcoPolo and Panda projects provided the more detailed estimates for China (<http://www.marcopolo-panda.eu>). The obtained top-down emission estimates are publicly available and will be updated in the follow-up efforts (see <http://airqast.com>).

There are multiple tools available to the community for performing emission inversions, some of them are listed below.

- The GEOS-Chem (http://wiki.seas.harvard.edu/geos-chem/index.php/Main_Page) and GEOS-Chem adjoint (http://wiki.seas.harvard.edu/geos-chem/index.php/GEOS-Chem_Adjoint) are used to perform global to regions variational inversions.
- The Data Assimilation Research Testbed (DART, <https://www.image.ucar.edu/DARes/DART/>) is a community facility for ensemble data assimilation supporting many models that has been used to perform inverse modeling at multiple scales.
- The Stochastic Time-Inverted Lagrangian Transport model (STILT, <http://stilt-model.org>), is a Lagrangian particle dispersion model for atmospheric transport frequently used for emission inversions.
- TM5 (<http://tm5.sourceforge.net/about-tm5/physics/>) is a global chemistry transport model with zooming capabilities and an adjoint implemented for the single-tracer version that is regularly used in greenhouse gas flux inversions and that is publicly available.
- SILAM (<http://silam.fmi.fi>, Sofiev et al, 2015) is a global-to-meso-scale model with embedded 3D- and 4D- variational and Ensemble Kalman Filter and Smoother techniques, which allow for solving the inverse atmospheric chemistry problems. Existing adjoint formulations are suitable for both emission estimation and model-state assimilation. The model is an open-code system, available on a request basis from the Finnish Meteorological Institute

10.6 Summary

- Air quality forecasting systems have been improving their skill over time but multiple uncertainties (e.g., meteorology, processes, emissions) still hinder their performance. Thus, there is often room for improving forecasts by using observed data, which can be used to enhance forecast models in a variety of ways.
- Data fusion is a post-processing technique for statistically combining air quality forecasts with a large variety of data sets, including dense air quality sensor networks, meteorological observations and models, and GIS-datasets to produce improved forecasts.
- Data assimilation within an air quality forecasting framework broadly refers to methods for combining model predictions and observations to adjust some aspect of the model (e.g., initial conditions, boundary conditions, emissions) such that the next forecasting cycle is improved. A large variety of techniques exist that vary in terms of computational expense, accuracy, and the nature of the adjustments made to the forecast. The most common data assimilation application in air quality forecast models is updating chemical initial conditions, which is commonly found to reduce uncertainty and bias in short-term forecasts.
- Inverse modeling in the air quality forecasting community refers to approaches for constraining emissions using observations, which can lead to more sustained forecast improvements. In contrast to data assimilation, wherein methods are often drawn directly from numerical weather prediction, emissions estimation poses unique sets of methodological challenges which often more closely mirror problems in geophysics and remote sensing, and often entails the use of auxiliary prior information, regularization, and extensive cross-validation. Inverse modeling has often been applied as an offline step for making adjustments to emissions that may be out of date (in the case of anthropogenic sources), uncertain (e.g., biomass burning), or both. Advanced methods and examples exist that allow for constraining emissions and initial concentrations simultaneously.

References

- Aster, R. C.; Borchers, B. & Thuber, C. H.; Parameter Estimation and Inverse Problems, Elsevier Academic Press, 2006.
- Anderson, J. L.: A local least squares framework for ensemble filtering, *Mon. Wea. Rev.*, 131, 634–642, 2003
- Arellano, A. F., Hess, P. G., Edwards, D. P., and Baumgardner, D.: Constraints on black carbon aerosol distribution from Measurement of Pollution in the Troposphere (MOPITT) CO, *Geophysical research letters*, 37, L17801, 10.1029/2010gl044416, 2010.
- Baklanov, A., A. Rasmussen, B. Fay, E. Berge, and S. Finardi (2002), Potential and Shortcomings of Numerical Weather Prediction Models in Providing Meteorological Data for Urban Air Pollution Forecasting, *Water, Air and Soil Poll.: Focus*, 2(5-6), 43-60.
- Baklanov, A., D. Brunner, G. Carmichael, J. Flemming, S. Freitas, M. Gauss, Hov, R. Mathur, K. Schlünzen, C. Seigneur, and B. Vogel, 2017: Key issues for seamless integrated chemistry-meteorology modeling. *Bull. Amer. Meteor. Soc.* doi:10.1175/BAMS-D-15-00166.1, in press.
- Baklanov, A., Schlünzen, K., Suppan, P., Baldasano, J., Brunner, D., Aksoyoglu, S., Carmichael, G., Douros, J., Flemming, J., Forkel, R., Galmarini, S., Gauss, M., Grell, G., Hirtl, M., Joffre, S., Jorba, O., Kaas, E., Kaasik, M., Kallos, G., Kong, X., Korsholm, U., Kurganskiy, A., Kushta, J., Lohmann, U., Mahura, A., Manders-Groot, A., Maurizi, A., Moussiopoulos, N., Rao, S. T., Savage, N., Seigneur, C., Sokhi, R. S., Solazzo, E., Solomos, S., Sørensen, B., Tsegas, G., Vignati, E., Vogel, B., and Zhang, Y.: Online coupled regional meteorology chemistry models in Europe: current status and prospects, *Atmos. Chem. Phys.*, 14, 317–398, doi:10.5194/acp-14-317-2014, 2014.
- Barré, J., Edwards, D., Worden, H., Arellano, A., Gaubert, B., Da Silva, A., Lahoz, W., and Anderson, J.: On the feasibility of monitoring carbon monoxide in the lower troposphere from a constellation of northern hemisphere geostationary satellites: Global scale assimilation experiments (Part II), 140, 188-201, 2016.
- Benedetti, A., et al. (2009), Aerosol analysis and forecast in the European Centre for Medium-Range Weather Forecasts Integrated Forecast System: 2. Data assimilation, *J. Geophys. Res.*, 114, D13205, doi:10.1029/2008JD011115.
- Berge, E., S.-E. Walker, A. Sorteberg, M. Lenkopane, S. Eastwood, H. I. Jablonska, and M. Ø. Koltzow (2002), A real-time operational forecast model for meteorology and air quality during peak air pollution episodes in Oslo, Norway, *Water, Air, and Soil Pollution: Focus*, 2, 745-757.
- Bhartia, P. K., McPeters, R. D., Mateer, C. L., Flynn, L. E., and Wellemeyer, C., Algorithm for the estimation of vertical ozone profiles from the backscattered ultraviolet technique, *J. Geophys. Res.*, 101, 18793–18806, 1996.
- Bocquet, M., and Wu, L.: Bayesian design of control space for optimal assimilation of observations. Part II: Asymptotic solutions, *Quarterly Journal of the Royal Meteorological Society*, 137, 1357-1368, 10.1002/qj.841, 2011.
- Bocquet, M., Elbern, H., Eskes, H., Hirtl, M., Žabkar, R., Carmichael, G. R., Flemming, J., Inness, A., Pagowski, M., Pérez Camaño, J. L., Saide, P. E., San Jose, R., Sofiev, M., Vira, J., Baklanov, A., Carnevale, C., Grell, G., and Seigneur, C.: Data assimilation in atmospheric chemistry models: current status and future prospects for coupled chemistry meteorology models, *Atmos. Chem. Phys.*, 15, 5325-5358, <https://doi.org/10.5194/acp-15-5325-2015>.
- Bocquet, M., Pires, C. A., and Wu, L.: Beyond Gaussian statistical modeling in geophysical data assimilation, *Monthly Weather Review*, 138, 2997-3023, 2010.

- Bocquet, M., Wu, L. and Chevallier, F.: Bayesian design of control space for optimal assimilation of observations. I: Consistent multiscale formalism *Q. J. R. Meteorol. Soc.*, 137, 1340-1356, 2011.
- Bocquet, M.: An introduction to inverse modeling and parameter estimation for atmosphere and ocean sciences *Advanced data assimilation for geosciences*, Blayo, É.; Bocquet, M.; Cosme, E. & Cugliandolo, L. F. (Eds.). Oxford University Press, 461-493, 2014.
- Bocquet, M.: Reconstruction of an atmospheric tracer source using the principle of maximum entropy. I: Theory: *Q. J. R. Meteorol. Soc.*, 131, 2191-2208, 2005.
- Boersma, K. F., Eskes, H. J., and Brinksma, E. J.: Error analysis for tropospheric NO₂ retrieval from space, *J. Geophys. Res.*, 109, D04311, doi: [10.1029/2003JD003962](https://doi.org/10.1029/2003JD003962), 2004.
- Boersma, K.F., H.J. Eskes, J.P. Veefkind, E.J. Brinksma, R.J. van der A, M. Sneep, G.H.J. van den Oord, P.F. Levelt, P. Stammes, J.F. Gleason and E.J. Bucsela, 2006. Near-real time retrieval of tropospheric NO₂ from OMI. *Atm. Chem. Phys. Discussions*, 6, 12301-12345.
- Borrego, C., Coutinho, M., Costa, A. M., Ginja, J., Ribeiro, C., Monteiro, A., Ribeiro, I., Valente, J., Amorim, J. H., Martins, H., Lopes, D., Miranda, A. I.: Challenges for a new air quality directive: the role of monitoring and modeling techniques, *Urban Climate*, doi: [10.1016/j.uclim.2014.06.007](https://doi.org/10.1016/j.uclim.2014.06.007), in press, 2015.
- Borsdorff, T., Aan de Brugh, J., Hu, H., Aben, I., Hasekamp, O., & Landgraf, J. (2018). Measuring carbon monoxide with TROPOMI: First results and a comparison with ECMWF-IFS analysis data. *Geophysical Research Letters*, 45, 2826–2832. <https://doi.org/10.1002/2018GL077045>
- Bousserez, N., and Henze, D. K.: Optimal and Scalable Methods to Approximate the Solutions of Large-Scale Bayesian Problems: Theory and Application to Atmospheric Inversion and Data Assimilation, *Q. J. R. Meteorol. Soc.*, in press, 2018.
- Brasseur, G., and Jacob, D. (2017) *Modeling of Atmospheric Chemistry*. Cambridge University Press.
- Brioude, J., G. Petron, G. J. Frost, R. Ahmadov, W. M. Angevine, E. Y. Hsie, S. W. Kim, S. H. Lee, S. A. McKeen, M. Trainer, F. C. Fehsenfeld, J. S. Holloway, J. Peischl, T. B. Ryerson and K. R. Gurney (2012). "A new inversion method to calculate emission inventories without a prior at mesoscale: Application to the anthropogenic CO₂ emission from Houston, Texas." *Journal of Geophysical Research-Atmospheres* 117.
- Buehner, M. P., Houtekamer, I., Charette, C., Mitchell, H. L., and He, B.: Intercomparison of variational data assimilation and the ensemble Kalman filter for global deterministic N.W.P., Part I. Description and single-observation experiments, *Mon. Wea. Rev.*, 138, 1550–1566, 2010a.
- Buehner, M. P., Houtekamer, I., Charette, C., Mitchell, H. L., and He, B.: Intercomparison of variational data assimilation and the ensemble Kalman filter for global deterministic N.W.P., Part II. One-month experiments with real observations, *Mon. Wea. Rev.*, 138, 1567–1586, 2010b.
- Butz, A., Hasekamp, O. P., Frankenberg, C., Vidot, J., and Aben, I.: CH₄ retrievals from space-based solar backscatter measurements: performance evaluation against simulated aerosol and cirrus loaded scenes, *J. Geophys. Res.*, 115, D24302, doi: [10.1029/2010JD014514](https://doi.org/10.1029/2010JD014514), 2010.
- Cai, C., C. Hogrefe, P. Katsafados, G. Kallos, M. Beauharnois, J.J. Schwab, X. Ren, W. Brune, X. Zhou, Y. He, and K. Demerjian (2008), Performance evaluation of an air quality forecast modeling system for a summer and winter season – Photochemical oxidants and their precursors, *Atmos. Environ.*, 42, 8585-8599, doi: [10.1026/j.atmosenv.2008.08.029](https://doi.org/10.1026/j.atmosenv.2008.08.029).

- Carmichael, G. R., Sandu, A., Chai, T., Daescu, D., Constantinescu, E., and Tang, Y.: Predicting air quality: Improvements through advanced methods to integrate models and measurements, *J. Comp. Phys.*, 227, 3540–3571, 2008.
- Chai T., G.R. Carmichael, Y. Tang, and A. Sandu: “Regional NOX emission inversion through a four-dimensional variational approach using SCIAMACHY tropospheric NO_2 column observations.” *Atmospheric Environment*, Vol. 43, Issue 32, pp. 5046--5055, 2009.
- Chai, T. F., Carmichael, G. R., Sandu, A., Tang, Y. H., and Daescu, D. N.: Chemical data assimilation of transport and chemical evolution over the Pacific (TRACE-P) aircraft measurements, *J. Geophys. Res.*, 111, D02301, doi:10.1029/2006JD007763, 2006.
- Chai, T., Carmichael, G. R., Tang, Y., Sandu, A., Hardesty, M., Pilewskie, P., Whitlow, S., Browell, E. V., Avery, M. A., Nédélec, P., Merrill, J. T., Thompson, A. M., and Williams, E.: Four-dimensional data assimilation experiments with International Consortium for Atmospheric Research on Transport and Transformation ozone measurements, *J. Geophys. Res.*, 112, D12S15, doi:10.1029/2006JD007763, 2007.
- Chen, J., J. Vaughan, J. Avise, S. O'Neill, and B. Lamb (2008), Enhancement and evaluation of the AIRPACT ozone and $\text{PM}_{2.5}$ forecast system for the Pacific Northwest, *J. Geophys. Res.*, 113, D14305, doi:10.1029/2007JD009554.
- Chen, C., Dubovik, O., Henze, D. K., Lapyonak, T., Chin, M., Ducos, F., Litvinov, P., Huang, X., and Li, L.: Retrieval of Desert Dust and Carbonaceous Aerosol Emissions over Africa from POLDER/PARASOL Products Generated by GRASP Algorithm, *Atmos. Chem. Phys.*, 18, 12551–12580, 2018, <https://doi.org/10.5194/acp-18-12551-2018>.
- Cheng H., M. Jardak, M. Alex, and A. Sandu: A Hybrid Approach to Estimating Error Covariances in Variational Data Assimilation. *Tellus Series A -- Dynamic Meteorology and Oceanography*, Vol. 62, Issue A, pp. 288--297, 2010.
- Chuang, M.-T., Y. Zhang, and D.-W. Kang (2011), Application of WRF/Chem-MADRID for Real-Time Air Quality Forecasting over the Southeastern United States, *Atmos. Environ.*, 45 (34), 6241-6250, doi: 10.1016/j.atmosenv.2011.06.071.
- Cioaca A., A. Sandu, and E. de Sturler: “Efficient Methods for Computing Observation Impact in 4D-Var Data Assimilation.” *Computational Geosciences*, Vol. 17, Issue 6, pp. 975--990, 2013.
- Clerbaux, C., Boynard, A., Clarisse, L., George, M., Hadji-Lazaro, J., Herbin, H., Hurtmans, D., Pommier, M., Razavi, A. Turquety, S., Wespes, C., and Coheur, P.-F.: Monitoring of atmospheric composition using the thermal infrared IASI/MetOpsounder, *Atmos. Chem. Phys.*, 9, 6041–6054, doi:10.5194/acp-9-6041-2009, 2009.
- Colarco, P. R., E. P. Nowottnick, C. A. Randles, B. Yi, P. Yang, K.-M. Kim, J. A. Smith, and C. G. Bardeen, 2014: Impact of radiatively interactive dust aerosols in the NASA GEOS-5 climate model: Sensitivity to dust particle shape and refractive index, *J. Geophys. Res. Atmos.*, 119, 753–786, doi:10.1002/2013JD020046.
- Constantinescu, E. M., Sandu, A., Chai, T., and Carmichael, G. R.: Ensemble-based chemical data assimilation. i: General approach, *Q. J. Roy. Meteorol. Soc.*, 133, 1229–1243, 2007a.
- Constantinescu, E. M., Sandu, A., Chai, T., and Carmichael, G. R.: Ensemble-based chemical data assimilation. ii: Covariance localization, *Q. J. Roy. Meteorol. Soc.*, 133, 1245–1256, 2007b
- Constantinescu, E.M., A. Sandu, T. Chai, and G.R. Carmichael: “Assessment of Ensemble-based Chemical Data Assimilation in an Idealized Setting.” *Atmospheric Environment*, Vol. 41, Issue 1, pp. 18--36, 2007c.

- Constantinescu, E.M., T. Chai, A. Sandu, and G.R. Carmichael: "Autoregressive Models of Background Errors for Chemical Data Assimilation." *Journal of Geophysical Research*, Vol. 112, D12309, 2007d.
- Cooper, M., R. V. Martin, A. Padmanabhan, and D. K. Henze (2017), Comparing mass balance and adjoint methods for inverse modeling of nitrogen dioxide columns for global nitrogen oxide emissions, *J. Geophys. Res. Atmos.*, 122, 4718-4734, doi: [10.1002/2016JD025985](https://doi.org/10.1002/2016JD025985).
- Cope, M. E., G. D. Hess, S. Lee, K. Tory, M. Azzi, J. Carras, W. Lilley, P. C. Manins, P. Nelson, L. Ng, K. Puri, N. Wong, S. Walsh, and M. Young (2004), The Australian Air Quality Forecasting System. Part I: Project description and early outcomes, *J. of Applied Meteorology*, 43, 649-662.
- Cope, M.E., and G.D. Hess (2005), Air quality forecasting: a review and comparison of the approaches used internationally and in Australia, *Clean Air and Environmental Quality*, 39 (1): 52-60.
- Courtier, P., Thépaut, J.-N., and Hollingsworth, A.: A strategy for operational implementation of 4D-Var, using an incremental approach, *Q. J. Roy. Meteorol. Soc.*, 120, 1367–1388, 1994.
- Crevoisier, C., Chédin, A., Matsueda, H., Machida, T., Armante, R., and Scott, N. A.: First year of upper tropospheric integrated content of CO₂ from IASI hyperspectral infrared observations, *Atmos. Chem. Phys.*, 9, 4797-4810, <https://doi.org/10.5194/acp-9-4797-2009>, 2009a.
- Crevoisier, C., Nobileau, D., Fiore, A. M., Armante, R., Chédin, A., and Scott, N. A.: Tropospheric methane in the tropics – first year from IASI hyperspectral infrared observations, *Atmos. Chem. Phys.*, 9, 6337-6350, <https://doi.org/10.5194/acp-9-6337-2009>, 2009a.
- Davoine, X., and Bocquet, M.: Inverse modeling-based reconstruction of the Chernobyl source term available for long-range transport, *Atmos. Chem. Phys.*, 7, 1549-1564, [10.5194/acp-7-1549-2007](https://doi.org/10.5194/acp-7-1549-2007), 2007.
- Deeter, M. N., D. P. Edwards, G. L. Francis, J. C. Gille, S. Martinez-Alonso, H. M. Worden, and C. Sweeney (2017), A Climate-scale Satellite Record for Carbon Monoxide: The MOPITT Version 7 Product, *Atmos. Meas. Tech. Discuss.*, 2017, 1–34, doi: [10.5194/amt-2017-71](https://doi.org/10.5194/amt-2017-71).
- De Foy, B., J. Heo, and J.J. Schauer, Estimation of direct emissions and atmospheric processing of reactive mercury using inverse modeling. *Atmospheric Environment*, 2014. 85: p. 73-82. 50.
- DelleMonache, L., Julie K. Lundquist, Branko Kosović, Gardar Johannesson, Kathleen M. Dyer, and Roger D. Aines, Bayesian Inference and Markov Chain Monte Carlo Sampling to Reconstruct a Contaminant Source on a Continental Scale, *JAMC*, 47, 2008, <https://doi.org/10.1175/2008JAMC1766.1>.
- Descombes, G., Auligné, T., Vandenberghe, F., Barker, D. M., and Barré, J.: Generalized background error covariance matrix model (GEN_BE v2.0), 8, 669-696, 2015.
- di Tomaso, E. [et al.]. Assimilation of MODIS Dark Target and Deep Blue observations in the dust aerosol component of NMMB-MONARCH version 1.0. *Geoscientific Model Development*, 10 March 2017, vol. 10, p. 1107-1129.
- Djalalova, I., J. Wilczak, S. McKeen, G. Grell, S. Peckham, M. Pagowski, L. DelleMonache, J. McQueen, Y. Tang, P. Lee, J. McHenry, W. Gong, V. Bouchet, and R. Mathur (2010), Ensemble and bias-correction techniques for air quality model forecasts of surface O₃ and PM_{2.5} during the TEXAQS-II experiment of 2006, *Atmos. Environ.*, 44, 455-467, doi: [10.1016/j.atmosenv.2009.11.007](https://doi.org/10.1016/j.atmosenv.2009.11.007).

- Doraiswamy, P., C. Hogrefe, W. Hao, B. Colle, M. Beauharnois, K. Demerjian, J.-Y. Ku, and G. Sistla (2009). Preliminary Experiences with the Multi-Model Air Quality Forecasting System for New York State, paper presented at the 8th Annual Community Modeling and Analysis System (CMAS) Conference, Chapel Hill, NC.
- Eder, B. K., D. Kang, R. Mathur, S. Yu, and K. Schere (2006), An operational evaluation of the Eta–CMAQ air quality forecast model, *Atmos. Environ.*, *40*, 4894–4905.
- Eder, B., D. Kang, R. Mathur, J. Pleim, S. Yu, T. Otte, and G. Pouliot (2009), A performance evaluation of the National Air Quality Forecast Capability for the summer of 2007, *Atmos. Environ.*, *43*, 2312–2320, doi:10.1016/j.atmosenv.2009.01.033.
- Elbern, H. and Schmidt, H.: A four-dimensional variational chemistry data assimilation scheme for Eulerian chemistry transport modeling, *J. Geophys. Res.*, *104*, 18583–18598, 1999.
- Elbern, H. and Schmidt, H.: Ozone episode analysis by four-dimensional variational chemistry data assimilation, *J. Geophys. Res.*, *106*, 3569–3590, 2001.
- Elbern, H., Strunk, A., Schmidt, H., and Talagrand, O.: Emission rate and chemical state estimation by 4-dimensional variational inversion, *Atmos. Chem. Phys.*, *7*, 3749–3769, 10.5194/acp-7-3749-2007, 2007.
- Evensen, G.: Sequential data assimilation with a nonlinear quasigeostrophic model using Monte Carlo methods to forecast error statistics, *J. Geophys. Res.*, *99*, 10143–10162, 1994.
- Fletcher S. J., and Zupanski M. A (2006), Data assimilation method for log-normally distributed observational errors, *Q. J. R. Meteorol. Soc.* doi:10.1256/qj.05.222 2006
- Findari, S., R. De maria, A. D'Allura, C. Cascone, G. Calori, and F. Lollobrigida (2008), A deterministic air quality forecasting system for Torino urban area, Italy, *Environmental Modeling & Software*, *23*, 344–355, doi:10.1016/j.envsoft.2007.04.001.
- Froidevaux, L., Jiang, Y. B., Lambert, A., Livesey, N. J., Read, W. G., Waters, J. W., Browell, E. V., Hair, J. W., Avery, M. A., McGee, T. J., Twigg, L. W., Sumnicht, G. K., Jucks, K. W., Margitan, J. J., Sen, B., Stachnik, R. A., Toon, G. C., Bernath, P. F., Boone, C. D., Walker, K. A., Filipiak, M. J., Harwood, R. S., Fuller, R. A., Manney, G. L., Schwartz, M. J., Daffer, W. H., Drouin, B. J., Cofield, R. E., Cuddy, D. T., Jarnot, R. F., Knosp, B. W., Perun, V. S., Snyder, W. V., Stek, P. C., Thurstans, R. P., and Wagner, P. A.: Validation of Aura Microwave Limb Sounder stratospheric ozone measurements, *J. Geophys. Res.* *113*, D15S20, doi:10.1029/2007JD008771 , 2008.
- Fu, T.-M., J. J. Ca, X. Y. Zhang, S. C. Lee, Q. Zhang, Y. M. Han, W. J. Qu, Z. Han, R. Zhang, Y. X. Wang, D. Chen, and D. K. Henze (2012), Carbonaceous Aerosols in China: Top-down Constraints on Primary Sources and Estimation of Secondary Contribution, *Atmos. Chem. Phys.*, *12*, 2725–2746.
- Ganesan, A. L., Rigby, M., Zammit-Mangion, A., Manning, A. J., Prinn, R. G., Fraser, P. J., Harth, C. M., Kim, K.-R., Krummel, P. B., Li, S., Mühle, J., O'Doherty, S. J., Park, S., Salameh, P. K., Steele, L. P., and Weiss, R. F.: Characterization of uncertainties in atmospheric trace gas inversions using hierarchical Bayesian methods, *Atmos. Chem. Phys.*, *14*, 3855–3864, <https://doi.org/10.5194/acp-14-3855-2014>.
- Gao, M., Saide, P.E., Xin, J., Wang, Y., Liu, Z., Wang, Z., Pagowski, M., Guttikunda, S., and Carmichael, G.R. Reduced Uncertainties in Health Impacts and Radiative Forcing Estimates in Winter Haze in eastern China through constraints of surface PM2.5 predictions. ES&T, 2017.
- George, M., Clerbaux, C., Hurtmans, D., Turquety, S., Coheur, P.-F., Pommier, M., Hadji-Lazaro, J., Edwards, D. P., Worden, H., Luo, M., Rinsland, C., and McMillan, W.: Carbon monoxide distributions from the IASI/METOP mission: evaluation with other space-borne remote sensors, *Atmos. Chem. Phys.*, *9*, 8317–8330, doi:10.5194/acp-9-8317-2009.

- Gilliam, R.C., C. Hogrefe, and S.T. Rao (2006), New methods for evaluating meteorological models used in air quality applications, *Atmos. Environ.*, 40, 5073-5086.
- Gou T.Y. and A. Sandu: "Continuous versus Discrete Advection Adjoints in Chemical Data Assimilation with CMAQ." *Atmospheric Environment*, Vol. 45, Issue 28, pp. 4868--4881, 2011.
- Groetsch, C. W.: *Inverse Problems in the Mathematical Sciences*, Vieweg and Verlag, 1993.
- Hassinen, S., Balis, D., Bauer, H., Begoin, M., Delcloo, A., Eleftheratos, K., Gimeno Garcia, S., Granville, J., Grossi, M., Hao, N., Hedelt, P., Hendrick, F., Hess, M., Heue, K.-P., Hovila, J., Jönch-Sørensen, H., Kalakoski, N., Kauppi, A., Kiemle, S., Kins, L., Koukoulis, M. E., Kujanpää, J., Lambert, J.-C., Lang, R., Lerot, C., Loyola, D., Pedergnana, M., Pinardi, G., Romahn, F., van Roozendaal, M., Lutz, R., De Smedt, I., Stammes, P., Steinbrecht, W., Tamminen, J., Theys, N., Tilstra, L. G., Tuinder, O. N. E., Valks, P., Zerefos, C., Zimmer, W., and Zyrichidou, I.: Overview of the O3M SAF GOME-2 operational atmospheric composition and UV radiation data products and data availability, *Atmos. Meas. Tech.*, 9, 383-407, <https://doi.org/10.5194/amt-9-383-2016>.
- Haussaire, J.-M. and Bocquet, M.: A low-order coupled chemistry meteorology model for testing online and offline data assimilation schemes: L95-GRS (v1.0), *Geosci. Model Dev.*, 9, 393-412, 2016.
- Henze, D. K., Seinfeld, J. H., and Shindell, D. T.: Inverse modeling and mapping US air quality influences of inorganic PM_{2.5} precursor emissions using the adjoint of GEOS-Chem, *Atmos. Chem. Phys.*, 9, 5877-5903, [10.5194/acp-9-5877-2009](https://doi.org/10.5194/acp-9-5877-2009), 2009.
- Hess, G. D., K. J. Tory, M. E. Cope, S. Lee, K. Puri, P. C. Manins, and M. Young (2004), The Australian Air Quality Forecasting System. Part II: Case study of Sydney 7-day photochemical smog event, *Journal of Applied Meteorology*, 43, 663-679.
- Hogrefe, C., W. Hao, K. Civerolo, J.-Y. Ku, G. Sistla, R.S. Gaza, L. Sedefian, K. Schere, A. Gilliland, and R. Mathur (2007), Daily simulation of ozone and fine particulates over New York State: findings and challenges, *Journal of Applied Meteorology and Climatology*, 46(7), 961-979, [doi:10.1175/JAM2520.1](https://doi.org/10.1175/JAM2520.1)
- Honoré, C., L. Rouil, R. Vautard, M. Beekmann, B. Bessagnet, A. Dufour, C. Elichegaray, J.-M. Flaud, L. Malherbe, F. Meleux, L. Menut, D. Martin, A., Peuch, V.-H. Peuch, and N. Poisson (2008), Predictability of European air quality: Assessment of 3 years of operational forecasts and analysis by the PREV'AIR system, *J. Geophys. Res.*, 113, D04301, [doi:10.1029/2007JD008761](https://doi.org/10.1029/2007JD008761).
- Houtekamer, P. L. and Mitchell, H. L.: A sequential ensemble Kalman filter for atmospheric data assimilation, *Mon. Wea. Rev.*, 129, 123-137, 2001.
- Hov, O; Terblanche, D Carmichael, G , Jones, S; Ruti, PM; Tarasova, O , Five priorities for weather and climate research *NATURE* , 552, 168-170 , 2017
- Hu, Y., M. T. Odman, M. E. Chang, W. Jackson, S. Lee, E. S. Edgerton, K. Baumann, and A. G. Russell (2008), Simulation of air quality impacts from prescribed fires on an urban area, *Environ. Sci. Technol.*, 42, 3676-3682.
- Inness, A., Baier, F., Benedetti, A., Bouarar, I., Chabrillat, S., Clark, H., Clerbaux, C., Coheur, P., Engelen, R. J., Errera, Q., Flemming, J., George, M., Granier, C., Hadji-Lazarou, J., Huijnen, V., Hurtmans, D., Jones, L., Kaiser, J. W., Kapsomenakis, J., Lefever, K., Leitão, J., Razinger, M., Richter, A., Schultz, M. G., Simmons, A. J., Suttie, M., Stein, O., Thépaut, J. N., Thouret, V., Vrekoussis, M., Zerefos, C., and the M. t.: The MACC reanalysis: an 8 yr data set of atmospheric composition, *Atmos. Chem. Phys.*, 13, 4073-4109, [10.5194/acp-13-4073-2013](https://doi.org/10.5194/acp-13-4073-2013), 2013.
- Jacobson, M. Z. (2002), Control of fossil-fuel particulate black carbon plus organic matter, possibly the most effective method of slowing global warming, *J. Geophys. Res.*, 107, (D19), 4410, [doi:10.1029/2001JD001376](https://doi.org/10.1029/2001JD001376).
- Jiménez, P., O. Jorba, R. Parra, and J. M. Baldasano (2006), Evaluation of MM5-

EMICAT2000-CMAQ performance and sensitivity in complex terrain: High-resolution application to the north-eastern Iberian Peninsula, *Atmos. Environ.*, *41*, 5056-5072, doi: [10.1016/j.atmosenv.2005.12.060](https://doi.org/10.1016/j.atmosenv.2005.12.060).

- Jiménez-Guerrero, P., C. Pérez, O. Jorba, and J. M. Baldasano (2008), Contribution of Saharan dust in an integrated air quality system and its online assessment, *Geophys. Res. Lett.*, *35*, L03814, doi: [10.1029/2007GL031580](https://doi.org/10.1029/2007GL031580).
- Johansson, L.O., Epitropou, V., Karatzas, K.D., Bassoukos, A., Karppinen, A., Kukkonen, K. and Wanner, L. The extraction and fusion of meteorological and air quality information for orchestrated services. *Env. Modeling & software*. Volume 64, p 143–155, February 2015.
- Kalnay, E.: Atmospheric modeling, data assimilation and predictability, Cambridge University Press, Cambridge, UK, 2003
- Kaminski, T., Rayner, P. J., Heimann, M. and Enting, I. G.: On aggregation errors in atmospheric transport inversions *J. Geophys. Res.*, *106*, 4703-4715, 2001.
- Kang, D., B. K. Eder, A. F. Stein, G. A. Grell, S. E. Peckham, and J. McHenry (2005), The New England Air Quality Forecasting Pilot Program: Development of an evaluation protocol and performance benchmark, *J. Air & Waste Manage. Assoc.*, *55*, 1782-1796.
- Konovalov, I.B., M. Beekmann, F. Meleux, A. Dutot, and G. Foret (2009), Combining deterministic and statistical approaches for PM₁₀ forecasting in Europe, *Atmos. Environ.*, *43*, 6425-6434, doi: [10.1016/j.atmosenv.2009.06.039](https://doi.org/10.1016/j.atmosenv.2009.06.039).
- Kopacz, M., Jacob, D. J., Fisher, J. A., Logan, J. A., Zhang, L., Megretskaia, I. A., Yantosca, R. M., Singh, K., Henze, D. K., Burrows, J. P., Buchwitz, M., Khlystova, I., McMillan, W. W., Gille, J. C., Edwards, D. P., Eldering, A., Thouret, V., and Nedelec, P.: Global estimates of CO sources with high resolution by adjoint inversion of multiple satellite datasets (MOPITT, AIRS, SCIAMACHY, TES), *Atmos. Chem. Phys.*, *10*, 855-876, [10.5194/acp-10-855-2010](https://doi.org/10.5194/acp-10-855-2010), 2010.
- Lahoz, W., Khattatov, B., and Ménard, R. (Eds.): Data assimilation – Making sense of observations, Springer, 718 pp., 2010.
- Lee, C., Richter, A., Weber, M., and Burrows, J. P.: SO₂ Retrieval from SCIAMACHY using the Weighting Function DOAS (WFDOAS) technique: comparison with Standard DOAS retrieval, *Atmos. Chem. Phys.*, *8*, 6137-6145, <https://doi.org/10.5194/acp-8-6137-2008>, 2008.
- Liu, X., Bhartia, P. K., Chance, K., Spurr, R. J. D., and Kurosu, T. P.: Ozone profile retrievals from the Ozone Monitoring Instrument, *Atmos. Chem. Phys.*, *10*, 2521–2537, doi: [10.5194/acp-10-2521-2010](https://doi.org/10.5194/acp-10-2521-2010), 2010.
- Liu, X., Mizzi, A. P., Anderson, J. L., Fung, I. Y., and Cohen, R. C.: Assimilation of satellite NO₂ observations at high spatial resolution using OSSEs, *Atmos. Chem. Phys.*, *17*, 7067-7081, <https://doi.org/10.5194/acp-17-7067-2017>, 2017.
- Liu, Y., Haussaire, J.-M., Bocquet, M., Roustan, Y., Saunier, O. and Mathieu, A.: Uncertainty quantification of pollutant source retrieval: comparison of Bayesian methods with application to the Chernobyl and Fukushima-Daiichi accidental releases of radionuclides *Q. J. R. Meteorol. Soc.*, *143*, 2886-2901, 2017.
- Liu, Z., Liu, Q., Lin, H. C., Schwartz, C. S., Lee, Y. H., and Wang, T.: Three-dimensional variational assimilation of MODIS aerosol optical depth: Implementation and application to a dust storm over East Asia, *Journal of Geophysical Research*, *116*, D23206, 2011.
- Lorenc, A. C.: The potential of the ensemble Kalman filter for NWP – a comparison with 4D-Var, *Q. J. Roy. Meteorol. Soc.*, *129*, 3183–3203, 2003.
- Makar, P. A., et al. (2009), Modeling the impacts of ammonia emissions reductions on North American air quality, *Atmos. Chem. Phys.*, *9*, 7183–7212, doi: [10.5194/acp-9-7183-2009](https://doi.org/10.5194/acp-9-7183-2009).

- Manders, A.M.M., M. Schaap, and R. Hoogerbrugge (2009), Testing the capability of the chemistry transport model LOTOS-EUROS to forecast PM₁₀ levels in the Netherlands, *Atmos. Environ.*, 43, 4050-4059, doi: [10.1016/j.atmosenv.2009.05.006](https://doi.org/10.1016/j.atmosenv.2009.05.006).
- Manins, P. C., M. E. Cope, G. D. Hess, P. F. Nelson, K. Puri, N. Wong, and M. Young (2002), The Australian Air Quality Forecasting System: prognostic air quality forecasting in Australia, *Clean Air and Environmental Quality*, 36 (2): 43-48.
- Manins, P. (2001a), Current Status, Preliminary Validation Study of the Australian Air Quality Forecasting System, Project Report, PSS : dh79, Department of the Environment and Heritage, CSIRO Atmospheric Research, PMB 1 Aspendale 3195, Australia.
- Manins, P. C. (2001b), Air Quality Forecasting For Australia's Major Cities, Final Report, PSS: dh79A, Department of Environment and Heritage, CSIRO Atmospheric Research, 341 pp., PMB 1 Aspendale 3195, Australia, November.
- Marchuk, G.I. (1995). Adjoint Equations and Analysis of Complex Systems, Springer Netherlands, 1995, ISBN 978-94-017-0621-6, p. 468p.
- Martin, R. V., D. J. Jacob, K. Chance, T. P. Kurosu, P. I. Palmer and M. J. Evans (2003). "Global inventory of nitrogen oxide emissions constrained by space-based observations of NO₂ columns." *Journal of Geophysical Research-Atmospheres* 108(D17).
- Mathur, R., S. Yu, D. Kang, and K. L. Schere (2008), Assessment of the wintertime performance of particulate matter forecasts with the Eta-Community Multiscale Air Quality modeling system, *J. Geophys. Res.*, 113, D02303, doi: [10.1029/2007JD008580](https://doi.org/10.1029/2007JD008580).
- McHenry, J. N., W. F. Ryan, N. L. Seaman, C. J. Coats Jr., J. Pudykiewics, S. Arunachalam, and J. M. Vukovich (2004), A real-time Eulerian photochemical model forecast system: Overview and initial ozone forecast performance in the Northeast U.S. corridor, *Bull. Amer. Meteor. Soc.*, 85, 525-548.
- McKeen, S., J. Wilczak, G. Grell, I. Djalova, S. Peckham, E.-Y. Hsie, W. Gong, V. Bouchet, S. Ménard, R. Moffet, J. McHenry, J. McQueen, Y. Tang, G. R. Carmichael, M. Pagowski, A. Chan, t. Dye, G. Frost, P. Lee, and R. Mathur (2005), Assessment of an ensemble of seven real-time ozone forecasts over eastern North America during the summer of 2004, *J. Geophys. Res.*, 110, D21307, doi: [10.1029/2005JD005858](https://doi.org/10.1029/2005JD005858).
- McKeen, S., S. H. Chung, J. Wilczak, G. Grell, I. Djalalova, S. Peckham, W. Gong, V. Bouchet, R. Moffet, Y. Tang, G. R. Carmichael, R. Mathur, and S. Yu (2007), Evaluation of several PM_{2.5} forecast models using data collected during the ICARTT/NEAQS 2004 field study, *J. Geophys. Res.*, 112, D10S20, doi: [10.1029/2006JD007608](https://doi.org/10.1029/2006JD007608).
- McKeen, S. et al. (2009), An evaluation of real-time air quality forecasts and their urban emissions over eastern Texas during the summer of 2006 Second Texas Air Quality Study field study, *J. Geophys. Res.*, 114, D00F11, doi: [10.1029/2008JD011697](https://doi.org/10.1029/2008JD011697).
- Meirink, J. F., Eskes, H. J., and Goede, A. P. H.: Sensitivity analysis of methane emissions derived from SCIAMACHY observations through inverse modeling, 6, 1275-1292, 2006.
- Mendoza-Dominguez, A. and A. G. Russell (2000). "Iterative inverse modeling and direct sensitivity analysis of a photochemical air quality model." *Environmental Science & Technology* 34(23): 4974-4981.
- Menut L., I. Chiapello, and C. Moulin (2009), Previsibility of mineral dust concentrations: The CHIMERE-DUST forecast during the first AMMA experiment dry season, *J. Geophys. Res.*, 114, D07202, doi: [10.1029/2008JD010523](https://doi.org/10.1029/2008JD010523).
- Messina, P., D'Isidoro, M., Maurizi, A., and Fierli, F.: Impact of assimilated observations on improving tropospheric ozone simulations, 45, 6674-6681, 2011.
- Michalak, A. M., Hirsch, A., Bruhwiler, L., Gurney, K. R., Peters, W. and Tans, P. P.: Maximum likelihood estimation of covariance parameters for Bayesian atmospheric

trace gas surface flux inversions *J. Geophys. Res.*, 110, D24107, 2005.

- Michalak, A., L. Bruhwiler, P. P. Tans, A geostatistical approach to surface flux estimation of atmospheric trace gases, *J. Geophys. Res.*, 109, D14109, doi: [10.1029/2003JD004422](https://doi.org/10.1029/2003JD004422).
- Miyazaki, K., Eskes, H. J., and Sudo, K.: Global NO_x emission estimates derived from an assimilation of OMI tropospheric NO₂ columns, *Atmos. Chem. Phys.*, 12, 2263-2288, 10.5194/acp-12-2263-2012, 2012a.
- Miyazaki, K., Eskes, H. J., Sudo, K., Takigawa, M., van Weele, M., and Boersma, K. F.: Simultaneous assimilation of satellite NO₂, O₃, CO, and HNO₃ data for the analysis of tropospheric chemical composition and emissions, *Atmos. Chem. Phys.*, 12, 9545-9579, <https://doi.org/10.5194/acp-12-9545-2012>, 2012b.
- Miyazaki, K., Eskes, H., Sudo, K., Boersma, K. F., Bowman, K., and Kanaya, Y.: Decadal changes in global surface NO_x emissions from multi-constituent satellite data assimilation, *Atmos. Chem. Phys.*, 17, 807-837, <https://doi.org/10.5194/acp-17-807-2017>, 2017.
- Navon, I. M.: Data assimilation for numerical weather prediction: A review, in: *Data Assimilation for Atmospheric, Oceanic and Hydrologic Applications*, edited by: Park, S. K. and Xu, L., Springer-Verlag, Berlin Heidelberg, Germany, 2009.
- Nesterov, Y., *Introductory Lectures on Convex Programming*, Basic course, Springer, ISBN 978-1-4419-8853-9, 2004.
- Niu, T., S. L. Gong, G. F. Zhu, H. L. Liu, X. Q. Hu, C. H. Zhao, and Y. Q. Wang (2008), Data assimilation of dust aerosol observations for the CUACE/dust forecasting system, *Atmos. Chem. Phys.*, 8, 3473-3482.
- OJEU: Directive 2008/50/EC of the European Parliament and of the Council of 21 May 2008, *Official Journal of the European Union*, L 152/1, 11 June 2008.
- Pagowski, M., Liu, Z., Grell, G. A., Hu, M., Lin, H. C., and Schwartz, C. S.: Implementation of aerosol assimilation in Gridpoint Statistical Interpolation (v. 3.2) and WRF-Chem (v. 3.4.1), 7, 1621-1627, 2014.
- Palmer, P. I., D. J. Jacob, A. M. Fiore, R. V. Martin, K. Chance, and T. P. Kurosu (2003), Mapping isoprene emissions over North America using formaldehyde column observations from space, *J. Geophys. Res.*, 108(D6), 4180, doi: [10.1029/2002JD002153](https://doi.org/10.1029/2002JD002153).
- Park, R. J., D. J. Jacob, M. Chin and R. V. Martin (2003). "Sources of carbonaceous aerosols over the United States and implications for natural visibility." *Journal of Geophysical Research* 108(D12).
- Park, S. K. and A. G. Russell, Regional Adjustment of Emission Strengths via Four Dimensional Data Assimilations, *Asia-Pacific J. Atmos. Sci.*, 49(3), 361-374, 2013.
- Peischl, J., et al. (2015), Quantifying atmospheric methane emissions from the Haynesville, Fayetteville, and northeastern Marcellus shale gas production regions, *J. Geophys. Res. Atmos.*, 120, 2119–2139, doi: [10.1002/2014JD022697](https://doi.org/10.1002/2014JD022697).
- Penenko, V., A. Baklanov, E. Tsvetova and A. Mahura (2012). Direct and Inverse Problems in a Variational Concept of Environmental Modeling, *Pure and Applied Geoph.* 169, 447.
- Penenko, V. and Obraztsov, N. (1976). A variational initialization method for the fields of the meteorological elements, *Soviet Meteorology and Hydrology*, 11: 1-11.
- Potempski, S., Galmarini, S. Est modus in rebus: analytical properties of multi-model ensembles. *Atmos. Chem. Phys.* 9, 9471e9489. <http://dx.doi.org/10.5194/acp-9-9471-2009>, 2009.
- Randles, C. A., da Silva, A. M., Buchard, V., Colarco, P. R., Darmenov, A., Govindaraju, R., Smirnov, A., Holben, B., Ferrare, R., Hair, J., Shinozuka, Y., and Flynn, C. J.: The MERRA-2 Aerosol Reanalysis, 1980 Onward. Part I: System Description and Data Assimilation Evaluation, *Journal of Climate*, 30, 6823-6850, 2017.

- Rodgers, C. D.: Inverse methods for atmospheric sounding, World Scientific, Series on Atmospheric, Oceanic and Planetary Physics, 2000.
- Rubin, J. I., and Co-authors, 2016: Development of the Ensemble Navy Aerosol Analysis Prediction System (ENAAPS) and its application of the Data Assimilation Research Testbed (DART) in support of aerosol forecasting. *Atmos. Chem. Phys.*, 16, 3927–3951, doi: <https://doi.org/10.5194/acp-16-3927-2016>.
- Rubin, J. I., J. S. Reid, J. A. Hansen, J. L. Anderson, B. N. Holben, P. Xian, D. L. Westphal, and J. Zhang, 2017: Assimilation of AERONET and MODIS AOT observations using variational and ensemble data assimilation methods and its impact on aerosol forecasting skill, *J. Geophys. Res. Atmos.*, 122, 4967–4992, doi: [10.1002/2016JD026067](https://doi.org/10.1002/2016JD026067).
- Saide, P. E., Carmichael, G. R., Liu, Z., Schwartz, C. S., Lin, H. C., da Silva, A. M., and Hyer, E.: Aerosol optical depth assimilation for a size-resolved sectional model: impacts of observationally constrained, multi-wavelength and fine mode retrievals on regional scale forecasts, *Atmos. Chem. Phys. Discuss.*, 13, 12213–12261, 10.5194/acpd-13-12213-2013, 2013.
- Saide, P. E., Kim, J., Song, C. H., Choi, M., Cheng, Y., and Carmichael, G. R.: Assimilation of next generation geostationary aerosol optical depth retrievals to improve air quality simulations, *Geophysical research letters*, 41, 2014GL062089, 10.1002/2014gl062089, 2014.
- Saide, P. E., Peterson, D., da Silva, A., Anderson, B., Ziemba, L. D., Diskin, G., Sachse, G., Hair, J., Butler, C., Fenn, M., Jimenez, J. L., Campuzano-Jost, P., Perring, A. E., Schwarz, J. P., Markovic, M. Z., Russell, P., Redemann, J., Shinozuka, Y., Streets, D. G., Yan, F., Dibb, J., Yokelson, R., Toon, O. B., Hyer, E., and Carmichael, G. R.: Revealing important nocturnal and day-to-day variations in fire smoke emissions through a multiplatform inversion, *Geophysical research letters*, 2015GL063737, 10.1002/2015gl063737, 2015.
- Saide, Pablo E.; Thompson, G.; Eidhammer, T., and G. Carmichael, Assessment of biomass burning smoke influence on environmental conditions for multiyear tornado outbreaks by combining aerosol-aware microphysics and fire emission constraints, *JGR*, 17, 10294–10311, 2016.
- Sandu A. and H. Cheng: "An Error Subspace Perspective on Data Assimilation." *International Journal for Uncertainty Quantification*, Vol. 5, No. 6, pp. 491--510, 2015.
- Sandu A. and P. Miehe: "Forward, Tangent Linear, and Adjoint Runge Kutta Methods in KPP--2.2 for Efficient Chemical Kinetic Simulations." *International Journal of Computer Mathematics*, Vol. 87, Issue 11, pp. 2458--2479, September 2010.
- Sandu A. and T.F. Chai: "Chemical Data Assimilation -- an Overview." *Atmosphere*, Vol. 2, No. 3, pp. 426--463, 2011.
- Sandu A., E.M. Constantinescu, G.R. Carmichael, T. Chai, D. Daescu, and J.H. Seinfeld: "Ensemble Methods for Dynamic Data Assimilation of Chemical Observations in Atmospheric Models." *Journal of Algorithms and Computational Technology*, Vol. 5, No. 4, DDDAS issue, pp. 667--692, 2011.
- Sandu A., K. Singh, M. Jardak, K.W. Bowman, and M. Lee: "A Practical Method to Estimate Information Content in the Context of 4D-Var Data Assimilation." *SIAM/ASA Journal on Uncertainty Quantification*, Vol. 1, pp. 106--138, 2013.
- Schmidt, H., C. Derognat, R. Vautard, and M. Beekmann (2001), A comparison of simulated and observed ozone mixing ratios for the summer of 1998 in western Europe, *Atmos. Environ.*, 35, 6277– 6297.
- Schwartz, C. S., Liu, Z., Lin, H. C., and McKeen, S. A.: Simultaneous three-dimensional variational assimilation of surface fine particulate matter and MODIS aerosol optical depth, *Journal of Geophysical Research*, 117, D13202, 2012.
- Schwartz, C. S., Liu, Z., Lin, H.-C., and Cetola, J. D.: Assimilating aerosol observations with a

“hybrid” variational-ensemble data assimilation system, *Journal of Geophysical Research: Atmospheres*, 2013JD020937, 10.1002/2013jd020937, 2014.

Seigneur, C. (2001), Current status of air quality modeling for particulate matter, *J. Air Waste Manage. Assoc.*, 51, 1508– 1821.

Sekiyama, T., T. Tanaka, A. Shimizu, and T. Miyoshi, 2010: Data assimilation of CALIPSO aerosol observations. *Atmos. Chem. Phys.*, 10, 39–49, doi: <https://doi.org/10.5194/acp-10-39-2010>

Shrivastava, M., J. Fast, R. Easter, W. I. Gustafson Jr., R. A. Zaveri, J. L. Jimenez, P. Saide, and A. Hodzic (2010), Modeling organic aerosols in a megacity: comparison of simple and complex representations of the volatility basis set approach, *Atmos. Chem. Phys. Discuss.*, 10, 30205–30277.

Singh K. and A. Sandu: “Variational Chemical Data Assimilation with Approximate Adjoint.” *Computers & Geosciences*, Vol. 40, pp. 10--18, 2012.

Singh K., M. Jardak, A. Sandu, K. Bowman, M. Lee, and D. Jones: Construction of Non-diagonal Background Error Covariance Matrices for Global Chemical Data Assimilation. *Geoscientific Model Development*, Vol. 4, pp. 299--314, 2011.

Snow, J.A., J. B. Dennison, D.A. Jaffe, H. U. Price, J. K. Vaughan, and B. Lamb (2003), Aircraft and surface observations of air quality in Puget Sound and a comparison to a regional model, *Atmos. Environ.*, 37, 4019-4032, doi: [10.1016/S1352-2310\(03\)00429-1](https://doi.org/10.1016/S1352-2310(03)00429-1).

Sofiev, M., P. Siljamo, H. Ranta, and A. Rantio-Lehtimäki (2006), Towards numerical forecasting of long-range air transport of birch pollen: theoretical considerations and a feasibility study, *Int. J. Biometeorol.*, 50, 392-402, 2006b.

Sofiev, M., Vira, J., Kouznetsov, R., Prank, M., Soares, J., Genikhovich, E. (2015) Construction of the SILAM Eulerian atmospheric dispersion model based on the advection algorithm of Michael Galperin, *Geosci. Model Developm.* 8, 3497-3522, doi: [10.5194/gmd-8-3497-2015](https://doi.org/10.5194/gmd-8-3497-2015)

Szopa, S., G. Foret, L. Menut, and A. Cozic (2009), Impact of large scale circulation on European summer surface ozone and consequences for modeling forecast, *Atmos. Environ.*, 43, 1189-1195, doi: [10.1016/j.atmosenv.2008.10.039](https://doi.org/10.1016/j.atmosenv.2008.10.039).

Tarantola, A.; *Inverse Problem Theory and Methods for Model Parameter Estimation*, SIAM, 2005.

Tombette, M., Mallet, V., and Sportisse, B.: PM10 data assimilation over Europe with the optimal interpolation method, *Atmos. Chem. Phys.*, 9, 57-70, <https://doi.org/10.5194/acp-9-57-2009>.

Turner, A. J., and Jacob, D. J.: Balancing aggregation and smoothing errors in inverse models, *Atmos. Chem. Phys. Discuss.*, 15, 1001-1026, 10.5194/acpd-15-1001-2015, 2015.

Turner, A., D. K. Henze, R. V. Martin, and A. Hakami (2012), The spatial extent of source influences on modeled column concentrations of short-lived species, *Geophys. Res. Lett.*, 39, L12806, doi: [10.1029/2012GL051832](https://doi.org/10.1029/2012GL051832).

Vira, J., Sofiev, M. (2012) On variational data assimilation for estimating the model initial conditions and emission fluxes for the short-term forecasting of SO_x concentrations. *Atmosph. Environ.*, 46, pp.318-328, doi: [10.1016/j.atmosenv.2011.09.066](https://doi.org/10.1016/j.atmosenv.2011.09.066)

Vira, J., Sofiev, M. (2015) Assimilation of surface NO₂ and O₃ observations into the SILAM chemistry transport model, *Geosci. Model Dev.*, 8, 191-203, www.geosci-model-dev.net/8/191/2015/, doi: [10.5194/gmd-8-191-2015](https://doi.org/10.5194/gmd-8-191-2015)

Vlemmix, T., Pijters, A. J. M., Stammes, P., Wang, P., and Levelt, P. F.: Retrieval of tropospheric NO₂ using the MAX-DOAS method combined with relative intensity measurements for aerosol correction, *Atmos. Meas. Tech.*, 3, 1287-1305, <https://doi.org/10.5194/amt-3-1287-2010>, 2010.

- von Clarmann, T., Glatthor, N., Grabowski, U., Höpfner, M., Kellmann, S., Kiefer, M., Linden, A., Mengistu Tsidu, G., Milz, M., Steck, T., Stiller, G. P., Wang, D. Y., Fischer, H., Funke, B., Gil-López, S., and López-Puertas, M.: Retrieval of temperature and tangent altitude pointing from limb emission spectra recorded from space by the Michelson Interferometer for Passive Atmospheric Sounding (MIPAS), *J. Geophys. Res.*, 108, 4736, doi:10.1029/2003JD003602, 2003.
- von Clarmann, T., Höpfner, M., Kellmann, S., Linden, A., Chauhan, S., Funke, B., Grabowski, U., Glatthor, N., Kiefer, M., Schieferdecker, T., Stiller, G. P., and Versick, S.: Retrieval of temperature, H₂O, O₃, HNO₃, CH₄, N₂O, ClONO₂ and ClO from MIPAS reduced resolution nominal mode limb emission measurements, *Atmos. Meas. Tech.*, 2, 159-175, <https://doi.org/10.5194/amt-2-159-2009>, 2009.
- Whitaker, J. S. and Hamill, T. M.: Ensemble data assimilation without perturbed observations, *Mon. Wea. Rev.*, 130, 1913–1924, 2002.
- WMO, 2017: Global Atmosphere Watch Workshop on Measurement-Model Fusion for Global Total Atmospheric Deposition (MMF-GTAD), Geneva, Switzerland, 28 February-2 March, 2017, 45 pp., May 2017.GAW Report No. 234.
https://library.wmo.int/opac/index.php?lvl=notice_display&id=19885
- Wu, L., Bocquet, M., Chevallier, F., Lauvaux, T. and Davis, K. Hyperparameter Estimation for Uncertainty Quantification in Mesoscale Carbon Dioxide Inversions *Tellus B*, 2013, 65, 20894, 2011.
- Wu, L., Bocquet, M., Lauvaux, T., Chevallier, F., Rayner, P. and Davis, K. Optimal representation of source-sink fluxes for mesoscale carbon dioxide inversion with synthetic data *J. Geophys. Res.*, 116, D21304, 2011.
- Yahya, K., Y. Zhang, and J. M. Vukovich, 2014, Real-Time Air Quality Forecasting over the Southeastern United States using WRF/Chem-MADRID: Multiple-Year Assessment and Sensitivity Studies, *Atmospheric Environment*, 92, 318-338, doi:10.1016/j.atmosenv.2014.04.024.
- Yang, K., N. A. Krotkov, A. J. Krueger, S. A. Carn, P. K. Bhartia, and P. F. Levelt (2007), Retrieval of large volcanic SO₂ columns from the Aura Ozone Monitoring Instrument: Comparison and limitations, *J. Geophys. Res.*, 112, D24S43, doi:10.1029/2007JD008825.
- Yu, S. C., R. Mathur, D. Kang, K. Schere, J. Pleim, and T. L. Otte (2007), A detailed evaluation of the Eta-CMAQ forecast model performance for O₃, its related precursors, and meteorological parameters during the 2004 ICARTT study, *J. Geophys. Res.*, 112, D12S14, doi:10.1029/2006JD007715.
- Yu, S., R. Mathur, K. Schere, D. Kang, J. Pleim, J. Young, D. Tong, G. Pouliot, S. A. McKeen, and S. T. Rao (2008), Evaluation of real-time PM_{2.5} forecasts and process analysis for PM_{2.5} formation over the eastern United States using the Eta-CMAQ forecast model during the 2004 ICARTT study, *J. Geophys. Res.*, 113, D06204, doi:10.1029/2007JD009226.
- Yumimoto, K., Uno, I., Sugimoto, N., Shimizu, A., Hara, Y., and Takemura, T.: Size-resolved adjoint inversion of Asian dust, 39, 2012
- Zhang, J., J. S. Reid, D. L. Westphal, N. L. Baker, and E. J. Hyer (2008), A system for operational aerosol optical depth data assimilation over global oceans, *J. Geophys. Res.*, 113, D10208, doi:10.1029/2007JD009065.
- Zhang, L., Chen, Y., Zhao, Y., Henze, D. K., Zhu, L., Song, Y., Paulot, F., Liu, X., Pan, Y., Lin, Y., and Huang, B.: Agricultural ammonia emissions in China: reconciling bottom-up and top-down estimates, 18, 339-355, 2018.
- Zhang, L., E.M. Constantinescu, A. Sandu, Y. Tang, T. Chai, G.R. Carmichael, D. Byun, E. Olaguer: An Adjoint Sensitivity Analysis and 4D-Var Data Assimilation Study of Texas Air Quality. *Atmospheric Environment*, Vol. 42, Issue 23, pp. 5787--5804, 2008.

- Zhang, Y., P. Liu, B. Pun, and C. Seigneur (2006a), A Comprehensive Performance Evaluation of MM5-CMAQ for the Summer 1999 Southern Oxidants Study Episode, Part-I. Evaluation Protocols, Databases and Meteorological Predictions, *Atmos. Environ.*, 40, 4825-4838.
- Zhang, Y., P. Liu, A. Queen, C. Misenis, B. Pun, C. Seigneur, and S.-Y. Wu (2006b), A Comprehensive Performance Evaluation of MM5-CMAQ for the Summer 1999 Southern Oxidants Study Episode, Part-II. Gas and Aerosol Predictions, *Atmos. Environ.*, 40, 4839-4855.
- Zhang, Y., C. Seigneur, M. Bocquet, V. Mallet, and A. Baklanov, 2012, Real-Time Air Quality Forecasting, Part I: History, Techniques, and Current Status, *Atmospheric Environment*, 60, 632-655, doi:10.1016/j.atmosenv.2012.06.031v.
- Zhang, Y., C.-P. Hong, K. Yahya, Q. Li, Q. Zhang, and K.-B. He, 2016, Comprehensive evaluation of multi-year real-time air quality forecasting using an online-coupled meteorology-chemistry model over southeastern United States, *Atmos. Environ.*, 138, 162-182, doi:10.1016/j.atmosenv.2016.05.006.
- Zupanski, M.: Maximum likelihood ensemble filter: Theoretical aspects, *Mon. Wea. Rev.*, 133, 1710–1726, 2005.
-

Chapter 11. Uncertainty Quantification and Probabilistic Forecasting

11.1 Introduction

In this chapter, fundamentals on uncertainty quantification and probabilistic forecasting are described in detail. Topics include different forms of ensembles (Section 11.2), attributes of probabilistic prediction (Section 11.3), post-processing and calibration (Section 11.4), forecast products from ensembles (Section 11.5), and uncertainty quantification and data assimilation (Section 11.6). Finally, Section 11.7 summarizes the key points.

11.2 Definitions

11.2.1 *The Challenge of Uncertainty*

Uncertainty is part of every chemical weather (CW) and air-quality (AQ) prediction. It is unavoidable. One part of that uncertainty comes from models of the atmosphere, the land surface, chemistry, and emissions, which will always be flawed no matter what their sophistication and accuracy. Another part of that uncertainty comes from the chaotic dynamics of the atmosphere and the non-linearity of chemical processes. Even if flawless models were to be created one day, atmospheric observations, information about emissions, initial and boundary conditions, and other data fed into those models to initiate simulations and constrain their solutions would always bear a degree of imprecision, creating uncertainty in forecasts. Errors in model simulations are familiar to anyone who uses forecasts. It is less easy to remember that observations have errors, too. It is tempting to regard observations as truth, as a measure of the atmosphere's real state, but they are not. Instruments are not infinitely precise and accurate, they are not placed in infinitely dense arrays everywhere, and the atmosphere is a chaotic system. Uncertainty in observations is no more avoidable than uncertainty in models.

11.2.2 *The Power of Probability*

Fortunately, there are ways to gauge uncertainty, to mitigate it, and even to put it to good use. Uncertainty in AQ forecasts - or, more generally, in the dispersion of non-passive pollutants - has proven manageable through probabilistic approaches (Galmarini et al., 2001; Delle Monache and Stull 2003; Galmarini et al., 2004; Delle Monache et al., 2006 a, c; McKeen et al., 2005; Pagowski et al., 2005; Potempski and Galmarini, 2009; Mallet, 2010; Solazzo et al., 2012; Kioutsioukis and Galmarini, 2014; Kioutsioukis et al., 2016; Delle Monache et al., 2018). For decision-makers, probabilistic predictions offer benefits that deterministic predictions cannot provide (Palmer, 2002; Buizza, 2008).

A primary tool for probabilistic prediction is the ensemble. In weather forecasting in general, and specifically in AQ forecasting, the term ensemble describes a collection of forecasts, differentiating them from just a single forecast, which is often called deterministic.

11.3 Different Forms of Ensembles

11.3.1 *Overview*

Ensemble prediction systems (EPSs) for forecasting CW and AQ take a variety of forms, each with advantages and disadvantages. Often practicality and pragmatism are the main drivers in constructing an EPS (Rao et al., 2011). In some respects, theory lags applications (Potempski and Galmarini, 2009). Delle Monache (2010) and Zhang et al. (2012) provided good reviews of the young history of EPSs in CW and AQ forecasting.

Galmarini et al. (2004) proposed a scheme to catalogue the various practices that allow construction of an ensemble starting from multiple circulation or dispersion inputs, and multiple dispersion/AQ models. The basic idea is that one can work on the diversity of weather fields and use one or more models, or can work on the diversity of the input parameters, or of

ways to model some aspects of the chemical process and transform limitations into benefits. Deficiencies that arise from limitations in monitoring atmospheric conditions and from the limitations in our ability to model them can be exploited from the probabilistic point of view to estimate the uncertainty that characterizes a forecast and its reliability.

No matter its form, in an ideal EPS the prediction from each member is equally plausible when evaluated over a statistically large number of cases, with each member's prediction differing from other members' predictions by a realistic amount. These characteristics are explained more in Section 11.4.

11.3.2 Dynamical Ensembles

One of the most traditional forms of EPS, sometimes described as dynamical, is based on a Monte Carlo approach. In a dynamical EPS, the discrete sampling of a probability distribution of a system's state (i.e., the atmosphere and its constituents) is achieved by running more than one deterministic simulation to generate meaningfully different predictions, all valid for the same location and time. There are a variety of methods to achieve those meaningful differences. Figure 11.1 illustrates five methods as they might be applied to transport-and-dispersion forecasting (Galmarini et al., 2004).

One method is to base each member of an EPS on the same model (or the same system of models) and configuration, but to provide that model (or that system) with different inputs. A simple, pragmatic example of this method is the lagged ensemble, which is often used in weather forecasting (Hoffman and Kalnay, 1983; Dalcher et al., 1988; Ebisuzaki and Kalnay, 1991; Mittermaier, 2007). In a lagged ensemble, a single deterministic model is used to compose an ensemble by creating members from a recent sequence of forecasts valid at the same time but initialized at different times (thus the term lagged). A 12-h forecast might be used as a base, then be combined with an 18-h forecast initialized 6 hours earlier than the base's initialization time, and with a 24-h forecast initialized 12 hours earlier, etc. This is a way to address uncertainty in initial conditions. Other single-model EPSs address the same uncertainty by choosing different sources of initial and boundary conditions (e.g., different large-scale models of the meteorology or different descriptions of emissions) or by perturbing the input of meteorological and/or chemical fields in plausible ways (Molteni et al., 1996; Delle Monache et al., 2006 a, b; Zhang et al., 2007). These methods correspond to columns 1 and 2 of Figure 11.1.

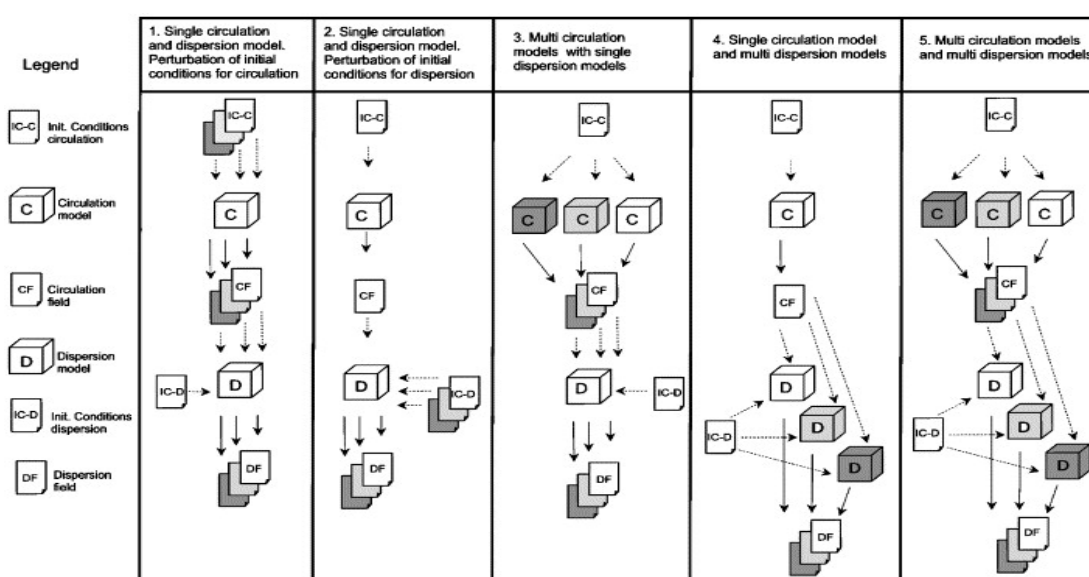


Figure 11.1. Schemata of five methods (columns labeled 1–5) for constructing a dynamical EPS for transport-and-dispersion forecasting (From Galmarini et al., 2004, used by permission).

A second method for achieving meaningful differences among members is to use the same inputs but different configurations of an atmospheric model and/or chemistry model, or to use different models entirely (columns 3–5 of Figure 11.1). The former of these alternatives is sometimes called a multi-physics EPS (e.g., Mallet and Sportisse, 2006 a, b; Wu et al., 2008; Bei et al., 2010). By varying parameterization schemes for the atmospheric surface and boundary layers, cloud microphysics, cumulus convection, short- and long-wave radiation, etc., a multi-physics EPS can partially account for uncertainty in how atmospheric processes are represented in the model code. If two or more entirely different models are used, it is called a multi-model EPS (Galmarini et al., 2001; McKeen et al., 2005, 2007; Potemski et al., 2008; Djalalova et al., 2010; Solazzo et al., 2012; Monteiro et al., 2013; Žabkar et al., 2013; Im et al., 2015). From one perspective, a multi-physics EPS is just a specific case of a multi-model EPS.

A third method is to combine the other two: different models and different inputs. The combined approach can lead to more diversity among members. In the case of meteorological EPSs, especially on the mesoscale for short lead times, achieving realistic diversity among ensemble members can be a challenge (Hamill et al., 2000; Eckel et al. 2010; Romine et al., 2014; Schwartz et al., 2014; Berner et al., 2015).

11.3.3 *Analog Ensembles*

Dynamical EPSs are complex and computationally expensive, so other methods of probabilistic prediction have also been developed. One of these is the analog ensemble (AnEn). AnEn is a hybrid dynamical-statistical approach to treating uncertainty (Delle Monache et al., 2013; Nagarajan et al., 2015; Delle Monache et al., 2018). AnEn starts with a current dynamical prediction from a model. Then an archive of output from the same model (or nearly the same model) is searched using a proper metric to find a subset of past predictions most like the current prediction. Those are the analogs. For each analog forecast from the archives, the corresponding archived observations are then used collectively as an ensemble from which the final statistical forecast is made. The method applied to AQ forecasts is described in detail by Delle Monache et al. (2018).

11.4 *Attributes of Probabilistic Prediction*

11.4.1 *Overview*

Attributes of probabilistic predictions include statistical consistency, reliability, sharpness, resolution, discrimination, and spread. These terms, which are explained below, are generally not in the lexicon of deterministic prediction or traditional forecasting with single model runs. By themselves the attributes are not skill metrics in the way one typically thinks of skill. For example, a probabilistic prediction can be perfectly reliable yet completely without skill if one uses climatology as a standard of reference. Yet each attribute provides insight into the character and utility of probabilistic forecasts, and what information they do and do not provide.

11.4.2 *Statistical Consistency*

The degree to which an EPS's predictions are indistinguishable from observations characterizes the predictions' statistical consistency (Anderson, 1996). Statistical consistency can be thought of as an ultimate measure of a statistically ideal ensemble prediction whose probability distribution is like that of the observed conditions.

11.4.3 *Reliability*

Probabilistic predictions are reliable if the frequency at which something is predicted to happen over many cases (e.g., concentration of PM_{2.5} > 10 μg m⁻³) is the frequency at which it actually happens (i.e., is found in observations), within the statistical limitations imposed by a

finite number of ensemble members, knowledge of the atmosphere's state, etc. (Leutbecher and Palmer, 2008). For a single case, frequency translates to probability (likelihood).

Reliability can be measured in several ways, including with the aptly named reliability diagram (Weisheimer and Palmer 2014), as shown in Figures 11.2 and 11.3. Reliability diagrams require a large set of predictions and corresponding observations to reveal a clear signal.

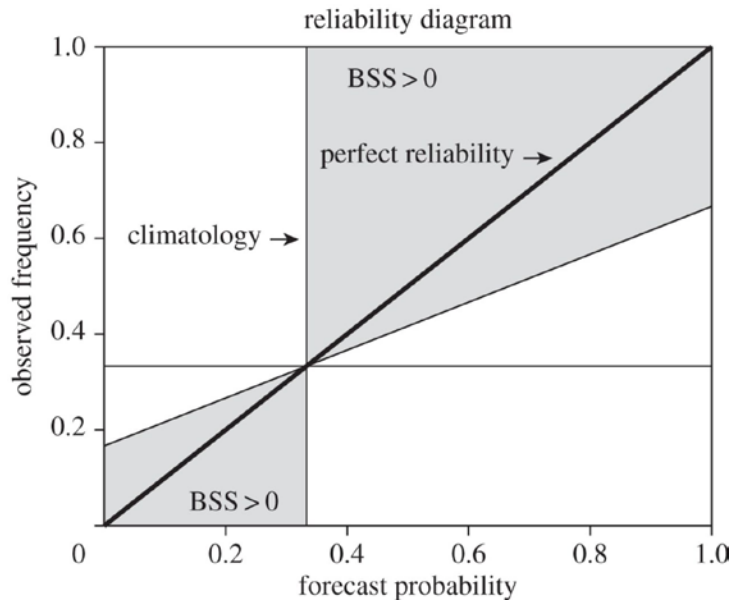


Figure 11.2. Schema of a reliability diagram

The frequency with which some condition is observed is plotted as a function of the predicted probability of that condition occurring. Perfect reliability is the 1:1 line (bold). Regions of positive Brier skill score (BSS) based on climatology as a reference are in gray. The thin horizontal line and thin vertical line (labeled “climatology”) respectively mark how frequently a condition was observed in climatological data and the probabilistic prediction of that condition over many cases. (From Weisheimer and Palmer, 2014, reprinted by permission.)

Rank histograms are also useful for assessing reliability (Anderson 1996; Hamill and Colucci 1997; Talagrand et al. 1997; Hamill 2001; Delle Monache 2010). In a rank histogram, each ensemble member's prediction of a variable valid at a specific time and place is rank-ordered, bounding intervals or bins between pairs of predictions. Beyond the lowest and highest ranked predictions are open-ended bins. The number of bins exceeds the number of predictions by one. Observations that correspond to each prediction are then placed within the bins. Reliable forecasts lead to a flat ranked histogram in which each bin contains approximately the same number of observations. A histogram that is concave up (shaped like a U) is a sign of under-dispersive predictions. Over-dispersive predictions produce a histogram that is convex up. If bars on the left of a histogram are longer than on the right, observations preferentially fall outside the lowest prediction by an ensemble member, so forecasts are biased high (Figure 11.4). Long bars on the right of a histogram are a sign of low bias.

Another way of measuring reliability is by examining the spread among an EPS's predictions. A perfectly reliable probabilistic prediction from an ensemble will have a spread (measured by standard deviation) equal to the root mean squared error (RMSE) in the mean forecast (Talagrand et al., 1997). Figure 11.5 is an example.

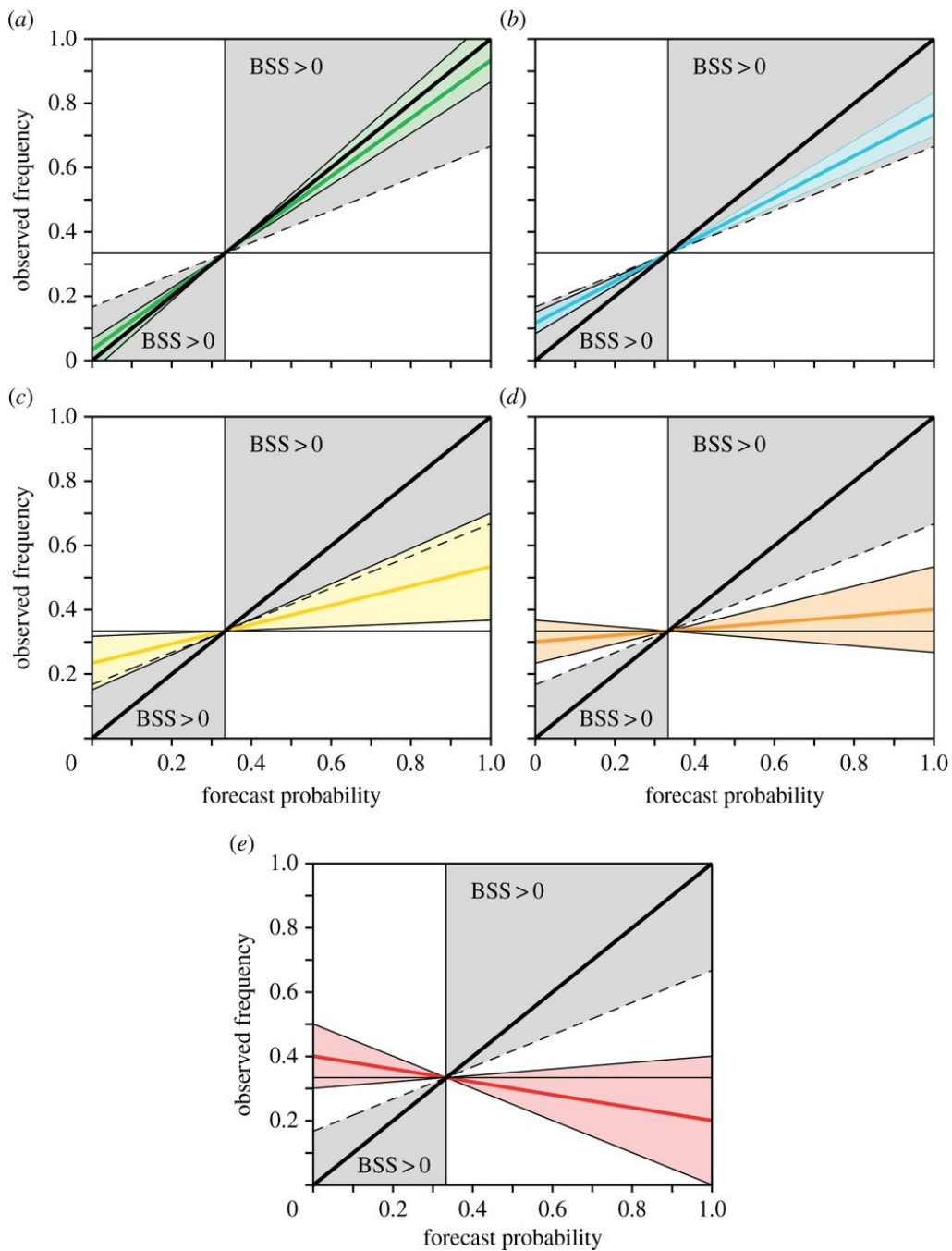


Figure 11.3. Five schematic examples of reliability

(a) completely reliable, (b) highly reliable, (c) marginally reliable, (d) unreliable, (e) unreliable and deceptive. Each bold colored line is the reliability slope for a hypothetical collection of probabilistic forecasts, around which the range of uncertainty is shaded. Other details of the panels are as in Figure 11.2. In (e) the predicted and observed probabilities are negatively related, which is why the predictions can be considered deceptive. (From Weisheimer and Palmer 2014, reprinted by permission. Terms for the five categories are re-interpreted herein.)

11.4.4 *Sharpness*

The narrower the distribution of an EPS's probabilistic prediction, the sharper it is (Gneiting et al., 2007). Sharp predictions are specific predictions (Hamill, 2001). They are not necessarily skillful predictions, however, because observations (i.e., for validation) play no role in the definition of sharpness (Wilks, 2006). Sharpness is only a property of forecasts, determining how distinct one forecast is from another, for example.

11.4.5 *Resolution and Discrimination*

Resolution is a measure of how distinctly different the observations are from one another, given differences among an EPS's predictions (Murphy, 1993; Bröcker 2015a). An example of perfect resolution is when a predicted probability is 100%, the predicted outcome (what is observed) occurs every time, and when the predicted probability is 0%, the outcome never occurs. More generally, better resolution means that observations are more distinctly different depending on whether A or B is predicted.

Discrimination is a measure of how distinctly different an EPS's predictions are from one another, given differences among the observations (Murphy, 1993; Bröcker, 2015a). An example of perfect discrimination is when a predicted outcome occurs (is observed), its predicted probability was 100%, and when the outcome does not occur, its predicted probability was 0%. More generally, better discrimination means that observations are more distinctly different depending on whether the outcome is A or B. A Receiver Operating Characteristic (ROC) diagram (Mason, 1982; Marzban, 2004; Wilks, 2006) is one method of quantifying discrimination (Figure 11.6). The abscissa and ordinate respectively are false-alarm rate and hit rate. With the ROC curve it is easy to visualize performance with respect to dichotomous predictions and outcomes.

Resolution and discrimination might at first appear to describe the same thing. Indeed, they are closely related. The difference between the two attributes rests on the starting point of each definition - on what circumstance the relationship between a prediction and an observation is conditioned. Resolution is conditioned on predictions. Discrimination is conditioned on observations.

11.4.6 *Spread-Skill Relationship*

The spread among an EPS's predictions indicates approximately how much confidence one can place in the predictions, assuming the ensemble that generated them is reasonably well calibrated (Figure 11.5). This rule of thumb is rooted in the so-called spread-skill relationship; under certain circumstances, the more skillful an EPS's probabilistic prediction, the narrower its spread (Murphy, 1988; Barker, 1991; Kalnay, 2003; Hopson, 2014), although the strength of this relationship is generally modest.

11.5 Post-Processing and Calibration

When raw predictions from an EPS are evaluated for the attributes listed above, the predictions are usually revealed to be deficient in some way. They might be biased low or high. The spread among members might be too large or (more likely) too small.

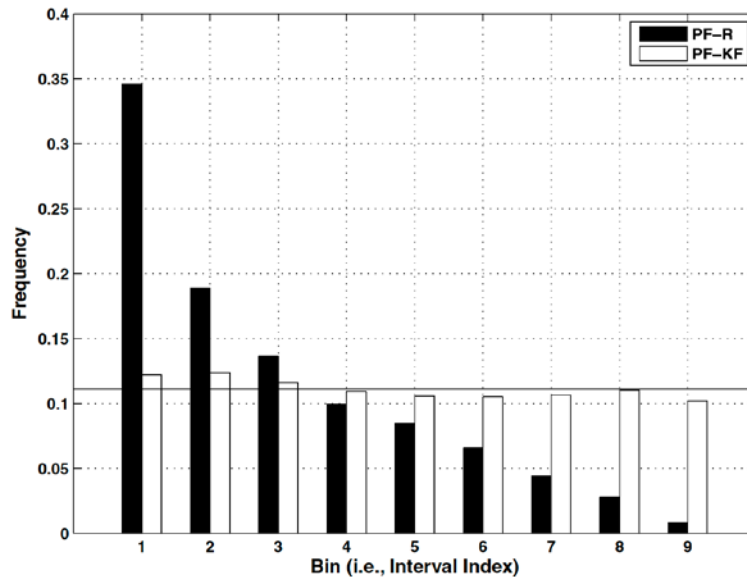


Figure 11.4. Example of how a rank histogram can be used to assess reliability. A reliable (i.e., unbiased and realistically dispersive) set of forecasts (white) was generated by post-processing a set of raw, high-biased probabilistic forecasts (black). (From Delle Monache et al., 2008a, used by permission.)

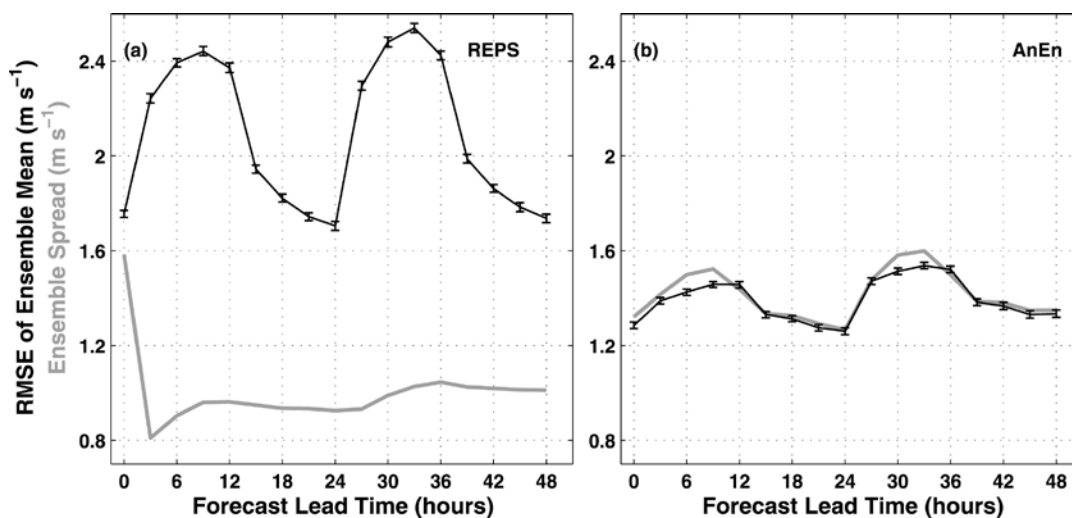


Figure 11.5. Dispersion diagram showing the root mean squared error (RMSE) of the ensemble mean (black) and the ensemble spread (gray) of predicted wind speed at 10 m (AGL) by (a) Canada's Regional Ensemble Prediction System (REPS) and (b) an analog ensemble (AnEn). The close match in (b) between the RMSE and spread signifies reliability of these AnEn forecasts. (From Delle Monache et al., 2013, used by permission.)

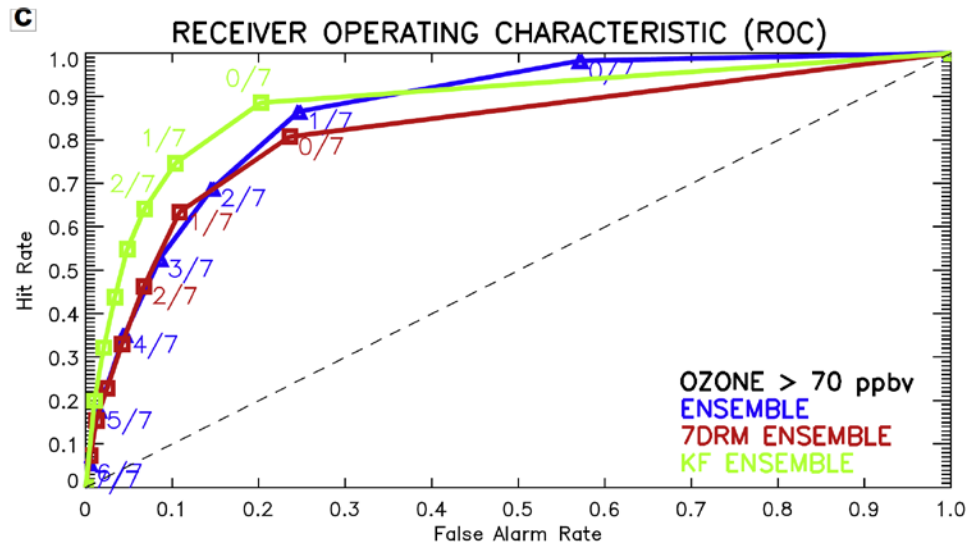


Figure 11.6. Example of a Receiver Operating Characteristic (ROC) diagram

Probabilistic forecasts are of O₃ > 70 ppbv from a raw ensemble (blue), the ensemble after bias-correction based on a 7-day running mean (red), and after bias-correction based on a Kalman filter (green). A perfect ROC curve (false alarm rate = 0%; hit rate = 100%) would trace the left and top axes. In this case, bias-correcting with the Kalman filter produced the superior result (From Djalalova et al., 2010, used by permission.).

Maybe some members' predictions are consistent outliers. Such deficiencies can be addressed by:

- (1) improving a model's numerical schemes or its representation of physical processes,
- (2) improving how diversity is introduced to ensemble members,
- (3) improving data assimilation,
- (4) increasing temporal and spatial resolution, etc.

Fundamental improvements in these areas are of course critical to advancing the science (Zhang et al., 2012), but those improvements are expensive, time-consuming, and difficult. Cheaper, faster, and easier approaches are also needed. For example, after an EPS is run and the raw model output generated, that output can be improved through what is called post-processing. One of the most powerful forms of post-processing is calibration.

Calibration improves the reliability, sharpness, resolution, and discrimination of an EPS's predictions. Mean predictions are made more skillful, partly because biases are reduced and random errors are filtered (Delle Monache, 2010; Solazzo et al., 2012, 2013; Kioutsioukis and Galmarini, 2014; Kioutsioukis et al., 2016). Well calibrated predictions produce more accurate guidance about rare, potentially hazardous conditions because ensemble spread is more realistic. Through the spread-skill relationship described above, calibration provides a better indication of predictions' uncertainty, which can be useful when applying forecasts directly to decision-making. There are many ways to calibrate probabilistic predictions. Garaud and Mallet (2011) showed how to build a calibrated ensemble of ozone forecasts. Kniviel et al. (2017) provided in their section 2b a brief list of more than a dozen calibration methods applied to meteorological prediction.

11.6 Forecast Products from Ensembles

Organizing the wealth of information produced by an EPS and presenting it in forms tailored to users' needs is critical to the system's success (Palmer, 2002; Buizza et al., 2005). This section provides some examples of deterministic and probabilistic products that can be generated from an ensemble's output.

11.6.1 Deterministic

As mentioned above, the mean of ensemble members is effectively a deterministic forecast - one that has smaller errors, on average, than even the best ensemble member. Many studies have demonstrated the value of ensemble means across many EPS designs (e.g., McKeen et al., 2005; Wilczak et al., 2006; Delle Monache et al., 2008a; Djalalova et al., 2010). The mean can be calculated based on equal contributions by all members. However, the mean can sometimes be improved through weighting members' contributions by, for example, minimizing the least squared error (Pagowski et al., 2005; Potempski and Galmarini, 2009), by applying a dynamic linear regression algorithm (Pagowski et al., 2006), or by applying learning algorithms (Mallet et al., 2009). The ensemble median can also be used as a deterministic forecast (e.g., McKeen et al., 2005). Figure 11.7 is an example. The median is less affected by extreme outliers than the mean (Galmarini et al., 2004).

11.6.2 Probabilistic

Most AQ forecast products traditionally based on deterministic predictions can also be applied to the mean or median prediction from an EPS, but it is with probabilistic products that EPSs truly revolutionize AQ forecasting. Predictions based on the mean or median can be supplemented with information about the ensemble spread (Figures 11.8 and 11.9). When the spread tightens with lead time, showing more agreement among members, one can infer decreasing uncertainty in the forecast, as described above. Broadening spread implies more uncertainty.

Uncertainty Quantification and Data Assimilation

Uncertainty quantification was originally barely developed in CW and AQ forecasting. Techniques such as optimal interpolation, 3D- and 4D-Var were not meant to estimate the uncertainty associated with the analysis of the control variables, not to mention with the many parameters of AQ models. However, with the advent of ensemble methods such as the ensemble Kalman filter and smoother (see Section 10.4.2), ensembles could become natural components of AQ forecast systems (Constantinescu et al., 2007a, b; Wu et al., 2008). With more advanced optimization techniques, it is now possible to extract uncertainty information from 4D-Var (Bousserez et al., 2015).

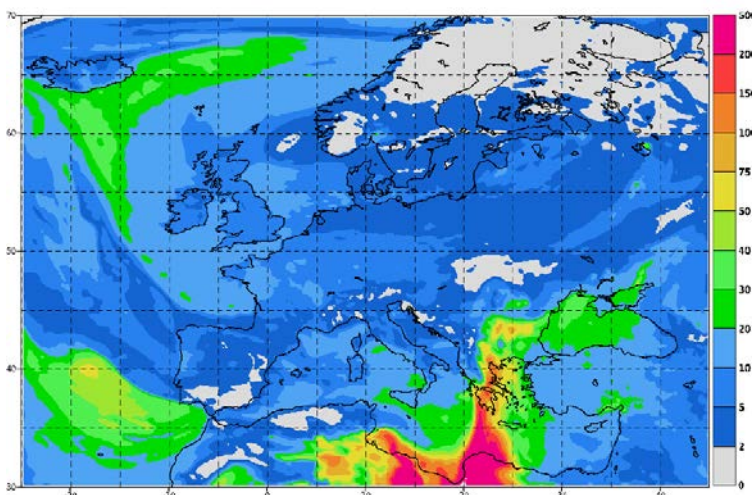


Figure 11.7. Example of a deterministic prediction from the median of an EPS. The shaded field is a 72-h forecast of PM₁₀ ($\mu\text{g m}^{-3}$ following color bar on right) at the surface valid 00 UTC 18 March 2018, generated by the CAMS (Copernicus Atmosphere Monitoring Service) regional EPS described at <https://atmosphere.copernicus.eu/>.

Uncertainty quantification is also better handled through the estimation of statistical parameters, often called hyperparameters, that are used directly or indirectly to tune uncertainty of the variables and parameters (see the discussion in Section 10.5.1). In statistics, this approach where some of the statistical parameters are optimally adjusted using observational data is called empirical Bayes. More complete Bayesian solutions to fully estimate uncertainty are usually based on a hierarchical Bayesian analysis, where statistical parameters are part of the analysis along with the control variables. MCMC techniques, such as the Metropolis-Hastings algorithm, are meant to implement such hierarchical strategy and are able to generate samples (large ensembles) that rigorously represent the uncertainty in the system. Their computational cost is high, but they have been successfully applied to simple problems with a few degrees of freedom or, more recently, to problems where transport and fate of the species are linear or almost linear such as CO₂, CO, or some VOC, coupled with efficient reduction techniques (Delle Monache et al., 2008b; Lunt et al., 2016; Liu et al., 2017).

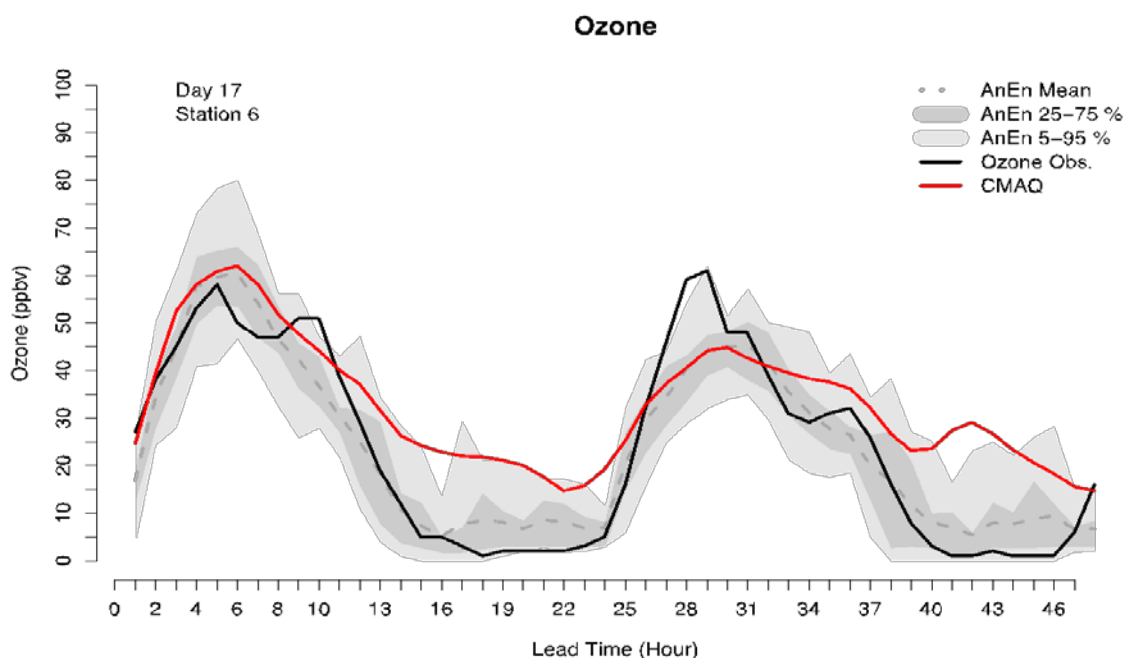


Figure 11.8. Forecasts of O₃ (ppbv) over lead times of 0–48 h at a point location

The ensemble mean from AnEn (gray dotted line) can be compared to the deterministic forecast by CMAQ (red solid line). Observations are in the solid black line. Additional probabilistic information is available from the AnEn members such as the 5%–95% and 25%–75% interquartile ranges shaded here.

(From Delle Monache et al., 2018, used by permission.)

Summary

Uncertainty is part of every chemical weather and air-quality prediction. Fortunately, as summarized below, ensemble prediction systems (EPSs) are powerful tools for characterizing uncertainty, mitigating it, and using it intelligently.

- EPSs frame predictions as probabilities.
- EPSs take several forms, among them dynamical and statistical; dynamics and statistics can be combined through analog ensembles, which sometimes provide very good results faster and with less computational cost than can be achieved with dynamical ensembles.
- There are specific attributes that describe the quality of probabilistic predictions:
 - Reliable means outcomes are predicted with the same frequency at which they are observed;
 - Sharp means predictions are distinctly different from one another;
 - Resolution refers to the extent of differences among observations, given different predictions;
 - Discrimination refers to the extent of differences among predictions, given different observations.
- Spread among predictions from members of an EPS is modestly correlated with predictive skill in certain circumstances, revealing when forecasts can be employed with more or less confidence.
- Raw predictions from an EPS can almost always be improved through calibration applied during post-processing, whereby the mean and higher moments of the distribution of forecasts are adjusted to be more statistically consistent with observations.
- The mean and/or median of an EPS can be treated like a simple deterministic forecast, with the benefit that such a forecast usually is superior to standard forecasts from a single model.
- Finally, the techniques of data assimilation more recently adapted to CW and AQ, such as the ensemble Kalman filter, naturally produce ensembles or finer estimations of the uncertainty of the control variables.
- In a few cases, by exploiting reduction techniques and the possible linearity of models, we are now closer to proposing a more complete Bayesian analysis, based for instance on Markov chain Monte Carlo techniques, whereby uncertainty is fully quantified.

Acknowledgements

L. Delle Monache and J. C. Knievel were supported by the NASA Earth Science Division Applied Science Program (Grant # NNX15AH03G). Thanks to Thomas Hopson (NCAR) for helpful input.

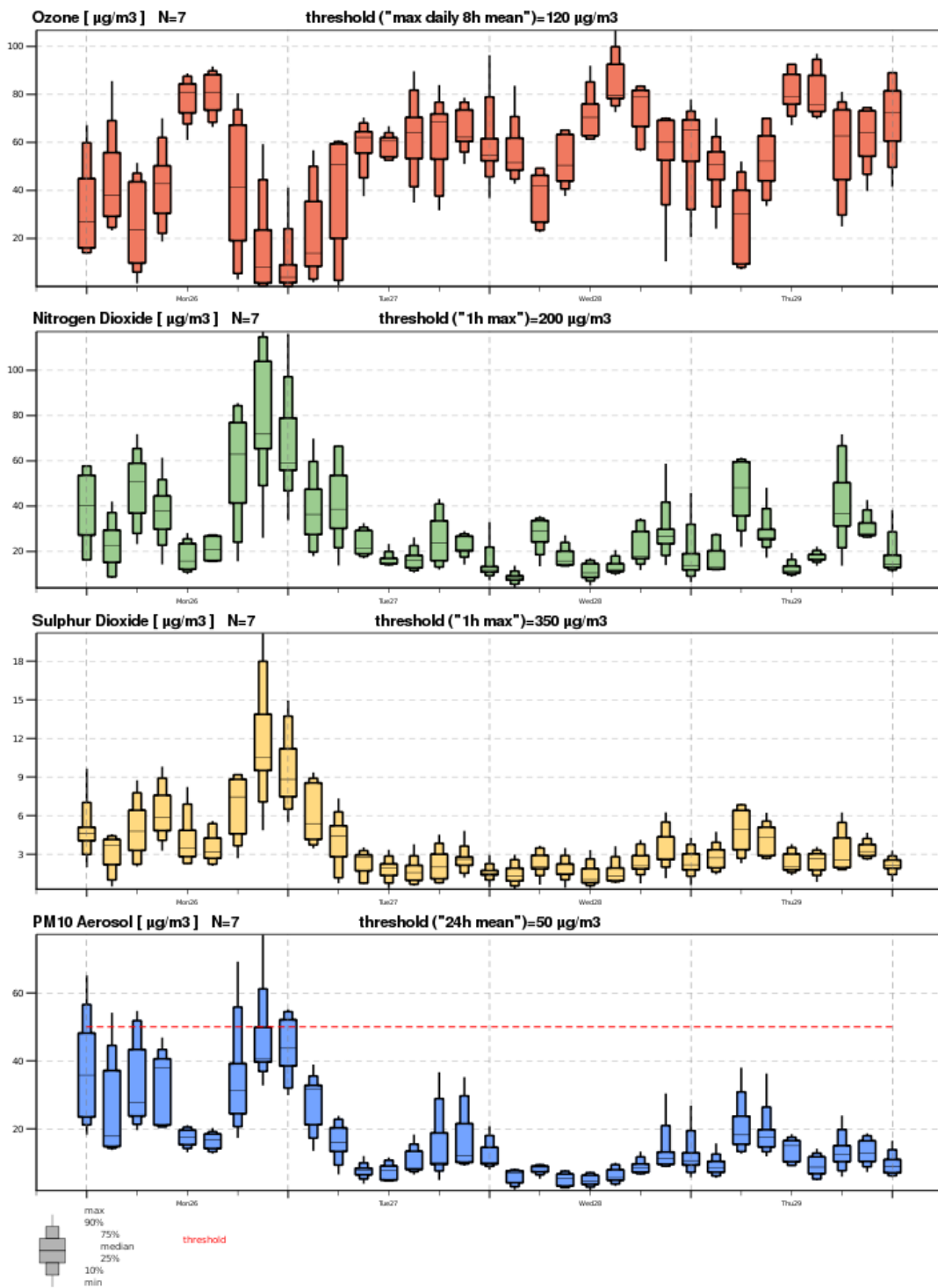


Figure 11.9. Example of probabilistic predictions of ozone (red), nitrogen dioxide (green), sulphur dioxide (yellow), and PM10 aerosols (blue) at Paris, France as a function of valid time from an EPS forecast initialize 00 UTC 26 March 2018, generated by the CAMS regional EPS. Each box shows the predicted minimum, median, maximum, 10th, 25th, 75th, and 90th-percentile (key on lower left). Each horizontal dashed red line is a pollutant's threshold.

References

- Anderson, J. L., 1996: A method for producing and evaluating probabilistic forecasts from ensemble model integrations. *J. Clim.*, 9, 1518–1530, doi:10.1175/1520-0442(1996)009<1518:AMFPAE>2.0.CO;2.
- Barker, T. W., 1991: The Relationship between Spread and Forecast Error in Extended-range Forecasts. *J. Clim.*, 4, 733–742, doi:10.1175/1520-0442(1991)004<0733:TRBSAF>2.0.CO;2.
- Bei, N., W. Lei, M. Zavala, and L. T. Molina, 2010: Ozone predictabilities due to meteorological uncertainties in the Mexico City basin using ensemble forecasts. *Atmospheric Chem. Phys.*, 10, 6295–6309, doi:10.5194/acp-10-6295-2010.
- Berner, J., K. R. Fossell, S.-Y. Ha, J. P. Hacker, and C. Snyder, 2015: Increasing the skill of probabilistic forecasts: understanding performance improvements from model-error representations. *Mon. Weather Rev.*, 143, 1295–1320, doi:10.1175/MWR-D-14-00091.1.
- Bousserez, N., D. K. Henze, A. Perkins, K. W. Bowman, M. Lee, J. Liu, F. Deng, and D. B. A. Jones, 2015: Improved analysis-error covariance matrix for high-dimensional variational inversions: application to source estimation using a 3D atmospheric transport model: Improved Analysis-Error Covariance Estimates. *Q. J. R. Meteorol. Soc.*, 141, 1906–1921, doi:10.1002/qj.2495.
- Bröcker, J., 2015a: Resolution and discrimination - two sides of the same coin. *Q. J. R. Meteorol. Soc.*, 141, 1277–1282, doi:10.1002/qj.2434.
- Bröcker, J., 2015b: Resolution and discrimination-two sides of the same coin: Resolution and Discrimination. *Q. J. R. Meteorol. Soc.*, 141, 1277–1282, doi:10.1002/qj.2434.
- Buizza, R., 2008: The value of probabilistic prediction. *Atmospheric Sci. Lett.*, 9, 36–42, doi:10.1002/asl.170.
- Buizza, R., P. L. Houtekamer, G. Pellerin, Z. Toth, Y. Zhu, and M. Wei, 2005: A comparison of the ECMWF, MSC, and NCEP global ensemble prediction systems. *Mon. Weather Rev.*, 133, 1076–1097.
- Constantinescu, E. M., A. Sandu, T. Chai, and G. R. Carmichael, 2007a: Ensemble-based chemical data assimilation. I: General approach. *Q. J. R. Meteorol. Soc.*, 133, 1229–1243, doi:10.1002/qj.76.
- Constantinescu, E. M., A. Sandu, T. Chai, and G. R. Carmichael, 2007b: Ensemble-based chemical data assimilation. II: Covariance localization. *Q. J. R. Meteorol. Soc.*, 133, 1245–1256, doi:10.1002/qj.77.
- Dalcher, A., E. Kalnay, and R. N. Hoffman, 1988: Medium Range Lagged Average Forecasts. *Mon. Weather Rev.*, 116, 402–416, doi:10.1175/1520-0493(1988)116<0402:MRLAF>2.0.CO;2.
- Delle Monache, L., 2010: Ensemble-based air quality predictions. *Air Quality: Theories, Methodologies, Computational Techniques, and Available Databases and Software*, P. Zannetti, Ed., Vol. IV (Advances and Updates) of, The EnviroComp Institute and the Air & Waste Management Association.
- Delle Monache, L., and R. B. Stull, 2003: An ensemble air-quality forecast over western Europe during an ozone episode. *Atmos. Environ.*, 37, 3469–3474, doi:10.1016/S1352-2310(03)00475-8.
- Delle Monache, L., X. Deng, Y. Zhou, and R. Stull, 2006a: Ozone ensemble forecasts: 1. A new ensemble design. *J. Geophys. Res.*, 111, doi:10.1029/2005JD006310. <http://doi.wiley.com/10.1029/2005JD006310> (Accessed November 22, 2016).
- Delle Monache, J. P. Hacker, Y. Zhou, X. Deng, and R. B. Stull, 2006b: Probabilistic aspects of meteorological and ozone regional ensemble forecasts. *J. Geophys. Res.*, 111, doi:10.1029/2005JD006917. <http://doi.wiley.com/10.1029/2005JD006917> (Accessed November 22, 2016).

- Delle Monache, T. Nipen, X. Deng, Y. Zhou, and R. Stull, 2006c: Ozone ensemble forecasts: 2. A Kalman filter predictor bias correction. *J. Geophys. Res.*, 111, doi:10.1029/2005JD006311. <http://doi.wiley.com/10.1029/2005JD006311> (Accessed November 22, 2016).
- Delle Monache, and Co-authors, 2008a: A Kalman-filter bias correction method applied to deterministic, ensemble averaged and probabilistic forecasts of surface ozone. *Tellus B*, 60, 238–249, doi:10.1111/j.1600-0889.2007.00332.x.
- Delle Monache, and Co-authors, 2008b: Bayesian inference and Markov Chain Monte Carlo sampling to reconstruct a contaminant source on a continental scale. *J. Appl. Meteorol. Climatol.*, 47, 2600–2613, doi:10.1175/2008JAMC1766.1.
- Delle Monache, F. A. Eckel, D. L. Rife, B. Nagarajan, and K. Searight, 2013: Probabilistic weather prediction with an analog ensemble. *Mon. Weather Rev.*, 141, 3498–3516, doi:10.1175/MWR-D-12-00281.1.
- Delle Monache, S. Alessandrini, I. Djalalova, J. Wilczak, and J. C. Knievel, 2018: Air quality predictions with an analog ensemble. *Atmospheric Chem. Phys.*, submitted.
- Djalalova, I., and Co-authors, 2010: Ensemble and bias-correction techniques for air quality model forecasts of surface O₃ and PM_{2.5} during the TEXAQS-II experiment of 2006. *Atmos. Environ.*, 44, 455–467, doi:10.1016/j.atmosenv.2009.11.007.
- Ebisuzaki, W., and E. Kalnay, 1991: Ensemble experiments with a new lagged average forecasting scheme. *WMO Res. Act. Atmospheric Ocean. Model. Rep.*, 15, 308.
- Eckel, F. A., H. R. Glahn, T. M. Hamill, S. Joslyn, W. M. Lapenta, and C. F. Mass, 2010: National mesoscale probabilistic prediction: status and the way forward. National Workshop on Mesoscale Probabilistic Prediction, Boulder, CO.
- Galmarini, S., R. Bianconi, R. Bellasio, and G. Graziani, 2001: Forecasting the consequences of accidental releases of radionuclides in the atmosphere from ensemble dispersion modeling. *J. Environ. Radioact.*, 57, 203–219, doi:10.1016/S0265-931X(01)00017-0.
- Galmarini, S., and Co-authors, 2004: Ensemble dispersion forecasting—Part I: concept, approach and indicators. *Atmos. Environ.*, 38, 4607–4617, doi:10.1016/j.atmosenv.2004.05.030.
- Garaud, D., and V. Mallet, 2011: Automatic calibration of an ensemble for uncertainty estimation and probabilistic forecast: Application to air quality. *J. Geophys. Res.*, 116, doi:10.1029/2011JD015780. <http://doi.wiley.com/10.1029/2011JD015780> (Accessed March 30, 2018).
- Gneiting, T., F. Balabdaoui, and A. E. Raftery, 2007: Probabilistic forecasts, calibration and sharpness. *J. R. Stat. Soc. Ser. B Stat. Methodol.*, 69, 243–268.
- Hamill, T. M., 2001: Interpretation of rank histograms for verifying ensemble forecasts. *Mon. Weather Rev.*, 129, 550–560.
- Hamill, T. M., and S. J. Colucci, 1997: Verification of Eta-RSM short-range ensemble forecasts. *Mon. Weather Rev.*, 125, 1312–1327.
- Hamill, T. M., S. L. Mullen, C. Snyder, D. P. Baumhefner, and Z. Toth, 2000: Ensemble forecasting in the short to medium range: Report from a workshop. *Bull. Am. Meteorol. Soc.*, 81, 2653–2664.
- Hoffman, R. N., and E. Kalnay, 1983: Lagged average forecasting, an alternative to Monte Carlo forecasting. *Tellus A*, 35A, 100–118, doi:10.1111/j.1600-0870.1983.tb00189.x.
- Hopson, T. M., 2014: Assessing the ensemble spread–error relationship. *Mon. Weather Rev.*, 142, 1125–1142, doi:10.1175/MWR-D-12-00111.1.
- Im, U., and Co-authors, 2015: Evaluation of operational online-coupled regional air quality models over Europe and North America in the context of AQMEII phase 2. Part I: Ozone. *Atmos. Environ.*, 115, 404–420, doi:10.1016/j.atmosenv.2014.09.042.

- Kalnay, E., 2003: Atmospheric Modeling, Data Assimilation and Predictability. 1st ed. Cambridge University Press, 364 pp.
- Kioutsioukis, I., and S. Galmarini, 2014: De praeceptis ferendis: good practice in multi-model ensembles. *Atmospheric Chem. Phys.*, 14, 11791–11815, doi:10.5194/acp-14-11791-2014, .
- Kioutsioukis, I., and Co-authors, 2016: Insights into the deterministic skill of air quality ensembles from the analysis of AQMEII data. *Atmospheric Chem. Phys.*, 16, 15629–15652, doi:10.5194/acp-16-15629-2016.
- Knievel, J. C., and Co-authors, 2017: Mesoscale ensemble weather prediction at U.S. Army Dugway Proving Ground, Utah. *Weather Forecast.*, 32, 2195–2216, doi:10.1175/WAF-D-17-0049.1.
- Leutbecher, M., and T. N. Palmer, 2008: Ensemble forecasting. *J. Comput. Phys.*, 227, 3515–3539, doi:10.1016/j.jcp.2007.02.014.
- Liu, Y., J.-M. Haussaire, M. Bocquet, Y. Roustan, O. Saunier, and A. Mathieu, 2017: Uncertainty quantification of pollutant source retrieval: comparison of Bayesian methods with application to the Chernobyl and Fukushima Daiichi accidental releases of radionuclides. *Q. J. R. Meteorol. Soc.*, 143, 2886–2901, doi:10.1002/qj.3138.
- Lunt, M. F., M. Rigby, A. L. Ganesan, and A. J. Manning, 2016: Estimation of trace gas fluxes with objectively determined basis functions using reversible jump Markov chain Monte Carlo. *Geosci. Model Dev. Discuss.*, 1–27, doi:10.5194/gmd-2016-41.
- Mallet, V., 2010: Ensemble forecast of analyses: Coupling data assimilation and sequential aggregation. *J. Geophys. Res.*, 115, doi:10.1029/2010JD014259. <http://doi.wiley.com/10.1029/2010JD014259> (Accessed December 20, 2016).
- Mallet, V., and B. Sportisse, 2006a: Ensemble-based air quality forecasts: A multimodel approach applied to ozone. *J. Geophys. Res.*, 111, doi:10.1029/2005JD006675. <http://doi.wiley.com/10.1029/2005JD006675> (Accessed December 20, 2016).
- Mallet, V., and B. Sportisse, 2006b: Uncertainty in a chemistry-transport model due to physical parameterizations and numerical approximations: An ensemble approach applied to ozone modeling. *J. Geophys. Res.*, 111, doi:10.1029/2005JD006149. <http://doi.wiley.com/10.1029/2005JD006149> (Accessed December 20, 2016).
- Mallet, V., G. Stoltz, and B. Mauricette, 2009: Ozone ensemble forecast with machine learning algorithms. *J. Geophys. Res.*, 114, doi:10.1029/2008JD009978. <http://doi.wiley.com/10.1029/2008JD009978> (Accessed December 20, 2016).
- Marzban, C., 2004: The ROC Curve and the Area under it as Performance Measures. *Weather Forecast.*, 19, 1106–1114, doi:10.1175/825.1
- Mason, I. B., 1982: A model for assessment of weather forecasts. *Aust. Meteorol. Mag.*, 30, 291–303.
- McKeen, S., and Co-authors, 2005: Assessment of an ensemble of seven real-time ozone forecasts over eastern North America during the summer of 2004. *J. Geophys. Res.*, 110, doi:10.1029/2005JD005858. <http://doi.wiley.com/10.1029/2005JD005858> (Accessed November 22, 2016).
- McKeen, S., and Co-authors, 2007: Evaluation of several PM 2.5 forecast models using data collected during the ICARTT/NEAQS 2004 field study. *J. Geophys. Res.*, 112, doi:10.1029/2006JD007608. <http://doi.wiley.com/10.1029/2006JD007608> (Accessed January 6, 2017).
- Mittermaier, M. P., 2007: Improving short-range high-resolution model precipitation forecast skill using time-lagged ensembles. *Q. J. R. Meteorol. Soc.*, 133, 1487–1500, doi:10.1002/qj.135.

- Molteni, F., R. Buizza, T. N. Palmer, and T. Petroliaigis, 1996: The ECMWF Ensemble Prediction System: methodology and validation. *Q. J. R. Meteorol. Soc.*, 122, 73–119, doi:10.1002/qj.49712252905.
- Monteiro, A., and Co-authors, 2013: Bias Correction Techniques to Improve Air Quality Ensemble Predictions: Focus on O3 and PM Over Portugal. *Environ. Model. Assess.*, 18, 533–546, doi:10.1007/s10666-013-9358-2.
- Murphy, A. H., 1993: What is a good forecast? An essay on the nature of goodness in weather forecasting. *Weather Forecast.*, 8, 281–293.
- Murphy, J. M., 1988: The impact of ensemble forecasts on predictability. *Q. J. R. Meteorol. Soc.*, 114, 463–493, doi:10.1002/qj.49711448010.
- Nagarajan, B., L. Delle Monache, J. P. Hacker, D. L. Rife, K. Searight, J. C. Knievel, and T. N. Nipen, 2015: An evaluation of analog-based post-processing methods across several variables and forecast models. *Weather Forecast.*, 151030091332000, doi:10.1175/WAF-D-14-00081.1.
- Pagowski, M., and Co-authors, 2005: A simple method to improve ensemble-based ozone forecasts: IMPROVING ENSEMBLE OZONE FORECASTS. *Geophys. Res. Lett.*, 32, n/a-n/a, doi:10.1029/2004GL022305.
- Pagowski, M., and Co-authors, 2006: Application of dynamic linear regression to improve the skill of ensemble-based deterministic ozone forecasts. *Atmos. Environ.*, 40, 3240–3250, doi:10.1016/j.atmosenv.2006.02.006.
- Palmer, T. N., 2002: The economic value of ensemble forecasts as a tool for risk assessment: from days to decades. *Q. J. R. Meteorol. Soc.*, 128, 747–774.
- Potempski, S., and S. Galmarini, 2009: Est modus in rebus: analytical properties of multi-model ensembles. *Atmos Chem Phys*, 19.
- Potempski, S., and Co-authors, 2008: Multi-model ensemble analysis of the ETEX-2 experiment. *Atmos. Environ.*, 42, 7250–7265, doi:10.1016/j.atmosenv.2008.07.027.
- Rao, S. T., S. Galmarini, and K. Puckett, 2011: Air Quality Model Evaluation International Initiative (AQMEII): Advancing the state of the science in regional photochemical modeling and its applications. *Bull. Am. Meteorol. Soc.*, 92, 23–30, doi:10.1175/2010BAMS3069.1.
- Romine, G. S., C. S. Schwartz, J. Berner, K. R. Fossell, C. Snyder, J. L. Anderson, and M. L. Weisman, 2014: Representing forecast error in a convection-permitting ensemble system. *Mon. Weather Rev.*, 142, 4519–4541, doi:10.1175/MWR-D-14-00100.1.
- Schwartz, C. S., G. S. Romine, K. R. Smith, and M. L. Weisman, 2014: Characterizing and optimizing precipitation forecasts from a convection-permitting ensemble initialized by a mesoscale ensemble Kalman filter. *Weather Forecast.*, 29, 1295–1318, doi:10.1175/WAF-D-13-00145.1.
- Solazzo, E., and Co-authors, 2012: Model evaluation and ensemble modeling of surface-level ozone in Europe and North America in the context of AQMEII. *Atmos. Environ.*, 53, 60–74, doi:10.1016/j.atmosenv.2012.01.003.
- Talagrand, O., R. Vautard, and B. Strauss, 1997: Evaluation of probabilistic prediction systems. Workshop on Predictability, 20–22 October 1997, Shinfield Park, Reading, ECMWF, 1–26.
- Weisheimer, A., and T. N. Palmer, 2014: On the reliability of seasonal climate forecasts. *J. R. Soc. Interface*, 11, 20131162–20131162, doi:10.1098/rsif.2013.1162.
- Wilczak, J., and Co-authors, 2006: Bias-corrected ensemble and probabilistic forecasts of surface ozone over eastern North America during the summer of 2004: BIAS-CORRECTED ENSEMBLE. *J. Geophys. Res. Atmospheres*, 111, n/a-n/a, doi:10.1029/2006JD007598.

- Wilks, D. S., 2006: *Statistical Methods in the Atmospheric Sciences*. 2nd ed. 467 pp.
- Wu, L., V. Mallet, M. Bocquet, and B. Sportisse, 2008: A comparison study of data assimilation algorithms for ozone forecasts. *J. Geophys. Res.*, 113, doi:10.1029/2008JD009991. <http://doi.wiley.com/10.1029/2008JD009991> (Accessed March 30, 2018).
- Žabkar, R., D. Koračin, and J. Rakovec, 2013: A WRF/Chem sensitivity study using ensemble modeling for a high ozone episode in Slovenia and the Northern Adriatic area. *Atmos. Environ.*, 77, 990–1004, doi:10.1016/j.atmosenv.2013.05.065.
- Zhang, F., N. Bei, J. W. Nielsen-Gammon, G. Li, R. Zhang, A. Stuart, and A. Aksoy, 2007: Impacts of meteorological uncertainties on ozone pollution predictability estimated through meteorological and photochemical ensemble forecasts. *J. Geophys. Res.*, 112, doi:10.1029/2006JD007429. <http://doi.wiley.com/10.1029/2006JD007429> (Accessed December 20, 2016).
- Zhang, Y., M. Bocquet, V. Mallet, C. Seigneur, and A. Baklanov, 2012: Real-time air quality forecasting, part II: State of the science, current research needs, and future prospects. *Atmos. Environ.*, 60, 656–676, doi:10.1016/j.atmosenv.2012.02.041.

Chapter 12. Demonstration Cases for Real-Time CW-AQF

12.1 Introduction

It is a considerable challenge to provide guidance and an educated explanation of the large range of chemical regimes and spikes of high concentration of air pollutants in a particular city or industrial district. It is exponentially more difficult to attempt to provide guidance and a discerned educated explanation of such high impact events and chronic detrimental chemical weather for the human populace in many populated areas of the world. This WMO document deals virtually with all populated continents of the world. Furthermore, ironically this chapter is dedicated to this herculean "mission impossible" of outlining examples and best practices for all these geographical locations concisely yet comprehensively. Physically-based air chemistry and air quality models are invariably the most popular and natural tools used to formulate chemical weather-air quality forecasting (CW-AQF) guidance. We believe that the underlying physics and their corresponding physical and chemical parameterizations are comparable despite their difference in model/module choices such as those pertinent to the difference between two gas-phase chemical mechanisms. In addition, along with our presentation of the sample cases and best practices, we hereafter delineate the demonstrative cases by climate, seasonal, and geographical (continental) categorizations. The large variability in the chemical and meteorological regimes of adverse air pollution events will be a pressing challenge for scientists to qualify and quantify at present and for the foreseeable future.

12.2 Arctic/Antarctic and High-Latitude Regions

Cold pools and multiple day stagnant conditions with shallow boundary layers are common causes of pollution scenarios in the high latitude cities and industrial regions. Particulate matter (PM) associated pollution events are common there. Photochemical generated O₃ is usually not the culprit pollution species but PM is the single dominant pollutant that causes human health detriment. In these high latitudes, the recent adverse change in albedo is due to black carbon deposition, precipitous rates of ice-melt, and glacial retreat feedbacks as climate modifications. Monitoring albedo and ice-sheet boundaries becomes critical for databases.

12.3 Mid-Latitude Regions

Almost half of the world's population lives in the largely temperate climate in the mid-latitude regions in the Northern Hemisphere. The mid-latitude region in both hemispheres is highly variable in meteorology and air chemistry regimes. Climate varies between extreme arid to extreme humid and tropical. Severe weather has a large role to play in causing wildfires, wind-blown dust storms, and strong variability of the polar and extra-tropical jet streams that result in air-mass intrusion from the stratosphere. On top of these natural variabilities, the anthropogenic elements such as pollutant emissions with complicated inter-play among themselves and with biogenic emissions and land use modifications impact air composition and climate. Both of these natural and man-made influences on air composition should all be considered for CW-AQF guidance. Air managers in this region are world leaders in regulatory and technological controls of air pollution and greenhouse gases. There have been scientific communities and inter-governmental agencies such as the United Nations and the European Commission that promote coordination of countries in this region to share data and technology to exploit CW-AQ technology for mutual benefits. CW-AQ is not only a local problem but is becoming increasingly more regional and global especially when weather and climate feedback are considered.

Mid-latitude regions are also characterized by cities and megacities where anthropogenic and local emissions strongly affect air quality. In European cities, the presence of densely built districts with street-canyon configuration may require different types of air-quality models to calculate air pollution at the street scale. Further to the requirements of multi-scale modeling from global to street scales, the inter-play among pollutants from different origins (e.g., industries, traffic, residential, agriculture, biogenic, etc.) is crucial to apprehend the formation of secondary pollutants in cities.

12.4 Tropical Regions of the Hemispheres

Over one third of the world's population lives in this region. Some countries in this region experience fast economic growth at the expense of rapidly deteriorating CW-AQ conditions. Large wildfires and enormous dust storms are frequent in this region. The trade wind does not vary as much as the westerly winds in the mid-latitudes. However, the intertropical convergence zone (ITCZ) and the air mass exchange is a binding science challenge for CW-AQ and climate. One cannot understand CW-AQ unless the monsoons and cyclone-genesis are taken into account. The ocean temperature variability in the region determines the onset and severity of El Niño occurrences that are affecting severe precipitation and drought around the globe. The focus rightfully belongs here as large latent heat exchanges from the tropical oceans play a major role in determining climate and weather change.

Wildfire and dust storm variability are partly due to these climate and weather changes. Air chemistry is modulated by such severe weather as well as by the rapidly changing emission fluxes due to fast economic growth. The region has a wealth of diversity of species of plants and animals forming a highly sensitive ecosystem – an added dimension of urgency and responsibility to understand CW-AQ well in this region.

12.5 Summary of Best Practices

It is evident from the examples given in this chapter (see also Tables 12.2-12.8) that the latest and greatest cutting-edge air chemistry, meteorological, emission and land-surface modeling science should be employed as practically as possible under an operational setting of a forecast institution. For some regions, there are multiple AQF systems from multiple institutions, whereas for others a lack of such expertise and/or resources hampers the delivery of such critical services to their constituents. Regardless of abundant or meagre availability, AQF modelers in a region should be sharing data, AQF systems, and any policy-relevant and emission changes in their domain of responsibility. Most AQF systems are developed under free software license, and AQF researchers share their knowledge through publishing and sharing publications. Information sharing between researchers and governmental institutions is crucial. For instance, prescribed burns for debris clearing practiced in many agricultural regions are regulated and their seasonality and permitting policies can be shared with AQF centers in their region and downwind regions. Such knowledge sharing has been proven helpful and timely and should be encouraged henceforth. Aforementioned chapters have accredited some of the inter-governmental technological and knowledge sharing to some international commissions. Regional and phenomonal specific measurement campaigns and establishment and/or deployment of observational network promoted by such commissions and international consortia often resulted in valuable data benefiting the region to resolve their specific air chemistry problems. It is also evident from the examples (see also Tables 12.2-12.8) that there is sufficient similarity in the state-of-science model physics and chemical packages across the different AQFs that a forum of scientist-to-scientist knowhow exchange has de-facto been organized internationally. The contributing authors of this WMO document should continue to spearhead this continual success of volunteerism in "exemplary sportsmanship of sharing our best for the advancement of science and societal welfare".

12.6 Demonstration Cases

Hereafter is a collection of demonstration cases with highlights of their meteorological, chemical, and geographical characteristics. At times, the choice of numerical modeling may give specific insight on certain aspects of CW-AQ. We hope to elaborate cases of general common interest as well as some of those insightful cases. These cases cover the globe and six major continents,

- (a) Global
- (b) North America
- (c) Europe
- (d) Asia
- (e) South America
- (f) Oceania
- (g) Africa

This section provides demonstration cases with a total of 24 cases including 3 on a global scale, 3 in North America, 4 in Europe, 5 in Asia, 2 in South America, 3 in Oceania, and 5 in Africa. Table 12.1 provides a list of all demonstration cases. Tables 12.2-12.8 summarize details for those demonstration cases. A case overview and significance is provided for each case study.

Table 12.1 List of Demonstration Cases for Real-Time CW-AQF

Domain	Case #	Case Title
Global	a1	Long-range transport of Sahara dust and smoke from Portuguese Wildfire emissions to North-West Europe forecast by the global CAMS forecasting system for atmospheric composition
	a2	A study of the 2016 post-monsoon air pollution event over India using the GEOS forecasting system
	a3	Impact of wildland fires on atmospheric aerosols in Northern Hemisphere in 2012
North America	b1	National Air Quality Forecasting Capability for the U.S.A.
	b2	Application of WRF/Chem-MADRID over Southeastern U.S.
	b3	Wildland fire smoke forecasting capability in the U.S.A.
Europe	c1	Application of Regional CAMS over Europe
	c2	Air quality forecasting and analysis for the United Kingdom
	c3.1-3.2	Multi-scale modeling down to street level
Asia	d1	Application of CUACE/Haze-fog over China
	d2	Application of HAQFS over China
	d3	Application of Hong Kong Air Quality Forecasting system over Hong Kong, China
	d4	The impact of urbanization in the Pearl River Delta Region, China under three different climate change scenarios
	d5	Development of a smoke forecasting system for Southeast Asia
South America	e1	Application of WRF-Chem over Southeast Brazil, South America
	e2	Particulate Matter forecasting capability in Peru
Oceania	f1-3	Numerical air quality forecasting of the May 2016 fires in the Sydney, Australia region
Africa	g1.1-1.2	Application of RegCM-CHEM4.5 for dust storm and air quality forecast over southern Africa
	g2	Performance of WRF-CHEM Model to simulate North African Aerosols: preliminary results
	g3	Application of ADMS Urban over the Grand Casablanca area, Morocco

Table 12.2. Demonstration Cases for Real-Time CW-AQF on Global Scale

Attributes	Case a1 (ECMWF)	Case a2 (NASA)	Case a3 (FMI)
Model System and Version	CAMS global forecasting system	GEOS composition forecast system	Finnish Meteorological Institute AQ Forecasting system v.5.5.1
Met Model	Integrated forecasting System of ECMWF	Goddard Earth Observing System Model, Version 5 (GEOS-5)	ECMWF IFS
Chemical Model	Chemical scheme CB05 and LMDz aerosol bin scheme (3 DD, 3 SS, 2 OM, 2 BC, SO42-)	GEOS-Chem v11-02e, GOCART aerosol scheme	SILAM v.5.5
Coupling method	Online	Online	Offline
Application			
Domain	global	global	global
Time Period	5-day forecast started at 00 and 12 UTC	5-day forecast started at 18z	Daily provision 5 days forwards
Nesting method	N/A	N/A	N/A
Horizontal Grid Resolution (km)	Reduced Gaussian grid T511 = 40 km × 40 km	Cubed sphere C360 = approx. 25km × 25km	0.5 °
Vertical Grid Resolutions (total number of layers) (x, y, z grid points)	60 vertical layers up to 0.1 hPa 1014 × 512 × 60	72 vertical layers up to 0.01 hPa 1440 × 540 × 72	720 × 356 × 29
Height of 1st layer (m)	17 m	60 m	20 m
Height of top layer (km)	60 km	78 km	10.5 Pa
Input			

Attributes	Case a1 (ECMWF)	Case a2 (NASA)	Case a3 (FMI)
Meteorological ICONs and BCONs	Meteorological analysis with the CAMS configuration of the IFS	Meteorological analysis with the GEOS FP-IT configuration	ECMWF IFS
Chemical ICONs and BCONs	Analysis (4DVAR) of previous forecast and satellite retrievals of AOD (MODIS), CO (MOPITT, IASI), NO ₂ and ozone retrievals from several sensors (MLS, SBUV-2, OMI, GOME used as initial conditions	Initial conditions from previous time analysis step, aerosol initial conditions from assimilation of AOD (MODIS and AVHRR)	Previous forecast, SILAM v.5.5.1
Anthropogenic Emissions	MACCITY, GFAS fire	HTAP v2.0, QFED v2.5	MACCITY 2016 + STEAM ships 2015 + GEIA lightning + GEIA aircraft + IS4FIRES fire PM + GFAS fire gases
Biogenic Emissions	MEGAN 2.0	MEGAN 2.1	MEGAN-MACC
Dust Emissions	Online	Online (Zender et al., 2003)	Own development (unpublished)
Sea-salt Emissions	Online	Online (Jaegle et al., 2011)	Own development (Sofiev et al., 2012)
Smoke Emissions	None	None	None
The use of WUDAPT data	None	None	None
Forecasting Products			
O ₃	✓	✓	✓
CO	✓	✓	✓
NO _x	✓	✓	✓
SO ₂	✓	✓	✓

Attributes	Case a1 (ECMWF)	Case a2 (NASA)	Case a3 (FMI)
VOCs	✓	✓	✓
PM2.5/PM10	✓ (diagnostics)	✓ (prognostic)	✓
Evaluation Datasets			
Surface	GAW surface, AIRBASE (EEA)	US EPA, EEA	
Satellite	As assimilated + ACE	OMI, MOPITT	MODIS AOD, OMI NO2, OMI O3,
Other (aircraft, sounding, etc.)	IAGOS, WOUDC and other ozone sondes	SEAC4RS, ozone sondes	AERONET AOD
Physics Options			
Longwave Radiation	Yes	Chou et al. (2001)	IFS
Shortwave Radiation	Yes	Chou and Suarez (1999)	IFS
PBL Scheme	Yes	Nonlocal scheme of Lock et al. (2000) in conjunction with the Richardson-number-based scheme of Louis et al. (1982)	IFS
Land Surface Scheme	Yes	Catchment model (Koster et al., 2000)	IFS
Urban Canopy Model	Yes	No	
Cumulus Parameterization	Yes	Relaxed Arakawa–Schubert (Moorthi and Suarez, 1992)	IFS
Microphysics	Yes	Single Moment scheme of Bacmeister et al (2006)	IFS
Aerosol Activation	No	No	IFS

Attributes	Case a1 (ECMWF)	Case a2 (NASA)	Case a3 (FMI)
Aerosol Direct Effect	No	Yes	IFS
Aerosol Indirect Effect	No	No	IFS
Cloud Feedbacks	No	No	IFS
Chemical Options			
Photolysis Scheme	Modified band approach	Fast-JX	Lookup table
Gas-Phase Chemistry	CB05	GEOS-Chem v11-02e	Updated CB04 + stratospheric set of Damski et al (2007) + SOA VBS species oxidation
Aqueous-Phase Chemistry	EQSAM	Sulfate-nitrate-ammonium aerosol simulation coupled to gas-phase chemistry (Park et al., 2004)	Own development, based on Sofiev, 2000
Heterogeneous Chemistry	N2O5, H2O2 on aerosol surfaces	Jacob (2000)	SIA based on updated Sofiev, 2000 + SOA VBS + PSC in the stratosphere
Aerosol Module	LMDz aerosol bin scheme (3 bins desert dust, 3 bins sea salt, 2 organic matter, 2 black carbon and SO4)	2 options: (a) GEOS-Chem (Park et al., 2003, Wang et al., 2014, Fairlie et al., 2007, Jaegle et al., 2011); (b) GOCART (Chin et al., 2002; Colarco et al., 2014).	Own development, sectional, 2-5 bins depending on species
Inorganic aerosol thermodynamics	No	ISORROPIA-II (Fountoukis and Nenes, 2007)	Equilibrium-based, Sofiev, 2000
Secondary organic model	No	Simplified Volatility Basis Set (VBS) scheme (Pye et al. [2010])	VBS
Contact info for case provider	http://atmosphere.copernicus.eu/johannes.flemming@ecmwf.int	https://gmao.gsfc.nasa.gov/christoph.a.keller@nasa.gov	mikhail.sofiev@fmi.fi

Table 12.3. Demonstration Cases for Real-Time CW-AQF in North America

Attributes	Case b1 (NOAA/ARL)	Case b2 (NC State University)	Case b3 (NOAA/ESRL)
Model System and Version	US National Air Quality Forecasting	Northeastern University Air Quality Forecasting Model	RAP-Chem/NOAA/ESRL/GSD
Met Model	NAM version 4.0	WRF/Chem-MADRID v3.0	WRF-Chem v3.7
Chemical Model	CMAQ5.0.2	WRF/Chem-MADRID v3.0	WRF-Chem v3.7
Coupling method	Offline	Online	Online
Application			
Domain	North America	Eastern U.S.	North America
Time Period	18 July 2017 and 21 Feb 2018	12-19 July 2017	12-19 July 2017
Nesting method	No	No	No
Horizontal Grid Resolution (km)	12 km	12 km	13.5 km
Vertical Grid Resolutions (total number of layers) (x, y, z grid points)	468 × 288 × 35	129 × 140 × 23	649 × 648 × 50
Height of 1st layer (m)	19 m	38 m	20 m
Height of top layer (km)	20 hPa	100 hPa	10 hPa
Input			
Meteorological ICONs and BCONs	NCEP GFS FNL	NCEP GFS FNL	NCEP GFS FNL

Attributes	Case b1 (NOAA/ARL)	Case b2 (NC State University)	Case b3 (NOAA/ESRL)
Chemical ICONs and BCONs	NEMS GFS Aerosol Component	Adapted from CMAQ and updated based on satellite measurements	Initial conditions from the previous forecast except for aerosols from 3D-Var assimilation of AIRNow observations, Lateral boundaries from RAQMS
Anthropogenic Emission	U.S. EPA NEI2011	U.S. EPA NEI 2011	U.S. EPA NEI 2011
Biogenic Emissions	BEIS3.16	MEGANv2.0	MEGANv2.0
Dust Emissions	FENGSHA (in CMAQ5.0)	Shaw (2008)	N/A
Sea-salt Emissions	Surf zone parameterization	Gong et al. (1997)	MADE/SORGAM
Smoke Emissions	None	None	None
The use of WUDAPT data	None	None	None
Forecasting Products			
O3	✓	✓	✓
CO	No	✓	✓
NOx	✓	✓	✓
SO2	✓	✓	✓
VOCs	✓	✓	✓
PM2.5/PM10	✓	✓	✓
Evaluation Datasets			
Surface	U.S. EPA AIRNow	U.S. EPA AIRNow	N/A

Attributes	Case b1 (NOAA/ARL)	Case b2 (NC State University)	Case b3 (NOAA/ESRL)
Satellite	GOES-R and Suomi	MODIS/OMI/MOPITT/GOME2	N/A
Other (aircraft, sounding, etc.)	ACARS for meteorology	N/A	N/A
Physics Options			
Longwave Radiation	RRTM similar to RRTMG	RRTM similar to RRTMG	RRTMG
Shortwave Radiation	GFDL	Goddard shortwave	RRTMG
PBL Scheme	Mellor-Yamada-Janjic 2o TKE	YSU	YSU
Land Surface Scheme	NOAH LSM with 1 km land-use	NOAH LSM	NOAH LSM
Urban Canopy Model		N/A	N/A
Cumulus Parameterization	ACM2 (Pleim, 2007)	Grell-Devenyi	Grell-Freitas
Microphysics	WSM6	Purdue-Lin	WSM 5-Class
Aerosol Activation	No	Abdul-Razzak and Ghan	
Aerosol Direct Effect	No	Yes	Yes
Aerosol Indirect Effect	No	Yes	No
Cloud feedbacks	No	Yes	No
Chemical Options			
Photolysis Scheme	F-TUV photolysis scheme	Fast-J photolysis	Madronich TUV
Gas-Phase Chemistry	CB05	CB05	RACM

Attributes	Case b1 (NOAA/ARL)	Case b2 (NC State University)	Case b3 (NOAA/ESRL)
Aqueous-Phase Chemistry	CMAQ5.0.2 aqueous phase chemistry	CMU aqueous-phase chemistry	CMAQ aqueous-phase chemistry
Heterogeneous Chemistry	N2O5 hydrolysis	N/A	N/A
Aerosol Module	CMAQ5.0.2 aero4 aerosol module	MADRID	MADE
Inorganic aerosol thermodynamics	ISORROPIA	ISORROPIA v1.7	MARS
Secondary organic model	VBS option (Robinson et al. 2007)	MADRID-SOA	VBS
Contact info for case provider	Pius Lee, NOAA, USA, pius.lee@noaa.gov	Yang Zhang, NEU; ya.zhang@northeastern.edu	Mariusz Pagowski, NOAA, USA mariusz.pagowski@noaa.gov

Table 12.4. Demonstration Cases for Real-Time CW-AQF in Europe

Attributes	Case c1 (Meteo-France)	Case c2 (Uni. of Hertfordshire)	Case c3.1 (ENPC)	Case c3.2 (ENPC)
Model System and Version	CAMS Regional ENSEMBLE, is the median of 7 different models in Europe	WRF-CMAQ	WRF/Polyphemus	WRF/Polyphemus/Street-in-Grid
Met Model	ECMWF IFS	WRF V3.4.1	WRF ARW 3.6.1	WRF ARW 3.6.1
Chemical Model	7 different schemes	CMAQ v4.7.1	Polyphemus 1.8.1 Technical Note: The air quality modeling system Polyphemus (Mallet et al., 2007)	Polyphemus-SinG multi-scale modeling of urban air pollution (Kim et al., 2018)
Coupling method	6 are offline and 1 online	Offline	Offline	Offline
Application				
Domain	[30° W-45° E] × [30° N-70° N]	Nested, D01: Europe 50km D02: UK 10km	Europe	Nesting From a regional scale (about 50 km) over western Europe to an urban scale (about 1 km) over Paris
Time Period	21-22 June 2017 4-day forecast each day Extension to any cases since October 2015 is possible since data have been freely accessible since then (see below)	Every day since Jan 2014	Daily prevision for 4 days	March 24 to Jun 14, 2014
Nesting method	1-way	1 way nesting	None	1-way nesting

Attributes	Case c1 (Meteo-France)	Case c2 (Uni. of Hertfordshire)	Case c3.1 (ENPC)	Case c3.2 (ENPC)
Horizontal Grid Resolution (km)	0.1°	10 km	about 50 km (0.5°)	western Europe (D01): 0.5° Northern/central France (D02): 0.15° Île-de-France region (D03): 0.04° Eastern Paris suburbs (D04): 0.01°
Vertical Grid Resolutions (total number of layers) (x, y, z grid points)	8 vertical layers 700 × 400 × 8	23 vertical layers D01: 97 × 87 × 23 D02: 117 × 147 × 23	14 100 × 70 × 14	10 D01: 35 × 35 × 10 D02: 40 × 40 × 10 D03: 20 × 20 × 10 D04: 31 × 31 × 10
Height of 1st layer (m)	~ 10 m	~10 m	30 m	50 m
Height of top layer (km)	5000m	15000m (15km)	12 km	6 km
Input				
Meteorological ICONs and BCONs	ECMWF IFS high-resolution deterministic forecast	NCEP GFS	GFS Forecasts 004 (0.5°) domain available at www.ncdc.noaa.gov	NCEP FNL Operation Global Analysis data available at rda.ucar.edu
Chemical ICONs and BCONs	ICONs from the day before BCONs from global CAMS (ECMWF)	MACC	MOZART-4/GEOS5 simulation results available at www.acom.ucar.edu/wrf-chem/mozart.shtml	MOZART-4/GEOS5 simulation results available at www.acom.ucar.edu/wrf-chem/mozart.shtml
Anthropogenic Emissions	TNO MACC-III inventory	TNO-TRANSPHORM inventory	EMEP emission database	EMEP emission database

Attributes	Case c1 (Meteo-France)	Case c2 (Uni. of Hertfordshire)	Case c3.1 (ENPC)	Case c3.2 (ENPC)
Biogenic Emissions	Included, MEGAN in most models	MEGAN v2.0.4	MEGAN v2.04 (Guenther et al., 2006)	MEGAN v2.04 (Guenther et al., 2006)
Dust Emissions	included	No	None	None
Sea-salt Emissions	included	Yes	Monahan et al., 1986	Monahan et al., 1986
Smoke Emissions	None	None	None	None
The use of WUDAPT data	None	None	None	None
Forecasting Products				
O3	✓	✓	✓	✓
CO	✓	✓	✓	✓
NOx	✓ (NO and NO2)	✓	✓	✓
SO2	✓	✓	✓	✓
VOCs	✓ (NMVOCs)	✓	✓	✓
PM2.5/PM10	✓	✓	✓	No
Evaluation Datasets				
Surface	O3, NO2, SO2, CO, PM2.5 and PM10 surface observations (from the EEA)	DEFRA Automatic Urban and Rural Network (AURN) UK	Airbase European database	Airparif French database TrafiPollu database (Kim et al., 2018)

Attributes	Case c1 (Meteo-France)	Case c2 (Uni. of Hertfordshire)	Case c3.1 (ENPC)	Case c3.2 (ENPC)
	https://atmosphere.copernicus.eu/validation-regional-systems			
Satellite	GOME-2 NO2 columns			
Other (aircraft, sounding, etc.)	Earlynet lidar profiles, MAX-DOAS NO2 columns			
Physics Options				
Longwave Radiation	May differ between the 7 models	RRTM scheme	RRTM scheme	RRTM scheme
Shortwave Radiation	May differ between the 7 models	RRTM scheme	Goddard shortwave	Goddard shortwave
PBL Scheme	May differ between the 7 models	Yonsei University scheme	Yonsei University scheme	Yonsei University scheme
Land Surface Scheme	May differ between the 7 models	Noah land-surface model	Noah Land Surface Model	Noah Land Surface Model
Urban Canopy Model	May differ between the 7 models	None	None	D01/D02: None D03/D04: UCM
Cumulus Parameterization	May differ between the 7 models	Grell-Freitas	Grell-Freitas (GF) scheme	Grell-Freitas (GF) scheme
Microphysics	May differ between the 7 models	Morrison double-moment scheme	Kessler scheme	Kessler scheme
Aerosol Activation	No	No	No	No

Attributes	Case c1 (Meteo-France)	Case c2 (Uni. of Hertfordshire)	Case c3.1 (ENPC)	Case c3.2 (ENPC)
Aerosol Direct Effect	No	No	No	No
Aerosol Indirect Effect	No	No	No	No
Cloud Feedbacks	No	No	No	No
Chemical Options				
Photolysis Scheme	May differ between the 7 models	JPROC	FastJX 5.7	FastJX 5.7
Gas-Phase Chemistry	Different for the 7 models	CB05	CB05	CB05
Aqueous-Phase Chemistry	Different for the 7 models	Yes	Variable Size-Resolved Model (VSRM) (Fahey and Pandis, 2001)	No
Heterogeneous Chemistry	Different for the 7 models	Yes	Heterogeneous chemistry and tropospheric ozone (Jacob, 2000)	No
Aerosol Module	Different for the 7 models	AERO5	Technical Note: A new Size Resolved Aerosol Model (SIREAM) (Debry et al., 2007)	No
Inorganic aerosol thermodynamics	May differ between the 7 models	Yes	ISORROPIA 1.7	No

Attributes	Case c1 (Meteo-France)	Case c2 (Uni. of Hertfordshire)	Case c3.1 (ENPC)	Case c3.2 (ENPC)
Secondary organic model	Different for the 7 models	Yes	Secondary Organic Aerosol Processor (SOAP) (Couvidat and Sartelet, 2015)	No
Contact info for case provider	Matthieu Plu Meteo-France Regional Copernicus Atmosphere Monitoring Service (CAMS) matthieu.plu@meteo.fr	Ranjeet S. Sokhi r.s.sokhi@herts.ac.uk	Youngseob Kim, CEREA/ENPC, France, youngseob.kim@enpc.fr Karine Sartelet, CEREA/ENPC, France, karine.sartelet@enpc.fr	Youngseob Kim, CEREA/ENPC, France, youngseob.kim@enpc.fr Karine Sartelet, CEREA/ENPC, France, karine.sartelet@enpc.fr

Table 12.5. Demonstration Cases for Real-Time CW-AQF in Asia

Attributes	Case d1 (CMA)	Case d2 (Zhejiang Univ)	Case d3 (HK EPD)
Model System and Version	CMA Haze-fog forecasting system: CUACE/Haze-fog	Hangzhou Air Quality Forecasting System	Hong Kong's Real-time Air Quality Forecasting System (R-t PATH) Air Modeling Section Air Science Group Environmental Protection Department
Met Model	Regional GRAPES	WRF version 3.4	WRF version 3.4.1
Chemical Model	CUACE	CMAQ5.0.2	CMAQ 5.0.2
Coupling method	Online	Online	Offline
Application			
Domain	East Asia	Most of China and parts of East Asia	Most of China and parts of East Asia Fine resolution on Hong Kong
Time Period	Jan 1-31, 2013	Aug 26, 2016 to present	Jan 2015 to present
Nesting method	None	None	1-way
Horizontal Grid Resolution (km)	0.25°	12 km	27km / 9km / 3km / 1km
Vertical Grid Resolutions (total number of layers) (x, y, z grid points)	460 × 200 × 31	395 × 345 × 27	26 layers 182 × 138 × 26 (27 km) 74 × 74 × 26 (9km / 3km / 1km)
Height of 1st layer (m)	About 30 m	About 57 m	17 m
Height of top layer (km)	35 km	16 km	6.3 km
Input			

Attributes	Case d1 (CMA)	Case d2 (Zhejiang Univ)	Case d3 (HK EPD)
Meteorological ICONs and BCONs	CMA global GRAPES	NCEP GFS	NCEP GFS and NHM (Non-hydrostatic model) from the Hong Kong Observatory
Chemical ICONs and BCONs	Restart	Default	Based on one set of year 2004 Geos-CHEM output
Anthropogenic Emissions	Inside China is the MEIC emission database, outside China is HTAP	MEIC emission database EDGAR: HTAP v2	MEIC emission database for 27 km, 9 km and 3 km grids; Hong Kong emission inventory for 1 km grid
Biogenic Emissions	Land surface based	MEGAN	MEGAN
Dust Emissions	MBA scheme	None	None
Sea-salt Emissions	Gong 1997	Gong 2003	Gong 2003 (AERO5)
Smoke Emissions	None	None	None
The use of WUDAPT data	None	None	None
Forecasting Products			
O3	✓	✓	✓
CO	✓	✓	✓
NOx	✓	✓	✓
SO2	✓	✓	✓
VOCs	✓	No	Based on Emissions
PM2.5/PM10	✓	✓	✓
Evaluation Datasets			

Attributes	Case d1 (CMA)	Case d2 (Zhejiang Univ)	Case d3 (HK EPD)
Surface	CMA surface PM10/PM2.5 data	Ministry of Environmental Protection in China (http://datacenter.mep.gov.cn/)	Hong Kong Air Quality Monitoring Data (http://www.aqhi.gov.hk/)
Satellite	CMA FENGYUN AOD data	None	None
Other (aircraft, sounding, etc.)	None	None	None
Physics Options			
Longwave Radiation	RRTMG	RRTMG	RRTM
Shortwave Radiation	RRTMG	RRTMG	Dudhia scheme
PBL Scheme	MRF	Asymmetric Convective Model (ACM2)	Mellor-Yamada-Janjic
Land Surface Scheme	SLAB	Pleim-Xiu	Noah land-surface model
Urban Canopy Model	none	None	None
Cumulus Parameterization	Kain-Fritsch 2	Kain-Fritsch (KF2)	Kain-Fritsch
Microphysics	WDM6	Two-moment scheme	WSM 3-class simple ice scheme
Aerosol Activation	Yes	Yes	No
Aerosol Direct Effect	Yes	Yes	No
Aerosol Indirect Effect	Yes	Yes	No
Cloud Feedbacks	None	Yes	No
Chemical Options			

Attributes	Case d1 (CMA)	Case d2 (Zhejiang Univ)	Case d3 (HK EPD)
Photolysis Scheme	RADM2	CB05	CB05
Gas-Phase Chemistry	RADM2	CB05	CB05
Aqueous-Phase Chemistry	RADM2	Regional Acid Deposition Model (RADM)	RADM
Heterogeneous Chemistry	None	Heterogeneous chemistry (B. Zheng et al., 2015)	None
Aerosol Module	CAM (Gong, 2003)	AERO6	AERO5
Inorganic aerosol thermodynamics	ISORROPIA	ISORROPIA	ISORROPIA
Secondary organic model	None	AERO6	AERO5 / SORGAM (Secondary Organic Aerosol Model)
Contact info for case provider	Chunhong Zhou, CMA, China Zhouch@cma.gov.cn	Shaocai Yu, Zhejiang University, China, shaocaiyu@zju.edu.cn	Kenneth Leung, Hong Kong EPD, kleung@epd.gov.hk Tsz-cheung Lee, HK Observatory, China, tcllee@hko.gov.hk

Table 12.5 [continued]

Attributes	Case d4 (HKUST)	Case d5 (NEA)
Model System and Version	WRF	Meteorological Service Singapore's smoke forecasting system – ASEAN Tropical Lagrangian Atmospheric System (ATLAS)
Met Model	WRF ARW V3.7.1	Unified Model (UM)
Chemical Model	None	Numerical Atmospheric-dispersion Modeling Environment (NAME)
Coupling method	N/A	Offline
Application		
Domain	China / South China / Guangdong Province / Pearl River Delta	Southeast Asia
Time Period	2010 June – July 2030 June – July	2013 to present – Daily provision for 2-day forecast
Nesting method	1-way	None
Horizontal Grid Resolution (km)	27 km/ 9 km / 3 km/ 1 km	10
Vertical Grid Resolutions (total number of layers) (x, y, z grid points)	283 × 184 × 48 / 223 × 163 × 48 / 172 × 130 × 48 / 190 × 133 × 48	396 × 361 × 53
Height of 1st layer (m)	14 m	10 m
Height of top layer (km)	20 km	20 km
Input		

Attributes	Case d4 (HKUST)	Case d5 (NEA)
Meteorological ICONs and BCONs	NCEP (bias-corrected and converted CESM1's output)	UM global forecast fields
Chemical ICONs and BCONs	None	None
Anthropogenic Emission	None	None.
Biogenic Emissions	None	None
Dust Emissions	None	None
Sea-salt Emissions	None	None
Smoke Emissions	None	Smoke emissions from biomass burning using modified GFAS approach (Kaiser et al., 2012, Hertwig et al., 2015)
The use of WUDAPT data	Yes	None
Forecasting Products		
O3	None	
CO	None	Optional
NOx	None	Optional
SO2	None	Optional
VOCs	None	
PM2.5/PM10	None	
Evaluation Datasets		Yes (primary PM)
Surface	Data from Hong Kong Observatory	Singapore air quality monitoring data (http://www.nea.gov.sg/anti-pollution-radiation-

Attributes	Case d4 (HKUST)	Case d5 (NEA)
		protection/air-pollution-control/)
Satellite	N/A	
Other (aircraft, sounding, etc.)	N/A	AERONET AOD (planned)
Physics Options		
Longwave Radiation	RRTM Scheme	Edwards and Slingo (1996)
Shortwave Radiation	Dudhia Scheme	Edwards and Slingo (1996)
PBL Scheme	Asymmetric Convection Model 2 (ACM2) (Pleim, 2007)	Lock et al. (2000; 2001), Brown et al. (2008)
Land Surface Scheme	Noah land-surface model	JULES (Best et al., 2011; Clark et al., 2011)
Urban Canopy Model	None	None
Cumulus Parameterization	Grell 3-D Ensemble Scheme for first two domains (27km/9km resolution); None for the last two domain (3km/1km resolution)	Gregory and Rowntree (1990) with modifications.
Microphysics	WSM 3-class simple ice scheme	Wilson and Ballard (1999) with extensive modification (Walters et al., 2017)
Aerosol Activation	No	No
Aerosol Direct Effect	No	No
Aerosol Indirect Effect	No	No
Cloud Feedbacks	No	No
Chemical Options		

Attributes	Case d4 (HKUST)	Case d5 (NEA)
Photolysis Scheme	No	STOCHEM (Collins et al., 1997) (Planned to be incorporated)
Gas-Phase Chemistry	No	STOCHEM (Collins et al., 1997) (Planned to be incorporated)
Aqueous-Phase Chemistry	No	STOCHEM (Collins et al., 1997) (Planned to be incorporated)
Heterogeneous Chemistry	No	No
Aerosol Module	No	No
Inorganic aerosol thermodynamics	No	Malcolm et al. (2000) Redington and Derwent (2002)
Secondary organic model	No	Redington and Derwent (2013)
Contact info for case provider	Jimmy Fung, HKUST majfung@ust.hk	Christopher Gan, Meteorological Service Singapore, christopher_gan@nea.gov.sg

Table 12.6. Demonstration Cases for Real-Time CW-AQF in South America

Attributes	Case e1 (USP)	Case e2 (SENAMHI)
Model System and Version	WRF-Chem v3.7.1	Air Quality Forecasting System in Lima, Peru
Met Model	WRF ARW	WRF-Chem v3.8.1
Chemical Model	WRF chemistry extension	WRF-Chem v3.8.1
Coupling method	Online	Online
Application		
Domain	South America	Lima, Peru
Time Period	Daily prevision for 3 days	Daily prevision for 1 day http://www.senamhi.gob.pe/?p=calidad-de-aire-numeric
Nesting method	None	None
Horizontal Grid Resolution (km)	50 km	5 km
Vertical Grid Resolutions (total number of layers) (x, y, z grid points)	120 × 150 × 35	50 × 50 × 30
Height of 1st layer (m)	30 m	38 m
Height of top layer (km)	20 km	50 hPa
Input		
Meteorological ICONs and BCONs	NCEP GFS 0.5	NCEP GFS 0.25 http://rda.ucar.edu/datasets/ds083.3/

Attributes	Case e1 (USP)	Case e2 (SENAMHI)
Chemical ICONs and BCONs	MOZART-4/GEOS5	Default
Anthropogenic Emission	HTAPv2.2 and MACCity global inventories	Vehicular emissions model developed by the IAG-USP Laboratory of Atmospheric Processes (Andrade et al., 2015; Vara-Vela et al., 2016)
Biogenic Emissions	MEGANv2.04	N/A
Dust Emissions	Jones and Creighton, 2011	N/A
Sea-salt Emissions	Gong et al. (1997)	N/A
Smoke Emissions	None	None
The use of WUDAPT data	No	N/A
Forecasting Products		
O3	✓	✓
CO	✓	✓
NOx	✓	✓
SO2	✓	✓
VOCs	✓	No
PM2.5/PM10	✓	✓
Evaluation Datasets		
Surface	Available ambient data (meteorology and air quality) from national weather services (e.g., from INMET in Brazil and from SENAMHI in Peru)	SENAMHI's Peru air quality station

Attributes	Case e1 (USP)	Case e2 (SENAMHI)
Satellite	NCDC and GPCP for meteorological fields and MODIS for AOD	N/A
Other (aircraft, sounding, etc.)	AERONET data for AOD evaluation; LIDAR data for aerosol extinction profile and PBL height evaluations	N/A
Physics Options		
Longwave Radiation	Rapid Radiative Transfer Model for GCMs (RRTMG)	Rapid radiative transfer model
Shortwave Radiation	RRTMG	Goddard
PBL Scheme	Yonsei University (YSU)	Yonsei University scheme
Land Surface Scheme	Unified Noah land-surface model	Noah Land Surface Model
Urban Canopy Model	Kusaka et al. (2001)	None
Cumulus Parameterization	Multi-Scale Kain-Fritsch (MSKF)	Grell three-dimensional ensemble cumulus scheme
Microphysics	Morrison double-moment	Lin
Aerosol Activation	No	No
Aerosol Direct Effect	No	No
Aerosol Indirect Effect	No	No
Cloud Feedbacks	No	No
Chemical Options		
Photolysis Scheme	Fast Troposphere Ultraviolet-Visible (FTUV)	Madronich photolysis (TUV)

Attributes	Case e1 (USP)	Case e2 (SENAMHI)
Gas-Phase Chemistry	Carbon Bond mechanism (CB05)	RADM2
Aqueous-Phase Chemistry	None	None
Heterogeneous Chemistry		
Aerosol Module	Modal for Aerosol Dynamics model for Europe (MADE)	MADE/SORGAN
Inorganic aerosol thermodynamics	Model for an Aerosol Reacting System (MARS)	None
Secondary organic model	Secondary Organic Aerosol Model (SORGAM)	None
Contact info for case provider	Maria de Fatima Andrade, USP, Brazil, maria.andrade@iag.usp.br ; Edmilson Freitas, USP, Brazil, efreitas@model.iag.usp.br	Odón Sanchez, SENAMHI, Peru, osanchezbr@gmail.com

Table 12.7. Demonstration Cases for Real-Time CW-AQF in Oceania

Attributes	Case f1 (CSIRO)	Case f2 (CSIRO)	Case f3 (CSIRO)
Model System and Version	AQFx- Tier 2	CCAM-CTM	AQFx- Tier 3
Met Model	Unified Model (UM)	Conformal Cubic Atmospheric Model (CCAM)	Unified Model
Chemical Model	C-CTM	C-CTM	C-CTM
Coupling method	Offline	Offline	Offline
Application			
Domain	Australia→Sydney	Australia→ Sydney	Greater Sydney
Time Period	1-25 May 2016	1-25 May 2016	1-25 May 2016
Nesting method	1-way	1-way	None
Horizontal Grid Resolution (km)	27 km, 9 km, 3 km	80 km, 9 km, 3 km	1.36 km
Vertical Grid Resolutions (total (x, y, z grid points))	400 × 300 × 20	60 × 60 × 20	700 × 500 × 20
Height of 1st layer (m)	20 m	20 m	20 m
Height of top layer (km)	11 km	11 km	11 km
Input			
Meteorological ICONs and BCONs	Australian Community Climate and Earth System Simulator (ACCESS) global analysis and forecast	ERA analysis/reanalysis	ACCESS global analysis and forecast
Chemical ICONs and BCONs	GLOMAP/obs; CCAMS	GLOMAP/obs	None

Attributes	Case f1 (CSIRO)	Case f2 (CSIRO)	Case f3 (CSIRO)
Anthropogenic Emission	NSW Greater Metropolitan Region 20 (vehicles; wood-heaters, elevated industrial sources adjusted for meteorology inline)	As per Case 1a	None
Biogenic Emissions	ABCGEM (inline) https://tinyurl.com/yaxwtbt8	ABCGEM (inline)	None
Dust Emissions	Lu and Shao (inline)	Lu and Shao	None
Sea-salt Emissions	Monahan/Gong (open ocean); Clark (surf break). Inline	As per Case 1a	None
Smoke Emissions	C-SEM (Phoenix; MODIS; VIIRS), GFA	C-SEM (Fire agency data)	C-SEM (Phoenix)
The use of WUDAPT data	None	None	None
Forecasting Products			
O3	✓	✓	No
CO	✓	✓	No
NOx	✓	✓	No
SO2	✓	✓	No
VOCs	✓	✓	No
PM2.5/PM10	✓	✓	✓ (PM2.5 tracers)
Evaluation Datasets			
Surface	OEH air quality network	OEH air quality network	N/A
Satellite	HIMAWARI-8; CALIPSO; VIIRS		N/A

Attributes	Case f1 (CSIRO)	Case f2 (CSIRO)	Case f3 (CSIRO)
Other (aircraft, sounding, etc.)	ACARS		N/A
Physics Options			
Longwave Radiation	Modified Edwards and Slingo (1996)	GFDL-AM3 (Freidenreich and Ramaswamy 1999)	N/A
Shortwave Radiation	Modified Edwards and Slingo (1996)	GFDL-AM3 (Schwarzkopf and Ramaswamy, 1999)	N/A
PBL Scheme	Adrian Lock's scheme	EDMF with k-e (Hurley, 2007), plus modifications for moisture	N/A
Land Surface Scheme	JULES	CABLE (Kowalczyk et al., 2006)	N/A
Urban Canopy Model	JULES single tile	UCLEM (renamed from aTEB, Thatch and Hurley, 2011)	N/A
Cumulus Parameterization	Modified Gregory and Rowntree (1999)	Mass flux (McGregor, 2003)	N/A
Microphysics	Prognostic cloud scheme (PC2; Wilson et al. 2008)	Prognostic condensate, single moment 5-class scheme (Rotstayn, 1997; Lin et al., 1983)	Prognostic cloud scheme (PC2; Wilson et al. 2008)
Aerosol Activation	No	CSIRO Mk3.6 Bulk scheme (Rotstayn and Lohmann 2002; Rotstayn et al., 2011)	N/A
Aerosol Direct Effect	No	GFDL-AM3	N/A
Aerosol indirect Effect	No	Modified Jones et al. (2001) to include hydrophilic carbonaceous aerosols	N/A
Cloud feedbacks	No	No	N/A
Chemical Options			

Attributes	Case f1 (CSIRO)	Case f2 (CSIRO)	Case f3 (CSIRO)
Photolysis Scheme	1-D photolysis scheme	1-D photolysis scheme	N/A
Gas-Phase Chemistry	CB05	CB05	N/A
Aqueous-Phase Chemistry	Seinfeld and Pandis	Seinfeld and Pandis	N/A
Heterogeneous Chemistry	GLOMAP- chemical ageing	No	N/A
Aerosol Module	GLOMAP	2-bin	1-bin. PM2.5 tracers
Inorganic aerosol thermodynamics	ISORROPIA	ISORROPIA	N/A
Secondary organic model	Volatility Basis Set	Volatility Basis Set	N/A
Contact info for case provider	Martin Cope, CSIRO, Australia, Martin.Cope@csiro.au ; Hiep Duc, OEH/NSW, Australia, Hiep.Duc@environment.nsw.gov.au	Martin Cope, CSIRO, Australia, Martin.Cope@csiro.au ; Hiep Duc, OEH/NSW, Australia, Hiep.Duc@environment.nsw.gov.au	Martin Cope, CSIRO, Australia, Martin.Cope@csiro.au ; Hiep Duc, OEH/NSW, Australia, Hiep.Duc@environment.nsw.gov.au

Table 12.8. Demonstration Cases for Real-Time CW-AQF in Africa.

Attributes	Case g1 (SAWS)	
Model System and Version		
Met Model	RegCM4.6	
Chemical Model	RegCM-CHEM4.6 (Shalaby et al., 2011; Solmon et al., 2006; Zakey et al., 2006, 2009)	
Coupling method	Online	
Application	We plan to do simulation for two domains	
Domain	Case 1.1 Southern Africa Domain	Case 1.2 Africa Domain
Time Period	22 August 2017	
Nesting method	None	
Horizontal Grid Resolution (km)	10 km (over Southern Africa Domain) and 20 km (over Africa Domain)	
Vertical Grid Resolutions (total number of layers) (x, y, z grid points)	19 layers	
Height of 1st layer (m)	1003.62 (mb) or 80.95 m	
Height of top layer (km)	50.00 (mb) or 30.37 km	
Input		
Meteorological ICONs and BCONs	ECMWF or GFS but NOAA Optimum Interpolation is used for SST)	
Chemical ICONs and BCONs	For gas phase species: MOZART CTM For aerosols from global simulations: CAM + EC-EARTH	

Attributes	Case g1 (SAWS)
Anthropogenic Emissions	Currently for forecasting purpose we use an emission climatology which is formed via processing and aggregating different sector of anthropogenic emissions from CMIP5 RCP and IASA. Note: using locally available emission data from some sectors, we also made some corrections in our emission climatology. For biomass burning we can use Global Fire Emissions Database
Biogenic Emissions	The land surface model used (CLM4.5) allow to calculate online biogenic volatile hydrocarbon emissions, as well as chemical deposition that can be used in RegCM.
Dust Emissions	Online coupled dust module based on Zaakey et al. (2006)
Sea-salt Emissions	Online coupled sea-salt module based on Zaakey et al. (2009)
Smoke Emissions	None
The use of WUDAPT data	No
Forecasting Products	
O3	✓
CO	✓
NOx	✓
SO2	✓
VOCs	✓
PM2.5/PM10	✓
Evaluation Datasets	
Surface	Data from South Africa air quality monitoring station

Attributes	Case g1 (SAWS)
Satellite	<p>MISR/MODIS/AERONET (for AOD evaluation)</p> <p>Depending on the time period of the simulation requested, in South Africa the LIDAR data can be used for aerosol extinction profile and PBL height evaluations</p> <p>Satellites which provide concentration of trace gases and/or air pollutants such as OMI, SCIAMACHY, TES and so on can also be used. Note: in our previous studies (over South Africa) the uncertainty range of trace gas observing satellites were much higher but for other parts of African regions it might not be the same.</p>
Other (aircraft, sounding, etc.)	For South Africa radiosonde measurements can be used for relative humidity profile evaluation
Physics Options	
Longwave Radiation	Based on the radiation scheme of Community Climate System Model (CCSM) (Note: the model is also configured to use computed long wave emissivity)
Shortwave Radiation	Based on the radiation scheme of Community Climate System Model (CCSM) (Note: for both LW and SW, it is also possible to use RRTM)
PBL Scheme	Currently based on the regional sensitivity study (over South Africa) we use non-local planetary boundary layer parameterization of Holtslag and Bouville (1993); however, for the bigger domain (i.e., Africa) we can also do sensitivity experiments, via comparing with UW PBL scheme (Bretherton and McCaa, 2004)
Land Surface Scheme	Community Land Model V4.5 (CLM4.5)
Urban Canopy Model	Community Land Model Urban (CLMU) (it is a component of CLM4.5) Oleson et al., (2013)
Cumulus Parameterization	Currently based on the regional sensitivity study (over South Africa), we use Emanuel (1991) parameterization with Cumulus closure scheme of Grell Scheme (Arakawa & Schubert, 1974)); however, for the bigger domain (i.e., Africa) we can also do sensitivity experiments, such as mixed Grell over land and Emanuel over ocean and so on
Microphysics	<p>Semi-Lagrangian advection scheme for tracers and humidity</p> <p>Moisture scheme: Explicit moisture (SUBEX; Pal et al., 2000)</p> <p>Convective precipitation scheme: Grell (Grell, 1993) with FritscheChappell assumption (Fritsch and</p>

Attributes	Case g1 (SAWS)
	<p>Chappell, 1980)</p> <p>Large-scale cloud and non-convective precipitation: Subgrid explicit moisture scheme (Pal et al., 2000)</p> <p>Ocean Flux scheme: Zeng et al. (1998)</p> <p>Pressure gradient force scheme uses a full fields with SST diurnal cycle scheme and desert seasonal albedo variability</p> <p>Coupled Lake Model</p>
Aerosol Activation	None
Aerosol Direct Effect	Yes
Aerosol Indirect Effect	Yes, sulfate aerosol indirect effect in radiation scheme is considered
Cloud Feedbacks	Yes
Chemical Options	
Photolysis Scheme	Based on 8-stream Tropospheric Ultraviolet-Visible Model (TUV) (Note: for determining photolysis rates, due to the 8-stream TUV computational demand, we usually use tabulated and interpolated values in our simulations).
Gas-Phase Chemistry	Carbon Bond Mechanism-Zaveri and Peters (CBM-Z) along with Radical Balance Method (RBM)
Aqueous-Phase Chemistry	The model uses simplified aqueous-phase chemistry approach based on Solmon et al. (2006) (i.e., Qian et al., 2001)
Heterogeneous Chemistry	Currently the model uses the external mixture assumption (i.e., it did not encompass heterogeneous chemistry). However, for computing relative humidity dependent ageing processes of carbonaceous aerosols, the model uses simplified hydrophobic/-philic aerosol scheme (Solmon et al., 2006)
Aerosol Module	RegCM-aerosol chemistry module (Solmon et al., 2006; Zakey et al., 2006, 2009)
Inorganic aerosol thermodynamics	ISORROPIA II (Fountoukis and Nenes, 2007)

Attributes	Case g1 (SAWS)
Secondary organic model	simplified parametrization within RegCM-aerosol chemistry module
Contact info for case provider	Melaku Yigiletu, SAWS, South Africa, Melaku.Yigiletu@weathersa.co.za Lucky Ntsangwane, SAWS, South Africa, lucky.ntsangwane@weathersa.co.za

Table 12.8 [Continued]

Attributes	Case g2 (Cairo University)	Case g3 (Maroc Météo)
Model System and Version		ADMS URBAN 3.1
Met Model	WRF-ARW	Al Bachir Morocco
Chemical Model	WRF-CHEM	The GRS (Generic Reaction Set) chemical model
Coupling method	Online	Online
Application		
Domain	North Africa	The Grand Casablanca Area, Morocco
Time Period	Summer and winter 2007	December 2016-January 2017
Nesting method	No	None
Horizontal Grid Resolution (km)	50 km	- 400 m on the whole domain; - 200 m on inhabited areas, industrial and airport zones; - A fine mesh around the main roads
Vertical Grid Resolutions (total number of layers) (x, y, z grid points)	217 × 151 × 51	Monin-Obukhov length = 100m
Height of 1st layer (m)	0 m	1.5
Height of top layer (km)	20296.08 (m)	2
Input		

Attributes	Case g2 (Cairo University)	Case g3 (Maroc Météo)
Meteorological ICONs and BCONs	NCEP/DOE Reanalysis Global Data	Based on predictions from the ALADIN Morocco operational weather prediction model used in Maroc Météo
Chemical ICONs and BCONs	MOZART	Pollutant concentrations from observation and from Mocage model (ongoing)
Anthropogenic Emissions	RETRO	Emissions from road traffic and other modes of transport (ships, airports), the main industrial sources and diffuse emissions (residential, tertiary, biogenic, etc.)
Biogenic Emissions	MEGAN	Yes
Dust Emissions	Provided through land usage produced by WPS	None
Sea-salt Emissions		None
Smoke Emissions	GFEDv2	None
The use of WUDAPT data	None	No
Forecasting Products		
O3	✓	✓
CO	✓	✓
NOx	✓	✓
SO2	✓	✓
VOCs	No	C6H6

Attributes	Case g2 (Cairo University)	Case g3 (Maroc Météo)
PM2.5/PM10	✓	PM10
Evaluation Datasets		
Surface	Some	Yes
Satellite	All available	Planned
Other (aircraft, sounding, etc.)	No	None
Physics Options		
Longwave Radiation	CAM radiation scheme	None
Shortwave Radiation	CAM radiation scheme	None
PBL Scheme	Yonsei University planetary boundary layer scheme (Hong et al., 2006)	From different input datasets: wind speed, date, time and coverage cloudy; or wind speed, surface heat flux, and boundary layer height
Land Surface Scheme	Noah Land Surface Model (LSM) four-layer soil temperature and moisture model with canopy moisture and snow-cover prediction (Tewari et al., 2004)	Complex terrain/FLOWSTAR model
Urban Canopy Model		Building module/Street Canyon
Cumulus Parameterization	Kain–Fritsch convective parameterization scheme (Kain et al., 2004)	None
Microphysics	Lin et al., 1983	None
Aerosol Activation	Yes	None
Aerosol Direct Effect	Yes	None

Attributes	Case g2 (Cairo University)	Case g3 (Maroc Météo)
Aerosol Indirect Effect	No	None
Cloud Feedbacks	No	None
Chemical Options		
Photolysis Scheme	F-TUV photolysis scheme	The chemistry of NO ₂ , NO, O ₃ and VOCs (7 reactions scheme)
Gas-Phase Chemistry	MOZART chemical mechanism	Yes (according to type of gas while modeling deposition)
Aqueous-Phase Chemistry	None	None
Heterogeneous Chemistry	None	None
Aerosol Module	Goddard Global Ozone Chemistry Aerosol Radiation and Transport (GOCART) simple aerosol scheme	None
Inorganic aerosol thermodynamics	None	None
Secondary organic model	None	None
Contact info for case provider	Magdy Abdelwahab, Cairo Uni, Egypt, magdy@sci.cu.edu.eg	Kenza Khomsi, Maroc Météo, Morocco, k.khomsi@gmail.com

12.6.1 Global

Case a1. Long-range transport of Sahara dust and smoke from Portuguese Wildfire emissions to North-West Europe forecast by the global CAMS forecasting system for atmospheric composition

Johannes Flemming

ECMWF, Shinfield Park, Reading, United Kingdom

Case overview and significance: A series of high publicity events of increased AOD and heightened spectacular sunsets due to large atmospheric aerosol loadings attributable to various causes occurred around mid-fall 2017 over Europe and North-western Africa. The ECMWF model was proven skillful in identifying the dominant causes of those deteriorated air quality conditions due to long range transport of desert dust and biomass burning aerosol. The long-range transport was well predicted due to the precision of the ECMWF meteorological model to forecast the track of Hurricane Ophelia over the Atlantic. The realistic forecast of winds over the Sahara causing the wind-blown dust emissions is a further contributing factor for the success. Finally, the routine observation of fire events from space made it possible to include adequate biomass burning emissions in the forecast.

a1.1 Introduction

Increased aerosol optical depth values were observed in the United Kingdom and Northern Germany in the period from 16-20 October 2017. This coincided with the reports of the “orange sky” phenomenon, which received a lot of media attention in the United Kingdom. The CAMS forecasting system of atmospheric composition, which is run by ECMWF, predicted the event and the results helped to attribute the increased aerosol values to a combination of causes.

a1.2 General Description of the Model

[Table 12.2 Global Case a1](#) summarizes the parameterization choices of the model used.

The Copernicus Atmosphere Monitoring Service (CAMS) NRT forecasting system uses the integrated forecasting system (IFS) of the European Centre for Medium Range Weather Forecasting (ECMWF) with online coupled modules for chemistry and aerosol simulation and data assimilation (Morcrette et al., 2009; Benedetti et al., 2009; Flemming et al., 2015; Inness et al., 2015). The CAMS IFS system is run at a lower horizontal and vertical resolution than the operational ECMWF high resolution NWP system because of the added computational cost for the simulation of the sink and source processes of atmospheric composition. The resolution of the IFS in CAMS configuration is about 40 km globally on 60 vertical levels, whereas the operational NWP forecast is carried out at a 9 km resolution on 137 vertical levels.

a1.3 Results and Discussion

The aerosols were advected in the wake of a hurricane, later storm, Ophelia, which after having developed in the subtropical Atlantic reached Ireland on 16 October (Figure 12.1). The good forecast of the track of Ophelia and the associated wind fields by the IFS was important for the accurate forecast of the long-range transport.

The high wind fields of Hurricane Ophelia caused very high but localized emissions of sea salt. The position of Ophelia at the South West coast of Ireland is therefore also visible in the AOD forecast (see Figure 12.2). The passing of Ophelia led in its southern inflow region to the transport of Sahara desert dust towards Europe. The dust had been previously advected westward from the Sahara to the subtropical Atlantic.

Between 14 and 16 October 2017 was a period of intense wildfires in northwest Portugal. The smoke plume of the fires was also transported towards northwest Europe in the flow following the passing of Ophelia. The CAMS NRT system uses the GFAS system (Kaiser et al., 2012) to

obtain NRT fire emissions based on satellite observations of fire radiative power. The fire emissions used in the CAMS forecast have therefore a good degree of accuracy with respect to their location and timing.

Biomass burning and desert dust aerosol were transported by the same flow pattern. The relative contribution of dust and biomass burning aerosol varied with location and time. The AERONET AOD observation site East Malling (UK) observed high AOD values on 16 October and 17-18 October 2017, which were well predicted by the CAMS system. According to the CAMS forecast, the high AOD values on 16 October were caused predominately by desert dust from the Sahara whereas the high AOD values on the 17-18 October 2017 were dominated by biomass burning aerosol (organic matter) from the fires in Portugal.

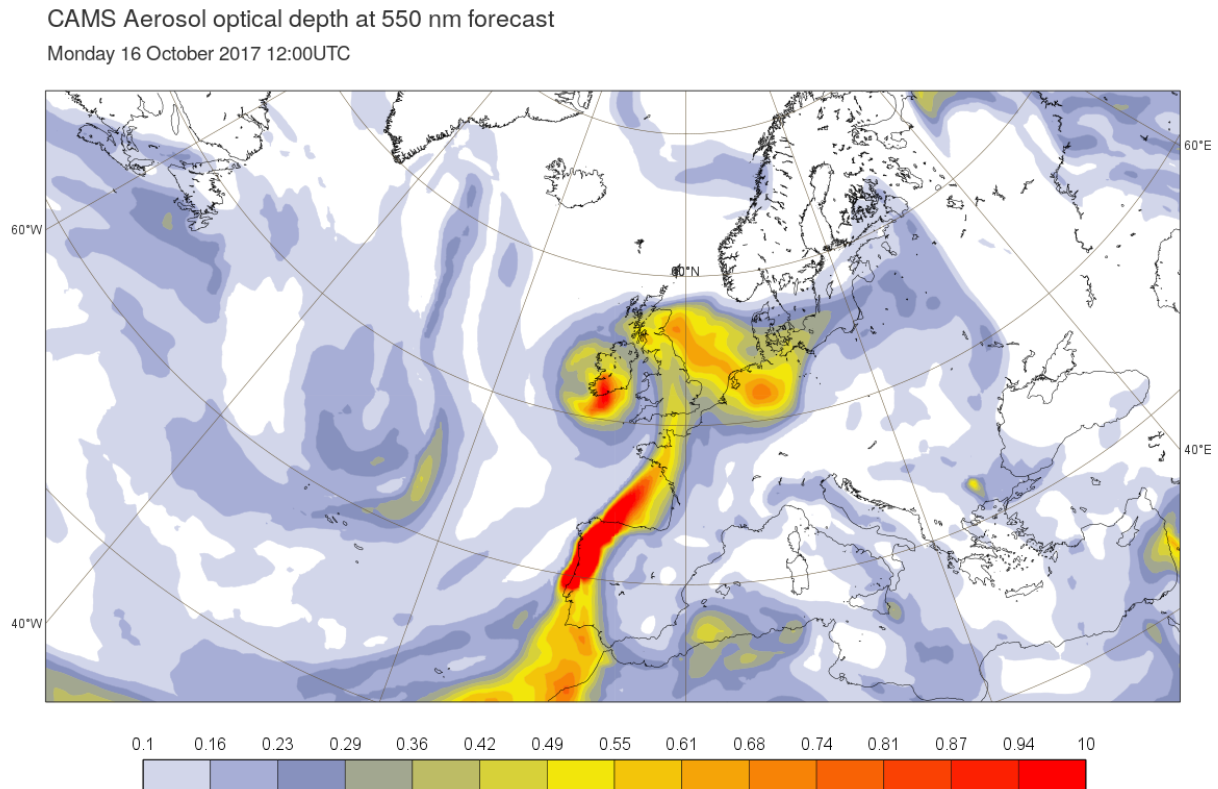


Figure 12.1. The aerosol optical depth forecast by the CAMS NRT forecasting system run by ECMWF for 12 UTC 16 October 2017

(source: <https://atmosphere.copernicus.eu/validation-regional-systems>). High AOD values over SW Ireland are caused by increased sea salt concentration and indicate the position of Ophelia. Saharan dust is transported toward Europe over the Atlantic next to the coast of Northwest Africa. Intense fire emissions increased the AOD further over Portugal.

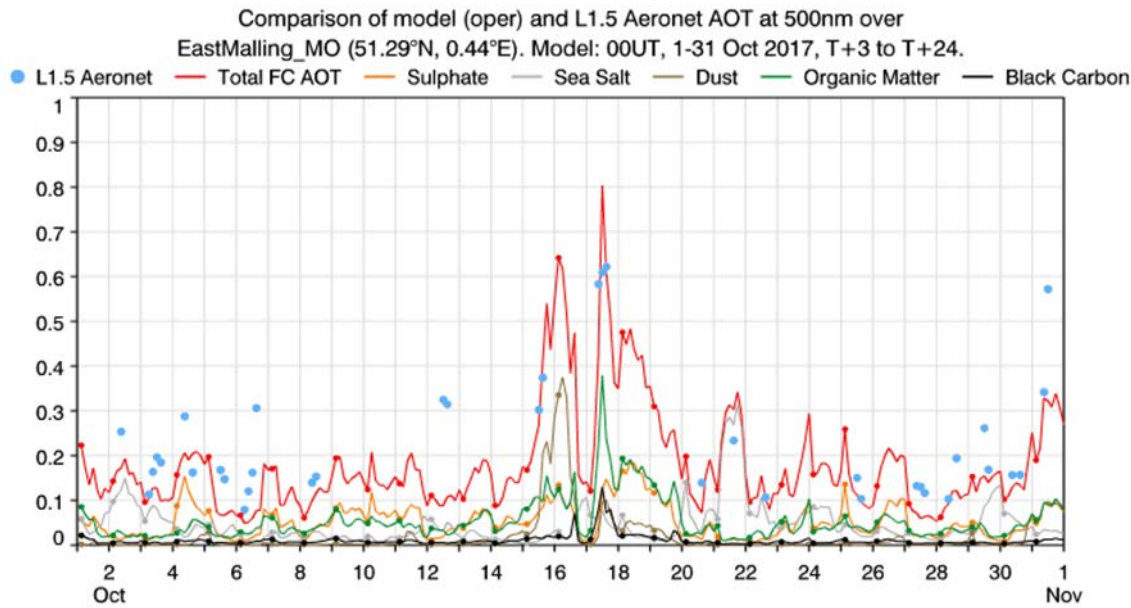


Figure 12.2. Observed (blue dots) and forecast total and component AOD (1 day forecast) over East Malling, U.K. (51.29N, 0.44E) in October 2017.

High AOD values on 16 October were caused predominately by desert dust, high AOD on 17-18 October 2017 were dominated by biomass burning aerosol (Organic Matter).

Person of contact: Johannes Flemming, email: Johannes.Flemming@ecmwf.int

References

- Benedetti, A., Morcrette, J.-J., Boucher, O., Dethof, A., Engelen, R. J., Fisher, M., Flentje, H., Huneus, N., Jones, L., Kaiser, J. W., Kinne, S., Mangold, A., Razinger, M., Simmons, A. J., Suttie, M., and the GEMS-AER team: Aerosol analysis and forecast in the European Centre for Medium-Range Weather Forecasts Integrated Forecast System: 2. Data assimilation, *J. Geophys. Res.*, 114, D13205, doi:10.1029/2008JD011115, 2009.
- Flemming, J., Huijnen, V., Arteta, J., Bechtold, P., Beljaars, A., Blechschmidt, A.-M., Diamantakis, M., Engelen, R. J., Gaudel, A., Inness, A., Jones, L., Josse, B., Katragkou, E., Marecal, V., Peuch, V.-H., Richter, A., Schultz, M. G., Stein, O., and Tsikerdekis, A.: Tropospheric chemistry in the Integrated Forecasting System of ECMWF, *Geosci. Model Dev.*, 8, 975-1003, doi:10.5194/gmd-8-975-2015, 2015.
- Inness, A., Blechschmidt, A.-M., Bouarar, I., Chabrillat, S., Crepulja, M., Engelen, R. J., Eskes, H., Flemming, J., Gaudel, A., Hendrick, F., Huijnen, V., Jones, L., Kapsomenakis, J., Katragkou, E., Keppens, A., Langerock, B., de Mazière, M., Melas, D., Parrington, M., Peuch, V. H., Razinger, M., Richter, A., Schultz, M. G., Suttie, M., Thouret, V., Vrekoussis, M., Wagner, A., and Zerefos, C.: Data assimilation of satellite retrieved ozone, carbon monoxide and nitrogen dioxide with ECMWF's Composition-IFS, *Atmos. Chem. Phys.*, 15, 5275-5303, doi:10.5194/acp-15-5275-2015, 2015.
- Kaiser, J. W., Heil, A., Andreae, M. O., Benedetti, A., Chubarova, N., Jones, L., Morcrette, J.-J., Razinger, M., Schultz, M. G., Suttie, M., and van der Werf, G. R.: Biomass burning emissions estimated with a global fire assimilation system based on observed fire radiative power, *Biogeosciences*, 9, 527-554, doi:10.5194/bg-9-527-2012, 2012.
- Morcrette, J.-J., Boucher, O., Jones, L., Salmond, D., Bechtold, P., Beljaars, A., Benedetti, A., Bonet, A., Kaiser, J. W., Razinger, M., Schulz, M., Serrar, S., Simmons, A. J., Sofiev, M., Suttie, M., Tompkins, A. M. and Untch, A.: Aerosol analysis and forecast in the ECMWF Integrated Forecast System. Part I: Forward modeling, *J. Geophys. Res.* 114, D06206. 1-17. Doi:10.1029/2008JD011235, 2009.

Case a2. A study of the 2016 post-monsoon air pollution event over India using the GEOS forecasting system

Christoph A. Keller and Anton Darmenov

NASA Global Modeling and Assimilation Office, Goddard Space Flight Center, Greenbelt, Maryland, U.S.A.

Case overview and significance: The NASA GMAO GEOS forward processing model has been enhanced with global atmospheric composition modeling capability-- dubbed herein as GEOS-CF. GEOS-CF was used to simulate an adverse air pollution event due to agricultural debris removal biomass burning during October and November 2016 over Northern India. This study verified the fidelity of the GEOS-CF prediction by comparing the simulated AOD against that retrieved by MODIS. GEOS-CF produced concentration surfaces for PM_{2.5}, NO₂ and O₃. The lowest level concentrations of these three constituent determined Air Quality Health Index (AQHI), a user friendly air quality health index used to advise the degree of mitigation measures to be taken to advert potentially health-harming consequences. This study further combined the distribution of AQHI with human population to estimate exposure of the populace during the biomass burning episode. Therefore, a health user end-point application of a global chemical composition model has been demonstrated by this pioneering study.

a2.1 Introduction

Extensive burning of crop residue during the post-monsoon season is a major source of air pollution over India. The NASA Goddard Earth Observing System Model (GEOS) provides a tool to predict and evaluate the severity of such events.

a2.2 General Description of the Model

[Table 12.2 Global Case a2](#) summarizes the parameterization choices of the model used.

The GEOS model consists of a group of components that can be connected in a flexible manner. The Global Modeling and Assimilation Office (GMAO) at NASA Goddard Space Flight Center uses variants of the GEOS system to produce an array of products such as near real-time weather analyses and forecasts (GEOS-FP) and decadal reanalysis (MERRA-2; for an overview of all products see https://gmao.gsfc.nasa.gov/GMAO_products/NRT_products.php). A new product is the GEOS composition forecast model (GEOS-CF), which produces global, daily air quality forecasts at a horizontal resolution of 25 × 25 km². GEOS-CF is an extension of the GEOS forward processing model GEOS-FP. The main difference between GEOS-CF and GEOS-FP is the inclusion of the extensive atmospheric chemistry module GEOS-Chem in GEOS-CF (Long et al., 2015; Hu et al., 2018). This allows simulation of reactive gases such as ozone (O₃), nitrogen dioxide (NO₂), formaldehyde, and benzene, along with aerosol species including sulfates, nitrates, dust, sea salt aerosols, and (organic and black) carbon. As such, GEOS-CF provides comprehensive information on many chemical species relevant to air quality.

a2.3 Results and Discussion

In October and November 2016, a large-scale air pollution event was observed from NASA EOS satellites. True color images from MODIS/Aqua over India and Pakistan reveal widespread fires in the Punjab region (left panel Figure 12.3). The computation of aerosols and fire emissions in GEOS incorporates near-real time fire locations and intensity (Darmenov and da Silva, 2015) and aerosol optical depths (AODs) derived from MODIS retrievals (Buchard et al., 2016). The middle panel of Figure 12.3 shows model AOD after blending it with the MODIS observations, and the right panel shows corresponding surface concentrations of PM_{2.5}.

The Air Quality Health Index (AQHI) is a commonly used tool to assess the impact of air pollution on human health. It combines surface concentrations of PM_{2.5}, O₃, and NO₂ and presents an overall measure of health risk associated with air pollution. Various definitions exist of the AQI (e.g., Stieb et al., 2008; US EPA AQI:

<https://airnow.gov/index.cfm?action=aqibasics.aqi>). While GEOS-CF does not offer a direct estimate of AQHI, the model produces all information required to compute it for the region and time period of interest. For illustration, we computed the AQHI over India for the time period 1 Oct – 20 Nov 2016. The left panel of Figure 12.4 shows the AQHI for 6 November 2016. By combining population density with the spatially gridded AQHI from the GEOS model, we can gather a detailed picture of the fraction of population affected by air pollution in general and agricultural fires in particular. The right panel of Figure 12.4 shows the fraction of the total Indian population exposed to various levels of air pollution. Prior to the onset of the agricultural burning season on 10 October 2016, approximately 25% of Indians are exposed to low air pollution, while the vast majority live in a region with moderate air pollution levels. During the peak of the burning season in mid-November, the fraction of people living in a low air pollution region drops to less than 5% and up to 25% of Indians are exposed to dangerously high levels of air pollution (right panel of Figure 12.4).

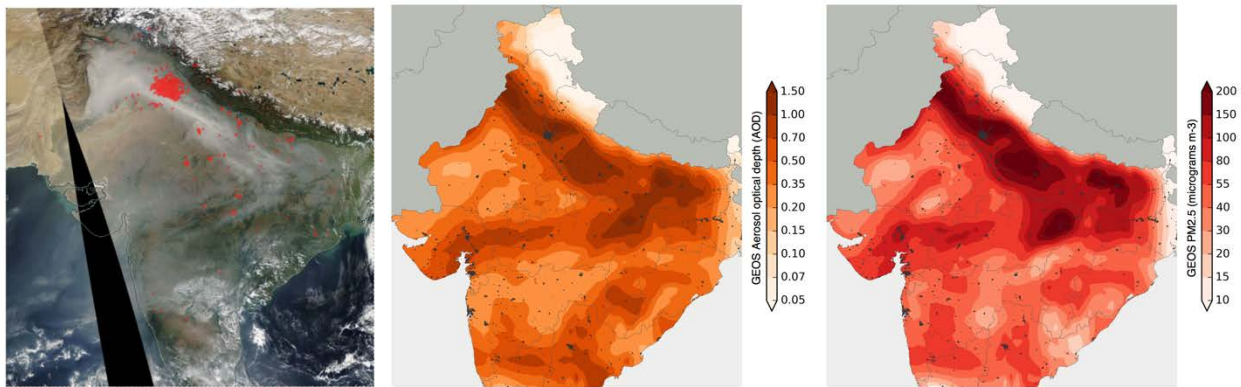


Figure 12.3. Air pollution over India on 6 November 2016 (08z).

The left panel shows the true color image from MODIS, with fires shown as red dots (from NASA World View: <https://worldview.earthdata.nasa.gov>); the corresponding model estimates of aerosol optical depth (AOD) and surface concentrations of fine particulate matter (PM2.5) are shown in the middle and right panel, respectively.

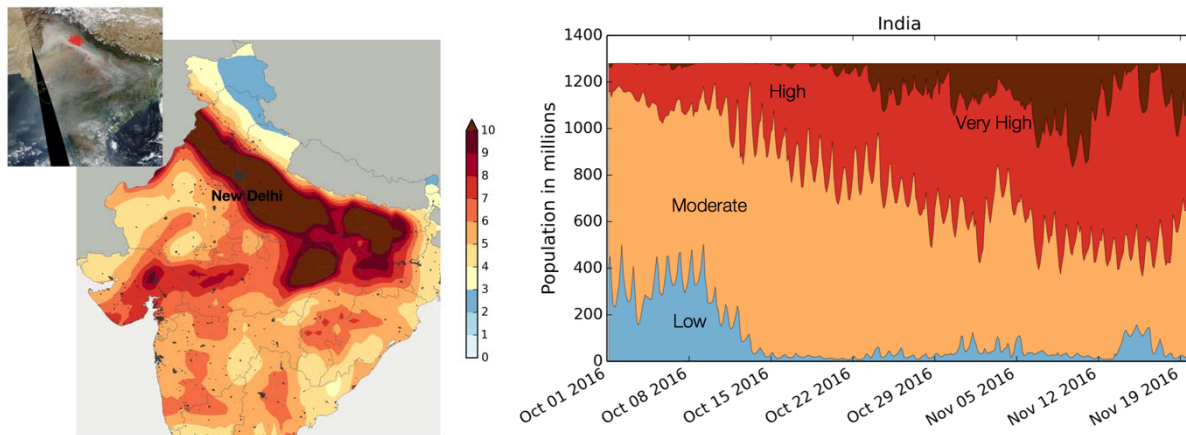


Figure 12.4. Air Quality Health Index (AQHI) over India on 6 November 2016 (08z).

The left panel shows the air quality index computed from model surface concentrations of PM2.5, O3, and NO2. AQHI values are quantitative measure of health effects caused by air pollution with higher values indicating increased risk to health, values less than 3 are categorized as low risk whereas values higher than 8 are categorized as high risk. The right panel shows the number of people exposed to low, moderate, high and very high levels of air pollution for the time period 1 October – 20 November 2016. The agricultural burning season started around 10 October.

Person of contact: Christoph A. Keller, email: christoph.a.keller@nasa.gov

References

- Buchard, V., A. M. da Silva, C. A. Randles, P. Colarco, R. Ferrare, J. Hair, C. Hostetler, J. Tackett, and D. Winker, 2016. Evaluation of the surface PM_{2.5} in Version 1 of the NASA MERRA Aerosol Reanalysis over the United States. *Atmos. Env.*, 125, Part A, 100-111. doi: 10.1016/j.atmosenv.2015.11.004.
- Darmenov, A. S., and A. M. Da Silva. 2015. The Quick Fire Emissions Dataset (QFED): Documentation of versions 2.1, 2.2 and 2.4. NASA Technical Report Series on Global Modeling and Data Assimilation 38 (NASA/TM–2015–104606).
- Hu, L., Keller, C. A., Long, M. S., Sherwen, T., Auer, B., Da Silva, A., Nielsen, J. E., Pawson, S., Thompson, M. A., Trayanov, A. L., Travis, K. R., Grange, S. K., Evans, M. J., and Jacob, D. J.: Global simulation of tropospheric chemistry at 12.5 km resolution: performance and evaluation of the GEOS-Chem chemical module (v10-1) within the NASA GEOS Earth System Model (GEOS-5 ESM), *Geosci. Model Dev.*, 11, 4603–4620, 2018
<https://doi.org/10.5194/gmd-11-4603-2018>.
- Long, M. S., Yantosca, R., Nielsen, J. E., Keller, C. A., da Silva, A., Sulprizio, M. P., Pawson, S., and Jacob, D. J.: Development of a grid-independent GEOS-Chem chemical transport model (v9-02) as an atmospheric chemistry module for Earth system models, *Geosci. Model Dev.*, 8, 595-602, <https://doi.org/10.5194/gmd-8-595-2015>, 2015.
- Stieb, D.M., R.T. Burnett, M. Smith-Doiron, O. Brion, H. Hyun Shin, V. Economou: A New Multipollutant, No-Threshold Air Quality Health Index Based on Short-Term Associations Observed in Daily Time-Series Analyses, *Journal of the Air & Waste Management Association*, 58:3, 435-450, 2008.

Case a3. Impact of wildland fires on atmospheric aerosols in Northern Hemisphere in 2012

Mikhail Sofiev

Finnish Meteorological Institute, Helsinki, Finland

Case overview and significance: Wildfire severity as measured by particulate matter (PM) burden into the atmosphere varied significantly in this century with its largest monthly total recorded in July 2012. Between July and September 2012 there was a record high number of incidences of wildfires in the Northern Hemisphere high latitudes and in the Southern subtropical and mid-latitudes. The Northern Hemispheric phenomena were attributable to dry and hot weather whereas the Southern Hemispheric phenomena were caused by the usual agricultural biomass burning. The dry and hot weather conditions were a common denominator in the synchronized and strengthened Northern Hemisphere high latitude wildfires resulting in a persistent “continuous fire smoke belt” in the high northern latitudes for days on end during July to September 2012 conspicuously seen by the polar orbiting satellites. This study applied the satellite-retrieval assisted Fire Information system (IS4FIRES) to estimate fire strength and injection characteristics for a simplified “tracer-mode-only” SILAM global model to determine wildfire smoke transport during those months. The model skillfully captured the observed smoke peaks spatiotemporally when atmospheric column integrated PM were compared against satellite retrievals. This lent the model credibility in its inferences of the wildfire emitted PM and their removal physical processes and the interplay feedback among the processes.

a3.1 Introduction

Strength and geographical distribution of fire seasons vary from year to year. On a global scale, the major contributor however is the fire season in the Northern Hemisphere, where vast forests of Siberia and Northern America can bring into the atmosphere up to 10 tons of fine PM per second. During all of the 21st century, the most-severe seasons were in 2002 and in three sequential years 2010 – 2012. The last of these years was additionally characterized by a very long season with several strong peaks, practically covering the whole summer of 2012.

The current section provides a brief outlook of that season. The next section describes the fire information system that provided the fire data and the dispersion model used for computing the global distribution of the fire plumes. The subsequent section considers the evolution and geographical redistribution of fires using both model computations and satellite observations of the smoke plumes.

a3.2 Tools Used in the Assessment

Fire information system IS4FIRES

The information on the fire distribution and intensity over the globe has been obtained from the Integrated System for wildland Fires (IS4FIRES, <http://is4fires.fmi.fi>, (Soares et al., 2015; Sofiev et al., 2009). It is based on the satellite observations of Fire Radiative Power (FRP) and follows the main principles described in the Fire Emission chapter for such type of systems.

The general structure of IS4FIRES is presented in <http://is4fires.fmi.fi/>. It includes the real-time component based on MODIS FRP products (<https://modis.gsfc.nasa.gov/data/dataproduct/mod14.php>) and offline calibration and evaluation input flows based on MODIS FRP and Aerosol Optical Depth (AOD) products together with the data from the MISR plume height project (<https://mISR.jpl.nasa.gov/getData/accessData/MISRPlumeHeight/>) and SEVIRI high-temporal resolution FRP products (<https://data.gov.uk/dataset/dfffd1c3-101b-44f1-bda9-0c43c6a281c9/seviri-spinning-enhanced-visible-and-infrared-imager-fire-radiative-power-frp-data-from-the-meteosat-second-generation-msg-satellite>).

Additional input flows included static land-cover data of the US Geological Survey (USGS, <http://www.usgs.gov>) and meteorological information from the European Centre of Medium-Range Weather Forecasts (ECMWF, <http://www.ecmwf.int>).

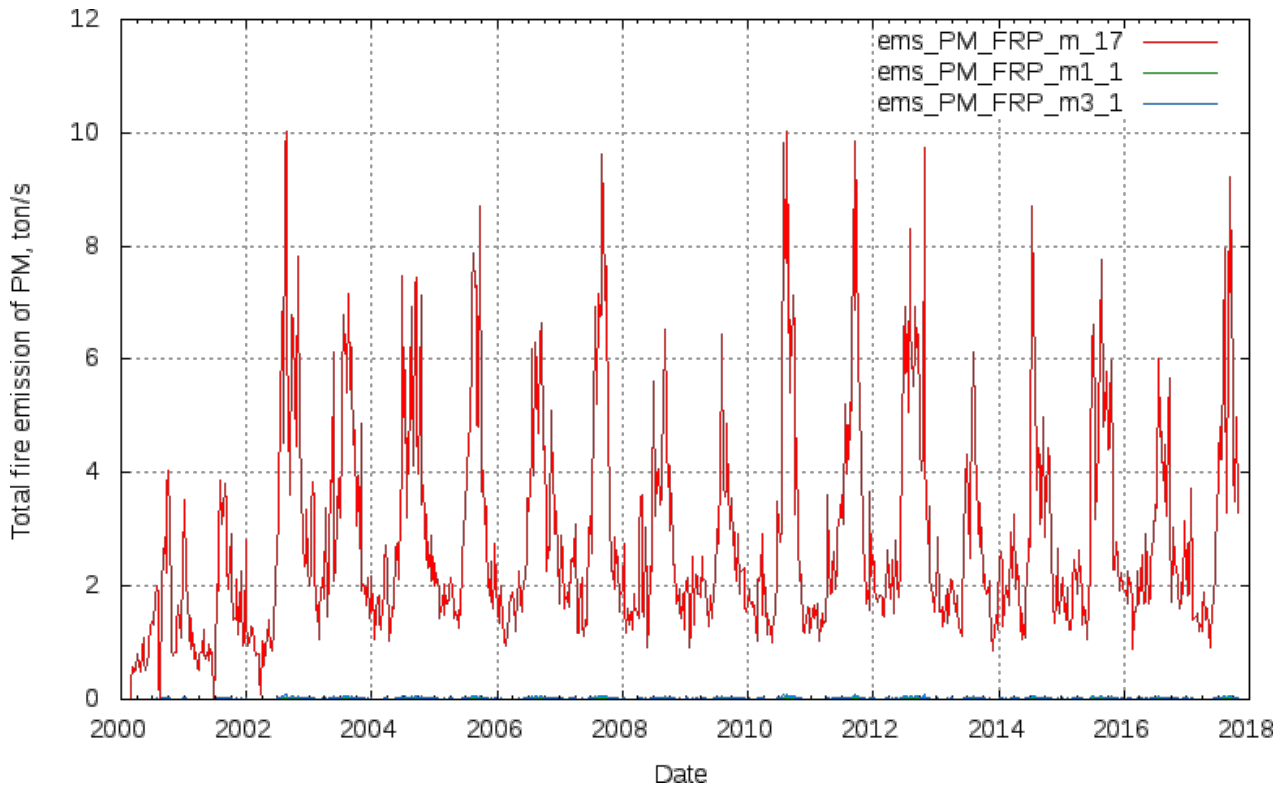


Figure 12.5. Global fire emission, IS4FIRES v.2.0, based on MODIS Aqua+Terra FRP observations. Unit: [ton sec⁻¹].

Obs. lower emission estimates for Terra-only period 2000-2002.

The output products of IS4FIRES consisted of the fluxes of the atmospheric pollutants computed for each MODIS fire pixel and the emission injection profile for this pixel (Sofiev et al., 2012, 2013). The temporal resolution of both datasets was one hour.

a3.3 Chemistry Transport Model SILAM

Table 12.2 Global Case a3 summarizes the parameterization choices of the model used. The information from IS4FIRES has been provided to the System of Integrated modeling of Atmospheric coMposition SILAM (<http://silam.fmi.fi>, (Sofiev et al., 2015)). A specific feature of SILAM is that it is interfaced to IS4FIRES and is capable of treating the individual fire pixels obtained directly from IS4FIRES, thus allowing for accurate computation of the vertical profile of the fire-induced emission and fire-by-fire submitting them to the dispersion computations.

SILAM is equipped with 7 chemistry transformation and 3 aerosol dynamic units but, for the sake of simplicity, the current assessment has treated the fire PM emission as an inert aerosol, which is only subjected to removal from the atmosphere via wet and dry deposition (Kouznetsov and Sofiev, 2012). The aerosols are assumed to be sub-2.5 μm (PM_{2.5}) with the dry mean diameter of 1.5 μm .

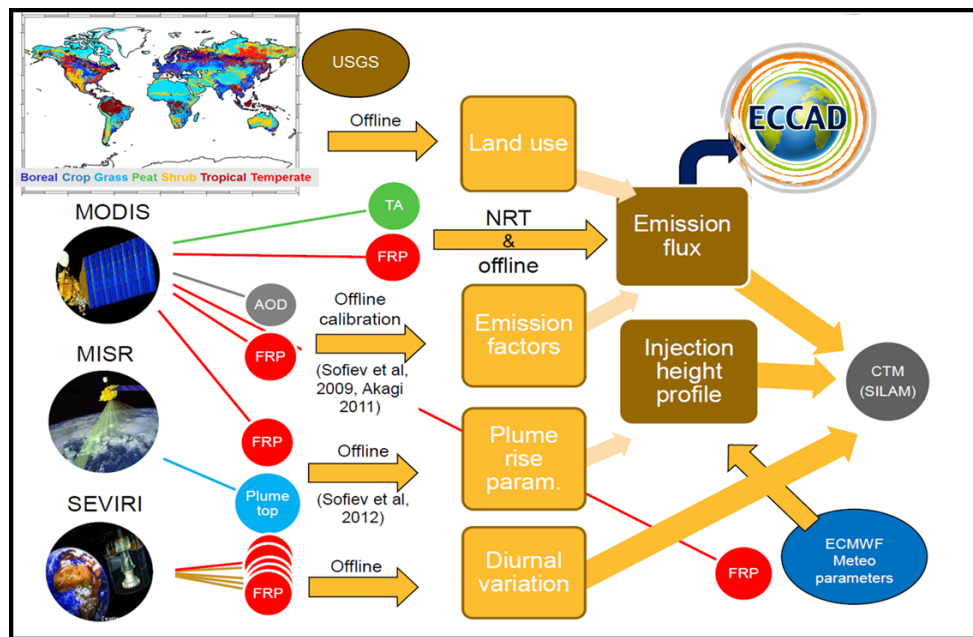


Figure 12.6. Structure and input data for IS4FIRES v.2.0.

Satellite observations of the fire plumes

Fire plumes are the strong and highly localized sources, which impact on the atmosphere and are comparatively easily observed from space. In the current example, information of MODIS on Aerosol Optical Depth (AOD) was used together with the CO column load of MOPIT instrument (<https://eosps.nasa.gov/sites/default/files/atbd/atbd-mop-02.pdf>). Both products observe also non-fire-induced pollutants: all kinds of aerosols in case of MODIS and all carbon monoxide emitted by combustion sources and produced as a result of chemical reactions in case of MOPITT. However, the non-fire contributions to their signals are largely (albeit not completely) independent: the powerful aerosol sources, such as deserts and sea surface area, do not emit CO. Therefore, their simultaneous usage can help delineate the fire plumes, especially if they are combined also with the model computations where the fire smoke can be separated precisely.

a3.4 Summer 2012: Hemispheric-scale fire smoke distribution

IS4FIRES – SILAM model predictions

The main part of the Northern-hemisphere fire season of 2012 started early in June when a large number of comparatively small fires was sprinkled over the whole of Eurasia, also rising in Canada and the US. In the Southern hemisphere, The development from that point was pretty strong and fast. Within just a couple of weeks, the Eurasian fires built up strength and new spots also showed up in the US and Canada.

Strength of the fires, especially in Siberia and on the Far East of Russia (Khabarovsk Krai region) was so high that their plumes were injected deep in the free troposphere, which facilitated their transcontinental transport. At the same time, fires were already starting in the European part of Russia south of Moscow and even in Western Europe, where the season is usually later. Together with the smoke from American fires, these plumes formed a “smoke belt” over the whole Northern hemisphere.

In the Southern hemisphere, African fires were at their usual location but were somewhat stronger than in other years. With burns in Amazonian forests and African and Australian grasslands, by mid-July strong fires were widespread over all continents. The main driving force of this spread was, of course, dry and hot weather, which synchronized and strengthened these events, which are usually somewhat smaller in scale and come at more diverse times. This especially refers to the Northern hemisphere, where the fires are not so much a result of agriculture or forestry practices as in Africa or Amazonia.

The season in the Northern hemisphere continued till the end of summer with fires gradually fading out only in September. At the same time, in the Southern hemisphere African and Amazonian fires just got their full strength.

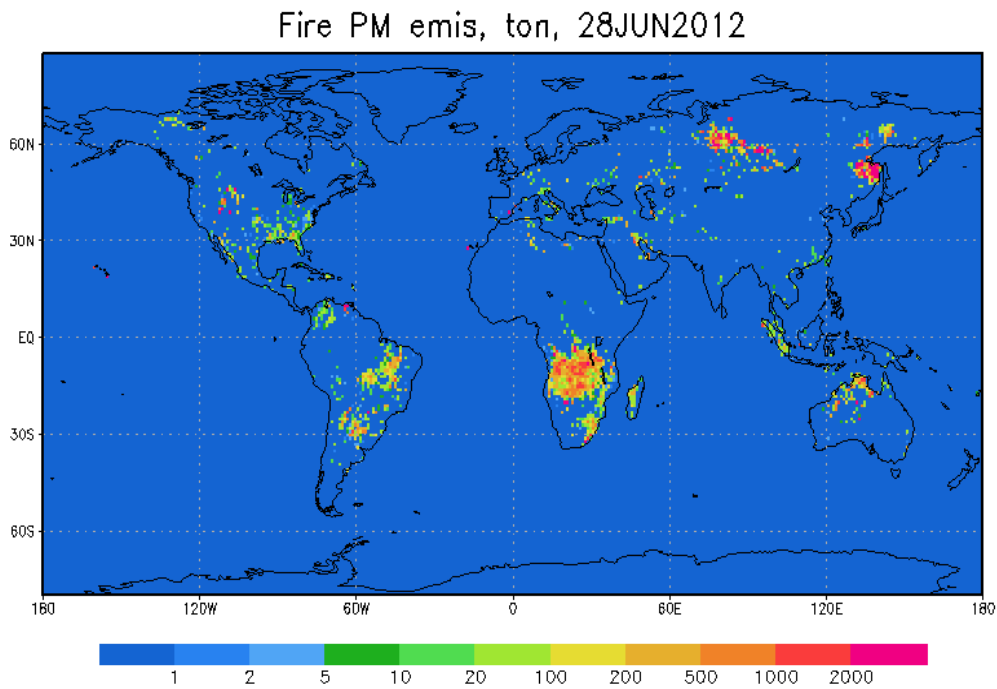


Figure 12.7. Daily fire PM emission distribution over the globe on 28 June 2012. Unit: [ton PM].

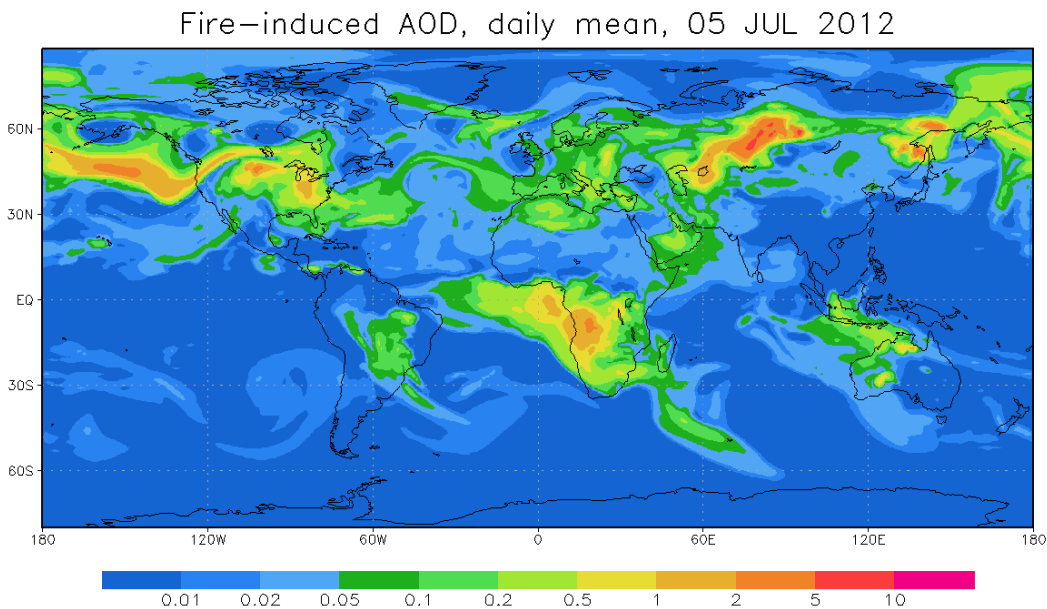


Figure 12.8. Fire-induced AOD on 5 July 2012. Daily mean predicted by SILAM. Relative unit.

a3.5 Satellite observations of the fire plumes

The above model predictions showed day-by-day the evolution of the fire season in 2012 and revealed the spatial distribution of the fire smoke, including its hemispheric-scale transport.

Verification of the model predictions at a global scale is comparatively straightforward using satellites, which provide arguably higher spatial homogeneity of the coverage and the quality of the signal as compares to in-situ networks. For the current outlook, MODIS AOD and MOPITT CO column-integrated retrievals were taken from the corresponding Websites “as-is” for the same date of 5 July 2012.

As one can see, the MODIS picture generally confirms the model predictions despite quite limited coverage over the northern Pacific, where SILAM provided much more information. However, the available retrievals show the same position and similar absolute AOD values for both model and the satellite.

A word of caution should be issued concerning the near-zero AOD over Australia despite a large number of fires noticed over that continent by the same MODIS instrument. This is a known feature of MODIS: it routinely shows practically zero AOD over Australia regardless the actual situation. One should also be careful not to mix the fire smoke with desert dust emitted from the Sahara and Middle East or sea salt released from the sea surface.

Analysis of MOPITT also has its own complexity (Figure). First of all, one has to exclude the industrial regions of Northern America, Europe and China. Secondly, CO has a nearly uniformly distributed background level (green color in Figure 12.10), which makes it not sensitive to small fires. With these two exceptions, the elevated-CO areas can be considered as the traces of wildland fire plumes.

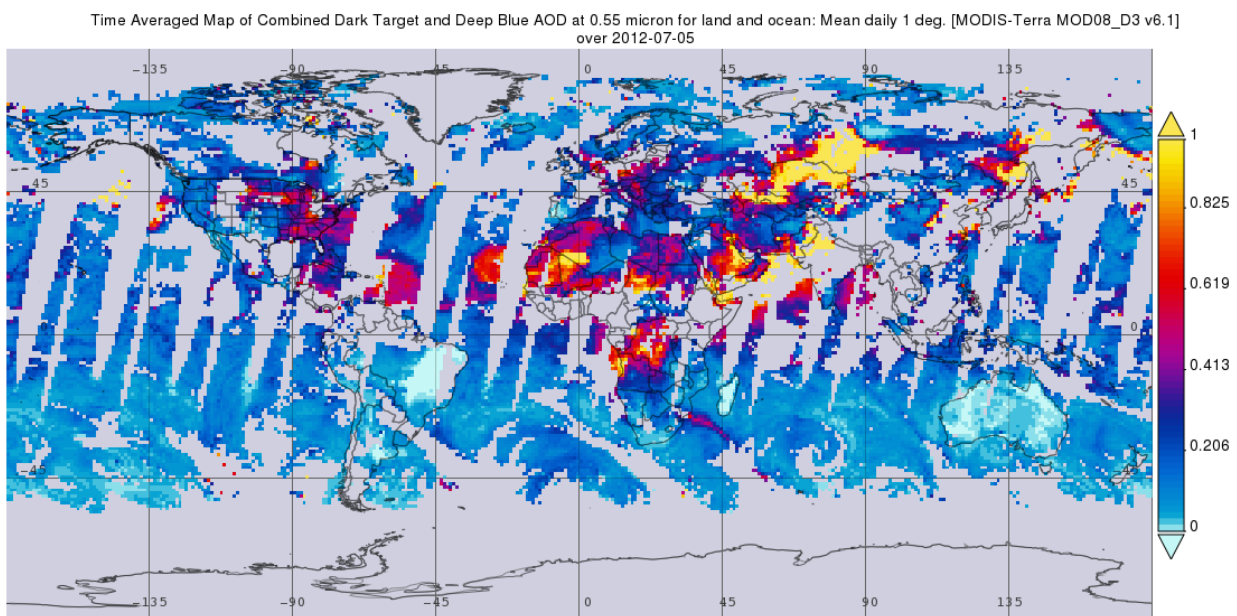


Figure 12.9. MODIS AOD, 5 July 2012, Terra only, daily composite. Source NASA Giovanni Web service: <https://giovanni.gsfc.nasa.gov>.

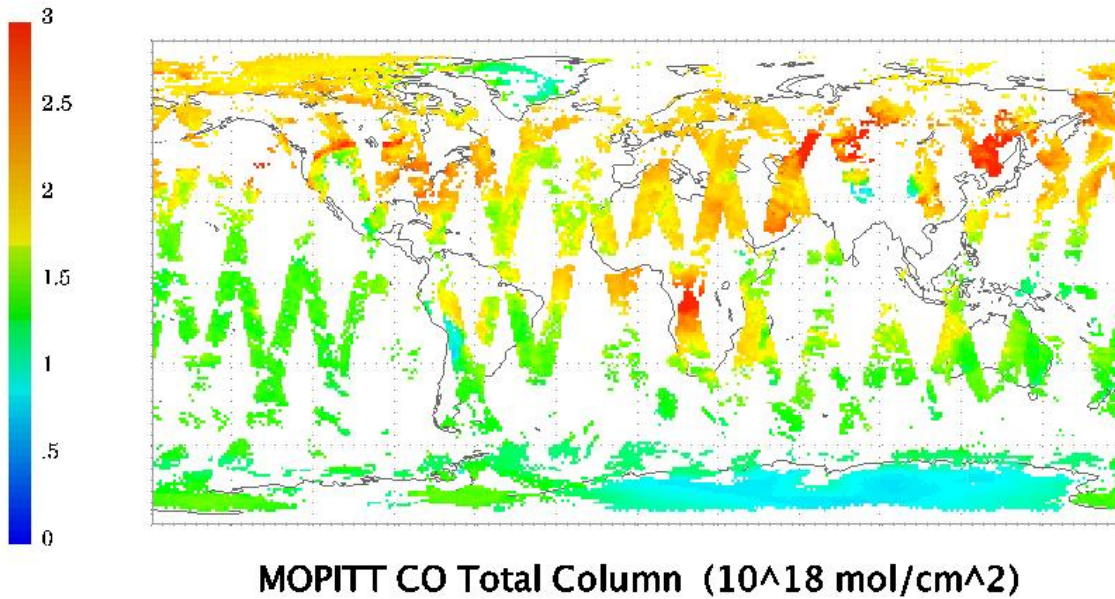


Figure 12.10. MOPITT CO total column, 5 July 2012.

On 5 July 2012, the strongest peaks of CO are visible over Africa, Siberia and Asia, the former two being mainly from fire sources and the last one originating from combination of Chinese industrial emission (southern part of the red area) and fire smoke (northern part). Due to the CO background, one cannot easily follow the “hemispheric smoke belt” but the main fire areas are very well seen. Noteworthy, MOPITT has firmly registered the elevated CO level downwind of Australian fires, in agreement with the SILAM predictions.

a3.6 Summary

The short outline of the fire season of 2012 in the Northern Hemisphere aimed at highlighting the variety of fire regions and reasons. Owing to seasonality of the large-scale meteorological processes, the fire seasons in different parts of the globe come in different times, which for some exceptional years can partly coincide – as it happened in the summer months of 2012 in the Northern hemisphere.

The current case was also used to demonstrate the synergy between different kinds of remote-sensing observations and modeling approaches that can be used for revealing such large-scale phenomena. Combined in an optimal way, they can provide a comparatively complete picture of the considered problem and suggest ways for discovering its underlying mechanisms.

Person of contact: Mikhail Sofiev, email: Mikhail.Sofiev@fmi.fi

References

- Kouznetsov, R. and Sofiev, M.: A methodology for evaluation of vertical dispersion and dry deposition of atmospheric aerosols, *J. Geophys. Res. Atmos.*, 117(1), doi:10.1029/2011JD016366, 2012.
- Soares, J., Sofiev, M. and Hakkarainen, J.: Uncertainties of wildland fires emission in AQMEII phase 2 case study, *Atmos. Environ.*, doi:10.1016/j.atmosenv.2015.01.068, 2015.
- Sofiev, M., Vankevich, R., Lotjonen, M., Prank, M., Petukhov, V., Ermakova, T., Koskinen, J. and Kukkonen, J.: An operational system for the assimilation of the satellite information on wildland fires for the needs of air quality modeling and forecasting, *Atmos. Chem. Phys.*, 9(18), 6833–6847, 2009.
- Sofiev, M., Ermakova, T. and Vankevich, R.: Evaluation of the smoke-injection height from wildland fires using remote-sensing data, *Atmos. Chem. Phys.*, 12(4), 1995–2006, doi:10.5194/acp-12-1995-2012, 2012.
- Sofiev, M., Vankevich, R., Ermakova, T. and Hakkarainen, J.: Global mapping of maximum emission heights and resulting vertical profiles of wildfire emissions, *Atmos. Chem. Phys.*, 13(14), 7039–7052, doi:10.5194/acp-13-7039-2013, 2013.
- Sofiev, M., Vira, J., Kouznetsov, R., Prank, M., Soares, J. and Genikhovich, E.: Construction of an Eulerian atmospheric dispersion model based on the advection algorithm of M. Galperin: dynamic cores v.4 and 5 of SILAM v.5.5, *Geosci. Model Dev.*, 8, 3497–3522, doi:10.5194/gmd-8-3497-2015, 2015.

12.6.2 North America

Case b1. National Air Quality Forecasting Capability for the U.S.A.

Pius Lee

Air Resources Laboratory (ARL), NOAA Center for Weather and Climate Prediction, College Park, Maryland; and CSISS, George Mason University (GMU), Fairfax, Virginia, U.S.A.

Case overview and significance: The U.S. NAQFC has been one of the main stays of air quality forecasting services of the world for roughly two decades. However, the dynamic evolution of fuel mix and energy consumption make-up of the U.S. has been a major challenge for NAQFC – an air quality forecasting operational system that customary can only be updated once a year. This is a typical challenge for national air quality forecasting services. This sample study illustrated the criticality of user feedback to constrain a large operational forecasting system with large variability. In this case the users were state and local forecasters from their respective air management agencies. Their 2017-2018 feedback exposed two grossly overlook emission problems: (1) recent increase trend of shale gas exploration, and (2) an erroneous chemical speciation match-up between the NAQFC emission model and NAQFC's chemical transport model. In both cases the local forecasters pin-pointed the spatially and temporally peculiarity of the NAQFC forecast resulting in upgrades to NAQFC for the problem areas and beyond.

b1.1 Introduction

The selected study case represents two high surface O₃ concentration scenarios over various parts of the conterminous U.S.A., as shown in Figure 12.11.

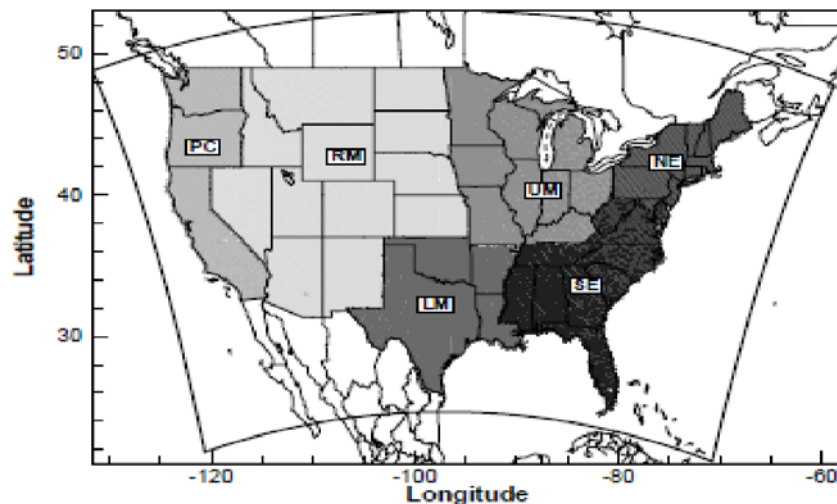


Figure 12.11. Domain map with abbreviation for the 6 evaluation regions labeled: (PC) Pacific Coast, (RM) Rocky Mountain, (UM) Upper Middle, (LM) Lower Middle, (NE) Northeast, and (SE) Southeast of the Conterminous U.S.A. (CONUS).

The establishment of the National Air Quality Forecasting Capability (NAQFC) of the U.S. was mandated by the U.S. Congress in 2002 to safeguard the public health, environmental and ecological assets of the U.S. The NAQFC provides a nationwide surface ozone (O₃) and particulate matter less than 2.5 μm in diameter (PM_{2.5}) with 48 h lead-time (Lee et al., 2017). The selected scenarios represent a perennial challenge in air quality forecasting (AQF) to capture many rapidly changing emissions in the industry. The exercise sheds insight on the subject area for a hands-on reader to delve into potential emission calculation deficiencies. We engage the reader in an exercise for possible remedies for such problems.

In this case study, the NAQFC was applied for two disjoint periods both with a 2-day forecast: 18-19 July 2017 and 21-22 February 2018, respectively. Both have 48 hours lead time. The

forecast products include surface level O₃ and PM_{2.5}. These products can be accessed at <http://www.emc.ncep.noaa.gov/mmb/aq/>

b1.2 General Description of the Model

NAQFC is comprised of the simulation of the fate of air pollutants using the US Environmental Protection Agency (EPA) Community Air Quality Multi-scale Model (CMAQ) driven by an offline coupling of the North American Mesoscale Forecasting System (NAM). Ideally, air quality and composition modeling should be an integral part of numerical weather prediction (NWP) modeling. Otherwise, geometric re-mapping and interpolation of grid structures between the models can be cumbersome. CMAQ and NAM have 12 km horizontal grid spacing. Both NAM and CMAQ dedicated fine vertical grid spacing at heights: near the surface, shallow convective layers just above the planetary boundary layer (PBL), and the tropopause to respectively capture surface-atmospheric directional exchanges, PBL venting and tropo-stratospheric O₃ entrainment. CMAQ was more CPU demanding than NAM. In order to meet the forecast-issuance time-requirements, the vertical structure for CMAQ was coarsened from that in NAM. The lowest five model layers below 1.5 km were identical between the two models assuring the near surface phenomena were best captured but were coarsened for the CMAQ grid at higher altitudes.

b1.2.1 Meteorological Model

NAM is the operational NWP forecast for the U.S. Its issuance is punctual and widely used (Rogers et al., 2014). The meteorological fields predicted by NAM is routinely used and familiarized by air quality forecasters. NAM's surface temperature, cloud fraction and precipitation distributions are fundamental input to CMAQ. NAM is benefited by the real time assimilation of many surface-, air- and space-borne observations (Wang et al., 2013). The NAM uses the RRTM radiation scheme for both long and short waves (Clough et al., 2005). NAM considers a climatology aerosol concentration but except for carbon dioxide, no trace gas is considered for radiation attenuation. The PBL-height, h , is determined by the lowest model layer that exhibits a critical bulk Richardson Number smaller than 0.25. Vertical eddy diffusivity used for mass flux is prescribed 0.2 m² s⁻¹ above the PBL. NAM is inline with the Noah Land Surface model (LSM) (Ek et al., 2002). The LSM provides surface characteristics such as soil moisture, canopy conductance, and vegetation greenness fraction to NAM. Many of these are sensitive parameters used by CMAQ for determining dry deposition velocities and biogenic and soil NO_x emissions.

b1.2.2 Chemical Transport Model (CTM)

Solar radiation and cloudiness constrain actinic flux strongly for the photolytic production of pollutants. Cloud fraction from NAM modulates downward short wave solar flux for photolytic reaction rates in CMAQ (Byun and Schere, 2006). Above cloud, enhanced photolytic rates due to reflection from clouds is accounted for by a multiplicative adjustment factor. The in-situ photolytic rate attenuation coefficient equals unity at the cloud top. The in-situ photolytic rate attenuation coefficient at each height at and below the cloud base is equal to the ratio of short wave solar radiation reaching that height to that would therein under clear sky conditions. Photolytic rates within the cloud are interpolated between cloud top and cloud base values using the in-situ cloud cover fraction at that height. The CB05-gas- and aero6-aerosol-phase mechanisms have been selected for NAQFC (Lee et al., 2017). Aqueous phase catalytic reactions represent a significant production pathway for inorganic compounds such as sulfate and organic compounds such as glyoxal in cloud droplets. Aqueous phase reaction is modeled in a reconstructed cloud column derived from the NAM predicted relative humidity vertical profile and the adiabatic lapse rate.

CMAQ derives convective boundary layer mixing of air pollutant using the Asymmetrical Convective Model version 2 (Pleim, 2007) PBL-scheme. The surface layer upward fluxes are allowed to transport pollutants to any layer within h by non-local mass exchange. For downward entrainment, a layer-by-layer local transport is prescribed. Cumulus cloud convective mixing of air pollutants is modeled by using a similar asymmetrical methodology with additional entrainment constraints (Pleim, 2007).

Removal processes of depositions are important in capturing the distributions of air pollutants, especially in surface levels. Rates of scavenging for gas and aerosol species by liquid and solid hydrometeors are often calculated by empirical uptake and accretion efficiency coefficients with considerable range of variability. Wet depositional speeds are determined by hydrometeor gravitational settling velocities. Dry deposition velocity for aerosol and trace gases are derived respectively basing on particle sedimentation velocity and canopy conductance and other surface resistances (Pleim and Xiu, 1995). These processes are highly spatially and temporally variable and are inherently less certain due to the empirical parameters used.

b1.3 Choices and Fine-Tuning of Model Parameterizations

Table 12.3 North America Case b1 summarizes the parameterization choices in NAQFC. These model selections involved synergies tested and tuned for various processes (e.g., Lee et al., 2009). In an operational forecasting system, the interplays of these processes and the preferred modeling choices are often systematically optimized based on long term performance statistics. For instance, modeling of wind-blown dust and soil nitrogen oxide (NO_x) emission are modulated by soil-wetness determined by precipitation. On the other hand, the formation and development of precipitation has strong dependencies on cloud microphysics and atmospheric aerosol concentration including suspended dust particles from wind-blown dust. This illustrates a possible complicated reciprocity in the feedback between cloud and precipitation, and aerosol and gaseous pollutant emissions. Furthermore, feedback is often nonlinear rendering the optimal selection of schemes and parameters challenging.

b1.4 Initialization, Boundary Conditions and Inputs for the Base and Sensitivity Simulations

Initialization of the CTM simulation were conducted from forecast fields from the previous NAQFC forecast cycle. Its boundary conditions were prescribed by monthly-varying concentration fields from a full-year retrospective simulation by the GEOS-Chem (Lee et al., 2017). In addition, there were three groups of input files: (a) Geometric data: `grd***` files, (b) Meteorological data: `met***` files, and (c) Emission files for the Base and two Sensitivity simulations. The three emission scenarios were: (Case_base) NAQFC operations (`emis_base***`), (Case_Oil_n_Gas) Updated shale oil and gas emission projections based on the actual US Energy Information Agency petroleum production data (`emis_O_n_G***`), and (Case_VOC_remap) Re-allocation for Volatile Organic Compound (VOCs) for the oil and gas area source sector (`emis_voc***`). They are available from the following anonymous ftp site: ftp.emc.ncep.noaa.gov/mmb/aq/WMO_NA_Case1 and a dedicated site assigned by WMO for this publication.

b1.5 Lessons Learned: Emission and PBL Dynamics

In NAQFC the most binding phenomena are those of meso-scale spatially and temporally close to the surface. We learned much from our years of attentive scrutiny of the NAQFC forecast. The two decisive modeled processes determining NAQFC accuracy are: (1) emission fluxes, and (2) planetary boundary layer (PBL) dynamics. The former is handled by emission inventory and projection calculation and the latter is dependent on the NAM's ability to accurately unravel movements of air and hydrometeor masses.

b1.6 Results and Discussion

During the 13th Annual Evaluation Conference for NAQFC Air Quality Forecasters in September 2017, forecasters expressed concern about the tightened U.S. national ambient O₃ standard at 70 ppb for the daily maximum 8 hours averaged concentration. NAQFC had difficulty to predict exceedances in the Northeastern US. It happened on July 18 2017 over Western Pennsylvania (PA) and its neighboring Northeastern West Virginia (WV). The NAQFC research team studied the failures in detecting exceedance events. It was likely that the large increase in shale field oil and gas exploration and production since 2010 in the Marcellus and Utica Shales in Western PA, WV and the State of Ohio caused the increase of surface O₃ concentration. Figure 12.12 shows the underprediction in NAQFC (background color shading) downwind of the shale fields valid at local noon time. The filled circles depict real-time measurement retrospectively

performed around 30 hours after the issued forecast. In the Case_Oil_n_Gas simulation, the oil and gas sector NOx and VOC emission were adjusted to the US Energy Information Agency 2016 actual energy production data in contrary with Base_Case's direct application of the U.S. EPA 2011 National Emission Inventory (NEI). NAQFC's underprediction at places downwind of the shale plays around the state border between PA and WV was reduced significantly (Figure 12.12). The missed exceedance on that day over Morgan Town, WV was remedied and correctly captured. Case_Oil_n_Gas results exhibited improvement.

A peculiarly high O3 concentration plume was reported by local forecasters over Northeastern Colorado in February 2018. It was unusual that it was in the middle of winter and O3 was typically not a problem, especially there was no snow then in Colorado to enhance photochemical reactions. To further mess up speculations, there was no other high O3 plume in the entire country for the month of February 2018 but only occasionally in Colorado, north of Denver? Further delving into the precursor concentration and speciation, it was discovered that the VOC assigned by NEI 2011 version 1 used by the Case_base has mistakenly apportioned too much reactive VOC to the total VOC. We adjusted the VOC speciation correspondence between Formaldehyde and other less non-reactive compounds. A parallel simulation was thus conducted for the month of February 2018. Figures 12.13 a and b show a snapshot prediction of surface O3 for July 20 2017 valid at 2:00 pm local time. The Case_VOC_remap was successful in removing the fictitious high O3 plume north of Denver, Colorado. The sensitivity case success was accredited to the reporting from forecasters.

Morgan Town, WV

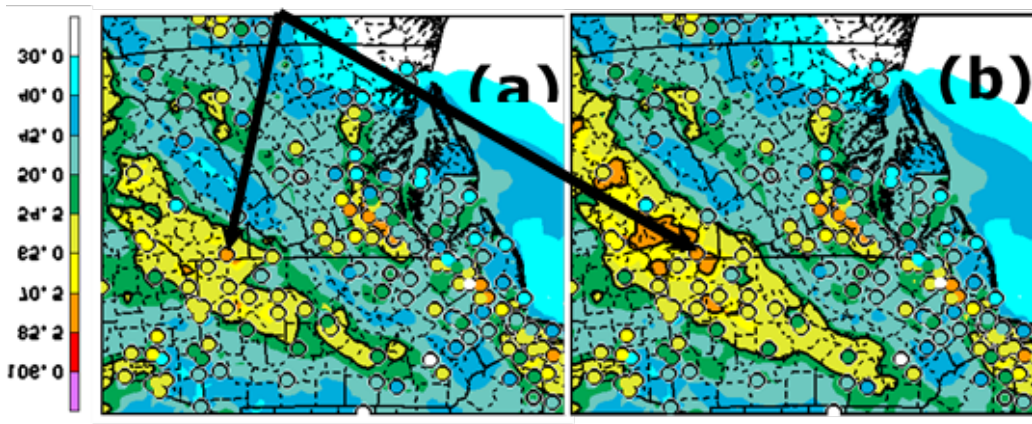


Figure 12.12. NAQFC 2nd day forecast (color shading) versus near real-time US EPA AIRNow measurements (filled solid circles) for July 18, 2017, 18:00 UTC by (a) Case_Base, and (b) Case_Oil_n_Gas.

(a) (b)

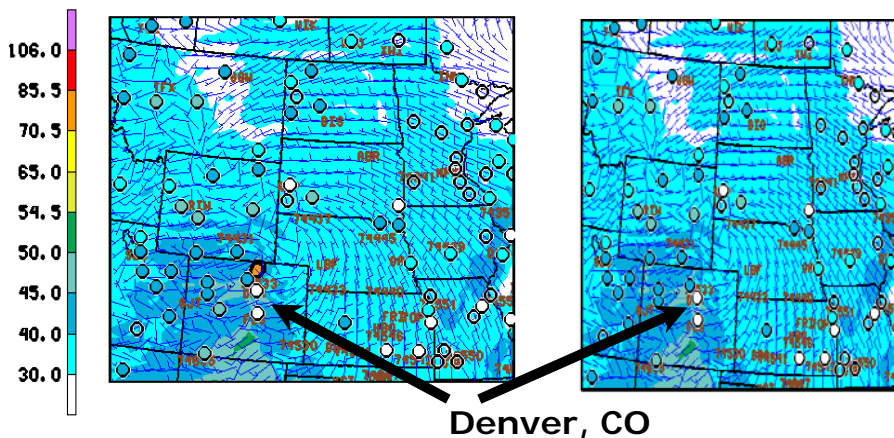


Figure 12.13. NAQFC 2nd day forecast (color shading) versus near real-time US EPA AIRNow measurements (filled solid circles) for Feb 21, 2017, 1800:00 UTC by (a) Operational, and (b) Corrected VOC speciation.

Denver, CO

References

- Byun D. and Schere K. 2006: Review of the governing equation, computational algorithms, and other components of the models-3 community multiscale air quality (CMAQ) modeling system, *Appl. Mech Rev.* 59, 51-57.
- Clough, S.A., M.W. Shephard, E.J. Mlawer, J.S. Delamere, M.J. Iacono, K. Cady-Pereira, S. Boukabara, and P.D. Brown, 2005: Atmospheric radiative transfer modeling: A summary of the AER codes, *J. Quant. Spectrosc. Radiat. Transfer*, 91, 233-244, doi:10.1016/j.jqsrt.2004.05.058. *J. Geophys. Res.*, 97, 15761-15785
- Ek, M. B., K. E. Mitchell, Y. Lin, E. Rogers, P. Grunmann, V. Koren, G. Gayno, and J. D. Tarpley, 2003: Implementation of Noah land surface model advances in the National Centers for Environmental Prediction operational mesoscale Eta model. *J. Geophys. Res.*, 108 (D22), 16.
- Lee, P., McQueen, J., Stajner, I., Huang, J., Pan, L., Tong, D., Kim, H., Tang, Y., Shafran, P., Huang, H.-C., Gorline, J., Upadhyay, S., and Artz, R., 2017: NAQFC developmental forecast guidance for fine particulate matter (PM_{2.5}), *Weather and Forecasting*, 32 no.1. pp 343-360,
- Lee, P., Y. H. Tang, D. Kang, J. McQueen, M. Tsidulko, H. C. Huang, S. Lu, M. Hart, H. M. Lin, S. Yu, G. DiMego, and P. Davidson, 2009: Impact of consistent boundary layer mixing approaches between NAM and CMAQ. *Environmental Fluid Mechanics* 9, 23-42, DOI 10.1007/s10652-008-9089-0.
- Pleim, J. 2007: A combined local and nonlocal closure model for the atmospheric boundary layer. Part I: model description and testing, *J. Appl. Meteor.* 46, 1383-1395.
- Pleim, J. E., and A. Xiu, 1995: Development and testing of a surface flux and planetary boundary layer model for application in mesoscale models. *J. Appl. Meteor.*, 34, 16-32.
- Rogers E., and co-authors, 2014: The NCEP North American Mesoscale (NAM) Analysis and Forecast System : Near-term plans and future evolution into a high-resolution ensemble, AMS 27th WAF/23rd NWP Conference, Atlanta, GA, viewable at <https://ams.confex.com/ams/94Annual/videogateway.cgi/id/26188?recordingid=26188> doi:10.1029/2002JD003296.
- Wang, Parrish, Kleist and Whitaker, *MWR*, 2013, 141, 4098-4117.

Case b2. Application of WRF/Chem-MADRID over Southeastern U.S.

Yang Zhang

Department of Civil and Environmental Engineering, Northeastern University, Boston, MA, U.S.A. (previously at North Carolina State University, Raleigh, North Carolina)

Case overview and significance: The online-coupled WRF/Chem-MADRID has been applied to real-time air quality forecasting (AQF) over the Southeastern U.S.A. for about a decade. There were two lessons learned during this deployment of the forecasting system: (a) Up-to-date emission was critical for forecast accuracy --- noticeably for the surface concentrations of the two criterion species: O₃ and PM_{2.5}; and (b) Application of satellite-constrained chemical lateral boundary condition could potentially improve forecast accuracy. WRF/Chem-MADRID is an advanced online-coupled system facilitating communication of relevant meteorological conditions in WRF and chemical composition dynamics in Chem-MADRID in each advection time step. The system's comprehensive physically based parameterization accounted for all major physical and chemical processes for AQF. The system extended its capability for two-way feedback between meteorology and chemical composition for direct, semi-direct, and indirect effects of aerosols which is not customarily included in AQF. Nonetheless, two-way feedback modeling systems replicate the reality and should represent a leading role in future AQF and other earth system modeling efforts.

b2.1 Introduction

An online-coupled meteorology-chemistry model, WRF/Chem with the Model of Aerosol Dynamics, Reaction, Ionization, and Dissolution (MADRID) (WRF/Chem-MADRID) (Zhang et al., 2010a, 2012), has been deployed for real-time air quality forecasting (RT-AQF) in southeastern U.S. since 2009 for O₃ seasons (May-September) and winter seasons (December, January, and February). The forecasting simulations are performed at a horizontal grid resolution of 12 km over an area in southeastern U.S. including the states of Mississippi (MI), Alabama (AL), Georgia (GA), Florida (FL), South Carolina (SC), North Carolina (NC), Tennessee (TN), Kentucky (KY), Virginia (VA), West Virginia (WV), and Delaware (DE), as well as small portions of Louisiana (LA), Arkansas (AR), Missouri (MS), Illinois (IL), Indiana (IN), Ohio (OH), and Maryland (MD). Figure 12.14 shows the forecasting domain. This case provides the forecasting testbed during July 1-10, 2017.

b2.2 General Description of the Model and Evaluation Protocol

WRF/Chem-MADRID is an online-coupled meteorology and chemistry model. It was developed based on WRF/Chem version 3.0 (Grell et al., 2005) and CMAQ-MADRID (Zhang et al., 2004) with updates in gas-phase chemistry and aerosol treatments by Zhang et al. (2010a, b, 2012). WRF/Chem-MADRID simulates all major atmospheric processes such as emissions, transport, chemistry in the gas-, aqueous-, and particulate-phases, aerosol and cloud processes, and removal. The aerosol module, MADRID, simulates detailed thermodynamic equilibrium for both inorganic and organic species and microphysics such as new particle formation, condensation/evaporation, coagulation, and gas/particle mass transfer. Unlike offline-coupled air quality models, WRF/Chem-MADRID simulates aerosol direct and semi-direct feedbacks to photolysis, radiation, and planetary boundary layer (PBL) meteorology, as well as aerosol indirect effects on cloud and precipitation formation via many aerosol-cloud interaction processes.

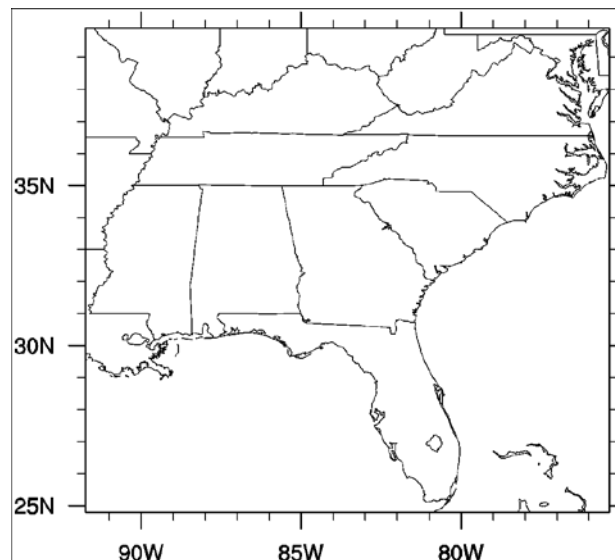


Figure 12.14. Simulated domain for RT-AQF using WRF/Chem-MADRID.

Since May 2009, WRF/Chem-MADRID has been deployed for RT-AQF in southeastern U.S. for ozone (O₃) season (May-September) and winter season (December-February) (Chuang et al., 2011; Yahya et al., 2014). Figure 12.15 shows a flowchart of the RT-AQF system based on WRF/Chem-MADRID. The hourly and daily forecast products are provided at https://coe.northeastern.edu/Research/CASCADE/Real_Time.html. The forecasts of air quality and meteorology since 2009 have been comprehensively evaluated against all available surface and satellite-derived observations. The model evaluation includes both discrete and categorical measures. In the discrete evaluation, mean bias (MB), normalized mean bias (NMB), root mean square error (RMSE), and normalized mean error (NME) are calculated based on Zhang et al. (2006). In the categorical evaluation, several indices including accuracy (A), critical success index (CSI), probability of detection (POD), bias (B), and false alarm ratio (FAR) are used to evaluate the model's ability to predict exceedances and non-exceedances (Kang et al., 2005).

b2.3 Choices and Fine-Tuning of Model Parameterizations

Table 12.3 North America Case b2 summarizes the parameterization choices in WRF/Chem-MADRID. The physics and chemistry options used in this study follow those of Chuang et al. (2011), Yahya et al. (2014) and Zhang et al. (2016); they are kept the same for all forecasting periods since 2009. The physics options include the cloud microphysics of Lin et al. (1983); the Rapid Radiative Transfer Model (RRTM) of Mlawer et al. (1997) for longwave radiation; the Goddard scheme of Chou et al. (1998) for shortwave radiation; the Yonsei University (YSU) PBL scheme of (Hong et al. 2006); the National Center for environmental Prediction, Oregon State University, Air Force, Hydrologic Research Lab (NOAH) LSM (Chen and Dudhia, 2001); and the Grell-Devenyi ensemble cumulus parameterization (Grell and Devenyi, 2002). The chemistry and aerosol-related options chosen include the 2005 Carbon Bond gas-phase chemical mechanism (CB05) (Yarwood et al., 2005); the Carnegie-Mellon (CMU) bulk aqueous-phase chemical kinetic mechanism (Fahey and Pandis, 2001), the MADRID1 aerosol module with 8 size sections over the PM aerodynamic diameter range of 0.025-11.630 μm of Zhang et al. (2004, 2010a, b, 2012), and the aerosol activation of Abdul Razzak and Ghan (2002). A more detailed description of the model can be found in Chuang et al. (2011) and Yahya et al. (2014).

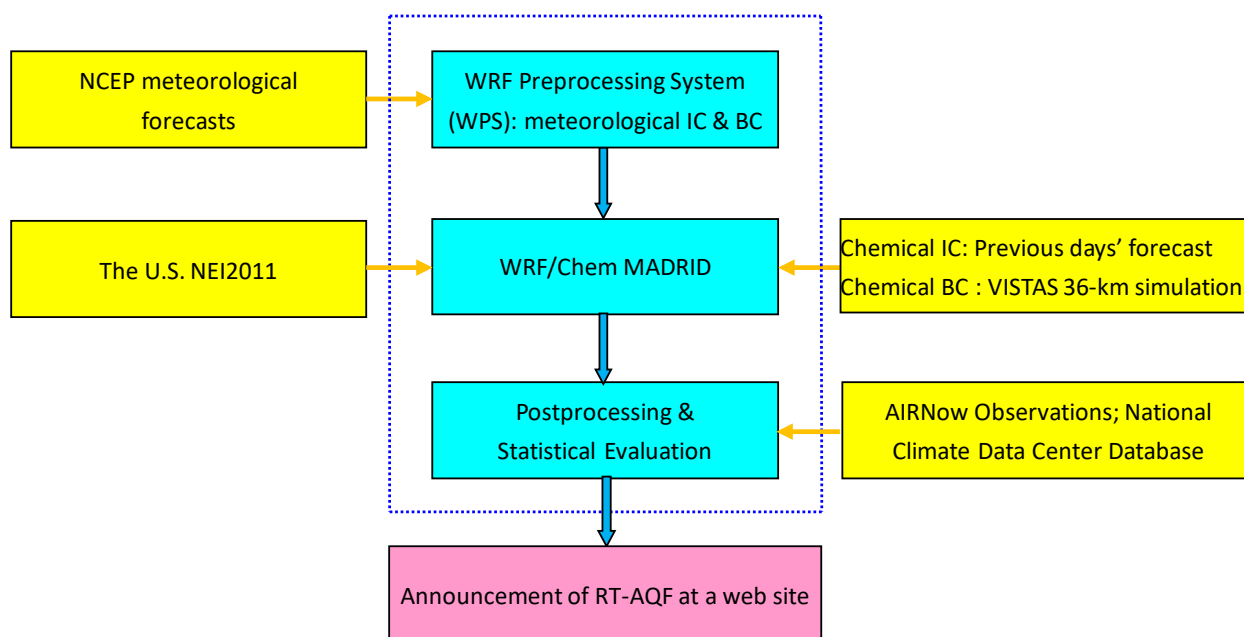


Figure 12.15. Flowchart of the RT-AQF system based on WRF/Chem-MADRID (VISTAS denotes the Visibility Improvement State and Tribal Association of the Southeast) (Figure was taken from Chuang et al., 2011 and updated based RT-AQF since 2015).

b2.4 Initialization, Boundary Conditions, and Inputs

The National Center for Environmental Prediction's (NCEP) meteorological forecast is downloaded at 7 p.m. (Local Standard Time) to initialize a 60-hr forecasting cycle using WRF/Chem-MADRID with 12-hr spin-up and 48-hr forecasting. The anthropogenic emissions are based on the 2011 U.S. National Emission Inventories (NEI). Those emissions vary hourly and account for seasonal variations. Biogenic emissions are simulated using the online module based on the Model for Gases and Aerosols from Nature (MEGAN) version 2. Mineral dust emissions are simulated using online dust emission of Shaw (2008). The Visibility Improvement State and Tribal Association of the Southeast's (VISTAS) 2009 36-km CMAQ simulation results and those from the previous day's simulation are used to provide daily chemical boundary and initial conditions (BCONs and ICONs), respectively. One-week spin up simulation is performed for the first day of the first 60-hr forecasting cycle for each forecasting season.

b2.5 Lessons Learned: Emission and Boundary Conditions

Several lessons were learned from our forecasting since 2009. For example, the anthropogenic emissions were based on the projected 2009 emissions by the VISTAS from the 1999 National Emission Inventories (NEI) version 2 during 2009-2014. The model evaluation for 2013 and 2014 forecasting products indicated overpredictions in O₃ and PM_{2.5} concentrations at some urban sites, which were mainly attributed to the use of out-of-date emissions. The anthropogenic emissions for forecasting since 2015 were updated based on the NEI2011, which help reduce such overpredictions. This illustrates the importance of using up-to-date emissions for RT-AQF. The model evaluation of column mass abundance of chemical species such as CO and O₃ shows large model biases, which were attributed to the use of the inaccurate BCONs. Two sensitivity simulations were performed: one during August 2012 using satellite-constrained BCONs for CO and a sensitive simulation during December 2012 using satellite-constrained BCONs for O₃. Those sensitivity simulations show large improvements in simulated column CO and tropospheric ozone residuals (TOR). As an example, Figure 12.16 compares the spatial distributions of satellite-derived CO simulated from baseline (Sim_base) and the sensitivity simulations in August 2012 (Sim_sen). The use of satellite-constrained BCONs improves the simulated CO substantially in terms of both magnitude and spatial

distribution. The MB, NMB, and NME of CO from Sim_sen are -0.2, -10.6%, and 18.2%, respectively, compared to -0.8, -40.6%, and 40.8% from Sim_base. The MB, NMB, and NME of TOR from Sim_sen are -0.2, -0.01%, and 0.1%, respectively, compared to 11.7, 44.8%, and 44.8% from the Sim_base. This illustrates the importance of using more realistic BCONs for RT-AQF.

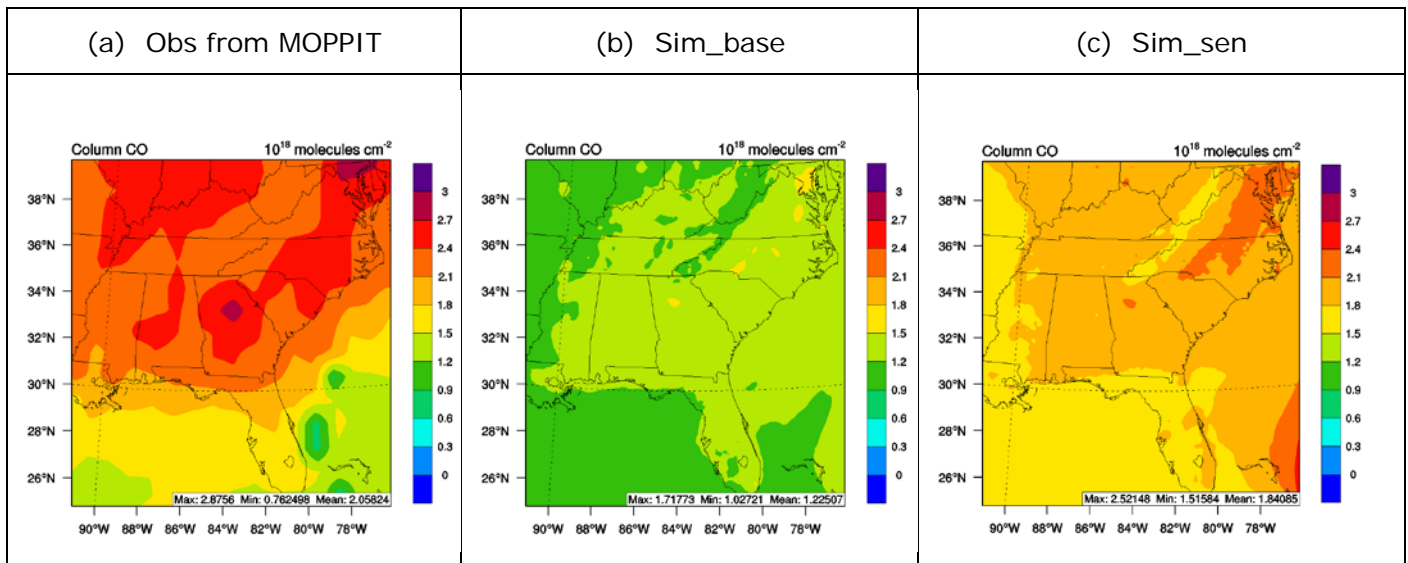


Figure 12.16. Comparison of CO spatial distributions in August, 2012: (a) satellite observation from MOPPIT, (b) baseline simulation, and (c) sensitivity simulation (Figure taken from Zhang et al., 2016).

b2.6 Results and Discussion

The forecasting products from WRF/Chem-MADRID during May-September 2017 are evaluated using surface concentration observations from AIRNow. The chemical species evaluated include maximum 1-hr and 8-hr O₃ and 24-hr average PM_{2.5}. Table 12.9 summarizes the performance statistics. Figure 12.17 shows the forecasted maximum 8-hr average O₃ and 24-hr average PM_{2.5} concentrations overlaid with observations from AIRNow during the 2017 O₃ seasons. The NMBs for O₃ and PM_{2.5} are within 4% and 7%, respectively, which are considered to be excellent performance based on the criteria of NMBs of 15% and 30%, respectively, for their good performance that are commonly used in the air quality communities. The forecasted spatial distributions of both species generally capture the gradients and hot spots, despite some underpredictions in the north-western corner for O₃ and in the northern and the southern areas for PM_{2.5}. These underpredictions may be caused by several factors such as uncertainties in the emissions over those areas, the use of a 12-km grid resolution, and the use of the older version of WRF/Chem as the host model for MADRID. Further improvement of the model and associated inputs can be performed when resources become available.

Table 12.9. Performance Statistics for Max 1-hr and 8-hr Average O3 and 24-hr Average PM2.5.

	Max 1-hr O3	Max 8-hr Average O3	24-hr Average PM2.5
Mean Obs	46.1	41.2	8.9
Mean Sim	47.5	44.0	9.2
MB	1.4	2.9	0.3
RMSE	19.6	12.3	4.6
NMB, %	3.1	7.0	3.8
NME, %	22.2	23.4	37.3

MB, RMSE, and Bias are in ppb for max 8-hr average O3 and $\mu\text{g m}^{-3}$ for 24-hr average PM2.5. The observations are taken from AIRNow.

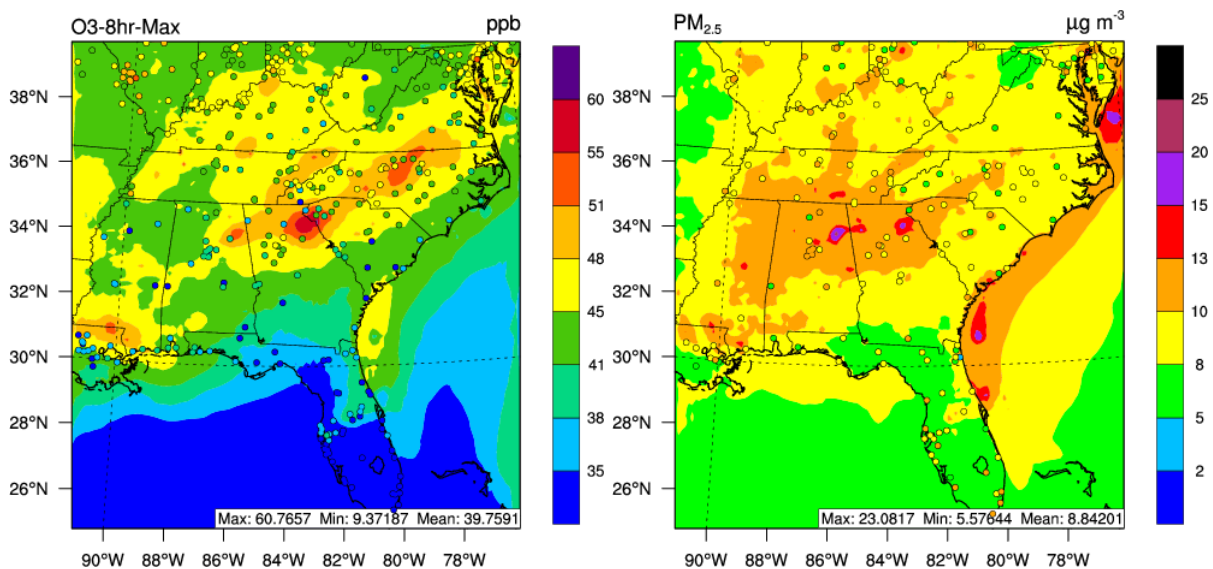


Figure 12.17. Spatial distributions of forecasted maximum 8-hr average O3 and 24-hr average PM2.5 concentrations during the 2017 O3 seasons. The observations are symbolled as circles, they were taken from AIRNow.

Person of Contact: Yang Zhang, email: ya.zhang@northeastern.edu

References

- Abdul-Razzak, H., and S. J. Ghan. 2002. A parameterization of aerosol activation, 3. Sectional representation. *J. Geophys. Res.* 107 (D3). doi:10.1029/2001JD000483.
- Chen, F., and J. Dudhia. 2001. Coupling an advanced land surface–hydrology model with the Penn State-NCAR MM5 modeling system. Part I: Model implementation and sensitivity. *Mon. Weather Rev.* 129 (4):569–585. doi:10.1175/1520-0493(2001)129<0569:CAALSH>2.0.CO;2.
- Chou, M. D., M. J. Suarez, C. Ho, M. M. Yan, and K. Lee. 1998. Parameterizations for Cloud Overlapping and Shortwave Single-Scattering Properties for Use in General Circulation and Cloud Ensemble Models. *J. Climate.* 11 (2):202-214. doi: http://dx.doi.org/10.1175/1520-0442(1998)011<0202:PFCOAS>2.0.CO;2.
- Chuang, M. T., Y. Zhang, and D. W. Kang. 2011. Application of WRF/Chem-MADRID for Real-Time Air Quality Forecasting over the Southeastern United States. *Atmos. Environ.* 45 (34):6241-6250. doi:10.1016/j.atmosenv.2011.06.071.
- Fahey, K.M., and S. N. Pandis. 2001. Optimizing model performance: variable size resolution in cloud chemistry modeling. *Atmos. Environ.* 35:4471-4478. doi:10.1016/S1352-2310(01)00224-2.
- Grell, G. A., and D. Devenyi. 2002. A generalized approach to parameterizing convection combining ensemble and data assimilation techniques. *Geophys. Res. Lett.* 29 (14): 1693. doi:10.1029/2002GL015311.
- Grell G. A., S. E. Peckham, R. Schmitz, S. A. McKeen, G. Frost, W. C. Skamarock, and B. Eder. 2005. Fully coupled 'online' chemistry in the WRF model. *Atmos. Environ.* 39:6957-6976. doi:10.1016/j.atmosenv.2005.04.027.
- Hong, S.-Y., Y. Noh, and J. Dudhia. 2006. A New Vertical Diffusion Package with an Explicit Treatment of Entrainment Processes. *Mon. Weather Rev.* 134:2318-2341. doi:10.1175/MWR3199.1.
- Kang, D., B. K. Eder, A. F. Stein, G. A. Grell, S. E. Peckham, and J. McHenry. 2005. The New England Air Quality Forecasting Pilot Program: Development of an evaluation protocol and performance benchmark. *J. Air & Waste Manage. Assoc.* 55:1782-1796. doi:10.1080/10473289.2005.10464775.
- Lin, Y.-L., R. D. Farley, and H. D. Orville. 1983. Bulk Parameterization of the Snow Field in a Cloud Model. *J. Appl. Met. Clim.* 22:1065-1092. doi:10.1175/1520-0450(1983)022.
- Mlawer, E.J., S. J. Taubman, P. D. Brown, M. J. Iacono, and S. A. Clough. 1997. Radiative transfer for inhomogeneous atmospheres: RRTM, a validated correlated-k model for the longwave. *J. Geophys. Res.* 102:16663-16682. doi: 10.1029/97JD00237.
- Shaw, W. J., K. Jerry Allwine, B. G. Fritz, F. C. Rutz, J. P. Rishel, and E. G. Chapman (2008), An evaluation of the wind erosion module in DUSTRAN, *Atmos. Environ.*, 42(8), 1907–1921,
- Yahya, K., Y. Zhang, and J. M. Vukovich. 2014. Real-Time Air Quality Forecasting over the Southeastern United States using WRF/Chem-MADRID: Multiple-Year Assessment and Sensitivity Studies. *Atmos. Environ.* 92:318-338. doi:10.1016/j.atmosenv.2014.04.024.
- Yarwood, G., S. Rao, M. Yocke, G. Z. Whitten, and S. Reyes. 2005. Final Report Updates to the Carbon Bond Chemical Mechanism CB05. Report to the U.S. Environmental Protection Agency, December 2005.
- Zhang, Y., B. Pun, K. Vijayaraghavan, S.-Y. Wu, C. Seigneur, S. Pandis, M. Jacobson, A. Nenes, and J. H. Seinfeld. 2004. Development and Application of the Model of Aerosol Dynamics, Reaction, Ionization and Dissolution (MADRID). *J. Geophys. Res.* 109:D01202. doi:10.1029/2003JD003501.
- Zhang, Y., P. Liu, B. Pun, and C. Seigneur. 2006. A comprehensive performance evaluation of MM5-CMAQ for the Summer 1999 Southern Oxidants Study episode-Part I: Evaluation protocols, databases, and meteorological predictions. *Atmos. Environ.* 40:4825-4838. doi:10.1016/j.atmosenv.2005.12.043.

- Zhang, Y., Y. Pan, K. Wang, J. D. Fast, and G. A. Grell. 2010a. WRF/Chem-MADRID: Incorporation of an aerosol module into WRF/Chem and its initial application to the TexAQS2000 episode. *J. Geophys. Res.* 115: D18202. doi:10.1029/2009JD013443.
- Zhang, Y., P. Liu, X.-H. Liu, B. Pun, C. Seigneur, M.Z. Jacobson, and W.-X. Wang. 2010b. Fine Scale Modeling of Wintertime Aerosol Mass, Number, and Size Distributions in Central California. *J. Geophys. Res.* 115:D15207. doi:10.1029/2009JD012950.
- Zhang, Y., Y. Chen, G. Sarwar, and K. Schere. 2012. Impact of gas-phase mechanisms on Weather Research Forecasting Model with Chemistry (WRF/Chem) predictions: Mechanism implementation and comparative evaluation. *J. Geophys. Res.* 117:D01301. doi:10.1029/2011JD015775.
- Zhang, Y., C.-P. Hong, K. Yahya, Q. Li, Q. Zhang, and K.-B. He, 2016. Comprehensive evaluation of multi-year real-time air quality forecasting using an online-coupled meteorology-chemistry model over southeastern United States, *Atmos. Environ.*, 138, 162-182, doi:10.1016/j.atmosenv.2016.05.006.

Case b3. Wildland fire smoke forecasting capability in the U.S.A.

Mariusz Pagowski and Stuart McKeen

Earth Research Laboratory, NOAA, Boulder, Colorado, U.S.A.

Cooperative Institute for Research in Environmental Sciences, Boulder, Colorado, U.S.A.

Case overview and significance: In this study, RAP-Chem provided near-real time air pollutant forecasts for North America at 12 km horizontal resolution. It was a regional application of WRF-Chem with ingestion of dynamic chemical boundary conditions from the RAQMS global atmospheric composition simulation. The regional meteorological simulation and the global chemical composition simulations were benefited by frequent data assimilation of observations and short latency in acquiring continuous observations. This study focused on demonstrating two high impact scenarios of adverse air quality conditions due to different pollutant sources and meteorological conditions. Both of these scenarios demanded increased attention by health and air managers: (a) Wildland fire smoke in the western U.S.A. that seemed to occur more frequently and severely in recent years were adversely impacting human health and the environment; (b) Increase of background O₃ due to stratospheric intrusion of air masses jeopardizing county-specific compliance of the ambient O₃ standards that has been tightened and projected to be further tightened by the U.S. EPA.

b3.1 Introduction

Two selected cases illustrate performance of RAP-Chem during wildfires over the north-western USA in September 2017 and a stratospheric intrusion that occurred in March of 2018 over Colorado. RAP-Chem is an implementation of the WRF-Chem meteorology-chemistry model (Grell et al., 2005) that provides near-real time forecasts for an extended North American domain at 12 km horizontal resolution. 48-hr forecasts are initialized at 00 UTC and displayed daily at <https://rapidrefresh.noaa.gov/RAPchem>.

RAP-Chem predicts meteorology and concentrations of gaseous and particulate pollutants. The details on domain set-up and choices of physical and chemical parameterizations are given in Table 12.3 North America Case b3. Lateral boundary conditions are obtained for meteorology from GFS, the US national global forecasting system, and the RAQMS model (<http://raqms.ssec.wisc.edu/>) for photochemical and aerosol variables.

b3.2 Tackling the Wildland Fire Forecast Challenge

Wildfires cost U.S. taxpayers millions of dollars that are spent on extinguishing fires, repairing damage to property and ecosystems, and healthcare due to air and water pollution. Predictions of smoke dispersion help to mitigate the effects of poor air quality on affected populations. Extensive fires over north-western U.S. occur with unwelcome regularity every summer. Success of their prediction is largely determined by the quality of emissions derived from satellite products. In RAP-Chem observations from GOES-West and MODIS determine the extent and intensity of the fire emission sources. Smoke plumes rise from the surface and disperse at a level determined by a one-dimensional cloud model. Temporal profiles of the intensity of surface emissions resemble a Gaussian during the day and are flat at night. In Figure 12.18 contours of surface concentration of PM_{2.5} opposite aerosol optical depth retrievals at 550 nm from VIIRS are shown. These quantities are not directly comparable, and it is difficult to verify the accuracy of model predicted surface PM_{2.5} without further analysis. But in our opinion the extent of the smoke plume matches the independent satellite observations well. We note that forecasts of surface concentrations of species are inherently difficult because of uncertainties of vertical mixing, and forecasts of vertically integrated quantities like AOD are generally more skillful.

A major uncertainty for tropospheric ozone forecasts within regional-scale models is the treatment of "background" ozone, and more specifically the contribution of ozone from the stratosphere. Ozone lidar observations often detect episodically high levels, sometimes reaching the ground, from stratospheric intrusion events associated with cyclogenesis.

Figure 12.19a shows an example from the TOPAZ ozone lidar over Boulder, CO on 3/16/18 (<https://www.esrl.noaa.gov/csd/groups/csd3/measurements/2018>). Surface pressure had minimized the previous evening as a deep cut-off low forms over the central U.S. The TOPAZ lidar saw high O₃ from the intrusion event below 500 mb starting at noon local time and lasting 2 to 4 hours on 3/16/18. Figure 12.19b shows the horizontal distribution of O₃ during the time of the event. Ozone boundary conditions for RAP/Chem are taken from the global RAQMS model, which assimilates observed O₃ above the middle troposphere from TES satellite data. Although the RAP/Chem model output is temporally too coarse to catch the observed O₃ maxima, the timing of the intrusion matches the TOPAZ observations quite well. Model O₃ increases at the 700mb level (see RAP/Chem web page) also match the timing in Figure 12.19b. One needs to average the observations over a model grid to compare statistically, but the 500mb model O₃ values (~90 ppbv) on the edges of the event are consistent with the TOPAZ data. The model results of Figure 9b3.2b put the TOPAZ measurements in a broader context: as the tail end of a much larger stratospheric impact over a major fraction of the U.S. Another intrusion was observed by TOPAZ on 3/23/18 (see the CSD measurement webpage), and again RAP/Chem captured the timing of elevated O₃ very well. However, the TOPAZ lidar showed the intrusion reaching the surface on this day, as confirmed by surface O₃ monitors, while the model did not.

Acknowledgement: S. Kondragunta and collaborators (NOAA/NESDIS) provided VIIRS retrievals.

Person of Contact: Mariusz Pagowski, email: mariusz.pagowski@noaa.gov

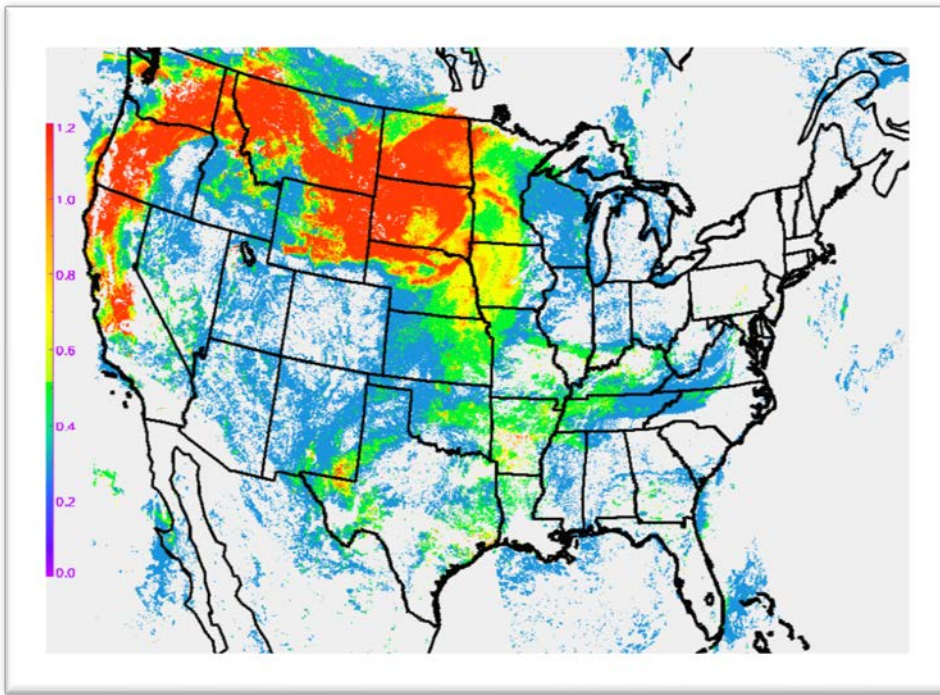
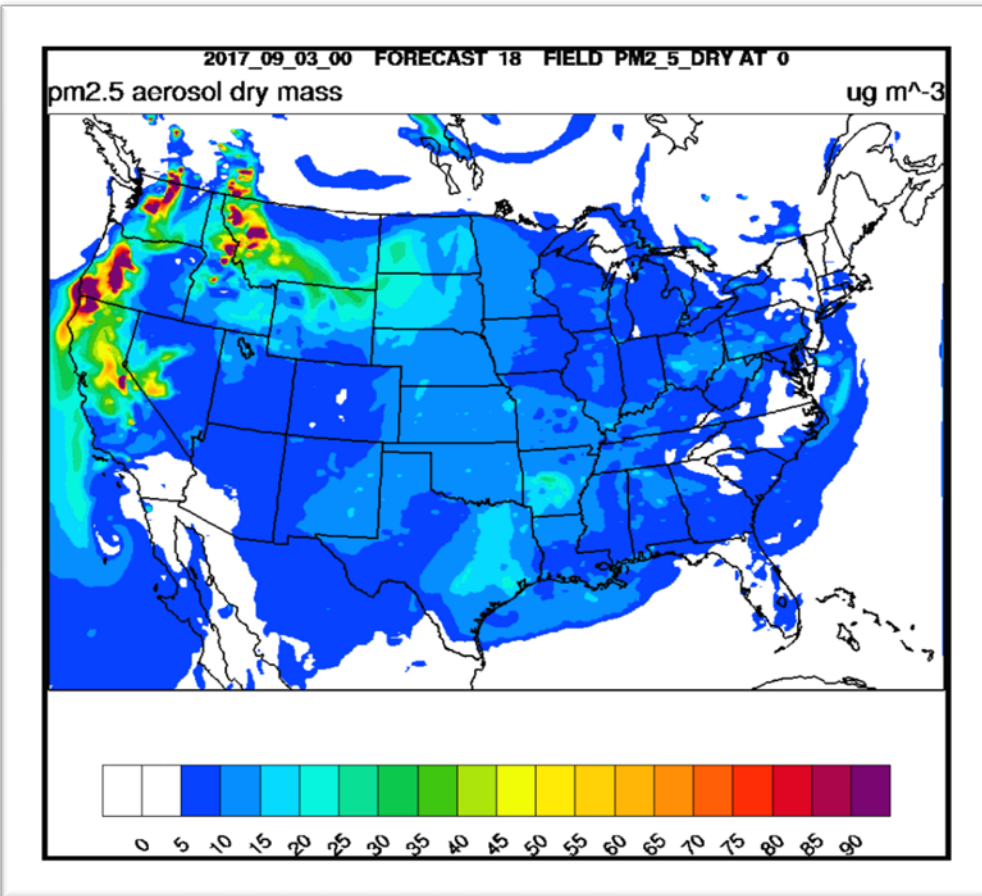


Figure 12.18

Top: retrievals of AOD at 550 nm from VIIRS – aggregated granules from 20170903 between 15-21UTC.



Bottom: 18-hr RAP-Chem forecast of surface PM_{2.5} concentration.

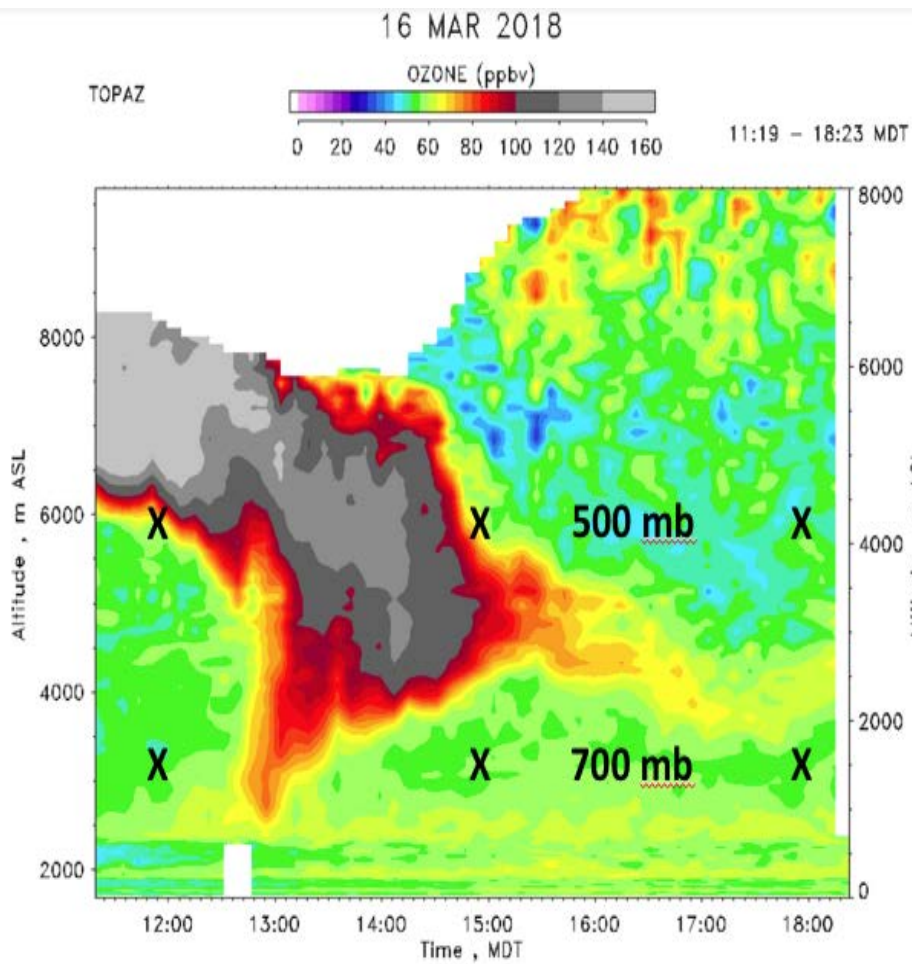
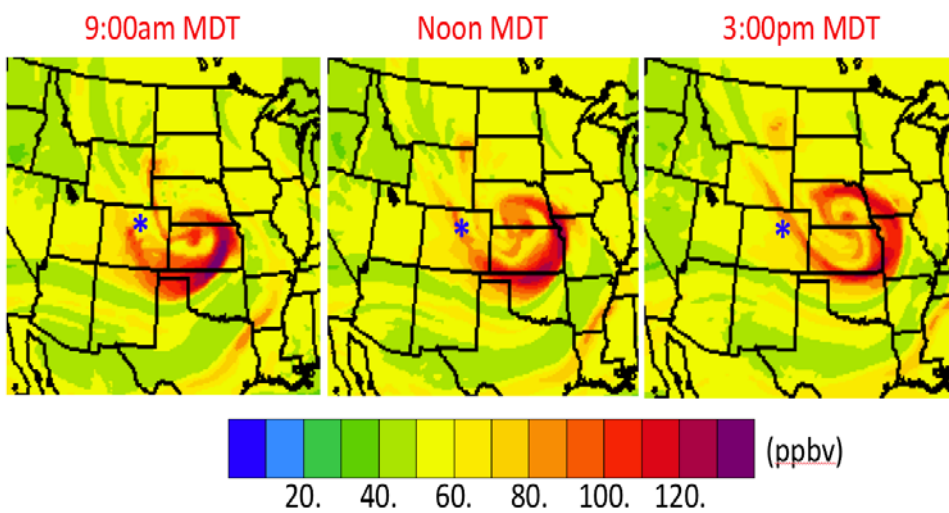


Figure 12.19. Top: Ozone from the TOPAZ lidar on 3/16/18 over Boulder, CO. Crosses denote the times and levels of the output fields displayed in the RAP/Chem forecast web page.



Bottom: 500mb ozone from the RAP/Chem model on 3/16/18 before and during the intrusion event. Blue stars denote the location of the TOPAZ ozone lidar.

12.6.3 Europe

Case c1. Application of Regional CAMS over Europe

Matthieu Plu

Meteo-France

Regional Copernicus Atmosphere Monitoring Service (CAMS), Toulouse, France

Case overview and significance: The regional air quality (RAQ) production forecasting and analysis suite (<http://www.regional.atmosphere.copernicus.eu/>) in the EU-funded Copernicus Atmosphere Monitoring Service (CAMS) is implemented by ECMWF after several years of research and development in MACC projects. The CAMS RAQ products are supplied by Météo-France by combining the outputs of seven chemistry-transport models from European countries. The products cover a large European domain at 0.1° resolution. The seven RAQ models use input: (a) from CAMS emissions for anthropogenic, biogenic and wildfire sources, and (b) the global ECMWF IFS and ECMWF global CAMS chemical composition simulations to provide meteorology and chemical lateral boundary conditions, respectively. Despite the RAQ's common input, the use of a seven-member ensemble system is useful to assess the uncertainty of the forecasts. The RAQ forecast showed considerable skill in capturing an elevated surface O3 concentration episode in 21-22 June 2017 across a large swath over the Po Valley, the Rhône valley and north-west Germany, during a stagnant high pressure system.

c1.1 Introduction

Regional CAMS data have been freely available since October 2015. Any pollution (ozone, PM, NO₂, SO₂) case over Europe since then can thus be investigated with regional CAMS data. This test case serves as an example of how regional CAMS data can be accessed and used, through <http://www.regional.atmosphere.copernicus.eu/>. The selected study case represents a high surface O₃ concentration continental-scale episode over Europe, on 21 and 22 June 2017.

During this 21-22 June 2017 pollution episode, the ozone concentration values reached and surpassed the 180 µg m⁻³ threshold (12.20). The maintenance during these two days of sunny anticyclonic conditions, with high temperatures (often above 30°C during the day) and light winds were favorable to high ozone concentration levels in several countries (Italy, Germany, France, Hungary, etc.). Photochemistry contributed to a high production of ozone. Some regions have been particularly affected, such as the Po plain, the Rhône valley and north-west Germany.

c1.2 CAMS regional data

[Table 12.4 Europe Case c1](#) summarizes the parameterization choices used in the model.

The regional air quality (RAQ) production of the Copernicus Atmosphere Monitoring Service (CAMS) is based on seven state-of-the-art numerical air quality models developed in Europe: CHIMERE from INERIS (France), EMEP from MET Norway (Norway), EURAD-IM from the University of Cologne (Germany), LOTOS-EUROS from KNMI and TNO (Netherlands), MATCH from SMHI (Sweden), MOCAGE from METEO-FRANCE (France) and SILAM from FMI (Finland). Common to all models, the meteorological parameter settings (coming from the ECMWF global weather operating system), the boundary conditions for chemical species (coming from the CAMS IFS-MOZART global production), the [emissions](#) coming from CAMS emission (for anthropic emissions over Europe and for biomass burning).

Thursday 22 June 2017 00UTC CAMS Forecast t+015 VT: Thursday 22 June 2017 15UTC
 Model: ENSEMBLE Height level: Surface Parameter: Ozone [$\mu\text{g}/\text{m}^3$]

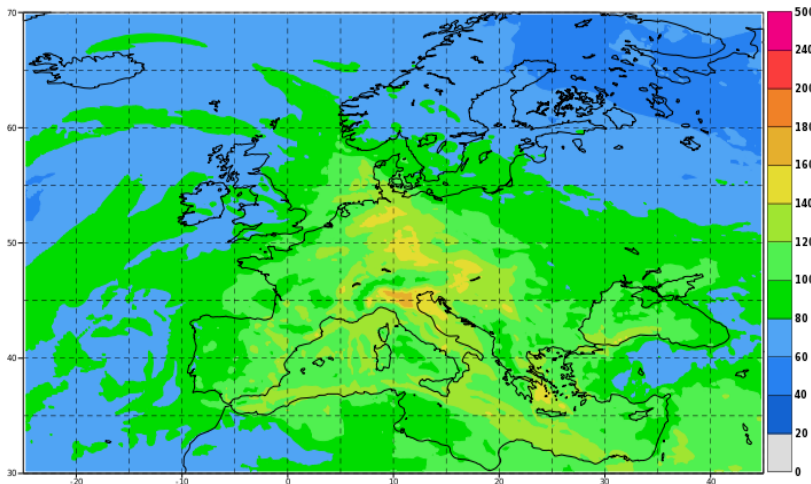


Figure 12.20. Regional CAMS ENSEMBLE forecast of ozone at surface, 22nd June 2017, when the concentrations reached the highest daily values (15h UTC).

The regional air quality models provide 4-day, daily forecasts of the main atmospheric pollutant concentrations, in the lowest layers of the atmosphere. Their horizontal coverage is approximately 10 to 20 km, allowing large-scale phenomena and background air pollution to be displayed. To get insight into your local area, please liaise with your national or local air quality agency.

Alongside forecasts, the models perform daily retrospective [analyses](#) of pollutants near the surface by assimilating, i.e., incorporating, day-old observations. For this purpose, they rely on their own data assimilation system. [Surface observations](#) are the main source of data used in the assimilation process, and also support statistical evaluations of forecasts. They are collected on a daily basis from the European Environmental Agency (EEA), and more precisely from its near-real time (NRT) service for air quality measurements over Europe.

The forecasts and analyses from all seven models are combined via an ensemble approach, consisting of calculating the median value of the individual outputs. Usually, better estimates of air pollutant concentrations are generated by resulting CAMS regional [Ensemble](#).

The models involved in regional CAMS and the ensemble methods are described there: <http://atmosphere.copernicus.eu/documentation-regional-systems>

The system was developed during the series of MACC projects, and it is described at: <https://www.geosci-model-dev.net/8/2777/2015/gmd-8-2777-2015.html>

Archive data (from October 2015) can be accessed through: <http://www.regional.atmosphere.copernicus.eu/>

From the archive it is possible to retrieve:

- daily forecasts, analyses and reanalyses at surface and up to 5 000 m altitude,
- every individual model outputs and the median ENSEMBLE at a 0.1° horizontal resolution,
- for the species: O₃, CO, NO, NO₂, SO₂, NMVOCs, PANs, PM₁₀, PM_{2.5}, NH₃.

The data can be used directly to investigate pollution cases or as boundary conditions for local-scale modeling. The multi-model ENSEMBLE may be used to assess the uncertainty of the forecasts.

Person of Contact: Matthieu Plu, email: matthieu.plu@meteo.fr

Case c2. Air quality forecasting and analysis for the United Kingdom

Ranjeet. S. Sokhi¹, Shital Rohekar¹, Vikas Singh², Aidan R. Farrow³ and Charles Chemel¹

¹ Centre for Atmospheric and Climate Physics Research (CACPR), School of Physics, Astronomy and Mathematics, University of Hertfordshire, College Lane, Hatfield, U.K.

² National Atmospheric Research Laboratory, Gadanki, Andhra Pradesh, India

³ Greenpeace Research Laboratories, College of Life and Environmental Sciences, Innovation Centre, University of Exeter, Exeter, U.K.

Case overview and significance: A two-tier nested grid was used for air quality forecasting with the parent grid covering Europe at 50 km and the child grid covering the UK at 10 km horizontal grid resolution, respectively. In an offline coupled configuration, with WRF/NCEP-GFS providing meteorology and MACC II restraining the chemical boundary conditions, CMAQ was used to simulate the chemical transport/concentration/deposition fields. Near-real time verification for the inner domain was conducted by comparison with measurements from 42 rural and urban background air quality automatic monitors. A full annual forecast was conducted between the winters of 2014 and 2015. An adverse air quality episode in the spring of 2014 was analysed to attribute the leading causes of the event. Analysis of regional air masses and local meteorology including low planetary boundary inhibition on ventilation along with composition analysis of simulated and monitored data implied that long range transport of air pollution from continental Europe was the likely cause of the event.

c2.1 Introduction

There are a number of air quality forecast (AQF) systems that have been reported in literature (e.g., see Kukkonen et al., 2012; Zhang et al., 2012). This paper reports on the use of the Community Multiscale Air quality (CMAQ) Modeling system (e.g., Byun and Schere, 2006) to understand air quality over the UK and Europe. The system has been based on previous work reported by Sokhi et al. (2006), Chemel et al. (2010), and Fisher et al. (2016).

This case briefly describes the AQF system for the UK and gives an indication of its performance by comparison with available observations for the period covering 1 December 2014 to 30 November 2015. An example of the analysis based on the forecast outputs is shown for a particulate matter (PM) episode that affected the UK during March/April 2014. This type of information is essential to understand the evolution of high air pollution events in terms of compositional and meteorological changes that can occur on an hourly timescale. In particular, this paper discusses some results that are applicable to forecasting air quality over urban areas in the UK.

c2.2 Description of the AQF System

Table 12.4 Europe Case c2 summarizes the parameterization choices used in the model.

CMAQ is a 'one atmosphere' chemistry-transport model that can simulate complex atmospheric processes that govern the transport and transformation of air pollutants including O₃, NO_x, and PM over a broad range of spatial and timescales (e.g., Chemel et al., 2010). A detailed description of CMAQ can be found on <https://www.epa.gov/air-research/community-multi-scale-air-quality-cmaq-modeling-system-air-quality-management>.

The Weather Research Forecasting (WRF) model acts as the meteorological driver for the CMAQ modeling system. A detailed description of the WRF model can be found on <http://www.wrf-model.org/index.php>. A Meteorology Chemistry Interface Processor (MCIP) is used to prepare the meteorological fields for use in the CMAQ (Otte and Pleim, 2010).

The WRF-CMAQ modeling system is run daily to produce 3-day forecasts with an outer coarser European domain (50 km x 50 km) and a one-way nested finer grid for the UK (10 km x 10 km) domain. Lateral boundary conditions are derived from the US National Centers for

Environmental Prediction (NCEP) Global Forecast System (GFS, <https://www.ncdc.noaa.gov/data-access/model-data/model-datasets/global-forcast-system-gfs>). Chemical boundary conditions for the outer European domain are derived from the Modeling Atmospheric Composition and Climate (MACC II). The overall domain is shown in Figure 12.21.

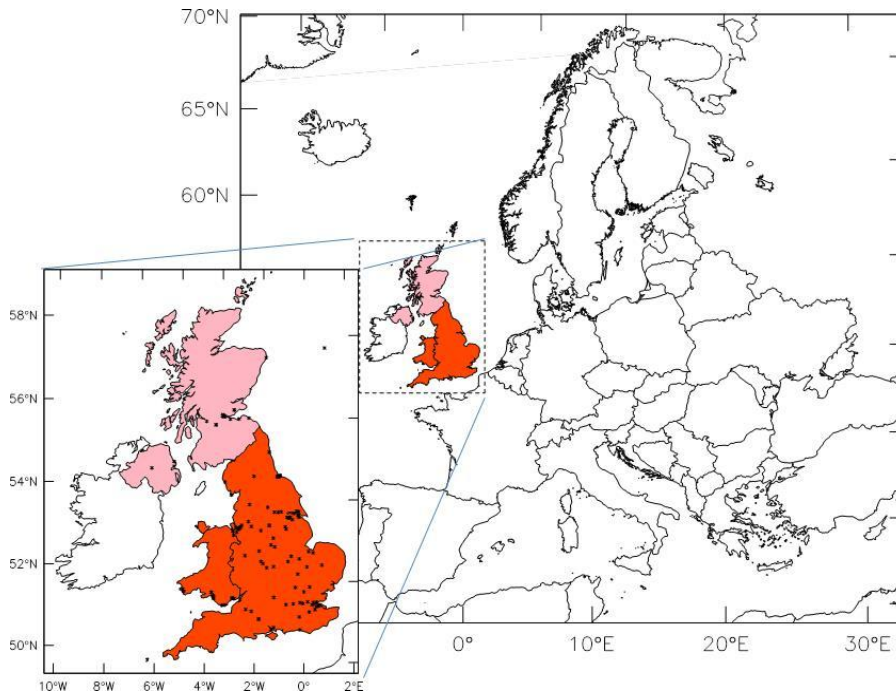


Figure 12.21. WRF-CMAQ Model Domain: Spatial coverage of the outer (coarser) European domain (50 km x 50 km) and the inner nested UK domain (10 km x 10 km).

Hourly measurements of NO, NO₂ and O₃ for 36 urban background (UB) sites were obtained from the Automatic Urban and Rural Network (https://uk-air.defra.gov.uk/data/data_selector#mid).

Observations of meteorological variables were obtained from the Met Office Integrated Data Archive System (MIDAS) (http://badc.nerc.ac.uk/search/midas_stations/).

c2.3. Results and Discussion

The annual mean diurnal profile of NO, NO₂ and O₃ from Day0, Day1 and Day2 of the forecast taken as a mean over UB station sites is shown in Figure 12.22 which shows the diurnal variation in the NO and NO₂ concentrations in both observations and the model simulations. The observed NO₂ concentration peaks reach their maxima between 0800 – 1000 hours and 1900 - 2100 hours. Analysis has indicated that the differences between observed and modeled NO₂ peak concentrations is possibly due to the emission profiles allocation during the SMOKE emission pre-processing stage. In the case of O₃, the model forecasts mimic the variations exhibited by the measurements although there is negative bias during nighttime and early day time.

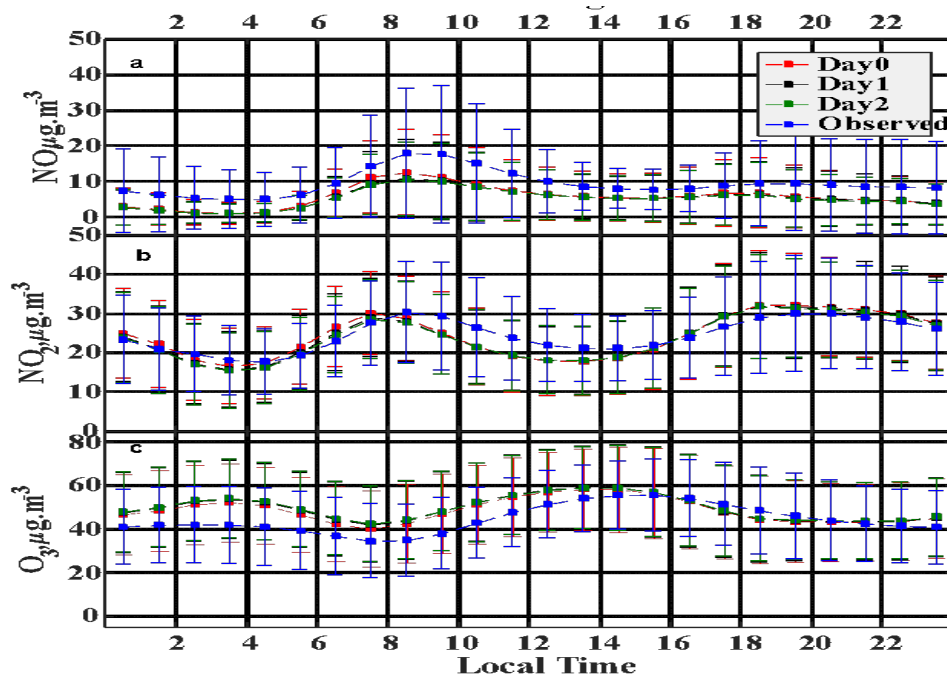


Figure 12.22. Annual mean diurnal variations of air pollutants (in $\mu\text{g m}^{-3}$) with error bars (as $\pm 1\sigma$) at UB sites.

Figure 12.23 shows the hourly trend of NO, NO₂ and O₃ for Day0 of the forecast for urban station sites. Comparison of the Day0 and observed O₃ concentrations at UB sites shows that the model replicates the hourly variations reasonably well at urban sites throughout the year although there is some over-prediction in the ozone concentrations during spring and autumn.

Daily mean variations for PM_{2.5} over 2014 is shown in Figure 12.24. The model reasonably replicates the variations although there is some underprediction in the highest peaks. Such a forecast can be used to explain the causes of high air pollution events (see Figure 12.25 below).

For this particular episode, analysis of the chemical composition showed that the first peak, centered around 13 March 2014, was due to incoming NO₃ rich PM_{2.5} most likely due to agricultural activities from continental Europe. The peak during 2 April exhibited a more mixed signal with contributions also from dust as well as NO₃. During the high air pollutant concentration days, the general planetary boundary layer height was much lower than during other periods.

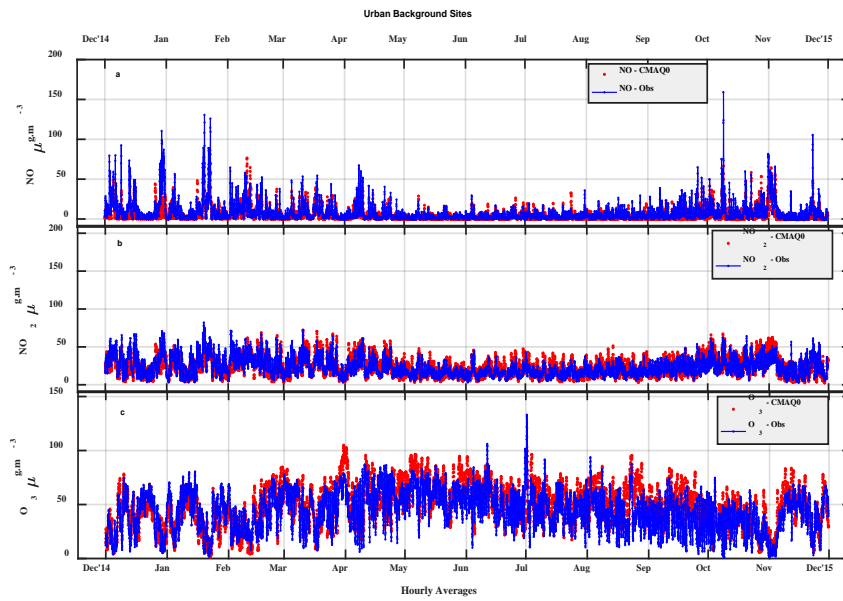


Figure 12.23. Hourly surface concentrations of a) NO b) NO₂ and c) O₃ for Day0 (red circles) and observations (blue lines) at UB sites.

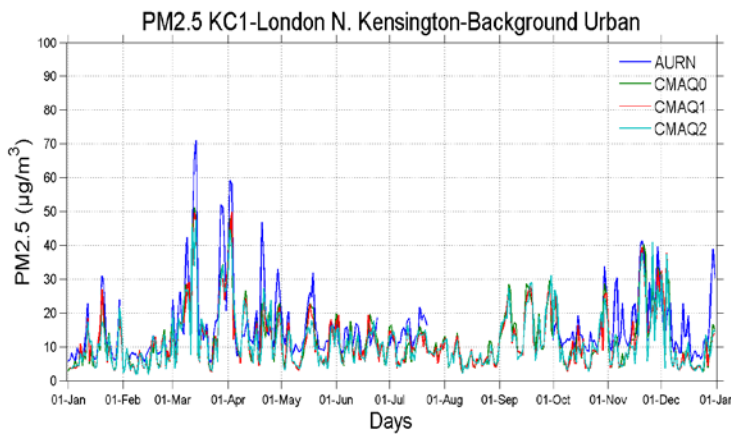


Figure 12.24. Daily variations of PM_{2.5} by WRF-CMAQ and AURN observations for the year 2014 showing the forecasts for Day0 (CMAQ0), Day1 (CMAQ1) and Day2 (CMAQ2).

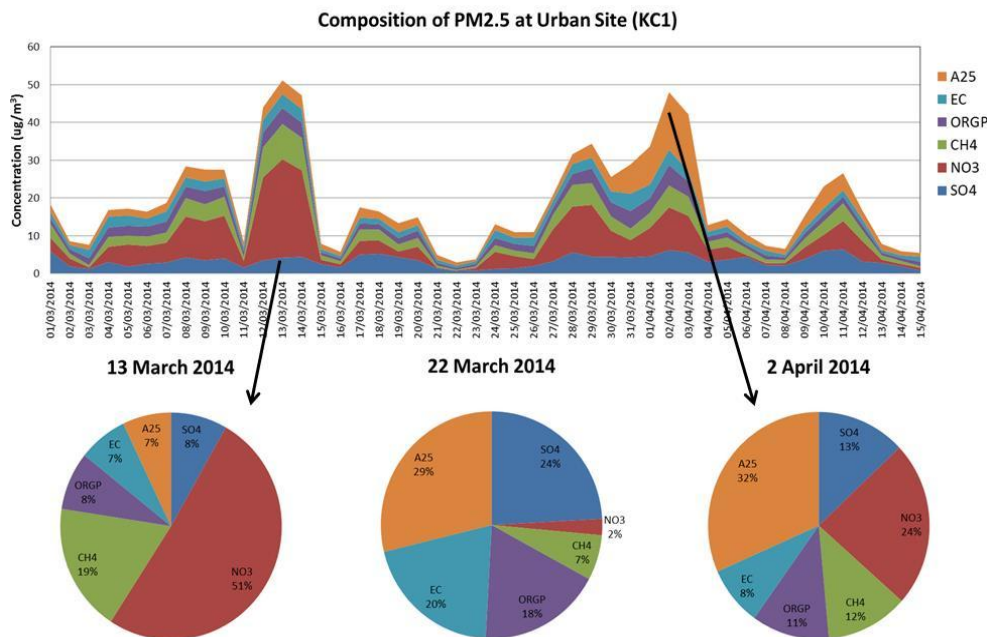


Figure 12.25. Compositional analysis of PM_{2.5} episodes during March/April 2014 over a London urban site in the UK (using output from WRF-CMAQ).

This paper has reported on the performance and application of the AQF system for the UK with an emphasis on urban areas. The period covered included 1 December 2014 to 30 November 2015 and an example of the analysis based on the forecast outputs is shown for a particulate matter (PM) episode that affected the UK during March/April 2014. The Day0 forecast for urban station sites demonstrates that the model replicates the hourly variations reasonably well. However, overprediction is seen in the forecasts for ozone concentrations during spring and autumn.

Analysis of an episode during March/April 2014, showed how the forecast is able to distinguish between an incoming NO₃ rich PM_{2.5} episode and one due to more mixed contributions from dust as well as NO₃. Meteorological analysis showed that planetary boundary layer height was much lower during the episode than during other periods.

Acknowledgement

This work has been supported by the NERC National Center for Atmospheric Science (NCAS), UK.

Person of Contact: R. S. Sokhi, email: r.s.sokhi@herts.ac.uk

References

- Byun, D., and Schere, K. L., 2006, Review of the governing equations, computational algorithms, and other components of the Models-3 Community Multiscale Air Quality (CMAQ) modeling system. *Appl. Mech. Rev.* 59(2), 51-77, doi:10.1115/1.2128636.
- Chemel, C., Sokhi, R.S., Yu, Y., Hayman, G.D., Vincent, K.J., Dore, A.J., Tang, Y. S., Prain, H.D., and Fisher, B. E. A., 2010, Evaluation of a CMAQ simulation at high resolution over the UK for the calendar year 2003, *Atmos. Environ.*, 44, 2927-2939, doi:10.1016/j.atmosenv.2010.03.029.
- Fisher, B., Chemel, C., Sokhi, R. S., Timmis, R., 2016, A risk based application of the regional model CMAQ to policy decisions, *Atmospheric Pollution Research* 7, 207-214.
- Kukkonen, J., Olsson, T., Schultz, D. M., Baklanov, A., Klein, T., Miranda, A. I., Monteiro, A., Hirtl, M., Tarvainen, V., Boy, M., Peuch, V.-H., Poupkou, A., Kioutsioukis, I., Finardi, S., Sofiev, M., Sokhi, R., Lehtinen, V.-H., Karatzas, K., San Jose, R., Astitha, M., Kallos, G., Schaap, M., Reimer, E., Jakobs, H., and Eben K., 2012, A review of operational, regional-scale, chemical weather forecasting models in Europe, *Atmos. Chem. Phys.*, 12, 1–87.
- Otte, T. L., and Pleim, J. E., 2010, The Meteorology-Chemistry Interface Processor (MCIP) for the CMAQ modeling system: updates through MCIP v3.4.1, *Geosci. Model Dev.*, 3, 243–256, doi: 10.5194/gmd-3-243-2010.
- Sokhi, R. S., San Jose, R., Kitwiroon, N., Fragkou, E., Perez, J. L., and Middleton, D.R., 2006, Prediction of ozone levels in London using the MM5-CMAQ modeling system, *Environ. Model. Softw.*, 21, 566-576, doi:10.1016/j.envsoft.2004.07.016.
- Zhang, Y., Bocquet, M., Mallet, V., Seigneur, C., and Baklanov, A., 2012, Real-time air quality forecasting, part I: History, techniques, and current status, *Atmos. Environ.*, 60, 632-655, doi: 10.1016/j.atmosenv.2012.02.041.

Cases c3.1-3.2. Multi-scale modeling down to street level

Youngseob Kim and Karine Sartelet

CEREA, Joint laboratory Ecole des Ponts ParisTech - EDF R&D, Champs-sur-Marne, France

Case overview and significance: The urban scale Street-in-Grid (SinG) model based on a coupled Polair3D/Polyphemus and the street-network model, MUNICH – with both the street canyon and street-intersection components have been applied to a multiple scale air quality simulation. The WRF model provided the meteorology for all the telescopic nested domains: 4 domains in all, starting from the outermost parent in regional scale for continental Europe at $0.5^\circ \times 0.5^\circ$ to the innermost $0.01^\circ \times 0.01^\circ$ resolution over an eastern Paris suburb: Le Perreux sur Marne. Expertise in meteorological and chemical variable communication between the multiple generation parent-child domains have been developed and demonstrated in this study. Dynamic hourly traffic emissions were pioneered in the innermost domain simulation where hundreds of streets and intersections have been simulated explicitly. Care not to double count emissions was vigorously applied in the 2-way feedback between the innermost domain and the streets. Recommendation to further test the system for aerosol species down to street level has been suggested. This study demonstrated that a street level air quality simulation as such has the potential to revolutionize air quality forecasting to street-level-resolution personalized health behavioral management regarding gaseous and aerosol pollutants.

This case study represents a multi-scale simulation from the European regional scale to an urban street scale using the Street-in-Grid (SinG) model. It combines a chemistry-transport model (CTM) that includes a comprehensive treatment of atmospheric chemistry and transport at spatial scales down to 1 km and a street-network model that describes the atmospheric concentrations of pollutants in an urban street network (Kim et al., 2018). SinG is conceived to conduct a multi-scale simulation, which estimates both grid-averaged concentrations at the urban scale and concentrations within each street segment. This combined model provides the following advantages:

- It allows one to estimate the influence of the background concentrations on the concentrations within the street network and vice-versa.
- There is no double counting of emissions, originating within the urban canopy: these emissions are removed from the grid-averaged emission inventory of CTM.
- There is consistency between the treatment of physical and chemical processes at different scales. Transport and dispersion of pollutants at the urban and street-network scales are calculated from the same meteorological data. Similarly, the same chemical kinetic mechanism is used at those different scales.

c3.1 Brief Description of the Model

Table 12.4 Europe Case c3 summarizes the parameterization choices used in the model.

The Street-in-Grid (SinG) model is composed of the CTM Polair3D of the Polyphemus air quality modeling platform (Mallet et al., 2007, <http://cerea.enpc.fr/polyphemus/>) and of the street-network model, MUNICH (Model of Urban Network of Intersecting Canyons and Highways). Figure 12.26 presents the schematic diagram for SinG model.

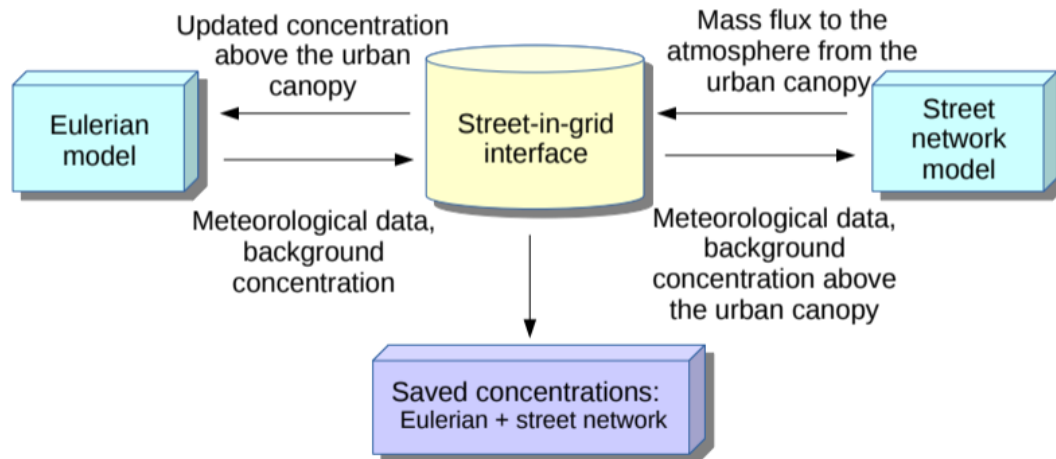


Figure 12.26. Schematic diagram of the Street-in-Grid model.

Polair3D/Polyphemus has been widely applied over Europe, North America, South America, Asia, and Africa (e.g., Sartelet et al., 2012). For the test case presented here, the following modules are used for atmospheric chemistry: the gaseous chemical scheme CB05 modified to represent the formation of secondary organic aerosols (Kim et al., 2011; Chrit et al., 2017), the scheme VSRM (Fahey and Pandis, 2003) for aqueous chemistry and the Size-Composition Resolved Aerosol Model (SCRAM) for aerosol dynamics (Zhu et al., 2015).

The street-network model, MUNICH (Model of Urban Network of Intersecting Canyons and Highways), is based conceptually on the SIRANE general formulation (Soulhac et al., 2011). MUNICH consists of two main components: the street-canyon component, which represents the atmospheric processes in the volume of the urban canopy, and the street-intersection component, which represents the processes in the volume of the intersection. These components are connected to the Polair3D model at roof level and are also interconnected.

c3.2 Regional-Scale (Polair3D) Set-Up and Input Data

Four simulation domains are used from the continental scale to the urban scale (see Figure 12.27). Domain 1 covers Western Europe with a horizontal resolution of $0.5^\circ \times 0.5^\circ$. Domains 2 and 3 cover northern/central France ($0.15^\circ \times 0.15^\circ$ resolution) and the Île-de-France region ($0.04^\circ \times 0.04^\circ$ resolution), respectively. The urban-scale domain 4 covers the eastern Paris suburbs ($0.01^\circ \times 0.01^\circ$ resolution) including the area where the street network is located. The street network neighborhood is covered by 12 grid cells of domain 4. The vertical resolution consists of 10 levels up to 6 km with the lowest level at 15 m.

For each simulation domain, ground data are generated using a pre-processing program with the Global Land Cover Facility (GLCF) data as input data. Meteorological data are obtained from WRF simulations for all domains. The urban canopy model (UCM) is used for the domains 3 and 4. WRF results need to be interpolated from WRF grid to a regular grid (latitude/longitude in the horizontal and altitudes in meters in the vertical). WRF results are interpolated in time and space using a pre-processing program.

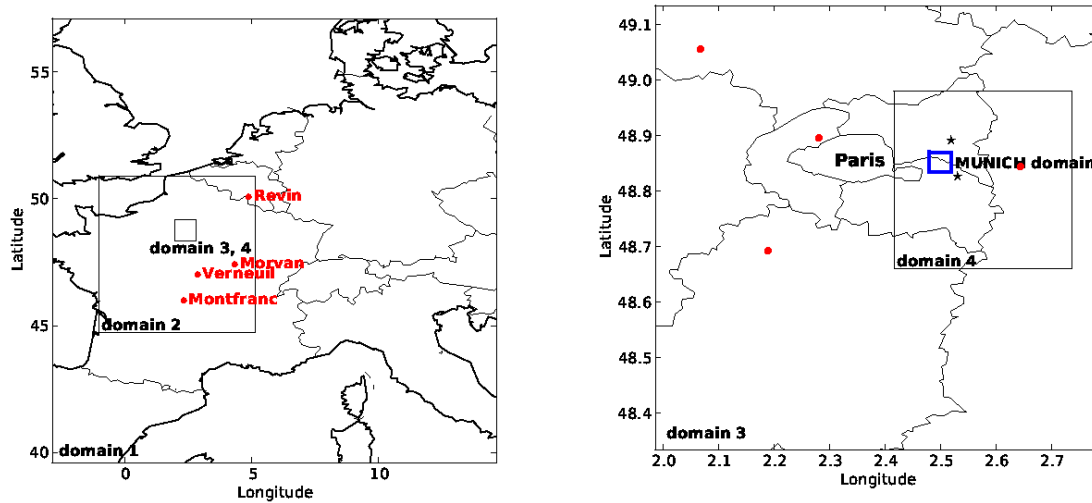


Figure 12.27. Modeling domains for the Polair3D, MUNICH and Street-in-Grid simulations. In the right panel, the blue box corresponds to the modeling area in suburban Paris for the MUNICH simulation. SinG is only used for domain 4.

Photolysis rates are computed using the photolysis scheme FAST-J (Wild et al., 2000). In this case, they are computed offline, and they are multiplied by an attenuation coefficient that parameterizes the impact of clouds on photolysis rates. Dry-deposition velocities, below cloud and in-cloud scavenging are generated on the basis of meteorological data and ground data, following the parameterizations described in Sartelet et al. (2007). Boundary conditions for the outer domain 1 and initial conditions for all domains are obtained from data simulated by the MOZART 4 global CTM (Emmons et al., 2010). The data can be downloaded from <https://www.acom.ucar.edu/wrf-chem/mozart.shtml> for a domain, which covers our domain 1. Then downloaded data are interpolated for domain 1 using a pre-processing program. For the other sub-domains (domains 2, 3 and 4), boundary conditions are obtained from the simulation on the larger domain.

Anthropogenic emissions are calculated using the EMEP inventory (EMEP/CEIP 2014 present state of emissions as used in EMEP models). First, you must download the data from <http://www.ceip.at>. Download emissions for CO, PM, NH₃, NMVOC, NO_x, SO_x for all countries, the year 2014 and all activity sectors (SNAP). EMEP emissions are provided as annual values. A typical time distribution of emissions, given for each month, day and hour is then applied to each emission sector or SNAP (Selected Nomenclature for Air Pollution) category. The inventory species are disaggregated into real species using speciation coefficients, which are thereafter aggregated into the model species. Primary particle emissions are also chemically speciated and size segregated by SNAP category or emission source. Biogenic emissions with the EFv2.1 dataset are calculated with MEGAN for domains 1 to 4 (Guenther et al., 2006).

c3.3 Street-Scale (MUNICH) Set-Up and Input Data

Geographic data are required to estimate pollutant transport in the street network. The necessary data are: street intersection coordinates in latitude/longitude, street width for each street, average building height for each street. Total street width includes the traffic lane width and the sidewalk width. Traffic lane widths and building heights are obtained from the BD TOPO database (<http://professionnels.ign.fr/bdtopo>).

The traffic emissions for the simulation domain are estimated using the dynamic traffic model, Symuvia (Leclercq et al., 2007) with the COPERT 4 emission factors (<http://emisias.com/products/copert-4/versions>), as part of the TrafiPollu project (<http://www.agence-nationale-recherche.fr/?Project=ANR-12-VBDU-0002>). The emission rates depend on the vehicle speed and composition of the fleet. Two typical days (25 March for a weekday and 30 March for a weekend) were chosen for the traffic simulation. The dynamic traffic model estimates the emission rates for each traffic direction of a two-way street. The traffic emissions of a two-way street are merged to obtain one emission rate for the street segment. Surface areas of intersections are not taken explicitly into account in MUNICH and streets are connected at the center of the intersection, i.e., an intersection is represented by a point using a latitude/longitude coordinate set. In this case, the traffic emissions are prepared for 577 street segments. Hourly traffic emissions are required for NO, NO₂ and VOC. If you do not have the traffic emissions, you can use a program to generate emissions (<https://github.com/pollemmission>) using COPERT4. In this case, you need the total vehicle number and the average speed for each street (in an hour). Optionally, if the information of the fleet in circulation is available (gas vs diesel, light-duty vs heavy-duty, etc.) more accurate input data can be obtained.

Meteorological data, including wind direction/speed, planetary boundary layer (PBL) height, and friction velocity, are obtained from WRF simulation conducted with a horizontal resolution of 1.5×1.5 km². The simulated meteorological data are compared to the measurements at urban background meteorological stations near the simulation domain 4 and showed satisfactory results (Thouron et al., 2017).

c3.4 Street-in-Grid Simulation

A SinG simulation is performed for domain 4. The same input data, prepared for MUNICH stand-alone simulation, are used for MUNICH except the boundary conditions over roof tops, which are obtained from the lowest layer of Polair3D. The input data for the Polair3D simulation are reused except the emission data. In order to avoid double counting of traffic emissions, the traffic emissions are removed from the grid-averaged emission inventory of Polair3D. In the simulation chain from the regional scale to the urban scale, one-way nesting simulations for domains 1 to 3 are conducted for the boundary conditions of Polair3D domain 4 simulation and SinG simulation. Output data of the SinG simulation consist of grid-averaged concentrations by Polair3D and street-level concentrations by MUNICH. The comparison of grid-averaged concentrations of Polair3D stand-alone simulation results and street-level concentrations of MUNICH stand-alone simulation results shows that multi-scale modeling with a tool as SinG is required to better model concentration in urban streets.

c3.5 Discussion

SinG is used to simulate the concentrations of nitrogen oxides (NO_x) and ozone (O₃) in a Paris suburb (Le Perreux sur Marne). Simulated concentrations are compared to NO_x concentrations measured at two monitoring stations within a street canyon. SinG shows better performance than Polair3D and MUNICH for nitrogen dioxide (NO₂) concentrations (Figure 12.28). However, both SinG and MUNICH underestimate NO_x. The extensions of MUNICH and SinG to aerosol modeling using the same models as in Polair3D are ongoing.

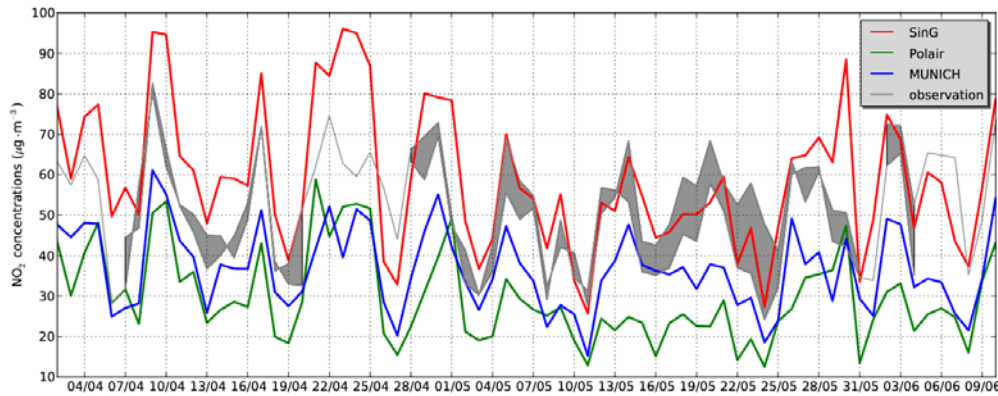


Figure 12.28. Temporal evolution of NO₂ daily-averaged concentrations modeled with MUNICH (blue line), Polair3D (green line), and the SinG model (red line). They are compared to the measured concentrations (gray shaded regions) at the stations nearby traffic on each sidewalk of the Boulevard Alsace-Lorraine. If the measurement is available at only one station, a black line is used instead.

Source code and configuration files: The source code including configuration files is available at <http://doi.org/10.5281/zenodo.1025629> and can be freely downloaded.

Person of Contact: Karine Sartelet, email: karine.sartelet@enpc.fr

References

- Chrit, M. and Sartelet, K. and Sciare, J. and Pey, J. and Marchand, N. and Couvidat, F. and Sellegri, K. and Beekmann, M. Modeling organic aerosol concentrations and properties during ChArMEx summer campaigns of 2012 and 2013 in the western Mediterranean region *Atmos. Chem. Phys.*, 17, 12509-12531, doi:10.5194/acp-2017-312, 2017.
- Emmons, L. K., Walters, S., Hess, P. G., Lamarque, J.-F., Pfister, G. G., Fillmore, D., Granier, C., Guenther, A., Kinnison, D., Laepple, T., Orlando, J., Tie, X., Tyndall, G., Wiedinmyer, C., Baughcum, S. L., and Kloster, S.: Description and evaluation of the Model for Ozone and Related chemical Tracers, version 4 (MOZART-4), *Geosci. Model Dev.*, 3, 43-67, <https://doi.org/10.5194/gmd-3-43-2010>, 2010.
- Fahey, K. and Pandis, S. Size-resolved aqueous-phase chemistry in a three-dimensional chemical transport model. *J. Geophys. Res.*, 108:4690, 2003.
- Guenther, A., Karl, T., Harley, P., Wiedinmyer, C., Palmer, P. I., and Geron, C.: Estimates of global terrestrial isoprene emissions using MEGAN (Model of Emissions of Gases and Aerosols from Nature), *Atmos. Chem. Phys.*, 6, 3181-3210, <https://doi.org/10.5194/acp-6-3181-2006>, 2006.
- Kim Y., Couvidat F., Sartelet K. and Seigneur C. Comparison of different gas-phase mechanisms and aerosol modules for simulating particulate matter formation. *J. Air Waste Manage. Assoc.*, 61, 1218-1226, doi:10.1080/10473289.2011.603999, 2011.
- Kim, Y., Wu, Y., Seigneur, C., and Roustan, Y.: Multi-scale modeling of urban air pollution: development and application of a Street-in-Grid model (v1.0) by coupling MUNICH (v1.0) and Polair3D (v1.8.1), *Geosci. Model Dev.*, 11, 611-629, <https://doi.org/10.5194/gmd-11-611-2018>, 2018.
- Leclercq L., Laval J., Chevallier E.: The Lagrangian coordinates and what it means for first order traffic flow models. In: Allsop RE, Bell MGH, Heydecker BG (eds) *Transportation and traffic theory 2007*. Elsevier, Oxford, pp 735–753, 2007
- Mallet, V., D. Quélo, B. Sportisse, M. Ahmed de Biasi, É. Debry, I. Korsakissok, L. Wu, Y. Roustan, K. Sartelet, M. Tombette and H. Foudhil: Technical Note: The air quality modeling system Polyphemus, *Atmos. Chem. Phys.*, 7 (20), 2007.
- Sartelet K., Debry E., Fahey K., Roustan Y., Tombette M., Sportisse B. Simulation of aerosols and gas-phase species over Europe with the Polyphemus system. Part I: model-to-data comparison for 2001. *Atmospheric Environment*, 41 (29), p6116-6131, doi:10.1016/j.atmosenv.2007.04.024, 2007.
- Sartelet, K. N., Couvidat, F., Seigneur, C., and Roustan, Y.: Impact of biogenic emissions on air quality over Europe and North America, *Atmos. Environ.*, 53, 131 – 141, doi:10.1016/j.atmosenv.2011.10.046, 2012.
- Soulhac, L., Salizzoni, P., Cierco, F.-X., and Perkins, R.: The model SIRANE for atmospheric urban pollutant dispersion; part I, presentation of the model, *Atmos. Environ.*, 45, 7379 – 7395, doi:10.1016/j.atmosenv.2011.07.008, 2011.
- Thouron, L., C. Seigneur, Y. Kim, C. Legorgeu, Y. Roustan, B. Bruge: Simulation of trace metals and PAH atmospheric pollution over Greater Paris: Concentrations and deposition on urban surfaces, *Atmos. Environ.*, 167, 360-376, 2017.
- Wild, O., Zhu, X. et Prather, M. Fast-j: Accurate simulation of in- and below-cloud photolysis in tropospheric chemical models. *J. Atmos. Chem.*, 37(3):245–282, 2000.
- Zhu S., Sartelet K., Seigneur C. A size-composition resolved aerosol model for simulating the dynamics of externally mixed particles: SCRAM (v 1.0) *Geosci. Model Dev.*, 8, 1595-1612, 2015

12.6.4 Asia

Case d1. Application of CUACE/Haze-fog over China

Chunhong Zhou

Key Laboratory for Atmospheric Chemistry (LAC), Institute of Atmospheric Composition

Chinese Academy of Meteorological Sciences (CAMS)

China Meteorological Administration (CMA)

Beijing, P.R. China

Case overview and significance: The persistency and frequency of urban haze impaired air quality conditions in Eastern China received public attention. Partly in response to such concerns CMA has developed the CUACE/Haze-fog system to facilitate Chemical Transport Model (CTMs) calculations of pollutants and a 2-way communication between GRACES -- the CMA meteorological simulation system and the CTM. CUACE/Haze-fog was based on the operational WMO-SDS-WAS CUACE/Dust with expanded capability to simulate sea salts, sand/dust, BC, OC, sulfates, nitrates and ammonium salts. CUACE included major organic and inorganic aerosol growth and activation processes capable of communicating direct, semi-direct and indirect effects on meteorology. The anthropogenic emission was derived by performing SMOKE simulations using CMA's EMIS inventories. The CUACE/Haze-fog system has been in the CMA's operations suite since 2012 and consistently demonstrated good forecast fidelity in capturing haze and fog. The captured January 2013 heavy haze and fog event over the North China Plain, the Yangtze River Delta, and the Pearl River Delta seemed to attribute air mass stagnation (PLAM in excess of 80) as a major factor in the prolonged haze episode.

d1.1 Introduction

The selected heavy haze-fog case was the long-lasting scenario in January 2013 that covers most parts of east China.

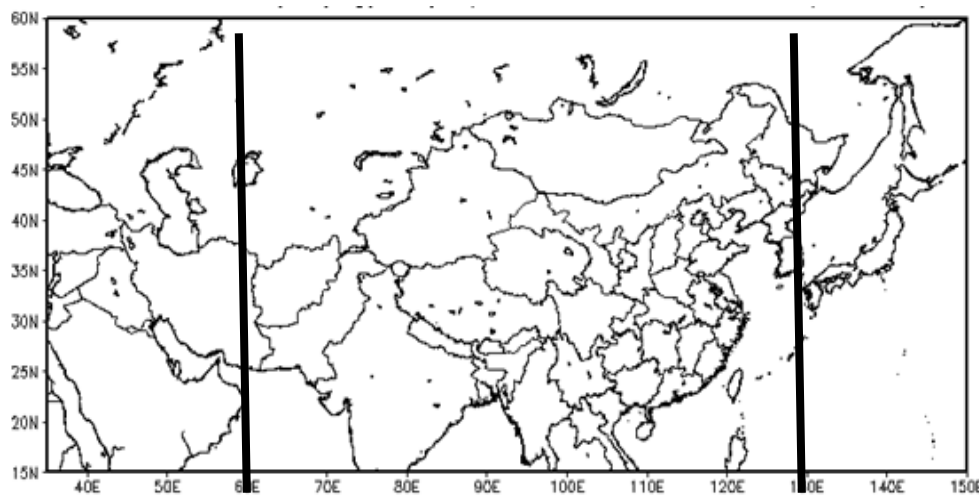


Figure 12.29. The domain map of CUACE/Haze-fog (15-60N, 35-150E), the targeting area is (15-60N, 70-140E).

d1.2 General Description of the Model

[Table 12.5 Asia Case d1](#) summarizes the parameterization choices used in the model.

CUACE is a CMA unified chemistry environment and has been designed as a unified chemical module, which can be easily coupled onto any atmospheric models at various temporal and spatial scales (Zhou et al., 2008, 2012, 2016, and 2018). It compasses a chemistry interface for tracers of aerosols and gases. The chemistry interface is to pass the atmospheric backgrounds like wind, temperature, and humidity together with model configurations into the chemistry module to calculate the chemical physics processes for the tracers. The chemical fields can also be fed back into the host model for post analysis through the interface. The chemistry module for aerosols in CUACE is a size-segregated multi-component one for all types of aerosols such as dust, sea salt, BC/OC, sulfate, nitrate and ammonium (Gong et al., 2003). It includes major aerosol processes in the atmosphere such as the generation, hygroscopic growth, coagulation, nucleation, condensation, dry depositions, scavenging and aerosol activations.

The CUACE/Dust system was developed based on a size-segregated dust aerosol module CAM (Canadian Aerosol Module) (Gong et al., 2003) that was coupled into a mesoscale meteorological model - MM5 to conduct real time SDS forecasting in Northeast Asia. A positive definite 3-D advection scheme called MPDATA has also been introduced and an anti-gradient diffusion scheme has been developed for dust advection and diffusion processes in the system, respectively. CUACE/Dust has been put into operation since 2007 and is the main operational dust storm forecasting model for WMO-SDS-WAS.

CUACE/Haze-fog is based on the model frame of CUACE/Dust and incorporating the Emission Subsystem (EMIS) provides through SMOKE (The Sparse Matrix Operator Kernel Emissions) module the hourly gridded offline emission intensity for 32 species including black carbon (BC), organic carbon (OC), sulfate, nitrate, fugitive dust particles and 19 volatile organic compounds (VOC), NH₃, CO, CO₂, SO_x and NO_x over the model domain. The gas chemistry module is based on the second generation of Regional Acid Deposition Model (RADM2) mechanism with 63 gaseous species through 21 photochemical reactions and 121 gas phase reactions applicable under a wide variety of environmental conditions especially for smog (Stockwell, Middleton et al. 1990). There are seven categories of aerosol species, i.e., sea salt, sand/dust, BC, OC, sulfates, nitrates and ammonium salts in the aerosol module. CUACE/Haze-fog has been in operation since 2012 and issues the PM_{2.5} and visibility products since then.

CUACE has also been fully coupled onto a China new generation NWP forecasting system GRAPES (a Global and Regional Assimilation and PrEdiction System) and China regional climate model BCC_AGCM2.0.1. The mechanism of aerosol direct and indirect impacts on weather have also been established.

d1.3 Results and Discussion

d1.3.1 Case Description

A series of long-lasting heavy haze-fog events hit the east part of China in January 2013. Climatology analysis shows that the mean number of hazy days in this period is much higher than the mean value from 1981 to 2010, especially in the three major pollution zones of the North China Plain, the Delta of the Yangtze River and the Zhu River (Zhang et al., 2013). Meanwhile, the values of the stagnant polluted parameter PLAM, a threshold value to distinguish clear and polluted weather, are over 80 in most parts of east China, which indicates strong stagnant weather conditions for pollutant accumulation (Wang et al., 2012; Zhang et al., 2013). Surface daily mean PM_{2.5} concentrations are in the range of 100-150 $\mu\text{g m}^{-3}$ and AOD is above 1.0 in many surface stations (Che et al., 2014; Wang et al., 2014).

d1.3.2 CUACE/Haze-fog's Performance

CUACE/Haze-fog successfully forecasted the development of the long lasting case and kept stable fine results routinely. The following were the real-time outputs for different forecast

lengths (24 hours, 48 hours and 72 hours) for 2013011200 UTC. It showed consistent results for different forecast lengths, showing a stable forecast ability of the modeling system.

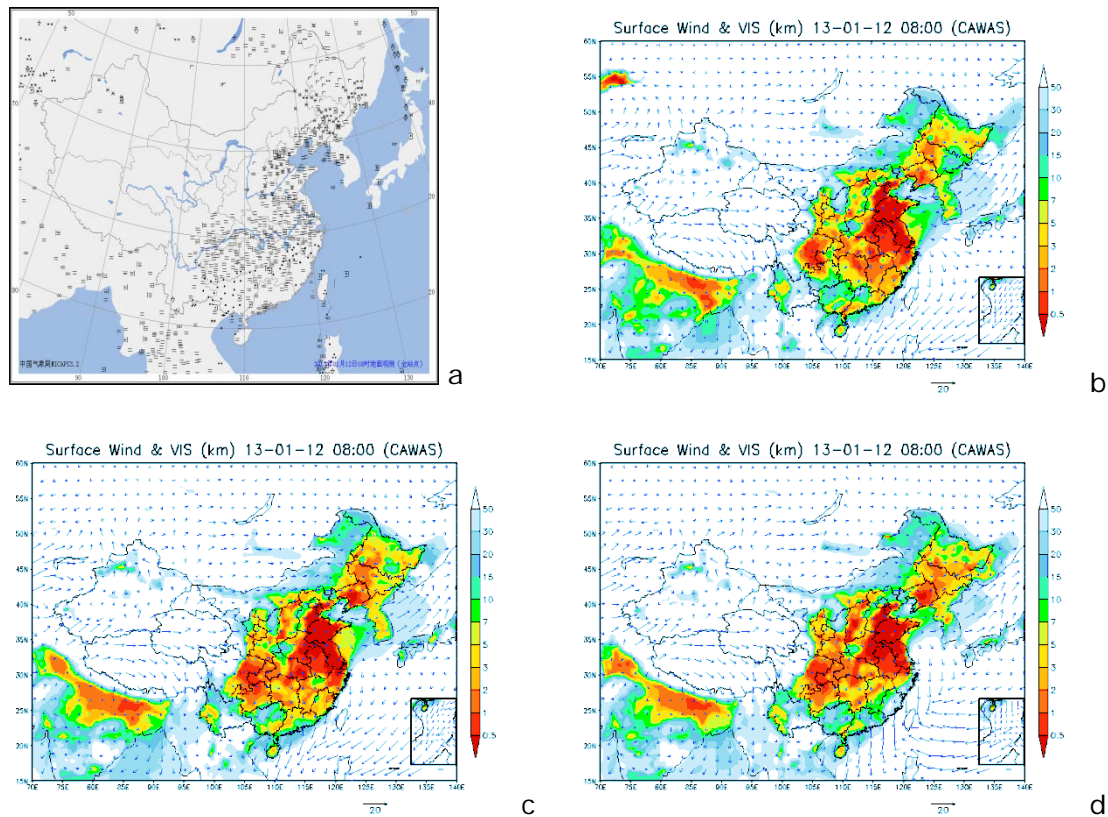


Figure 12.30. visibility from CUACE/Haze-fog for forecast length of (b) 24 hours, (c) 48 hours, and (d) 72 hours. (a) shows the haze observation meteorological stations in CMA.

Person of Contact: Chunhong Zhou, email: zhouch@cma.gov.cn

References

- Che, H., X. Xia, et al. (2014). "Column aerosol optical properties and aerosol radiative forcing during a serious haze-fog month over North China Plain in 2013 based on ground-based sun photometer measurements." *Atmos. Chem. Phys.* 14: 3125-2138.
- Gong, S. L., L. A. Barrie, et al. (2003). "Canadian Aerosol Module: A size-segregated simulation of atmospheric aerosol processes for climate and air quality models 1. Module development." *J. Geophys. Res.* 108(D1): 4007, doi:4010.1029/2001JD002002.
- Stockwell, W. R., P. Middleton, et al. (1990). "The second generation Regional Acid Deposition Model Chemical Mechanism for Regional Air Quality Modeling." *J. Geophys. Res.* 95: 16343~16376.
- Wang, H., X. Y. Zhang, S. L. Gong, et al., 2010: Radiative feedback of dust aerosols on the East Asian dust storms. *J. Geophys. Res.*, 115, D23214, doi: 10.1029/2009JD013430
- Wang, J. Z., S. L. Gong, et al. (2012). "A Parameterized Method for Air-Quality Diagnosis and Its Applications." *Advances in Meteorology* 2012: 1-10.
- Wang, Y., L. Yao, et al. (2014). "Mechanism for the formation of the January 2013 heavy haze pollution episode over central and eastern China." *Sci China Earth Sci* 57: 14-25.
- Zhang, R. H., Q. Li, et al. (2013). "Meteorological conditions for the persistent severe fog

and haze event over eastern China in January 2013." *Science China: Earth Sciences* 57: 26-35.

Zhang, X. Y., J. Y. Sun, et al. (2013). "Factors contributing to haze and fog in China (in Chinese)." *Chin Sci Bull (Chin Ver)* 58: 1178-1187.

Zhou, C. H., X. J. Shen, Z. R. Liu., et al., 2018: Simulating aerosol size distribution and mass concentration with simultaneous nucleation, condensation/coagulation, and deposition with the GRAPES–CUACE. *J. Meteor. Res.*, 32(2), 1–14, doi: 10.1007/s13351-018-7116-8.

Zhou, C., X. Zhang, et al. (2016). "Improving aerosol interaction with clouds and precipitation in a regional chemical weather modeling system." *Atmospheric Chemistry and Physics* 16(1): 145-160.

Zhou, C.-H., Gong, S., Zhang, X.-Y., Liu, H. L., Xue, M., Cao, G. L., An, X. Q., Che, H. Z., Zhang, Y. M., and Niu, T.: Towards the improvements of simulating the chemical and optical properties of Chinese aerosols using an online coupled model CUACE/Aero, *Tellus B*, 64, 18965, <http://dx.doi.org/10.3402/tellusb.v64i0.18965>, 2012.

Zhou, C. H., Gong, S. L., Zhang, X. Y., Wang, Y. Q., Niu, T., Liu, H. L., Zhao, T. L., Yang, Y. Q., and Hou, Q.: Development and Evaluation of an Operational SDS Forecasting System for East Asia: CUACE/Dust *Atmos. Chem. Phys*, 8, 1-12, 2008.

Case d2. Application of HAQFS over China

Shaocai Yu

Zhejiang University, Hangzhou, Zhejiang, China

Case overview and significance: The operational deployment of the HAQFS has been effective in assisting the local government agencies to safeguard the public health of the residents of Hangzhou and vicinity. The HAQFS is an offline coupling between the WRF and CMAQ models providing daily air quality forecasts 72 hours into the future over most of China and Eastern Asia. The HAQFS was also effective in ensuring the air quality in Hangzhou during the G-20 summit on 4-5 September 2016. This study focused on HAQFS' performance across the temporal span around the G-20 summit: (prior) 4 August – 3 September; (during) 4-5 September; and (after) 6-15 September. Subtracting the reality projected emission in compliance with the stringent emission control prior and during the G-20 from a baseline HAQFS simulation with "business-as-usual", significant surface pollutant concentration difference was determined. A reduction of 25% in surface ozone and 56% in PM_{2.5} during the G-20 summit were derived by comparing these two simulations by the HAQFS. Although the brute force emission control was enforced in Hangzhou and its vicinity, its air chemistry impact was noticeable in Shanghai and localities hundreds of kilometers downwind of Hangzhou indicative of the regional footprints of emission control.

d2.1 Introduction

The selected study case represents a high reduction of ozone and particulate matter during the 2016 G-20 summit in Hangzhou by forced emission controls of industry and traffic.

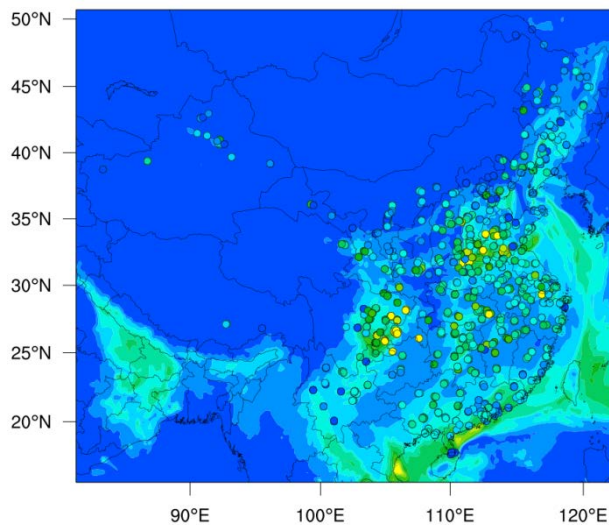


Figure 12.31. Domain map, a single domain, it covers most of China and parts of East Asia. The dots in the figure represent the monitoring sites.

The establishment of the Hangzhou Air Quality Forecasting System (HAQFS) was mandated by the Environmental Protection Agency of Hangzhou to safeguard public health and ensure the air quality of Hangzhou during the 2016 G-20. The HAQFS started to provide a nationwide air pollutants (O₃, CO, NO₂, SO₂, PM_{2.5}, PM₁₀) with 72-h lead-time. The selected case study represents a simulation results by HAQFS of high reduction of ozone and particular matter during the 2016 G-20 summit in Hangzhou by forced emission controls of industry and traffic.

In this case study, the HAQFS result was evaluated by comparing the simulation results with observation data, the observation data was obtained on 'China Air Quality Online Monitoring and Analysis Platform' (<https://www.aqistudy.cn/>). The evaluation results showed the HAQFS is accurate enough to do the research. And we selected three different periods according to different emission reduction.

d2.2 General Description of the Model

Table 12.5 Asia Case d2 summarizes the parameterization choices used in the model.

HAQFS is comprised of the simulation of the fate of air pollutants using the U.S. Environmental Protection Agency (EPA) Community Air Quality Multi-scale Model (CMAQ) driven by the modeled meteorological fields given hourly by the Weather Research and Forecasting Model (WRF). Ideally, air quality and composition modeling is an integral part of meteorology or numerical weather prediction (NWP) modeling. Otherwise, geometric re-mapping and interpolation of grid structures between the models can be cumbersome. Both CMAQ and WRF are at 12 km horizontal grid spacing. Both WRF and CMAQ should afford fine vertical grid spacing at heights near the surface, shallow convective layers just above the planetary boundary layer (PBL), and the tropopause to capture directional exchanges, PBL venting and tropo-stratospheric O₃ entrainment. CMAQ is much CPU demanding than that of WRF. In order to meet the forecast-issuance time requirements, the vertical structure for CMAQ is coarsened from that in WRF. The lowest five model layers below 1.5 km are identical between the two models assuring the near surface phenomena are best captured but are coarsened for the CMAQ grid at higher altitudes.

d2.2.1 Meteorology Model

WRF is a widely used meteorological model. The meteorological fields predicted by WRF is routinely used and knowledgeably familiarized by air quality forecasters. WRF's surface temperature, cloud fraction and precipitation distributions are fundamental input to CMAQ. WRF is benefited by 3-D and 4-D assimilation systems and can be computed simultaneously by supercomputers, which greatly accelerates the computational wall-clock capability. The WRF uses the RRTMG radiation scheme for both long and short waves (Iacono et al., 2008). The AER broadband models can calculate longwave forcing within a range of 0.08 to 0.23 W m⁻² of LBL calculations and shortwave forcing within a range of 0.16 to 0.38 W m⁻² of LBL results. The PBL scheme used in the WRF model is ACM2, it is able to represent both the supergrid- and subgrid-scale components of turbulent transport in the convective boundary layer (Pleim, 2007). The land surface scheme used in the WRF model is Pleim-Xiu, it includes explicit soil moisture, which is based on the Interactions between Soil, Biosphere, and Atmosphere (ISBA) model, and three pathways for evaporation: soil evaporation, evaporation from the wet canopy, and vegetative transpiration (Xiu and Pleim, 2001).

d2.2.2 Chemical transport Model (CTM)

Solar radiation and cloudiness constrain actinic flux for the photolytic production of photochemical pollutants. Cloud fraction from WRF modulates downward short-wave solar flux contributing to photolytic reaction rates in CMAQ. Above cloud enhanced photolytic rates due to reflection from clouds has been accounted for by a multiplicative adjustment factor. The in-situ photolytic rate attenuation coefficient equals unity at the cloud top. The in-situ photolytic rate attenuation coefficient at each height at and below the cloud base is equal to the ratio of short-wave solar radiation reaching that height to the radiation that would reach that height under clear sky conditions. Photolytic rates within the cloud are interpolated between cloud top and cloud base values using the in-situ cloud cover fraction at that height. Aqueous phase catalytic reactions represent a significant production pathway for inorganic compounds such as sulfate and organic compounds such as glyoxal in cloud droplets. Aqueous phase reaction is modeled in a reconstructed cloud column derived from the WRF predicted relative humidity vertical profile and the adiabatic lapse rate.

CMAQ derives convective boundary layer mixing of air pollutant using the Asymmetrical Convective Model version 2 (Pleim, 2007) PBL-scheme. The surface layer upward fluxes are allowed to transport pollutants to any layer within the PBL by non-local mass exchange. For downward entrainment, a layer-by-layer local transport is prescribed. Cumulus cloud convective mixing of air pollutants is modeled by using a similar asymmetrical methodology with additional entrainment constraints (Pleim, 2007).

Removal processes of depositions are likewise important in capturing the distributions of air pollutants in surface levels. Rates of scavenging for gas and aerosol species by liquid and solid hydrometeors are often calculated by empirical uptake and accretion efficiency coefficients with considerable range of conditions and applicability ranges. Wet depositional speeds are determined by hydrometeor gravitational settling velocities. Dry deposition velocity for aerosol and trace gases are derived respectively basing on particle sedimentation velocity and canopy conductance and other surface resistances (Xiu and Pleim, 2001). These processes are highly spatial and temporal variable and inherently less certain due to the empirical parameters used.

d2.3 Choices and Fine-Tuning of Model Parameterizations

Table 12.5 Asia Case d2 summarizes the parameterization choices in HAQFS for the meteorological and chemical of the numerical simulation system. It is worthwhile to explain some of these model selections as the choice of physical or chemical parameterization often lend synergies with one another in a one-way or two-way feedback relationship. In an operational forecasting system, the interplays of these processes and the preferred modeling choices are often systematically tuned to optimize performance accuracy.

d2.4 Initialization, Boundary Conditions and Inputs for the Base and Sensitivity Simulations

Initialization of the CTM simulation were conducted from forecast fields from the previous HAQFS forecast cycle. Its boundary conditions were prescribed by monthly-varying concentration fields from a full-year retrospective simulation by the WRF. In addition, there were three groups of input files: (a) Geometric data: `grd**` files, (b) Meteorological data: `met**` files, and (c) Emission files.

d2.5 Lessons Learned: Emission and PBL Dynamics

In HAQFS the most binding phenomena are those of meso-scale in length and hourly-averages in temporal scales close to the surface. We have learned much from our years of daily attentive scrutiny of HAQFS forecasting accuracy. The two decisive classes of modeled processes determining HAQFS accuracy are: (1) emission fluxes, and (2) planetary boundary layer (PBL) dynamics. The former is handled by emission inventory and projection calculation and the latter is dependent on the WRF's ability to accurately unravel movements of air and hydrometeor masses.

d2.6 Results and Discussion

During the G-20 2016 Hangzhou summit, emission controls included a forced closure of highly polluting industries, and limiting traffic and construction emissions in the cities and surroundings were applied. Figure 12.32 shows spatial distributions of simulated O₃ and PM_{2.5} overlaid with observed data before and during the G-20 Summit at 14:00 LT on August 30, September 1 and 5, 2016. As shown, there is essential consistency between the model predictions and observations, indicating that the spatial patterns of observed O₃ and PM_{2.5} are captured reasonably well. Figure 12.33 shows time series of observations and simulations for O₃ and PM_{2.5} in the absence and presence of emission reductions during the period from August 26 to September 15. Model predictions with emission reduction ("model-ctr") give a much closer agreement with the observations for both O₃ and PM_{2.5} than those without emission reductions. In addition, predictions under the targeted emission controls are much closer to the observations of O₃ and PM_{2.5} than those without the emission controls, as indicated by both time series and scatter plots in Figure 12.33.

To assess the effects of emission reductions during the G-20 Summit 2016 in Hangzhou, the entire study period was separated into three subperiods: before the G-20 Summit (from August 4 to September 3), namely the start of the implementation of emission reduction; during the G-20 Summit (from September 4 to September 5), during which the more stringent emission reduction strategy was carried out, and after the G-20 Summit (from September 6 to September 15), during which the emission reduction was stopped (Figure 12.33). The very low O₃ concentrations for the periods of September 9-12 and September 14-15 caused the

average low O₃ concentration after the G-20 Summit as indicated in Figure 12.33a. Figure 12.33b shows that the average observed PM_{2.5} concentration during the G-20 Summit was somewhat lower than that before the G-20 Summit because of more stringent emission reduction strategies during the G-20 Summit. The average simulated concentrations of O₃ and PM_{2.5} without emission reductions were significantly higher than the observed values during the G-20 Summit (Figures 12.33a and b), indicating significant improvement of air quality.

Figure 12.34 shows the geographical distributions of predicted reduction of hourly O₃ and PM_{2.5} concentrations in the Yangtze River Delta region during three periods (i.e., August 31-September 2, September 3-5 and September 6-9, 2016) obtained by the difference between the model simulations in the presence and absence of emission controls. During the G-20 Summit period, O₃ concentrations were reduced by more than 20 $\mu\text{g m}^{-3}$ (or 25.4%) in Hangzhou and to a lesser extent in surrounding areas such as Shanghai (Figure 12.34). PM_{2.5} reductions exceed 20 $\mu\text{g m}^{-3}$ (or 56.1%) in Hangzhou and to a lesser extent in surrounding Yangtze River Delta region. Reductions of hourly O₃ and PM_{2.5} in Figure 12.33 showed noticeable trends; reduction of hourly levels increased gradually during August 31-September 3, and reaching a maximum during the G-20 Summit.

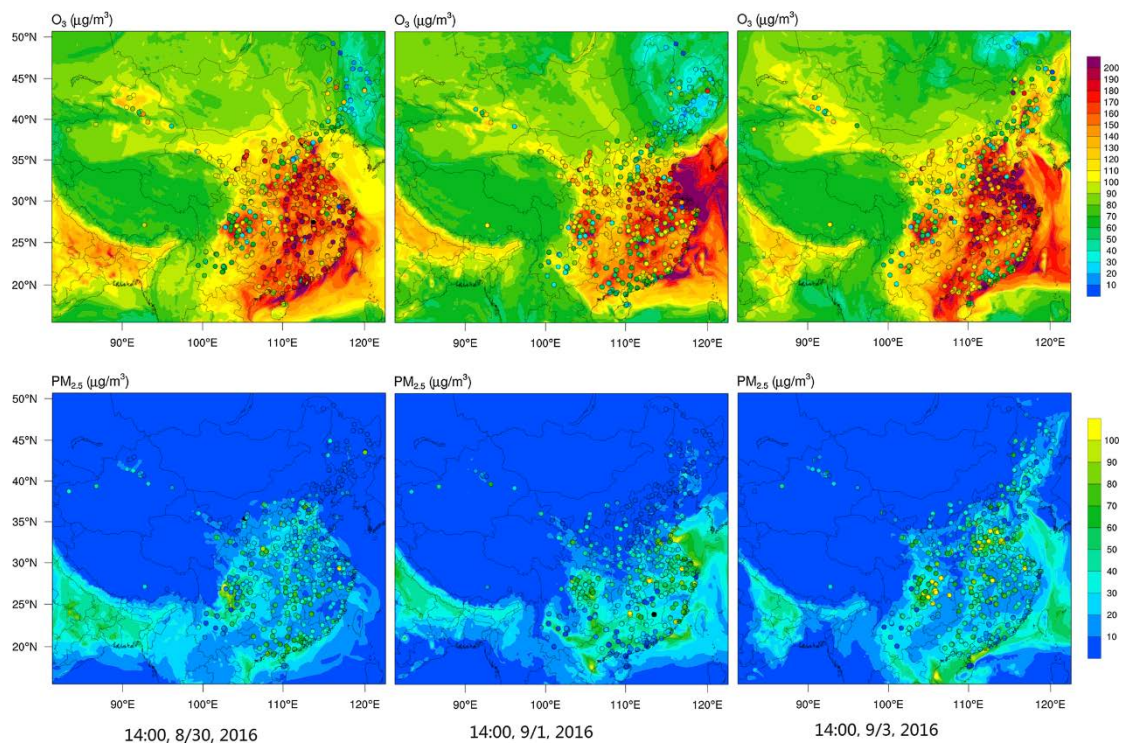


Figure 12.32. Concentrations of ozone (O₃) and PM_{2.5} (particles with aerodynamic diameter lower than 2.5 μm) simulated by the WRF-CMAQ (based on the emission controls) with observed data overlaid (circles) at 14:00 (local time) on August 30, September 1 and September 3, 2016. The essential consistency between the model predictions and observations indicates that the spatial patterns of observed O₃ and PM_{2.5} are captured reasonably well.

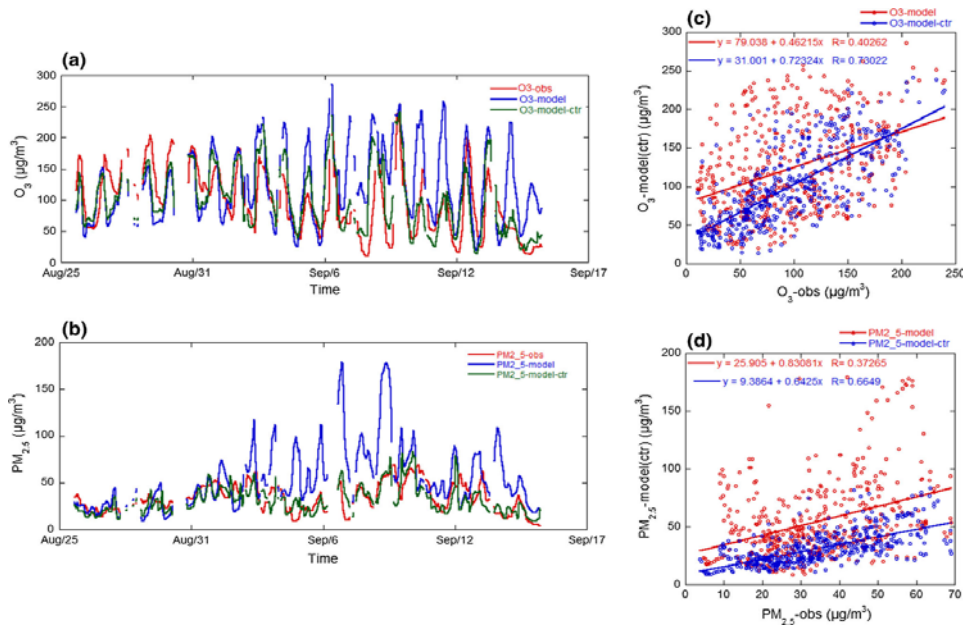


Figure 12.33. Time series of observations and simulations with (O3-model-ctr, PM2_5-model-ctr) and without (O3-model, PM2_5-model) emission controls and the corresponding scatter plots between observations and predictions during August 26-September 15, 2016; a time series comparison for O3, b time series comparison for PM2.5, c scatter plots for O3 and d scatter plots for PM2.5. The correlation equations are also shown in the scatter plots. The “model” and “model-ctr” represent the results in the absence and presence of emission reductions, respectively. The “Obs” represents observations. The average simulated concentrations of O3 and PM2.5 without emission reductions were significantly higher than the observed values during the G-20 Summit (a, b), indicating significant improvement of air quality.

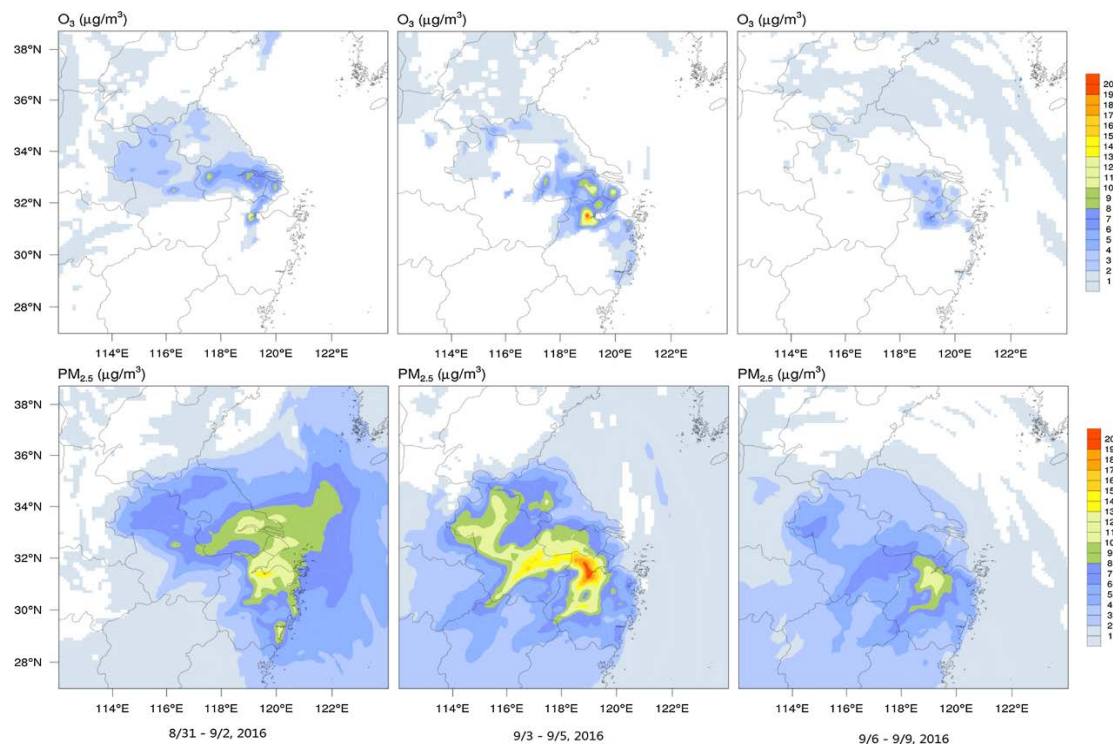


Figure 12.34. Predicted reductions of hourly O3 (top) and PM2.5 (bottom) concentrations in the Yangtze River Delta region with and without the emission controls for the three period

(i.e., August 31-September 2, September 3-5 and September 6-9, 2016). During the G-20 Summit period, O₃ concentrations were reduced by more than 20 $\mu\text{g m}^{-3}$ (or 25.4%) in Hangzhou and to a lesser extent in surrounding areas such as Shanghai. PM_{2.5} reductions exceeded 20 $\mu\text{g m}^{-3}$ (or 56.1%) in Hangzhou and to a lesser extent in surrounding Yangtze River Delta region.

Person of Contact: Shaocai Yu, email: shaocaiyu@zju.edu.cn

References

- Iacono, M. J., Delamere, J. S., Mlawer, E. J., Shephard, M. W., Clough, S. A., & Collins, W. D. (2008). Radiative forcing by long-lived greenhouse gases: calculations with the air radiative transfer models. *Journal of Geophysical Research Atmospheres*, 113(D13), -.
- Pleim, J. E. (2007). A combined local and nonlocal closure model for the atmospheric boundary layer. part i: model description and testing. *Journal of Applied Meteorology & Climatology*, 46(9), 1383--1395.
- Xiu, A., & Pleim, J. E. (2001). Development of a land surface model. part i: application in a mesoscale meteorology model'. *j. appl. meteorol.* 40, 192-209. *Journal of Applied Meteorology*, 40(2), 192-209.

Case d3. Application of Hong Kong Air Quality Forecasting system over Hong Kong, China

Kenneth Leung

Hong Kong Environmental Protection Department, Wan Chai, Hong Kong

Case overview and significance: The Hong Kong EPD has developed a real-time air quality forecasting capability dubbed PATH that has been serving the Hong Kong residents since 2003. PATH is comprised of an offline coupling of WRF and CMAQ applied to a four-tier telescopic nested domain at 27, 9, 3, and 1 km horizontal grid spacing with the Hong Kong territory simulated in the innermost grid. Chemical lateral boundary condition (LBC) was given by monthly varying data derived from an annual Geos-CHEM global simulation for 2004. Emissions were determined from local inventories. This study illustrated a somewhat counter-intuitive notion that: "occurrence of typhoon or tropical storms exacerbates ozone exceedance --strong winds from these systems should clean the air?" Focusing on the emergence of two tropical depressions impacting Hong Kong in 2017, PATH showed mixed skill in capturing high ozone and PM_{2.5} concentration in the territory immediately prior to their passing: (a) Typhoon Hato passed on August 23; and (b) Tropical Storm Sanyu passed on August 31. The strong subsidence ahead of the depression systems inhibited convective mixing resulted in multiple day stagnant conditions that were conducive for pollutant accumulation resulting in extreme ozone exceedance. Indeed, had dynamic chemical LBC been implemented, PATH could show aggravated pollution conditions due to cyclonic transport importing additional pollution from the industrialized regions north of Hong Kong.

d3.1 Introduction

The selected study case represents high surface O₃ and PM_{2.5} episode scenarios over Hong Kong affected by tropical typhoons.

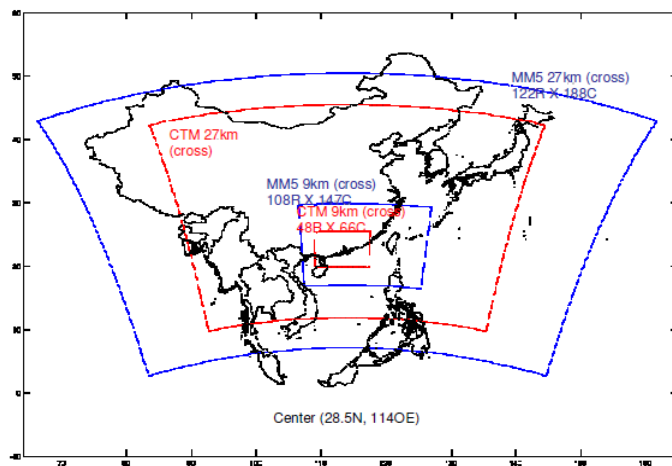


Figure 12.35. Domain map of the two coarse modeling domain with 27 km and 9 km horizontal resolution used for the meteorological module WRF and chemical transport model CMAQ of the Hong Kong EPD forecasting system.

The establishment of the Hong Kong Air Quality Forecasting System (PATH) of Hong Kong was funded by the Hong Kong Environmental Protection Department since 2003 to protect public health against air pollution and to support daily forecasting operations. The PATH system provides territory-wide surface gaseous pollutants (NO, NO₂, SO₂ and O₃) and particulate matters (PM₁₀ and PM_{2.5}) with 120 h lead-time.

In this case study, the PATH system was applied for a period over the month of August 2017. On August 21, Typhoon Hato emerged over the northern portion of the South China Sea and reached typhoon intensity. As one of the strongest typhoons to affect Macao and Hong Kong in the past 50 years, Hato caused significant damage and a total of 24 fatalities. The approach of the typhoon also caused an ozone pollution episode to Hong Kong with hourly concentration over 300 $\mu\text{g m}^{-3}$ measured at the monitoring stations. On August 30, later in the month, there was another ozone episode in Hong Kong with hourly concentration over 400 $\mu\text{g m}^{-3}$ record while tropical storm Sanyu was approaching from the Pacific and a low pressure system was

developing above Philippines. Although the model is capable of capturing trends and timing of these occurrences, it is still challenging to predict the actual pollution level accurately during these episode scenarios.

d3.2 General Description of the Model

[Table 12.5 Asia Case d3](#) summarizes the parameterization choices used in the model.

The PATH forecasting system is based on air quality predictions made by simulation using the USEPA CMAQ model as the chemistry and transport module (Byun and Schere, 2006). The meteorology is computed offline without aerosol feedback using the weather research forecast (WRF) from the National Center for Atmospheric Research (NCAR) (Skamarock et al., 2008). The meteorological initial and boundary conditions were provided by Global Forecast System by the National Centers for Environmental Prediction (GFS-NCEP) as well as input from the Non-hydrostatic model (NHM) from the Hong Kong Observatory. The CMAQ and WRF have 4 levels of nested domain from 27 km down to 1 km horizontal grid spacing with nesting ratio of 3. Both WRF and CMAQ models have fine vertical grid spacing at heights near the surface. At upper levels, the vertical structure for CMAQ was coarsened to reduce computing cost.

d3.2.1 Meteorological Model

The WRF model provides operational meteorological input for the CMAQ in the Hong Kong Environmental Protection Department. The WRF model surface temperature, cloud fraction and precipitation distributions are input to the CMAQ in air quality predictions. Currently, real time assimilation of surface observations were not applied directly to the WRF model but instead applied to the NHM by the Hong Kong Observatory before input into WRF as initial and boundary conditions. The direct assimilation of surface observations is currently in development and may be added to the system in the future. The Noah land-surface model with appropriate land surface data for Hong Kong was input into the WRF model (Xiu and Pleim, 2000).

d3.2.2 Chemical Transport Model (CTM)

The CB05-gas- and aero5-aerosol-phase mechanisms are used in the PATH forecasting system. The CMAQ Version 4.6 was used initially in the HK/PRD modeling. The Piecewise Parabolic Method (Coella and Woodward, 1984) advection solver was used along with the spatially varying horizontal diffusion approach and K-theory for vertical diffusion. The Asymmetric Convective Mixing (ACM2) planetary boundary layer (PBL) scheme was used for vertical turbulent exchange. The CMAQ configuration used the CB05 gas-phase, RADM aqueous-phase, and AERO5/ISORROPIA aerosol chemistry schemes. Treatment of reversible secondary organic aerosols was simulated by the SORGAM implementation in CMAQ.

d3.2.3 Initialization, Boundary Conditions and Inputs for the Base and Sensitivity Simulations

Initialization of the CMAQ simulation were conducted from forecast fields from the previous CMAQ forecast cycle. Its boundary conditions were prescribed by monthly-varying concentration fields based on one set of year 2004 Geos-CHEM (Jacob et al., 2005) output. One set of emission files based on local data was used to provide the air quality forecasts.

d3.3 Results and Discussion

The PATH forecasting system simulation starts every day to provide routine prediction to forecast operations. The results are stored in archive and can be retrieved from time to time for analysis and investigation.

Figure 12.36 shows a surface contour plot of the simulation on August 21 2017 before Typhoon Hato approaches the South China Sea. It can be seen that the typhoon caused North to North-westerly wind to Hong Kong, bringing along air pollutants downstream from Guangdong affecting the Pearl River Delta estuary. The subsiding air ahead of the typhoon

brought fine and light wind condition, causing sharp rise in air temperature and poor dispersion of air pollutants. The temperature reached around 34.4 degree Celsius measured at King's Park station during the episode.

Figure 12.37 shows the monthly time series of model predicted ozone levels against observations during the two ozone episodes in August 2017 using the PATH forecasting system. The episode from August 20 to 22 lasted for three consecutive days before the typhoon landed and dissipated. The ozone level reached $300 \mu\text{g m}^{-3}$ for two consecutive days. For this type of ozone episode affected by typhoons, the model seems capable of predicting ozone levels that match with observations.

Another episode occurred later in the month from August 29 to 31. The ozone reached $400 \mu\text{g m}^{-3}$ on August 30th. The model predicted a lower ozone level on this day, which may be due to discrepancy in model meteorology or emissions. The weather chart of August 30 is shown in Figure 12.38, there is no clear evidence showing the ozone episode was due to approaching typhoon. For this type of complicated weather situations, the model may predict ozone level that match with observation less well. Nonetheless, although there are discrepancies, the model can capture trends and timings of these occurrences quite reasonably over monthly time spans.

Figure 12.39 shows the same time series but for PM_{2.5}. The PM_{2.5} concentrations increased during the episodes but did not reach very high levels. The forecasting system seems to predict the trends of these increases reasonably.

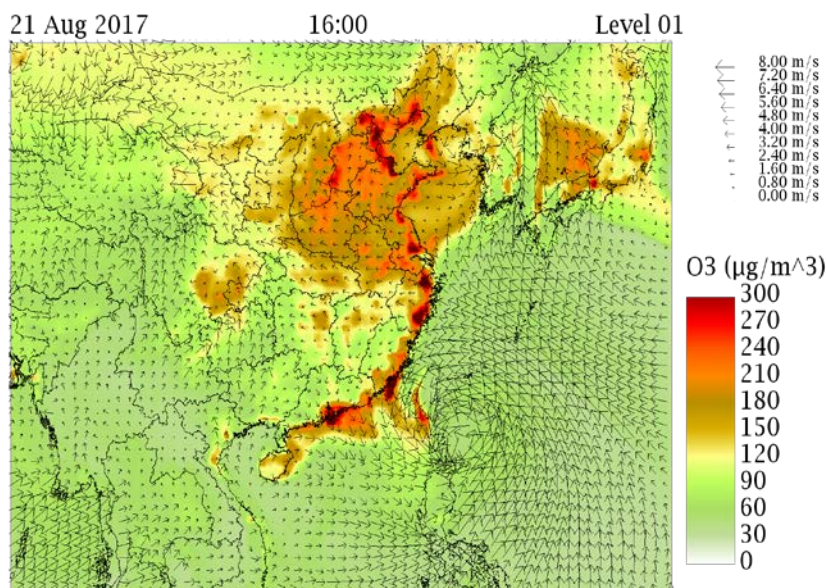


Figure 12.36. Predicted ozone levels and wind vectors on 21 August 2017 before Typhoon Hato approaches the Guangdong coast using the PATH forecasting system.

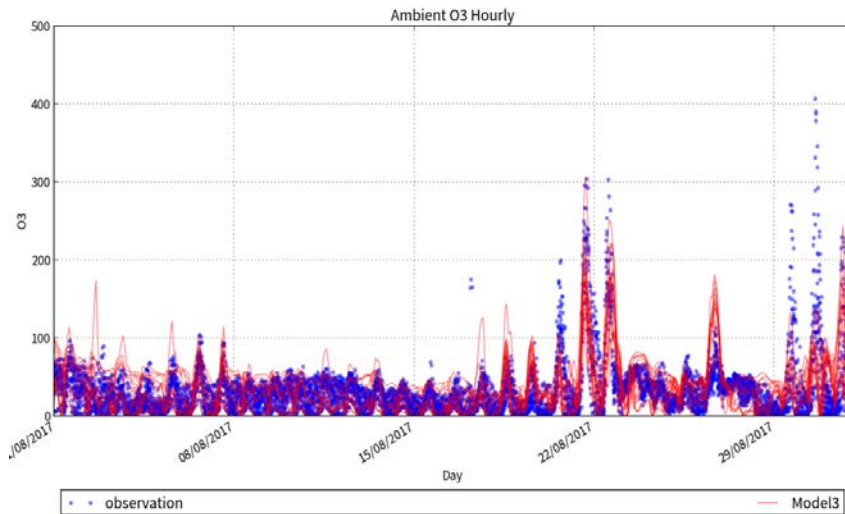


Figure 12.37. Predicted ozone levels (red) and observation (blue) during two air pollution episodes in August 2017 using the PATH forecasting system.

日期/Date: 30.08.2017 香港時間/HK Time: 08:00 香港天文台 Hong Kong Observatory

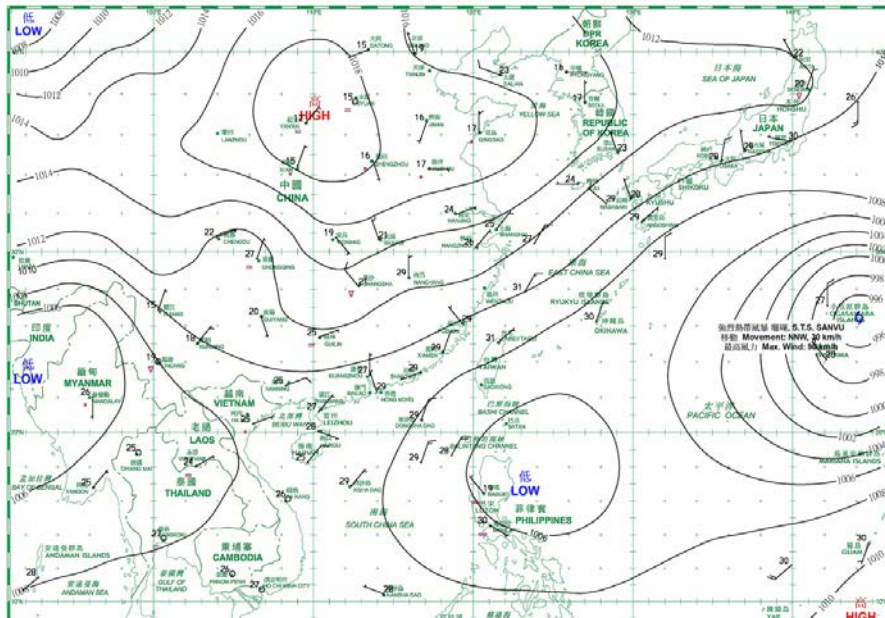


Figure 12.38. Weather chart at August 30, 2017, of an ozone episode day with concentration reached 400 $\mu\text{g m}^{-3}$.

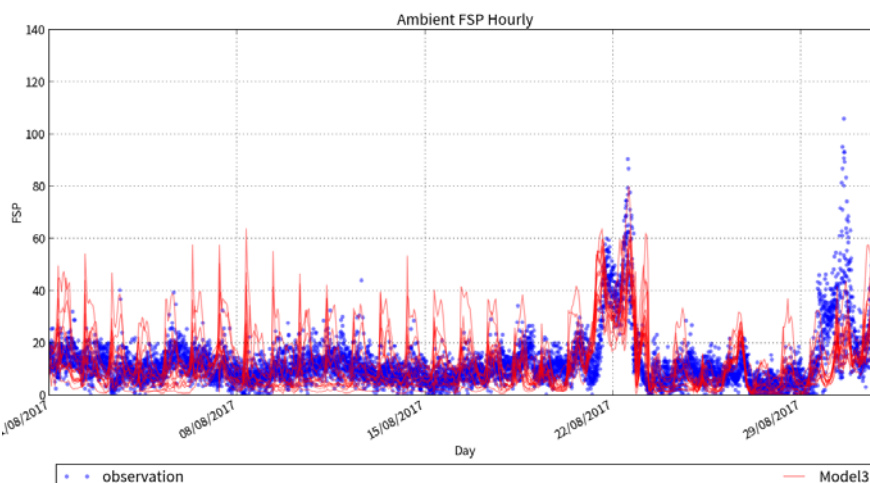


Figure 12.39. Predicted PM2.5 levels (red) and observation (blue) during two air pollution episodes in August 2017 using the PATH forecasting system.

Person of Contact: Kenneth Leung, email: kleung@epd.gov.hk

References

- Byun, D.W., and K.L. Schere, 2006: Description of the Models-3 Community Multiscale Air Quality (CMAQ) Model: System overview, governing equations, and science algorithms. *Appl. Mech. Rev.* 59(2), 51-77, doi:10.1115/1.2128636.
- Coella, P., and P. L., Woodward. 1984. "The Piecewise Parabolic Method (PPM) for Gas-Dynamical Simulations", *J. Comp. Physics*, Vol. 54, pp. 174-201.
- Jacob, D.J., R. Park and J.A. Logan. 2005. Documentation and Evaluation of the GEOS CHEM Simulation for 2002 Provided to the VISTAS Group. Harvard University. June 24.
- Skamarock, W. C., J. B. Klemp, J. Dudhia, D. O. Gill, D. M. Barker, W. Wang, and J. G. Powers, 2008: A description of the Advanced Research WRF version 3. NCAR Tech. Note NCAR/TN-475+STR, 113 pp.
- Xiu, A., and J.E. Pleim. 2001. Development of a land surface model. Part I: Application in a mesoscale meteorology model. *Journal of Applied Meteorology*, 40, 192-209.

Case d4. The impact of urbanization in the Pearl River Delta Region, China under three different climate change scenarios

Peter Yeung, Jimmy Chi-Hung Fung, and Chao Ren

Department of Mathematics, Hong Kong University of Science and Technology, Clearwater Bay, Kowloon, Hong Kong

Case overview and significance: The WMO Representative Concentration Pathway (RCP) scenarios: (a) RCP4.5, (b) RCP6.0; and (c) RCP8.5 were studied to investigate how urbanization in the Pearl River Delta (PRD) impact climate change by models using a specifically configured WRF. The modeled tendency trajectory on climate change confined to land-use and land-cover parameters was verified to a satisfactory degree retrospectively for a few decadal time points between 1988 and 2010. Future climate change tendency was conjectured for 2030 by inputting projected land-use and land-cover scenarios basing on the proposed RCPs by applying the GeoSOS Future Land Use Simulation model. These sensitivity simulations projected an impact envelop for a possible urban-landscape-to-climate-change response relationship. Urban planning officials and other policymakers may take advantage of such cause-and-effect relationships for informed decision-making to alleviate adverse effects from unwise urbanization practices and safeguard public health and the environment.

d4.1 Introduction

The selected study case represents three future CO₂ emission scenarios over the Pearl River Delta (PRD) Region in China. Low, medium and high CO₂ emission scenarios as the representative concentration pathway (RCP) were adopted to capture the potential climate change in the PRD region given its future urbanization in terms of land use land cover change.

In this case study, land use data in the year of 1988, 1999 and 2010 is collected and detected based on the Landsat images by using the WUDAPT level 0 method (Bechtel, 2015). Future land use in 2030 (Figure 12.40) is predicted based on the developed historical land use data by using the Geographical Simulation and Optimization System (GeoSOS) – the Future Land Use Simulation (FLUS) model (Liu et al., 2017).

By integrating the updated land use data from WUDAPT with the Weather Research and Forecast Model, the impact of urbanization in the Pearl River Delta regions is evaluated and compared between the year 2010 and 2030 respectively.

The exercise not only provides a scientific understanding of urban-environment relationship (Seto et al., 2017), but also sheds an insight into the future and select adaptive measures to alleviate the potential health risks and improve urban living quality.

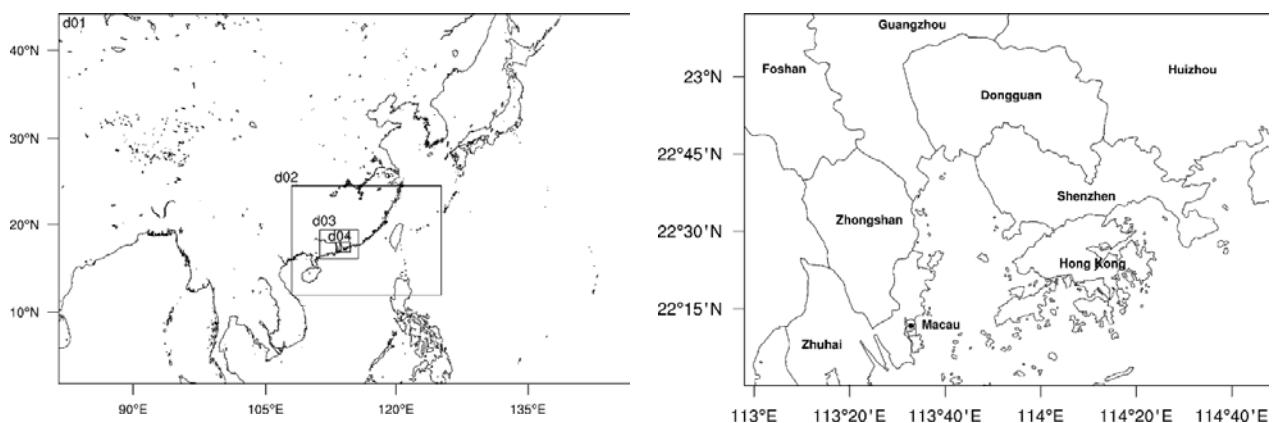


Figure 12.40. (Left) The coverage of the domains configured in WRF. "d01" represents domain 1 and so on. (Right) The innermost domain ("d04") is the area of interest for this study.

d4.2 General Description of the Model

[Table 12.5 Asia Case d4](#) summarizes the parameterization choices used in the model.

The Weather Research and Forecast Model (hereafter “WRF”) with Advanced Research WRF (ARW) Version 3.7.1 is employed in this study. WRF is a mesoscale, non-hydrostatic numerical weather prediction, which is the successor of the Fifth-Generation Penn State/NCAR Mesoscale Model (MM5). WRF provides different schemes for various physical interaction, including microphysics, surface physics and so on. Such flexibility allowed models to be used in by other research in different areas. For example, pollution dispersion modeling (WRF-Chem) (Grell et al., 2005) and Large Eddy Simulation for microscale simulation (WRF-LES).

d4.3 Choices and Fine-Tuning of Model Parameterizations

A total of four domains are configured, with the innermost domain is the study domain covering the Pearl River Delta region (Figure 12.40). The following physics schemes are employed for the simulation. MM5 Similarity Scheme (Zhang and Anthes, 1982) is used for the surface layer physics; RRTM Shortwave and Longwave Schemes are applied for the shortwave and longwave radiation. Grell 3D Ensemble Scheme (Grell & Dévényi, 2002) is responsible for the cumulus parameterization in domain 1 and 2 only. The resolution of domain 3 and 4 is small enough to resolve cumulus physics by itself. Asymmetric Convection Model 2 (ACM2) (Pleim, 2007) is employed for the calculation for planetary boundary layer. According to Xie, Fung, Chan and Lau (2012), it is found that ACM2 performs better for the Pearl River Delta. Unified Noah Land Surface Model (Noah-LSM) (Tewari et al., 2004) is chosen for the land surface. Noah-LSM is modified so as to extend the bulk parameterization to the newly added urban-type land use. Following Liu, Chen, Warner and Basara (2006), the roughness length and volumetric heat capacity is also adjusted for these land use categories so as to reflect the urban effects.

d4.4 Initialization, Boundary Conditions, and Inputs

Initial and lateral boundary conditions provided from National Center for Environmental Prediction (NCEP) are employed. They are the outputs from NCAR’s Community Earth System Model (CESM1). It is bias-corrected and as well as converted for the dynamical downscaling in WRF. The dataset has forecasted the global climate until the end of the 21st century under three different Representative Concentration Pathways (RCPs), which are “RCP4.5”, “RCP6.0” and “RCP8.5” (Moss et al., 2010) respectively. Each of these represents different radiative forcing at the year 2100. RCP4.5 represents the radiative forcing will reach 4.5 W m⁻², and similarly for other cases. By applying the dataset, 2010 RCP6.0 is chosen as control run which represents the current scenario. 2030 RCP4.5, RCP6.0, and RCP8.5 are chosen to represent future scenario with the low, medium and high emission of greenhouse gases respectively. These data are in 6 hours interval with the horizontal resolution approximately 10.

Moreover, land use data covering area of interest are also updated from the WUDAPT data for the simulation of year 2010 and year 2030 respectively (Figure 9.d4.2). Through updating the land use, it helps to realistically forecast the future heat stress contributed by both global warming and urbanization.

Throughout the simulations, WRF is run with consecutive integration by re-initialization for every 4 days so as to prevent the model drifting from forcing. Moreover, the first day after the initialization is treated as model spin-up time and excluded from the analysis.

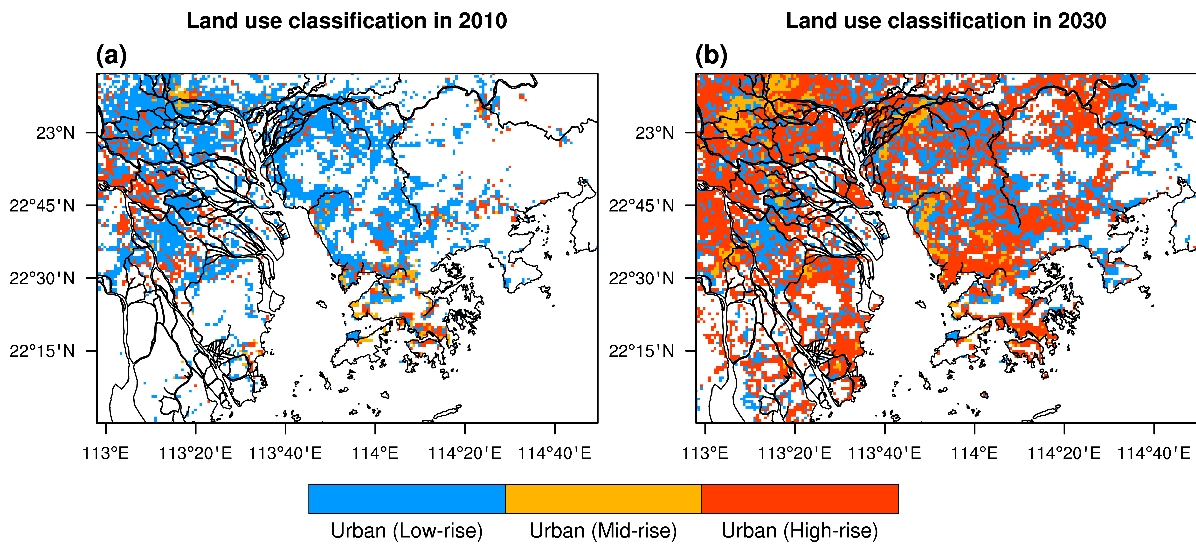


Figure 12.41. The land use classification in (a) 2010 and (b) 2030 used in WRF.

d4.5 Lesson Learned: Physical Properties of Urban Land use

Due to the heterogeneity of the buildings pattern in urban areas of the Pearl River Delta, the original setting for the urban land use is not representative. For example, a single value of roughness length may represent low-rise buildings appropriately, but not for skyscrapers in urban cores. As such, it is important to differentiate the urban land use and adjust their physical properties correspondingly. To achieve so, one of the approaches is to update the land use data and Noah-LSM in WRF apart from coupling urban canopy models with WRF. It is found that the overestimation of wind speed and underestimation of temperature during night-time are both alleviated due to the better representation of urban areas.

d4.6 Results and Discussion

When comparing with the current (year 2010) and future (year 2030) scenarios, a warming trend can be observed. Overall, there are 1 – 2°C increases in temperature during both daytime and night-time (Figures 12.42 and 12.43). A significant temperature increase in inland areas can be observed, particularly regions with appreciable urbanization causing the pronounced urban heat island effect. For instance, the north-eastern part of the simulation domain, where rural areas are predicted to become urban (high-rise) according to Figure 12.41, is able to have 2-3°C temperature rises when comparing Figure 12.42 (a) with (b), (c), and (d).

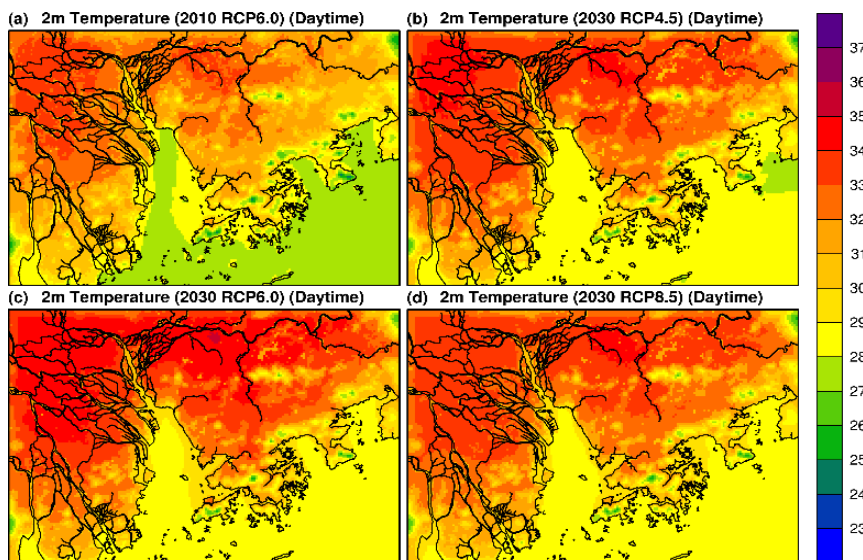


Figure 12.42. Spatial distributions of averaged 2-meters temperature during 1400 LST and 1600 LST in June - July.

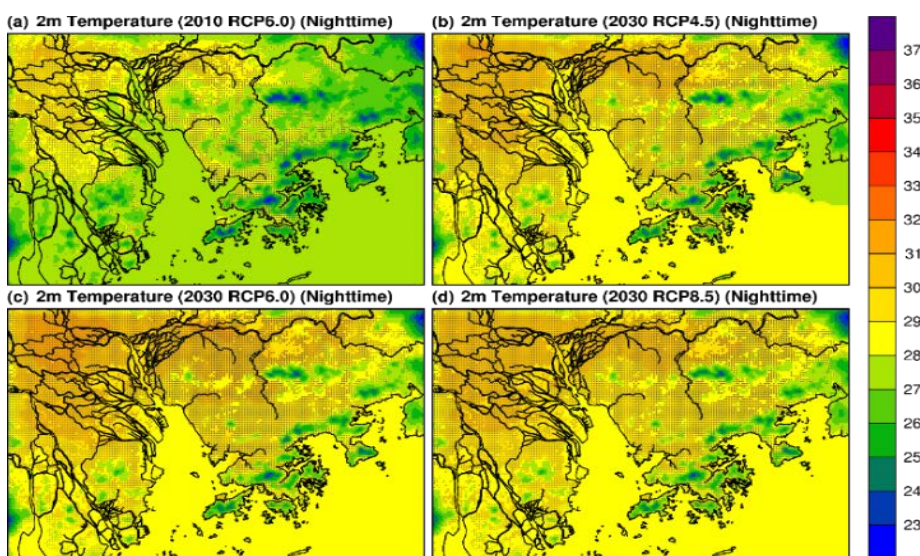


Figure 12.43. Spatial distributions of averaged 2-meters temperature during 2000 LST and 2200 LST in June - July. Gray dots on the map indicate model grid with urban land use.

There is a widespread of weakened wind speed in inland areas, particularly during the daytime, due to the appreciable urbanization predicted from year 2010 to 2030. However, the weakening is less obvious during the night-time (Figure 12.44). This can be explained the diurnal variation of the boundary layer, which is the dominant factor to diminish the wind during night-time. After sunset, ground surface loses heat faster than the air, and most of the time a stable boundary layer is formed at the lower part of atmosphere. Consequently, the wind speed to be weakened at night-time across all the scenarios. In the control run, the magnitude of the wind speed can be 1 m s^{-1} or lower (Figure 12.44(a)). Given the already weakened wind speed due to the boundary layer, the further urbanization is less impactful towards the weaker wind speed during night-time.

Apart from the declining wind speed, land sea breeze can be observed at various locations in the model domain. In particular, the one at the Pearl River Estuary have been analysed by Lo et al. (2006). By comparing the wind speed at coastal areas between the control (Figure 12.45(a)) and the future scenarios (Figure 12.45(b), (c), and (d)), it is found that the land sea breeze is intensified at the coastal areas during daytime. At the Pearl River Estuary, the wind speed is increased from 5.5 m s^{-1} to 6.0 m s^{-1} , and 2030 RCP6.0 has a widespread of 7.0 m s^{-1} (Figure 12.45(c)).

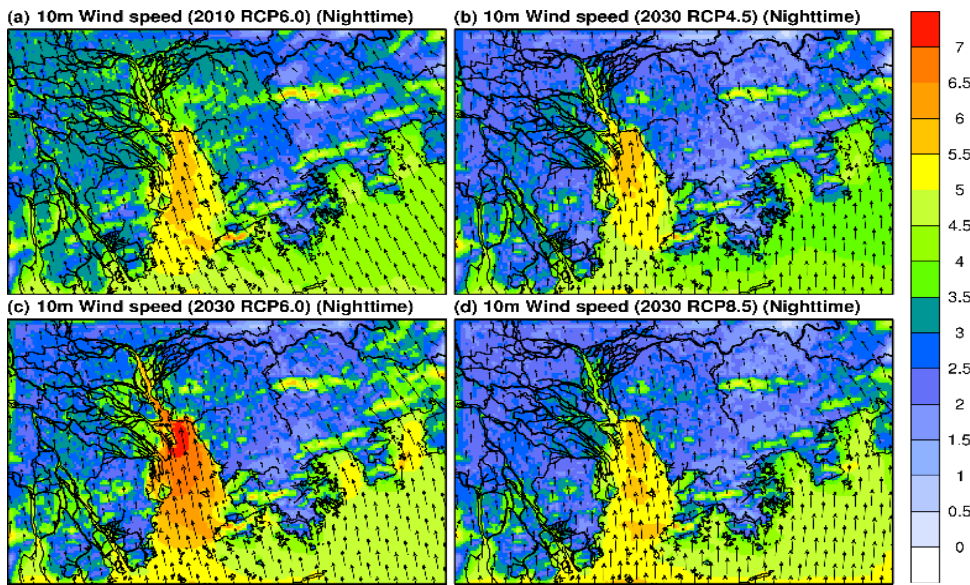


Figure 12.44. Spatial distributions of averaged 10-meters wind speed during 2000 LST and 2200 LST in June - July. Gray dots on the map indicate model grid with urban land use.

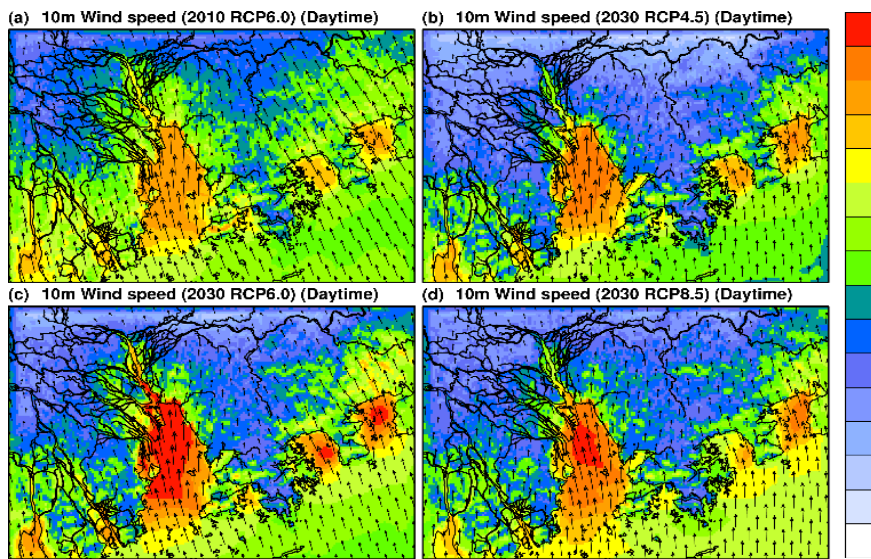


Figure 12.45. Spatial distributions of averaged 10-meters wind speed during 1400 LST and 1600 LST in June - July.

Person of Contact: Jimmy Chi-Hung Fung, email: majfung@ust.hk

References

- Bechtel, B., Mícheál Foley, Gerald Mills, Jason Ching, Linda See, Paul Alexander, Martin O'Connor et al. (2015). CENSUS of Cities: LCZ Classification of Cities (Level 0) – Workflow and Initial Results from Various Cities. Paper presented at the 9th International Conference on Urban Climate (ICUC9), Toulouse, France.
- Grell, G. A., & Dévényi, D. (2002). A generalized approach to parameterizing convection combining ensemble and data assimilation techniques. *Geophysical Research Letters*, 29(14), 38-31-38-34 [doi: 10.1029/2002GL015311](https://doi.org/10.1029/2002GL015311)
- Grell, G. A., Peckham, S. E., Schmitz, R., McKeen, S. A., Frost, G., et al. (2005). Fully coupled "online" chemistry within the WRF model. *Atmospheric Environment*, 39(37), 6957-6975. doi: <https://doi.org/10.1016/j.atmosenv.2005.04.027>
- Liu, X., Liang, X., Li, X., Xu, X., Ou, J., et al. (2017). A future land use simulation model (FLUS) for simulating multiple land use scenarios by coupling human and natural effects. *Landscape and Urban Planning*, 168, 94-116. doi: <https://doi.org/10.1016/j.landurbplan.2017.09.019>
- Liu, Y., Chen, F., Warner, T., & Basara, J. (2006). Verification of a Mesoscale Data-Assimilation and Forecasting System for the Oklahoma City Area during the Joint Urban 2003 Field Project. *Journal of Applied Meteorology and Climatology*, 45(7), 912-929. doi: 10.1175/jam2383.1
- Moss, R. H., Edmonds, J. A., Hibbard, K. A., Manning, M. R., Rose, S. K., et al. (2010). The next generation of scenarios for climate change research and assessment. [Perspective]. *Nature*, 463, 747. doi: 10.1038/nature08823
- Pleim, J. E. (2007). A Combined Local and Nonlocal Closure Model for the Atmospheric Boundary Layer. Part I: Model Description and Testing. *Journal of Applied Meteorology and Climatology*, 46(9), 1383-1395. doi: 10.1175/jam2539.1
- Seto, K. C., Golden, J. S., Alberti, M., & Turner, B. L. (2017). Sustainability in an urbanizing planet. *Proceedings of the National Academy of Sciences*, 114(34), 8935-8938. doi: 10.1073/pnas.1606037114
- Tewari, M., Chen, F., Wang, W., Dudhia, J., LeMone, M. A., et al. (2004). Implementation and verification of the unified NOAA land surface model in the WRF model (Formerly Paper Number 17.5). Paper presented at the 20th conference on weather analysis and forecasting/16th conference on numerical weather prediction, Seattle, Washington. https://ams.confex.com/ams/84Annual/techprogram/paper_69061.htm
- Xie, B., Fung, J. C. H., Chan, A., & Lau, A. (2012). Evaluation of nonlocal and local planetary boundary layer schemes in the WRF model. *Journal of Geophysical Research: Atmospheres*, 117(D12). doi: [doi: 10.1029/2011JD017080](https://doi.org/10.1029/2011JD017080)
- Zhang, D., & Anthes, R. A. (1982). A High-Resolution Model of the Planetary Boundary Layer—Sensitivity Tests and Comparisons with SESAME-79 Data. *Journal of Applied Meteorology*, 21(11), 1594-1609. doi: 10.1175/1520-0450(1982)021<1594:ahrmot>2.0.co;2

Case d5. Development of a smoke forecasting system for Southeast Asia

Christopher Gan

Center for Climate Research, Singapore

Case overview and significance: Man-started biomass burning in South Eastern Asia had gone disastrously out of control in recent past and caused severe smoke plumes jeopardized the public health and land, sea and aviation transportation of the region. The occurrence of such disasters seemed to have been amplified by dry spells coincident of El Niño events. It was a significant upheaval and economic loss when the busy international shipping lanes in the Strait of Malacca and nearby airports had to be closed for many days due to severe biomass burning smoke. Partly motivated to understand these phenomena and other regulatory concerns, the government of Singapore in collaboration of the UK Met Office had developed ATLAS, an operational Lagrangian-framework-based regional forecasting system to project the evolution of smoke concentration in terms of PM10 out two days into the future to support decision on mitigation advisory. Biomass-burning-emission detection depended on satellite retrieval of hot spots which could have significant underestimation due to various obscurations including retrieval blockage by cloud and smoke-plume. This study reported an application of ATLAS during a severe smoke event during June 1- 30 2013 with smoke plumes from biomass burning in Central Sumatra infringed over much of Southeastern Asia. ATLAS was under-predicting in the onset of the plumes, but captured the peak concentrations rather skillfully around June 20 and the waning phases of the event. This study illustrated a high stake forecast influential for regional and international policy decisions.

d5.1 Introduction

Smoke resulting from hundreds of simultaneously emitting vegetation fires regularly deteriorates air quality in Southeast Asia and can result in particularly hazardous conditions in densely populated urban areas. The large-scale burning of biomass (e.g., forests, crop residue, or peat) is mostly of anthropogenic origin. Resulting emissions of particulate aerosols and greenhouse gases, including carbon dioxide and methane, into the atmosphere are of great environmental and political concern regarding the short- and long-term consequences for human health, the stability of local ecosystems, and global climate change.

The potential of local fires to develop beyond control into disastrous burns with smoke affecting regions over large distances is strongly intertwined with the complex meteorology of the tropics (Reid et al., 2013). In particular, drier conditions brought about by El Niño events can significantly amplify fire occurrence. For example, the strong El Niño events in 1997 and 2015 brought about widespread unprecedented levels of smoke across the region. Regional precipitation patterns are governed by the monsoons with two distinct dry seasons when burning is prevalent. From January to April, fires are common in mainland Southeast Asia whereas from June to October burning is focused in maritime Southeast Asia where Singapore is located. The annual cycle of fire activity, however, is subject to strong local variations due to the complex distribution of land, sea, and terrain in the region.

d5.2 Modeling System

[Table 12.5 Asia Case d5](#) summarizes the parameterization choices used in the model.

The Meteorological Service Singapore (MSS) has been developing the ASEAN Tropical Lagrangian Atmospheric System (ATLAS) in collaboration with the UK Met Office, with the aim to establish a reliable forecast system that can adequately simulate smoke transport from fires in the region (Hertwig et al., 2015). One advantage of the Lagrangian framework is that smoke plumes can be better resolved near to source areas. ATLAS is the first operational, Lagrangian-based modeling system in Southeast Asia and has been running operationally since 2013.

At the core of the system lies the Lagrangian dispersion model NAME (Numerical Atmospheric-dispersion Modeling Environment; Jones et al., 2007), driven with Numerical Weather Prediction (NWP) meteorological fields from the global configuration of the Unified Model (UM; Davies et al., 2005) and satellite-based emission products based on active fire detections available in near real time. Model outputs are verified and bias corrected against ground-based measurement stations.

d5.3 Forecast Configuration

The dispersion domain has been defined to include key source regions in Southeast Asia, extended in the meridional and zonal directions to prevent smoke that is released near the edges of the domain from being immediately lost and allowing for recirculation of pollutants. The top of the dispersion domain is set to 20 km above ground level to allow dispersion within the tropical troposphere to be fully accounted for.

NAME has been set up to represent only the dispersion and deposition of primary PM₁₀ and PM_{2.5} particles that are emitted from biomass burning sources, with its chemistry scheme switched off. Contributions to the ambient PM₁₀ levels from other natural or anthropogenic (e.g. sea salt, industry or traffic) sources and from secondary aerosol formation have not been accounted for. In future versions, the inclusion of other emissions sources as well as running with the chemistry scheme switched on will be considered.

The modeled PM particles are subject to wet and dry deposition mechanisms. In order to ensure an acceptable level of statistical noise in the output from the Lagrangian dispersion simulations, the model has been set up to release large numbers of particles for each source location. Depending on the overall number of fire sources, the average number of computational particles present in the domain over 1 hour of simulated time is typically in the range of approximately 0.5–50 million.

The maximum travel time of each particle is set to 96 hours for the benefit of computational efficiency. After this time, it is reasonable to assume that most particles will have left the domain and those that have not would have travelled a significant distance away from the source, been well dispersed and affected by deposition processes, thereby contributing to comparatively low concentration levels. A spin-up time of 4 days is implemented in order to create realistic initial PM₁₀ levels resulting from biomass burning prior to retrieving the first model output. The model forecast extends out to 2 days.

d5.4 Smoke Emissions

Smoke emissions are calculated based on the Global Fire Assimilation System (GFAS, Kaiser et al., 2012) v1.2 daily gridded fire radiative power (FRP) and smoke injection height products, integrated with high resolution peatland maps and land classification data (Miettinen et al., 2016). Within the model, fire sources are represented as cuboid-shaped releases with horizontal dimensions of 0.1°, reflecting the horizontal resolution of GFAS v1.2. The vertical extent of the emissions from the ground is determined by the injection height available in GFAS with Lagrangian particles being uniformly released within this layer.

Emissions based on the latest observation day are persisted into the future. This simplified assumption is applied in the absence of a dynamical fire model and also stems from the difficulty in predicting the evolution of smoke emissions from human ignited fires. As the fire situation can be highly dynamic, the validity of the persistence assumption could significantly impact forecast results.

Smoke emissions could potentially be underestimated by a factor of 3.4 (Kaiser et al., 2012), though this value is expected to vary by region. The underestimation is related to challenges in satellite detection and monitoring of fires (Reid et al., 2013) and uncertainties in calculating emissions through the FRP method. For example, abundant cloud cover in Southeast Asia, including ubiquitous high cirrus clouds, frequently obscures fires from satellite sensors. Further obscuration can also be expected by thick smoke plumes during severe fire episodes.

d5.5 Meteorology

The global configuration of the UM has been used to supply the three-dimensional deterministic input meteorology to NAME. The model atmosphere of the UM is compressible and non-hydrostatic. Various processes including convection, boundary layer turbulence, radiation, cloud microphysics and orographic drag are parameterized to varying degrees of sophistication. The UM uses a hybrid ensemble 4-D variational data assimilation system (Clayton et al., 2013) to assimilate available observations into the model initial state. Model fields are output for NAME at a temporal resolution of 3 hours. The global UM currently has a horizontal resolution of about 10 km and 70 levels non-uniformly distributed in the vertical with a model top at an altitude of 80 km. Meteorology in NAME for the smoke forecast set-up extends to an altitude of 20 km, using the lowest 53 UM model levels. Within NAME, meteorological data are interpolated in both space and time.

The accuracy of the modeled smoke dispersion is influenced by uncertainties in the emissions, the NWP inputs in representing the actual state of the atmosphere, and in the transport and dispersion processes modeled within NAME. These uncertainties would include aspects such as the turbulent exchanges at the top of the boundary layer, which require an accurate estimate of boundary layer depth from the NWP, vertical transport by moist convection and pollutant washout by rainfall. In NAME, the use of unrealistic NWP boundary layer depths is avoided by constraining the allowable boundary layer depth to a predetermined range between 80 m and 4 km.

Given the moderate resolution of the global configuration of UM, coastal regions and smaller islands, including Singapore, are not reproduced in detail or, in some cases, not at all. Not fully representing the complex juxtaposition of land, sea and terrain in Southeast Asia is expected to impact local dispersion features by under-representing for instance, local orographic-induced flow and land-sea breeze circulations. Global NWP models are known to face limitations in representing the multiscale convective organization in the tropics (Arakawa and Jung, 2011) and the diurnal cycles in Southeast Asia, particularly over land (Yang and Slingo, 2001). As a result, inaccuracies in the modeled precipitation rates and rainfall locations could lead to erroneous wet deposition rates of pollutants in the dispersion simulation.

d5.6 June 2013 Case Study

The severe smoke event of June 2013 resulting from fires in central Sumatra was investigated by modeling the smoke dispersion during the period 15 May to 15 July 2013 and compared to hourly-averaged PM10 data from Singapore (Hertwig et al., 2015). Figure 9.d5.1 shows modeled PM10 concentration plumes during the onset, peak, and decline of the smoke episode. Concentrations shown are 24-hour averages valid at 00 UTC and represent boundary layer averaged fields. During the peak period of fire activity around 20 June, smoke was transported across the Strait of Malacca into Malaysia and Singapore by anomalous strong westerlies enhanced by the presence of a tropical cyclone in the South China Sea. When the tropical cyclone subsequently made landfall over Vietnam, low-level winds over Singapore shifted to a south-southeasterly direction, resulting in a huge improvement in the local air quality. At the same time, convective activity picked up in the region and the rainfall quickly helped to subdue most of the fires in Sumatra. A significant improvement in the regional smoke situation was observed during the last days of June (Figure 12.46) when light and variable winds confined the remaining smoke close to the fire sources.

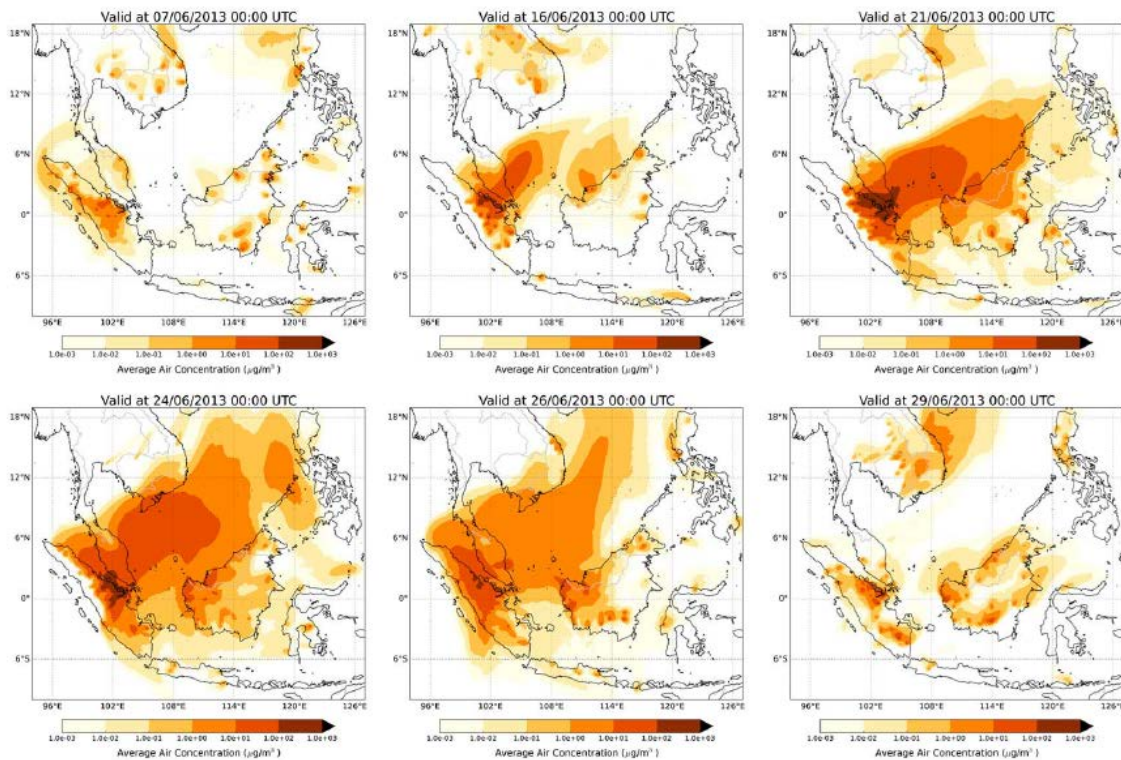


Figure 12.46. 24-hour averaged modeled PM10 concentrations within the boundary layer during the onset, peak, and end of the June 2013 smoke episode in Southeast Asia.

The early phase of the event starting around 15 June, the model simulation underpredicts concentration levels (Figure 9.d5.2) possibly due to a too strong southerly flow component in the UM. During the peak period, however, the model is able to simulate the timing and the magnitude of the highest concentrations of PM10 and accurately predicts the worst of the haze event. Towards the end of the event, increased cloud cover over the region is likely to have significantly contributed to the differences between the model and local observations, through reducing the number of fires detected by satellite and hence the calculated smoke emissions (Figure 12.47).

d5.7 Real-Time Bias Correction

Operationally, a real-time bias correction based on observations can help improve air quality and pollutant dispersion forecasts. Systematic and random model errors introduced, for example, by regionally varying uncertainties in emissions or NWP skill can be addressed through such a correction process. The real-time bias correction approach used at MSS is applied as a post-processing step and does not attempt to adjust the original smoke emission terms.

As the dispersion simulations are purely driven by emissions from biomass burning, the forecast lacks local baseline pollution levels associated with other natural or anthropogenic sources of particulate matter. The impact of such local or regional sources on near-surface air quality in Singapore can vary on a range of different spatio-temporal scales. The bias correction takes into account the local background pollution based on observations from the past 24 hours, which are then projected into the forecast period (Hertwig et al., 2015). The skill of the bias-corrected smoke prediction, however, can be further influenced by short-term changes of anthropogenic emissions taking place during the forecast period.

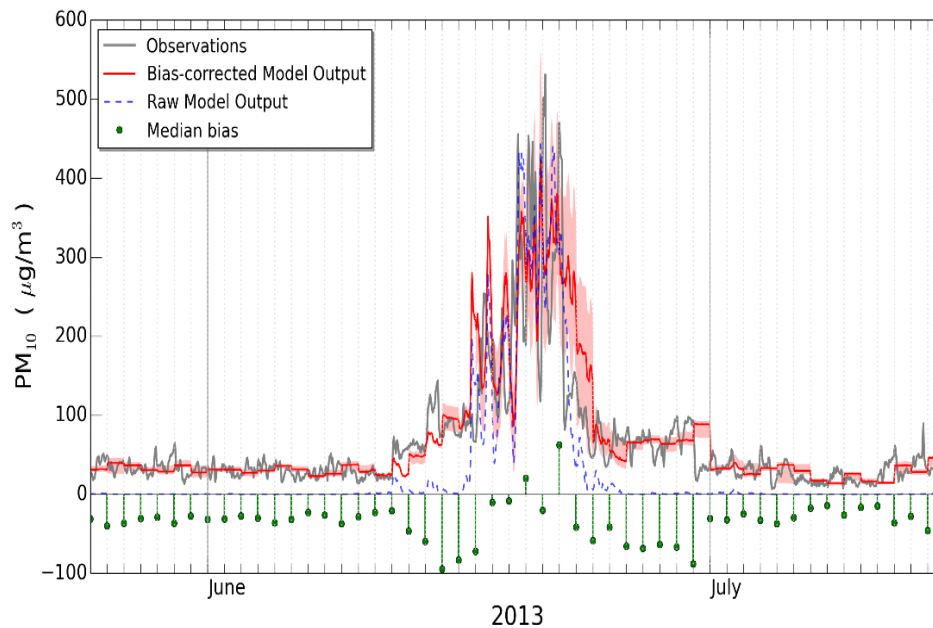


Figure 12.47. Bias-correction of the June 2013 smoke episode in Singapore based on the median bias determined over a 24-hour analysis window. Hourly simulation and observation data represent averages over 12 local monitoring sites in Singapore. Red areas indicate forecast margins based on the 25th and 75th bias quantiles.

Person of Contact: Christopher Gan, email: Christopher_GAN@nea.gov.sg

References

- Arakawa, A., & Jung, J. H., 2011. Multiscale modeling of the moist-convective atmosphere—A review. *Atmospheric research*, 102(3), 263-285.
- Clayton, A. M., Lorenc, A. C., & Barker, D. M., 2013. Operational implementation of a hybrid ensemble/4D-Var global data assimilation system at the Met Office. *Quarterly Journal of the Royal Meteorological Society*, 139(675), 1445-1461.
- Davies, T., M. J. P. Cullen, A. J. Malcolm, M. H. Mawson, A. Staniforth, A. A. White, and N. Wood, 2005. A new dynamical core for the Met Office's global and regional modeling of the atmosphere, *Q. J. R. Meteorol. Soc.*, 131(608), 1759–1782, doi:10.1256/qj.04.101.
- Hertwig, D., Burgin, L., Gan, C., Hort, M., Jones, A., Shaw, F., Witham, C., Zhang, K., 2015. Development and demonstration of a Lagrangian dispersion modeling system for real-time prediction of smoke haze pollution from biomass burning in Southeast Asia. *J. Geophys. Res.-Atmos.* 120 (24), 12605–12630.
- Jones, A., D. Thomson, M. Hort, and B. Devenish, 2007. The U.K. Met Office's next-generation atmospheric dispersion model, NAME III, in *Air Pollution Modeling and Its Application XVII*, edited by C. Borrego and A.-L. Norman, pp. 580–589, Springer, New York.
- Kaiser, J.W., Heil, A., Andreae, M.O., Benedetti, A., Chubarova, N., Jones, L., Morcrette, J.J., Razinger, M., Schultz, M.G., Suttie, M., Van Der Werf, G.R., 2012. Biomass burning emissions estimated with a global fire assimilation system based on observed fire radiative power. *Biogeosciences* 9 (1), 527–554.
- Miettinen, J., C. Shi, W. J. Tan, and S. C. Liew, 2016. 2015 land cover map of insular Southeast Asia in 250m spatial resolution, *Remote Sens. Lett.*, 7:7, 701–710, doi:10.1080/2150704X.2016.1182659.
- Reid, J. S., et al., 2013. Observing and understanding the Southeast Asian aerosol system by remote sensing: An initial review and analysis for the Seven Southeast Asian Studies (7SEAS) program, *Atmos. Res.*, 122, 403–468, doi:10.1016/j.atmosres.2012.06.005.
- Yang, G. Y., & Slingo, J., 2001. The diurnal cycle in the tropics. *Monthly Weather Review*, 129(4), 784-801.

12.6.5 South America

Case e1. Application of WRF-Chem over the Southeast Brazil, South America

Maria de Fatima Andrade and Edmilson Dias de Freitas

Atmospheric Sciences Department, University of São Paulo, São Paulo, Brazil

Case overview and significance: This study presented a regional air quality forecasting capability for Southeastern Brazil demonstrated for austral summer 2014. The University of Sao Paulo (USP) provided the daily forecast in terms of concentration of Ozone, PM2.5 and PM10 48 hours out into the future. USP's forecasting capability was based on WRF-Chem with the chemical mechanism package option: CBM-Z for gas and MOSAIC for aerosol modeling. The Sao Paulo MASP field campaign provided constraint for aerosol size and composition characterizations. MASP data showed peculiarly large quantity of ethanol prevalent over Sao Paulo perhaps due to vehicular emissions and fuel evaporation. In January and February 2014 Southeastern Brazil experienced anomaly in warmer temperature and smaller amount of precipitation than a baseline 1933-2013 climatology. However, diagnostic analysis of the speciation data pointed to a possible emission estimate deficiency that resulted with a counter-intuition forecast with both over-estimations in nitrogen oxides and ozone in the surface layer. Emission from diesel vehicles and fuel evaporation seemed to be areas warranting further investigation to address this inconsistency.

e1.1 Introduction

There is an Air Quality forecasting Laboratory at the Atmospheric Sciences Department of the Institute of Astronomy, Geophysics and Atmospheric Sciences from the University of São Paulo that provides the forecast of the Ozone and Particles (PM2.5 and PM10) for 48 hours. The forecast is made for the Southeastern part of Brazil. The domain of the simulation is presented in Figure 12.48.

The selected case study represents two months in the summer season in 2014 when the concentration of fine particulate matter (PM2.5) and Ozone (O3) reached high values. These months are not usually associated to the occurrence of high concentration of pollutants but during that year the summer was very dry and with high temperatures facilitating the formation of secondary pollutants.

It was a good case to be analysed due to the lack of precipitation and the high availability of radiation to process the photochemical formation of pollutants. In Figure 12.48b it is presented the location of the air quality stations that provided the data for the comparison between simulated and measured values.

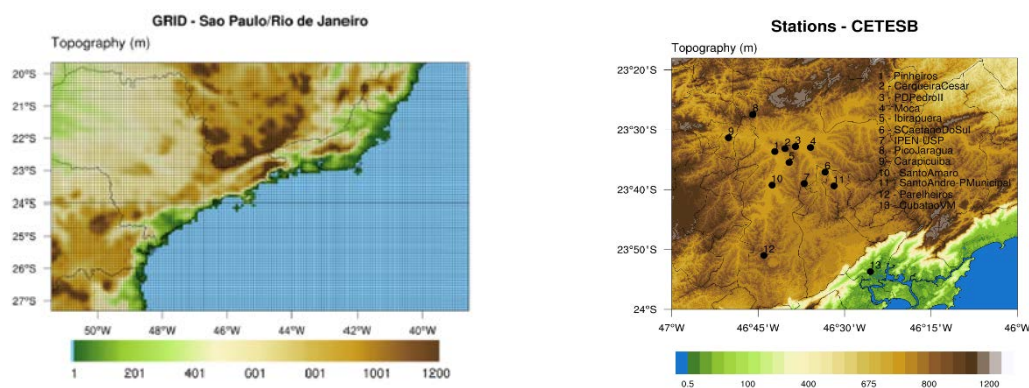


Figure 12.48. a) Area considered in the simulations, showing elevations (m). b) Location of the Air Quality Stations from the Environmental Agency of São Paulo.

The Meteorological Services in Brazil are not committed to present a National Air Quality Forecasting. Most of the forecasts are performed by the universities and the Centro de Previsão do Tempo e Estudos Climáticos from the Institute for Space Research (CPTEC-INPE). Atmospheric Sciences Department from the University of Sao Paulo (ASD-USP) has Air Quality Forecasting Capability. The example that will be presented here is from the ASD-USP, that makes the forecast available in a daily basis at www.lapat.iag.usp.br/.

The case study was for the period of January-February 2014 when there was considerably less precipitation and humidity and high concentration of pollutants in the Southeast region of Brazil. The data considered for the evaluation of the simulation was provided by the Air Quality network from the Environment Agency of Sao Paulo (CETESB). Data related to the mass and number size distribution of aerosol and its composition were from experimental campaigns performed at MASP (Brito et al., 2013; Miranda and Andrade, 2005). Details of this simulation were described by (Andrade et al., 2015).

e1.2 Description of the Modeling Application

[Table 12.6 South America Case e1](#) summarizes the parameterization choices used in the model. The modeling that is being used for Air Quality Forecast at the ASD-USP is the WRF-Chem model (Grell et al., 2005). The chemistry mechanism for the gas phase is the carbon-bond mechanism, version Z (CBM-Z), (Vara-Vela et al., 2016) and the Model for Simulation Aerosol Interactions and Chemistry (MOSAIC, Zaveri et al., 2008) for the description of aerosols. The characteristics intervals for the size distribution of the fine and coarse aerosol were obtained from the cascade impactors sampled in the Metropolitan Area of Sao Paulo (MASP). The composition of the gaseous and particulate compounds were also obtained from experimental campaigns in MASP (Vara-Vela et al., 2016).

e1.3 Anthropogenic Emissions

According to official reports from the CETESB Environmental Agency, the main source of air pollutants in the MASP is the vehicular emission. Due to the lack of detailed emission inventory, experiments were carried out inside traffic tunnels in the city to evaluate the emission factors from the light- and heavy-duty vehicles (Nogueira et al., 2015; Pérez-Martínez et al., 2014). The spatial and temporal distribution of mobile emissions are being performed through an emission model developed in R language (R CORE TEAM, 2017) with open data, as Open street maps, data from Traffic Engineering Company of the Sao Paulo city, and any other available option of emission factors.

The relative fractions of the VOC's emissions from different process were considered based on the same tunnel experiments, considering explicitly the ethanol, formaldehyde and acetaldehyde, due to the large amounts of ethanol emission.

e1.4 Meteorological and Air quality Data

The air quality data was provided by CETESB air quality network and measurements from experimental campaigns from IAG-USP's Laboratory of Atmospheric Process, including Volatile Organic Compounds and particles. To evaluate particle size distributions for mass, number of fine particles, and cloud condensation nuclei, a micro-orifice uniform deposit impactor was employed (Souto-Oliveira et al., 2016), whereas particle concentrations and composition were evaluated with receptor modeling (Andrade et al., 2012).

e1.5 Results from the Simulation for the Summer 2013/2014

During January-February 2014 there was considerably less precipitation and humidity than would be expected on the basis of the historical climatological data (for 1933-2013). During this period the temperature was also above the climatological mean. The quality of the simulation in comparison with direct measurements was evaluated with statistical parameters (Andrade et al., 2015). The strongest and weakest correlations found were for ozone and PM_{2.5} respectively. The high concentrations were associated to the high insolation and lack of precipitation during the period. In Figure 12.49 the comparison between modeled and

simulated values for the IPEN air quality station during January and February is presented. The results showed that there are problems with the representation of the sources. The simulated values for NOx are higher than the measured ones and the ozone is also overestimated by the model. It is important to observe that efforts have been done to improve the sources representation.

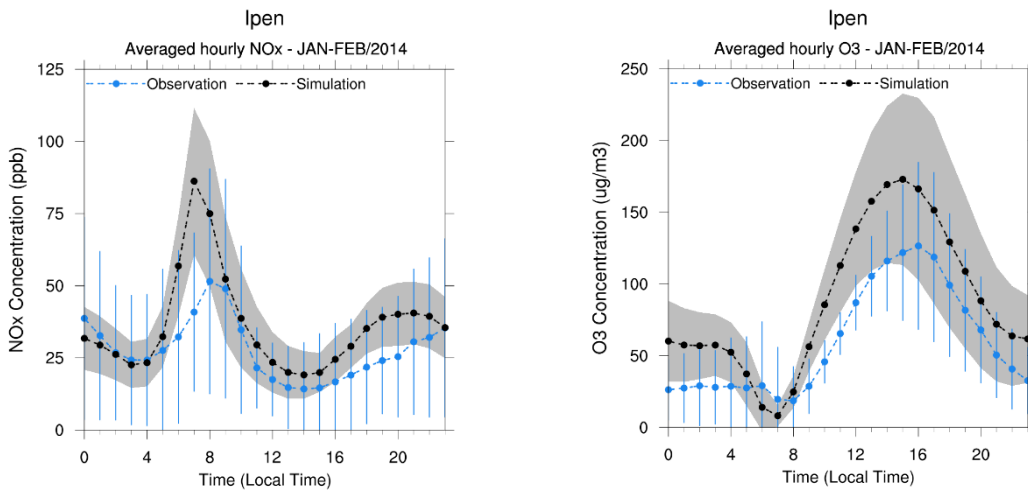


Figure 12.49. Comparison between modeled and simulated values for NOx and O3 at the air quality station IPEN, during the period of January-February 2014.

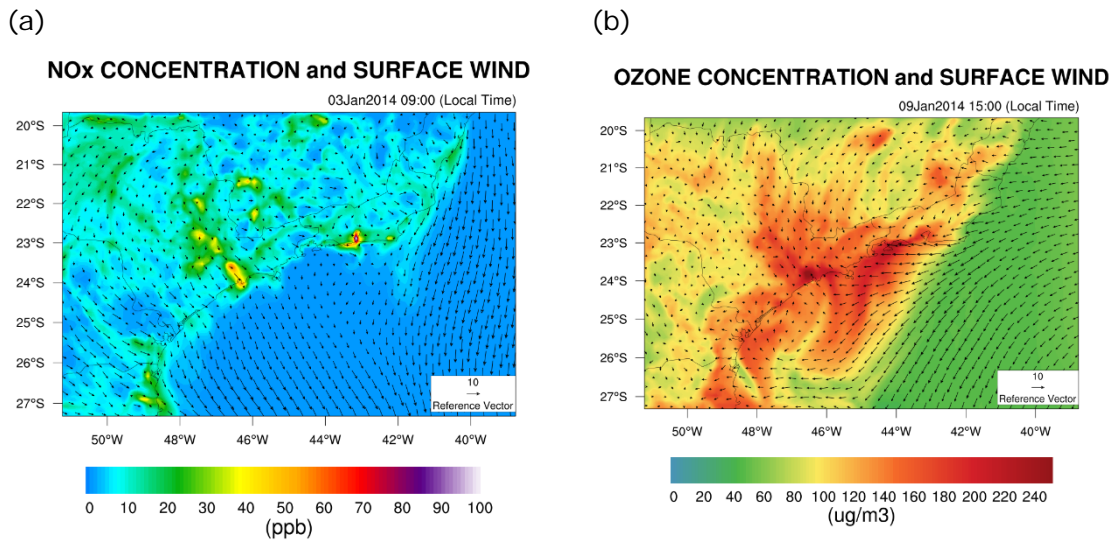


Figure 12.50. (a) Illustration of the NOx at 9 am (Local Time - LT) showing the emission by the vehicular fleet in the region and (b) ozone in the area during the hour of the maximum values (3 pm LT).

In Figure 12.50 it is presented the spatial distribution of NOx and Ozone in the modeled area. The NOx in the region is associated to the vehicular emission. The highest values occurred in the rush hours (as observed in Figure 12.49) at 8 am and 8 pm associated to the commuting of the population to work. NOx is mainly emitted by the diesel vehicles exhaust, according to CETESB, while the COV emissions are associated to the light-duty fleet, from exhaust and evaporative process.

The representation of the emissions by the evaporative process is where we can find a great part of the uncertainties. The evaporative emissions can be associated to the diurnal losses from fuel tanks, running losses or evaporation from the fuel system when the engine is running, hot soak emissions or evaporation from fuel systems after a warm engine is turned off and resting losses or evaporation of fuel after permeation through plastic and rubber components of fuel systems. Due to the high amount of fuel consumed, the contribution from evaporative process can be even higher than from exhaust (Nogueira et al., 2015). However, the representation of this source is not completely adequate in the modeling system.

Person of Contact: Maria de Fatima Andrade, email: maria.andrade@iag.usp.br

References

- Andrade, M. D. F., Ynoue, R. Y., Freitas, E. D., Todesco, E., Vara Vela, A., Ibarra, S., ... Carvalho, V. S. B. (2015). Air quality forecasting system for Southeastern Brazil. *Frontiers in Environmental Science*, 3(February), 1–14. <https://doi.org/10.3389/fenvs.2015.00009>
- Andrade, M., de Miranda, R. M., Fornaro, A., Kerr, A., Oyama, B., de Andre, P. A., & Saldiva, P. (2012). Vehicle emissions and PM_{2.5} mass concentrations in six Brazilian cities. *Air Quality, Atmosphere and Health*, 5, 79–88. <https://doi.org/10.1007/s11869-010-0104-5>
- Brito, J., Rizzo, L. V., Herckes, P., Vasconcellos, P. C., Caumo, S. E. S., Fornaro, a., ... Andrade, M. F. (2013). Physical-chemical characterization of the particulate matter inside two road tunnels in the São Paulo Metropolitan Area. *Atmospheric Chemistry and Physics Discussions*, 13, 20839–20883. <https://doi.org/10.5194/acpd-13-20839-2013>
- Grell, G. A., Peckham, S. E., Schmitz, R., Mckeen, S. A., Frost, G., Skamarock, W. C., & Eder, B. (2005). Fully coupled “online” chemistry within the WRF model, *Atmospheric Environment*, 39, 6957–6975. <https://doi.org/10.1016/j.atmosenv.2005.04.027>
- Kochanski, a. K., Beezley, J. D., Mandel, J., & Clements, C. B. (2013). Air pollution forecasting by coupled atmosphere-fire model WRF and SFIRE with WRF-Chem. *Proceedings of 4th Fire Behavior and Fuels Conference*, February 18-22, 1–12.
- Miranda, R. M., & Andrade, M. F. (2005). Physico-chemical characteristics of atmospheric aerosol during winter in the Sao Paulo Metropolitan area in Brazil. *Atmospheric Environment*, 39(33), 6188–6193. <https://doi.org/10.1016/j.atmosenv.2005.06.055>
- Nogueira, T., Ferreira, K., Souza, D., & Fornaro, A. (2015). On-road emissions of carbonyls from vehicles powered by biofuel blends in traffic tunnels in the Metropolitan Area of Sao Paulo , Brazil. *Atmospheric Environment*, 108, 88–97. <https://doi.org/10.1016/j.atmosenv.2015.02.064>
- Pérez-Martínez, P. J., Miranda, R. M., Nogueira, T., Guardani, M. L., Fornaro, a., Ynoue, R., & Andrade, M. F. (2014). Emission factors of air pollutants from vehicles measured inside road tunnels in São Paulo: case study comparison. *International Journal of Environmental Science and Technology*, (Cetesb 2013). <https://doi.org/10.1007/s13762-014-0562-7>.
- R CORE TEAM (2017). R: A language and environment for statistical computing. R Foundation for Statistical Computing, Vienna, Austria. ISBN: 3-900051-07-0. URL: <https://www.R-project.org/>
- Souto-Oliveira, C. E., Andrade, M. D. F., Kumar, P., Juliano, F., Lopes, S., Babinski, M., ... Paulo, S. (2016). Effect of local and remote sources and new particle formation events on the activation properties of cloud condensation nuclei in the Brazilian megacity of São Paulo. *Atmospheric Chemistry and Physics Discussions*,, <https://doi.org/10.5194/acp-2016-241>
- Vara-Vela, A., Andrade, M. F., Kumar, P., Ynoue, R. Y., & Muñoz, A. G. (2016). Impact of vehicular emissions on the formation of fine particles in the Sao Paulo Metropolitan Area : a numerical study with the WRF-Chem model, *Atmospheric Chemistry and Physics*, 16, 777–797. <https://doi.org/10.5194/acp-16-777-2016>
- Zaveri, R. a., Easter, R. C., Fast, J. D., & Peters, L. K. (2008). Model for Simulating Aerosol Interactions and Chemistry (MOSAIC). *Journal of Geophysical Research: Atmospheres*, 113(April 2007), 1–29. <https://doi.org/10.1029/2007JD008782>

Case e2. Particulate Matter forecasting capability in Peru

Odón R. Sánchez-Ccoyllo

Universidad Nacional Tecnológica de Lima Sur (UNTELS), Lima, Perú

Case overview and significance: Peru's Ministry of the Environment had tightened the national ambient air quality standards (NAAQS): 100 $\mu\text{g m}^{-3}$ for PM10 and 50 $\mu\text{g m}^{-3}$ for PM2.5 the 24-hour primary standards. This NAAQS update was among other policies attempted to rein in pollution. A WRF-Chem based air quality modeling system was built to help reconstructing some of the pollution episodes in Lima, Peru. Optimal physical packages were selected in WRF-Chem. However, only vehicular emissions were considered for this initiative application of the WRF-Chem system for Peru (Sánchez-Ccoyllo et al., 2018). The forecast showed there existed strong correlation between the vehicular traffic and pollutant concentration clustered around rush hours across Lima-Callao.

e2.1 Introduction

The establishment of the National Ambient Air Quality Standards (NAAQS) of the Peru was approved in 2017 by Ministerio del Ambiente del Peru (Ministry of the Environment of Peru) that particulate matter less than 10 μm in diameter (PM10) and PM2.5 for 24 hours is 100 $\mu\text{g m}^{-3}$ and 50 $\mu\text{g m}^{-3}$ respectively. The selected study case represents one high surface PM10 and PM2.5 concentration case over Metropolitan area of Lima, Peru.

e2.2 General Description of the Model

Table 12.6 South America Case e2 summarizes the parameterization choices used in the model. The Weather Research and Forecasting model coupled with chemistry (WRF-Chem) is an online meteorology-chemistry model, which is widely used in air quality and atmospheric chemistry applications (Grell et al., 2005; Bahreini et al., 2018). The model includes multiple gas and aerosol chemistry parameterizations with varying levels of complexity, photolysis and removal (dry and wet) mechanisms (Bahreini et al., 2018).

e2.3 Parameterizations Choices

Table 12.6 Case e2 summarizes the parameterization choices in WRF-Chem version 3.8.1 for the meteorological and chemical of the numerical simulation system. In an operational forecasting system, it included only anthropogenic vehicular emission inventory (Vara et al., 2016; Andrade et al., 2015). The meteorological fields predicted by Global Forecast System (GFS) with 0.250 resolution horizontal is routinely used (<https://rda.ucar.edu/datasets/ds084.1/#!access>) for input to wrf-chem model version 3.8.1.

e2.4 Chemical Transport, Transformation, Removal and Fate of Air Pollutants Aerosol direct effect through interaction with atmospheric radiation, photolysis, and microphysics routines. More detail see user's guide for wrf-chem.

e2.5 Lessons learned: Emission and PBL Dynamics

We have learned much from daily evaluation with measures statistics of forecasting accuracy. The two decisive classes of modeled processes determining air quality forecast accuracy are: (1) emission fluxes, and (2) planetary boundary layer (PBL) dynamics.

Run script and input data for Base and Sensitivity Cases

The following files are given in the Supplementary Material: (a) WPS and WRF name list (b) wrf-chem run script. The one emission set-ups are: (Case base) wrf-chem operations.

e2.6 Results and Discussion

A case analysed was March 25 2018 over Metropolitan Area of Lima-Callao. Figure 12.51 shows the PM10 concentration and surface wind performed around 37 hours after the started run model forecast. That is available at web site of SENAMHI-Peru (<http://www.senamhi.gob.pe/?p=calidad-de-aire-numeric>). It observed high concentration of PM10 forecast at around the Metropolitan area of Lima-Callao, it because mainly vehicular emission in the urban area of Metropolitan area of Lima-Callao.

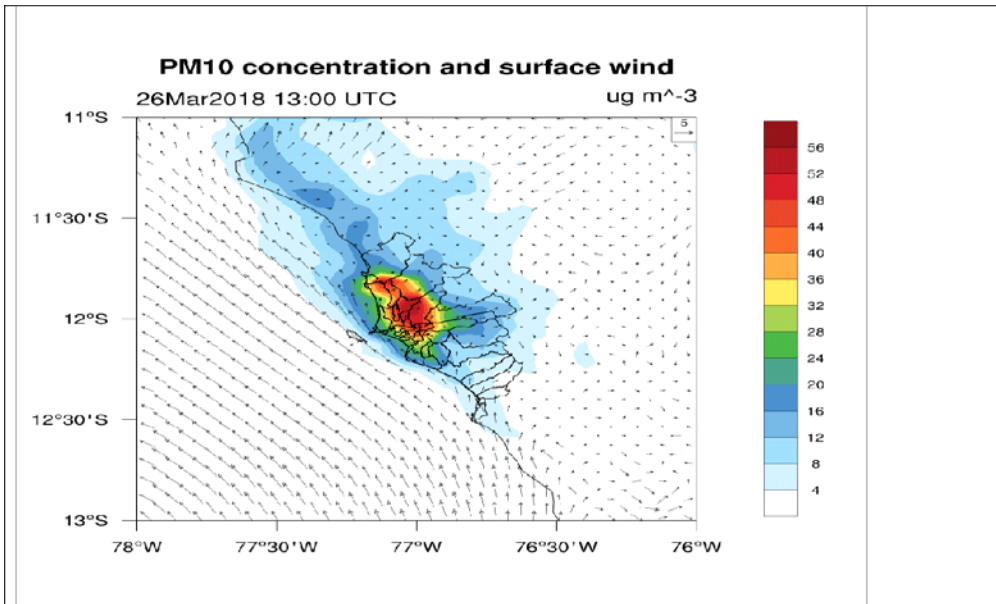


Figure 12.51. PM10 and surface wind 2nd day forecast for March 25, 2018, 1300:00 UTC by operational.

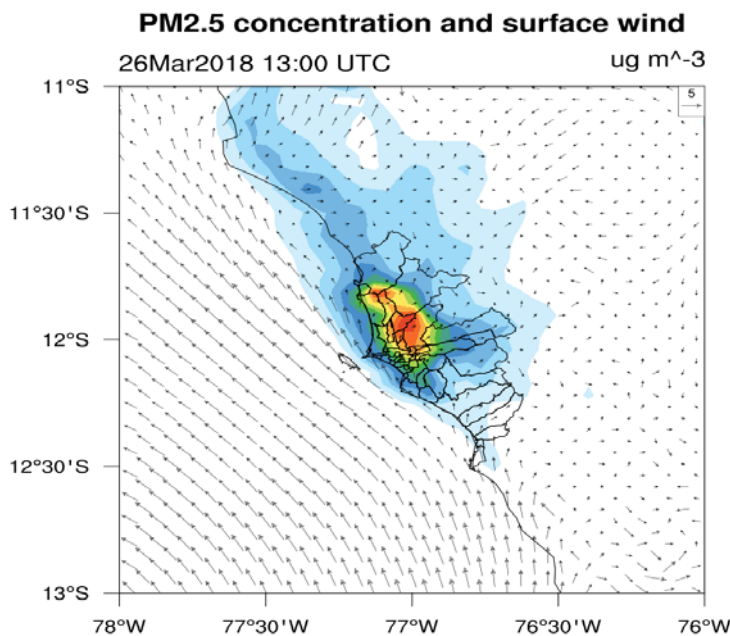


Figure 12.52. PM2.5 and surface wind 2nd day forecast for March 25, 2018, 1300:00 UTC by operational.

Source: SENAMHI (<http://www.senamhi.gob.pe/?p=calidad-de-aire-numeric>).

Figure 12.52 shows the PM_{2.5} concentration and surface wind performed around 37 hours after the started run model forecast. That is available at web site of SENAMHI-Peru (<http://www.senamhi.gob.pe/?p=calidad-de-aire-numeric>). It observed also high concentration of PM_{2.5} forecast at around the Metropolitan area of Lima-Callao, it because mainly vehicular emission in the urban area of Metropolitan area of Lima-Callao.

Person of Contact: Odón R. Sánchez-Ccoyllo, email: osanchezbr@gmail.com

References

- Andrade, R. Ynoue, E. Dias, T. E., A. Vara, S. Ibarra, L. Dropinchinski, J. Martins and V. Barreto, "Air quality forecasting system for southeastern Brazil," *Frontiers in Environmental Sciences*, 23, 1-14, doi.org/10.3389/fenvs.2015.00009,, 2015.
- Bahreini, R., Ahmadov, R., McKeen, S. A., Vu, K. T., Dingle, J. H., Apel, E. C., Blake, D. R., Blake, N., Campos, T. L., Cantrell, C., Flocke, F., Fried, A., Gillman, J. B., Hills, A. J., Hornbrook, R. S., Huey, G., Kaser, L., Lerner, B. M., Mauldin, R. L., Meinardi, S., Montzka, D. D., Richter, D., Schroeder, J. R., Stell, M., Tanner, D., Walgea, J., Weibring, P., and Weinheimer, A.: Sources and Characteristics of Summertime Organic Aerosol in the Colorado Front Range: Perspective from Measurements and WRF-Chem Modeling, *Atmos. Chem. Phys.*, 18, 8293–8312, 2018
<https://doi.org/10.5194/acp-18-8293-2018>.
- Sánchez-Ccoyllo, O., Ordoñez-Aquino, C., Muñoz, A., Alan Llacza, A., Andrade, M., Liu, Y., Reátegui, W. and Brasseur, G. (2018) Modeling Study of the Particulate Matter in Lima with the WRF-Chem Model: Case Study of April 2016. *International Journal of Applied Engineering Research*, 13, 10129-10141.
- Vara, M. Andrade, P. Kumar, R. Ynoue and A. Muñoz, "Impact of vehicular emissions on the formation of fine particles in the Sao Paulo Metropolitan Area: a numerical study with the WRF-Chem model," *Atmospheric Chemistry. Physics.*, 16, pp. 777-797, doi:10.5194/acp-16-777-2016, 2016.

12.6.6 Oceania

Cases f1-f3. Numerical air quality forecasting of the May 2016 fires in the Sydney, Australia regionMartin Cope¹ and Hiep Duc²¹ Climate Science Center, Ocean & Atmosphere, CSIRO, Aspendale Victoria, Australia² Science Division, NSW Office of Environment and Heritage, Sydney, Australia

Case overview and significance: The Australian Bureau of Meteorology is keen on *understanding the causes and magnitudes of elevated health risk of the Sydney populace by hazard reduction burning (HRB). In particular the bureau spearheaded a multiple agency study on the 2016 Mother's Day weekend HRB-induced smoke that was attributed the cause of significant adverse health consequences. The study focused over the Greater Metropolitan Sydney Region (GMR) across two back-to-back smoke events in May 2016: (a) 2-10, and (b) 14-15. Both Eulerian-framework models such as AQFx and Lagrangian-framework models such as the Rural Fire Service's HYSPLIT-like tracer transport model were used. In biomass smoke emission from HRB, sophisticated emission forecasting models with various capability accounting for fuel type, dynamically available loadings, burn scar, and flaming and smoldering pyrolysis were exploited: cases in point are the OSEFS and C-SEM emission models. The study concluded a stunning 500% exceedance of CO emission (a proxy for biomass burn emission) by HRB than to all anthropogenic sources combined in the GMR. The study also identified potential uncertainties in the modeling systems through the exploitation of satellite-based observations. Australia's systematic and concerted effort in mobilizing multiple government bureaus to advance knowledge about HRB and biomass burning is establishing cutting edge science.*

f1.1 Introduction

Hazard reduction burning (HRB) is widely used in Australia as a technique for reducing the risk of large wildfire development. In the southern states, HRB is usually undertaken in the autumn months when the prevalence of stable, slow moving synoptic high-pressure systems and moderate ambient temperatures and fuel moisture support the planning and management of landscape fires. However, HRB can also lead to the attendant risk of poor air quality and the exposure of significant populated regions to fine particle pollution. Such an event occurred in Sydney (over 4 million people), Australia in May 2016 when smoke from hazard reduction burns were implicated with poor air quality across the airshed. The period surrounding the Mother's Day weekend (6–9 May 2016) was of note- with high concentrations of smoke over Sydney being widely reported in the media. Concerns regarding the health impacts of the smoke exposure were investigated by Broome, Johnstone et al. (2016) who estimated that elevated concentrations of PM_{2.5} resulting from hazard reduction burning around Sydney led to between 5 and 23 premature deaths, and an increase in cardiovascular and respiratory hospitalizations.

To help manage the risk of smoke exposure from HRB, Australian land management agencies have been investing in the science and application of chemical transport models for air quality forecasting. For example, the Australian Bureau of Meteorology operates AQFx with a current focus on the southern-states Australian states; the NSW Office of Environment and Heritage OEHS Smoke Emission Forecasting System (OSEFS) is used as part of a suite of methodologies to aid in air quality forecasting in the state of NSW; the NSW Rural Fire Service (RFS) operate a high resolution meteorological forecasting and tracer transport model.

In the case study presented below, we stress test the AQFx model by modeling two periods of high smoke concentrations and complex meteorology (2–10 and 14–25 May 2016). The purpose of such testing is to identify, and where possible, correct biases in the model forecasts. Such an approach should lead to steady improvements in the robustness, accuracy and utility of the system.

f1.2 Description of the Model

Table 12.7 Oceania Cases f1-f3 summarize the parameterization choices used in the model. AQFx is a three-tiered numerical smoke forecasting system. The first tier delivers an ensemble forecast of fire weather and fire danger indices extending over a 5–10 day outlook. The second tier is a traditional AQF system, which delivers a multi-species air quality forecast for the Australian region for a 24–72 hour outlook, and the third tier delivers a tagged tracer forecast for any likely HRB within 24 hour outlook.

Here we focus on the second tier of AQFx which comprises a Chemical Transport Model (CTMs), (Lawson et al., 2017)) which is run offline using meteorological fields generated from the Bureau's Australian Community Climate and Earth-System Simulator (ACCESS) 3. C-CTM treats gas-phase photochemistry using the Carbon Bond V chemical mechanism (Yarwood et al., 2005). Inorganic aerosol partitioning is modeling using ISORROPIA-II (Fountoukis and Nenes 2007), and organic aerosol partitioning is modeling using the volatility basis set approach (Tsimpidi et al., 2014). C-CTM can either be run in a two-bin configuration (PM_{2.5}, PM_{2.5-10}), or coupled to GLOMAP (Mann et al., 2010), a 2-moment, multi-mode, multi-component aerosol model. Tracer advection is undertaken using the Walcek scheme (Walcek, 2000), tracer diffusion and wet and dry deposition follows the approaches in Hysplit (Stein et al., 2015).

C-CTM is limited area and thus one-way nesting is used to focus on a region of interest. For example, Figure 12.53 shows the 3-grid configuration used by AQFx to forecast air pollution in the Sydney region. Data from the ACCESS regional forecasts (ACCESS-R, ~15 km grid spacing) and the city-scale forecast for Sydney (ACCESS-C 1–3 km grid spacing) are used drive the estimates of meteorologically dependent emission fields such as volatile organic compound (VOC) emissions from vegetation; plume rise from buoyant industrial sources; and evaporative emissions from motor vehicles. Anthropogenic emissions are sourced from the NSW EPA and OEH 2008 air emissions inventory⁴. Biogenic VOCs, ammonia, sea salt aerosol, NO_x and ammonia from soils are all calculated by C-CTM inline as the forecast advances. The treatment of emissions from hazard reduction burns is discussed in the next section.

f1.3. Smoke Emissions from Hazard Reduction Burns

The emissions of smoke from HRBs are estimated using C-SEM, a model which can be configured to either run in a forecasting mode forced by Phoenix Rapid-fire, a prognostic fire behavior model (Tolhurst, Chong et al. 2007), or run in a diagnostic mode for case studies using after-the-event information including the area burned and the time period for which flaming combustion of fuels was underway. In either case C-SEM relies on information about the loading of fine ($d < 6 \mu\text{m}$), and coarse woody debris (CWD, $6 \mu\text{m} < d < 50 \mu\text{m}$), the fuel burning efficiency and patchiness (Meyer et al., 2008), and observations of the emission rates of smoke-related gases and aerosols from flaming and smoldering pyrolysis (Andreae et al., 1988; Akagi et al., 2013). Smoke from the flaming component of a HRB is injected at the top of the boundary layer and emissions from smoldering pyrolysis are mixed into the surface layer.

³ http://www.bom.gov.au/charts/about/about_access.shtml

⁴ <http://www.epa.nsw.gov.au/air/airinventory.htm>

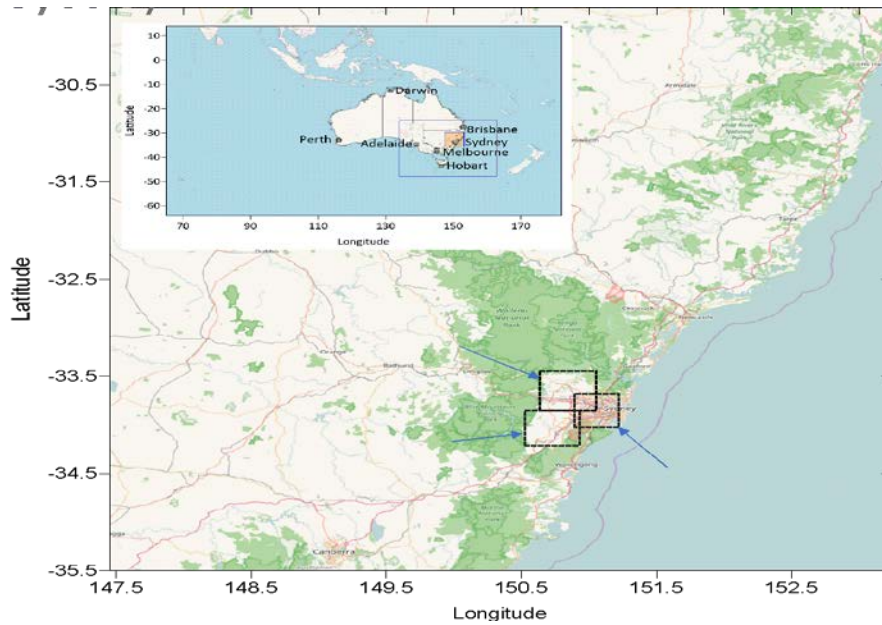


Figure 12.53. The 3-grid configuration used by AQF to model air pollution Australian region, focusing on greater Sydney.

The outer domain (see inset) has a grid spacing of 0.27° and includes, Australia, New Zealand and Papua New Guinea. The second domain has a grid spacing of 0.09° and covers south-eastern Australia. The third domain has a grid spacing of 0.03° and includes the Greater Metropolitan Sydney Region (GMR).

For the May 2016 case study, C-SEM was run in diagnostic mode with fire scar data provided by the NSW Rural Fire Service. Figure 12.54 shows the time series of carbon monoxide emission estimates from the HRBs for the inner AQF domain for 2–10 May 2016. The carbon monoxide emissions from the fires peak early afternoon on each day as fine fuels are ignited and are followed by a long tail of emissions from the smoldering of coarse woody debris. Total surface-based anthropogenic emissions for the GMR are also plotted for comparison and suggest that the emissions from the hazard reduction burns exceeded the ground level emissions for the entire Sydney region by about a factor of five.

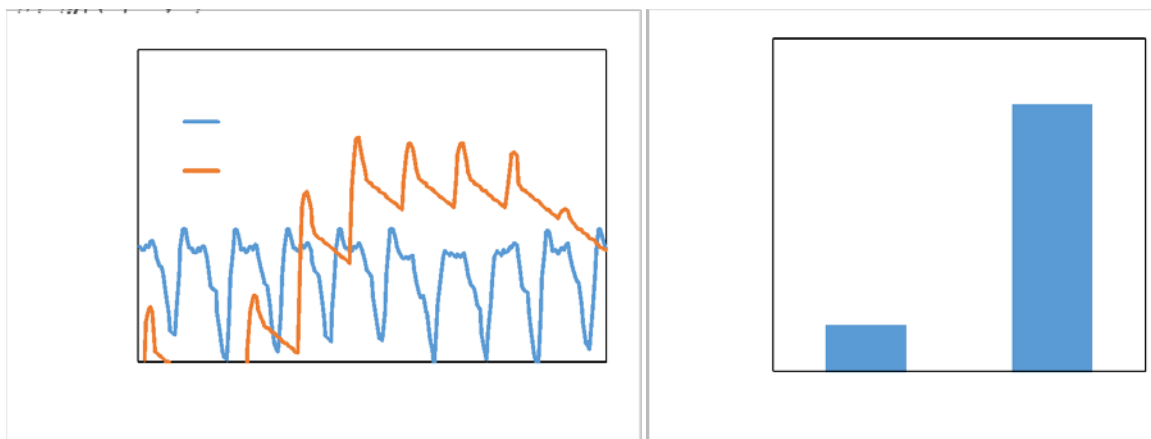


Figure 12.54. Left- hourly time series of carbon monoxide emissions estimated for the hazard reduction burns and for all other anthropogenic ground sources in the Greater Sydney Region 2-10 May 2016.

Right- total carbon monoxide emissions summed across the same period.

f1.4 Model Results for PM2.5

Figures 12.55 a and b show the observed and modeled near surface PM2.5 concentrations for the two study periods. The spatial plots show the locations of the largest prescribed burns, with AQFx predicting average concentrations of $5 \mu\text{g m}^{-3}$ to greater than $50 \mu\text{g m}^{-3}$ within the vicinity of each burn. AQFx is biased to some under prediction when comparing the observed and modeled concentrations in the spatial plots, with a larger bias apparent for the 14–25 May study period.

Figure 12.55c shows the time series of Sydney average 24-h PM2.5 concentration and demonstrates that that AQFx has captured the first smoke event (7 and 8 May), however has under predicted the magnitude of the event by about 30% when averaged across all stations and modeled days. Figure 12.55c also shows that AQFx has predicted the highest PM2.5 concentrations for the observed day of the second smoke event (May 22) but has under predicted the magnitude of the PM2.5 concentrations (40% average under prediction).

f1.5 Identifying and Reducing Uncertainties

Our analysis of the modeling results for the May 2016 case study suggests that biases in the modeled PM2.5 are in part due to uncertainties in the modeled meteorology- leading to smoke plume trajectory errors. Figure 12.56 shows how biases in the near-surface wind fields contributed to the model missing a PM2.5 smoke event observed in Sydney on 19th May. Over the Sydney region the near surface winds for both hours indicate a north-westerly flow pattern while the forecast winds are from the west to south-west. Imagery from the Himawari satellite (geostationary, 1–2 km resolution, 10-minute updates) show the transport of a smoke plume to the south-east and then to the south- resulting in observed high concentrations of PM2.5 over the Sydney region. On the other hand, the modeled smoke is transported to the north of Sydney and thus the observed smoke impact over Sydney is missed. We are fortunate that the OSEFS is now deployed and will provide a second air quality forecast. Additionally, the Bureau of Meteorology have been testing a high-resolution rapid update cycle configuration of ACCESS which in the future may provide additional meteorological forecasts which could be used for an ensemble AQF.

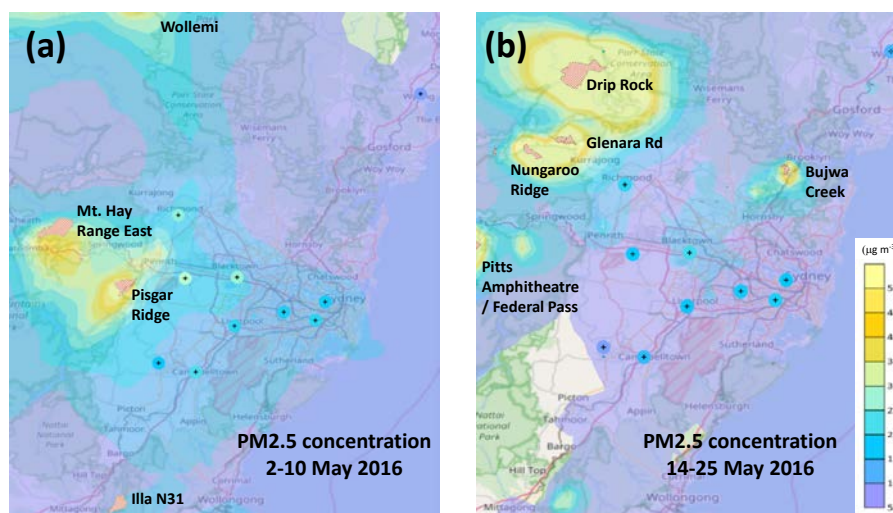
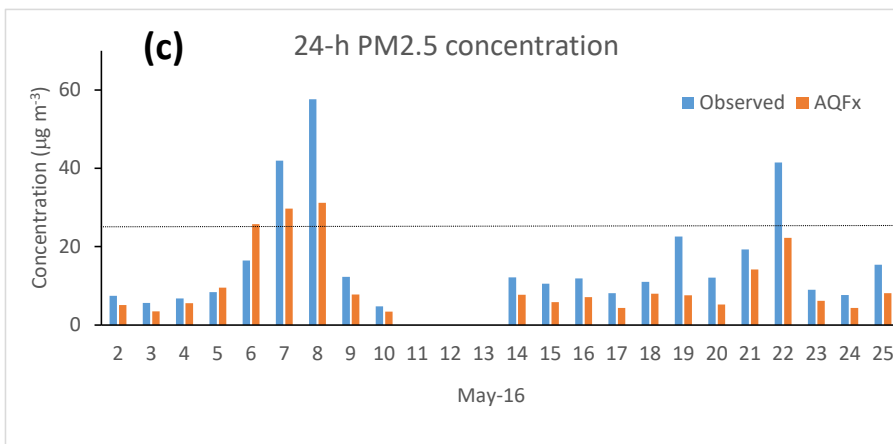


Figure 12.55. (a) The modeled average PM2.5 concentration for the Sydney region for 2-10 May 2016, with the most significant hazard reduction burns also shown and named. The observed PM2.5 concentrations are represented by the colored circles. The horizontal spatial scale is about 100 km. (b) the same except for 14-25 May 2016.



(c) The Sydney region average observed and modeled 24-h concentration time series for the two study periods. The national air quality standard of $25 \mu\text{g m}^{-3}$ for $\text{PM}_{2.5}$ is also shown.

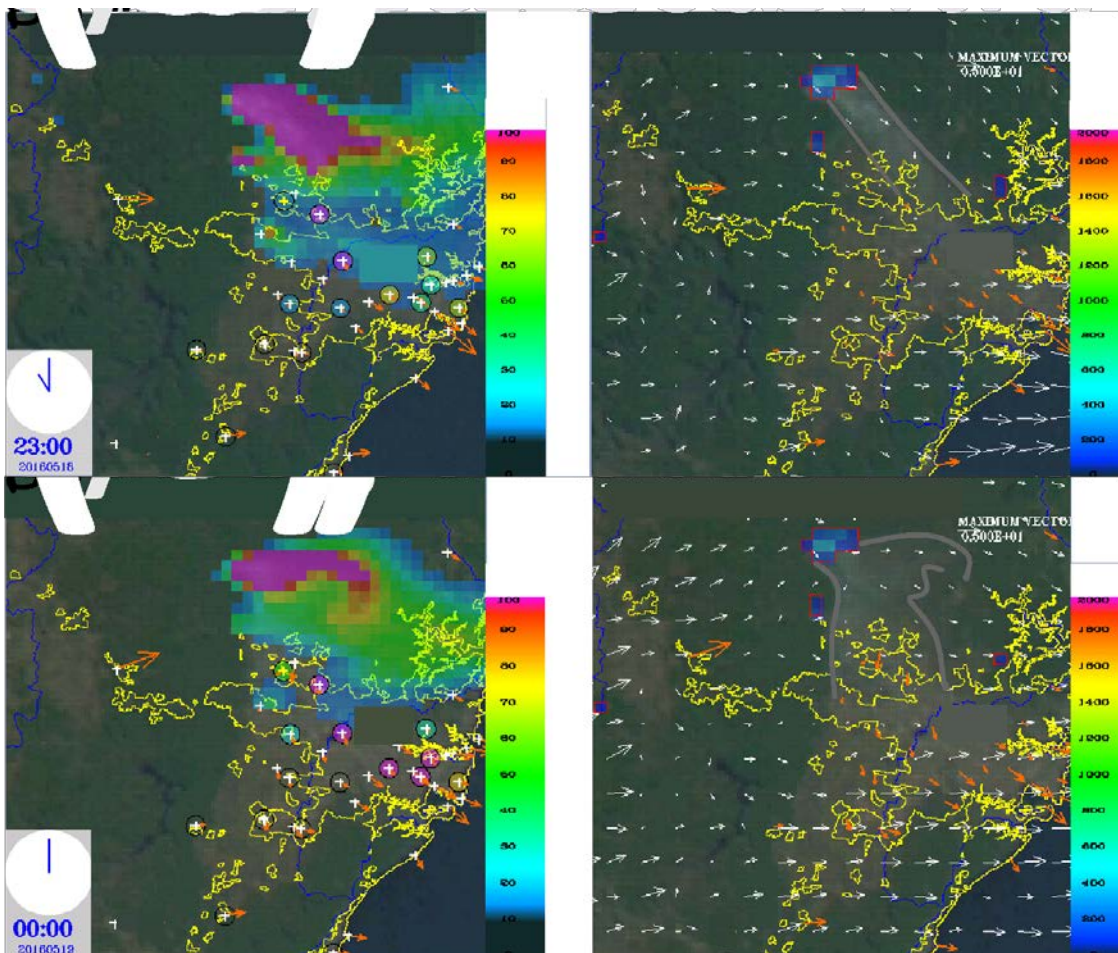


Figure 12.56. Output from the AQFx diagnostic tool showing (a, c) modeled and observed (filled circles) near-surface 1-h $\text{PM}_{2.5}$ concentrations; (b, c) fire locations (red polygons), Himawari smoke plume envelopes (gray lines); forecast wind field (white vectors); observed winds (orange vectors). Times are in UTC and the horizontal spatial scale is about 100 km.

It is also likely that the modeled regional background $\text{PM}_{2.5}$ concentrations may be biased low because the existing smoke emission methodology is not capturing the many small private land burns (i.e. stubble burning) that were also taking place during the May 2016 hazard reduction burns. Figure 12.57 shows VIIRS (reference) hot spot imagery for May 2016 for a region in NSW, which extends 300 km to the west of Sydney. The farming areas to the west of the Blue Mountains are dotted by hundreds of fires, which in total are likely to sum to a significant flux of smoke into the lower atmosphere. Extension of the smoke emissions layer to include a VIIRS (and MODIS) hot spot database has recently been completed and thus the contribution of stubble burns to regional $\text{PM}_{2.5}$ concentrations can now be assessed.

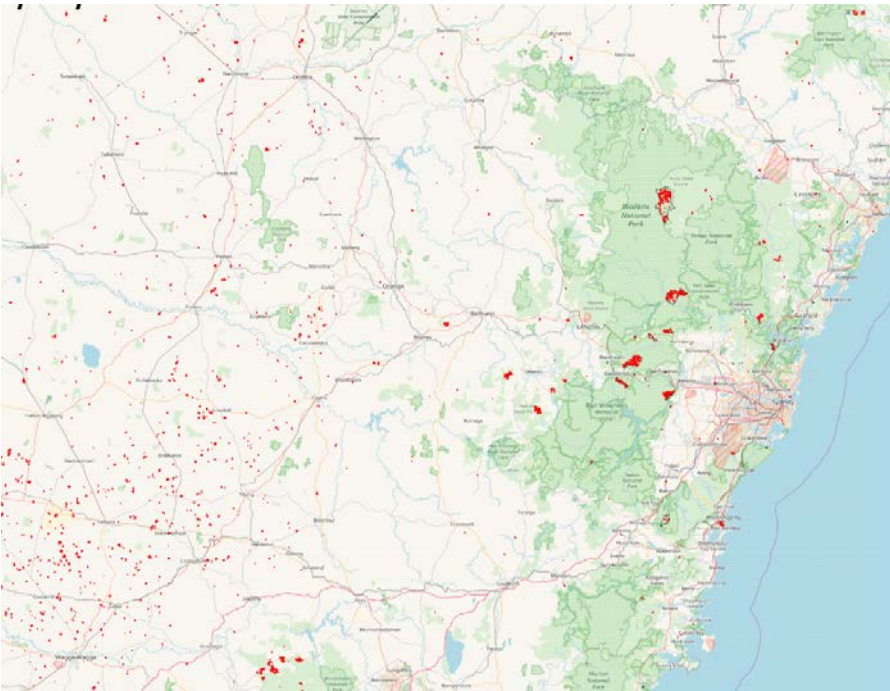


Figure 12.57. VIIRS satellite hotspots (red) for May 2016. The horizontal scale is 300 km.

Person of Contact: Martin Cope, email: Martin.Cope@csiro.au

References

- Akagi, S. K., R. J. Yokelson, I. R. Burling, S. Meinardi, I. Simpson, D. R. Blake, G. R. McMeeking, A. Sullivan, T. Lee, S. Kreidenweis, S. Urbanski, J. Reardon, D. W. T. Griffith, T. J. Johnson and D. R. Weise (2013). "Measurements of reactive trace gases and variable O-3 formation rates in some South Carolina biomass burning plumes." *Atmospheric Chemistry and Physics*, 13(3): 1141-1165.
- Andreae, M. O., E. V. Browell, M. Garstang, G. L. Gregory, R. C. Harriss, G. F. Hill, D. J. Jacob, M. C. Pereira, G. W. Sachse, A. W. Setzer, P. L. S. Dias, R. W. Talbot, A. L. Torres and S. C. Wofsy (1988). "Biomass-Burning Emissions and Associated Haze Layers over Amazonia." *Journal of Geophysical Research-Atmospheres*, 93(D2): 1509-1527.
- Broome, R. A., F. H. Johnstone, J. Horsley and G. G. Morgan (2016). "A rapid assessment of the impact of hazard reduction burning around Sydney, May 2016." *Medical Journal of Australia*, 205(9): 407-408.
- Fountoukis, C. and A. Nenes (2007). "ISORROPIA II: a computationally efficient thermodynamic equilibrium model for K^+ - Ca^{2+} - Mg^{2+} - NH_4^+ - Na^+ - SO_4^{2-} - NO_3^- - Cl^- - H_2O aerosols." *Atmospheric Chemistry and Physics*, 7(17): 4639-4659.
- Lawson, S. J., M. Cope, S. Lee, I. E. Galbally, Z. Ristovski and M. D. Keywood (2017). "Biomass burning at Cape Grim: exploring photochemistry using multi-scale modeling." *Atmospheric Chemistry and Physics*, 17(19): 11707-11726.
- Mann, G. W., K. S. Carslaw, D. V. Spracklen, D. A. Ridley, P. T. Manktelow, M. P. Chipperfield, S. J. Pickering and C. E. Johnson (2010). "Description and evaluation of GLOMAP-mode: a modal global aerosol microphysics model for the UKCA composition-climate model." *Geoscientific Model Development*, 3(2): 519-551.
- McGregor, J. L. and M. R. Dix (2008). "An updated description of the Conformal-Cubic atmospheric model." In *High Resolution Numerical Modeling of the Atmosphere and Ocean*: 51-75.
- Meyer, C. P., A. K. Luhar and R. M. Mitchell (2008). "Biomass burning emissions over northern Australia constrained by aerosol measurements: I—Modeling the distribution of hourly emissions." *Atmospheric Environment*, 42(7): 1629-1646.
- Paugam, R., M. Wooster, S. Freitas and M. V. Martin (2016). "A review of approaches to estimate wildfire plume injection height within large-scale atmospheric chemical transport models." *Atmospheric Chemistry and Physics*, 16(2): 907-925.
- Stein, A. F., R. R. Draxler, G. D. Rolph, B. J. B. Stunder, M. D. Cohen and F. Ngan (2015). "Noaa's Hysplit Atmospheric Transport and Dispersion Modeling System." *Bulletin of the American Meteorological Society*, 96(12): 2059-2077.
- Tolhurst, K., D. Chong and A. Pitts (2007). PHOENIX - a dynamic fire characterization simulation tool. Bushfire CRC Fire Behaviour Workshop, Hobart, Australia, September 18 2007.
- Tsimpidi, A. P., V. A. Karydis, A. Pozzer, S. N. Pandis and J. Lelieveld (2014). "ORACLE (v1.0): module to simulate the organic aerosol composition and evolution in the atmosphere." *Geoscientific Model Development*, 7(6): 3153-3172.
- Walcek, C. J. (2000). "Minor flux adjustment near mixing ratio extremes for simplified yet highly accurate monotonic calculation of tracer advection." *Journal of Geophysical Research-Atmospheres*, 105(D7): 9335-9348.
- Yarwood, G., S. Rao, M. Yocke and G. Z. Whitten (2005). Updates to the carbon bond mechanism: CB05. Report to the U.S. Environmental Protection Agency.
<http://www.camx.com>

12.6.7 Africa

Cases g1.1-1.2. Application of RegCM-CHEM4.5 for dust storm and air quality forecast over southern Africa

Melaku Tesfaye Yigiletu

South African Weather Service, Pretoria, South Africa

Case overview and significance: The wide spectrum of emission sources and meteorological variability over the vast territories of Africa poses unique challenges to air managers. This study superbly demonstrated some of such challenges over Southern Africa during austral winters. Austral winter in South Africa is often dry and windy subject to outbreaks of forest fire and wind-blown dust storms causing abrupt and considerable deterioration on air quality. The South African Weather Service (SAWS) has developed an ambient air quality forecasting capability for South Africa basing on the RegCM-CHEM4.5 model to forecast O₃, CO, BC, and wind-blown dust. The RegCM-CHEM4.5 model has the option for a non-hydrostatic dynamical core for fine horizontal resolution likely necessary for the online handling of dynamical dust, sea-salt and intricate circulation around large biomass burns. The lack of emission database was worked around by using a 1990-2010 integrated emission climatology. Static chemical boundary condition obtained from ICTP was complemented by 6 hourly output of the MOZART global chemical transport model. The RegCM-CHEM4.5 model forecast for August 22 2017 over South Africa was studied. The forecast skillfully captured the poor air quality episode resulted from perennial savannahs and grassland fires there accounted by climatology, and from successful reconstruction of heatwave and anticyclonic advection of polluted air from northern South Africa. The lack of emission database in South Africa and her laboring countries was a significant holdback in forecast accuracy. To its resolution, international and regional efforts are warranted.

g1.1 Introduction

Africa has a substantial amount of land mass in both the southern and northern hemispheres. Trace gas and aerosol emissions from this vast continent have important climatic, health and environmental implications. Geographically speaking, southern Africa is most frequently described as the region south of approximately 10° S. Most of southern Africa is situated in the subtropics experiencing dry and windy winters as well as hot and humid summers. Besides emissions from industrial activities, which fluctuate little throughout the year; during the dry austral winter season, emission from biomass burning events are high over most areas of southern Africa (Tesfaye et al., 2014a). Furthermore, although dust activity in Africa occurs year round (especially over the northern parts of the continent), the peak dust activity over southern Africa occurs during the winter season, when soils are dry and surface wind speeds are at a maximum (Tesfaye et al., 2015). As a result of the aforementioned simultaneous events, during austral winter season (June to September), most of the southern Africa regions experience strong air quality deterioration. This case study aims to briefly exhibit the combined air quality effects of anthropogenic, biomass burning and desert dust emissions in southern Africa (see Figure 12.58). This case study is conducted at the South African Weather Service (SAWS), and its main focuses are forecast products of surface level ozone (O₃), carbon monoxide (CO), black carbon (BC) and dust storm, on 22 August 2017.

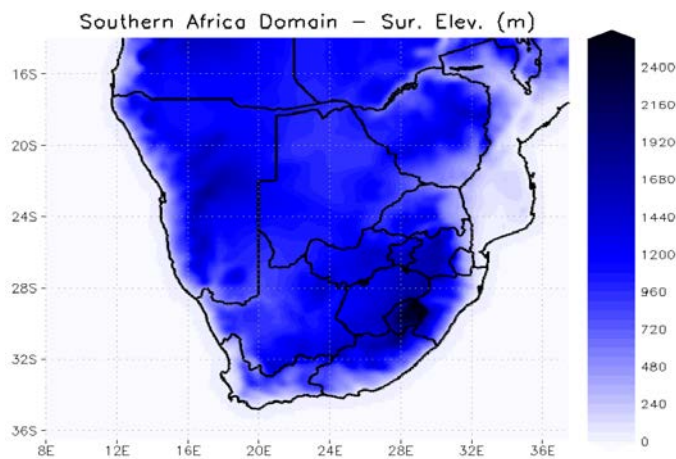


Figure 12.58. Southern Africa air quality forecast model domain and topography (unit: m).

South Africa is one of the most industrialized regions of the continent, accordingly emissions from various industrial activities are much higher when compared with other countries on the continent. Besides these, South Africa experiences both trace gas and aerosol emissions from different anthropogenic activities, biomass burning events and dust load from southern Africa desert regions via anticyclonic surface air circulation (Tesfaye et al., 2016). Accordingly, the effect of South African air quality deterioration on health, environment, ecological resources and socio-economic activities has become one of the major concerns of the country. Recently, the South African Department of Environmental Affairs (SA-DEA) mandated the SAWS to establish ambient air quality forecast products as well as services in provision of scientifically quantified information to decision makers and resource managers. Currently, SAWS is conducting regional optimization of coupled climate–chemistry modeling system, and soon it is expected to be deployed for a national air quality forecast as well as for other services. SA-DEA is also completing the SA industrial emissions compilation system. This case study – besides showing the combined effects of different emission sources on air quality – also provides important insights to the possibilities of using integrated emission climatology, during the absence of well-established regional/national emission database.

g1.2 RegCM-CHEM4.5 Model

g1.2.1 General Description of the Model

Table 12.8 Africa Case g1 summarizes the parameterization choices used in the model. In this case study, RegCM-CHEM4.5 model is used. The RegCM-CHEM is online coupled climate–chemistry model. The climate component of the coupled model is the RegCM4.5, a model developed at the Abdus Salam International Center for Theoretical Physics (ICTP) (Giorgi et al., 2012). RegCM4.5 comprises both Mesoscale Model (MM5) hydrostatic and non-hydrostatic dynamical cores, with sigma vertical coordinate system. The hydrostatic core is cheaper computationally, but physically it should be limited to a resolution greater than 20 km. For higher resolutions, the non-hydrostatic core is preferable. Under the current model configuration, the initialization and boundary conditions prepared for non-hydrostatic core cannot be used for the hydrostatic run. The non-hydrostatic can be nested into both hydrostatic and non-hydrostatic domains, however the hydrostatic can only be nested into hydrostatic core. There are no strict rules in RegCM domain and resolution selections; rather this process is usually determined by the area of interest, nature of the problem and the availability of computing resources. Generally, the model resolution should be high enough to allow the model to develop its own circulations, to include all relevant forcing processes and to capture local processes of interest. The computational cost increases rapidly with resolution, domain size as well as on model internal time-steps used to trigger internal parametric schemes; thus, one needs to make compromises based on experience and experimental trials. Being a limited area model, RegCM-CHEM4.5 requires the provision of meteorological initial and time dependent lateral boundary conditions as well as chemical boundary conditions. These are obtained from global climate model simulations, which thus drive the regional climate model. Furthermore, the chemical emission data are crucial for running the coupled model.

The model contains several options for the parameterization of model physics, and it is well known that there is no scheme that works best everywhere. Hence one needs to run some experiments with different schemes and conduct tuning on some scheme parameters before finding out the best model set-up for the area of interest. By solving the tracer mass continuity equation within the RegCM dynamical core, the model can simulate atmospheric processes, surface emission, transportation, physico-chemical transformations, and removal processes of different aerosols (Solmon et al., 2006), gas-phase species (Shalaby et al., 2012), dust (Zakey et al., 2006) and sea salt particles (Zakey et al., 2008). The anthropogenic and biomass burning aerosol schemes account for sulfur dioxide, sulfate, hydrophobic and hydrophilic components of black carbon and organic carbon particles; as well as it takes into account the chemical conversion of sulfur dioxide to sulfate through both gaseous-phase and aqueous-phase pathways. The essential steps and mechanisms, which are considered for developing and implementing the online dynamical dust and sea salt production schemes, are respectively described in Zakey et al. (2006) and (2008). For each wavelength of the RegCM4 radiation scheme and for each aerosol species, the aerosol size distribution and optical properties are computed using the Mie theory and employed in the model. Using prognostic dust bin concentrations, long-wave refractive indices, and absorption cross sections, the dust particles long-wave emissivity/absorptivity influences are also implemented (Giorgi et al., 2012). Tropospheric gas-phase chemistry is integrated into the model using the photochemical mechanism of version 5 of the Carbon Bond Mechanism (CBM-Z). The model applied rapid radical balance method to solve the tendency equation for photochemical production and loss (Shalaby et al., 2011). Applying tabulation and interpolation techniques, the model determines photolysis rates as a function of several meteorological and chemical inputs including altitude, solar zenith angle, and column densities for O₃, SO₂ and NO₂, surface albedo, aerosol optical depth, aerosol single scattering albedo, cloud optical depth and cloud altitude. The model considers both resolvable scale and cumulus precipitation wet removal processes as well as the dry deposition of tracers. Particularly the dry deposition process of gas phase species is modeled following the Community Land Model dry deposition model and their wet deposition is parameterized as in the Model for Ozone And Related chemical Tracers: Chemistry Transport Model (MOZART: CTM) global model. For a more detailed description of RegCM, the reader is referred to (Giorgi et al., 2012; Tesfaye et al., 2013 and references therein).

g1.2.2 The Case Study Model Set-up

Among different model physics parameterization schemes of RegCM4, this case study employs the following scheme: for the radiative transfer computation – the Community Climate Model – radiative transfer package is used. The radiative flux calculations include 18 spectral intervals, which are within a wavelength range of 0.2 to 4.5 μm . Among these 18 spectral bands, seven of them are situated in the ultraviolet spectral interval (0.2–0.35 μm), one is in the visible band (0.35–0.64 μm) and the remaining spectral bands cover the infrared/special absorption windows. The ocean surface fluxes are computed according to the scheme of Zeng et al. (1998), and surface processes are treated using the Community Land Model version 4.5. The study employs the mass-flux cumulus scheme of Emanuel (1991), the resolvable precipitation scheme of Pal et al. (2000) and the non-local planetary boundary layer parameterization of Holtslag and Bouville (1993). The simulation presented here uses a horizontal grid resolution of 20 km and 18 vertical layers, with a dynamical model time step of 30 s and the land model called every 600 s. Forecast products of the European Centre for Medium-Range Weather Forecasts (such as profile of wind components, temperature, relative humidity, geopotential height) are implemented for time-dependent initial and lateral boundary conditions. This case study uses online dynamical dust and sea salt production schemes of RegCM.

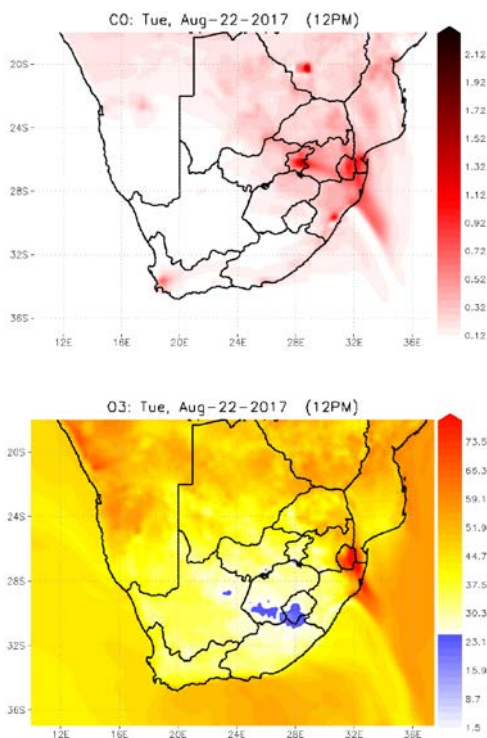
The emission inventories implemented in RegCM-CHEM4.5 include emissions from anthropogenic, biomass burning and biogenic. Since we did not have a well-established regional emission database, following the ICTP procedure, this case study uses an integrated emission climatology approach. Aggregating different sectors of emissions that are present in the global Representative Concentration Pathways (RCP), an integrated emission climatology (20 year: 1990 to 2010) for anthropogenic and biogenic isoprene emissions has been produced. Furthermore, based on emission information gathered from local municipalities in South Africa, the anthropogenic emission climatology has been realigned for certain tracer species (such as SO₂). The biomass burning emission climatology has been established based

on version 3 of Global Fire Emissions Database (14 year: 1997 to 2010). These two climatological emission datasets consider all species that are needed for CBM-Z chemical processing. Moreover, these climatological emission datasets were combined into one file before used as input into the model pre-processor code, which re-grids and interpolates the emission data to the same model projection and resolution as needed by RegCM-CHEM4. In addition, this case study uses climatological chemical boundary conditions that are generated at ICTP, based on CAM + EC-EARTH global simulations for aerosols, and six hourly chemical boundary conditions climatology coming from MOZART: CTM. In order to validate our forecast, surface observation station located in the northern part of South Africa has also been used.

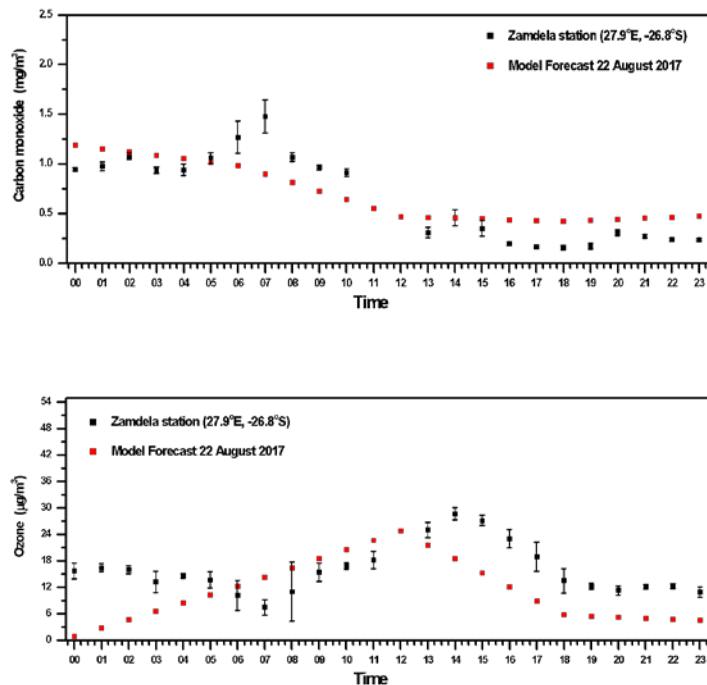
g1.3 Results and Discussion

Southern Africa is generally characterized as dry and windy during austral winter season (June to September). Figure 12.59 column (a) shows the air quality forecast of 22 August 2017 at 12:00 pm for: CO, O3 and BC surface concentration spatial distributions. Generally, southern Africa is well known for winter season savannahs and grassland fires. Accordingly, poor air quality incidences have been noted over the eastern and central parts of the region which extends from ~ 18°S to 27°S. Particularly, strong air quality deterioration is forecasted over South African provinces of Gauteng, Mpumalanga and Limpopo; where ~75% of the South African industrial infrastructures are situated. Higher surface concentration of CO, O3 and BC were forecasted over southern parts of Zambia as well as the northern areas of South Africa and Mozambique, where biomass burning and/or industrial activities are strong. The forecast also exhibited that, due to regionally dominant anticyclonic surface air circulation patterns, most of the BC and CO were dispersed towards the northern and eastern parts of South Africa. This worsened the air quality deterioration over these regions.

(a)



(b)



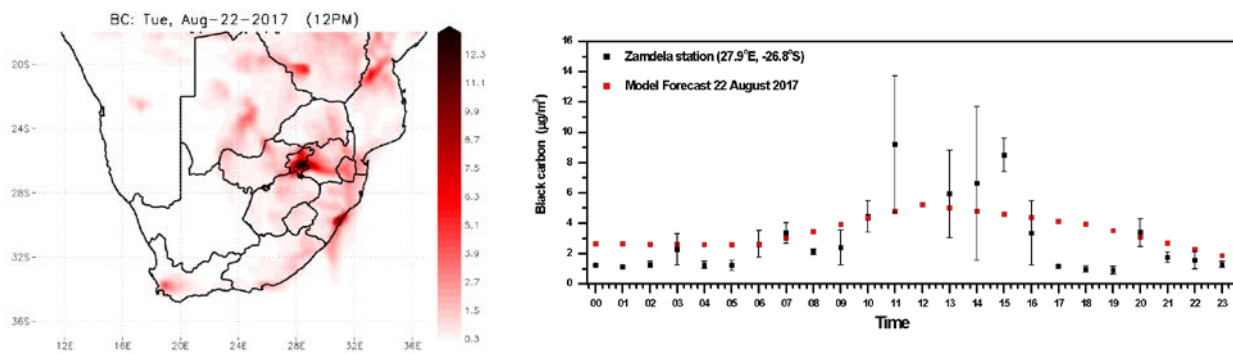


Figure 12.59. Air quality forecast on 22 August 2017: column (a) forecasted CO, O₃ and BC surface concentration spatial distributions; column (b) comparison of surface observation and forecasted surface concentration.

Industrial activities over the southern Africa western arid areas are sporadic as well as vegetation cover is sparse (Tesfaye et al., 2014b). Therefore, over these parts of the subcontinent, the forecast exhibits small loads of BC and CO. On the other hand, on 22 August, relative to the north and eastern parts of the subcontinent, the western arid areas experience hot weather and heatwave incidences. These regional circumstances strongly amplify the ozone production rate and reduce its dry deposition. As a result, O₃ forecast exhibits higher concentrations over the central areas of Namibia and Botswana. However, due to south-westerly blowing Atlantic cold front, the central areas of South Africa are expected to experience less amount of O₃ concentration.

Figure 12.59 column (b) shows the comparison of surface observation with that of forecasted concentration of O₃, BC and CO at Zamdela station: 27.9° E, 26.8° S. In overall, the model reasonably captures the observed trend of air pollution episodes. Notably, RegCM-CHEM captures the decrease in BC and CO during the evening hours. In the case of O₃, mainly during night hours, the forecast exhibits smaller concentrations than observed. This O₃ bias (night-time chemical loss) may be biased by the lack of regionally determined diurnal cycle in NO_x emissions and other O₃ precursors. There are several physical and emission processes that could contribute to these modeled-observed discrepancies. Thus, further analysis on this matter is important for establishing better prediction systems.

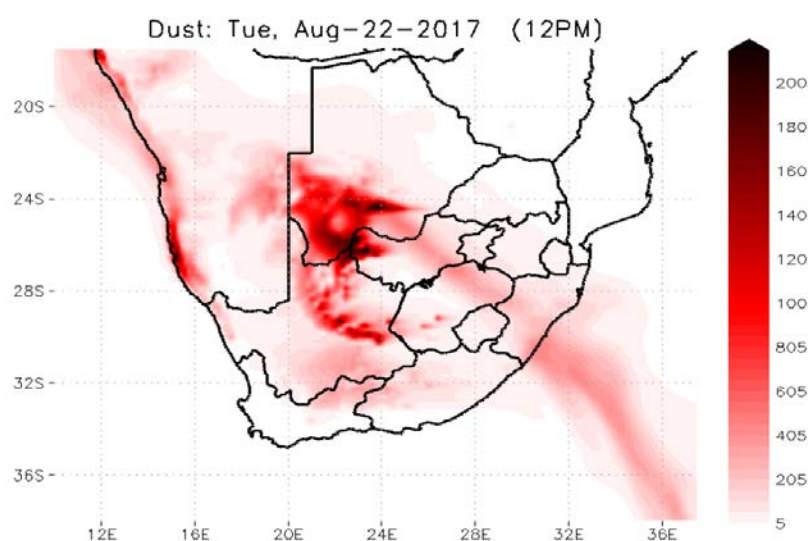


Figure 12.60. Southern Africa dust storm forecast on 22 August 2017 at 12:00.

Generally, the southern Africa anticyclonic circulation system – which swept through the Namib and Kalahari Basin desert regions – is responsible for the dispersion of desert dust particles towards South Africa (Tesfaye et al., 2015). Figure 12.60 shows the dust storm forecast on 22 August 2017 at 12:00. The forecast displays that on August 22nd 2017, both Kalahari and Namib Deserts are the most prominent source zones of wind driven desert dust particles, which mainly burdens the western parts of southern Africa. Also, as shown in Figure 12.60, following the anticyclonic circulation, the dust plume dispersed towards the central regions of South Africa, before migrating into the Indian Ocean. In terms of spatio-temporal distribution, the dust storm predicted on 22 August were more realistic. On this day, the SAWS satellite application division noted the passage of dust storm through central regions of South Africa (almost in alignment with the forecasted time) and provided visibility degradation warnings. In overall, this case study, besides exhibiting the applicability of RegCM-CHEM4.5 for dust storm and air quality forecasts – also provide insights into the possibilities of using integrated emission climatology, during the absence of well-established regional/national emission database. However, we also would like to emphasize the need of regionally/nationally quantified emission inventories for establishing more robust air quality forecast system.

Person of Contact: Melaku Tesfaye Yigiletu, email: Melaku.Yigiletu@weathersa.co.za

References

- Giorgi, F., et al., 2012: RegCM4: model description and preliminary tests over multiple CORDEX domains. *Clim. Res.* 52, 7–29.
- Shalaby, A., et al., 2012: Implementation and evaluation of online gas-phase chemistry within a regional climate model (RegCM-CHEM4), *Geosci. Model Dev.*, 5, 741–760, doi:10.5194/gmd-5-741-2012, 2012.
- Solmon, F., et al., 2006: Aerosol modeling for regional climate studies: application to anthropogenic particles and evaluation over a European/African domain. *Tellus*. 58B. 51-72.
- Tesfaye, M., et al., 2013: Evaluation of regional climatic model simulated aerosol optical properties over South Africa using ground-based and satellite observations. *ISRN Atmos. Sci.* 2013, 2013. <http://dx.doi.org/10.1155/2013/237483>.
- Tesfaye, M., et al., 2014a: Simulation of biomass burning aerosols mass distributions and their direct and semi-direct effects over South Africa using a regional climate model. *Meteorol. Atmos. Phys.* 125, 177–195. <http://dx.doi.org/10.1007/s00703-014-0328-2>.
- Tesfaye, M., et al., 2014b: Simulation of anthropogenic aerosols mass distributions and analysing their direct and semi-direct effects over South Africa using RegCM4. *Int. J. Climatol.* 35, 3515–3539. <http://dx.doi.org/10.1002/joc.4225>.
- Tesfaye, M., et al., 2015: Mineral dust aerosol distributions, its direct and semi-direct effects over South Africa based on regional climate model simulation. *J. Arid Environ.* 114, 22–40. <http://dx.doi.org/10.1016/j.jaridenv.2014.11.002>.
- Tesfaye, M., et al., 2016: Simulation of bulk aerosol direct radiative effects and its climatic feedbacks in South Africa using RegCM4. *Journal of Atmospheric and Solar-Terrestrial Physics*, 142, 1-19.
- Zakey, A. S., et al., 2008: Modeling of sea salt in a regional climate model: fluxes and radiative forcing, *J. Geophys. Res.*, 113, D14221, doi:10.1029/2007JD009209.
- Zakey, A.S., et al., 2006: Implementation and testing of a desert dust module in a regional climate model. *Atmos. Chem. Phys.* 6, 4687–4704. <http://dx.doi.org/10.5194/acp-6-4687-2006>.

Case g2. Performance of WRF-CHEM Model to simulate North African Aerosols: preliminary results

Aboubakr Abdallah¹ and Magdy M. Abdel Wahab²

¹ Astronomy and Meteorology Department, Faculty of Science, Al-Azhar University, Cairo, Egypt

² Astronomy and Meteorology Department, Faculty of Science, Cairo University, Giza, Egypt

Case overview and significance: Northern Africa region has many potential sources of atmospheric aerosols. Atmospheric aerosols are a major primary climate forcing. This study applied WRF-CHEM to reproduce aerosol species fields including BC, OC, dust, ammonia and nitrate during summer and winter in 2007 over Northern Africa by using reanalysis meteorology and climatology-assisted emission estimates as input. Horizontal grid spacing was 50 km with 51 vertical levels reaching a model top of 10 hPa. This study postulated that atmospheric aerosols could induce radiative, microphysical modifications and modulate precipitation patterns across the Greater Cairo and the Nile River Delta in the nested scheme.

g2.1 Introduction

One of the major forcing for climate change is aerosols, in case of Egypt and North Africa the major form of aerosol are air pollutants and sand particles carried away with the storms; respectively. Cairo city in Egypt is a major source of industrial pollutants in the region. Due to lack of rain, it has a very poor dispersion pattern and its buildings and narrow streets create a bowl effect. Over the last years full attention has been given to the modeling of aerosols by the scientific community, this work is an effort to simulate the regional climate aerosols over a large domain covering most African continent, especially North Africa and Egypt using WRF-CHEM model. This experiment concerned with the spatial distribution of aerosols and their emissions over the simulation domain as well as their impact on the regional climate precipitation patterns. This work describes the preliminary results and discusses the special distributions of some species of aerosols such as nitrogen oxides ($\text{NO}_x = \text{NO} + \text{NO}_2$), Black and Organic Carbon (BC+OC), and Ammonia (NH_3) over North Africa and Egypt. We here stated just a sample of the results for this experiment and the details of this experiment will be documented in the future work.

g2.2 Model, Data, and Experimental Design

g2.2.1 Model Description

Table 12.8 Africa Case g2 summarizes the parameterization choices used in the model. The Weather Research and Forecasting (WRF) model is a numerical weather prediction (NWP) and atmospheric simulation system designed for both atmospheric research needs and operational applications (e.g., that advances both the understanding and prediction of weather (Skamarock et al., 2008). WRF reflects flexible, state-of-the-art, it is suitable for a broad span of applications across scales ranging from large-eddy to global simulations (e.g., from the scale of convective storms to the scale of continental weather patterns (Michalakes et al., 2005). Recently, WRF model has been increasingly used as RCM for the most applications of downscaling, climate simulations, and parameterizations studies. The possible applications of the current modeling system include prediction and simulation of weather, or regional and local climate, data assimilation development, atmosphere-ocean coupling, idealized simulations, coupled weather prediction/dispersion model to simulate release and transport of constituents, coupled weather/dispersion/air quality model with full interaction of chemical species with prediction of O₃ and UV radiation as well as particulate matter (PM), and study of processes that are important for global climate change issues.

WRF-Chem extends WRF by incorporating a chemistry module that interactively simulates emissions of aerosols and gases, their transport, turbulent and convective mixing, and chemical and microphysical transformations of trace gases and aerosols (Grell et al., 2005). The version 3.5 of WRF-Chem model will be used in this study.

g2.2.2 Data Forcing

g2.2.2.1 Meteorological Input Data

The reanalysis dataset that provide the initial and lateral boundary meteorological conditions to the WRF-Chem model is the NCEP/DOE Reanalysis-2 global dataset (Kanamitsu et al., 2002). This dataset was created in cooperation between the National Centers for Environmental Prediction (NCEP) and Department of Energy (DOE). NCEP/DOE Reanalysis-2 is an improved version of the NCEP Reanalysis-1 model that fixed errors and updated parameterizations of physical processes. The NCEP/DOE Reanalysis-2 dataset is split into 2-D and 3-D files, the 2-D dataset has T63 horizontal spectral resolution ($1.875^\circ \times 1.875^\circ$) while 3-D has horizontal spectral resolution ($2.5^\circ \times 2.5^\circ$), the temporal coverage is 4-times daily, and 17 vertical levels, with the top extending to 10 hPa. The global sea surface temperature SST dataset used has weekly of temporal coverage and ($1^\circ \times 1^\circ$) horizontal resolution and updated in the model every 6 hr.

g2.2.2.2 Chemical Input Data

The initial and lateral boundary chemical conditions are considered from the most recent databases of urban/industrial, biogenic, biomass burning, biofuel use, and burning from agricultural waste sources, as shown in Table 12.10.

One of the global anthropogenic emissions inventories dataset used is the REanalysis of the TROpospheric (RETRO) chemical composition over the past 40 years (Schultz et al., 2007). The emission dataset has a $0.5^\circ \times 0.5^\circ$ spatial resolution and global coverage, with monthly temporal resolution, and is based on the year 2000. The second database proposed for anthropogenic emission is provided by the Emission Database for Global Atmospheric Research (EDGAR v4.2), (Janssens-Maenhout et al., 2010).

The EDGAR emission dataset provide global annual emissions for several chemical species with a $1^\circ \times 1^\circ$ spatial resolution, with daily temporal resolution, and is based on the year 2008. The third global anthropogenic aerosol emissions provided from the Goddard Chemistry Aerosol Radiation and Transport (GOCART). The dataset has $1^\circ \times 1^\circ$ spatial resolution on a monthly temporal resolution. The dataset provides emissions of organic carbon (OC), black carbon (BC).

Table 12.10. The input datasets used for the initial and lateral boundary conditions for meteorological parameters and chemical species.

Meteorological ICONs and BCONs	Chemical ICONs and BCONs
NCEP/DOE Reanalysis-2, 2-D ($1.875^\circ \times 1.875^\circ$), 3-D ($2.5^\circ \times 2.5^\circ$), 4-times daily, 17 vertical levels, top extending to 10 hPa, SST, $1^\circ \times 1^\circ$, weekly, updated in the model every 6 hr.	<ul style="list-style-type: none"> • Dust emissions dataset is provided through land usage information produced by the WPS. • RETRO, $0.5^\circ \times 0.5^\circ$, monthly, 2000. • EDGAR, $0.1^\circ \times 0.1^\circ$, daily, 2008. • GOCART, $1^\circ \times 1^\circ$, monthly. • MEGAN, $0.5^\circ \times 0.5^\circ$, monthly, 2003. • GFEDv2, $1^\circ \times 1^\circ$, 8-d / 1-month, 2004. • Yevich and Logan, $1^\circ \times 1^\circ$, annually per grid box.

The alternative biogenic emissions database is derived by the Model of Emissions of Gases and Aerosols from Nature (MEGAN, Guenther et al., 2006). MEGAN is a modeling system for estimating the net emission of gases and aerosols from terrestrial ecosystems into the atmosphere. Driving variables used by MEGAN to calculate the fluxes include land cover,

weather, and atmospheric chemical composition. The dataset covers the entire world with a $0.5^\circ \times 0.5^\circ$ spatial resolution, compiled for 2003 with a monthly temporal resolution.

The biomass burning emissions is based on (Giglio and van der Werf et al., 2006). In these dataset the burnt-area estimates from remote sensing, a biogeochemical model, and emission factors from the literature to estimate fire emissions during the 8-year period from 1997-2004. This dataset, called the Global Fire Emissions Database (GFEDv2), has $1^\circ \times 1^\circ$ spatial resolution and 8-day or one-month temporal resolution.

Finally, the biofuel use and agriculture waste burning emission inventories developed by (Yevich and Logan, 2003). This inventory covers the developing world with $1^\circ \times 1^\circ$ spatial resolution, and provides the amount of biomass burned annually per grid box.

g2.3.2 Experiments Design

g2.3.3 Model Domain

The selected domain that covers the extent of North Africa domain is presented in Figure 12.61(b), includes other important sources of emissions of gas and aerosol species that can affect Egypt. This domain is rich in aerosols from various origins, such as desert dust, urban continent, maritime areas, and forest fires. The model domain is centered over 17.5° N (latitude) and 17.5° E (longitude) and the area is covered the most African continent with 217×151 grid points with horizontal grid spacing of 50 km, and 51 vertical levels, with the model top at 10 hPa and time step of 200 sec.

The simulation experiment extended for winter and summer seasons 2007, in addition to one month of spin-up time for each season, which excluded from our analysis. The output is stored every 6 h (00, 06, 12, 18 UTC) and monthly fields are therefrom derived.

d2.3.4 Model Configuration

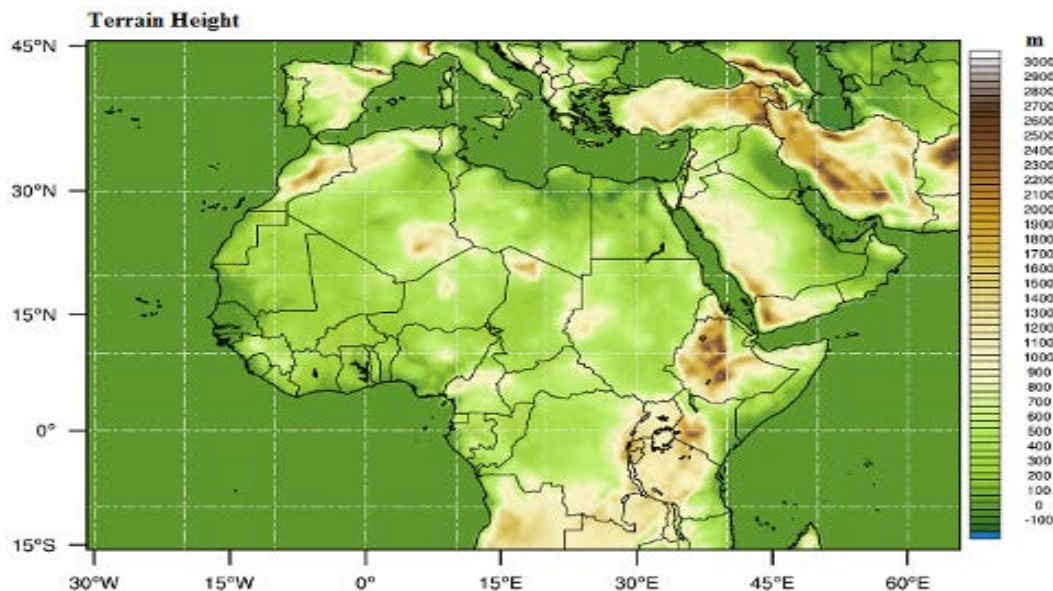


Figure 12.61. Terrain height of model domain over African continent with a 50 km resolution grid.

In this work the physics options include the Lin et al. Microphysics scheme (Lin et al., 1983), Kain–Fritsch convective parameterization scheme (Kain et al., 2004), CAM Shortwave and Longwave schemes (Collins et al., 2004), the Yonsei University planetary boundary layer scheme (Hong et al., 2006), the Noah Land Surface Model (LSM) four-layer soil temperature and moisture model with canopy moisture and snow-cover prediction (Tewari et al., 2004),

and MM5 Similarity Surface Layer Scheme (Beljaars et al., 1994; Zhang et al., 1982). A summary of the selected model physics and chemistry options is given in Table 12.11.

Table 12.11. The model physics and chemistry options used in all experiments.

Compartment		Selected Schemes
Met. Options	Microphysics	Lin
	LW Radiation	CAM
	SW Radiation	CAM
	BPL	YSU
	Land Surface	NOAH LSM
	Convective Parameterization	Kain-Fritch (KF)
Chem. Options	Chemical Mechanism	GOCART simple aerosol
	Photolysis Option	F-TUV
	anthropogenic emissions	GOCART RACM_KPP

The chemical options include the Goddard Global Ozone Chemistry Aerosol Radiation and Transport (GOCART) simple aerosol scheme for chemical mechanism, the F-TUV photolysis scheme will be used, this scheme, also from Sasha Madronich, is faster than the previous Madronich scheme option as shown in Table 12.11.

g2.5 Analysis Processes

This work will focus on the distribution of aerosols concentration and its impact on the regional climate precipitation patterns. The aerosol species used here are Nitrates NO_x, Black Carbon (BC), Organic Carbon (OC), and Ammonia (NH₃). For distribution of aerosol species concentration, we showed here the average of winter and summer seasons for 2007 as a preliminary result while the discussions of this simulation will be in more details in the future work.

g2.6 Results and Discussions

As mentioned, this chapter describes the preliminary results and discusses the special distributions of some species of aerosols over North Africa and Egypt. The following section will discuss the chemical species aerosols of nitrogen oxides (NO_x = NO + NO₂), Black and Organic Carbon, and Ammonia (NH₃).

g2.7 Nitrogen oxides NO_x

Figure 12.62 shows the spatial distribution of modeled NO_x concentrations over the model domain as a climatological average (DJF and JJA; Figure 12.62 (a) and (b) and Figure 12.62 (c) and (d), respectively).

Seasonal mean NO_x concentrations are typically less than 10 ppb as simulated by the model, with larger concentrations in the tropics due to biomass burning emissions. During the summer, NO_x concentrations remain relatively low (< 2 ppb) over northern Africa with higher concentrations (up to 10 ppb) in the winter due to an increase in OH lifetime, with a clear urban NO_x signal in Greater Cairo and the Nile Delta of Egypt.

g2.8 Black and Organic Carbon

Black carbon (BC) and organic carbon (OC) are particulate aerosols formed by incomplete combustion. The co-emission ratio of BC to OC varies by fuel type, combustion efficiency, and the extent of emissions control. When fossil fuels, such as oil and coal, are incompletely combusted (i.e., not completely oxidized to carbon dioxide [CO₂]), BC tends to be formed in much larger amounts than OC. When biomass fuels, such as wood, are incompletely combusted, OC is formed in greater amounts than BC. Black carbon remains in the atmosphere for about a week (Parungo et al., 1994), while CO₂ lingers for several decades. However, because BC is such a potent warmer, the immediate warming impacts are much greater than those of CO₂. It has been proposed that reductions of light-absorbing particles may assist in slowing the rate of global warming (Hansen et al., 2000). BC is emitted simultaneously with organic carbon (OC), which has a net negative climate forcing. Heating of the atmosphere by BC may reduce cloudiness (Ackerman et al., 2000); the addition of light absorbing particles to the aerosol mix may cause circulation and rainfall shifts (Menon et al., 2002). Open biomass burning in Africa is the largest contribution to both BC and OC emissions such as Savanna burning. Figure 12.63 shows the spatial distribution of modeled BC+OC concentrations over the model domain as a climatological average for (a) DJF 2007 and (b) JJA 2007.

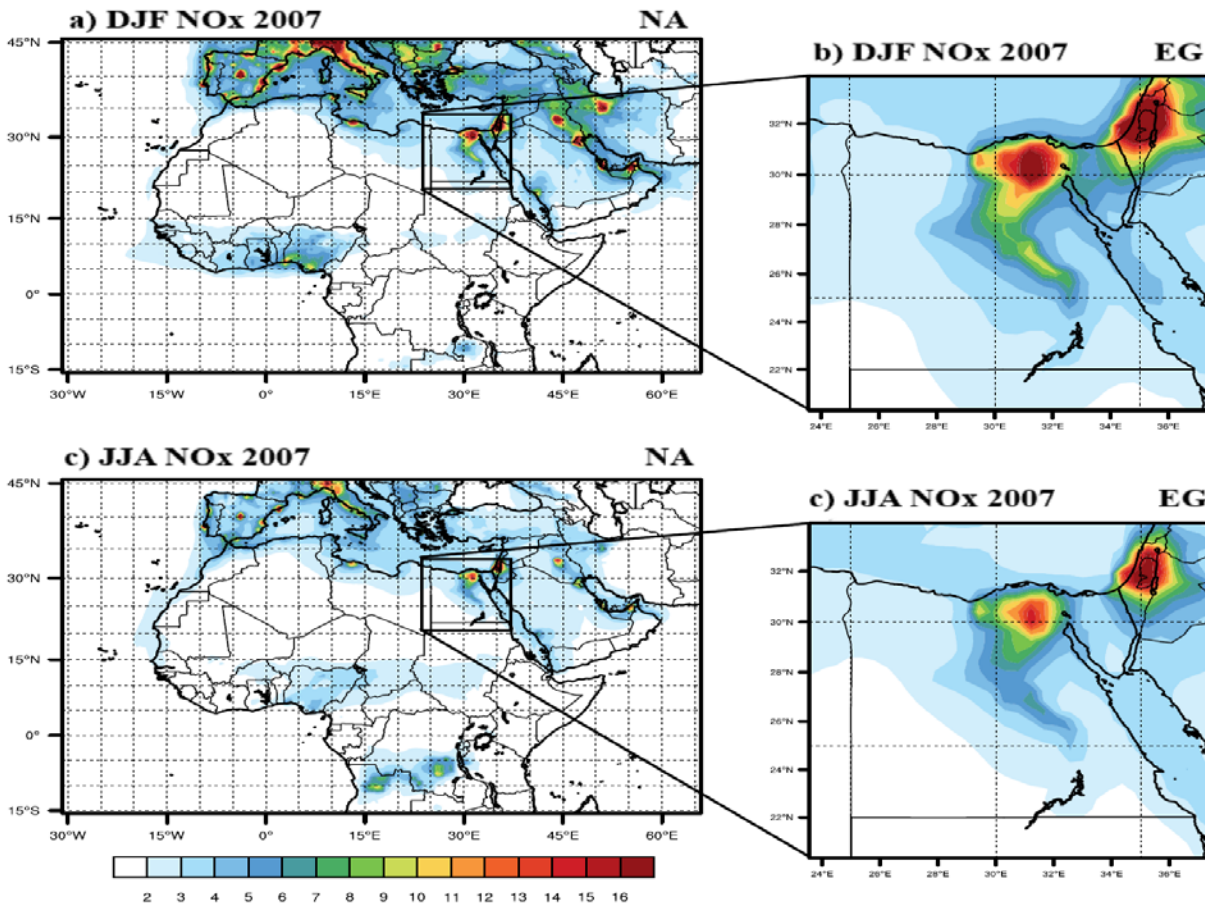


Figure 12.62. The spatial distribution of modeled NO_x (ppb) concentrations over the model domain as a climatological average for (a) and (b) DJF 2007 and (c) and (d) JJA 2007.

Black and organic carbon as simulated by the model provides relatively same contributions to the overall aerosol burden. Anthropogenic BC and OC emissions from Egypt domain especially from the Greater Cairo and Nile Delta areas are evident in JJA as in Figure 12.63 (b), with low concentrations in the winter as in Figure 12.63 (a). Despite larger emissions of OC, the model captures this truth and the differences in atmospheric concentrations was large in magnitude. The model simulation captures the main distribution of BC and OC concentrations over the model domain.

Figure 12.64 is just samples from the simulation of winter and summer seasons for 2007.

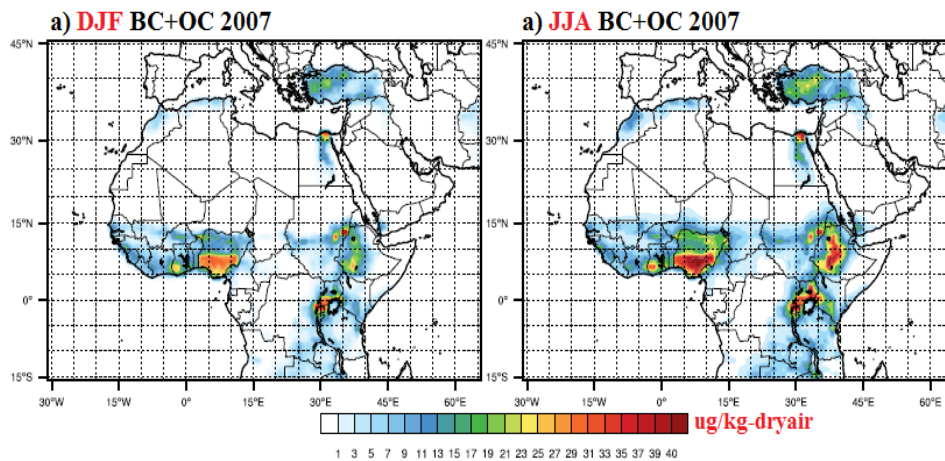
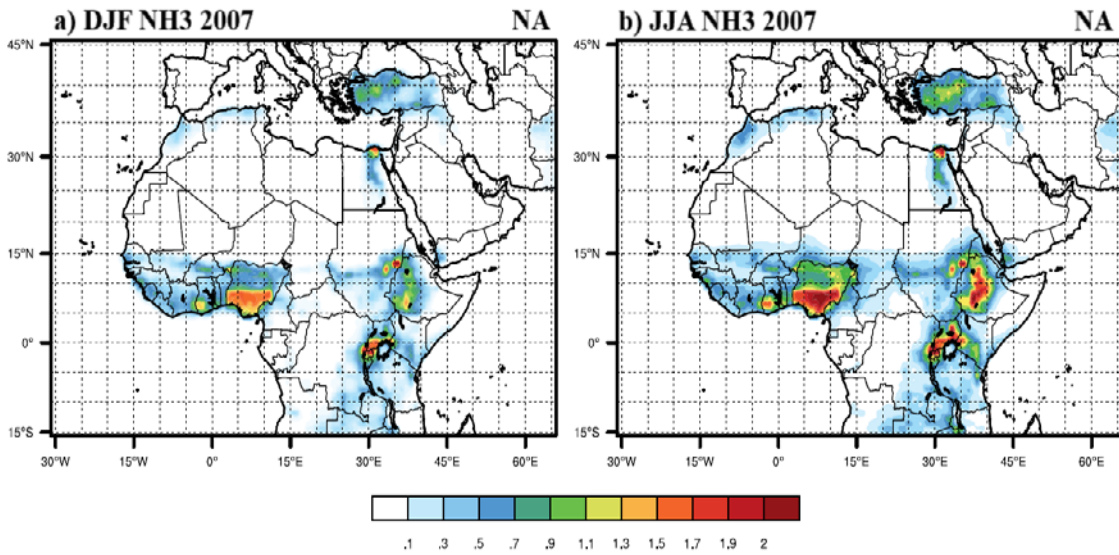


Figure 12.63. The spatial distribution of modeled BC+OC concentrations over the model domain as a climatological average for a) DJF 2007 and b) JJA 2007.



Person of contact: M. M. Abdel Wahab, email: magdy@sci.cu.edu.eg

References

- Ackerman A. S., Toon O. B., Taylor J. P., Johnson D. W., Hobbs P. V., and Ferek R. J., (2000): "Effects of Aerosols on Cloud Albedo: Evaluation of Twomey's Parameterization of Cloud Susceptibility Using Measurements of Ship Tracks". *Physics* 5577 (16): 2684–2695.
- Beljaars, A. C. M., (1994): The parameterization of surface fluxes in large-scale models under free convection. *Quart. J. Roy. Meteor. Soc.*, 121, 255–270.
- Collins, William D., Philip J. Rasch, Byron A. Boville, James J. Hack, James R. McCaa, David L. Williamson, Jeffrey T. Kiehl, and Bruce Briegleb, (2004): Description of the NCAR Community Atmosphere Model (CAM 3.0). NCAR Tech. Note NCAR/TN–464+STR. 214 pp.
- Giglio L., G. R. van der Werf, J. T. Randerson, G. J. Collatz, and P. Kasibhatla, (2006): Global Estimation of Burned Area Using MODIS Active Fire Observations. *Atmos. Chem. Phys.*, 6, 957-974.
- Grell, G. A., Peckham, S. E., Schmitz, R., McKeen, S. A., Frost, G., et al. (2005). Fully coupled "online" chemistry within the WRF model. *Atmospheric Environment*, 39(37), 6957-6975. doi: <https://doi.org/10.1016/j.atmosenv.2005.04.027>.
- Guenther, T. Karl, P. Harley, C. Wiedinmyer, P. I. Palmer, and Geron, (2006): Estimates of Global Terrestrial isoprene emissions using MEGAN (Model of Emissions of Gases and Aerosol from Nature). *Atmospheric Chemistry and Physics*, 6, 11, 3181-3210.
- Hansen, J. E., M. Sato, R. Ruedy, A. Lacis, and V. Oinas, (2000): Global warming in the twenty-first century: An alternative scenario, *Proc. Natl. Acad. Sci. U. S. A.*, 97(18), 9875– 9880.
- Hong, Song–You, Yign Noh, and Jimmy Dudhia, (2006): A new vertical diffusion package with an explicit treatment of entrainment processes. *Mon. Wea. Rev.*, 134, 2318–2341.
- Janssens-Maenhout Greet, Frank Dentener, John Van Aardenne, Suvi Monni, Valerio Pagliari, Lorenzo Orlandini, Zbigniew Klimont, Jun-ichi Kurokawa, Hajime Akimoto, Toshimasa Ohara, Robert Wankmuller, Bill Battye, Doug Grano, Andre Zuber, and Terry Keating, (2010): EDGAR-HTAP: A Harmonized Gridded Air Pollution Emission Dataset Based on National Inventories. JRC Scientific and Technical Reports, EUR 25229, doi: 10.2788/14102.
- Kain, John S., (2004): The Kain–Fritsch convective parameterization: An update. *J. Appl. Meteor.*, 43, 170–181.
- Kanamitsu M., W. Ebisuzaki, J. Woollen, S-K Yang, J.J. Hnilo, M. Fiorino, and G. L. Potter, (2002): NCEP–DOE AMIP-II REANALYSIS: An updated NCEP–NCAR reanalysis, covering 1979–present, features newer physics and observed soil moisture forcing and also eliminates several previous errors, *Bulletin of the American Meteorological Society*. (R-2)1631-1643.
- Lin, Yuh–Lang, Richard D. Farley, and Harold D. Orville, (1983): Bulk Parameterization of the Snow Field in a Cloud Model. *J. Climate Appl. Met.*, 22, 1065–1092.
- Menon, S., J. Hansen, and L. Nazarenko, (2002): Climate effects of black carbon aerosols in China and India, *Science*, 297, 2250– 2253.
- Michalakes, J., Duhia, D., Gill, D., Henderson, T., Klemp, J., and Wang, W., (2005): The weather research and forecast model: software architecture and performance, in: *Proceedings of the 11th ECMWF Workshop on the Use of High Performance Computing in Meteorology*, edited by Zwiefelhofer, W. and Mozdzyński, G., World Scientific, Singapore, 156–168.
- Parungo, F., C. Nagamoto, M.-Y. Zhou, A. D. A. Hansen, and J. Harris, (1994): Aeolian transport of aerosol black carbon from China to the ocean, *Atmos. Environ.*, 27,

3251– 3260.

- Schultz, M. and Rast, S., (2007): Emission Datasets and Methodologies for Estimating Emissions, Available at: http://accent.aero.jussieu.fr/RETRO_metadata.php, RETRO Report Di-6.
- Skamarock, W.C., Klemp, J. B., Dudhia, J., Gill, D. O., Barker, D. M., Duda, M. G., Huang, X.-Y., Wang, W., and Powers, J.G., (2008): A Description of the Advanced Research WRF Version 3, NCAR/TN-475+STR, NCAR TECHNICAL NOTE, June 2008.
- Tewari, M., F. Chen, W. Wang, J. Dudhia, M. A. LeMone, K. Mitchell, M. Ek, G. Gayno, J. Wegiel, and R. H. Cuenca, (2004): Implementation and verification of the unified NOAA land surface model in the WRF model. 20th conference on weather analysis and forecasting/16th conference on numerical weather prediction, pp. 11–15. ISSN 2320-5407 International Journal of Advanced Research (2016), Volume 3, Issue 1, 1011- 1023 1023.
- Yevich, R., and J. A. Logan, An assessment of biofuel use and burning of agricultural waste in the developing world, *Global Bio. Geo. chem. Cycles*, 17(4), 1095, doi:10.1029/2002GB001952, 2003.
- Zhang, D.-L., and R.A. Anthes, (1982): A high-resolution model of the planetary boundary layer- sensitivity tests and comparisons with SESAME-79 data. *J. Appl. Meteor.*, 21, 1594–1609.

Case g3. Application of ADMS Urban over the Grand Casablanca area, Morocco

Kenza Khomsi

National Meteorological Directorate, National Climate Center, Air Quality Department, Morocco

Case overview and significance: This study highlighted an application of the ADMS-Urban model adopted by Maroc Météo based on ADMS. ADMS-Urban is an urban air modeling tool for prescribing air quality 48 hour out in terms of NO₂, SO₂, O₃ and PM₁₀ concentrations. The Morocco official ALADIN meteorology forecast model provided the state and stability-regime variables for ADMS-Urban. A condensed semi-empirical chemical scheme following the concept of Generic Reaction Set of equations (GRS) formed the chemical processing portion of ADMS-Urban. ADMS-Urban partitioned calculation of pollutant concentration in two steps: (a) background concentrations; and (b) dispersion plume center-line concentration resulted from chemical and physical changes. An SO₂ pollution episode in winter 2016 over Casablanca was simulated by ADMS-Urban. It was reasonably captured by ADMS-Urban. Higher scores of fidelity of ADMS-Urban associated with non-dispersive and stable meteorological conditions.

g3.1 Introduction

In 2012, the meteorological services in Morocco (Maroc Météo) has implemented the Casablanca Air project whose main purpose was the implementation of a high-resolution monitoring and forecasting platform of air quality in the Casablanca metropolitan area.

The Casablanca Air has used the Urban Air tool which is based on the street scale model ADMS Urban and is allowing 48 hours forecasting of air quality (including NO₂, SO₂, O₃ and PM₁₀) at the scale of the Casablanca agglomeration. It uses the topographic data of the city, weather conditions, local emissions (emissions inventory on the city) and observations from 13 measuring stations implemented in the area.



Figure 12.65. The Grand Casablanca Area: the Domain map for Urban Air.

Many partners have participated in the establishment of the Air Casablanca tool in Maroc Météo and the modeling project was funded by the FASEP green fund donation for pilot projects that demonstrate "green" and / or innovative technologies. Maroc Météo is not committed to produce air quality forecasting at the national level and most of its modeling activities are performed for research purposes.

The selected case study represents an SO₂ episode forecasting over the Grand Casablanca Area in Morocco using the Urban Air tool. The episode has begun on the 19 December 2016 and reached its peak between the 29 December 2016 and the 3 January 2017.

g3.2 General Description of the Model

The Urban Air tool is comprised of the simulation of the fate of air pollutants using the ADMS Urban which is the most comprehensive version of the Atmospheric Dispersion Modeling System (ADMS) (Carruthers et al., 1997; McHugh et al., 1997). The main features of ADMS-Urban are:

An advanced dispersion model in which the boundary layer structure is characterized by the height of the boundary layer and the Monin-Obukhov length, a length scale dependent on the friction velocity and the heat flux at the surface;

A non-Gaussian vertical profile of concentration in convective conditions which allows for the skewed nature of turbulence within the atmospheric boundary layer that can lead to high concentrations near the source;

A meteorological pre-processor which calculates boundary layer parameters from a variety of input data, meteorological input data are issued from the ALADIN Morocco forecasting model;

An integrated street canyon model;

The calculation of flow and dispersion over complex terrain.

The model uses the National Ambient Air Quality Standards set by the Morocco Secretary of State to the Minister of Energy, Mines and Sustainable Development, responsible for sustainable development to compare its forecast and produce its colored maps.

g3.2.1 Parameterizations Choices

[Table 12.8 Africa Case g3](#) summarizes the parameterization choices in ADMS-Urban version 3.1 for meteorological and chemical simulation systems.

g3.2.2 Meteorological Model

The ALADIN System⁵ is the set of pre-processing, data assimilation, forecast model and post-processing–verification software codes shared and developed by the partners of the ALADIN consortium⁶ to be used for running a high resolution limited-area model (LAM). The ALADIN consortium is a collaboration between the national meteorological services of 16 European and northern African countries among which Morocco (Termonia et al., 2018). ALADIN Morocco is the operational weather prediction model in Maroc Météo. ALADIN is benefiting from the real time assimilation of many observations and its surface temperature, cloud fraction, precipitation distributions and wind are fundamental inputs to ADMS-Urban.

g3.3 Chemical Model

A scheme is used which models the important reactions involving Nitrogen, VOC's and Ozone. The Generic Reaction Set of equations (GRS) (Venkatram et al., 1994) is a semi-empirical photochemical model which reduces the complicated series of chemical reactions involving NO, NO₂, Ozone and many hydrocarbons to just seven (Carruthers et al., 1997).

The chemistry scheme in ADMS-Urban consists of two modules. The first models chemical reactions that occur only in the main model domain. The main model domain contains all individually defined sources, receptor points and output grids. For each set of input meteorological data, the time taken (Δt) for background pollutants to travel from the most upwind point of the main model domain to the first (most upwind) source is calculated. The

⁵ The ALADIN acronym stands for Aire Limitée Adaptation Dynamique Développement International (International development for limited-area dynamical adaptation)

⁶ <http://www.umr-cnrm.fr/aladin/>

chemistry scheme is then applied to the background pollutants over the period Δt to calculate background concentrations at the first source.

The second module consists of a simple Lagrangian box model, which is used to calculate background concentrations for the air approaching the main model domain. This allows the main ADMS model to be nested within a larger domain such as a large urban conurbation, where the effects of NO_x and VOC emissions over the whole area need to be considered.

g3.4 Results and Discussion

According to the model, the SO₂ episode has begun on the 19 December 2016 (Figure 12.66) in the north of the study area which is under the influence of industrial emissions, the peak was reached between the 29th December 2016 and the 3rd January 2017. Figure 12.67 shows the forecasted plume on December 2016.

The forecasted “star” that appears penetrating the city on the 30 December 2016 shows no prevailing directions and informs about weak winds and flow, this is confirmed while checking the wind at 10 m and at vertical levels (Figures 12.68 and 12.69). No temperature inversion was noticed as well.

The results from the model were compared to the observed daily average SO₂ recorded by the air quality background fixed station located at the (-7.56° E, 33.6° N) (Figure 12.70). During the first 3 days, the model alerted to the important SO₂ concentrations that were confirmed by observations. The model overestimated the concentrations of the 4th day and underestimated the concentrations of the end of the event.

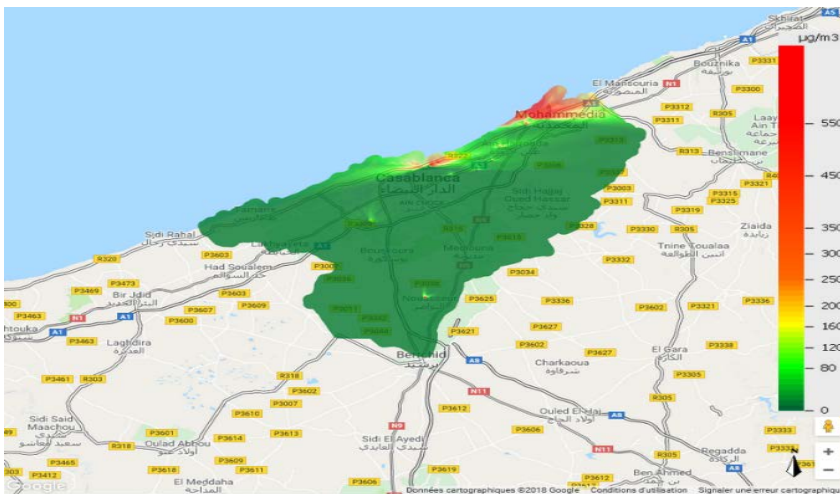


Figure 12.66. The forecasted beginning of the SO₂ episode on the 19th December 2016.

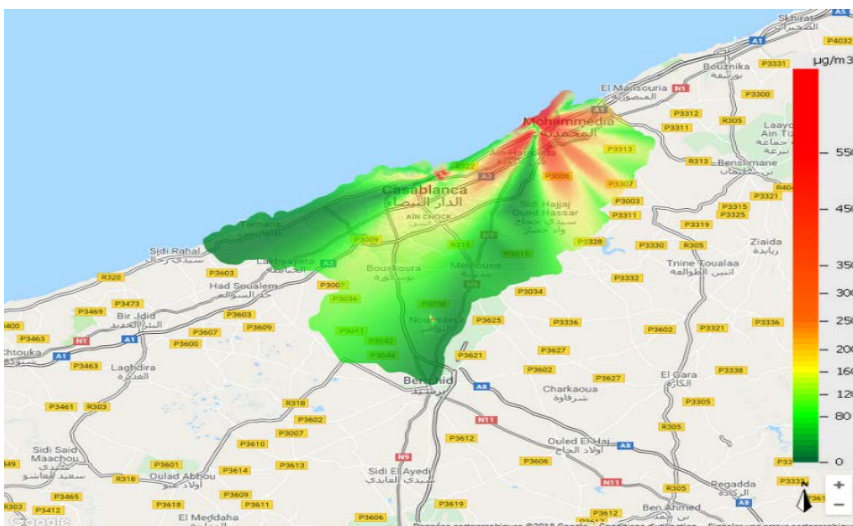


Figure 12.67. The forecasted SO₂ episode for the 30th December 2016.

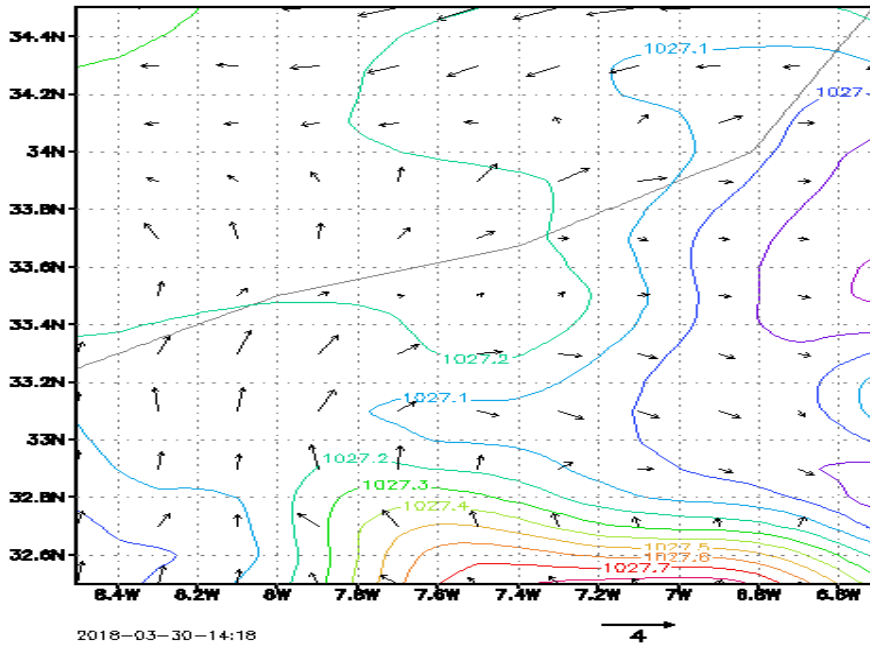


Figure 12.68. Weather map and 10 m wind (30 December 2016).

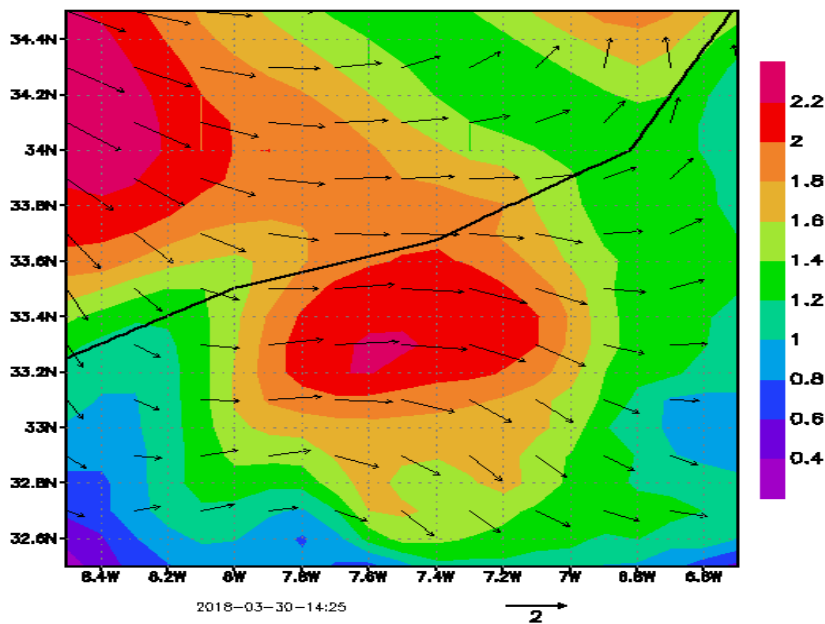


Figure 12.69. Wind direction and intensity at the 850 hPa level (30 December 2016).

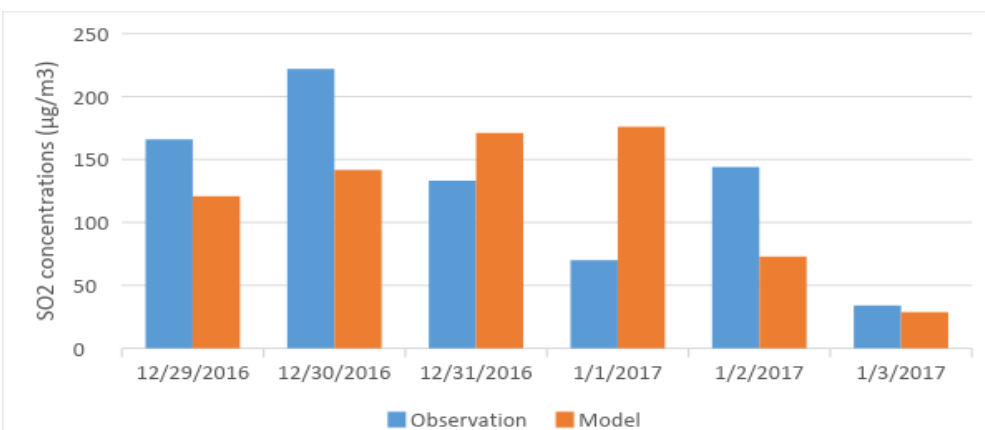


Figure 12.70. Comparison between modeled and observed values of SO₂ at the air quality station located at the (-7.56° E, 33.6° N) between 29 December

2016 and 3
January 2017.

g3.5 Lessons Learned

This type of episodes is mainly fostered by the non-dispersive meteorological situations and the dynamics of the boundary layer. Thus, the direction of the dispersion of the pollution is mostly influenced by the rate and the velocity of emissions from the activities nearby. The input emission inventory to the model needs to be updated.

Person of Contact: Kenza Khomsi, email: k.khomsi@gmail.com

References

- Carruthers, D.J., Edmunds, H.A., McHugh, C.A., Riches, P.J., Singles, R.J. (1997): ADMS Urban - an integrated air quality modeling system for local government. *Air Pollut. V* 45–58.
- McHugh, C.A., Carruthers, D.J., Edmunds, H.A. (1997): ADMS and ADMS-Urban. *Int. J. Environ. Pollut. 8*, 438–440.
- Termonia, P., Fischer, C., Bazile, E., Bouyssel, F., Brožková, R., Bénard, P., Bochenek, B., Degrauwe, D., Derková, M., El Khatib, R., Hamdi, R., Mašek, J., Pottier, P., Pristov, N., Seity, Y., Smolíková, P., Španiel, O., Tudor, M., Wang, Y., Wittmann, C., Joly, A. (2018): The ALADIN System and its canonical model configurations AROME CY41T1 and ALARO CY40T1. *Geosci. Model Dev. 11*, 257–281.
- Venkatram, A., Karamchandani, P., Pai, P., Goldstein, R. (1994): The development and application of a simplified ozone modeling system (SOMS). *Atmos. Environ. 28*, 3665–3678.

12.7 Summary

A total of 24 cases were tabulated in Tables 12.2-12.8. Table 12.2 summarizes case studies using 3 global models. The remainder were regional models where they collectively nearly covered the entire globe including 3 North American cases (Table 12.3), 4 European case studies with one of them nested to urban scale (Table 12.4), 5 East Asian case studies (Table 12.5), 2 South American case studies (Table 12.6), (3 Oceanian case studies (Table 12.7), and 6 African case studies (Table 12.8). The largest grid used in Case a.1 had over 3.1×10^7 grid cells. The regional models averaged about 2×10^6 grid cells. Most regional models utilized global chemical models to provide chemical boundary conditions. Some of these global models were providing near real-time simulations constraint by satellite-based observation.

There are multiple models for the ensemble approach in Case c1 with the seven-member ensemble gave the diversity in physics and chemistry in the Chemical Transport Model (CTM) models despite uniformity in their boundary conditions and emission fluxes. Tables 12.2-12.8 lists 32 CTMs. Among the 32 CTMs used, half of them were offline-coupled with a meteorology model, whereas the remainder were online-coupled with a meteorology model. Two-way feedback between meteorology and chemical composition in CTMs in the online models enabled air constituent direct, semi and indirect forcing in meteorology.

The commonly reiterated emphases in order of descending important and frequency expressed by the authors from this chapter are as follows:

Online modeling is a future requirement: 2-way feedback to model direct and indirect effort of aerosol (cases b2, d1, g2);

Verification is key to confirming forecast accuracy. Therefore, as much as possible, quality assured data should be used: space-, air-, and surface-based (all cases);

Emission uncertainty is binding and needs all eyes and ears to minimize it (cases a3, b1, b2, e1, g1);

Meteorological uncertainty; e.g., PBL height, etc. can be as large an uncertainty as emissions (cases a1, b1, d1, d3, g3);

Observation from space will become increasingly more important for emission modeling and verification (all cases);

Satellite constraint chemical LBC is critical (cases b1, b2, b3, c1, d3, g1);

Biomass burning is a major source of aerosol that subject to Long Range Transport (LRT) (cases a1, a2, a3, d5, f1, f2, f3, g1);

Pollution is transcontinental and transboundary (LRT is a strong component in many episodes) (cases a1, a3, d1);

Street canyon and fine resolution dispersion modeling drives home to health end-points: personalized air management (cases c3, d5, f3, g3);

Multiple tier grid nesting technique is common (cases c2, c3, d3, g1);

Application to health end-points is key to good service; e.g., AQHI (case a2);

Tackling wildfire and prescribed fires take efforts from multiple government agencies (cases f1, f2, f3);

Tropopause air mass folding can be important as O3 standard further being tightened (case b3);

Major international festivals, economic summits and athletic events requires good air quality -
- impact of brute force emission controls (case d2);

Region Haze can have a LRT component (case d1);

Pre-frontal subsidence ahead of deep depressions could be inductive to poor air quality (case d3);

Atmospheric composition models are key in Earth modeling systems – climate modification experiments (case d4);

Fire behavior modeling will be important to characterize fire plumes (case f3);

There exists interplay El Niño events and air quality events (case d5);

Ensemble approach (case c1);

There is large vehicular emission uncertainty: large ethanol emission was suspected of diesel fuel and fuel evaporation, and mobile sources can be locally dominant (cases e1, e2).

This above list is hardly exhaustive from the diverse study presented. Nonetheless the expert recommendations ranked priorities and cross-cutting sciences their advance expand understanding of atmospheric composition impacting a vast spectrum of time and space scales as fine as hourly personal respiratory health care by street blocks to climate modifications around the globe.

References

- Ackermann, I.J., Hass, H., Memmesheimer, M., Ebel, A., Binkowski, F.S., Shankar, U., 1998. Modal aerosol dynamics model for Europe: development and first applications. *Atmos. Environ.* 32, 2981e2999.
- Andrade, M. F., Ynoue, R. Y., Freitas, E. D., Todesco, E., Vara-Vela, A., Ibarra, S., Martins, L. D., Martins, J. A., and Carvalho, V. S. B.: Air quality forecasting system for Southeastern Brazil, *Front. Environ. Sci.*, 3, 1–14, 2015.
- Anthes R.A., E. Y. Hsie, and Y. H. Kuo, 1987: Description of the Penn State/ NCAR Mesoscale Model Version 4 (MM4). NCAR Tech. Note, NCAR/TN-282+STR.
- Arakawa A, Schubert WH. 1974. Interaction of a cumulus ensemble with the large-scale environment. Part 1. *J. Atmos. Sci.* 31: 674–701.
- Bacmeister, J. T., Suarez, M. J., and Robertson, F. R.: Rain Reevaporation, Boundary Layer-Convection Interactions, and Pacific Rainfall Patterns in an AGCM, *J. Atmos. Sci.*, 63, 3383–3403, doi:10.1175/jas3791.1, 2006.
- Best, M. J., Pryor, M., Clark, D. B., Rooney, G. G., Essery, R. L. H., Ménard, C. B., Edwards, J. M., Hendry, M. A., Porson, A., Gedney, N., Mercado, L. M., Sitch, S., Blyth, E., Boucher, O., Cox, P. M., Grimmond, C. S. B., and Harding, R. J.: The Joint UK Land Environment Simulator (JULES), model description – Part 1: Energy and water fluxes, *Geosci. Model Dev.*, 4, 677–699, doi:10.5194/gmd-4-677-2011, 2011.
- Bretherton, C. S., J. R. McCaa, and H. Grenier, 2004: A new parameterization for shallow cumulus convection and its application to marine subtropical cloud-topped boundary layers. Part I: Description and 1-D results. *Mon. Wea. Rev.*, 132, 864-882.
- Brown, A. R., 1996: Evaluation of parameterization schemes for the convective boundary layer using large-eddy simulation results. *Bound.-Layer Meteor.*, 81, 167–200.
- Brown, A. R., R. J. Beare, J. M. Edwards, A. P. Lock, S. J. Keogh, S. F. Milton, and D. N. Walters (2008), Upgrades to the boundary layer scheme in the Met Office numerical weather

- prediction model, *Bound. Lay. Meteorol.*, 128(1), 117–132, doi:10.1007/s10546-008-9275-0.
- Chang, J., et al.; 1987: A three-dimensional Eulerian and deposition model, Physical concepts and formulation, *J. Geophys. Res.*, 92, 14 681-14 700.
- Chin, M., Ginoux, P., Kinne, S., Torres, O., Holben, B. N., Duncan, B. N., Martin, R. V., Logan, J. A., Higurashi, A., and Nakajima, T.: Tropospheric aerosol optical thickness from the GOCART model and comparisons with satellite and sun photometer measurements, *J. Atmos. Sci.*, 59, 461–483, doi:10.1175/1520-0469(2002)0592.0.CO;2, 2002.
- Chou, M.-D. and Suarez, M. J.: A solar radiation parameterization for atmospheric studies, Technical Report Series on Global Modeling and Data Assimilation, 40 pp., available at: <http://gmao.gsfc.nasa.gov/pubs/docs/Chou136.pdf> (last access: 4 March 2014), 1999.
- Chou, M.-D., Suarez, M. J., Liang, X.-Z., and Yan, M. M.-H.: A thermal infrared radiation parameterization for atmospheric studies, Technical Report Series on Global Modeling and Data Assimilation, 56 pp., available at: <http://gmao.gsfc.nasa.gov/pubs/tm/docs/Chou137.pdf> (last access: 4 March 2014), 2001.
- Clark D.B., Mercado L.M., Sitch S., Jones C.D., Gedney N., Best M., Pryor M., Rooney G.G., Essery R.L.H., Blyth E., Boucher O., Harding R.J., Huntingford C. & Cox P.M. 2011. The Joint UK Land Environment Simulator (JULES), model description. Part 2: Carbon fluxes and vegetation dynamics. *Geosci. Model Dev.* 4: 701–722.
- Colarco, P. R., Nowottnick, E. P., Randles, C. A., Yi, B., Yang, P., Kim, K.-M., Smith, J. A., and Bardeen, C. G.: Impact of radiatively interactive dust aerosols in the NASA GEOS-5 climate model: Sensitivity to dust particle shape and refractive index, *J. Geophys. Res.-Atmos.*, 119, 753–786, doi:10.1002/2013JD020046, 2014.
- Collins, W. , .S. Stevenson, C.E. Johnson, R.G. Derwent, Tropospheric ozone in a Global-Scale Three- Dimensional Lagrangian Model and its response to NO_x emission controls *J. Atmos. Chem.*, 26 (3) (1997), pp. 223-27.
- Couvidat, F. and Sartelet, K.: The Secondary Organic Aerosol Processor (SOAP v1.0) model: a unified model with different ranges of complexity based on the molecular surrogate approach, *Geosci. Model Dev.*, 8, 1111–1138, <https://doi.org/10.5194/gmd8-1111-2015>, 2015.
- Damski, J., Thölix, L., Backman, L., Kaurola, J., Taalas, P., Austin, J., Butchart, N., and Kulmala, M.: A chemistry-transport model simulation of middle atmospheric ozone from 1980 to 2019 using coupled chemistry GCM winds and temperatures, *Atmos. Chem. Phys.*, 7, 2165-2181, <https://doi.org/10.5194/acp-7-2165-2007>, 2007.
- Debry, E., Fahey, K., Sartelet, K., Sportisse, B., and Tombette, M.: Technical Note: A new Size REsolved Aerosol Model (SIREAM), *Atmos. Chem. Phys.*, 7, 1537-1547, <https://doi.org/10.5194/acp-7-1537-2007>, 2007.
- Dickinson, R. E., A. Henderson-Sellers, and P. J. Kennedy, 1993: Biosphere–Atmosphere Transfer Scheme (BATS) Version 1e as coupled to the NCAR community climate model. NCAR Tech. Note NCAR/TN-3871STR, 72 pp. [Available from National Center for Atmospheric Research, P. O. Box 3000 Boulder, CO 80307.]
- Edwards, J. M. and A. Slingo. Studies with a flexible new radiation code. I: Choosing a configuration for a large-scale model. *Quart. J. Roy. Meteor. Soc.*, 1996, 122 (531): 689-719.
- Emanuel, K. A., 1991: A scheme for representing cumulus convection in large-scale models. *J. Atmos. Sci.*, 48, 2313-2335.
- Emanuel, K.A. and M. Zivkovic-Rothman, 1999: Development and evaluation of a convection scheme for use in climate models. *J. Atmos. Sci.*, 56, 1766–1782.
- Fahey, K. and Pandis, S.: Optimizing model performance: variable size resolution in cloud chemistry modeling, *Atmos. Environ.*, 35, 4471–4478, 2001.
- Fairlie, T.D., D.J. Jacob, and R.J. Park, The impact of transpacific transport of mineral dust in the United States, *Atmos. Environ.*, 1251-1266, 2007.

- Freidenreich, S.M., and V. Ramaswamy, 1999: A new multiple-band solar radiative parameterization for general circulation models. *J. Geophys.*
- Fritsch, J. M., and C. F. Chappell, 1980: Numerical prediction of convectively driven mesoscale pressure systems. Part I: Convective parameterization. *J. Atmos. Sci.*, **37**, 1722–1733.
- Fountoukis, C. and Nenes, A.: ISORROPIA II: a computationally efficient thermodynamic equilibrium model for K^+ – Ca^{2+} – Mg^{2+} – NH_4^+ – Na^+ – SO_4^{2-} – NO_3^- – Cl^- – H_2O aerosols, *Atmos. Chem. Phys.*, **7**, 4639–4659, <https://doi.org/10.5194/acp-7-4639-2007>, 2007.
- Giorgi, A. P., & Giorgi, B. M. (2003). Chapter 13: The descriptive phenomenological psychological method. In P. M. Camic, J. E. Rhodes & L. Yardley (Eds.), *Qualitative research in psychology: Expanding perspectives in methodology and design* (pp. 243–273). Washington, DC: American Psychological Association.
- Gong, S. L., L. A. Barrie, and J.-P. Blanchet, Modeling sea-salt aerosols in the atmosphere: 1. Model development, *J. Geophys. Res.*, **102**(D3), 3805–3818, 1997.
- Gong, S.L., 2003. A parameterization of sea-salt aerosol source function for sub- and super-micron particles. *Global Biogeochemical Cycles* **17** (4), 1097. doi:10.1029/2003GB002079.
- Gregory, D., and P. R. R. Rowntree, 1990: A mass flux convection scheme with representation of cloud ensemble characteristics and stability dependent closure. *Mon. Wea. Rev.*, **118**, 1483–1506.
- Grell, G. A., 1993: Prognostic evaluation of assumptions used by cumulus parameterizations. *Mon. Wea. Rev.*, **121**, 764–787.
- Grell, G. A. and Freitas, S. R.: A scale and aerosol aware stochastic convective parameterization for [weather](#) and air quality modeling, *Atmos. Chem. Phys.*, **14**, 5233–5250, <https://doi.org/10.5194/acp-14-5233-2014>, 2014.
- Guenther, A., T. Karl, P. Harley, C. Wiedinmyer, P.I. Palmer, and C. Geron (2006), Estimates of global terrestrial isoprene emissions using MEGAN (Model of Emissions of Gases and Aerosols from Nature), *Atmospheric Chemistry and Physics*, **6**, 3181–3210.
- Hertwig, D. et al. Development and demonstration of a Lagrangian dispersion modeling system for real-time prediction of smoke haze pollution from biomass burning in Southeast Asia. *J. Geophys. Res. Atmos.* **120**, doi: 10.1002/2015JD023422 (2015).
- Holtlag, A. A. M., and B. A. Boville, 1993: Local versus nonlocal boundary-layer diffusion in a global model. *J. Climate*, **6**, 1825–1842.
- Hong, S. Y., Y. Noh, and J. Dudhia (2006), A new vertical diffusion package with an explicit treatment of entrainment processes, *Mon. Weather Rev.*, **134**(9), 2318–2341, doi:10.1175/Mwr3199.1
- Hurley P. 2007. Modelling mean and turbulence fields in the dry convective boundary layer with the eddy diffusivity/mass flux approach. *Boundary-Layer Meteorol.* **125**: 525–536. *Res.*, **104**, 31,389–31,409.
- Jacob, D.J., Heterogeneous chemistry and tropospheric ozone, *Atmos. Environ.*, **34**, 2131–2159, 2000.
- Jaeglé, L., P.K. Quinn, T. Bates, B. Alexander, and J.-T. Lin, Global distribution of sea salt aerosols: New constraints from in situ and remote sensing observations, *Atmos. Chem. Phys.*, **11**, 3137–3157, doi:10.5194/acp-11-3137-2011, 2011.
- Jones, S. L., Creighton, G. A., Kuchera, E. L., Rentschler, S. A., 2011. Adapting WRF-CHEM GOCART for Fine-Scale Dust Forecasting. In: American Geophysical Union, Fall Meeting 2011.
- Jones, A., D. L. Roberts, M. J. Woodage, and C. E. Johnson (2001), Indirect sulphate aerosol forcing in a climate model with an interactive sulphur cycle, *J. Geophys. Res.*, **106**, 20,293–20,310.
- Kain, John S., (2004): The Kain–Fritsch convective parameterization: An update. *J. Appl. Meteor.*, **43**, 170–181.

- Kaiser, J. W., Heil, A., Andreae, M. O., Benedetti, A., Chubarova, N., Jones, L., Morcrette, J. J., Razinger, M., Schultz, M. G., Suttie, M., and van der Werf, G. R. (2012): Biomass burning emissions estimated with a global fire assimilation system based on observed fire radiative power, *Biogeosciences*, 9, 527-554.
- Kiehl, J. T., J. J. Hack, G. B. Bonan, B. A. Boville, B. P. Briegleb, D. L. Williamson, and P. J. Rasch, 1996: Description of the NCAR Community Climate Model (CCM3). NCAR/TN-420+STR, 152 pp.
- Kiehl, J. T., and C. S. Zender, 1995: A prognostic ice water scheme for anvil clouds. Proc. Workshop on Cloud Microphysics Parameterizations in Global Atmospheric Circulation Models of the Atmosphere, Kananaskis, AB, Canada, WMO, 167–188.
- Kim, Y, Wu, Y., Seigneur, C., Roustan, Y, (2018): Multi-scale modeling of urban air pollution: development and application of a street-in-grid model (v1.0) by coupling MUNICH (v1.0) and Polair (v1.8.1), *Geo Model Dev.* 2018. DOI: 10.5194/ gmd-11-611-2018, 2018.
- Koster, R. D., Suarez, M. J., Ducharne, A., Stieglitz, M., and Kumar, P.: A catchment-based approach to modeling land surface processes in a general circulation model: 1. Model structure, *J. Geophys. Res.-Atmos.*, 105, 24809–24822, doi:10.1029/2000jd900327, 2000.
- Kowalczyk, E. A., Y. P. Wang, R. M. Law, H. L. Davies, J. L. McGregor, and G. Abramowitz, 2006: The CSIRO Atmosphere Biosphere Land Exchange (CABLE) model for use in climate models and as an offline model. CSIRO Marine and Atmospheric Research Paper 013, 42 pp. [Available online at http://www.cmar.csiro.au/e-print/open/kowalczykea_2006a.pdf.]
- Kusaka, H., F. Kimura, Coupling a single-layer urban canopy model with a simple atmospheric model: impact on urban heat island simulation for an idealized case *J. Meteorol. Soc. Jpn.*, 82 (2004), pp. 67-80.
- Lin, Y.-L., R.D. Farley, H.D. Orville, Bulk parameterization of the snow field in a cloud model, *J. Clim. Appl. Meteorol.*, 22 (1983), pp. 1065-1092
- Liu, X. H., Penner, J. E., and Herzog, M.: Global modeling of aerosol dynamics: Model description, evaluation, and interactions between sulfate and non-sulfate aerosols, *J. Geophys. Res.- Atmos.*, 110, D18206, doi:10.1029/2004jd005674, 2005.
- Liu, X., et al. "Toward a minimal representation of aerosols in climate models: description and evaluation in the Community Atmosphere Model CAM5," *Geosci. Model Dev.* 5 709-739 (2012).
- Lock, A. P., Brown, A. R., Bush, M. R., Martin, G. M., and Smith, R. N. B.: A New Boundary Layer Mixing Scheme. Part I: Scheme Description and Single-Column Model Tests, *Mon. Weather Rev.*, 128, 3187–3199, doi:10.1175/1520- 0493(2000)1282.0.co;2, 2000.
- Louis, J., Tiedtke, M., and Geleyn, J.: A short history of the PBL parameterization at ECMWF, Workshop on Planetary Boundary Layer Parameterization, ECMWF, Reading, England, 5– 27 November 1981, 59–79, 1982.
- Madronich, S., and Flocke, S.: The Role of Solar Radiation in Atmospheric Chemistry, in: 4 Environmental Photochemistry, edited by: Boule, P., *The Handbook of Environmental Chemistry*, 5 Springer Berlin Heidelberg, 1-26, 1999.
- Mallet, V., Quélo, D., Sportisse, B., Ahmed de Biasi, M., Debry, É., Korsakissok, I., Wu, L., Roustan, Y., Sartelet, K., Tombette, M., and Foudhil, H.: Technical Note: The air quality modeling system Polyphemus, *Atmos. Chem. Phys.*, 7, 5479-5487, <https://doi.org/10.5194/acp-7-5479-2007>, 2007.
- McGregor, J. L. (2006). Regional climate modelling using CCAM. In "The Australian Community Climate and Earth System Simulator (ACCESS) – challenges and opportunities", BMRC Research Report 123, 118–122. <https://www.cawcr.gov.au/bmrc/pubs/researchreports/RR123.pdf>
- Monahan, E.C. (1986), The ocean as a source for atmospheric particles, *The Role of Air-Sea Exchange in Geochemical Cycling*, P. Buat-Menard, ed., Springer, 129-163.

- Moorthi, S. and Suarez, M. J.: Relaxed Arakawa-Schubert. A Parameterization of Moist Convection for General Circulation Models, *Mon. Weather Rev.*, 120, 978–1002, doi:10.1175/1520-0493(1992)120<0978>2.0.co;2, 1992.
- Oleson KW, Monaghan A, Wilhelmi O, Barlage M, Brunzell N, Feddema J, Hu L, Steinhoff DF. 2013. Interactions between urbanization, heat stress, and climate change. *Climatic Change* doi:10. 1007/s10584-013-0936-8.
- Pal, J.S., Small, E. & Elthair, E., 2000: Simulation of regional-scale water and energy budgets — Representation of subgrid cloud and precipitation processes within RegCM. *Journal of Geophysical Research*, 105, 29, 567-594.
- Park, R.J., D.J. Jacob, M. Chin and R.V. Martin, Sources of carbonaceous aerosols over the United States and implications for natural visibility, *J. Geophys. Res.*, 108(D12), 4355, doi:10.1029/2002JD003190, 2003.
- Park, R.J., D.J. Jacob, B.D. Field, R.M. Yantosca, and M. Chin, Natural and transboundary pollution influences on sulfate-nitrate-ammonium aerosols in the United States: implications for policy, *J. Geophys. Res.*, 109, D15204, 10.1029/2003JD004473, 2004.
- Pleim, J. E.: A combined local and nonlocal closure model for the atmospheric boundary layer. Part I: Model description and testing, *J. Appl. Meteorol. Clim.*, 46, 1383–1395, 2007.
- Pye, H. O. T., H. Liao, S. Wu, L.J. Mickley, D.J. Jacob, D. K. Henze, and J. H. Seinfeld, Effect of changes in climate and emissions on future sulfate-nitrate-ammonium aerosol levels in the United States, *J. Geophys. Res.*, 114, D01205, 2009.
- Pye, H.O.T., Chan, A. W.H., Barkley, M.P., and Seinfeld, J.H., Global modeling of organic aerosol: the importance of reactive nitrogen (NO_x and NO₃), *Atmos. Chem. Phys.*, 10, 11261-11276, doi:10.5194/acp-10-11261-2010, 2010.
- Qian, Y., Giorgi, F., Huang, Y., Chameides, W., Luo, C., 2001. Regional simulation of anthropogenic sulfur over East Asia and its sensitivity to model parameters. *Tellus* 53B, 171–191.
- Redington, A. L., R.G. Derwent, C.S. Witham, A.J. Manning, Sensitivity of modelled UK sulphate and nitrate aerosol to cloud, pH and ammonia emissions, *Atmos. Env.*, 43 (2009), pp. 3227-3234.
- Robinson, L.D., A. L., Donahue, N. M., Shrivastava, M. K., Weitkamp, E. A., Sage, A. M., Grieshop, A. P., Lane, T. E., Pierce, J. R., and Pandis, S. N.: Rethinking Organic Aerosols: Semivolatile Emissions and Photochemical Aging, *Science*, 315, 1259–1262, doi:10.1126/science.1133061, 2007
- Rotstayn, Wenju Cai, Martin R. Dix, Graham D. Farquhar, Yan Feng, Paul Ginoux, Michael Herzog, Akinori Ito, Joyce E. Penner, Michael L. Roderick and Minghui Wang, Have Australian rainfall and cloudiness increased due to the remote effects of Asian anthropogenic aerosols?, *Journal of Geophysical Research: Atmospheres*, 112, D9, (2007).
- Rotstayn, L. D., & Liu, Y. (2009). Cloud droplet spectral dispersion and the indirect aerosol effect: Comparison of two treatments in a GCM. *Geophysical Research Letters*, 36, L10801. <https://doi.org/10.1029/2009GL038216>.
- Rotstayn, L. D. and Lohmann, U.: Simulation of the tropospheric sulfur cycle in a global model with a physically based cloud scheme, *J. Geophys. Res.*, 107, 4592, doi:10.1029/2002JD002128, 2002
- Rotstayn, L. D., Collier, M. A., Mitchell, R. M., Qin, Y., Camp-bell, S. K., and Dravitzki, S. M.: Simulated enhancement of ENSO-related rainfall variability due to Australian dust, *Atmos. Chem. Phys.*, 11, 6575–6592, doi:10.5194/acp-11-6575- 2011,
- Rotstayn, L. D., and U. Lohmann, 2002: Simulation of the tropospheric sulfur cycle in a global model with a physically based cloud scheme. *J. Geophys. Res.* 107, 4592, doi:10.1029/2002JD002128, 2002.
- Rotstayn, L. D., Collier, M. A., Mitchell, R. M., Qin, Y., Camp- bell, S. K., and Dravitzki, S. M.: Simulated enhancement of ENSO-related rainfall variability due to Australian dust, *Atmos. Chem. Phys.*, 11, 6575–6592, doi:10.5194/acp-11-6575- 2011

- Schell, B., Ackermann, I.J., Hass, H., Binkowski, F.S., Ebel, A., 2001. Modeling the formation of secondary organic aerosol within a comprehensive air quality model system. *J. Geophys. Res.* 106, 28,275e28,293.
- Schwarzkopf, M. D., and V. Ramaswamy (1999), Radiative effects of CH₄, N₂O, halocarbons, and the foreign-broadened H₂O continuum: A GCM experiment, *J. Geophys. Res.*, 104, 9467 – 9488.
- Shalaby, A; Zakey, A. S; Tawfik, A. B; Solmon, F; Giorgi, F; et al. Geoscientific Model Development; Katlenburg-Lindau Vol. 5, Iss. 3, (2012): 741. DOI:10.5194/gmd-5-741-2012.
- Shaw, W.J., Allwine, K.J., Fritz, B.G., Rutz, F.C., Rishel, J.P., Chapman, E.G., 2008. An evaluation of the wind erosion module in DUSTAN. *Atm. Environ.* 42 (8), 1907–1921.
- Sillman, S., A numerical solution to the equations of tropospheric chemistry based on an analysis of sources and sinks of odd hydrogen, *J. Geophys. Res.*, 96, 20,735 – 20,744, 1991.
- Sofiev, M., J. Soares, M. Prank, G. de Leeuw, and J. Kukkonen (2011), A regional-to-global model of emission and transport of sea salt particles in the atmosphere, *J. Geophys. Res.*, 116, D21302, doi:10.1029/2010JD014713.
- Sofiev, M. (2000). A model for the evaluation of long-term airborne pollution transport at regional and continental scales. *Atmospheric Environment*, 34 (15), 2481–2493.
- Solmon, F., et al., 2006: Aerosol modelling for regional climate studies: application to anthropogenic particles and evaluation over a European/African domain. *Tellus*. 58B. 51-72.
- Steiner, A.L., A.J. Davis, S. Sillman, R.C. Owen, A.M. Michalak, A.M. Fiore Observed suppression of ozone formation at extremely high temperatures due to chemical and biophysical feedbacks *Proc. Natl. Acad. Sci. U. S. A.*, 107 (2010), pp. 19685-19690
- Tewari, M., and Co-authors, 2004: Implementation and verification of the unified Noah land surface model in the WRF model. 20th Conf. on Weather Analysis and Forecasting/16th Conf. on Numerical Weather Prediction, Seattle, WA, Amer. Meteor. Soc., 14.2a
- Thatcher M and Hurley P. Simulating Australian urban climate in a mesoscale atmospheric numerical model. *Boundary-Layer Meteorol* 2012; 142: 149–175.
- Tiedtke, M., 1993: Representation of clouds in large-scale models. *Mon. Wea. Rev.*, 121, 3030-3061.
- Vara-Vela, A., Andrade, M. F., Kumar, P., Ynoue, R. Y., and Muñoz, A. G.: Impact of vehicular emissions on the formation of fine particles in the Sao Paulo Metropolitan Area: a numerical study with the WRF-Chem model, *Atmos. Chem. Phys.*, 16, 777-797, <https://doi.org/10.5194/acp-16-777-2016>, 2016.
- Walters, D. N., Best, M. J., Bushell, A. C., Copsey, D., Edwards, J. M., Falloon, P. D., Williams, K. D. (2011). The Met Office Unified Model Global Atmosphere 3.0/3.1 and JULES Global Land 3.0/3.1 configurations. *Geoscientific Model Development*, 4, 919–941.
- Walters W. (2017) The Microphysics of Power Redux. In: Bonditti P., Bigo D., Gros F. (eds) Foucault and the Modern International. The Sciences Po Series in International Relations and Political Economy. Palgrave Macmillan, New York. DOI: https://doi.org/10.1057/978-1-137-56153-4_4
- Wilson, D. R., et al. (2008). "PC2: A prognostic cloud fraction and condensation scheme. I: Scheme description." *Quarterly Journal of the Royal Meteorological Society* 134(637): 2093-2107.
- Sofiev, M., J. Soares, M. Prank, G. de Leeuw, and J. Kukkonen (2011), A regional-to-global model of emission and transport of sea salt particles in the atmosphere, *J. Geophys. Res.*, 116, D21302, doi:10.1029/2010JD014713.
- Wang, Q., D.J. Jacob, J.R Spackman, A.E. Perring, J.P. Schwarz, N. Moteki, E.A. Marais, C. Ge, J. Wang, and S.R.H. Barrett, Global budget and radiative forcing of black carbon aerosol: constraints from pole-to-pole (HIPPO) observations across the Pacific, *J. Geophys. Res.*, 119, 195-206, 2014.

- Wilson, D. R., and S. P. Ballard, 1999: A microphysically based precipitation scheme for the UK Meteorological Office Unified Model. *Quart. J. Roy. Meteor. Soc.*, 125, 1607–1636, doi:10.1002/qj.49712555707
- Zakey, A. S., F. Solmon, and F. Giorgi (2006), Development and testing of a desert dust module in a regional climate model, *Atmos. Chem. Phys.*, 6, 1749 – 1792.
- Zakey, A.S., F. Giorgi, and X. Bi (2008) “Modeling of sea salt in a regional climate model: Fluxes and radiative forcing”, *Journal of Geophysical Research*, Vol. 113, D14221, doi:10.1029/2007JD009209.
- Zaveri R.A. and L.K. Peters, 1999: A new lumped structure photochemical mechanism for large-scale applications. *J. Geophys. Res.*, Vol. 104, D23, 30,387-30, 415.
- Zaveri, R.A., Easter Jr., R.C., Fast, J.D., Peters, L.K., 2008. Model for Simulating Aerosol Interactions and Chemistry (MOSAIC). *J. Geophys. Res.* 113, D13204. <http://dx.doi.org/10.1029/2007JD008782>
- Zender, C. S., H. Bian, and D. Newman (2003b), Mineral Dust Entrainment and Deposition (DEAD) model: Description and 1990s dust climatology, *J. Geophys. Res.*, 108(D14), 4416, doi:10.1029/2002JD002775.
- Zeng, X., R. E. Dickinson, and Y. He, 1998: Effect of surface sublayer on surface skin temperature and fluxes. *J. Climate*, 11, 537–550.
- Zheng, B., Zhang, Q., Zhang, Y., He, K. B., Wang, K., Zheng, G. J., Duan, F. K., Ma, Y. L., and Kimoto, T.: Heterogeneous chemistry: a mechanism missing in current models to explain secondary inorganic aerosol formation during the January 2013 haze episode in North China, *Atmos. Chem. Phys.*, 15, 2031-2049, <https://doi.org/10.5194/acp-15-2031-2015>, 2015.

APPENDICES

Final Contributors to the WMO's Training Materials and Best Practices for Chemical Weather/Air Quality Forecasting (CW-AQF)

Appendix I. List of Scientific Editors

#	Name	Affiliation	Country	Email
1	Yang Zhang	Northeastern University, previously at North Carolina State University	USA	ya.zhang@northeastern.edu
2	Alexander Baklanov	WMO	Switzerland	Abaklanov@wmo.int

Appendix II. List of Authors for Chapters 1-12

#	Name	Affiliation	Country	Email
1	Dan Aliaga	Purdue University	USA	Aliaga@cs.purdue.edu
2	Maria de Fatima Andrade	USP	Brazil	maria.andrade@iag.usp.br
3	Wyat Appel	EPA	USA	Appel.Wyat@epa.gov
4	Alexander Baklanov	WMO	Switzerland	Abaklanov@wmo.int
5	Sara Basart	BSC	Spain	sara.basart@bsc.es
6	Angela Benedetti	ECWMF	UK	Angela.Benedetti@ecmwf.int
7	Marc Bocquet	CEREA/ENPC	France	bocquet@ceresa.enpc.fr
8	Gregory Carmichael	Uni of Iowa	USA	gcarmich@engineering.uiowa.edu
9	Oriol Jorba Casellas	BSC	Spain	oriol.jorba@bsc.es
10	Jason Ching	UNC-Chapel Hill	USA	jksching@gmail.com
11	Martin Cope	CSIRO	Australia	Martin.Cope@csiro.au
12	Arlindo DA SILVA	NASA	USA	arlindo.dasilva@nasa.gov
13	José Luis Santiago Del Río	CIEMAT	Spain	jl.santiago@ciemat.es
14	Hiep Duc	OEH/NSW	Australia	Hiep.Duc@environment.nsw.gov.au
15	Johannes Flemming	ECMWF	UK	johannes.flemming@ecmwf.int
16	Edmilson Freitas	USP	Brazil	edmilson.freitas@iag.usp.br
17	Carlos Pérez García-Pando	BSC	Spain	carlos.perez@bsc.es
18	Stefano Galmarini	JRC	EU	stefano.galmarini@jrc.ec.europa.eu
19	Daven Henze	University of Colorado	USA	Daven.Henze@colorado.edu
20	Antje Inness	ECMWF	UK	a.inness@ecmwf.int
21	Johannes Kaiser	MPIC	German	j.kaiser@mpic.de
22	Ari Karppinen	FMI	Finland	Ari.Karppinen@fmi.fi
23	Christoph Keller	NASA	USA	christoph.a.keller@nasa.gov
24	Zak Kipling	ECMWF	UK	zak.kipling@ecmwf.int
25	Jason Knievel	NCAR	USA	knievel@ucar.edu
26	Lasse Johansson	FMI	Finland	Lasse.Johansson@fmi.fi

#	Name	Affiliation	Country	Email
27	Pius Lee	NOAA	USA	pius.lee@noaa.gov
28	Paul Makar	Environ Canada	Canada	paul.makar@canada.ca
29	Alberto Martilli	CIEMAT	Spain	alberto.martilli@ciemat.es
30	Valéry Masson	Meteo-France	France	alberto.martilli@ciemat.es
31	Gerald Mills	UCD	Ireland	gerald.mills@ucd.ie
32	Luca Delle Monache	NCAR	USA	lucadm@ucar.edu
33	Mariusz Pagowski	NOAA	USA	mariusz.pagowski@noaa.gov
34	Gabi Pfister	NCAR	USA	pfister@ucar.edu
35	Chao Ren	CUHK	China	renchao@cuhk.edu.hk
36	Glenn Rolph	NOAA	USA	glenn.rolph@noaa.gov
37	Pablo Saide	UCLA	USA	saide@atmos.ucla.edu
38	Odón R. Sánchez-Ccoyllo (UNTELS)	Universidad Nacional Tecnológica de Lima Sur	Peru	osanchezbr@gmail.com
39	Beatriz Sanchez	CIEMAT	Spain	Beatriz.Sanchez@ciemat.es
40	Adrian Sandu	Virginia Tech	USA	asandu7@vt.edu
41	Karine Sartelet	CEREA/ENPC	France	karine.sartelet@enpc.fr
42	Mikhail Sofiev	FMI	Finland	Mikhail.Sofiev@fmi.fi
43	Ranjeet Sokhi	University of Hertfordshire	UK	r.s.sokhi@herts.ac.uk
44	William Stockwell	DRI/UTEP	USA	william.r.stockwell@gmail.com
45	Daniel Tong	NOAA/George Mason Uni	USA	daniel.tong@noaa.gov
46	Shaocai Yu	Zhejiang University	China	shaocaiyu@zju.edu.cn
47	Chunhong Zhou	CMA	China	Zhouch@cma.gov.cn
48	Sergej Zilitinkevich	FMI	Finland	Sergej.zilitinkevich@fmi.fi
49	Yang Zhang	Northeastern University, previously at North Carolina State University	USA	ya.zhang@northeastern.edu

Appendix III. List of Providers for Demonstration Cases in Chapter 12

#	Name	Affiliation	Country	Email
1	Aboubakr Abdallah	Al-Azhar University	Egypt	beeker79@azhar.edu.eg
2	Maria de Fatima Andrade	USP	Brazil	maria.andrade@iag.usp.br
3	Charles Chemel	University of Hertfordshire	U.K.	c.chemel@herts.ac.uk
4	Martin Cope	CSIRO	Australia	Martin.Cope@csiro.au
5	Anton Darmenov	NASA	USA	christoph.a.keller@nasa.gov
6	Hiep Duc	OEH/NSW	Australia	Hiep.Duc@environment.nsw.gov.au
7	Aidan R. Farrow	University of Exeter	U.K.	Aidan.farrow@bristol.ac.uk
8	Johannes Flemming	ECMWF	U.K.	johannes.flemming@ecmwf.int
9	Edmilson Freitas	USP	Brazil	edmilson.freitas@iag.usp.br
10	Jimmy Chi-Hung Fung	Hong Kong University of Science and Technology	Hong Kong, China	majfung@ust.hk
11	Christopher Gan	NEA	Singapore	Christopher_GAN@nea.gov.sg
12	Christoph Keller	NASA	USA	christoph.a.keller@nasa.gov
13	Kenza Khomsi	Maroc Météo	Morocco	k.khomsi@gmail.com
14	Youngseob Kim	CEREA	France	youngseob.kim@enpc.fr
15	Pius Lee	NOAA	USA	pius.lee@noaa.gov
16	Kenneth Leung	Hong Kong EPD	China	kleung@epd.gov.hk
17	Paul Makar	Environ Canada	Canada	paul.makar@canada.ca
18	Alberto Martilli	CIEMAT	Spain	alberto.martilli@ciemat.es
19	Valéry Masson	Meteo-France	France	Valery.masson@meteo.fr
20	Stuart McKeen	NOAA ESRL	USA	Stuart.A.McKeen@noaa.gov
21	Mariusz Pagowski	NOAA ESRL	USA	mariusz.pagowski@noaa.gov
22	Matthieu Plu	Meteo-France	France	matthieu.plu@meteo.fr
23	Chao Ren	CUHK	China	renchao@cuhk.edu.hk

#	Name	Affiliation	Country	Email
24	Shital Roheka	University of Hertfordshire	U.K.	sheetal.shirsat@gmail.com
25	Glenn Rolph	NOAA	USA	glenn.rolph@noaa.gov
26	Karine Sartelet	CEREA/ENPC	France	karine.sartelet@enpc.fr
27	Vikas Singh	National Atmospheric Research Laboratory	India	vikas@narl.gov.in
28	Mikhail Sofiev	FMI	Finland	Mikhail.Sofiev@fmi.fi
29	Ranjeet Sokhi	University of Hertfordshire	U.K.	r.s.sokhi@herts.ac.uk
30	Magdy Abdel Wahab	Cairo University	Egypt	magdy@sci.cu.edu.eg
31	Melaku Tesfaye Yigiletu	SAWS	South Africa	Melaku.Yigiletu@weathersa.co.za
32	Shaocai Yu	Zhejiang University	China	shaocaiyu@zju.edu.cn
33	Peter Yeung	Hong Kong University of Science and Technology	Hong Kong, China	peter.yeung@hkstp.org
34	Chunhong Zhou	CMA	China	Zhouch@cma.gov.cn
35	Yang Zhang	Northeastern University, previously at North Carolina State University	USA	ya.zhang@northeastern.edu

Appendix IV. List of Authors and Reviewers

Chapter	Authors	Chapter Title	Reviewers
1	Yang Zhang and Alexander Baklanov	Introduction	Frank Dentener, Michaela Hegglin, Chunhong Zhou
2	Yang Zhang, Johannes Flemming, and Alexander Baklanov	History and Characteristics of CW-AQF	Frank Dentener
3		Fundamentals of 3-D CW-AQF Models	
3.1	Yang Zhang, Edmilson Freitas, Christoph Keller, and Alexander Baklanov	Introduction	
3.2	Yang Zhang, Edmilson Freitas, Christoph Keller, and Alexander Baklanov	Model Types and Existing Models	Ranjeet_Sokhi
3.3	Edmilson Freitas, Alexander Baklanov, and Yang Zhang	Meteorological and NWP Models for Air Quality Forecasting	Ranjeet_Sokhi
3.4	Alexander Baklanov and Sergej Zilitinkevich	Atmospheric Planetary Boundary Layer and Parameterizations of Boundary-Layer Processes	Ranjeet_Sokhi
3.5	William Stockwell and Yang Zhang	Atmospheric Chemistry	Frank Dentener
3.6	Yang Zhang, Karine Sartelet, Zak Kipling, Maria de Fatima Andrade, and Ranjeet Sokhi	Atmospheric Aerosol	Ranjeet_Sokhi, Frank Dentener
3.7	Yang Zhang, Zak Kipling, and Karine Sartelet	Atmospheric Removal	Frank Dentener,
3.8	Paul Makar	Interactions of Aerosol Species with Radiation via the Direct Effect for CW-AQF Models	Frank Dentener,
3.9	Carlos Pérez García-Pando, Oriol Jorba, and Yang Zhang	Interactions of Aerosol Chemical Species with Clouds for CW-AQF Models	Alexander Baklanov
4	Chunhong Zhou and Shaocai Yu	Model Deployment and Application	Michaela Hegglin, Taichu Tanaka, Alexander Baklanov

Chapter	Authors	Chapter Title	Reviewers
5		Special Considerations for Urban Applications	
5.1	Edmilson Freitas, Jason Ching, Valéry Masson, and Jose-Luis Santiago	Introduction	
5.2	Edmilson Freitas, Jason Ching, and Alexander Baklanov	Characteristics of Urban Scale Forecasting	Michaela Hegglin, Taichu Tanaka, Véronique Bouchet
5.3	Edmilson Freitas, Chao Ren, Alexander Baklanov, and Jason Ching	Consideration of Urban Induced Thermal and Air Quality Patterns and Circulations for CW-AQF	Michaela Hegglin, Taichu Tanaka, Heinke Schluenzen
5.4	Valéry Masson and Jason Ching	Urban Canopy Models	Michaela Hegglin, Taichu Tanaka, Jianguo_Tan
5.5	Jose-Luis Santiago, Beatriz Sanchez, and Alberto Martilli	Coupling with Parameterized or Computational Fluid Dynamics Models	Michaela Hegglin, Taichu Tanaka, Ranjeet Sokhi
5.6	Jason Ching, Gerald Mills, and Dan Aliaga	Infrastructure: World Urban Database and Access Portal Tools (WUDAPT)	Michaela Hegglin, Taichu Tanaka, Sue Grimmond
6	Daniel Tong, Mikhail Sofiev, Glenn Rolph, Sara Basart, Johannes W. Kaiser, Georg Grell, Hiep Duc, Martin Cope, and Alexander Baklanov	Special Considerations for Extreme Events	Michaela Hegglin, Taichu Tanaka, Alexander Baklanov
7	Mikhail Sofiev, Maria de Fatima Andrade, Gabi Pfister, and Edmilson Freitas	Model Input and Preparation	Chunhong Zhou, Alexander Baklanov
8	Christoph A. Keller	Model Output and Data Management	Chunhong Zhou, Alexander Baklanov
9	K. Wyatt Appel, Johannes Flemming, and Yang Zhang	Model Evaluation	Alexander Baklanov
10	Pablo Saide, Daven K. Henze, Angela Benedetti, Marc Bocquet, Gregory Carmichael, Arlindo da Silva, Antje Inness, Lasse Johansson, Ari Karppinen, Mariusz Pagowski, Adrian Sandu, Mikhail Sofiev, and Yang Zhang	Bias Correction and Forecast Skill Improvement Methods	Alexander Baklanov
11	Jason C. Knierel, Luca Delle Monache, Marc Bocquet, Stefano Calmarini, and Yang Zhang	Uncertainty Quantification and	Alexander Baklanov

Chapter	Authors	Chapter Title	Reviewers
12	Pius Lee, Karine Sartelet, and Yang Zhang	Probabilistic Forecasting Demonstration Cases for Real-Time CW-AQF	

Appendix V. List of Demonstration Cases and Providers

Domain	Case #	Case Title	Providers
Global	a1	Long-range transport of Sahara dust and smoke from Portuguese Wildfire emissions to North-West Europe forecast by the global CAMS forecasting system for atmospheric composition	Johannes Flemming
	a2	A study of the 2016 post-monsoon air pollution event over India using the GEOS forecasting system	Christoph A. Keller and Anton Darmenov
	a3	Impact of wildland fires on atmospheric aerosols in Northern Hemisphere in 2012	Mikhail Sofiev
North America	b1	National Air Quality Forecasting Capability for the U.S.A.	Pius Lee
	b2	Application of WRF/Chem-MADRID over Southeastern U.S.	Yang Zhang
	b3	Wildland fire smoke forecasting capability in the U.S.A.	Mariusz Pagowski and Stuart McKeen
Europe	c1	Application of Regional CAMS over Europe	Matthieu Plu
	c2	Air quality forecasting and analysis for United Kingdom	Ranjeet. S. Sokhi, Shital Rohekar, Vikas Singh, Aidan R. Farrow and Charles Chemel
	c3.1-3.2	Multi-scale modeling down to street level	Youngseob Kim and Karine Sartelet
Asia	d1	Application of CUACE/Haze-fog over China	Chunhong Zhou
	d2	Application of HAQFS over China	Shaocai Yu
	d3	Application of Hong Kong Air Quality Forecasting system over Hong Kong, China	Kenneth Leung
	d4	The impact of urbanization in the Pearl River Delta Region, China under three different climate change scenarios	Peter Yeung, Jimmy Chi-Hung Fung, and Chao Ren
	d5	Development of a smoke forecasting system for Southeast Asia	Christopher Gan
South America	e1	Application of WRF-Chem over the Southeast Brazil, South America	Maria de Fatima Andrade and Edmilson Dias de Freitas

Domain	Case #	Case Title	Providers
	e2	Particulate Matter forecasting capability in Peru	Odón R. Sánchez-Ccoyllo
Oceania	f1-3	Numerical air quality forecasting of the May 2016 fires in the Sydney, Australia region	Martin Cope ¹ and Hiep Duc ²
Africa	g1.1-1.2	Application of RegCM-CHEM4.5 for dust storm and air quality forecast over southern Africa	Melaku Tesfaye Yigiletu
	g2	Performance of WRF-CHEM Model to simulate North African Aerosols: preliminary results	A. Abdallah and Magdy M. Abdel Wahab
	g3	Application of ADMS Urban over the Grand Casablanca area, Morocco	Kenza Khomsi

List of Tables

Table 1.1	Ambient air quality standards of WHO, the European Union (EU), and several countries	5
Table 2.1	Impacts of meteorology on atmospheric pollution and chemistry	16
Table 2.2	Major differences between weather forecasting and air quality forecasting	21
Table 2.3	Examples of CW-AQ Forecast Models used by NMHSs.....	23
Table 2.4.	Major differences between air quality backcasting and forecasting.	26
Table 3.1	Component Models, Spatial Scale, and Coupling of Meteorology and Chemistry in Global CW-AQF Model Systems.....	40
Table 3.2	Component Models, Spatial Scale, and Coupling of Meteorology and Chemistry in Regional/Urban CW-AQF Model Systems.....	42
Table 3.3	Some meteorological observational networks used for CW-AQF models	58
Table 3.4	The impact of atmospheric variables and processes on atmospheric composition ..	60
Table 3.5	Impacts of atmospheric pollutants on atmospheric variables and processes	61
Table 3.6	Selected main characteristics of the numerical weather prediction models used for CTMs	63
Table 3.7	A summary of highly significant reactions that affect ozone concentrations over a range of polluted conditions	84
Table 3.8	Gas-phase chemical mechanisms used in 3-D air quality models.....	86
Table 3.9	An example of typical assignments of VOCs in an emissions inventory to classes and subcategories.....	94
Table 3.10	The assignment of chemical subcategories into model species using the RADM chemistry mechanism as an example.	96
Table 3.11	Comparison of several aqueous-phase chemical mechanisms (Zhang, 2020)	100
Table 3.12	Aqueous-phase and heterogeneous chemical mechanisms used in CW-AQF models	101
Table 3.13	Representation of aerosol processes in global CW-AQF models	117
Table 3.15	Representation of atmospheric removal processes in global CW-AQF models.....	146
Table 3.16	Representation of atmospheric removal processes in regional/urban CW-AQF models	147
Table 3.17	Radiative forcing impact of different aerosol components by composition	166
Table 3.18	..Methodologies used in simulating aerosol direct and indirect effects and feedbacks in global CW-AQF models.....	176
Table 3.19	Methodologies used in simulating aerosol direct and indirect effects and feedbacks in regional/urban CW-AQF models	178
Table 3.20	Treatments of Cloud Properties in Global CW-AQF Models	197

Table 3.21	Treatments of Cloud Properties in Regional/Urban CW-AQF Models	198
Table 4.1	Chemical Options selected for GRAPES-CUACE.	211
Table 5.1	Properties of Building Materials.....	218
Table 5.2	Urban canopy parameter (UCP) values associated with Local Climate Zone (LCZ) types	258
Table 9.1	Example routine surface-level observation data available.....	302
Table 9.2	Example absolute bias/error metrics	307
Table 9.3	Example relative bias/error metrics.....	308
Table 9.4	Example categorical forecast metrics.....	309
Table 9.5	Examples of existing air quality modelling specific evaluation tools/software	313
Table 10.1	Discrete and categorical evaluation of RT-AQF results for O ₃ predictions.....	320
Table 10.2	Discrete and categorical evaluation of RT-AQF results for PM _{2.5} predictions	323
Table 10.3	Aerosol remote-sensing observations	336
Table 10.4	Reactive and GHG remote sensing retrievals. TC: Total column, TRC: Tropospheric column, PROF: profiles, PC: Partial columns, ColAv: Column average mixing ratio	337

List of Figures

Figure 2.1.	An automated RT-AQF system from global to urban scales.....	27
Figure 3.1.	Illustration of the nesting grid procedure in numerical models.	65
Figure 3.2.	Diurnal evolution of PBL (after Stull, 2000).	69
Figure 3.3.	Recent Evaluations of Aerosol Feedback CW-AQF models for Forest Fire Smoke.	167
Figure 3.4.	WRF-Chem simulations comparing (a, b) direct effect only simulations with (c, d) direct + indirect effect simulations, during the Russian forest fires of 2010. ...	169
Figure 3.5.	Approximate fractional light transmission from equation (1) using the data of Hale and Querry (1973) and Krekov (1993) presented in Jacobson (1999).....	171
Figure 3.6.	Comparison of extinction coefficient values for a dry (a) and wet (b) aerosol, as a function of $2\pi r\lambda$. Note that both scales are logarithmic.	173
Figure 3.7.	Radiative mechanisms associated with cloud effects identified as significant in relation to aerosols (IPCC, 2007)	195
Figure 4.1	A uniform domain (left) and graded domain or adaptive mesh refinement (right) (Zarzycki and Jablonowski, 2014, 2015).....	208
Figure 4.2	A nested domain covering most of China and parts of East Asia (An et al., 2011).	209
Figure 5.1.	Urban effects and idealized urban canopy structure and scales incorporated as science codes into urbanized mesoscale forecasting modeling systems	215
Figure 5.2.	View of the city of São Paulo, Brazil, illustrating the very complex 3-D structure of an urban area.....	217
Figure 5.3.	Three-dimensional urban structure and the main components of energy budget.	218
Figure 5.4.	Satellite picture in a very heterogeneous urban region. Yellow line grid was constructed using 1 km spacing.....	219
Figure 5.5.	Example of a land use/land class file used in numerical models to identify surface characteristics, including urban features. As in Figure 5.4, grid was constructed using 1 km spacing.	220
Figure 5.6.	View of the city center of the Metropolitan Area of São Paulo, Brazil.....	226
Figure 5.7.	Left panel - Urban Heat Island Intensity over the Metropolitan Area of São Paulo, Brazil.	226
Figure 5.8.	View of heterogeneity observed in the city of São Paulo, Brazil, showing a region of a large number of high-rise buildings in the vicinity of low-rise constructions in a greener area.....	227
Figure 5.9.	Multi-model average of heat wave days (averaged for the period 1971–2000 (left: (a) and the 2071–2100 period (right: b) under scenario RCP8.5-SSP3...)	228
Figure 5.10.	Characteristics used to classify models. QF is the anthropogenic heat flux, QH is the sensible heat flux, QE is the latent heat flux, Q^* is the net all-wave radiation, and ΔQS is the net heat storage.	229

Figure 5.11.	Vehicular CO emissions ($\text{kg}\cdot\text{m}^{-2}\cdot\text{s}^{-1}$) in the Metropolitan Area of Sao Paulo for (a) Monday at 00:00:00 LT, estimated with the VEIN model (Ibarra-Espinosa et al., 2018), and (b) the emissions of road transport for the same area from the Emission Database for Global Atmospheric Research (EDGAR).....	231
Figure 5.12.	Spatial distribution of pollutant concentrations in $1\text{ km} \times 1\text{ km}$ with a full CFD model. This domain is the equivalent to a grid cell of a mesoscale model.	247
Figure 5.13.	Simplified scheme of the numerical approach of the multiscale system.....	250
Figure 5.14	(a) Schematic depicting the role of UCPs to represent urban effects incorporated into science options in contemporary urban canopy models. (b) Form based building UCPs (from Oke et al., 2017).	255
Figure 5.15.	Local Climate Zones	256
Figure 5.16.	Examples of classifying LCZs: (a) Sao Paulo, (b) Madrid, (c) Shanghai, (d) Mumbai.....	257
Figure 5.17.	Computing scale dependent UCPs based on outputs of DSC	259
Figure 6.1.	Overview of a potential Vegetation Fire and Smoke Pollution Warning and Advisory System (WMO VFSP-WAS, 2018).	263
Figure 6.2	Interannual variability and trend of dust storms from the NASA NCA Dust Indicator observations (Tong et al., 2017).	267
Figure 6.3.	Surface SO_2 concentration predicted on 19 May 2018 over Hawaii, United States.	276
Figure 8.1.	Global air quality model forecasts are available online from a variety of sources, such as the Copernicus Atmosphere Monitoring Service (CAMS, https://atmosphere.copernicus.eu/charts/cams/) or the NASA Global Modeling and Assimilation Office (GMAO, https://fluid.nccs.nasa.gov/wxmaps/chem2d/).	296
Figure 11.1.	Schemata of five methods (columns labeled 1–5) for constructing a dynamical EPS for transport-and-dispersion forecasting (From Galmarini et al., 2004, used by permission).	358
Figure 11.2.	Schema of a reliability diagram.....	360
Figure 11.3.	Five schematic examples of reliability.....	361
Figure 11.4.	Example of how a rank histogram can be used to assess reliability A reliable (i.e., unbiased and realistically dispersive) set of forecasts (white) was generated by post-processing a set of raw, high-biased probabilistic forecasts (black). (From Delle Monache et al., 2008a, used by permission.)	363
Figure 11.5.	Dispersion diagram showing the root mean squared error (RMSE) of the ensemble mean (black) and the ensemble spread (gray) of predicted wind speed at 10 m (AGL) by (a) Canada's Regional Ensemble Prediction System (REPS) and (b) an analog ensemble (AnEn). The close match in (b) between the RMSE and spread signifies reliability of these AnEn forecasts. (From Delle Monache et al., 2013, used by permission.).....	363
Figure 11.6.	Example of a Receiver Operating Characteristic (ROC) diagram	364
Figure 11.7.	Example of a deterministic prediction from the median of an EPS.	365

Figure 11.8.	Forecasts of O ₃ (ppbv) over lead times of 0–48 h at a point location.....	366
Figure 11.9.	Example of probabilistic predictions of ozone (red), nitrogen dioxide (green), sulphur dioxide (yellow), and PM ₁₀ aerosols (blue) at Paris, France as a function of valid time from an EPS forecast initialize 00 UTC 26 March 2018, generated by the CAMS regional EPS. Each box shows the predicted minimum, median, maximum, 10th, 25th, 75th, and 90th-percentile (key on lower left). Each horizontal dashed red line is a pollutant's threshold.....	368
Figure 12.1.	The aerosol optical depth forecast by the CAMS NRT forecasting system run by ECMWF for 12 UTC 16 October 2017	418
Figure 12.2.	Observed (blue dots) and forecast total and component AOD (1 day forecast) over East Malling, U.K. (51.29N, 0.44E) in October 2017.	419
Figure 12.3.	Air pollution over India on 6 November 2016 (08z).	421
Figure 12.4.	Air Quality Health Index (AQHI) over India on 6 November 2016 (08z).	421
Figure 12.5.	Global fire emission, IS4FIRES v.2.0, based on MODIS Aqua+Terra FRP observations. Unit: [ton sec ⁻¹].	424
Figure 12.6.	Structure and input data for IS4FIRES v.2.0.....	425
Figure 12.7.	Daily fire PM emission distribution over the globe on 28 June 2012.	426
Figure 12.8.	Fire-induced AOD on 5 July 2012. Daily mean predicted by SILAM. Relative unit.	426
Figure 12.9.	MODIS AOD, 5 July 2012, Terra only, daily composite.....	427
Figure 12.10.	MOPITT CO total column, 5 July 2012.....	428
Figure 12.11.	Domain map with abbreviation for the 6 evaluation regions labeled: (PC) Pacific Coast, (RM) Rocky Mountain, (UM) Upper Middle, (LM) Lower Middle, (NE) Northeast, and (SE) Southeast of the Conterminous U.S.A. (CONUS).	430
Figure 12.12.	NAQFC 2nd day forecast (color shading) versus near real-time US EPA AIRNow measurements (filled solid circles) for July 18, 2017, 18:00 UTC by (a) Case_Base, and (b) Case_Oil_n_Gas.....	433
Figure 12.13.	NAQFC 2nd day forecast (color shading) versus near real-time US EPA AIRNow measurements (filled solid circles) for Feb 21, 2017, 1800:00 UTC by (a) Operational, and (b) Corrected VOC speciation.	433
Figure 12.14.	Simulated domain for RT-AQF using WRF/Chem-MADRID.....	436
Figure 12.15.	Flowchart of the RT-AQF system based on WRF/Chem-MADRID (VISTAS denotes the Visibility Improvement State and Tribal Association of the Southeast) (Figure was taken from Chuang et al., 2011 and updated based RT-AQF since 2015).	437
Figure 12.16.	Comparison of CO spatial distributions in August, 2012: (a) satellite observation from MOPITT, (b) baseline simulation, and (c) sensitivity simulation (Figure taken from Zhang et al., 2016).....	438
Figure 12.17.	Spatial distributions of forecasted maximum 8-hr average O ₃ and 24-hr average PM _{2.5} concentrations during the 2017 O ₃ seasons. The observations are symbolled as circles, they were taken from AIRNow.	439
Figure 12.18	Retrievals of AOD at 550 nm from VIIRS	444

- Figure 12.19. Top: Ozone from the TOPAZ lidar on 3/16/18 over Boulder, CO. Crosses denote the times and levels of the output fields displayed in the RAP/Chem forecast web page. 445
- Figure 12.20. Regional CAMS ENSEMBLE forecast of ozone at surface, 22nd June 2017, when the concentrations reached the highest daily values (15h UTC)..... 447
- Figure 12.21. WRF-CMAQ Model Domain: Spatial coverage of the outer (coarser) European domain (50 km x 50 km) and the inner nested UK domain (10 km x 10 km). 449
- Figure 12.22. Annual mean diurnal variations of air pollutants (in $\mu\text{g m}^{-3}$) with error bars (as $\pm 1\sigma$) at UB sites. 450
- Figure 12.23. Hourly surface concentrations of a) NO b) NO₂ and c) O₃ for Day0 (red circles) and observations (blue lines) at UB sites. 451
- Figure 12.24. Daily variations of PM_{2.5} by WRF-CMAQ and AURN observations for the year 2014 showing the forecasts for Day0 (CMAQ0), Day1 (CMAQ1) and Day2 (CMAQ2). 451
- Figure 12.25. Compositional analysis of PM_{2.5} episodes during March/April 2014 over a London urban site in the UK (using output from WRF-CMAQ)..... 451
- Figure 12.26. Schematic diagram of the Street-in-Grid model. 455
- Figure 12.27. Modeling domains for the Polair3D, MUNICH and Street-in-Grid simulations. In the right panel, the blue box corresponds to the modeling area in suburban Paris for the MUNICH simulation. SinG is only used for domain 4..... 456
- Figure 12.28. Temporal evolution of NO₂ daily-averaged concentrations modeled with MUNICH (blue line), Polair3D (green line), and the SinG model (red line). They are compared to the measured concentrations (gray shaded regions) at the stations nearby traffic on each sidewalk of the Boulevard Alsace-Lorraine. If the measurement is available at only one station, a black line is used instead..... 458
- Figure 12.29. The domain map of CUACE/Haze-fog (15-60N, 35-150E), the targeting area is (15-60N, 70-140E). 460
- Figure 12.30. visibility from CUACE/Haze-fog for forecast length of (b) 24 hours, (c) 48 hours, and (d) 72 hours. (a) shows the haze observation meteorological stations in CMA. 462
- Figure 12.31. Domain map, a single domain, it covers most of China and parts of East Asia. The dots in the figure represent the monitoring sites..... 464
- Figure 12.32. Concentrations of ozone (O₃) and PM_{2.5} (particles with aerodynamic diameter lower than 2.5 μm) 467
- Figure 12.33. Time series of observations and simulations with (O₃-model-ctr, PM_{2.5}-model-ctr) 468
- Figure 12.34. Predicted reductions of hourly O₃ (top) and PM_{2.5} (bottom) concentrations in the Yangtze River Delta region with and without the emission controls for the three period 468
- Figure 12.35. Domain map of the two coarse modeling domain with 27 km and 9 km horizontal resolution used for the meteorological module WRF and chemical transport model CMAQ of the Hong Kong EPD forecasting system. 470

Figure 12.36. Predicted ozone levels and wind vectors on 21 August 2017 before Typhoon Hato approaches the Guangdong coast using the PATH forecasting system.	472
Figure 12.37. Predicted ozone levels (red) and observation (blue) during two air pollution episodes in August 2017 using the PATH forecasting system.	473
Figure 12.38. Weather chart at August 30, 2017, of an ozone episode day with concentration reached 400 $\mu\text{g m}^{-3}$	473
Figure 12.39. Predicted PM _{2.5} levels (red) and observation (blue) during two air pollution episodes in August 2017 using the PATH forecasting system.	473
Figure 12.40. (Left) The coverage of the domains configured in WRF. "d01" represents domain 1 and so on. (Right) The innermost domain ("d04") is the area of interest for this study.	475
Figure 12.41. The land use classification in (a) 2010 and (b) 2030 used in WRF.	477
Figure 12.42. Spatial distributions of averaged 2-meters temperature during 1400 LST and 1600 LST in June - July.	478
Figure 12.43. Spatial distributions of averaged 2-meters temperature during 2000 LST and 2200 LST in June - July. Gray dots on the map indicate model grid with urban land use.	478
Figure 12.44. Spatial distributions of averaged 10-meters wind speed during 2000 LST and 2200 LST in June - July. Gray dots on the map indicate model grid with urban land use.	479
Figure 12.45. Spatial distributions of averaged 10-meters wind speed during 1400 LST and 1600 LST in June - July.	479
Figure 12.46. 24-hour averaged modeled PM ₁₀ concentrations within the boundary layer during the onset, peak, and end of the June 2013 smoke episode in Southeast Asia.	484
Figure 12.47. Bias-correction of the June 2013 smoke episode in Singapore based on the median bias determined over a 24-hour analysis window. Hourly simulation and observation data represent averages over 12 local monitoring sites in Singapore. Red areas indicate forecast margins based on the 25th and 75th bias quantiles.	485
Figure 12.48. (a) Area considered in the simulations, showing elevations (m). b) Location of the Air Quality Stations from the Environmental Agency of São Paulo.	486
Figure 12.49. Comparison between modeled and simulated values for NO _x and O ₃ at the air quality station IPEN, during the period of January-February 2014.	488
Figure 12.50. (a) Illustration of the NO _x at 9 am (Local Time - LT) showing the emission by the vehicular fleet in the region and (b) ozone in the area during the hour of the maximum values (3 pm LT).	488
Figure 12.51. PM ₁₀ and surface wind 2nd day forecast for March 25, 2018, 1300:00 UTC by operational.	491
Figure 12.52. PM _{2.5} and surface wind 2nd day forecast for March 25, 2018, 1300:00 UTC by operational.	491
Figure 12.53. The 3-grid configuration used by AQFx to model air pollution Australian region, focusing on greater Sydney.	495

Figure 12.54. Left- hourly time series of carbon monoxide emissions estimated for the hazard reduction burns and for all other anthropogenic ground sources in the Greater Sydney Region 2-10 May 2016.	495
Figure 12.55 The modeled average PM2.5 concentration for the Sydney region	496
Figure 12.56 Output from the AQFx diagnostic tool.....	497
Figure 12.57. VIIRS satellite hotspots (red) for May 2016. The horizontal scale is 300 km. ...	498
Figure 12.58. Southern Africa air quality forecast model domain and topography (unit: m)..	501
Figure 12.59. Air quality forecast on 22 August 2017: column (a) forecasted CO, O3 and BC surface concentration spatial distributions; column (b) comparison of surface observation and forecasted surface concentration.	504
Figure 12.60. Southern Africa dust storm forecast on 22 August 2017 at 12:00.....	504
Figure 12.61. Terrain height of model domain over African continent with a 50 km resolution grid.....	508
Figure 12.62. The spatial distribution of modeled NOx (ppb) concentrations over the model domain as a climatological average for (a) and (b) DJF 2007 and (b) and d) JJA 2007	511
Figure 12.63. The spatial distribution of modeled BC+OC concentrations over the model domain as a climatological average for a) DJF 2007 and b) JJA 2007.....	511
Figure 12.64. The spatial distribution of modeled NH3 (ppb) concentrations over the model domain as a climatological average for a) DJF 2007 and b) JJA 2007.....	512
Figure 12.65. The Grand Casablanca Area: the Domain map for Urban Air.....	515
Figure 12.66. The forecasted beginning of the SO2 episode on the 19th December 2016.....	517
Figure 12.67. The forecasted SO2 episode for the 30th December 2016.	517
Figure 12.70. Comparison between modeled and observed values of SO2 at the air quality station located at the (-7.56° E, 33.6° N) between 29 December 2016 and 3 January 2017.	518

Nomenclature

Acronym	Definition
1-D	One dimensional
2-D	Two dimensional
3-D	Three dimensional
3D-VAR	A three-dimensional variational data assimilation
4-D	Four dimensional
4D-VAR	A four-dimensional variational data assimilation
A	Accuracy
AAQFS	The Australian air quality forecasting system
ACARS	The aircraft communications addressing and reporting system
ACCMIP	The emissions for atmospheric chemistry and climate model intercomparison project
ACI	Aerosol-cloud interactions
ACM2	The asymmetric convective mixing planetary boundary layer scheme
ACOM	Atmospheric chemistry observations & modeling laboratory
ACT	Atmospheric chemical transport
ADAM	Air force dispersion assessment model
ADMS-Urban	The atmospheric diffusion modeling system for urban planning
ADOM	The acid deposition and oxidants model
ADOM-IIb	The gas-phase mechanism of ADOM-IIb
the AEC model	The AER/EPRI/Caltech aerosol model
AERO5	Aerosol module 5 in CMAQ
AERO6	Aerosol module 6 in CMAQ
AERONET	Aerosol network
AIM2	The aerosol inorganics model version 2
AIOMFAC	Aerosol inorganic–organic mixtures functional groups activity coefficients
AIRNow	The aerometric information retrieval now
AIRPACT3	Air-quality forecasting for the Pacific Northwest
AIRPARIF	Air quality monitoring network in Île-de-France
AirQUIS	Air quality information system
ALADIN	The aire limitée adaptation dynamique développement international
ALD	Aldehydes
ALOHA	Areal locations of hazardous atmospheres
AMET	The atmospheric model evaluation tool
AMO	Atlantic multidecadal oscillation
AMON	Ammonia monitoring network
AMWFG	Atmospheric modeling and weather forecasting group at the university of Athens

Acronym	Definition
AnEn	The analog ensemble
AOD	The aerosol optical depth
APC	The analytical predictor of condensation
API	Application programming interfaces
AQ	Air quality
AQB	Air quality backcasting
AQFMS	Air quality forecast modeling system
AQFx	The AQF system
AQHI	The air quality health index
AQI	The air quality index
AQMs	Air quality models
AQMEII	The air quality model evaluation international initiative
AQS	Air quality system
AQUM	Air quality in the unified model: limited area forecast configuration of the U.K. met office unified model which uses the UKCA (U.K. chemistry and aerosols) sub-model
ARGOS/DEMA	The accident reporting and guidance operational system of the Danish emergency management agency
ARO	Aromatic rings
ARL	Air resources laboratory
ARW	The advanced research WRF with the Eulerian mass
ASEAN-NAME	The association of southeast Asian nations-numerical atmospheric dispersion modeling environment
ASTEEM	The adaptive step time-split explicit Euler method
ATLAS	ASEAN tropical Lagrangian atmospheric system
AURAMS	A unified regional air-quality modeling system
AUT	Aristotle university of Thessaloniki
B	Bias
BAMS	The Aaron Advanced Meteorological System, Inc.
BEM	Building energy module
BEP	Building environment parameterization
BC	Black carbon
BCONs	The boundary conditions
BDFC	Barcelona dust forecast center
BIGALK	Alkanes with four or more carbon atoms and other higher-carbon VOCs with similar reactivity
BIGENE	Alkenes with four or more carbon atoms and other higher-carbon VOCs with similar reactivity
BOLAM	Bologna limited area model
BOLCHEM	Bologna limited area model for meteorology and chemistry

Acronym	Definition
BS	Brier score
BSS	Brier skill score
BSC-CNS	Barcelona Supercomputing center -centro nacional de supercomputación
BUM	The background urban model
BVOCs	Biogenic volatile organic compounds
C ₆ H ₆	Benzene
Ca ²⁺	Calcium
CACM	The California atmospheric chemical mechanism
CALIOP	Satellite sensor developed under the Caliope project funded by the Spanish ministry of the environment
CALIOPE	An air quality forecasting system for Spain developed under the Caliope project funded by the Spanish ministry of the environment
CAM	Canadian aerosol module
CAM3, 5	The community atmospheric model versions 3 and 5
CAMS	The European Copernicus atmosphere monitoring service
CAMx	Comprehensive air quality model with extensions
CAQI	The common air quality index
CAPRAM	Chemical aqueous phase radical mechanism
CAR	Carbonyl group
CAR-FMI	Contaminants in the air from a road of the Finnish meteorological institute
CASTNET	Clean air status and trends network
CATT-BRAMS	The coupled aerosol and tracer transport model to the Brazilian developments on the regional atmospheric modeling system
CCATT-BRAMS	The chemistry coupled aerosol and tracer transport model to the Brazilian developments on the regional atmospheric modeling system
CB05/CBM-05	The 2005 version of carbon bond mechanism
CB05Clx	Cb05 with chlorine extension
CB05-TUL	Cb05 with toluene chemistry
CB06	The carbon bond mechanism version 6
CBM-EX	The Stanford university's extended carbon bond mechanism
CBM-IV/CB4	The carbon-bond mechanism version 4
CBM-Z	The carbon-bond mechanism version z
CCAM	Conformal cubic atmospheric model
CCMM	Coupled chemistry-meteorology/climate modeling
CCN	Cloud condensation nuclei
CCSR/NIES/FRCGC	The center for climate system research/national institute for environmental study/frontier research center for global change, japan
CDA	Chemical data assimilation

Acronym	Definition
CDC	Centers for disease control and prevention
CEREA	Atmospheric environment center
CESM	Community earth system model
CETEMPS	The center of excellence for the integration of remote sensing techniques and numerical modeling for the prediction of severe weather
CFD	Computational fluid dynamics model
CFL	Courant-Friedrichs-Lewy
CFORS	The chemical weather forecast system
CH ₄	Methane
CH ₃ •	A methyl radical
CH ₃ CH ₂ CH ₂ CH ₃	Butane
CH ₃ CHO	Acetaldehyde
CH ₃ COOH	Acetic acid
CH ₃ HC=CH ₂	Propene
CH ₃ O ₂	Methyl peroxy radical
CHASER	Atmospheric environment and radiative forcing
CHIMERE	The chimere air quality model
CHO•	Formyl radical
CHRONOS	The Canadian hemispheric and regional ozone and NO _x system
Cl-	Chloride
CMA	China meteorological administration
CMAQ	The community multiscale air quality (CMAQ) modeling system
CMAQ-MADRID	CMAQ with the model of aerosol dynamics, reaction, ionization, and dissolution
CMU	Carnegie Mellon university
CNR-ISAC	The institute of atmospheric sciences and climate
CO	Carbon monoxide
CO ₂	Carbon dioxide
CO _x	Carbon oxides
CONUS	The conterminous or continental U.S.A.
COPD	Chronic obstructive pulmonary disease
COSMO-ART	Consortium for small-scale modeling- aerosols and reactive trace gases
COSMO-MUSCAT	Consortium for small-scale modeling-multi-scale chemistry aerosol transport
COST	The European cooperation in science and technology
CPBL	The convective planetary boundary layer
CPTEC	Center for weather forecasting and climate studies of Brazil, Centro de previsão do tempo e estudos climáticos
CRIMech	Common reactive intermediates gas-phase mechanism

Acronym	Definition
CSAPPs	Crowdsourced apps
CSI	Critical success index
CSIRO	The commonwealth scientific and industrial research organization
CSL	Phenols and cresols
CSN	Chemical speciation network
CSP	Concentrating solar-thermal power systems
csv	Comma separated values
CTMs	Chemical transport models
CW-AQ	Chemical weather and air quality
CW-AQF	Chemical weather and air quality forecasting
CWF	Chemical weather forecasting
DACFOS	The Danish atmospheric chemistry forecasting system
DART	The data assimilation research testbed
DDM	Decoupled direct method
DEHM	The Danish eulerian hemispheric model
DEOM	The Danish eulerian operational model
DERMA	The Danish emergency response model of the atmosphere
DMS	Dimethyl sulfide
DMU-ATMI THOR	Denmark/danmarks miljøundersøgelser (dmu)- afdelingen for atmosfærisk miljø (the national environmental research institute (neri)- department of atmospheric environment) an integrated air pollution forecasting and scenario management system
DREAM	The Danish Rimpuff and Eulerian accidental release model
DSC	Digital synthetic city
EC	Elemental carbon
ECCAD portal	Emissions of atmospheric compounds and compilation of ancillary data
ECHAM5	A global climate model developed based on ECMWF global forecast model by max planck institute for meteorology, Hamburg , version 5
ECHAM5/6-HAMMOZ	ECHAM versions 5/6 with the Hamburg MOZART chemical mechanisms developed by Hamburg with the MOZART mechanism
ECLIPSE	Evaluating the climate and air quality impacts of short-lived pollutants
ECMWF	The European center for medium-range weather forecast
ECMWF IFS	ECMWF integrated forecasting system
EDGAR	Global atmospheric research
EEA	European environmental agency
EM	The Europa-model
EMA	The Egyptian meteorological authority
EMEP	The European monitoring and evaluation programme model
EmChem09	The European monitoring and evaluation programme for chemistry version 9, chemical mechanism

Acronym	Definition
EMEP-unified	The EMEP unified model that unifies previous versions of EMEP for acidification and oxidant modeling developed by the Norwegian meteorological institute
EnKF	The ensemble Kalman filter
ENIAC	The electronic numerical integrator and computer
Environ Canada	Environment Canada
EnviroHirnam	The environment – high resolution limited area model
ENVISAT	Environmental satellite
EPA	The U.S. environmental protection agency
EPSs	Ensemble prediction systems
EQSAM	Equilibrium simplified aerosol model
EQUISOLV II	The equilibrium solver version 2
ESA	Ecological society of America
Eta scheme	Eta-Mellor-Yamada scheme
ESMERALDA	Études multi régionales de l'atmosphère (multi regional studies of the atmosphere)
ESRL	Earth system research laboratory, NOAA
ETH	Ethene
ETHA	Ethane
EU	The European union
EULAG	Eulerian/semi-Lagrangian fluid solver
EURAD	The European air pollution dispersion model
FAR	False alarm rate or ratio
FARM	The flexible air quality regional model
Fe ³⁺	Iron
FINN	Fire inventory from NCAR
FLEXPART	Flexible particle dispersion model
FLUS	The future land use simulation model
FMI	Finnish meteorological institute
ForeChem	The Italian air quality forecasting model
FRIUUK	Status of work at RIU at university of cologne
FRP	Fire radiative power
FTP	File transfer protocol
F-TUV	The fast tropospheric ultraviolet and visible radiation model
FU-Berlin	The Free University of Berlin (freie universität berlin)
FWI	The Canadian fire weather index
GACM	The global atmospheric chemistry mechanism
GAINS	The greenhouse gas and air pollution interactions and synergies
GATORG	The gas, aerosol, transport, radiation, and general circulation model

Acronym	Definition
GATOR-GCMOM	The gas, aerosol, transport, radiation, general circulation, mesoscale, ocean model
GATOR/MCCM	The gas, aerosol, transport, and radiation air quality model/multiscale climate–chemistry model
GATOR/MMTD (or GATORM)	The gas, aerosol, transport, and radiation air quality model/a mesoscale meteorological and tracer dispersion model
GAW SAG APP	The global atmosphere watch program, with the scientific advisory groups on applications
GCM	General circulation model
GCTM	The global chemical transport model
GDPFS	Global data-processing and forecasting system
GEM-AQ	The global environmental multiscale weather prediction model with air quality processes
GEM-MACH	Global environmental multiscale model - modeling air quality and chemistry
GEM-MACH15	A limited-area 15-km version of global environmental multiscale model-modeling air quality and chemistry
GEMS	Global and regional earth-system (atmosphere) monitoring using satellite and in-situ data
GEOS-5	The Goddard earth observing system model, version 5 (geos-5)
G5CHEM	Geos-5 with geos-chem
GEOS-5 ESM	Geos-5 earth system model
GEOS-Chem	A global model of tropospheric chemistry and transport
GFAS	The global fire assimilations system
GeoSOS	The geographical simulation and optimization system
GFED4s	The global fire emission database
GISS GCM Model II	The Goddard institute for space studies general circulation model II
GLCF	The global land cover facility
GLOMAP	The global model of aerosol processes
GME	The German national meteorological service's operational global numerical weather prediction model
GMES	The global monitoring for environment and security programme
GMR	The greater metropolitan Sydney region
GOCART	The Goddard chemistry aerosol radiation and transport
GOCI	The geostationary ocean color imager
GOME	The global ozone monitoring experiment
GRAPES - CUACE	Global/regional assimilation and prediction system coupled with the china meteorological administration unified atmospheric chemistry environmental forecasting system
GRIB	Gridded binary or general regularly-distributed information in binary form

Acronym	Definition
GRIB 2	Gridded binary or general regularly-distributed information in binary form 2
GRS	The generic reaction set of equations
GSI	The grid point statistical interpolation system
GURME	Urban research meteorology and environment
H	Hydrogen atom
H ₂	Molecular hydrogen
HAQFS	The Hangzhou air quality forecasting system
HC3	Low reactive alkane based on ho-rate coefficients
HC5	Middle reactive alkane based on ho-rate coefficients
HC8	High reactive alkane based on ho-rate coefficients
HCl	Hydrogen chloride
HCHO	Formaldehyde
HCOOH	Formic acid
HDF5	Hierarchical data format 5
The HEMEN scheme	The hybrid of Euler-mass and Euler- number scheme
HR	Hit rate
HNO ₃	Nitric acid
H ₂ O	Water
H ₂ O ₂	Hydrogen peroxide
HO ₂	Hydroperoxy radical
HO _x	Odd hydrogen
HONO	Nitrous acid
HSO ₃ ⁻	Bisulfate anion
H ₂ SO ₃	Sulfurous acid
H ₂ SO ₄	Sulfuric acid
HTTPs	Hypertext transfer protocol
HWDs	Heat wave days
HRB	Hazard reduction burning
HYDE	History database of the global environment
HYSPLIT	Hybrid single-particle Lagrangian integrated trajectory
IAP-CAS	The institute of atmospheric physics, Chinese academy of sciences
IASI	The infrared atmospheric sounding interferometer
IBBI	The interdisciplinary biomass burning initiative
ICAO	The international civil aviation organization
ICAP	The international cooperative for aerosol prediction
ICAP MME	The international cooperative for aerosol prediction multi model ensemble

Acronym	Definition
ICONS	The initial conditions
ICTP	The Abdus Salam international Center for theoretical physics
IDN	Ice deposition nuclei
IIASA	The international institute for applied systems analysis
IMK-IFU	The institute of meteorology and climate research- atmospheric environmental research
IMK-TRO	The Institute of Meteorology and Climate Research - department troposphere research, German
IMPROVE	Interagency monitoring of protected environments
IN	Ice nuclei
INERIS	The French national institute for industrial environment and risks
INPs	The ice nucleation parameterizations
INPE	The national institute of spatial research
IPCC	Intergovernmental panel on climate change
IS4FIRES	The integrated monitoring and modeling system for wildland fires
ISORROPIA	"Equilibrium" in Greek, refers to the ISORROPIA thermodynamic module
ITCZ	The intertropical convergence zone
JMA	The japan meteorological agency
KET	Higher ketones
KF	Kain-Fritch
KIT	Karlsruhe institute of technology, German
LAI	Leaf area index
LAMI	The limited area model Italy
LCZ	The local climate zones
LES	Large-eddy simulations
LITR	Leibniz institute for tropospheric research
LMDzt-INCA	The Laboratoire de Météorologie Dynamique (dynamic meteorology laboratory) – zoom tracers GCM with interaction of chemistry and aerosol
LOC	Level of concern
LOTOS-EUROS	Long term ozone simulation - European operational smog model
LSM	Land surface model
LUCY	The large-scale urban consumption of energy model
LVOCs	Low-volatile organic compounds
LW	The longwave radiation
M	Third molecule
M7	The dynamical aerosol model in 7 modes)
M2UE	The Microscale Model for Urban Environment
MACC	Monitoring atmospheric composition & climate

Acronym	Definition
MADE/SORGAM	The Modal Aerosol Dynamics Model for Europe (MADE) with the secondary organic aerosol model (SORGAM)
MADRID	The model of aerosol dynamics, reaction, ionization, and dissolution
MADRID 2	The model of aerosol dynamics, reaction, ionization, and dissolution version 2
MAQSIP-RT	The multiscale air quality simulation platform—real time
MARS-A	The model for an Aerosol Reacting System (MARS) –version a
MARS-aero	The Eulerian photochemical dispersion model with aerosol
MASINGAR	The model of aerosol species in the global atmosphere
MASP	The metropolitan area of Sao Paulo
MATCH	Multiple-scale Atmospheric Transport and Chemistry Modeling System (Sweden)
MB	Mean bias
MCCM (or MM5/Chem)	The Multiscale Climate–Chemistry Model
MCM	Master chemical mechanism
ME	Mean error
MEGAPOLI	Megacities: emissions, urban, regional and global atmospheric pollution and climate effects, and integrated tools for assessment and mitigation
MECCA1	Module efficiently calculating the Chemistry of the Atmosphere, Version 1
MECTM	The mesoscale chemistry model
MELCHIOR1 and 2	The Mode Le Lagrangien De La Chimie De l'Ozone A l'échelle régionale Versions 1 and 2
MEMO/MARS	The mesoscale model/the Eulerian photochemical dispersion model
MEMO/MARS-aero	The mesoscale model/the Eulerian photochemical dispersion model with aerosol
MERRA	The Modern-era Retrospective Analysis for Research and Applications
MERRA 2	The Modern-era Retrospective Analysis for Research and Applications 2
MESSy	Modular Earth submodel system
Météo France- CNRM	The French meteorological office, centre national de recherches météorologiques
METRAS	Mesoscale meteorology model with passive tracer and pollen transport
Meso-NH	The Mesoscale Non-hydrostatic Chemistry (Meso-Nh-C) Model The Mesoscale Air Quality Mesoscale Non-hydrostatic Model
Meso-NH-C	The Mesoscale Non-hydrostatic Chemistry (Meso-Nh-C) Model The Mesoscale Air Quality Mesoscale Non-hydrostatic Chemistry Model
MetUM	The Met Office's Unified Model
MHEWS	Multi-hazard Early Warning Systems
MICROSYS	Micro-scale air quality modeling system
MIDAS	Met Office Integrated Data Archive System
MIR	The middle infrared

Acronym	Definition
MLS	Microwave limb sounder
MM5	The Penn State University/NCAR mesoscale model version 5
Mn ²⁺	Manganese
MNB	Mean normalized bias
MNE	Mean normalized error
MFB	Mean fractional bias
MFE	Mean fractional error
MOCAGE	The Météo-France multi-scale Chemistry and Transport model, modèle de chimie atmosphérique de grande échelle
MODIS	Moderate-resolution imaging spectroradiometer
MOPITT	Measurements of pollution in the troposphere
MOSAIC	The model for simulating aerosol interactions and chemistry
MOST	The Monin-Obukhov similarity theory
MOZART2	The model for ozone and related chemical tracers version 2
MOZART3	The model for ozone and related chemical tracers version 3
MOZART4	The model for ozone and related chemical tracers version 4
MPAS-A	The model for prediction across scales for atmosphere
MPIC	Max-Planck-Institute for Chemistry
MPIM	The Max Planck Institute for Mathematics
MRF	Medium range forecast
MSA	Methane sulfonic acid
MSC	The Meteorological Service of Canada
MSS	Meteorological Service Singapore
M-SYS	The Multiscale Model System
MUNICH	The Model of Urban Network of Intersecting Canyons and Highways
Na ⁺	Sodium
NAAQSs	The National Ambient Air Quality Standards
NAM	North American mesoscale
NAME	Numerical atmospheric-dispersion modeling environment
NA-ME-E	Northern Africa-Middle East-Europe Regional Center.
NAPS	National air pollution surveillance
NAQPMS	The IAP/CAS nested air quality prediction modeling system
netCDF	The network Common Data Form
NHM	The non-hydrostatic model
NMB	Normalized mean bias
NME	Normalized mean error
NMM	Non-hydrostatic mesoscale model
NMMB	Non-hydrostatic multi-scale meteorological model on the B grid

Acronym	Definition
NMMB-MONARCH	The multiscale online nonhydrostatic atmosphere chemistry model
NMVOCs	Non-methane volatile organic compounds
NCAR	The National Center for Atmospheric Research
NAAPS	Navy aerosol analysis and prediction system
NAQFC	The national air quality forecast capability
NASA	The National Aeronautics and Space Administration
NCDC	National climatic data center
NCEP	National centers for environmental prediction
NCEP-NGAC	NCEP NEMS GFS aerosol component
NEI	National Emissions Inventory
NEU	Northeastern University
NEMS/GFS	NOAA environmental modeling system/the global forecast system
Netherlands/KNMI, TNO, RIVM, PBL/KN	Royal Netherlands meteorological institute (KNMI), Netherlands organization for applied scientific research (TNO) , National Institute for Public Health and the Environment (RIVM) , the Netherlands environmental assessment agency (PBL)
NGM	The nested gridded model
NH3	Ammonia
NH4HSO4	Ammonium bisulfate
NH4NO3	Ammonium nitrate
(NH4)2SO4	Ammonium sulfate
NIAR	Norwegian Institute for air research
NINFA	North Italian network to forecast aerosol pollution
NKUA	National and Kapodistrian University of Athens
NMBs	Normalized mean biases
NMHC)	Non-methane hydrocarbon
NMHSs	National meteorological and hydrological services
NMM	The nonhydrostatic mesoscale model
NWP	Numerical weather prediction
NWP-chem	The NWP chemical gas mechanism
NWS	The U.S. National Weather Service
NO3	Nitrate radical
NO	Nitric oxide
NO2	Nitrogen dioxide
NOx	Nitrogen oxides
N2O5	Dinitrogen pentoxide
NOAA	The National Oceanic and Atmospheric Administration
NOAH	The National Center for Environmental Prediction, Oregon State University, Air Force, Hydrologic Research Lab. land surface module

Acronym	Definition
NRT	Near-real time
NTN	National trends network
O ₂	Molecular oxygen
O ₃	Ozone
O(3P)	Ground state oxygen atom
O(1D)	Energetically excited oxygen atom
OA	Organic aerosol
OC	Organic carbon
ODEs	Ordinary differential equations
OH	Hydroxyl radical
OLE	Double bonded carbon atoms
OLI	Internal alkenes
OLT	Primary alkenes
OM	Organic matter
OMI	Ozone monitoring instrument
OMPS	Ozone mapping profiler suite
OPAC	The optical properties of aerosols and clouds software library module
OPANA	Operational version of the atmospheric numerical pollution model for urban and regional areas
OPPIO	Ozone and PM ₁₀ polynomial inference based on observations
ORA	Organic acids
OR&R	Office of Response and Restoration
OSPM	The operational street pollution model
OSSEs	The observing system simulation experiments
PA	Pennsylvania
PAHs	Polycyclic aromatic hydrocarbons
PAN	Peroxyacetyl nitrate
PANX	Higher molecular weight pan analog
PAR	Alkane carbon atoms
PATH	The Hong Kong air quality forecasting system
Pb	Lead
PBL	The planetary boundary layer
PM _{2.5}	Particles with aerodynamic diameters less than or equal to 2.5 μm
PM ₁₀	Particles with aerodynamic diameters less than or equal to 10 μm
PMCAMx	Comprehensive air quality model with extensions for PM
POA	Primary organic aerosol
POD	Probability of detection
POI	Selected point of interest

Acronym	Definition
Polair3D	3D Eulerian CTM for regional air quality
POLYPHEMUS	The French air quality modeling system
Prev'air	Prévision de l'air (Air Forecast)
PRD	The Pearl River delta
PRO	Propane and all less reactive alkanes
PV	Photovoltaic
QFED	The quick-fire emissions dataset
QUIC	The quick urban and industrial complex plume modeling system
r	Correlation
RACM1	The regional atmospheric chemistry mechanism version 1
RACM2	The regional atmospheric chemistry mechanism version 2
RACM-ESRL	RACM-Earth system research laboratory
RACM-MIM	RACM-Mainz Isoprene Mechanism
RADM	The Regional Acid Deposition model
RADM2	The gas-phase chemical mechanism of Regional Acid Deposition model, version 2
RADMK	The gas-phase chemical mechanism of Regional Acid Deposition model version Karlsruhe Institute of Technology Institute of Meteorology and Climate Research
RAMS	The Regional Atmospheric modeling system
RAMS/ICLAMS	RAMS/integrated community limited area modeling system
RANS	Reynolds-averaged Navier-Stokes
RAQ	Regional air quality (chemistry scheme)
RAQMS	A regional aerosol assimilation/forecast model
RETRO	The reanalysis of the tropospheric chemical composition emission inventory
RCG	REM_Calgrid
RCO3	Acyl peroxy radicals
RCP 8.5	The Representative Concentration Pathways 8.5
REAS	Regional Emission Inventory in Asia
RegCM-CHEM4.5	Online gas-phase chemistry within the regional climate model system version 4.5
ReLACS	Regional lumped atmospheric chemical scheme
ReLACS2	Regional lumped atmospheric chemical scheme version 2
ReLACS-AQ	Regional lumped atmospheric chemical scheme - aqueous chemistry
REM-CALGRID	Regional Eulerian model - California grid model
REPS	Canada's regional ensemble prediction system
RFS	The NSW rural fire service
RH	Reactive hydrocarbons
RMSE	The root mean square error

Acronym	Definition
RIs	Refractive indices
RIU	Rhenish Institute for Environmental Research at Cologne University
RO	Alkoxy radical
RO ₂	Organic peroxy radicals
ROC diagram	Receiver operating characteristic diagram
RRTM	The rapid radiative transfer model
RSMC-ASDF	Regional specialized meteorological centers with activity specialization on atmospheric sand and dust forecast
RT	Real time
RT-AQF	Real-time air quality forecasting
S(IV)	Dissolved sulfur compounds with oxidation state IV
S(VI)	Sulfur compounds with oxidation state VI
SA-DEA	The south African department of environmental affairs
SAPRC-90	The 1990 statewide air pollution research center gas-phase mechanism
SAPRC-99	The 1999 statewide air pollution research center gas-phase mechanism
SAPRC-07	The 2007 statewide air pollution research center gas-phase mechanism
SAWS	South African Weather Service
SBUV2	The solar backscatter ultraviolet radiometer 2
SCAPE2	Simulating composition of atmospheric particles in equilibrium, version 2
SCIAMACHY	Scanning imaging absorption spectrometer for atmospheric cartography
SCRAM	The size and composition resolved aerosol model
SDS	The sand and dust storm
SDS-WAS	The sand and dust storm warning advisory and assessment system
SEARCH	Southeastern aerosol research and characterization
SILAM	The system for integrated modeling of atmospheric composition
SinG	The street-in-grid model
SIREAM	The size resolved aerosol model
SIRANE	An operational street network model
SKIRON/Dust	The SKIRON forecasting model with dust
SKIRON/TAPM	The SKIRON forecasting model/the air pollution model
SLCP	Short-lived climate pollutant
SMHI	Swedish meteorological and hydrological institute
SMOKE	The sparse matrix operator kernel emissions
SO ₂	Sulfur dioxide
SO ₄ ²⁻	Sulfate
SO _x	Sulphur oxides
SOA	Secondary organic aerosol

Acronym	Definition
SOAP	The secondary organic aerosol processor model
SPBL	The stable planetary boundary layer
SS	Sea-salt
SSA	The single scattering albedo
SSE	The sum of squared error
SSP3	Shared socio-economic pathways scenario 3
SST	Sea surface temperature
StdTrop	Standard tropospheric chemistry mechanism
STEM I	The sulfur transport Eulerian model, version 1
STEM-2K3	The sulfur transport and emissions model 2003
STILT	The stochastic time-inverted Lagrangian transport model
SUEWS	The surface urban energy and water balance schemes
SUNY-Albany	The state university of New York at Albany
SVOCs	Semi-volatile organic compounds
SW	The shortwave radiation
TEB	The town energy balance
TexAQS II/GoMACCS	The second Texas air quality study (TexAQS II)/Gulf of Mexico atmospheric composition and climate study (GoMACCS)
TKE	Turbulent kinetic energy
TM5 (KNMI-cy3-GEMS)	Tracer model version 5 (Koninklijk Nederlands Meteorologisch Instituut (knmi), Royal Netherlands Meteorological Institute –cy3 - global and regional earth-system (atmosphere) monitoring using satellite and in-situ data)
TANSO	Thermal and near infrared sensor for carbon observation
TOLUENE, TOL	Lumped aromatic species (including toluene, benzene and xylenes)
TOR	Tropospheric ozone residuals
TROPOMI	The tropospheric monitoring instrument
TUM (or UPM)	Technical University of Madrid (Universidad Politécnica De Madrid, Madrid)
TUV	The tropospheric ultraviolet and visible radiation model
txt	Text format
UAQIFS	Urban air quality information and forecasting system
UCAR	The University Corporation For Atmospheric Research
UCLA-GCM	The University of Los Angeles General Circulation Model
UCL	The Urban Canopy Layer
UCM	Urban Canopy Model
UCP	Urban Canopy Parameterization Or Parameter
UHI	The Urban Heat Island
UKAEA	The United Kingdom Atomic Energy Authority
UKAQ	United Kingdom Air Quality Model

Acronym	Definition
UKCA	United Kingdom Chemistry And Aerosols Model
UKMO	UK Met Office
UM	Unified Model
UNIFAC	The Universal Functional Activity Coefficient Method
USDA	U.S. Department Of Agriculture
US/FNMOC/NRL	The Fleet Numerical Meteorology and Oceanography Center/ Naval Research Laboratory
USP	The University of Sao Paulo
UTC	Coordinated Universal Time
VAACs	The Volcanic Ash Advisory And Assessment Centers
VBS	Volatility Basis Set Approach
VEI	Volcanic Explosivity Index
VFSP-WAS	Vegetation Fire And Smoke Pollution Warning And Advisory System
VISTAS	The Visibility Improvement State and Tribal Association of the Southeast
VOCs	Volatile Organic Compounds
VIIRS	The Visible Infrared Imaging Radiometer Suite
VRSM	Variable Size-Resolution Model
WHO	World Health Organization
WMO	World Meteorological Organization
WRF	The Weather Research And Forecasting
WRF/Chem	The Weather Research Forecast Model With Chemistry
WRF/Chem-MADRID	WRF/Chem with the model of aerosol dynamics, reaction, ionization, and dissolution
WSU	Washington State University
WUDAPT	The World Urban Database And Access Port Tool
WWOSC	World Weather Open Science Conference
xls	Microsoft excel
XYL	High reactive aromatic compounds
YSU	The Yonsei University PBL scheme
ZAMG	Zentralanstalt für meteorologie und geodynamik
ZSR	The Central Institution for Meteorology and Geodynamics of Austria, Zdanovskii-Stokes-Robinson

For more information, please contact:

World Meteorological Organization

7 bis, avenue de la Paix – P.O. Box 2300 – CH 1211 Geneva 2 – Switzerland

Strategic Communications Office

Tel.: +41 (0) 22 730 87 40/83 14 – Fax: +41 (0) 22 730 80 27

Email: communications@wmo.int

public.wmo.int